

# *NEUTRINO 2006*

*Proceedings of the XXIIth International Conference on Neutrino  
Physics and Astrophysics*

*Santa Fe, New Mexico, June 13-19, 2006*

*Edited by:*

*Geoffrey B. Mills*

*Steve Elliott*

*Terrance Goldman*

*Thomas Bowles*

*Los Alamos National Laboratory, Los Alamos, NM*

Single photocopies of single articles may be made for personal use or educational purposes as allowed by national copyright laws. Figures and tables may be reproduced for the purposes of derivative presentations and papers as long as they are properly referenced. Permission by the publisher is required for resale of material.

Notice: No responsibility is assumed by the Publisher for any injury and/or damages to persons or property as a matter of products liability, negligence or otherwise, or from any use herein.

## ***Forward***

The Neutrino 2006 conference held in Santa Fe by all reports was a great success in almost all respects due to the diligent work of the international and local organizing committees. Many thanks are in order for Tom Bowles, whose guidance tireless efforts lead to the conferences success. The one area which fell by the wayside was the publishing of these proceedings. The reason for the delay is not simple, but changes in LANL leadership and Tom's subsequent departure to full time service in the government of the great state of New Mexico certainly played a role.

The high quality of the presentations and proceedings of Neutrino 2006 have demanded that they be preserved and published before they are lost in the sands of time. These proceedings are an attempt to make that a reality. The work to create these proceedings was performed without a budget and during whatever spare time the editors could find. While this does not do justice to the fine work contained in the proceedings, it is where the project now stands.

We would like to thank Los Alamos National Laboratory, the Lensic Theater, and the International Advisory Committee for their support and patience with the conference and its proceedings.

*The Editors*

# *INVITED TALKS*

# Galactic sources of high energy neutrinos

**Felix Aharonian**

Dublin Institute for Advanced Studies, 5 Merrion Square, Dublin 2, Ireland &  
Max Planck Institut für Kernphysik, Saupfercheckweg 1, 69117 Heidelberg, Germany

E-mail: [felix.aharonian@mpi-hd.mpg.de](mailto:felix.aharonian@mpi-hd.mpg.de)

**Abstract.** The undisputed galactic origin of cosmic rays at energies below the so-called knee implies an existence of a nonthermal population of galactic objects which effectively accelerate protons and nuclei to TeV-PeV energies. The distinct signatures of these cosmic PeVatrons are high energy neutrinos and  $\gamma$ -rays produced through hadronic interactions. While  $\gamma$ -rays can be produced also by directly accelerated electrons, high energy neutrinos provide the most straightforward and unambiguous information about the nucleonic component of accelerated particles. The planned km<sup>3</sup>-volume class high energy neutrino detectors are expected to be sensitive enough to provide the first astrophysically meaningful probes of potential VHE neutrino sources. This optimistic prediction is based on the recent discovery of high energy  $\gamma$ -ray sources with hard energy spectra extending to 10 TeV and beyond. Amongst the best-bet candidates are two young shell-type supernova remnants – RXJ 1713.7-4946 and RXJ 0852.0-4622, and perhaps also two prominent plerions - the Crab Nebula and Vela X. Because of strong absorption of TeV  $\gamma$ -rays, one may expect detectable neutrino fluxes also from (somewhat fainter) compact TeV  $\gamma$ -ray emitters like the binary systems LS 5039 and LS I+61 303, and, hopefully, also from hypothetical "hidden" or "orphan" neutrino sources.

## 1. Introduction

Very High Energy ( $E \geq 0.1$  TeV; VHE) neutrinos are unique messengers of nonthermal phenomena in the Universe related to the hadronic interactions of protons and nuclei in cosmic TeVatrons and PeVatrons - Nature's masterly designed machines accelerating particles to TeV and PeV energies. In this regard VHE neutrinos are complementary to  $\gamma$ -rays which are produced both in electromagnetic and hadronic interactions. On the other hand, unlike  $\gamma$ -rays, neutrinos are not fragile; they interact only weakly with the ambient medium - gas, radiation and magnetic fields, and thus carry information about high energy processes occurring in "hidden" regions where the particle accelerators could be located. This concerns, first of all, the regions associated with compact objects - black holes, pulsars, the initial epochs of supernovae explosions, *etc.* The penetrating potential of neutrinos is important not only for extremely dense environments in which  $\gamma$ -rays are dramatically absorbed, but also moderately opaque sources from which we do see  $\gamma$ -rays, but after significant distortion due to internal and external absorption.

Ironically, this nice (from an astrophysical point of view) feature of neutrinos makes, at the same time, their detection extremely difficult. This explains why, over several decades high energy neutrino astronomy has remained essentially a theoretical discipline with many exciting ideas and predictions but without the detection of a single VHE neutrinos source. However, it is expected that, with arrival of the km<sup>3</sup>-volume class scale detectors like IceCube and KM3NeT (see e.g. [1, 2]), the status of the field will be changed dramatically. Generally, prediction of VHE

neutrino fluxes from astrophysical objects contain many assumptions and free parameters and, therefore, often contain large (orders of magnitude!) uncertainties. This leaves a significant freedom in speculations on the "best-bet neutrino sources", and consequently allows a broad spectrum of opinions concerning the prospects for detecting the first astrophysical neutrinos - from very enthusiastic statements to rather careful predictions prevailed by a healthy scepticism (see e.g. [3]).

Presently extragalactic objects like Active Galactic Nuclei (AGN) and sources of Gamma Ray Bursts (GRBs) are believed to be the most likely objects to be detected as neutrino sources, and therefore the driving force of experimental VHE neutrino astronomy (see e.g. [4]). The current models of AGN and GRBs indeed contain many attractive components (concerning the conditions of particle acceleration and their interactions) which make these objects *potentially detectable* sources of VHE neutrinos. On the other hand, the poor understanding of many aspects of the physics of AGN and especially GRBs, as well as the lack of constraints on neutrino productions rates from  $\gamma$ -ray observations (because of intrinsic and intergalactic absorption of VHE  $\gamma$ -rays), formally allow calculations in extreme model-parameter segments which often lead to rather high (over-optimistic) neutrino flux predictions.

The models of potential galactic neutrino sources, in particular the shell type Supernova Remnants (SNRs), Pulsar Wind Nebulae (PWNe), Star Formations Regions and the dense molecular clouds related to them, are robustly constrained by  $\gamma$ -ray observations of the galactic disk in very-high energy ( $\geq 1$  TeV) [5, 6] and ultra-high energy ( $\geq 100$  TeV) [7] domains. Typically, the expected fluxes from these objects are below the detection threshold of the planned neutrino detectors. However, the recent HESS discoveries of several TeV  $\gamma$ -ray sources at the flux level of "1 Crab", which can be interpreted within the hadronic models of gamma-ray emission, sustain a hope that that the first TeV galactic sources will be detected in foreseeable future by km<sup>3</sup>-volume class instruments like IceCube and Km3NeT.

## 2. On the detectability of galactic VHE neutrino sources

The recent performace studies of the km<sup>3</sup>-volume scale detectors show that the detection of a persistent point-like (for a typical angular resolution of VHE neutrino detectors the "point-like" source implies an object of angular size  $\leq 1^\circ$ ) neutrino sources for a realistic exposure time (typically, a few years continuous observations) is limited by a flux  $F(\geq 1\text{TeV}) \approx 10^{-11} \nu/\text{cm}^2\text{s}$  (see e.g. [8, 9, 10, 11]). The corresponding energy flux is  $f_E \approx 10^{-10} \text{erg}/\text{cm}^2\text{s}$  or somewhat less, depending on the spectrum in the most relevant energy band between 1 TeV and 100 TeV. This exceeds, by two orders of magnitude, the minimum  $\gamma$ -ray flux detectable in the same energy band. On the other hand, the sensitivity of the km<sup>3</sup>-scale detectors is comparable or better than the minimum detectable energy flux achieved by the Compton Gamma Ray Observatory detectors (COMPTEL, EGRET) in the MeV/GeV  $\gamma$ -ray band. For an isotropic VHE source located at a distance  $d$ , the luminosity of TeV neutrinos can be probed at the level

$$L_\nu \simeq 10^{34} (d/1 \text{ kpc})^2 \text{ erg/s} . \quad (1)$$

At first glance, this is a quite modest luminosity, at least for a powerful hadronic source located in a dense environment. Indeed, for production of TeV neutrinos in  $p$ - $p$  interactions with ambient gas of density  $n_0 = n/1\text{cm}^{-3}$ , the required total energy in multi-TeV protons is estimated  $W_p \simeq t_{\text{pp}} c_{p \rightarrow \nu} L_\nu \simeq 3 \times 10^{48} n_0 d_{\text{kpc}}^2 \text{ erg}$ , where  $t_{\text{pp}} \approx 5 \times 10^{14} n_0^{-1} \text{ s}$  is the radiative cooling time of protons due to inelastic  $p$ - $p$  interactions, and  $c_{p \rightarrow \nu} \approx 0.1$  is the fraction of average energy of a proton transferred to muon neutrinos. One may conclude that even in a relatively low density environment,  $n_0 \sim 1$ , the required total energy can be readily produced in young SNRs through diffusive shock acceleration (see e.g. [12]) or by a powerful pulsar assuming that a major fraction of the spin-down luminosity of the pulsar is converted to an ion-dominated wind (see e.g. [13]). However, these kinds of estimates can be misleading since they are based on a

silent assumption that all particles accelerated during the life-time of the source are effectively confined in a relatively compact region inside or nearby the accelerator. In fact, production of TeV neutrinos requires protons with energies well beyond 10 TeV the escape of which from the source is difficult to prevent. This, of course, would lead to a significant reduction of the neutrino production efficiency which in the case of  $p$ - $p$  interactions can be expressed in the following form:  $\eta = L_\nu/\dot{W}_p = \min[1, t_{\text{esc}}/t_{\text{pp}}] \times c_{p \rightarrow \nu}$ , where  $t_{\text{esc}}$  is the escape time of nonthermal particles. If the escape proceeds in the diffusion regime, then  $t_{\text{esc}} = R^2/2D(E)$ . It is convenient to write the diffusion coefficient  $D(E)$  in the following form  $D(E) = \xi r_L c/3 = 3.3 \times 10^{20} \xi E_{\text{TeV}} B_{\text{mG}}^{-1} \text{ cm}^2/\text{s}$ ;  $E_{\text{TeV}} = E/1 \text{ TeV}$  is the proton energy normalized to 1 TeV, and  $B_{\text{mG}} = B/10^{-3} \text{ G}$  is the magnetic field in units of mG. Generally the parameter  $\xi \geq 1$  is a function of energy. In the most effective confinement regime corresponding to the Bohm diffusion,  $\xi = 1$ . Thus, in a source of size  $R_{\text{pc}} = R/1 \text{ pc}$ , the production efficiency of TeV neutrinos, assuming that the hard spectrum of protons extends effectively to 100 TeV, is

$$\eta \approx 10^{-2} c_{p \rightarrow \nu} \xi^{-1} R_{\text{pc}}^2 n_0 B_{\text{mG}} . \quad (2)$$

The maximum possible efficiency of the TeV neutrino source,  $\eta \rightarrow c_{p \rightarrow \nu} \approx 0.1$  can in principle be achieved if  $R_{\text{pc}}^2 n_0 B_{\text{mG}} \geq 10^2 \xi$ . Such a condition can be best fulfilled in objects like giant molecular clouds, with a size  $R \sim 10 \text{ pc}$ , mass  $10^5 M_\odot$ , and magnetic field  $B \geq 0.1 \text{ mG}$ , provided that the propagation of multi-TeV protons proceeds close the Bohm diffusion regime. However, Bohm diffusion hardly can be realized in molecular clouds, thus  $\eta \ll c_{p \rightarrow \nu}$ , typically  $\eta \leq 10^{-3}$ , which implies that the acceleration power should exceed  $\dot{W}_p = \eta L_\nu \geq 10^{37} d_{\text{kpc}}^2 \text{ erg/s}$ . This significantly reduces the number of potentially detectable neutrino sources to the most powerful representatives of nonthermal source populations in our Galaxy. In addition to young SNRs and PWNe, possible emitters of TeV neutrinos are compact binary systems in which the compact object (a black hole or a pulsar) plays the role of particle accelerator, and the dense gas regions, e.g. the atmosphere of the companion star [14, 15, 16, 17] or the accretion plasma around the compact object [18], play the role of the target.

Moreover, in binary systems containing a luminous optical star and a compact object, the photomeson interactions could provide an additional channel for neutrino production, provided that protons are accelerated to energies exceeding the interaction threshold,  $E_{\text{th}} \approx (200 \text{ MeV}/3kT) m_p c^2 \approx 10^4 \text{ TeV}$  in the case of interactions with the starlight, and three orders of magnitude less for interactions with photons of the accretion disk. For a photon field with thermal a (Planckian) distribution, the interaction and escape times of protons are  $t_{\text{esc}} \approx 10^{10} \xi^{-1} R_{\text{pc}}^2 B_{\text{mG}} (kT/3eV) \text{ s}$ , and  $t_{p\gamma} \approx 10^{18} L_{37} R_{\text{pc}}^2 (kT/3eV) \text{ s}$ , respectively. It is remarkable that both timescales are proportional, although for completely different reasons (!), to the product  $R^2 kT$ , therefore the neutrino production efficiency appears independent, for a given luminosity of thermal radiation, of both the source size and the temperature of radiation, but strongly depends on the magnetic field

$$\eta \approx 10^{-9} \xi^{-1} L_{37} B_{\text{mG}} . \quad (3)$$

Thus we arrive at the conclusion that the neutrino production can be effective only in the compact objects with strong magnetic fields ( $B \geq 10 \text{ kG}$ ) and high turbulence (for confinement of protons with  $\xi \sim 1$ ). The immediate proximity of the luminous star (i.e. its photosphere) or the compact object, e.g the accretion disk or the base of the jet [19, 20], can be sites where the neutrino production proceeds with a reasonably high efficiency.

### 3. Detectability of neutrino sources in the context of multiwavelength observations

The *high efficiency* of neutrino production is a key condition for the detectability of the potential VHE neutrino sources given the *limited budget* of available energy and the *limited sensitivity* of

detectors. The above qualitative estimates show that this condition can be achieved only with certain combinations of a few key model parameters. Therefore, a careful inspection of these conditions before any detailed numerical calculations is highly advisable.

Independent constraints on the detectability of a VHE neutrino source can be obtained also from analysis of multi-wavelength observations, in particular in the most relevant VHE  $\gamma$ -ray band. Indeed, TeV  $\gamma$ -ray fluxes can be safely used as upper limits for neutrino fluxes, provided, of course, that the internal and external absorption of  $\gamma$ -rays is negligible. Generally, the production of VHE neutrinos is accompanied by the production of  $\gamma$ -rays, but not *vice versa*;  $\gamma$ -rays are copiously produced also in electromagnetic interaction both by electrons (through bremsstrahlung, inverse Compton scattering) and protons (e.g. through the synchrotron and curvature radiations). Moreover, since the main channels of neutrino and "hadronic" gamma-ray production are decays of charged  $\pi^\pm$  and  $\pi^0$  mesons, with decay time of charged pions significantly longer than the decay time of neutral pions, at certain conditions the production of neutrinos can be suppressed compared to  $\gamma$ -ray production. Indeed, in the lab frame, the decay time of charged pions responsible for TeV neutrino production is  $t_{\pi^\pm} = (E_\pi/m_\pi c^2) \tau_{\pi^\pm} \approx 2.5 \times 10^{-3} (E_\pi/10 \text{ TeV}) \text{ s}$ . On the other hand, the cooling time of pions due to inelastic  $\pi p$  and  $\pi\gamma$  interactions depends on the densities of the ambient gas  $n_p$  and X-ray photons  $n_x$ :  $t_{\pi p} \sim 10^{14} (n_p/1\text{cm}^{-3})^{-1} \text{ s}$ , and  $t_{\pi\gamma} \sim 10^{18} (n_x/1\text{cm}^{-3})^{-1} \text{ s}$ , respectively. Thus, charged pions would decay to  $\mu$  and  $\nu_\mu$  before interacting with the ambient photons and protons if  $n_x \leq 10^{21} \text{ cm}^{-3}$  and  $n_p \leq 10^{17} \text{ cm}^{-3}$ . Finally, the production of neutrinos from the subsequent muon decay would proceed with high probability as long as the magnetic field does not exceed  $B \approx 10^6 \text{ G}$ . This follows directly from the comparison of the decay time of muons,  $t_\mu = (E_\mu/m_\mu c^2) \tau_\mu \simeq 0.2 (E_\mu/10\text{TeV}) \text{ s}$ , with their synchrotron cooling time  $t_{\text{sy}} \approx 0.07 (B/10^6\text{G})^{-2} (E_\mu/10 \text{ TeV})^{-1} \text{ s}$ .

Thus, the ratio of  $\gamma$ -ray and neutrino production rates in a VHE source is expected to be of order of 1 or more,  $\gamma/\nu \geq 1$ . The absorption of  $\gamma$ -rays can, of course, significantly change the initial  $\gamma/\nu$  ratio. While for galactic sources the external  $\gamma$ -ray absorption (due to interactions with the interstellar IR photon fields) is not dramatic up to several tens of TeV [21], in compact galactic objects like X-ray binaries the internal absorption can be huge. However, the absorption of gamma-rays does not mean that the information is lost; the secondary electrons initiate a cascade in the same radiation field and/or are cooled via synchrotron radiation. In the first case, which happens when the radiation density  $w_r$  exceeds the energy density of the magnetic field,  $B^2/8\pi$ , the energy of the initial  $\gamma$ -rays is gradually reprocessed, down to energies at which the source becomes transparent. In binary systems containing luminous optical stars (like LS 5039) the main energy is released at GeV energies [20, 22], while in the case of particle acceleration in the accretion disk around a black hole (like Cygnus X-1), the initial energy is released mainly at MeV energies [23]. So far the MeV and GeV  $\gamma$ -ray sky has been explored at a depth corresponding to the energy flux  $\geq 10^{-10} \text{ erg/cm}^2\text{s}$ ; the data available in the MeV-GeV band from the VHE neutrino candidate sources associated with X-ray binaries provide important, although not very restrictive, upper limits on the energy flux of VHE neutrinos. With the arrival of GLAST, the MeV/GeV  $\gamma$ -ray observations will play a more decisive role in predictions of VHE neutrinos from compact objects.

#### 4. "Orphan" TeV neutrino sources?

The multiwavelength approach to the estimates of VHE neutrino fluxes expected from potential cosmic accelerators indicate that the fluxes of the best-candidate *persistent* galactic neutrino sources cannot significantly exceed  $\sim 10^{-11} \nu/\text{cm}^2\text{s}$ , i.e. most likely these sources are expected to be revealed at the level of statistically marginal signals. A possible exception could be "hidden" sources - proton accelerators completely shielded from us by a very thick ( $\gg 1000 \text{ g/cm}^2$ ) gas material in which the energy of ultrarelativistic protons is converted with 100 % efficiency

to secondaries, and, at the same time, the high energy electromagnetic radiation completely dissipates, and thus becomes invisible because of much stronger background and foreground thermal emission components. In such objects, the (highly unknown) total acceleration power of the source is the only model parameter that determines the neutrino flux; the source would be detectable by VHE neutrino detectors if the power of the "hidden" PeVatron exceeds, approximately by a factor of 10, the estimate given by Eq. (1).

There is another (more sophisticated) scenario of realization of "orphan" neutrino sources, i.e. objects with neutrino fluxes not accompanied by electromagnetic radiation. Such a possibility is related to the features of acceleration and radiation of particles in optically thick (with respect to the photon-photon pair production) relativistic flows which can be formed by hot plasma left behind a relativistic shock or exist in the form of jets. Generally it is silently assumed that nonthermal particles and hence their radiation are isotropically distributed in the comoving frame. However, this assumption can easily be violated in relativistic shocks and jets with a strong impact on the emission properties, especially at very high energies. Namely, the beam pattern of relativistic jets with a bulk motion Lorentz factor  $\Gamma$  in this energy domain appears much broader than the inverse Lorentz factor,  $\Gamma^{-1}$ . This results in an *off-axis* high energy emission [24] which is expected to be much brighter compared to the predictions derived from the standard Doppler boosting considerations applied to an isotropic (in the frame of the jet) source. However, in optically thick sources, the electromagnetic radiation from super-critical particles is reprocessed through the electron-photon cascades, becomes isotropic in the jet frame, and, therefore, strongly collimated in the lab-frame. Consequently, the reprocessed electromagnetic radiation cannot be observable at large viewing angles. Since this does not concern the high energy neutrinos, the jet when viewed off-axis, may appear as an *over-bright* neutrino source with an arbitrarily large ratio of the neutrino luminosity to the total electromagnetic luminosity. It should be noted that acceleration of protons in relativistic shocks and shear flows can be significantly enhanced when it proceeds through the so-called "converter" mechanism [25]. This mechanism, which utilizes multiple conversions of protons to neutrons through photomeson reactions, has certain advantages compared to the standard diffusive shock acceleration scenario. It greatly diminishes particle losses downstream and provides penetration of particles deep into the upstream region allowing a highly desirable energy boost by a factor of  $\Gamma^2$  at *each* shock encounter. Since the copious neutrino production is an intrinsic feature of this scenario, the realization of the converter mechanism in relativistic flows with large aspect angles would naturally lead to the appearance of an "orphan" VHE neutrino source.

### 5. First galactic TeV neutrino sources to be detected...

A possible hadronic origin of gamma-radiation of some of the TeV  $\gamma$ -ray sources discovered by HESS in the galactic plane [27] makes them also potential emitters of high energy neutrinos (see e.g. [26]). Recently, Vissani [8] Kistler and Beacom [9] and Kappes et al.[11] performed detailed calculations of the neutrino signal and background rates for the future 1km<sup>3</sup>-volume scale neutrino telescopes based on the energy spectra and source-morphologies of galactic TeV  $\gamma$ -ray sources reported by HESS. The potential of the km<sup>3</sup>-volume class detectors is limited, as mentioned above, by the detection of  $\geq 1$  TeV neutrino fluxes at the flux level of  $10^{-11}$   $\nu/\text{cm}^2\text{s}$  confined within an angle  $\leq 1^\circ$ . The related  $\gamma$ -ray flux in the same energy interval, for a proton spectra with power-law index  $\alpha \approx 2 - 3$ , is slightly, by a factor of 1 to 2, higher [28], i.e. quite close to the gamma-ray flux of the Crab Nebula - the standard candle of TeV  $\gamma$ -ray astronomy. Thus, the accompanied  $\gamma$ -ray flux in units of "1 Crab" can be treated as the detection threshold of the *galactic* neutrino astronomy with km<sup>3</sup>-volume class detectors. Presently, in addition to the Crab Nebula itself, three more TeV  $\gamma$ -ray sources are detected at the "1 Crab" level - two young shell-type SNRs RXJ 1713.7-3946 [29] and RXJ 0852.0-4622 [30] (Vela Jr), as well as a nearby PWN - Vela X [31].

### 5.1. Shell type Supernova Remnants

Young SNRs have been predicted, within a hadronic model, as extended TeV  $\gamma$ -ray and neutrino sources with shell type morphology and hard energy spectra extending to 100 TeV [32]. The morphological and spectroscopic studies of SNRs RXJ 1713.7-3946 and RXJ 0852.0-4622 by the HESS array of telescopes perfectly agree with these predictions, but ironically cannot yet be considered as an ultimate proof the hadronic model. The "trouble makers" are the alternative leptonic models which relate the TeV  $\gamma$ -rays to inverse Compton scattering of electrons responsible also for the nonthermal X-ray emission. Although these models do not provide satisfactory explanations of the energy spectra of  $\gamma$ -rays, and require very low magnetic field of order of 10  $\mu$ G [29, 30], they unfortunately cannot be safely excluded. This prevent us from making a robust statement of detection of SNRs as sources of cosmic ray protons and nuclei. Although it is believed that detailed theoretical studies of SNRs in the context of their multiwavelength properties should allow us to arrive at certain conclusions concerning the origin of TeV  $\gamma$ -ray emission, formally only the detection of TeV neutrinos from these objects can be considered as straightforward and unambiguous proof of acceleration of protons and nuclei. The predicted detection rates of  $\geq 1$  TeV neutrinos (of order of a few events per one year) from the brightest  $\gamma$ -ray SNRs RAJ1713.7-3946 and RAJ0852.0-4622 by a km<sup>3</sup>-volume detector in the Mediterranean Sea, make the prospects of detection of TeV neutrinos from these SNRs rather realistic. Unfortunately the location of these two SNRs is not favorable for IceCube. The existence of SNRs of similar brightness in TeV  $\gamma$ -rays located in the Northern Hemisphere will be explored, hopefully soon, by the VERITAS and MAGIC telescope systems. The search for TeV  $\gamma$ -ray sources in the Cygnus region - one of the most prominent and promising pieces of the galactic plane - is of a special interest. The recent Milagro observations of this region revealed a diffuse  $\gamma$ -ray component with several hot spots [33], the strongest of which, MGRO J2019+37 could be a neutrino source with a flux close to the detection threshold of IceCube [34].

### 5.2. Pulsar Wind Nebulae

The close associations of some of the extended TeV galactic sources discovered by HESS with several well established synchrotron X-ray nebulae (MSH 15-52, PSR J1826-1334, Vela X, *etc.*) confirm the early theoretical predictions about visibility of young PWNe in TeV  $\gamma$ -rays. The broad-band spectral energy distributions of these sources are readily explained by the standard PWN model which assumes acceleration of ultrarelativistic electrons by the pulsar wind termination shock. Yet, in some of these systems particle acceleration could be driven by ions present in the relativistic pulsar wind [13]. These ions are expected to produce  $\gamma$ -rays and neutrinos via inelastic interactions with the ambient medium [35, 36, 37, 38]. In this regard, the extended TeV source associated with the pulsar PSR B0833-45 (Vela X) is a possible candidate for such a "hadronic plerion". Indeed, although the observed  $\gamma$ -ray emission can be interpreted as inverse Compton emission of nonthermal electrons [31], one needs to make some strong (non-trivial) assumptions in order to explain the rather unusual spectrum of this source with photon index  $\Gamma \simeq 1.5$  and exponential cutoff around 14 TeV. The steady-state electron distribution constrained by  $\gamma$ -ray data requires an  $E^{-2}$  type power-law spectrum with a sharp cutoff around 70 TeV. Such a spectrum of electrons can be interpreted only in terms of negligible synchrotron cooling, which would be possible only in the case of unusually low nebular magnetic field (a few  $\mu$ G or less). Moreover, total energy in relativistic electrons and in the magnetic field required to match the observations is only a negligible fraction  $\sim 0.1\%$  of the pulsar spin-down energy released over the pulsar's life-time  $1.1 \times 10^4$  yr. This begs the question as to where the remaining energy has gone? Interestingly if we assume that a large fraction of the spin-down luminosity of the pulsar is carried out by relativistic protons and nuclei, one can satisfactorily explain both the absolute flux and the spectrum of TeV  $\gamma$ -rays of this unusual source [39]. Remarkably, the TeV neutrino flux expected within this scenario should be detectable by KM3NeT [11]. This

makes the Vela X as one of the best-bet candidates to be the first *detected* astronomical TeV neutrino source. For the IceCube detector an obvious target representing this source population is the Crab Nebula.

### 5.3. Compact Binary Systems

The recent detections of TeV  $\gamma$ -rays from two binary systems tentatively called microquasars – LS 5039 by HESS [40] and LSI 61 303 by MAGIC [41] – are amongst the most exciting discoveries of observational gamma-ray astronomy in the very high energy regime. This result clearly demonstrates that the galactic binaries systems containing a luminous optical star and a compact object (a black hole or a pulsar/neutron star), are sites of effective acceleration of particles (electrons and/or protons) to multi-TeV energies. As usual, whether the  $\gamma$ -rays are of hadronic or leptonic origin is a key question which however does not have a simple answer [42]. The critical analysis of conditions of particle acceleration and radiation in these sources, based on the temporal and spectral behavior of TeV  $\gamma$ -ray emission, in particular on the modulation of the TeV flux of LS 5039 with a period of 3.9 day, and the extension of its energy spectrum to 10 TeV and beyond, reduces the possible interpretations to a few options. One of them gives a preference to the hadronic origin of TeV photons, especially if they are produced within the binary system[20]. If so, the detected  $\gamma$ -rays should be accompanied by a flux of high energy neutrinos emerging from the decays of  $\pi^\pm$  mesons produced by  $p$ - $p$  and/or  $p\gamma$  interactions. The neutrino fluxes, which can be estimated on the basis of the detected TeV  $\gamma$ -ray fluxes, taking into account the severe internal  $\gamma\gamma \rightarrow e^+e^-$  absorption, depend significantly on the location of  $\gamma$ -ray production region(s) [43, 44]. The minimum neutrino flux above 1 TeV is expected to be at the level of  $10^{-12} \text{ cm}^{-2}\text{s}^{-1}$ ; however, it could be much higher - by a factor of 10, or even more. The detectability of the TeV neutrino signals significantly depends on the high energy cutoff in the spectrum of parent protons; if the spectrum of accelerated protons continues to 100 TeV and beyond, the predicted neutrino fluxes of LS 5039 and LSI 61 303 can be probed by KM3NeT [20] and IceCube [45, 46] detectors.

## 6. References

- [1] Halzen F 2007 *Science* **315** 66
- [2] Katz U F 2006 *NIMPA* **567** 457
- [3] Lipari P 2006 *NIMPA* **567** 405
- [4] Waxman E 2007 *Science* **315** 63
- [5] HESS collaboration 2006 *Astrophys J* **636** 777
- [6] Atkins R et al. (Milagro collaboration) 2005 *Phys. Rev. Lett.* **95** 251103
- [7] McKay T A et al. (CASA-MIA collaboration) 1993 *Astrophys. J* **417** 742
- [8] Vissani F 2006 *Astropart. Physics* **26** 310
- [9] Kistler M and Beacom J F *Phys. Rev. D* **74** id. 063007
- [10] Distefano C 2007 *Astrophys Space Sci*, in press, astro-ph/0608514
- [11] Kappes A, Hinton J, Stegmann Ch and Aharonian F A 2007 *Astrophys. J.* **656** 870
- [12] Malkov M A and Drury L 2001 *Report on Progress in Physics* **64** 429
- [13] Arons J 1995 *Space Sci. Rev.* **75** 235
- [14] Berezhinsky V S 1977, in Proc. "Ultra High Energy Neutrinos and Detection Possibilities by DUMAND" (FERMILAB, Batavia) 229
- [15] Vestrand W T and Eichler D 1982 *Astrophys. J.* **261** 251
- [16] Hillas A M 1984 *Nature* **312** 50
- [17] Gaisser T K and Stanev T 1985 *Phys. Rev. Lett.* **54** 2265
- [18] Anchordoqui L A, Torres D F, McCauley T P, Romero G E and Aharonian F A 2003 *Astrophys. J.* **589** 481
- [19] Distefano C, Guetta D, Waxman E and Levinson A 2002 *Astrophys. J.* **575** 378
- [20] Aharonian F, Anchordoqui L, Khangulyan D and Montaruli T 2006 *J of Physics: Conf. Ser.* **39** 408
- [21] Moskalenko I V, Porter T A and Strong A W 2006 *Astrophys. J.* **640** L155
- [22] Bednarek W 2006 *MNRAS* **368** 579
- [23] Aharonian F A and Vardanian V V 1985 *Astrophys. Space Sci.* **115** 31

- [24] Derishev E V, Aharonian F A and Kocharovsky, VI V 2007 *Astrophys. J.* **655** 980
- [25] Derishev E V, Aharonian F A, Kocharovsky, V V and Kocharovsky, VI V 2003 *Phys. Rev. D* **68** id.043003
- [26] Dermer C D 2007 *Proc. of TeV-Particle Astrophysics II*, in press
- [27] Aharonian F A 2007 *Science* **315** 70
- [28] Kelner S R, Aharonian F A and Bugayov V V 2006 *Phys. Rev. D* **74** id.034018
- [29] HESS collaboration 2004 *Nature* **432** 75; 2006 *Astron. Astrophys.* **449** 223
- [30] HESS collaboration 2005 *Astron. Astrophys.* **437** L7
- [31] HESS collaboration 2006 *Astron. Astrophys.* **448** L43
- [32] Drury L, Aharonian F A and Völk H J 1994 *Astron. Astrophys* **287** 959
- [33] Abdo A A et al (Milagro collaboration) 2006, *Astrophys. J.*, submitted, astro-ph/0611691
- [34] Beacom J F, Kistler M D 2007 *Phys Rev. D* (submitted), astro-ph/0701751
- [35] Atoyan A M and Aharonian F A 1996 *MNRAS* **278** 525
- [36] Bednarek W and Protheroe R J 1997 *Phys. Rev. Lett.* **79** 2616
- [37] Bednarek W 2003 *Astron. Astrophys* **407** 1
- [38] Amato E, Guetta D and Blasi P 2003 *Astron. Astrophys.* **402** 827
- [39] Horns D, Aharonian F, Santangelo A, Hoffmann A and Masterson C 2006 *Astron. Astrophys* **451** L51
- [40] HESS collaboration 2005 *Science* **309** 746; *Astron. Astrophys* **460** 743
- [41] Albert J et al (MAGIC collaboration) 2006 *Science* **312** 1771
- [42] Paredes J M 2007, in "Frontier Objects in Astrophysics and Particle Physics"; astro-ph/0609168
- [43] Dubus G 2006 *Astron. Astrophys.* **451** 9
- [44] Boettcher M 2007 *Astropart. Physics.*, in press: astro-ph/0609136
- [45] Christiansen H R, Orellana M and Romero G E 2006 *Phys. Rev. D* **73** 063012
- [46] Torres D F and Halzen Francis 2006 astro-ph/0607368

# Dark Matter Detection: Current Status

**Daniel S. Akerib**

Dept. of Physics, Case Western Reserve University, Cleveland, Ohio 44106, USA

E-mail: [akerib@case.edu](mailto:akerib@case.edu)

**Abstract.** Overwhelming observational evidence indicates that most of the matter in the Universe consists of non-baryonic dark matter. One possibility is that the dark matter is Weakly-Interacting Massive Particles (WIMPs) that were produced in the early Universe. These relics could comprise the Milky Way’s dark halo and provide evidence for new particle physics, such as Supersymmetry. This talk focuses on the status of current efforts to detect dark matter by testing the hypothesis that WIMPs exist in the galactic halo. WIMP searches have begun to explore the region of parameter space where SUSY particles could provide dark matter candidates.

## 1. Dark Matter and the WIMP Hypothesis

The previous talk by L.M. Krauss [1] covered the broad evidence for dark matter along with a survey of the candidates from particle physics. In this talk the focus is the specific class of particles he referred to as WIMPs, or Weakly Interacting Massive Particles. Their detection relies on the hypothesis that they populate the galactic halo at the local dark matter density of about  $0.3 \text{ GeV}/\text{cm}^3$  with a Maxwellian velocity distribution with a RMS speed of about 220 km/s and that they would scatter from atomic nuclei resulting in detectable energy depositions.

Figure 1a shows the standard “progress” plot in this field, in which the elastic cross section normalized to the nucleon is plotted against the WIMP mass. Theoretical regions for specific models sample appropriate regions of parameter space, including WMAP constraints of the relic density, known accelerator bounds on particle parameters, as well as specific imposed constraints that define the model, *e.g.*, minimal Supergravity which assumes a high degree of degeneracy in the SUSY masses and couplings. Other than the unconfirmed claim by the DAMA collaboration, which observes an annual modulation expected due to seasonal kinematic variations corresponding to the heart-shaped  $3\sigma$  contour [2], experimental upper limits are shown as curves that exclude the parameter space above them at 90% C.L.. That is, cross sections higher than a given limit curve would have been observed in the given experiment. Further experimental bounds are shown below in Figure 1b.

## 2. Searching for Dark Matter

If WIMPs are indeed the dark matter, their local density in the galactic halo inferred from the Milky Way’s gravitational potential may allow them to be detected via elastic scattering from atomic nuclei in a suitable terrestrial target [3]. Owing to the WIMP-nucleus kinematics assuming a WIMP RMS-speed of about 220 km/s (typical of bound objects in the halo), the energy transferred to the recoiling nucleus is on the order of 10 keV [9]. The expected rate of WIMP interactions is  $\sim 10^{-16}$  per nucleon per year [10],

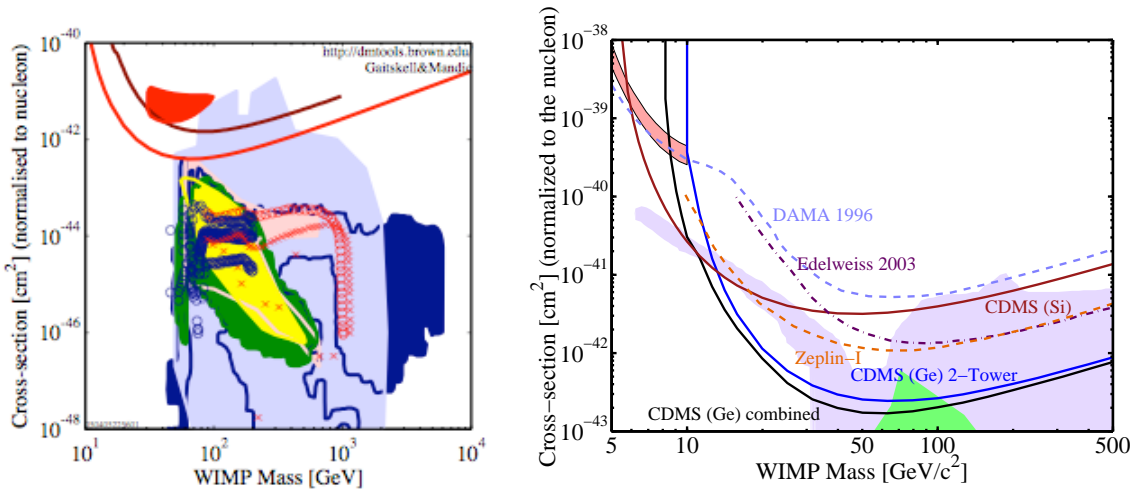


**Figure 1.** (a) Left: The plot of WIMP-nucleon cross section versus WIMP mass includes various theoretical predictions for different SUSY models, including “Split Supersymmetry” (circles [4, 5]), post-LEP LHC Benchmarks (X’s [6]), and minimal supergravity with and without the muon  $g-2$  constraint (medium grey and black; [7]). The closed contour at upper left is the DAMA annual modulation signal [2]. For illustration, some experimental bounds are shown: the upper from EDELWEISS [16] and the lower from CDMS’s 2003 data [8]. (b) Right: On a reduced scale, this version shows the present state of experimental bounds for 90 % C.L. limits on the WIMP-nucleon scalar cross section. The upper CDMS Ge curve uses only the most recent data of 34kg-days [10]; the lower Ge curve includes data from the previous run [11]. Supersymmetric models allow the largest shaded region [12], and the smaller shaded region [13]. The shaded region in the upper left is a sodium-recoil interpretation [15] of the DAMA NaI claim, and experimental limits are from DAMA [14], EDELWEISS [16], and ZEPLIN [18].

tends to be exceeded in this energy range by the rate of interactions from natural radiation. Therefore, WIMP search experiments must be located deep underground for protection from cosmic rays, made of high purity materials with low natural radioactivity, and have the ability to reject residual backgrounds.

A common technique to accomplish this background rejection is to use so-called “recoil discrimination.” The WIMP mass is well-matched kinematically to depositing energy on the order of 10 keV to an atomic nucleus in a detection medium. On the other hand, the dominant sources of background are electromagnetic, namely, gammas and betas from uranium and thorium decay chains, environmental radon, potassium-40, etc. Since these backgrounds deposit energy in the electrons in the detection medium, discriminating between, say, a recoiling germanium or xenon nucleus with 10 keV versus a 10 keV electron from a Compton scatter is an important tool for defeating the background.

Also taking into account the relatively low rate of WIMP-induced recoils, and the intrinsic inability of a detector to discriminate between neutrons and WIMPs, as well as other issues pertaining to the signal, the desirable characteristics of a dark matter experiment follow:

- High purity to minimize residual background.
- Recoil discrimination to reject residual background.
- Great depth to minimize cosmic-ray related backgrounds, primarily high-energy neutrons produced by unvetted muon interactions in the cavern walls, because neutrons with energy above

- Large instrumented detector mass to maximize the interaction rate. Good statistics on the signal also allow for the study of a secondary characteristic of the signal, that of seasonal modulation due to a kinematic effect from the Earth's variation between prograde and retrograde motion with respect to the Sun's orbit about the Galactic center.<sup>1</sup>
- Low energy threshold, also to maximize the rate, given that the nucleus's recoil energy spectrum is roughly a falling exponential.
- Position information of the interaction site since WIMPs will interact uniformly (and some backgrounds may not).
- Information on the recoiling nucleus direction, because the Earth's rotation combined with a preferred direction of the lab's velocity vector with respect to the Galaxy, results in a diurnal modulation in the incoming WIMP "wind" direction.

### 3. Dark Matter Experiments: CDMS

In this section, I discuss the methods and results obtained by the Cryogenic Dark Matter Search (CDMS) Collaboration, of which I am a member and which currently has the world-leading sensitivity. In section 4, I survey some of the other techniques and experiments that are under way or under development, which will illustrate the both the broad range of approaches to meet the criteria described above and the great level of activity aimed at detecting dark matter.

The primary distinction of the CDMS experiment is our novel ionization and athermal-phonon detectors, which provide detailed information about each event. A key parameter, the "ionization yield," is determined for each event through the simultaneous measurement of an ionization signal and a phonon-mediated signal, and is defined as the ratio of the ionization signal per unit recoil energy. Recoil energy is determined by the phonon signal with a correction for the phonons produced by the drifting ionization. The ionization yield is useful because nuclear-recoil events have typically a one-third lower yield than electron recoils, as is illustrated in Figure 2. The discrimination power is well demonstrated by exposing the detector to gammas and neutrons.

Briefly, the detectors consist of 1-cm-thick 3-inch-diameter germanium or silicon puck-like cylinders upon which metals are photolithographically deposited. The electrode structures collect the ionization signal in a standard capacitor-like geometry. The phonons are collected by superconducting aluminum quasi-particle traps which in turn funnel the broken Cooper pairs into thin superconducting tungsten meanders. The tungsten meanders are maintained in the middle of their 80 mK superconducting transition with a stable voltage bias. Events are sensed by change in the film resistance, which results in a current signal coupled to a SQUID amplifier. To maintain appropriate operating temperature, the detectors are operated in a shieldable cryostat at a temperature of 50 mK. The shield consists of lead shielding for gammas, polyethylene for moderating neutrons, and scintillator to tag muon-coincident events.

While the ionization yield is effective at rejecting electron recoils in the bulk, betas that have energy in the range of WIMP recoils are not very penetrating and suffer a reduced yield in a few-micron-thick "dead layer" typical of semi-conductor ionization detectors. Fortunately, this loss of yield, which can cause a false-positive nuclear recoil, is compensated by a difference in pulse shape between surface events and bulk events owing to the differing phonon propagation velocities of the two types of events. This effect is illustrated in Figure 3, which shows the onset of the phonon pulse relative to the prompt ionization signal (or "start time") versus the ionization yield.

Experiment runs in the underground setup in the Soudan Mine in 2003 and 2004 resulted in total exposures in germanium after cuts of 53 kg-days. No events above estimated background

<sup>1</sup> This effect has been observed by the DAMA collaboration, resulting in the contour of Figure 1a, but remains controversial and contested by other searches.

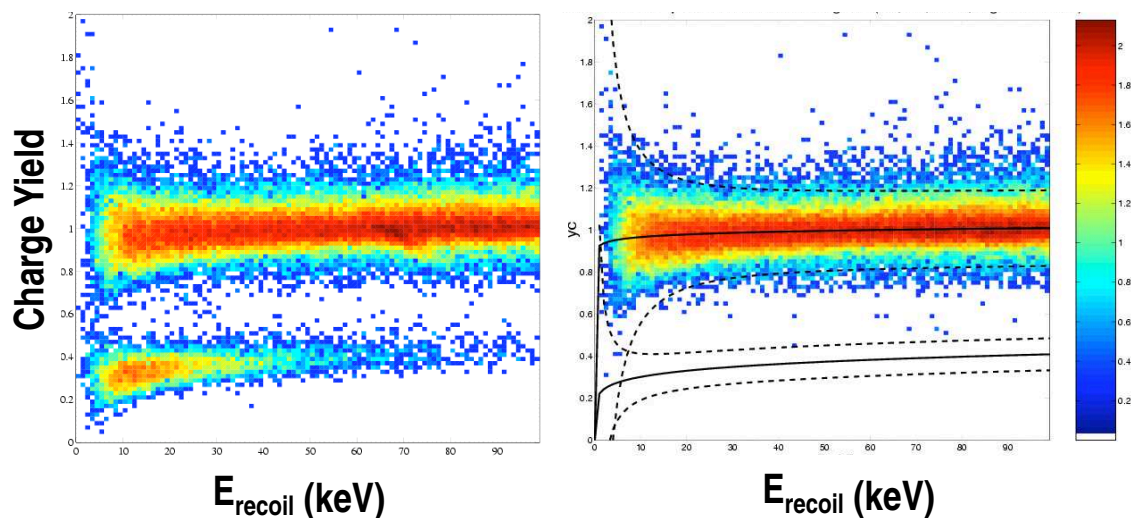


**Figure 2.** These scatter plots of yield versus recoil energy illustrate the discrimination capability of the detectors when exposed to gamma + neutron source ( $^{252}\text{Cf}$ ) on the left and gammas only ( $^{60}\text{Co}$ ) on the right. The plot on the right contains over 50,000 events in the “gamma” band, none of which is falsely identified as a nuclear recoil event in the lower “neutron” band.

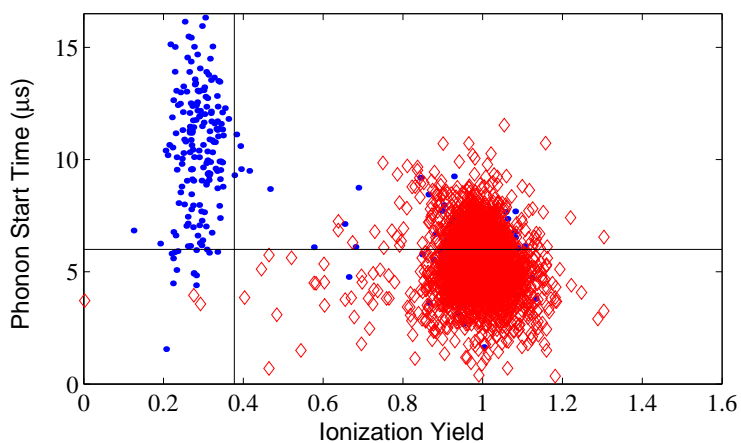


**Figure 3.** This plot of start time versus yield shows the improved 2-parameter discrimination between gamma-induced events from  $^{133}\text{Ba}$  calibration (diamonds), including a tail of surface events, and neutron induced events from  $^{252}\text{Cf}$  (dots). The two lines define the approximate acceptance region for nuclear recoils (upper right) with high rejection of both bulk and surface gamma-induced and electron recoils.

were observed, where background expectations were less than one event in each of the two exposures. (See [10] and references therein for a complete discussion.) These data led to the limits on the WIMP-nucleon cross section for spin-dependent couplings shown in Figure 1b. In addition to ruling out some regions of SUSY parameter space, these limits contradict the claim by DAMA [2] assuming a standard halo and couplings.

#### 4. A Survey of Some Other Techniques

Some of the other leading experiments searching for dark matter use recoil discrimination techniques and cryogenic detectors similar to CDMS. The EDELWEISS collaboration also uses a combination of ionization and phonons, but the phonon signal is purely thermal (based on NTD thermistors), and so there is no discrimination between bulk and surface events in the thermal channel. Instead, the focus of that group has been to emphasize minimizing the effects of the dead layer by experimenting with different types of charge contacts. While some progress was made, the performance limitations have led to them to pursue highly-resistive metal contacts that promise some surface discrimination in the thermal signal. The limit set by EDELWEISS's 2002/2003 was a then-best result [16], and is shown in Figure 1b.

The CRESST collaboration uses cryogenic detectors as well, but instead of ionization as the second parameter, they use scintillating substrates and the ratio of light to charge to discriminate the type of recoil. The thermal signal from the calcium tungstate ( $\text{CaWO}_4$ ) targets are read out with a tungsten superconducting thermometer, and the light signal is absorbed and converted to heat in a second thin crystal with a similar read out. Limits from their 2004 data show a neutron background, which was identified with the oxygen recoils. Under that interpretation, that is, in which no nuclear recoils are attributed to the tungsten nuclei, the resulting limit [17] is similar to the limit curve of EDELWEISS.

Liquid nobles, namely, neon, argon and xenon are all generating interest as dark matter detectors. Several programs to develop new detectors are underway, and one, the Zeplin collaboration, has produced a limit (again, see Figure 1b on the cross section [18]). This limit is based on the Zeplin-I detector, which detects scintillation pulses in liquid xenon. For more details on the current results of Zeplin-I, and a comprehensive overview of the liquid nobles dark matter program, see the following talk by Nigel Smith [19].

A completely different approach to gaining immunity to electromagnetic backgrounds is the revival of the bubble chamber by the COUPP Collaboration [20]. The idea here is to operate the chamber in a thermodynamic regime in which the lower energy density tracks from electron recoils and minimum ionizing radiation are insufficient to nucleate bubbles, but where the higher energy density recoils of nuclei are above the nucleation-energy threshold. A technical challenge, which has been met, was to passivate the walls of the vessel so that microcracks in the walls were not a cause of spontaneous nucleations, allowing the chamber to remain stable. The present configuration of the experiment is a 2-kg  $\text{CF}_3\text{I}$  bubble chamber being setup in a modest-depth site in the MINOS near-detector gallery at Fermilab for a demonstration test.

Finally, as mentioned earlier, it is possible to establish the galactic origin of a signal if the direction of the recoil nucleus can be detected. The only demonstrated method of performing such a measurement has been in the low-pressure TPC technology developed by the DRIFT collaboration [21]. In this device, recoiling nuclei ionize the TPC gas in the presence of  $\text{CS}_2$ , which is highly electronegative. The  $\text{CS}_2$  negative ions that form are drifted through the gas to read out MWPC's with very little diffusion and so the primary ionization track is preserved. Also, a measure of the ionization per unit pathlength is a good identifier of the recoil type. Unfortunately, to match the physical size of the track with the position resolution of the read out, the chamber must be run at low pressure (about a 1/20th of an atmosphere) and so a very large target volume is required. Furthermore, to have sufficient statistics to observe the diurnal modulation in the directional distribution of the tracks, on the order of a hundred detected

events is needed [22]. This presents a daunting challenge, since the cross section is not even known. However, ongoing R&D is attempting to address this challenge with superior read out schemes. For example, the required statistics are reduced approximately by a factor of ten if the head of the track can be identified.

## 5. Summary and Outlook

The outlook for WIMP detection looks very promising. Following more than a decade of detector development in cryogenic detectors, significant strides have been made in sensitivity. The challenge to cryogenic detectors, which I believe we will be able to meet with sufficient R&D efforts, is to continue scaling the detector mass; clearly the technology itself performs extremely well with regard to background rejection. Within the CDMS collaboration, the technology is already capable of an additional factor of ten at Soudan, and plans for a “SuperCDMS” 25-kg experiment for a factor beyond that have been proposed. Plans for further scale up and cryogenic detector improvements are also underway among the CRESST and EDELWEISS collaborations. On the liquid nobles front, intensive efforts are being brought to bear and we should see some important technology demonstrations in the coming year or two, in particular by the XENON, ZEPLIN and XMASS groups using xenon, and the DEAP and WARP collaborations using argon and/or neon. The COUPP bubble chamber, and also the PICASSO experiment, are using innovative techniques based on superheated liquids, for background immunity.

The advancing of this work, and the possibility of producing WIMP candidates in the lab as the LHC era begins, offer the potential for much exciting science as we attempt to unravel the nature of dark matter.

\ack I thank my valued colleagues on the CDMS experiment for a most enjoyable and successful experiment. My research has or is being supported by the National Science Foundation under Grant Nos. AST-9978911, PHY-9722414, and PHY-0503729.

- [1] L.M. Krauss, these proceedings.
- [2] R. Bernabei *et al.* (DAMA Collaboration), *Phys. Lett.* **B480**, 23-31 (2000); R. Bernabei *et al.* , astro-ph/0405282.
- [3] M.W. Goodman and E. Witten, *Phys. Rev.* **D31**, 3059 (1985).
- [4] N. Arkani-Hamed and S. Dimopoulos, hep-th/0405159.
- [5] G.F. Giudice and A. Romanino, hep-ph/0406088.
- [6] J. Ellis, K. A. Olive, Y. Santoso and V.C. Spanos, *Phys. Lett.* **B565**, 176-182 (2003).
- [7] E.A. Baltz and P. Gondolo, hep-ph/0407039.
- [8] D.S. Akerib *et al.* (CDMS Collaboration), *Phys. Rev. Lett.* **93**, 211301 (2004).
- [9] J.D. Lewin and P.F. Smith, *Astropart. Phys.* **6**, 87 (1996).
- [10] D.S. Akerib *et al.* (CDMS Collaboration), *Phys. Rev. Lett.* **96**, 011302 (2006).
- [11] D.S. Akerib *et al.* (CDMS Collaboration), *Phys. Rev. Lett.* **93**, 211301 (2004).
- [12] A. Bottino *et al.* , *Phys. Rev.* **D69**, 037302 (2004).
- [13] J. Ellis *et al.* , *Phys. Rev.* **D71**, 095007 (2005).
- [14] R. Bernabei *et al.* (DAMA Collaboration), *Phys. Lett.* **B389**, 757 (1996).
- [15] P. Gondolo and G. Gelmini, *Phys. Rev.* **D71**, 123520 (2005).
- [16] V. Sanglard, *et al.* (EDELWEISS Collaboration), *Phys. Rev.* **D71**, 122002 (2005).
- [17] G. Angloher, *et al.* (CRESST Collaboration), *Astropart. Phys.* **23**, 325-339 (2005).
- [18] G.J. Alner *et al.* (UK Dark Matter Collab.), *Astropart. Phys.* **23**, 444 (2005).
- [19] N.J.T. Smith, these proceedings.
- [20] W.J. Bolte *et al.* (COUPP Collaboration), astro-ph/0503398.
- [21] D.P. Snowden-Ifft, C.J. Martoff, J.M. Burwell, *Phys. Rev.* **D61**, 101301 (2000).
- [22] C.J. Copi, L.M. Krauss, D. Simmons-Duffin, S.R. Stroiney, astro-ph/0508649.

# Neutrino oscillations: theory and phenomenology

**E K Akhmedov**<sup>1</sup>

Department of Theoretical Physics, Royal Institute of Technology, AlbaNova University Center, SE-106 91 Stockholm, Sweden

E-mail: akhmedov@ictp.trieste.it

**Abstract.** A brief overview of selected topics in the theory and phenomenology of neutrino oscillations is given. These include: oscillations in vacuum and in matter; phenomenology of 3-flavour neutrino oscillations; CP and T violation in neutrino oscillations in vacuum and in matter; matter effects on  $\nu_\mu \leftrightarrow \nu_\tau$  oscillations; parametric resonance in neutrino oscillations inside the earth; oscillations below and above the MSW resonance; unsettled issues in the theory of neutrino oscillations.

## 1. A bit of history...

The idea of neutrino oscillations was first put forward by Pontecorvo in 1957 [1]. Pontecorvo suggested the possibility of  $\nu \leftrightarrow \bar{\nu}$  oscillations, by analogy with  $K^0 \bar{K}^0$  oscillations (only one neutrino species –  $\nu_e$  – was known at that time). Soon after the discovery of muon neutrino, Maki, Nakagawa and Sakata [2] suggested the possibility of neutrino flavour transitions (which they called “virtual transmutations”).

## 2. Theory

### 2.1. Neutrino oscillations in vacuum

Neutrino oscillations are a manifestation of leptonic mixing. For massive neutrinos, weak (flavour) eigenstates do not in general coincide with mass eigenstates but are their linear combinations. The diagonalization of the leptonic mass matrices leads to the emergence of the leptonic mixing matrix  $U$  in the expression for the charged current interactions. This matrix relates the left-handed components of the neutrino mass eigenstates and flavour eigenstates:

$$|\nu_a^{\text{fl}}\rangle = \sum_i U_{ai}^* |\nu_i^{\text{mass}}\rangle \quad (a = e, \mu, \tau; i = 1, 2, 3). \quad (1)$$

For relativistic neutrinos, the oscillation probability in vacuum is

$$P(\nu_a \rightarrow \nu_b; L) = \left| \sum_i U_{bi} e^{-i \frac{m_i^2}{2p} L} U_{ai}^* \right|^2. \quad (2)$$

For 2-flavour (2f) oscillations, which are a good first approximation in many cases, one has  $|\nu_e\rangle = \cos \theta |\nu_1\rangle + \sin \theta |\nu_2\rangle$ ,  $|\nu_\mu\rangle = -\sin \theta |\nu_1\rangle + \cos \theta |\nu_2\rangle$ , and eq. (1) yields the 2f transition

<sup>1</sup> On leave from the National Research Center “Kurchatov Institute”, Moscow, Russia

probability

$$P_{\text{tr}} = \sin^2 2\theta \sin^2 \left( \frac{\Delta m^2}{4E} L \right). \quad (3)$$

The modes of neutrinos oscillations depend on the character of neutrino mass terms:

- Dirac mass terms ( $\bar{\nu}_L m_D N_R + h.c.$ ): active - active oscillations  $\nu_{aL} \leftrightarrow \nu_{bL}$  ( $a, b = e, \mu, \tau$ ) Neutrinos are Dirac particles.
- Majorana mass terms ( $\bar{\nu}_L m_L (\nu_L)^c + h.c.$ ): active - active oscillations  $\nu_{aL} \leftrightarrow \nu_{bL}$ . Neutrinos are Majorana particles.
- Dirac + Majorana mass terms ( $\bar{\nu}_L m_D N_R + \bar{\nu}_L m_L (\nu_L)^c + \bar{N}_R M (N_R)^c + h.c.$ ): active - active oscillations  $\nu_{aL} \leftrightarrow \nu_{bL}$ ; active - sterile oscillations  $\nu_{aL} \leftrightarrow (N_{bR})^c \equiv (N_b^c)_L$ . Neutrinos are Majorana particles.

Would an observation of active - sterile neutrino oscillations mean that neutrinos are Majorana particles? Not necessarily! In principle, one can have active - sterile oscillations with only Dirac - type mass terms at the expense of introducing additional species of sterile neutrinos with opposite lepton number  $L$ .

### 2.2. Neutrino oscillations in matter – the MSW effect [3]

Matter can change the pattern of neutrino oscillations drastically. In particular, a resonance enhancement of oscillations and resonance flavour conversion become possible (Wolfenstein, 1978; Mikheyev & Smirnov, 1985 [3]). Matter effect on neutrino oscillations is due to the coherent forward scattering of neutrinos on the constituents of matter. Charged current interactions between  $\nu_e$  and the electrons of matter yields an effective potential of the electron neutrinos  $V_e^{\text{CC}} \equiv V = \sqrt{2} G_F N_e$ , which leads to a modification of the nature of neutrino oscillations in matter. The 2f neutrino evolution equation in matter is

$$i \frac{d}{dt} \begin{pmatrix} \nu_e \\ \nu_\mu \end{pmatrix} = \begin{pmatrix} -\frac{\Delta m^2}{4E} \cos 2\theta + V & \frac{\Delta m^2}{4E} \sin 2\theta \\ \frac{\Delta m^2}{4E} \sin 2\theta & \frac{\Delta m^2}{4E} \cos 2\theta \end{pmatrix} \begin{pmatrix} \nu_e \\ \nu_\mu \end{pmatrix}. \quad (4)$$

The mixing angle in matter  $\theta_m$ , which diagonalizes the Hamiltonian on the r.h.s. of eq. (4), is different from the vacuum mixing angle  $\theta$ :

$$\sin^2 2\theta_m = \frac{\sin^2 2\theta \cdot \left(\frac{\Delta m^2}{2E}\right)^2}{\left[\frac{\Delta m^2}{2E} \cos 2\theta - \sqrt{2} G_F N_e\right]^2 + \left(\frac{\Delta m^2}{2E}\right)^2 \sin^2 2\theta}. \quad (5)$$

The flavour eigenstates can now be written as  $|\nu_e\rangle = \cos \theta_m |\nu_{1m}\rangle + \sin \theta_m |\nu_{2m}\rangle$ ,  $|\nu_\mu\rangle = -\sin \theta_m |\nu_{1m}\rangle + \cos \theta_m |\nu_{2m}\rangle$ , where  $|\nu_{1m}\rangle$  and  $|\nu_{2m}\rangle$  are the eigenstates of the neutrino Hamiltonian in matter (matter eigenstates). The Mikheyev - Smirnov - Wolfenstein (MSW) resonance condition is

$$\sqrt{2} G_F N_e = \frac{\Delta m^2}{2E} \cos 2\theta. \quad (6)$$

At the resonance  $\theta_m = 45^\circ$  ( $\sin^2 2\theta_m = 1$ ), i.e. the mixing in matter becomes maximal. For the case of constant-density matter, the fact that the mixing in matter becomes maximal at a certain neutrino energy was first pointed out in [4].

If the matter density changes slowly enough (adiabatically) along the neutrino trajectory, neutrinos can undergo a flavour conversion (see fig. 1). In the adiabatic regime the transitions between the matter eigenstates  $|\nu_{1m}\rangle$  and  $|\nu_{2m}\rangle$  are strongly suppressed, i.e. these states evolve independently. However, their flavour composition, which is determined by the mixing angle  $\theta_m$ , varies with density. The adiabaticity (slow density change) condition can

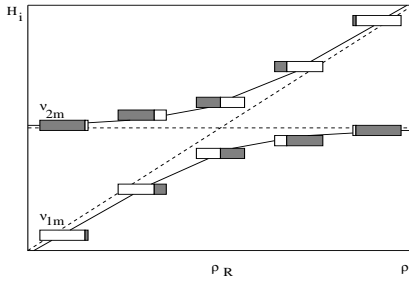


**Figure 1.** Adiabatic neutrino flavour conversion. Solid curves show the energy levels of neutrino matter eigenstates, dashed curves illustrate level crossing in the absence of mixing. Black and white filling corresponds to the weights of neutrino flavour eigenstates in given matter eigenstates.

be written as  $(\sin^2 2\theta / \cos 2\theta)(\Delta m^2 / 2E)L_\rho \gg 1$ , where  $L_\rho$  – electron density scale height:  $L_\rho = |(1/N_e)dN_e/dx|^{-1}$ .

A simple and useful formula for 2f conversion probability, averaged over production/detection positions (or small energy intervals), was derived in [5]:

$$\overline{P}_{\text{tr}} = \frac{1}{2} - \frac{1}{2} \cos 2\theta_i \cos 2\theta_f (1 - 2P'). \quad (7)$$

Here  $\theta_i$  and  $\theta_f$  are the mixing angles in matter in the initial and final points of the neutrino path, and  $P'$  is the hopping probability, which takes into account possible deviations from adiabaticity: in the adiabatic regime  $P' \ll 1$ , whereas in the extreme non-adiabatic regime  $P' = \sin^2(\theta_i - \theta_f)$ .

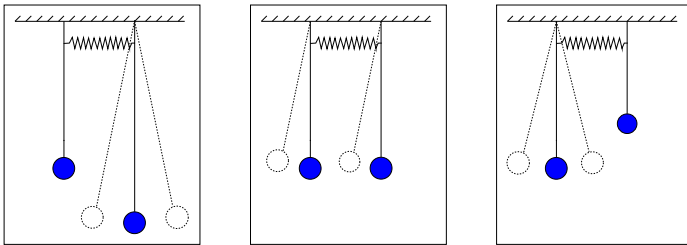


**Figure 2.** Mechanical analogue of neutrino flavour conversion in matter – two coupled pendula of variable lengths.

An illuminating analogy of neutrino flavour conversion in matter is provided by a system of two coupled pendula (see fig. 2). When the right pendulum gets a kick, it starts oscillating, but the left pendulum is almost at rest because the eigenfrequencies of the two pendula are very different. With the length  $l_2$  of the right pendulum slowly decreasing, its eigenfrequency approaches that of the left one, and when  $l_2 = l_1$  the two frequencies coincide (the resonance occurs): both pendula oscillate with the same amplitude. When the length of the right pendulum decreases further, the amplitude of its oscillations decreases too, while the left pendulum starts oscillating with a large amplitude. This adiabatic transfer of the oscillation energy from one pendulum to another is analogous to the adiabatic neutrino flavour conversion.

Analysis of the solar neutrino data and the results of the KamLAND and CHOOZ reactor neutrino experiments has convincingly demonstrated that the (large mixing angle) MSW effect is responsible for the flavour conversion of solar neutrinos, thus resolving the long-standing problem of the deficiency of the observed flux of solar neutrinos. This is illustrated by the analysis of the Bari group, in which the strength of the matter-induced potential of electron neutrinos was considered a free parameter (fig. 3). For more on MSW effect, see the talk of A. Friedland [7].

### 3. Phenomenology

All the available neutrino data except those of the LSND experiment can be explained in terms of oscillations between the 3 known neutrino species –  $\nu_e$ ,  $\nu_\mu$  and  $\nu_\tau$ . If the LSND results are correct, they would most likely require the existence  $\geq 1$  light sterile neutrinos. The MiniBooNE experiment was designed to confirm or refute the LSND claim, and the results are expected very soon. From now on I will concentrate on 3-flavour (3f) oscillations of active neutrinos. For a review on sterile neutrinos, see the talk of A. Kusenko [8].

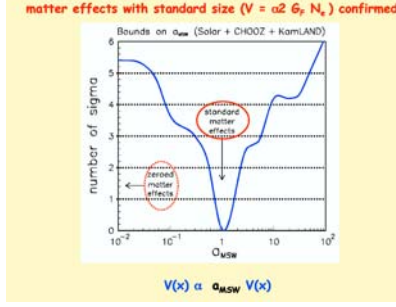


**Figure 3.** Results of the analysis of the solar, CHOOZ and KamLAND data with the standard matter-induced potential rescaled by a factor  $a_{MSW}$ , treated as a free parameter. The value  $a_{MSW} \approx 1$  is strongly favoured [6].

### 3.1. 3-flavour neutrino mixing and oscillations

For 3 neutrino species the mixing matrix depends in general on 3 mixing angles  $\theta_{12}$ ,  $\theta_{23}$  and  $\theta_{13}$ , one Dirac-type CP-violating phase  $\delta_{CP}$ , and two Majorana-type CP violating phases  $\sigma_{1,2}$ . The Majorana-type phases do not affect neutrino oscillations, and the relevant part of the leptonic mixing matrix can be written in the standard parameterization as

$$U = \begin{pmatrix} c_{12}c_{13} & s_{12}c_{13} & s_{13}e^{-i\delta_{CP}} \\ -s_{12}c_{23} - c_{12}s_{13}s_{23}e^{i\delta_{CP}} & c_{12}c_{23} - s_{12}s_{13}s_{23}e^{i\delta_{CP}} & c_{13}s_{23} \\ s_{12}s_{23} - c_{12}s_{13}c_{23}e^{i\delta_{CP}} & -c_{12}s_{23} - s_{12}s_{13}c_{23}e^{i\delta_{CP}} & c_{13}c_{23} \end{pmatrix}, \quad (8)$$

where  $s_{ij} = \sin\theta_{ij}$  and  $c_{ij} = \cos\theta_{ij}$ .

Neutrino oscillations probe the neutrino mass squared differences, which satisfy  $\Delta m_{sol}^2 \equiv \Delta m_{21}^2 \ll \Delta m_{32}^2 \simeq \Delta m_{31}^2 \equiv \Delta m_{atm}^2$ . Accordingly, there are two possible orderings of the neutrino masses: normal hierarchy, when the mass eigenstate  $\nu_3$ , separated from  $\nu_1$  and  $\nu_2$  by the largest mass gap, is the heaviest one, and inverted hierarchy, when  $\nu_3$  is the lightest state.

In many cases 2f description of neutrino oscillations gives a good first approximation. The reasons for this are (i) the hierarchy of  $\Delta m^2$ :  $\Delta m_{sol}^2 \ll \Delta m_{atm}^2$ , and (ii) the smallness of  $|U_{e3}|$ . There are exceptions, however: when oscillations due to the solar frequency ( $\propto \Delta m_{sol}^2$ ) are not frozen, the probabilities  $P(\nu_\mu \leftrightarrow \nu_\tau)$ ,  $P(\nu_\mu \rightarrow \nu_\mu)$  and  $P(\nu_\tau \rightarrow \nu_\tau)$  do not have a 2f form [9]. However, even for the probabilities of oscillations involving  $\nu_e$ , the corrections due to 3-flavourness can be as large as  $\sim 10\%$ , i.e. are at the same level as the accuracy of the present-day data, and so cannot be ignored. In addition, there is a number of very interesting pure 3f effects in neutrino oscillations. Therefore, 3f analyses are now a must.

### 3.2. Genuine 3f effects in neutrino oscillations

These are, first of all, CP and T violation. CP violation results in  $P(\nu_a \rightarrow \nu_b) \neq P(\bar{\nu}_a \rightarrow \bar{\nu}_b)$ , whereas T violation leads to  $P(\nu_a \rightarrow \nu_b) \neq P(\nu_b \rightarrow \nu_a)$ . Under the standard assumptions, quantum field theory conserves CPT. CPT invariance of neutrino oscillations in vacuum gives  $P(\nu_a \rightarrow \nu_b) = P(\bar{\nu}_b \rightarrow \bar{\nu}_a)$ , therefore CP violation implies T violation and vice versa.

One can consider the following probability differences as measures of CP and T violation:

$$\Delta P_{ab}^{CP} \equiv P(\nu_a \rightarrow \nu_b) - P(\bar{\nu}_a \rightarrow \bar{\nu}_b), \quad \Delta P_{ab}^T \equiv P(\nu_a \rightarrow \nu_b) - P(\nu_b \rightarrow \nu_a). \quad (9)$$

From CPT invariance, for oscillations in vacuum one has  $\Delta P_{ab}^{CP} = \Delta P_{ab}^T$ ,  $\Delta P_{aa}^{CP} = 0$ . In the 3f case  $\Delta P_{e\mu}^{CP} = \Delta P_{\mu\tau}^{CP} = \Delta P_{\tau e}^{CP}$ . Experimental observation of CP violation in neutrino oscillations represents a significant challenge (for more on that, see the talk of O. Mena [10]).

*CP violation and T violation in  $\nu$  oscillations in matter.* Normal matter (with number of particles  $\neq$  number of antiparticles) violates C, CP and CPT, which leads to a fake (extrinsic) CP violation in neutrino oscillations. It exists even in the 2f limit and may complicate the study of the fundamental (intrinsic) CP violation.

The situation with T-violation in matter is different: matter with density profile symmetric w.r.t. the midpoint of neutrino trajectory does not induce any fake T violation. Asymmetric profiles do, but only for  $N > 2$  flavors [11, 12]. Matter-induced T violation may fake fundamental T violation and complicate its study (extraction of  $\delta_{\text{CP}}$  from the experiment). However, it is absent when either  $U_{e3} = 0$  or  $\Delta m_{\text{sol}}^2 = 0$  and thus is doubly suppressed by both these small parameters. Therefore its effects in terrestrial experiments are expected to be very small [12].

*Matter effects on  $\nu_\mu \leftrightarrow \nu_\tau$  oscillations.* In the 2f limit, matter does not affect  $\nu_\mu \leftrightarrow \nu_\tau$  oscillations. However, this is not true in the full 3f framework [13]. In particular, for oscillations inside the earth there are ranges of baselines and neutrino energies for which the matter effect can be very large (fig. 4, left panel,  $E \sim 5 - 10$  GeV). If one ignores them, one may end up with a negative expected flux of oscillated  $\nu_\mu$  in atmospheric neutrino experiments (right panel).

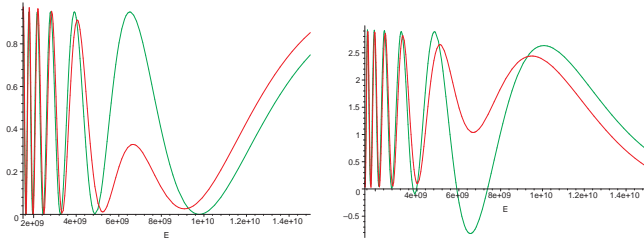


**Figure 4.** Left panel:  $P_{\mu\tau}$ . Right panel: oscillated flux of atmospheric  $\nu_\mu$ .  $\Delta m_{31}^2 = 2.5 \times 10^{-3} \text{ eV}^2$ ,  $\sin^2 \theta_{13} = 0.026$ ,  $\theta_{23} = \pi/4$ ,  $\Delta m_{21}^2 = 0$ ,  $L = 9400 \text{ km}$ . Red (dark) curves – with matter effects, green (light) curves – without matter effects on  $P_{\mu\tau}$ .

### 3.3. Parametric resonance in neutrino oscillations in matter

The MSW effect is not the only possible way matter can influence neutrino oscillations. Another interesting possibility is a parametric enhancement of neutrino oscillations in matter [14, 15]. Parametric resonance in oscillating systems with varying parameters occurs when the rate of the parameter change is correlated in a certain way with the values of the parameters themselves. A well-known mechanical example is a pendulum with vertically oscillating suspension point (fig. 5): at the resonance, the pendulum turns upside down and starts oscillating around the vertical, normally unstable, equilibrium point. Neutrino oscillations in matter can undergo parametric

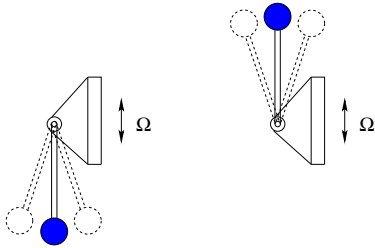


**Figure 5.** Parametric resonance in oscillations of a pendulum with vertically oscillating point of support. For small-amplitude oscillations the resonance condition is  $\Omega_{\text{res}} = 2\omega/n$  ( $n = 1, 2, 3, \dots$ ).

enhancement if the length and size of the density modulation is correlated in a certain way with neutrino parameters. This enhancement is completely different from the MSW effect; in particular no level crossing is required. An example admitting an exact analytic solution is the “castle wall” density profile [15, 16]. The resonance condition in this case can be written as [16]  $X_3 \equiv -(\sin \phi_1 \cos \phi_2 \cos 2\theta_{1m} + \cos \phi_1 \sin \phi_2 \cos 2\theta_{2m}) = 0$ , where  $\phi_{1,2}$  are the oscillation phases acquired in layers 1 and 2 and  $\theta_{m1,2}$  are the corresponding mixing angles in matter.

The earth’s density profile seen by neutrinos with core-crossing trajectories can be well approximated by a piece of this castle wall profile. Interestingly, the parametric resonance condition  $X_3 = 0$  can be satisfied for oscillations of core-crossing neutrinos in the earth for a rather wide range of zenith angles both at intermediate energies [17, 18, 16] and high energies [19] (see fig. 6). The parametric resonance of neutrino oscillations in the earth can be observed in future atmospheric or accelerator experiments if  $\theta_{13}$  is not too much below its current upper limit.

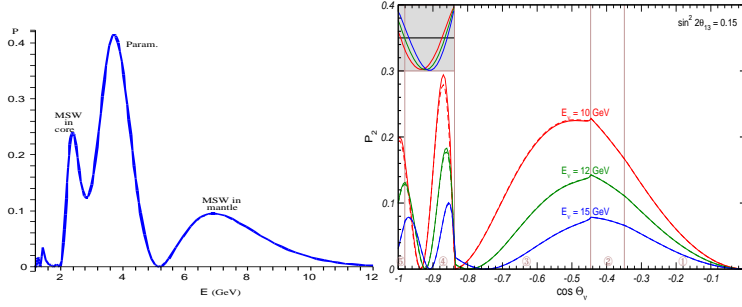


**Figure 6.** Parametric resonance in oscillations of core-crossing neutrinos. Left panel:  $\cos \Theta = -0.89$ ,  $\sin^2 2\theta_{13} = 0.01$ ; right panel:  $\sin^2 2\theta_{13} = 0.15$ , small window shows the values of  $X_3$ .

### 3.4. Some recent developments

When  $V \ll \Delta m^2/2E$  (oscillations of low- $E$  neutrinos in matter or, equivalently, oscillations in low-density matter), matter effects on neutrino oscillations are small and can be considered in perturbation theory. This gives simple and transparent formulas describing, in particular, oscillations of solar and supernova neutrinos in the earth. The earth matter effects can be expressed through the regeneration factor  $f_{reg} = P_{2e}^\oplus - P_{2e}^{vac}$ , where  $P_{2e}$  is the probability for  $\nu_2$  to become  $\nu_e$  upon traversing the earth. In the 3f framework one has [20]

$$P_{2e}^\oplus - P_{2e}^{vac} = \frac{1}{2} c_{13}^4 \sin^2 2\theta_{12} \int_0^L dx V(x) \sin \left[ 2 \int_x^L \omega(x') dx' \right], \quad (10)$$

where  $\omega(x) = \sqrt{[\cos 2\theta_{12} \delta - c_{13}^2 V(x)/2]^2 + \delta^2 \sin^2 2\theta_{12}}$ ,  $\delta = \Delta m_{21}^2/4E$ . The 2f ( $\theta_{13} = 0$ ) version of these equations was derived in [21] (see also [22]).

Oscillations of high energy neutrinos in matter or, equivalently, oscillations in dense matter ( $V > \delta \equiv \Delta m^2/4E$ ), can also be very accurately described analytically. The transition probability for oscillations in a matter of an arbitrary density profile is given by [19]

$$P = \delta^2 \sin^2 2\theta \left| \int_0^L dx e^{-2i\phi(x)} \right|^2, \quad \phi(x) = \int_0^x dx' \omega(x'). \quad (11)$$

The accuracy of this approximation is quickly increasing with neutrino energy (see the right panel of fig. 6, where the exact results are shown by solid curves and the analytic results, by dashed curves).

## 4. Unsettled issues?

The theory of neutrino oscillations is quite mature and well developed now. However, it is far from being complete or finished, and a number of basic questions are still being debated. Below I list some of these questions (given in italics), along with my short answers to them:

- *Equal energies or equal momenta?*
  - Neither equal  $E$  nor equal  $p$  assumptions, normally used in the derivations of the oscillation probability, are exact. But for relativistic neutrinos, both give the correct answer.
- *Evolution in space or in time?*
  - This is related to the previous question. For relativistic neutrinos both are correct and equivalent. Fortunately, in practice we only deal with relativistic neutrinos. In the non-relativistic case the very notion of the oscillation probability is ill-defined (the probability depends on both the production and detection processes).
- *Claim: evolution in time is never observed*
  - Incorrect. Examples: K2K, MINOS (and now also CNGS) experiments, which use the neutrino time of flight in order to suppress the background.

- *Is wave packet description necessary?*
  - Yes, if one wants to rigorously justify the standard oscillation probability formula. Once this is done, the wave packets can be forgotten unless the issues of coherence become important.
- *Do charged leptons oscillate?*
  - No, they don't.
- *Is the standard oscillation formula correct?*
  - Yes, it is. In particular, there is no extra factor of two in the oscillation phase, which is sometimes claimed to be there. However, it would be theoretically interesting and important to study the limits of applicability of the standard approach.

A number of subtle issues of the neutrino oscillation theory still remain unsettled (e.g., rigorous wave packet treatment, oscillations of non-relativistic neutrinos, etc). At present, this is (rightfully) of little concern for practitioners.

What are interesting future tasks for the theory and phenomenology of neutrino oscillations? These include the search for the best strategies for measuring neutrino parameters, study of subleading effects and effects of non-standard neutrino interactions and of the domains of applicability and limitations of the current theoretical framework. Future experimental results may also bring some new surprises and pose more challenging problems for the theory!

## Acknowledgments

The author was supported by the Wenner-Gren Foundation as the Axel Wenner-Gren visiting professor at the Royal Institute of Technology.

## References

- [1] Pontecorvo B 1957 *Zh. Eksp. Teor. Fiz.* **34** 247 [1958 *Sov. Phys. JETP* **7** 172]
- [2] Maki Z, Nakagawa M and Sakata S 1962 *Prog. Theor. Phys.* **28** 870
- [3] Wolfenstein L 1978 *Phys. Rev. D* **17** 2369;  
Mikheev S P and Smirnov A Y 1985 *Yad. Fiz.* **42** 1441 [Sov. J. Nucl. Phys. **42** 913]
- [4] Barger V D, Whisnant K, Pakvasa S and Phillips R J N 1980 *Phys. Rev. D* **22** 2718
- [5] Parke S J 1986 *Phys. Rev. Lett.* **57** 1275
- [6] Fogli G L, Lisi E, Palazzo A and Rotunno A M 2003 *Phys. Rev. D* **67** 073001 [arXiv:hep-ph/0211414];  
Fogli G L, Lisi E, Marrone A and Palazzo A 2004 *Phys. Lett B* **583** 149 [arXiv:hep-ph/0309100];  
Fogli G and Lisi E 2004 *New J. Phys.* **6** (2004) 139
- [7] Friedland A, talk at this Conference
- [8] Kusenko A, talk at this Conference, arXiv:hep-ph/0609158
- [9] Akhmedov E K *et al.* 2004 *JHEP* **0404** 078 [arXiv:hep-ph/0402175]
- [10] Mena O, talk at this Conference, arXiv:hep-ph/0609031
- [11] de Gouvêa A 2001 *Phys. Rev. D* **63** 093003 [arXiv:hep-ph/0006157]
- [12] Akhmedov E K, Huber P, Lindner M and Ohlsson T 2001 *Nucl. Phys. B* **608** 394 [arXiv:hep-ph/0105029]
- [13] Akhmedov E K 2003 *Nucl. Phys. Proc. Suppl.* **118** 245 [arXiv:hep-ph/0207342];  
Gandhi R *et al.*, 2005 *Phys. Rev. Lett.* **94** 051801 [arXiv:hep-ph/0408361]
- [14] Ermilova V K, Tsarev V A and Chechin V A 1986 *Kr. Soob. Fiz. [Short Not. Lebedev Institute]* **5**, 26
- [15] Akhmedov E K 1988 *Yad. Fiz.* **47** 475 [Sov. J. Nucl. Phys. **47** (1988) 301]; preprint IAE-4470/1, 1987
- [16] Akhmedov E K 1999 *Nucl. Phys. B* **538** 25 [arXiv:hep-ph/9805272]
- [17] Liu Q Y and Smirnov A Y 1998 *Nucl. Phys. B* **524** 505 [arXiv:hep-ph/9712493];  
Liu Q Y, Mikheyev S P and Smirnov A Y 1998 *Phys. Lett. B* **440** 319 [arXiv:hep-ph/9803415]
- [18] Petcov S T 1998 *Phys. Lett. B* **434** 321 [arXiv:hep-ph/9805262]
- [19] Akhmedov E K, Maltoni M and Smirnov A Y 2005 *Phys. Rev. Lett.* **95** 211801 [arXiv:hep-ph/0506064]
- [20] Akhmedov E K, Tortola M A and Valle J W F 2004 *JHEP* **0405** 057 [arXiv:hep-ph/0404083]
- [21] Ioannisian A N and Smirnov A Y 2004 *Phys. Rev. Lett.* **93** (241801) [arXiv:hep-ph/0404060]
- [22] de Holanda P C, Liao W and Smirnov A Y 2004 *Nucl. Phys. B* **702** 307 [arXiv:hep-ph/0404042]

# Double beta decay experiments: past and present achievements

**Alexander Barabash**

Institute of Theoretical and Experimental Physics, B.Cheremushkinskaya 25, 117218 Moscow, Russia

E-mail: barabash@itep.ru

**Abstract.** A brief history of double beta decay experiments is presented. The best currently running experiments (NEMO-3 and CUORICINO) and their latest results are described. The best measurements and limits for the  $2\nu\beta\beta$ ,  $0\nu\beta\beta$  and  $0\nu\chi^0\beta\beta$  are summarized.

## 1. Historical introduction

### 1.1. Theory

The double beta decay problem arose practically immediately after the appearance of W. Pauli's neutrino hypothesis in 1930 and the development of  $\beta$ -decay theory by E. Fermi in 1933. In 1935 M. Goeppert-Mayer identified for the first time the possibility of two neutrino double beta decay, in which there is a transformation of an  $(A, Z)$  nucleus to an  $(A, Z+2)$  nucleus that is accompanied by the emission of two electrons and two anti-neutrinos [1]:

$$(A, Z) \rightarrow (A, Z + 2) + 2e^- + 2\bar{\nu} \quad (1)$$

It was demonstrated theoretically by E. Majorana in 1937 [2] that if one allows the existence of only one type of neutrino, which has no antiparticle (i.e.  $\nu \equiv \bar{\nu}$ ), then the conclusions of  $\beta$ -decay theory are not changed. In this case one deals with a Majorana neutrino. In 1939 B. Furry introduced a scheme of neutrinoless double beta decay through the virtual state of intermediate nuclei [3]:

$$(A, Z) \rightarrow (A, Z + 2) + 2e^- \quad (2)$$

In 1981 a new type of neutrinoless decay with Majoron emission was introduced [4]:

$$(A, Z) \rightarrow (A, Z + 2) + 2e^- + \chi^0 \quad (3)$$

### 1.2. Experiment

The first experiment to search for  $2\beta$ -decay was done in 1948 using Geiger counters. In this experiment a half-life limit for  $^{124}\text{Sn}$  was established,  $T_{1/2} > 3 \cdot 10^{15}$  y [5]. During the period 1948 to 1965  $\sim 20$  experiments were carried out with a sensitivity to the half-life on the level  $\sim 10^{16} - 10^{19}$  y (see reviews [6, 7]). The  $2\beta$ -decay was thought to have been "discovered" a few times, but each time it was not confirmed by new (more sensitive) measurements. The

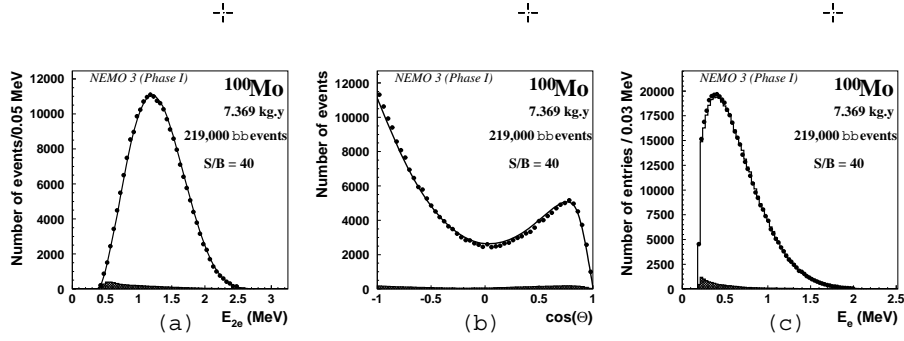


**Figure 1.** (a) Energy sum spectrum of the two electrons, (b) angular distribution of the two electrons and (c) single energy spectrum of the electrons, after background subtraction from  $^{100}\text{Mo}$  with 7.369 kg-years exposure [22].

exception was the geochemical experiment in 1950 where two neutrino double beta decay of  $^{130}\text{Te}$  was really detected [8].

At the end of the 1960s and beginning of 1970s significant progress in the sensitivity of double beta decay experiments was realized. E. Fiorini et al. carried out experiments with Ge(Li) detectors and established a limit on neutrinoless double beta decay of  $^{76}\text{Ge}$ ,  $T_{1/2} > 5 \cdot 10^{21}$  y [9]. Experiments with  $^{48}\text{Ca}$  and  $^{82}\text{Se}$  using streamer chamber with a magnetic field and plastic scintillators were done by C. Wu's group and led to impressive limits of  $2 \cdot 10^{21}$  y [10] and  $3.1 \cdot 10^{21}$  y [11] respectively. During these years many sensitive geochemical experiments were done and  $2\nu\beta\beta$  decay of  $^{130}\text{Te}$ ,  $^{128}\text{Te}$  and  $^{82}\text{Se}$  were detected (see reviews [12, 7, 13]).

The important achievements in the 1980s were connected with the first evidence of two neutrino double beta decay in direct counting experiments. This was done by M. Moe's group for  $^{82}\text{Se}$  using a TPC [14]. There was also the first use of semiconductor detectors made of enriched Ge in the ITEP-ErPI experiment [15].

During the 1990s the two neutrino decay process was detected in many experiments for different nuclei (see [16, 17]), two neutrino decay to an excited state of the daughter nuclei was also detected [18]. In addition, the sensitivity to  $0\nu\beta\beta$  decay in experiments with  $^{76}\text{Ge}$  (Hidelberg-Moscow [19] and IGEX [20]) was increased up to  $\sim 10^{25}$  y.

Since 2002 the progress in double beta decay searches has been connected with the two best present experiments, NEMO-3 and CUORICINO (see Section 2).

## 2. Best present experiments

### 2.1. NEMO-3

This is a tracking experiment that, in contrast to experiments with  $^{76}\text{Ge}$ , detects not only the total energy deposition, but also other parameters of the process, including the energy of the individual electrons, angle between them, and the coordinates of the event in the source plane. Since June of 2002, the NEMO-3 detector [21] has operated at the Frejus Underground Laboratory (France) located at a depth of 4800 m w.e. The detector has a cylindrical structure and consists of 20 identical sectors. A thin (about 30-60 mg/cm<sup>2</sup>) source containing double beta decaying nuclei and having a total area of 20 m<sup>2</sup> and a weight of up to 10 kg was placed in the detector. The energy of the electrons is measured by plastic scintillators (1940 individual counters), while the tracks are reconstructed on the basis of information obtained in the planes of Geiger cells (6180 cells) surrounding the source on both sides. In addition, there is a magnetic field of 25 G parallel to the detector axis which is created by a solenoid surrounding the detector.

At the present time, studies are being performed on seven double beta decay isotopes; these are  $^{100}\text{Mo}$  (6.9 kg),  $^{82}\text{Se}$  (0.93 kg),  $^{116}\text{Cd}$  (0.4 kg),  $^{150}\text{Nd}$  (37 g),  $^{96}\text{Zr}$  (9.4 g),  $^{130}\text{Te}$  (0.45 kg),

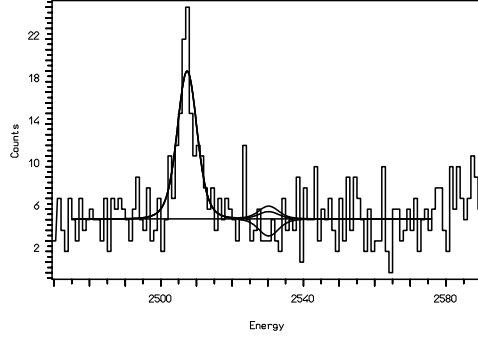


**Figure 2.** The sum spectra of all  $^{nat}\text{TeO}_2$  crystals in the region of the  $2\beta(0\nu)$  energy of  $^{130}\text{Te}$  [23].

and  $^{48}\text{Ca}$  (7 g).

Fig. 1 displays the spectrum of  $2\beta(2\nu)$  events in  $^{100}\text{Mo}$  that were collected over 389 days [22]. The total number of events is about 219,000, which is much greater than the total statistics of all of the preceding experiments. Given the calculated values for the detection efficiencies for  $2\beta(2\nu)$  events, the following half-life value was obtained for  $^{100}\text{Mo}$ :

$$T_{1/2}(^{100}\text{Mo}; 2\nu) = [7.11 \pm 0.02(\text{stat}) \pm 0.54(\text{syst})] \cdot 10^{18} \text{ y} \quad (4)$$

Using 690 days of data the following limits on neutrinoless double beta decay of  $^{100}\text{Mo}$  and  $^{82}\text{Se}$  (mass mechanism; 90% C.L.) have been obtained:  $> 5.8 \cdot 10^{23} \text{ y}$  and  $> 2.1 \cdot 10^{23} \text{ y}$ .

The corresponding limits on  $\langle m_\nu \rangle$  are presented in Table 2.

## 2.2. CUORICINO

This program is the first stage of the larger experiment CUORE. The experiment is running at the Gran Sasso Underground Laboratory. The detector consists of low-temperature devices based on  $^{nat}\text{TeO}_2$  crystals. The detector consists of 62 individual crystals, their total mass being 40.7 kg. The energy resolution is  $\sim 8 \text{ keV}$  (FWHM) at 2.6 MeV.

The experiment has been running since March of 2003. The summed spectra of all crystals in the region of the  $2\beta(0\nu)$  energy is shown in Fig. 2. The total exposure is  $8.3 \text{ kg} \cdot \text{y}$  ( $^{130}\text{Te}$ ). The background at the energy of the  $2\beta(0\nu)$  decay is  $0.18 \text{ keV}^{-1} \cdot \text{kg}^{-1} \cdot \text{y}^{-1}$ . No peak is evident and the limit is  $T_{1/2} > 2.4 \cdot 10^{24} \text{ y}$  (90% CL) [23]. The corresponding limits on  $\langle m_\nu \rangle$  are presented in Table 2.

## 3. Best achievements

### 3.1. Two neutrino double beta decay

As discussed above this decay was first recorded in 1950 in a geochemical experiment with  $^{130}\text{Te}$  [8]. In 1967, it was also found for  $^{82}\text{Se}$  [24]. Attempts to observe this decay in a direct measurement employing counters were unsuccessful for a long time. Only in 1987 could M. Moe, who used a time-projection chamber (TPC), observe  $2\beta(2\nu)$  decay in  $^{82}\text{Se}$  for the first time [14]. Within the next few years, experiments employing counters were able to detect  $2\beta(2\nu)$  decay in many nuclei. In  $^{100}\text{Mo}$  [18, 25, 26], and  $^{150}\text{Nd}$  [27]  $2\beta(2\nu)$  decay to the  $0^+$  excited state of the daughter nucleus was also recorded. The  $2\beta(2\nu)$  decay of  $^{238}\text{U}$  was detected in a radiochemical experiment [28], and in a geochemical experiment for the first time the ECEC process was detected in  $^{130}\text{Ba}$  [29]. Table 1 displays the present-day averaged and recommended values of  $T_{1/2}(2\nu)$  from [30].

**Table 1.** Average and recommended  $T_{1/2}(2\nu)$  values (from [30]).

Isotope	$T_{1/2}(2\nu)$
$^{48}\text{Ca}$	$4.2^{+2.1}_{-1.0} \cdot 10^{19}$
$^{76}\text{Ge}$	$(1.5 \pm 0.1) \cdot 10^{21}$
$^{82}\text{Se}$	$(0.92 \pm 0.07) \cdot 10^{20}$
$^{96}\text{Zr}$	$(2.0 \pm 0.3) \cdot 10^{19}$
$^{100}\text{Mo}$	$(7.1 \pm 0.4) \cdot 10^{18}$
$^{100}\text{Mo}$ - $^{100}\text{Ru}(0_1^+)$	$(6.8 \pm 1.2) \cdot 10^{20}$
$^{116}\text{Cd}$	$(3.0 \pm 0.2) \cdot 10^{19}$
$^{128}\text{Te}$	$(2.5 \pm 0.3) \cdot 10^{24}$
$^{130}\text{Te}$	$(0.9 \pm 0.1) \cdot 10^{21}$
$^{150}\text{Nd}$	$(7.8 \pm 0.7) \cdot 10^{18}$
$^{150}\text{Nd}$ - $^{150}\text{Sm}(0_1^+)$	$1.4^{+0.5}_{-0.4} \cdot 10^{20}$
$^{238}\text{U}$	$(2.0 \pm 0.6) \cdot 10^{21}$
$^{130}\text{Ba}$ ; ECEC( $2\nu$ )	$(2.2 \pm 0.5) \cdot 10^{21}$

### 3.2. Neutrinoless double beta decay

In contrast to two-neutrino decay, neutrinoless double-beta decay has not yet been observed <sup>1</sup>.

The present-day constraints on the existence of  $2\beta(0\nu)$  decay are presented in table 2. In calculating constraints on  $\langle m_\nu \rangle$ , the nuclear matrix elements from [34, 35, 36] were used (3-d column). In column four, limits on  $\langle m_\nu \rangle$  are given, which were obtained using the NMEs (QRPA and RQRPA calculations) from a recent paper [37]. In this paper  $g_{pp}$  values ( $g_{pp}$  is a parameter in QRPA theory) were fixed using experimental half-life values for  $2\nu$  decay and then  $\text{NME}(0\nu)$  were calculated. The authors [37] analyzed the results of all existing QRPA calculations which demonstrates that their approach gives the most accurate and reliable values for NMEs. There is criticism to this claim in [40]).

### 3.3. Neutrinoless double beta decay with Majoron emission

Table 3 displays the best present-day constraints for an ordinary Majoron (spectral index  $n = 1$ ). For nonstandard models of the Majoron ( $n = 2, 3$  and  $7$ ) the strongest limits were obtained with the NEMO-3 detector [41].

### 3.4. Improvements in experimental methods

The dominate experimental achievements are connected with the following methods:

- 1) Low background HPGe detectors made of enriched Ge (HM [19] and IGEX [20]).
- 2) Low background low temperature detectors ( $\text{TeO}_2$  crystals; CUORICHINO [22]).
- 3) Low background crystal scintillators ( $^{116}\text{CdWO}_4$ ; SOLOTVINO [39]).
- 4) Low background tracking detectors (TPC [45], NEMO-3 [22]).

The key point is the level of the background, because high sensitivity experiments can only operate under low background conditions. The important achievements were done during the

<sup>1</sup> A fraction of the Heidelberg-Moscow Collaboration published a "positive" result for  $^{76}\text{Ge}$ ,  $T_{1/2} \approx 1.2 \cdot 10^{25}$  y [31] (see table 2). The Moscow portion of the Collaboration does not agree with this conclusion [32] and there is independent criticism of this result (see, for example [33]). Thus at the present time this "positive" result is not accepted by the " $2\beta$  decay community" and it has to be checked by new experiments.

**Table 2.** Best present results on  $2\beta(0\nu)$  decay (limits at 90% C.L.). \*) See text.

Isotope	$T_{1/2}, y$	$\langle m_\nu \rangle, eV$ [34, 35, 36]	$\langle m_\nu \rangle, eV$ [37]	Experiment
$^{76}\text{Ge}$	$> 1.9 \cdot 10^{25}$	$< 0.33 - 0.84$	$< 0.46 - 0.59$	HM [19]
	$\simeq 1.2 \cdot 10^{25} (?)^*$	$\simeq 0.5 - 1.3 (?)^*$	$\simeq 0.6 - 0.7 (?)^*$	Part of HM [31]
	$> 1.6 \cdot 10^{25}$	$< 0.36 - 0.92$	$< 0.51 - 0.64$	IGEX [20]
$^{130}\text{Te}$	$> 2.4 \cdot 10^{24}$	$< 0.4 - 0.8$	$< 0.7 - 1.3$	CUORICINO [23]
$^{100}\text{Mo}$	$> 5.8 \cdot 10^{23}$	$< 0.6 - 0.9$	$< 2.0 - 2.7$	NEMO- 3 (this work)
$^{136}\text{Xe}$	$> 4.5 \cdot 10^{23}$	$< 0.8 - 4.7$	$< 2.8 - 5.6$	DAMA [38]
$^{82}\text{Se}$	$> 2.1 \cdot 10^{23}$	$< 1.2 - 2.5$	$< 2.3 - 3.2$	NEMO-3 (this work)
$^{116}\text{Cd}$	$> 1.7 \cdot 10^{23}$	$< 1.4 - 2.5$	$< 2.9 - 4.3$	SOLOTVINO [39]

**Table 3.** Best present limits on  $2\beta(0\nu\chi^0)$  decay (ordinary Majoron) at 90% C.L.

Isotope	$T_{1/2}, y$	$\langle g_{ee} \rangle, [34, 35, 36]$	$\langle g_{ee} \rangle, [37]$
$^{76}\text{Ge}$	$> 6.4 \cdot 10^{22}$ [19]	$< (1.2 - 3.0) \cdot 10^{-4}$	$< (1.9 - 2.3) \cdot 10^{-4}$
$^{82}\text{Se}$	$> 1.5 \cdot 10^{22}$ [41]	$< (0.66 - 1.4) \cdot 10^{-4}$	$< (1.3 - 1.8) \cdot 10^{-4}$
$^{100}\text{Mo}$	$> 2.7 \cdot 10^{22}$ [41]	$< (0.4 - 0.7) \cdot 10^{-4}$	$< (1.3 - 1.8) \cdot 10^{-4}$
$^{116}\text{Cd}$	$> 8 \cdot 10^{21}$ [39]	$< (1.0 - 2.0) \cdot 10^{-4}$	$< (2.3 - 3.5) \cdot 10^{-4}$
$^{128}\text{Te}$	$> 2 \cdot 10^{24}(\text{geochem})[42]$	$< (0.7 - 1.6) \cdot 10^{-4}$	$< (1.7 - 2.8) \cdot 10^{-4}$

period of  $2\beta$ -decay searches. In table 4 one can find the best background levels reached which were obtained in the different experiments. In 2-nd column, is the background  $B$  in  $(keV \cdot kg \cdot y)^{-1}$ . For a better comparison of the experiments with different energy resolutions and efficiencies, a so called effective background value  $\langle B \rangle$  has been introduced.

**Table 4.** Lowest levels of background in double beta decay experiments.  $\Delta E$  is energy resolution (FWHM) in keV and  $\eta$  is efficiency;  $PSD$  is pulse shape discrimination.

Experiment	$B, (keV \cdot kg \cdot y)^{-1}$	$\langle B \rangle = B \cdot \Delta E / \eta, (kg \cdot y)^{-1}$
HM [19], IGEX [20]; $^{76}\text{Ge}$	$\sim 0.2$	$\sim 0.8$
	$\sim 0.06(PSD)$	$\sim 0.25(PSD)$
CUORICINO [44]; $\text{TeO}_2$	$\sim 0.18$	$\sim 1.4$
NEMO-3 [22]; $^{100}\text{Mo}$	$\sim 0.001$	$\sim 2.5$
SOLOTVINO [39]; $^{116}\text{CdWO}_4$	$\sim 0.037$	$\sim 10$
TPC [45]; $^{136}\text{Xe}$	$\sim 0.02$	$\sim 15$
DAMA [38]; $^{136}\text{Xe}$	$\sim 0.06$	$\sim 30$

#### 4. Conclusion

The principle achievements of past and present experiments are the following:

- 1) A conservative limit on the effective Majorana neutrino mass has been established as  $< 0.9$  eV (90% C.L.).
- 2) A conservative limit on the coupling constant of Majoron to neutrino (ordinary Majoron) has been established as  $< 1.8 \cdot 10^{-4}$  (90% C.L.).
- 3) The two neutrino double beta decay has been detected in 10 nuclei. In addition this type of decay to the  $0^+$  excited state of daughter nuclei has been detected (for  $^{100}\text{Mo}$  and  $^{150}\text{Nd}$ ). Finally, the ECEC( $2\nu$ ) process has been detected in geochemical experiment.

#### 5. References

- [1] Goepfert-Mayer M 1935 *Phys. Rev.* **48** 512
- [2] Majorana E 1937 *Nuovo Cimento* **14** 171
- [3] Farry W H 1939 *Phys. Rev.* **56** 1184
- [4] Georgi H, Glashow S and Nussinov S 1981 *Nucl. Phys. B* **193** 297
- [5] Firemann E L 1948 *Phys. Rev.* **74** 1238
- [6] Lazarenko V R 1966 *Uspechi* **90** 601
- [7] Haxton W C and Stephenson G J 1984 *Prog. Part. Nucl. Phys.* **12** 409
- [8] Inghram M G and Reynold J H 1950 *Phys. Rev.* **78** 822
- [9] Fiorini E et al. 1973 *Nuovo Cimento* **13A** 747
- [10] Bardin R K Gollon P J Ullman J D and Wu C S 1970 *Nucl. Phys. A* **158** 337
- [11] Cleveland B T et al. 1975 *Phys. Rev. Lett.* **35** 757
- [12] Kirsten T 1983 *AIP Conference Proceedings* **96** 396
- [13] Manuel O K 1986 *Proc. Int. Work. Nuclear beta decays and the neutrino (Osaka)* (Singapore: World Scientific) p 71
- [14] Elliott S R Hahn A A and Moe M K 1987 *Phys. Rev. Lett.* **59** 2020
- [15] Vasenko A A et al. 1990 *Mod. Phys. Lett. A* **5** 1299
- [16] Barabash A S 2002 *Czech. J. Phys.* **52** 567 (*Preprint nucl-ex/0203001*)
- [17] Barabash A S 2004 *Phys. At. Nucl.* **67** 438
- [18] Barabash A S et al. 1995 *Phys. Lett. B* **345** 408
- [19] Klapdor-Kleingrothaus H V et al. 2001 *Eur. Phys. J. A* **12** 147
- [20] Aalseth C E 2002 *Phys. Rev. C* **65** 092007
- [21] Arnold R et al. 2005 *Nucl. Instr. Meth. A* **536** 79
- [22] Arnold R et al. 2005 *Phys. Rev. Lett.* **95** 182302
- [23] Capelli S 2006 *Poster presentation at NEUTRINO'06 Conference (Santa Fe, USA)*
- [24] Kirsten T Gentner W and Schaeffer O A 1967 *Z. Phys.* **202** 273
- [25] Barabash A S et al. 1999 *Phys. At. Nucl.* **62** 2039
- [26] De Braeckelee L et al. 2001 *Phys. Rev. Lett.* **86** 3510
- [27] Barabash A S 2004 *Phys. At. Nucl.* **79** 10
- [28] Turkevich A L Economou T E and Cowan G A 1991 *Phys. Rev. Lett.* **67** 3211
- [29] Meshik A P 2001 *Phys. Rev. C* **64** 035205
- [30] Barabash A S 2006 *Czech. J. Phys.* **56** 437 (*Preprint nucl-ex/0602009*)
- [31] Klapdor-Kleingrothaus H V et al. 2004 *Phys. Lett. B* **586** 198
- [32] Bakalyarov A M et al. 2005 *Phys. Part. Nucl. Lett.* **2** 77 (*Preprint hep-ex/03090160*)
- [33] Strumia A and Vissani F 2005 *Nucl. Phys. B* **726** 294
- [34] Simkovic F et al. 1999 *Phys. Rev. C* **60** 055502
- [35] Stoica and Klapdor-Kleingrothaus H V 2001 *Nucl. Phys. A* **694** 269
- [36] Civitarese O and Suhonen J 2003 *Nucl. Phys. A* **729** 867
- [37] Rodin V A et al 2006 *Nucl. Phys. A* **766** 107
- [38] Bernabei R et al. 2002 *Phys. Lett. B* **546** 23
- [39] Danevich F A et al. 2003 *Phys. Rev. C* **67** 035501
- [40] Suhonen J 2005 *Nucl. Phys. A* **752** 53c
- [41] Arnold R et al. 2006 *Nucl. Phys. A* **765** 483
- [42] Manuel O K 1991 *J. Phys. G* **17** 221
- [43] Gunther M et al. 1997 *Phys. Rev. D* **55** 54
- [44] Arnaboldi C et al. 2005 *Phys. Rev. Lett.* **95** 142501
- [45] Luescher R et al. 1998 *Phys. Lett. B* **434** 407

## First data from the ANTARES neutrino telescope

V. Bertin<sup>1</sup> on behalf of the ANTARES Collaboration

<sup>1</sup>C.P.P.M., CNRS/IN2P3 et Université de la Méditerranée,  
Case 902, 163, avenue de Luminy, 13288 Marseille cedex 9, France

E-mail: bertin@cppm.in2p3.fr

**Abstract.** This contribution reviews the recent progress achieved towards building the ANTARES neutrino telescope. The first results obtained by the operation of a Mini Instrumentation Line with Optical Modules, “MILOM”, and the first complete detector line are highlighted.

### 1. The ANTARES detector

The European Collaboration ANTARES aims at building and operating a large undersea neutrino telescope located at a depth of 2500 m in the Mediterranean Sea, offshore from Toulon in France [1]. Neutrinos will be detected through their interaction in the matter surrounding the detector, producing muons radiating Cherenkov light while propagating in the sea water. Photons are recorded by a lattice of Optical Modules (OMs) [2], consisting of 10” hemispherical photomultiplier tubes (PMTs) [3] housed in pressure resistant glass spheres, installed on a set of mooring lines. The reconstruction of the muon track direction, pointing to a fraction of a degree towards the direction of the parent neutrino source for high energy neutrinos, is achieved from the measurement of the arrival times of the Cherenkov photons on the OMs, as well as their position in space.

The complete ANTARES detector will consist of 12 lines of 25 storeys, each storey being equipped with a triplet of Optical Modules looking at 45° downward and an electronics container mounted on a titanium frame, giving a grand-total of 900 OMs. On each storey, the local electronics container includes the front-end electronics of the PMTs, an Ethernet board for the data acquisition and the detector Slow Control, electronics boards for clock distribution and for Dense Wavelength Division Multiplexing of the Ethernet transmission, and a tiltmeter-compass board measuring the local tilt and orientation of the storey. Some storeys also support a hydrophone for acoustic positioning or an LED Optical Beacon used for inter-string time calibration.

The vertical distance between storeys is 14.5 m, the first one being placed at 100 m above the sea bed, leading to a total height of the detector strings of 480 m. Each string is anchored on the sea floor at a distance of 70 m from its neighbours. Every line is individually connected to a Junction Box by an interconnection cable a few hundred metres long. The Junction Box is itself linked to the shore by a 40 km long electro-optical cable equipped with 48 optical fibres.

The construction of the ANTARES detector started in October 2001 with the deployment of the main electro-optical cable from the ANTARES site, located in the Mediterranean Sea (42°48’N-6°10’E) offshore Toulon (France) at a depth of 2475 m, to the beach of La Seyne-sur-Mer where the shore station of the experiment is situated. In December 2002, the Junction Box was connected at the end of this cable and immersed on the site. In Spring 2003, two small test lines, the Prototype Sector

Line (PSL) and the Mini Instrumentation Line (MIL), were installed, connected and operated for a few months. The genuine operation of the ANTARES neutrino telescope really started in April 2005 after the connection of the Mini Instrumentation Line with Optical Modules (MILOM) and more recently the installation of the first full complete detector line, Line 1, in March 2006. The second line, Line 2, was in integration phase in June 2006, at the time of the Neutrino'06 Conference, it has been successfully deployed on the ANTARES site at the end of July 2006 as scheduled. Thanks to two assembly sites running in parallel, the ANTARES detector is foreseen to be fully deployed and operational by the end of 2007 for several years of physics data taking.

The main performance parameters expected for the complete ANTARES neutrino telescope are summarized in figure 1. The left plot shows the effective area for neutrinos as a function of the neutrino energy for various incident angles. The effective area reaches 1 m<sup>2</sup> for  $E_\nu > 100$  TeV, the energy above which the Earth shadowing starts to be of some importance. The right plot shows the angular resolution for the reconstructed muon compared to the true muon direction and to the parent neutrino direction, as a function of the neutrino energy. While the angular resolution is dominated by the physical angle between the muon and the parent neutrino at low energy, it is dominated by the reconstruction for  $E_\nu \geq 10$  TeV and is expected to be as good as 0.3°. In this regime, the angular resolution is mainly dominated by two effects: the scattering and the chromatic dispersion of the Cherenkov light during its travel into the sea water, contributing for a time arrival spread of  $\sigma \sim 1$  ns; the transit time spread (TTS) of the PMT signals being  $\sigma \sim 1.3$  ns.

To achieve this good angular resolution, the ANTARES detector is designed such as additional electronics contributions to the time calibration contribute for less than  $\sim 0.5$  ns to the time-stamping of the detected photons. In addition, the relative position reconstruction of the OM has to be controlled with a precision of  $\sim 10$  cm.

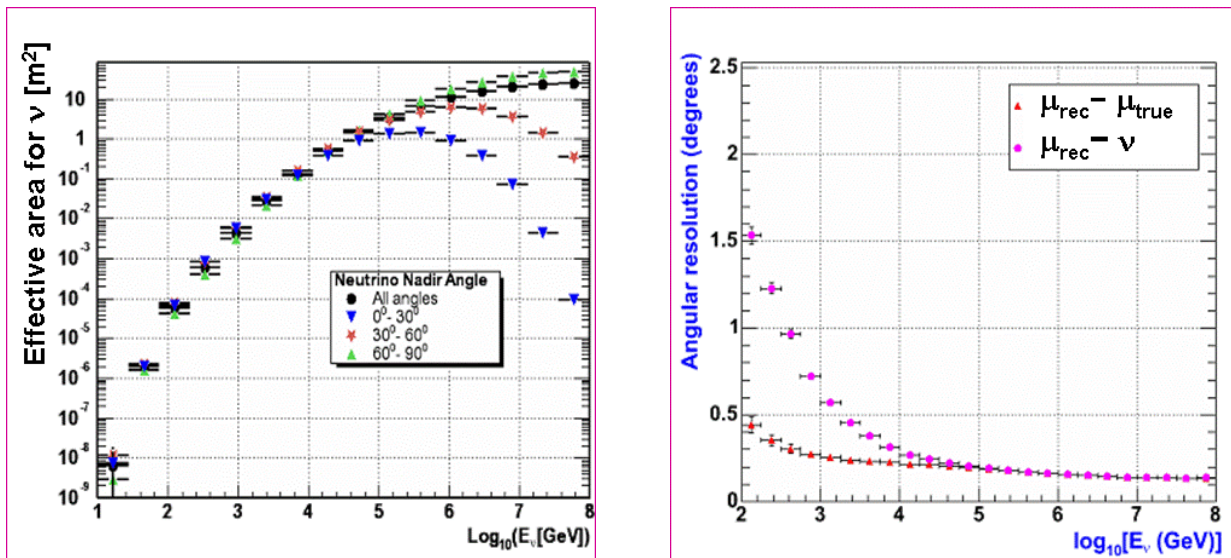


**Figure 1.** Expected performance for the complete 12 lines ANTARES neutrino telescope. The left figure shows the effective area for neutrinos as a function of the neutrino energy for several incident angles. The right figure shows the angular resolution of the reconstructed muon compared to the true muon direction and to the parent neutrino as a function of the neutrino energy.

## 2. Results from the first ANTARES lines

### 2.1. The MILOM line

The current data taking of the ANTARES detector started in March 2005 with the operation of the MILOM [4]. This instrumentation line, partly devoted to multi-disciplinary and environmental studies,

consists of an instrumented releasable anchor, the Bottom String Socket (BSS), and three storeys respectively located at 100 m, 117 m and 169 m above the sea bed. The middle storey is a standard ANTARES storey housing a triplet of Optical Modules. The main other devices are a water current profiler located on the top storey, an LED Optical Beacon held on the bottom storey, an acoustic positioning transducer attached to the BSS and a seismometer buried into the sea floor 50 m away from the MILOM.

2.1.1. *Optical background measurements.* The operation of the MILOM allowed a continuous monitoring of the background rates of the Optical Modules. A typical OM counting rate display exhibits a baseline of  $\sim 60\text{--}80$  kHz largely dominated by optical background due to  $^{40}\text{K}$  decays and bioluminescence activities coming from bacteria, as well as bursts of a few seconds duration produced by bioluminescent emission of macro-organisms [5]. Figure 2 (left) shows the baseline rates recorded by the three OMs of the MILOM during a period of three months in Autumn 2005. A seasonal variation of the bioluminescence component of the baseline is clearly observed. The 15% higher counting rate of OM1 during the full period is due to a lower threshold set on the readout of this Optical Module. Figure 2 (right) shows the burstfraction, defined as the fraction of the time when the counting rate is higher than the baseline by 20% during a 15 min interval, as a function of the water current intensity. A strong correlation of these two quantities is clearly observed.

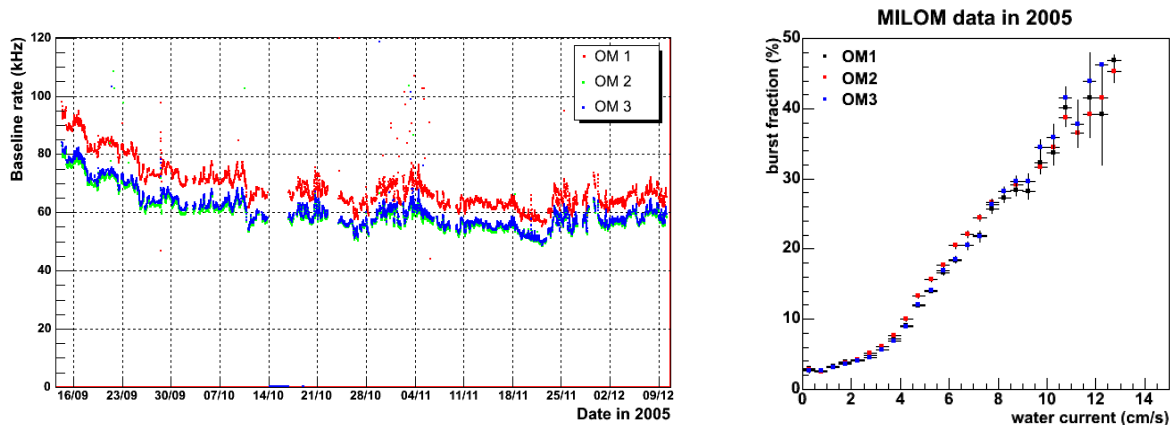


**Figure 2.** Baseline rates recorded by the three OMs of the MILOM during Autumn 2005 (left) and burstfraction as function of the water current intensity (right).

The time coincidences between pairs of neighbouring Optical Modules have also been studied. These distributions exhibit a flat background of random coincidences and a Gaussian peak of few ns width due to genuine coincidences of  $^{40}\text{K}$  radioactive decays producing two detected photons. The  $^{40}\text{K}$  coincidence rate is measured to be  $13.0 \pm 0.5$  Hz and is in good agreement with a simulation the signals induced by  $^{40}\text{K}$  decays which leads to a coincidence rate of 12 Hz with a 4 Hz systematic error due to uncertainties in the effective area and angular response of the OMs.

2.1.2. *Time calibration with the LED Optical Beacon.* The time calibration of the MILOM Optical Modules has been checked by flashing the LED Optical Beacon located on the bottom storey. This device consists of a glass cylinder container containing 36 blue LEDs synchronised in time in order to produced intense light flashes with a time dispersion  $< 0.5$  ns. The time calibration of the OMs can be checked either by looking at the arrival time of the signal on the PMT relative to the time of the flash, or by the time difference of the flash arrival time measured by two adjacent OMs. Due to the large intensity of the light flashes and the short 15 m distance of propagation of the light into the water, the time stamping of the OM signal is dominated by its electronics contribution and not by the TTS of the

PMT in this case. The measured distributions confirm that the electronics contribution to the time calibration is  $\leq 0.5$  ns as expected.

## 2.2. The Line 1

The first complete line of the ANTARES neutrino telescope, Line 1, has been deployed on the site on February 14<sup>th</sup> 2006 and connected two weeks later on March 2<sup>nd</sup> by using the Remote Operated Vehicle *Victor* of IFREMER. This line is made of a BSS and of 25 storeys, holding a total of 75 OMs. It also includes 4 LED Optical Beacons and 5 acoustic positioning hydrophones spread along the line, as well as an acoustic transducer on its BSS.

**2.2.1. Time calibration with the MILOM LED Optical Beacon.** The time calibration of the Line 1 OMs can also be checked by flashing the LED Optical Beacon located on the MILOM bottom storey. Figure 3 (left) shows the detection time spread of the LED Optical Beacon flashes by an OM of Line 1 located on a storey at the same altitude than the MILOM LED Optical Beacon. In this case, the measured distribution width is  $\sigma = 0.7$  ns for a “horizontal” travel path of  $\sim 80$  m of the light in the sea water. Figure 3 (right) shows in comparison the detection time spread for an OM of Line 1 located at a higher altitude corresponding to a “diagonal” travel path of the flash light of  $\sim 150$  m. A wider distribution is clearly observed due to the smaller intensity of the detected signal, as well as a tail of delayed photons coming from scattering light. All measured distributions have been found in good agreement with expectations.

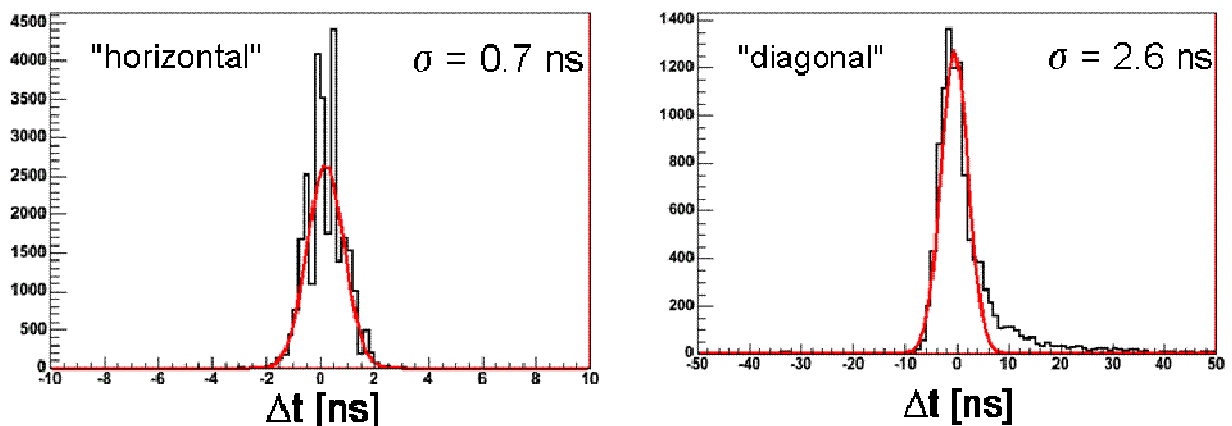


**Figure 3.** Detection time spread of the MILOM LED Optical Beacon flashes by an OM of Line 1 located at the same altitude as the LED Optical Beacon at an “horizontal” distance of  $\sim 80$  m (left) and by an OM at a higher altitude at a “diagonal” distance of  $\sim 150$  m (right).

**2.2.2. Acoustic positioning measurements.** The reconstruction of the detector geometry in real time is primarily based on acoustic triangulation of a small number of hydrophones scattered along every line. The triangulation is performed from distance measurements of each hydrophone to several fixed acoustic emitters located either on every line anchor base (transducers) or on autonomous pyramidal structures anchored around the detector field (transponders). A relative positioning of the hydrophones in space with a precision of few cm is necessary in order to obtain a precision of  $\sim 10$  cm on the OM positions as a result of the line shape reconstruction performed by the addition of the tilts and heading measurements of every storey. The concomitant operation of MILOM and Line 1 has allowed a check of the acoustic system performance by performing the Line 1 hydrophone triangulation based on the acoustic emission of the MILOM transducer and two autonomous transponders. The good resolution of the acoustic system, found to be well within the specification, can be appreciated on figure 4 which shows the radial displacement of the lowest hydrophone of Line 1, located on its bottom storey at 100 m above the sea bed, with respect to the line axis during a period of two weeks.

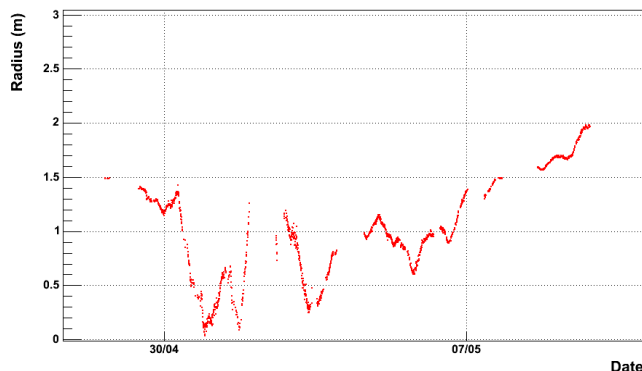


**Figure 4.** Radial displacement of the Line 1 lowest hydrophone with respect to the line axis measured by the acoustic relative positioning system during a period of two weeks.

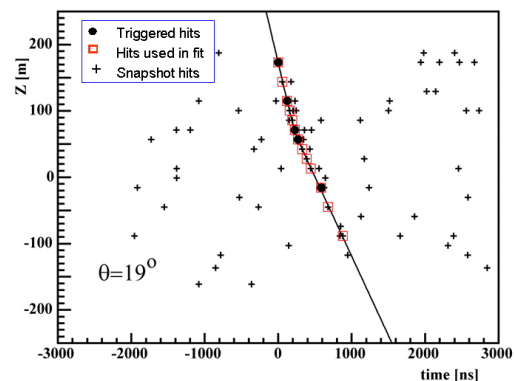


**Figure 5.** Example of a downward-going atmospheric muon track reconstruction with the ANTARES Line 1.

**2.2.3. Reconstruction of atmospheric muons.** Although the OMs point at  $45^\circ$  downwards, the ANTARES detector has a none negligible efficiency for the detection and the reconstruction of downward-going atmospheric muons. The event selection is first performed by an online filter algorithm, running at the shore station, which looks for a set of  $\geq 4$  local coincidence hits, the triggered hits, causally compatible with a muon track passing through the detector during a  $4 \mu\text{s}$  time window. The muon reconstruction is then performed with a  $\chi^2$  fit of the hit times as function of their altitudes, to a hyperbola corresponding to the intersection of the muon Cherenkov light front with the line plane, in order to determine the zenith angle of the muon track. An example of such a muon track fit is shown on figure 5. Several thousand of atmospheric muons have already been reconstructed after a few weeks of operation of the Line 1, the first being detected only two days after its connection. The study of the muon angular distribution is in progress. The preliminary results already show that the muon reconstruction is working well and that the hunt for the first undersea neutrino can be started.

### 3. Conclusion

The ANTARES Collaboration has made a major step forward during the last year by the operation of a Mini Instrumentation Line with Optical Modules, the MILOM, for more than a year, and the installation of the first complete line of the detector in Spring 2006. All studies performed with these two lines show that the detector behaves well within the design specification and that all technical problems are solved. The detector should be fully installed by the end of 2007 and in operation for science during at least five years. It is also considered as a milestone towards the building of a  $\text{km}^3$  underwater detector for which a design study is under preparation.

### References

- [1] Aslanides E *et al.*, ANTARES Collaboration 1999 the ANTARES Proposal *Preprint astro-ph/9907432*
- [2] Amram P *et al.* ANTARES Collaboration 2002 *Nucl. Inst. Meth. A* **484** 369 (*Preprint astro-ph/0112172*)
- [3] Aguilar J A *et al.* ANTARES Collaboration 2005 *Nucl. Inst. Meth. A* **555** 132 (*Preprint physics/0510031*)
- [4] Aguilar J A *et al.* ANTARES Collaboration 2006 First results of the Instrumentation Line for the deep-sea ANTARES neutrino telescope *Preprint astro-ph/0606229*
- [5] Amram P *et al.* ANTARES Collaboration 2000 *Astropart. Phys.* **13** 127 (*Preprint astro-ph/9910170*)

# Neutrinos from WIMP annihilations in the Sun including neutrino oscillations

Mattias Blennow<sup>1</sup>, Joakim Edsjö<sup>2</sup> and Tommy Ohlsson<sup>1</sup>

<sup>1</sup> Department of Theoretical Physics, School of Engineering Sciences, Royal Institute of Technology (KTH) – AlbaNova University Center, SE-106 91 Stockholm, Sweden

<sup>2</sup> Department of Physics, Stockholm University – AlbaNova University Center, SE-106 91 Stockholm, Sweden

E-mail: emb@kth.se, edsjo@physto.se, tommy@theophys.kth.se

**Abstract.** The prospects to detect neutrinos from the Sun arising from dark matter annihilations in the core of the Sun are reviewed. Emphasis is placed on new work investigating the effects of neutrino oscillations on the expected neutrino fluxes.

## 1. WIMP capture and annihilation in the Sun

Weakly Interacting Massive Particles (WIMPs) in the Milky Way halo can scatter in the Sun and be gravitationally bound to it. Eventually, they will scatter again and sink to the core of the Sun. In the core, WIMPs will accumulate and can annihilate and produce neutrinos.

## 2. Neutrino interactions

On the way out of the Sun, neutrinos can participate in both charged- and neutral-current interactions. Neutral-currents degrade the energy of the neutrinos, whereas charged-currents give a charged lepton. Electrons and muons are stopped before they can give neutrinos, which means that electron and muon neutrinos are lost, while tau leptons will decay and produce new neutrinos (regeneration).

Then, what about the spectra beyond the Sun? At the surface of the Sun, some of the neutrinos have interacted, and thus, the flux at high energies is degraded. However, some of these neutrinos reappear at low energies both from neutral-current interactions and tau decays.

## 3. Neutrino oscillations

We use a completely general three-flavor neutrino oscillation scheme (with matter effects included) and a realistic solar model [1]. Thus, at the surface of the Sun, we obtain the fluxes in a general format (including both amplitudes and phases of the neutrino oscillations). Furthermore, in our computations, neutrino oscillations and interactions are treated simultaneously. We have used the following values of standard neutrino oscillation parameters (which are the central values from Ref. [2] with no CP violation in neutrino oscillations and a normal neutrino mass hierarchy):  $\theta_{12} = 33.2^\circ$ ,  $\theta_{13} = 0$ ,  $\theta_{23} = 45.0^\circ$ ,  $\delta = 0$ ,  $\Delta m_{21}^2 = 8.1 \cdot 10^{-5} \text{ eV}^2$ ,  $\Delta m_{31}^2 = 2.2 \cdot 10^{-3} \text{ eV}^2$ .

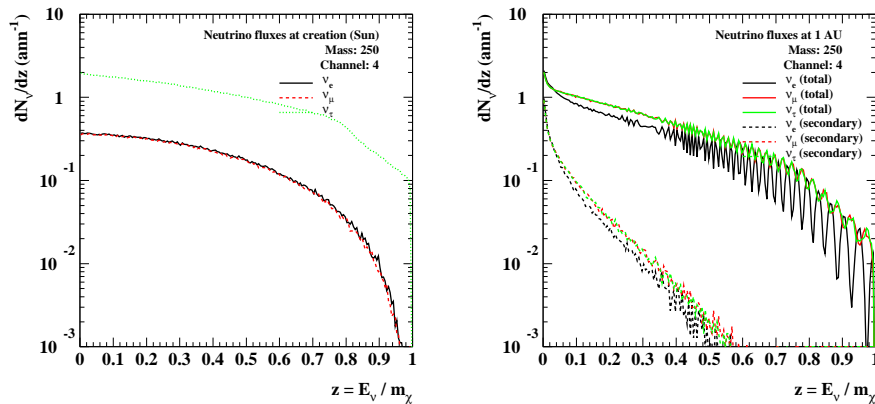


**Figure 1.** *Left:* Initial neutrino fluxes at the center of the Sun. *Right:* Neutrino fluxes at 1 AU.

#### 4. Propagation to and in the Earth

First, for the propagation to the Earth, vacuum neutrino oscillations to the Earth are included in the same three-flavor neutrino setup. In addition, effects of the eccentricity of the Earth's orbit are included. In Fig. 1, we plot the initial neutrino fluxes at the center of the Sun, *i.e.*, at the point of production, as well as we show an example of the propagation of neutrinos from the center of the Sun to the distance of the Earth, *i.e.*, on the distance of 1 AU).

Second, for the propagation in the Earth, matter effects are included in the neutrino oscillations as well. Our simulations are made with a time stamp to include effects of the Earth's distance to the Sun (due to the eccentricity of the orbit) and rotation (affects the distance traversed in the Earth).

#### 5. Summary and conclusions

For typical WIMP masses (*i.e.*,  $10\text{--}10^5$  GeV), neutrino oscillations effectively: 1. average  $\nu_\mu$  and  $\nu_\tau$  on the way out of the Sun, 2. average  $\nu_e$  and  $\nu_\mu/\nu_\tau$  on the way to the Earth, and 3. wash out the remaining oscillation patterns in the spectra due to the eccentricity of the Earth's orbit.

Note that the full scheme described above is implemented as a complete event-based Monte Carlo code. In addition, it should be mentioned that other computations of neutrinos from WIMP annihilations have been performed, such as the study by Cirelli *et al.* [3]. However, their results are not event-based.

#### Acknowledgments

This work was supported by the Royal Swedish Academy of Sciences (KVA) and the Swedish Research Council (Vetenskapsrådet), Contract No. 621-2002-3577, 621-2003-6025, 621-2005-3588.

#### References

- [1] J. N. Bahcall, A. M. Serenelli and S. Basu, "New solar opacities, abundances, helioseismology, and neutrino fluxes," *Astrophys. J.* **621** (2005) L85 [arXiv:astro-ph/0412440].
- [2] M. Maltoni, T. Schwetz, M. A. Tortola and J. W. F. Valle, "Status of global fits to neutrino oscillations," *New J. Phys.* **6** (2004) 122 [arXiv:hep-ph/0405172].
- [3] M. Cirelli, N. Fornengo, T. Montaruli, I. Sokalski, A. Strumia and F. Vissani, "Spectra of neutrinos from dark matter annihilations," *Nucl. Phys. B* **727** (2005) 99 [arXiv:hep-ph/0506298].

# Evidence for Sterile Neutrinos from Solar Neutrino Flux Modulation

**David O. Caldwell**

Physics Department, University of California, Santa Barbara, CA 93106, USA

E-mail: [caldwell@slac.stanford.edu](mailto:caldwell@slac.stanford.edu)

**Abstract.** Solar neutrino fluxes measured by the Cl, Ga, and Super-Kamiokande (SK) experiments reveal modulations at frequencies related to solar rotation rates of the solar magnetic field. The modulations produced by Resonant-Spin-Flavor Precession (RSFP) cannot be explained by the three known neutrinos, as a sterile neutrino is required which couples to the active neutrinos only via a large transition magnetic moment. Such a sterile with no mixing avoids all known constraints, is compatible with the time-varying solar data, and improves the fit to the time-averaged data. The subdominant RSFP process occurs in the solar convection zone in series with the LMA MSW effect at a smaller radius. Since the magnetic field in the convection zone changes with solar cycle, a rotation frequency in GALLEX data (solar cycle 23) would not be in GNO data (cycle 24). An analysis lumping these data together shows the same frequency not significantly, whereas GALLEX data shows it at the 99.9% CL, using more of the experimental information. Use of insufficient information is a problem in the SK analysis, which sees at low significance the same 3 frequencies (one of rotation and two of related r-modes) we find even at the 99.9% CL when more experimental information is used. SNO looked unsuccessfully for one of these r-mode peaks, but SK data shows this very episodic process had died out before SNO turned on. A rotation frequency of the magnetic field seen in SK data does appear also in SNO data.

Statistically significant frequencies of solar neutrino flux modulation, all of which are related to known solar processes, have been found in the data of the Cl, Ga, and Super-Kamiokande experiments. These modulations can be understood if Resonant-Spin-Flavor Precession (RSFP) occurs in the solar convection zone, producing a sterile neutrino via  $\nu_e \rightarrow \bar{\nu}_s$ . This  $\nu_s$  does not require any mixing with active neutrinos, avoiding all known constraints, but it does couple via a large transition magnetic moment. Since the dominant LMA MSW process occurs at a small solar radius, the RSFP effect follows the MSW one in series. Because these modulations have small amplitude and are of limited time duration, the analysis must utilize all available experimental information. After a brief summary of evidence for flux modulation and for this type of sterile neutrino, the lack of significant observation of these effects in other analyses is explained.

Initial analyses[1] of solar neutrino flux variability was done on the radiochemical experiments, starting with discovering that the variance of the Homestake (Cl) experiment's data[2] is larger than expected at the 99.9% CL. A subsequent power spectrum analysis showed that the main frequency involved was  $12.88 \pm 0.02 \text{ y}^{-1}$  (28.4 d period), which came from regions above the solar equator. In contrast, the Ga experiments (particularly GALLEX[3]) showed a main frequency of  $13.59 \pm 0.04 \text{ y}^{-1}$ , an equatorial rotation rate of the deep convective zone. Helioseismology

data give rotation frequencies as a function of solar radius and latitude, and these match the  $13.59 \text{ y}^{-1}$  rate on the solar equator at about 0.8 of the solar radius,  $R_{\odot}$ .

The influence of these rotation frequencies extends even to the corona, since the SXT instrument[4] on the Yohkoh spacecraft provides evidence for two rotation rates, one ( $13.55 \pm 0.02 \text{ y}^{-1}$ ) mainly at the equator, and the other ( $12.86 \pm 0.02 \text{ y}^{-1}$ ) mainly at high latitudes, in remarkable agreement in rate and location with the neutrino data, as shown in Fig. 1. That the Cl and Ga experiments should respond differently to these two frequencies arises from the difference in solar radii at which their neutrinos are produced and the tilt of the solar axis relative to the ecliptic. The neutrinos the Cl experiment detects come from a small sphere ( $\sim 0.05 R_{\odot}$ ), so those reaching the earth mainly miss the equatorial region at  $0.8 R_{\odot}$  and are modulated instead at higher solar latitudes. The Ga experiments detect pp neutrinos which are produced at  $\sim 0.2 R_{\odot}$ , so this wide beam is insensitive to axis tilt and can be modulated by the equatorial region.

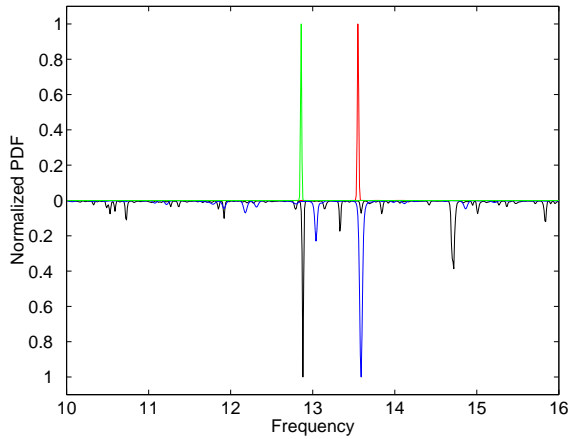


**Figure 1.** Comparison of normalized probability distribution functions formed from power spectra of data from SXT (plotted upwards) and Homestake and GALLEX (plotted downwards). At the frequency  $13.6 \text{ y}^{-1}$  the SXT and GALLEX data are equatorial, while the other two are not. All frequencies are in cycles per year.

The GALLEX data show another manifestation of this modulation when the flux values of individual runs are plotted, as these have a double peak. That this structure is related to the  $13.59 \text{ y}^{-1}$  modulation is shown by reordering runs according to the phase of that frequency, since lower flux values appear in the descending part of the cycle and higher flux values in the ascending portion.

How can these observations be understood? Since the modulations correspond to rotations of the solar magnetic field, Resonant-Spin-Flavor Precession[5] (RSFP) must be involved. The RSFP process is subdominant to the main suppression of solar  $\nu_e$  via the Large-Mixing-Angle (LMA) MSW effect, and the two occur in series at different solar radii. For simplicity, one would like to utilize just the three known light neutrinos. Their measured mass differences would force the RSFP process to occur at a smaller solar radius than the MSW effect, which is contrary to our analyses. Also the RSFP modulations are calculated[6] to be much too small and to have the wrong energy dependence. Thus one is forced to introduce a fourth neutrino, which cannot have the weak interactions, as required by the width of the  $Z^0$  boson. The RSFP process is then  $\nu_e \rightarrow \bar{\nu}_s$ , with a mass-squared difference between the two states,  $\Delta m^2 \sim 10^{-8} \text{ eV}^2$ , to provide a resonant density in the solar convection zone at a much larger radius than that at which the similar MSW resonance occurs.

A model was suggested[1] in which the sterile neutrino couples to active neutrinos via only a large transition magnetic moment, with no mixing required. This lack of mixing avoids all known limitations on sterile neutrinos, and constraints on RSFP from null observations of solar antineutrinos are also irrelevant. This model, when used[7] with the LMA MSW solution, (1) predicted correctly the magnitude and energy dependence of the flux modulation, (2) gave the right location of the equatorial RSFP resonance at  $\sim 0.8 R_{\odot}$ , and (3) improved the fit to the time-averaged solar data. The fit improvement results from the resonant dip in the RSFP  $\nu_e$  survival probability, which suppresses the 0.86 MeV  ${}^7\text{Be}$  neutrino line, reduces the  $2.5\sigma$  excess in the predicted Cl rate over the Homestake observation, and eliminates the rise below  $\sim 8$  MeV predicted by the LMA solution but not observed by the Super-Kamiokande[8] and SNO[9] experiments.

Especially because understanding these results on flux variability requires a sterile neutrino, there has been reluctance to accept them. This reaction has been exacerbated by analyses from the experimental groups involved, which generally find the same modulation frequencies we do but not at a significant level. This problem arises mainly from two causes: this subdominant effect usually produces a very small flux modulation (e.g.,  $\sim 7\%$  in the  ${}^8\text{B}$  neutrino energy range) and the effects are only transient. These two issues are illustrated below by comparing our analyses with those of the experimental groups.

An analysis[10] of GALLEX-GNO data shows the  $13.6 \text{ y}^{-1}$  modulation frequency peak we see, but not so significantly. The main problem is that the two data sets occurred in different solar cycles, and the magnetic field in the convection zone changes drastically with solar cycle. We find the  $13.6 \text{ y}^{-1}$  peak increases in power until near the end of GALLEX running, when there is a change in solar cycle, and it disappears (as does the double flux peak) during GNO data taking. Using only GALLEX data, a search band ( $12.5\text{--}13.8 \text{ y}^{-1}$ ) compatible with solar rotation rates, full information on run durations, and the existence of a harmonic, we establish the peak at the 99.96% CL[11]. The harmonic is unique, since a search for pairs of peaks with frequencies in a 2:1 ratio yields a single peak at a fundamental of  $13.6 \text{ y}^{-1}$ , the probability of which by chance is 0.7% for a  $0\text{--}26 \text{ y}^{-1}$  search band, or 0.04% for the rotational band.

Super-Kamiokande (SK) sees at low significance the same three peak frequencies we[12] see:  $9.43 \pm 0.05$  (A),  $39.28 \pm 0.05$  (B), and  $43.22 \pm 0.06$  (C)  $\text{y}^{-1}$ , as shown in Fig. 2. To understand the difference in the two analyses, we concentrate on peak A and show how the power of the peak increases as more experimental information is used, where the probability of obtaining a power  $P$  or more by chance at a specified frequency is  $e^{-P}$ . SK[8], using a Lomb-Scargle procedure in which all the data collected in a 5-day data run is taken to be at one time, got  $P = 5.90$  when using the midtime, but  $P = 6.18$  when using a mean live time. If, instead[12], one uses in addition a symmetrized experimental error,  $P = 9.56$ . Including also the start and end times of each run raises  $P$  to 11.67. Finally, if the asymmetry in the error is taken into account[13],  $P = 13.24$ . The significance of  $P$  from a Monte Carlo shows 71% of the simulations exceed  $P = 6.18$ , SK's result, whereas only 0.1% of simulations exceed  $P = 13.24$ . Thus SK's result is correctly not significant, but ours, using more experimental information, certainly is.

Even if the peaks are significant, one needs to understand their origin. Help comes from the power spectrum[1, 13] of the photospheric magnetic field during the SK data-acquisition interval, when the field had considerable lumpiness. The fundamental and first harmonic of the rotation frequency are almost absent, but there is a remarkable series of higher harmonics, with the second ( $P = 19$ ) and sixth ( $P = 20$ ) being especially prominent. Using the second through sixth harmonics gives  $13.20 \pm 0.19 \text{ y}^{-1}$  for the synodic rotation frequency of the field. Then neutrino peak B, at  $39.28 \text{ y}^{-1}$ , falls within the band of frequencies,  $39.60 \pm 0.42 \text{ y}^{-1}$ , of the second harmonic at the 99.5% CL for  $P = 8.91$  of peak B. Also, the second harmonic and peak B have the same time dependence during the solar cycle.

To understand neutrino peaks A and C, we need retrograde waves, or r-modes which move

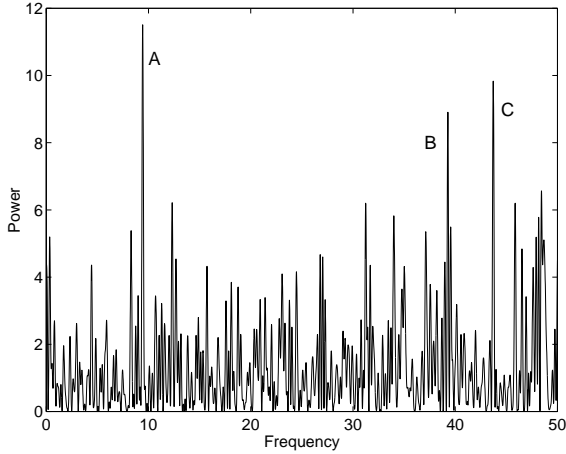


**Figure 2.** Power spectrum of Super-Kamiokande 5-day data computed taking into account the symmetrized error and start time and end time of each bin. Note that subsequent analyses using more experimental information increased the peak powers.

magnetic field regions in and out of the  $\nu_e$  path. We found evidence for r-modes in Homestake (and to a lesser extent, GALLEX) data that appear to be the origin of the well-known Rieger and Rieger-type oscillations[14]. Such modulations, resulting from the interference of an r-mode frequency and the magnetic field rotation, produce frequencies

$$\nu = \left| m\nu_R - \frac{2m}{\ell(\ell+1)}(\nu_R + 1) \pm m\nu_R \right|, \quad (1)$$

where  $\nu_R$  is the synodic rotation frequency, and  $\ell$ ,  $m$  are the usual spherical harmonic indices, with  $\ell \geq 2$  for a rotating sphere. The solution with the + sign,  $\nu = 2m(\nu_R + 1)/\ell(\ell + 1)$ , was used with  $\ell = 3$ ,  $m = 1, 2, 3$  and  $\nu_R = 12.88 \text{ y}^{-1}$  (as found by Homestake especially) to give the three Rieger frequencies to at least the accuracy they are known from sunspots and solar flares. In the SK case, where  $\nu_R = 13.20 \pm 0.14 \text{ y}^{-1}$ , using  $\ell \equiv m = 2$  this relation gives  $9.47 \pm 0.09$ , while the solution to (1) with the + sign gives  $43.33 \pm 0.47 \text{ y}^{-1}$ . Using the powers with just symmetrized errors, peak A falls in the band of the first solution at the 99.98% CL, and peak C falls into the band of the second solution at the 99.7% CL. Thus the origins of all these peaks are understood.

While frequencies dependent upon rotation rates change with solar cycle, r-modes are even more ephemeral, as is known from solar flares, sunspots, etc. Because of its prominence in the SK data, the SNO collaboration particularly searched for r-mode peak A without success. We agree with that result, but we also find that peak similarly does not appear in the SK data in the 1.6 y overlap of the two experiments. SNO, using all its data, assumed the modulation effects are constant in time. The salt data has a particularly bad background of neutral-current events, and even the D<sub>2</sub>O data has an appreciable admixture of these events which in our model are not modulated. The results are preliminary, but in the D<sub>2</sub>O data we see some evidence for rotation peak B ( $3\nu_R$ ) and also for the sixth harmonic peak at  $7\nu_R$ , which can appear in these one-day data, but not in SK's 5-day data.

Even the sample of the evidence presented above makes a very strong case for solar neutrino flux modulation, presumably requiring a sterile neutrino. Such a neutrino with very little or no mixing could be produced at a cosmologically convenient time, helping to understand small-scale structure, and contributing much more to dark matter than is presently considered possible. It also would

## 1. References

- [1] D.O. Caldwell, P.A. Sturrock, *Astropart. Phys.* 23 (2005) 543, and earlier references therein.
- [2] B.T. Cleveland *et al.*, *Astrophys. J.* 496 (1998) 505.
- [3] W. Hampel *et al.*, *Phys. Lett. B* 447 (1999) 127; M. Altmann *et al.*, *Phys. Lett. B* 616 (2005) 174.
- [4] S. Tsuneta *et al.* *Solar Phys.* 136 (1991) 37.
- [5] C.-S. Lim, W.J. Marciano, *Phys. Rev. D* 37 (1988) 1368; E.Kh. Akhmedov, *Phys. Lett. B* 213 (1988) 64.
- [6] A. Friedland, A. Gruzinov, *Astropart. Phys.* 19 (2003) 575; A.B. Balantekin, C. Volpe, *Phys. Rev. D* 72 (2005) 033008.
- [7] B.C. Chauhan, J. Pulido, *J. High Energy Phys.* 06 (2004) 008.
- [8] J. Yoo *et al.*, *Phys. Rev. D* 68 (2003) 092002.
- [9] B. Aharmim *et al.*, *Phys. Rev. D* 72 (2005) 052010.
- [10] L. Pandola, *Astropart. Phys.* 22 (2004) 219.
- [11] P.A. Sturrock, D.O. Caldwell, J.D. Scargle *Astropart. Phys.* (in press).
- [12] P.A. Sturrock, D.O. Caldwell, J.D. Scargle, M.S. Wheatland, *Phys. Rev. D* 72 (2005) 113004.
- [13] P.A. Sturrock and J.D. Scargle, hep-ph/0601251.
- [14] E. Rieger *et al.*, *Nature* 312 (1984) 623; J.N. Kile, E.W. Cliver, *Astrophys. J.* 370 (1991) 442; T. Bai, *Astrophys. J.* 388 (1992) L69; T. Bai, *Solar Phys.* 150 (1994) 385.

# Low energy Superbeams, Beta beams and the Neutrino Factory

**Leslie Camilleri**

CERN, 1211 Geneva 23, Switzerland

E-mail: [Leslie.Loris.Camilleri@cern.ch](mailto:Leslie.Loris.Camilleri@cern.ch)

**Abstract.** The world neutrino community is currently investigating the best way forward to address the value of  $\theta_{13}$ , the mass hierarchy and possible CP violation in the neutrino sector. This presentation describes the status of performance studies and R&D concerning Low energy Superbeams, Beta beams and a Neutrino Factory.

## 1. Introduction

Determining the value of  $\theta_{13}$  is currently being addressed by reactor [1] and accelerator [2], [3], [4], [5] experiments either at the running or planning stages. Some of these, especially if extended through the use of upgraded accelerators, could even begin to address the mass hierarchy question. However observing CP violation in the neutrino sector would require more sensitive experiments and therefore a more intense neutrino source. At this stage candidate sources are either a beta beam complex, possibly including a low energy superbeam, or a neutrino factory. The method of choice is the comparison, at the atmospheric  $\Delta m^2$  of  $2.5 \times 10^{-3} \text{ eV}^2$ , of the rate of appearance of  $\nu_e$  in a  $\nu_\mu$  beam with that of  $\bar{\nu}_e$  in a  $\bar{\nu}_\mu$  beam, or conversely the rate of appearance of  $\nu_\mu$  in a  $\nu_e$  beam with that of  $\bar{\nu}_\mu$  in a  $\bar{\nu}_e$  beam

## 2. Low energy superbeams

A typical example is the Superconducting Proton Linac(SPL) [6] being considered at CERN, a 4MW machine with a kinetic energy up to 5 GeV. The pulse length is shortened to decrease atmospheric neutrino contamination by reducing the duty cycle. The protons impinge on a liquid mercury target as a solid target would not withstand the stress. The pions produced are focused by a horn and reflector system towards a decay tunnel. A far detector will be located in a new cavern off the Frejus road tunnel, 130 km away. The recent approval of a safety gallery for this tunnel provides an opportunity for excavating a new cavern. At this distance the neutrino energy to be at oscillation maximum is 260 MeV, but it seems that 350 MeV provides better sensitivity due to larger neutrino interaction cross sections and lower backgrounds. A near detector will also be required, as in all schemes described in this talk.

### 2.1. The detector and its performance

The civil engineering requires the cavern, located at a depth of 4800 m.w.e., to be subdivided into shafts 57m in both diameter and height. Three such shafts could be excavated and each would house a 145 ktons water Cerenkov detector, amounting to a total mass close to 0.5 Mton,

the MEMPHYS detector [7]. Each detector would use 81000 12 in. photomultipliers and would cost 80 Meuros in addition to the 80 Meuros civil engineering costs for each shaft.

Several options have been studied [8]: 3.5 and 4.5 GeV proton beams as well as 260 and 350 MeV neutrinos. The sensitivity to  $\theta_{13}$  is shown in Figure 1a for a 5 year neutrino run and can be seen to depend on the value of  $\delta_{CP}$  because of correlations. This dependence can be reduced, Figure 1b, by running both neutrinos (2 years) and antineutrinos (8 years). A 90% C.L. limit on  $\sin^2 2\theta_{13}$  of 0.001 can then be achieved. Matter effects and therefore the mass hierarchy are not important at this energy and distance.

### 3. Beta beams

This was an idea introduced [9] by Piero Zucchelli some years ago. It consists [10] in accelerating radioactive ions decaying either via  $\beta^-$  such as  ${}^6\text{He}$  or  $\beta^+$  such as  ${}^{18}\text{Ne}$ . Because of the Lorentz boost the decay  $\nu_e$  or  $\bar{\nu}_e$  will be focused forward into a narrow beam. The signal is to look for  $\nu_\mu$  or  $\bar{\nu}_\mu$  appearance via their charged current (CC) interactions producing  $\mu^-$  or  $\mu^+$  in a far detector. The advantages are a clean beam without an oscillated flavour intrinsic background and a neutrino energy tunable through the acceleration of the parent ions. A conceptual design for EURISOL [11], a nuclear physics facility using radioactive ions, is currently being funded by the European Union. Because many components of EURISOL would be similar to a beta beam facility, this study, to be completed in 2010, includes the production of beta beams. Protons, accelerated in the SPL, would impinge on the appropriate source to produce  ${}^6\text{He}$  giving  $\nu_e$  or  ${}^{18}\text{Ne}$  giving  $\bar{\nu}_e$ . The current production rates are adequate for  ${}^6\text{He}$  but an order of magnitude too small for  ${}^{18}\text{Ne}$ . However a possible solution [12] is in sight. The ions will be bunched to reduce the atmospheric neutrino background, accelerated in the PS and SPS and finally injected as 8 bunches into a race-track shaped storage ring with its straight sections pointing to the far detector. They could either be stored together provided  $\gamma({}^{18}\text{Ne}) = 1.67\gamma({}^6\text{He})$ , allowing both neutrino flavours to be studied simultaneously or stored separately, thus removing the  $\gamma$  constraint. Since the front-end would be needed by EURISOL and the PS and SPS already exist at CERN, the only additional component would be the storage ring.

#### 3.1. The detector and its performance

It would be the same as for an SPL, thus allowing both types of beams to use it. The distance would require the radioactive ions to be accelerated such as to boost the 3 MeV beta decay neutrinos to a few hundred MeV to be at oscillation maximum. The basic design assumes  $\gamma$ 's of 60 and 100 for  ${}^6\text{He}$  and  ${}^{18}\text{Ne}$  respectively.

Assuming the above  $\gamma$ 's,  $2.9 \times 10^{18}$   ${}^6\text{He}$  ions and  $1.2 \times 10^{18}$   ${}^{18}\text{Ne}$  ions decaying per year in the straight sections and a 2% systematic uncertainty, the sensitivity to  $\delta_{CP}$  was calculated [13], [14] for a 10 year exposure of a 440 kton detector. It is shown in Figure 2 as a function of  $\sin^2 2\theta_{13}$ . At low values of  $\theta_{13}$  it degrades because of statistics. It does not continue to improve as  $\theta_{13}$  increases because the effect of CP violation decreases with increasing  $\theta_{13}$ , cancelling the effect of better statistics. A 99% discovery potential of  $\delta_{CP}$  of  $30^\circ$  can be achieved. The performance has also been optimized [14] by storing ions separately and thus going to higher energies. Accelerating both ion types to  $\gamma$ 's of 120, the discovery potential of  $\delta_{CP}$  can be improved to  $15^\circ$ . This is also shown in Figure 2 which also displays sensitivities achievable with either a new lab at 300km or a higher energy SPS and a detector at the Gran Sasso.

#### 3.2. Comparisons of SPL and beta beams performance

A study of the relative performance of T2K, SPL, and a beta beam has been performed [15]. The same 440 kton detector was assumed for each. A 2 year neutrino run and an 8 year antineutrino run was assumed for the SPL and 5 years each of neutrinos and antineutrinos for the beta beam.

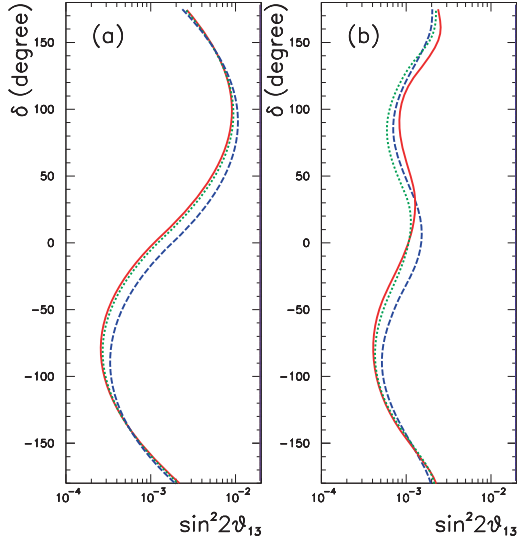


**Figure 1.** The 90% C.L. limit on  $\sin^2 2\theta_{13}$  as a function of  $\delta_{CP}$  that can be set by an SPL run for various combinations of neutrino and proton energies. (a) For a 5 year neutrino run and (b) for a two year neutrino and 8 year antineutrino run.

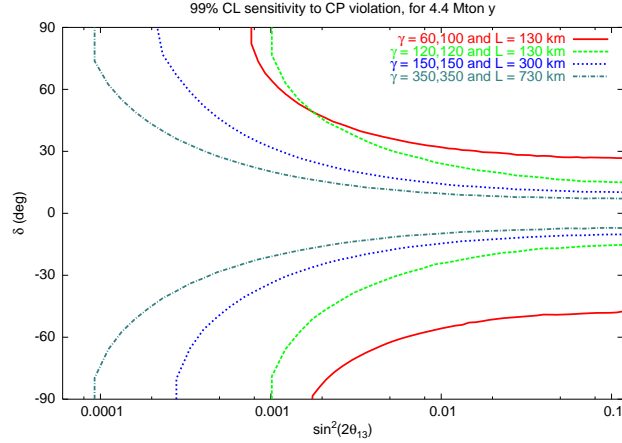


**Figure 2.** The 99% C.L. discovery potential on  $\delta_{CP}$  as a function of  $\sin^2 2\theta_{13}$ , achievable with beta beams obtained with stored ions of different  $\gamma$ 's and for different baselines.

The resulting  $3\sigma$  discovery potential on  $\sin^2 2\theta_{13}$  is shown in Figure 3 as a function of  $\delta_{CP}$ . Systematics were varied between 2% and 5%. One can conclude that:

- The SPL and T2K are comparable in sensitivity.
- The beta beam is more sensitive than both over most of the range of  $\delta_{CP}$ .
- A combination of SPL and beta beam, also shown in Figure 3 for 2% systematics is considerably more sensitive than any of the other three schemes. This can be envisaged as the SPL would only be used for radioactive ion production for a fraction of its time.

The energy envisaged for both the SPL and the beta beam is too low to determine the mass hierarchy. However combining these results with the large number of atmospheric neutrino events that can be accumulated with a 0.5 Mton detector, could lead to appreciable sensitivity to the mass hierarchy [16] because of its influence, through matter effects, on atmospheric neutrinos going through the core of the earth. The expected  $\nu_\mu/\nu_e$  ratio changes by 7% depending on the mass hierarchy for values of  $\sin^2 2\theta_{13}$  of 0.05. In combination with these atmospheric results, SPL and the beta beam could resolve the mass hierarchy at a significance of better than  $2\sigma$  for 50% of the range of  $\delta_{CP}$  for values of  $\sin^2 2\theta_{13}$  larger than 0.04, as shown in Figure 4.

#### 4. The Neutrino Factory

The concept [17] of a neutrino factory is to produce pions using a high intensity proton beam, let them decay to muons, cool these muons to reduce their angular and momentum spread, accelerate the muons and inject them in a storage ring where they decay producing neutrinos. A suitably shaped storage ring will send most of the neutrinos towards one or two far detectors. If  $\mu^+$ , which decay to  $e^+ + \bar{\nu}_\mu + \nu_e$ , are stored, the CC interaction of the two final state neutrinos will result in  $\mu^+$  and  $e^-$ . The signal for a  $\nu_e$  to  $\nu_\mu$  oscillation will then be the observation of  $\mu^-$ , the so called golden channel, requiring the use of a magnetic detector to measure the muon

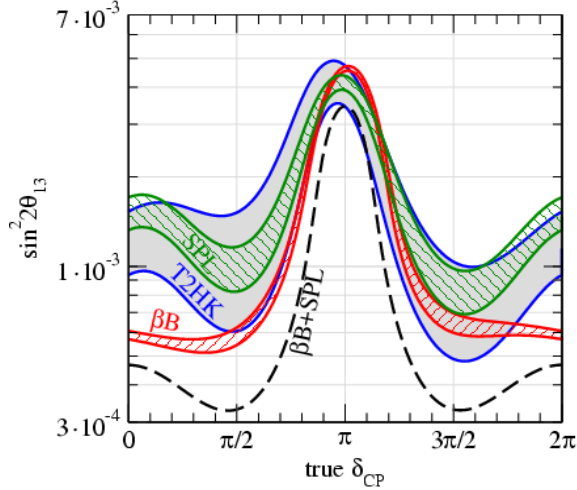


**Figure 3.** The region of parameter space over which  $\sin^2 2\theta_{13}$  can be determined at better than  $3\sigma$  for T2HK, SPL and Beta beams. The top edge of each band is for 5% systematic uncertainty and the bottom edge for 2%. The dashed black curve is for beta beams in conjunction with an SPL assuming 2% systematics.

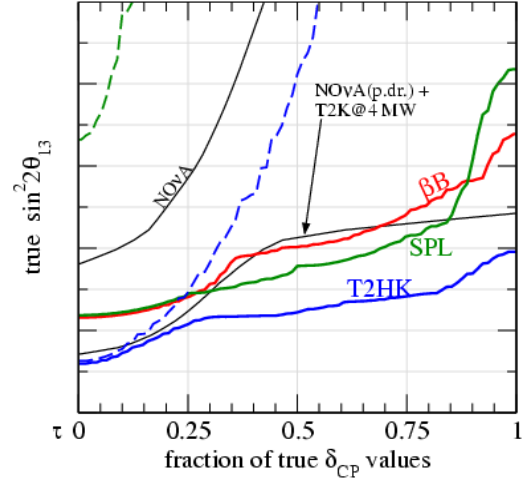


**Figure 4.** The range of parameter space over which the mass hierarchy can be determined with a significance of better than  $2\sigma$ . Dashed and dotted lines for the facilities shown on the plot, solid lines for the same facilities but including atmospheric neutrino data.

charge. If the charge of an electron can also be measured, the study of the platinum channel,  $\bar{\nu}_\mu$  to  $\bar{\nu}_e$ , would allow the search for T violation.

#### 4.1. Technical design

The study of a neutrino facility and its performance is being carried out in the context of the International Scoping Study (ISS). Some preliminary conclusions have already been reached [18]: a proton energy of 5-15 GeV, a liquid mercury target, a bunch length of 2 ns and a horn instead of a solenoid for pion collection. Longitudinal cooling would be obtained by phase rotation using the Neuffer scheme. This entails capturing multi bunches of muons with a very high frequency RF and rotating them with decreasing RF along the cooling channel. Transverse cooling will be provided through ionization and RF. No decision on the muon acceleration scheme has been taken yet. The use of the Neuffer scheme and that of a solenoid for pion collection allows the simultaneous collection of  $\mu^+$  and  $\mu^-$ . Their interaction would be distinguished by separating them by 400 ns in the storage ring for which two configurations have been studied. A race-track would have both straight sections pointing to the same detector and could supply both signs to it simultaneously. Two rings would be needed if two detectors at different locations would be active at the same time. A triangle could supply simultaneously the same sign to two detectors each lined up with one of its straight sections. Two rings would be required if both signs are needed at the same time. With these parameters,  $10^{21}$  ( $\mu^+ + \mu^-$ ) decays per year in each straight section of the storage ring may be achieved.

#### 4.2. The performance and the detectors

At the first oscillation maximum the  $\nu_\mu \rightarrow \nu_e$  oscillation probability in matter for neutrinos of energy  $E_\nu$ , is related to the vacuum oscillation probability by

$$P(\nu_\mu \rightarrow \nu_e)_{\text{matt}} = [1 \pm (2E_\nu/E_R)]P(\nu_\mu \rightarrow \nu_e)_{\text{vac}}$$

where the  $\pm$  sign depends on the mass hierarchy and  $E_R = 12$  GeV and depends on  $\Delta m^2$  and the density of matter the beam goes through. The dependence on the mass hierarchy increases with energy and therefore with distance, if one wants to remain at the first oscillation maximum. This is seen in Figure 5 which shows an increase with distance of the dependence on the mass hierarchy of the ratio of antineutrino to neutrino oscillation probabilities. The figure also shows that at 7000 km this ratio does not depend on the CP phase, making this distance a “magic” distance at which correlations are minimized [19]. However at these long distances the earth density must be well understood. It is estimated that it can be known to 2%.

From Figure 6, it can be seen that an experiment using  $\nu$  and  $\bar{\nu}$  at a single baseline would deduce a clone solution [20] as well as the correct one. A second baseline, at which the clone solution would occur at different values of the parameters, is needed to deduce the correct solution. Alternatively, both  $\nu_\mu \rightarrow \nu_e$  and  $\nu_e \rightarrow \nu_\tau$ , which have opposite CP violation effects could be studied [21] with a detector, using the DONUT [22] and OPERA [3] emulsion technology, which provides the ability to observe  $\tau$ 's through their mm long decay path.

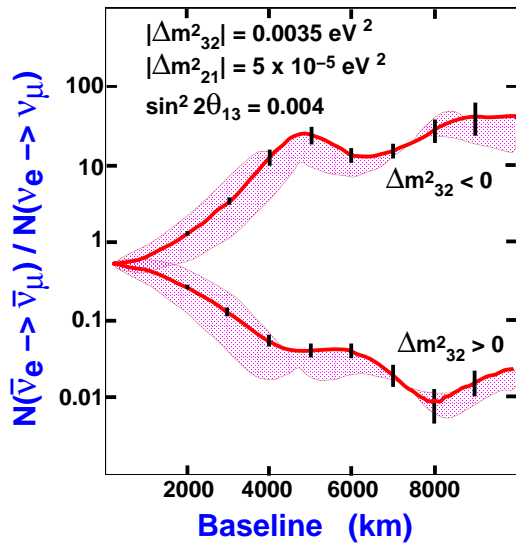


**Figure 5.** The ratio  $(\bar{\nu}_e \rightarrow \bar{\nu}_\mu) / (\nu_e \rightarrow \nu_\mu)$  as a function of baseline, for the two mass hierarchies. The width of the bands is the effect of  $\delta_{CP}$ .

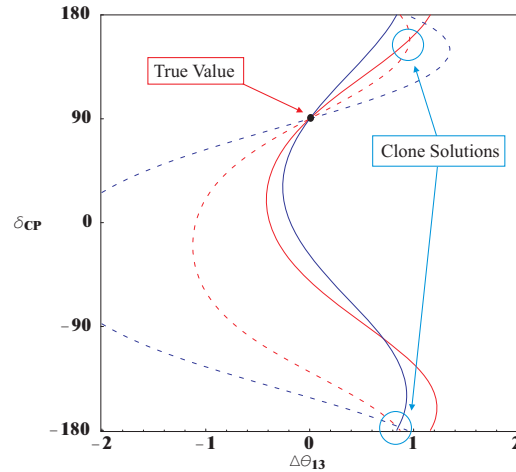


**Figure 6.** The result of measurements of the oscillation probability  $\nu_e \rightarrow \nu_\mu$  with both neutrinos (solid) line and antineutrinos (dashed lines) for a 3000km (red) and a 730km (blue) baseline.

Several detector technologies are being considered [18]. A 50kton detector consisting of magnetized iron plates interleaved with planes of liquid scintillator filled PVC tubes is an attractive possibility. Another one is a liquid argon detector [23]. This promising technology needs to be adapted to reach large masses. Its mass would be limited to 15ktons by the coil needed to magnetize it. However its superior efficiency, especially to electrons, would make it competitive even with a reduced mass. A fully active detector such as NOvA [5], enclosed in a magnetic field is also a possibility but again would be limited by realistic magnet sizes. An emulsion detector [21] could also be included in such a magnetic detector and would be used for  $\nu_e \rightarrow \nu_\tau$  searches and for identifying the charge of electrons over very short distances.

## 5. Comparison of the different options

A GLOBES analysis [24] was used to determine and compare [25] the capabilities of beta beams ( $\gamma = 100, 100$ ) in conjunction with an SPL or not, of a neutrino factory with baselines of 3000 and 7000 km and of T2HK [26]. The parameter space over which CP violation can be determined at a significance of better than  $3\sigma$  is shown in Figure 7. It is clear that the neutrino factory is sensitive to smaller values of  $\sin^2 2\theta_{13}$ . However for values of  $\sin^2 2\theta_{13}$  above 0.01 the SPL and SPL + beta beams seem to be more appropriate. This comparison is currently being addressed again in the ISS.

The advantages of beta beams are its synergy with EURISOL, the lack of intrinsic background, negligible matter effects and no need for an analyzing magnet. Its disadvantages are mostly due to the low energy of its neutrinos resulting in low interaction rates, poorly known cross sections (nuclear effects), larger atmospheric backgrounds and the impossibility to study the  $\nu_e \rightarrow \nu_\tau$  channel. In addition it would require an SPL neutrino beam to achieve its ultimate sensitivity.

The advantages of a neutrino factory are its reach, the ability to determine the mass hierarchy, the presence of both  $\nu_e$  and  $\nu_\mu$  in the beam which allows the measurement of all the required cross sections in a near detector, the higher energy resulting in better known cross sections and lower atmospheric background. Its disadvantages are its more challenging technology, the need to understand the earth density over long distances and the need for a magnetic detector.

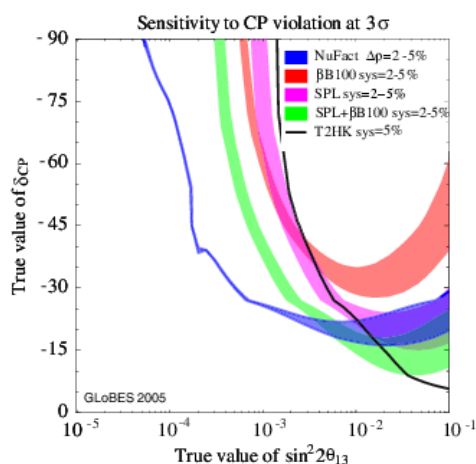


**Figure 7.** A comparison of the  $\delta_{CP}$  discovery potential of the various neutrino facilities described in the text as calculated using GLOBES, shown for one quadrant of  $\delta_{CP}$  values. The width of the curves reflect systematic uncertainties. See Ref..

## 6. Ongoing R&D efforts

MERIT [27], an experiment at the CERN PS, is designed to measure the effects of a  $2 \times 10^{13}$  protons/pulse 24 GeV beam impinging on a mercury jet target in a 15T magnetic field. Its aim is to measure jet dispersal and the effect of the magnetic field on the jet flow. It is scheduled to run in Spring 2007. MICE [28], the muon cooling experiment at RAL, with its strong synergy with MUCOOL [29] at Fermilab, is intended to demonstrate the feasibility of muon cooling using liquid hydrogen absorbers interleaved with sets of RF cavities. Incoming and outgoing spectrometers will measure the effectiveness of the cooling on the incident muon beam. It is to start in Spring 2007 and will have its full setup in 2009.

## 7. Conclusions

The year 2010 will be critical in many ways: a possible ILC decision, the conclusion on CLIC possibilities, LHC results, decisions on LHC upgrades and on the location of EURISOL and a possible first indication from MINOS and Double CHOOZ of the value of  $\theta_{13}$ . It will be

crucial to know by that date which neutrino facility is favoured. Its approval in this crowded international context will be difficult but it is definitely worth fighting for, given all the surprises neutrino physics have provided us with of late.

### Acknowledgments

I would like to acknowledge the studies done by J-E. Campagne, M. Lindroos and M. Mezzetto on which the section on SPL and beta beams are based. The studies and presentations of A. Blondel, Y. Nagashima, R. Palmer and P.Soler on the Neutrino Factory are also gratefully acknowledged.

### References

- [1] Ardellie F *et al* hep-ex/0606025  
Cao J 2006 Nucl. Phys. Proc. Suppl. **155** 229  
<http://braidwood.uchicago.edu>  
<http://kaska.hep.sc.niigata-u.ac.jp/scientists>
- [2] Michael D G *et al* hep-ex/0607088 and references therein
- [3] Guler M *et al* CERN SPSC 2000-028 SPSC/P318 LNGS P25/2000
- [4] Itow Y *et al* hep-ex/0106019
- [5] Ayres D *et al* hep-ex/0503053
- [6] Gerigk F *et al* *Conceptual Design of the SPL II* CERN Yellow Report CERN 2006 -006
- [7] de Bellefon A *et al* hep-ex/0607026
- [8] Campagne J-E and Cazes A 2006 Eur. Phys. J. C **45** 643, hep-ex/0411062
- [9] Zucchelli P 2002 Phys. Lett.B **532** 166
- [10] Autin B *et al* physics/0306106
- [11] *European Isotope Separation Online* <http://ganinfo.in2p3.fr/eurisol/>
- [12] Rubbia C, Ferrar A, Kadi Y and Vlachoudis V hep-ph/0602032
- [13] Bouchez J, Lindroos M and Mezzetto M hep-ex/0310059
- [14] Burguet-Castell J, Casper D, Couce E, Gomez-Cadenas J J and Hernandez P 2005 Nucl. Phys. B **725** 306, hep-ph/0503021
- [15] Campagne J-E *et al* hep-ph/0603172, LAL-06-35, IC/2006/11, SISSA 16/2006/EP
- [16] Bernabeu J, Palomares-Ruiz S and Petcov S T hep-ph/0305152, SISSA 28/03/EP, FTUV-03-0513, IFIC/03-21
- [17] Geer S 1998 Phys. Rev. D **57** 6989  
De Rujula A, Gavela M B and Hernandez P 1999 Nucl. Phys.B **547** 21
- [18] *International Scoping Study* <http://www.hep.ph.ic.ac.uk/iss/>
- [19] Barger V, Geer G, Raja R, Whisnant K hep-ph/0003184
- [20] Rigolin S hep-ph/0407009
- [21] Autiero D *et al* hep-ph/0305185
- [22] Kodama K *et al* 2002 NIM A **493** 45 and references therein
- [23] Rubbia A 2005 Nucl. Phys. Proc. Suppl. B **147** 103
- [24] Huber P, Lindner M and Winter M 2005 Comput. Phys. Commun. **167** 195, hep-ph/0407333
- [25] Blondel A *et al* hep-ph/0606111
- [26] Kobayashi T 2005 Nucl. Phys. Proc. Suppl. B **143** 303
- [27] Bennett J *et al* CERN-INTC 2004-16
- [28] *The International Muon Ionization Cooling Experiment MICE* <http://hep04.phys.iit.edu/cooldemo>
- [29] *The Muon Cooling Experiment R&D* [http://www.fnal.gov/projects/muon\\_collider/cool/cool.html](http://www.fnal.gov/projects/muon_collider/cool/cool.html)

# What we can learn from atmospheric neutrinos

**Sandhya Choubey**

Harish-Chandra Research Institute, Chhatnag Road, Jhansi, Allahabad 211019, India

E-mail: sandhya@mri.ernet.in

**Abstract.** Physics potential of future measurements of atmospheric neutrinos is explored. Observation of  $\Delta m_{21}^2$  driven sub-dominant effects and  $\theta_{13}$  driven large matter effects in atmospheric neutrinos can be used to study the deviation of  $\theta_{23}$  from maximality and its octant. Neutrino mass hierarchy can be determined extremely well due to the large matter effects. New physics can be constrained both in standard atmospheric neutrino experiments as well as in future neutrino telescopes.

## 1. Introduction

Atmospheric neutrinos observed in the Super-Kamiokande (SK) experiment provided the first unambiguous signal for neutrino flavor oscillations [1]. The observed zenith angle and energy dependent depletion of atmospheric  $\nu_\mu/\bar{\nu}_\mu$  in SK can be explained only by  $\nu_\mu$ - $\nu_\tau$  oscillations with  $\Delta m_{31}^2 = 2.1 \times 10^{-3} \text{ eV}^2$  and almost maximal mixing angle,  $\sin^2 2\theta_{23} = 1$ . The results of the SK experiment was subsequently corroborated by the MACRO and Soudan-2 atmospheric neutrino experiments and more recently by the K2K and MINOS long baseline (LBL) experiments. In this talk we will expound the physics potential of future atmospheric neutrino experiments using larger and better detectors.

## 2. Confirming oscillations of atmospheric neutrinos

The “smoking gun” signal for  $\nu_\mu$ - $\nu_\tau$  oscillations is the observation of the characteristic “dip” in  $L/E$ , predicted by neutrino flavor mixing. Although the analysis of the  $L/E$  binned atmospheric neutrino data in SK has been found to support the oscillation hypothesis [2], it would be worthwhile to make an unambiguous check using a detector with better  $E$  and  $L$  resolution. This can be done in large magnetized detectors, such as the proposed ICAL detector at the India-based Neutrino Observatory (INO) [3]. Analysis of results obtained from detailed simulations by the INO collaboration show that oscillations can be confirmed with a significant C.L. with just 250 kTy data.

## 3. Precision measurement of $\Delta m_{31}^2$ and $\sin^2 \theta_{23}$

Both  $\Delta m_{31}^2$  and  $\sin^2 2\theta_{23}$  are expected to be measured very accurately by the forthcoming LBL experiments. A statistical analysis of the combined data set with five years of running of MINOS, ICARUS, OPERA, T2K and NO $\nu$ A each, reveals that  $\Delta m_{31}^2$  and  $\sin^2 \theta_{23}$  could be measured with a spread of 4.5% and 20% respectively at  $3\sigma$  [4]. The future prospective data from water Cerenkov atmospheric neutrino experiments with a statistics 20 times the current SK statistics could measure  $\Delta m_{31}^2$  and  $\sin^2 \theta_{23}$  with a spread of  $\sim 17\%$  and  $\sim 24\%$  respectively [5]. A large

magnetized iron calorimetric detector such as the proposed INO detector ICAL [3], could use atmospheric neutrinos to measure  $\Delta m_{31}^2$  and  $\sin^2 \theta_{23}$  within 10% and 30% respectively at  $3\sigma$  with a statistics of 250 kTy [3].

#### 4. Atmospheric neutrino experiments: Subdominant effects

The effect of the sub-dominant terms in the Super-Kamiokande (SK) atmospheric neutrino data is not yet at the statistically significant level. However, the sub-dominant terms, if observed in a future high statistics atmospheric neutrino experiment, can be used to give information on:

- Deviation of  $\theta_{23}$  from its maximal value
- Octant of  $\theta_{23}$
- $\text{sgn}(\Delta m_{31}^2)$

Assuming a constant density for the earth matter, the excess of electron type events in a water Cerenkov experiment such as SK is given by [6, 7]

$$\frac{N_e}{N_e^0} - 1 \simeq \sin^2 2\theta_{12}^M \sin^2 \left( \frac{(\Delta m_{21}^2)^M L}{4E} \right) \times (r \cos^2 \theta_{23} - 1) \quad (1)$$

$$+ \sin^2 2\theta_{13}^M \sin^2 \left( \frac{(\Delta m_{31}^2)^M L}{4E} \right) \times (r \sin^2 \theta_{23} - 1) \quad (2)$$

$$+ \sin \theta_{23} \cos \theta_{23} r \text{Re} \left[ A_{13}^* A_{12} \exp(-i\delta_{CP}) \right], \quad (3)$$

where  $L$  is the baseline,  $E$  is the energy of the neutrino,  $r = N_e/N_\mu$ ,  $N_e$  and  $N_\mu$  being the number of e and  $\mu$  events respectively in the detector in absence of oscillations and  $\theta_{12}^M$ ,  $\theta_{13}^M$ ,  $(\Delta m_{21}^2)^M$  and  $(\Delta m_{31}^2)^M$  are the mixing angle and mass squared differences in matter.

- (i) The first term in Eq. (3) is the  $\Delta m_{21}^2$  driven oscillation term – which is obviously more important for the sub-GeV neutrino sample. Since  $r \simeq 0.5$  in the sub-GeV regime, this term brings an excess (depletion) of sub-GeV electron events if  $\theta_{23} < \pi/4$  ( $\theta_{23} > \pi/4$ ). It can thus be used to study the maximality and octant of  $\theta_{23}$  through the sub-GeV electron sample [6, 5].
- (ii) The second term is the  $\theta_{13}$  driven oscillation term. Being dependent on  $\sin^2 \theta_{23}$ , this term goes in the opposite direction to the first term. Therefore for sub-GeV neutrinos, larger  $\theta_{13}$  would imply that the effect of the first term would get negated by this term. However for multi-GeV neutrinos, there will be large matter effects inside the earth and this term dictates the electron excess. The  $\sin^2 \theta_{23}$  dependence of this term could then be used to study the maximality and octant of  $\theta_{23}$  through the multi-GeV electron sample (see also [8]). Since matter effects bring in sensitivity to the  $\text{sgn}(\Delta m_{31}^2)$ , this term can be used to study the mass hierarchy.
- (iii) The last term is the “interference” term [7], which depends on  $\delta_{CP}$ . The effect of this term could be to dilute the effect of the first two terms and spoil the sensitivity of the experiment. However, being directly dependent on  $\delta_{CP}$ , this term also brings in some sensitivity to the CP phase itself [7, 9].

The depletion of the muon events in the limit of  $\Delta m_{21}^2 = 0$  is given by<sup>1</sup>

$$1 - \frac{N_\mu}{N_\mu^0} = (P_{\mu\mu}^1 + P_{\mu\mu}^2) + (P_{\mu\mu}^3)' \sin^2 \theta_{23} (\sin^2 \theta_{23} - \frac{1}{r}), \quad (4)$$

<sup>1</sup> The approximation of taking a vanishing  $\Delta m_{21}^2$  has been made in Eq. (7) only for the sake of simplicity, since the main subdominant effect in the muon neutrino channel comes from earth matter effects, which are large for multi-GeV neutrinos for which  $\Delta m_{21}^2$  dependence is less importance. The results presented in the later sections have been obtained using the full numerical solution of the three-generation equation of the atmospheric neutrinos.

$$P_{\mu\mu}^1 = \sin^2 \theta_{13}^M \sin^2 2\theta_{23} \sin^2 \frac{[(A + \Delta m_{31}^2) - (\Delta m_{31}^2)^M] L}{8E}, \quad (5)$$

$$P_{\mu\mu}^2 = \cos^2 \theta_{13}^M \sin^2 2\theta_{23} \sin^2 \frac{[(A + \Delta m_{31}^2) + (\Delta m_{31}^2)^M] L}{8E}, \quad (6)$$

$$(P_{\mu\mu}^3)' = \sin^2 2\theta_{13}^M \sin^2 \frac{(\Delta m_{31}^2)^M L}{4E}, \quad (7)$$

where  $A = 2\sqrt{2}G_F N_e E$  is the matter potential. For very small values of  $\theta_{13}$ , there is very little matter effect and we can see that  $P_{\mu\mu}^2$  is the dominant term in the survival probability. Since this term depends on  $\sin^2 2\theta_{23}$  we do not expect octant sensitivity in absence of matter effects from experiments probing the  $P_{\mu\mu}$  channel alone. However, if  $\theta_{13}$  is not too small, neutrinos which travel through large baselines and hence large matter densities inside the earth, undergo large matter effects. The mixing angle  $\theta_{13}^M$  increases in matter and the third term  $(P_{\mu\mu}^3)'$  becomes important as well. Since this term has a strong dependence on  $\sin^2 \theta_{23}$  rather than  $\sin^2 2\theta_{23}$ , we expect the  $P_{\mu\mu}$  channel to develop sensitivity to the octant of  $\theta_{23}$  in presence of large matter effects [10]. Probing matter effects in the resultant muon signal in the detector will also provide us with information on the neutrino mass hierarchy [11, 12].

Since matter effects are large for higher energy neutrinos, we expect that multi-GeV atmospheric  $\nu_\mu/\bar{\nu}_\mu$  events can be used for this purpose. However, unlike in the case for matter effects in the  $P_{\mu e}$  channel, both the magnitude and sign of the earth matter effects in the  $P_{\mu\mu}$  channel depends crucially on  $L$  and  $E$ . The largest effect of earth matter comes for neutrino travelling  $L \simeq 7000$  km with  $E \sim 5$  GeV. The matter effects changes sign rapidly with  $L$  and  $E$  – with  $\Delta(P_{\mu\mu}) < 0$  and  $\Delta(P_{\mu\mu}) > 0$  at the maximum and minimum respectively of  $P_{\mu\mu}$ . Thus, in order to see the matter effects one needs to bin the data judiciously both in energy and zenith angle.

Very good energy and zenith angle detector resolution is expected for the magnetized iron calorimeters. Therefore, fine binning would allow such detectors to observe matter effects in the muon signal. Since large matter effects appear only in either the neutrino or the antineutrino channel, the magnetic field which allows for charge discrimination, further helps these type of detectors to observe earth matter effects in the muon channel. However, unless the iron plates of the detector are thin enough, it would not be possible to detect electrons in these type of detectors. The current INO-ICAL design does not allow for it and therefore would observe muon events only. Another restriction for these detectors come from the relatively higher threshold, which allows for the detection of only multi-GeV  $\nu_\mu/\bar{\nu}_\mu$ .

Water Cerenkov detectors have the advantage that sub-GeV neutrinos can be detected. However, the energy resolution is worse than that for iron calorimeters. For the results shown here, the data is binned in sub-GeV and multi-GeV bins and therefore the matter effects in the  $P_{\mu\mu}$  channel get largely averaged out. This means that one would see very small residual matter effects in the multi-GeV muon sample. However, matter effects in the  $P_{\mu e}$  channel do not change sign over most of the relevant range of  $E$  and  $L$  in the multi-GeV regime. Therefore, multi-GeV electron sample has large matter effects and can be used to study the deviation of  $\theta_{23}$  from maximality and its octant as well as the neutrino mass hierarchy.

### 5. Is the mixing angle $\theta_{23}$ maximal?

The measurement of both the magnitude and sign of the deviation of  $\sin^2 \theta_{23}$  from its maximal value 0.5 is of utmost theoretical importance. To quantify the deviation of the true value of  $\theta_{23}$  from its maximal value, we introduce the function  $D \equiv \frac{1}{2} - \sin^2 \theta_{23}$ . The magnitude  $|D|$  gives the deviation of  $\sin^2 \theta_{23}$  from its maximal value, while  $sgn(D)$  gives the octant of  $\sin^2 \theta_{23}$ . The best current limit on  $|D|$  comes from the SK atmospheric neutrino experiment

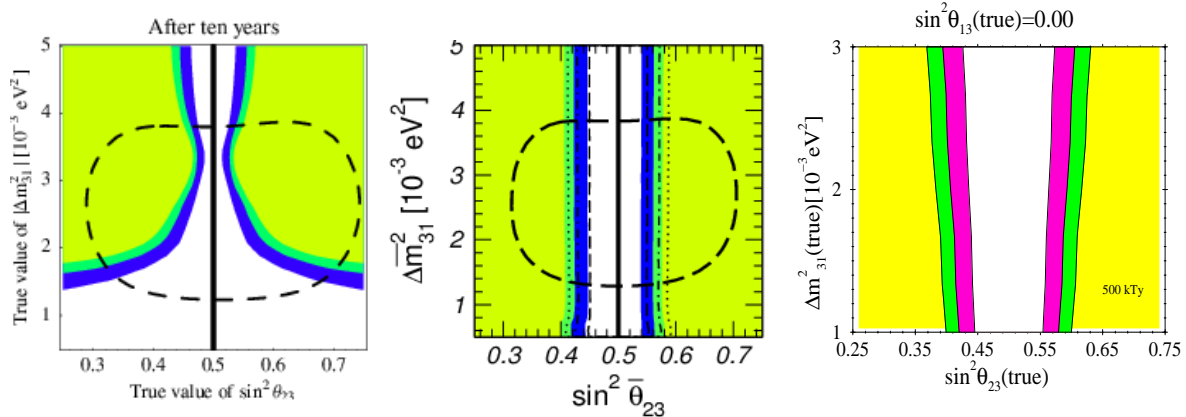


**Figure 1.** The regions of  $\Delta m_{31}^2(\text{true})$  and  $\sin^2 \theta_{23}(\text{true})$  where maximal  $\theta_{23}$  mixing can be rejected at  $1\sigma$  (inner bands),  $2\sigma$  (middle bands) and  $3\sigma$  (outer bands) C.L. The left-hand panel [13] shows the sensitivity expected from the combined data from the LBL experiments. The middle panel [5] shows the sensitivity expected with atmospheric neutrinos in a megaton water detector (SK50). The extreme right-hand panel [10] shows the corresponding reach expected from 500 kTy atmospheric neutrino data in large magnetized iron detectors. The true value of  $\theta_{13}$  is assumed to be zero.

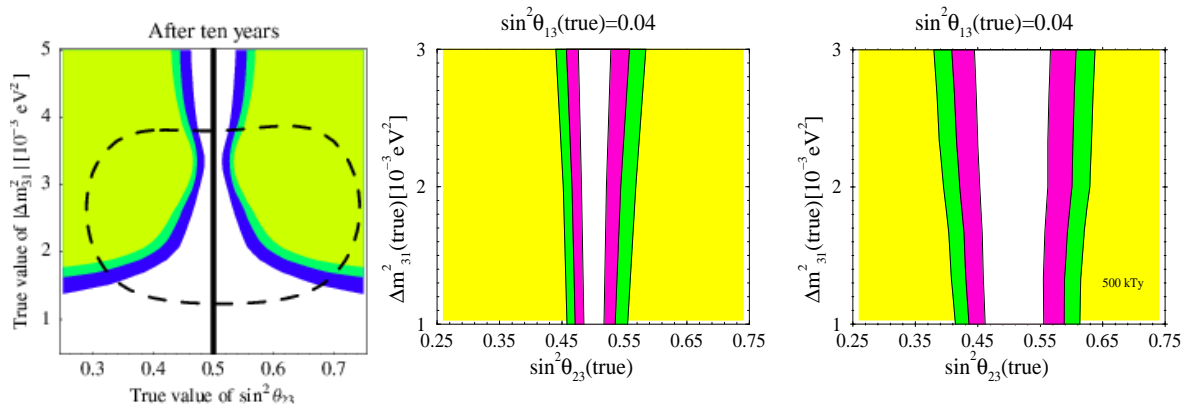


**Figure 2.** Left-hand panel same as in Fig. 1. Middle panel (for water detector) and right-hand panel (for magnetized iron detector) have been drawn assuming that  $\sin^2 \theta_{13}(\text{true}) = 0.04$ .

giving  $|D| \leq 0.16$  at  $3\sigma$  [1] while  $\text{sgn}(D)$  is almost unknown at present. Fig. 1 shows the potential of atmospheric neutrino experiments to test the deviation of  $\theta_{23}$  from maximality and compares it with the reach of the combined data from the current and next generation long baseline experiments. The combined long baseline data include five years of running each of the MINOS, ICARUS, OPERA, T2K and NO $\nu$ A experiments. The middle panel gives the sensitivity to  $|D|$  of atmospheric neutrino experiments with water detectors for a 4.6 Megaton-yr statistics, while the left panel shows the corresponding sensitivity of atmospheric neutrino data in large magnetized iron detectors with 500 kTy statistics. At  $\Delta m_{31}^2(\text{true}) = 2.5 \times 10^{-3} \text{ eV}^2$ , it should be possible to measure  $|D|$  within 19% and 25% at  $3\sigma$  with atmospheric neutrinos in water and iron detectors respectively. This is slightly weaker than the sensitivity of the combined long baseline experiments, where it should be possible to measure  $|D|$  within 14% at  $3\sigma$ . However, note that all the results presented in Fig. 1 have been obtained assuming that the true value of  $\theta_{13}$  was zero. Results for atmospheric neutrino experiments when the true value of  $\theta_{13}$  is not zero is shown in Fig. 2. For non-zero  $\theta_{13}$ , presence of earth matter effects in the  $P_{\mu\mu}$  channel

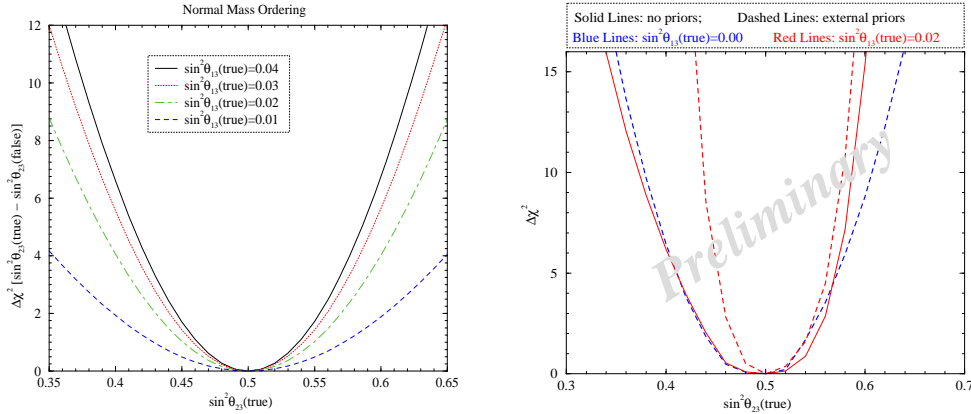


**Figure 3.** Plot showing the octant sensitivity as a function of  $\sin^2 \theta_{23}(\text{true})$ , for an atmospheric neutrino experiment with large magnetized iron calorimeter (left-hand panel) and megaton water detector (right-hand panel).

Type of Experiment	$\sin^2 \theta_{23}(\text{false})$ excluded at $3\sigma$ if:	for
Magnetized Iron (0.5 MTy)	$\sin^2 \theta_{23}(\text{true}) < 0.402$ or $> 0.592$	$\sin^2 \theta_{13}(\text{true}) = 0.02$
	$\sin^2 \theta_{23}(\text{true}) < 0.421$ or $> 0.573$	$\sin^2 \theta_{13}(\text{true}) = 0.04$
Water Cerenkov (4.6 MTy)	$\sin^2 \theta_{23}(\text{true}) < 0.383$ or $> 0.600$	$\sin^2 \theta_{13}(\text{true}) = 0.00$
	$\sin^2 \theta_{23}(\text{true}) < 0.438$ or $> 0.573$	$\sin^2 \theta_{13}(\text{true}) = 0.02$

**Table 1.** A comparison of the potential of different experiments to rule out the wrong  $\theta_{23}$  octant at  $3\sigma$  (1 dof). The third column gives the condition on the true value of  $\sin^2 \theta_{13}$  needed for the  $\theta_{23}$  octant resolution.

brings in a marginal improvement in the sensitivity of atmospheric neutrino experiment with the magnetized iron detector. For the megaton water atmospheric neutrino experiment, very large earth matter effects in the  $P_{\mu e}$  channel bring in significant improvement in the determination of  $|D|$ , making this experiment comparable/better than the long baseline experiments for studying the deviation of  $\theta_{23}$  from maximality.

## 6. Resolving the $\theta_{23}$ Octant Ambiguity

If the true value of  $\theta_{23}$  is not  $45^\circ$ , then the question arises whether  $\theta_{23} > (D \text{ positive})$  or  $< \pi/4$  ( $D$  negative). This leads to an additional two-fold degeneracy in the measurement of the mixing angle  $\theta_{13}$  and the CP phase  $\delta_{CP}$  in LBL experiments. This ambiguity is generally regarded as the most difficult to resolve. As discussed before, the presence of earth matter effects in the zenith angle and energy binned atmospheric  $\nu_\mu/\bar{\nu}_\mu$  data in magnetized iron detectors opens up the possibility of probing the octant of  $\theta_{23}$  [10]. On the other hand atmospheric  $\nu_e/\bar{\nu}_e$  data in water detectors could also give information on the octant of  $\theta_{23}$ , both through the  $\Delta m_{21}^2$  dependent subdominant term in the sub-GeV sample [6, 5], as well as through earth matter effect in the multi-GeV events, as discussed above. One could hence combine the atmospheric neutrino data, in either megaton water detectors [8, 14], or in large magnetized iron calorimeters with data from long baseline experiments to resolve parameter degeneracies.

In order to obtain the limiting value of  $\sin^2 \theta_{23}(\text{true})$  which could still allow for the determination of  $\text{sgn}(D)$  we define

$$\Delta\chi^2 \equiv \chi^2(\sin^2 \theta_{23}(\text{true}), \sin^2 \theta_{13}(\text{true}), \text{others}(\text{true})) - \chi^2(\sin^2 \theta_{23}(\text{false}), \sin^2 \theta_{13}, \text{others}), \quad (8)$$

with  $\sin^2 \theta_{23}$ (false) restricted to the wrong octant and ‘others’ comprising  $\Delta m_{31}^2$ ,  $\Delta m_{21}^2$ ,  $\sin^2 \theta_{12}$  and  $\delta_{CP}$ . These, along with  $\sin^2 \theta_{13}$  as well as  $\sin^2 \theta_{23}$ (false), are allowed to vary freely in the fit. Fig. 3 shows the results of a statistical analysis based on simulated data from atmospheric neutrinos with 500 kiloton-yr exposure in a large magnetized iron calorimeter (left-hand panel) and 4.6 Megaton-yr exposure in a water Cerenkov experiment (right-hand panel). For large magnetized iron detector we show results for four different values of  $\sin^2 \theta_{13}$ (true), assuming a normal mass ordering. For a given  $\sin^2 \theta_{13}$ (true), the range of  $\sin^2 \theta_{23}$ (true), for which  $\sin^2 \theta_{23}$ (false) can be ruled out with atmospheric neutrinos in magnetized iron detector is given in Table 1. This can be compared to the sensitivity possible with water Cerenkov detectors, shown for a true normal hierarchy in the right-hand panel of Fig. 3 and Table 1, where octant determination can be done reasonably well even if  $\sin^2 \theta_{13}$ (true) was zero [5]. However, if  $\sin^2 \theta_{13}$ (true) was non-vanishing and reasonably large, the octant sensitivity of this experiments gets significantly boosted through earth matter effects appearing in the multi-GeV electron sample.

### 7. Resolving the Ambiguity in Neutrino Mass Hierarchy

Large earth matter effects in atmospheric neutrinos can be exploited to probe the sign of  $\Delta m_{31}^2$ . Fig. 4 [12] shows the sensitivity to  $sgn(\Delta m_{31}^2)$  expected in a magnetized iron calorimeter, with 4000 observed upward going events. The data corresponds to a normal (solid lines) and inverted (dashed lines) hierarchy and the curves show the  $\chi^2$  and hence the C.L. with which the wrong hierarchy can be ruled out. The red lines correspond to an analysis method where all the oscillation parameters are fixed in the fit. The blue lines show the results of the fit where external priors for the oscillation parameters have been used. The green lines correspond to the case where all oscillation parameters are allowed to vary freely in the fit. The left-hand panel is for muon events in a detector with 15% energy and 15° zenith angle resolution, the middle panel is for muon events with 5% energy and 5° zenith angle resolution, while the right-hand panel is for electron events. For vanishing  $\theta_{13}$  the matter effects vanish giving  $\chi^2 = 0$ . As  $\theta_{13}$  increases, matter effects increase, thereby increasing the sensitivity of the experiment to hierarchy determination. For a INO-ICAL like detector, where energy resolution is expected to be around 15% and zenith angle resolution of about 15°, the wrong hierarchy can be ruled out at  $2\sigma$  using the muon events, if  $\sin^2 2\theta_{13}$ (true)= 0.1 and  $\sin^2 \theta_{23}$ (true)= 0.5, and where the information from the other long baseline experiments on the oscillation parameters have been included through the priors. Comparison of the left-hand with the middle panel shows that the sensitivity to hierarchy increases if the detector resolution is improved. Comparison of the left-hand with the right-hand panel shows that the sensitivity to hierarchy increases if the detector could detect electron type events as well. And of course since matter effects increase with  $\theta_{23}$ , the sensitivity to hierarchy increases as the true value of  $\theta_{23}$  increases.

The  $sgn(\Delta m_{31}^2)$  can be done using the excess in the multi-GeV electron sample due to earth matter effects in water Cerenkov detectors. The wrong hierarchy can be ruled by a 4.6 Megaton-yr data in such an experiment at more than the  $2\sigma$  limit if  $\sin^2 2\theta_{13}$ (true)= 0.1 and  $\sin^2 \theta_{23}$ (true)= 0.5 (see also [8]). This is comparable to the sensitivity of the magnetized iron detectors as discussed above. However, since water detectors use the excess in electron events for multi-GeV neutrinos, which in turn have large matter effects in the  $P_{\mu e}$  channel, they therefore depend also on the CP phase  $\delta_{CP}$  as discussed before. If the value of  $\delta_{CP}$  is allowed to vary freely in the fit then the sensitivity gets affected and decreases appreciably.

### 8. Looking for new physics

There are a variety of new physics scenarios which could manifest themselves as subdominant effects in oscillations of atmospheric neutrinos. Each one of these have a distinctive  $L/E$  behavior, while oscillations go linearly with  $L/E$ . This can be probed directly using the  $L/E$

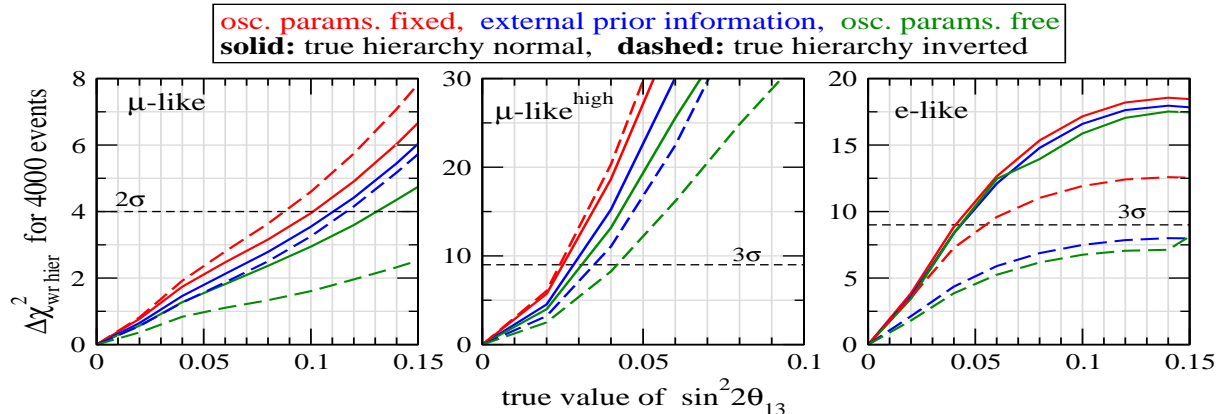


**Figure 4.**  $\Delta\chi^2$  for the wrong hierarchy as a function of  $\sin^2 2\theta_{13}(\text{true})$ . See [12] for details.

binned data in large iron detectors [15] or by comparing the low energy contained events with the high energy upward going muons in large water detectors [16]. Atmospheric neutrino events which constitute a background for the neutrino telescopes such as IceCube, can also be used effectively to constrain new physics. Neutrino telescopes look for neutrinos in the  $(10^{-1} - 10^4)$  TeV range, for which standard oscillations of atmospheric neutrinos are negligible. Hence, any  $E$  or  $L$  dependence in the data would signify new physics. Likewise, the absence of any  $E$  and  $L$  dependence can be used to constrain the new physics parameters [17].

## 9. Conclusions

In this talk we explored the physics potential of future measurements of atmospheric neutrinos. Observation of  $\Delta m_{21}^2$  driven sub-dominant effects and  $\theta_{13}$  driven large matter effects in atmospheric neutrinos can be used to study the deviation of  $\theta_{23}$  from maximality and its octant. Neutrino mass hierarchy can be determined extremely well due to the large matter effects. New physics can be constrained both in standard atmospheric neutrino experiments as well as in future neutrino telescopes.

- [1] Y. Ashie *et al.* [Super-Kamiokande Collaboration], Phys. Rev. D **71**, 112005 (2005).
- [2] Y. Ashie *et al.* [Super-Kamiokande Collaboration], Phys. Rev. Lett. **93**, 101801 (2004).
- [3] M. S. Athar *et al.* [INO Collaboration], *India-based Neutrino Observatory: Project Report*.
- [4] P. Huber *et al.*, Phys. Rev. D **70**, 073014 (2004).
- [5] M. C. Gonzalez-Garcia, M. Maltoni and A. Y. Smirnov, Phys. Rev. D **70**, 093005 (2004).
- [6] O. L. G. Peres and A. Y. Smirnov, Phys. Lett. B **456**, 204 (1999).
- [7] O. L. G. Peres and A. Y. Smirnov, Nucl. Phys. B **680**, 479 (2004).
- [8] P. Huber, M. Maltoni and T. Schwetz, Phys. Rev. D **71**, 053006 (2005).
- [9] G. L. Fogli, E. Lisi, A. Marrone and A. Palazzo, Prog. Part. Nucl. Phys. **57**, 742 (2006).
- [10] S. Choubey and P. Roy, Phys. Rev. D **73**, 013006 (2006).
- [11] J. Bernabeu *et al.*, Nucl. Phys. B **669**, 255 (2003); S. Palomares-Ruiz and S. T. Petcov, Nucl. Phys. B **712**, 392 (2005); D. Indumathi and M. V. N. Murthy, Phys. Rev. D **71**, 013001 (2005); R. Gandhi *et al.*, Phys. Rev. D **73**, 053001 (2006); R. Gandhi *et al.*, arXiv:hep-ph/0506145.
- [12] S. T. Petcov and T. Schwetz, Nucl. Phys. B **740**, 1 (2006).
- [13] S. Antusch, P. Huber, J. Kersten, T. Schwetz and W. Winter, Phys. Rev. D **70**, 097302 (2004).
- [14] J. E. Campagne, M. Maltoni, M. Mezzetto and T. Schwetz, arXiv:hep-ph/0603172.
- [15] A. Datta *et al.*, Phys. Lett. B **597**, 356 (2004).
- [16] M. C. Gonzalez-Garcia and M. Maltoni, Phys. Rev. D **70**, 033010 (2004) and references therein.
- [17] M. C. Gonzalez-Garcia *et al.*, Phys. Rev. D **71**, 093010 (2005); D. Morgan *et al.*, Astropart. Phys. **25**, 311 (2006).

## First physics results from WARP 2.3 litre prototype

P Benetti<sup>1</sup>, R Acciarri<sup>6</sup>, M Belluco<sup>1</sup>, E Calligarich<sup>1</sup>, F Calaprice<sup>4</sup>,  
 M Cambiaghi<sup>1</sup>, F Carbonara<sup>2</sup>, F Cavanna<sup>3</sup>, A G Cocco<sup>2</sup>,  
 F Di Pompeo<sup>3</sup>, N Ferrari<sup>3</sup>, G Fiorillo<sup>2</sup>, C Galbiati<sup>4</sup>, L Grandi<sup>1</sup>,  
 A Ianni<sup>3</sup>, G Mangano<sup>2</sup>, C Montanari<sup>1</sup>, O Palamara<sup>3</sup>, L Pandola<sup>3</sup>,  
 G L Raselli<sup>1</sup>, M Rossella<sup>1</sup>, C Rubbia<sup>1</sup>, A M Szelc<sup>5</sup> and C Vignoli<sup>1</sup>

<sup>1</sup> Dipartimento di Fisica Nucleare e Teorica, INFN e Università di Pavia, Via A. Bassi 6, I-27100, Pavia, Italy

<sup>2</sup> Dipartimento di Scienze Fisiche, INFN e Università Federico II, Via Cinthia, I-80126, Napoli, Italy

<sup>3</sup> Laboratori Nazionali del Gran Sasso dell'INFN, S.S. 17 bis km 18.910, I-67010, Assergi (AQ), Italy

<sup>4</sup> Department of Physics, Princeton University, Princeton, New Jersey 08544, USA

<sup>5</sup> Instytut Fizyki Jadrowej PAN, ul. Radzikowskiego 152, 31-342, Krakow, Poland

<sup>6</sup> Dipartimento di Fisica, INFN e Università dell'Aquila, v. Vetoio loc. Coppito, I-67010, L'Aquila, Italy

*Presented by Alfredo G. Cocco*

### Abstract.

A method to measure the low energy nuclear recoils induced by weakly interactive massive particles (WIMPs) has been achieved by means of an ultra pure Liquid Argon detector. The simultaneous observation of scintillation and ionization occurring in the liquid Argon allow to obtain a very high rejection power against background sources. The first preliminary upper bounds on WIMP parameters obtained with a small 2.3 liter test chamber with an accumulated fiducial exposure of about 100 kg·day at the Gran Sasso Underground Laboratory is reported. This supports the validity of this method for a larger detector presently under construction with correspondingly increased sensitivities.

### 1. Introduction

Latest experimental results on cosmic microwave background [1], supernova [2] and gravitational weak lensing studies have strengthened the evidence of a large ( $\Omega_{nb} \approx 0.23$ ) non-baryonic dark matter component of the Universe [3]. The candidate to solve this dark matter puzzle are the so-called Weakly Interacting Massive Particles (WIMPs); these particles could provide the required present cosmological abundance and, at the same time, justify the observed galactic structures formation [4]. The role of WIMPs could be played by the lightest particles present in most of the supersymmetric models (neutralinos). These models, together with cosmological constraints, predict a wide range of possible masses and cross sections, which may become accessible to direct detection experiments. Up to now, the best sensitivities have been obtained by detectors operating at very low temperatures [5, 6, 7] and no evidence has been found for a WIMP-like signal. We will show here that the detection method based on the use of liquid Argon is suitable to increase the present sensitivity by orders of magnitude.

## 2. Experimental setup

The 2.3 litre detector is a two-phase drift chamber with a lower liquid Argon volume and an upper region with Argon in the gaseous phase, both viewed by the same set of photo-multipliers (PMTs). A detailed description of the experimental setup can be found in [8]. Ionization electrons generated in the liquid are drifted toward the liquid-gas interface, extracted by means of an electric field, and detected by the proportional scintillation light generated in a high electric field. The drift volume, 7.5 cm long, is delimited by a 20 cm diameter stainless steel cathode and by a system of field-shaping electrodes that generate very uniform electric drift fields (1 kV/cm). A system of three grids provides both extraction of the drifting electrons from the liquid to the gas and their acceleration in the gas phase to generate a secondary proportional scintillation light. Residual concentration of electronegative impurities of the Argon is kept at a level of  $\lesssim 1$  ppb ( $O_2$  equiv.), achieving a free electron mean free path well in excess of 0.5 m. In order to shield the detector from  $\gamma$ -rays and fast neutrons coming from the outside the detector is completely surrounded by 10 cm thick Lead walls and by a polyethylene shield with a thickness of 60 cm. Seven 12-stage 2" PMTs are placed about 4 cm above the last grid and detect both the primary and the proportional scintillation light. A wavelength-shifter (Tetra-Phenyl-Butadiene) is used to convert the 128 nm wavelength Argon scintillation light to the photo-multiplier sensitive region (q.e. of about 18%). The signal from the anode of each photo-multiplier is integrated through a charge preamplifier (40  $\mu$ s time shaping constant) and then sent to a 10 bit flash ADC with 20 MHz sampling frequency.

## 3. Data taking and calibration

We report data collected with  $2.8 \times 10^7$  triggers, in a total live time of 52.76 days. The sensitive volume of the chamber is 1.87 liters (2.57 kg) and the fiducial volume is of 1.32 liters (1.82 kg). This corresponds to a total exposure of 96.5 kg·day. The trigger is generated by at least three PMTs being above a threshold of 1.5 photoelectrons, which corresponds to about 2.5 keV<sub>ion</sub> (ion recoil energy). The trigger efficiency is estimated to be close to unity above 20 photoelectrons (about 12 keV<sub>ion</sub>). The resulting trigger rate is of the order of 6 counts/s.

We select events consisting of both a primary light pulse (S1), from the collection of the direct scintillation light, and one or more secondary light pulses (S2) from the proportional light produced by the ionization electrons after extraction from the liquid into the gas phase. The time between the primary pulse (S1) and the secondary pulse (S2) is related to the drift time  $T_{drift}$  of the electrons traveling across the liquid ( $z$ -coordinate). Given the dimensions of the chamber and the applied electric fields,  $T_{drift} \lesssim 40$   $\mu$ s.

### 3.1. Light yield

Primary (S1) signals were studied in a dedicated calibration run with a weak Am-Be neutron source inserted near the inner detector, inside the shield. The observed S1 distribution for Argon recoils is well reproduced by MonteCarlo assuming a constant light yield of  $Y_{Ar} = (1.65 \pm 0.25)$  phe/keV. The error is mainly due to uncertainties in the evaluation of the Monte Carlo simulated neutron flux induced in the chamber.

Nuclear recoils of Radon daughters from the cathode are due to traces of  $^{222}\text{Rn}$  present in the liquid Argon at the time of filling and decaying with a half-life of 3.8 days. Alpha particles are emitted in a chain by the initial  $^{222}\text{Rn}$  decay (5.5 MeV) and by the subsequent  $^{218}\text{Po}$  decay (6.0 MeV) and  $^{214}\text{Po}$  decay (7.7 MeV). The last two decays occur mainly at the bottom of the detector producing a visible ion recoil when the corresponding  $\alpha$  particle is emitted toward the cathode. In the case of  $^{214}\text{Po}$  (110 keV recoil) and  $^{210}\text{Po}$  (144 keV recoil) a preliminary result of  $Y_{Po} = 1.70 \pm 0.03$  phe/keV (statistical error only) is found, the analysis being still in progress.

During the early running the large shield around the detector was not yet installed and a significant rate of neutron events was observed. In spite of the small statistics, the S1 distribution

is in good agreement with the Monte Carlo simulation of neutron flux from the rock [9] for  $Y_{Ar} = (1.6 \pm 0.4)$  phe/keV.

### 3.2. Background rejection criteria

The main luminescence signal from high density noble liquid scintillation excited by charged particles is attributed to low excited molecular states ( $^1\Sigma_u^+$  and  $^3\Sigma_u^+$ ) to the ground state [10, 11]. The primary signal (S1) is consequently characterized by the presence of two components with very different time constants [12]:  $\tau_{singlet} = 7.0 \pm 1.0$  ns and  $\tau_{triplet} = 1.6 \pm 0.1$   $\mu$ s respectively for  $^1\Sigma_u^+$  and  $^3\Sigma_u^+$ . The scintillation light intensity ratio  $I_{singlet}/I_{triplet}$  are found to be 0.3, 1.3 and 3 for electrons,  $\alpha$ -particles and fission fragments excitation, respectively [12]. We introduce the pulse shape discrimination parameter  $F = I_{singlet}/(I_{singlet} + I_{triplet})$ . The parameter  $F$  is found to be centered on  $F = 0.31$  for electrons and on  $F = 0.75$  for Argon from neutron recoils, both with nearly Gaussian distributions. The observed value of  $F$  for electrons corresponds to  $I_{singlet}/I_{triplet} \approx 0.44$  while that for nuclear recoils to  $I_{singlet}/I_{triplet} \approx 3$ . In order to achieve a meaningful separation the number of collected photoelectrons must be adequate: S1 signals with more than 50 phe (about 30 keV<sub>ion</sub>) have been considered in the analysis.

Another criteria for background rejection is based on the ratio S2/S1. This ratio depends on the values of the electric fields and is typically of the order of 180 for minimum ionizing particles, 3 for  $\alpha$ -particles, and 10 for Ar-recoils. The experimental observation of neutron induced Argon recoils (20  $\div$  150 keV<sub>ion</sub>) shows that the S2/S1 ratio is much larger than in the case of  $\alpha$ -particles and that the S2/S1 ratio is inversely proportional to the recoil energy. For very low energies neutron induced events S2/S1 is roughly proportional to 1/E, being described in a first approximation by a function of the form:  $S2/S1 = a + b/E(\text{keV})$  where  $a = 2.1$  and  $b = 510$  keV<sub>ion</sub>.

The two mentioned criteria, namely the shape in time of the primary signal S1 and the comparison of the primary to the secondary signal coming from the gas S2/S1, employed simultaneously achieve a powerful background rejection power in all cases of interest.

## 4. Results

We shall make in the following the assumption that weakly interacting WIMP events produce the same signal pattern as observed for the neutron-induced recoils. Therefore the efficiency of the selection cuts for WIMP candidate events is assumed to be equal to that from the neutron calibration data (for energies above 40 keV<sub>ion</sub> it is of the order of 90%). The cuts defined to select elastic scattering on Argon due to WIMP interactions are: single-hit event in the relevant energy domain,  $10 \mu\text{s} \leq T_{drift} \leq 35 \mu\text{s}$ ,  $0.68 \leq F \leq 0.87$ , S2/S1 contained in the single recoil selection band (energy dependent) and visual scanning to reject mis-reconstructed or noisy events. The importance of using both discrimination techniques is illustrated in Figure 1: the low energy window (30  $\div$  50 keV) sample collected during the WIMP exposure of 96.5 kg-day shows 5 events in the region previously selected with the Am-Be calibration. In the region 42  $\div$  100 keV<sub>ion</sub> no candidate events are present.

Following the prescription of Ref. [13] the 90% C.L. upper limit has been derived from the observation of zero events in the energy region above 42 keV<sub>ion</sub>. It is shown in Figure 2 where the estimated WIMP-nucleon spin-independent cross section in cm<sup>2</sup> vs. an hypothetical WIMP mass in GeV/c<sup>2</sup> is also compared with the results coming from the mentioned cryogenic detectors. A slightly lower limit is also presented for the case of 30 keV<sub>ion</sub> threshold, under the (optimistic) assumption that the observed events are due to background. The dominant systematic effect is given by the uncertainty on the nuclear recoil light yield. Considering an error of 15% on the light yield, the variation on the limit is of the order of 20% for 100 GeV/c<sup>2</sup> WIMP mass, reaching 30% for 50 GeV/c<sup>2</sup>.

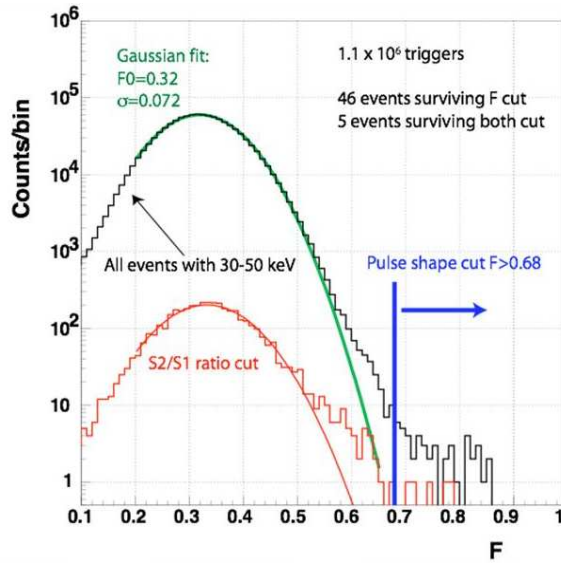


**Figure 1.** Effect of the cuts on  $F$  and  $S2/S1$  on the sample of reconstructed events in the energy region 30-50 keV. The 5 residual events have energy less than 42 keV.

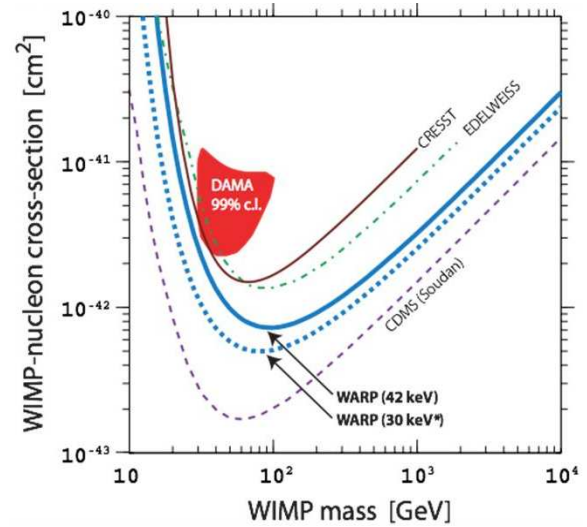


**Figure 2.** Evaluated upper limit on spin-independent WIMP–nucleon cross section as a function of the WIMP mass, as explained in the text.

## 5. Conclusions

The main achievements of the 2.3 litre WARP prototype detector have been: (1) perfecting the sensitivity of liquid Argon ensuring a sufficient luminescence for Argon recoils in the energies of interest and (2) demonstrating the validity of the techniques that will be used in the future. In particular we find that in actual underground conditions both discrimination methods, namely the pulse shape discrimination parameter  $F$  and the ratio  $S2/S1$  between the delayed electrons signal extracted from the liquid to the gas and the initial luminescence, are absolutely necessary in order to ensure a sufficient robustness to the identification of a possible WIMP signal.

## References

- [1] P de Berbaradis et al., *Astrophys. J.* **564** (2002) 559; C L Bennett et al., *Astrophys. J.* **583** (2003) 1
- [2] A G Riess et al., *Astron. J.* **116** (1998) 1009; S Perlmutter et al., *Astrophys. J.* **517** (1999) 565
- [3] A Morales, *Nucl. Phys. B (Proc. Suppl.)* **114** (2003) 39; M Roos, arXiv.org:astro-ph/0509089
- [4] M Srednicki and N. I. C. Spooner, *Phys. Rev. D* **66** (2002) 173
- [5] D S Akerib et al., *Phys. Rev. Lett.* **96** (2006) 011302
- [6] V Sanglard et al., *Phys. Rev. D* **71** (2005) 122002
- [7] Angloher et al., *Astropart. Phys.* **23** (2005) 325
- [8] P Benetti et al., WARP Coll., in preparation
- [9] H Wulandari et al., *Astrop. Phys.* **22** (2004) 313
- [10] S Kubota et al., *Phys. Rev. B* **20** (1979) 3486; S Kubota et al., *Phys. Rev. B* **17** (1978) 2762
- [11] T Doke et al., *Nucl. Instr. and Meth. A* **291** (1990) 617
- [12] A Hitachi et al., *Phys. Rev. B* **27** (1983) 5479 and references therein
- [13] J D Lewin and P F Smith, *Astropart. Phys.* **6** (1996) 87

## Reactor monitoring with Neutrinos

**Michel Cribier**

Astroparticule & Cosmologie  
10, rue Alice Domon et Léonie Duquet  
F-75205 Paris Cedex 13  
France

mcribier@cea.fr

**Abstract.** The fundamental knowledge on neutrinos acquired in the recent years open the possibility of applied neutrino physics. Among it the automatic and non intrusive monitoring of nuclear reactor by its antineutrino signal could be very valuable to IAEA in charge of the control of nuclear power plants. Several efforts worldwide have already started.

### 1. IAEA interest

The International Atomic Energy Agency (IAEA) is the United Nations agency in charge of the development of peaceful use of atomic energy. In particular IAEA is the verification authority of the Treaty on the Nonproliferation of Nuclear Weapons (NPT). To do that jobs inspections of civil nuclear installations and related facilities under safeguards agreements are made in more than 140 states. IAEA uses many different tools for these verifications, like neutron monitor, gamma spectroscopy, but also book keeping of the fuel element composition before and after their use in the nuclear power station. In particular it verify that weapon-origin and other fissile materials that Russia and USA have released from their defence programmes are used for civil application.

Looking for innovative methods, the IAEA ask members states to make a feasibility study to determine whether antineutrino detection methods might provide practical safeguards tools for selected applications. If this method proves to be useful, IAEA has the power to decide that any new nuclear power plants built has to include an antineutrino monitor.

### 2. Physic basis

In a new reactor with normal water the initial fuel consist of enriched uranium rods, with an  $^{235}\text{U}$  content typically at 3.5%, the rest is  $^{238}\text{U}$ . As soon as the reactor is operating, reactions of neutron capture on  $^{238}\text{U}$  produce  $^{239}\text{Pu}$  (and  $^{241}\text{Pu}$ ), which then contribute also to the energy production. Nevertheless the net balance in plutonium is positive and a standard pressurized water power reactor produces around 200 kg of plutonium per year.

Every fission of a fissile isotope produce two fissions fragments of unequal masses. The distribution of the lightest fragment is centred around  $A = 94$  for fission of  $^{235}\text{U}$ , and centred around  $A = 102$  in the case of  $^{239}\text{Pu}$ . All these nuclei, too rich in neutrons, are extremely unstable and thus beta decay toward stable nuclei with an average of 6  $\beta$  decays and thus with 6 antineutrinos. In these processes several hundreds of unstable nuclei, with their excited states are involved, which makes very difficult to understand details of the physics; moreover, the most energetic antineutrinos, which are detected more easily by the neutrinos detectors, are produced in the very first decays, involving nuclei with typical lifetime much smaller than a second.

	<sup>235</sup> U	<sup>239</sup> Pu
released energy per fission	201.7 MeV	210.0 MeV
Mean energy of $\nu$	2.94 MeV	2.84 MeV
$\nu$ per fission > 1.8 MeV	1.92	1.45
average inter. cross section	$\approx 3.2 \cdot 10^{-43} \text{ cm}^2$	$\approx 2.76 \cdot 10^{-43} \text{ cm}^2$

Table. Main characteristics of antineutrinos originating from <sup>235</sup>U and <sup>239</sup>Pu fission

Nevertheless based on predicted and observed  $\beta$  spectra, the number of antineutrinos per fission from <sup>239</sup>Pu is known to be less than the number from <sup>235</sup>U, and the energy released bigger by 5%. Hence an hypothetical reactor able to use only <sup>235</sup>U would induce in a detector an antineutrino signal 60% higher than the same reactor producing the same amount of energy but burning only <sup>239</sup>Pu (see table 1). This sizeable difference offer a handle to monitor changes in the relative amounts of <sup>235</sup>U and <sup>239</sup>Pu in the core. Merged with the high penetration power of antineutrinos, this provide a new mean to make remote, nonintrusive measurements of plutonium content in reactors [1].

In most of the presently considered detectors, antineutrinos are detected via the inverse beta decay process on quasi-free protons in hydrogenous scintilla tor:  $\bar{\nu}_e + p \rightarrow e^+ + n \square \nu_e$ , with a threshold at 1.8 MeV. The positron and the neutron are detected in a delayed coincidence, allowing strong rejection of the much more frequent singles backgrounds due to natural radioactivity.

Because the antineutrino signal from the reactor decreases as the square of the distance from the reactor to the detector a precise "remote" measurement is really only practical at distances of a few tens of meters if one is constrained to "small" detectors of the order of few cubic meter in size.

### 3. Pioneers in Kurchatov

The potentiality to address certain safeguards applications was recognized long time ago by Mikaelian et al. [2]. The correlation of the antineutrino signal with the thermal power and the burn-up was demonstrated by the Bugey [3] and Rovno experiments [4]. What makes this old idea possible today is our present understanding of the oscillation mechanism which guarantee that the signal recorded by a neutrino detector at less than 200 meters from a reactor is not significantly affected, or could be corrected for. In this respect the results of KamLAND detector [5] as a global monitor of remote ( $\approx 180 \text{ km}$ ) power plants is impressive.

### 4. Efforts in the USA

The experimental program for development of nonproliferation detectors in the United States is led by Lawrence Livermore National Laboratory and Sandia National Laboratories. The LLNL/SNL work has consisted of installing and operating a prototype detector at the 3.46 GWth San Onofre Nuclear Generating Station (SONGS) in Southern California. The detector [6], now operating at SONGS at a distance of 24.5 meters from the core in the tendon gallery (fig. 1a), and with an overburden of about 25 m.w.e., is shown in figure 1b. The shielding consists of a muon veto system for rejecting cosmic ray backgrounds, a water/polyethylene shield to reject neutron and gamma backgrounds. The central detector, which registers antineutrino interactions, has a one cubic meter active liquid scintillator doped with gadolinium ( $0.64 \pm 0.06 \text{ ton}$ ), seen by eight 9" PMTs. The overall footprint including shielding is 2.5 meter  $\times$  3 meter.

In this condition the rate predicted at the beginning of the reactor fuel cycle is approximately  $3800 \pm 440$  antineutrino interactions per day for a perfectly efficient detector. The overall efficiency to detect antineutrino interaction via positron neutron delayed coincidence is 10.7% with a signal to background close to 4. The number of antineutrino events observed,  $459 \pm 16/\text{day}$  is in good agreement with the expected rate deduced from simulation.

Changes in reactor power can quickly (within a few hours) be detected by tracking the antineutrino rate. The plot of daily rate versus time (Figure 2) also shows a two sigma deviation of the antineutrino rate from a constant value over a six month period, with the linear reduction in total rate consistent with a prediction that includes a fuel burn up estimate. Current effort is focused on confirming the

indications of fuel burn up seen in this data. Already these results, although modest for neutrino specialists, are convincing enough for external viewers which correlate usually a neutrino detector with a huge apparatus.

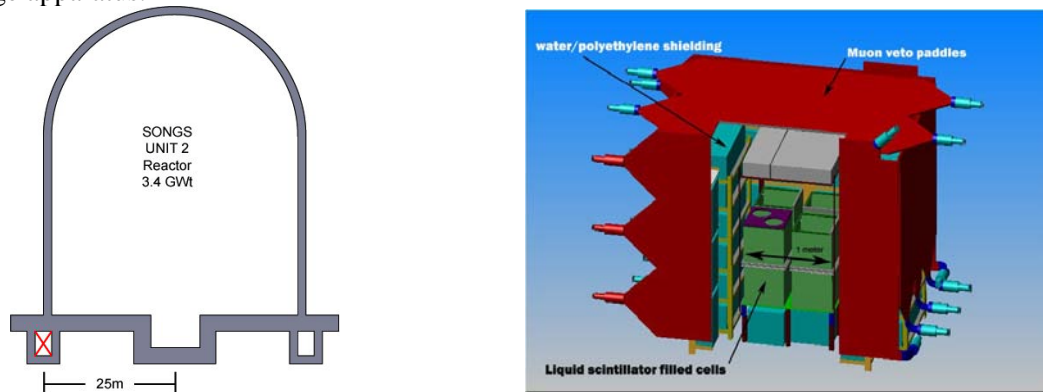


Figure 1. The SONGS detector (right) located in the tendon gallery (left)

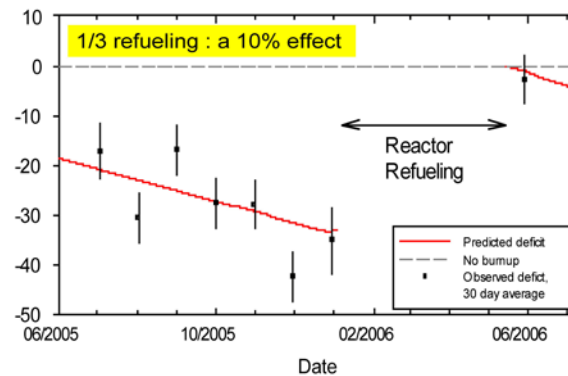


Figure 2. The impact of the refueling is clearly seen on the antineutrino record

## 5. Efforts in France

The Double Chooz collaboration, an experiment [7] mainly devoted to study the fundamental properties of neutrinos, is also in a good position to evaluate the interest of using antineutrino detection to remotely monitor nuclear power station. Indeed, without any extra experimental effort, the near detector of the Double Chooz experiment will provide the most important data set of antineutrino detected ( $5 \times 10^5$   $\nu$  per year). The precise energy spectrum recorded at a given time will be correlated to the fuel composition and to the thermal power provided by EDF; it is expected that individual component due to fissile element ( $^{235}\text{U}$ ,  $^{239}\text{Pu}$ ) could be extracted with some modest precision and serve as a benchmark of this techniques.

### 5.1. Toward a better understanding of the antineutrino spectrum

The IAEA recommends the study of specific safeguards scenarios. Among its concerns are the confirmation of the absence of unrecorded production of fissile material in declared reactors and the monitoring of the burn-up of a reactor core. The time required to manufacture an actual weapon estimated by the IAEA (conversion time), for plutonium in partially irradiated or spent fuel, lies between 1 and 3 months. The significant quantity of plutonium is 8 kg, to be compared with the 3 tons of  $^{235}\text{U}$  contained in a Pressurized Water Reactor (PWR) of power 900MWe enriched to 3%. The small magnitude of the expected signal requires a careful feasibility study.

The proliferation scenarios of interest involve different kinds of nuclear power plants such as light water or heavy water reactors (PWR, BWR, Candu...), it has to include isotope production reactors of

a few tens of MWth, and future reactors (e.g., PBMRs, Gen IV reactors, accelerator-driven sub-critical assemblies for transmutation, molten salt reactors). To perform these studies, core simulations with dedicated Monte-Carlo codes are being developed in France. The particle transport code MCNPX coupled with an evolution code solving the Bateman equations for the fission products are combined within a package called MURE (MCNP Utility for Reactor Evolution) [8]. It computes accurately the amount of all  $\beta$ -emitters produced during the operation of a nuclear power plant.

To fulfil the goal of nonproliferation, additional laboratory tests and theoretical calculations should also be performed to more precisely estimate the underlying neutrino spectra of plutonium and uranium fission products, especially at high energies. As concluded by P. Huber and Th. Schwetz [9] to achieve this goal a reduction of the present errors on the antineutrino fluxes of about a factor of three is necessary. This is the basis to the important effort to better understand the antineutrino spectrum. More details can be found in S. Cormon contribution [10].

A careful evaluation and propagation of all sources of error is under study in french groups. When building the total spectra, experimental data on the energy and spin and parity of all known nuclear levels are used to determine the shape and error of individual  $\beta$ -branches. In the case of nonunique forbidden  $\beta$  transition, different levels of approximation are used to parameterize the spectrum shape. When computing the amount of  $\beta$ -emitters present in the reactor core at a given time, the effect of the uncertainty on fission yields can be estimated numerically via a limited number of MURE simulations.

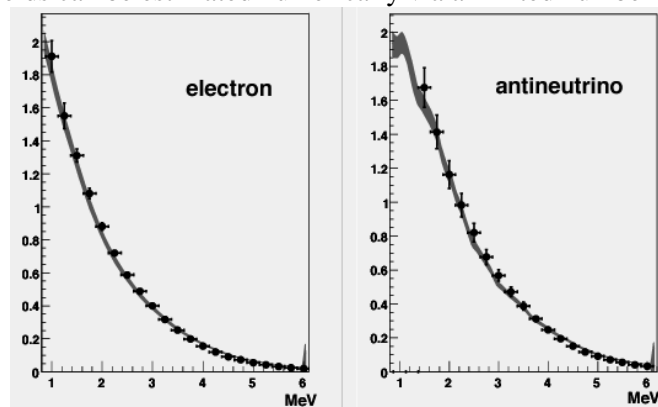


Figure 3. Comparison (Preliminary) with the simulation (shaded area) and Schreckenbach's data [11] for electrons and antineutrino

Thanks to the description of each single  $\beta$ -branch, no extra error is involved when converting the electron total spectrum to an antineutrino spectrum. Once a final error is quoted in each 100 keV bin, this method will allow quantifying for the first time the sensitivity of the neutrino probe to the isotopic composition of the reactor core, that is what minimum change of the  $^{235}\text{U}/^{239}\text{Pu}$  ratio is detectable. Uncertainties in the normalization and the large amount of common nuclei in the  $^{235}\text{U}$  and  $^{239}\text{Pu}$  decay chains induce large error correlations, which, if treated properly, will increase the sensitivity of the neutrino probe when comparing two spectra.

This promising study will also provide the error budget for an independent measurement of the total nuclear power released by the core. In the low energy part of the spectrum ( $<4$  MeV) one expects the final accuracy to be high enough to provide useful constraints on the total spectrum shape for the neutrino oscillation analysis. At higher energy these simulations can tag few critical poorly known isotopes and trigger an experimental program in order to complete the existing databases.

Finally, the computed energy spectrum of antineutrino can be coupled to a detailed GEANT4 simulation of the Double-Chooz detector or of a small prototype antineutrino detector.

## 6. Toward a prototype of neutrino monitor

If we want to propose to the IAEA a neutrino detector able to help in monitoring future nuclear power plants, the next step in this effort has to merge the two present experimental approaches: the Double

Chooz approach with a good energy measurement, a good signal to noise ratio, but expensive and sophisticated; and the SONGS approach with a robust, simple, automatic, cheap, but with poor antineutrino detection efficiency, a modest signal to background ratio, and poor energy resolution. We thus are considering a new prototype with a size small enough to be installed very close to the reactor core (30 meters or so), but using a technique able to clearly sign antineutrinos. Such a prototype will be considered as a demonstrator to be shown to the IAEA and at the same time it is already usable tool to measure the thermal power.

As an intermediate goal, we can foresee measurements with this prototype at ILL with its core of roughly pure  $^{235}\text{U}$ . It would allow the recording of a very pure neutrino signal from  $^{235}\text{U}$  fission only followed by the evolution due to burn-up. Such a clean experiment would help to calibrate the neutrino signal versus the thermal power, and will also give some confidence for the simulation effort.

A Brazilian team is currently developing an antineutrino detector to be installed in the close vicinity of a new power plant in Angra [12]. This detector will be used to monitor the reactor activity, and to provide an additional tool on verification of safeguards on Nonproliferation. The planned turnon dates are 2008 for the very near detector and 2013 for the Angra complete configuration.

### 7. Distant monitoring

Neutrinos travels long distance through dense materials without being stopped. Hence it forbids to totally hide some nuclear activities involving fission like a clandestine nuclear power or nuclear test. Moreover, in the case of a test, the unique signature given by the antineutrino interaction, in coincidence with other methods like seismic waves, transform an hint into a proof.

Based on this principal several groups around the world propose network of huge detectors able to detect, locate and measure the power of nuclear reactors and of bombs test. In the mean time a more modest neutrino detector used in coincidence with the standard seismic network could sign unambiguously the real nature of a kton test. This aspect of the use of antineutrinos was covered in the previous proceeding of Neutrino 04 [13] and was the subject of a dedicated workshop [14]. In this approach HanoHano is a good example of such detector [15].

### 8. Neutrinos for Peace

All the applications of our knowledge of neutrinos seems surprising for physicists which, for many years, consider this particle as the most elusive one. It is remarkable that so quickly a very fundamental research could turn into applications: it is even more enjoyable that the first applications envisaged for this unusual particle is the control of arm races and not a new weapon. For all these reasons, I would gladly propose to name these worldwide efforts: Neutrinos for Peace.

### References.

- [1] A. Bernstein, et. al., J. Appl. Phys. 91 (2002) 4672
- [2] Mikaelian L.A., Proc. Int. Conference Neutrino-77, v. 2, p. 383-387
- [3] Y. Declais et al., Nucl. Phys. B434 (1995) 503
- [4] Yu. V. Klimov, et. al., Atomic Energy, 76 (1994) 123
- [5] K. Eguchi et al., KamLAND Collab., Phys. Rev. Lett. 90 (2003) 021802
- [6] N.S. Bowden et al., ArXiv:physics/0612152
- [7] F. Ardellier et al., ArXiv:hep-ex/0606025
- [8] Mal'plan O. et al. In Proceedings of the ENC 2005 (CD-Rom) (2005) 1-7.
- [9] P. Huber, Th. Schwetz, Phys.Rev. D70 (2004) 053011
- [10] S. Cormon et al., *these Proceedings*
- [11] K. Schreckenbach et al., Phys. Lett. B160 (1985) 325
- [12] J.C. Anjos et al., Nucl.Phys.Proc.Suppl.155:231-232,2006. ; ArXiv: hep-ex/0511059
- [13] J.C. Learned, Nucl. Phys. B (Proc. Suppl.) 143 (2005) 152-156
- [14] Neutrino Science 2005, <http://www.phys.hawaii.edu/~sdye/hnsc.html>
- [15] S. Dye, ArXiv:hep-ex/0611039

## MUNU final results

Zornitza Daraktchieva<sup>1</sup>

Institute de Physique, A.-L. Breguet 1, CH-2000 Neuchâtel, Switzerland

E-mail : Zornitza.Daraktchieva@unine.ch

**Abstract.** The MUNU detector has been designed to study  $\bar{\nu}_e e^-$  elastic scattering at low energy. The central tracking detector is a 1 m<sup>3</sup> Time Projection Chamber surrounded by an anti-Compton detector. In this paper the results from final analysis of the data recorded at 3-bar and 1-bar pressure are presented. At 3-bar a new upper limit on the neutrino magnetic moment  $\mu_\nu < 9 \times 10^{11} (7 \times 10^{11}) \mu_B$  at 90 (68%) C.L. is derived. At 1-bar pressure electron tracks down to 80 keV are measured in the TPC. A <sup>137</sup>Cs photopeak is reconstructed by measuring both the energy and direction of the Compton electrons in the TPC.

### 1. MUNU experiment

Technical details of the MUNU detector have already been presented in references [1, 2]. Here are given only the essentials. Briefly the detector is located at 18 m from the core of a 2.75 GW reactor in Bugey serving as an antineutrino source. The lab has overburden of steel, concrete and water corresponding to 20 meter of water. The central part of the detector is a cylindrical Time Projection Chamber (TPC). As shown in figure 1 the acrylic vessel TPC, 90 cm diameter and 160 cm long contains 11.4 (3.8 kg) of CF<sub>4</sub> gas at 3 (1) bar pressure. The gas was chosen because of its high density, low Z, which leads to less multiple scattering and its absence of free protons, which excludes the background from the inverse beta decay. The drift volume of the TPC acts at the same time as a target for the neutrinos and as a detector for the recoiling electrons. An anode plane with 20 μm wires and pitch of 4.95 mm is used to amplify the ionization charge. The integrated anode signal gives the total deposited energy. An *x* - *y* plane behind the anode plane provides the spatial information of the tracks in the *x* and *y* directions. The third projection *z* is obtained from the time evolution of the signal. The acrylic vessel is immersed in a steel tank (2 m diameter and 3.8 m long), filled with 10 m<sup>3</sup> of liquid scintillator (NE235) and viewed by 48 photomultipliers (PMT). The liquid scintillator acts as an anti-Compton detector and as a veto against the cosmic muons with an efficiency of 98 %. In addition, the detector is shielded against local activities by 8 cm of boron loaded polyethylene and 15 cm of Pb.

In [3] we presented an analysis of the data taken at a pressure of 3-bar, amounting to 66.6 days reactor-on and 16.7 days reactor-off. Here is presented the final analysis of 3-bar data, which takes better advantage of the electron kinematics. Also an analysis of 5.3 days of reactor-on data taken at 1-bar pressure is given.

<sup>1</sup> On behalf of the MUNU collaboration (LPSC Grenoble, INFN Padova, Institute de Physique Neuchâtel and Physik Institut Zurich)

We define a neutrino candidate as a single electron fully contained in a 42 cm fiducial radius with no energy deposited above 90 keV in the anti-Compton detector. The initial direction of the electrons is obtained by a visual fit [3]. From this fit the angles  $\theta_{det}$ ,  $\theta_{reac}$  and  $\varphi_{det}$  are determined in the  $x-z$  and  $y-z$  projections. Here  $\theta_{det}$  is the angle with respect to the detector axis,  $\theta_{reac}$  is the scattering angle with respect to the reactor-detector axis and  $\varphi_{det}$  is the angle between the projection of the initial track direction on the  $x-y$  plane and the vertical  $y$  axis (see figure 2). The background from the activities on the readout plane side of the TPC is suppressed by applying the angular cut  $\theta_{det} < 90^\circ$  [3].

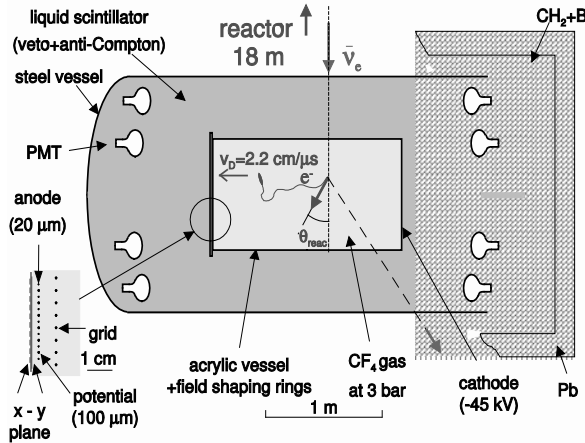


Figure 1. The MUNU detector

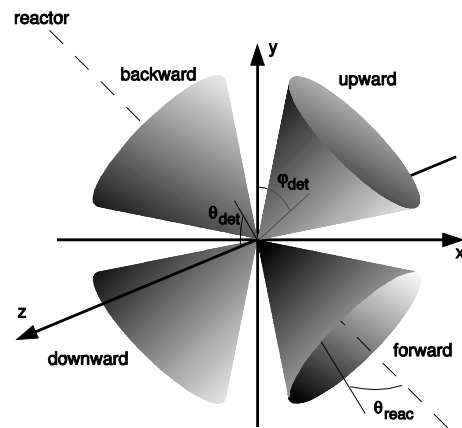


Figure 2. The four kinematical cones

## 2. Results from 3-bar forward-normalized background analysis

At 3-bar we select electron events with kinetic energies  $T_e > 700$  keV. For each electron track the neutrino energy  $E_\nu$  is reconstructed from the scattering angle  $\theta_{reac}$  and measured electron recoil energy  $T_e$ . The selected events with  $E_\nu > 0$  and beginning of the track within a forward cone are the forward electrons (figure 2). The axis of the forward cone coincides with the reactor-detector axis. In the same way the electrons in the three background cones: backward, upward and downward are selected to estimate the background. The backward cone is defined as opposite to the forward cone while upward and downward cones are perpendicular. To avoid overlap of the cones, which can occur for  $T_e < 2m_e c^2$ , we require in addition that the angle  $\varphi_{det}$  is within less than  $\pm 45^\circ$  of the cone axis.

The forward electrons are signal plus background events. The backward, upward and downward electrons are all background events. The background rates in the backward, upward and downward cones are normalised by dividing by 3 to the rate in the forward cone. This normalized background (NB) is then directly compared with the event rate in the forward cone [4].

The energy distributions of both forward ( $455 \pm 21$ ) and NB ( $384 \pm 11$ ) electrons are given in figure 3. There is a clear excess of the events in forward direction from  $\bar{\nu}_e e^-$  scattering. The total forward minus NB above 700 keV is  $71 \pm 23$  counts for 66.6 days live time reactor-on. We make the same analysis with the data taken during the reactor-off period as a cross check (16.7 days live time). The energy distributions of both forward ( $133 \pm 11$ ) and NB electrons ( $147 \pm 7$ ) are given in figure 4. The integrated forward minus NB rate above 700 keV is  $-0.8 \pm 0.8$  counts per day (cpd), consistent with zero.

Now we estimate the expected rate from weak interactions. The Monte Carlo simulations (GEANT 3) are used for calculation of various acceptances of the electron selection procedure [3]. The detector containment efficiency in the 42 cm fiducial radius was found to vary from 63 % at 700 keV, 50 % at 1 MeV to 12 % at 2 MeV, with an error of 2 %.

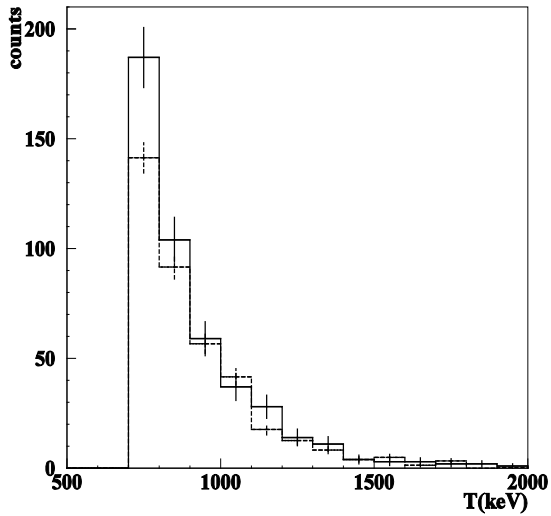


**Figure 3.** Forward (solid line) and NB (dashed line) electrons, 3 bar, reactor on

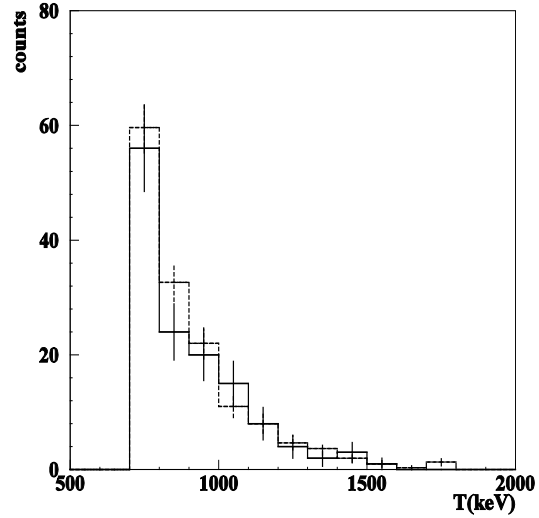


**Figure 4.** Forward (solid line) and NB (dashed line) electrons, 3 bar, reactor off

The reactor neutrino spectrum was calculated using the procedure described in [3, 6]. The uncertainties in the neutrino spectrum are 5 % above 900 keV and 20 % below that. The errors on the global acceptance, including track reconstruction efficiency (4 %), are of order of 7 %. The expected event rate above 700 keV is found to be  $1.02 \pm 0.1$  cpd, in good agreement with the measured one  $1.05 \pm 0.36$  (cpd).

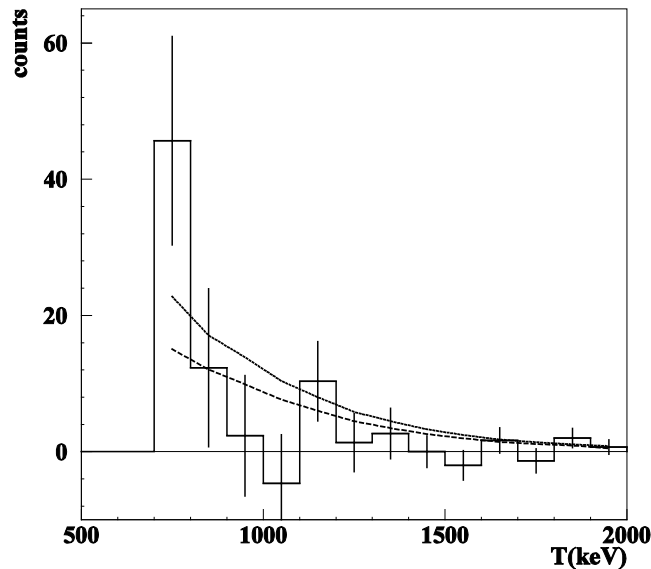


**Figure 5.** Energy distribution of forward minus NB electrons, 3 bar, reactor on (solid line), expected spectrum from weak interactions alone (dashed line) and estimated for a magnetic moment of  $9 \times 10^{-11} \mu_B$  (dotted line).

Both the measured and expected rates are displayed in figure 5. The large excess of events in the first two bins (700 – 900 keV) observed in our previous analysis has to a large extent disappeared. It

is thus most likely due to a statistical fluctuation in the background, more precisely determined in the present analysis.  $\chi^2$  method was used as in [3], with the same binning to compare the measured and expected spectra. The minimum  $\chi^2$  is 11.5 for 7 degrees of freedom for a squared magnetic moment  $\mu^2 = -0.72 \times 10^{20} \mu_B^2$ . We find in 90 % confidence interval  $\mu^2 = (-0.72 \pm 1.25) \times 10^{20} \mu_B^2$ . This result is compatible with the weak interaction alone, and there is no indication of a magnetic moment. To estimate the limit on the magnetic moment we renormalize the result to the physical region ( $\mu^2 > 0$ ) and obtain the limit  $\mu_\nu < 9(7) \times 10^{11} \mu_B$  at 90 (68) % C.L.

### 3. 1-bar analysis

#### 3.1. Results from 1 bar forward – normal background analysis

During the 1-bar data taking period the threshold on the electron recoil was lowered to 100 keV. Events in the TPC which are not in coincidence with a gamma above 90 keV in the scintillator in an 80  $\mu$ s time window are accepted. The neutrino trigger rate is 0.4 Hz with 50 % deadtime, mostly due to the data read-out and data transfer time. The measurements with radioactive sources showed that the energy resolution of the TPC at 1-bar is following an empirical  $T^{0.57}$  law, being about 2 times better than the energy resolution at 3-bar [5].

An example of a low energy single electron of 170 keV in 1bar of CF4 is displayed in figure 6. For single electrons fully contained inside the TPC above 200 keV the rate is 760 cpd/kg. We used the same kinematical procedure as abovementioned to determine the background and to select the neutrino candidates. After applying the fiducial, geometrical and kinematical cuts we have measured the signal from neutrino electron interaction, corresponding to  $2.89 \pm 2.39$  counts per day.

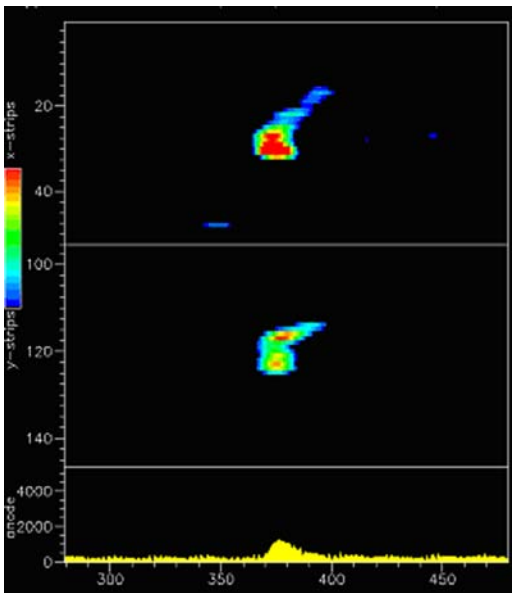


**Figure 6.** A 170 keV electron in the TPC at 1 bar of CF4:  $x-z$ ,  $y-z$  projections as well as the integrated anode signal are displayed as a function of time ( $z$ ). The binning is 3.5 mm for  $x$  and  $y$  and 80 ns for  $z$ .

#### 3.2. Reconstruction of Cs photopeak

Here is given the reconstruction of the incident photon energy obtained with the 662 keV  $^{137}\text{Cs}$  source at 1 bar of CF4. The photons interact with electrons in the TPC via Compton scattering. The scatter photon is measured in the scintillator. The recoil electron track and energy are measured in the TPC. The electron direction is coinciding with the incident photon direction in the first centimetres of the track. The Compton electrons initial direction is obtained with a visual fit. The angle  $\theta_{source}$  which is the angle with respect to the source axis (being perpendicular to detector-reactor axis) is calculated

from this fit. The initial photon energy  $E_\gamma$  is reconstructed from the scattering angle  $\theta_{source}$  and the electron recoil energy  $T_e$ , measured in the TPC. The reconstructed photopeak is compared with Monte Carlo simulations in figure. 7. The width of the peak at  $1\sigma$  is 220 keV at 662 keV. The angular resolution of the Compton recoil spectrum above 150 keV is  $\sigma_\theta = 11.6^\circ \pm 0.9$ .

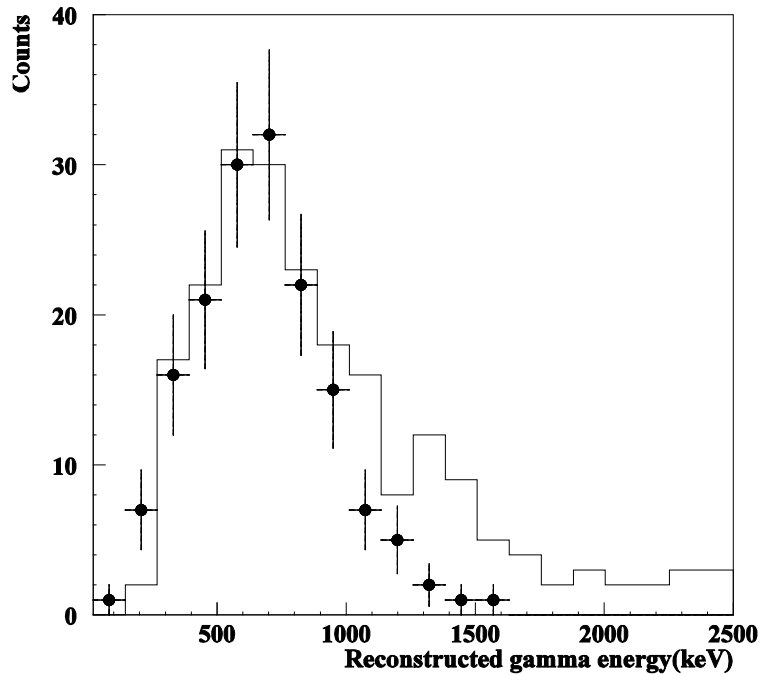


Figure 7. Reconstructed  $^{137}\text{Cs}$  photopeak of 662 keV.

#### 4. Conclusion

The MUNU experiment studied neutrino electron scattering at low energy using a nuclear reactor as an antineutrino source. Both the energy and scattering angle are measured. A reduction of the statistical errors is achieved due to a better estimation of the background in the entire chamber. A good agreement is seen between the measured and expected from weak interactions spectra above 700 keV for operation of 3-bar. A limit of  $\mu_\nu < .9 \times 10^{11} \mu_B$  at 90 % CL is derived. At 1 bar pressure, the direction and energy of the electron tracks are reconstructed above 200 keV. Also at 1 bar, a 662 keV  $^{137}\text{Cs}$  photopeak is reconstructed from Compton scattering.

#### References

- [1] MUNU Collaboration, C. Amsler, et al., *Nucl. Instr. and Meth. A* **396**, 115 (1997).
- [2] MUNU Collaboration, M. Avenier, et al., *Nucl. Instr. and Meth. A* **482**, 408 (2002).
- [3] MUNU Collaboration, Z. Daraktchieva, et al., *Phys. Lett. B* **564**, 190 (2003).
- [4] MUNU Collaboration, Z. Daraktchieva, et al., *Phys. Lett. B* **615**, 153 (2005).
- [5] Z. Daraktchieva, *Thesis*, University of Neuchatel, 2004.
- [6] G. Zacek, et al., *Phys. Rev. D* **34**, 2621 (1986).

# Direct measurement of the neutrino mass

**Peter J. Doe**

Center for Experimental Nuclear Physics and Astrophysics, Box 354290, University of Washington, Seattle, WA 98195-4290, USA

E-mail: pdoe@u.washington.edu

**Abstract.** The absolute values of the neutrino masses are important to the evolving models of particle physics, and cosmology. Experimental limits on the neutrino masses have been established by neutrino oscillation and nuclear beta decay experiments. Improved, model dependent limits are being provided by a range of cosmological observations and neutrinoless double beta decay experiments. This document reports on the status of experiments investigating neutrino mass in a direct, model independent, way. These experiments are approaching a sensitivity that will offer guidance and constraint to models of both cosmology and particle physics. The prospect for pushing the sensitivity of direct measurements still further is considered.

## 1. Introduction

Experiments conducted using natural and man-made sources of neutrinos have shown conclusively that neutrinos undergo flavor oscillation and therefore possess mass. The neutrino flavor states ( $\nu_e, \nu_\mu, \nu_\tau$ ) are not states of fixed mass ( $\nu_1, \nu_2, \nu_3$ ) but a coherent superposition of these mass states given by  $|\nu_l\rangle = \sum_i U_{li} |\nu_i\rangle$ . The oscillations experiments do not tell us the absolute value of the neutrino mass states, only the mass squared differences e.g.  $\Delta m_{ij}^2 = |m_j^2 - m_i^2|$ . From this we can deduce that at least one neutrino has a mass  $\geq 45$  meV, i.e. very small compared to the mass of the other fermions.

Knowing the absolute value of the neutrino masses is crucial to our understanding of the fermion masses in general. Whether the ordering of these masses is "hierarchical" ( $m_1 < m_2 < m_3$ ) or "quasi degenerate" ( $m_1 \approx m_2 \approx m_3$ ) is currently unknown. In the standard model (SM) of particle physics neutrinos are massless, left handed particles. Theories beyond the SM with massive neutrinos can be divided broadly into two classes, distinguished by either hierarchical or degenerate mass schemes. An experimental sensitivity of  $\sim 200$  meV would distinguish between these schemes and provide guidance for model development. Similarly, experimental confirmation as to whether the neutrino is a Dirac or Majorana particle will provide both constraint and guidance to model development.

Relic neutrinos, the second most abundant particles in the universe, are candidates for hot dark matter (HDM). Their influence on the formation of large scale structure in the early universe is quite distinct from that of the cold dark matter (CDM) candidates. Currently, the contribution of the neutrino density  $\Omega_\nu$  to the total density of the universe,  $\Omega$  ranges from 0.001 to 0.15. Improving this limit and knowing the contribution of  $\nu$ HDM to the total DM would lead to a better understanding of the role of neutrinos in the formation of large scale structure.

## 2. Techniques to determine neutrino mass

Techniques to determine the neutrino mass can be broadly divided into two classes, model dependent and model independent, see [1] for a detailed discussion.

Model dependent techniques are based on either cosmological observations [2] or neutrino-less double beta decay ( $0\nu\beta\beta$ ) [3]. Cosmological techniques make use of fluctuations in the cosmic microwave background, large scale structure, galactic red-shifts, Lyman- $\alpha$  forest and other astronomical observations. The *total* neutrino mass ( $\sum_i \nu_i$ ) appears as one of many parameters in the models that describe these observations. Parameter degeneracy introduces a degree of arbitrariness to the value of the neutrino mass obtained. Combinations of these model dependent data sets offer the most stringent limits on the total neutrino mass and the upcoming experiments will soon be able to distinguish between the hierarchical and degenerate mass schemes.  $0\nu\beta\beta$  techniques offer limits comparable to that of the current cosmological techniques.  $0\nu\beta\beta$ , which requires the neutrino be its own antiparticle (a Majorana particle), is the only realistic way to determine the nature of the neutrino. If the neutrino is a Dirac particle,  $0\nu\beta\beta$  will not occur and therefore provides no information concerning the neutrino mass. Current  $0\nu\beta\beta$  experiments are approaching the sensitivity required to distinguish between the hierarchical and degenerate mass schemes and subsequent experiments could, in principle, cover the entire range allowed by the oscillation experiments.

Model independent, or *direct* techniques are purely kinematical, relying only on the principles of energy and momentum conservation to obtain information on  $m(\nu_e)$ ,  $m(\nu_\mu)$ , and  $m(\nu_\tau)$ . The most sensitive of these techniques use nuclear beta decay and are approaching the sensitivity necessary to distinguish between the hierarchical and degenerate mass schemes. The technique of utilizing neutrino time-of-flight from a nearby supernova could, under ideal conditions, obtain limits on the order of  $\sim 1\text{eV}$  and is therefore not considered to be competitive.

Both model dependent and independent techniques are approaching a sensitivity that is of importance to extensions of the SM and a measurement or limit of the neutrino mass would help break the parameter degeneracies that handicap cosmological models. A direct measurement used in conjunction with results from  $0\nu\beta\beta$  experiments will throw light on the Majorana or Dirac nature of the neutrino. These techniques are complimentary and both are needed to fully understand the nature of the neutrino mass.

## 3. Direct mass measurement via nuclear beta decay

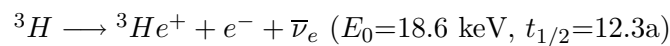
This technique requires precise measurement of the shape of the  $\beta$  decay spectrum near its end point in order to discern distortions attributed to the neutrino mass. The electron energy spectrum of  $\beta$  decay for an  $\nu_e$  with component masses  $m_1, m_2, m_3$  is given by [8]:

$$dN/dE = C \times F(Z, E) p E (E_0 - E) \sum_{i=1}^3 |\langle \nu_{ei} | \rangle|^2 [(E_0 - E)^2 - m_i^2]^{\frac{1}{2}} \theta(E_0 - E - m_i)$$

The neutrino mass is the only unknown and the reaction is independent of whether the neutrino is Dirac or Majorana. The number of counts near the end-point of the spectrum is  $\propto (1/E_0)^3$ , thus, to maximize statistics in the region of interest requires isotopes with low end-point energy, i.e.  $^{187}\text{Re}$  and Tritium. Investigations using  $^{187}\text{Re}$  employ micro-calorimeters while tritium based experiments employ magnetic/electrostatic spectrometers. Both techniques offer different advantages and disadvantages and, importantly, have very different systematics.

### 3.1. Tritium electrostatic spectrometer technique

In this technique, the source of beta decay electrons is separate from the detector, as shown schematically in figure 1. Electrons from the decay



are guided towards the detector by traveling along the magnetic field lines connecting two superconducting solenoids. In doing so they must surmount an electrostatic retarding potential. This type of spectrometer is referred to as a MAC-E-filter (Magnetic Adiabatic Collimation combined with Electrostatic filter). Only electrons whose energy exceeds this potential pass into the detector. The beta spectrum near the end point is mapped out by varying the retarding potential. The advantages of this technique are that only electrons in the region of interest are

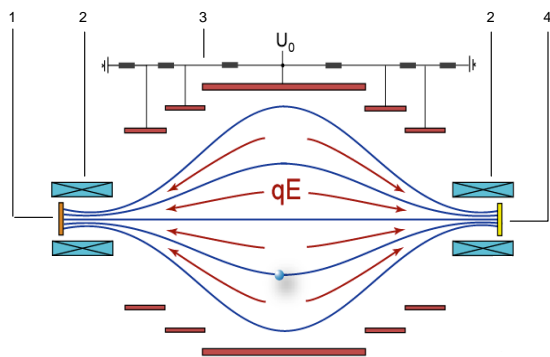


**Figure 1.** The MAC-E spectrometer where the source and the detector are separate. 1 source, 2 super-conducting solenoids, 3 retarding potential electrodes, 4 detector.

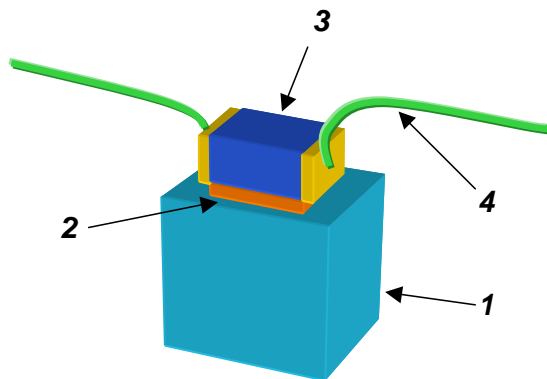


**Figure 2.** The micro-bolometer where the source and the detector are the same. 1 absorber ( $^{187}\text{Re}$ ), 2 thermal contact, 3 thermistor, 4 electrical connection and heat sink

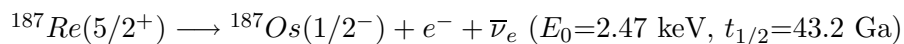
selected, allowing use of intense sources yielding high statistics. Further, the energy resolution (essentially the stability of the retarding potential) may surpass 1 eV for the tritium end point energy of 18.6 keV.

The disadvantages of this technique are that one must understand very precisely the response function of the instrument in order to separate these effects from the quantity being measured. Sources of systematic error must be carefully understood by use of calibration sources and other techniques. Failure to account for a systematic error results in an unphysical negative mass squared reported by experiments pioneering this technique.

Example of the electrostatic MAC-E technique are the Mainz [4] and Troitsk [5] experiments which have established the current limits of  $\sim 2.3$  eV on the neutrino mass.

### 3.2. $^{187}\text{Re}$ micro-calorimeter technique

In this technique the detector is also the source of the beta decay electrons from the decay



Detector masses on the order of a few 100  $\mu\text{gm}$  are cooled to  $\sim 100$  mK, at which temperature the thermal capacity is very low. Small energy depositions result in a temperature rise that can be recorded with precision thermometers as shown in figure 2.

The advantage of the calorimetric technique is that because of the detectors long integration time all the decay energy, except that attributed to the neutrino, is measured. This includes energy stored in excited states.

The disadvantage of the technique is also associated with the long integration time. Since the detector is also the source, one is forced to count the entire spectrum of beta particles, not just the region of interest. This can lead to very high rates and pulse pile-up. To avoid these high

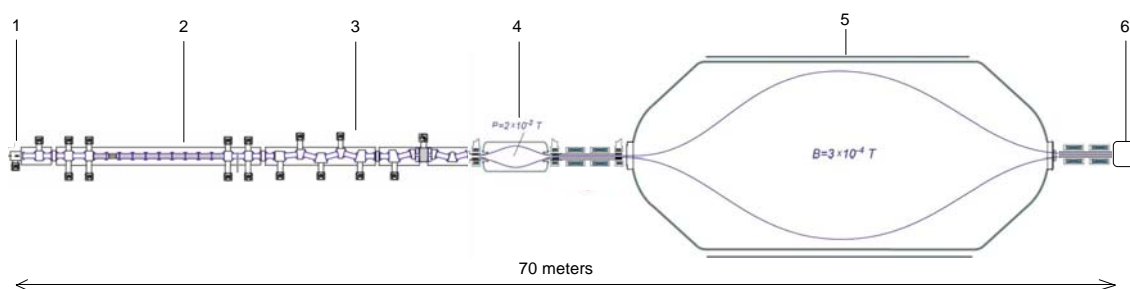


**Figure 3.** Schematic layout of the main KATRIN components. 1 calibration electron gun, 2 windowless gaseous tritium source, 3 transport and cryo-pumping section, 4 pre-spectrometer, 5 main spectrometer, 6 detector

decay rates one is restricted to very small detectors and poor statistics in the region of interest, unless one is able to produce and operate large numbers of detectors.

Current examples of the micro-calorimeter technique using small numbers (1-10) of crystals are the MANU [6] and MIBETA [7] experiments which have achieved mass limits of 19 eV and 15 eV (90% CL) respectively.

#### 4. Next generation of direct mass measurement experiments

A mass sensitivity of a few hundred meV will enable the next generation experiments to distinguish between hierarchical and quasi degenerate mass schemes and reach a sensitivity comparable to the current model dependent cosmological and  $0\nu\beta\beta$  experiments. These limits will be achieved by building on the experiences of the earlier experiments.

##### 4.1. KATRIN

The Karlsruhe Tritium Neutrino experiment [8] is under construction at the Tritium Laboratory Karlsruhe (TLK), Germany. The TLK has unique capabilities to handle the intense ( $\sim 10^{11}$  Bq) source intensity. KATRIN will achieve an order of magnitude improvement in sensitivity by means of a very intense, stable and well understood source, by reducing backgrounds and by controlling systematic errors. The apparatus, shown in figure 3, consists of: a windowless gaseous tritium source (WGTS), a highly stable and pure source of gaseous molecular tritium at a temperature of 27 K and pressure of  $3 \times 10^{-3}$  mbar. Approximately  $5 \times 10^{10} \beta$  decay electrons per second are transported by a magnetic flux of  $191 \text{ Tcm}^2$  towards a pair of MAC-E filter spectrometers. Tritium gas entering the transport system is returned to the source by an array of turbo molecular pumps. Any gas escaping this closed loop is captured by a cryogenic pumping system consisting of argon frost deposited on the walls of the transport pipe. This reduces the partial pressure of tritium, a source of background, to  $10^{-20}$  mbar at the entrance of the spectrometers. The first, low resolution, spectrometer, reduces the flux of electrons from  $10^{10}$  to  $10^3$ . Electrons of energy greater than  $\sim 18.4$  keV enter the main spectrometer which achieves an energy resolution of  $\sim 0.97$  eV by maintaining the retarding potential to a part in  $10^6$ . To achieve this resolution and reduce sources of background the pressure in this vessel must be maintained to  $\leq 10^{-11}$  mbar. Another source of background arises from electrons emitted from the wall of the vessel, either due to cosmic rays or natural radioactivity. To reduce this background the interior of the vessel is lined with a low mass wire electrode held at a potential that repels these electrons back to the wall of the vessel, while optimizing the field shape of the retarding potential and screening against stray fields. Electrons passing through the main spectrometer are guided to the detector which consists of a

10 cm diameter monolithic array of  $\sim 100$  PIN diodes. The pixels are configured in a dart-board arrangement which images and monitors the source, allowing study and control of sources of systematic error. Environmental backgrounds are controlled by surrounding the detector with passive shielding and a scintillator veto. At the most upstream end of the beam line is the control and monitoring system consisting of an electron gun which monitors the transmission function of electrons as they pass from the source to the detector and also used to investigate systematics. Located upstream of the source is a detector which is used to monitor the activity of the source.

#### 4.2. Status of KATRIN

Most major components of the KATRIN experiment are under construction or already in hand. The pre-spectrometer has been used to demonstrate vacuums of better than  $10^{-11}$  mBar can be achieved and is now being used to study the efficacy of the inner electrode system to control backgrounds. The Test of Inner LOop (TILO) experiment has successfully demonstrated that the design parameters of the closed loop WGTS can be achieved. The TRitium ARgon frost PUMP (TRAP) experiment has demonstrated the tritium trapping efficiency required by the cryogenic pumping system. A voltage source, stable to a part in  $10^6$  has been demonstrated. Construction of the main experimental hall will be finished in time to receive the main spectrometer in Fall 2006. Tritium data taking will commence in Spring 2010. After 5 calendar years, a sensitivity to a neutrino mass of 350 meV ( $5\sigma$ ) or a limit of 200 meV (90% CL) is expected to be reached.

#### 4.3. MANU2 + MIBETA2 $\rightarrow$ MARE

Recent technical advances in micro-machining techniques, experience in the fabrication of large detector arrays for astronomy, improvements in sensor technology and a better understanding of systematic sources have presented new possibilities to improve the sensitivity of the micro-calorimeter technique. To take advantage of these possibilities the MANU and MIBETA experiments propose MARE (Micro-calorimeter Arrays for a Rhenium Experiment) [9] which aims to achieve  $\sim 10^2$  improvement in sensitivity to make an independent test of the spectrometer results at a sensitivity of 200 meV. This sensitivity will be reached in two stages. The first stage, MARE-1, involves two second generation experiments, MANU2 and MIBETA2. Each experiment will increase their size to  $\sim 300$  detector elements of several  $100\mu\text{g}$  each, with energy resolution and response times of  $\sim 10$  eV and  $\sim 100\mu\text{s}$  respectively. An example of a prototype array is shown in figure 4. A total of  $10^{10}$  events collected over 4 years is expected to yield a sensitivity of  $m_\nu < 2.5\text{eV}$  (90% CL) by 2010. In parallel with this an R&D program will investigate 3 new technologies; Metallic magnetic calorimeters which promise improved energy resolution and response time; Multiplexed kinetic induction detectors which allow  $10^3 \rightarrow 10^4$  detectors to be read out per amplifier; Super-conducting transition edge sensors which promise factors of  $\sim 60$  improvement in energy resolution and  $\sim 100$  in response time. If MARE-1 and the the R&D program are successful, the plan is to initiate MARE-2, consisting of  $\sim 5 \times 10^4$  detector elements arranged in 5 independent arrays. The dilution refrigerators for these arrays exist and the arrays will be increase in size incrementally as the micro-fabrication techniques make new detectors available. If the R&D programs achieve, as anticipated, energy resolution and response times of  $\sim 5$  eV and  $\sim 1\mu\text{s}$  respectively, then a total of  $10^{14}$  events collected over 3 years should yield a sensitivity of  $m_\nu < 0.2\text{eV}$  (90% CL). Because of the different systematics this result would compliment that of the KATRIN experiment on a similar time scale.

### 5. Future prospects

The prospects appear good that at least one direct measurement technique will achieve the important limit of  $\sim 200$  meV. What are the prospects of pushing the direct measurement technique into the sub 200 meV region, currently the preserve of the model dependent techniques

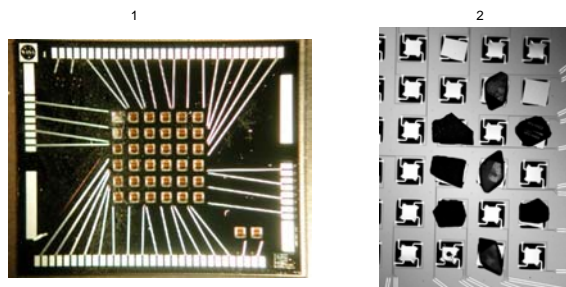


**Figure 4.** The very small - a prototype bolometer array. 1 micro-machined 36 element array, 2  $\text{AgReO}_4$  absorbers mounted on array.



**Figure 5.** The very large - the KATRIN main spectrometer vessel nears completion.

of cosmology and  $0\nu\beta\beta$ ? For spectrometers maximum sensitivity requires that the column density and isotopic purity of the source be optimized and the area of the analyzing plane, and therefore the spectrometer vacuum vessel, be maximized. The KATRIN spectrometer vessel, shown in figure 5, is 10 meters in diameter and 24 meters long. To make a significantly larger vessel that is compatible with a vacuum of  $< 10^{-11}$  mbar is a technological challenge. Aside from the technological challenges, the ultimate limit of this technique is probably set by the ability to calculate to sufficient accuracy the excited final states of the tritium beta decay. For micro-calorimeters, the sensitivity to neutrino mass is proportional to the pulse-pair resolving times (the pile-up problem) and the energy resolution. If MARE-1 is successful in demonstrating the technological improvements and MARE-2 does not encounter insurmountable systematic problems, then, naively, one need only increase the number of detectors to improve the mass sensitivity. Whether the future of direct measurements beyond KATRIN lies with micro-calorimeters remains to be seen from the outcome of the MARE program.

### Acknowledgments

The author wishes to thank his KATRIN collaborators and colleagues on the MANU and MIBETA experiments for providing information.

- [1] Aalseth C 2004, Neutrinoless double beta decay and direct searches for neutrino mass, hep-ph/0412300v1
- [2] Lesgourgues J and Pastor S 2006 Massive neutrinos and cosmology <http://arxiv.org/abs/astro-ph/0603494> to be published in *Physics Reports*
- [3] Elliott S R and Engel J 2004 Double-beta decay *J. Phys. G: Nucl. Part. Phys.***30** R183 - R215
- [4] Kraus Ch *et al.* 2005 *Eur. Phys. J.* **40** 447, hep-ex/0412056
- [5] Lobashev V *et al.* 2003 *Nucl. Phys.* **A719** 153
- [6] Galeazzi M *et al.* 2001 *Phys. Review C* 63-1 0114302
- [7] Sisti M *et al.* 2004 *Nucl. Instr. Meth* A520, 125
- [8] 2004 KATRIN design report. A copy of this report can be downloaded from <http://www-ik.fzk.de/%7Ekatrin/publications/index.html#publications>
- [9] Gatti F *et al.* 2005 Mare Proposal. A copy of the proposal can be downloaded from <http://crio.mib.infn.it/wig/silicini/proposal/>

# Introduction to the Double-Beta Decay Experimental Program

**Steven R. Elliott**

Los Alamos National Laboratory, Los Alamos, NM 87506, USA

E-mail: [elliotts@lanl.gov](mailto:elliotts@lanl.gov)

**Abstract.** This document gives an overview of the technical issues and goals facing future double-beta decay experiments.

## 1. Introduction

The science of double-beta decay has been described in detail in a number of good review articles [1, 2, 3, 4]. In addition, these proceedings contain a lot of more current information on this rich and exciting field. Previous experimental results are summarized in Ref.[5], and the theoretical situation concerning the matrix elements is summarized in Ref.[6]. Here we just list the very impressive experimental accomplishments to date in Table 1.

In this article, we describe the issues facing the  $0\nu\beta\beta$  experimental program of the future. Table 2 lists the active proposals for the future projects of which the author is aware. It presents an amazing variety of experimental techniques and expertise and is a tribute to the skill and ingenuity of the scientists involved. Many of these projects are well underway and many others have vigorous research programs, hence, the situation is extremely encouraging. While issues specific to a given project are described in other articles within these proceedings, there are numerous issues that are common to all these projects and it is these issues that are the focus of this article.

## 2. Producing a Result with Confidence

The recent claim for positive evidence for  $0\nu\beta\beta$  in  $^{76}\text{Ge}$ [34] has been controversial. One must ask why this result was not universally accepted and what types of evidence are required to ensure that future claims are embraced by the community. Even though a peak is arguably present in the spectrum of this work, the signal was very weak and immersed in a large background. The background model had a fair amount of uncertainty including some unidentified lines near the region of interest. Supporting evidence to prove the peak was indeed due to  $0\nu\beta\beta$  and not some competing process was insufficient. Although future experiments will certainly have improved signal/background ratios, the supporting evidence question is more complicated. By noting that the physical process of  $0\nu\beta\beta$  has distinct characteristics, one can make a subjectively ordered list of potential supporting criteria.

- To show that  $0\nu\beta\beta$  likely exists, one needs a combination of:

- a clear peak at the correct  $0\nu\beta\beta$  energy value

**Table 1.** A summary of the recent  $0\nu\beta\beta$  results. The  $\langle m_{\beta\beta} \rangle$  limits are those deduced by the authors. All limits are at 90% confidence level unless otherwise indicated. The columns providing the exposure and background are based on arithmetic done by the author of this paper, who takes responsibility for any errors in interpreting data from the original sources.

Isotope	Exposure (kmole-y)	Background (counts)	Half-Life Limit (y)	$\langle m_{\beta\beta} \rangle$ (meV)
$^{48}\text{Ca}$	$5 \times 10^{-5}$	0	$> 1.4 \times 10^{22}$	$< 7200 - 44700$ [7]
$^{76}\text{Ge}$	0.467	21	$> 1.9 \times 10^{25}$	$< 350$ [8]
$^{76}\text{Ge}$	0.117	3.5	$> 1.6 \times 10^{25}$	$< 330 - 1350$ [9]
$^{76}\text{Ge}$	0.943	61	$= 1.2 \times 10^{25}$	$= 440$ [12]
$^{82}\text{Se}$	0.022	7	$> 2.1 \times 10^{23}$	$< 1200 - 3200$ [13, 5]
$^{100}\text{Mo}$	0.131	14	$> 5.8 \times 10^{23}$	$< 600 - 2700$ [13, 5]
$^{116}\text{Cd}$	$1 \times 10^{-3}$	14	$> 1.7 \times 10^{23}$	$< 1700$ [10]
$^{128}\text{Te}$	Geochem.	NA	$> 7.7 \times 10^{24}$	$< 1100 - 1500$ [11]
$^{130}\text{Te}$	0.07	12	$> 2.4 \times 10^{24}$	$< 400 - 1400$ [14]
$^{136}\text{Xe}$	$7 \times 10^{-3}$	16	$> 4.4 \times 10^{23}$	$< 1800 - 5200$ [15]
$^{150}\text{Nd}$	$6 \times 10^{-5}$	0	$> 1.2 \times 10^{21}$	$< 3000$ [16]

**Table 2.** A summary of the  $0\nu\beta\beta$  proposals.

Collaboration	Isotope	Detector Description
CANDLES[17]	$^{48}\text{Ca}$	CaF <sub>2</sub> crystals in liq. scint.
COBRA[18]	$^{116}\text{Cd}$	CdTe semiconductors
CUORE[19]	$^{130}\text{Te}$	TeO <sub>2</sub> bolometers
DCBA[20]	$^{82}\text{Se}$	Nd foils and tracking chambers
EXO[21]	$^{136}\text{Xe}$	Xe TPC
GeH <sub>4</sub> [22]	$^{76}\text{Ge}$	GeH <sub>4</sub> tracking ionization chamber
GEM[23]	$^{76}\text{Ge}$	Ge detectors in LN
GSO[24, 25]	$^{160}\text{Gd}$	Gd <sub>2</sub> SiO <sub>5</sub> crystals in liq. scint.
Majorana[26]	$^{76}\text{Ge}$	Segmented Ge detectors
MOON[27]	$^{100}\text{Mo}$	Mo foils and plastic scintillator
GERDA[28]	$^{76}\text{Ge}$	Ge detectors in LN
Nano-crystals[29]		suspended nanoparticles
SeF <sub>6</sub> [30]	$^{82}\text{Se}$	negative ion drifting SeF <sub>6</sub> TPC
Super-NEMO[31]	$^{82}\text{Se}$	foils with tracking
Xe[32]	$^{136}\text{Xe}$	Xe dissolved in liq. scint.
XMASS[33]	$^{136}\text{Xe}$	liquid Xe

- a demonstration that the event is a single-site energy deposit
- measured event distributions (spatial, temporal) are representative of  $0\nu\beta\beta$
- a demonstration that the measured decay rate scales with isotope fraction
- To present a convincing case, one needs:
  - an observation of the 2-electron nature of the  $0\nu\beta\beta$  event
  - a demonstration that the kinematic distributions (electron energy sharing, opening angle) match those of  $0\nu\beta\beta$
  - to observe the daughter nucleus appear in real time with the  $0\nu\beta\beta$  decay

- to observe the excited state decay process with parameters indicative of  $0\nu\beta\beta$
- To remove all doubt, many of the above  $0\nu\beta\beta$  indicators should be:
  - measured in several isotopes

Although no experiment can demonstrate the entire list, the projects listed in Table 2 all exploit a number of these.

### 3. Experimental Requirements

Table 3 shows expected signal count rates in  $0\nu\beta\beta$  experiments as a function of neutrino mass. Present experiments are reporting half-life limits near  $10^{25}$  years or  $\approx 500$  meV, whereas the next round of experiments hope to reach 100 meV. Such experiments should cover the degenerate mass region. Beyond that, experiments hoping to have sensitivity near the atmospheric mass scale will need about 1 ton of isotope. To obtain a signal-to-noise ratio of 1 will require a background level of  $\approx 1$  count/ton-year, which will be extremely challenging. Processes that are typically considered when estimating contributions to the background for  $0\nu\beta\beta$  include  $2\nu\beta\beta$ , naturally occurring radioactive isotopes, neutron-induced processes, and long-lived cosmogenic activities.

For the current generation of experiments, energy resolutions are sufficient to prevent the tail of the  $2\nu\beta\beta$  energy spectrum from intruding into the  $0\nu\beta\beta$  peak region. Resolution will become a concern, however, as we approach the ton scale. Even so, resolution is a critical issue for the signal-to-noise ratio at any level of sensitivity. For example, an experiment with a factor 2 worse resolution will require a corresponding lower background for an equivalent ratio.

Naturally occurring radioactive materials, such as U and Th chain isotopes, occur as impurities in virtually all materials that make up an apparatus. The challenge is to ensure that the level of impurity is sufficiently low such that the decays of these isotopes won't mask the desired signal. The solution to this problem is mostly understood, but it is difficult to implement. Great progress has been made understanding materials and their associated U/Th contamination. Furthermore, purification and assay techniques have also improved. Even so, elaborate QA/QC programs will be required. In addition, to reach the ton scale, future purity levels will continue to greatly challenge assay capabilities. Materials with purity levels of  $\approx 1\mu\text{Bq/kg}$  or less will be required for ton scale experiments. It is difficult to assay materials to this level. Hence, improvements are needed in the sensitivity of assay techniques such as mass spectroscopy, direct counting, and neutron activation analysis. Problems associated with long-lived cosmogenic isotopes are material dependent, but the problematic isotopes have been identified. Minimizing the surface exposure of detector materials and performing selected construction activities underground can mitigate much of this background contribution.

Unfortunately, neutron-induced backgrounds are more subtle. Neutrons originate from a number of sources. Those arising from  $(\alpha, n)$  and fission processes in a laboratory's surrounding rock have an energy up to  $\approx 10$  MeV and can be shielded effectively. Those arising from high-energy  $\mu$  interactions in the rock and the detector shield materials can have very high energies and therefore are very penetrating. Unlike naturally-occurring radioactive isotopes, neutron-induced processes often don't have a unique signature that identifies the background process, which in turn provides clues to a mitigation plan. Instead, neutron related backgrounds are more likely to be a sum of a large number of processes, each of which is small by itself. This is especially true of  $(n, n'\gamma)$  reactions. To fully understand and plan for these backgrounds, the low-energy nuclear physics needs to be fully implemented into the simulation codes and verified. In some cases, the data required to do this doesn't yet exist. Moving to a deep site that shields the experiment from  $\mu$ 's will effectively reduce this background. Reference [35] estimates that a depth of  $\approx 5000$  m.w.e. will certainly suffice.

**Table 3.** A summary of the approximate  $0\nu\beta\beta$  signal rate for a number of neutrino masses. These estimates are for Ge, but are qualitatively similar for most of the proposed isotopes.

Neutrino Mass Scale	$\langle m_{\beta\beta} \rangle$	Representative half life	Signal
	meV	years	counts/ton-year
Degenerate	400	$10^{25}$	530
	100	$5 \times 10^{26}$	10
Atmospheric	40	$5 \times 10^{27}$	1
Solar	2	$10^{29}$	0.05

Figure 1 shows a flow chart indicating possible outcomes of future experiments and what they indicate for the future path of the overall  $0\nu\beta\beta$  program. After the current generation of experiments (100-200 kg) are complete, there will be a decision point regarding the following generation. If these experiments are null, then it will be necessary to build experiments with a ton of isotope to search for a signal at the atmospheric scale. Alternatively, if the experiments see a signal, there is different choice to make depending on the precision of the result. If the result is not a precision result ( $\sim 10\%$ ), then an expansion to the 1-ton scale is again warranted. Otherwise, if the result is a precision result, a follow-up experiment to measure the statistical distributions of kinematic parameters would be desired. Because the experimental design for measuring kinematic parameters may not be congruent with a simple scale up for a search experiment, planners will have to decide which direction to proceed after the current experiments are completed.

To reach a sensitivity at the solar scale, an experiment with 100 tons of isotope will be required. Such an experiment is not yet feasible for numerous reasons. Enrichment costs and production rates are not presently practical. Achieving the required excellent energy resolution (better than 1%) in such a large experiment is also daunting. Schemes involving  $10^6$  solid state detectors are conceivable, but costs would need to be greatly reduced to make that number of detectors affordable. Encouragingly, large multi-element detector electronics are improving and would not likely be a show-stopper. Alternatively, large volume detectors using metal-loaded liquid scintillator or Xe scale more easily and cost effectively. However, the energy resolution of such detectors is still too poor for this application. Significant research will be required on these technical difficulties if such an experiment is to be realized.

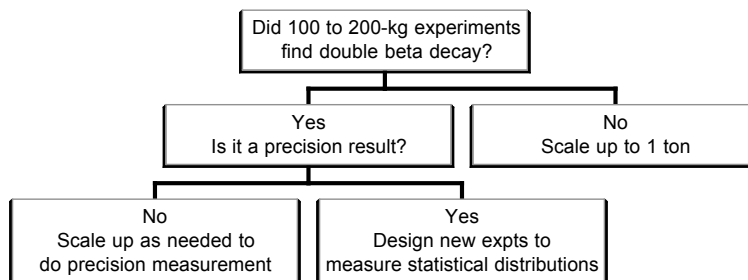


**Figure 1.** A cartoon of a decision tree for how the  $\beta\beta$  program should proceed after the currently proposed generation of experiments.

If  $0\nu\beta\beta$  is observed, we will want to extract all the underlying physics. The existence of the process would imply that neutrinos have a Majorana mass, but it doesn't necessarily mean that light neutrinos are Majorana particles. **Proceedings of Neutrino Physics and Astrophysics, July 13-19, 2006**

R-parity violating super-symmetry particle exchange. See Ref. [2] and references therein for a discussion of alternative decay mechanisms. The matrix elements, however, are different for differing processes and this leads to a possible technique for isolating the dominate one. By comparing  $0\nu\beta\beta$  rates in several isotopes one might be able to identify the underlying physics. If one uses the present theoretical values for the matrix elements as a guide, it appears that 3 or more experiments, each with a total uncertainty (theory, statistical, systematic) of less than about 40% will be required.

#### 4. The Majorana Phases

The linear combination of the neutrino mass eigenstates ( $\nu_k$ ) that mix to form the weak interaction eigenstates ( $\nu_\alpha$ ) is given by a mixing matrix,  $U_{\alpha k}$ . This matrix may contain as many as 3 physically meaningful phases, two of which (the Majorana phases  $\alpha_{21}, \alpha_{31}$ ) contribute to the effective double-beta decay mass ( $\langle m_{\beta\beta} \rangle$ ). These phases do not contribute to the effective beta decay mass ( $\langle m_\beta \rangle$ ) or the differences in the squares of the neutrino masses ( $\Delta m_{\text{sol}}^2$ ) as measured in oscillation experiments.

If  $U_{e3} \neq 0$ , then both phases contribute to  $\langle m_{\beta\beta} \rangle$  and since no other experiment has been identified that is sensitive to the phases, there will be an ambiguity in trying to extract the phase values. You can't deduce two parameters from one data point. However, if  $U_{e3} = 0$ , only one of the Majorana phases contribute to  $\langle m_{\beta\beta} \rangle$  and it could, in principle be extracted. To show this we compare measurements of  $\langle m_{\beta\beta} \rangle$ ,  $\langle m_\beta \rangle$ , and  $\Delta m_{\text{sol}}^2$  for a toy model. Figure 2 was drawn for  $m_1 = 300$  meV,  $\Delta m_{\text{sol}}^2 = (9 \text{ meV})^2$ ,  $U_{e1} = 0.866$ ,  $U_{e2} = 0.5$ , and  $\alpha_{21} = 2.5$  radians. These result in  $\langle m_\beta \rangle = 300$  meV and  $\langle m_{\beta\beta} \rangle = 171$  meV. Note that the 3 measured parameters are all plotted as functions of the mass eigenvalues and they agree at only one point and then only if the correct value for  $\alpha_{21}$  is chosen.

However, to determine the value of the phase with any precision requires great accuracy on  $\langle m_{\beta\beta} \rangle$ . Figure 3 shows  $\langle m_{\beta\beta} \rangle$  as a function of the value of the phase for the above toy model. Its clear that if the uncertainty on  $\langle m_{\beta\beta} \rangle$  is 50%, no information regarding  $\alpha$  is obtained. For a useful determination of the phase, even in this simplistic two-flavor model, a precision nearing 10% is required. Note that a similar analysis can be found in Reference [36] and a three-neutrino-species example is presented in Reference [2].

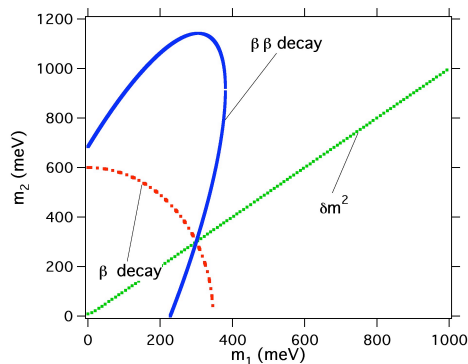


**Figure 2.** A consistency plot for the neutrino mass eigenvalues  $m_1$  and  $m_2$ , for various hypothetical measurements. This set of curves indicates how measured values of  $\Sigma$ ,  $\langle m_{\beta\beta} \rangle$ ,  $\Delta m_{\text{sol}}^2$ , and  $\langle m_\beta \rangle$  constrain the mass eigenvalues. See text for a description of the chosen input parameters.

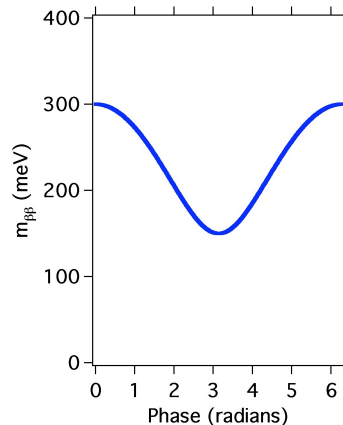


**Figure 3.** For the same parameters as those in Fig. 2, a plot of  $\langle m_{\beta\beta} \rangle$  as a function of the Majorana phase.

## 5. Conclusions

This is a very exciting time for  $\beta\beta$ . The experimental program is poised to make great strides into a region that will greatly impact neutrino physics. Since neutrino oscillations imply that neutrinos have mass, even null  $0\nu\beta\beta$  experiments will constrain the possible neutrino mass spectra. If one sees  $0\nu\beta\beta$  in the upcoming experiments, the qualitative physics conclusion will be extremely exciting. However, to fully understand all the underlying physics, precision measurements in several nuclei will be needed.

## Acknowledgments

Acknowledgments This work was supported in part by Laboratory Directed Research and Development at LANL. I thank Peter Doe and Petr Vogel for careful readings of this manuscript.

## 6. References

- [1] Elliott Steven R, and Petr Vogel, 2002 *Annu. rev. Nucl. Part. Sci.* **52** 115
- [2] Elliott S R and J Engel, 2004 *J. Phys.* **G30** R183
- [3] Barabash A S, 2004 *Physics of Atomic Nuclei* **67**, No. 3, 438
- [4] F.T Avignone III, G.S. King III and Yuri Zdesenko, 2005 *New Journal of Physics* **7** 6
- [5] Barabash A S, "Double beta decay experiments: Past and present results", presented at Neutrino 2006
- [6] Simkovic Fedor 2006, "The nuclear matrix elements for double-beta decay ", presented at Neutrino 2006
- [7] Ogawa I *et al* 2004 *Nucl. Phys. A* **730** 215; S. Umehara, "CANDLES for double beta decay of  $^{48}\text{Ca}$ ", presented at TAUP 2005
- [8] Klapdor-Kleingrothaus H V, Päs H and Smirnov A Yu 2001 *Phys. Rev. D* **63** 073005
- [9] Aalseth C E *et al* 2002 *Phys. Rev. D* **65** 092007
- [10] Danevich F A *et al* 2003 *Phys. Rev. C* **68** 035501
- [11] Bernatowicz T *et al* 1993 *Phys. Rev. C* **47** 806
- [12] Klapdor-Kleingrothaus H V, Dietz A, Krivosheina I V and O. Chkvorets 2004 *Phys. Lett. B* **586** 198; *Nucl. Instrum. Meth. A* **522** 371
- [13] Arnold R *et al* 2005 *Phys. Rev. Lett.* **95** 182302
- [14] Arnaboldi C *et al* 2005 *Phys. Rev. Lett.* **95** 142501; R. Maruyama, "Cuore and Cuoricino: A bolometric search for neutrinoless double beta decay", presented at Neutrino 2006
- [15] Luescher R *et al* 1998 *Phys. Lett. B* **434** 407
- [16] De Silva A *et al* 1997 *Phys. Rev. C* **56** 2451
- [17] Kishimoto T 2004, private communication
- [18] Zuber K 2001 *Phys. Lett. B* **519** 1; J. Wilson, "The COBRE experiment", presented at Neutrino 2006
- [19] Arnaboldi C *et al* 2004a *Nucl. Instrum. Meth.* **A518** 775
- [20] Ishihara N *et al* 2000 *Nucl. Instrum. Meth. A* **443** 101
- [21] Danilov M *et al* 2000 *Phys. Rev. C* **62** 044501; A. Piepke, "New techniques: EXO, MOON, SuperNEMO", presented at Neutrino 2006
- [22] Robertson RGH 2005, private communication
- [23] Zdesenko Yu G, Ponkratenko O A and Tretyak V I 2001 *J. Phys.* **G27** 2129
- [24] Danevich F A *et al* 2001 *Nucl. Phys. A* **694** 375
- [25] Wang S C, Wong H T and Fujiwara M 2000 *Nucl. Instrum. Meth. A* **479** 498-510
- [26] Gaitskell R *et al* 2003 *Preprint nucl-ex/0311013*
- [27] Ejiri H *et al* 2000 *Phys. Rev. Lett.* **85** 2917; H. Nakamura, "MOON for double beta decay experiment and MOON-1 prototype detector status", presented at TAUP 2005
- [28] Abt I *et al* 2004 LNGS-LOI 35/04, *Preprint hep-ex/0404039*; S. Schöenert, "New techniques in  $0\nu\beta\beta$  germanium experiments", presented at Neutrino 2006
- [29] McDonald A 2004 private communication for members of the SNO Collaboration
- [30] Nygren D 2005, private communication
- [31] Sarazin X *et al* 2000 *Preprint hep-ex/0006031*
- [32] Caccianiga B and Giammarchi M G 2001 *Astropart. Phys.* **14** 15
- [33] Moriyama S *et al* 2001 presented at XENON01 Workshop, Dec., Tokyo, Japan
- [34] Klapdor-Kleingrothaus H V, A Dietz, I V Krivosheina and O Chkvorets, 2004 *Nucl. Instrum. Meth.* **A522** 371
- [35] Mei D-M, and A Hime 2006 *Phys. Rev.* **D73** 053004
- [36] Barger V, S L Glashow, P Langacker, D Marfatia 2002 *Phys.Lett.* **B540** 247

# MSW Oscillations - LMA and Subdominant Effects

**Alexander Friedland**

Theoretical Division, T-8, MS B285, Los Alamos National Laboratory, Los Alamos, NM 87545

**Abstract.** These notes, based on a talk given at the Neutrino 2006 conference [1], review the sensitivity of solar neutrinos to certain types of new physics, namely modifications of neutrino-matter interactions by the exchange of a new heavy particle and a large neutrino transition moment. Both were first proposed in the 1970's as possible explanations for the solar neutrino "problem" and were actively investigated for many years. While since ruled out as the dominant mechanisms of the solar neutrino flavor conversion, they remain of great interest as subdominant effects, which, if observed, would open a window to new physics. We outline the sensitivity of the current experiments and describe progress that may be expected in the near future.

## 1. Standard LMA solution: basic features

We begin by reviewing the standard Large Mixing Angle (LMA) MSW [2, 3] solution to the solar neutrino "problem". The basic experimental result is that the electron neutrino survival probability  $P_{ee}^{std} \equiv P(\nu_e \rightarrow \nu_e)$  varies across the solar neutrino energy spectrum. At high energy,  $E_\nu \gtrsim 6 - 7$  MeV,  $P_{ee}^{std}$  is about  $\sim 34 \pm 3\%$ , as measured by SNO [4] and Super-Kamiokande [5], while at lower energies it rises to  $58 \pm 6\%$ , as measured by the gallium experiments [6]. How is this behavior accommodated in the standard LMA solution?

To answer this, consider the expression for  $P_{ee}^{std}$ , which, without the Earth effect, is given by

$$P_{ee}^{std, 2\nu} = \cos^2 \theta_\odot \cos^2 \theta + \sin^2 \theta_\odot \sin^2 \theta. \quad (1)$$

The probability of finding the neutrino in eigenstate 1(2) is  $\cos^2 \theta_\odot (\sin^2 \theta_\odot)$ , where  $\theta_\odot$  is the mixing angle at the production point; in turn, the probability of detecting the neutrino already in eigenstate 1(2) as  $\nu_e$  is  $\cos^2 \theta (\sin^2 \theta)$ . The key physical ideas here are that the evolution is adiabatic (no level jumping) and incoherent (interferences between 1 and 2 disappear upon integration over energies for  $\Delta m^2 \gtrsim 10^{-9} - 10^{-8}$  eV<sup>2</sup> [7, 8] and over the production region).

The angle  $\theta_\odot$  is determined from the oscillation Hamiltonian  $H_{\text{tot}} = H_{\text{vac}} + H_{\text{mat}}$ , where

$$H_{\text{vac}} = \begin{pmatrix} -\Delta \cos 2\theta & \Delta \sin 2\theta \\ \Delta \sin 2\theta & \Delta \cos 2\theta \end{pmatrix}, \quad H_{\text{mat}} = \begin{pmatrix} \sqrt{2}G_F n_e & 0 \\ 0 & 0 \end{pmatrix}. \quad (2)$$

Here  $\Delta \equiv \Delta m^2 / (4E_\nu)$  and  $\Delta m^2$  is the mass splitting between the first and second neutrino mass states:  $\Delta m^2 \equiv m_2^2 - m_1^2$ . The two limiting values are  $\theta_\odot = \theta$  ( $H_{\text{tot}}$  is dominated by  $H_{\text{vac}}$ ) and  $\theta_\odot = \pi/2$  ( $H_{\text{tot}}$  is dominated by  $H_{\text{mat}}$ ). The probability  $P_{ee}^{std}$  then varies from  $\cos^4 \theta + \sin^4 \theta$  ( $= 1 - (1/2)\sin^2 2\theta$ , averaged vacuum oscillations) to  $\sin^2 \theta$ .

The transition from one regime to another occurs when  $\sqrt{2}G_F n_e \sim 2\Delta$  at the production point. To accommodate the data on  $P_{ee}$ , this transition must occur *right in the middle of the solar neutrino spectrum*, implying  $\Delta m^2 \sim$  a few  $\times 10^{-5}$  eV<sup>2</sup>. Moreover,  $\Delta m^2$  cannot be lower

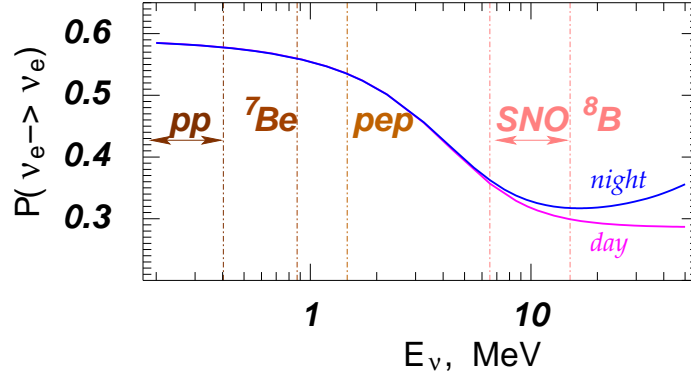


**Figure 1.** The  $\nu_e$  survival probability and day/night asymmetry for the LMA solution.

than  $\sim 3 \times 10^{-5} \text{ eV}^2$  to avoid being close to the resonance condition in the Earth and resulting large day/night variations of  $P_{ee}$ . The situation is illustrated in Fig. 1. Evidently, Nature chose to “tune” the mass splitting involved in solar neutrino oscillations to the density in the solar core! Remarkably, KamLAND [9] showed that  $\Delta m^2$  is indeed in this range.

The preceding discussion assumed that mass eigenstate 3 is not involved in the evolution of solar neutrinos. The correction due its presence is trivially computed if we notice that the splitting between this state and eigenstates 1 and 2 is significantly larger than the matter potential even in the center of the Sun ( $\Delta m_{atm}^2/2E \gg \sqrt{2}G_F N_e(0)$ ), so that the  $\nu_e$  content of that state is always given by  $\sin^2 \theta_{13}$ . Repeating the arguments that led to Eq. (1), we can write

$$P_{ee}^{std, 3\nu} = \sin^4 \theta_{13} + \cos^4 \theta_{13} P_{ee}^{std, 2\nu}. \quad (3)$$

Given the bound  $\sin^2 \theta_{13} \lesssim 0.02$  from CHOOZ [10], the first term is negligibly small. The effect of the third state then is to multiply the two-neutrino survival probability by  $\cos^4 \theta_{13}$ . The resulting correction is at most 4%; this correction is basically the probability that the original electron neutrino “disappears” into state 3. See, *e.g.*, [11, 12] for recent data analyses and further references.

## 2. Searching for nonstandard neutrino interactions

The impact of nonstandard neutrino-matter interactions on solar neutrino oscillations was discussed already in the classical paper by L. Wolfenstein [2] and subsequently elaborated on by many authors ([13, 14, 15] and many others). The idea is that novel interactions due to a heavy vector and scalar exchange could modify the neutrino forward scattering amplitude and hence the oscillation Hamiltonian in matter. Regardless of their origin, at low energies relevant to neutrino oscillations, nonstandard interactions (NSI) are described by the effective Lagrangian

$$L^{NSI} = -2\sqrt{2}G_F(\bar{\nu}_\alpha \gamma_\rho \nu_\beta)(\epsilon_{\alpha\beta}^{fL} \bar{f}_L \gamma^\rho f_L + \epsilon_{\alpha\beta}^{fR} \bar{f}_R \gamma^\rho f_R) + h.c. \quad (4)$$

Here  $\epsilon_{\alpha\beta}^{fL}$  ( $\epsilon_{\alpha\beta}^{fR}$ ) denotes the strength of the NSI between the neutrinos  $\nu$  of flavors  $\alpha$  and  $\beta$  and the left-handed (right-handed) components of the fermions  $f$ .

Neutrino scattering tests, like those of NuTeV [16] and CHARM [17], mainly constrain the NSI couplings of the muon neutrino, *e.g.*,  $|\epsilon_{e\mu}| \lesssim 10^{-3}$ ,  $|\epsilon_{\mu\mu}| \lesssim 10^{-3} - 10^{-2}$ . Their limits on  $\epsilon_{ee}$ ,  $\epsilon_{e\tau}$ , and  $\epsilon_{\tau\tau}$  are remarkably loose, *e. g.*,  $|\epsilon_{\tau\tau}^{uuR}| < 3$ ,  $-0.4 < \epsilon_{ee}^{uuR} < 0.7$ ,  $|\epsilon_{\tau e}^{uu}| < 0.5$ ,  $|\epsilon_{\tau e}^{dd}| < 0.5$  [18]. Stronger constraints exist on the corresponding interactions involving the charged leptons. Those, however, are model-dependent and do not apply if the NSI come from the underlying operators containing the Higgs fields [19]. Here we only consider direct experimental bounds.

Even with the addition of NSI the splitting  $\Delta m_{atm}^2/2E$  remains much greater than the matter potential anywhere along the neutrino trajectory. This means the solar neutrino analysis can still be reduced to two neutrino states, following the arguments of Sect. 1. Neglecting small corrections of order  $\sin \theta_{13}$  or higher, the corresponding matter contribution to the two-neutrino oscillation Hamiltonian can be written as

$$H_{\text{mat}}^{NSI} = \frac{G_F n_e}{\sqrt{2}} \begin{pmatrix} 1 + \epsilon_{11} & \epsilon_{12}^* \\ \epsilon_{12} & -1 - \epsilon_{11} \end{pmatrix}, \quad \text{where} \quad \begin{aligned} \epsilon_{11} &= \epsilon_{ee} - \epsilon_{\tau\tau} \sin^2 \theta_{23}, \\ \epsilon_{12} &= -2\epsilon_{e\tau} \sin \theta_{23}. \end{aligned} \quad (5)$$

The epsilons are the sums of the contributions from the matter constituents:  $\epsilon_{\alpha\beta} \equiv \sum_{f=u,d,e} \epsilon_{\alpha\beta}^f n_f/n_e$ . In turn,  $\epsilon_{\alpha\beta}^f \equiv \epsilon_{\alpha\beta}^{fL} + \epsilon_{\alpha\beta}^{fR}$ . Observe that only the vector component of the NSI enters the propagation effect; in contrast, the NC detection process at SNO depends on the axial coupling. The propagation and detection effects of the NSI are thus sensitive to different parameters, and the corresponding searches could be complementary.

Eq. (5) shows that the flavor changing NSI effect in solar neutrino oscillations comes from  $\epsilon_{e\tau}$ , while the flavor preserving NSI effect comes from both  $\epsilon_{ee}$  and  $\epsilon_{\tau\tau}$ . A useful parameterization is

$$H_{\text{mat}}^{NSI} = \begin{pmatrix} A \cos 2\alpha & Ae^{-2i\phi} \sin 2\alpha \\ Ae^{2i\phi} \sin 2\alpha & -A \cos 2\alpha \end{pmatrix}, \quad \text{where} \quad \begin{aligned} \tan 2\alpha &= |\epsilon_{12}|/(1 + \epsilon_{11}), \\ 2\phi &= \text{Arg}(\epsilon_{12}), \\ A &= G_F n_e \sqrt{[(1 + \epsilon_{11})^2 + |\epsilon_{12}|^2]/2}. \end{aligned} \quad (6)$$

The effect of  $\alpha$  is to change the mixing angle in the medium of high density from  $\pi/2$  to  $\pi/2 - \alpha$ . The angle  $\phi$  (related to the phase of  $\epsilon_{e\tau}$ ) is a source of CP violation. Solar neutrino experiments, just like terrestrial beam experiments [20, 21], are sensitive to its effects [22], while atmospheric neutrinos are not [23, 24].

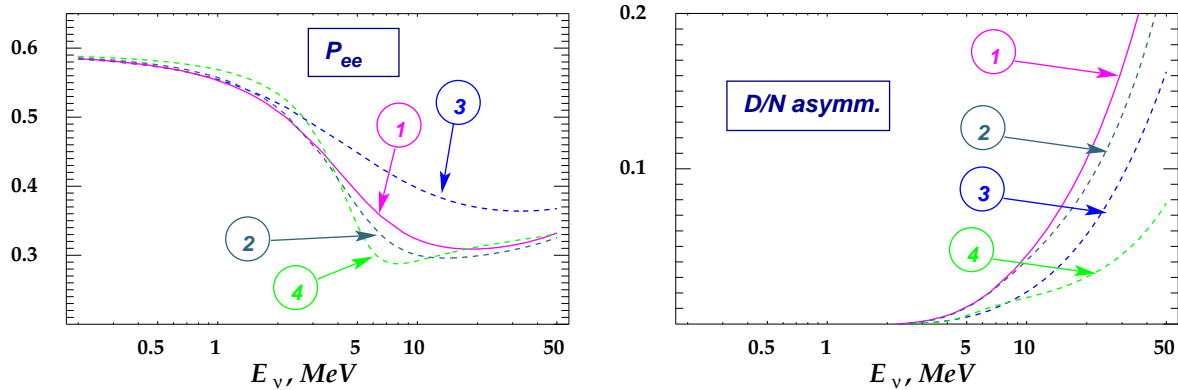


**Figure 2.** The electron neutrino survival probability (*left*) and day/night asymmetry (*right*) for  $\Delta m^2 = 7 \times 10^{-5} \text{ eV}^2$ ,  $\tan^2 \theta = 0.4$  and several representative values of the NSI parameters: (1)  $\epsilon_{11}^u = \epsilon_{11}^d = \epsilon_{12}^u = \epsilon_{12}^d = 0$ ; (2)  $\epsilon_{11}^u = \epsilon_{11}^d = -0.008$ ,  $\epsilon_{12}^u = \epsilon_{12}^d = -0.06$ ; (3)  $\epsilon_{11}^u = \epsilon_{11}^d = -0.044$ ,  $\epsilon_{12}^u = \epsilon_{12}^d = 0.14$ ; (4)  $\epsilon_{11}^u = \epsilon_{11}^d = -0.044$ ,  $\epsilon_{12}^u = \epsilon_{12}^d = -0.14$ . Reproduced from [22].

The main effects of NSI on  $P_{ee}$  are as follows [22]: (i) the low-energy limit stays the same (vacuum oscillations); (ii) the high-energy limit changes, according to Eq. (1),  $P_{ee} \rightarrow \sin^2 \alpha \cos^2 \theta + \cos^2 \alpha \sin^2 \theta$ ; (iii) at intermediate energies, the transition from vacuum to matter dominated regime can shift in energy, with changing  $A$ , and can become more or less abrupt, with changing  $\alpha$  and  $\phi$ . The nonadiabatic regime occurs when  $\theta \rightarrow \alpha$ , rather than  $\theta \rightarrow 0$ . Also, very importantly, the day/night effect can change with *all three parameters*. In particular, it becomes small either as  $A \rightarrow 0$  [25, 26] or as  $\alpha \rightarrow \theta$  [22]. Thus, the LMA-0 region that is normally excluded by the non-observation of day/night asymmetry may become allowed [22, 25, 26].

Fig. 2 illustrates the impact of the NSI on  $P_{ee}$  and the day/night asymmetry. Curve 3 gives an example of parameters that can be excluded already by the existing data. Curve 4 illustrates the suppression of the Earth effect described above. For technical details, including approximate analytical expressions for  $P_{ee}$  and day/night asymmetry, see [22].

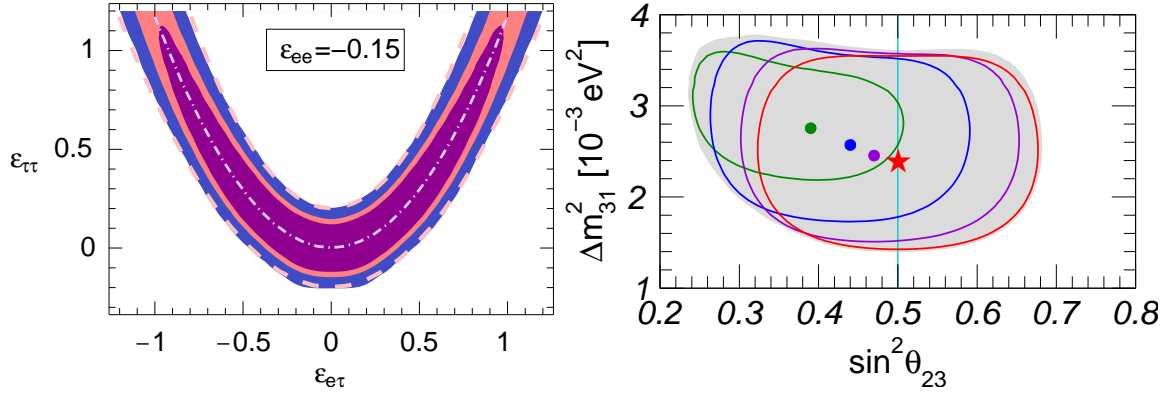


**Figure 3.** *Left panel:* A 2-D section ( $\epsilon_{ee} = -0.15$ ) of the allowed region of the NSI parameters (shaded). We assumed  $\Delta m_{\odot}^2 = 0$  and  $\theta_{13} = 0$ , and marginalized over  $\theta$  and  $\Delta m^2$ . The dashed contours indicate our analytical predictions. See text for details. *Right panel:* The effect of the NSI on the allowed region and best-fit values of the oscillation parameters. From [23].

The solar neutrino analysis of NSI cannot be done in isolation: the same NSI can also be probed with atmospheric neutrinos. Indeed, on general grounds, one expects the atmospheric neutrinos – particularly the high energy ones for which nonstandard matter effects can dominate over the vacuum oscillation effects – to be a very sensitive probe of NSI. Early two-neutrino ( $\nu_{\mu}, \nu_{\tau}$ ) numerical studies [27] yielded  $\epsilon_{\mu\tau} \lesssim 0.08 - 0.12$  and  $\epsilon_{\tau\tau} \lesssim 0.2$ <sup>1</sup>. Clearly, these are very strong bounds; if they were to extend to  $\epsilon_{e\tau}$ , the NSI effects on solar neutrinos discussed in the previous subsection would be excluded. It turns out, however, that this is not the case: when the analysis is properly extended to three flavors, one finds that very large values of both  $\epsilon_{e\tau}$  and  $\epsilon_{\tau\tau}$  are still allowed by the data [23]. This is illustrated in Fig. 3 (*left panel*), which shows that NSI with strengths comparable to the Standard Model interactions can be compatible with all atmospheric data. It must be noted that the compatibility is achieved as a result of adjusting the vacuum oscillation parameters: large NSI imply a smaller mixing angle and larger  $\Delta m_{atm}^2$ , as can be seen in the *right panel* of Fig. 3.

The addition of the K2K data helps constrain the allowed NSI region somewhat [24], while the addition of the first data from MINOS brings no further improvement [28]. Importantly, the future high-statistics MINOS dataset will be a very valuable probe of this parameter space [28].

### 3. Searching for neutrino transition moments

The idea that solar neutrinos could be affected by the neutrino spin precession (NSP) in the solar magnetic fields is even older [29] than the NSI idea. Remarkably, this idea – much improved with time [30, 31, 32, 33, 34, 35] – remained viable for the next three decades. While, by the late 1990’s, the lack of time variations in the Super-Kamiokande data gave strong evidence against NSP in the solar convective zone, NSP in the radiative zone continued to give a good fit to all solar data [36].

Even after the confirmation of the LMA oscillation solution by KamLAND [9], the possibility of the NSP happening at a *subdominant* level remains of great interest, as a probe of the neutrino

<sup>1</sup> Notice the difference in normalization: our  $\epsilon$ ’s are normalized per electron, while [27] gives  $\epsilon$ ’s per  $d$  quark.

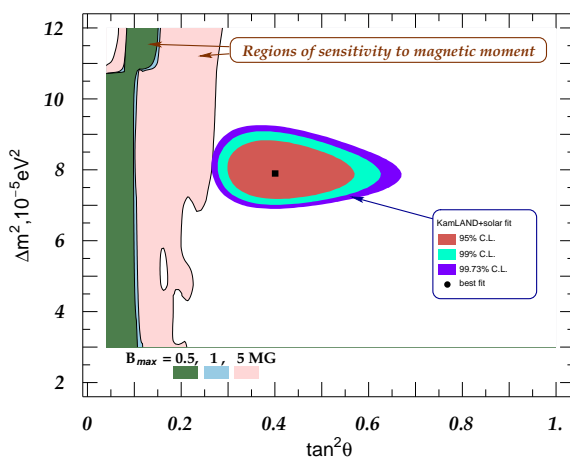


**Figure 4.** The regions of the oscillation parameter space where one may expect the electron antineutrino flux above the KamLAND bound [37] (three different shadings correspond to three different normalizations of the magnetic field, up to the upper bound [38]). An optimistic value of the transition moment,  $\mu = 1 \times 10^{-11} \mu_B$ , was taken. For comparison, the region allowed by the combined analysis of the KamLAND and solar neutrino data [39] is also shown. From [40].

electromagnetic properties and, at the same time, of the magnetic fields in the solar interior. NSP combined with flavor oscillations could lead to conversion  $\nu_e \rightarrow \bar{\nu}_e$  in the Sun, on which recently KamLAND [37] reported a strong upper bound ( $< 0.03\%$ ). It is very important to understand what this bound implies for the neutrino magnetic (transition) moment.

It turns out that *for the measured LMA oscillation parameters* NSP in the radiative zone cannot produce the  $\bar{\nu}_e$  flux above the KamLAND bound. This is illustrated in Fig. 4. This is a remarkable example that knowing neutrino oscillation parameters precisely can be very valuable: the answer would have qualitatively changed, had the mixing angle been  $16^\circ$  instead of  $32^\circ$ .

For NSP in the convective zone, the analysis is different, though in the end the conclusion is similar: one should not have expected the flux of  $\bar{\nu}_e$  in excess of the published KamLAND bound. Put another way, the bound on the neutrino transition moment from the published KamLAND bound is weaker than that from analysis of the red giant cooling [41]. This could change, however, if KamLAND releases an updated bound, with higher statistics/better background rejection. For lack of space, we refer the reader to [40] for details and further references.

- [1] Neutrino 2006, Santa Fe, New Mexico, USA, <http://neutrinosantafe06.com/>.
- [2] L. Wolfenstein, *Neutrino oscillations in matter*, *Phys. Rev.* **D17** (1978) 2369.
- [3] S. P. Mikheev and A. Y. Smirnov, *Resonance enhancement of oscillations in matter and solar neutrino spectroscopy*, *Sov. J. Nucl. Phys.* **42** (1985) 913–917.
- [4] SNO Collaboration, B. Aharmim *et al.*, *Electron energy spectra, fluxes, and day-night asymmetries of b-8 solar neutrinos from the 391-day salt phase sno data set*, *Phys. Rev.* **C72** (2005) 055502, [[nucl-ex/0502021](#)].
- [5] Super-Kamiokande Collaboration, M. B. Smy *et al.*, *Precise measurement of the solar neutrino day/night and seasonal variation in super-kamiokande-i*, *Phys. Rev.* **D69** (2004) 011104, [[hep-ex/0309011](#)].
- [6] GNO Collaboration, M. Altmann *et al.*, *Gno solar neutrino observations: Results for gno i*, *Phys. Lett.* **B490** (2000) 16–26, [[hep-ex/0006034](#)].
- [7] S. Pakvasa and J. T. Pantaleone, *Direct probes of neutrino properties using solar neutrino lines*, *Phys. Rev. Lett.* **65** (1990) 2479–2482.
- [8] A. Friedland, *Msw effects in vacuum oscillations*, *Phys. Rev. Lett.* **85** (2000) 936–939, [[hep-ph/0002063](#)].
- [9] KamLAND Collaboration, K. Eguchi *et al.*, *First results from kamland: Evidence for reactor anti-neutrino disappearance*, *Phys. Rev. Lett.* **90** (2003) 021802, [[hep-ex/0212021](#)].
- [10] M. Apollonio *et al.*, *Search for neutrino oscillations on a long base-line at the chooz nuclear power station*,

- Eur. Phys. J.* **C27** (2003) 331–374, [[hep-ex/0301017](#)].
- [11] S. Goswami and A. Y. Smirnov, *Solar neutrinos and 1-3 leptonic mixing*, *Phys. Rev.* **D72** (2005) 053011, [[hep-ph/0411359](#)].
- [12] G. L. Fogli, E. Lisi, A. Marrone, and A. Palazzo, *Global analysis of three-flavor neutrino masses and mixings*, *Prog. Part. Nucl. Phys.* **57** (2006) 742–795, [[hep-ph/0506083](#)].
- [13] J. W. F. Valle, *Resonant oscillations of massless neutrinos in matter*, *Phys. Lett.* **B199** (1987) 432.
- [14] E. Roulet, *Mikheyev-smirnov-wolfenstein effect with flavor-changing neutrino interactions*, *Phys. Rev.* **D44** (1991) 935–938.
- [15] M. M. Guzzo, A. Masiero, and S. T. Petcov, *On the msw effect with massless neutrinos and no mixing in the vacuum*, *Phys. Lett.* **B260** (1991) 154–160.
- [16] NuTeV Collaboration, G. P. Zeller *et. al.*, *A precise determination of electroweak parameters in neutrino nucleon scattering*, *Phys. Rev. Lett.* **88** (2002) 091802, [[hep-ex/0110059](#)].
- [17] CHARM-II Collaboration, P. Vilain *et. al.*, *Precision measurement of electroweak parameters from the scattering of muon-neutrinos on electrons*, *Phys. Lett.* **B335** (1994) 246–252.
- [18] S. Davidson, C. Pena-Garay, N. Rius, and A. Santamaria, *Present and future bounds on non-standard neutrino interactions*, *JHEP* **03** (2003) 011, [[hep-ph/0302093](#)].
- [19] Z. Berezhiani and A. Rossi, *Limits on the non-standard interactions of neutrinos from  $e^+e^-$  colliders*, *Phys. Lett.* **B535** (2002) 207–218, [[hep-ph/0111137](#)].
- [20] M. C. Gonzalez-Garcia, Y. Grossman, A. Gusso, and Y. Nir, *New  $cp$  violation in neutrino oscillations*, *Phys. Rev.* **D64** (2001) 096006, [[hep-ph/0105159](#)].
- [21] M. Campanelli and A. Romanino, *Effects of new physics in neutrino oscillations in matter*, *Phys. Rev.* **D66** (2002) 113001, [[hep-ph/0207350](#)].
- [22] A. Friedland, C. Lunardini, and C. Pena-Garay, *Solar neutrinos as probes of neutrino - matter interactions*, *Phys. Lett.* **B594** (2004) 347, [[hep-ph/0402266](#)].
- [23] A. Friedland, C. Lunardini, and M. Maltoni, *Atmospheric neutrinos as probes of neutrino matter interactions*, *Phys. Rev.* **D70** (2004) 111301, [[hep-ph/0408264](#)].
- [24] A. Friedland and C. Lunardini, *A test of tau neutrino interactions with atmospheric neutrinos and  $k2k$* , *Phys. Rev.* **D72** (2005) 053009, [[hep-ph/0506143](#)].
- [25] M. M. Guzzo, P. C. de Holanda, and O. L. G. Peres, *Effects of non-standard neutrino interactions on  $msw$ - $lma$  solution*, *Phys. Lett.* **B591** (2004) 1–6, [[hep-ph/0403134](#)].
- [26] O. G. Miranda, M. A. Tortola, and J. W. F. Valle, *Are solar neutrino oscillations robust?*, [[hep-ph/0406280](#)].
- [27] N. Fornengo, M. Maltoni, R. T. Bayo, and J. W. F. Valle, *Probing neutrino non-standard interactions with atmospheric neutrino data*, *Phys. Rev.* **D65** (2002) 013010, [[hep-ph/0108043](#)].
- [28] A. Friedland and C. Lunardini, *Two modes of searching for new neutrino interactions at minos*, *Phys. Rev.* **D74** (2006) 033012, [[hep-ph/0606101](#)].
- [29] A. Cisneros, *Effect of neutrino magnetic moment on solar neutrino observations*, *Astrophys. Space Sci.* **10** (1971) 87–92.
- [30] M. B. Voloshin and M. I. Vysotsky, *Neutrino magnetic moment and time variation of solar neutrino flux*, *Sov. J. Nucl. Phys.* **44** (1986) 544.
- [31] L. B. Okun, *On the electric dipole moment of neutrino*, *Sov. J. Nucl. Phys.* **44** (1986) 546.
- [32] L. B. Okun, M. B. Voloshin, and M. I. Vysotsky, *Neutrino electrodynamics and possible consequences for solar neutrinos*, *Sov. Phys. JETP* **64** (1986) 446–452.
- [33] E. K. Akhmedov, *Resonant amplification of neutrino spin rotation in matter and the solar-neutrino problem*, *Phys. Lett.* **B213** (1988) 64–68.
- [34] C.-S. Lim and W. J. Marciano, *Resonant spin-flavor precession of solar and supernova neutrinos*, *Phys. Rev.* **D37** (1988) 1368.
- [35] R. S. Raghavan *et. al.*, *Direct tests for solar neutrino mass, mixing and majorana magnetic moment*, *Phys. Rev.* **D44** (1991) 3786–3790.
- [36] A. Friedland and A. Gruzinov, *Has super-kamiokande observed antineutrinos from the sun?*, *Astropart. Phys.* **19** (2003) 575–582, [[hep-ph/0202095](#)].
- [37] KamLAND Collaboration, K. Eguchi *et. al.*, *A high sensitivity search for anti- $\nu$ / $e$ 's from the sun and other sources at kamland*, *Phys. Rev. Lett.* **92** (2004) 071301, [[hep-ex/0310047](#)].
- [38] A. Friedland and A. Gruzinov, *Bounds on the magnetic fields in the radiative zone of the sun*, *Astrophys. J.* **601** (2004) 570–576, [[astro-ph/0211377](#)].
- [39] KamLAND Collaboration, T. Araki *et. al.*, *Measurement of neutrino oscillation with kamland: Evidence of spectral distortion*, *Phys. Rev. Lett.* **94** (2005) 081801, [[hep-ex/0406035](#)].
- [40] A. Friedland, *Do solar neutrinos probe neutrino electromagnetic properties?*, [[hep-ph/0505165](#)].
- [41] G. G. Raffelt, *New bound on neutrino dipole moments from globular cluster stars*, *Phys. Rev. Lett.* **64** (1990) 2856–2858.

# Atmospheric Neutrinos<sup>1</sup>

**Thomas K. Gaisser**

Bartol Research Institute and Department of Physics and Astronomy  
University of Delaware, Newark, DE 19716 USA

E-mail: gaisser@bartol.udel.edu

**Abstract.** This paper is a brief overview of the theory and experimental data of atmospheric neutrino production at the fiftieth anniversary of the experimental discovery of neutrinos.

## 1. Introduction

Atmospheric neutrinos are of interest as a beam for the study of neutrino oscillations and as the background and calibration beam in the search for neutrinos from astrophysical sources. The basic features of the flux of atmospheric neutrinos have been known since 1961. Fig. 1 is a plot of the numerical formulas of Zatsepin & Kuz'min [2], which shows the main features of the flux of atmospheric neutrinos at production. At low energy there are approximately two  $\nu_\mu + \bar{\nu}_\mu$  produced for each  $\nu_e + \bar{\nu}_e$  as a consequence of the decay sequence,

$$\pi^\pm \rightarrow \mu^\pm + \nu_\mu(\bar{\nu}_\mu) \rightarrow e^\pm + \nu_e(\bar{\nu}_e) + \bar{\nu}_\mu(\nu_\mu).$$

The flavor ratio

$$r \equiv \frac{\nu_\mu + \bar{\nu}_\mu}{\nu_e + \bar{\nu}_e} \quad (1)$$

increases with energy above a GeV because muons begin to reach the ground before they decay. Some modern calculations of the muon flavor ratio [3, 4, 5] are shown in Fig. 2.

The first detections of atmospheric neutrinos were made in the early sixties in deep mines by Reines *et al.* in South Africa [6] and by Menon *et al.* in the Kolar Gold Fields in India [7]. I have reviewed the history of atmospheric neutrino calculations and measurements in more detail elsewhere [8]. The modern era began in the 1980's with the construction of large underground detectors to search for proton decay. Interactions of atmospheric neutrinos are most numerous in the GeV range and hence constitute the main background for nucleon decay. Increasingly precise measurements of the atmospheric neutrino beam led to the discovery of oscillations [15] in the  $\nu_\mu \leftrightarrow \nu_\tau$  sector, as is well-known.

After a brief discussion of the current level of uncertainties in the flux of atmospheric neutrinos and the implications for atmospheric neutrinos as a beam for the study of oscillations, I conclude with some comments on atmospheric neutrinos as background for searches for astrophysical neutrinos.

<sup>1</sup> Research supported in part by the U.S. Department of Energy under DE-FG02 91ER40626.

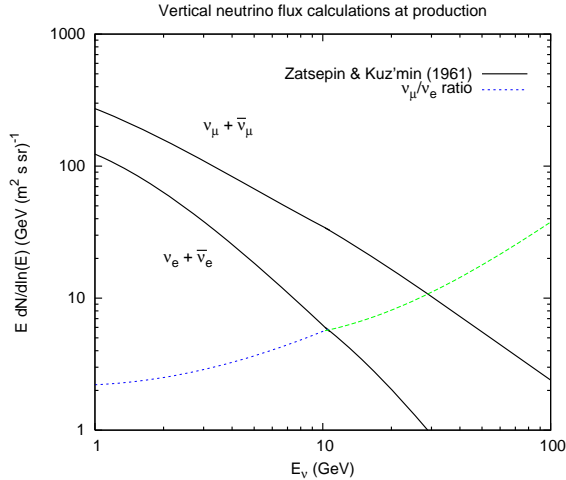


**Figure 1.** Plots of the numerical formulas of Ref. [2].

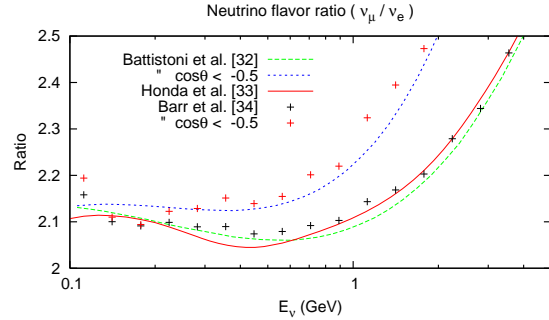


**Figure 2.** Comparison of the flavor ratio  $r$  from three calculations [3, 4, 5].

## 2. Uncertainties in the flux of atmospheric neutrinos

I want to distinguish three approaches to this subject. The first is to compare various calculations of the atmospheric neutrino flux, as in Fig. 2. Other examples of such comparison plots are given in Refs. [8, 9, 10]. There is now a large number of calculations that use different approaches, different interaction models and different representations of the primary cosmic-ray spectrum [3, 4, 5, 11, 12, 13, 14]. The size of differences among the various calculations can be used to gauge the uncertainty in the neutrino flux. The general conclusion of such exercises is that ratios agree to better than 5% while the uncertainty in normalization is larger and increases with energy. Differences among the three calculations shown in Fig. 2 for the flavor ratio  $r$  are at the level of 2%.

A related approach [16] is to vary the input parameters within the framework of a single calculational scheme. This approach seeks to avoid the danger of different calculations converging on similar results because they use common input assumptions. Uncertainties in hadronic interaction model dominate at low energy, while uncertainties in the primary spectrum become the dominant source of uncertainty above a few GeV. Within the set of parameters that characterize uncertainties in hadron production, those related to production of pions dominate at lower energy, while uncertainties in strange particle production dominate above 10 GeV, becoming comparable to the uncertainties from the primary spectrum in the TeV region. The importance of kaons is a consequence of the kinematics of meson decay convolved with a steep primary proton beam, which has the effect of making kaon production relatively more important for neutrinos than for muons. For  $E_\nu > 100$  GeV, kaons become the dominant source of atmospheric neutrinos. (See e.g. Fig. 8 of Ref. [9]). For analogous reasons, neutrinos from decay of charmed hadrons must eventually become the most abundant at sufficiently high energy even though charmed hadrons are produced much less often than strange hadrons. At some point (e.g. around several hundred TeV), uncertainties in hadro-production of charm will become the biggest source of uncertainty.

Overall uncertainty is at the level of  $\pm 15\%$  in the GeV range, rising to  $\pm 40\%$  for  $E_\nu = 1$  TeV. In contrast, uncertainties in the ratios are much smaller because uncertainties in the primary spectrum and in hadronic interactions cancel in lowest order in the ratios. The uncertainty in the flavor ratio of Eq. 1 is of order  $\pm 1\%$  for  $E_\nu < 30$  GeV, as illustrated in Figs. 3,4. These figures also show the ratios of neutrinos to anti-neutrinos, which are somewhat larger than the

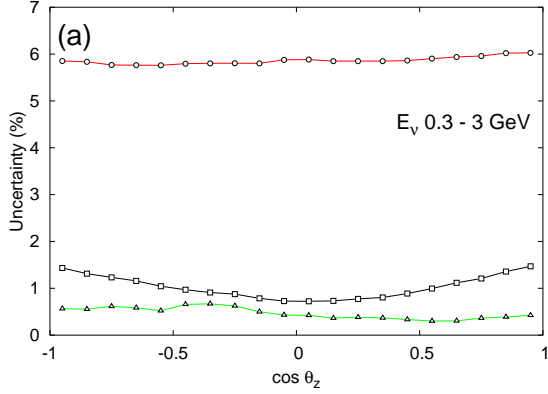


**Figure 3.** Uncertainties in neutrino ratios as estimated in Ref. [16] (0.3-3 GeV). (See text.)

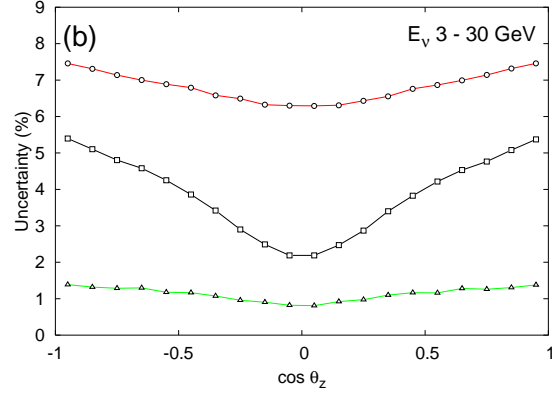


**Figure 4.** Same as (a) for 3-30 GeV. Lowest curve in (a) and in (b) shows  $r$ .

uncertainty in  $r$  (6-7% for  $\nu_e/\bar{\nu}_e$  and 1-5% for  $\nu_\mu/\bar{\nu}_\mu$ ) because they are more sensitive to the charge ratio of the parent mesons.

A precise knowledge of the flavor ratio  $r$  is particularly important in searching for subdominant oscillation effects with atmospheric neutrinos. For example, oscillations driven by the solar parameters are suppressed in the atmospheric neutrino beam by a factor that depends on the near equality of the three neutrino flavors in the *oscillated* atmospheric neutrino beam [17]. The observed number of  $\nu_e$  ( $N_e$ ) deviates from its value in the absence of solar effects by [17]

$$\frac{N_e}{N_e(0)} - 1 = P_2 \times (r \cos^2 \theta_{23} - 1), \quad (2)$$

where  $P_2(\delta m_{12}^2, \theta_{12})$  is the two-flavor mixing of  $\nu_e$  with the orthogonal combination of  $\nu_\mu$  and  $\nu_\tau$  [17]. In the sub-GeV region where pathlengths comparable to  $R_\oplus$  are long enough so that oscillations in the solar parameters can occur,  $r$  is close to two. Since the atmospheric mixing is characterized by  $\theta_{23} \sim 45^\circ$  and  $\cos^2 \theta_{23} \sim 0.5$ , the cancellation is nearly complete. As shown in Fig. 2, however,  $r_{\text{sub-GeV}}$  is somewhat larger than two (more so for atmospheric neutrinos in the vertically upward quadrant of phase space, which have pathlength  $> R_\oplus$ ), making a measurement of the octant of  $\theta_{23}$  possible in principle with sufficient statistics.

A similar suppression factor occurs in the atmospheric neutrino beam for effects that depend on the deviation of  $\sin^2 \theta_{13}$  from zero [18]. Such effects are, however, expected to be most important for  $E_\nu \sim 5$  GeV [18], where the flavor ratio is already significantly larger than two. In this case, the limiting factor is the intrinsically small size of  $\sin^2 \theta_{13}$  [18].

A different and complementary approach to determining the flux of atmospheric neutrinos accurately is to consider the analysis of the data of Super-K I [19] as a measurement of the flux of atmospheric neutrinos. The Super-K analysis proceeds by simultaneously fitting their data with the oscillation parameters together with a large set of parameters that characterize experimental and theoretical uncertainties. The theoretical parameters reflect deviations from the assumed production spectrum of atmospheric neutrinos (i.e. before oscillations). Shifts in the fitted parameters that describe the trial production spectrum of atmospheric neutrinos can be considered as a measurement of the atmospheric neutrino flux at production. This approach may be of greatest value for  $E_\nu \sim 100$  GeV to 1 TeV, because the normalization and oscillation parameters are primarily determined by the data at lower energy. In this regard, the adjustment of the spectral index found in the Super-K fit suggests that the neutrino spectrum continues into the high-energy range at a higher level than some calculations. A recent analysis [20] confirms this conclusion, as does the new analysis of Honda *et al.* [21].

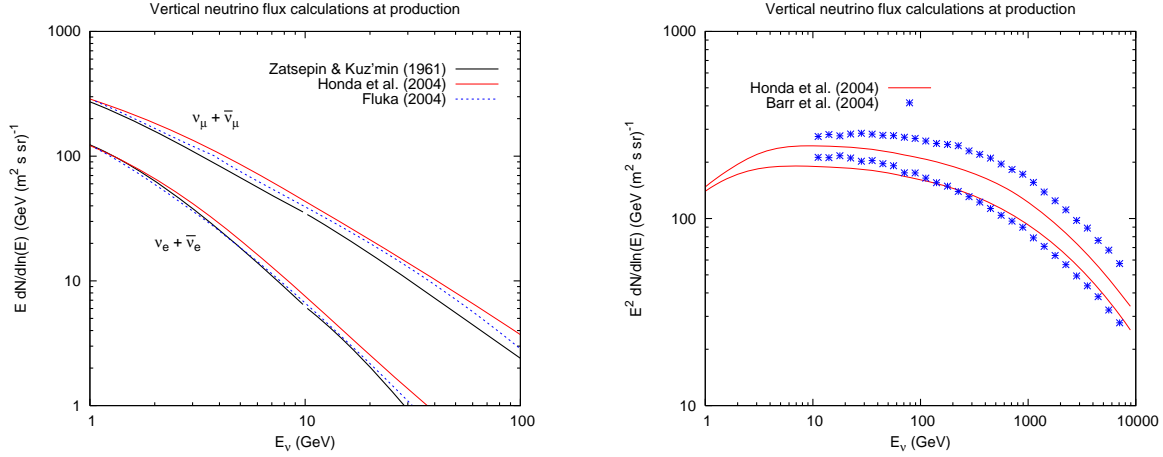


**Figure 5.** Neutrino flux from several calculations. The right panel shows muon neutrinos only, with  $\nu_\mu$  and  $\bar{\nu}_\mu$  plotted separately for each calculation. (Note the difference in energy ranges and powers of  $E$  in the two plots.)

### 3. Background for astrophysical neutrinos

Neutrino telescopes designed to search for astrophysical neutrinos generally have thresholds in the range of  $\sim 100$  GeV or higher. Figure 5 is a compilation of several calculations, including two that extend to high energy. The hard spectral index that comes out of the Super-K analysis [19] suggests that higher intensities should be preferred in the TeV region. The much larger ratio of  $\nu_\mu/\bar{\nu}_\mu$  in Ref. [5] as compared to that of Ref. [4] reflects the large associated production ( $p \rightarrow \Lambda K^+$ ) assumed by Barr et al. [5] at high energy. The production of strange and charmed particles is a significant source of uncertainty and needs more investigation. Decay of charmed hadrons is expected to become the dominant source of atmospheric neutrinos at sufficiently high energies,  $\sim 100$  TeV. At some level it will become the limiting factor in a search for a diffuse flux of extra-terrestrial neutrinos.

A well-understood feature of the atmospheric neutrino flux that may be useful in distinguishing signal from background is its characteristic dependence on zenith angle. A standard form for the differential spectrum of  $\nu_\mu + \bar{\nu}_\mu$  at high energy is

$$\phi_\nu(E_\nu) = \frac{\phi_N(E_\nu)}{1 - Z_{NN}} \times \sum_{i=1}^3 \frac{A_i}{1 + B_i \cos \theta E_\nu / \epsilon_i}, \quad (3)$$

where the three terms correspond respectively to neutrinos from decay of pions, kaons and charmed hadrons. The overall flux is proportional to the primary spectrum of nucleons,  $\phi_N(E_\nu)$ , evaluated at the energy of the neutrino and scaled by a factor  $1/(1 - Z_{NN})$  related to the nucleon attenuation length. Each flavor of hadron has a characteristic critical energy,  $\epsilon_i$ , above which the hadron is more likely to interact than to decay. The shape of each contribution also depends on a numerical factor ( $B_i$ ) and on the cosine of the zenith angle. The latter is the “secant theta” effect. For  $E_\nu \gg \epsilon_i / (B_i \cos \theta)$  the contribution is inversely proportional to  $\cos \theta$  and asymptotically one power of energy steeper than the primary spectrum. At very large angles ( $\sim \theta > 70^\circ$ ) the secant theta term is limited by the curvature of the Earth.

Neutrinos from astrophysical sources do not depend on the local zenith angle at which they are observed. Therefore in principle the known zenith angle dependence of the atmospheric background is available as an extra parameter to distinguish background from signal. The most obvious example would be the contrast between atmospheric background and an isotropic, diffuse extraterrestrial flux of high-energy neutrinos. Because the contribution from charm is

also isotropic (until extremely high energy), the distinction disappears when the intensity of the extraterrestrial neutrinos is at the level of atmospheric neutrinos from decay of charmed hadrons.

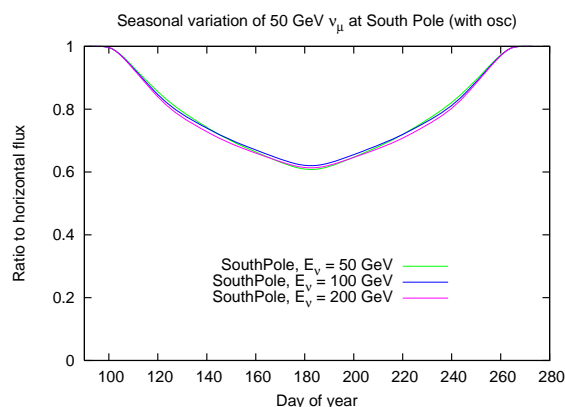


**Figure 6.** Relative variation of the intensity of atmospheric  $\nu_\mu + \bar{\nu}_\mu$  from the direction of the Sun as viewed from the South Pole during Austral winter (including oscillations).

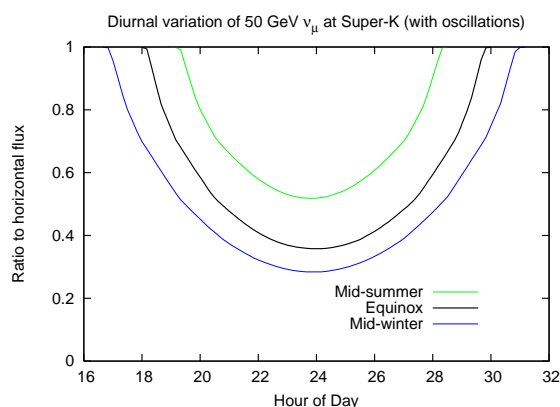


**Figure 7.** Relative variation of the intensity of 50 GeV atmospheric  $\nu_\mu + \bar{\nu}_\mu$  from the direction of the Sun as viewed from Super-K, including oscillation effects.

For point sources of neutrinos observed from mid-latitude detectors, variation of the background in the direction of a potential source as it rises and sets can in principle also help to distinguish background from signal. A related example is the indirect search for neutrinos from WIMP annihilation in the Sun. Figures 67 show the expected diurnal variation of the atmospheric background from the direction of the Sun as seen from the South Pole and from Super-K.

- [1] Zatsepin, G.T. & Kuz'min, V.A. Sov. Phys. JETP 12, 1171 (1961).
- [2] Zatsepin, G.T. & Kuz'min, V.A. Sov. Phys. JETP 14, 1294 (1962).
- [3] Battistoni, G. et al., Astropart. Phys. 19, 269 (2003) (Erratum pp 291-294).  
<http://www.mi.infn.it/~battist/nuetrino.html>
- [4] Honda, M. et al., Phys. Rev. D 70, 043008 (2004).  
<http://www.icrr.u-tokyo.ac.jp/~mhonda/>
- [5] Barr, G.D. et al., Phys. Rev. D 70, 023006 (2004).  
<http://www-pnp.physics.ox.ac.uk/~barr/fluxfiles/>
- [6] Reines, F. et al., Phys. Rev. Letters 15, 429 (1965).
- [7] Achar, C.V. et al., Phys. Lett. 18, 196 (1965).
- [8] T.K. Gaisser, Physica Scripta T121 (2005) 51 (astro-ph/0502380).
- [9] T.K. Gaisser, Nucl. Phys. B (Proc. Suppl.) 118 (2003) 109.
- [10] Giles Barr, Nucl. Phys. (Proc. Suppl.) 143 (2005) 89.
- [11] Wentz, J. et al., Phys. Rev. D 67, 073020 (2003).
- [12] Liu, Y. et al., Phys. Rev. D 67, 073022 (2003).
- [13] Favier, J. et al., Phys. Rev. D 68, 093006 (2003).
- [14] See T.K. Gaisser & M. Honda, Ann. Revs. Nucl. Part. Sci. 52 (2002) 153 for a review of earlier calculations.
- [15] Fukuda, Y. et al., Phys. Rev. Lett. 81, 1562 (1998).
- [16] G. Barr et al., Phys. Rev. D 74 (2006) 094009.
- [17] O.L.G. Perez & A. Yu. Smirnov, Nucl. Phys. B456 (1999) 204 and B680 (2004) 479.
- [18] S.T. Petcov & T. Schwetz, Nucl. Phys. B740 (2006) 1.
- [19] Ashie, Y. et al., Phys. Rev. D 71 (2005) 112005.
- [20] M.C. Gonzalez-Garcia, M. Maltoni & J. Rojo, hep-ph/0607324.
- [21] M. Honda *et al.*, astro-ph/0611418.

# Radiochemical solar neutrino experiments

V N Gavrin<sup>1</sup> and B T Cleveland<sup>2,3</sup>

<sup>1</sup> Institute for Nuclear Research of the Russian Academy of Sciences, Moscow 117312, Russia

<sup>2</sup> Department of Physics, University of Washington, Seattle Washington 98195, USA

E-mail: <sup>1</sup> gavrin@dionis.iasnet.ru, <sup>2</sup> bclevela@snolab.ca

## Abstract.

Radiochemical experiments have been crucial to solar neutrino research. Even today, they provide the only direct measurement of the rate of the proton-proton fusion reaction,  $p + p \rightarrow d + e^+ + \nu_e$ , which generates most of the Sun's energy. We first give a little history of radiochemical solar neutrino experiments with emphasis on the gallium experiment SAGE – the only currently operating detector of this type. The combined result of all data from the Ga experiments is a capture rate of  $67.6 \pm 3.7$  SNU. For comparison to theory, we use the calculated flux at the Sun from a standard solar model, take into account neutrino propagation from the Sun to the Earth and the results of neutrino source experiments with Ga, and obtain  $67.3_{-3.5}^{+3.9}$  SNU. Using the data from all solar neutrino experiments we calculate an electron neutrino  $pp$  flux of  $\phi_{pp}^{\bar{\nu}} = (3.41_{-0.77}^{+0.76}) \times 10^{10}/(\text{cm}^2\text{-s})$ , which agrees well with the prediction from a detailed solar model of  $\phi_{pp}^{\bar{\nu}} = (3.30_{-0.14}^{+0.13}) \times 10^{10}/(\text{cm}^2\text{-s})$ . Four tests of the Ga experiments have been carried out with very intense reactor-produced neutrino sources and the ratio of observed to calculated rates is  $0.88 \pm 0.05$ . One explanation for this unexpectedly low result is that the cross section for neutrino capture by the two lowest-lying excited states in  $^{71}\text{Ge}$  has been overestimated. We end with consideration of possible time variation in the Ga experiments and an enumeration of other possible radiochemical experiments that might have been.

## 1. Introduction and a little history

Our knowledge of neutrinos from the Sun is based on seven experiments: Homestake, Kamiokande, SAGE, Gallex, GNO, Super-Kamiokande and SNO. More than half of these are radiochemical experiments.

The detection of neutrinos by use of the inverse  $\beta$  decay reaction was proposed 60 years ago by Bruno Pontecorvo [1]. This method of detection, which is the basis for radiochemical experiments, has played a fundamental role in solar neutrino investigation. The idea to use neutrino capture in  $^{37}\text{Cl}$  to observe the “undetectable” new particle proposed by Wolfgang Pauli was brilliantly realized to observe solar neutrinos by R. Davis and collaborators in the world-famous experiment at the Homestake Gold Mine [2, 3, 4]. The  $^{37}\text{Cl}$  experiment was built 4200 m.w.e. (meters of water equivalent) underground and began to collect data in 1967. Between 1970–1994, 108 extractions of Ar were made from a tank that contained 615 tons of  $\text{C}_2\text{Cl}_4$ . The number of  $^{37}\text{Ar}$  atoms collected in each run was measured in a miniature proportional counter. The result for the first measured capture rate of solar neutrinos at the Earth was  $2.56 \pm 0.23$  SNU. The SNU unit (defined as 1 neutrino capture per day in a target that contains  $10^{36}$  atoms of the neutrino-absorbing isotope) was specially introduced by John Bahcall, who had a fundamental role in the funding of the Cl experiment and the interpretation of its results, and whose contributions cannot be overestimated. Bahcall was the first to fully develop a solar model that included

<sup>3</sup> Present address: SNOLAB, PO Box 159, Lively, Ontario P3Y 1M3, Canada

all the physical parameters needed to calculate the solar neutrino flux at the Earth. He worked tirelessly to refine his calculations and it was the robustness of his solar model that eventually led all people to understand the significance of the discrepancy between the result of the Cl experiment and standard solar model (SSM) predictions.

The discrepancy identified in the Cl experiment attracted the attention of a significant number of scientists and it soon became known as “the solar neutrino problem”. This problem continued to bother the mind of scientists for more than 30 years. Especially important was the confirmation of the discrepancy by the Kamiokande experiment [5], a real-time detector of solar neutrinos that used a completely different method of detection – electron scattering, and which began to collect data in 1987. As a result there were no doubts that the flux of neutrinos in the high-energy part of the solar neutrino spectrum was significantly less than the calculations of the SSM. Kamiokande, with an analysis threshold of 7 MeV, was sensitive only to the high-energy  $^8\text{B}$  neutrinos and the Cl experiment, whose major response was from the superallowed analog state at an excitation energy of 5.0 MeV in  $^{37}\text{Ar}$ , was also mostly sensitive to the  $^8\text{B}$  neutrinos. Another significant development during this time was the confirmation of the results of the Bahcall SSM by a solar model independently developed by Sylvaine Turck-Chièze and collaborators [6].

Despite many attempts, the combination of these two experiments could not be explained on the basis of solar physics; rather, many scientists began to believe that it was necessary to reject some of our old ideas about neutrino properties and to develop new ones. Conclusive evidence for this suggestion could be obtained by measuring the low-energy part of the solar neutrino spectrum, which is produced in reactions that provide the vast majority of the Sun’s energy, and whose flux can be well predicted from the measured solar luminosity combined with a simple solar model. The need for experiments sensitive to low-energy solar neutrinos was recognized shortly after the first results from the Cl experiment were announced and many people began to consider radiochemical experiments with low-energy sensitivity, such as those shown in Table 1.

**Table 1.** Radiochemical solar neutrino detectors considered in 1972 [7] The relative response is given to the various sources of solar neutrinos. The mass of target element is the number of tons required to yield 1 neutrino capture/day from the sum of the  $pp$  and  $pep$  reactions. The relative response and mass were calculated from the 1972 values of solar flux and used cross sections that neglected excited states.

Target	Product	Relative response (%)					Mass (tons)
		$pp$	$pep$	$^7\text{Be}$	$^8\text{B}$	CNO	
$^{87}\text{Rb}$	$^{87\text{m}}\text{Sr}$	74	2	21	1	3	32
$^{55}\text{Mn}$	$^{55}\text{Fe}$	67	3	25	1	3	420
$^{71}\text{Ga}$	$^{71}\text{Ge}$	69	2	26	0	3	19
$^7\text{Li}$	$^7\text{Be}$	0	18	15	51	16	17

From these possibilities attention focused on  $^7\text{Li}$ , proposed in 1969 by John Bahcall [8], and on  $^{71}\text{Ga}$ , proposed in 1965 by Vadim Kuzmin [9]. Because of its high capture rate, low energy threshold of 233 keV and favorable half-life of 11.4 days, a Ga experiment appeared to be a most attractive possibility. The main problems with the Ga experiment were the acquisition of several tens of tons of the expensive element gallium and the development of a nearly lossless procedure for the extraction and purification of  $^{71}\text{Ge}$ .

## 2. The Ga experiment

Laboratory research to develop a gallium experiment began approximately in 1975. In the United States this work took place at Brookhaven National Laboratory under the direction of Ray Davis with

participation of B. Cleveland, J. Evans, G. Friedlander, K. Rowley, R. Stoener from Brookhaven, and W. Frati and K. Lande from the University of Pennsylvania [10]. Methods were developed to extract germanium from liquid gallium metal and from a  $\text{GaCl}_3$  solution. After a few years, this group achieved success in development of these methods and chose the method based on  $\text{GaCl}_3$  solution. To carry out the experiment a collaboration was initiated with a group from the Max Planck Institute at Heidelberg. Despite repeated requests and favorable reviews, the Ga experiment was, however, not funded in the United States. Rather, a special subcommittee of the Nuclear Science Advisory Committee recommended that interested scientists associate themselves with groups in Western Europe and/or the Soviet Union. The western European group, called Gallex, had been formed by the Heidelberg group under the direction of Till Kirsten when it became apparent that the experiment would not be funded in the US.

In the Soviet Union, at the Institute for Nuclear Research, laboratory investigations to develop a gallium experiment began about the same time in 1975. It was initially based on a  $\text{GaCl}_3$  solution, but when it was learned that Soviet industry could not provide the necessary radioactive purity in 50 tons of solution, the project was changed to gallium metal. Using Davis's idea, the extraction of minute quantities of  $^{71}\text{Ge}$  from many tons of metallic gallium was independently developed. One advantage of metallic Ga is that it is significantly less sensitive to radioactive impurities. In 1980 an installation was built that contained 300 kg of Ga metal. In addition to testing the technology, this work also yielded a new limit on the law of conservation of electric charge [11]. By 1985 a pilot installation containing 7.5 tons of metallic gallium had been constructed at Troitsk.

The Soviet group built their experiment at the Baksan Neutrino Observatory in the Caucasus mountains. The first Ga exposure began in December 1989 and data collection has continued since that time. The Gallex built their experiment at the Gran Sasso tunnel in Italy and collected data from 1991-1997. In 1998 they were reconstituted as the Gallium Neutrino Observatory (GNO) and they continued operation until 2003 [12].

### 3. SAGE

In 1986 the Soviet-American collaboration SAGE was officially established to carry out the gallium solar neutrino experiment at the Baksan Neutrino Observatory. The experiment is situated in a specially built deep underground laboratory where the measured muon flux is  $(3.03 \pm 0.10) \times 10^{-9}/(\text{cm}^2 \text{ s})$ . It is located 3.5 km from the entrance of a horizontal adit excavated into the side of a mountain. The rock gives an overhead shielding equivalent to 4700 m of water and reduces the muon flux by a factor of  $10^7$ .

The mass of gallium used in SAGE at the present time is about 50 tonnes. It is in the form of liquid metal and is contained in 7 chemical reactors. A measurement of the solar neutrino capture rate begins by adding to the gallium a stable Ge carrier. The carrier is a Ga-Ge alloy with a known Ge content of approximately  $350 \mu\text{g}$  and is distributed equally among all reactors. The reactor contents are stirred thoroughly to disperse the Ge throughout the Ga mass. After a typical exposure interval of four weeks, the Ge carrier and  $^{71}\text{Ge}$  atoms produced by solar neutrinos and background sources are chemically extracted from the Ga using procedures described in [13, 14]. The final step of the chemical procedure is the synthesis of germane ( $\text{GeH}_4$ ), which is used as the proportional counter fill gas with an admixture of (90–95)% Xe. The total efficiency of extraction is the ratio of mass of Ge in the germane to the mass of initial Ge carrier and is typically  $(95 \pm 3)\%$ . The systematic uncertainty in this efficiency is 3.4%, mainly arising from uncertainties in the mass of added and extracted carrier. The proportional counter is placed in the well of a NaI detector that is within a large passive shield and is counted for a typical period of 4–6 months.

Based on criteria described in [13], a group of events is selected from each extraction that are candidate  $^{71}\text{Ge}$  decays. These events are fit to a maximum likelihood function [15], assuming that they originate from an unknown but constant-rate background and the exponentially decaying rate of  $^{71}\text{Ge}$ . A single run result has little significance because of its large statistical uncertainty.

The global best fit capture rate for all SAGE data from January 1990 through December 2005 (139

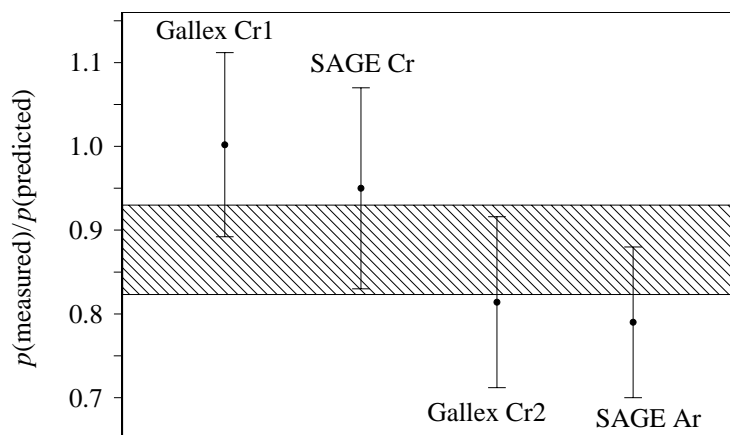


**Figure 1.** Results of all neutrino source experiments with Ga. The hashed region is the weighted average of the four experiments. See [20] for details.

runs and 264 separate counting sets) is  $66.2^{+3.5}_{-3.4}$  SNU, where the uncertainty is statistical only. If one considers the *L*-peak and *K*-peak data separately, the results are  $67.6^{+5.5}_{-5.3}$  SNU and  $65.5^{+4.7}_{-4.5}$  SNU, respectively. The agreement between the two peaks serves as a strong check on the robustness of the event selection criteria. The systematic effects fall into three main categories: those associated with extraction efficiency, with counting efficiency and with backgrounds. For a complete description of these effects see [13]. Including all uncertainties, our overall result is thus  $66.2^{+3.5}_{-3.4}$  (stat) $^{+3.8}_{-3.4}$  (syst) SNU. If we combine the SAGE statistical and systematic uncertainties in quadrature, the result is  $66.2^{+5.2}_{-4.8}$  SNU.

The final result from 123 runs in the Gallex and GNO experiments is  $69.3 \pm 5.5$  (stat + syst) SNU [12]. The weighted combination of all the Ga experiments, SAGE, Gallex and GNO, is thus

$$67.6 \pm 3.7 \text{ SNU.} \quad \text{Present Ga experiment result.} \quad (1)$$

It was very good that for many years there were two Ga experiments operating at the same time and it is indeed unfortunate that the GNO experiment was terminated for non-scientific reasons.

#### 4. Source experiments

The experimental procedures of both Ga experiments, including the chemical extraction, counting and analysis techniques, have been checked by exposing the gallium target to reactor-produced neutrino sources whose activity was close to 1 MCi. Gallex has twice used  $^{51}\text{Cr}$  sources to irradiate their entire target; SAGE has irradiated about 25% of their target with a  $^{51}\text{Cr}$  source and an  $^{37}\text{Ar}$  source [16, 17]. The results, expressed as the ratio *R* of the measured  $^{71}\text{Ge}$  production rate to that expected due to the source strength, are shown in Figure 4. The weighted average value of the ratio for the four experiments is  $R = 0.88 \pm 0.05$ , more than two standard deviations less than unity.

Since other auxiliary tests, especially the  $^{71}\text{As}$  experiment of Gallex, have given great confidence in the knowledge of the various efficiencies in the Ga experiments, the combined result of these source tests should not be considered to be a measurement of the entire throughput of the Ga experiments. Rather, we believe that, although not statistically conclusive, the combination of these experiments suggests that the predicted rates may be overestimated. The most likely hypothesis<sup>4</sup> is that the cross sections for neutrino capture to the lowest two excited states in  $^{71}\text{Ge}$ , both of which can be reached using either  $^{51}\text{Cr}$  or  $^{37}\text{Ar}$  sources, have been overestimated [19]. If the contribution of these two excited states to the predicted rate is set to zero, then  $R = 0.93 \pm 0.05$ , reasonably consistent with unity. A new experiment with a considerably higher rate from the neutrino source is needed to settle this question.

As a side note, during the time of the SAGE  $^{37}\text{Ar}$  source experiment, which used 26 tonnes of Ga, solar neutrino extractions were also made from the remaining 22 tonnes of Ga. Since the SAGE counting

<sup>4</sup> For an alternative explanation, based on transitions to sterile neutrinos, see [18].

**Table 2.** Factors needed to compute the capture rate in  $^{71}\text{Ga}$  solar neutrino experiments. The units of flux are  $10^{10}(pp)$ ,  $10^9(^7\text{Be})$ ,  $10^8(pep, ^{13}\text{N}, ^{15}\text{O})$ ,  $10^6(^8\text{B}, ^{17}\text{F})$ , and  $10^3(hep)$   $\text{cm}^{-2}\text{s}^{-1}$ . The uncertainty values are at 68% confidence.

Spectrum comp. $i$	Flux $\phi_i^\odot$		$\langle P_i^{ee} \rangle$	$\langle \sigma_i \rangle$ ( $10^{-46}$ $\text{cm}^2$ )	Capture rate $R_i$ (SNU)	
	BP04	BP04+			BP04	BP04+
$pp$	$5.94(1^{+0.01}_{-0.01})$	5.99	$0.555(1^{+0.038}_{-0.040})$	$11.75(1^{+0.024}_{-0.023})$	$38.7(1^{+0.046}_{-0.047})$	39.1
$pep$	$1.40(1^{+0.02}_{-0.02})$	1.42	$0.517(1^{+0.033}_{-0.034})$	$194.4(1^{+0.17}_{-0.024})$	$1.41(1^{+0.17}_{-0.046})$	1.43
$^7\text{Be}$	$4.86(1^{+0.12}_{-0.12})$	4.65	$0.537(1^{+0.036}_{-0.037})$	$68.22(1^{+0.070}_{-0.023})$	$17.8(1^{+0.14}_{-0.13})$	17.0
$^{13}\text{N}$	$5.71(1^{+0.37}_{-0.35})$	4.06	$0.539(1^{+0.036}_{-0.038})$	$56.86(1^{+0.099}_{-0.023})$	$1.75(1^{+0.38}_{-0.35})$	1.24
$^{15}\text{O}$	$5.03(1^{+0.43}_{-0.39})$	3.54	$0.531(1^{+0.035}_{-0.036})$	$107.2(1^{+0.13}_{-0.023})$	$2.86(1^{+0.45}_{-0.39})$	2.02
$^{17}\text{F}$	$5.91(1^{+0.44}_{-0.44})$	3.97	$0.531(1^{+0.035}_{-0.036})$	$107.8(1^{+0.13}_{-0.023})$	$0.03(1^{+0.46}_{-0.44})$	0.02
$^8\text{B}$	$5.79(1^{+0.23}_{-0.23})$	5.26	$0.374(1^{+0.044}_{-0.039})$	$21580(1^{+0.32}_{-0.15})$	$4.67(1^{+0.40}_{-0.28})$	4.25
$hep$	$7.88(1^{+0.16}_{-0.16})$	8.04	$0.347(1^{+0.061}_{-0.054})$	$66300(1^{+0.33}_{-0.16})$	$0.02(1^{+0.37}_{-0.23})$	0.02
Total					$67.3^{+3.9}_{-3.5}$	65.1

system was filled with samples from the  $^{37}\text{Ar}$  source, we transported the  $^{71}\text{Ge}$  extracted from the solar runs to Gran Sasso, where  $\text{GeH}_4$  was synthesized and the samples were counted in the GNO counting system. The combined result of six such solar runs was  $64^{+24}_{-22}$  SNU [21], in excellent agreement with the overall result of the Ga experiments.

## 5. Comparison of gallium result to predictions of standard solar model

The capture rate  $R_i$  of component  $i$  of the solar neutrino spectrum is given in a radiochemical experiment by

$$R_i = \phi_i^\odot \langle P_i^{ee} \rangle \langle \sigma_i \rangle \quad (2)$$

where  $\phi_i^\odot$  is the amplitude of the flux from this solar component at the production point in the Sun,  $\langle P_i^{ee} \rangle$  is the integral over the solar spectrum of the probability of survival of the electron neutrino during its travel from where it is produced in the Sun to where it is detected at the Earth, and  $\langle \sigma_i \rangle$  is the integral of the cross section for neutrino capture over the spectrum at the Earth. The physical origin for the reduction of the electron component of the solar neutrino flux is the now well-established mechanism of MSW neutrino oscillations [22].

Values of  $\phi_i^\odot$ ,  $\langle P_i^{ee} \rangle$  and  $\langle \sigma_i \rangle$  are given for each neutrino component in Table 2. The fluxes are from two solar models with differing composition [23]. The other quantities were calculated assuming three-neutrino mixing to active neutrinos with parameters  $\Delta m_{12}^2 = (7.92 \pm 0.36) \times 10^{-5} \text{ eV}^2$ ,  $\theta_{12} = 34.1^{+1.7}_{-1.5}$  degrees and  $\theta_{13} = 5.44^{+2.79}_{-5.44}$  degrees [24]. The approximate formulae given in [25] were used for the survival probability  $P_i^{ee}(E)$ . Since radiochemical experiments average over a long exposure interval, regeneration in the Earth was neglected. The cross sections  $\sigma(E)$  were taken from [26] but were modified to delete the effect of the lowest two excited states in  $^{71}\text{Ge}$  according to the results of the neutrino source experiments as given in the previous section. The neutrino spectra were taken from [26] ( $pp$  and CNO), [27] ( $^8\text{B}$ ) and [28] ( $hep$ ).

There is excellent agreement between the calculated ( $67.3^{+3.9}_{-3.5}$  SNU) and observed ( $67.6 \pm 3.7$  SNU) capture rates in  $^{71}\text{Ga}$ .

## 6. The $pp$ neutrino flux

One of the main purposes of the Ga experiment is to provide information that leads directly to the experimental determination of the flux of  $pp$  neutrinos at the Earth. In this Section we will assume the Sun is generating energy by the  $pp$  cycle, and not dominantly by the CNO cycle, and will derive the present best value for the  $pp$  flux directly from the results of neutrino experiments.

To obtain the  $pp$  flux we begin with the combined capture rate from the SAGE and GALLEX/GNO experiments given above of  $67.6 \pm 3.7$  SNU. This rate is the sum of the rates from all the components of the solar neutrino flux, which we denote by  $[pp+{}^7\text{Be}+\text{CNO}+pep+{}^8\text{B}|\text{Ga}]$ . (We ignore the *hep* contribution.)

The only one of these flux components that is known from direct experiment is the  ${}^8\text{B}$  flux, measured by SNO to be  $[{}^8\text{B}|\text{SNO}] = (1.68 \pm 0.11) \times 10^6$  electron neutrinos/( $\text{cm}^2\text{-s}$ ) [29] at the Earth. We multiply this flux by the cross section for  ${}^8\text{B}$  given in Table 2 and find that the contribution to the Ga experiment is  $[{}^8\text{B}|\text{Ga}] = 3.7^{+1.2}_{-0.7}$  SNU. Subtracting this measured value from the total Ga rate gives  $[pp+{}^7\text{Be}+\text{CNO}+pep|\text{Ga}] = 64.0^{+3.7}_{-3.9}$  SNU.

The measured capture rate in the Cl experiment is  $[{}^7\text{Be}+\text{CNO}+pep+{}^8\text{B}|\text{Cl}] = 2.56 \pm 0.23$  SNU [4]. In a manner analogous to Ga we can calculate the cross section for  ${}^8\text{B}$  neutrinos on  ${}^{37}\text{Cl}$ , including the suppression factor, to be  $1.02(1 \pm 0.046) \times 10^{-42}$   $\text{cm}^2$ . We multiply this by the flux measured by SNO and deduce that the contribution of  ${}^8\text{B}$  to the Cl experiment is  $[{}^8\text{B}|\text{Cl}] = 1.72 \pm 0.14$  SNU. Subtracting this component from the total leaves  $[{}^7\text{Be}+\text{CNO}+pep|\text{Cl}] = 0.84 \pm 0.27$  SNU, all of which is due to neutrinos of medium energy.

We assume the Sun is generating its energy via the  $pp$  cycle so these medium-energy neutrinos are dominated by  ${}^7\text{Be}$ . We can thus make the approximation that  $[{}^7\text{Be}+\text{CNO}+pep|\text{Ga}] = [{}^7\text{Be}+\text{CNO}+pep|\text{Cl}] \times \text{cross section for } {}^7\text{Be on Ga} / \text{cross section for } {}^7\text{Be on Cl} = (0.84 \pm 0.27) \times [71.9(1^{+0.07}_{-0.03})] / [2.40(1 \pm 0.02)] = 23.9^{+7.9}_{-7.6}$  SNU. There is an additional error due to the approximation used, which is estimated to be 10%, giving the result  $[{}^7\text{Be}+\text{CNO}+pep|\text{Ga}] = 23.9^{+8.1}_{-8.0}$  SNU.

We subtract this contribution from the rate given above and get the result for the measured  $pp$  rate in the Ga experiment  $[pp|\text{Ga}] = [pp+{}^7\text{Be}+\text{CNO}+pep|\text{Ga}] - [{}^7\text{Be}+\text{CNO}+pep|\text{Ga}] = 40.1^{+6.6}_{-9.0}$  SNU. Dividing this capture rate by the cross section for capture of  $pp$  neutrinos of  $11.8(1^{+0.024}_{-0.023}) \times 10^{-46}$   $\text{cm}^2$  gives the measured electron neutrino  $pp$  flux at Earth of  $\phi_{pp}^{\dagger} = (3.41^{+0.76}_{-0.77}) \times 10^{10}/(\text{cm}^2\text{-s})$ . The major component of the error in this  $pp$  flux measurement is due to the poor knowledge of the medium-energy neutrinos which was inferred from the Cl experiment.

For comparison, the standard solar model calculates the  $pp$  flux produced in the Sun to be  $\phi_{pp}^{\odot} = 5.94(1 \pm 0.01) \times 10^{10}/(\text{cm}^2\text{-s})$  [23]<sup>5</sup>. If we multiply this rate by the average survival probability for  $pp$  neutrinos, which from Table 2 is  $0.555(1^{+0.038}_{-0.040})$ , we obtain a  $pp$  flux at the Earth of  $\phi_{pp}^{\dagger} = (3.30^{+0.13}_{-0.14}) \times 10^{10}/(\text{cm}^2\text{-s})$ , in excellent agreement with the value determined above from solar neutrino experiments.

In the future it will be possible to reduce the error in this flux measurement when there are new experiments that directly measure the  ${}^7\text{Be}$  flux, as anticipated by Borexino and KamLAND, and the CNO flux, as anticipated by SNO+. The dominant error should eventually be due to the inaccuracy of the Ga measurement itself.

## 7. Is the neutrino capture rate in Ga constant?

Short-term variations in the Gallex-GNO rate with periods from 15 days to a few 100 days have been considered by Pandola [30] and Sturrock *et al.* [31]. Pandola's analysis finds no variability but Sturrock *et al.* see evidence for variation if one considers the Gallex and GNO data sets separately.

The possibility of variability over longer time periods has been considered by several authors [32, 33]. In a plot of the data there appears to be a difference between early and late time periods, which gives a visual hint of a long-term decrease, as illustrated in Figure 2. The Gallex-GNO data is shown on the left

<sup>5</sup> The error here is only 1% because the measured solar luminosity was used in this calculation.

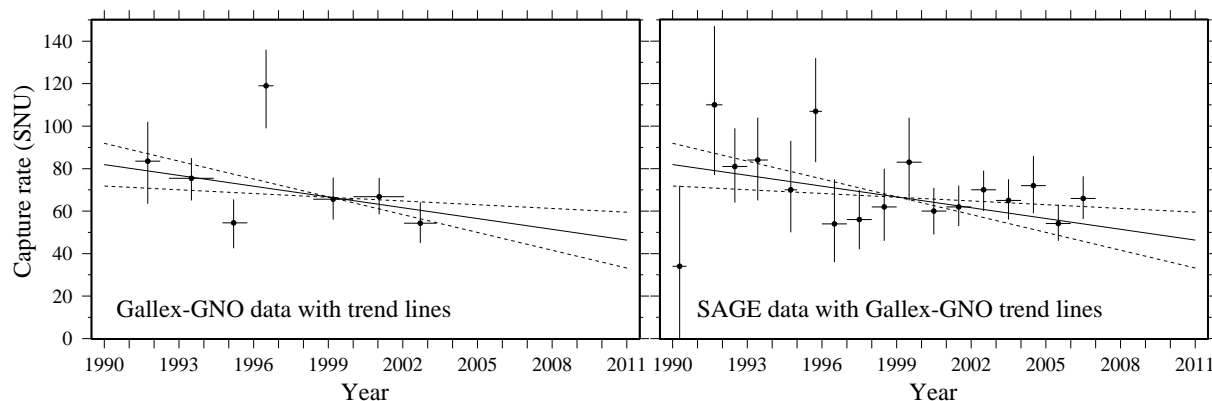


**Figure 2.** Gallex-GNO results (left panel) and SAGE results (right panel) vs time. See text for further explanation.

of this Figure where the data have been grouped by the experimenters into 7 intervals. The SAGE data, divided into intervals of one calendar year, is shown on the right of Figure 2. The average rate prior to 1997 is higher in both experiments than in the data after 1997.

If one assumes the rate in Gallex-GNO varies linearly in time then the best fit gives [12]

$$\text{Capture rate} = 82 \pm 10 - (1.7 \pm 1.1) \times [t(\text{year}) - 1990]. \quad (3)$$

These trend lines are plotted for both experiments in Figure 2 and there is reasonably good visual agreement with the measured data.

When examined quantitatively, however, the evidence for long-term variability becomes less convincing. A  $\chi^2$  test applied to the Gallex-GNO data with (without) the assumed time variation yields  $\chi^2/\text{dof} = 10.8/5$  ( $13.2/6$ ), prob. = 5.6% (4.0%), i.e., the fit to both the time-varying rate and to a constant rate is more or less equally bad. For the SAGE data the fit to a constant rate gives  $\chi^2/\text{dof} = 11.7/16$ , prob. = 76%, whereas the fit to the central Gallex-GNO trend line yields  $\chi^2/\text{dof} = 11.4/17$ , prob. = 83%, i.e., the fit to both rate hypotheses is quite good. At the present time we cannot differentiate between these two hypotheses, but it should become possible to do so with considerable additional data.

Up to now it is not known if this apparent variability is a statistical fluctuation or an indication of a real effect, such as has been considered by Pulido *et al.* [34].

## 8. Other radiochemical experiments

Several other radiochemical experiments to measure solar neutrinos have been developed to various degrees. These include  $^{127}\text{I} \rightarrow ^{127}\text{Xe}$  [35, 36] and  $^{81}\text{Br} \rightarrow ^{81}\text{Kr}$  [37] experiments that would in many ways be similar to the  $^{37}\text{Cl}$  experiment, and a  $^{97}\text{Mo} \rightarrow ^{97}\text{Tc}$  [38] experiment that could measure the long-term history of the  $^8\text{B}$  solar neutrino flux. Although very considerable efforts were expended in the United States on the  $^{127}\text{I}$  and  $^{97}\text{Mo}$  experiments, they were never brought to fruition, mainly because of a lack of funding.

The  $^7\text{Li} \rightarrow ^7\text{Be}$  experiment has continued to be pursued in Russia. Methods for the efficient extraction of Be from metallic Li have been proven [39] and an experiment could, in principle, be built [40].

At the present time interest in radiochemical experiments has greatly decreased and it is only direct-counting experiments that are under development. Nonetheless, the radiochemical experiments stimulated great interest in the solar neutrino problem, which led to the real-time experiments Super-Kamiokande, SNO and KamLAND.

## Acknowledgments

We thank Thomas Bowles for leading the American side of the SAGE collaboration for many years and for organizing this excellent conference. We are grateful to our SAGE colleagues for their hard work and perseverance. We wish to thank Victor Matveev, Valery Rubakov and Albert Tavkhelidze of the Institute for Nuclear Research RAS, Russia for their vigorous and continuous support.

## References

- [1] Pontecorvo B M 1946 *Inverse  $\beta$  Process Chalk River Laboratory Report PD-205*
- [2] Davis R Jr 1964 *Phys Rev Lett* **12** 303
- [3] Davis R Jr, Harmer D S and Hoffman K C 1968 *Phys Rev Lett* **20** 1205
- [4] Cleveland B T *et al.* 1998 *Astrophys J* **496** 505
- [5] Fukuda Y 1996 *Phys Rev Lett* **77** 1683
- [6] Turck-Chièze S *et al.* 2004 *Phys Rev Lett* **93** 211102 (*Preprint astro-ph/0407176*)
- [7] Evans J C 1972 *Proc Solar Neutrino Conf* (25-26 February, Irvine: unpublished) p B-6E
- [8] Bahcall J N 1969 *Phys Rev Lett* **23** 251
- [9] Kuzmin V A 1965 *Zh Eksp Teor Fiz* **49** 1532 [*1966 Sov Phys JETP* **22** 1051]
- [10] Bahcall J N *et al.* 1978 *Phys Rev Lett* **40** 1351
- [11] Barabanov I R *et al.* 1980 *Pis'ma Zh Eksp Teor Fiz* **32** 384
- [12] Altmann M *et al.* 2005 *Phys Lett B* **616** 174 (*Preprint hep-ex/0504037*)
- [13] Abdurashitov J N *et al.* 1999 *Phys Rev C* **60** 055801 (*Preprint astro-ph/9907113*)
- [14] Abdurashitov J N *et al.* 2002 *J Exp Theor Phys* **95** 181 [*Zh Eksp Teor Fiz* **122** 211] (*Preprint astro-ph/0204245*)
- [15] Cleveland B T 1983 *Nucl Instrum Methods Phys Res* **214** 451
- [16] Haxton W C 1988 *Phys Rev C* **38** 2474
- [17] Gavrin V N *et al.* 1992 *Institute for Nuclear Research of the Russian Academy of Sciences Preprint No. P-777*
- [18] Giunti C and Laveder M 2006 *Preprint hep-ph/0610352*
- [19] Haxton W C 1998 *Phys Lett B* **431** 110 (*Preprint nucl-th/9804011*)
- [20] Abdurashitov J N *et al.* 2006 *Phys Rev C* **73** 045805 (*Preprint nucl-ex/0512041*)
- [21] Abdurashitov J N *et al.* 2006 *Astropart Phys* **25** 349 (*Preprint nucl-ex/0509031*)
- [22] Smirnov A Yu 2003 *Proc 10th Int Workshop on Neutrino Telescopes* (11-14 March, Venice) and references therein. (*Preprint hep-ph/0305106*)
- [23] Bahcall J N and Pinsonneault M H 2004 *Phys Rev Lett* **92** 121301 (*Preprint astro-ph/0402114*)
- [24] Fogli H L *et al.* 2006 *Prog in Part and Nucl Phys* **57** 742 (*Preprint hep-ph/0506083*)
- [25] Barger V, Marfatia D and Whisnant K 2005 *Physics Letters B* **617** 78 (*Preprint hep-ph/0501247*)
- [26] Bahcall J N 1997 *Phys Rev C* **56** 3391 (*Preprint hep-ph/9710491*)
- [27] Bahcall J N *et al.* 1996 *Phys Rev C* **54** 411 (*Preprint nucl-th/9601044*)
- [28] Bahcall J N web site [www.sns.ias.edu/~jnb](http://www.sns.ias.edu/~jnb)
- [29] Aharmim B *et al.* 2005 *Phys Rev C* **72** 05502 (*Preprint nucl-ex/0502021*)
- [30] Pandola L 2004 *Astropart Phys* **22** 219 (*Preprint hep-ph/0406248*)
- [31] Sturrock P A, Caldwell D O and Scargle J D 2006 *Astropart Phys* **26** 174 (*Preprint hep-ph/0409064*)
- [32] Strumia A, Cattadori C, Ferrari N and Vissani F 2002 *Phys Lett B* **541** 327 (*Preprint hep-ph/0205261*)
- [33] Cattadori C, Ferrari N and Pandola L 2005 *Nucl Phys (Proc Suppl)* **B 143** 3
- [34] Pulido J, Chauhan B and Picariello M 2006 (*Preprint hep-ph/0611331*)
- [35] Haxton W C 1988 *Phys Rev Lett* **60** 768
- [36] Engel J, Krastev P L and Lande K 1995 *Phys Rev C* **51** 2837
- [37] Hurst G S *et al.* 1984 *Phys Rev Lett* **53** 1116
- [38] Cowan G A and Haxton W C 1982 *Science* **216** 51
- [39] Veretenkin E P, Gavrin V N and Yanovich E A 1985 *Sov J Atom Energy* **58** 82 [*Atomniya Energia* **58** 65]
- [40] Kopylov A *et al.* 2004 *Phys Atom Nucl* **67** 1182 [*Yad Fiz* **67** 1204] (*Preprint hep-ph/0310163*)

# The KATRIN sensitivity to the neutrino mass and to right-handed currents in beta decay

J Bonn<sup>1</sup>, K Eitel<sup>2</sup>, F Glück<sup>3,4</sup>, D Sevilla-Sanchez<sup>1</sup> and N Titov<sup>5,6</sup>

<sup>1</sup> Johannes Gutenberg-Universität Mainz, Institut für Physik, Germany

<sup>2</sup> Forschungszentrum Karlsruhe, Institut für Kernphysik, Germany

<sup>3</sup> Universität Karlsruhe (TH), Institut für Experimentelle Kernphysik, Germany

<sup>4</sup> Research Institute for Nuclear and Particle Physics, Theory Dep., Budapest, Hungary

<sup>5</sup> Westfälische Wilhelms-Universität Münster, Institut für Kernphysik, Germany

<sup>6</sup> Institute for Nuclear Research, Troitsk, Russia

E-mail: jbonn@uni-mainz.de, Klaus.Eitel@ik.fzk.de, Ferenc.Glueck@ik.fzk.de, sevilla@uni-mainz.de, titov@inr.ru

## Abstract.

The aim of the Karlsruhe TRItium Neutrino experiment KATRIN is the determination of the absolute neutrino mass scale down to 0.2 eV, with smaller model dependence than from cosmology and neutrinoless double beta decay. For this purpose, the integral electron energy spectrum is measured close to the endpoint of molecular tritium beta decay. The endpoint, together with the neutrino mass, should be fitted from the KATRIN data as a free parameter. The right-handed couplings change the electron energy spectrum close to the endpoint, therefore they have some effect also to the precise neutrino mass determination. The statistical calculations show that, using the endpoint as a free parameter, the unaccounted right-handed couplings constrained by many beta decay experiments can change the fitted neutrino mass value, relative to the true neutrino mass, by not larger than about 5-10 %. Using, incorrectly, the endpoint as a fixed input parameter, the above change of the neutrino mass can be much larger, order of 100 %, and for some cases it can happen that for large true neutrino mass value the fitted neutrino mass squared is negative. Publications using fixed endpoint and presenting large right-handed coupling effects to the neutrino mass determination are not relevant for the KATRIN experiment.

## 1. Neutrino mass determination and the endpoint

In the KATRIN experiment the absolute neutrino mass is determined by the measurement of the integral energy spectrum of the electrons coming from beta decay of tritium molecules. The electrons are guided from the tritium source to the detector by magnetic field. Between the source and the detector a large negative potential (-18.6 kV) is applied at the main spectrometer, with the aim that only those electrons can reach the detector that have a decay kinetic energy above the value corresponding to this potential. The transversal energy component (relative to magnetic field) of the electrons is converted into longitudinal energy by using the inverse magnetic mirror effect, due to small magnetic field inside the main spectrometer (the electric field can change only the longitudinal energy component of the electrons). Thus it is possible to measure the integral electron energy spectrum simultaneously with high statistics and with high precision. For further information about the KATRIN experiment see Refs. [1] and [2].

The differential electron energy spectrum can be written (in a first approximation, close to the endpoint) as

$$w_{diff}(E) = E_\nu \sqrt{E_\nu^2 - m_\nu^2}, \quad (1)$$

where  $E$  is the relativistic total electron energy,  $E_\nu = E_0 - E$  and  $m_\nu$  denote the neutrino energy and mass, and  $E_0$  is the nominal endpoint (maximum of  $E$ , if the neutrino mass is zero). There are several theoretical modifications to this simplified spectrum, the most important of them is due to the recoil molecular ion final state distribution (see Ref. [3] for a recent calculation). Degenerate neutrino masses are assumed (the KATRIN experiment is able to find a non-zero neutrino mass only above 0.2 eV).

The KATRIN experiment measures the integral energy spectrum, therefore one has to multiply the differential spectrum by the response function of the spectrometer (see Ref. [2] for details), and to integrate from the minimal electron energy  $E_U = e|U_A - U_S|$ , where  $U_A$  and  $U_S$  denote the electric potential in the middle of the main spectrometer and in the tritium source, respectively. The expected absolute detection rate of the KATRIN experiment can be seen in Fig. 1 for different neutrino mass and endpoint values. The most sensitive region for the neutrino mass determination is around  $E_U - E_0^* \approx -5$  eV, where the signal is twice as large as the background (Ref. [4]). It is clear from the figure that there is a positive correlation between the neutrino mass and the endpoint: a larger fixed endpoint value results in a larger fitted neutrino mass value.

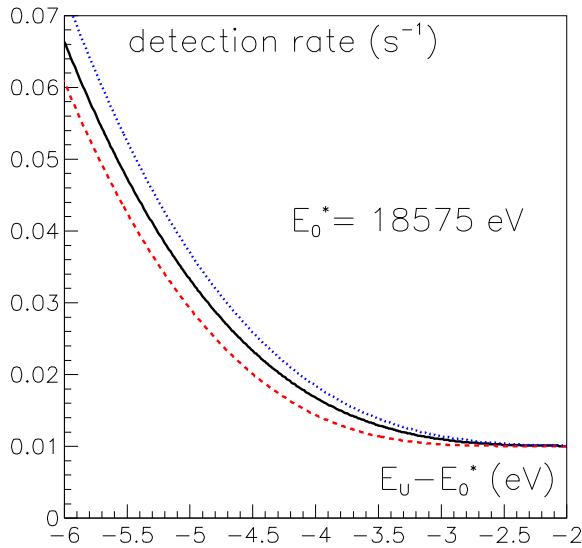


**Figure 1.** Expected detection rate of the KATRIN experiment as function of the minimal detected electron energy  $E_U$ , for different neutrino mass and endpoint values. Full (black) curve:  $m_\nu = 0$ ,  $E_0 = E_0^*$ ; dashed (red) curve:  $m_\nu = 1$  eV,  $E_0 = E_0^*$ ; dotted (blue) curve:  $m_\nu = 0$ ,  $E_0 = E_0^* + 0.15$  eV. The new KATRIN design parameters of Ref. [2] together with  $0.01$   $s^{-1}$  background rate have been employed.

In the KATRIN experiment (like in several earlier neutrino mass experiments) the endpoint is a free parameter, to be determined from the KATRIN spectrum data. Nevertheless, let us assume for a moment that the endpoint is a fixed input parameter. Then a  $\Delta E_0$  error of the endpoint results in a  $\Delta m_\nu^2$  ( $eV^2$ )  $\approx 7\Delta E_0$  (eV) error for the neutrino mass squared (using the last 20 eV of the spectrum for the data analysis). From the triton-Helium3 nuclear mass differences one has at present a  $\Delta E_0 = 1.2$  eV error for the endpoint [5]. In addition, it is difficult to determine the absolute potential values with a precision better than 100 mV. On the other hand, the KATRIN experiment aims to measure the neutrino mass squared with an accuracy of  $\sigma(m_\nu^2) = 0.025$   $eV^2$ . To obtain this precision, the accuracy of the endpoint value (as fixed parameter) should be at least 4 meV. Therefore, it is obvious: **for the data analysis of the KATRIN experiment the endpoint cannot be used as an external fixed input parameter; it should be used necessarily as a free parameter, determined from**

the KATRIN data. Analyses assuming the endpoint as a fixed parameter are not relevant for the KATRIN experiment.

## 2. Right-handed couplings and the electron energy spectrum

In the presence of right-handed weak couplings the differential electron spectrum is changed to the following form:

$$w_{diff}(E) = E_\nu \sqrt{E_\nu^2 - m_\nu^2} \left( 1 + b' \frac{m_\nu}{E_\nu} \right). \quad (2)$$

This formula is valid close to the endpoint. A similar change of the electron spectrum is due to the Fierz parameter  $b$ . The parameter  $b'$  is a linear combination of the right-handed vector ( $R_V$ ), axial-vector ( $R_A$ ), scalar ( $R_S$ ) and tensor ( $R_T$ ) couplings:

$$b' \approx -2 \frac{\Re e(L_V R_V^* + L_V R_S^*) |M_F|^2 + \Re e(L_A R_A^* + L_A R_T^*) |M_{GT}|^2}{|L_V|^2 |M_F|^2 + |L_A|^2 |M_{GT}|^2} \quad (3)$$

(only the dominant terms are shown in this formula, which is in agreement with Ref. [6]). The left-handed  $L_j$  and right-handed  $R_j$  couplings have the following simple relations with the widely used couplings  $C_j$  and  $C'_j$  introduced by Lee and Yang in Ref. [7]:  $C_j = (L_j + R_j)/\sqrt{2}$ ,  $C'_j = (L_j - R_j)/\sqrt{2}$ . As it is explained in Ref. [8], there are several advantages using the couplings  $L_j$  and  $R_j$ . In the Standard Model only the left-handed vector and axial-vector couplings  $L_V$  and  $L_A$  are non-zero.

There are many experimental observables (like beta asymmetry, neutrino-electron correlation, beta polarization etc.) that provide constraints for the couplings  $R_j$ . Unfortunately, these observables are quadratic in the  $R_j$  couplings (with zero neutrino mass the right-handed couplings have no interference with the dominant left-handed couplings), therefore the 95 % confidence limits are not too small:  $|R_V| < 0.08$ ,  $|R_A| < 0.10$ ,  $|R_S| < 0.07$ ,  $|R_T| < 0.10$  (see the recent overview in Ref. [9]; the  $L_V = 1$  normalization is used here). The signs of the couplings  $R_j$  are not known; in order to obtain conservative limit for  $b'$  we assume that these signs are equal (in this case there is no sign cancellation in Eq. 3). Then we get the following constraints for  $b'$ :

$$|b'| < 0.26 \quad (95\% \text{ CL}); \quad |b'| < 0.31 \quad (99.7\% \text{ CL}). \quad (4)$$

## 3. Right-handed couplings and neutrino mass determination in KATRIN

Let us assume that the real value of the parameter  $b'$  is nonzero, and the KATRIN data are analyzed with  $b' = 0$  theory (Standard Model). In this case, the fitted neutrino mass value should deviate from the real mass value. Fig. 2 shows the  $\Delta m_\nu/m_\nu = (m_\nu^{(\text{fit})} - m_\nu^{(\text{real})})/m_\nu^{(\text{real})}$  relative deviation due to the unaccounted right-handed parameter  $b' = \pm 0.28$ . The KATRIN design parameters and the statistical method described in Ref. [2] have been used for this calculation. The fitted parameter in these calculations is the neutrino mass squared, not the mass. One has to emphasize also that the endpoint was taken as a free parameter. According to Fig. 2 **the relative change of the neutrino mass due to the unaccounted right-handed couplings is of order of 5-10 %**. For small neutrino mass values (below 0.5 eV) the shift  $m_\nu^{(\text{fit})} - m_\nu^{(\text{real})}$  is smaller than the expected experimental error of the mass, for larger mass values (above 0.5 eV) the shift of the mass is larger than the experimental error.

Taking the endpoint as a fixed input parameter, the results are completely different. To illustrate this difference, let us consider a special numerical example: we assume that the real neutrino mass is  $m_\nu^{(\text{real})} = 0.35$  eV, and the real value of the parameter  $b'$  is  $b'_{\text{real}} = \pm 0.28$ . Then we make a computer experiment: we generate the KATRIN data by using these real values, but

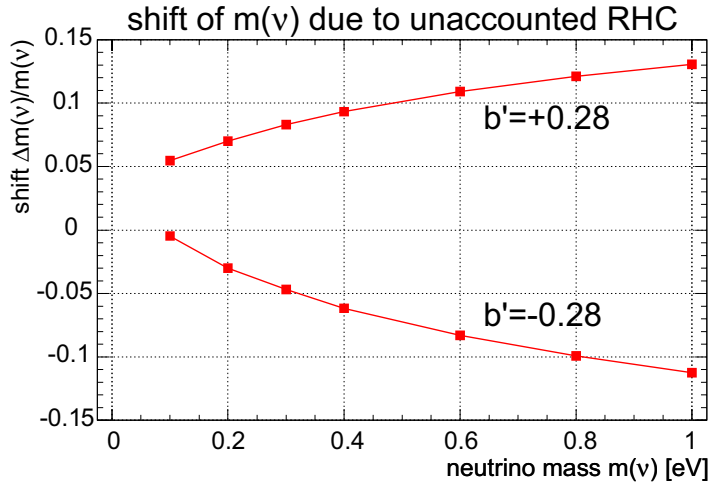


**Figure 2.** Relative shift  $(m_\nu^{(\text{fit})} - m_\nu^{(\text{real})})/m_\nu^{(\text{real})}$  of neutrino mass due to unaccounted right-handed couplings, as function of  $m_\nu^{(\text{real})}$ .

we analyze the data assuming  $b' = 0$ . Table 1 shows the fitted neutrino mass values of these calculations with fixed and with free endpoint. **With free endpoint the fitted mass values are close to the real mass. On the other hand, in the case of fixed endpoint the fitted neutrino mass with  $b'_{\text{real}} = -0.28$  is completely different from the real mass value. In the case of  $b'_{\text{real}} = +0.28$  the fitted mass squared becomes negative, in spite of the positive real mass value. Using the endpoint as a free parameter such a large deviation between real and fitted mass or mass squared values does not occur.**

$b'_{\text{real}}$	$E_0$ fixed	$E_0$ free
-0.28	$m_\nu^{(\text{fit})} = 0.6$ eV	$m_\nu^{(\text{fit})} = 0.33$ eV
+0.28	$m_\nu^{2(\text{fit})} = -0.1$ eV <sup>2</sup>	$m_\nu^{(\text{fit})} = 0.38$ eV

**Table 1.** Fitted neutrino mass (or mass squared) values with  $m_\nu^{(\text{real})} = 0.35$  eV.

Several theoretical publications present large right-handed coupling effects to the neutrino mass determination (Refs. [10, 11, 12]). Refs. [10, 11] tried to explain the negative mass squared anomaly of several neutrino mass experiments by assuming the presence of non-zero right-handed couplings. **Nevertheless, all these 3 publications used in their analyses fixed endpoint, therefore they are not relevant for the neutrino mass experiments (like KATRIN) using free endpoint.** We mention that in Ref. [13] right-handed couplings were searched in the data of the Mainz neutrino mass experiment, using free endpoint in the analysis; the data did not favor the existence of non-zero right-handed couplings.

## References

- [1] Doe P 2006, Direct neutrino mass measurements, *in this proceedings*.
- [2] KATRIN Collaboration, KATRIN Design Report 2004, Wissenschaftliche Berichte FZK 7090 (2004); NPI ASCR Rez EXP-01/2005; MS-KP-0501; see also in: <http://www-ik.fzk.de/~katrin/index.html>.
- [3] Doss N et al. 2006 *Phys. Rev. C* **73** 025502.
- [4] Otten E W, Bonn J and Weinheimer Ch. 2006 *Int. J. Mass Spectrom.* **251** 173.
- [5] Nagy Sz. et al. 2006 *Europhys. Lett.* **74** 404.
- [6] Enz C P 1957 *Nuovo Cimento* **6** 250.
- [7] Lee T D and Yang C N 1956 *Phys. Rev.* **104** 254.
- [8] Glück F, Joo I and Last J 1995 *Nucl. Phys. A* **593** 125.
- [9] Severijns N, Beck M and Naviliat-Cuncic O 2006 *Rev. Mod. Phys.*, to appear.

- [10] Stephenson G J and Goldman T 1998 *Phys. Lett. B* **440** 89.
- [11] Stephenson G J, Goldman T and McKellar B H J 2000 *Phys. Rev. D* **62** 093013.
- [12] Ignatiev A Yu and McKellar B H J 2006 *Phys. Lett. B* **633** 89.
- [13] Kraus C 2000 *Diplomework, Mainz* .

## K2K cross section results

**Richard Gran, for the K2K collaboration**

Department of Physics, University of Minnesota Duluth, 1023 University Dr. MWAH 371,  
Duluth, MN 55804

E-mail: [rgran@d.umn.edu](mailto:rgran@d.umn.edu)

**Abstract.** This paper contains results from several cross section studies made using the near detectors in the K2K neutrino beam. These include an estimate of neutral current single  $\pi^0$  production, an upper limit on the cross section for charged current coherent  $\pi^+$  production, and an analysis of the axial vector form factor for quasi-elastic interactions.

### 1. Introduction

The neutrino experiments which have been running during the first half of this decade have accumulated hundreds of thousands of neutrino interactions at energies around 1 GeV. The K2K experiment was designed to study neutrino oscillation phenomena, but we have also used our high statistics samples to study neutrino cross sections. For K2K, these neutrino interactions occur on water ( $\text{H}_2\text{O}$ ), scintillator (HC), and iron (Fe), and come from a beam that peaks around 1.2 GeV, and averages 1.3 GeV. In these proceedings, we summarize the results of three such cross section studies.

We are challenged to understand neutrino interactions in the region around 1 GeV because this is the energy of the expected oscillation signal for several neutrino oscillation experiments [1,2,3] as well as future neutrino oscillation initiatives. At the same time, it is the most complicated region for neutrino interactions: this is where quasi-elastic, resonance production, and deep inelastic scattering all contribute significantly. Finally, because of the difficulty in designing beams and detectors for these energies, previous experimental measurements have significant uncertainties in the cross sections. By necessity, neutrino oscillation experiments at these energies must make their own measurements and arrange their experiments to minimize these uncertainties.

The K2K near detectors were designed to measure the features of the neutrino beam right after it was produced. The spectrum of neutrinos at the far detector can then be compared to the near detector spectrum to observe the characteristic distortion caused by neutrino oscillations. From upstream to downstream, the near detector system consists of a 1000 ton water Cerenkov detector (1kT), a scintillating fiber detector which uses tanks of water as a target (SciFi), a fully active plastic scintillator detector (SciBar), and a muon range detector (MRD).

The 1kT detector is designed to be a small scale version of Super-Kamiokande, in order to partially cancel systematics due to the Cerenkov technique and uncertainties in the neutrino-water interactions. The SciFi also uses water as the primary neutrino interaction target, but its fine grained design and the use of the MRD to get muon momentum from range give it sensitivity to higher energy neutrino interactions and yields different information about those reactions than

the 1kT. The SciBar works on the same principle, but uses a fully active scintillator design, and is even more sensitive to the protons and pions that come out of the interaction.

These detectors took data in several running periods between 1999 and 2004 in the K2K neutrino beam, though, for technical reasons, the analyses below use data from different portions of this run time. This beam is produced when 12 GeV protons are extracted from the proton synchrotron at the KEK accelerator in Tsukuba, Japan, and bent toward the Super Kamiokande detector. A proton spill 1.1  $\mu\text{s}$  wide hits an aluminum target every two seconds. Among the resulting hadrons, the  $\pi^+$  are focused into a decay region filled with helium where they decay to  $\mu^+$  and  $\nu_\mu$ . The muons and undecayed pions are absorbed by earth, while the neutrinos continue to the near detector hall, 300 meters from the target, and eventually to Super Kamiokande, 250 km away. The resulting neutrino beam is 98% pure  $\nu_\mu$ .

More details about the experimental setup, with additional specifications and references, are available in [1].

## 2. Neutral current single $\pi^0$ production in the 1kT detector

This study is described more completely in Ref. [4]. The 1kT detector has excellent ability to observe and reconstruct the  $\pi^0$  interactions. The neutral pions decay to two gamma rays, each of which initiate an electromagnetic shower. These appear in the detector as two electron-like Cerenkov rings, but no visible muon. In addition, any recoil proton will nearly always be below threshold as well. From the two Cerenkov rings, it is possible to estimate the implied invariant mass and select a sample of candidate  $\pi^0$  events.

This measurement is of the neutral current single  $\pi^0$  production. It includes as signal neutral pions from resonance production events, coherent production, as well as from deep inelastic scattering events in which only one neutral pion was produced. In the context of this measurement, it is the outgoing pion, after intranuclear processes such as charge exchange and absorption have occurred. The signal, after selections, is expected to be about 70% of the total sample. The backgrounds to these processes are from charged current interactions in which the muon is not seen, as well as from multi pion production in which the other particles are below detection threshold.

Starting from this sample, we estimate the detection efficiency for the signal, and make the appropriate calculation. Also, we use the Monte Carlo simulation (MC) to estimate the background, and subtract it. After these corrections, the measurement for NC single  $\pi^0$  interactions yields  $(3.61 \pm 0.07 \text{ stat.} \pm 0.36 \text{ syst.}) \times 10^3$  events in the 25 ton fiducial volume. We form the ratio with all muon-like (i.e. charged current) interactions observed in the same samples:  $(5.65 \pm 0.03 \text{ stat.} \pm 0.26 \text{ syst.}) \times 10^4$  events.

Thus, the measured neutral current single  $\pi^0$  ratio at an average neutrino energy of 1.3 GeV is  $0.064 \pm 0.001 \text{ stat.} \pm 0.007 \text{ syst.}$  This can be compared to the ratio predicted from our Monte Carlo simulation which is 0.065. Systematic errors dominate; they come from model errors (DIS model 5.6%, NC/CC cross section 3.2%) which affect the background subtraction. The two largest detector uncertainties are in identifying and counting Cerenkov rings (5.4% uncertainty in the ratio) and the separation of electron-like and muon-like Cerenkov rings (4.2%). There is an additional uncertainty in the denominator of the ratio of 4%, which comes from the interplay between vertex reconstruction and the definition of the fiducial volume.

## 3. Charged current coherent pion production in the SciBar detector

Another study we have done is a search for charged current coherent pion production in the SciBar plastic scintillator detector. This study was reported in [5]. In coherent production, the neutrino interacts coherently with the nucleus as a whole, rather than with an individual nucleon. For the charged current reaction on carbon  $\nu_\mu + C \rightarrow \mu^- + C + \pi^+$ , no recoil nucleon is present, so the only observable products are the charged pion and the muon. This interaction

is characterized by very forward going muons, equivalently a small momentum transfer. These final states, with little or no other activity at the vertex of the interaction, combined with the kinematics, give a signature that can be isolated in the SciBar detector data.

One motivation for looking at this reaction is that the K2K experiment, among others, had observed that our MC over-predicts the number of events at very low square of the momentum transfer  $Q^2$ , which for our beam energies correspond to muons at very forward angles or the lowest energies. In principle this discrepancy could come from any of the relevant interactions, such as quasi-elastic, or resonance production events. It could be something fundamental to the neutrino-nucleon cross section, or to the application of nuclear effects such as Pauli blocking. However, since coherent production always happens at low momentum transfer, this offers a unique probe of this discrepancy.

The first step in isolating coherent pion enhanced samples is to make a subsample of events which have two tracks. This sample can be further divided into quasi-elastic enhanced and non-quasi-elastic enhanced subsamples. Because quasi-elastic interactions are a two-body scattering process, it is possible to use the muon angle and momentum to predict the angle at which the recoil proton should be found. If the observed second track matches this prediction, within 25 degrees, it is likely to be QE. If it does not match, then it is likely to be a proton or pion from a resonance, coherent, or DIS interaction.

Because of the fully-active design of the SciBar scintillator detector, it is possible to identify the products of the interaction. For a charged current coherent interaction, there should be a muon and a  $\pi^+$ , but there should be no recoil nucleon. The muon is easy to identify from its long range, and second tracks can be identified as a proton or pion from the  $dE/dx$  along the track. In this way, the non-quasi-elastic subsample is further divided into samples where that second track is proton like or pion like.

This latter sample can be further examined. Because nothing comes out of the nucleus in a coherent interaction, there should be little or no vertex activity apart from the two tracks. For ordinary two-track interactions, there is often another particle present: a recoil nucleon or pion. A cut on this feature further purifies the CC coherent sample.

Finally, we estimate the reconstructed  $Q^2$  of this interaction. Actually, this is done using the quasi-elastic kinematic assumptions, so the reconstructed  $Q^2$  does not exactly correspond to the correct momentum transfer, but it gives a method to treat the data and the MC the same without knowing the underlying interaction kinematics, so that they data and MC may be compared. The expected bias is  $0.008 \text{ (GeV/c)}^2$  for CC coherent pion events. We select events with reconstructed  $Q^2 < 0.1 \text{ (GeV/c)}^2$ . We again take the ratio to all the CC events and obtain  $\sigma_{CC\text{coh}\pi}/\sigma_{\text{AllCC}} = (0.04 \pm 0.29\text{stat.}_{-0.35}^{+0.32}\text{sys.}) \times 10^{-2}$ . This is consistent with zero CC Coherent Pion production.

Because the value is consistent with zero, we compute an upper bound on the CC coherent pion cross section. Again, relative to all CC events:  $\sigma_{CC\text{coh}\pi}/\sigma_{\text{AllCC}} < 0.60 \times 10^{-2}$  at 90% C.L. This is approximately 30% of the former Rein and Sehgal prediction [6]. It is important to note that this bound is set by two large systematics: the cross section for resonance pion events (including Pauli blocking effects) and the model for pion reinteractions in carbon. It is possible that the observed  $Q^2$  distribution is a combination of unexpectedly small coherent cross section and an overestimation of resonance production due to one or both of these systematic effects.

Since the original publication of this result, there has been a renewed look at the very low  $Q^2$  cross section calculations. Of principle interest is the inclusion of terms that depend on the muon mass in the calculation, which suppress the cross section below  $Q^2 < 0.2 \text{ (GeV/c)}^2$  for interactions that produce  $\pi^+$ , including coherent production. In a very recent paper, Rein and Sehgal [7] give a discussion of the size of this effect, not included in their original publication. We have not yet quantified how this recent work impacts the interpretation of these data.

#### 4. Axial vector form factors in the SciFi detector

Our final topic summarized in these proceedings is a study of quasi-elastic interactions measured by the SciFi detector. A full description of the technique and results can be found in [8].

Quasi-elastic interactions,  $\nu_\mu + n \rightarrow \mu^- + p$  are the simplest kinematics available. This is a two-body scattering process, which means that the muon momentum and angle are sufficient to reconstruct the details of the interaction. In our analysis we take advantage of this to get an estimate of the incident neutrino energy  $E_\nu$ , the square of the momentum transfer  $Q^2$  to the nucleon, and a prediction for the angle of the recoil proton.

The expected cross section can be calculated following Llewellyn-Smith [9]. The interesting feature of this calculation is that it involves vector form factors and other constants that are relatively precisely determined from electron scattering data and neutron decay. In this analysis, we assume the axial vector form factor can be approximated with a dipole form which has only one free parameter, and fit to find the value for this parameter, the axial vector mass  $M_A$ , that best matches the data.

The parameter  $M_A$  has two effects on the cross section. A 10% larger value increases the QE cross section by about 10%. However, uncertainties in absolute normalization of the flux for this experiment are significant. Instead, the fit we will do is a fit to the shape of the  $Q^2$  distribution. In this case, a 10% larger value of  $M_A$  produces a shape that is flatter, has relatively more high  $Q^2$ , high  $\theta_\mu$  events.

The SciFi detector is made of aluminum tanks filled with water. In between these tanks are scintillating fiber tracker. Thus, the neutrinos are incident primarily on  $H_2O$ , but 22% (by mass) of the material is Al, and 8% is plastic. In our interaction model, neutrino quasi-elastic interactions can only occur on neutrons, changing them to protons; there is no allowed final state for the CC interaction on hydrogen. In this sense, we consider our result to be a measurement of the effective  $M_A$  for oxygen. Because of the fiber tracker design, this detector has outstanding angle resolution for tracks that go three or more layers.

As with the SciBar samples in the previous section, we separate events into samples with one track, two tracks where the second track matches the QE assumption, and a two-track sample that is non-QE enhanced. The SciFi detector does not have strong capability to differentiate protons from pions via  $dE/dx$ , so that additional cut is not used. We further concern ourselves with the low  $Q^2$  discrepancy, as above. Regardless of the source of the discrepancy, resonance production or coherent production cross sections, or Pauli blocking, or another nuclear effect, we disregard all events with reconstructed  $Q^2 < 0.2$  (GeV/c)<sup>2</sup>.

Another feature of the analysis is that we are using the updated vector form factors from electron scattering data [10,11]. Changing this part of the cross section calculation has a significant effect on the shape, and thus affects the  $M_A$  parameter extracted from fits to this shape.

We then divide the data into five energy regions and bin it by  $Q^2$ . We fit the entire collection of samples. Because this includes the non-QE enhanced sample, the fit will constrain the size of the non-QE background in the one-track and the two-track QE samples. In the end, we obtain a fit value of  $M_A = 1.20 \pm 0.12$  GeV, with a  $\chi^2 = 261$  for 235 degrees of freedom. Our default MC uses a value of  $M_A = 1.1$ , so the data prefer a flatter  $Q^2$  spectrum than the MC.

We have investigated several systematic errors, and have a couple interesting conclusions. First, nuclear effects that are understood at this time seem to have a small effect on the shape of the  $Q^2$  distribution. However, the muon momentum scale has a very significant effect on the measurement. Its contribution to this measurement is  $M_A \pm 0.07$  GeV. How this is constrained is described in more detail in [8], but can be roughly simplified to an unknown potential bias of  $\pm 1.5\%$  in the reconstructed muon momentum. A small bias has a large effect on the shape of the  $Q^2$  distribution, stretching or compressing it significantly. The final uncertainty is from the relative flux and normalization of the neutrino beam, which is included in the fit as a sequence

of five unconstrained parameters.

Though most of these QE interactions occur on oxygen, it is relevant to compare this result to measurements on deuterium from bubble chamber experiments [12,13,14]. In order to make this comparison, it is easiest to reproduce their assumptions about the vector form factors and other constants. The resulting fit value is higher:  $M_A = 1.23 \pm 0.12$ . The bubble chamber measurements, which were also primarily shape fits, are usually taken together and give  $M_A = 1.03 \pm 0.03$ . These two values agree at about the two-sigma level, though there is no expectation that they should be the same. One other comment: because these results were obtained primarily through shape fits, consumers of neutrino interaction generators should be very cautious when assigning an uncertainty in  $M_A$ . The small error from a shape fit may hide a larger error in the absolute cross section, and it is the latter that is relevant for most oscillation analyses.

## 5. Oscillation measurements

At the Neutrino 2006 conference, we are also pleased to present the final oscillation results from the K2K oscillation analysis. Compared to the previous published results [15], these results include small changes to the Super Kamiokande reconstruction and the inclusion of information from the HARP measurement of the hadron production off a thin (5% interaction length) version of the K2K target [16]. The K2K best fit result in the physical region is at  $\Delta m^2 = 2.8 \times 10^{-3}$  (eV)<sup>2</sup> and maximal  $\sin^2 2\theta = 1$ . The 90% confidence contour crosses the maximal mixing axis at  $\Delta m^2 = 1.9 \times 10^{-3}$  and  $3.5 \times 10^{-3}$ . In addition, a full paper with extensive description of the experiment, analysis, and results is now published [1]. Another paper describing the upper limits on  $\nu_\mu$  to  $\nu_e$  oscillation obtained from an electron neutrino appearance search is also available [17].

## 6. Conclusion

The K2K experiment has completed a program to measure neutrino oscillations, but also to make measurements of neutrino interactions on nuclei. These measurements, combined with upcoming cross section results from MiniBooNE, MINOS, and later SciBooNE and MINERvA, will be vital to the continuing program to understand neutrino mixing and its implications for particle physics, astrophysics, and cosmology.

## References

- [1] Ahn M H, *et al.* (K2K) 2006 *Phys. Rev. D* **74** 072003, hep-ex/0606032
- [2] Michael D G, *et al.* (MINOS) 2006 *Phys. Rev. Lett.* **97** 191801, hep-ex/0607088
- [3] Tayloe R. and Fleming B. (MiniBooNE) each a paper in these proceedings.
- [4] Nakayama S, Mauger C, *et al.* (K2K) 2005 *Phys. Lett. B* **619** 255, hep-ex/0408134
- [5] Hasegawa M, *et al.* (K2K) 2005 *Phys. Rev. Lett.* **95** 252301, hep-ex/0506008
- [6] Rein D and Sehgal L 1981 *Ann. Phys.* **133** 79
- [7] Rein D and Sehgal L 2006, hep-ph/0606185
- [8] Gran R, Jeon E J, *et al.* (K2K) 2006 *Phys. Rev. D* **74** 052002, hep-ex/0603034
- [9] Llewellyn Smith C 1972 *Phys. Rep.* **3C** 262
- [10] Bosted P E 1995 *Phys. Rev. C* **51** 409
- [11] Budd H, Bodek A, Arrington J 2003 (NuInt02), hep-ex/0308005
- [12] Miller K, *et al.* 1982 *Phys. Rev. D* **26** 537
- [13] Kitagaki T, *et al.* 1983 *Phys. Rev. D* **28** 436
- [14] Kitagaki T, *et al.* 1990 *Phys. Rev. D* **42** 1331
- [15] Aliu E, *et al.* (K2K) 2005 *Phys. Rev. Lett.* **94** 081802 hep-ex/0411038
- [16] Catanesi M G, *et al.* (HARP) 2006 *Nucl. Phys. B* **732** 1 hep-ex/0510039
- [17] Yamamoto S, Zalipska J, *et al.* (K2K) 2006 *Phys. Rev. Lett.* **96** 181801, hep-ex/0603004

# Neutrino astronomy with IceCube and AMANDA

Gary C. Hill, for the IceCube collaboration [1]

Department of Physics, University of Wisconsin, Madison

E-mail: ghill@icecube.wisc.edu

**Abstract.** Since the early 1990s, the South Pole has been the site of the construction of the world's first under-ice Cherenkov neutrino telescopes - AMANDA and IceCube. The AMANDA detector was completed in 2000, and its successor IceCube, a kilometre scale neutrino detector, began construction in 2005. Completion of IceCube is scheduled for 2011. This paper will give an overview of the history, construction, latest physics results and potential of these detectors.

## 1. The appeal of neutrino astronomy

The road to a kilometre scale neutrino detector, pioneered by the DUMAND collaboration, has seen the operation of the first generation experiments, AMANDA and Lake Baikal, as well as initial construction and planning for IceCube, ANTARES, NESTOR, NEMO and KM3NET. The discovery of neutrinos with these detectors will hopefully extend and complement the knowledge of the universe to date gained through cosmic ray and gamma ray observations. While the nature and location of the cosmic ray sources are unknown, there are many confirmed sources of TeV gamma-rays. If one of these turned out to also be a neutrino source, then a hadronic accelerator central engine might be driving cosmic ray, gamma and neutrino production [2].

A neutrino detector like IceCube or AMANDA uses an array of photomultipliers to record Cherenkov light from through-going muons, or from point-like shower ("cascade") events. Muons result from charged current interactions of neutrinos in the detector volume, or in the surrounding ice and rock. Cascade events result from charged and neutral current interactions of all neutrino flavours.

The backgrounds to a search for a flux of high-energy extra-terrestrial neutrinos at the earth are atmospheric muons and neutrinos from the interaction of cosmic rays in the earth's atmosphere. The atmospheric muons are eliminated by looking for events moving upward through the detector – only neutrinos can penetrate the earth. A small fraction of the large downgoing muon flux will be falsely reconstructed in the upward direction. These are removed by tight requirements on the fitted track. After atmospheric muons are eliminated, there is a flux of atmospheric neutrinos seen in a detector. This can be used as a calibration test beam to check the understanding of the detector, or be used to look for new neutrino physics. A search for point sources of neutrinos is made by looking for an excess of events from a direction in the sky. Electromagnetic observations by other detectors may provide information to reduce the time over which such a search is made - for instance in a search for neutrinos correlated with a gamma-ray burst. One can also look for a diffuse excess of neutrinos from the sum of all sources in the universe. Since the extra-terrestrial flux predictions tend to go as  $dN/dE \sim E^{-2}$ , one looks for higher energy events in the detector to separate them from the more steep atmospheric neutrino spectrum ( $dN/dE \sim E^{-3.7}$ ).

## 2. Physics results from AMANDA

The first detection of muon Cherenkov radiation in polar ice was made in Greenland in 1990 [3], using three photomultipliers deployed to a depth of about 200 metres. Following this success, similar tests were made at the South Pole over the next years, with the AMANDA-A detector deployed in 1993-94 [4]. Construction of the presently operating AMANDA detector took place from 1995 to 2000, over which time 677 optical modules were deployed over 19 strings, to depths ranging from 1500 to 2000 metres. The properties of the polar ice, critical for understanding of the detector, have been measured using light sources in the array [5]. Although most of AMANDA used analogue signal technology, digital technology, eventually chosen for IceCube, was tested on one string [6].

### 2.1. Atmospheric neutrinos

While three neutrino candidates were observed with the first four strings of AMANDA [7], the first compelling evidence of high-energy atmospheric neutrinos came from the 10 string 1997 data set, where 16 upgoing events were left after data reduction [8]. Dramatic improvements in the analysis techniques [9] increased this number to about 300 [10, 11]. Over the entire life of AMANDA-II, many thousands of atmospheric neutrinos have now been observed [12, 13]. These are the highest energy neutrinos ever observed. The observed rate is consistent with the uncertainties in theoretical predictions [14, 15]. A regularised unfolding technique has been used to make a best-fit to the originating energy spectrum; again consistency with expectation is seen [16]. The agreement of the atmospheric neutrino measurements with expectations shows that the detector is working as expected.

### 2.2. Point sources

Several searches for northern hemisphere point sources of neutrinos have been conducted with the AMANDA detector, for the 1997 [17], 2000 [18] and 2000-02 [19] data sets. The most recent search used data from 2000-04, corresponding, after correction for down-time of the detector, to 1001 days of live time [12, 13]. The final event set consists of 4282 upward moving events, believed to be atmospheric neutrinos. Several search methods were used to look for point sources in the northern sky. For each, the expected background for any source is found from off-source data from the same declination band. The expected sensitivity is found from simulations of neutrino interactions, muon propagation, and the full detector response to the Cherenkov light emitted. Full-sky searches (looking for a hot spot anywhere in the sky), specific source searches, and stacking searches were conducted. The full-sky and specific source searches were optimised in an unbiased fashion to produce the best limit setting potential [20]. The 90% confidence level sensitivity of the full-sky search to an  $E^{-2}$  flux (assumed to have a  $\nu_\mu : \nu_\tau$  ratio of 1:1), relatively constant with declination, is about  $E_\nu^2 \times dN_\nu/dE_\nu < 10^{-10} \text{ TeV cm}^{-2} \text{ s}^{-1}$ . The numbers of observed events across the sky were consistent with the background expectations, leading to the same result for the average all-sky experimental limit. The highest significance seen was  $3.7\sigma$  and, via scrambled random sky maps, the probability of seeing something this significant or higher was found to be 69%. Searches for 32 specific candidate sources, and searches made where the events from objects belonging to common classes were summed, were made. Limits were placed on the neutrino fluxes from the objects [21, 13]. For a source above the horizon, SGR 1806-20, a search for muons from both neutrinos and gamma-rays was made. With no significant signal seen, limits were placed on the gamma and neutrino fluxes from the source [22]. While not truly a point source, the galactic plane was searched for an excess of neutrinos from cosmic ray interactions with the dust, using similar methods as employed in the point source searches. No excess of events was seen and limits on models were set [23].

### 2.3. GRBs

Gamma-ray bursts are some of the most energetic phenomena in the universe, with emission timescales as short as seconds. During the life of AMANDA, satellites such as the CGRO, with the BATSE detector, and the IPN satellites, including HETE and Swift, have recorded gamma emissions from many GRBs. Waxman and Bahcall theorised that GRBs may be the source of the highest energy cosmic rays [24]. In this “fireball” model, neutrinos would also be produced. The AMANDA data has been searched for neutrinos in spatial and temporal coincidence with about 400 GRBs [25]. The addition of a time cut on the search greatly reduces the expected background to of order one event over the sum of all GRBs searched. No event has been observed in coincidence with a GRB, consistent with this small total expected background. Limits on the fluxes from all bursts, classes of bursts, and individual bursts, have been placed. The limits from all bursts are within a factor 4 of the Waxman-Bahcall prediction. In another analysis, the observations from each individual burst are interpreted in light of all information known about that burst from other wavelengths, via an individually calculated neutrino flux. An analysis of this type has been performed for GRB030329 [26]. The study of further GRBs is in progress. Searches for cascade like events from GRBs have been made [27]. All-time and rolling time window searches have been performed and limits placed on models of neutrino production.

### 2.4. WIMPs

The mystery of the dark matter, responsible for some 23% of the energy density of the universe, is a target of the search for WIMPs (Weakly Interacting Massive Particles) with AMANDA. A likely dark matter candidate is the neutralino - the lightest supersymmetric particle in most supersymmetric extensions of the standard model. After some time, these would become gravitationally trapped in the centre of the earth and sun, where they could pair-wise annihilate via several paths to produce neutrinos. Thus, AMANDA searches for excesses of neutrinos from the centre of the earth (1997-99 data [28, 29]), and from the sun (2001 data [30]). To date, neither the earth nor sun has been revealed as an annihilation site for neutralinos, and these non-observations place bounds on various parameters in the supersymmetric extensions of the standard model. Once all current data is analysed, these bounds will be competitive and complementary with those from direct detection experiments like CDMS.

### 2.5. Diffuse searches

To search for a diffuse flux of neutrinos from the sum of sources in the universe, one must look for neutrinos in excess of the expectation for atmospheric neutrinos. The extra-terrestrial flux is expected to have a harder spectrum ( $\sim E^{-2}$ ) than the atmospheric neutrinos ( $\sim E^{-3.7}$ ), so searches are designed where event energies are estimated. Three types of diffuse search are conducted with AMANDA, one sensitive to muon-neutrinos, and the other two sensitive to all flavours. The muon search seeks to isolate muon tracks and use event observables related to the energy. One style of all-flavour search focuses on cascade-like events - and is thus sensitive to neutral and charged current interactions of all flavours. Cascades from charged current interactions come from electron and tau neutrinos, and from some muon-neutrinos where most of the energy goes into the cascade, leaving only a short track from a low energy muon. These searches are mostly sensitive to cascade events contained in the detector volume. The second type of all-flavour search looks for large cascade and muon events from extremely high energy neutrino interactions, including events where the cascade or muon is well outside the volume of the detector. Due to attenuation of neutrinos in the earth, these searches are most sensitive to horizontal events, with the main background being energetic cosmic ray muon bundles.

Unlike a point source search, a diffuse search strictly has no “off-source” region where data can be used to estimate the background. Thus the analysis relies on theoretical predictions of the atmospheric neutrino fluxes for background estimations. In practice, the observed lower

energy events are used to place some constraint on the atmospheric models before they are used to estimate the high energy background. As for other analyses, downgoing muons are used as a calibration beam to check that the detector would be sensitive to the types of high-energy events expected from extra-terrestrial neutrinos.

Table 1 summarises the results of the different searches for a diffuse flux of neutrinos with the AMANDA data sets, taken from 1997 to 2003. In the results reported here, the all-flavour analyses assume a 1:1:1 electron, muon and tau flavour mixture at the earth, due to maximal neutrino oscillations. These limits can be converted (and compared) to muon limits by dividing by three.

Two *all-flavour cascade* searches have been performed, on the 1997 [31] and 2000 [32] data sets. The limit for the 2000 data improved by an order of magnitude over that for 1997. In a similar energy range ( $20 - 5 \times 10^4$  TeV), the Baikal collaboration has recently analysed 1038 days (1998-2003) of data from the NT-200 experiment, leading to a slightly better limit of  $E_\nu^2 \times dN_\nu/dE_\nu = 8.1 \times 10^{-7}$  GeV cm<sup>-2</sup> s<sup>-1</sup> sr<sup>-1</sup> [33].

At higher energies, these data sets have been analysed with the *all-flavour UHE* method [34, 35, 36]. Although the sensitivity of the 2000 search ( $E_\nu^2 \times dN_\nu/dE_\nu = 3.7 \times 10^{-7}$  GeV cm<sup>-2</sup> s<sup>-1</sup> sr<sup>-1</sup>) was improved over 1997, the experimentally obtained limit for 2000 turned out to be the same as that for 1997, due to the observation of a non-significant excess of events. These limits are the best of any detector at energies up to  $\sim 1$ PeV.

Searches for a diffuse flux, using reconstructed contained muon events, have been made on the 1997 [37], 2000 and 2000-03 data sets. For the year 2000 data set, a regularised unfolding of the energy spectrum was conducted. This spectrum was statistically compared with the atmospheric neutrino expectation and a limit on a diffuse  $E^{-2}$  flux derived [16]. For the 2000-03 data, the muon analysis used the number of optical module channels per event that reported at least one Cherenkov photon ( $N_{\text{ch}}$ ) as an energy estimator. The harder expected extra-terrestrial flux would produce a flatter  $N_{\text{ch}}$  distribution than that for atmospheric neutrinos (see figure 1). Before looking at the data, an optimal cut of  $N_{\text{ch}}$  was found in order to produce the best limit setting sensitivity of the search [20, 38]. The data above this cut ( $N_{\text{ch}} > 100$ ) were kept blind while the lower  $N_{\text{ch}}$  events were compared to atmospheric neutrino expectations. The Bartol [14] and Honda [15] atmospheric neutrino fluxes were varied to account for systematic uncertainties, then constrained by normalisation with the low  $N_{\text{ch}}$  data. The remaining spread in the high  $N_{\text{ch}}$  region was used to calculate an error on the expected number of events above the  $N_{\text{ch}} > 100$  cut. The results are shown in figure 1 and compared to the data. Above the cut, 6 events were seen, where 6.1 were expected. Using the range of atmospheric uncertainty (shaded band in figure 1) in the limit calculation [39] leads to a limit on an  $E^{-2}$  flux of muon-neutrinos, at the earth, of  $E_\nu^2 \times dN_\nu/dE_\nu = 8.8 \times 10^{-8}$  GeV cm<sup>-2</sup> s<sup>-1</sup> sr<sup>-1</sup>. This limit is valid in the energy range 16-2500 TeV and is the best limit of any neutrino detector to date. Limits were also placed on specific extra-terrestrial models and on the flux of prompt, charm-meson neutrinos from the earth's atmosphere [40].

### 2.6. Supernovae, cosmic ray composition, monopoles and new physics

AMANDA is a supernova detector, with sensitive coverage of our galaxy [41]. A burst of low energy electron-neutrinos from a supernova would produce an increase in the rates of all optical modules over a short time ( $\sim 10$  seconds). The AMANDA supernova system is part of the Supernova Early Warning System (SNEWS). AMANDA, in conjunction with the SPASE surface air shower detector, has been used to study the composition of cosmic rays near the knee [42]. Searches for magnetic monopoles have been made, and Lorentz invariance and decoherence are two of the “new physics” tests being conducted with atmospheric neutrino data from AMANDA.

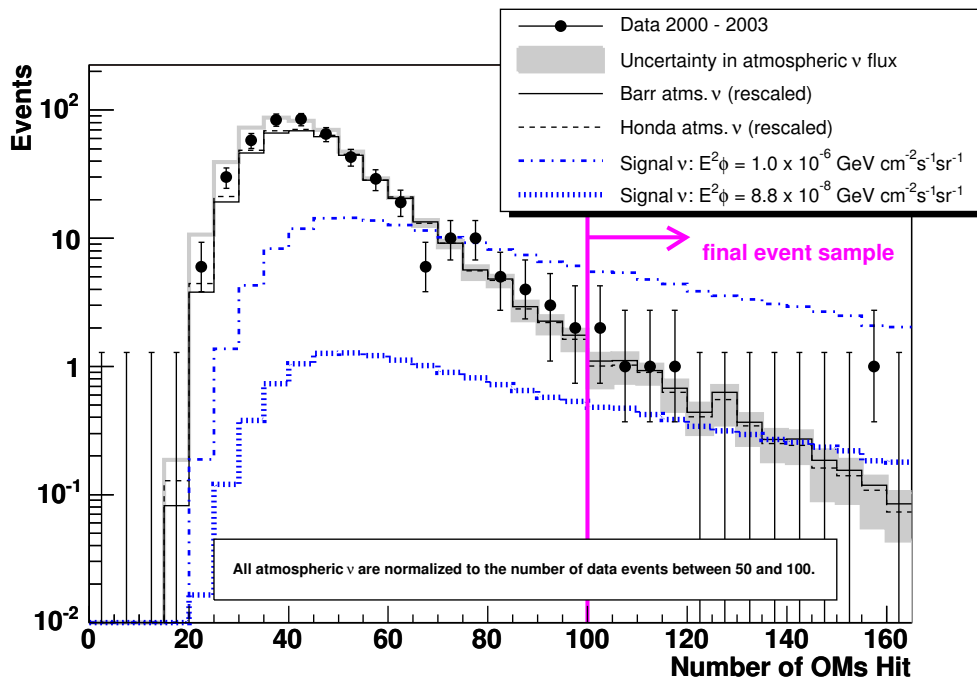


**Figure 1.**  $N_{\text{ch}}$ , the number of OMs triggered, for the AMANDA 2000-03 muon track diffuse analysis. The data is compared to atmospheric neutrino expectations [14, 15]. The signal prediction for an  $E^{-2}$  flux is rescaled to reflect the event limit derived from the background and events above  $N_{\text{ch}} = 100$ .

**Table 1. Summary of AMANDA diffuse neutrino flux results, 1997-2003.** The results labelled “muon” are for analyses sensitive to neutrino-induced muon tracks in the detector, and give limits on the muon-neutrino flux at earth. The “all-flavour” analyses are sensitive to events from muon, electron and tau neutrinos, and place limits on the total neutrino flux at the earth, assuming a 1:1:1 flavour ratio due to maximal mixing neutrino oscillations during propagation to the earth. Assuming this 1:1:1 flavour ratio, the muon-neutrino limits may be converted to all-flavour limits by multiplying by three.

Data set	Detection channel	Neutrino energy range TeV	Limit $E_\nu^2 \times dN_\nu/dE_\nu$ (90% c.l.) $\text{GeV cm}^{-2} \text{s}^{-1} \text{sr}^{-1}$
1997	muon [37]	$6 - 10^3$	$8.4 \times 10^{-7}$
1997	all flavour, UHE [34]	$10^3 - 3 \times 10^6$	$9.9 \times 10^{-7}$
1997	all flavour, cascade [31]	$5 - 300$	$98.0 \times 10^{-7}$
2000	all flavour, cascade [32]	$50 - 5 \times 10^3$	$8.6 \times 10^{-7}$
2000	all flavour, UHE [35, 36]	$1.8 \times 10^2 - 1.8 \times 10^6$	$9.9 \times 10^{-7}$
2000	muon, unfolding [16]	$100 - 300$	$2.6 \times 10^{-7}$
2000-03	muon	$16 - 2.5 \times 10^3$	$0.88 \times 10^{-7}$

### 3. IceCube: The future is now

#### 3.1. Construction and Performance

The first of the next generation kilometre scale neutrino telescopes, IceCube, will consist of an in-ice cubic kilometre neutrino detector, and a kilometre square surface cosmic ray air shower detector (IceTop). Construction began at the South Pole during the austral summer 2004-05, with 1 in-ice string, and 4 IceTop stations deployed [43]. During the second summer season, 8 more strings and 12 IceTop stations were installed. The goal is to complete construction in early 2011, with 80 strings (4800 modules) and stations (320 modules) completed. The in-ice strings will instrument a kilometre volume between 1500 and 2500 metres depth, and the IceTop array will cover a square kilometre at the surface. The same design of DOM (Digital Optical Module) is used throughout the detector. These consist of pressure spheres containing 10 inch photomultiplier tubes, the signals of which are digitised inside the module and then sent to the surface data acquisition system. The DOMs differ from the AMANDA modules in that the full time series of photons (the “waveform”) is captured.

The holes are drilled with a hot water system, taking about 30 hours to drill to the final depth, then 10 hours to ream back up, depositing more energy to leave a hole at the correct size during the string deployment. Deployment of a string takes about 12 hours - 8 hours for module attachment, 4 hours to lower to the final depth. IceTop tanks are installed in shallow trenches dug near each string location, and are filled with water, which is allowed to slowly freeze back about the modules, to prevent formation of bubbles.

The deployed hardware has performed up to expectations to date. Detailed studies of the first string and IceTop tank behaviour has been published [43]. Two upward moving events were detected with the single string, consistent with an atmospheric neutrino origin. The presently operating 9 string and 16 station detector is performing well. Upward moving neutrino events have been seen. Atmospheric muons have been tracked in the in-ice array. Air showers have been reconstructed with IceTop, and coincident events, where IceTop sees an air shower and the in-ice array sees the penetrating muons, have been studied. First physics analyses are well underway.

#### 3.2. Physics potential

An initial potential performance study for the in-ice array of IceCube was completed before construction began [44]. The simulation and reconstruction programs were those used in AMANDA, adapted to the larger IceCube detector. As such, no usage of the DOM waveform information was made in the reconstruction. The assumed flux of charm atmospheric neutrinos [45] was chosen conservatively; if in reality this background turns out smaller, then the predicted sensitivities will be better than those quoted. A median angular resolution of better than  $1^\circ$  is seen for muon energies greater than 1 TeV. The effective area for muon detection exceeds the geometric kilometre area at 10 TeV, rising to 1.4 square kilometres for events in the 1 to 100 PeV energy range. The sensitivity to diffuse and point sources of neutrinos has been estimated. For three to five years of observation, the limit on an  $E^{-2}$  flux of diffuse neutrinos would be about thirty times smaller than the AMANDA-II four-year muon limit (section 2.5), and a flux one-tenth of the AMANDA-II limit would be detectable at  $5\sigma$  significance in that time. For point sources, similar results are obtained. For GRBs, the Waxman-Bahcall flux would be constrained after the observation of about 100 GRBs, and 500 GRBs would be needed to observe that flux at a  $5\sigma$  significance.

### 4. Conclusions

The long-held dream of a large volume, high energy neutrino detector is finally a reality at the South Pole. The last decade has been one of technology, deployment, and analysis development with the AMANDA detector, leading to the design and construction of IceCube. IceCube,

slated for completion in 2011, is already producing physics data, and once completed, will have unprecedented sensitivity to sources of extra-terrestrial neutrinos, hopefully leading to new discoveries about the nature of the cosmos.

## References

- [1] For more information, see the IceCube website: <http://icecube.wisc.edu>
- [2] Gaisser T K, Halzen F and Stanev T 1995 *Phys. Rept.* **258** 173 [*Erratum* 1995 **271** 355 ], hep-ph/9410384; Learned J G and Mannheim K 2000 *Ann. Rev. Nucl. Part. Science* **50** 679; Halzen F and Hooper D 2002 *Rept. Prog. Phys.* **65** 1025, arXiv:astro-ph/0204527; Halzen F 2006 *Proc. of 'The multi-messenger approach to high-energy gamma ray sources,'* Barcelona
- [3] Lowder D M, Miller T, Price P B, Westphal A, Barwick S W, Halzen F and Morse R 1991 *Nature* **353** 331
- [4] Askebjerg P *et al* 1995 *Science* **267** 1147-1150
- [5] Ackermann M *et al* 2006 *Journal of Geophysical Research* **111** D13203
- [6] Ackermann M *et al* 2006 *Nucl. Inst. and Meth. in Phys. Res., A.* **556** 169
- [7] Andres E *et al* 2000 *Astropart. Phys.* **13** 1
- [8] Karle A, for the AMANDA collaboration 1999 *Proc. 26th ICRC, Salt Lake City, Utah*
- [9] Ahrens J *et al* 2004 *Nuclear Instruments and Methods in Physics Research A* **524** 169
- [10] Ahrens J *et al* 2002 *Phys. Rev. D* **66**, 012005
- [11] Andres E *et al* 2001 *Nature* **410** 441
- [12] Ackermann M, for the IceCube Collaboration 2006 *Proc. of 'The multi-messenger approach to high-energy gamma ray sources,'* Barcelona
- [13] Achterberg A *et al* 2006 to be submitted to *Phys. Rev. D.*
- [14] Barr G D, Gaisser T K, Lipari P, Robbins S and Stanev T 2004 *Phys. Rev. D* **70**, 023006
- [15] Honda M, Kajita T, Kasahara K and Midorikawa S 2004 *Phys. Rev. D* **70**, 043008
- [16] K. Münich for the IceCube Collaboration 2005 2005 Proc. 29th Int. Cosmic Ray Conf., Pune
- [17] Ahrens J *et al* 2003 *Astrophys. J* **583** 1040
- [18] Ahrens J *et al* 2004 *Phys. Rev. Lett.* **92** 071102
- [19] Ackermann M *et al* 2005 *Phys. Rev. D* **71** 077102
- [20] Hill G C and Rawlins K 2003 *Astropart. Phys.* **19** 393
- [21] Achterberg A *et al* 2006 *Astroparticle Physics*, accepted
- [22] Achterberg A *et al* 2006 *Phys. Rev. Lett.* accepted for publication
- [23] Kelley J L for the IceCube Collaboration 2005 Proc. 29th Int. Cosmic Ray Conf., Pune
- [24] Waxman E and Bahcall J 1997 *Phys. Rev. Lett.* **78** 2292-2295
- [25] Kuehn K for the IceCube Collaboration and the IPN Collaboration 2005 Proc. 29th Int. Cosmic Ray Conf., Pune
- [26] Stamatikos M, Kurtzweil J and Clarke M J for the IceCube Collaboration (*Preprint*: astro-ph/0510336)
- [27] Hughey B and Taboada I for the IceCube Collaboration, 2005 Proc. 29th Int. Cosmic Ray Conf., Pune
- [28] Ahrens J *et al* 2002 *Phys. Rev. D* **66** 032006
- [29] Achterberg A *et al* 2006 *Astropart. Phys.* in press
- [30] Achterberg A *et al* 2006 *Astropart. Phys.* **24** 456-466
- [31] Ahrens J *et al* 2003 *Phys. Rev. D* **67** 012003
- [32] Ackermann M *et al* 2004 *Astropart. Phys.* **22** 127
- [33] Dzhilkibaev Z *et al* 2006 *Astropart. Phys.* **25** 140
- [34] Ackermann M *et al* 2005 *Astropart. Phys.* **22** 339
- [35] Gerhardt L for the IceCube Collaboration, 2005 Proc. 29th Int. Cosmic Ray Conf., Pune
- [36] Gerhardt L for the IceCube Collaboration 2006 Proc. SUSY06
- [37] Ahrens J *et al* 2003 *Phys. Rev. Lett.* **90** 251101
- [38] Hodges J for the IceCube Collaboration, 2005 Proc. 29th Int. Cosmic Ray Conf., Pune
- [39] Cousins R D and Highland V L 1992 *Nucl. Ins. Meth. Phys. Res.* **A320** 331, Feldman G and Cousins R 1998 *Phys. Rev. D* **57** 3873, Conrad J, Botner O, Hallgren A and de los Heros C 2003 *Phys. Rev. D* **67** 012002, Hill G C 2003 *Phys. Rev. D* 118101
- [40] Hodges J for the IceCube Collaboration 2006 *Proc. TeV Particle Astrophysics II*, Madison, to appear in *J. Phys.: Conf. Series*
- [41] Ahrens J *et al* 2002 *Astropart. Phys.* **16** 345
- [42] Ahrens J *et al* (AMANDA and SPASE Collaborations) 2004 *Astropart. Phys.* **21** 565
- [43] Achterberg A *et al* 2006 *Astropart. Phys.* doi:10.1016/j.astropartphys.2006.06.007
- [44] Ahrens J *et al* 2004 *Astropart. Phys.* **20** 507
- [45] Bugaev E V *et al* 1998 *Phys. Rev. D* **58** 054001

# Measurements of $^8\text{B}$ Solar Neutrinos – Results and Prospects from SNO and SuperKamiokande

**Andrew Hime**

Physics Division, MS H803, Los Alamos National Laboratory, Los Alamos, NM 87545, USA

ahime@lanl.gov

**Abstract.** Measurements of  $^8\text{B}$  solar neutrinos at the Sudbury Neutrino Observatory (SNO) and at SuperKamiokande (SK) result in a model independent proof that electron neutrinos born in the Sun undergo active flavor transformation. Large mixing angle, matter enhanced neutrino oscillations are responsible for this flavor transformation and the total flux of  $^8\text{B}$  solar neutrinos measured is in agreement with standard solar model predictions. The long-standing solar neutrino problem is resolved. In this paper the salient results from measurements of  $^8\text{B}$  solar neutrinos at SNO and SK are summarized, including recent analyses looking for potential temporal variations in the solar neutrino fluxes and a new limit on the *hep* solar neutrino flux. The field of solar neutrino physics has entered a new era of precision with measurements aimed at the elucidation of fundamental neutrino properties and our basic understanding of how the Sun shines. Future goals and prospects of the SNO and SK experiments are discussed.

## 1. Introduction

This XXII<sup>th</sup> International Conference on Neutrino Physics and Astrophysics marks an historic occasion in a distinguished series with the 50<sup>th</sup> anniversary of the discovery of the electron antineutrino by Fred Reines and Clyde Cowan. We were privileged with the warm account from Herald Kruse at this meeting and equally so for the discovery of muon and tau neutrinos presented by Jack Steinberger. Solar neutrinos have played an equal and vital role in the history of neutrino physics. The pioneering work of Ray Davis Jr. provided the first experimental information about solar neutrinos in the Chlorine radiochemical experiment operating in the Homestake gold mine [1]. During the period of 20 years from 1968 to 1988 this effort was paralleled only by the dedicated and steadfast efforts of John Bahcall and collaborators who continued to refine the theoretical predictions of solar neutrino production rates in what is now commonly known as the Standard Solar Model (SSM). At this meeting Lincoln Wolfenstein reminded us of the original purpose of this pioneering work, namely to test the basic notion that the Sun is powered by nuclear fusion. The deficit of solar neutrinos that Davis measured relative to Bahcall's calculations provided the first hint of either a fundamental problem with our basic understanding of how the Sun shines or the possibility of something anew in the fundamental behavior of neutrinos.

The concept that neutrino properties themselves were responsible for the solar neutrino problem [2] was first met with skepticism. Nonetheless, the field endured with refined calculations and new experiments. In 1989, the Kamoiokande collaboration, following an upgrade to their proton decay experiment, observed a deficit of  $^8\text{B}$  solar neutrinos and was the first to make a real-time measurement of elastic-scattering (ES) interactions of neutrinos with the ability to point to the Sun as their origin

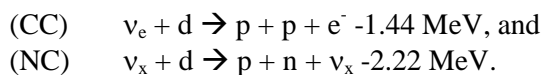
[3]. Soon thereafter, an initiative at the newly established Baksan Laboratory in the Soviet Union gave forth to the SAGE (Soviet American Gallium Experiment) project, a radiochemical experiment exploiting Gallium (Ga) capable to measure the low-energy and dominant (*pp-fusion*) component of the solar neutrino flux. Another experiment (Gallex) to exploit Ga as a solar neutrino target was also staged at the Grann Sasso Laboratory with a mainly European collaboration. Results from these Ga experiments, discussed at this meeting by Vladimir Gavrin, provided a vital ingredient to understanding the solar neutrino puzzle. Bahcall's SSM predicted that Ga experiments should observe a signal of 136 SNU [4]. An observed rate above 69 SNU would indicate a flaw in the SSM while a smaller rate would require new physics at the responsibility of the neutrinos themselves. Nature grinned since the first results from SAGE [5] and Gallex [6] produced a result of exactly 69 SNU.

All results from the solar neutrino experiments at this stage found rates well below the expectations of the SSM. In addition, the deficit of solar neutrinos appeared to be energy dependent and difficult to reconcile within the basic concepts of stellar evolution, nuclear, and particle physics. While the original purpose of the Davis experiment was to test the basic concept that the Sun is powered by nuclear fusion, the suite of experimental results pointed more strongly towards neutrino physics as the source of the solar neutrino deficit. This possibility was strengthened further with the realization of the Mikheyev-Smirnov-Wolfenstein (MSW) effect that would allow neutrino oscillations to be significantly enhanced in dense matter [7]. Nonetheless, there was no smoking gun that could differentiate between a flaw in the SSM or the discovery of new science associated with the neutrino sector. In 1985, Herb Chen and collaborators realized the smoking gun required to solve the problem by exploiting a real-time Cerenkov detector using heavy water to measure the  $^8\text{B}$  rate via both charged-current (CC) and neutral-current (NC) interactions on deuterium [8]. The realization of this concept in SNO (Sudbury Neutrino Observatory) has enabled a solution to the solar neutrino problem by decoupling neutrino properties *per se* from the physics determining their production rate in the Sun.

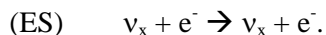
The results from SNO and SuperKamiokande (SK) discussed below resolve the longstanding solar neutrino problem. The deficit of electron neutrinos born in the Sun as observed in the pre-SNO experiments have reappeared as muon and tau neutrinos through the direct detection of their NC interactions. This active flavor transformation of solar neutrinos is well described by the phenomena of matter enhanced neutrino oscillations and this scenario is confirmed by the observation of electron antineutrino disappearance in the KamLAND experiment [9]. Furthermore, the SSM stands triumphant by predicting with remarkable accuracy the total flux of  $^8\text{B}$  solar neutrinos.

## 2. Results from SNO and SuperKamiokande

The SNO detector [10] was filled with heavy water in May 1999 to commence its first phase of operations using pure- $\text{D}_2\text{O}$ . Unique to SNO is its ability to measure purely electron neutrinos via CC interactions and the total flux of active neutrinos via NC interactions, both on deuterium:



Both SNO and SK also measure ES interactions of solar neutrinos from electrons in  $\text{D}_2\text{O}$  and  $\text{H}_2\text{O}$ , respectively:



The first results from SNO were reported in 2001[11], which compared its CC-rate to the ES-rate measured in SK [12]. It was concluded for the first time that the total flux of  $^8\text{B}$  solar neutrinos agrees with SSM predictions but that  $\sim 2/3$  of the electron neutrinos had been transformed to muon and tau neutrinos. This fact was determined directly after lowering the energy threshold in SNO to reveal the neutrons liberated from the NC disintegration of deuterium [13,14].

The SNO experiment was constructed to operate in three separate phases distinguished by the technique to detect neutrons liberated from the NC interactions. In its second phase, the addition of NaCl significantly enhanced SNO's sensitivity to the NC interaction and allowed extraction of the CC-energy spectrum independent of assumptions regarding its shape [15]. A detailed record and analysis of the complete (391 day) dissolved-salt data set from SNO appears in ref. [16]. More recently, an archival account of the initial pure-D<sub>2</sub>O phase (306.4 days) has been provided in ref. [17]. SNO has completed data taking from its third and final phase using a discrete array of ultra-low background Neutral-Current-Detectors (NCDs). The SK collaboration has also published a detailed account of their first phase of operations (SK-I), which collected 1496 days of solar neutrino data (see Fig.1) between April 1996 and July 2001[18]. At this meeting, preliminary results from SK-II were presented based upon 791 days of solar neutrino data following a tragic loss of a significant fraction of PMTs in their Nov.12, 2001 accident. Fortunately, the SuperKamiokande detector is now fully restored and taking data in SK-III.

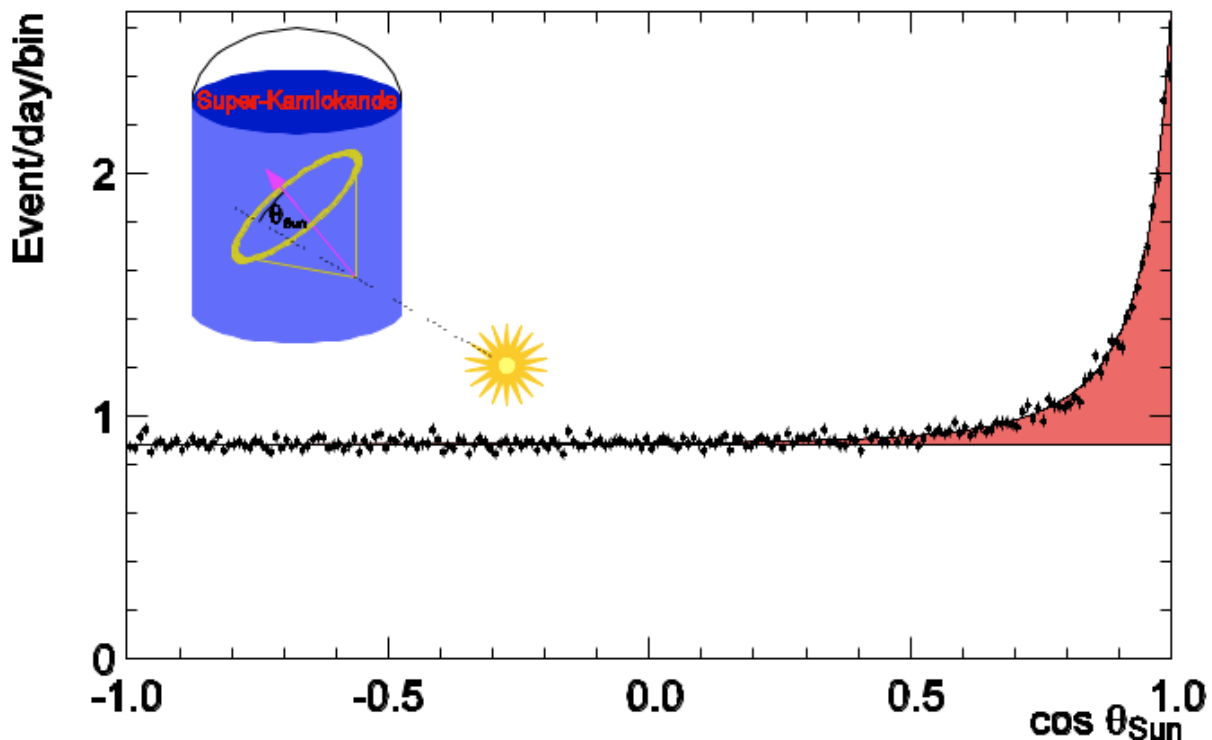


**Figure 1:** The 1496-day data set from SK-I (ref. [18]) containing 22400 solar neutrino events extracted from the characteristic elastic scattering peak.

In units of  $10^6 \text{ cm}^{-2} \text{ s}^{-1}$ , the measured  $^8\text{B}$  solar neutrino fluxes are shown below. These fluxes can be used to deduce the flavor content of the B flux as shown in Fig.2. The total active flux obtained directly from SNO's NC measurement is in good agreement with the SSM value of  $(5.69 \pm 0.91) \times 10^6 \text{ cm}^{-2} \text{ s}^{-1}$  [19] and the experimental value is determined now with a precision roughly two times better than the predicted value.

$$\phi_{\text{CC}}^{\text{SNO}} = 1.68 \pm 0.06 \pm 0.09 \text{ (ref. [16])}$$

$$\phi_{\text{NC}}^{\text{SNO}} = 4.94 \pm 0.21 \pm 0.36 \text{ (ref. [16])}$$

$$\phi_{\text{ES}}^{\text{SNO}} = 2.35 \pm 0.22 \pm 0.15 \text{ (ref. [16])}$$

$$\phi_{\text{ES}}^{\text{SK-I}} = 2.35 \pm 0.02 \pm 0.08 \text{ (ref. [18])}$$

$$\phi_{\text{ES}}^{\text{SK-II}} = 2.38 \pm 0.05 \pm 0.16 \text{ (preliminary)}$$

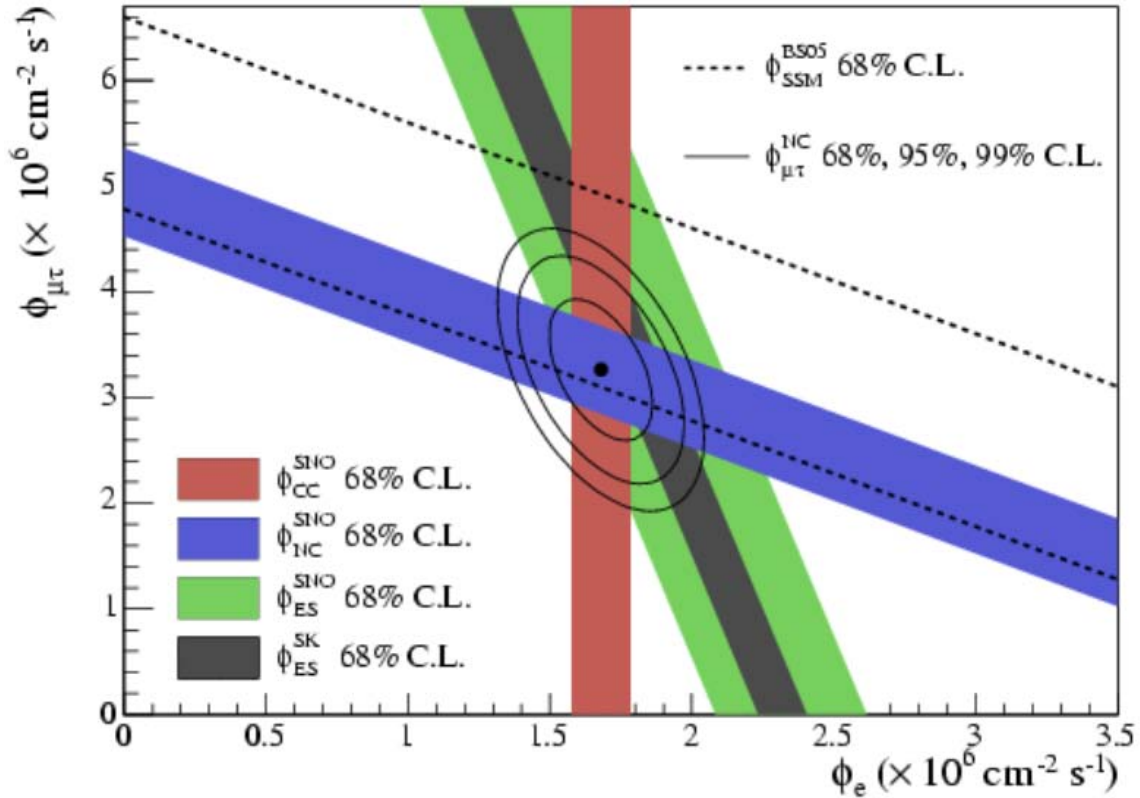


**Figure 2:** Flavor content of the  $^8\text{B}$  solar neutrino flux from ref. [16]. The total flux is measured by the NC rate in SNO (blue band), which agrees well with the SSM prediction shown as the dotted lines. The electron neutrino flux is extracted directly from the CC measurement in SNO (red band). When combined, the solid ellipses constrain the muon/tau *versus* electron flux plane as shown. Approximately 2/3 of the electron neutrino flux is actively converted to muon/tau neutrinos. Also shown are the ES measurements made both at SNO and SK.

Interpreted as two-neutrino flavor oscillations, the LMA (Large Mixing Angle) solution is the only survivor in a global analysis of the solar neutrino data (see Fig.3) and maximal mixing is ruled out with a confidence exceeding five standard deviations. The solar neutrino data and KamLAND data are highly complementary in pinpointing the neutrino parameters. The baseline and energy spectrum of reactor antineutrinos allow KamLAND to zero in on the neutrino mass splitting,  $\Delta m_{12}^2$ , while the solar neutrino data, in particular the NC/CC ratio measured in SNO, provides the best measure of the mixing angle,  $\theta_{12}$ . Matter-enhanced neutrino oscillations as described by the MSW mechanism predict that electron neutrinos originally converted to muon and tau neutrinos in the Sun would be regenerated as they pass through the Earth. This effect would give rise to an asymmetry in the electron component of the solar neutrino flux as measured in the daytime *versus* the nighttime,  $A_{\text{ND}} \equiv 2(\phi_{\text{N}} - \phi_{\text{D}}) / (\phi_{\text{N}} + \phi_{\text{D}})$ . Unfortunately, SNO and SK predict this effect to be small for the established LMA parameter space and the  $^8\text{B}$  neutrino energies accessible:

$$A_{CC}^{SNO} = 0.037 \pm 0.040 \text{ (ref. [16])}$$

$$A_{ES}^{SK-I} = 0.021 \pm 0.020 \pm 0.013 \text{ (ref. [18])}$$

$$A_{ES}^{SK-II} = 0.014 \pm 0.049 \pm 0.025 \text{ (preliminary)}$$

In principle, distortions could also be observable in electron energy spectra owing to the energy dependence of the electron neutrino survival probability. Again, this effect is predicted to be small for the established LMA parameter space and the  $^8\text{B}$  neutrino energies accessible by SNO and SK (Fig.3). As discussed in section 5 below, efforts to combine data from the various phases of SNO and to accumulate more and more data from SK-III aim to improve the precision of these fundamental measurements and extend the scientific reach accessible with  $^8\text{B}$  solar neutrinos.

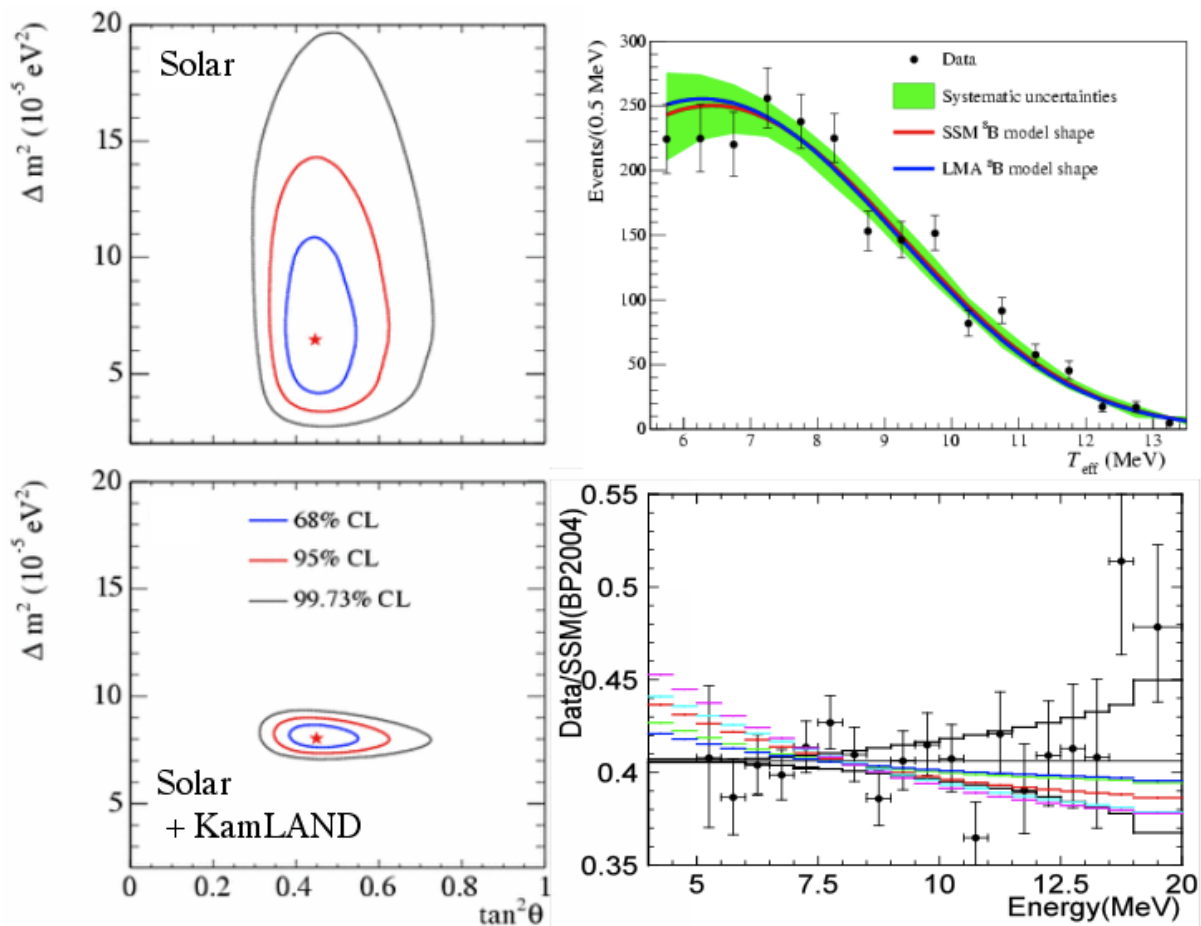


**Figure 3:** The left panels show the two-neutrino mixing parameters from ref. [16] in a global analysis of the solar neutrino data (upper left) and when combined with the results from the KamLAND experiment (lower left). The CC electron energy spectrum extracted from the SNO dissolved-salt phase (ref. [16]) is shown in the upper right panel. Also shown are the spectral shapes predicted in SNO for the standard, undistorted,  $^8\text{B}$  spectrum along with that predicted for the central LMA solution. The recoil electron energy spectra extracted from the ES measurement in SK-I (ref. [18]) is shown in the lower right panel along with systematic spread associated with energy-related systematic uncertainties. The colored lines show the expected distortions in the SK spectrum within the allowed regions of the LMA solution.

### 3. Temporal Modulations and Flux Periodicities

At this meeting David Caldwell discussed recent reports of periodic variations in the measured solar neutrino fluxes associated with the solar rotational period. On the one hand, since solar rotation should not produce variations in the nuclear fusion rate, periodicities in the solar neutrino flux would indicate new physics such as electron neutrino conversion to sterile neutrinos due to coupling through a transition magnetic moment to harmonics of the Sun's rotating magnetic field. On the other hand, analyses including those of the experimental collaborations themselves, do not find evidence for such periodicities. Particularly relevant to this paper is the claim by Sturrock *et al* of a 7% amplitude modulation in SK's  ${}^8\text{B}$  neutrino flux [20]. The period of this modulation is  $9.43 \text{ yr}^{-1}$  with a claimed significance exceeding 99%. The SK collaboration reports no such evidence in their analysis using the Lomb-Scargle periodogram method [21]. Ranucci analyzed the same data using both maximum likelihood and Lomb-Scargle methods [22] and attributes the contradictory claims to differences in the treatment of uncertainties but does not confirm or directly rule out the possibility of the claimed effect. More recently the SK collaboration performed another study of their data using a  $\Delta\chi^2$  technique in order to account directly for the error bar associated with each of the 5-day binned data points. As shown in Fig.4, structure is present in the data including the claimed frequency of  $9.43 \text{ yr}^{-1}$ , however, it corresponds only to 8.4% statistical significance and the SK collaboration concludes that no significant periodicity is observed.

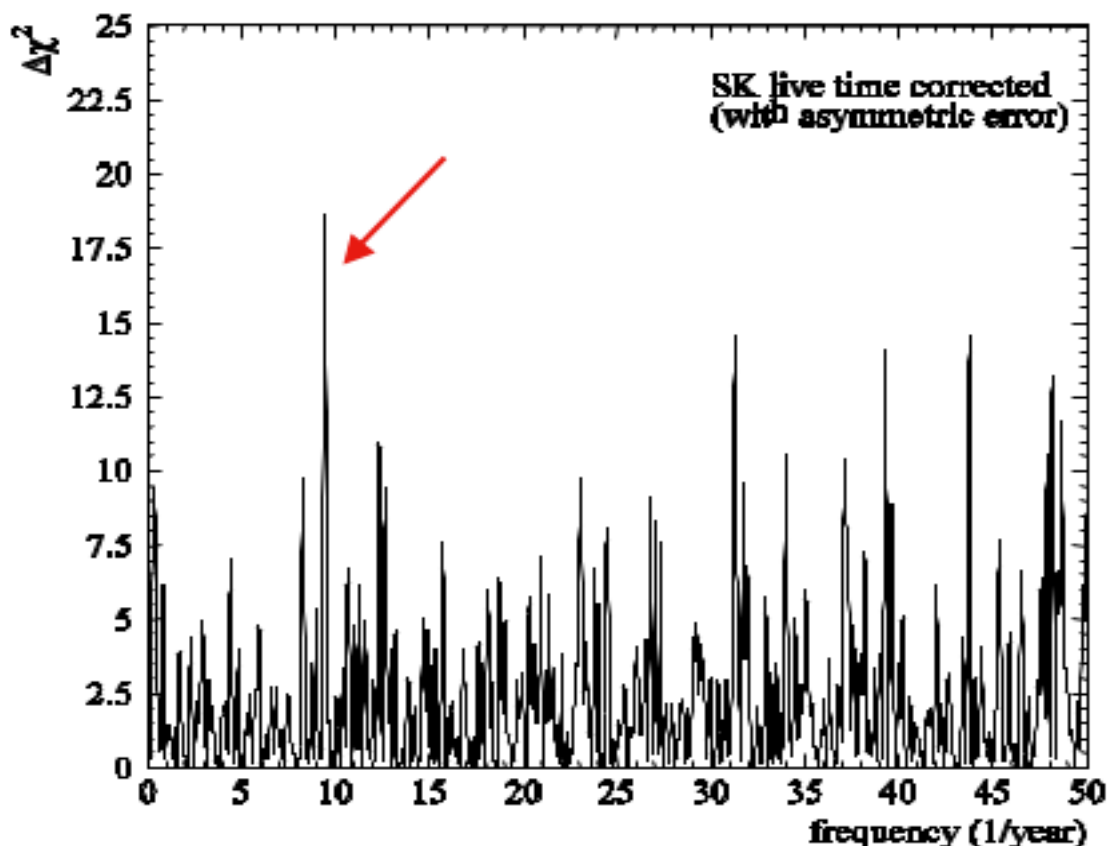
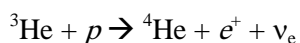


**Figure 4:** The  $\Delta\chi^2$  analysis of the SK-I data set provided by the SK collaboration at this meeting. The arrow points to the potential peak in the frequency spectrum at  $9.43 \text{ yr}^{-1}$  claimed by Sturrock *et al*. to be present at a high C.L. in an independent analysis. The study provided here by the SK collaboration claims a probability of only 8.4% that this peak is more than a statistical fluctuation and that such fluctuations are consistent with those found at other frequencies spanned by the data set.

The SNO collaboration has published its own periodicity analysis of its D<sub>2</sub>O and dissolved-salt data sets using both a Lomb-Scargle periodogram and an unbinned maximum likelihood fit [23]. For the combined data sets the largest effect occurs at a period of 2.4 days and Monte Carlo shows that a peak at least this large would occur 35% of the time. At the claimed frequency of 9.43 yr<sup>-1</sup>, SNO's best-fit amplitude is  $(1.3 \pm 1.6)\%$  and inconsistent with a 7% modulation of the <sup>8</sup>B flux. While any evidence for non-standard periodicities in the SNO and SK data sets appears waning, studies can also be performed at other frequencies of interest. In particular, a seasonal variation is expected owing to the Earth-Sun orbital eccentricity of 1.67%. An eccentricity of  $(2.1 \pm 0.3)\%$  has been extracted from the SK-I data [18] and  $(1.43 \pm 0.86)\%$  from SNO [23], both in agreement with the expected value.

#### 4. Search for *hep* Solar Neutrinos

Five reactions in the primary *pp* fusion chain lead to solar neutrinos, the highest energies of which ensue from the *hep* reaction with endpoint energy of 18.77 MeV:



An observation of these *hep* neutrinos has so far eluded experiments owing to their small-predicted flux of  $(7.97 \pm 1.24) \times 10^3 \text{ cm}^{-2} \text{ s}^{-1}$  [24], some 700 times lower than even the <sup>8</sup>B flux. A limit on the *hep* flux of  $7.3 \times 10^4 \text{ cm}^{-2} \text{ s}^{-1}$  at 90% C.L. was set by the SK collaboration [25]. Accounting for neutrino oscillations this can be interpreted as an upper bound on the total *hep* flux of  $1.5 \times 10^5 \text{ cm}^{-2} \text{ s}^{-1}$ . SNO has recently improved this limit by a factor of  $\sim 6.5$  in an analysis of their initial, pure-D<sub>2</sub>O data set [26]. As can be seen in Fig.5 the dominant background for the *hep* neutrinos is the <sup>8</sup>B neutrinos themselves. Consequently, a low energy (6 to 12 MeV) energy window is chosen to normalize the <sup>8</sup>B spectrum with an account for neutrino oscillations. A signal box for *hep* neutrinos was then optimized using Monte Carlo simulations while blinding the data on the energy interval from 12 to 35 MeV. An optimum window of 14.3 to 20 MeV was found where  $3.1 \pm 0.6$  background events were expected and a SSM signal of  $0.99 \pm 0.09$  events. With 2 events observed in the signal box, this leads to SNO's upper limit of the total *hep* flux of  $2.3 \times 10^4 \text{ cm}^{-2} \text{ s}^{-1}$  at 90% C.L.

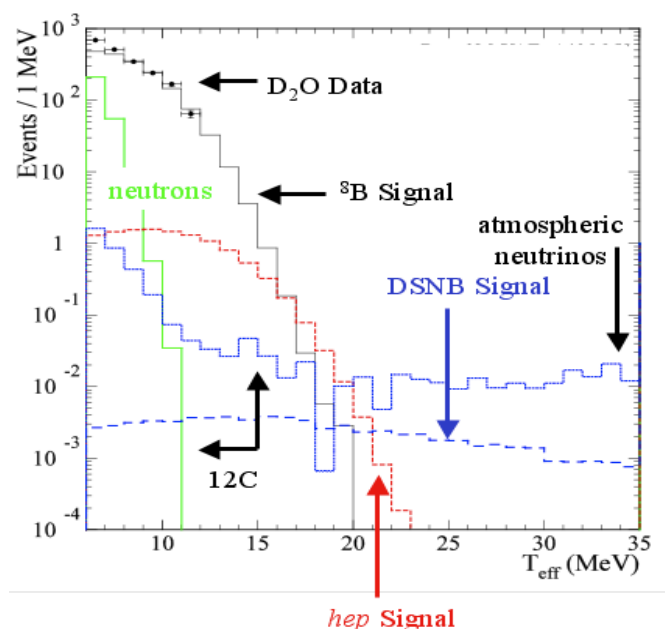


**Figure 5:** The signal region and backgrounds for the pure-D<sub>2</sub>O data set from SNO recently used to set a limit of  $2.3 \times 10^4 \text{ cm}^{-2} \text{ s}^{-1}$  at 90% C.L. on the *hep* solar neutrino flux (ref. [26]).

## 5. Future Prospects

With the solar neutrino problem resolved, the field of solar neutrino physics has evolved to one of precision measurements aimed at the elucidation of the new paradigm of neutrino oscillations. At  $^8\text{B}$  energies, the SNO and SK programs continue to push their envelope of sensitivity both by the analysis of new data as well in perfecting analysis methods to improve systematic uncertainties. Improved precision in the  $^8\text{B}$  fluxes alone directly impacts the precision with which the fundamental neutrino parameters can be extracted. This is particularly true for the mixing angles since the ratio of CC to NC fluxes as measured in SNO is a direct measure of the electron neutrino survival probability. For active neutrino oscillations we have:

$$\phi_{\text{CC}} / \phi_{\text{NC}} \sim \text{Cos}^4\theta_{13}\text{Sin}^2\theta_{12} = 0.34 \pm 0.23 \pm 0.031 \text{ (ref. [16])}.$$

Consequently, in a simple 2-component mixing scenario (*ie.*  $\theta_{13}=0$ ), the solar neutrino measurements directly constrain the mixing probability  $\text{Sin}^2\theta_{12}$ . Interestingly, the solar neutrino data also play a role in constraining  $\theta_{13}$  in a 3-component analysis of neutrino oscillation data as can be seen by the additional  $\text{Cos}^4\theta_{13}$  weighting above. The solar neutrino data are particularly important in this regard for the region of small values of the atmospheric neutrino mass splitting [27,28].

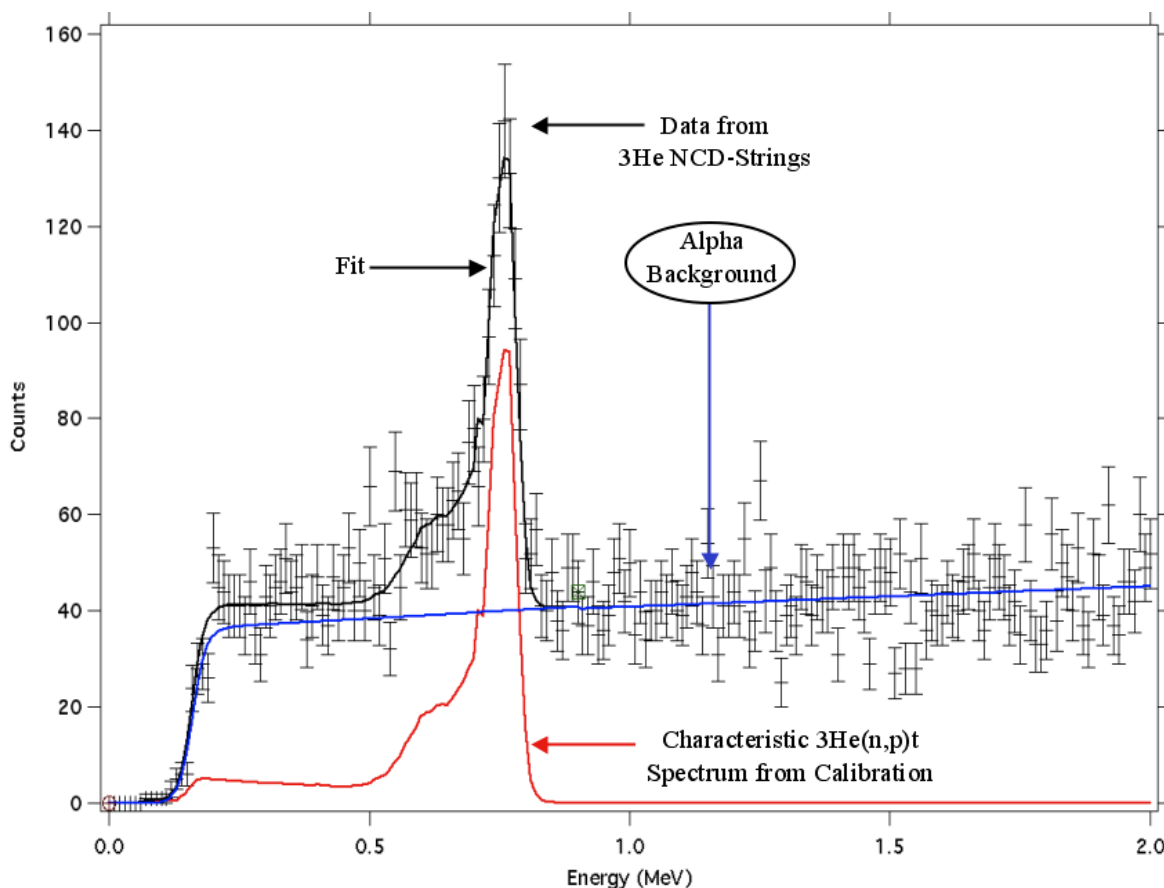


**Figure 6:** The  $^3\text{He}(n, p)t$  spectrum extracted from the blind data set in SNO's third and final phase with discrete Neutral Current Detectors (NCDs) deployed in the central detector. Shown are the experimental data points with statistical error bars. The data clearly contain neutron capture events distributed as expected based upon the neutron calibration data (shown in red). These events sit upon a continuum of alpha-particle background associated with U and Th contained within the bulk material comprising the proportional counters.

Of particular interest is the possibility to directly demonstrate what is now a fundamental prediction of the new paradigm of LMA neutrino oscillations, namely the presence of matter effects and the energy dependence of the electron neutrino survival probability. The former would be revealed in a measurement of a non-zero day-night asymmetry while the latter would be manifest as a distortion in the electron neutrino energy spectrum. Unfortunately, as described above, these effects are now predicted to be small in the SNO and SK experiments. The possibility to reveal a day-night asymmetry will benefit mainly through the accumulation of statistics through further running of the SK-III experiment and by combining the data accumulated from the various stages of the SNO experiment. More data will also aid studies of the spectral shape, however, improvements are required to also reduce systematic uncertainties associated with energy-dependent correlations. Both the SK and SNO collaborations are developing methods to do just this and there are positive indications that analyses of  $^8\text{B}$  solar neutrinos will be extended to a threshold as low as  $\sim 4$  MeV in both cases. Ultimately, the extraction of CC and NC signals in SNO will be enhanced with data from its third and final NCD phase. The NCD experiment allows a measurement of the NC independent of the Cerenkov signal and thus offers a unique method to break the statistical correlation between CC and NC signals characteristic of previous phases of the experiment. As can be seen in Fig.6 the quality of the data is high and the collaboration is presently engaged in a blind analysis of the NCD data set.

## References

- [1] B.T. Cleveland *et al.*, *Astrophys. J.* **496**, 505 (1998).
- [2] V.N. Gribov and B. Pontecorvo, *Phys. Lett.* **B28**, 493 (1969).
- [3] K.S. Hirata *et al.*, *Phys. Rev. Lett.* **63**, 16 (1989).
- [4] J.N. Bahcall, *Revs. Mod. Phys.* **50**, 881 (1978).
- [5] A.I. Abazov *et al.*, *Phys. Lett.* **B328**, 234 (1994); *Nucl. Phys. B (Proc. Suppl.)* **19**, 77 (1991).
- [6] P. Anselmann *et al.*, *Nucl. Phys. Proc. Suppl.* **31**, 117 (1993).
- [7] S.P. Mikheyev and A.Y. Smirnov, *Prog. Part. Nucl. Phys.* **23**, 41 (1989); L. Wolfenstein, *Phys. Rev. D* **17**, 2369 (1978).
- [8] H.H. Chen, *Phys. Rev. Lett.* **55**, 1534 (1985); G. Aardsma *et al.*, *Phys. Lett.* **B194**, 321 (1987).
- [9] KamLAND Collaboration, *Phys. Rev. Lett.* **94**, 081801 (2005); *Phys. Rev. Lett.* **90**, 021802 (2003).
- [10] SNO Collaboration, *Nucl. Instrum. Meth.* **A449**, 172 (2000).
- [11] SNO Collaboration, *Phys. Rev. Lett.* **87**, 071301 (2001).
- [12] S. Fukuda *et al.*, *Phys. Lett.* **B539**, 179 (2002); *Phys. Rev. Lett.* **86**, 5651 (2001).
- [13] SNO Collaboration, *Phys. Rev. Lett.* **89**, 011301 (2002).
- [14] SNO Collaboration, *Phys. Rev. Lett.* **89**, 011302 (2002).
- [15] SNO Collaboration, *Phys. Rev. Lett.* **92**, 181301 (2004).
- [16] SNO Collaboration, *Phys. Rev.* **C72**, 055502 (2005).
- [17] SNO Collaboration, arXiv:nucl-ex/0610020, *accepted for publication in Phys. Rev. C*.
- [18] SuperKamiokande Collaboration, arXiv:hep-ph/0508053.
- [19] J.N. Bahcall, A.M. Serenelli, and S. Basu, *Astrophys. J.* **621**, L85 (2005).
- [20] P.A. Sturrock *et al.*, *Astrophys. J.* **605**, 568 (2004); arXiv:hep-ph/0501205; *Phys. Rev.* **D72**, 113004 (2005); arXiv:hep-ph/0601251.
- [21] SuperKamiokande Collaboration, *Phys. Rev.* **D68**, 092002 (2003).
- [22] G. Ranucci, *Phys. Rev.* **D73**, 103003 (2006).
- [23] SNO Collaboration, *Phys. Rev.* **D72**, 052010 (2005).
- [24] J.N. Bahcall, A.M. Serenelli, and S. Basu, *ApJS.* **165**, (2006).
- [25] J. Hosaka *et al.*, (SK Collaboration), *Phys. Rev.* **D73**, 112001 (2006).
- [26] SNO Collaboration, *Astrophys. J.* **653**, 1545 (2006).
- [27] M. Maltoni, *et al.*, arXiv:hep-ph/0309130; G.L. Fogli *et al.*, *Phys. Rev.* **D62**, 013002 (2000).
- [28] J.F.W. Valle, arXiv:hep-ph/0509262.

# Phenomenology of neutrinoless double beta decay

**Martin Hirsch**

AHEP Group, IFIC/CSIC, Edificio Institutos de Paterna, Apt 22085, E-46071 Valencia, Spain

E-mail: mahirsch@ific.uv.es

**Abstract.** Neutrinoless double beta decay ( $0\nu\beta\beta$ ) violates lepton number by two units, a positive observation therefore necessarily implies physics beyond the standard model. Here, three possible contributions to  $0\nu\beta\beta$  decay are briefly reviewed: (a) The mass mechanism and its connection to neutrino oscillations; (b) Left-right symmetric models and the lower limit on the right-handed  $W$  boson mass; and (c) R-parity violating supersymmetry. In addition, the recently published “extended black box” theorem is briefly discussed. Combined with data from oscillation experiments this theorem provides proof that the  $0\nu\beta\beta$  decay amplitude must receive a non-zero contribution from the mass mechanism, if neutrinos are indeed Majorana particles.

## 1. Introduction

Since the discovery of neutrino oscillations [1] most papers on neutrinoless double beta decay ( $0\nu\beta\beta$ ) have exclusively concentrated on its implications for Majorana neutrino masses. However, as is well-known, *any* model beyond the standard model of particle physics, which allows for lepton number violation, potentially contributes to  $0\nu\beta\beta$  decay. Thus, the basic physics of  $0\nu\beta\beta$  decay can be summarized as:

$$\left[T_{1/2}^{0\nu\beta\beta}\right]^{-1} = \left(\sum_i \langle\epsilon_i\rangle \mathcal{M}_{\epsilon_i}\right)^2 F^{0\nu\beta\beta}. \quad (1)$$

The factor  $\langle\epsilon_i\rangle$  contains some (unknown, but lepton number violating) particle physics parameters. To determine the numerical value of  $\langle\epsilon_i\rangle$  input from both, experiment and theoretical nuclear physics, is needed. Experiments limit (or measure)  $T_{1/2}^{0\nu\beta\beta}$ , for a discussion of various different experiments see, for example [2].  $\mathcal{M}_{\epsilon_i}$  in eq. (1) stands for a nuclear structure matrix element. Different particle physics contributions to  $0\nu\beta\beta$  decay depend on different matrix elements. No definite consensus about the value and, most importantly, the error of nuclear matrix elements exist up to now. For a thorough discussion see [3]. Finally,  $F^{0\nu\beta\beta}$  is a leptonic phase space integral, its value can be calculated quite precisely [4].

This talk concentrates exclusively on particle physics aspects of  $0\nu\beta\beta$  decay. The classic “black box” [5] theorem and its recently published “extended” version [6] are briefly discussed, before reviewing constraints on left-right symmetric models and supersymmetry with R-parity violation derived from a lower limit on the  $0\nu\beta\beta$  decay half-life. Last but not least, expectations for the mass mechanism of  $0\nu\beta\beta$  decay in light of neutrino oscillation data are discussed. It is curious to note, that combining the “extended black box” with oscillation data [6] already today demonstrates that there must be a non-zero contribution from the mass mechanism to the  $0\nu\beta\beta$  decay amplitude, if neutrinos are indeed Majorana particles.

## 2. $0\nu\beta\beta$ decay and the Black Box

From the experimental point of view lepton number violation in  $0\nu\beta\beta$  decay is observed through the appearance of two electrons in the final state with **no** missing energy. Many different, possible mechanisms have been discussed in the literature. Interestingly, however, one can show [5] that independent of which contribution to  $0\nu\beta\beta$  decay is the dominant one, neutrinos are guaranteed to have a non-zero Majorana mass, if  $0\nu\beta\beta$  decay is observed. The proof of this “black box” theorem [5] essentially follows from the observation that any effective low-energy  $\Delta L \neq 0$  operator inducing  $0\nu\beta\beta$  decay will contribute also - possibly at the some order in perturbation theory, for sure in some higher order - to the  $(\nu_e - \nu_e)$  entry of the Majorana neutrino mass matrix ( $M_{ee}^\nu$ ). A perfect cancellation of all different contributions to  $M_{ee}^\nu$  would then require a special symmetry and the proof of the black box theorem is completed by showing that no such symmetry can exist [7] in any gauge model containing the standard model charged current interaction.

This well-known theorem has recently been extended to the case of three generations of neutrinos and arbitrary lepton number and lepton flavour violating processes [6]. Combined with data from oscillation experiments this “extended” black box theorem can be used to show that  $M_{ee}^\nu \neq 0$ . The proof involves two steps. In the first step it is shown that any effective operator generating lepton number violating processes of the form  $\Phi_k \rightarrow \Phi_m l_\alpha l_\beta$ , where  $\Phi_k$  and  $\Phi_m$  stand symbolically for any set of SM particles with  $L = 0$ , necessarily generates a non-zero  $M_{\alpha\beta}^\nu$  entry in the Majorana neutrino mass matrix in higher order of perturbation theory. As for the original black box, one can show that there is no possible symmetry allowing for a perfect cancellation of different contributions to this entry. In the second step, then all allowed neutrino mass matrices with  $M_{ee}^\nu \equiv 0$  are constructed. It is then easy to show that none of the possible five structures is consistent with oscillation data. One can thus conclude that  $M_{ee}^\nu \neq 0$  is guaranteed for Majorana neutrinos [6] already today.

The above theorem(s) do not state which mechanism of  $0\nu\beta\beta$  decay is the dominant one. Two instructive examples, in which the mass mechanism might indeed not be the dominant contribution to  $0\nu\beta\beta$  decay, are therefore discussed next.

### 2.1. Left-right symmetry

For  $0\nu\beta\beta$  decay, with its typical low energy scale of a few MeV, all calculations can be done with the effective Hamiltonian [4]

$$\mathcal{H}_W^{CC} = \frac{G_F}{\sqrt{2}} \left\{ J_{\mu L}^\dagger j_{\mu L}^- + \kappa J_{\mu R}^\dagger j_{\mu L}^- + \eta J_{\mu L}^\dagger j_{\mu R}^- + \lambda J_{\mu R}^\dagger j_{\mu R}^- \right\}. \quad (2)$$

Here,  $J_{\mu\alpha}^\dagger = \bar{u}\gamma_\mu d_\alpha$  and  $j_{\mu\alpha}^- = \bar{e}\gamma_\mu \nu_\alpha$  are the hadronic and leptonic charged currents,  $L/R$  stands for  $P_{L/R} = \frac{1}{2}(1 \mp \gamma_5)$ .  $G_F$  is the Fermi constant,  $\kappa \simeq \eta \simeq \tan \zeta$ , i.e. the mixing angle between the  $W_L$  and  $W_R$  bosons, and  $\lambda \simeq (m_{W_L}/m_{W_R})^2$ .

The Hamiltonian of eq. (2) gives rise to the diagrams in fig. (1). The graphs on the left and the middle represent so-called “long-range” contributions. The graph to the left is due to a product of two  $j_{\mu L}^-$  and corresponds to the mass mechanism of  $0\nu\beta\beta$  decay, proportional to  $\langle m_\nu \rangle = \sum_i U_{ei}^2 m_{\nu_i}$  (see discussion in the next section). The graph in the middle is proportional to  $\langle \lambda \rangle = \lambda \sum_i U_{ei} V_{ei}$  and  $\langle \eta \rangle = \eta \sum_i U_{ei} V_{ei}$ . The graph to the right is proportional to  $\langle \xi \rangle = \left[ \lambda^2 + \eta^2 - 2\lambda\eta \left( \frac{M_{GT}^N + M_F^N}{M_{GT}^N - M_F^N} \right) \right] / \langle m_N \rangle$  [8]. Here,  $\langle \frac{1}{m_N} \rangle = \sum_j V_{ej}^2 \left( \frac{m_p}{m_j} \right)$ .

Formally, the long-range contribution in LR models are suppressed only by one power of  $\lambda/\eta$ , compared to the short-range contribution, which is quadratic in  $\lambda/\eta$ . Many calculations therefore have taken into account only the long-range LR contributions. However, as first pointed out by Mohapatra [9] and confirmed by a detailed calculation of the relevant nuclear matrix elements [8], the short-range contribution can be much more important than the long-range one. This at

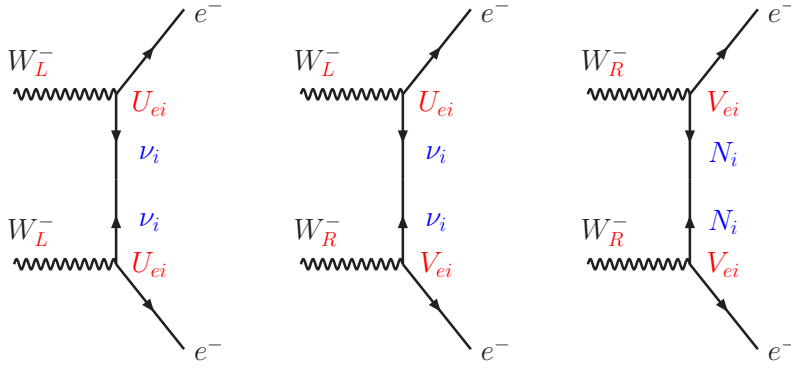


**Figure 1.** Leptonic parts of the  $0\nu\beta\beta$  decay amplitude in left-right symmetric models. The graph to the left represents the mass mechanism. The graph in the middle is long-range, but suppressed by  $\sum_i U_{ei}V_{ei}$ . The graph to the right is the so-called short range contribution for heavy Majorana neutrinos.

first sight contradictive statement can be easily understood. In left-right symmetric models the mixing between the active, left (and light) neutrinos with the heavy, sterile ones can be estimated “à la seesaw” to be very roughly of the order  $\sum_i U_{ei}V_{ei} \sim \frac{m_D}{M_M} \sim \sqrt{\frac{m_\nu}{M_M}}$ . Then, with a limit of  $\langle \lambda \rangle \lesssim 8 \cdot 10^{-7}$  one gets  $m_{W_R} \gtrsim 1.1 m_{W_L} \left(\frac{m_\nu}{1\text{eV}}\right)^{1/4} \left(\frac{M_M}{1\text{TeV}}\right)^{-1/4}$ . In the short range contribution, although some cancellation of terms in  $\langle m_N \rangle$  might occur, no such strong suppression is expected. From [8] and assuming a limit on the  $^{76}\text{Ge}$  half-life of  $T_{1/2}^{0\nu\beta\beta} \geq 1.2 \cdot 10^{25}$  ys a limit of

$$m_{W_R} \gtrsim 1.3 \left(\frac{\langle m_N \rangle}{[1\text{TeV}]}\right)^{-1/4} \text{ TeV} \quad (3)$$

can then be derived. Note that the limit disappears as  $\langle m_N \rangle$  goes to infinity, as it should. Note also that the uncertainty in this limit due to the uncertainty in the nuclear matrix element calculation scales only as  $\Delta m_{W_R} \sim (\Delta \mathcal{M})^{-1/4}$  and thus is quite insensitive to the details of the nuclear model.

## 2.2. R-parity violation

In the standard model lepton number is conserved, because there is (a) no right-handed neutrino and (b) only one Higgs doublet with  $L = 0$ . In supersymmetric models, on the other hand, if one does not assume lepton number conservation a priori, one can write down the following (trilinear) lepton number violating terms

$$\begin{aligned} \mathcal{L}_{\mathcal{R}P} = & - \lambda'_{ijk} \left[ (\tilde{u}_L \tilde{d}_R)_j \cdot \begin{pmatrix} e_R^c \\ -\nu_R^c \end{pmatrix}_i (\tilde{d}_R)_k + (\tilde{e}_L \tilde{\nu}_L)_i (d_R)_k \cdot \begin{pmatrix} \tilde{u}_L^* \\ -\tilde{d}_L^* \end{pmatrix}_j \right. \\ & \left. + (\tilde{u}_L \tilde{d}_L)_j (d_R)_k \cdot \begin{pmatrix} \tilde{e}_L^* \\ -\tilde{\nu}_L^* \end{pmatrix}_i + h.c. \right] \end{aligned} \quad (4)$$

Here, the tilde indicates the scalar superpartners of the usual quarks and leptons. A product of two of the terms in eq. (4), together with an MSSM neutralino and/or gluino interaction lead to  $0\nu\beta\beta$  decay diagrams without *any* virtual neutrinos being exchanged, as first pointed out in [10, 11]. A dedicated calculation of all diagrams [12], together with a limit of  $T_{1/2}^{0\nu\beta\beta} \geq 1.2 \cdot 10^{25}$  y for  $^{76}\text{Ge}$  leads to

$$\lambda'_{111} \leq 3.2 \times 10^{-4} \left(\frac{m_{\tilde{q}}}{100\text{GeV}}\right)^2 \left(\frac{m_g}{100\text{GeV}}\right)^{1/2}. \quad (5)$$

It is interesting to note, that such a small value of  $\lambda'_{111}$  generates at 1-loop level an entry in the Majorana neutrino mass matrix of  $M_{ee}^\nu \simeq 10^{-6}$  eV only.

### 3. Neutrino oscillations and $0\nu\beta\beta$ decay

If the mass mechanism is dominant, the  $0\nu\beta\beta$  decay half-life is proportional to the (square of the)  $(\nu_e - \nu_e)$  element of the Majorana neutrino mass matrix. For three generations of light neutrinos, this so-called “effective Majorana” mass can be expressed as:

$$M_{ee}^\nu \equiv \langle m_\nu \rangle = c_{12}^2 c_{13}^2 m_1 + s_{12}^2 c_{13}^2 e^{i\alpha} m_2 + s_{13}^2 e^{i\beta} m_3 \quad (6)$$

Eq.(6) contains a priori seven unknowns: Three mass eigenstates, two angles and two phases. With the help of data from neutrino oscillation experiments, one can trade two mass eigenstates for the observed  $\Delta m_{\text{Atm}}^2$  and  $\Delta m_{\odot}^2$  and relate the two angles to the solar ( $\theta_{\odot}$ ) and reactor angle ( $\theta_R$ ). For the case of normal hierarchy,  $m_{\nu_1} \leq m_{\nu_2} \leq m_{\nu_3}$ , eq.(6) can then be written as

$$\langle m_\nu \rangle = c_{\odot}^2 c_R^2 m_{\nu_1} + s_{\odot}^2 c_R^2 e^{i\alpha} \sqrt{m_{\nu_1}^2 + \Delta m_{\odot}^2} + s_R^2 e^{i\beta} \sqrt{m_{\nu_1}^2 + \Delta m_{\odot}^2 + \Delta m_{\text{Atm}}^2}, \quad (7)$$

while for the case of inverse hierarchy,  $m_{\nu_3} \leq m_{\nu_1} \leq m_{\nu_2}$ , it is given by

$$\langle m_\nu \rangle = c_{\odot}^2 c_R^2 \sqrt{m_{\nu_3}^2 - \Delta m_{\odot}^2 + \Delta m_{\text{Atm}}^2} + s_{\odot}^2 c_R^2 e^{i\alpha} \sqrt{m_{\nu_3}^2 + \Delta m_{\text{Atm}}^2} + s_R^2 e^{i\beta} m_{\nu_3} \quad (8)$$

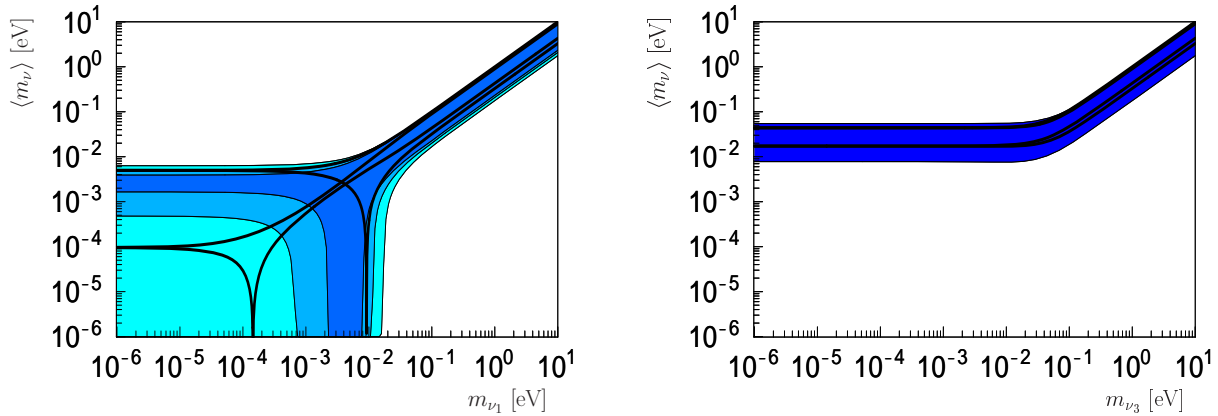


**Figure 2.** Allowed range of  $\langle m_\nu \rangle$  as a function of the lightest neutrino mass eigenvalue. To the left normal hierarchy, to the right inverse hierarchy. To calculate the allowed range of  $\langle m_\nu \rangle$  the  $3\sigma$  c.l. intervals on the oscillation parameters have been used [13], except for the case of normal hierarchy, for which 3 different cases for the upper limit on  $s_R^2$  are shown. These are  $s_R^2 \leq 0.04$  (light blue),  $s_R^2 \leq 0.025$  (medium blue),  $s_R^2 \leq 0.005$  (darker blue).

Fig. (2) shows the resulting allowed range of  $\langle m_\nu \rangle$  for both, normal and inverse hierarchy, taking into account the latest results from a global fit to all neutrino oscillation data [13]. The lower limit on  $\langle m_\nu \rangle$ , which appears in the case of inverse hierarchy, can be understood trivially. For  $m_{\nu_3} = 0$  and  $\alpha = \pi$  eq. (8) reads approximately

$$\langle m_\nu \rangle \simeq c_R^2 (c_{\odot}^2 - s_{\odot}^2) \sqrt{\Delta m_{\text{Atm}}^2}. \quad (9)$$

Thus, as soon as data tells us that  $s_{\odot}^2 < \frac{1}{2}$ , exact cancellation is no longer a possibility. This statement remains true for any finite  $m_{\nu_3}$ , simply because  $s_R^2 < \cos(2\theta_{\odot})$  is guaranteed by data nowadays. Fig. (3) shows how this lower limit evolves with future data from neutrino oscillation experiments. A possible future smaller upper bound on  $s_{\odot}^2$  would make it easier for  $0\nu\beta\beta$  decay experiments to rule out inverse hierarchy.

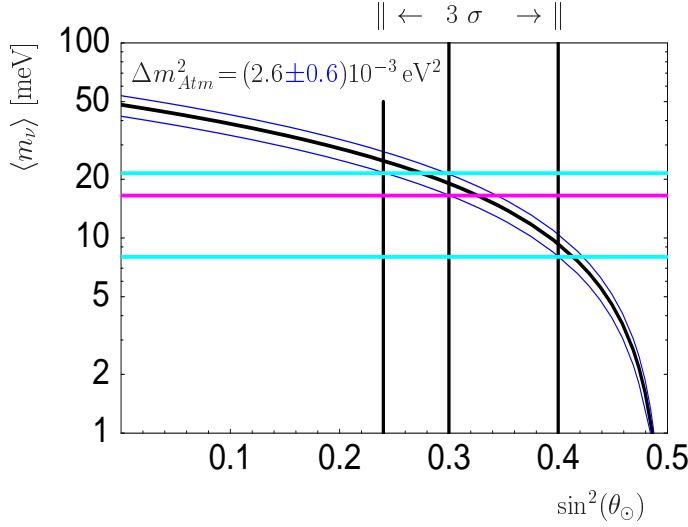


**Figure 3.** Lower Limit on  $\langle m_\nu \rangle$  in the case of inverse hierarchy as a function of the solar mixing angle  $\sin^2 \theta_\odot$  for three different values of  $\Delta m_{Atm}^2$ , i.e. best fit point  $\pm 3 \sigma$  allowed range. The vertical black lines indicate the current best fit point and the  $3 \sigma$  c.l. allowed range of  $s_\odot^2 \equiv \sin^2(\theta_\odot)$ . The worst case, i.e. the most conservative limit, is found for  $\sin^2 \theta_\odot^{\text{Max}}$  and  $(\Delta m_{Atm}^2)^{\text{Min}}$ , currently  $\langle m_\nu \rangle \geq 8$  meV.

There is no such simple quantitative lower limit for the case of normal hierarchy. Fig. (2), to the left, aims at demonstrating this point. If  $m_{\nu_1} \equiv 0$ , a lower limit appears if

$$s_R^2 \leq \frac{\sqrt{\Delta m_\odot^2 s_\odot^2}}{\sqrt{\Delta m_\odot^2 + \Delta m_{Atm}^2} + \sqrt{\Delta m_\odot^2 s_\odot^2}} \sim 0.034 \quad (10)$$

However, from this superficial look at the data at the point  $m_{\nu_1} = \tan^2 \theta_\odot m_{\nu_2}$  exact cancellation yielding  $\langle m_\nu \rangle \equiv 0$  seems possible. However, this is equivalent to saying  $M_{ee}^\nu \equiv 0$  and it is exactly this possibility which is ruled out by the “extended black box” theorem [6].

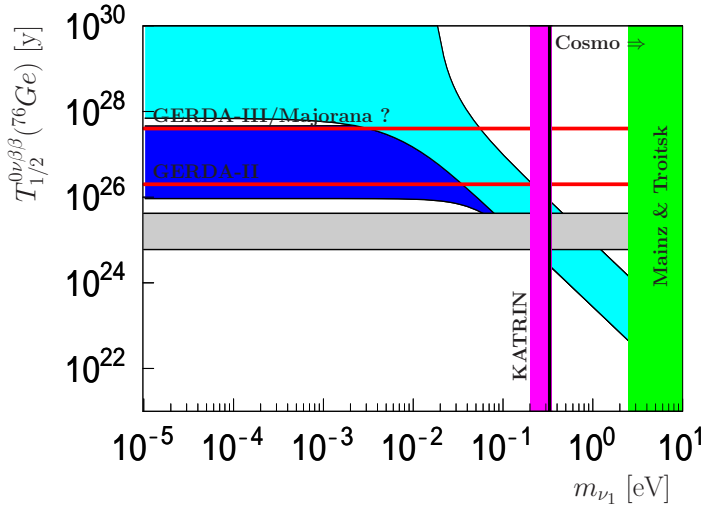


**Figure 4.** Summary of experimental data on the absolute neutrino mass scale and the half-life of  ${}^{76}\text{Ge}$   $0\nu\beta\beta$  decay. For discussion see text.

In fig. (4) finally a summary of the current status of various experimental attempts on measuring/limiting the absolute scale of neutrino masses is given. The light and darker blue areas are allowed for the  $0\nu\beta\beta$  decay half live of  ${}^{76}\text{Ge}$  for normal and inverse hierarchy, calculated with matrix elements from [14]. Note, that matrix elements from [15] lead to slightly larger half-lives, see also the discussion in [3]. The green area labeled “Mainz & Troitsk” shows the latest upper limits derived from endpoint measurements in  ${}^3\text{H}$  decay [16, 17]. The bar labeled

“KATRIN” represents the expected sensitivity of the next generation  $^3\text{H}$  experiment KATRIN [18]. Note, that KATRIN claims a final sensitivity of  $m_{\nu_e} \sim 0.2$  eV (@ 90 % c.l.) or a  $5\sigma$  discovery threshold of  $m_{\nu_e} \sim 0.35$  eV. Various limits on the absolute neutrino mass scale from cosmology have been published recently, derived from CMB data combined with information from large scale structure surveys. For three generations of neutrinos numbers ranging from  $\sum_i m_{\nu_i} \sim 0.4 - 2.0$  eV, depending on input and bias, have been published. For a detailed discussion see, for example, the review [19]. The horizontal gray band indicates the range of the finite  $T_{1/2}^{0\nu\beta\beta}$  claimed by some members of the Heidelberg-Moscow experiment [20]. Note that this result is highly controversial, see for example the discussion by Barabash in [2]. The vertical red lines indicate the sensitivity of two future Ge experiments. GERDA [21] is currently in phase I, phase II is funded. In the future Majorana [22] and/or GERDA phase III can test the range allowed by inverse hierarchy.

#### 4. Conclusions

Lower limits on the  $0\nu\beta\beta$  decay half live can be used to constrain various particle physics parameters. However, from the point of view of particle physics it would be interesting to determine the *dominant* contribution to  $0\nu\beta\beta$  decay. Very little work has been done in this direction. Angular correlations between the electrons [4] or a comparative study of  $0\nu\beta^-\beta^-$  and  $0\nu\beta^+/EC$  decay [23] might be able to disentangle left-left and left-right-handed combinations of currents (of the long range type). However, other contributions to  $0\nu\beta\beta$  decay possibly exist and ultimately it might be that only a combination of various different pieces of experimental data will provide the correct and final answer.

#### Acknowledgments

I would like to thank S.G. Kovalenko and J.W.F. Valle for various discussions on the subject. Financial support by Spanish grant FPA2005-01269, by European Commission Human Potential Program RTN network MRTN-CT-2004-503369 and the EU Network of Astroparticle Physics (ENTApP) WP1, as well as the spanish MCyT Ramon y Cajal program is acknowledged.

- [1] Y. Fukuda *et al.* [Super-Kamiokande Collaboration], Phys. Rev. Lett. **81**, 1562 (1998)
- [2] S. Elliott, A. Barabash, S. Schönert, A. Piepke, R. Maruyama and J. Wilson, these proceedings
- [3] F. Simkovic, these proceedings
- [4] M. Doi, T. Kotani and E. Takasugi, Prog. Theor. Phys. Suppl. **83**, 1 (1985).
- [5] J. Schechter and J. W. F. Valle, Phys. Rev. D **25**, 2951 (1982).
- [6] M. Hirsch, S.G. Kovalenko and I. Schmidt, hep-ph/0608xxx
- [7] E. Takasugi, Phys. Lett. B **149**, 372 (1984).
- [8] M. Hirsch, H. V. Klapdor-Kleingrothaus and O. Panella, Phys. Lett. B **374**, 7 (1996)
- [9] R. N. Mohapatra, Phys. Rev. D **34**, 909 (1986).
- [10] R. N. Mohapatra, Phys. Rev. D **34**, 3457 (1986).
- [11] J. D. Vergados, Phys. Lett. B **184**, 55 (1987).
- [12] M. Hirsch, H. V. Klapdor-Kleingrothaus and S. G. Kovalenko, Phys. Rev. D **53**, 1329 (1996)
- [13] M. Maltoni, T. Schwetz, M. A. Tortola and J. W. F. Valle, New J. Phys. **6**, 122 (2004) [arXiv:hep-ph/0405172]. (V5) in the archive provides updated numbers taking into account all relevant data as of June 2006.
- [14] K. Muto, Phys. Lett. B **391**, 243 (1997).
- [15] V. A. Rodin, A. Faessler, F. Simkovic and P. Vogel, Nucl. Phys. A **766**, 107 (2006).
- [16] C. Kraus *et al.*, Eur. Phys. J. C **40**, 447 (2005) [arXiv:hep-ex/0412056].
- [17] V. M. Lobashev *et al.*, Nucl. Phys. Proc. Suppl. **91**, 280 (2001).
- [18] A. Osipowicz *et al.* [KATRIN Collaboration], arXiv:hep-ex/0109033; see also: <http://www-ik.fzk.de/katrin/index.html>
- [19] J. Lesgourgues and S. Pastor, Phys. Rept. **429**, 307 (2006) [arXiv:astro-ph/0603494].
- [20] H. V. Klapdor-Kleingrothaus, A. Dietz, I. V. Krivosheina and O. Chkvorets, Nucl. Instrum. Meth. A **522**, 371 (2004) [arXiv:hep-ph/0403018].
- [21] I. Abt *et al.*, arXiv:hep-ex/0404039. See also the GERDA web page <http://www.mpi-hd.mpg.de/ge76/>
- [22] R. Gaitskell *et al.* [Majorana Collaboration], arXiv:nucl-ex/0311013.
- [23] M. Hirsch, K. Muto, T. Oda and H. V. Klapdor-Kleingrothaus, Z. Phys. A **347**, 151 (1994).

## **Henderson Deep Underground Science and Engineering Lab: *Unearthing the secrets of the Universe, underground***

**C K Jung for the HUSEP collaboration**

Department of Physics and Astronomy, Stony Brook University, Stony Brook, NY

alpinist@nngroup.physics.sunysb.edu

**Abstract.** The Henderson Mine near Empire, Colorado is proposed to be the site to host a Deep Underground Science and Engineering Laboratory (DUSEL), which will have a rich program for forefront research in physics, biology, geosciences, and mining engineering. The mine is owned by the Climax Molybdenum Company (CMC). It is located about 50 miles west of Denver and is easily accessible via major highways. The mine is modern and has extensive infrastructure with reserve capacity well-suited to the demands of DUSEL. CMC owns all land required for DUSEL, including the tailings site. It also has all environmental and mining permits required for DUSEL excavation, core drilling, and rock disposal. The mine owners are enthusiastic supporters of this initiative. In support of the Henderson DUSEL project, the State of Colorado has pledged substantial funding for surface construction.

### **1. Introduction**

In the past decade, large-scale underground physics laboratories in Canada, Europe, and Japan have made major discoveries in neutrino physics, but the United States lacks a comparable facility. When established, the Henderson laboratory will help American researchers regain lost leadership not only in this one area of physics but in several important fields of underground science and engineering while also providing the infrastructure for international cooperation in a broad range of disciplines.

The Henderson mine, one of the largest operating underground mines in the world, offers a superb location and infrastructure for such a laboratory. Established by Climax Molybdenum Company (CMC) in the 1970's at a cost of \$500 million and modernized in 1999 for \$150 million, it offers high-capacity rock removal (40 ktons/day), ample electric power (48 MW), water, and water treatment facilities. The opportunity to share this infrastructure and benefit from the world-class mine-staff's expertise will make the design, construction and operation of this underground laboratory highly efficient, cost effective, environmentally sound and safe.

CMC personnel have been active and enthusiastic participants in the development of this proposal. To ensure that the company has been well-educated on the potential impact of hosting a scientific laboratory, senior managers from Henderson visited the Kamioka Laboratory in Japan, SNOLab in Canada, Gran Sasso National Laboratory in Italy and Brookhaven National Laboratory in New York.

#### **1.1. Why DUSEL at Henderson?**

This site's core advantages derive from the proximity of an efficient modern mine with large capacity to a large metropolitan area and several prominent universities. Even a cursory visit to the mine reveals impressive assets for establishing a new science and engineering laboratory. A large-capacity

shaft and hoisting system, one of the largest in the U.S., can accommodate 20-ft ISO sea-containers and up to 50-ton loads. This system will ease construction, and lower the cost, of large underground experiments. A massive underground crusher feeding a fast, high capacity conveyor system can remove 40,000 tons of rock daily. This system can easily handle DUSEL loads including a 2.5-million ton excavation for a neutrino-physics and nucleon-decay experiment with minimal impact on the mine's commercial operations. A less obvious, but essential, Henderson strength is its well-established and environmentally sound tailing site available to deposit rock excavated during DUSEL construction. (Indeed, there is minimal environmental concern for any aspect of laboratory construction or operation.) This vast physical plant is supported by an enthusiastic high-tech corporate partner with all needed underground and environmental permits and an excellent safety and management record. Successful laboratories in working mines elsewhere include the Kamioka Observatory in Japan, SNOLab in Canada, and the Boulby Mine in England. These facilities all began with the cooperation of friendly, science-sympathetic and image-conscious mine owners who furnished safety and environmental expertise – exactly the relationship enjoyed with the Henderson Mine and its parent company. Area residents, and local and state government officials are involved and are extremely supportive. In two years of presenting the project to varied constituencies, not a single serious concern has been raised.

Easy access to the site is another strength. The mine is less than two miles from U.S. highway 40 on a well-maintained paved road, and just ten miles from I-70. Based on the past three decades of experience, the mine is generally accessible year-round by two-wheel drive vehicles without requiring four-wheel drive or snow tires/chains. Denver International Airport, providing nonstop flights to all major U.S. and Canadian cities and with international connections, is a 1.5-hour drive. So there will be economies of travel time and expense for researchers and other visitors.

The academic, technical, commercial, and industrial resources available near this site are outstanding. Through hubs in Denver, a high bandwidth optical fiber network provides access to the national Internet2 backbone. The three primary Colorado education and research institutions with core participation in this proposal (the University of Colorado at Boulder, Colorado State University, and Colorado School of Mines) have underground research programs and will provide access to equipment, services, and personnel. And finally, the breathtaking scenery of the Rocky Mountains, with related recreational opportunities, will help attract gifted researchers from around the world.

## **2. Henderson DUSEL Vision and Conceptual Design**

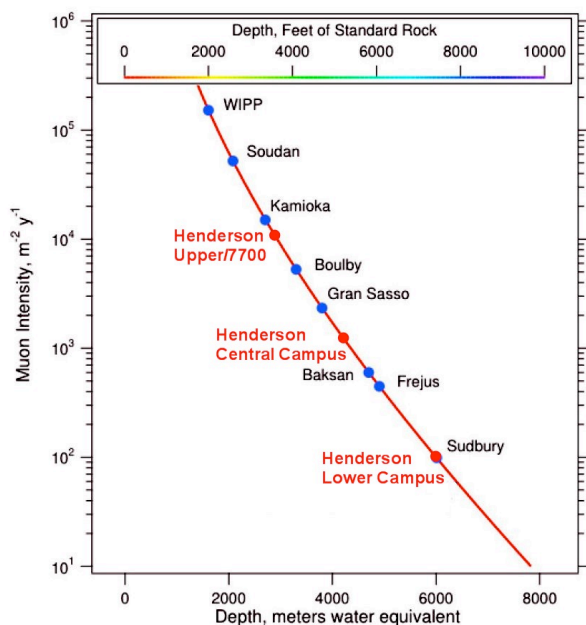
Henderson DUSEL [1] will be a comprehensive laboratory for neutrino physics and astrophysics, dark matter and proton decay searches, geoscience and bioscience explorations, and mining engineering development. It will also have state-of-the-art low background counting facilities and vigorous outreach and education programs. It will embody a unique multidisciplinary and cross-disciplinary effort that will optimize science output and complement the characteristics and capacity of laboratories in other countries. It will be the scene of multinational efforts lasting many decades, providing continuous access and long-term research opportunities. At the same time, its dynamic program and underground cavern network will enable it to adapt to rapidly changing scientific landscapes in the short term. There will be a flexible, staged, meet-the-need approach that will allow experiments to be carried out as the laboratory is being built while minimizing the initial investment.

Figure 1 shows muon background reduction as a function of the depth in existing laboratories at their operating depths. It shows also the planned Henderson DUSEL campuses that will offer muon reduction rates appropriate for a wide range of crucial experiments. The Upper Campus (UC) at 3000 mwe overburden uses existing mine caverns where experiments can be installed within a year of groundbreaking; the Central Campus (CC) at 4300 mwe will be available in 3 years; and the Lower Campus (LC) at 5800 mwe will be operational in 5 years. Figure 2 shows the conceptual design layout of the Henderson DUSEL with schematic geologic cross-section. Also shown in Figure 2 are the Geoscience/Engineering Campus beneath the molybdenum ore body, which includes outposts for

biological research, and the Deep Exploration Station at the deepest level, where core drilling to extreme depths will extract samples for biological and geological studies.

The conceptual design includes a baseline approach and a faster option (should circumstances support it) and desired future expansions. In the Fast-Track scenario, the UC has seven clean-area experimentation halls totaling nearly 15,900 ft<sup>2</sup>. The baseline UC also has seven halls, all located in currently existing excavations, totaling 6,600 ft<sup>2</sup>. At CC there will be seven clean-area halls, including two that are 10,000 ft<sup>2</sup> each, totaling 44,200 ft<sup>2</sup>. The LC has 25,300 ft<sup>2</sup>, including one 10,000 ft<sup>2</sup> hall and the Deep Exploration Station. The baseline design provides a 76,100 ft<sup>2</sup> total research area, and future expansions with much larger research area would be readily accommodated. In comparison, Halls A, B and C at Gran Sasso National Laboratories at 3800 mwe overburden have about 68,000 ft<sup>2</sup> in total, and SNOLab at 6000 mwe has about 11,800 ft<sup>2</sup>.

For geological and/or hydrological characterization of the site, we have performed two core drillings: a 762-m drilling to the CC site and a 1152-m drilling to the LC site. We saw no show-stoppers from the cores, and the rock quality was found to be good to very good.



**Figure 1.** Muon intensities at various underground laboratories and proposed Henderson DUSEL campuses.

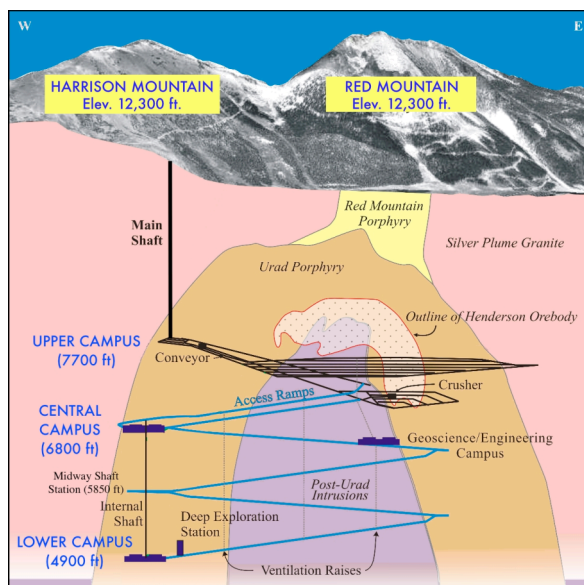


**Figure 2.** Henderson DUSEL conceptual design layout with schematic geologic cross-section, view to north.

### 3. Science at Henderson DUSEL

#### 3.1. Physics

Physics experiments planned for this lab will address some of the deepest questions about our understanding of the fundamental nature of particle interactions and the universe: What is the nature of the dark matter that comprises some 80% of the matter in the universe? Is the neutrino its own antiparticle and did it play a unique role in generating the matter universe we know today? Do protons decay, and what does this tell us about the “grand unification” of forces? [2]

We present two possible schemes for developing facilities needed to address such questions. One is a Baseline Design based on our current understanding of the technical and funding status of candidate experiments; the other is a Fast-Track Option that could be implemented if high-priority experiments make rapid progress in the next few years.

In the Baseline Design, existing mine space is developed into a modest UC for early experiments, low-background counting facilities, and prototyping that does not require extreme overburden. Primary support facilities and first-stage laboratory space for experiments requiring greater depth are developed at a CC. Space for sensitive experiments requiring the greatest depth will be developed at LC. This strategy is driven partially by the needs of the initial suite of experiments, which includes two neutrinoless double beta decay experiments, two dark matter search experiments, and a nuclear accelerator experiment for astrophysics-related measurements. Some experiments initially slated for the CC may make rapid technical progress and be able to operate at UC depth before completion of the CC. In order to accommodate this possibility, the Fast-Track option emphasizes early operation of these experiments at the UC with the creation of new larger cavities to accommodate water shielding.

In the long term, we envision a large multi-purpose proton decay and neutrino detector at the CC. Excavation of the large cavity required for this 500 kton-plus detector is well suited to the rock quality and the unique Henderson infrastructure and rock removal capacity. The primary US proponents of such a detector, the UNO collaboration, have identified Henderson as the most promising site to build the experiment. The working group on long baseline neutrino oscillation experiments, co-sponsored by Fermilab and Brookhaven National Laboratory, has identified Henderson as a suitable location for a detector used in conjunction with a neutrino superbeam generated at Fermilab to probe first and third generation mixing and CP violation in the lepton sector. The lab's flexible design will allow effective pursuit of these opportunities, and others not yet conceived of.

### 3.2. Other Science and Engineering

Henderson DUSEL geoscience plan will address fundamental questions about the deformation of rock, transport of heat and mass, and interactions between inert rock and living organisms in the deep subsurface. The Henderson DUSEL is ideal for studying geoscience because it offers a combination of pristine homogeneous conditions, which are perfect for experiments involving basic natural processes, along with important heterogeneities, which hold the answers to many current questions in geoscience. The geoscience plan includes a major exploration drilling program, a Fracture Processes Laboratory, a Coupled Processes Laboratory and a Deep Flow Hydrology Laboratory.

Geochemical heterogeneity at Henderson makes it an excellent site for long-term study of biogeochemistry, biodiversity, and evolution. Preliminary analyses of deep fracture water in the mine have already revealed diverse water chemistry and a concomitant diversity of life forms, including entirely novel bacterial phyla. These data, combined with the interests of our collaborators, are focusing attention on four initial research themes: energy sources and nutrients that support life; analyses of reactions at rock-water interfaces; characterization of subsurface biodiversity; and metagenomic and proteomic analyses of the diversity of metabolic pathways and enzymes that adapt life to deep environments. Experiments will be conducted using drilling and coring at distributed outposts to access diverse fracture-water chemistry and mineralogy. Also, from our Deep Exploration Station we will bore to an approximate depth of 4.7 km, where the temperature will approach 120°C.

The lab will provide a large lateral area (11.7 km<sup>2</sup>) and depth (2.25 km) encompassing pristine homogeneous granitic rock under Harrison Mountain and a variety of pristine and perturbed granitic rocks under Red Mountain for research in mining and engineering. Massive excavation to create science caverns will provide a superb opportunity to address unanswered geo-engineering questions.

Many high-priority scientific investigations must minimize interference from background radiation. For this reason, Henderson DUSEL will have a modern Low Background Counting Facility (LBCF). The installation will have counting stations with detector arrays surrounded by shielding designed to eliminate background radiation. There will be the necessary infrastructure to fabricate and clean samples and detector components, as well as methods to store samples that satisfy acceptance criteria.

We envision DUSEL at Henderson as transcending disciplinary boundaries to become a truly interdisciplinary enterprise. Indeed, that process has already begun. Physicists, geologists, and engineers are collaborating to design large facilities at depth; biologists and geologists will join in the study of deep subsurface ecosystems; geologically based applications such as earth imaging and

drilling will serve multiple scientific communities and are being planned by interdisciplinary teams; and education and outreach efforts (e.g., the planned Mining Academy) will be a shared endeavor among all the disciplines. Henderson DUSEL will nurture these and other connections and synergies.

#### **4. The HUSEP Collaboration**

Founded in 2004 the collaboration now has 224 members from 98 institutions or organizations in 14 countries. It has a well-established organizational structure with an Executive Committee (EC) at its core. The EC is advised by a 24-member International Advisory Board that includes researchers experienced in underground science and engineering from Canada, Europe, Japan and the United States. Eleven standing committees cover all DUSEL science and engineering topics, broader impacts, environmental safety and health, local community and government relations, industry relations, and management. Our engineering team is composed of groups from the Henderson Mine, the Colorado School of Mines, CNA Engineers and its partners (Dunham Associates and Miller-Dunwiddie Architects), Itasca Consulting Group Inc., and ILF Consulting Engineers.

#### **5. Support from Collaborating Universities, State of Colorado and the Local Community**

The relationship between HUSEP and local community and government groups is excellent at all levels. In 2005, Colorado Governor Bill Owens established the State Advisory Commission for HUSEP, and in May 2006, the Colorado legislature passed a bipartisan bill allocating \$20M to fund a visitor center and other DUSEL surface facilities if Henderson is chosen as the DUSEL site. The State has contributed \$145,000 toward core drillings in the proposed site and has identified potential additional funds of more than \$1 million. Members of Colorado's Congressional delegation and both of the state's U.S. Senators have expressed strong support. Local supporters have established the Arapaho Project Inc., which has raised money for a broad range of activities and facilitated interactions with local and state officials, neighboring communities and schools.

#### **6. Conclusions**

A national DUSEL will house experiments that will address some of the most important science questions of today with potential for major discoveries. As envisioned, the Henderson facility will: house particle, nuclear and astro-particle experiments (examining dark matter, neutrinoless double beta decay, proton decay, and supernova neutrinos) that are regarded as among the highest priority research topics in the particle and nuclear physics community; establish a "4-D" geoscience/bioscience observatory, *i.e.* one involving large scale ( $\text{km}^3$ ) and long term (multi-decade) access; provide an opportunity for the American mining and engineering community to take a leading role in developing deep underground construction techniques; and enable U.S. researchers to lead the world in particle physics using a Large Multi-Purpose Detector and a neutrino superbeam.

Henderson DUSEL will be a unique facility serving the interdisciplinary science community on a national and international basis. The Henderson Mine presents an excellent practical, cost-effective site with great support from the local community and with no environmental concerns during construction or operation. As an operating mine with a modern and vast infrastructure, it has many advantages for DUSEL construction and operation.

#### **Acknowledgements**

This work was supported by the National Science Foundation; State of Colorado; U. of Colorado, Boulder; Colorado School of Mines, Colorado State U.; Stony Brook U. The author, on behalf of the HUSEP collaboration, acknowledges the cooperation of the Climax Molybdenum Company/Phelps Dodge Corporation, and support from the Colorado State Special Commission for HUSEP.

#### **References**

- [1] For more information on the Henderson DUSEL, see: <http://nngroup.physics.sunysb.edu/husep/>
- [2] For more extensive discussion of science and engineering research, see: <http://www.dusel.org/>

# Underwater Neutrino Detection in the Mediterranean Sea: From Present to Future

**Ulrich F. Katz**

University of Erlangen-Nuremberg, Physics Institute,  
Erwin-Rommel-Str. 1, D-91058 Erlangen, Germany

E-mail: [katz@physik.uni-erlangen.de](mailto:katz@physik.uni-erlangen.de)

**Abstract.** The observation of high-energy extraterrestrial neutrinos is one of the most promising future options to increase our knowledge of non-thermal processes in the universe. Neutrinos are e.g. unavoidably produced in environments where high-energy hadrons collide; in particular this is almost certainly true at astrophysical accelerators of cosmic rays, which thus could be identified unambiguously by sky observations in “neutrino light”. To establish neutrino astronomy beyond the detection of single events, neutrino telescopes of  $\text{km}^3$  scale are needed. In order to obtain full sky coverage, a corresponding detector in the Mediterranean Sea is required to complement the IceCube experiment currently under construction at the South Pole. The groups pursuing the current neutrino telescope projects in the Mediterranean Sea, ANTARES, NEMO and NESTOR, have joined to prepare this future installation in a 3-year, EU-funded Design Study named KM3NeT (in the following, this name will also denote the future detector). This report highlights some scientific key questions, addresses the status of current projects and outlines the path towards the realization of KM3NeT.

## 1. The scientific case

The energy range accessible to neutrino telescopes is intrinsically limited by the detection method to some 10 GeV at its lower end, while at energies beyond roughly  $10^{17}$  eV the neutrino flux is expected to fade below detection thresholds even for future  $\text{km}^3$ -scale detectors. The lower-energy region is dominated by the flux of *atmospheric neutrinos* produced in reactions of cosmic rays with the atmosphere. There are three approaches to identify cosmic neutrino signals on top of this background: (i) Neutrinos from specific astrophysical objects (*point sources*) produce excess signals associated to particular celestial coordinates; (ii) Neutrinos not associated to specific point sources (*diffuse flux*) are expected to have a much harder energy spectrum than the atmospheric neutrinos and to dominate the neutrino flux above  $10^{14} - 10^{15}$  eV; (iii) Exploitation of coincidences in time and/or direction of neutrino events with observations by telescopes (e.g. in the radio, visible, X-ray or gamma regimes) and possibly also by cosmic ray detectors (*multi-messenger method*).

The various astro- and particle physics questions to be addressed with the resulting data have been summarised e.g. in [1] and the references therein. Here, we will focus on a few central topics.

### 1.1. Neutrinos from galactic sources

The recent observation of various types of TeV gamma ray sources in the Galactic plane by H.E.S.S. (see [2] and references therein) allows us, for the first time, to estimate expected neutrino fluxes and spectra with rather small uncertainties, provided the production of gamma rays is due to hadronic processes [3]. Detailed calculations [4, 5] indicate that neutrinos from some of these sources could be detected with a km<sup>3</sup>-scale detector in the Mediterranean Sea, even though with limited statistics. Promising candidate sources are e.g. the two shell-type supernova remnants RX J1713.7-3946 and RX J0852.0-4622, for which the observations by H.E.S.S. [6] disfavour explanations of the gamma flux by purely electromagnetic processes. The detection of neutrinos from any of these sources would identify unambiguously specific cosmic accelerators.

Note that this requires a Northern-hemisphere neutrino telescope which, in contrast to the South Pole detectors, covers the relevant part of the Galactic plane in its field of view (see Fig. 1).

### 1.2. The diffuse neutrino flux

The sensitivity of current and future experiments is sufficient to test various predictions of diffuse neutrino fluxes (see e.g. [7, 8]). Whereas some of the models are already now severely constrained by the data, others require km<sup>3</sup>-size neutrino telescopes for experimental assessment and potential discoveries. The measurement of the diffuse neutrino flux would allow for important clues on the properties of the sources, on their cosmic distribution, and on more exotic scenarios such as neutrinos from decays of topological defects or superheavy particles (*top-down scenarios*).

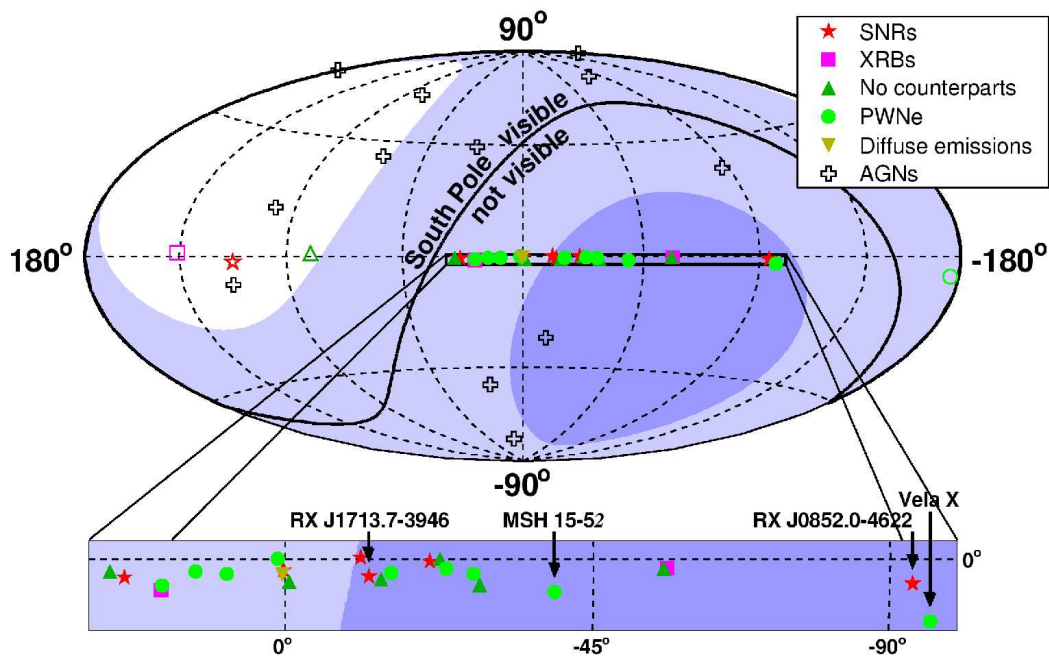


**Figure 1.** Field of view of a neutrino telescope in the Mediterranean Sea, assuming a  $2\pi$  downward sensitivity appropriate for neutrino energies up to about 100 TeV. The dark shaded area indicates visibility above 75% of the time, the light shaded area above 25%. From the South Pole, the region marked “South Pole visible” can be observed (100% visibility). The symbols indicate the known TeV gamma ray sources (SNRs: super nova remnants; XRBs: x-ray binaries; PWNe: pulsar wind nebulae; AGNs: active galactic nuclei). The enlarged insert indicates the Galactic plane. Figure taken from [5].

### 1.3. Search for dark matter annihilation

The major part of the matter content of the universe is nowadays thought to be non-baryonic, weakly interacting massive particles (WIMPs), such as the hypothetical lightest supersymmetric particle, the neutralino. Complementary to direct searches, indirect WIMP observations may be possible by detecting neutrinos produced in WIMP annihilations in regions with enhanced WIMP density, e.g. due to gravitational trapping in the Sun or the Galactic Centre. The signal would be an enhanced neutrino flux from these directions, with a characteristic upper cut-off in the energy spectrum below the WIMP mass,  $M_{\text{WIMP}}$ . Although there is no generic upper constraint on  $M_{\text{WIMP}}$ , supersymmetric theories prefer values below 1 TeV. Substantial detection efficiency down to neutrino energies of about 100 GeV is therefore essential. The expected sensitivity depends strongly on assumptions on the WIMP density profile, on  $M_{\text{WIMP}}$  and on the energy spectrum of neutrinos from WIMP annihilations. At least for some supersymmetric scenarios this sensitivity is compatible or even better than for direct searches [1, 9]

## 2. Current neutrino telescope projects in the Mediterranean Sea

The pioneering neutrino telescopes, AMANDA at the South Pole [10, 11] – now embedded in its growing, km<sup>3</sup>-scale successor IceCube (see e.g. [12]) – and the Lake Baikal experiment [13], are already taking data for several years.

Three current Mediterranean pilot projects are reporting progress: By early 2007, more than 40% of the foreseen detector modules of ANTARES [14, 15] have been deployed and connected; ANTARES has reported the detection of first neutrinos with this setup [16]. A further neutrino telescope, NESTOR [17]), is under construction. Preparatory work for a future large-scale installation in the Mediterranean Sea is being performed in the R&D project NEMO [18]; a first successful deployment of a prototype detector modules was achieved in December 2006. All groups involved in these projects have now joined into a 3-year EU-funded Design Study towards the future km<sup>3</sup>-scale neutrino telescope in the Northern hemisphere (KM3NeT) [19].

### 2.1. ANTARES

The ANTARES neutrino telescope [14] is situated in 2500 m depth about 40 km from the French coast of the Mediterranean Sea near Toulon. It will consist of 12 lines (“strings”) that are anchored to the sea bed at distances of about 70 m from each other and kept vertical by buoys. Each string is equipped with 75 optical modules (OMs) [20] arranged in triplets (*storeys*) sustained by titanium frames that also support water-tight titanium containers for the electronic components. The OMs are glass spheres housing one 10-inch photomultiplier each, directed at an angle of 45° towards the sea bed. The storeys are spaced at a vertical distance of 14.5 m and are interconnected with an electro-optical-mechanical cable supplying the electrical power and the control signals and transferring the data to the string bottom. Submersible-deployed electro-optical link cables connect the strings to the *junction box (JB)*, which acts as a fan-out between the main electro-optical cable to shore and the strings.

For a detailed description of ANTARES and its current status see [21].

### 2.2. NESTOR

The site selected for the NESTOR neutrino telescope is off Pylos at the West coast of the Peloponnese, at a depth of 3800 m. The NESTOR design is based on rigid, hexagonal star-like structures (*floors*) with a diameter of 32 m, carrying 6 pairs of upward- and downward-looking photomultipliers each as well as a titanium sphere for the readout electronics in the centre (see Fig. 2). 12 floors are foreseen to be connected vertically at a distance of 30 m to form a *tower*. The deployment operations are performed by lifting the existing structure to the surface, connecting the new module(s) and redeploying the extended set-up, thus avoiding the use of submersibles.



**Figure 2.** Reduced-size NESTOR floor during preparation for deployment.

In 2003, a single floor of reduced size has been deployed, connected to the cable to shore and operated for more than a month [22]. In this time, more than 2 million 4- or higher-fold coincidence triggers have been collected [23]. From these data the angular distribution of the atmospheric muons was reconstructed. The good agreement of the results with simulations and previous measurements confirms that the functionality of the detector complies with the specifications and that a detailed level of detector understanding has been reached.

### 2.3. NEMO

In the framework of the Italian R&D project NEMO, a candidate site for a future  $\text{km}^3$ -scale detector has been identified at a depth of 3340 m off the East coast of Sicily near Capo Passero, and new solutions for various detector components have been developed. Amongst these is a new design of a mechanical structure, consisting of 20 m-long rigid arms connected to each other by cables and kept vertical by a buoy. The cables form a tetrahedral structure, sustaining successive arms orthogonally to each other at a distance of 40 m (see Fig. 3). Each arm carries 2 pairs of upward- and downward-looking photomultipliers. One advantage of this flexible tower structure is that a tower can be deployed folded into a compact structure which unfurls when released after reaching the sea bottom. A further NEMO development is a composite junction box, consisting of an inner, pressure-resistant steel vessel embedded in an oil-filled plastic tank, thus separating the resistance against pressure and salt water.

For assessing the newly developed components, a test site at a depth of 2000 m has been identified and connected to the shore station by an electro-optical cable. In December 2006, a junction box and a prototype of a flexible tower have been successfully deployed and connected to this cable; since then, data taking with the prototype module is in progress.

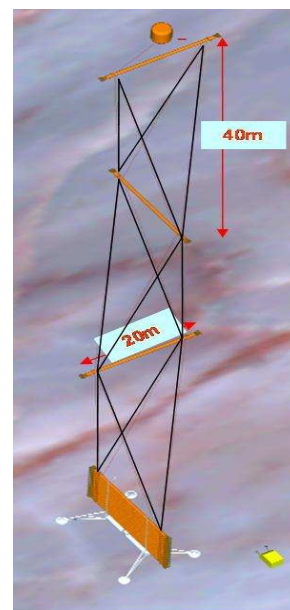


**Figure 3.** Schematic view of a flexible NEMO tower.

## 3. Towards a $\text{km}^3$ neutrino telescope in the Mediterranean Sea

In 2002 the *High Energy Neutrino Astronomy Panel (HENAP)* of the *Particle and Nuclear Astrophysics and Gravitation International Committee (PaNAGIC)* of the *International Union of Pure and Applied Physics (IUPAP)* has concluded that “a  $\text{km}^3$ -scale detector in the Northern hemisphere should be built to complement the IceCube detector being constructed at the South Pole” [24]. This has triggered a joint activity of the groups involved in the Mediterranean neutrino telescopes towards a common future project. The KM3NeT Design Study (see below)

has been approved to prepare this project. Concurrently, the *European Strategy Forum for Research Infrastructures (ESFRI)* has included KM3NeT into the *European Roadmap for Research Infrastructures* [25], thus assigning high maturity and priority to this project.

The vision of the proponents is that KM3NeT will be a pan-European research infrastructure, giving open access to the neutrino telescope data, allowing to assign “observation time” to external users by adapting the online filter algorithms to be particularly sensitive in predefined celestial directions, and providing access to long-term deep-sea measurements to the marine sciences communities.

### 3.1. The KM3NeT Design Study

The 3-year KM3NeT Design Study is funded with 9 million Euro through the 6th Framework Programme of the European Union and has an overall volume of about 20 million Euro, which will mainly be used for personnel and costs for prototyping, deployment tools and tests, etc. It started in February 2006 and is conducted by a consortium of 30 particle/astroparticle physics and 7 sea science/technology institutes from Cyprus, France, Germany, Greece, Ireland, Italy, the Netherlands, Spain and the United Kingdom. The Design Study comprises, amongst others, the groups involved in ANTARES, NEMO and NESTOR, and is coordinated by the University of Erlangen, Germany.

The major objective of the KM3NeT Design Study is to work out the technical foundation for the construction of the neutrino telescope, to be documented in an intermediate *Conceptual Design Report (CDR)* and the final *Technical Design Report (TDR)*. The goal is to design a neutrino telescope with sensitivity down to neutrino energies  $E_\nu$  of a few 100 GeV. The low level of light scattering in deep-sea water is to be exploited to reach a pointing resolution limited by the average angle between incoming neutrino and secondary muon up to  $E_\nu \sim 10$  TeV and better than  $0.1^\circ$  above this energy.

Some technical key questions to be addressed during the Design Study are:

*Detector architecture:* Although all first-generation projects use large-diameter photomultipliers (PMs), they pursue different approaches for the arrangement and mechanical support of the PMs. A choice has to be made between flexible strings (ANTARES), towers formed by rigid structures (NESTOR), towers formed by rigid arms connected to each other by cables (NEMO), a combination of these, or yet other solutions. This question is closely related to a variety of aspects, such as the physics sensitivity (which strongly depends on the geometrical arrangement of the photosensors, see [26]), the deep-sea infrastructure (cables, power distribution, data transport), deployment procedures, calibration methods, readout and data acquisition.

*Photodetection:* The KM3NeT time-line (see Sect. 3.2) is too tight to embark on alternative photodetection developments, such as silicon PMs. Nevertheless, different options have to be assessed. It has e.g. been suggested to use multiple smaller PMs arranged in spherical glass vessels. Careful studies are required to investigate the physics sensitivity of such arrangements, to optimise the readout and to assess the implications for the overall detector cost.

*Deployment and deep-sea infrastructure:* Different deployment approaches have been developed by the first-generation projects (e.g. connections performed by remotely-operated submersibles or at surface, deployment from ships or dedicated platforms, etc.) which need to be adapted to the needs of the KM3NeT infrastructure. Also to be addressed are the architecture of the deep-sea cable net, the choice of its components and the installation and maintenance procedures.

The current projects offer three possible sites for the KM3NeT infrastructure. The existing studies on the characteristics of these sites (water transparency, currents, sedimentation, bioluminescence, etc.) will be consolidated during the Design Study, and the site parameters (depth, distance to shore, etc.) will be taken into account in the optimisation of the physics sensitivity, where the figure of merit will be *physics output per Euro*. The results of these studies will provide the scientific input to the political site decision process.

### 3.2. The Path to KM3NeT Construction

In the 7th Framework Programme of the EU, a call for *Preparatory Phase* projects focusing on the political, legal and strategic questions that need to be solved in order to proceed with the construction has been issued; this scheme is restricted to research infrastructures of the ESFRI roadmap. In case of a successful application, this project would run concurrently with the KM3NeT Design Study and could lead to a start of the construction as early as 2010 or 2011. First data would thus become available concurrently with data from the IceCube telescope.

## 4. Conclusions

Neutrino astronomy is an emerging field in astroparticle physics offering exciting prospects for gaining new insights into the high-energy, non-thermal processes in our universe. The current neutrino telescope projects in the Mediterranean Sea are yielding exciting first data. They have reached a level of technical maturity allowing for the preparation of the next-generation cubic-kilometre detector to complement the IceCube telescope currently being installed at the South Pole.

The technical design of the future Mediterranean km<sup>3</sup> neutrino telescope will be worked out in the 3-year EU-funded KM3NeT Design Study that started in Feb. 2006. The construction of the KM3NeT neutrino telescope during the first years of the next decade appears to be in reach.

## Acknowledgments

The author wishes to thank the Neutrino06 organisers for a memorable and perfectly organised conference and for their patience with his delayed contribution to these proceedings.

## References

- [1] Spiering C 2005 *Phys. Scripta* T **121** 112 .
- [2] H.E.S.S. Coll., Rowell G *et al* 2006 *J. Phys. Conf. Ser* **47** 21 .
- [3] Aharonian F 2007 *Preprint* astro-ph/0702680; Aharonian F 2007 *these proceedings* .
- [4] Vissani F 2006 *Astropart. Phys* **26** 310; Kistler M and Beacom J 2006 *Phys. Rev. D* **74** 063007; NEMO Coll., Distefano C *et al* 2006 *Preprint* astro-ph/0608514 .
- [5] Kappes A, Hinton J, Stegmann C and Aharonian F 2007 *Astrophys. J* **656** 870; .
- [6] H.E.S.S. Coll., Aharonian F *et al* 2006 *Astron. Astrophys* **449** 223; and *Astron. Astrophys.* **437**, L7 .
- [7] Spiering C 2003 *J. Phys. G* **29** 843 .
- [8] Learned J G and Mannheim K 2000 *Ann. Rev. Nucl. Part. Sci.* **50** 679L .
- [9] Carr J, Lamanna G and Lavalley J 2006 *Rept. Prog. Phys* **69** 2475 .
- [10] AMANDA Coll., Andrés E *et al* 2000 *Astropart. Phys.* **13** 1 .
- [11] AMANDA Coll., Ahrens J *et al* 2004 *Phys. Rev. Lett.* **92** 071102 .
- [12] IceCube Coll., Achterberg A *et al* 2006 *Astropart. Phys* **26** 155 .
- [13] BAIKAL Coll., Belolaptikov I A *et al* 1997 *Astropart. Phys.* **7** 263; BAIKAL Coll., Balkanov V A *et al* 2000 *Phys. Atom. Nucl.* **63** 951 .
- [14] ANTARES Coll., Aslanides E *et al* 1999 *Report* CPPM-P-1999-02 (*Preprint* astro-ph/9907432) .
- [15] ANTARES Coll. 2001 *Technical Design Report* <http://antares.in2p3.fr/Publications/TDR/v1r0> .
- [16] ANTARES homepage, <http://antares.in2p3.fr/> .
- [17] NESTOR Coll., Grieder P *et al* 2001 *Nuovo Cimento* **24** C 771; and *Proc. ICRC 2003, Tsukuba* 1377 (<http://www-rccn.icrr.u-tokyo.ac.jp/icrc2003/PROCEEDINGS/PDF/343.pdf>) .
- [18] NEMO Coll., Piattelli P *et al* 2005 *Nucl. Phys. Proc. Suppl.* **143** 359 NEMO homepage, <http://nemoweb.lns.infn.it/>.
- [19] KM3NeT homepage, <http://www.km3net.org>.
- [20] ANTARES Coll., Amran P *et al* 2002 *Nucl. Inst. Meth. A* **484** 369 .
- [21] Bertin V 2007 *these proceedings* .
- [22] NESTOR Coll., Aggouras G *et al* 2005 *Nucl. Inst. Meth. A* **552** 420 .
- [23] NESTOR Coll., Aggouras G *et al* 2005 *Astropart. Phys.* **23** 377 .
- [24] [http://www.lngs.infn.it/lngs\\_infn/contents/docs/pdf/panagic/henap2002.pdf](http://www.lngs.infn.it/lngs_infn/contents/docs/pdf/panagic/henap2002.pdf) .
- [25] [ftp://ftp.cordis.europa.eu/pub/esfri/docs/esfri-roadmap-report-26092006\\_en.pdf](ftp://ftp.cordis.europa.eu/pub/esfri/docs/esfri-roadmap-report-26092006_en.pdf) .
- [26] Kuch S 2006 *Nucl. Inst. Meth. A* **567** 498 (*Proc. VLVnT2 Workshop, Catania, Nov. 2005*) .

# Searches for Astrophysical and Dark-Matter Axions

D. Kinion<sup>a</sup> \*

<sup>a</sup>Lawrence Livermore National Laboratory, 7000 East Ave., Livermore, CA 94550

I describe three on-going experiments to detect axions, light pseudoscalar particles which arise from the Peccei-Quinn solution to the Strong-CP problem. The Axion Dark-Matter Experiment (ADMX) has been searching for dark-matter axions using the Sikivie microwave cavity technique. The CARRACK experiment plans to use the same technique while employing a very sensitive photon detector using Rydberg Atoms. Finally, the Cern Axion Solar Telescope (CAST) is searching for axion-like particles with a two-photon interaction which could be produced in the Sun by the Primakoff process. The most recent exclusion regions from these experiments will be presented.

## 1. INTRODUCTION

Axions, a promising cold dark matter candidate, arise from a minimal extension of the Standard Model to enforce CP conservation in the strong interactions. The Peccei-Quinn solution to the Strong-CP problem in QCD [1] involves an approximate  $U_{PQ}(1)$  global symmetry. This  $U_{PQ}(1)$  symmetry is spontaneously broken at some unknown symmetry-breaking scale  $f_a$ , and the axion is the associated pseudo-Goldstone Boson [2].

The properties of the axion depend mainly on the symmetry breaking scale  $f_a$ . Its mass is inversely proportional to  $f_a$  and given by

$$m_a [eV] \approx 0.6 \text{ eV} \frac{10^7 \text{ GeV}}{f_a [\text{GeV}]} \quad (1)$$

All of the axion's couplings are proportional to  $m_a$ . The coupling relevant for detection is the two-photon coupling described by

$$L_{a\gamma\gamma} = g_\gamma \frac{\alpha\phi_a}{4\pi f_a} F_{\mu\nu} \tilde{F}^{\mu\nu} = -g_{a\gamma\gamma} \phi_a \mathbf{E} \cdot \mathbf{B} \quad (2)$$

where  $\alpha$  is the fine structure constant,  $\phi_a$  is the axion field,  $g_\gamma$  is a model-dependent constant of order unity, and  $g_{a\gamma\gamma} = (\alpha g_\gamma / \pi f_a)$ . For the two most important axion models, KSVZ [3] and DFSZ [4],  $g_\gamma \sim 0.97$ , and  $g_\gamma \sim -0.36$  respectively.

\*Work performed under the auspices of the U.S. Department of Energy by the University of California Lawrence Livermore National Laboratory under contract W-7405-ENG-48.

Since  $f_a$  is unknown and arbitrary,  $m_a$  could have any value. Fortunately, astrophysical and cosmological considerations help constrain  $m_a$ . These constraints are described in [5], which result in the allowed mass range, or axion window:

$$10^{-6} < m_a < 10^{-2} \text{ eV}. \quad (3)$$

## 2. Microwave-Cavity Axion Searches

To date, the most sensitive method of searching for axions is the microwave cavity technique originally proposed by Sikivie [6]. In a static background magnetic field, axions will decay into single photons via the Primakoff effect. The energy of the photons is equal to the rest mass of the axion with a small contribution from its kinetic energy, hence their frequency is given by  $hf = m_a c^2 (1 + O(10^{-6}))$ . At the lower end of the axion window (3), the frequency of the photons lies in the microwave regime. A high-Q resonant cavity, tuned to the axion mass serves as the detector for the converted photons. The expected signal power varies with the experimental parameters as [6,7]

$$P_{a \rightarrow \gamma} \propto B^2 V C Q f \rho_a \quad (4)$$

where  $B$  is the background magnetic field,  $V$  is the cavity volume,  $C$  is a mode dependent form factor,  $Q$  is the loaded quality factor,  $f$  is the resonant frequency, and  $\rho_a$  is the local halo axion density. Axions couple most strongly to the

2

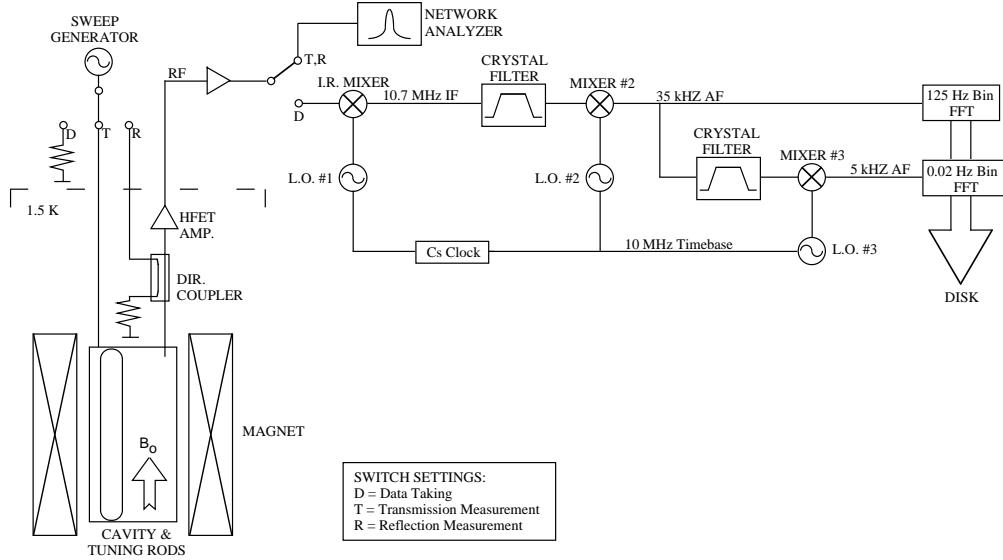


Figure 1. The ADMX detector.

$TM_{010}$  cavity mode ( $C \sim 0.5$ ), so it is the only mode used in most searches. For the parameters of the ADMX experiment, the power from KSVZ axions is typically  $5 \times 10^{-22} W$ .

Since the axion mass is unknown, the frequency of the cavity must be tunable. The signal-to-noise ratio (SNR) is related to the integration time  $t$ , and signal bandwidth  $B$  by Dicke's radiometer equation

$$\frac{S}{N} = \frac{P_{a \rightarrow \gamma}}{P_N} \sqrt{Bt} = \frac{P_{a \rightarrow \gamma}}{k_B T_s} \sqrt{\frac{t}{B}} \quad (5)$$

where  $k_B$  is Boltzmann's constant, and  $T_s$  is the system noise temperature. This expression can be inverted to give the scan rate which scales as

$$\frac{df}{dt} \propto \frac{f_o^2 Q_u C^2 B^4 V^2}{T_s^2}. \quad (6)$$

Equation 6 demonstrates the need for large magnetic fields and low temperatures.

### 2.1. The Axion Dark-Matter Experiment (ADMX)

The Axion Dark-Matter Experiment (ADMX) is a microwave cavity search currently under-

way at Lawrence Livermore National Laboratory (LLNL). The ADMX collaboration includes LLNL, the University of Florida, the University of Washington, and the University of California at Berkeley. Figure 1 is a schematic of the ADMX detector. The magnet employed in this search is an 8 T superconducting NbTi solenoid.

The microwave cavity is a right-circular cylinder 50 cm in diameter and 1 m long constructed from stainless steel and plated with ultra-high purity, oxygen-free copper. The resonant frequency of the empty single-cavity is 460 MHz and the unloaded  $Q$  is approximately 200000. Moving a combination of metal and dielectric rods, running the full length of the cavity, changes the resonant frequency. The entire system is cooled to 1.5 K by pumping on a bath of superfluid  $^4\text{He}$ .

The cryogenic amplifiers currently used are double-balanced GaAs HFET amplifiers supplied by NRAO [8]. The *in situ* measured noise temperatures range from 1.7 - 4.5 K. Cascading two of these amplifiers achieves sufficient gain (35 dB) to render downstream noise contributions negligible.

Before data is taken at a given frequency, a transmission measurement is made. A fit of the transmission curve to the sum of a Lorentzian and constant background determines the resonant frequency and  $Q$ .

The double-heterodyne receiver shown in Figure (1) mixes a small bandwidth centered on the cavity frequency down to 35 kHz. This audio frequency signal is then sent to medium and high-resolution spectrum analyzers.

The medium-resolution search channel consists of a commercial FFT spectrum analyzer. The sampling interval of the analyzer is 80 msec, giving a frequency resolution of 125 Hz. These data are coadded and the result searched for Maxwellian peaks a few bins wide (about 700 Hz) characteristic of thermalized axions in the halo [9].

An independent, high-resolution search channel operates in parallel to explore the possibility of fine-structure in the axion signal [10,11]. The 35 kHz signal passes through a third mixing stage to shift the center frequency to 5 kHz. A PC based DSP takes a single 50 second spectrum and performs an FFT with 20 mHz frequency resolution, about the limit imposed by the Doppler shift due to the earth's rotation. These data are searched for coincidences between different scans, as well as coincidences with peaks in the medium resolution data.

Positive fluctuations in the power spectrum are identified as candidate peaks and rescanned. Peaks which are statistical in nature will not reappear and can be eliminated as axion signals. Candidates which survive the rescan are considered persistent, and must be checked in other ways. Those few that remained have all been linked to external sources by using an antenna in the room. If a peak were to survive all of these checks, the definitive test would be to see if it appears only when the magnetic field is on.

So far, no axion signal has been detected. Based on these results, we exclude at 90% confidence a KSVZ axion of mass between 1.9 and 3.3  $\mu eV$ , assuming that thermalized axions comprise a major fraction of our galactic halo ( $\rho_a = 450 \text{ MeV/cm}^3$ ). This exclusion region is shown in Figure 4. For more details see Refs. [12,13].

## 2.2. Phase I Upgrade

As seen in Equation 6, the scan rate depends strongly on the parameters  $B$ ,  $V$ ,  $Q$  and  $T_S$ .  $B$  and  $V$  are both constrained by financial and material considerations, and the cavity  $Q$  is already very close to the theoretical limit for copper in the anomalous skin-depth regime. There is, however, room for significant improvement in the system noise temperature  $T_S$ .

Although the NRAO HFET amplifiers are state-of-the-art, their noise temperatures are still more than an order of magnitude higher than the Standard Quantum Limit ( $T_N = h\nu/k_B$ )[5]. In the past several years a group at Berkeley led by John Clarke has developed dc SQUID amplifiers in the 100 - 3000 MHz range specifically for the ADMX experiment.

A dc SQUID consists of two Josephson junctions connected in parallel on a superconducting loop. The SQUID produces an output voltage in response to a small input flux, and is a very sensitive flux-to-voltage transducer. Flux is coupled into the SQUID through a microstrip resonator. Near the fundamental frequency of the resonator, the gain of the amplifier is strongly enhanced. The noise temperature of the SQUID amplifiers was determined by measuring the Nyquist noise from a tuned tank circuit at the input and found to be more than an order-of-magnitude lower than that of the GaAs HFETs. More details can be found in Ref. [5].

The second, almost equal, contribution to the current value of  $T_S$  comes from the 1.5 K physical temperature. This can be reduced below 100 mK by cooling the entire experiment with a dilution refrigerator.

These two pursuits have been divided into a two-phase upgrade. Phase I is just underway with the goal of getting a SQUID amplifier working in the current experiment at 1.5 K. When this is accomplished, Phase II will be installing the dilution refrigerator.

## 2.3. The CARRACK Experiment

Another microwave-cavity axion search is under development at the University of Kyoto ('CARRACK' for Cosmic Axion Research with Rydberg Atoms in a Resonant Cavity in Ky-

4

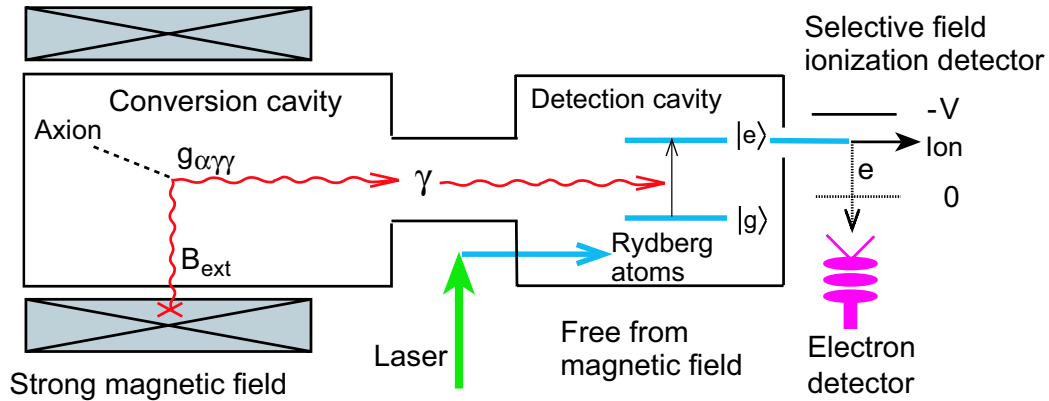


Figure 2. Experimental principle of the Kyoto axion detector with the Rydberg-atom cavity detector.

oto). This effort seeks to exploit the extremely low-noise photon counting capability of Rydberg atoms in a Sikivie-type microwave cavity experiment. The initial goal is to sweep out a 10% mass window around  $2.4\mu\text{eV}$ .

Rydberg atoms are atoms (usually alkali metals) where one electron is promoted to a principal quantum number  $n \gg 1$ , near the ionization limit. The valence electron of such highly excited atoms is hydrogen-like.

The experimental principle of the Kyoto experiment is shown in figure 2. Similar to ADMX, axions are converted to photons in the conversion cavity which is permeated by a strong magnetic field. The conversion cavity is a copper cylinder (4.5 cm radius, 72.5 cm long) which fits inside a superconducting solenoid (15 cm diameter, 50 cm long, 7 T peak field). Power from the conversion cavity is coupled to a superconducting Nb cavity, where the magnetic field is canceled by the combination of a compensation coil and the Meissner effect. The frequency of both cavities are made to track by means of 6 mm sapphire rods inserted axially into them. The cavities are cooled to  $< 15$  mK by means of a dilution refrigerator.

A beam of Rb atoms is accelerated, neutralized and directed through the detection cavity. Just before entering the detection cavity, the atoms are excited to a Rydberg state with principal

quantum number near 110 by triple optical excitation with three collinear diode laser beams. In the detection cavity, the Rydberg atoms are Stark-tuned so that the transition from the initial Rydberg state  $|g\rangle$  to an excited state  $|e\rangle$  is matched to the cavity frequency. Rydberg atoms have large transition dipole moments, and therefore have a high quantum efficiency for absorbing photons corresponding to an allowed transition. Upon exiting the cavity, most of the atoms are still in state  $|g\rangle$ , but a few of them are in state  $|e\rangle$  by virtue of having absorbed a microwave photon.

The key to this technique is selective field ionization. After exiting the detection cavity, an electric field is applied to the atoms, the combined atomic + coulomb potential is such that the electrons in state  $|e\rangle$  are unbound while those in state  $|g\rangle$  remain bound. The liberated electrons are counted in the electron detector and in principle this counts the number of photons in the detection cavity.

Studies have been performed to confirm that the experiment is sensitive to single blackbody photons in the  $< 15$  mK range. These include verifying the temperature dependence, and the number and velocity of the Rydberg atoms. For more details, see Ref. [?].

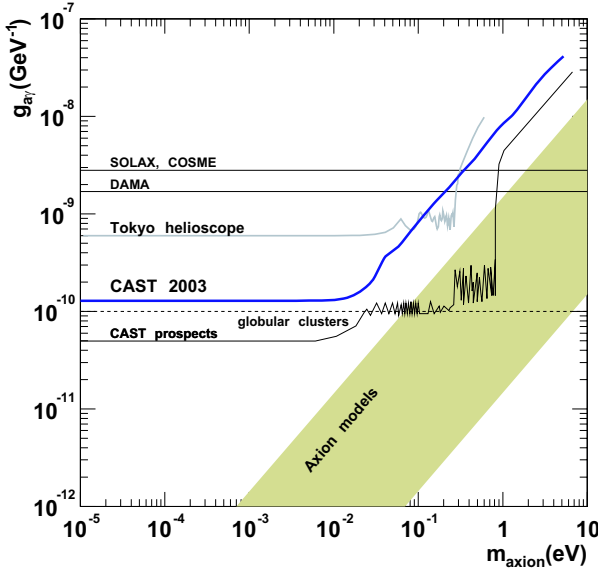


Figure 3. 95% CL exclusion line obtained from the analysis of the 2003 CAST data [21].

### 3. Axion helioscopes

Axions or other hypothetical axion-like particles with a two-photon interaction can also be produced in the interiors of stars by Primakoff conversion of the plasma photons. This axion emission would open new channels of stellar energy drain so energy loss arguments may significantly constrain axion properties in order not to conflict with our knowledge of solar physics or stellar evolution[15].

The solar axion flux can be estimated [16,17] within the standard solar model. The expected number of solar axions at the Earth surface is  $\Phi_a = (g_{a\gamma\gamma}/10^{-10} \text{ GeV}^{-1})^2 3.54 \times 10^{11} \text{ cm}^{-2} \text{ s}^{-1}$  (being  $g_{a\gamma\gamma}$  the axion-photon coupling) and their energies follow a broad spectral distribution around  $\sim 4$  keV, determined by solar physics (Sun's core temperature). Solar axions, unlike galactic ones, are therefore relativistic particles.

These particles can be converted back into photons in a laboratory electromagnetic field. This

technique was first experimentally applied in [18] and later on by the Tokyo helioscope [19], which provided the first "self-consistent" limit to solar axions, i.e, compatible with solar physics. Currently, the same basic concept is being used by the CAST collaboration at CERN [20] with some original additions that provides a considerable step forward in sensitivity to solar axions.

The CAST experiment is making use of a de-commissioned LHC test magnet that provides a magnetic field of 9 Tesla along its two parallel pipes of  $2 \times 14.5 \text{ cm}^2$  area and 10 m long. These values provide an axion-photon conversion probability that is a factor of 100 higher than in the Tokyo helioscope. The CAST magnet has been mounted on a platform that allows it to point toward the Sun and track it during  $\sim 3$  h per day on average. The rest of the time is devoted to measuring the background. CAST operates three different X-ray detectors with complementary approaches: a TPC, a MICROMEAS and a CCD. An X-ray focussing mirror system, designed and built as a spare system for the X-ray astronomy mission ABRIXAS, focusses the X-rays coming out of the magnet down to a spot of a few  $\text{mm}^2$  on the CCD, increasing the sensitivity of the experiment.

The experiment operated for about 6 months in 2003 and the results of the first analysis have been recently released [21]. No signal above background was observed, implying an upper limit to the axion-photon coupling  $g_{a\gamma} < 1.16 \times 10^{-10} \text{ GeV}^{-1}$  at 95% CL for the low mass (coherence) region  $m_a \lesssim 0.02 \text{ eV}$ . This limit, shown in Figure 3 is a factor 5 more restrictive than the limit from the Tokyo axion helioscope and already comparable to the one derived from stellar energy-loss arguments.

A better limit for the coherence region is expected after the analysis of the full body of data of CAST phase I, including 2004 data and especially the data taken with the focusing mirror. Later, a second data taking phase of CAST is foreseen with a buffer gas ( $\text{He}^4$  and/or  $\text{He}^3$ ) inside the magnet pipes. Varying the pressure of the gas matches the coherence condition for a range of axion masses up to  $\sim \text{eV}$ . As can be seen in Figure 4, CAST phase II sensitivity will enter for the first

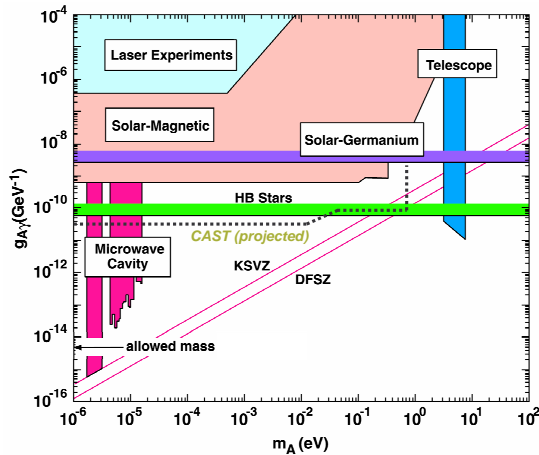


Figure 4. Combined exclusion region for axion search experiments.

time the region of the parameter space where the theoretically best-motivated axion models lie.

#### 4. CONCLUSION

After twenty five years, the axion remains the most elegant solution to the Strong-CP problem in QCD. In the meantime, a number of experiments have searched for axions via the Primakoff interaction, the resulting exclusion regions are shown in Figure 4. For more details, see Ref. [22].

#### REFERENCES

1. R. Peccei and H. Quinn, *Phys. Rev. Lett.* **38**, 1440 (1977).
2. S. Weinberg, *Phys. Rev. Lett.* **40**, 223 (1978); F. Wilczek, *ibid.* 279 (1978).
3. J.E. Kim, *Phys. Rev. Lett.* **43**, 103 (1979); M.A. Shifman, A.I. Vainshtein, and V.I. Zakharov, *Nucl. Phys.* **166**, 493 (1980).
4. M. Dine, W. Fischler, and M. Srednicki, *Phys. Lett.* **104**, 199 (1981); A.R. Zhitnitsky, *Sov. J. Nucl. Phys.* **31**, 260 (1980).
5. R. Bradley *et al.*, *Rev. Mod. Phys.* **75**, 777 (2003).
6. P. Sikivie, *Phys. Rev. Lett.* **51**, 1415 (1983).

7. L. Krauss *et al.*, *Phys. Rev. Lett.* **55**, 1797 (1985).
8. E. Daw and R.F. Bradley, *J. Appl. Phys.* **82**, 1925 (1997).
9. M.S. Turner, *Phys. Rev. D* **42**, 3572 (1990).
10. P. Sikivie and J. Ipser, *Phys. Lett. B* **291**, 288 (1992).
11. P. Sikivie *et al.*, *Phys. Rev. Lett.* **75**, 2911 (1995).
12. S. Asztalos *et al.*, *Phys. Rev. D* **64**, 092003 (2001).
13. L. Duffy *et al.*, *Phys. Rev. Lett.* **00**, 000000 (2006).
14. M. Mück, M., J. B. Kycia, and J. Clarke, 2001, *Appl. Phys. Lett.* **78**, 967 (2001).
15. G. G. Raffelt, *Ann. Rev. Nucl. Part. Sci.* **49**, 163 (1999) [hep-ph/9903472].
16. K. van Bibber, P. M. McIntyre, D. E. Morris and G. G. Raffelt, *Phys. Rev. D* **39** (1989) 2089.
17. R. J. Creswick, F. T. Avignone, H. A. Farach, J. I. Collar, A. O. Gattone, S. Nussinov and K. Zioutas, *Phys. Lett. B* **427** (1998) 235 [hep-ph/9708210].
18. D. M. Lazarus *et al.*, *Phys. Rev. Lett.* **69** (1992) 2333.
19. S. Moriyama *et al.*, *Phys. Lett. B* **434**, 147 (1998) [hep-ex/9805026].
20. K. Zioutas *et al.*, *Nucl. Instrum. Meth. A* **425** (1999) 482 [arXiv:astro-ph/9801176].
21. K. Zioutas *et al.*, *Phys. Rev. Lett.* **94**, 121301 (2005).
22. L. J Rosenberg and K. van Bibber *Phys. Rep.* **325**, 1 (2000).

# Dark Matter Candidates: What Cold, ..and What's Not

**Lawrence M. Krauss**

CERCA, Physics Department, Case Western Reserve University, 10900 Euclid Ave, Cleveland OH 44106-7079, and Physics Department, Vanderbilt University, Nashville TN.

E-mail: [krauss@cwru.edu](mailto:krauss@cwru.edu)

**Abstract.** In this brief review of recent theoretical developments associated with the search for dark matter I describe the following: why baryons are now ruled out as dark matter candidates; SUSY WIMPS and signatures in the MSSM and NMSSM why claimed indirect signatures are probably not WIMP related, why axions may be of new interest, how WIMP detection might tell us about the galactic halo, and how theorists are preparing to avoid the next generation of experimental constraints. (Invited review talk, Neutrino 2006, Santa Fe 2006)

## 1. Introduction

Determining the nature and origin of the dark matter dominating almost all clustered systems in the universe remains, some 40 years after strong evidence of the existence of dark matter was first presented, one of most important outstanding questions in physics and cosmology. While light neutrinos were the first natural non-baryonic candidate for dark matter, there is now ample evidence that this material, while definitely non-baryonic as I shall describe, must also be 'cold', i.e. non-relativistic at the time the first large scale structures in the universe began to form. Perhaps the favored Cold Dark Matter candidate is the Lightest Supersymmetric Particle (LSP), which not only arises naturally in extensions of the Standard Model, but also has a mass scale and interaction strength (making it a WIMP-Weakly Interacting Massive Particle) which naturally falls in the range allowing it to possibly dominate the mass density of the universe today. Nevertheless, as collider experiments continue to constrain the scale of SUSY breaking, the LSP allowed range is shrinking, and questions of fine tuning have arisen. For this reason, as I shall describe, extensions of the Minimal Supersymmetric Standard Model are now being considered. For all such WIMPS, there has been potential excitement associated with possible indirect signatures from annihilation in the galaxy, and I review why such excitement is misplaced. At the same time, as the second generation of WIMP detectors is coming online and beginning to seriously probe the LSP parameter space, it is worth considering how the uncertainties associated with our lack of knowledge of our galactic halo might impact upon such experiments, and also how one might design experiments that can separate astrophysical uncertainties from particle physics uncertainties. Next, as I shall describe, axions, the 'other' well motivated CDM candidate are once again returning from obscurity, as particle physicists are finding new ways of making unnatural acts natural. Finally, of course, there are a host of unmotivated dark matter candidates that are being discussed, demonstrating once again that beauty, even in science, is in the eye of the beholder.

## 2. Baryons Aren't

From the moment that Dark Matter was first inferred, using the motion of galaxies in clusters, and then, more solidly, by the rotation curves of spiral galaxies, the natural suspicion was that it could easily be explained as being due to non-luminous baryons, like snowballs, planets, or brown dwarfs. Over time these possibilities became more and more constrained. By the 1990's, one of the most severe constraints came from Big Bang Nucleosynthesis (BBN).

Observations of absorption of light from distant quasars by intervening hydrogen gas clouds allowed for the first time a measurement of the fraction of primordial deuterium in these clouds. While the measurements are quite difficult, and subject to large possible systematic uncertainties, the measured deuterium to hydrogen fraction settled on a value of approximately  $3 \times 10^{-5}$ . Comparing this to the predictions of standard BBN calculations yields a baryon fraction (compared to the critical density) of  $\Omega_B h^2 = .02 \pm .002$ , where  $h$  represents the Hubble constant in units of  $100 \text{ km/s/Mpc}$ , and HST values suggest  $h \approx 0.7$ .

At the same time, separate astrophysical observations, ranging from X-Ray studies of galaxy clusters to gravitational lensing observations of these system began to converge on an inferred dark matter fraction that was statistically incompatible with this fraction, in the range  $\Omega h^2 = 0.1 - 0.15$ .

While this inconsistency was apparent, there were still loopholes. First, could BBN estimates be trusted? Second, large scale structure observations had often been subject to large systematic uncertainties that had caused cosmologists to refine estimates of  $\Omega_{clustered}$  on numerous occasions.

Happily, whatever nagging doubts may have existed have largely been laid to rest following the WMAP observations of the CMB, which have independently confirmed both of the above estimates for  $\Omega_B$  and  $\Omega_{clustered}$  [1]. As a result, we now have definitive evidence that dark matter *cannot* be baryonic, and therefore is likely composed from a gas of more exotic elementary particles.

## 3. The Usual Suspects

I like to categorize non-baryonic dark matter candidates by the different mechanisms by which they may have arisen. In this case, dark matter candidates fall into one of the following categories:

- **BORN TO BE DARK,**
- **ACHIEVE DARK MATTERDOM**
- **HAVE DARK MATTERDOM THRUST UPON THEM**

### 3.1. Born to be Dark

The prototypical such candidate is a light neutrino. Present in roughly the same thermal equilibrium numbers in the early universe as photons, which have an energy fraction of roughly  $\Omega \approx 10^{-5}$ , if  $m_\nu/T \approx 10^5$  then neutrinos will automatically close the universe. Unfortunately they don't. Or rather, fortunately, they don't, because if they did it is not clear that galaxies would have formed in time for us to be here today.

### 3.2. Achieve Dark Matterdom

Here, WIMPS are the prototypical candidate. Like neutrinos, they were present with thermal equilibrium densities comparable to photons at early times. However, their annihilation cross-sections, which scale with their mass, are much larger. As a result, before their interactions freeze out, the temperature of the universe would have decreased below their mass. As a result, their number density will be suppressed by a factor of roughly  $\exp[-M/T_{freezeout}]$  compared to photons. This produces a roughly critical mass today if  $M \approx O(\text{GeV})$

and  $\exp[-M/T_{\text{freezeout}}] \approx 1/20$ , which requires interaction cross sections that are roughly comparable to weak interaction cross sections.

### 3.3. Have Dark Matterdom Thrust Upon Them

Axions are the prototypical candidate in this regard. With predicted masses much less than 1 eV, axions by all rights should be cosmologically irrelevant. However, cosmic axions are not be produced just thermally. Since axions are the pseudo-Goldstone boson associated with a global phase transition, they can exist as a Bose condensate at early times. If, for example, the Peccei-Quinn phase transition happens before Inflation, the axion field, described by an angular variable,  $\theta = a/F$ , where  $F$  is the PQ symmetry breaking scale, can have a non-zero expectation value throughout the entire universe. While the potential is strictly flat, when QCD effects break the symmetry, the axion field gets a mass. This induced curvature implies that there is non-zero energy density stored in the coherent axion field. It is miniscule at early times, but if the axion mass is very small, the axion field does not begin to relax down the potential until late times. Until it relaxes, the energy density stored in the field looks like a cosmological term, and remains constant, while the matter density of the rest of the universe falls as  $R^{-3}$ . Once the field starts to relax, the coherent field energy gets converted into non-relativistic matter, whose energy begins to redshift. Ultimately, if the initial value of  $\theta$  is  $O(1)$  then the axion can dominate the energy density of the universe, with a contribution to  $\Omega$  of

$$\Omega_a \approx (10^{-5} \text{ eV}/m_a)(200 \text{ MeV}/\Lambda_{\text{QCD}}) \quad (1)$$

## 4. Problems in SUSY Paradise: SUSY Dark Matter and the NMSSM

The Minimal Supersymmetric Standard Model (MSSM) provides an elegant framework in which to attempt to understand two central issues in elementary particle physics, the hierarchy problem, and the possibility of Grand Unification. It is remarkable that at the same time the energy scale associated with low energy supersymmetry breaking can naturally result in stable particles whose interaction strength is precisely in the range described above as required for WIMPs.

And if nature were an impressionist painting the MSSM would, without question, be considered the most likely candidate for physics beyond the standard model. However, when examined in detail, certain issues arise which suggest some fine tuning might be necessary. These are:

- The  $\mu$  problem: A SUSY conserving mass term for the two higgs superfields in the MSSM with mass parameter  $\mu$  can have values ranging from zero to the Planck Scale. Why it should be fine-tuned at the electroweak scale is not clear
- Non observation of the Higgs: The upper bound on a neutral Higgs in the MSSM at LEP requires that the Higgs exist very close to its upper bound, requiring fine tuning
- How to get  $\Omega \ll 1$ ?: Because annihilation of LSP's determines their remnant abundance, in order to get sufficient annihilation for relatively heavy LSP's, one has to have light intermediate annihilation channels. But collider constraints on sleptons and squarks, as well as the Higgs particles make this increasingly difficult.
- small flavor changing rates require fine tuning
- parameter space squeezed: the parameter space of the MSSM is being increasingly squeezed, especially if dark matter LSP's is desired

Within the context of the MSSM, a number of authors have examined what the implications of existing collider constraints are for dark matter searches. It has been claimed that constraints on  $\Omega$ , combined with collider constraints drive the allowed range of models to be those with

small  $\mu$  parameter. In some cases this gives a lower bound on the WIMP spin-independent cross section with nucleons, the parameter of relevance to direct dark matter detectors [2]. It has also been claimed [3] that Tevatron searches for the neutral Higgs, which are sensitive to large  $\tan\beta$  and small  $m_A$  are precisely the parameter range probed by dark matter experiments like the CDMS experiment [4]. Thus, direct dark matter constraints will impact on what is observable at the Tevatron.

As an alternative to this possibility, a number of authors have examined a next-to-minimal version of the SSM, in which a gauge singlet Higgs superfield is added. If this superfield gets a VEV of the order the the SUSY breaking scale, it leads to an effective  $\mu$  parameter that is also of the order of the EW scale. It also allows the upper bound on the neutral Higgs to be increased, and allows for a very light Higgs boson which is not experimentally excluded, and which also provides an additional annihilation channel for SUSY WIMPs, increasing the allowed parameter space as a function of LSP mass [5, 6]. In particular, very light LSP dark matter masses are now possible.

Recently, my collaborators and I carried out a comprehensive examination of the possibility that these additional phenomenological attractions in the NMSSM might lead to new indirect signatures for the detection of SUSY dark matter. We have found that extra one-loop amplitudes for NMSSM annihilation into photons and gluons is enhanced, and that low mass antimatter experiments should be a good probe of such NMSSM WIMPs, and that the possibility of the detection of a monochromatic gamma-ray line within the NMSSM is more promising than the MSSM [7]. It is also possible that NMSSM WIMPs might form an additional solar system dark matter contribution which could enhance detection of annihilation in the Earth [8].

### 5. Looking for Dark Matter in All the Wrong Places?

While the direct and indirect signatures for SUSY WIMPs in the MSSM and NMSSM are exciting, motivation for considering the added flexibility of light WIMPs allowed by the NMSSM was provided by several claimed direct and indirect hints of halo dark matter in experiments. The DAMA experiment, for example, claimed to observe an annual modulation signal in excess of noise in their Sodium Iodide scintillation experiment. This, however, was inconsistent with limits from the original CDMS experiment unless the WIMP mass was very small. However, this rationale turns out to have been misplaced, as it now appears that the DAMA experiment, which has its own consistency problems, appears inconsistent improved limits from direct search experiments, even for low mass WIMPs.

At the same time, positron annihilation signals have been observed from the Galactic Core [9, 10], which was thought might be possibly due to annihilation of very light WIMPs in the sub-GeV range.

It turns out however that detailed analyses have shown that WIMP annihilation cannot account for this signature. In particular, any mechanism which produces energetic positrons will also be accompanied by internal bremsstrahlung photon emission, and if the positrons are created with an energy greater than 20 MeV, this will violate the COMPTEL/EGRET constraints [11]. Moreover, if positrons are produced a mildly relativistic energies, then higher energy gamma rays will be produced due to in-flight annihilations, requiring that the positrons must be injected with  $E < 3MeV$  [12].

At the opposite SUSY extreme of very high WIMP masses, a claimed signature of dark matter annihilation came from claims of an excess in high energy gamma rays in the 100 GeV-TeV range. However, a careful analysis of the energy spectrum expected from such annihilations does not match the observed flux [13].

Thus, for the moment at least, it appears that there is as of yet no compelling direct or indirect evidence for signatures for SUSY WIMPs, and that the next generation of direct and indirect detectors, searching for the signals described in the last section, provide our best bet of

constraining the SUSY parameter space in a way that will complement the upcoming searches at the LHC.

## 6. Using Halo Uncertainties to distinguish Dark Matter from Noise

If direct search experiments ever do detect a signal, it will in fact resemble noise. Indeed this fact is one of the reasons that the DAMA claimed detection is so difficult to interpret. Clearly it will be necessary to consider a second generation of experiments that will be more sensitive to the halo properties of the dark matter, in particular the fact that the Earth and Sun are moving with respect to the galactic rest frame. A detector with full directional information would be optimal in order to distinguish a preferred direction for nuclear recoils from WIMP interactions. There are, however, no detectors with such sensitivity. Happily, we have recently explored the efficacy of using detectors with a two dimensional directional sensitivity, as may be achieved by the proposed DRIFT experiment. We have shown, as can be seen in the table below [14], that *if and only if* forward backward sensitivity is possible, i.e. the head of the recoil track can be distinguished from the tail, that 2D detectors which can rotate in the laboratory frame are almost as efficient as full 3D detectors for distinguishing motion through an isothermal halo from a flat laboratory background.

**Table 1.** The number of events required to identify a WIMP signal above a flat background for different types of detectors and a WIMP mass of  $m_\chi = 100\text{GeV}$ .

Detector Type	$v_0$ (km/s)		
	170	220	270
3D (full)	6	11	18
3D without FB	176	1795	> 35,000
2D—best/worst	19/45	34/75	61/123
2D rotating	13	24	43

## 7. Axions are Back?

Axions, while by far the most elegant solution of the strong CP problem, have been less favored of late as dark matter candidates because the parameter range for allowed axion masses does naturally lie in the range in which axions would be dark matter. If the Peccei-Quinn scale is near the GUT scale then if  $\theta \approx 1$ , axions would close the universe today. Moreover, constraints from axion emission by supernovae, red giants and white dwarfs put a limit on axion masses of less than  $O(10^{-3}\text{eV})$ , so that axion masses are being squeezed from the high end as well.

However, it is true that if  $\langle \theta \rangle \ll 1$  in our universe then GUT scale axions could be dark matter. Until recently this possibility was viewed as unnatural. However, recently, due to the inability to naturally explain what appears to be a cosmological constant dominating the energy density of the Universe with an absurdly small and non-zero value, theorists have been driven to the last refuge of scoundrels, namely the anthropic principle.

While much of the discussion regarding anthropics is tantamount to metaphysics, it is true that if inflation occurs after the PQ transition, then the value of  $\theta$  will be a random variable over different causally disconnected regions. Recently it has been argued that if one is to average over universes with sufficient clustered matter, then the expected value of  $\theta$  that is favored is such that the axion dark matter density would be comparable to the observed density of dark matter today [15]. This is amusing, but like all anthropic arguments, far from compelling. Nevertheless, it has boosted axion stock on futures markets around the world.

## 8. Conclusions: From the Sublime to the Ridiculous

Light SUSY WIMPs and axions remain as highly motivated and potentially detectable dark matter candidates. The possibility of future discoveries in direct and indirect dark matter searches can complement the range accessible at terrestrial accelerators, meaning that the beautiful complementarity between non-accelerator and accelerator physics continues. Of course, as mentioned, beauty is in the eye of the beholder, and the possibility of dark matter that might arise naturally in particle physics has not stopped theorists from imagining a host of dark matter particles that are both undetectable and unmotivated. I see no good reason to review these possibilities here.

**Acknowledgments** I thank the organizers of Neutrino 2006 for producing a very interesting meeting, and my collaborators, in particular Francesc Ferrer and Craig Copi, for their important contributions to our projects, and for educating me about many things. My research is supported in part by DOE and NASA grants.

- [1] Spergel, D.N., et al, 2006, astro-ph/0603449, 2006
- [2] Kitano, R, Nomura, Y., 2006, *Phys. Rev D* **73**, 095004
- [3] Carena, M, Hooper, D, Skands, P., 2006, *Phys. Rev. Lett.* **97**, 051801
- [4] Akerib, D.S., et al, 2006, *Phys. Rev. Lett.* **96**, 011302
- [5] Belanger, G., et al, 2005 *J. Cosm. and AstroPart. Phys* **9**, 001
- [6] Gunion, J. F., Hooper, D., McElrath, B., 2006, *Phys. Rev D* **73**, 005011
- [7] Ferrer, F, Krauss, L.M., Profumo, S., 2006, *Phys. Rev D* **74**, 115007
- [8] Damour, T, Krauss, L.M., 1999, *Phys. Rev. D* **59**, 3509
- [9] Knodlseder, J., et al, 2003, astro-ph/0309442
- [10] , Knodlseder, J., et al, 2005, *Astr. Astrophys.*, **441**, 513
- [11] Beacom, J.F., Bell, N., Bertone G., 2005, *Phys. Rev. Lett.* **94**, 171301
- [12] Beacom, J.F.,Yuksel H., 2006, *Phys. Rev. Lett.* **97**, 071102
- [13] Zaharijas, G, Hooper, D, 2005, *Phys. Rev. D* **73**, 103501
- [14] Copi, C., Krauss, L.M.,Simmons-Duffin, D, Stroiney, S. , 2007, *Phys. Rev. D* **75**, 023514
- [15] Tegmark, M., et al, 2006, *Phys. Rev. D* **73**, 023505

## Reines-Cowan team discovery of the electron neutrino

**Herald W Kruse**

Los Alamos, New Mexico, USA Email: [herald@cybermesa.com](mailto:herald@cybermesa.com)

**Abstract.** Personal perspective and recollections by the author discuss the Reines-Cowan team discovery of the electron neutrino at a Savannah River reactor in 1956. First presented at the Neutrino Santa Fe 2006 Conference.

I am honored to participate with you in this Celebration of the Neutrino on the 50<sup>th</sup> year anniversary of its detection! I understand that some of you are searching for relic neutrinos left over from the Big Bang. So it seems fitting that I should stand before you as a token relic of the team that first detected the neutrino! (Of course, we detected antineutrinos, but I do not distinguish between the two types in this paper).

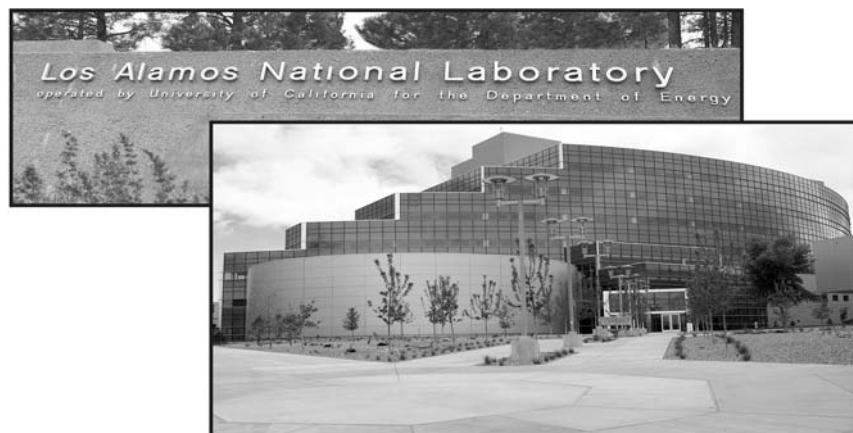


Figure 1. Newly constructed Los Alamos National Laboratory administration building.

It all started up on the Hill at Los Alamos. (figure 1) In fact, Reines stated that neutrino detection could only have happened at Los Alamos. I list a few factors which may have been relevant:

- Excellent financing and support for electronics, detector fabrication, and computer facilities. Through persuasive discussions, Reines convinced his Division Leader, Carson Mark, and Laboratory Director, Norris Bradbury that such an effort, if successful, would be well justified by the scientific importance of confirming Pauli's hypothesis of a new particle with unique properties.
- Easy availability of the security clearance required at large reactors. It was fortuitous that we needed to find such an excellent facility as Savannah River at a time soon after the reactor had come on line.
- Experience with large scintillators which were developed at Los Alamos to measure whole-body radioactivity.
- An extensive history at Los Alamos of successful, large-scale experiments and operations.

- Above all, we had Reines (figure 2).

He was the driving force for the experiment. I admired his strong focus, articulation, enthusiasm, and the steadfast effort he devoted to the work at hand. He excelled in explaining a plan for action and the reason for that action. He was born in New Jersey of immigrants from a small town in Russia. His first interest in science occurred during a moment of boredom at a religious grade school, when he noticed something peculiar (it turned out to be diffraction) when he looked at light through his closed fist. As a Boy Scout, he built radios from scratch. He earned his M.A. in science from Stevens Institute of Technology and Ph.D. in theoretical physics from New York University. He was recruited for work in the Theoretical Physics Division at Los Alamos by none other than Richard Feynman, even before he had finished his Ph.D. dissertation!



Figure 2. Fred Reines



Figure 3. Clyde Cowan, Jr.

After a chance meeting while waiting in an airport, Reines and Cowan established a firm partnership; they complimented each others' scientific expertise (figure 3). They communicated together, even late at night, discussing the merits of new ideas. Cowan was the administrative leader of our Neutrino Group but he also handled the instrumentation design and configuration details with inventive insight. Reines and Cowan first took a team to the Hanford reactor and the detector they used there is on display here at the Conference. Reines considered the Hanford experiment to have achieved tentative detection of the neutrino, and he titled our first paper announcing results from Savannah River a confirmation of the Hanford experiment. But I think, in general, our team thought of the Hanford result as justification for a far better experiment because the Hanford results suffered from a poor signal/noise ratio and poor statistics.

None of the Savannah River team had been a part of the Hanford team, except for Reines and Cowan. The Savannah River team (figure 4) included Kiko Harrison, an expert in large scintillators; Marty Warren, assisting in logistic details; two machinists who installed the detectors, assembled lead shielding, etc.; a young fellow in the lower corner of figure 4 who looks like I did 50 years ago; and Mac McGuire, an experienced physicist who designed the tank farm that housed the liquid scintillator. Mac was invaluable in many other phases of the project. Besides, he was our entertainer at social events at which he played a neat guitar and sang fun songs which he had composed. From his days in

Pacific nuclear tests, he sang “Don’t stand under a coconut tree when the bomb goes off out here ---” and a clever neutrino song “Oh, the little neutrino, of which there may be no --” in this one I think verse four was about living in fame with a Nobel Prize! There were two other team members who did not travel to Savannah River. One was Armand Brousseau, who was an exceptionally competent electronics technician. The other member was Tony Ronzio, a chemist who developed the cadmium chloride used in the scintillator for neutron capture. Tony loved to grow all kinds of huge crystals. In addition, a young woman living in Aiken, Linda Smith (to the best of my recollection) skillfully analyzed recorded traces on film each day.



Figure 4. The neutrino discovery team at the Savannah River reactor site. Clyde Cowan Jr., F.B. ‘Kiko’ Harrison, Austin McGuire, Fred Reines, Martin Warren, Herald Kruse, Forrest Rice, Richard Jones (Top left clockwise)

I came to Los Alamos as a graduate student at Kansas State at the suggestion of my graduate professor, Max Fowler, who had worked at Los Alamos for a few summers and who later came to LA full-time. He was a giant in the area of mega Gauss magnetic fields. I am sorry to say that he passed away earlier this year.

In just a few more years, you graduate students in the audience may experience the same feelings I had in coming to LA. I came in the summer of ‘53 to work in the cyclotron group. A few days after arrival, I answered the phone and the caller said he wanted to speak to John Brolley, a well-known physicist in the group. I said, “I’m sorry but Dr. Brolley is out for lunch right now. Could I take a message?” He said, “Just have him call me.” I said, “Who shall I say is calling?” He said -----“Fermi.” You could have blown me away with a feather and I realized what Moses had felt when he heard the voice of God on the mountaintop!

I came again in the summer of ‘54, when I was ushered into the Physics building and was told we were going to detect the neutrino! You can imagine how my brain was buzzing as I recalled the crisis of missing energy and spin in beta decay, the desperate hypothesis of Pauli, and his reluctance to

suggest his concept of the neutrino because, as he said, IT PROBABLY COULD NEVER BE DETECTED! At first, it seemed as if I was joining a lost cause, but then I decided it might be a great adventure!

I also recalled a joke or two. A group of protesters appeared at the fence surrounding the reactor with signs “No Nukes”, etc. You know the scene. A guard called to their attention that the neutrino shield had not yet been installed. So they all left. I’m sure each of you can recall a few more similar stories about neutrinos.

One of my tasks that summer was to test over 300 5” photomultiplier tubes for gain, noise level, and to seal the bases, since these tubes were to be mounted in an air/liquid interface. We also assembled the electronics that we would need in a trailer such as amplifiers, high voltage supplies, and coincidence circuits. (figure 5). These were all designed and fabricated in Los Alamos. Remember, this was a time before transistors; so all the electronics were bulky.



Figure 5. The electronics trailer used at the Savannah River reactor.

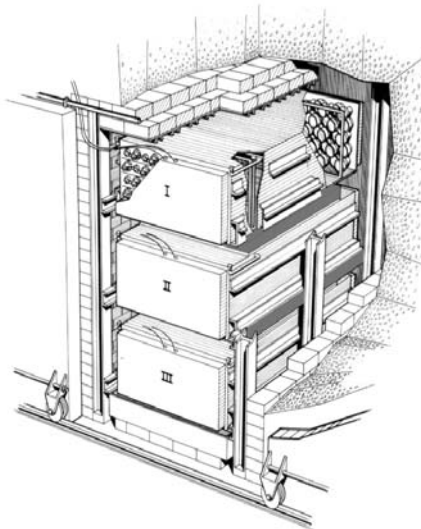


Figure 6. Detector design: Two target tanks (blue) between three scintillation detectors.

Some team members brought their families to Savannah River since we intended to stay for an extensive although unknown length of time. We all stayed in Aiken, a small but delightful town with beautiful flowers, sometimes a parade with beauty queens, and polo ponies. I spent weekends during the summer swimming somewhere; my favorite beach was at Beaufort State Park.

Reines and I both sang with the local choral society in a performance of *The Messiah*. Fred was a soloist, reflecting his earlier interest in music. He said he had once considered a career in music and at one point he had received free lessons from a musician at the Metropolitan Opera. Fortunately for all of us, he decided on a different direction! We also sang with an excellent chorus in Augusta, performing the *St. Matthew Passion* by Bach, accompanied by Virgil Fox, a famous organist in those days. Again Fred sang solo in that performance. I was asked to do a solo but I turned it down.

At the Savannah River reactor, we assembled our apparatus, tons of lead shielding, the pneumatic operated doors of lead bricks, the detectors, the scintillator plumbing, etc. Two target tanks containing

water and cadmium chloride were located between 3 tanks of liquid scintillator (figure 6). As all of you know, our goal was to examine a certain reaction:



I have seen Reines write this reaction on a blackboard countless times in various discussions, and it is so familiar now that I fear it has become prosaic. But in 1956 this reaction was hypothetical and to our team it presented an enormous challenge. We were attempting to establish the reaction either as a reality or a figment of a “desperate” imagination, both possibilities with far reaching results.

The reaction above was chosen by Reines because it had been computed to have such a high cross-section! Of course, that is facetious since it was several decades below the value of cross sections in previously observed interactions. Reines had first intended that just the positron signals were to be recorded which likely would have resulted in a failed experiment. Later, Reines and Cowan realized the very powerful technique of a delayed coincidence - detecting both the positron and the neutron signal within a short time (typically a few microseconds), offering a way to discriminate strongly against unwanted backgrounds. A typical event looked like this (figures 7 and 8): a pair of small pulses from each of 2 adjacent tanks, due to gammas from positron annihilation, followed by a pair of larger pulses, due to gammas resulting from neutron capture in Cd. These experimental details are described more fully in our original papers as well as in a thorough review of the experimental details published in Los Alamos Science. [1] [2] and [3]

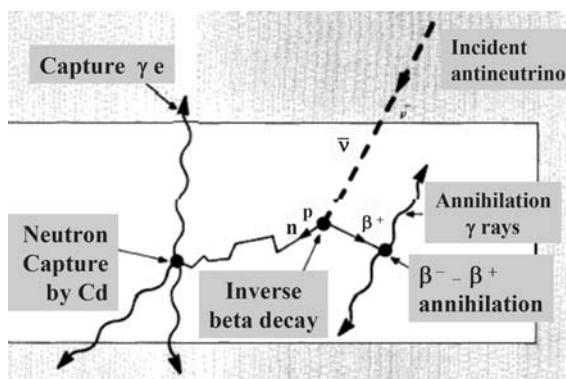


Figure 7. The reaction investigated by the Savannah River experiment.



Figure 8. A typical scope trace of a delayed-coincidence signal.

Finally, everything was ready for our first data recording session. When we turned on the main switch, nothing happened! We expected a scalar to trigger on possible events of interest, and we expected to hear the camera advancing the 35 mm film for each triggered event. We all stared at the electronics for a while and finally called the control room to see if the reactor was really on. Yes, it was, and after an agonizing wait, our first trigger happened, and we all relaxed a little.

One evening I accompanied Clyde and Fred to Columbia where we presented a talk to physics students at University of South Carolina. Clyde’s theme was that we were searching for the smallest particle in the world; and it took the largest detector in the world to detect it.

It was easy to determine that there was a reactor associated signal rate that was larger than the nonreactor rate. And we were pleased that this kind of signal/noise ratio was about a factor of 3 or 4, depending on many adjustable factors. Numerous checks followed which led to conclusions that the counting rate of just a few per hour was proportional to the number of protons in the target tank, that

the first small signal was due to positron annihilation, and the second was caused by neutron capture in Cd. I am certain that Reines spent many hours during the days and many nights, wondering what additional checks and tests would be necessary and sufficient to provide convincing evidence for neutrino detection. Team members were aware of the chasm that separated, on one hand, our results being consistent with the reaction under investigation, and on the other hand the conclusion that a neutrino had been detected. After significant amount of review of data in hand and soul searching, Reines and Cowan crossed that chasm and sent a wire to Pauli that “neutrinos were definitely detected from fission fragments by observing inverse beta decay of protons.” As I understand and paraphrase, Pauli announced in a surprised tone - “the neutrino is real after all” -as if anybody doubted it. Then they celebrated with champagne. I think our team celebrated with Florida orange juice!

In my personal view, it may have been venturesome to announce the first detection of the neutrino in 1956, even though no alternative was thought to be reasonable. I feel that the term “detection” or “discovery” is largely in the eye of the beholder. So, after having withstood the test of 50 years and receiving support from other experiments and the scientific community, it seems fair at this time to recognize our result as first detection of the neutrino.

Word of the neutrino detection spread, and I took a call one day from Life magazine. They wanted pictures, of course, and I offered some of a detector or photomultipliers or some hardware items- really exciting stuff! But they particularly wanted, of all things, you could never guess - baby pictures of Cowan! I said we didn't have any of those, and I tried to steer them to Cowan's family.

After we packed up and returned to Los Alamos, Reines and Cowan wrote publications, and I set up two of the detector tanks in an underground facility called the “ice house”, and proceeded to record a new lower limit for proton decay. Reines and I published a paper concerning this result and he continued to pursue this particular topic for years to come, including a project with a giant-sized detector, the IMB experiment.

Reines and Cowan were also busy preparing a proposal for another neutrino experiment using an accelerator instead of the reactor. Reines said he was puzzled by the Lab's response: “You all have had too much fun already and it 's time to get back to work.” I guess that's why they proceeded to move, in separate directions, to other locations in the country.

The experimental value of the cross section for the reaction studied is an important factor in a discussion about validity of our neutrino experiment. I believe that our experiment was designed to provide a valid test of the existence of the neutrino through concentration on the unique characteristics of inverse beta decay. But the features of the experimental configuration resulted in an unacceptably large uncertainty in the observed cross section, primarily due to the difficulties in determining the neutrino spectrum and detector efficiencies. I believe that Reines and Cowan considered that the test of uniqueness over-rode the need for cross section determination, in this first experiment. They probably argued that a cross section resulting from observed counting rates, no matter how precise, has no value unless a **real** neutrino caused the reaction. At the same time, it seems understandable that Reines, a theoretician, would have wanted to report a cross section! I feel that more details of this topic are intricate enough so as to be beyond the scope of this presentation. For further discussion, I refer you to a thorough review of our experiment by Robert Arns who is the only person, as far as I know, who has talked to team members and has reviewed in great detail the data recorded in the Savannah River notebooks, now on file at UC-Irvine. He pointed out an error that resulted in publication of apparent counting rate differences and discussed possible reasons for the belated Nobel Prize. [4]

Later in my own career, I returned to neutrino physics with a goal of detecting neutrinos from

underground nuclear tests. I wanted to demonstrate a practical application of measuring fission yields in a nonintrusive manner (such techniques were under investigation in order to assure treaty compliance) and to extend the technique to pursue evidence of neutrino oscillations. Reines had intended, originally, to use this approach, although I thought I had a better scheme! We organized a team, built a detector, computed in detail the neutrino spectrum expected, and studied effects of shock waves on photomultipliers and the detector to evaluate survivability. We expected to record about 100 neutrino events for each nuclear event during a 30 sec time duration. While we never fielded this experiment in Nevada, we used the detector in neutrino experiments at the Meson Facility (LAMPF) with a collaboration of scientists.

You recall that I previously mentioned the importance of the “delayed coincidence.” When the Nobel Prize was announced in 1995, another “delayed coincidence” occurred. Word was received at Savannah River with understandable excitement, in view of their considerable support. At that instant, my daughter, Deanna, was there in a conference, on LANL business. She stood up and said, “Hey, my Dad was on that team.” And she is here today! Stand up, please, Deanna.

When Reines left Los Alamos, he suggested that I follow him to Case Institute of Technology. At moments like this, I think perhaps I should have done that. There was only one reason that I remained in Los Alamos. Her name is Peggy Jo and she will stand for recognition now, please!

In behalf of the neutrino detection team, we and the Los Alamos National Laboratory are proud to have been a part of a very important experiment. Our only regret is that Clyde Cowan was not able to share the honor of receiving the Nobel Prize along with Fred Reines. We take pride that we were able to open a door that ushered in a whole new field of particle physics which raises so many questions that must be answered. We are gratified and have enormous satisfaction that so many of you are able to engage in challenging experiments in such interesting places all over the world! We know you will try, as we have tried, to advance our knowledge of the universe in which we live.

Long live the little neutrino!

#### Acknowledgements

I thank Deanna Kruse for Figure 1, and the Los Alamos National Laboratory for Figure 2 through Figure 8. I am indebted to Patricia Mendius for editing the text and Robert Kelly for technical review.

#### References

- [1] Cowan, C. L., Jr., F. Reines, F. B. Harrison, H. W. Kruse, and A. D. McGuire 1956 Detection of the Free Neutrino: A Confirmation *Science* **124** (3212): 103
- [2] Reines, F., C. L. Cowan, Jr., F. B. Harrison, A. D. McGuire, and H. W. Kruse 1960 Detection of the Free Antineutrino *Physical Review* **117** (1): 159
- [3] N. Cooper (Editor) Celebrating the Neutrino *Los Alamos Science* 1997 **25**
- [4] R. G. Arns Detecting the Neutrino 2001 *Physics in Perspective* **3** 314-334

# Sterile neutrino states

**Alexander Kusenko**

Department of Physics and Astronomy, University of California, Los Angeles, CA 90095, USA

**Abstract.**

Neutrino masses are likely to be a manifestation of the right-handed, or sterile neutrinos. The number of sterile neutrinos and the scale of their Majorana masses are unknown. We explore theoretical arguments in favor of the high and low scale seesaw mechanisms, review the existing experimental results, and discuss the astrophysical hints regarding sterile neutrinos.

## 1. Sterile neutrinos in particle physics

The term *sterile neutrino* was coined by Bruno Pontecorvo, who hypothesized the existence of the right-handed neutrinos in a seminal paper [1], in which he also considered vacuum neutrino oscillations in the laboratory and in astrophysics, the lepton number violation, the neutrinoless double beta decay, some rare processes, such as  $\mu \rightarrow e\gamma$ , and several other questions that have dominated the neutrino physics for the next four decades. Most models of the neutrino masses introduce sterile (or right-handed) neutrinos to generate the masses of the ordinary neutrinos via the seesaw mechanism [2]. The seesaw lagrangian

$$\mathcal{L} = \mathcal{L}_{\text{SM}} + \bar{N}_a (i\gamma^\mu \partial_\mu) N_a - y_{\alpha a} H \bar{L}_\alpha N_a - \frac{M_a}{2} \bar{N}_a^c N_a + h.c., \quad (1)$$

where  $\mathcal{L}_{\text{SM}}$  is the lagrangian of the Standard Model, includes some number  $n$  of singlet neutrinos  $N_a$  with Yukawa couplings  $y_{\alpha a}$ . Here  $H$  is the Higgs doublet and  $L_\alpha$  ( $\alpha = e, \mu, \tau$ ) are the lepton doublets. Theoretical considerations do not constrain the number  $n$  of sterile neutrinos. In particular, there is no constraint based on the anomaly cancellation because the sterile fermions do not couple to the gauge fields. The experimental limits exist only for the larger mixing angles [3]. To explain the neutrino masses inferred from the atmospheric and solar neutrino experiments,  $n = 2$  singlets are sufficient [4], but a greater number is required if the lagrangian (1) is to explain the LSND [5], the r-process nucleosynthesis [6], the pulsar kicks [7, 8], dark matter [9, 10, 11, 12], and the formation of supermassive black holes [13].

The scale of the right-handed Majorana masses  $M_a$  is unknown; it can be much greater than the electroweak scale [2], or it may be as low as a few eV [5, 14]. The seesaw mechanism [2] can explain the smallness of the neutrino masses in the presence of the Yukawa couplings of order one if the Majorana masses  $M_a$  are much larger than the electroweak scale. Indeed, in this case the masses of the lightest neutrinos are suppressed by the ratios  $\langle H \rangle / M_a$ .

However, the origin of the Yukawa couplings remains unknown, and there is no experimental evidence to suggest that these couplings must be of order 1. In fact, the Yukawa couplings of the charged leptons are much smaller than 1. For example, the Yukawa coupling of the electron is as small as  $10^{-6}$

One can ask whether some theoretical models are more likely to produce the numbers of order one or much smaller than one. The two possibilities are, in fact, realized in two types of theoretical models. If the Yukawa couplings arise as some topological intersection numbers in string theory, they are generally expected to be of order one [15], although very small couplings are also possible [16]. If the Yukawa couplings arise from the overlap of the wavefunctions of fermions located on different branes in extra dimensions, they can be exponentially suppressed and are expected to be very small [17].

In the absence of the fundamental theory, one may hope to gain some insight about the size of the Yukawa couplings using 't Hooft's naturalness criterion [18], which states essentially that a number can be naturally small if setting it to zero increases the symmetry of the lagrangian. A small breaking of the symmetry is then associated with the small non-zero value of the parameter. This naturalness criterion has been applied to a variety of theories; it is, for example, one of the main arguments in favor of supersymmetry. (Setting the Higgs mass to zero does not increase the symmetry of the Standard Model. Supersymmetry relates the Higgs mass to the Higgsino mass, which is protected by the chiral symmetry. Therefore, the light Higgs boson, which is not natural in the Standard Model, becomes natural in theories with softly broken supersymmetry.) In view of 't Hooft's criterion, the *small* Majorana mass is natural because setting  $M_a$  to zero increases the symmetry of the lagrangian (1) [19, 5].

One can ask whether cosmology can provide any clues as to whether the mass scale of sterile neutrinos should be above or below the electroweak scale. It is desirable to have a theory that could generate the matter-antimatter asymmetry of the universe. In both limits of large and small  $M_a$  one can have a successful leptogenesis: in the case of the high-scale seesaw, the baryon asymmetry can be generated from the out-of-equilibrium decays of heavy neutrinos [20], while in the case of the low-energy seesaw, the matter-antimatter asymmetry can be produced by the neutrino oscillations [21]. The Big-Bang nucleosynthesis (BBN) can provide a constraint on the number of light relativistic species in equilibrium [22], but the sterile neutrinos with the small mixing angles may never be in equilibrium in the early universe, even at the highest temperatures [9]. Indeed, the effective mixing angle of neutrinos at high temperature is suppressed due to the interactions with plasma [23], and, therefore, the sterile neutrinos may never thermalize. High-precision measurements of the primordial abundances may probe the existence of sterile neutrinos and the lepton asymmetry of the universe in the future [24].

While many seesaw models assume that the sterile neutrinos have very large masses, which makes them unobservable, it is worthwhile to consider light sterile neutrinos in view of the above arguments, and also because they can explain several experimental results. In particular, sterile neutrinos can account for cosmological dark matter [9], they can explain the observed velocities of pulsars [7, 8], the x-ray photons from their decays can affect the star formation [25]. Finally, sterile neutrinos can explain the LSND result [5, 26, 27], which is currently being tested by the MiniBooNE experiment.

## 2. Experimental limits

Laboratory experiments are able to set limits or discover sterile neutrinos with a large enough mixing angle. Depending on the mass, they can be searched in different experiments.

The light sterile neutrinos, with masses below  $10^2$  eV, can be discovered in one of the neutrino oscillations experiments [28]. In fact, LSND has reported a result [29], which, in combination with the other experiments, implies the existence of at least one sterile neutrino, more likely, two sterile neutrinos [5, 26]. It is also possible that sterile neutrino decays, rather than oscillations, are the explanation of the LSND result [27].

In the eV to MeV mass range, the "kinks" in the spectra of beta-decay electrons can be used to set limits on sterile neutrinos mixed with the electron neutrinos [30]. Neutrinoless double beta decays can probe the Majorana neutrino masses [31].

For masses in the MeV–GeV range, peak searches in production of neutrinos provide the limits. The massive neutrinos  $\nu_i$ , if they exist, can be produced in meson decays, e.g.  $\pi^\pm \rightarrow \mu^\pm \nu_i$ , with probabilities that depend on the mixing in the charged current. The energy spectrum of muons in such decays should contain monochromatic lines [30] at  $T_i = (m_\pi^2 + m_\mu^2 - 2m_\pi m_\mu - m_{\nu_i}^2)/2m_\pi$ . Also, for the MeV–GeV masses one can set a number of constraints based on the decays of the heavy neutrinos into the “visible” particles, which would be observable by various detectors. These limits are discussed in Ref. [3].

### 3. Sterile neutrinos in astrophysics and cosmology

Sterile neutrinos can be produced in supernova explosions. The observations of neutrinos from SN1987A constrain the amount of energy that the sterile neutrinos can take out of the supernova, but they are still consistent with the sterile neutrinos that carry away as much as a half of the total energy of the supernova. A more detailed analysis shows that the emission of sterile neutrinos from a cooling newly born neutron star is anisotropic due to the star’s magnetic field [7]. The anisotropy of this emission can result in a recoil velocity of the neutron star as high as  $\sim 10^3$  km/s. This mechanism can be the explanation of the observed pulsar velocities [8]. The range of masses and mixing angles required to explain the pulsar kicks is shown in Fig. 1.

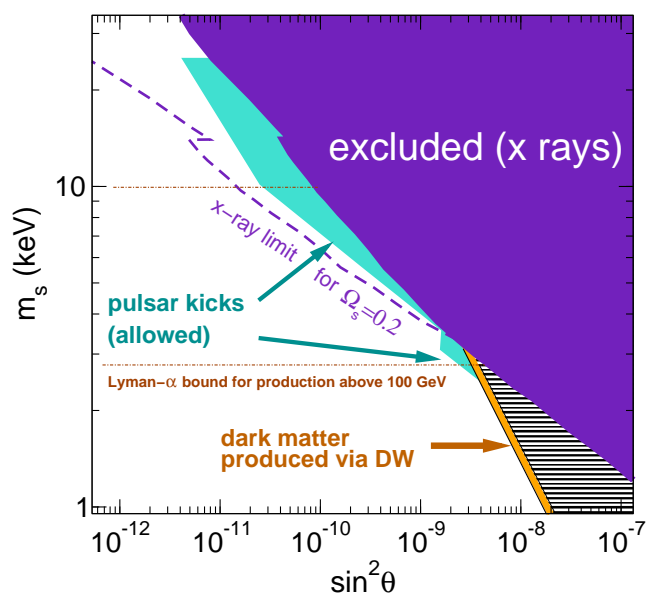


**Figure 1.** Sterile neutrinos in the keV mass range can be dark matter; their emission from a supernova can explain the observed velocities of pulsars. If the sterile neutrinos account for all dark matter, they must be sufficiently cold to satisfy the cosmological bounds on the mass. The limit depends on the production mechanism in the early universe. The lower bound of 2.7 keV corresponds to production at the electroweak scale [33].

The sterile neutrinos could play an important role in Big-Bang nucleosynthesis [24], as well as in the synthesis of heavy elements in the supernova, by enhancing the r-process [6].

The sterile neutrinos can be the cosmological dark matter [9, 10, 11, 12]. The interactions already present in the lagrangian (1) allow for the production of relic sterile neutrinos via the Dodelson-Widrow (DW) mechanism [9] in the right amount to account for all dark matter, i.e.  $\Omega_s \approx 0.2$ . The x-ray limits on the photons from the decays of the relic sterile neutrinos [34] forces them to have mass of at least a few keV if they are produced a la DW. However, these neutrinos appear to be too warm to agree with the Lyman- $\alpha$  bound [35], which is  $m_s > 10$  keV in this scenario (see Fig. 1).

If the lepton asymmetry of the universe is relatively large, the resonant oscillations can produce the requisite amount of dark matter even for smaller mixing angles, for which there are no x-ray limits. (The x-ray flux is proportional to the square of the mixing angle.)

It is also possible that some additional interactions, not present in eq. (1) can be responsible for the production of relic sterile neutrinos. The mass of the sterile neutrino  $m_s \sim 10$  keV is

not a fundamental constant of nature, but is the result of some symmetry breaking via the Higgs mechanism, the Lyman- $\alpha$  bound can be relaxed to well below the current x-ray limits [33]. In this case the same sterile neutrino can simultaneously explain the pulsar kicks and dark matter (Fig. 1). The Higgs field giving the sterile neutrinos their Majorana mass, the so called *singlet Majoron*, can be discovered at the Large Hadron Collider (LHC).

As was mentioned above, the relic sterile neutrinos can decay into the lighter neutrinos and into the x-ray photons [36], which can be detected by the x-ray telescopes [34]. The flux of x-rays depends on the sterile neutrino abundance. If all the dark matter is made up of sterile neutrinos,  $\Omega_s \approx 0.2$ , then the limit on the mass and the mixing angle is given by the dashed line in Fig. 1. However, the interactions in the lagrangian (1) cannot produce such an  $\Omega_s = 0.2$  population of sterile neutrinos for the masses and mixing angles along this dashed line, unless the universe has a relatively large lepton asymmetry [11]. If the lepton asymmetry is small, the interactions in eq. (1) can produce the relic sterile only via the neutrino oscillations off-resonance at some sub-GeV temperature [9]. This mechanism provides the lowest possible abundance (except for the low-temperature cosmologies, in which the universe is never reheated above a few MeV after inflation [32]). The model-independent bound [33] based on this scenario is shown as a solid (purple) region in Fig. 1. It is based on the flux limit from Ref. [34] and the analytical fit to the numerical calculation of sterile neutrino production by Abazajian [37]. This calculation may have some hadronic uncertainties [38]

Of course, the sterile neutrinos can have some additional couplings [39, 33], and the additional production can take place at higher temperatures. In particular, if the relic sterile neutrinos are produced above the electroweak scale, the Lyman- $\alpha$  bound is relaxed from 10 keV to 2.7 keV [33]. Of course, if the sterile neutrinos constitute only a small part of dark matter, the Lyman- $\alpha$  bounds do not apply at all.

The x-ray photons from sterile neutrino decays in the early universe could have affected the star formation. Although these x-rays alone are not sufficient to reionize the universe, they can catalyze the production of molecular hydrogen and speed up the star formation [25], which, in turn, could cause the reionization. Molecular hydrogen is a very important cooling agent necessary for the collapse of primordial gas clouds that gave birth to the first stars. The fraction of molecular hydrogen must exceed a certain minimal value for the star formation to begin [40]. The reaction  $H+H \rightarrow H_2 + \gamma$  is very slow in comparison with the combination of reactions  $H^+ + H \rightarrow H_2^+ + \gamma$  and  $H_2^+ + H \rightarrow H_2 + H^+$ , which are possible if the hydrogen is ionized. Therefore, the ionization fraction determines the rate of molecular hydrogen production. If dark matter is made up of sterile neutrinos, their decays produce a sufficient flux of photons to increase the ionization fraction by as much as two orders of magnitude [25]. This has a dramatic effect on the production of molecular hydrogen and the subsequent star formation.

#### 4. Conclusions

The underlying physics responsible for the neutrino masses is likely to involve right-handed, or sterile neutrinos. The Majorana masses of these states can range from a few eV to values well above the electroweak scale. Theoretical arguments have been made in favor of both the high-scale and low-scale seesaw mechanisms: the high-scale seesaw may be favored by the connection with the Grand Unified Theories, while the low-scale seesaw is favored by 't Hooft's naturalness criterion. Cosmological considerations are consistent with a vast range of mass scales. The laboratory bounds do not provide significant constraints on the sterile neutrinos, unless they have a large mixing with the active neutrinos. The atmospheric and solar neutrino oscillation results cannot be reconciled with the LSND result, unless sterile neutrinos (or other new physics) exist.

There are several indirect astrophysical hints in favor of sterile neutrinos at the keV scale. Such neutrinos can explain the observed velocities of pulsars, they can be the dark matter, and

they can play a role in star formation and reionization of the universe.

The preponderance of indirect astrophysical hints may be a precursor of a major discovery, although it may also be a coincidence. One can hope to discover the sterile neutrinos in the x-ray observations. The mass around 3 keV and the mixing angle  $\sin^2 \theta \sim 3 \times 10^{-9}$  appear to be particularly interesting because the sterile neutrino with such parameters could simultaneously explain the pulsar kicks and dark matter (assuming the sterile neutrinos are produced at the electroweak scale). However, it is worthwhile to search for the signal from sterile dark matter in other parts of the allowed parameter space shown in Fig. 1. The existence of a much lighter sterile neutrino, with a much greater mixing angle can be established experimentally if MiniBooNE confirms the LSND result.

### Acknowledgments

This work was supported in part by the DOE grant DE-FG03-91ER40662 and by the NASA ATP grants NAG 5-10842 and NAG 5-13399. The author thanks Theory Unit at CERN and ITP, EPFL, for hospitality.

### References

- [1] B. Pontecorvo, JETP, 53, 1717 (1967).
- [2] P. Minkowski, Phys. Lett. **B67**, 421 (1977); M. Gell-Mann, P. Ramond, and R. Slansky, *Supergravity* (P. van Nieuwenhuizen et al. eds.), North Holland, Amsterdam, 1980, p. 315; T. Yanagida, in *Proceedings of the Workshop on the Unified Theory and the Baryon Number in the Universe* (O. Sawada and A. Sugamoto, eds.), KEK, Tsukuba, Japan, 1979, p. 95; S. L. Glashow, *The future of elementary particle physics*, in *Proceedings of the 1979 Cargèse Summer Institute on Quarks and Leptons* (M. Lévy et al. eds.), Plenum Press, New York, 1980, pp. 687; R. N. Mohapatra and G. Senjanović, Phys. Rev. Lett. **44**, 912 (1980).
- [3] A. Kusenko, S. Pascoli and D. Semikoz, JHEP **0511**, 028 (2005).
- [4] P. H. Frampton, S. L. Glashow and T. Yanagida, Phys. Lett. B **548**, 119 (2002).
- [5] A. de Gouvea, Phys. Rev. D **72**, 033005 (2005).
- [6] G. C. McLaughlin, J. M. Fetter, A. B. Balantekin and G. M. Fuller, Phys. Rev. C **59**, 2873 (1999); D. O. Caldwell, G. M. Fuller and Y. Z. Qian, Phys. Rev. D **61**, 123005 (2000); J. Fetter, G. C. McLaughlin, A. B. Balantekin and G. M. Fuller, Astropart. Phys. **18**, 433 (2003).
- [7] A. Kusenko and G. Segrè, Phys. Lett. B **396**, 197 (1997); A. Kusenko and G. Segrè, Phys. Rev. D **59**, 061302 (1999). G. M. Fuller, A. Kusenko, I. Mocioiu, and S. Pascoli, Phys. Rev. D **68**, 103002 (2003); M. Barkovich, J. C. D'Olivo and R. Montemayor, Phys. Rev. D **70**, 043005 (2004); C. L. Fryer and A. Kusenko, Astrophys. J. Suppl. **163**, 335 (2006).
- [8] For review, see, e.g., A. Kusenko, Int. J. Mod. Phys. D **13**, 2065 (2004).
- [9] S. Dodelson and L. M. Widrow, Phys. Rev. Lett. **72**, 17 (1994).
- [10] K. Abazajian, G. M. Fuller and M. Patel, Phys. Rev. D **64**, 023501 (2001); A. D. Dolgov and S. H. Hansen, Astropart. Phys. **16**, 339 (2002).
- [11] X. d. Shi and G. M. Fuller, Phys. Rev. Lett. **82**, 2832 (1999). C. T. Kishimoto, G. M. Fuller and C. J. Smith, arXiv:astro-ph/0607403.
- [12] T. Asaka, S. Blanchet and M. Shaposhnikov, Phys. Lett. B **631**, 151 (2005)
- [13] F. Munyaneza, P.L. Biermann, P. L., Astron and Astrophys., 436, 805 (2005)
- [14] A. de Gouvea, J. Jenkins and N. Vasudevan, arXiv:hep-ph/0608147.
- [15] P. Candelas and S. Kalara, Nucl. Phys. B **298**, 357 (1988). D. Gepner, Nucl. Phys. B **311**, 191 (1988).
- [16] O. J. Eyton-Williams and S. F. King, JHEP **0506**, 040 (2005).
- [17] E. A. Mirabelli and M. Schmaltz, Phys. Rev. D **61**, 113011 (2000) [arXiv:hep-ph/9912265].
- [18] G. 't Hooft, *Naturalness, chiral symmetry, and spontaneous chiral symmetry breaking*, in *Recent Developments in Gauge Theories, Cargese 1979*, eds. G. 't Hooft et al., Plenum Press, New York, 1980.
- [19] K. Fujikawa, Prog. Theor. Phys. **113**, 1065 (2005).
- [20] M. Fukugita and T. Yanagida, Phys. Lett. B **174** (1986) 45.
- [21] E. K. Akhmedov, V. A. Rubakov and A. Y. Smirnov, Phys. Rev. Lett. **81**, 1359 (1998); T. Asaka and M. Shaposhnikov, Phys. Lett. B **620**, 17 (2005).
- [22] R. Barbieri and A. Dolgov, Phys. Lett. B **237**, 440 (1990); K. Kainulainen, Phys. Lett. B **244**, 191 (1990); K. Enqvist, K. Kainulainen and M. J. Thomson, Nucl. Phys. B **373**, 498 (1992); D. P. Kirilova and M. V. Chizhov, Phys. Rev. D **58**, 073004 (1998); A. D. Dolgov, Phys. Lett. B **506**, 7 (2001); M. Cirelli, G. M. Fuller, A. Strumfa and F. Vissani, Nucl. Phys. B **708**, 315 (2005).

- [23] L. Stodolsky, Phys. Rev. D **36**, 2273 (1987); R. Barbieri and A. Dolgov, Nucl. Phys. B **349** (1991) 743.
- [24] C. J. Smith, G. M. Fuller, C. T. Kishimoto and K. N. Abazajian, arXiv:astro-ph/0608377.
- [25] P. L. Biermann and A. Kusenko, Phys. Rev. Lett. **96**, 091301 (2006); M. Mapelli, A. Ferrara and E. Pierpaoli, Mon. Not. Roy. Astron. Soc. **369**, 1719 (2006); J. Stasielak, P. L. Biermann and A. Kusenko, Astrophys. J., in press [arXiv:astro-ph/0606435].
- [26] M. Sorel, J. M. Conrad and M. Shaevitz, Phys. Rev. D **70**, 073004 (2004).
- [27] S. Palomares-Ruiz, S. Pascoli and T. Schwetz, JHEP **0509**, 048 (2005) [arXiv:hep-ph/0505216].
- [28] A. Y. Smirnov and R. Zukanovich Funchal, Phys. Rev. D **74**, 013001 (2006).
- [29] C. Athanassopoulos *et al.* [LSND Collaboration], Phys. Rev. Lett. **77**, 3082 (1996); Phys. Rev. C **58**, 2489 (1998); Phys. Rev. Lett. **81**, 1774 (1998).
- [30] R. E. Shrock, Phys. Rev. D **24**, 1232 (1981).
- [31] S. R. Elliott and P. Vogel, Ann. Rev. Nucl. Part. Sci. **52**, 115 (2002).
- [32] G. Gelmini, S. Palomares-Ruiz and S. Pascoli, Phys. Rev. Lett. **93**, 081302 (2004).
- [33] A. Kusenko, arXiv:hep-ph/0609081.
- [34] K. Abazajian, G. M. Fuller and W. H. Tucker, Astrophys. J. **562**, 593 (2001); A. Boyarsky, A. Neronov, O. Ruchayskiy and M. Shaposhnikov, arXiv:astro-ph/0512509; A. Boyarsky, A. Neronov, O. Ruchayskiy and M. Shaposhnikov, JETP Lett. **83**, 133 (2006); A. Boyarsky, A. Neronov, A. Neronov, O. Ruchayskiy and M. Shaposhnikov, arXiv:astro-ph/0603368; A. Boyarsky, A. Neronov, O. Ruchayskiy, M. Shaposhnikov and I. Tkachev, arXiv:astro-ph/0603660; S. Riemer-Sorensen, S. H. Hansen and K. Pedersen, arXiv:astro-ph/0603661; K. Abazajian and S. M. Koushiappas, arXiv:astro-ph/0605271; C. R. Watson, J. F. Beacom, H. Yuksel and T. P. Walker, arXiv:astro-ph/0605424.
- [35] M. Viel, *et al.*, Phys. Rev. D **71**, 063534 (2005); U. Seljak, A. Makarov, P. McDonald and H. Trac, arXiv:astro-ph/0602430; M. Viel, J. Lesgourgues, M. G. Haehnelt, S. Matarrese and A. Riotto, Phys. Rev. Lett. **97**, 071301 (2006).
- [36] P. B. Pal and L. Wolfenstein, Phys. Rev. D **25**, 766 (1982).
- [37] K. Abazajian, Phys. Rev. D **73**, 063506 (2006).
- [38] T. Asaka, M. Laine and M. Shaposhnikov, JHEP **0606**, 053 (2006).
- [39] M. Shaposhnikov and I. Tkachev, Phys. Lett. B **639**, 414 (2006).
- [40] M. Tegmark, J. Silk, M. J. Rees, A. Blanchard, T. Abel and F. Palla, Astrophys. J. **474**, 1 (1997).

## The Homestake Interim Laboratory and Homestake DUSEL

**Kevin T. Lesko<sup>1</sup>**

University of California, Berkeley and Lawrence Berkeley National Laboratory

ktlesko@lbl.gov

**Abstract.** The former Homestake gold mine in Lead South Dakota is proposed for the National Science Foundation's Deep Underground Science and Engineering Laboratory (DUSEL). The gold mine provides expedient access to depths in excess of 8000 feet below the surface (>7000 mwe). Homestake's long history of promoting scientific endeavours includes the Davis Solar Neutrino Experiment, a chlorine-based experiment that was hosted at the 4850 Level for more than 30 years. As DUSEL, Homestake would be uncompromised by competition with mining interests or other shared uses. The facility's 600-km of drifts would be available for conversion for scientific and educational uses. The State of South Dakota, under Governor Rounds' leadership, has demonstrated exceptionally strong support for Homestake and the creation of DUSEL. The State has provided funding totalling \$46M for the preservation of the site for DUSEL and for the conversion and operation of the Homestake Interim Laboratory. Motivated by the strong educational and outreach potential of Homestake, the State contracted a Conversion Plan by world-recognized mine-engineering contractor to define the process of rehabilitating the facility, establishing the appropriate safety program, and regaining access to the facility. The State of South Dakota has established the South Dakota Science and Technology Authority to oversee the transfer of the Homestake property to the State and the rehabilitation and preservation of the facility. The Homestake Scientific Collaboration and the State of South Dakota's Science and Technology Authority has called for Letters of Interest from scientific, educational and engineering collaborations and institutions that are interested in hosting experiments and uses in the Homestake Interim Facility in advance of the NSF's DUSEL, to define experiments starting as early as 2007. The Homestake Program Advisory Committee has reviewed these Letters and their initial report has been released. Options for developing the Homestake Interim Laboratory and evolving this facility into DUSEL are presented.

### **1. Deep Underground Science and Engineering Laboratory Objectives and Goals**

The US National Science Foundation is aggressively pursuing the creation of a Deep Underground Science and Engineering Laboratory (DUSEL) to promote and to assist underground research and to support the related goals of education and public outreach. The NSF has established a three-step process to identify and to select a site for DUSEL. This process will consider many potential sites and provide a process for selection of a site for DUSEL. Professor Bernard Sadoulet of UC Berkeley is leading the first solicitation (S-1) to assess the scientific questions of the greatest impact that require a dedicated laboratory and to determine the approximate requirements for the facility. This effort is a site-independent assessment and will integrate the needs of the physics, earth science, biology, engineering, educational uses and applications of DUSEL. The second step (S-2) projects this general program of scientific uses for DUSEL onto specific sites to produce a conceptual design report tailored for each site, considering the assets and potential programs for that location. Two sites

received funding from the NSF to produce conceptual design reports, Homestake and Henderson. The third step (S-3) will produce a detailed design for DUSEL.

DUSEL's focus for physics experiments includes dark matter and neutrinoless double beta decay searches, solar neutrinos and geoneutrinos experiments, long baseline neutrino studies, nucleon decay, nuclear astrophysics and supporting technologies and applications such as low background counting.

Our focus for Homestake is the development of appropriate laboratory and supporting space to stimulate a diverse program in all of these physics topics, as well as supporting the earth science, biology, engineering, and education goals. The Homestake Interim Laboratory scientific program, described below, is already developing synergistic ties among these disciplines.

## **2. Homestake Strategy to Developing DUSEL**

The mining activities in Homestake ceased in 2001 and, later that same year, the Barrick Mining Corporation assumed control of the Homestake site. As part of the original Homestake Mining Corporation plans, the site was environmentally remediated, closed, and sealed. A consequence of the closure was that in-flowing water was no longer pumped from the underground facility. The ~ 700 gpm in-flow of water has been characterized. Approximately 2/3 of the in-flow water is essentially surface water entering into the underground workings from above the 5300 Level of the facility. (Levels refer to the elevation of the particular section of the mine in feet below the surface, thus the 5300 Level is 5300 feet below the surface at the Yates lift.) The remaining 1/3 of the in-flow water originates from deeper sources. The lower levels of the facility are submerged as the facility accumulates this water. The water is currently at the 6200 Level. The accumulation of water does not place the mining infrastructure at serious risk (the water is nearly neutral pH). However, if the water were to reach the 4850 Level, then significant facility infrastructure would be submerged and reentry into the mine would be complicated and delayed. It is anticipated that the in-flowing water will reach the 4850 Level in 2008. Thus, the State of South Dakota, in an effort to preserve the site for future consideration as DUSEL, has drafted a preliminary plan that outlines the necessary engineering steps required to safely re-enter Homestake, rehabilitate the shafts, conveyances, and levels, and to establish appropriate ventilation and dewatering facilities. Initially these efforts will reestablish the Yates and Ross shafts as the primary safe conveyances to the 4850 Level. Pumps will be installed at the 5300 Level to maintain the water below this level, while the upper facility (from the surface to 4850 Level) is inspected, secured and rehabilitated.

Before the rehabilitation could begin the State was required to obtain title to the property and satisfy the requirements in the Donation Agreement between the former owners, Barrick and South Dakota. These requirements included establishing indemnification statues, providing necessary insurance, and providing adequate operational support for the facility while the NSF's DUSEL process progressed.

It was soon realized that in preserving Homestake for DUSEL, that all the necessary components were in place to consider establishing a modest interim facility and hosting scientific, engineering, and educational uses at Homestake, with the facility being a state-operated facility.

Title to the facility was transferred to the South Dakota in May 2006. The South Dakota Authority has remodeled some of the surface buildings and moved their offices to the Homestake site. A ribbon cutting for the Homestake Interim Laboratory facility is scheduled for June 2006.

## **3. Laboratory Structure**

The Homestake Interim Laboratory will initially focus on developing the surface campus on the 186 acres of property transferred to the State. This property has been fully remediated and inspected as part of the transfer agreement. It includes the main administration buildings, Yates and Ross shafts and associated buildings, and many of the original Homestake shops and support buildings. In all ~ 50 buildings were transferred to the South Dakota Authority.

At the 300 Level there are portals providing drive-in access to the underground that connects to the Ross or Yates shafts. We recognized that the development of a relatively shallow campus with

exceptional drive-in access was strongly desired by various R&D activities and scientific collaborations, for certain educational uses, and for support services such as refining and storing low activity materials for dark matter and neutrinoless double beta decay experiments.

The main focus for stationary experiments will be the 4850 Level, the site of the original Davis Experiment. Initial experiments will be sited in proximity to the Davis-cavity near the Yates lift. We envision developing a new campus of laboratories in the "triangle" of rock formed by the existing drifts connecting the Yates and the Ross shafts.

As part of DUSEL we plan to develop a deep campus at the 7400 Level ( $\sim 7000$  mwe).

The earth science and engineering research efforts will be distributed throughout the facility. There is particular interest in several of the long cross drifts at the 2000 Level, 3900 Level, laboratories at the 4850 Level, obtaining access to large intact blocks of rock at different levels, and a very deep facility at the 8000 Level. The existing rooms and drifts enable some experiments and uses to obtain beneficial occupancy soon after rehabilitation in 2007. Custom built modules are being designed and developed both as part of the Homestake Interim Laboratory but also to make expanded space available as part of DUSEL. Our current plans call for 900 m<sup>2</sup> of laboratory space at the 300 Level, 11,000 m<sup>2</sup> of laboratory and common space at the 4850 Level, and 4500 m<sup>2</sup> of laboratory space at the 7400 Level as the full DUSEL is developed at Homestake. Additional rooms and space can be made available as the laboratory design advances. Figure 1 presents an isometric view of the Homestake facility and the approximate locations and sizes of the laboratories discussed above.

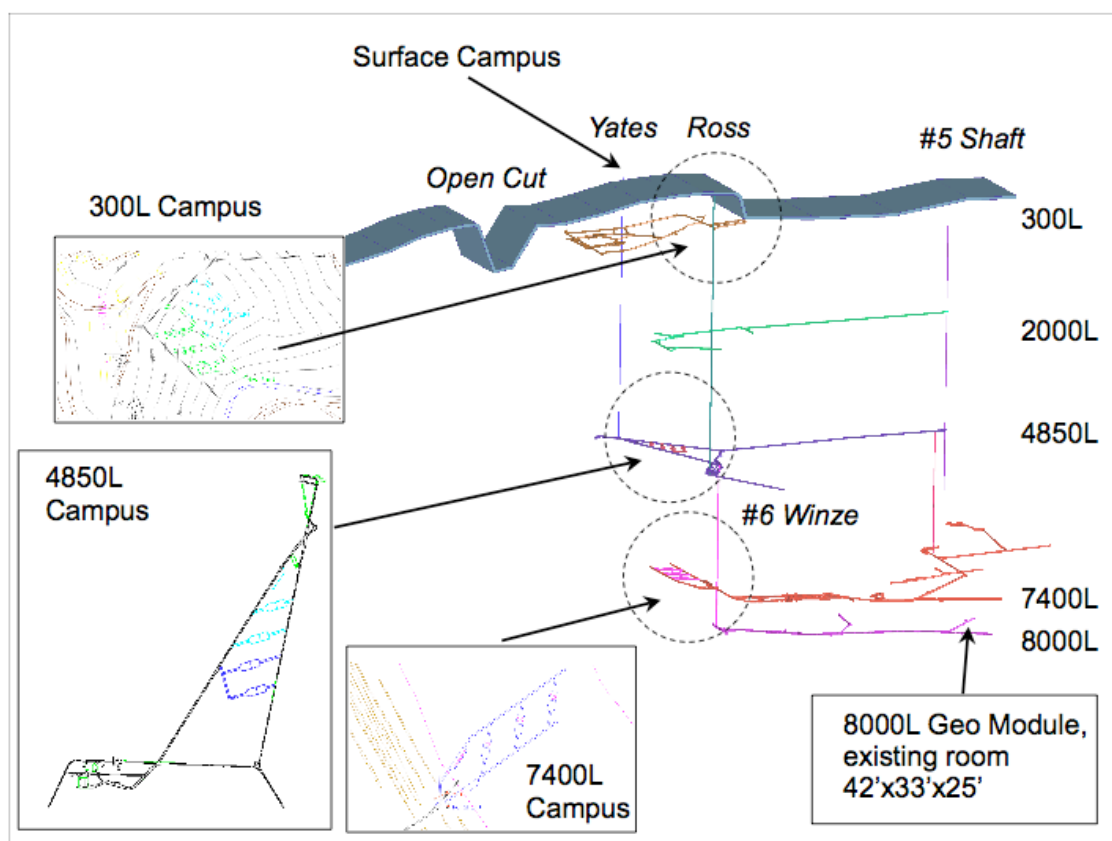


Figure 1. The Homestake plans for developing laboratory space on the surface, the 300 Level, 4850 Level, 7400 Level, and 8000 Level.



To help define the scientific uses for Homestake, the requisite infrastructure and approximate time-lines, Homestake issued a call for Letters of Interest to be submitted to the South Dakota Authority. By February 2006, 85 letters had been received. The letters were grouped into Earth Science: 60%, Physics: 25%, and Education and Engineering: 15%. The Program Advisory Committee has reviewed the letters and their recommendations can be found at: <http://www.lbl.gov/nsd/homestake> . The Letters have been assembled into an initial roadmap for Homestake, shown in Figure 2.

### **5. Summary**

The State of South Dakota has accomplished many of the steps necessary to develop DUSEL. These include obtaining title to the property, satisfying the initial insurance and indemnification requirements for a laboratory, and providing adequate financing to rehabilitate and to operate the facility in advance of the NSF's DUSEL. With the establishment of the Homestake Interim Laboratory in advance of the NSF's DUSEL, the process of assembling the scientific program for Homestake has begun. This diverse program involves excellent synergistic links between physics and the other DUSEL disciplines. The program includes dark matter searches, neutrinoless double beta decay, solar neutrino and geoneutrino experiments, experimental nuclear astrophysics, and the initial R&D for a very long baseline neutrino program and nucleon decay experiments.

The South Dakota has dealt with issues of ownership, insurance, liability and has launched the Homestake Interim Laboratory to take advantage of the efforts to preserve Homestake for DUSEL. This program will naturally evolve into the NSF's Initial Suite of Experiments for DUSEL. Homestake's initial focus will be on the 300 Level and 4850 Level laboratories with additional and deeper labs being developed in the coming years. Most recently, the Yates shaft was inspected from the surface to the bottom at 4850 and was found to be in good condition. Homestake offers a low risk and lower cost option for developing a DUSEL that addresses a full spectrum of physics, earth science, and engineering questions of the highest importance and provides an unequalled opportunity to couple education and public outreach into the scientific program at Homestake.

[1] For the Homestake Scientific Collaboration

# The diffuse supernova neutrino flux

**Cecilia Lunardini**

Institute for Nuclear Theory and University of Washington, Seattle, WA 98195

E-mail: [lunardi@phys.washington.edu](mailto:lunardi@phys.washington.edu)

**Abstract.** I review the status and perspectives of the research on the diffuse flux of (core collapse) supernova neutrinos (DSN $\nu$ F). Several upper bounds exist on this flux in different detection channels. The strongest is the limit from SuperKamiokande (SK) of 1.2 electron antineutrinos  $\text{cm}^{-2}\text{s}^{-1}$  at 90% confidence level above 19.3 MeV of neutrino energy. The predictions of the DSN $\nu$ F depend on the supernova rate and on the neutrino emission in a individual supernova. Above the SK threshold, they range between 0.05 electron antineutrinos  $\text{cm}^{-2}\text{s}^{-1}$  up to touching the SK limit. The SK bound constrains part of the parameter space of the supernova rate – and indirectly of the star formation rate – only in models with relatively hard neutrino spectra. Experimentally, a feasible and very important goal for the future is the improvement of background discrimination and the resulting lowering of the detection threshold. Theory instead will benefit from reducing the uncertainties on the supernova neutrino emission (either with more precise numerical modeling or with data from a galactic supernova) and on the supernova rate. The latter will be provided precisely by next generation supernova surveys up to a normalization factor. Therefore, the detection of the DSN $\nu$ F is likely to be precious chiefly to constrain such normalization and to study the physics of neutrino emission in supernovae.

## 1. Introduction

What are our chances to detect neutrinos from core collapse supernovae in the near future? With current and upcoming neutrino telescopes, a high statistics signal is possible if a supernova occurs in our immediate galactic neighborhood. Such event would be as exciting as it is rare: indeed it could require decades of waiting time, since the rate of core collapse in our galaxy is as low as 1-3 supernovae per century (see e.g. [1, 2]). A different option is to look for the flux of neutrinos from all supernovae, i.e., integrated over the whole sky. Recently it was shown that the detection of this diffuse supernova neutrino flux (DSN $\nu$ F) is a concrete possibility [3], which, if realized, could turn the field of supernova neutrinos from the realm of rare events to the territory of a moderately paced and steady progress.

Aside from practical advantages, the study of the DSN $\nu$ F has an interest of its own, because it would give complementary information, on supernovae and on neutrinos, with respect to an individual supernova burst. Since it contains contributions from several supernovae at different distance and of different morphology, the DSN $\nu$ F reflects the supernova population of the universe. Thus, from it we could learn about the distribution of core collapse supernovae with the redshift and with the mass of the progenitor. It is known that the supernova rate (SNR) increases with the redshift: supernovae were more numerous in the past than at present, so that as much as  $\sim 40\%$  of the DSN $\nu$ F above the SuperKamiokande detection threshold of 19.3 MeV come from cosmological sources, with redshift  $z > 0.5$ . The distribution in mass goes

roughly as the power -2.3 of the progenitor mass, meaning that about 60% of the DSN $\nu$ F is produced by relatively small stars with mass between the lower cutoff of  $8 M_{\odot}$  (the minimum mass to have core collapse) and  $15M_{\odot}$ , with  $M_{\odot} = 1.99 \cdot 10^{30}$  kg being the mass of the Sun. Thus, data from the diffuse flux would complement those we already have from SN1987A, which had a  $\sim 15 - 20M_{\odot}$  progenitor.

By testing the SNR, the DSN $\nu$ F also probes, indirectly, the history of star formation. Indeed, the SNR is proportional to the star formation rate (SFR), because supernovae progenitors have a very short lifetime, only  $\sim 10^7$  years (three orders of magnitude shorter than the Sun's lifetime), negligible with respect to their formation time. Specifically, neutrinos would be precious to learn about the normalization of the SNR, since they are not affected by dust extinction, in contrast with electromagnetic probes. The diffuse flux also offers the theoretical possibility to study the first (Population III) stars [4], since these are believed to have died as core collapse supernovae, and therefore to have contributed to the DSN $\nu$ F

Similarly to a neutrino burst from an individual galactic source, a detected signal from the DSN $\nu$ F would provide a large amount of information on the physics of neutrino production, propagation and emission from a supernova. I refer to other contributions for those [5]; focusing here on the aspects that are distinctive of the diffuse flux.

## 2. Experimental status: upper limits

**Table 1.** Summary of the most stringent bounds on the DSN $\nu$ F from currently active detectors, with their confidence level (C.L.). The limit on the  $\nu_e$  component labeled as “indirect” proceeds from the SK  $\bar{\nu}_e$  limit with considerations of similarity of the detected  $\nu_e$  and  $\bar{\nu}_e$  fluxes due to neutrino oscillations in the star [6]. The result in the channel  $\nu_e - ^{16}\text{O}$  is given as an interval of limits, corresponding to the range of neutrino spectra used in the analysis. The SNO result is also spectrum-dependent: the quoted bound is the median of several 90% C.L. limits found with different neutrino spectra.

Experiment,species	channel	energy interval	upper limit ( $\text{cm}^{-2}\text{s}^{-1}$ )
KamLAND, $\bar{\nu}_e$ [7]	$\bar{\nu}_e + p \rightarrow n + e^+$	$8.3 < E/\text{MeV} < 14.8$	$3.7 \times 10^2$ (90% C.L.)
SK, $\bar{\nu}_e$ [3]	$\bar{\nu}_e + p \rightarrow n + e^+$	$E/\text{MeV} > 19.3$	1.2 (90% C.L.)
SK/indirect, $\nu_e$ [6]		$E/\text{MeV} > 19.3$	5.5 ( $\sim 98\%$ C.L.)
SK, $\nu_e$ [8]	$\nu_e + ^{16}\text{O} \rightarrow ^{16}\text{F} + e^-$	$E/\text{MeV} > 33$	61-220 (90% C.L.)
SNO, $\nu_e$ [9]	$\nu_e + ^2_1\text{H} \rightarrow p + p + e^-$	$22.9 < E/\text{MeV} < 36.9$	70
LSD, $\nu_{\mu} + \nu_{\tau}$ [10]	$\nu_{\mu,\tau} + ^{12}\text{C} \rightarrow ^{12}\text{C} + \nu_{\mu,\tau}$	$20 < E/\text{MeV} < 100$	$3 \cdot 10^7$ (90% C.L.)
LSD, $\bar{\nu}_{\mu} + \bar{\nu}_{\tau}$ [10]	$\bar{\nu}_{\mu,\tau} + ^{12}\text{C} \rightarrow ^{12}\text{C} + \bar{\nu}_{\mu,\tau}$	$20 < E/\text{MeV} < 100$	$3.3 \cdot 10^7$ (90% C.L.)

So far, the DSN $\nu$ F has escaped detection. In Table 1 I summarize the most stringent bounds available on this flux. Thanks to their larger volumes, currently active detectors [3, 7, 12, 9] have improved dramatically on the limits set by the previous generation of experiments [13, 10]. In particular, the 50 kt of water of SuperKamiokande (SK) has allowed to push the limit on both the  $\bar{\nu}_e$  and  $\nu_e$  components of the DSN $\nu$ F within an order of magnitude or so from theoretical predictions (see Sec. 3 for those).

The main challenge and limiting factor of experimental searches of the diffuse flux is background reduction. At a water Cerenkov detector like SK a search for the diffuse flux requires to cut all events with energy below 18 MeV (positron energy), due to the high spallation background below that threshold. This excludes the bulk of the flux, which is concentrated at

lower energy,  $\sim 5$  MeV, causing a huge loss of sensitivity with respect to the ideal case of no background. In the remaining energy window one has to look for the signal induced by the DSN $\nu$ F ( $\bar{\nu}_e$  component) on top of the ineliminable background from invisible muons and atmospheric neutrinos, which limit the sensitivity further. Similar considerations hold for heavy water. Liquid scintillator allows to single out inverse beta decay events by observing the positron and neutron capture signals in coincidence. This results in a better background reduction and thus explains the sensitivity of KamLAND down to energy of about 8 MeV, which is where the ineliminable background of reactor neutrinos ends.

### 3. Status of theory: flux predictions

The recipe to estimate the DSN $\nu$ F is relatively simple: consider the neutrino output of an individual supernova, apply the relevant propagation effects – such as redshift of energy and neutrino oscillations – and then sum over the supernova population of the universe. Formally, this corresponds to the following integral:

$$\Phi(E) = \frac{c}{H_0} \int_0^{z_{max}} R_{SN}(z) \sum_{w=e,\mu,\tau} \frac{dN_w(E')}{dE'} P_{we}(E, z) \frac{dz}{\sqrt{\Omega_m(1+z)^3 + \Omega_\Lambda}}, \quad (1)$$

which describes the  $\nu_e$  component of the flux differential in the neutrino energy at Earth,  $E$ . There  $dN_w(E')/dE'$  is the flux of neutrinos of flavor  $w$  emitted by an individual supernova, differential in the neutrino energy at production,  $E'$ .  $P_{we}$  is the probability that a neutrino produced as  $\nu_w$  is detected as  $\nu_e$  at Earth, and  $R_{SN}$  describes the SNR per comoving volume.  $\Omega_m \simeq 0.3$  and  $\Omega_\Lambda \simeq 0.7$  represent the fractions of energy density of the universe in matter and dark energy respectively,  $c$  is the speed of light and  $H_0 \simeq 70 \text{ Km s}^{-1} \text{ Mpc}^{-1}$  is the Hubble constant.

Many estimates of the DSN $\nu$ F according to Eq. (1) have been published in the literature [14, 15, 16, 17, 18, 19, 20, 21, 22, 23, 24, 11, 25, 26, 27]. Fig. 1 shows a sample of results for the  $\bar{\nu}_e$  component of the flux above the SK threshold, compared with the current SK limit (see Table 1.) The spread between them reflects the different approaches used by different authors. Specifically, Hartmann and Woosley [20], Ando and Sato [24, 11], Strigari et al. [23] and Olive et al. [27] have used the SNR as it is inferred from measurements of the SFR, while Kaplinghat et al. [21] have estimated the SNR considering the constraints on the universal metal enrichment history. Lunardini [26] used information on the SNR from direct supernova observations only. Different were also the choices of the neutrino spectrum: all the references take the spectra from numerical simulations, with the exception of ref. [26], where only the (softer) spectra that fit the SN1987A data are considered, following the earlier example of Fukugita and Kawasaki [28].

Predictions exist also for the flux of  $\bar{\nu}_e$  above energy thresholds lower than the current SK one. These could be relevant for future neutrino telescopes, e.g. SK with Gadolinium addition (see Sec. 5). Table 2 shows the results obtained in ref. [26] for the  $\bar{\nu}_e$  flux and the corresponding rate of events from inverse beta decay in SK. From it, one concludes that a lowering of the energy threshold down to  $\sim 10$  MeV would represent a large improvement in the flux captured, with no guarantee of a detection, however, due to the smallness of the number of events.

### 4. What have we learned on supernovae and on neutrinos? What will we learn?

Undoubtedly, the best piece of information that we have, at present, on the DSN $\nu$ F is the negative result of SK. Is this upper limit strong enough to give any information? The answer can be read off from fig. 1: there one can see that the SK limit touches some of the theoretical predictions but not others, with the conclusion that only conditional bounds can be put on the SNR (or, indirectly, on the SFR) or on the neutrino emission in a supernova. The situation is illustrated well in fig. 2 taken from ref. [28]. The figure shows how the exclusion region for the

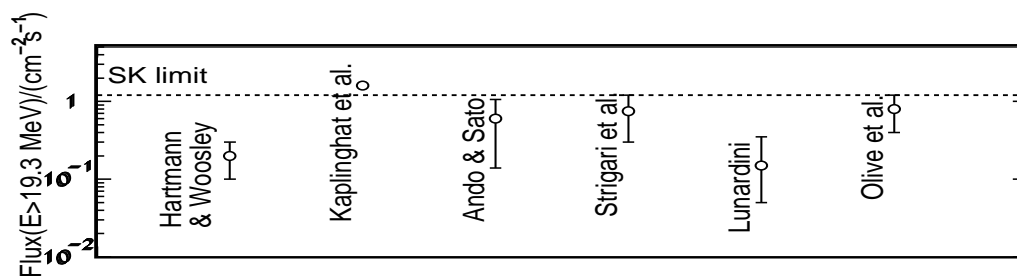


**Figure 1.** A sample of theoretical predictions [20, 21, 24, 11, 23, 26, 27] for the  $\bar{\nu}_e$  component of the DSN $\nu$ F above the SK energy threshold (figure adapted from ref. [26]). The number by Lunardini is quoted with a 99% C.L. error bar. For the other results, the error bars are an indicative description of the uncertainty due to uncertain input parameters; they have no statistical meaning. The SK limit (see Table 1) is shown for comparison.

**Table 2.** Predictions for the  $\bar{\nu}_e$  diffuse flux and for the corresponding rate of inverse beta decay events in SK for different energy thresholds, from ref. [26]. The intervals correspond to 99% C.L.. These results were obtained using soft neutrino spectra compatible with the SN1987A data, and therefore lie on the conservative side with respect to predictions that used harder neutrino spectra, motivated by numerical simulations.

	$E > 19.3$ MeV	$E > 11.3$ MeV	$E > 5.3$ MeV
flux ( $\text{cm}^{-2}\text{s}^{-1}$ )	0.05 - 0.35	0.33 - 2.1	3.2 - 22.6
events/year at SK	0.09 - 0.7	0.27 - 1.6	0.43 - 2.2

SFR varies by varying the neutrino spectrum in the region allowed by SN1987A and the minimum progenitor mass between 8 and 10  $M_{\odot}$ . The space allowed by astrophysical measurements of the SFR, also shown in the figure, is only marginally touched by the most conservative exclusion line, corresponding to the softest neutrino spectrum and 10  $M_{\odot}$  minimum progenitor mass (“SK Limit Min” in the figure). Some restriction of this space is obtained if the hardest spectrum is used with 8  $M_{\odot}$  minimum progenitor mass. The conclusions of ref. [26] are analogous. The exclusion found by Strigari et al. [29] is not in contrast with what shown in fig. 2, since these authors relied on a harder neutrino spectrum, with respect to refs. [28] and [26], motivated by numerical simulations.

On the side of neutrino physics, the DSN $\nu$ F could be the best probe of exotic effects that could manifest themselves only on cosmological distances. An example of this is neutrino decay: it was shown [30, 31] that data from the diffuse flux would be sensitive to a ratio of neutrino lifetime over mass as large as  $\tau/m \simeq 10^{10}$  s/eV. It was also pointed out [32] that the DSN $\nu$ F could reveal the existence of new, light gauge bosons that could be produced in the resonant annihilation of a neutrino and an antineutrino, one of them from a supernova and the other from the cosmological relic neutrino background. A test of dark energy, complementary to astrophysical measurements, is also possible in principle [33].

## 5. Discussion: perspective of future research

What are the likely developments in the study of the DSN $\nu$ F in the next 5-10 years?

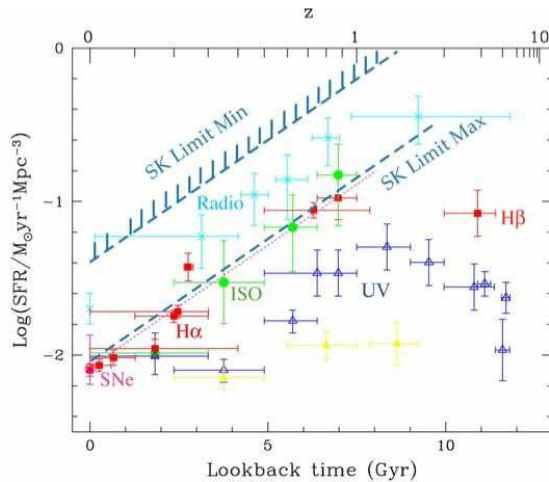


**Figure 2.** Measurements of the SFR compared with the exclusion region obtained from the SK limit on the  $\bar{\nu}_e$  diffuse flux (see Table 1), from ref. [28]. The figure shows how the exclusion region changes by varying the input neutrino spectrum in the range allowed by SN1987A. The less stringent exclusion barely touches the astrophysical measurements.

Progress will be made with new, more sensitive neutrino telescopes. The first to become operational could be the GADZOOKS project [34], based on adding Gadolinium trichloride to the water of SK. Gadolinium would enhance neutron capture, resulting in better background discrimination for the search of the  $\bar{\nu}_e$  flux. This would make it feasible to lower the energy threshold to 11.3 MeV in neutrino energy and therefore to have a larger event rate (up to 2 [26] or even 6 [34] events/year). The GADZOOKS initiative is progressing with the creation of a dedicated committee internal to the SK collaboration and the construction of a new test tank made of stainless steel [35].

In the space of a decade from now, water Cerenkov detectors of megaton mass, 20 times larger than SK, could become a reality. Projects of this type are under study: these are HyperKamiokande [36], UNO [37] and MEMPHYS [38]. According to a very conservative estimate [26], these should have an event rate between 2 and 44 events/year above the current SK threshold of 19.3 MeV.

A rather intense activity is ongoing to plan large non-water neutrino detectors. One of these is LENA [39], which, with its 50 kt of liquid scintillator, would have a better background rejection than SK and a comparable event rate. Detectors using  $\sim 100$  kt of liquid Argon, like GLACIER [40] and LANDD [41] would be precious for their sensitivity to the  $\nu_e$  component of the DSN $\nu$ F.

On the side of theory, much work has to be done to improve the predictions of the DSN $\nu$ F.

To reduce the uncertainty on the estimated diffuse flux, it would be crucial to reduce the uncertainties on the neutrino fluxes and spectra emitted by an individual supernova. This could be offered by the advancement of numerical simulations or by data from a future galactic supernova. Besides knowing better the neutrino emission by a single star, it would be important to generalize the calculation of the diffuse flux, Eq. (1), to include individual variations of the neutrino output between different stars, depending on various factors like the progenitor mass, rotation, magnetic fields, etc.. The uncertainty on the diffuse flux associated with the SNR will be dramatically reduced when results become available from the next generation supernova surveys like SNAP [42] and JWST [43]. While primarily designed to study type Ia supernovae, these would see thousands of core collapse supernovae up to redshift  $\sim 1$  and beyond [42].

Finally, let us review the scenarios that could be realized with new experimental results on the  $\bar{\nu}_e$  component of the DSN $\nu$ F and the current theoretical predictions as in fig. 1. Evidence of the diffuse flux above the SK limit would point in the direction of a neutrino spectrum much harder than what used in the analysis of the current SK data [3], or would indicate a fluctuation in the flux due to an extragalactic supernova at moderate distance [2]. The latter case could

be distinguished on the basis of the time distribution of the excess flux. A detection of the neutrino flux anywhere below the SK limit would be very important to discriminate between the different predictions. To constrain the SNR unambiguously (i.e., to obtain a constraint in every framework of theory considered so far), would require upper limits on the diffuse  $\bar{\nu}_e$  at the level of  $\sim 0.3 \text{ cm}^{-2}\text{s}^{-1}$  above the current SK threshold.

## Acknowledgments

I acknowledge support from the INT-SCiDAC grant number DE-FC02-01ER41187. I warmly thank the organizers and the participants of the Neutrino 2006 conference for the intellectually fertile atmosphere I enjoyed there.

## References

- [1] N. Arnaud *et al.*, *Astropart. Phys.* **21**, 201 (2004).
- [2] S. Ando, J. F. Beacom, and H. Yuksel, *Phys. Rev. Lett.* **95**, 171101 (2005).
- [3] M. Malek *et al.*, *Phys. Rev. Lett.* **90**, 061101 (2003).
- [4] F. Iocco, these proceedings .
- [5] G. G. Raffelt, these proceedings .
- [6] C. Lunardini, *Phys. Rev.* **D73**, 083009 (2006).
- [7] K. Eguchi *et al.*, *Phys. Rev. Lett.* **92**, 071301 (2004).
- [8] C. Lunardini and O. L. G. Peres, in preparation. See talk by O. L. G. Peres at the PHENO workshop, Madison, Wisconsin, USA, May 2006; <http://agenda.hep.wisc.edu/fullAgenda.php?ida=a0611> .
- [9] B. Aharmim *et al.*, hep-ex/0607010 (2006).
- [10] M. Aglietta *et al.*, *Astropart. Phys.* **1**, 1 (1992).
- [11] S. Ando and K. Sato, *New J. Phys.* **6**, 170 (2004).
- [12] B. Aharmim *et al.*, *Phys. Rev.* **D70**, 093014 (2004).
- [13] W. Zhang *et al.*, *Phys. Rev. Lett.* **61**, 385 (1988).
- [14] G. S. Bisnovatyi-Kogan and Z. F. Seidov, *Soviet Astronomy (Tr: A. Zhurn.)* **26**, 1982 (132).
- [15] L. M. Krauss, S. L. Glashow, and D. N. Schramm, *Nature* **310**, 191 (1984).
- [16] W. J. R. M. R. Woosley, S. E., *Astrophys. Jour.*, Part 1 **302**, 19 (1986).
- [17] T. Totani and K. Sato, *Astropart. Phys.* **3**, 367 (1995).
- [18] T. Totani, K. Sato, and Y. Yoshii, *Astrophys. J.* **460**, 303 (1996).
- [19] R. A. Malaney, *Astropart. Phys.* **7**, 125 (1997).
- [20] D. H. Hartmann and S. E. Woosley, *Astropart. Phys.* **7**, 137 (1997).
- [21] M. Kaplinghat, G. Steigman, and T. P. Walker, *Phys. Rev.* **D62**, 043001 (2000).
- [22] S. Ando, K. Sato, and T. Totani, *Astropart. Phys.* **18**, 307 (2003).
- [23] L. E. Strigari, M. Kaplinghat, G. Steigman, and T. P. Walker, *JCAP* **0403**, 007 (2004).
- [24] S. Ando, *Astrophys. J.* **607**, 20 (2004).
- [25] F. Iocco *et al.*, *Astropart. Phys.* **23**, 303 (2005).
- [26] C. Lunardini, *Astropart. Phys.* **26**, 190 (2006).
- [27] F. Daigne, K. A. Olive, P. Sandick, and E. Vangioni, *Phys. Rev.* **D72**, 103007 (2005).
- [28] M. Fukugita and M. Kawasaki, *Mon. Not. Roy. Astron. Soc.* **340**, L7 (2003).
- [29] L. E. Strigari, J. F. Beacom, T. P. Walker, and P. Zhang, *JCAP* **0504**, 017 (2005).
- [30] S. Ando, *Phys. Lett.* **B570**, 11 (2003).
- [31] G. L. Fogli, E. Lisi, A. Mirizzi, and D. Montanino, *Phys. Rev.* **D70**, 013001 (2004).
- [32] H. Goldberg, G. Perez, and I. Sarcevic, (2005).
- [33] L. J. Hall, H. Murayama, M. Papucci, and G. Perez, (2006).
- [34] J. F. Beacom and M. R. Vagins, *Phys. Rev. Lett.* **93**, 171101 (2004).
- [35] M. R. Vagins, , private communication. See also talk by R. Svoboda at the NNN06 conference, Seattle, Washington, USA, September 2006; [http://neutrino.phys.washington.edu/nnn06/slides/Svoboda\\_GdCl\\_v2.pdf](http://neutrino.phys.washington.edu/nnn06/slides/Svoboda_GdCl_v2.pdf).
- [36] K. Nakamura, *Int. J. Mod. Phys.* **A18**, 4053 (2003).
- [37] C. K. Jung, hep-ex/0005046 (1999).
- [38] L. Mosca, *Nucl. Phys. Proc. Suppl.* **138**, 203 (2005).
- [39] T. Marrodan Undagoitia *et al.*, *Prog. Part. Nucl. Phys.* **57**, 283 (2006).
- [40] <http://neutrino.ethz.ch/GLACIER/bodyintro.html> .
- [41] D. B. Cline, F. Raffaelli, and F. Sergiampietri, *JINST* **1**, T09001 (2006).
- [42] SNAP letter of intent, at <http://snap.lbl.gov/> .
- [43] <http://www.jinst.tokyo.ac.jp/>

# Intense Neutrino Beams and Leptonic CP Violation

William J. Marciano and Zohreh Parsa

Brookhaven National Laboratory<sup>1</sup>Upton, New York 11973

E-mail: marciano@bnl.gov, parsa@bnl.gov

**Abstract.** Effects of the Leptonic CP violating phase,  $\delta$ , on 3 generation neutrino oscillation rates and asymmetries are discussed. A figure of merit argument is used to show that our ability to measure the phase  $\delta$  is rather insensitive to the value of  $\theta_{13}$  (for  $\sin^2 2\theta_{13} \gtrsim 0.01$ ) as well as the detector distance (for very long oscillation baselines). Using a study of  $\nu_\mu \rightarrow \nu_e$  oscillations for BNL-Homestake (2540 km) we show that a conventional horn focused wide band neutrino beam generated by an intense 1-2 MW proton source combined with a very large water Cherenkov detector (250-500 kton) should be able to determine  $\delta$  to about  $\pm 15^\circ$  in  $5 \times 10^7 sec.$  of running. In addition, such an effort would also measure the other oscillation parameters ( $\theta_{ij}$ ,  $\Delta m_{ij}^2$ ) with high precision. Similar findings apply to a Fermilab-Homestake (1280 km) baseline. We also briefly discuss features of Superbeams, Neutrino Factories and Beta-Beams.

## 1. Status Of 3 Generation Lepton Mixing

The known weak interaction states  $|\nu_\ell\rangle$ ,  $\ell = e, \mu, \tau$  produced in charged current interactions are related to the neutrino mass eigenstates  $|\nu_i\rangle$ ,  $i = 1, 2, 3$  with masses  $m_i$  by the  $3 \times 3$  unitary matrix  $U$ .

$$\begin{pmatrix} |\nu_e\rangle \\ |\nu_\mu\rangle \\ |\nu_\tau\rangle \end{pmatrix} = U \begin{pmatrix} |\nu_1\rangle \\ |\nu_2\rangle \\ |\nu_3\rangle \end{pmatrix} \quad (1)$$

$$U = \begin{pmatrix} c_{12}c_{13} & s_{12}c_{13} & s_{13}e^{-i\delta} \\ -s_{12}c_{23} - c_{12}s_{23}s_{13}e^{i\delta} & c_{12}c_{23} - s_{12}s_{23}s_{13}e^{i\delta} & s_{23}c_{13} \\ s_{12}s_{23} - c_{12}c_{23}s_{13}e^{i\delta} & -c_{12}s_{23} - s_{12}c_{23}s_{13}e^{i\delta} & c_{23}c_{13} \end{pmatrix}$$

$$c_{ij} = \cos \theta_{ij} \quad , \quad s_{ij} = \sin \theta_{ij}$$

(Our phase convention differs in sign from the PDG, but is more consistent with  $V_{CKM}$ ).

Studies of atmospheric,  $K2K$  and recent MINOS  $\nu_\mu \rightarrow \nu_\mu$  disappearance indicate[1]

$$\Delta m_{32}^2 = m_3^2 - m_2^2 = \pm 2.6(3) \times 10^{-3} eV^2 \quad (2a)$$

$$\sin^2 2\theta_{23} \simeq 1.0 \quad \theta_{23} \simeq 45 \pm 5^\circ \quad (2b)$$

<sup>1</sup> This work is supported by the U.S. Department of Energy under contract number DE-AC02-98-CH-10886.

The sign of  $\Delta m_{32}^2$  is undetermined. For  $m_3 > m_2$ , normal ordering, neutrinoless double beta decay is highly suppressed, while for  $m_2 > m_3$ , inverted hierarchy, there is a chance that it could be observable in the next generation of experiments. So, determining the sign of  $\Delta m_{32}^2$  is important. In the case of  $\theta_{23}$ , maximal mixing,  $\theta_{23} \simeq 45^\circ$  is favored. How close that angle is to  $45^\circ$  and whether it is less than or greater than  $45^\circ$  (currently only  $\sin^2 2\theta_{23}$  is determined) is a key issue for model building. A very precise measurement is strongly warranted.

Solar neutrino and the Kamland reactor oscillation experiments indicate[1]

$$\Delta m_{21}^2 = m_2^2 - m_1^2 = 8 \pm 1 \times 10^{-5} \text{eV}^2 \quad (3a)$$

$$\sin^2 2\theta_{12} \simeq 0.84 \pm 0.10, \quad \theta_{12} \simeq 33^\circ \pm 4^\circ \quad (3b)$$

The angle  $\theta_{12}$  is large but not maximal.

Within the 3 generation formalism, what remains to be determined are the value of  $\theta_{13}$ , which is currently bounded[1]

$$0 \leq \sin^2 2\theta_{13} \lesssim 0.14, \quad (4)$$

by reactor experiments, along with the phase,  $\delta$ , about which nothing is currently known

$$-180^\circ \leq \delta < 180^\circ \quad (5)$$

After those parameters are determined, one will have an intrinsic measure of leptonic CP violation via the Jarlskog invariant[2]

$$J_{CP} \equiv \frac{1}{8} \sin 2\theta_{12} \sin 2\theta_{13} \sin 2\theta_{23} \cos \theta_{13} \sin \delta. \quad (6)$$

From the known angles ( $\sin^2 2\theta_{12} \approx 0.8$ ,  $\sin^2 2\theta_{23} \simeq 1$ )

$$J_{CP} \simeq 0.23 \sin \theta_{13} \sin \delta, \quad (7)$$

which suggests it is potentially enormous in comparison with the quark CKM matrix value

$$J_{CP}^{CKM} \simeq 3 \pm 1 \times 10^{-5} \quad (8)$$

Besides determining the  $\Delta m_{ij}^2$ , their signs,  $\theta_{ij}$  and  $\delta$  as precisely as possible, one would also like to have precision redundancy in those studies which probes deviations due to “new physics” such as sterile neutrino mixing, extra dimensions, exotic neutrino interactions, etc.

## 2. CP Violation

The flavor changing oscillations  $\nu_\mu \rightarrow \nu_e$  and  $\bar{\nu}_\mu \rightarrow \bar{\nu}_e$  have a very rich structure which includes CP violation. The oscillation probability is given by 3 important contributions as well as matter effects and smaller terms (which we neglect)[3, 4]

$$P(\nu_\mu \rightarrow \nu_e) = P_I(\nu_\mu \rightarrow \nu_e) + P_{II}(\nu_\mu \rightarrow \nu_e) + P_{III}(\nu_\mu \rightarrow \nu_e) + \text{matter} + \text{smaller terms} \quad (9)$$

$$P_I(\nu_\mu \rightarrow \nu_e) = \sin^2 \theta_{23} \sin^2 2\theta_{13} \sin^2 \left( \frac{\Delta m_{31}^2 L}{4E_\nu} \right) \quad (10)$$

$$P_{II}(\nu_\mu \rightarrow \nu_e) = \frac{1}{2} \sin 2\theta_{12} \sin 2\theta_{13} \sin 2\theta_{23} \cos \theta_{13} \sin \left( \frac{\Delta m_{21}^2 L}{2E_\nu} \right) \times \left[ \sin \delta \sin^2 \left( \frac{\Delta m_{31}^2 L}{4E_\nu} \right) + \cos \delta \sin \left( \frac{\Delta m_{31}^2 L}{4E_\nu} \right) \cos \left( \frac{\Delta m_{31}^2 L}{4E_\nu} \right) \right] \quad (11)$$

$$P_{III}(\nu_\mu \rightarrow \nu_e) = \sin^2 2\theta_{12} \cos^2 \theta_{13} \cos^2 \theta_{23} \sin^2 \left( \frac{\Delta m_{21}^2 L}{4E_\nu} \right) \quad (12)$$

while for  $\bar{\nu}_\mu$ ,  $\delta \rightarrow -\delta$  and matter effects change sign.

The rich structure of  $\nu_\mu \rightarrow \nu_e$  oscillations is nicely illustrated in Figs. 1-4 for BNL-Homestake and Fermilab-Homestake distances. Matter modifies the oscillation amplitudes and peak positions (the effect is opposite for an inverted hierarchy), making it straight forward to determine the sign of  $\Delta m_{31}^2$  with only a  $\nu_\mu$  beam. Also, the effect of  $\delta$  is important even for  $\delta = 0$ , no CP violation. By measuring the  $\nu_\mu$  oscillation probability as function of a  $\frac{L}{E_\nu}$  over a broad range, one can in principle measure all the parameters of neutrino oscillations with no degeneracies in  $\delta$ ,  $\theta_{23}$  and the mass hierarchy by a fit to Eq(9). For that reason, we favor[3, 4, 5] using an on axis broad band neutrino beam for  $0.5 \text{ GeV} \leq E_\nu \leq 5 \text{ GeV}$ .

Do we need to know the value of  $\theta_{13}$  before we embark on measuring  $\delta$ ? Not really, since the degree of difficulty for measuring  $\delta$  is to a large extent independent of  $\theta_{13}$  (unless it is very small) and the baseline distance (for  $1200 \text{ km} \lesssim L \lesssim 4000 \text{ km}$ ) if we use the wide band beam. To see that feature, consider the CP violation asymmetry.

$$A_{CP} \equiv \frac{P(\nu_\mu \rightarrow \nu_e) - P(\bar{\nu}_\mu \rightarrow \bar{\nu}_e)}{P(\nu_\mu \rightarrow \nu_e) + P(\bar{\nu}_\mu \rightarrow \bar{\nu}_e)} \quad (13)$$

It is given to leading order in  $\Delta m_{21}^2$  (assuming  $\sin^2 2\theta_{13}$  is not too small) by

$$A_{CP} \simeq \frac{\cos \theta_{23} \sin 2\theta_{12} \sin \delta}{\sin \theta_{23} \sin \theta_{13}} \left( \frac{\Delta m_{21}^2 L}{4E_\nu} \right) + \text{matter effects} \quad (14)$$

For fixed  $E_\nu$ , the asymmetry grows linearly with distance and increases as  $\theta_{13}$  gets smaller. Of course  $|A_{CP}|$  is bounded by 1; so, if it exceeds that value, e.g. if  $\sin^2 2\theta_{13} \lesssim 0.003$ , a breakdown in our assumption about the dominance of  $P_I$  in the denominator of eq.(13) is occurring.

The statistical figure of merit[3] is given by

$$F.O.M. = \left( \frac{\delta A_{CP}}{A_{CP}} \right)^{-2} = \frac{A_{CP}^2 N}{1 - A_{CP}^2} \quad (15)$$

where  $N$  is the total number of  $\nu_\mu \rightarrow \nu_e + \bar{\nu}_\mu \rightarrow \bar{\nu}_e$  events (properly normalized). Since  $N$  falls (roughly) as  $\sin^2 \theta_{13}$  and  $A_{CP}^2 \sim 1/\sin^2 \theta_{13}$ , we see that to a first approximation the F.O.M. is independent of  $\sin \theta_{13}$ . Similarly, for a given  $E_\nu$  the neutrino flux and consequently  $N$  falls as  $1/L^2$  but that is canceled by  $L^2$  in  $A_{CP}^2$ . So, to a good approximation, our ability to measure CP violation Proceedings of Neutrino Physics and Astrophysics, July 13-19, 2006

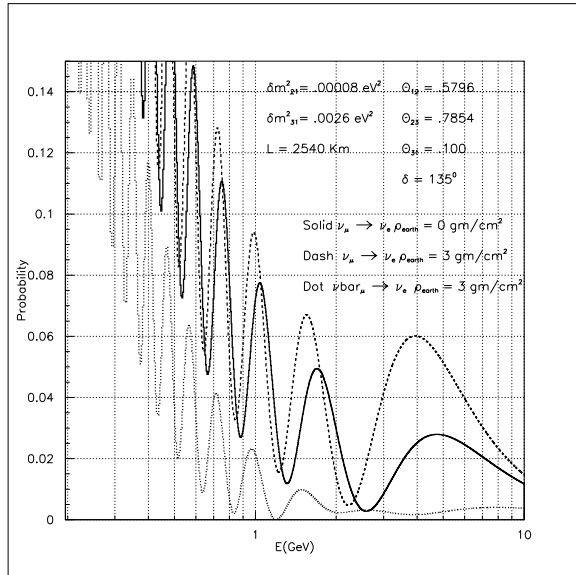


Figure 1.

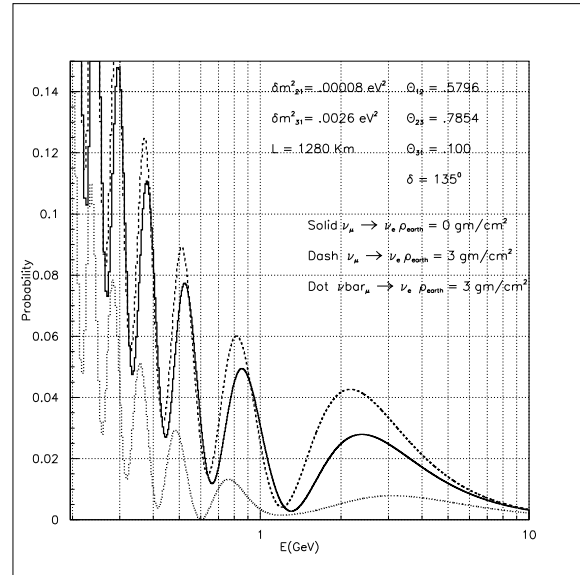


Figure 2.

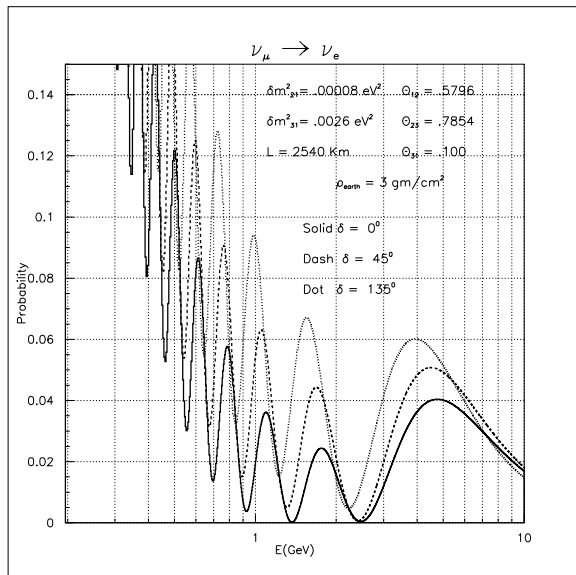


Figure 3.

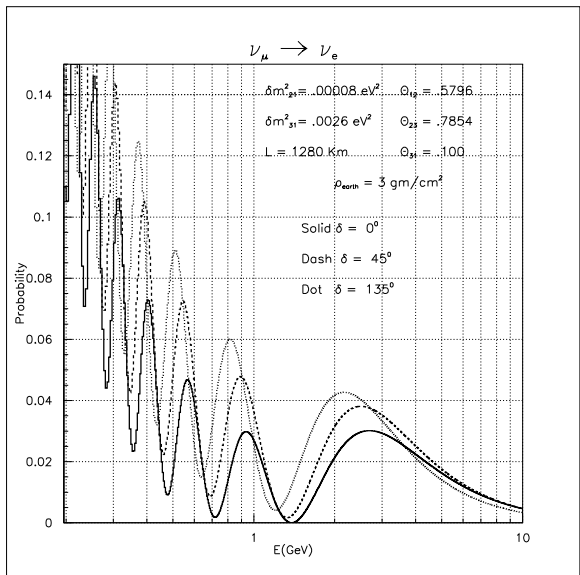


Figure 4.

Fig 1-4. Neutrino oscillations,  $\nu_\mu$  to  $\nu_e$ , as a function of energy for (Figs. 1 & 3) BNL-Homestake (2540 km) and (Figs. 2 & 4) FNAL - Homestake (1280 km). Effects of matter for neutrinos & antineutrinos relative to neutrinos with no matter are illustrated in Figs. 1 & 2, for  $\delta = 135^\circ$ . A comparison of different phases  $\delta = 0, 45^\circ, 135^\circ$  is given in Figs. 3 & 4. In all cases, we assume a normal mass hierarchy,  $\theta_{12} = 0.5796$ ,  $\theta_{23} = 0.7854$  &  $\theta_{13} = 0.1$  radians.

Another way of seeing the insensitivity to  $L$  in determining  $\delta$  is to consider the 3 terms in eqs. (10-12) separately. Each contributes to  $\nu_\mu \rightarrow \nu_e$  oscillations. The number of events from  $P_I$  falls as  $1/L^2$  due to flux reduction while those from  $P_{II}$  fall as  $1/L$  and from  $P_{III}$  they are approximately constant (assuming  $\sin \frac{\Delta m_{21}^2 L}{4E\nu} \sim \frac{\Delta m_{21}^2 L}{4E\nu}$ ). Viewing  $P_I$  and beam induced

backgrounds (which also fall as  $1/L^2$ ) together as a total background for measuring  $P_{II}$  and  $P_{III}$ , we see that the determination of  $P_{II}$  and therefore  $\delta$  relative to those backgrounds is independent of  $L$  for fixed  $E_\nu$  while the  $P_{III}$  signal to background increases linearly with  $L$ . So, longer distances have some advantages for  $P_{III}$ . In addition, we see from eq. (11) that we can measure both  $\sin \delta$  and  $\cos \delta$  just by mapping out  $\nu_\mu \rightarrow \nu_e$  oscillations (without antineutrinos) over a broad energy region. For those reasons, along with matter enhancement effects, larger  $E_\nu$  high energy cross-sections, larger total neutrino flux etc. we advocate a wide band neutrino beam (on axis)  $0.5 \lesssim E_\nu \lesssim 5$  GeV and a large detector at  $1200 - 4000 km$  for the measurement of  $\delta$ . Our study of that idea has shown many added benefits from the very long distance and broad band beam. Indeed, in principle it allows measurement of  $\Delta m_{31}^2$ ,  $\Delta m_{21}^2$ ,  $sign \Delta m_{31}^2 \sin^2 2\theta_{12}$ ,  $\sin^2 2\theta_{13}$ ,  $\sin^2 2\theta_{23}$  and  $\delta$  with outstanding to good precision in one experiment, possibly with only  $\nu_\mu$  running (i.e. no  $\bar{\nu}_\mu$ ). The basic features of that proposal[6] and some of its advantages are outlined below using a BNL-Homestake baseline, but first we explain why a conventional horn focused neutrino beam is currently the only viable way to explore leptonic CP violation.

### 3. Other Intense Neutrino Beams[5]

#### 3.1. Neutrino Superbeams:

By definition, a neutrino superbeam would require a 4MW or more proton driver. Such a facility would deliver 4 times as much neutrino flux as a more conventional 1MW source. However, because of heat and increased radiation loads it would require liquid targets, robotic handling and special focusing horns or solenoids. The engineering requirements for 4MW are much more demanding, requiring significant R&D to be realized[5]. The cost for such a facility would be much higher than the more conventional 1MW proton driver and horn envisioned above. Preliminary discussions of 4MW sources for neutrino superbeams and their anticipated oscillation studies are[7, 8] JPARC (Phase II)  $\rightarrow$  Hyper K (1000 kton  $H_2O$ ),  $L = 295 km$ , CERN (Super linac)  $\rightarrow$  Frejus (1000kton  $H_2O$ ),  $L = 130 km$ . Because of the relatively short baseline distances, those proposals would employ only low energy neutrino flux  $E_\nu < 1$  GeV for their oscillation studies. That corresponds to only a fraction of the potentially available neutrino flux and the cross-section is lower. To compensate, they must employ enormous detectors (1000 Kton), a more powerful source, and long running time. We have argued that it is much more cost effective and richer in physics to use a wide band beam of higher energy neutrinos and a much longer detector baseline distance[3, 4, 5, 6].

#### 3.2. Neutrino Factory[9]

Starting with an intense proton beam on target, the neutrino factory concept envisions capturing the  $\mu^\pm$  from  $\pi^\pm \rightarrow \mu^\pm \nu$  decays, cooling them and then accelerating them to 20-50 GeV. At that point they are placed in a storage ring with long straight sections where the decays  $\mu^+ \rightarrow e^+ \nu_e \bar{\nu}_\mu$  or  $\mu^- \rightarrow e^- \bar{\nu}_e \nu_\mu$  produce clean fluxes of high energy neutrinos with  $\langle E_\nu \rangle \simeq 0.7 - 0.8 E_\mu$ . Neutrino factories are expected to yield about  $0.03 \nu_\mu$ /proton; i.e. about 1/5 the flux of a conventional horn focused neutrino beam. The neutrino factories advantage (if it can be utilized) is the higher energy[9]. The beam solid angle will scale as  $\sim 1/E_\mu^2$  and deep-inelastic cross-sections grow as  $E_\nu$ . Hence, at fixed distance one can gain  $\sim E_\mu^3$  in event rate. However, in the case of oscillation studies, higher energies demand longer distance requirements for a fixed  $L/E$  and a flux fall-off by  $1/L^2$ . That means, for  $E_\nu \simeq 20$  GeV to sit at the first oscillation peak requires a detector at 12,000 km which is not possible. Hence, neutrino factories must do their studies primarily at shorter distances ( $\sim 3000 km$ ) where the first oscillation is only fractional. For measuring  $\theta_{13}$ , the relative nearness is actually an advantage, but it is a drawback for CP violation studies which are optimized at oscillation peaks. If  $\theta_{13}$  is extremely small,  $\sin^2 2\theta_{13} \lesssim 0.003$ , Neutrino Factories may be our best hope for measuring it. However, in that case, ~~Proceedings of Neutrino Physics and Astrophysics, July 13-19, 2006~~

### 3.3. Beta Beam

The interesting possibility of producing intense  $\nu_e$  or  $\bar{\nu}_e$  beams from nuclear beta decays was originally suggested by P. Zucchelli[10]. It is particularly well matched to CERN's radioactive beams capabilities and accelerator complex. To be competitive with other intense neutrino facilities, the radioactive nuclei must be copiously produced  $\gtrsim 10^{13}/sec$ , cooled, accelerated to  $\gamma \simeq 100$  and kept in a large storage ring (with a long straight section) where a highly collimated  $\nu_e$  or  $\bar{\nu}_e$  beams is produced by the decay  $N \rightarrow N' e \bar{\nu}_e$ . Such a feat is extremely challenging, but the resulting beam has some very attractive features. It is absolutely clean, containing pure  $\nu_e$  or  $\bar{\nu}_e$  with a precisely calculable energy spectrum. Unlike the neutrino factory, it does not require a magnetized detector; so, a very large  $H_2O$  Detector can be used. The neutrino energy spectrum is relatively low but broad, which are favorable characteristics for studying CP violation and measuring  $\delta$ . On the negative side, the flux is limited to  $O(10^{18}\nu/yr)$  and the  $\nu_\mu$  appearance cross-section is small. CP violation studies lack statistics but may be marginally viable because of the potentially tiny backgrounds.

## 4. BNL-HOMESTAKE NEUTRINO OSCILLATION EXPERIMENT

We have written a white[6] paper and had several follow-up studies extolling the virtues of a very long baseline BNL-Homestake (2540 km) neutrino oscillation experiment. (Actually, any distance[3] from about 1200–4000 km will do.) Its basic requirements are: 1) A conventional horn focused intense  $\nu_\mu$  beam using an upgraded 1-2 MW AGS proton beam on a standard target. The cost and technical requirements [6] needed for the upgrade are modest in comparison with ideas for 4MW superbeams or neutrino-factory sources described above. The resulting neutrino beam (on axis at  $0^\circ$ ) would be broad band,  $0.5 \text{ GeV} \lesssim E_\nu \lesssim 5 \text{ GeV}$ , peaking near 1.5 GeV. 2) The detector[11] would be about a 250–500 kton water cherenkov detector and would likely be somewhat modular in design. This is again modest (about half the cost) in comparison with the 1000 kton behemoth detectors being considered by others. To reconstruct the neutrino energy on an event by event basis and reject  $\pi^0$  background, we would primarily use quasi-elastic events  $\nu_e n \rightarrow e^- p$  in the analysis. They represent less than 1/4 of all neutrino events; therefore, a detector with better resolution and acceptance such as liquid Argon or Scintillator could be smaller, in principle, of order 100–200 kton by using a larger fraction of events to do the job. 3) The run time would be about  $5 \times 10^7$  sec with a  $\nu_\mu$  beam. Two types of oscillation measurements would be made  $\nu_\mu \rightarrow \nu_\mu$  disappearance and  $\nu_\mu \rightarrow \nu_e$  appearance. At a later time  $\bar{\nu}_\mu$  studies might be carried out; however, they may not be necessary because the wide band beam allows sensitivity to all neutrino oscillation parameters, even  $\delta$ , without actually measuring a CP violating effect such as  $A_{CP}$  directly. Instead a fit is done to the data assuming 3 generation mixing.

Because of the long distance and broad band beam, many physics studies are possible. The measurement of  $\nu_\mu \rightarrow \nu_\mu$  disappearance

$$P(\nu_\mu \rightarrow \nu_\mu) = 1 - \sin^2 2\theta_{23} \sin^2 \left( \frac{\Delta m_{31}^2 L}{4E_\nu} \right) + \text{smaller terms} \quad (16)$$

over the range  $0.5 \leq E_\nu \leq 5 \text{ GeV}$  would be sensitive to 3 or 4 oscillation cycles [6]. Such measurements would determine  $\sin^2 2\theta_{23}$  and  $\Delta m_{31}^2$  to better than  $\pm 1\%$  statistically. Such a study will tell us if  $\theta_{23} \simeq 45^\circ$  to within about  $\pm 2^\circ$ . Also, by comparing values of  $\Delta m_{31}^2$  obtained at different  $E_\nu$ , one can search for indications of “new physics”.

The study of  $\nu_\mu \rightarrow \nu_e$  oscillations can be divided into three domains: 1) High Energy,  $3 \text{ GeV} \leq E_\nu \lesssim 5 \text{ GeV}$ , 2) Intermediate Energy,  $1 \text{ GeV} \leq E_\nu \leq 3 \text{ GeV}$  and 3) Low Energy,  $E_\nu \lesssim 1 \text{ GeV}$ . Roughly speaking, the high energy  $\nu_e$  events will be matter enhanced (suppressed) for the normal (inverted) mass hierarchy. The effect is very pronounced (see Figs. 1 & 2), making a

determination of the sign of  $\Delta m_{31}^2$  relatively easy (for  $\sin^2 2\theta_{13} \geq 0.01$ ) and allowing for a good measurement or bound on  $\theta_{13}$  (via  $P_I$ ) which is better than any other proposed experiment [6]. Intermediate energy events will measure both  $\sin\delta$  and  $\cos\delta$  via  $P_{II}$ . In that way we expect  $\delta$  to be determined to within  $\pm 15^\circ$  independent of its value with no ambiguity [6] (again assuming  $\sin^2 2\theta_{13} \gtrsim 0.01$ ). That type of  $\delta$  determination is more robust and statistically more powerful than  $A_{CP}$ . Note, that the energy peaks are also displaced by matter effects. Their positions can in principle be used to determine the sign of  $\Delta m_{31}^2$ . (see fig. 1.) Finally, the low energy  $\nu_e$  events will determine the combination  $\Delta m_{21}^2 \sin 2\theta_{12}$  to about  $\pm 5\%$  via  $P_{III}$ . Altogether, this single experiment will measure or constrain all parameters of 3 generation leptonic mixing with unprecedented sensitivity and without parameter degeneracies. It would put leptonic mixing on about the same level of precision as quark mixing. Specific details of detector optimization and running strategy still need to be ironed out, but the basic idea of determining all oscillation parameters via one experiment is very compelling. We also note, a Fermilab-Homestake (1280 km) and wideband beam experiment would exhibit less dramatic effects (see Fig. 2), but would have about 4 times the statistics because of the shorter distance. Overall, it would have similar discovery potential. Figs. 3 & 4 illustrate the dependence on the phase  $\delta$  for BNL and Fermilab distances.

## 5. OUTLOOK

It appears that the combination of intense conventional wide band  $\nu_\mu$  beam, powered by a 1-2 MW proton accelerator, large detector and very long baseline provides an opportunity to measure  $\Delta m_{31}^2$ , sign  $\Delta m_{31}^2$ ,  $\Delta m_{21}^2$ , all  $\theta_{ij}$  and  $\delta$  with good to high precision. The intense proton source required for this effort is a straightforward upgrade of the AGS or Fermilab Main Injector. The large detector (= 500 kton  $H_2O$  or its equivalent) could be sited at either of the national underground lab sites being considered (Homestake or Henderson). It would also search for proton decay, supernova, atmospheric neutrinos etc. to unprecedented levels. The facility would probably be at the forefront of particle physics research for 50 years or more. Of course, proton sources at JPARC or CERN are also options for such a long baseline effort.

What remains to be done? Detector R&D to reject backgrounds such as  $\pi^0$  and reduce the cost are needed. An underground lab site needs to be developed and the horn generated wide band beam flux should be optimized. After the first phase of  $\nu_\mu$  is completed, one might run  $\bar{\nu}_\mu$  for a few years if one wants to actually observe CP violation (rather than just a determination of  $\delta$ ) or if an inverted mass hierarchy turns out to be correct. During that time further upgrades of the AGS or Main Injector to 2MW or more might be appropriate.

The strategy for long baseline neutrino oscillations outlined here is based on novel concepts: broad band beam, very long distance and large detector. It is bold, ambitious and doable. The opportunity is within our community's grasp and should be seized.

## References

- [1] See talks in Neutrino 2006 Proceedings.
- [2] C. Jarlskog, Z. Phys. **C29**, 491 (1985)
- [3] W. Marciano, "Extra Long Baseline Neutrino Oscillations and CP Violation", hep-ph/0108181.
- [4] W. Marciano, Nucl. Phys. **B138**, 370 (2005).
- [5] Z. Parsa "Physics of an Intense Neutrino Beam from BNL to a Very Long Baseline Detector" AIP CP **698** 307 (2003).
- [6] BNL Neutrino Working Group: M. Diwan *et al.*, hep-ex/0211001; Phys. Rev. **D68**, 012002 (2003).
- [7] Y. Itow *et al.*, "The JHF-Kamioka Neutrino Project", hep-ex/0106019.
- [8] B. Autin *et al.*, (SPL Study Group) CERN 2000-012 (2000) Report.
- [9] Z. Parsa, "Neutrino Factories-Physics Potential", AIP CP **549**, in Intersections of Particle and Nuclear Physics, Quebec City (2000) p. 781; *ibid* earlier papers.
- [10] P. Zucchelli, Phys. Lett. **B532**, 166 (2002).
- [11] M. Diwan *et al.*, Proposal for an Experimental Program in Neutrino Physics and Proton Decay in the Homestake Laboratory, hep-ex/0608023 (2006). W. Fratt and Z. Parsa, unpublished.

# Geophysics with Hawaiian Anti-neutrino Observatory (Hanohano)

## J. Maricic for the Hanohano Collaboration

Drexel University, Philadelphia, PA, 19104, University of Hawaii, Honolulu, HI, 96822

jelena.maricic@physics.drexel.edu

**Abstract.** The design studies are under way for the deep ocean anti-neutrino observatory located in the vicinity of the Big Island (Hawaii) with the main goal of measuring geo-neutrino flux from the mantle and core which can exclusively be done in a location far from the continental plates such is Hawaiian Islands chain. Hanohano will also accomplish the definitive measurement of the electron anti-neutrino signal from the core to observe or eliminate a hypothetical natural reactor in the Earth's core.

## 1. Introduction

Uranium and thorium content of the Earth is directly related to the Earth's heat flow, which is not a well known quantity [1]. One suggested way of estimating the uranium and thorium content of the Earth is via detection of anti-neutrinos produced in the radioactive decays of these elements [2] which has been done in [3] for the first time. The hypothetical nuclear reactor in the Earth's core can also be detected through its anti-neutrino flux and attempt has been made in [4]. Hawaiian Anti-neutrino Observatory (Hanohano) will be a liquid scintillator detector designed with a goal to make a definitive measurement of geo-neutrino flux due to uranium and thorium in the Earth's mantle and core and to observe or eliminate a putative reactor in the Earth's core via its anti-neutrino flux. Experience from the KamLAND detector in Japan is used to estimate needed baseline to achieve desired sensitivity as well as for the background rate estimates.

## 2. Hanohano detector

In order to accomplish 16% measurement of the U/Th content of the mantle plus core, Hanohano must have at least 10 kiloton-years of exposure. It should be placed at 4 km depth to reduce cosmic ray induced backgrounds, thus the suggested location is in the vicinity of the Big Island in Hawaii. It is expected that Hanohano should reach the same level of radio-purity levels as in KamLAND, except for radon where the significant improvement is need (at least a factor of 40). 1 TW or larger core nuclear reactor may be detected with  $5\sigma$  confidence level with Hanohano detector.

## References

- [1] D.L. Anderson, *Theory of Earth*, Blackwell Science (1990).
- [2] G. Eder, *Terrestrial Neutrinos*, Nucl. Phys. **78**, 657 (1966).
- [3] T. Araki et al., Nature (London) **436**, 499 (2005).
- [4] Jelena Maricic, Ph.D. Thesis, University of Hawaii (2005).



# Cryogenic Double Beta Decay Experiments: CUORE and CUORICINO

**Reina Maruyama, for the CUORE Collaboration [1]**

Lawrence Berkeley National Laboratory & University of Wisconsin, Madison, USA

E-mail: rmaruyama@lbl.gov

**Abstract.** Cryogenic bolometers, with their excellent energy resolution, flexibility in material, and availability in high purity, are excellent detectors for the search for neutrinoless double beta decay. Kilogram-size single crystals of  $\text{TeO}_2$  are utilized in CUORICINO for an array with a total detector mass of 40.7 kg. CUORICINO currently sets the most stringent limit on the halflife of  $^{130}\text{Te}$  of  $T_{1/2}^{0\nu} \geq 2.4 \times 10^{24}$  yr (90% C.L.), corresponding to a limit on the effective Majorana neutrino mass in the range of  $\langle m_\nu \rangle \leq 0.2\text{--}0.9$  eV. Based on technology developed for CUORICINO and its predecessors, CUORE is a next-generation experiment designed to probe  $\langle m_\nu \rangle$  in the range of 10–100 meV. Latest results from CUORICINO and overview of the progress and current status of CUORE are presented.

## 1. Introduction

The search for neutrinoless double beta decay ( $0\nu\beta\beta$ ) has become one of the top priorities in the field of neutrino physics since the discovery of neutrino oscillations in atmospheric[2], solar[3], and reactor[4] experiments. An overview and current status of double-beta decay physics and experiments were given in earlier talks by Hirsch, Simkovic, Elliott, and Barabash[5]. The need to verify the claim of the observation of  $0\nu\beta\beta$  by a subset of Heidelberg-Moscow germanium experiment[6] has also been presented in these talks. The most stringent limit on the effective mass of Majorana neutrinos comes from two  $^{76}\text{Ge}$  experiments, Heidelberg-Moscow[7] and IGEX[8]. CUORICINO which is searching for  $0\nu\beta\beta$  in  $^{130}\text{Te}$  follows closely behind[9]. NEMO-3 is capable of a multiple-isotope search for double-beta decay events, and with its tracking capabilities, has excellent sensitivity to  $2\nu\beta\beta$ [11].

A number of experiments are currently at various stages of development to probe the degenerate mass hierarchy region of the neutrino mass spectrum and into the inverted hierarchy, many of which are represented at this conference[12]. CUORE (Cryogenic Underground Observatory for Rare Events) is one such experiment, to be located at the Gran Sasso National Laboratory (LNGS). It will consist of 988 bolometers of  $\text{TeO}_2$  crystals, with a total mass of 741 kg. Because of the high isotopic abundance of 34%, 204 kg of  $^{130}\text{Te}$  is available for  $0\nu\beta\beta$  without isotopic enrichment, making CUORE both timely and significantly less expensive than other experiments. CUORE's modular design and flexibility will also allow future searches in other isotopes of interest. It is imperative to carry out double beta decay searches in multiple isotopes, both to improve the nuclear matrix calculations necessary to extract the effective neutrino mass, and to ensure that the observation of a line at the expected energy is not a result of an unidentified background.

Double beta decay experiments can be divided into three categories: indirect measurements such as geochemical analyses, direct measurements with the source being separate from the detector, and direct measurements with a detector that also acts as the source. Bolometers belong to the last category[16]. When the source is the same as the detector, the source mass is maximized while materials that could potentially contribute to the background are minimized. In bolometers, the deposited energy is measured thermally, therefore the entire energy of a decay event is fully accounted for. At low temperatures (the operating temperature for CUORICINO is 8 mK), the heat capacity of crystals is proportional to the cube of the ratio of the operating and Debye temperatures. The energy released in a single particle interaction within the crystal is clearly measurable as change in temperature of the entire crystal. The temperature change is measured by neutron transmutation doped (NTD) germanium thermistors which are optimized to operate at these temperatures[14, 15]. The energy resolution of cryogenic bolometers rivals that of germanium detectors, and 5 keV FWHM resolution at 2.5 MeV is readily achievable.

## 2. CUORICINO: Results and Performance

CUORICINO started taking data in April 2003 at LNGS and is now producing competitive results with those achieved by the germanium experiments. It will continue to run until CUORE has been constructed and is ready to take data. First results from CUORICINO were published recently which included data from a total exposure of 3.09 kg·yr of  $^{130}\text{Te}$ [9]. Here we report on an update that includes the data up to May 2006 with a total of 8.38 kg·yr of  $^{130}\text{Te}$  (see Fig. 1)[17]. No evidence for excess counts is observed at 2530 keV, the expected Q-value for  $0\nu\beta\beta$  for  $^{130}\text{Te}$ . The absence of any excess events above backgrounds in the region of interest gives a limit of  $T_{1/2}^{0\nu} \geq 2.4 \times 10^{24}$  yr (90% C.L.) on the  $0\nu\beta\beta$  decay rate of  $^{130}\text{Te}$ . This corresponds to an effective neutrino mass of  $\langle m_\nu \rangle \leq 0.18 - 0.94$  eV, the range reflecting the spread in QRPA nuclear matrix element calculations (see [9] for list). The background measured in the  $0\nu\beta\beta$  region of interest is  $0.18 \pm 0.01$  counts/keV·kg·yr.

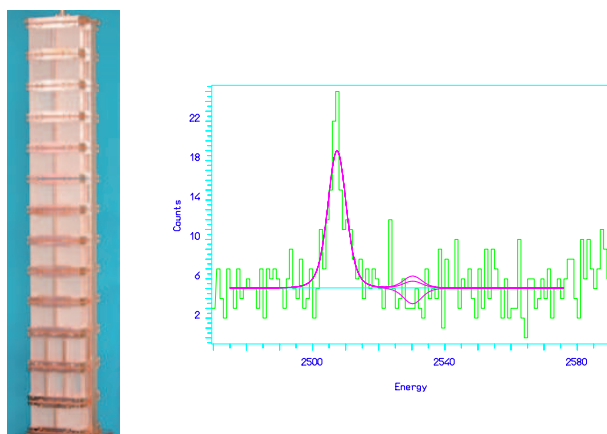


**Figure 1.** Left: Photo of the CUORICINO tower before Cu thermal shields were installed. Right: CUORICINO summed background energy spectrum in the  $^{130}\text{Te}$   $0\nu\beta\beta$  region. The peak at 2505 keV is the sum peak from two  $^{60}\text{Co}$  gamma lines.  $0\nu\beta\beta$  signal from  $^{130}\text{Te}$  is expected at 2530 keV. No evidence of DBD is seen.

CUORICINO is roughly one-twentieth the size of CUORE, and much of the technology that will be used in CUORE was used to build CUORICINO. It consists of 62  $\text{TeO}_2$  crystals with a total mass of 40.7 kg. The crystals are arranged in a tower, 11 levels each containing four crystals  $5 \times 5 \times 5 \text{ cm}^3$  in

size, weighing  $\sim 330$  g (see Fig. 1). All  $5 \times 5 \times 5$  cm<sup>3</sup> crystals and all but four of the  $3 \times 3 \times 6$  cm<sup>3</sup> crystals are made from tellurium of natural abundance. Two of the  $3 \times 3 \times 6$  cm<sup>3</sup> crystals are enriched to 75% <sup>130</sup>Te and two are enriched to 82.3% <sup>128</sup>Te. The average resolution in the  $0\nu\beta\beta$  region, measured with the 2615 keV <sup>208</sup>Tl line during calibration runs, is  $\sim 8$  keV. In 3 years of running with the present background level, CUORICINO will achieve a half-life sensitivity for  $0\nu\beta\beta$  decay of  $7.1 \times 10^{24}$  yr, corresponding to an effective mass on the order of 300 meV.

### 3. CUORE

CUORICINO also serves as an excellent test bed and prototype for CUORE. All critical subsystems of the proposed CUORE detector are based on the design of CUORICINO. CUORE will consist of an array of 988,  $5 \times 5 \times 5$  cm<sup>3</sup> TeO<sub>2</sub> bolometers arranged in 19 CUORICINO-like towers. The total crystal mass of TeO<sub>2</sub> will be 741 kg, with 204 kg of <sup>130</sup>Te (see Fig. 2). The entire detector will be housed in a single dilution refrigerator at 10 mK.

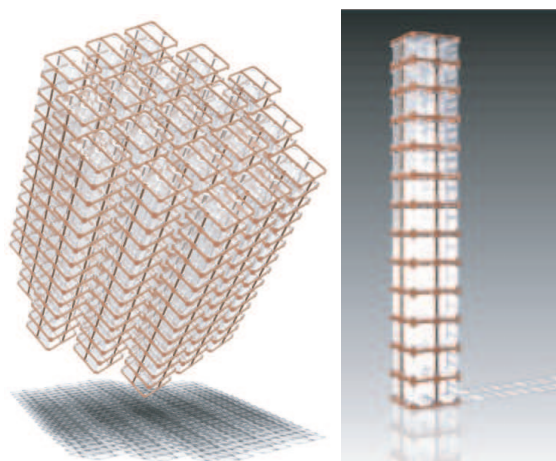


**Figure 2.** Left: The CUORE detector consisting of a close-packed array of 19 towers with a total of 988 crystals. Right: One of the 19 towers of the CUORE detector array, similar to the one operating in the CUORICINO experiment.

In 5 years of running with a background of 0.01 counts/keV·kg·yr and a resolution of 5 keV, CUORE expects to have a sensitivity to the half-life of  $0\nu\beta\beta$  of  $T_{1/2}^{0\nu} \sim 2.1 \times 10^{26}$  yr. This corresponds to an effective neutrino mass of  $\langle m_\nu \rangle \leq 19 - 100$  meV, with the spread coming from the uncertainty in matrix element calculations. If we are able to reduce the background to 0.001 counts/keV·kg·yr, the sensitivity will extend to  $T_{1/2}^{0\nu} = 6.5 \times 10^{26}$  yr (11–57 meV). The main technical challenges will be to control the background levels, ensure that the narrow energy resolution achieved with many of the crystals are uniformly implemented in all crystals, and that all crystals are well calibrated for energy.

A combination of CUORICINO background data, measurements from an independent R&D setup in Hall C in LNGS, direct counting with germanium detectors on- and off-site, neutron activation analysis, and other techniques are used to characterize materials and components to be used in CUORE. The results of these measurements as well as other potential sources of radioactive background (e.g. environmental activity) are used as input for Monte Carlo simulation. Estimates of the relative contributions of the main background sources in the ROI in CUORICINO is as follows:  $10 \pm 5\%$  from U/Th contaminations on the TeO<sub>2</sub> surfaces,  $50 \pm 20\%$  from Cu surfaces (both from the crystal support structure and thermal shielding), and  $30 \pm 10\%$  from the bulk of the Cu shields.

The sources of backgrounds are divided into three main categories: contamination in the bulk, surfaces, and environmental radioactivity. Because the Q-value for <sup>130</sup>Te  $0\nu\beta\beta$  decay is higher than most gamma-lines from U and Th, the only tails of known lines that may contribute to the background are <sup>60</sup>Co and <sup>208</sup>Tl. <sup>60</sup>Co and <sup>208</sup>Tl are expected to contribute, respectively,

Alpha events with lines at higher energies can contribute if they deposit only a part of their energy in the crystals, therefore surface contaminations on or near the crystals is of particular concern.

Other components facing the detector (Teflon stand-offs, heaters used for gain stabilization, and gold wires for signal and other electrical controls) were also tested in the R&D setup in Hall C by covering crystal surfaces with a large amount of these materials. The background seen from these materials was found to be negligible.

Simulations are being refined as more data are being collected with the CUORICINO detector and elsewhere. As of April 2006, we have demonstrated that background reductions of a factor of  $\sim 8$  and detector resolutions of 5 keV are achievable. Figure 3 shows the background spectrum obtained from CUORICINO and the R&D setup in Hall C. The shielding around the Hall C setup is insufficient to shield much of the  $\gamma$ 's below 2.6 MeV, however significant reduction in the  $\alpha$  events above 2.6 MeV is clearly seen. Effort is underway to further reduce the background by careful material selection and handling procedures. In addition, background rejection through anticoincidence among adjacent crystals will be more effective in the much larger CUORE array and will aid in achieving the background goals.

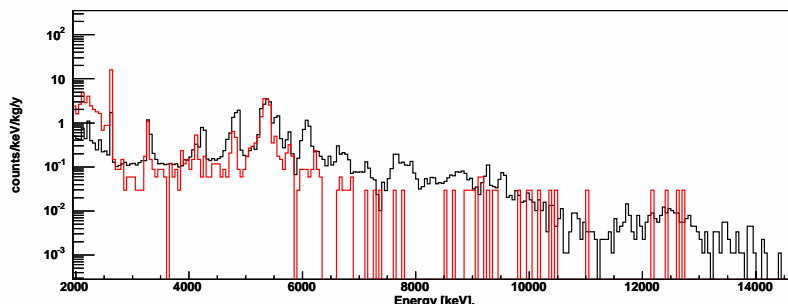


**Figure 3.** CUORICINO background energy spectrum (black) and background spectrum from the R&D setup in Hall C (red).

We have estimated that for the muon flux observed in LNGS ( $2.5 \times 10^{-8} \mu/(\text{cm}^2 \text{s})$ ), muons would produce  $\sim 0.04$  neutrons/day in the polyethylene shield and  $\sim 25$  neutrons/day in the lead shield. This indicates that neutrons will play a secondary role in the total background compared with other sources of background. In addition, we are planning a series of experiments at the GEANIE facility at Los Alamos National Laboratory to measure cross-sections for neutron-induced reactions on the abundant Te isotopes for neutrons from 1-100 MeV[18]. The results of these measurements will then be used in our MC calculations to refine background estimates.

#### 4. Beyond CUORE

The main goal and design of CUORE is to search for  $0\nu\beta\beta$  decay in  $^{130}\text{Te}$ . Its sensitivity can be increased three times ( $\sim 60\%$  improvement in the sensitivity to neutrino mass) by replacing the detectors with enriched crystals. Event identification using multiple signatures from a single event is a powerful tool in reducing backgrounds. Work is underway to further reduce backgrounds by using Surface Sensitive Bolometers (SSB) and/or scintillating bolometers[18]. Every factor of ten reduction in background would increase the halflife sensitivity by a factor of three.

SSB allows us to distinguish surface events and bulk events, especially for  $\alpha$ -particles. It consists of the main DBD absorber and thin absorbers attached to the crystal surfaces. The

surface events from either the main crystal absorber or elsewhere would trigger the SSB, and those events could be rejected. In addition, the additional heat capacity from the thin absorbers alters the pulse shape of the signal from the main absorber[19].

Scintillating bolometers would combine heat and scintillation approach already successfully applied in dark matter experiments such as CRESST and ROSEBUD. Scintillation and heat signals have different sensitivities for nuclear recoils,  $\alpha$  particles, and ionizing events such as  $0\nu\beta\beta$  decay. A  $\text{CaF}_2$  bolometer has successfully been used[20], and the collaboration is currently investigating  $\text{TeO}_2$  doped with Nb and Mn[21].

The modular design of the CUORE detector also allows for searches of  $0\nu\beta\beta$  in other isotopes. It is possible to create thermal detectors from a variety of materials, and CUORE could investigate  $0\nu\beta\beta$  in other nuclei. Several DBD candidates have been tested as thermal detectors:  $\text{CaF}_2$ , Ge,  $\text{MoPbO}_4$ ,  $\text{CdWO}_4$ , and  $\text{TeO}_2$ . Possible crystals for Nd are under development.

## 5. Conclusion

Cryogenic bolometers, with their flexibility in material choice and the ability to scale up to the ton-scale are ideal for large-scale detectors for double-beta physics experiments. CUORE aims to probe the Majorana nature of the neutrino, with a sensitivity to the neutrino mass deep into the inverted mass hierarchy. CUORICINO is currently running as the most sensitive  $0\nu\beta\beta$  experiment, and will continue until CUORE comes online. Much of the technology has been tested for CUORE, and a factor of 8 reduction from the radioactive background observed in CUORICINO has been achieved. CUORE has been approved by the advisory Commissione II of INFN (Italian Institute of Nuclear Physics) and funding has been allocated in 2005. The CUORE experiment was approved by the Scientific Committee of LNGS in 2004, and preparations of the laboratory space and the construction of CUORE are underway.

## References

- [1] For more information and complete list of authors, see the CUORE website: <http://crio.mib.infn.it/wig/Cuorepage/CUORE.php>.
- [2] Super-Kamiokande Collaboration, S. Fukuda *et al.*, Phys. Rev. Lett. **86** (2001) 5656.
- [3] SNO Collaboration, Q.R. Ahmad *et al.*, Phys. Rev. Lett. **89** (2002) 011301.
- [4] KamLAND Collaboration, K. Eguchi *et al.*, Phys. Rev. Lett. **90** (2003) 021802.
- [5] See presentations at Neutrino'06 by M. Hirsch, F. Simkovic, S. Elliott, and A. Barabash.
- [6] H.V. Klapdor-Kleingrothaus *et al.*, Mod. Phys. Lett. A **16** (2001) 2409; H.V. Klapdor-Kleingrothaus, A. Dietz, I. Krivosheina and O. Chkvorets, Phys. Lett. B **586** (2004) 198; H.V. Klapdor-Kleingrothaus *et al.*, Nucl.Instrum.and Meth. **522** (2004) 367.
- [7] H.V. Klapdor-Kleingrothaus *et al.* Eur. Phys. J. A **12** (2001) 147.
- [8] C.E. Aalseth *et al.*, Phys. Rev. D **65** (2002) 092007.
- [9] CUORICINO Collaboration, C. Arnaboldi *et al.*, Phys. Rev. Lett. **95** (2005) 142501.
- [10] CUORE Collaboration, R. Ardito *et al.*, hep-ex/0501010.
- [11] R. Arnold *et al.* Phys. Rev. Lett. **95** (2005) 182302.
- [12] See presentations at Neutrino'06 by S. Schoenert, A. Piepke, and J. Wilson.
- [13] C. Arnaboldi *et al.*, Phys. Lett. B **584** (2004) 260.
- [14] E.E. Haller *et al.*, Proc. Fourth Int. Conf. on Neutron Transmutation Doping of Semiconductor Materials, Nat. Bureau of Standards, June 1,2 1982, Gaithersburg MD, R.D. Larrabee ed., (Plenum Press 1984) p 21.
- [15] E. Haller, J. Appl. Phys. **77** (1995) 2857.
- [16] S.H. Moseley, J.C. Mather and D. McCammon, J. Appl. Phys. **56** (1994) 1257.
- [17] S. Capelli, Poster presentation at Neutrino'06 Conference (Santa Fe, NM, USA).
- [18] M. Dolinski, S. Sangiorgio, P. Gorla, Poster presentations at Neutrino'06 Conference (Santa Fe, NM, USA);
- [19] I. Bandac *et al.*, submitted to Journal of Applied Physics (2006).
- [20] A. Alessandrello *et al.*, Phys.Lett. B **420** (1998) 109
- [21] I. Dafinei *et al.*,  $\text{TeO}_2$  scintillating crystal growth and properties, presented at the Int.Conf. on Inorganic Scintillators and their Industrial Applications SCINT2005,; Crimea, Alushta (Ukraine), Sept.19-23, 2005

# Neutrinos from Supernovae and Gamma Ray Bursts: Nucleosynthesis and Detection

**G. C. McLaughlin**

Department of Physics, North Carolina State University, Raleigh, NC 27695-8202

E-mail: [Gail\\_McLaughlin@ncsu.edu](mailto:Gail_McLaughlin@ncsu.edu)

**Abstract.** We discuss the way in which neutrino oscillations, sterile neutrinos and ambient conditions impact the nucleosynthesis in extreme astrophysical environments such as supernovae and gamma ray bursts. We focus first on r-process nucleosynthesis and supernovae and the role of neutrinos. Secondly, we discuss active sterile neutrino oscillations in this environment. We then turn to gamma ray bursts and examine the nucleosynthesis that can be produced by accretion disk winds, and the impact of the neutrinos. Finally we comment on the prospects for detecting such an accretion disk if it were to occur in the Galaxy with existing neutrino detectors.

## 1. Introduction

In both supernovae and gamma ray bursts, an essential part of the energetics is dominated by neutrinos. In supernovae, most of the gravitational binding energy from the gravitational collapse of the star is released in the form of neutrinos, which leak out of the proto-neutron star core on a timescale of about ten seconds, see e.g. [1]. Long duration gamma ray bursts may be a rare form of supernovae, while short duration bursts may be produced by neutron star mergers [2, 3]. In both of these cases, it is likely that an accretion disks forms around a black hole, which becomes hot enough to emit large numbers of neutrinos, see the sketch in Fig 1. Neutrino fluxes become large when the neutrinos are emitted from regions where the mean free path is small. In Fig. 2 we show the neutrino trapped region for a proto-neutron star and for an accretion disk. As can be seen from the figure, all types of neutrinos are produced in the proto-neutron star, while primarily  $\nu_e$  and  $\bar{\nu}_e$  types are produced in the accretion disk.

A wind flows away from both the proto-neutron star and from the accretion disk. Close to these objects, the material is sufficiently hot that it is composed of free nucleons, as it flows away it cools, and nucleons combine into nuclei. The type of nuclei that are formed in this way depends sensitively on the outflow timescale, the entropy, and in particular the electron fraction,  $Y_e = 1/(1 + n/p)$ . Since there is an intense flux of neutrinos emitted in each case, the electron fraction will be influenced by both the backward and forward reactions below:



If these reactions equally matched, then the material has roughly equal numbers of neutrons and protons, which makes an environment favorable for forming iron peak elements, such as

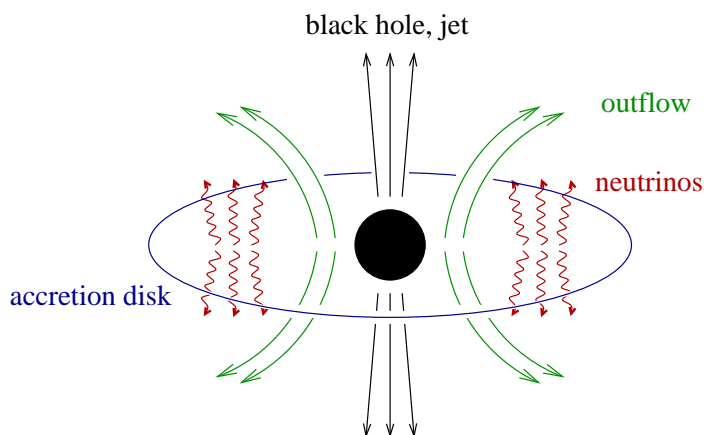


**Figure 1.** Sketch of an accretion disk, the jet and the wind.

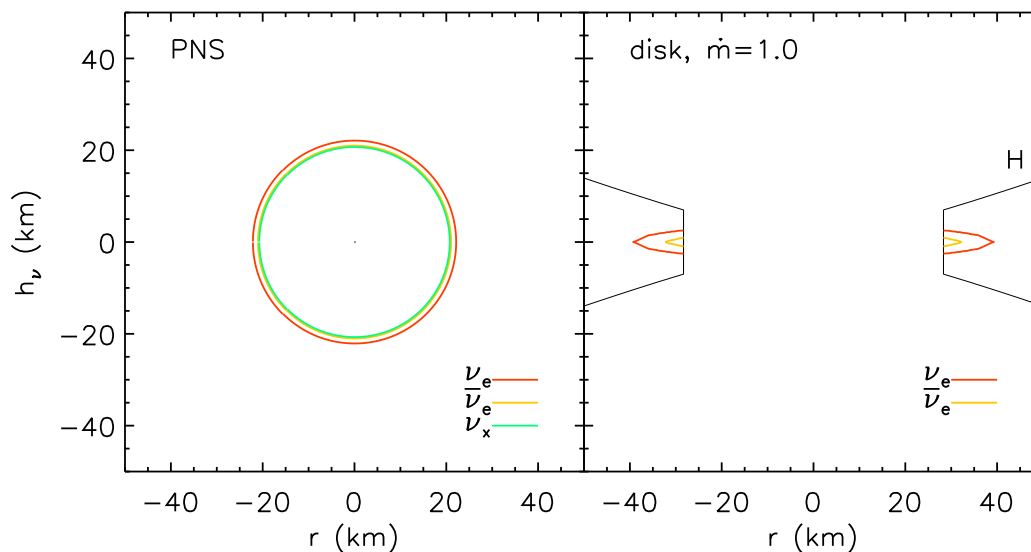


**Figure 2.** Shows the neutrino surfaces for a proto-neutron star and a  $1 M_{\odot}/s$  accretion disk. Figure from [21].

Nickel-56. In addition, for an intense  $\nu_e$  flux, with little  $\bar{\nu}_e$ , proton rich conditions would occur, while for the reverse situation, neutron rich conditions occur. Neutron rich conditions are favorable for the formation of the rapid neutron capture (r-process) elements. The observed abundance pattern of the heavy elements is shown in as the upper line in Fig. 3.

## 2. Proto-neutron Star Supernovae

Since the electron antineutrinos that are released from proton-neutron stars have slightly higher energy than the electron neutrinos, it was originally speculated that the “neutrino driven wind” of the supernova would be a good site for the r-process [4, 5]. However, self-consistent calculation shows that the standard scenario falls short of this expectation [6] as seen in by the lower left line in Fig 3.

The inclusion of one additional species of sterile neutrino which mixes with the electron

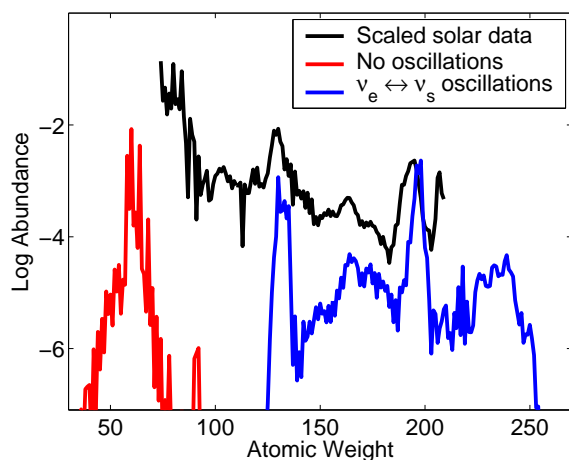


**Figure 3.** Abundance plot showing solar system data (top line), the nucleosynthesis products in a “standard” supernova neutrino driven wind (left line) and nucleosynthesis products when one sterile neutrino is included (lower right line) Figure from [9].

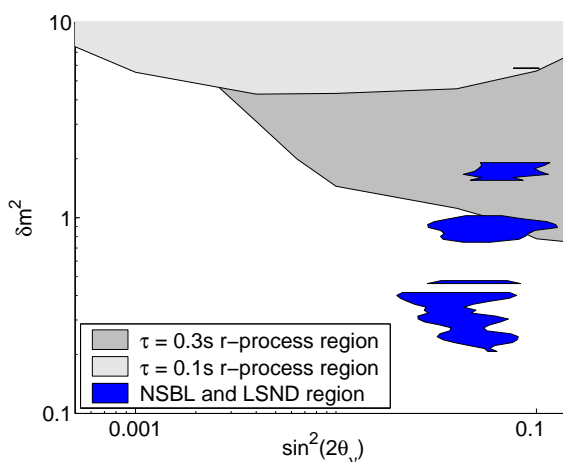


**Figure 4.** Shows the active sterile neutrino mixing parameter space which produces a rapid neutrino capture process for two different neutrino driven wind models. Also shown is the parameter space to be probed by MiniBooNE. Figure from [9]

neutrino can improve the situation [7, 8]. The lower right curve in Fig. 3 shows the nucleosynthesis products from a calculation which includes the mixing at the level of  $\delta m^2 = 2 \text{ eV}^2$ ,  $\sin^2 2\theta = 10^{-2}$ , for a neutrino driven wind with parameters entropy per baryon  $s = 100$ , and outflow timescale  $\tau = 0.3 \text{ s}$  [9]. The reason for this success is that the flux of electron neutrinos during the critical period of alpha particle formation is decreased, allowing the outflowing material to remain neutron rich. The parameter space which would allow for conditions which produce the r-process (in the absence of the inclusion of neutrino self interactions) is shown in Fig. 4 [9]. Part of this space is coincident with the positive LSND [10] result and will be tested in the future by MiniBooNE [11].

### 3. Accretion Disks

If accretion disks produce gamma ray bursts, the jet will occur on axis above the black hole, but there will be an additional much less relativistic outflow from the sides (see Fig. 1). For very rapidly accreting disks, the average energy of  $\nu_e$  is much less than that of the  $\bar{\nu}_e$  [12] and this much less relativistic outflow does become neutron rich [13]. It produces an r-process for a wide range of entropy,  $s$  and outflow conditions as can be seen in Fig. 5. In this figure we show the nucleosynthesis products for outflow coming from a disk accreting at a rate of  $10 M_\odot/s$  [14]. The peaks of the r-process distribution are labeled. The most complete r-process is labeled as  $A=195$ , while conditions which produce only the lightest r-process elements are labeled as  $A=80$ . The parameter  $\beta$  is a measure of the acceleration of the outflow. For small  $\beta$  the acceleration is the most rapid and the neutrinos have the smallest influence on the nucleosynthesis.

Such rapidly accreting disks are at present theoretically suggested to come from neutron star mergers [15, 16]. Lower accretion rate disks, of the order of  $0.1 M_\odot/s$  are predicted to come from the collapse of massive stars in the collapsar model [17, 18]. These disks produce a great deal of Nickel-56. One can see from Fig. 6 where the overproduction factors of Nickel are shown, that the amount of Nickel produced quite closely tracks the electron fraction (solid lines). Nickel-56 is an element which is important to produce in gamma ray bursts, since the supernova light curve “bumps” which are observed to occur with a few long duration gamma ray bursts, have

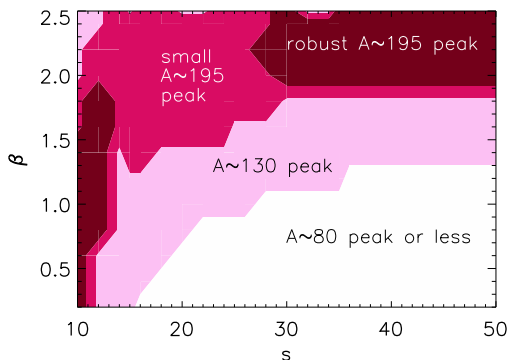


**Figure 5.** Shows the type of r-process produced by accretion disk outflow for a disk accreting at a rate of  $10 M_{\odot}/s$ . Figure from [12]

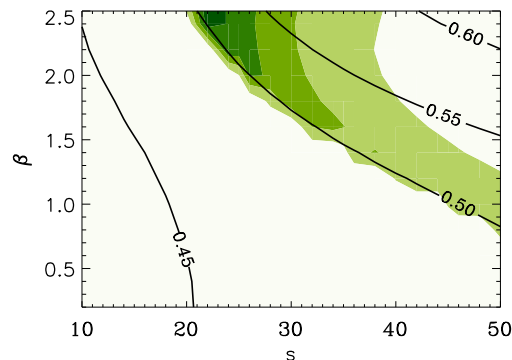


**Figure 6.** Shows the mass fraction of Nickel-56 from the outflow of a disk of  $0.1 M_{\odot}/s$ . Shaded Contours represent mass fractions greater than 0.1, 0.2, 0.3, 0.4, 0.5 From [12]

spectra which are associated with Type Ic supernova. The light curve of the supernova is driven by the decay of nickel to cobalt and then iron. In addition these disks may produce certain rare elements, including some p-process elements [19, 14, 20].

#### 4. Detection of Disk Neutrinos

The neutrinos from the accretion disks just discussed in the context of nucleosynthesis may also be considered in the context of supernova neutrino detection. Currently on line neutrino detectors would only detect these neutrinos if the event occurred within our Galaxy. Gamma ray bursts are several orders of magnitude more rare than supernovae, and at present one does not expect such an event to occur in our lifetime. However, it is likely that the rate of disk formation is considerably higher than the rate of burst formation, since not all disk may produce bursts.

If such a disk occurred in the Galaxy, it would produce events in currently on-line detectors. Rates of such events in the disk of our Galaxy in SuperKamiokande are given in Table 1. In comparison with the proto-neutron star supernova neutrinos the spectrum is quite similar (see Fig. 7).

Timescale and energetics are two possible ways to distinguish the proto-neutron star from the accretion disk. Total energetics however, would require a distance measurement to the object, which may be difficult as much of the Galaxy is obscured by dust. Neutrinos from the proto-neutron star are emitted on a characteristic diffusion timescale. The timescale of the accretion disk is set instead by the time the material is accreted onto the disk. Timescale is therefore an important observable, but uncertainties in the models of both the proto-neutron star supernova (fallback, black hole formation) and accretion disks (uncertain time in steady state), make it desirable to look for an additional test.

A better test is the flavor content of the neutrinos because the emitted flavor content of the neutrino signal would differ significantly in the cases of accretion disk neutrinos and proto-neutron star neutrinos. Proto-neutron stars produce neutrinos in all flavors with roughly equipartition of energy. In contrast, accretion disks produce primarily  $\nu_e$  and  $\bar{\nu}_e$ . Although oscillations will mix these spectra, it is unlikely that this mixing will mimic the roughly equipartition of energy of the proto-neutron star [21]. However in order to distinguish the two, in addition to a  $\bar{\nu}_e + p$  measurement, it is necessary to have a measurement in the  $\nu_e$  or neutral current channel, preferably both.

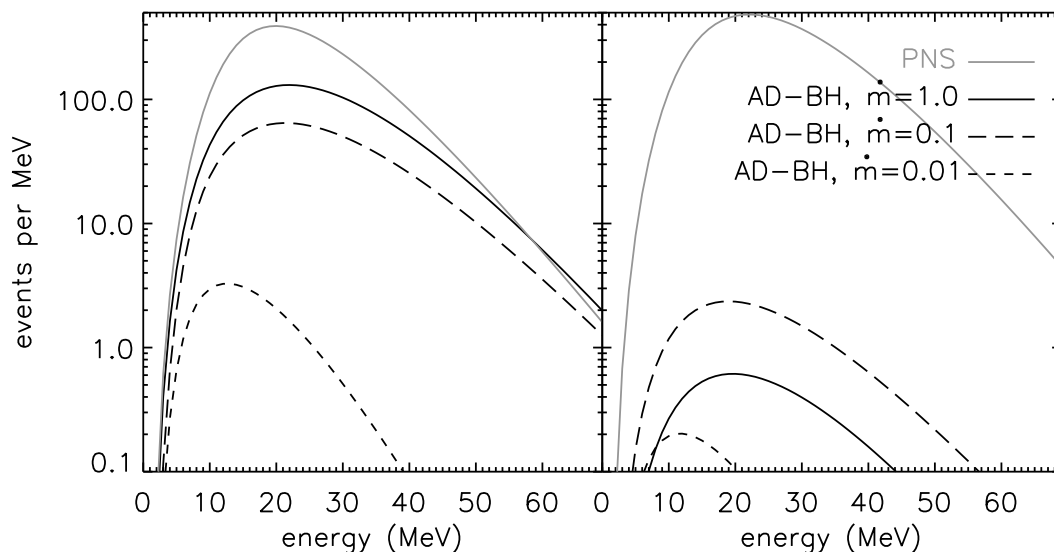


**Figure 7.** Comparison between the counts for  $\bar{\nu}_e + p \rightarrow e^+ + n$  at SuperKamiokande as a function of positron energy for the two oscillation scenarios. Plotted are the signals from the proto-neutron star and accretion disks ranging from  $0.01 M_\odot/s$  to  $1.0 M_\odot/s$ . With a normal hierarchy (left panel) and an inverted hierarchy (right panel). Figure from [21]

**Table 1.** Approximate numbers of events for a supernova with a proto-neutron star at 10 kpc and various accretion disks which process one solar mass of material at 10 kpc.

Type of Astrophysical Object	Events in Detector	Time
Protoneutron Star	7000	10 seconds
Accretion Disk of $\dot{M} = 1M_\odot/s$	2800	1 second
Accretion Disk of $\dot{M} = 0.1M_\odot/s$	1400	10 seconds
Accretion Disk of $\dot{M} = 0.01M_\odot/s$	50	100 seconds

## 5. Conclusions

Both proto-neutron stars and accretion disks produce nucleosynthesis in winds driven from their inner regions. The type of elements produced are strongly influenced by the neutrinos. In the proto-neutron star, the prospects for the production of the r-process elements are greatly improved by active sterile neutrino transformation. In the accretion disk scenario, the disk must be quite rapidly accreting to become hot enough to produce sufficiently neutron rich conditions to create the r-process elements. These disks would also produce a neutrino signal in currently on-line neutrino detectors, such as Super-Kamiokande.

## 6. Acknowledgments

This work was supported in part by the Department of Energy, under contract DE-FG02-02ER41216.

- [1] M. Liebendoerfer, M. Rampp, H. T. Janka and A. Mezzacappa, “Supernova simulations with Boltzmann neutrino transport: A comparison of *Astrophys. J.* **620**, 840 (2005) [arXiv:astro-ph/0310662].
- [2] P. Podsiadlowski, P. A. Mazzali, K. Nomoto, D. Lazzati and E. Cappellaro, *Astrophys. J.* **607**, L17 (2004) [arXiv:astro-ph/0403399].

- [3] J. Hjorth et al., *Nature* **437** 859 (2005).
- [4] B.S. Meyer et al, *Astrophys J.* **399** 656 (1992).
- [5] S. E. Woosley, J. R. Wilson, G. J. Mathews, R. D. Hoffman and B. S. Meyer, *Astrophys. J.* **433**, 229 (1994).
- [6] B. S. Meyer, G. C. McLaughlin and G. M. Fuller, *Phys. Rev. C* **58**, 3696 (1998) [arXiv:astro-ph/9809242].
- [7] G. C. McLaughlin, J. M. Fetter, A. B. Balantekin and G. M. Fuller, “An Active-Sterile Neutrino Transformation Solution for r-Process *Phys. Rev. C* **59**, 2873 (1999) [arXiv:astro-ph/9902106].
- [8] J. Fetter, G. C. McLaughlin, A. B. Balantekin and G. M. Fuller, “Active-sterile neutrino conversion: Consequences for the r-process and *Astropart. Phys.* **18**, 433 (2003) [arXiv:hep-ph/0205029].
- [9] J. Beun, G. C. McLaughlin, R. Surman and W. R. Hix, “Fission cycling in supernova nucleosynthesis: Active-sterile neutrino *Phys. Rev. D* **73**, 093007 (2006) [arXiv:hep-ph/0602012].
- [10] C. Athanassopoulos *et al.* [LSND Collaboration], *Phys. Rev. C* **54**, 2685 (1996) [arXiv:nucl-ex/9605001].
- [11] M.K. Sharp, J.F. Beacom, J.A. Formaggio, *Phys. Rev. D* **66**, 013012 (2002).
- [12] R. Surman and G. C. McLaughlin, *Astrophys. J.* **603**, 611 (2004) [arXiv:astro-ph/0308004].
- [13] R. Surman and G. C. McLaughlin, “Neutrino interactions in the outflow from gamma ray burst accretion *Astrophys. J.* **618**, 397 (2004) [arXiv:astro-ph/0407206].
- [14] R. Surman, G. C. McLaughlin and W. R. Hix, *Astrophys. J.* **643**, 1057 (2006) [arXiv:astro-ph/0509365].
- [15] M. Ruffert and H. T. Janka, arXiv:astro-ph/9809280.
- [16] S. Rosswog, arXiv:astro-ph/0508138.
- [17] A. MacFadyen and S. E. Woosley, *Astrophys. J.* **524**, 262 (1999) [arXiv:astro-ph/9810274].
- [18] D. Proga, A. I. MacFadyen, P. J. Armitage and M. C. Begelman, *AIP Conf. Proc.* **727**, 384 (2004)
- [19] J. Pruet, R. Surman and G. C. McLaughlin, “On the Contribution of Gamma Ray Bursts to the Galactic Inventory of Some *Astrophys. J.* **602**, L101 (2004) [arXiv:astro-ph/0309673].
- [20] S. i. Fujimoto, M. a. Hashimoto, K. Kotake and S. Yamada, arXiv:astro-ph/0602460.
- [21] G. C. McLaughlin and R. Surman, arXiv:astro-ph/0605281.

# Getting the most from NO $\nu$ A and T2K

**Olga Mena**

Theoretical Physics Department, Fermi National Accelerator Laboratory, P.O.Box 500,  
Batavia, IL 60510, USA

E-mail: omena@fnal.gov

**Abstract.** The determination of the ordering of the neutrino masses (the hierarchy) is probably a crucial prerequisite to understand the origin of lepton masses and mixings and to establish their relationship to the analogous properties in the quark sector. In this talk, we follow an alternative strategy to the usual neutrino–antineutrino comparison: we exploit the combination of the neutrino-only data from the NO $\nu$ A and the T2K experiments by performing these two off-axis experiments at different distances but at the same  $\langle E \rangle / L$ ,  $\langle E \rangle$  being the mean neutrino energy and  $L$  the baseline. This would require a minor adjustment to the proposed off-axis angle for one or both of the proposed experiments.

## 1. Introduction

During the last several years the physics of neutrinos has achieved a remarkable progress. The experiments with solar [1, 2, 3, 4, 5, 6], atmospheric [7], reactor [8], and also long-baseline accelerator [9, 11] neutrinos, have provided compelling evidence for the existence of neutrino oscillations, implying non zero neutrino masses. The data quoted above require two large mixing angles ( $\theta_{12}$  and  $\theta_{23}$ ) and may involve a small third one ( $\theta_{13}$ ) in the neutrino mixing matrix and two mass squared differences,  $\Delta m_{ji}^2 \equiv m_j^2 - m_i^2$ , with  $m_{j,i}$  the neutrino masses, one driving the atmospheric ( $\Delta m_{31}^2$ ) and the other one the solar ( $\Delta m_{21}^2$ ) neutrino oscillations. The mixing angles  $\theta_{12}$  and  $\theta_{23}$  control the solar and the atmospheric neutrino oscillations, while  $\theta_{13}$  is the angle limited by the data from the CHOOZ and Palo Verde reactor experiments [12, 13].

The Super-Kamiokande [7] and K2K [9] data are well described in terms of dominant  $\nu_\mu \rightarrow \nu_\tau$  ( $\bar{\nu}_\mu \rightarrow \bar{\nu}_\tau$ ) vacuum oscillations. The MINOS Collaboration has recently reported their first neutrino oscillation results from  $1.27 \times 10^{20}$  protons on target exposure of the MINOS far detector [11]. A recent global fit [14] (see also Ref. [15]) provides the following  $3\sigma$  allowed ranges for the atmospheric mixing parameters:

$$|\Delta m_{31}^2| = (1.9 - 3.2) \times 10^{-3} \text{eV}^2, \quad 0.34 < \sin^2 \theta_{23} < 0.68 . \quad (1)$$

The sign of  $\Delta m_{31}^2$ ,  $\text{sign}(\Delta m_{31}^2)$ , cannot be determined with the existing data. The two possibilities,  $\Delta m_{31}^2 > 0$  or  $\Delta m_{31}^2 < 0$ , correspond to two different types of neutrino mass ordering: normal hierarchy and inverted hierarchy. In addition, information on the octant in which  $\theta_{23}$  lies, if  $\sin^2 2\theta_{23} \neq 1$ , is beyond the reach of present experiments.

The 2-neutrino oscillation analysis of the solar neutrino data, in combination with the KamLAND spectrum data [16], shows that the solar neutrino oscillation parameters lie in the low-LMA (Large Mixing Angle) region, with best fit values [14]  $\Delta m_{21}^2 = 7.9 \times 10^{-5} \text{eV}^2$  and  $\sin^2 \theta_{12} = 0.30$ .

A combined 3-neutrino oscillation analysis of the solar, atmospheric, reactor and long-baseline neutrino data [14] constrains the third mixing angle to be  $\sin^2 \theta_{13} < 0.041$  at the  $3\sigma$  C.L.

The future goals in the study of neutrino properties will be to measure precisely the already known oscillation parameters and to obtain information on the unknown ones, namely  $\theta_{13}$ , the CP-violating phase  $\delta$  and the neutrino mass hierarchy (or equivalently  $\text{sign}(\Delta m_{31}^2)$ ). In this talk [17], we concentrate on the extraction of the neutrino mass hierarchy by combining the Phase I (neutrino-data only) of the long-baseline  $\nu_e$  appearance experiments T2K [18] and NO $\nu$ A [19], both exploiting the off-axis technique [20]. For our analysis, unless otherwise stated, we will use a representative value of  $|\Delta m_{31}^2| = 2.4 \times 10^{-3} \text{ eV}^2$  and  $\sin^2 2\theta_{23} = 1$ . For the solar oscillation parameters  $\Delta m_{21}^2$  and  $\theta_{12}$ , we will use the best fit values quoted in this introductory section.

## 2. Formalism

The mixing angle  $\theta_{13}$  controls  $\nu_\mu \rightarrow \nu_e$  and  $\bar{\nu}_\mu \rightarrow \bar{\nu}_e$  conversions in long-baseline  $\nu_e$  appearance experiments and the  $\bar{\nu}_e$  disappearance in short-baseline reactor experiments. Present and future reactor neutrino experiments [21], conventional neutrino beams and future long baseline neutrino experiments could measure, or set a stronger limit on,  $\theta_{13}$ . Therefore, with the possibility of the first measurement of  $\theta_{13}$  being made by a 1-to 2-km baseline reactor experiment, the long-baseline off-axis  $\nu_e$  appearance experiments, T2K [18] and NO $\nu$ A [19], need to adjust their focus to emphasize other physics topics. The most important of these questions is the form of the mass hierarchy, normal versus inverted and the measurement of leptonic CP violation, which in a three neutrino oscillation framework is directly related to the existence of a CKM-like CP-phase,  $\delta$ . Consider the probability  $P(\nu_\mu \rightarrow \nu_e)$  in the context of three-neutrino mixing in the presence of matter [22], represented by the matter parameter  $a$ , defined as  $a \equiv G_F n_e / \sqrt{2}$ , where  $n_e$  is the average electron number density over the baseline, taken to be constant throughout the present study. Defining  $\Delta_{ij} \equiv \frac{\Delta m_{ij}^2 L}{4E}$ , a convenient and precise approximation is obtained by expanding to second order in the following small parameters:  $\theta_{13}$ ,  $\Delta_{21}/\Delta_{32}$ ,  $\Delta_{21}/aL$  and  $\Delta_{21}$ . The result is (details of the calculation can be found in Ref. [23], see also Ref. [24])<sup>1</sup>:

$$P_{\nu_\mu \nu_e} \simeq \left| \sin \theta_{23} \sin 2\theta_{13} \left( \frac{\Delta_{31}}{\Delta_{31} - aL} \right) \sin(\Delta_{31} - aL) e^{-i(\Delta_{32} + \delta)} + \cos \theta_{23} \sin 2\theta_{12} \left( \frac{\Delta_{21}}{aL} \right) \sin(aL) \right|^2 \quad (2)$$

where  $L$  is the baseline and  $a \rightarrow -a$ ,  $\delta \rightarrow -\delta$  for  $P_{\bar{\nu}_\mu \bar{\nu}_e}$ . Suppose  $P_{\nu_\mu \nu_e} < P_{\bar{\nu}_\mu \bar{\nu}_e}$ : in vacuum, this implies CP violation. On the other hand, in matter, this implies CP violation only for the normal hierarchy but not necessarily for the inverted hierarchy around the first oscillation maximum. The different index of refraction for neutrinos and antineutrinos induces differences in the  $\nu$ ,  $\bar{\nu}$  propagation that could be misinterpreted as CP violation [25]. Typically, the proposed long baseline neutrino oscillation experiments have a single detector and plan to run with the beam in two different modes, neutrinos and antineutrinos. In principle, by comparing the probability of neutrino and antineutrino flavor conversion, the values of the CP-violating phase  $\delta$  and of  $\text{sign}(\Delta m_{31}^2)$  could be extracted. However, different sets of values of CP-conserving and violating parameters,  $(\theta_{13}, \theta_{23}, \delta, \text{sign}(\Delta m_{31}^2))$ , lead to the same probabilities of neutrino and antineutrino conversion and provide a good description of the data at the same confidence level. This problem is known as the problem of degeneracies in the neutrino parameter space [26, 27, 28, 29, 30] and severely affects the sensitivities to these parameters in future long-baseline experiments. Many strategies have been advocated to resolve this issue. Some of the degeneracies might be eliminated with sufficient energy or baseline spectral information. In practice, statistical errors and realistic efficiencies and backgrounds limit considerably the

<sup>1</sup> The author would like to thank S. Parke for the shorter version of the oscillation probability below.

capabilities of this method. Another detector [27, 31, 32, 33, 34] or the combination with another experiment [35, 36, 37, 38, 39, 40, 41, 42, 43, 44] would, thus, be necessary.

The use of only a neutrino beam could help in resolving the type of hierarchy when two different long-baselines are considered [36, 37, 45, 46]. It was shown in ref. [37] that if the  $\langle E \rangle / L$  for the two different experiments is approximately the same then the allowed regions for the two hierarchies are disconnected and thus this method for determining the hierarchy is free of degeneracies. Naively, we can understand this method in the following way for  $\sin^2 2\theta_{13} > 0.01$ : assume that matter effects are negligible for the short baseline, then at the same  $\langle E \rangle / L$ , if the oscillation probability at the long baseline is larger than the oscillation probability at the short baseline, one can conclude that the hierarchy is normal, since matter effects enhance the neutrino oscillation probabilities for the normal hierarchy. For the inverted hierarchy the oscillation probability for the long baseline is suppressed relative to the short baseline

### 3. Our strategy: only neutrino running and two detectors

Following the line of thought developed by Minakata, Nunokawa and Parke [37], we exploit the neutrino data from two experiments at different distances and at different off-axis locations [17]. The off-axis location of the detectors and the baseline must be chosen such that the  $\langle E \rangle / L$  is the same for the two experiments. Here we explain the advantages of such an strategy versus the commonly exploited neutrino-antineutrino comparison.

Suppose we compute the oscillation probabilities  $P_{\nu_\mu \nu_e}$  and  $P_{\bar{\nu}_\mu \bar{\nu}_e}$  for a given set of oscillation parameters and the CP-phase  $\delta$  is varied between 0 and  $2\pi$ : we obtain a closed CP trajectory (an ellipse) in the bi-probability space of neutrino and antineutrino conversion [28]. In general, the ellipses overlap for a large fraction of values of the CP-phase  $\delta$  for every allowed value of  $\sin^2 2\theta_{13}$ . This indicates that, generically, a measurement of the probability of conversion for neutrinos and antineutrinos cannot uniquely determine the type of hierarchy in a single experiment. This makes the determination of  $\text{sign}(\Delta m_{31}^2)$  extremely difficult, i. e., the  $\text{sign}(\Delta m_{31}^2)$ -extraction is not free of degeneracies.

In the case of bi-probability plots of neutrino-neutrino conversions at different distances (which will be referred as near (N) and far (F)), the overlap of the two bands, which implies the presence of a degeneracy of the type of hierarchy with other parameters, is controlled by the slope and the width of the bands. Using the fact that matter effects are small ( $aL \ll \Delta_{13}$ ), we can perform a perturbative expansion and assuming that the  $\langle E \rangle / L$  of the near and far experiments is the same, at first order, the ratio of the slopes reads [37]

$$\frac{\alpha_+}{\alpha_-} \simeq 1 + 4(a_N L_N - a_F L_F) \left( \frac{1}{\Delta_{31}} - \frac{1}{\tan(\Delta_{31})} \right), \quad (3)$$

where  $\alpha_+$  and  $\alpha_-$  are the slopes for normal and inverted hierarchies, and  $a_F$  and  $a_N$  are the matter parameters for the two experiments. The separation among the ellipses for the two hierarchies increases as the matter parameter times the path length for the two experiments does. The width of the ellipses is crucial: even when the separation between the central axes of the two regions is substantial, unless the ratio  $\langle E \rangle / L$  is kept close to constant, the width of the ellipses will grow rapidly and the ellipses will overlap. Consequently, we have to satisfy two conditions in order to optimize the determination of the neutrino mass hierarchy: (a) maximize the difference in the factor  $aL$  for both experiments and (b) minimize the ellipses width by performing the two experiments at the same  $\langle E \rangle / L$ .

The most promising way to optimize the sensitivity to the hierarchy with relatively near term data is therefore to focus on the neutrino running mode and to exploit the Phase I data of the long-baseline off-axis  $\nu_e$  appearance experiments, T2K and NO $\nu$ A. T2K utilizes a steerable neutrino beam from JHF and Super-Kamiokande and/or Hyper-Kamiokande as the far detector. The beam will peak at 0.65 GeV by placing the detector off-axis by an angle of  $2.5^\circ$  at 295 km.

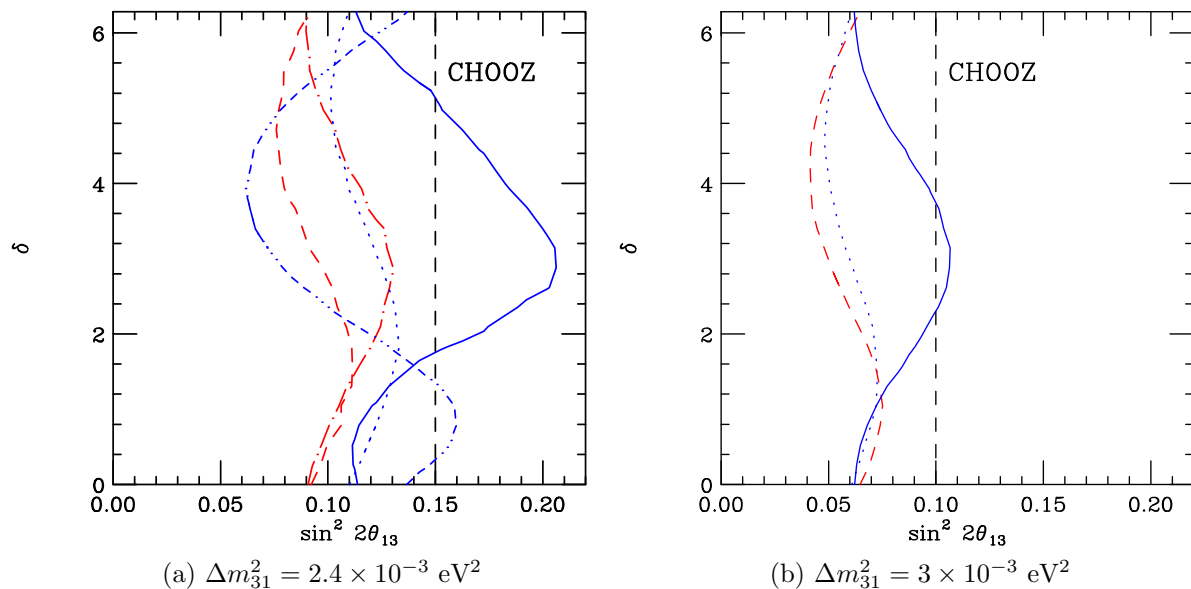


**Figure 1.** (a) 90% CL hierarchy resolution (2 d.o.f) for different possible combinations: the default one (T2K at an off-axis angle of  $2.5^\circ$  and NO $\nu$ A far detector at 12 km off-axis, in solid blue), T2K at an off-axis angle of  $2.5^\circ$  and NO $\nu$ A far detector at 13 km off-axis (long dash-dot red curve), at 14 km off-axis (short dashed red curve), at 16 km off-axis (three dots-three dashes blue curve) and T2K at an off-axis angle of  $2^\circ$  and NO $\nu$ A far detector at 12 km off-axis (dotted blue curve). (b) The same as (a) but assuming that  $\Delta m_{31}^2 = 3.0 \times 10^{-3} \text{ eV}^2$  and only for the three most representative combinations.

NO $\nu$ A proposes to use the Fermilab NuMI beam with a baseline of 810 km with a 30 kton low density tracking calorimeter with an efficiency of 24%. Such a detector would be located 12 km off-axis, resulting in a mean neutrino energy of 2 GeV. While for the T2K experiment matter effects are non negligible, albeit small [47], matter effects are quite significant for NO $\nu$ A. Therefore, the condition (a) is satisfied, since  $(aL)_{\text{NO}\nu\text{A}} \simeq 3(aL)_{\text{T2K}}$ . What about the condition (b)? A back-of-the-envelope calculation indicates that the current off-axis detector locations are not such that  $\langle E \rangle / L$  of the two experiments is the same. However, by placing the detector(s) in slightly different off-axis location(s), one can manage the  $\langle E \rangle / L$  of the two experiments to be exactly the same. This neutrino-data strategy would only need half of the time of data taking (because we avoid the antineutrino running), when compared to the standard one (i.e. running in neutrinos and antineutrinos at a fixed energy,  $E$ , and baseline,  $L$ ).

#### 4. Optimizing the NO $\nu$ A and T2K detector locations

In this section we present what could be achieved if NO $\nu$ A and T2K setups are carefully chosen, focusing on the physics potential of the combination of their future data. We define the Phase I of the experiments as follows. For the T2K experiment, we consider 5 years of neutrino running and SK as the far detector with a fiducial mass of 22.5 kton and 70% detection efficiencies. For the NO $\nu$ A experiment, we assume  $6.5 \times 10^{20}$  protons on target per year, 5 years of neutrino running and the detector described in the previous section.

We summarize the results in Figs. (1), where we present the exclusion plots in the  $(\sin^2 2\theta_{13}, \delta)$  plane for a measurement of the hierarchy at the 90% CL for the several possible combinations, assuming that nature's solution is the normal hierarchy and  $\Delta m_{31}^2 = 2.4 \times 10^{-3} \text{ eV}^2$  (left panel) and  $\Delta m_{31}^2 = 3 \times 10^{-3} \text{ eV}^2$  (right panel) (in light of the recent MINOS results, we explore here

the impact of a larger  $\Delta m_{31}^2$ ). We show as well the corresponding CHOOZ bound for  $\sin^2 2\theta_{13}$ . A larger value of  $\Delta m_{31}^2$  implies more statistics and consequently a sensitivity improvement: see Fig. (1) (b), where for the sake of illustration only the three most representative configurations are shown.

If both T2K and NO $\nu$ A run in their *default* configurations the combination of their future Phase I data (only neutrinos) will not contribute much to our knowledge of the neutrino sector, see the solid blue line in Figs. (1). If we fix the T2K off-axis location to its *default* value of  $2.5^\circ$  but we change the location of the NO $\nu$ A detector to 14 km the improvement is quite remarkable, see the short dashed red line in Figs. (1): the sensitivity to the mass hierarchy has a milder dependence on the CP-phase  $\delta$  once that the  $\langle E \rangle/L$  of the two experiments is chosen to be the same. The best sensitivity to the hierarchy extraction is clearly achieved when the NO $\nu$ A experiment is at 14 km off-axis and the T2K off-axis angle is the *default* one. If the T2K off-axis angle is slightly modified to  $2^\circ$ , see the dotted lines in Figs. (1) it would be possible to reproduce the results from the combination of the data from T2K located at  $2.5^\circ$  off-axis and the NO $\nu$ A detector placed at 13 km off-axis.

The combination of data from an upgraded phase (Phase II) of the T2K and/or NO $\nu$ A experiments (by increasing the proton luminosities, the years of neutrino running and/or the mass of the far detectors) will obviously increase the statistics and will shift the sensitivity curves depicted in Fig. (1) (a), similarly to the effect of increasing  $\Delta m_{31}^2$ .

If the nature's choice for the neutrino mass ordering is the inverted hierarchy, the sensitivity curves depicted in Fig. (1) (a) will be shifted but in the opposite direction, making the case for the Phase II of both experiments stronger, especially if  $\Delta m_{31}^2 = 2.4 \times 10^{-3} \text{ eV}^2$ .

## 5. Conclusions

The most promising way to extract the neutrino mass hierarchy is to make use of the matter effects and exploit the neutrino data from two near-term long baseline  $\nu_e$  appearance experiments performed at the same  $\langle E \rangle/L$ , provided  $\sin^2 2\theta_{13}$  is within their sensitivity range or within the sensitivity range of the next-generation  $\bar{\nu}_e$  disappearance reactor neutrino experiments. Such a possibility could be provided by the combination of the data from the Phase I of the T2K and NO $\nu$ A experiments. We conclude that the optimal configuration for these experiments would be 14 km off-axis for the NO $\nu$ A far detector and  $2.5^\circ$  off-axis for the T2K experiment. The combination of their expected results could provide a 90% confidence level resolution of the neutrino mass hierarchy if  $\sin^2 2\theta_{13} > 0.11$  (for  $\Delta m_{31}^2 = 2.4 \times 10^{-3} \text{ eV}^2$ ) or if  $\sin^2 2\theta_{13} > 0.07$  (for  $\Delta m_{31}^2 = 3 \times 10^{-3} \text{ eV}^2$ ). A modest upgraded next Phase of both NO $\nu$ A and T2K experiments (by increasing a factor of five their expected Phase I statistics) could shift the 90% CL limits quoted above to  $\sin^2 2\theta_{13} > 0.03$  (for  $\Delta m_{31}^2 = 2.4 \times 10^{-3} \text{ eV}^2$ ) and to  $\sin^2 2\theta_{13} > 0.025$  (for  $\Delta m_{31}^2 = 3 \times 10^{-3} \text{ eV}^2$ ).

## Acknowledgments

The material presented here is based on work developed in collaboration with H. Nunokawa, S. Palomares-Ruiz, S. Parke and S. Pascoli. Fermilab is operated by URA under DOE contract DE-AC02-76CH03000.

## References

- [1] Cleveland B T *et al.* 1998 *Astrophys. J.* **496** 505; Fukuda Y *et al.* [Kamiokande Collaboration] 1996 *Phys. Rev. Lett.* **77** 1683; Abdurashitov J N *et al.* [SAGE Collaboration] 2002 *J. Exp. Theor. Phys.* **95** 181; Hampel W *et al.* [GALLEX Collaboration] 1999 *Phys. Lett. B* **447** 127; Kirsten T A [GNO Collaboration] 2003 *Nucl. Phys. Proc. Suppl.* **118** 33.
- [2] Fukuda S *et al.* [Super-Kamiokande Collaboration] 2002 *Phys. Lett. B* **539** 179
- [3] Ahmad Q R *et al.* [SNO Collaboration] 2001 *Phys. Rev. Lett.* **87** 071301
- [4] Ahmad Q R *et al.* [SNO Collaboration] 2002 *Phys. Rev. Lett.* **89** 011301; and *ibid.* **89** 011302.

- [5] Ahmed S N *et al.* [SNO Collaboration] 2004 *Phys. Rev. Lett.* **92** 181301
- [6] Aharmim B *et al.* [SNO Collaboration] 2005 *Phys. Rev. C* **72** 055502
- [7] Ashie Y *et al.* [Super-Kamiokande Collaboration] 2005 *Phys. Rev. D* **71** 112005
- [8] Eguchi K *et al.* [KamLAND Collaboration] 2003 *Phys. Rev. Lett.* **90** 021802
- [9] Ahn M H [K2K Collaboration] *Preprint* hep-ex/0606032
- [10] Ables E *et al.* [MINOS Collaboration] FERMILAB-PROPOSAL-0875.
- [11] MINOS Collaboration *Preprint* hep-ex/0607088.
- [12] Apollonio M *et al.* 1999 *Phys. Lett. B* **466** 415
- [13] Boehm F *et al.* 2000 *Phys. Rev. Lett.* **84** 3764 and *Phys. Rev. D* **62** 072002
- [14] Schwetz T *Preprint* hep-ph/0606060
- [15] Fogli G L *et al.* *Preprint* hep-ph/0608060
- [16] Araki T *et al.* [KamLAND Collaboration] 2005 *Phys. Rev. Lett.* **94** 081801
- [17] Mena O, Nunokawa H and Parke S *Preprint* hep-ph/0609011
- [18] Hayato Y *et al.*, Letter of Intent, available at <http://neutrino.kek.jp/jhfnu/>
- [19] Ayres D S *et al.* [NOvA Collaboration] *Preprint* hep-ex/0503053
- [20] Para A and Szleper M *Preprint* hep-ex/0110032
- [21] Anderson K *et al.* *Preprint* hep-ex/0402041 Ardellier F *et al.* *Preprint* hep-ex/0405032 Abouzaid E *et al.* "Report of the APS Neutrino Study Reactor Working Group", LBNL-56599, available at <http://www-library.lbl.gov/docs/LBNL/565/99/>; Huber P *et al.* "From Double Chooz to Triple Chooz: Neutrino physics at the Chooz reactor 2006" *JHEP* **0605** 072
- [22] Wolfenstein L 1978 *Phys. Rev. D* **17** 2369; Barger V D, Whisnant K, Pakvasa S and Phillips R J N 1980 *Phys. Rev. D* **22** 2718; Mikheev S P and Smirnov A Y 1985 *Sov. J. Nucl. Phys.* **42** 913; Parke S J 1986 *Phys. Rev. Lett.* **57** 1275; Zaglauer H W and Schwarzer K H 1988 *Z. Phys. C* **40** 273; Banuls M C, Barenboim G and Bernabeu J 2001 *Phys. Lett. B* **513** 391; Freund M, Lindner M, Petcov S T and Romanino A 2000 *Nucl. Phys. B* **578** 27
- [23] Cervera A *et al.* 2000 *Nucl. Phys. B* **579** 17 [Erratum-*ibid.* 2001 B **593** 731]
- [24] Akhmedov E K *et al.* 2004 *JHEP* **0404**, 078
- [25] Arafune J, Koike M and Sato J 1997 *Phys. Rev. D* **56** 3093 [Erratum-*ibid.* 1999 D **60**, 119905]; Minakata H and Nunokawa H 1997 *Phys. Lett. B* **413** 369; Donini A *et al.* 2000 *Nucl. Phys. B* **574** 23
- [26] Fogli G L and Lisi E 1996 *Phys. Rev. D* **54** 3667
- [27] Burguet-Castell J *et al.* 2001 *Nucl. Phys. B* **608** 301
- [28] Minakata H and Nunokawa H 2001 *JHEP* **0110** 001
- [29] Barger V Marfatia D and Whisnant K 2002 *Phys. Rev. D* **65** 073023
- [30] Kajita T, Minakata H and Nunokawa H 2002 *Phys. Lett. B* **528** 245; Minakata H, Nunokawa H and Parke S J 2002 *Phys. Rev. D* **66** 093012; Freund M, Huber P and Lindner M 2001 *Nucl. Phys. B* **615** 331; Huber P, Lindner M and Winter W 2002 *Nucl. Phys. B* **645** 3; Donini A, Meloni D and Rigolin S 2004 *JHEP* **0406** 011; Aoki M, Hagiwara K and Okamura N 2005 *Phys. Lett. B* **606** 371; Yasuda O 2004 *New J. Phys.* **6** 83;
- [31] Minakata H and Nunokawa H 1997 *Phys. Lett. B* **413** 369;
- [32] Donini A, Meloni D and Migliozi P 2002 *Nucl. Phys. B* **646** 321; Autiero D *et al.* 2004 *Eur. Phys. J. C* **33** 243
- [33] Barger V, Marfatia D and Whisnant K 2002 *Phys. Rev. D* **66** 053007
- [34] Ishitsuka M *et al.* 2005 *Phys. Rev. D* **72** 033003; Hagiwara K, Okamura N and Senda K 2006 *Phys. Lett. B* **637** 266
- [35] Burguet-Castell J *et al.* 2002 *Nucl. Phys. B* **646** 301
- [36] Huber P, Lindner M and Winter W 2003 *Nucl. Phys. B* **654** 3
- [37] Minakata H, Nunokawa H and Parke S J 2003 *Phys. Rev. D* **68** 013010
- [38] Barger V, Marfatia D and Whisnant K 2003 *Phys. Lett. B* **560** 75
- [39] Whisnant K, Yang J M and Young B L 2003 *Phys. Rev. D* **67** 013004; Huber P *et al.* 2003 *Nucl. Phys. B* **665** 487; Huber P *et al.* 2004 *Phys. Rev. D* **70** 073014; Donini A *et al.* 2005 *Nucl. Phys. B* **710** 402; ; Donini A, Fernández-Martínez E and Rigolin S 2005 *Phys. Lett. B* **621** 276 Narayan M and Uma Sankar S 2000 *Phys. Rev. D* **61** 013003
- [40] Mena O and Parke S J 2004 *Phys. Rev. D* **70** 093011
- [41] Huber P, Maltoni M and Schwetz T 2005 *Phys. Rev. D* **71** 053006
- [42] Mena O 2005 *Mod. Phys. Lett. A* **20** 1
- [43] Huber P *et al.* *Preprint* hep-ph/0606119
- [44] Blondel A *et al.* *Preprint* hep-ph/0606111
- [45] Mena Requejo O, Palomares-Ruiz S and Pascoli S 2005 *Phys. Rev. D* **72** 053002;
- [46] Mena Requejo O, Palomares-Ruiz S and Pascoli S 2006 *Phys. Rev. D* **73** 073007

[47] Aoki M, Hagiwara K and Okamura N 2003 *Phys. Lett. B* **554** 121

# Phenomenology of neutrinoless double beta decay

**Martin Hirsch**

AHEP Group, IFIC/CSIC, Edificio Institutos de Paterna, Apt 22085, E-46071 Valencia, Spain

E-mail: mahirsch@ific.uv.es

**Abstract.** Neutrinoless double beta decay ( $0\nu\beta\beta$ ) violates lepton number by two units, a positive observation therefore necessarily implies physics beyond the standard model. Here, three possible contributions to  $0\nu\beta\beta$  decay are briefly reviewed: (a) The mass mechanism and its connection to neutrino oscillations; (b) Left-right symmetric models and the lower limit on the right-handed  $W$  boson mass; and (c) R-parity violating supersymmetry. In addition, the recently published “extended black box” theorem is briefly discussed. Combined with data from oscillation experiments this theorem provides proof that the  $0\nu\beta\beta$  decay amplitude must receive a non-zero contribution from the mass mechanism, if neutrinos are indeed Majorana particles.

## 1. Introduction

Since the discovery of neutrino oscillations [1] most papers on neutrinoless double beta decay ( $0\nu\beta\beta$ ) have exclusively concentrated on its implications for Majorana neutrino masses. However, as is well-known, *any* model beyond the standard model of particle physics, which allows for lepton number violation, potentially contributes to  $0\nu\beta\beta$  decay. Thus, the basic physics of  $0\nu\beta\beta$  decay can be summarized as:

$$\left[T_{1/2}^{0\nu\beta\beta}\right]^{-1} = \left(\sum_i \langle\epsilon_i\rangle \mathcal{M}_{\epsilon_i}\right)^2 F^{0\nu\beta\beta}. \quad (1)$$

The factor  $\langle\epsilon_i\rangle$  contains some (unknown, but lepton number violating) particle physics parameters. To determine the numerical value of  $\langle\epsilon_i\rangle$  input from both, experiment and theoretical nuclear physics, is needed. Experiments limit (or measure)  $T_{1/2}^{0\nu\beta\beta}$ , for a discussion of various different experiments see, for example [2].  $\mathcal{M}_{\epsilon_i}$  in eq. (1) stands for a nuclear structure matrix element. Different particle physics contributions to  $0\nu\beta\beta$  decay depend on different matrix elements. No definite consensus about the value and, most importantly, the error of nuclear matrix elements exist up to now. For a thorough discussion see [3]. Finally,  $F^{0\nu\beta\beta}$  is a leptonic phase space integral, its value can be calculated quite precisely [4].

This talk concentrates exclusively on particle physics aspects of  $0\nu\beta\beta$  decay. The classic “black box” [5] theorem and its recently published “extended” version [6] are briefly discussed, before reviewing constraints on left-right symmetric models and supersymmetry with R-parity violation derived from a lower limit on the  $0\nu\beta\beta$  decay half-life. Last but not least, expectations for the mass mechanism of  $0\nu\beta\beta$  decay in light of neutrino oscillation data are discussed. It is curious to note, that combining the “extended black box” with oscillation data [6] already today demonstrates that there must be a non-zero contribution from the mass mechanism to the  $0\nu\beta\beta$  decay amplitude, if neutrinos are indeed Majorana particles.

## 2. $0\nu\beta\beta$ decay and the Black Box

From the experimental point of view lepton number violation in  $0\nu\beta\beta$  decay is observed through the appearance of two electrons in the final state with **no** missing energy. Many different, possible mechanisms have been discussed in the literature. Interestingly, however, one can show [5] that independent of which contribution to  $0\nu\beta\beta$  decay is the dominant one, neutrinos are guaranteed to have a non-zero Majorana mass, if  $0\nu\beta\beta$  decay is observed. The proof of this “black box” theorem [5] essentially follows from the observation that any effective low-energy  $\Delta L \neq 0$  operator inducing  $0\nu\beta\beta$  decay will contribute also - possibly at the some order in perturbation theory, for sure in some higher order - to the  $(\nu_e - \nu_e)$  entry of the Majorana neutrino mass matrix ( $M_{ee}^\nu$ ). A perfect cancellation of all different contributions to  $M_{ee}^\nu$  would then require a special symmetry and the proof of the black box theorem is completed by showing that no such symmetry can exist [7] in any gauge model containing the standard model charged current interaction.

This well-known theorem has recently been extended to the case of three generations of neutrinos and arbitrary lepton number and lepton flavour violating processes [6]. Combined with data from oscillation experiments this “extended” black box theorem can be used to show that  $M_{ee}^\nu \neq 0$ . The proof involves two steps. In the first step it is shown that any effective operator generating lepton number violating processes of the form  $\Phi_k \rightarrow \Phi_m l_\alpha l_\beta$ , where  $\Phi_k$  and  $\Phi_m$  stand symbolically for any set of SM particles with  $L = 0$ , necessarily generates a non-zero  $M_{\alpha\beta}^\nu$  entry in the Majorana neutrino mass matrix in higher order of perturbation theory. As for the original black box, one can show that there is no possible symmetry allowing for a perfect cancellation of different contributions to this entry. In the second step, then all allowed neutrino mass matrices with  $M_{ee}^\nu \equiv 0$  are constructed. It is then easy to show that none of the possible five structures is consistent with oscillation data. One can thus conclude that  $M_{ee}^\nu \neq 0$  is guaranteed for Majorana neutrinos [6] already today.

The above theorem(s) do not state which mechanism of  $0\nu\beta\beta$  decay is the dominant one. Two instructive examples, in which the mass mechanism might indeed not be the dominant contribution to  $0\nu\beta\beta$  decay, are therefore discussed next.

### 2.1. Left-right symmetry

For  $0\nu\beta\beta$  decay, with its typical low energy scale of a few MeV, all calculations can be done with the effective Hamiltonian [4]

$$\mathcal{H}_W^{CC} = \frac{G_F}{\sqrt{2}} \left\{ J_{\mu L}^\dagger j_{\mu L}^- + \kappa J_{\mu R}^\dagger j_{\mu L}^- + \eta J_{\mu L}^\dagger j_{\mu R}^- + \lambda J_{\mu R}^\dagger j_{\mu R}^- \right\}. \quad (2)$$

Here,  $J_{\mu\alpha}^\dagger = \bar{u}\gamma_\mu d_\alpha$  and  $j_{\mu\alpha}^- = \bar{e}\gamma_\mu \nu_\alpha$  are the hadronic and leptonic charged currents,  $L/R$  stands for  $P_{L/R} = \frac{1}{2}(1 \mp \gamma_5)$ .  $G_F$  is the Fermi constant,  $\kappa \simeq \eta \simeq \tan \zeta$ , i.e. the mixing angle between the  $W_L$  and  $W_R$  bosons, and  $\lambda \simeq (m_{W_L}/m_{W_R})^2$ .

The Hamiltonian of eq. (2) gives rise to the diagrams in fig. (1). The graphs on the left and the middle represent so-called “long-range” contributions. The graph to the left is due to a product of two  $j_{\mu L}^-$  and corresponds to the mass mechanism of  $0\nu\beta\beta$  decay, proportional to  $\langle m_\nu \rangle = \sum_i U_{ei}^2 m_{\nu_i}$  (see discussion in the next section). The graph in the middle is proportional to  $\langle \lambda \rangle = \lambda \sum_i U_{ei} V_{ei}$  and  $\langle \eta \rangle = \eta \sum_i U_{ei} V_{ei}$ . The graph to the right is proportional to  $\langle \xi \rangle = \left[ \lambda^2 + \eta^2 - 2\lambda\eta \left( \frac{M_{GT}^N + M_F^N}{M_{GT}^N - M_F^N} \right) \right] / \langle m_N \rangle$  [8]. Here,  $\langle \frac{1}{m_N} \rangle = \sum_j V_{ej}^2 \left( \frac{m_p}{m_j} \right)$ .

Formally, the long-range contribution in LR models are suppressed only by one power of  $\lambda/\eta$ , compared to the short-range contribution, which is quadratic in  $\lambda/\eta$ . Many calculations therefore have taken into account only the long-range LR contributions. However, as first pointed out by Mohapatra [9] and confirmed by a detailed calculation of the relevant nuclear matrix elements [8], the short-range contribution can be much more important than the long-range one. This at

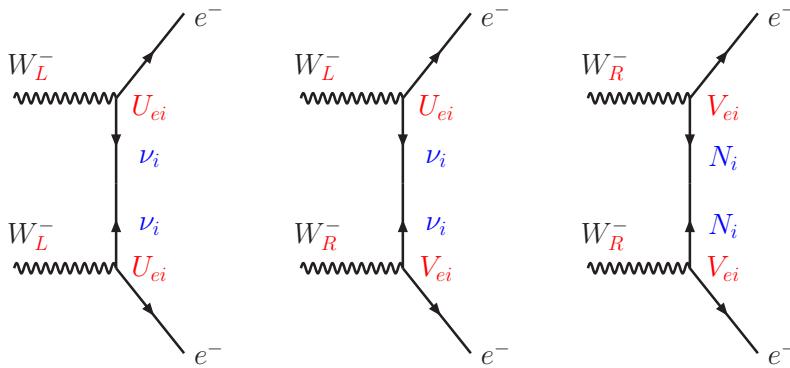


**Figure 1.** Leptonic parts of the  $0\nu\beta\beta$  decay amplitude in left-right symmetric models. The graph to the left represents the mass mechanism. The graph in the middle is long-range, but suppressed by  $\sum_i U_{ei}V_{ei}$ . The graph to the right is the so-called short range contribution for heavy Majorana neutrinos.

first sight contradictive statement can be easily understood. In left-right symmetric models the mixing between the active, left (and light) neutrinos with the heavy, sterile ones can be estimated “à la seesaw” to be very roughly of the order  $\sum_i U_{ei}V_{ei} \sim \frac{m_D}{M_M} \sim \sqrt{\frac{m_\nu}{M_M}}$ . Then, with a limit of  $\langle \lambda \rangle \lesssim 8 \cdot 10^{-7}$  one gets  $m_{W_R} \gtrsim 1.1 m_{W_L} \left(\frac{m_\nu}{1\text{eV}}\right)^{1/4} \left(\frac{M_M}{1\text{TeV}}\right)^{-1/4}$ . In the short range contribution, although some cancellation of terms in  $\langle m_N \rangle$  might occur, no such strong suppression is expected. From [8] and assuming a limit on the  $^{76}\text{Ge}$  half-life of  $T_{1/2}^{0\nu\beta\beta} \geq 1.2 \cdot 10^{25}$  ys a limit of

$$m_{W_R} \gtrsim 1.3 \left(\frac{\langle m_N \rangle}{[1\text{TeV}]}\right)^{-1/4} \text{ TeV} \quad (3)$$

can then be derived. Note that the limit disappears as  $\langle m_N \rangle$  goes to infinity, as it should. Note also that the uncertainty in this limit due to the uncertainty in the nuclear matrix element calculation scales only as  $\Delta m_{W_R} \sim (\Delta \mathcal{M})^{-1/4}$  and thus is quite insensitive to the details of the nuclear model.

## 2.2. R-parity violation

In the standard model lepton number is conserved, because there is (a) no right-handed neutrino and (b) only one Higgs doublet with  $L = 0$ . In supersymmetric models, on the other hand, if one does not assume lepton number conservation a priori, one can write down the following (trilinear) lepton number violating terms

$$\begin{aligned} \mathcal{L}_{\mathcal{R}P} = & - \lambda'_{ijk} \left[ (\tilde{u}_L \tilde{d}_R)_j \cdot \begin{pmatrix} e_R^c \\ -\nu_R^c \end{pmatrix}_i (\tilde{d}_R)_k + (\tilde{e}_L \tilde{\nu}_L)_i (d_R)_k \cdot \begin{pmatrix} \tilde{u}_L^* \\ -\tilde{d}_L^* \end{pmatrix}_j \right. \\ & \left. + (\tilde{u}_L \tilde{d}_L)_j (d_R)_k \cdot \begin{pmatrix} \tilde{e}_L^* \\ -\tilde{\nu}_L^* \end{pmatrix}_i + h.c. \right] \end{aligned} \quad (4)$$

Here, the tilde indicates the scalar superpartners of the usual quarks and leptons. A product of two of the terms in eq. (4), together with an MSSM neutralino and/or gluino interaction lead to  $0\nu\beta\beta$  decay diagrams without *any* virtual neutrinos being exchanged, as first pointed out in [10, 11]. A dedicated calculation of all diagrams [12], together with a limit of  $T_{1/2}^{0\nu\beta\beta} \geq 1.2 \cdot 10^{25}$  y for  $^{76}\text{Ge}$  leads to

$$\lambda'_{111} \leq 3.2 \times 10^{-4} \left(\frac{m_{\tilde{q}}}{100\text{GeV}}\right)^2 \left(\frac{m_g}{100\text{GeV}}\right)^{1/2}. \quad (5)$$

It is interesting to note, that such a small value of  $\lambda'_{111}$  generates at 1-loop level an entry in the Majorana neutrino mass matrix of  $M_{ee}^\nu \simeq 10^{-6}$  eV only.

### 3. Neutrino oscillations and $0\nu\beta\beta$ decay

If the mass mechanism is dominant, the  $0\nu\beta\beta$  decay half-life is proportional to the (square of the)  $(\nu_e - \nu_e)$  element of the Majorana neutrino mass matrix. For three generations of light neutrinos, this so-called “effective Majorana” mass can be expressed as:

$$M_{ee}^\nu \equiv \langle m_\nu \rangle = c_{12}^2 c_{13}^2 m_1 + s_{12}^2 c_{13}^2 e^{i\alpha} m_2 + s_{13}^2 e^{i\beta} m_3 \quad (6)$$

Eq.(6) contains a priori seven unknowns: Three mass eigenstates, two angles and two phases. With the help of data from neutrino oscillation experiments, one can trade two mass eigenstates for the observed  $\Delta m_{\text{Atm}}^2$  and  $\Delta m_{\odot}^2$  and relate the two angles to the solar ( $\theta_{\odot}$ ) and reactor angle ( $\theta_R$ ). For the case of normal hierarchy,  $m_{\nu_1} \leq m_{\nu_2} \leq m_{\nu_3}$ , eq.(6) can then be written as

$$\langle m_\nu \rangle = c_{\odot}^2 c_R^2 m_{\nu_1} + s_{\odot}^2 c_R^2 e^{i\alpha} \sqrt{m_{\nu_1}^2 + \Delta m_{\odot}^2} + s_R^2 e^{i\beta} \sqrt{m_{\nu_1}^2 + \Delta m_{\odot}^2 + \Delta m_{\text{Atm}}^2}, \quad (7)$$

while for the case of inverse hierarchy,  $m_{\nu_3} \leq m_{\nu_1} \leq m_{\nu_2}$ , it is given by

$$\langle m_\nu \rangle = c_{\odot}^2 c_R^2 \sqrt{m_{\nu_3}^2 - \Delta m_{\odot}^2 + \Delta m_{\text{Atm}}^2} + s_{\odot}^2 c_R^2 e^{i\alpha} \sqrt{m_{\nu_3}^2 + \Delta m_{\text{Atm}}^2} + s_R^2 e^{i\beta} m_{\nu_3} \quad (8)$$

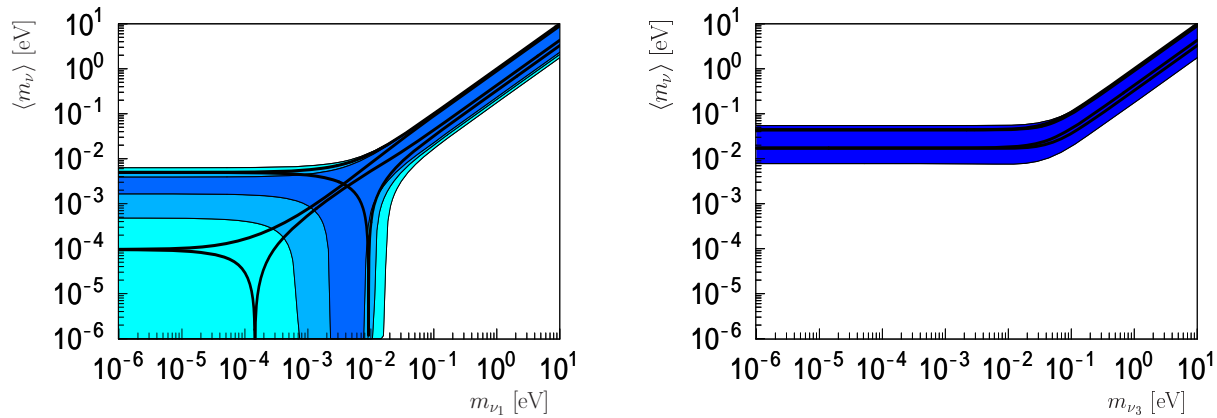


**Figure 2.** Allowed range of  $\langle m_\nu \rangle$  as a function of the lightest neutrino mass eigenvalue. To the left normal hierarchy, to the right inverse hierarchy. To calculate the allowed range of  $\langle m_\nu \rangle$  the  $3\sigma$  c.l. intervals on the oscillation parameters have been used [13], except for the case of normal hierarchy, for which 3 different cases for the upper limit on  $s_R^2$  are shown. These are  $s_R^2 \leq 0.04$  (light blue),  $s_R^2 \leq 0.025$  (medium blue),  $s_R^2 \leq 0.005$  (darker blue).

Fig. (2) shows the resulting allowed range of  $\langle m_\nu \rangle$  for both, normal and inverse hierarchy, taking into account the latest results from a global fit to all neutrino oscillation data [13]. The lower limit on  $\langle m_\nu \rangle$ , which appears in the case of inverse hierarchy, can be understood trivially. For  $m_{\nu_3} = 0$  and  $\alpha = \pi$  eq. (8) reads approximately

$$\langle m_\nu \rangle \simeq c_R^2 (c_{\odot}^2 - s_{\odot}^2) \sqrt{\Delta m_{\text{Atm}}^2}. \quad (9)$$

Thus, as soon as data tells us that  $s_{\odot}^2 < \frac{1}{2}$ , exact cancellation is no longer a possibility. This statement remains true for any finite  $m_{\nu_3}$ , simply because  $s_R^2 < \cos(2\theta_{\odot})$  is guaranteed by data nowadays. Fig. (3) shows how this lower limit evolves with future data from neutrino oscillation experiments. A possible future smaller upper bound on  $s_{\odot}^2$  would make it easier for  $0\nu\beta\beta$  decay experiments to rule out inverse hierarchy.

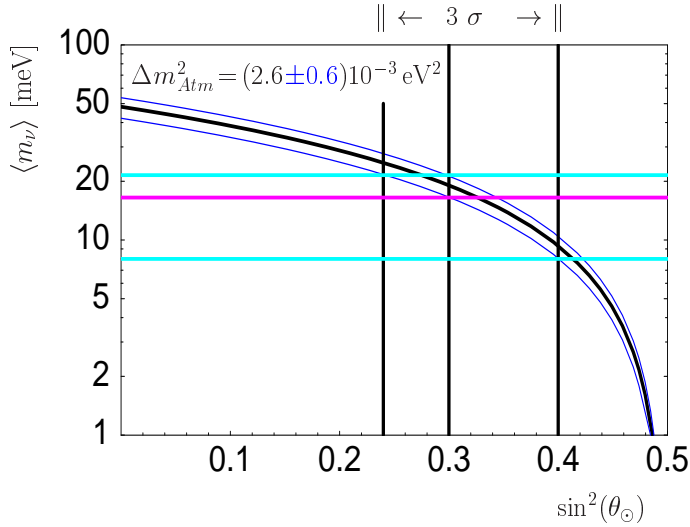


**Figure 3.** Lower Limit on  $\langle m_\nu \rangle$  in the case of inverse hierarchy as a function of the solar mixing angle  $\sin^2 \theta_\odot$  for three different values of  $\Delta m_{Atm}^2$ , i.e. best fit point  $\pm 3 \sigma$  allowed range. The vertical black lines indicate the current best fit point and the  $3 \sigma$  c.l. allowed range of  $s_\odot^2 \equiv \sin^2(\theta_\odot)$ . The worst case, i.e. the most conservative limit, is found for  $\sin^2 \theta_\odot^{\text{Max}}$  and  $(\Delta m_{Atm}^2)^{\text{Min}}$ , currently  $\langle m_\nu \rangle \geq 8$  meV.

There is no such simple quantitative lower limit for the case of normal hierarchy. Fig. (2), to the left, aims at demonstrating this point. If  $m_{\nu_1} \equiv 0$ , a lower limit appears if

$$s_R^2 \leq \frac{\sqrt{\Delta m_\odot^2 s_\odot^2}}{\sqrt{\Delta m_\odot^2 + \Delta m_{Atm}^2} + \sqrt{\Delta m_\odot^2 s_\odot^2}} \sim 0.034 \quad (10)$$

However, from this superficial look at the data at the point  $m_{\nu_1} = \tan^2 \theta_\odot m_{\nu_2}$  exact cancellation yielding  $\langle m_\nu \rangle \equiv 0$  seems possible. However, this is equivalent to saying  $M_{ee}^\nu \equiv 0$  and it is exactly this possibility which is ruled out by the “extended black box” theorem [6].

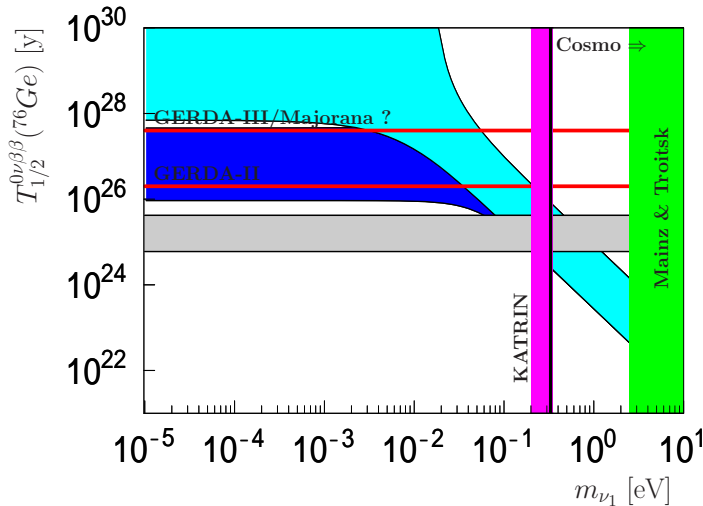


**Figure 4.** Summary of experimental data on the absolute neutrino mass scale and the half-life of  $^{76}\text{Ge}$   $0\nu\beta\beta$  decay. For discussion see text.

In fig. (4) finally a summary of the current status of various experimental attempts on measuring/limiting the absolute scale of neutrino masses is given. The light and darker blue areas are allowed for the  $0\nu\beta\beta$  decay half live of  $^{76}\text{Ge}$  for normal and inverse hierarchy, calculated with matrix elements from [14]. Note, that matrix elements from [15] lead to slightly larger half-lives, see also the discussion in [3]. The green area labeled “Mainz & Troitsk” shows the latest upper limits derived from endpoint measurements in  $^3\text{H}$  decay [16, 17]. The bar labeled

“KATRIN” represents the expected sensitivity of the next generation  ${}^3\text{H}$  experiment KATRIN [18]. Note, that KATRIN claims a final sensitivity of  $m_{\nu_e} \sim 0.2$  eV (@ 90 % c.l.) or a  $5\sigma$  discovery threshold of  $m_{\nu_e} \sim 0.35$  eV. Various limits on the absolute neutrino mass scale from cosmology have been published recently, derived from CMB data combined with information from large scale structure surveys. For three generations of neutrinos numbers ranging from  $\sum_i m_{\nu_i} \sim 0.4 - 2.0$  eV, depending on input and bias, have been published. For a detailed discussion see, for example, the review [19]. The horizontal gray band indicates the range of the finite  $T_{1/2}^{0\nu\beta\beta}$  claimed by some members of the Heidelberg-Moscow experiment [20]. Note that this result is highly controversial, see for example the discussion by Barabash in [2]. The vertical red lines indicate the sensitivity of two future Ge experiments. GERDA [21] is currently in phase I, phase II is funded. In the future Majorana [22] and/or GERDA phase III can test the range allowed by inverse hierarchy.

#### 4. Conclusions

Lower limits on the  $0\nu\beta\beta$  decay half live can be used to constrain various particle physics parameters. However, from the point of view of particle physics it would be interesting to determine the *dominant* contribution to  $0\nu\beta\beta$  decay. Very little work has been done in this direction. Angular correlations between the electrons [4] or a comparative study of  $0\nu\beta^-\beta^-$  and  $0\nu\beta^+/EC$  decay [23] might be able to disentangle left-left and left-right-handed combinations of currents (of the long range type). However, other contributions to  $0\nu\beta\beta$  decay possibly exist and ultimately it might be that only a combination of various different pieces of experimental data will provide the correct and final answer.

#### Acknowledgments

I would like to thank S.G. Kovalenko and J.W.F. Valle for various discussions on the subject. Financial support by Spanish grant FPA2005-01269, by European Commission Human Potential Program RTN network MRTN-CT-2004-503369 and the EU Network of Astroparticle Physics (ENTApP) WP1, as well as the spanish MCyT Ramon y Cajal program is acknowledged.

- [1] Y. Fukuda *et al.* [Super-Kamiokande Collaboration], Phys. Rev. Lett. **81**, 1562 (1998)
- [2] S. Elliott, A. Barabash, S. Schönert, A. Piepke, R. Maruyama and J. Wilson, these proceedings
- [3] F. Simkovic, these proceedings
- [4] M. Doi, T. Kotani and E. Takasugi, Prog. Theor. Phys. Suppl. **83**, 1 (1985).
- [5] J. Schechter and J. W. F. Valle, Phys. Rev. D **25**, 2951 (1982).
- [6] M. Hirsch, S.G. Kovalenko and I. Schmidt, hep-ph/0608xxx
- [7] E. Takasugi, Phys. Lett. B **149**, 372 (1984).
- [8] M. Hirsch, H. V. Klapdor-Kleingrothaus and O. Panella, Phys. Lett. B **374**, 7 (1996)
- [9] R. N. Mohapatra, Phys. Rev. D **34**, 909 (1986).
- [10] R. N. Mohapatra, Phys. Rev. D **34**, 3457 (1986).
- [11] J. D. Vergados, Phys. Lett. B **184**, 55 (1987).
- [12] M. Hirsch, H. V. Klapdor-Kleingrothaus and S. G. Kovalenko, Phys. Rev. D **53**, 1329 (1996)
- [13] M. Maltoni, T. Schwetz, M. A. Tortola and J. W. F. Valle, New J. Phys. **6**, 122 (2004) [arXiv:hep-ph/0405172]. (V5) in the archive provides updated numbers taking into account all relevant data as of June 2006.
- [14] K. Muto, Phys. Lett. B **391**, 243 (1997).
- [15] V. A. Rodin, A. Faessler, F. Simkovic and P. Vogel, Nucl. Phys. A **766**, 107 (2006).
- [16] C. Kraus *et al.*, Eur. Phys. J. C **40**, 447 (2005) [arXiv:hep-ex/0412056].
- [17] V. M. Lobashev *et al.*, Nucl. Phys. Proc. Suppl. **91**, 280 (2001).
- [18] A. Osipowicz *et al.* [KATRIN Collaboration], arXiv:hep-ex/0109033; see also: <http://www-ik.fzk.de/katrin/index.html>
- [19] J. Lesgourgues and S. Pastor, Phys. Rept. **429**, 307 (2006) [arXiv:astro-ph/0603494].
- [20] H. V. Klapdor-Kleingrothaus, A. Dietz, I. V. Krivosheina and O. Chkvorets, Nucl. Instrum. Meth. A **522**, 371 (2004) [arXiv:hep-ph/0403018].
- [21] I. Abt *et al.*, arXiv:hep-ex/0404039. See also the GERDA web page <http://www.mpi-hd.mpg.de/ge76/>
- [22] R. Gaitskell *et al.* [Majorana Collaboration], arXiv:nucl-ex/0311013.
- [23] M. Hirsch, K. Muto, T. Oda and H. V. Klapdor-Kleingrothaus, Z. Phys. A **347**, 151 (1994).

# Some Recent Secondary Production Measurements for Neutrino Flux Determination

**Geoffrey B. Mills**

Physics Division, MS-H846, Los Alamos NL, Los Alamos, NM, 87544

mills@lanl.gov

**Abstract.** Recent measurements of meson production in proton-nucleus interactions have made possible reliable neutrino flux determinations at modern neutrino experiments. This article discusses preliminary results from the HARP, MIP, and E910 are discussed along with some of their implications for the MINOS, K2K, and MiniBooNE neutrino experiments.

## 1. Introduction

Modern accelerator-neutrino experiments require a precise knowledge of the flux of neutrinos passing through the experimental apparatus in order to extract the most information from their data. Neutrinos beams from accelerators are generally produced by the decays of secondary mesons which in turn are produced by proton interactions with the nuclei in specially designed targets. The mesons are focused by pulsed magnetic field devices like magnetic horns which generate powerful toroidal focusing fields. That is the case for the two neutrino experiments that currently operate at Fermilab, MINOS [1] and MiniBooNE [2] and the experimental efforts.

With the use of second generation Monte Carlo transport codes [3], all electro-magnetic processes such as charged particle tracking in magnetic fields, energy loss, and multiple scattering are well characterized. The complex geometry of production targets, magnetic horn systems, decay tunnels and beam stops can be easily managed in today's computer simulation codes. The dominant source of uncertainty has become the knowledge of hadronic processes during particle transport, especially the yield of mesons in the primary proton interaction. The difficulty in modeling hadronic processes originates in the lack of a predictive theory for the underlying fundamental processes. The ability to predict hadronic processes rests on a foundation of empirical data that has been taken over a period of nearly 50 years.

While the empirical data can provide accurate information at measured values of beam energies, secondary momenta and angles, a model is usually needed to interpolate or extrapolate to other values. It was long ago noticed that at incident proton beam energies above 12 GeV, inclusive hadronic cross sections obeyed scaling laws [4] that allowed reliable interpolation and extrapolation over significant energy ranges. Feynman [5] in particular noticed that the scaling was most evident in "Feynman  $x$ " variable ( $x_F$ ). While the theoretical motivation for this scaling is somewhat qualitative, it has been shown to be reasonably accurate over a large range of energies above 12 GeV. It has been shown that below 12 GeV simple scaling models are less reliable and other methods are necessary.

Neutrino experiments, which are typically designed to use the primary beam of an accelerator, are interested in a precise knowledge of secondary production at the accelerator's primary beam energy. In order to avoid extrapolation errors, measurements must be made at the same proton beam energy as the experiment is operated at and on the same material the target is constructed from. Empirical data with the appropriate combination of beam energy, secondary momentum-and-angle, and target material is quite often not available. This makes it necessary to perform hadron production measurements with the precise conditions of the neutrino beam.

Ideally, one would make secondary measurements after the entire target and focusing system, but this is usually not practical as the magnetic focusing systems generally have an expensive physical plant of pulsed power supplies and associated equipment. The dominant uncertainties are in the primary production cross sections, and then related to the scattering and absorption of secondary particles in the thick targets required for neutrino production. The approaches that have been taken attempt to use thin targets to measure production cross sections and thick replica targets to measure effects related to secondary interactions.

## 2. Strategies for Mitigating Flux Uncertainties in Accelerator Neutrino Experiments

There are a number of strategies for minimizing the effects of hadro-production uncertainties in neutrino beams. The heart of the problem is lack of knowledge of the phase-space distribution of the secondary particles. The uncertainty can be reduced by either modifying the secondary phase-space distribution to a known configuration by cooling or momentum selection or by measuring it carefully in an experiment.

### 2.1. Decay-at-Rest Beams

One approach is to stop (cool) the mesons in a beam stop. The neutrino flux shape is perfectly understood in this case since the decays of mesons are well understood in the rest frame of the meson (e.g. muon, pion, or kaon decays). All that remains is to constrain the overall normalization, which can be achieved via one known reaction channel. Examples of this are KARMEN [6] or LSND [7], where the experiments were conducted in a stopped  $\pi/\mu$  beam. The  $^{12}\text{C}(\nu, e)^{12}\text{N}_{\text{GS}}$  reaction serves to normalize the flux and the decay-at-rest fluxes were completely understood. The advantage of that situation cannot be emphasized enough; the flux is *completely* determined by a single, known cross section measurement.

### 2.2. Decay-in-Flight Beams

Decay-in-flight experiments use several techniques to improve meson phase space distributions. One method is to momentum-select the secondary mesons in order to create a narrow-band beam. This approach yields a narrower, better understood momentum distribution at the expense of overall flux. A more costly alternative is to use phase space cooling techniques on long lived secondary particles (e.g. muons), and insert them into a storage ring, which can potentially yield a well defined neutrino beam.

When flux and cost are both an issue, broadband neutrino beams such as MiniBooNE or MINOS are often used. In this situation it can be crucial to understand the initial phase-space distribution of the primary mesons and follow its evolution in the decay region, by taking into account magnetic focusing and secondary interactions until they either decay or are absorbed by material. Often the primary production cross section is not completely understood and the secondary interactions even less well understood making broadband beam lines difficult to engineer.

### 3. Hadron Production Experiments

Hadron production experiments play an important role in decay-in-flight neutrino beam design and utilization. Several have become relevant to neutrino beams in the recent past. In this article I will discuss recent progress related to the operating neutrino experiments at Fermilab and KEK, the K2K beam line, the NUMI beam line, and the MiniBooNE beam line. Those experiments are E910 at Brookhaven, HARP at CERN, and MIPP at Fermilab. There are other recent experiments such as SPY how I will leave out of this discussion, if only for a lack of time.

While experimental design varies to some extent due to incident beam energies, the experiments generally place a TPC system around an interchangeable target, followed by a forward spectrometer arrangement with drift chamber tracking, a dipole magnet, a Cerenkov system, time-of-flight system, and finally an electro-magnetic calorimeter system. The E910 and MIPP experiments in fact used the same TPC provided by LBL.

#### 3.1. E910 at BNL

The E910 experiment [8] at Brookhaven was designed and operated to test intra-nuclear cascade models that are employed in understanding heavy ion experiments. Most of its running was in a triggered mode not ideally suited for unbiased hadron production measurements. However, it did record some proton-Be data at 6 GeV/c and 12 GeV/c incident beam momenta which could be used for the purposes of constraining fluxes at the 8.9 GeV/c MiniBooNE beam line. A preliminary analysis of this data for MiniBooNE purposes [8] is shown in Figure 1.

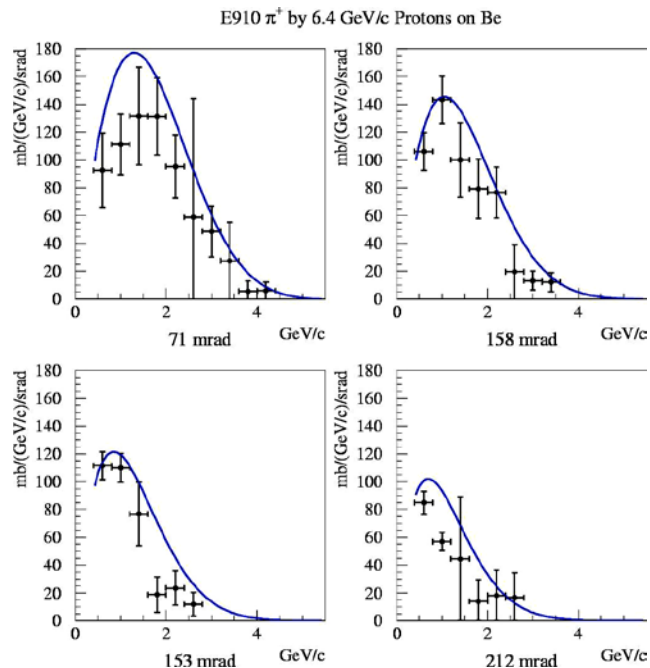


Figure 1: The results of a preliminary analysis of E910 positive pion production from 6.4 GeV/c proton-Be data [8]. The histogram results from a fit to a Sanford-Wang model.

### 3.2. HARP (PS214) at CERN

The HARP experiment was constructed for the express purpose of surveying a large number of target materials in proton-nucleus interactions with incident beam momenta in the range 2 GeV/c to 15 GeV/c. It was situated in the East Hall of the CERN PS on the T9 beam line. A schematic of the experimental apparatus is shown in Figure 2.

The MiniBooNE collaboration was graciously allowed to operate the HARP detector for a one week period in August of 2002 in order to record proton-Be data at the appropriate beam momentum of 8.9 GeV/c. In the subsequent week the K2K was allowed to do the same at 12.9 GeV/c. In both cases, thin ( $0.05 \lambda$ ) and thick target-replica data were accumulated.

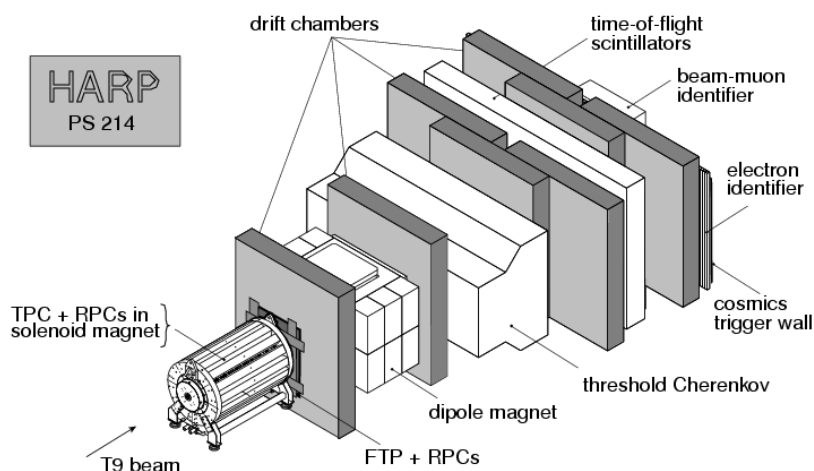


Figure 3: The HARP apparatus

The results of analyses of the thin target 8.9 GeV/c Be data [9] and for 12.9 GeV/c Al data [10] are shown in Figure 3 and Figure 4 respectively. In that analysis the forward spectrometer system was used exclusively because it covers the most important part of the production phase space for the MiniBooNE and K2K.

It is clear from the fits of a Sanford-Wang model [4] to E910 and HARP data above and below 12 GeV/c, that the model has difficulty at 8.9 GeV/c. The model was developed prior to the understanding gained by using Feynman  $x$  ( $x_F$ ) as the scaling variable, never-the-less, it is still employed by some neutrino experiments. With the analysis of the remainder of the HARP data, taken on many types of targets ranging from hydrogen and deuterium to lead and tantalum, it is hoped that an empirically based model will allow the description of hadro-production over a wide range of incident proton momenta.

### 3.3. MIPP (E907) at Fermilab

The MIPP experiment is designed to measure secondary production cross sections at beam momenta in the range below 120 GeV/c. Figure 5 shows a preliminary momentum distribution from several beam energies. MIPP ran with a replica NUMI target and is expected to help constrain MINOS fluxes and aid in the Minerva cross section measurements and NUMI.

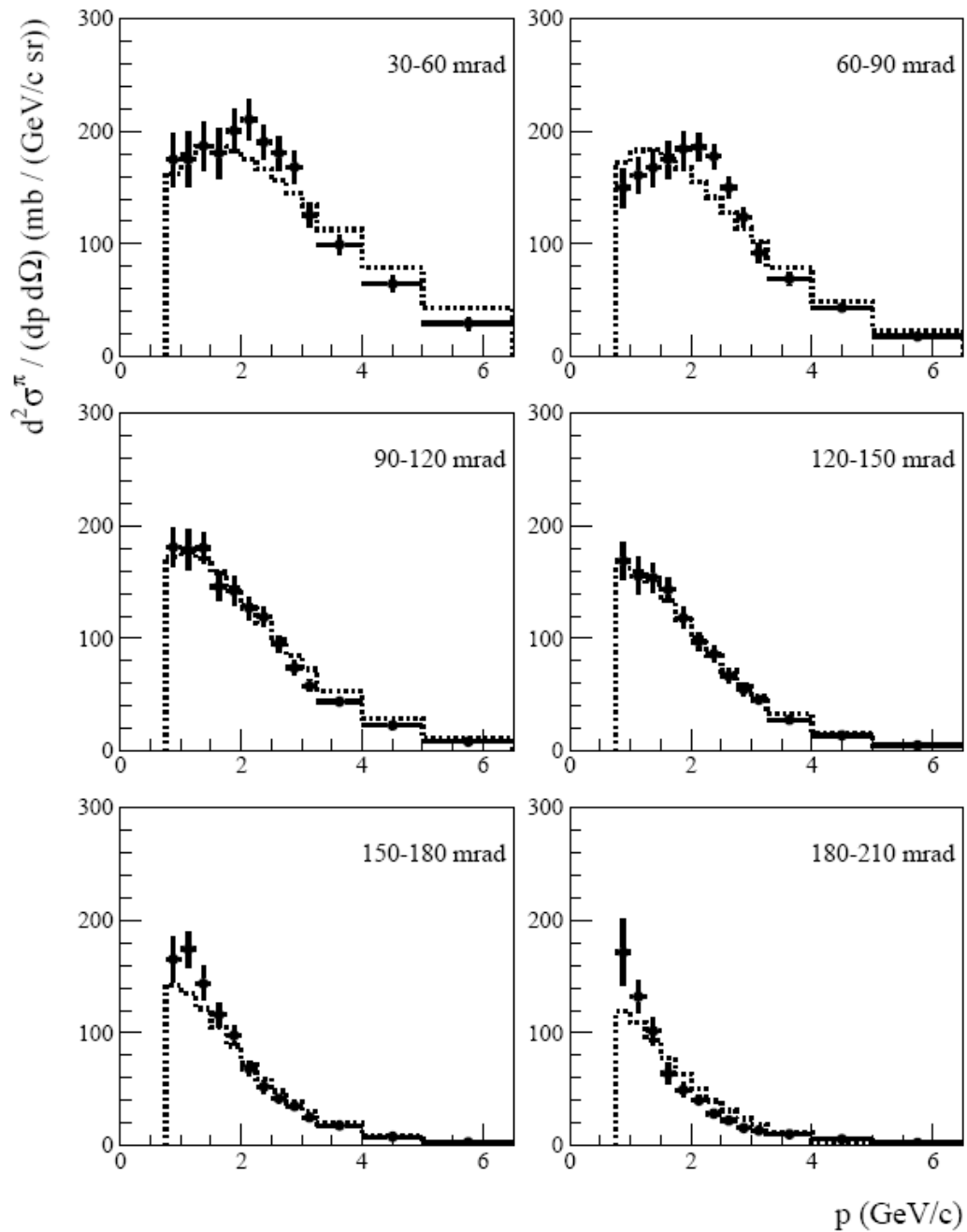


Figure 3

Positive pion production cross sections from the HARP experiment [9] for incident protons of 8.9 GeV/c on a beryllium target are shown in 30 mrad bins of angle. The data are fit to a Sanford-Wang [4] model which clearly has difficulty describing the data at 8.9 GeV/c. The  $\chi^2/\text{dof}$  of the fit is 248/70 indicating the inability of the model to describe the data when full systematic error correlations are accounted for in the data.

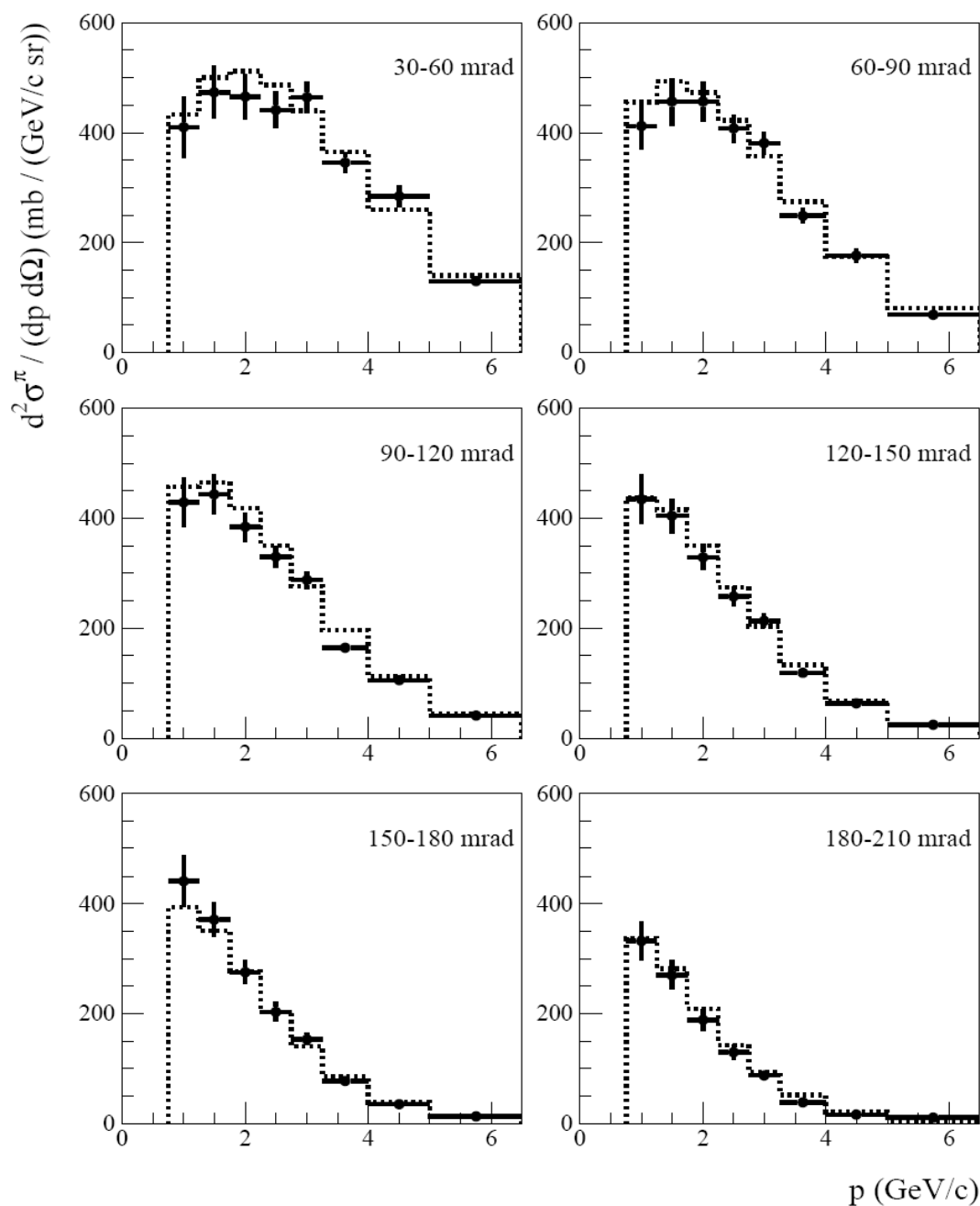


Figure 4

Positive pion production cross sections from the HARP experiment [10] for incident 12.9 GeV/c protons on an aluminium target are shown in 30 mrad bins in angle. At this incident proton momentum, the Sanford-Wang model seems to describe the data reasonably well.

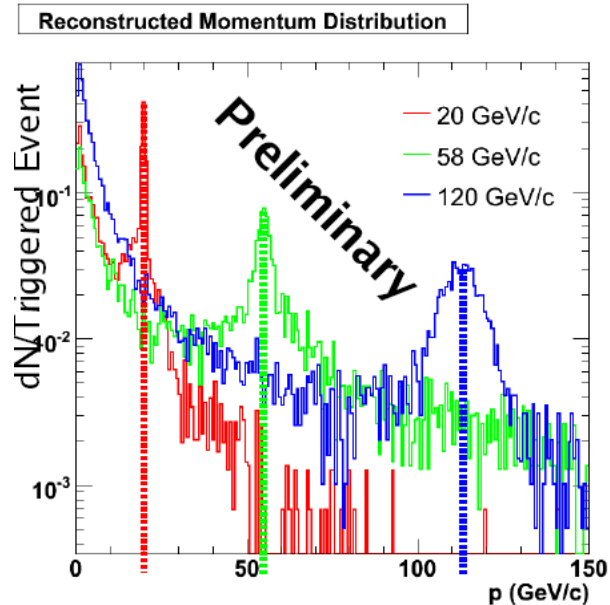


Figure 5

Preliminary raw momentum distributions from the MIPP experiment [11] at incident proton energies of 20 GeV/c, 58 GeV/c, and 120 GeV/c are shown that demonstrate the MIPP tracking system capabilities.

#### 4. Summary

The engineering and design of future neutrino beams for experiments like Nova [12] and T2K [13] will prove to be a challenge. Only with the best tools in hand will those experiments bear their full potential. A detailed understanding of neutrino flux enables the understanding of neutrino-nuclear cross sections. A detailed understanding of those cross sections enables the observation of new phenomena like neutrino oscillations, leptonic CP violation, and possibly exotic effects like violation of Lorentz invariance and CPT violation. Only with steadfast determination will these become a reality.

Acknowledgements: The author wishes to acknowledge the efforts of the HARP collaboration, the MiniBooNE collaboration, the E910 collaboration, and the MIPP collaboration that carry on this work.

#### References

- [1] MINOS proposal (1995), cf. hep-ex/0701049 and references therein
- [2] BooNE proposal ( Dec. 7, 1997) available at : ( <http://www-boone.fnal.gov/publicpages> )
- [3] GEANT3 ( CERN libraries ), GEANT4 ( <http://geant4.web.cern.ch/geant4> )
- [4] J. R. Sanford and C. L. Wang, BNL AGS internal report # BNL11299 and # BNL11479 (1967)
- [5] R. P. Feynman, Phys. Rev. Lett., 23, 1415 (1969)
- [6] KARMEN Experiment (<http://www-ik1.fzk.de/www/karmen>)  
Cf. [Phys. Rev. D66, 013001 \(2002\)](#)
- [7] LSND Collaboration, Phys.Rev.D64:112007,2001
- [8] E910 Collaboration, private communication
- [9] HARP Collaboration, hep-ex/0702024
- [10] HARP Collaboration, Nucl.Phys.B732:1-45,2006

- [11] MIPP Collaboration, private communication
- [12] Nova Collaboration, hep-ex/0503053
- [13] T2K collaboration ( <http://jnusrv01.kek.jp/public/t2k> )  
hep-ex/0106019

# KamLAND Results and Future

**Tadao Mitsui for the KamLAND Collaboration**

Research Center for Neutrino Science, Tohoku University, Sendai 980-8578, Japan

E-mail: mitsui@awa.tohoku.ac.jp

**Abstract.** KamLAND results, current status, and near-future plans are reviewed. For reactor and geoneutrino physics, reduction of the systematic uncertainties is underway, while taking subsequent data. For the detection of  ${}^7\text{Be}$  solar neutrinos, purification of the scintillator by distillation will start soon.

## 1. Introduction

KamLAND is a detector for low-energy electron-anti-neutrinos ( $\bar{\nu}_e$ ) with very high sensitivity. By employing 1 kton of ultra-pure liquid scintillator, as well as the powerful background suppression by neutron inverse  $\beta$ -decay ( $\bar{\nu}_e + p \rightarrow e^+ + n$ , Figure 1), KamLAND can identify as rare as  $\sim 1$  event per month of  $\bar{\nu}_e$  interaction in the detector, corresponding to the  $\bar{\nu}_e$  flux, for example,  $\sim 10^7 \text{ cm}^{-2} \text{ s}$  in the energy range  $2 < E_\nu < 3 \text{ MeV}$ , or higher sensitivity for higher  $E_\nu$ . With this sensitivity and flavor identification, KamLAND succeeded in detecting  $\bar{\nu}_e$  from distant ( $\sim 180 \text{ km}$ ) nuclear reactors to establish reactor neutrino oscillation, and also performed first experimental study of geologically produced  $\bar{\nu}_e$  (“geoneutrinos”) which come from Earth’s interior.

KamLAND is located at 2700 m.w.e. (Kamioka mine, Japan). The liquid scintillator (1200  $\text{m}^3 \sim 1 \text{ kton}$ ) consists of 1,2,4-trimethylbenzene 20%, dodecane 80% and PPO 1.52g/l as a fluor, which is contained in a plastic balloon (Figure 1). The light output of the liquid scintillator is 8000 photons/MeV, which are detected by 1879 PMTs with 34% photo-coverage, providing 500 p.e./MeV. With water extraction, and nitrogen purge, the scintillator has been purified before filled into the balloon. The present impurity level is  $3.5 \pm 0.5 \times 10^{-18} \text{ g/g}$  for Uranium and  $5.2 \pm 0.8 \times 10^{-17} \text{ g/g}$  for Thorium.

## 2. Reactor neutrino

The data taking of KamLAND started in 2002, to confirm or reject the Large Mixing Angle solution (MSW-LMA solution) of the “solar neutrino problem”, at that point, by using artificial antineutrinos from commercial reactors, which are fortunately distributed around Kamioka with a typical distance  $\sim 180 \text{ km}$ . First results of KamLAND [1, 2] has been reported in 2002, in which reactor neutrino disappearance is observed for the first time. This disappearance is only consistent with LMA solution, excluding other solutions at 99.95% confidence level (C.L.) under the assumption of CPT invariance. The second result [3, 4, 5] is reported in Neutrino 2004 conference, in which the energy spectral distortion is observed (Figure 2). The observed sinusoidal pattern is consistent with neutrino oscillation and is not consistent with hypotheses to explain neutrino disappearance without appearing again, such as neutrino decay or decoherence.

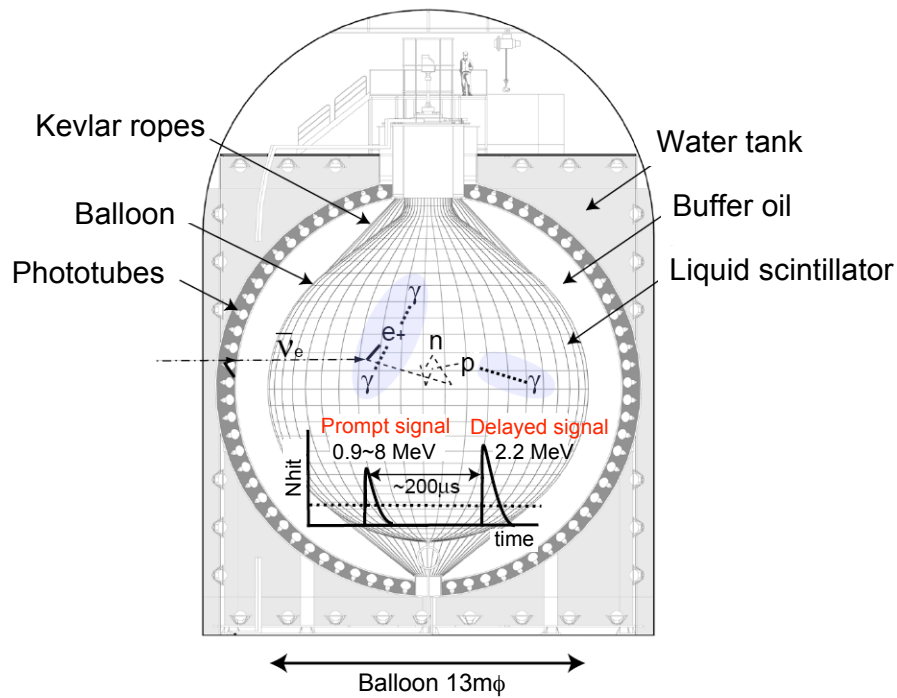


**Figure 1.** KamLAND detector and neutron inverse  $\beta$ -decay to detect electron-anti-neutrinos.

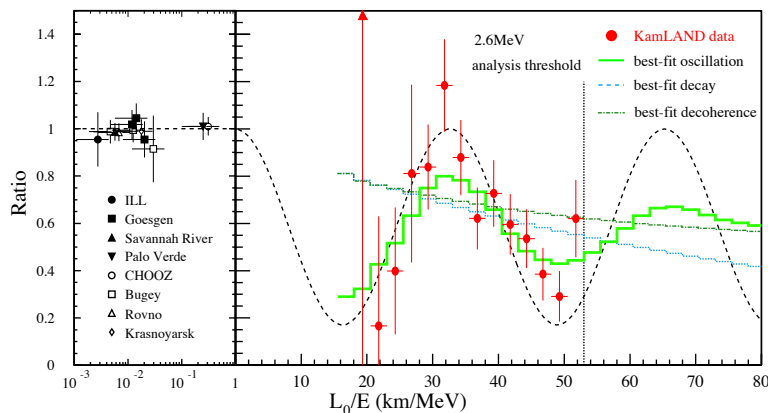


**Figure 2.** Energy spectral distortion of reactor neutrinos. KamLAND data are shown as a ratio of observed and expected (no oscillation) number of events as a function of  $L_0/E_\nu$ , where  $L_0$  is fixed at 180 km which is a typical distance between KamLAND and dominantly contributing reactors.

These second data have also constrained the neutrino oscillation parameters precisely;  $\Delta m^2 = 7.9^{+0.6}_{-0.5} \times 10^{-5} \text{ eV}^2$  and  $\tan^2 \theta = 0.40^{+0.10}_{-0.07}$  [4] in a combined analysis with solar neutrino data. For further improvement of the precision of the oscillation parameters, improved statistics with subsequent data and reduction of the systematic uncertainty are important. To reduce the uncertainty of the fiducial volume, which is the dominant source of the systematic uncertainty at present, the all volume calibration is now being performed using a device that can access almost all points in the fiducial volume, called “ $4\pi$  system”. If the total systematic uncertainty of the absolute number of events is reduced to 3% (6.5% at present) by this  $4\pi$  system and other efforts, the mixing angle  $\theta$  will also be constrained by KamLAND data alone (Figure 3) with a precision similar to the current solar neutrino data. Then, KamLAND and solar neutrino data

will provide independent measurements of oscillation parameters of  $\nu_e$  and  $\bar{\nu}_e$ , for an exciting test of CPT principle.

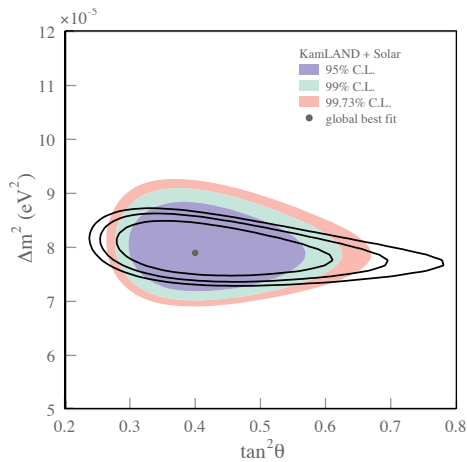


**Figure 3.** Present and future sensitivity for  $\Delta m^2$  and  $\tan^2 \theta$ . Shaded area shows current allowed region with KamLAND and solar neutrino data. Solid lines are expected sensitivity of KamLAND data alone with 3 kton-yr exposure and 3% systematic uncertainty for absolute number of detected neutrinos. For both, contours are 95, 99 and 99.73% C.L.

### 3. Geoneutrinos

KamLAND is the first detector sensitive enough to measure geologically produced antineutrinos (geoneutrinos), which are produced in the Earth interior from the  $^{238}\text{U}$  and  $^{232}\text{Th}$  decay chains. The decay chains are also sources of Earth's power. In the standard geological understanding, radiogenic heat from  $^{238}\text{U}$ ,  $^{232}\text{Th}$ , and  $^{40}\text{K}$  should contribute about 40% to Earth's total power. The source of Earth's power is a key to understanding the plate tectonics, thus understanding the mechanisms of continental drift, earthquakes, and volcanoes. Although  $^{238}\text{U}$  and  $^{232}\text{Th}$  are the dominant contributions to the radiogenic heat,  $^{40}\text{K}$  neutrino may be important to solve the puzzle of geomagnetism. KamLAND is only sensitive to  $^{238}\text{U}$  and  $^{232}\text{Th}$  neutrinos because energies of  $^{40}\text{K}$  neutrinos are lower than the threshold of inverse  $\beta$ -decay 1.8 MeV.

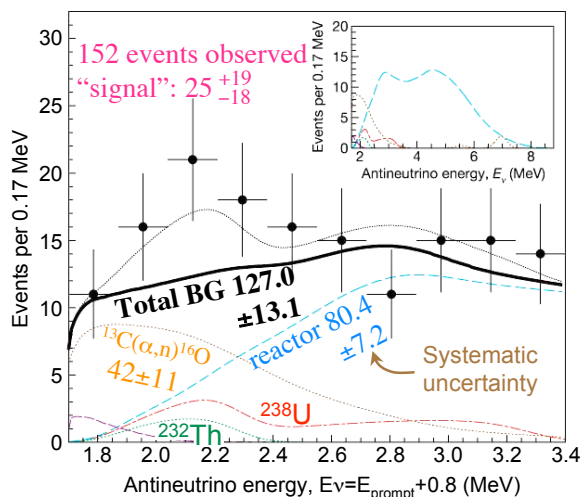


**Figure 4.** Observed spectrum below 3.4 MeV ( $E_{\text{prompt}} < 2.6$  MeV). Points are data, lines with labels and numbers estimated background (thin line around 1.8 MeV is random coincidence), lines labeled as  $^{238}\text{U}$  and  $^{232}\text{Th}$  best-fit geoneutrino signals. Thick black line is the estimated total background, thin black line that with the best-fit signals added.

Figure 4 shows the observed energy spectrum [6] in the signal region of geoneutrinos. The total number of  $\bar{\nu}_e$  candidates is 152, while the number of expected background  $127 \pm 13.1$ , which are due mainly to reactor neutrinos and  $\alpha$ -induced neutron background ( $^{13}\text{C}(\alpha, n)^{16}\text{O}$ )

[5]. Considering all systematic and statistical errors, the number of geoneutrino candidates is  $25_{-18}^{+19}$  [6], being consistent with the “reference model” [7] that predicts  $\sim 19$  events in the present data. Further analysis [6] using energy spectral shape and the fixed Th/U ratio are also consistent with the standard geological models, although statistical significance is not high.

In the near future, systematic uncertainty of the background will be reduced by the following efforts. For reactor neutrino, the main uncertainty is from oscillation parameters which will be determined more precisely by subsequent KamLAND and solar neutrino data. For  $^{13}\text{C}(\alpha, n)^{16}\text{O}$  background [4, 5], we will improve the rate and spectral estimation by (i) using new data of the  $^{13}\text{C}(\alpha, n)^{16}\text{O}$  cross section [8], (ii) performing direct measurement of the quenching factor for protons recoiled by  $\alpha$ -induced neutrons. For the latter one, the present estimation is deduced from  $\alpha$  quenching factor, so quite conservative systematic error is applied in the analysis. We already performed the direct measurement by using a monochromatic neutron beam from OKTAVIAN [9], which we utilized by courtesy of Osaka University. Now the precise analysis is underway.

Moreover, after the purification of the scintillator described in the next section, reduction of  $\alpha$  source for  $^{13}\text{C}(\alpha, n)^{16}\text{O}$  is expected, because the dominant  $\alpha$  source is  $^{210}\text{Po}$  that is a daughter of  $^{210}\text{Pb}$  (see the next section).

#### 4. Low energy solar neutrinos

Figure 5 shows the current single spectrum of KamLAND together with the identified background spectra (lines), whose intensities are fitted to the data. Also shown is the expected spectrum from the  $^7\text{Be}$  solar neutrinos via elastic scattering with an electron  $\nu + e \rightarrow \nu + e$ . As seen, the expected signal is 4 to 5 orders of magnitude lower than the background from  $^{210}\text{Bi}$ ,  $^{210}\text{Po}$ , and  $^{85}\text{Kr}$ . Then, the long-lived  $^{210}\text{Pb}$  and  $^{85}\text{Kr}$  should be removed from the scintillator, considering the decay chains  $^{210}\text{Pb}$  ( $T_{1/2} = 22.3$  yr)  $\rightarrow$   $^{210}\text{Bi}$  (5.01 day)  $\rightarrow$   $^{210}\text{Po}$  (138 day)  $\rightarrow$   $^{206}\text{Pb}$  (stable), and  $^{85}\text{Kr}$  (10.8 yr)  $\rightarrow$   $^{85}\text{Rb}$  (stable).

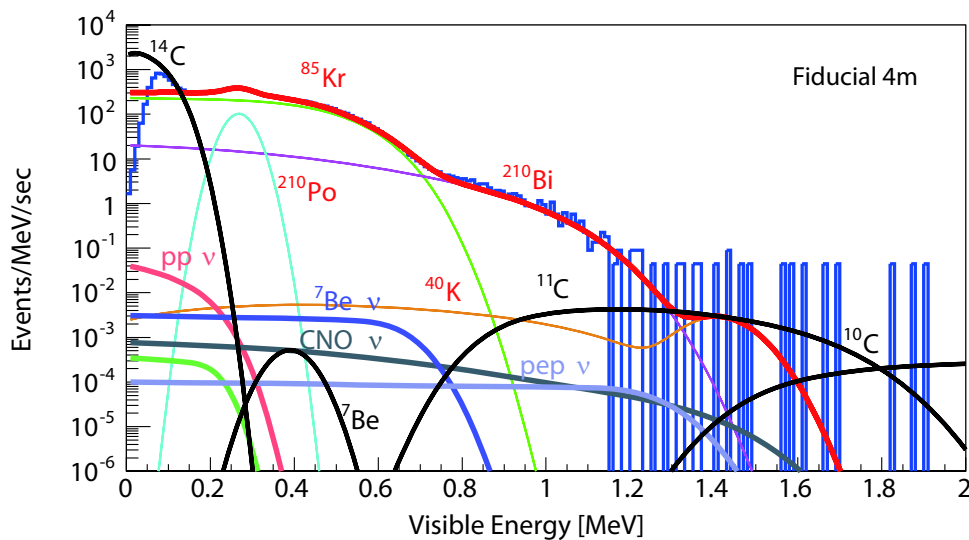


**Figure 5.** KamLAND single spectrum. Identified background and expected solar neutrino spectra.

We found the most effective way of scintillator purification is combination of distillation and nitrogen purge. As described already, KamLAND scintillator consists of 1,2,4-trimethylbenzene

(pseudocumene, PC) 20%, dodecane (a kind of normal paraffin, NP) 80%, and PPO 1.52g/l. The boiling points are PC 168, NP 216, and PPO 360 °C under one Atmosphere. For lower boiling points, vacuum distillation is chosen. Nitrogen purge works to remove inert gases  $^{85}\text{Kr}$  and  $^{222}\text{Rn}$ . The present  $^{210}\text{Pb}$  is resulted from  $^{222}\text{Rn}$ , so its removal is important not to pollute the scintillator again.

Three separate distillation towers will be installed for PC, NP and PPO. Each tower extracts each component only and discards, in principle, any of contaminants having different boiling points. The first tower boils the scintillator, then PC and more volatile contaminants are evaporated. At the top of the tower, PC is condensed while more volatile contaminants including  $^{222}\text{Rn}$ ,  $^{85}\text{Kr}$  and some of the possibly existing organic lead compounds are not condensed and exhausted. The next tower will boil the mixture of NP and PPO drawn from the bottom of the first tower, then NP is evaporated and condensed at the top. Contaminants having boiling points between NP and PC will not be condensed and exhausted here. The third tower will perform the same thing for PPO, and the contaminants having higher boiling points than PPO will be discarded as residue.

For R&D [10] of distillation,  $^{212}\text{Pb}$  is used as a substitute for  $^{210}\text{Pb}$ , because  $^{212}\text{Pb}$  can be identified much more easily than  $^{210}\text{Pb}$  by tagging  $^{212}\text{Bi}$ - $^{212}\text{Po}$  coincidence ( $T_{1/2} = 299$  ns). The decay curve of  $^{212}\text{Pb}$  (10.6 hr) also helps to identify it. Figure 6 is an example of PPO distillation, in which reduction of  $^{212}\text{Pb}$  by 4 orders of magnitude is observed.

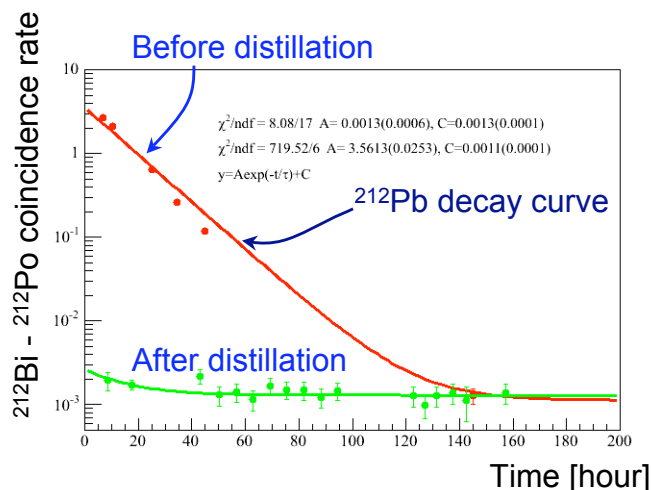


**Figure 6.** A typical result of PPO distillation test-bench. By tagging  $^{212}\text{Bi}$ - $^{212}\text{Po}$  coincidence and fitting the decay curve, concentration of  $^{212}\text{Pb}$  is measured before and after distillation. Reduction by 4 orders of magnitude is confirmed.

Constructions of the real distillation system started in 2006. Main civil engineering is excavating a new tunnel for the system, and construction of the power line for  $\sim 1$  MW consumption during distillation. A 1-ton liquid scintillator detector is also created to measure  $^{222}\text{Rn}$  concentration of the purified scintillator, before it is filled into KamLAND.

For *pep* and CNO neutrinos, cosmogenic  $^{11}\text{C}$  is a serious source of background (Figure 5) even after purification is quite successful. To reject  $^{11}\text{C}$  events in off-line analysis, three-fold coincidence [11] between parent muon, neutron capture and  $^{11}\text{C}$  signal is studied with KamLAND data, finding that  $^{11}\text{C}$  production accompanying more than one neutrons can be tagged efficiently. To perform this technique for real solar neutrino data, highly efficient detection of spallation neutrons soon after muon events is needed. To reduce dead time of electronics after large signals from muons, development of backup electronics has been started.

To measure low-energy part of  $^8\text{B}$  solar neutrino spectrum for possible detection of MSW effect,  $^{208}\text{Tl}$  background should be reduced. To reject those distributed  $^{208}\text{Tl}$  events, further

removal of Thorium from the scintillator is required, which may be achieved with distillation hopefully.

### 5. Exotic $\bar{\nu}_e$ and nucleon decay

With the high sensitivity for low-energy events, search for rare phenomena is one of the important tasks of KamLAND. Exotic antineutrinos are searched for in the energy range  $8.3 < E_{\bar{\nu}_e} < 14.8$  MeV (above the tail of reactor antineutrinos) and upper limit of  $3.7 \times 10^2 \text{cm}^{-2}\text{s}^{-1}$  (90% C.L.) on the  $\bar{\nu}_e$  flux is obtained [12] assuming  $^8\text{B}$  solar  $\nu_e$  energy spectrum. The result can be interpreted for any of exotic  $\bar{\nu}_e$  sources.

As one of the possible mode of nucleon decay, invisible decay of neutron is searched for [13] by tagging signals from highly excited  $^{11}\text{C}$  or  $^{10}\text{C}$  nuclei, which should be created when one or two neutrons disappear from  $^{12}\text{C}$  nuclei abundant in the KamLAND scintillator. No significance is found and limits for one- and two-neutron disappearance:  $\tau(n \rightarrow \text{inv}) > 5.8 \times 10^{29}$  years and  $\tau(nn \rightarrow \text{inv}) > 1.4 \times 10^{30}$  years at 90% C.L. is obtained.

- [1] Suzuki A 2002 The solar neutrino problem and first results from KamLAND *The XXIth Texas Symposium on Relativistic Astrophysics* 9-13, December, 2002, Florence
- [2] Eguchi K *et al.* 2003 First results from KamLAND: evidence for reactor antineutrino disappearance *Phys. Rev. Lett.* **90** 021802
- [3] Gratta G 2004 New results from KamLAND *The XXI International Conference on Neutrino Physics and Astrophysics* 14-19, June 2004, Paris
- [4] Araki T *et al.* 2005 Measurement of neutrino oscillation with KamLAND: evidence of spectral distortion *Phys. Rev. Lett.* **94** 081801
- [5] KamLAND collaboration 2005 Data release accompanying the 2nd KamLAND reactor result (<http://www.awa.tohoku.ac.jp/KamLAND/datarelease/2ndresult.html>)
- [6] Araki T *et al.* 2005 Experimental investigation of geologically produced antineutrinos with KamLAND *Nature* **436** 499
- [7] Enomoto S, Ohtani E, Inoue K and Suzuki A 2005 Neutrino geophysics with KamLAND and future prospects (arXiv:hep-ph/0508049)
- [8] Harissopoulos S *et al.* 2005 Cross section of the  $^{13}\text{C}(\alpha, n)^{16}\text{O}$  reaction: A background for the measurement of geo-neutrinos *Phys. Rev. C* **72** 062801(R)
- [9] OKTAVIAN, Osaka University (<http://www.eng.osaka-u.ac.jp/nuc/03/oktavian/japanese/home.html>, in Japanese)
- [10] Kishimoto Y 2004 Liquid scintillator purification *Topical Workshop on Low Radioactivity Techniques: LRT 2004* AIP Conference Proceedings vol 785, ed B Cleveland, R Ford and M Chen (AIP) p 193
- [11] Galbiati C *et al.* 2005 Cosmogenic  $^{11}\text{C}$  production and sensitivity of organic scintillator detectors to *pep* and CNO neutrinos *Phys. Rev. C* **71** 055805
- [12] Eguchi K *et al.* 2004 High sensitivity search for  $\bar{\nu}_e$ 's from the Sun and other sources at KamLAND *Phys. Rev. Lett.* **92** 071301
- [13] Araki T *et al.* 2006 Search for the invisible decay of neutrons with KamLAND *Phys. Rev. Lett.* **96** 101802

# Neutrino Mass Theory: Where We Stand ?

**R. N. Mohapatra**

Department of Physics, University of Maryland, College Park, USA

E-mail: [rmohapat@physics.umd.edu](mailto:rmohapat@physics.umd.edu)

**Abstract.** A brief overview of the progress in understanding neutrino masses and their implications for new physics is given with special emphasis on the seesaw mechanism and its implications.

## 1. Introduction

Two major puzzles of the successful standard model are : (i) origin of mass and (ii) origin of flavor. The first deals with understanding why the Higgs field of the standard model has a nonzero vacuum expectation value giving rise to masses for all particles. Attempts to answer this question is at the heart of the theoretical developments such as supersymmetry, extra dimensions etc. The large hadron collider machine is expected to provide an answer to this question. On the other hand, the origin flavor deals with the question of why there are three generations of fermions with the given pattern of masses and mixings, what is the origin of CP violation etc. ? A full understanding of neutrino masses and mixings will shed light on this important question of particle physics.

In the standard model neutrinos are massless making the entire lepton sector “flavor sterile” which leaves all flavor related questions to be probed by quark physics. The discovery of neutrino masses and their unusual mixing patterns has changed this picture and made the leptons “flavor active” turning them into important players in the flavor game specially when they are combined with ideas such as quark-lepton unification or grand unification. This brief review is an assessment of how far we have come in our understanding of neutrinos and the integrated approach to the flavor puzzle[1].

We start by outlining the major challenges for theory posed by neutrino observations: (i) why are neutrino masses so much smaller than the masses of the quarks and leptons i.e.  $m_\nu \ll m_{u,d,e}$  ? (ii) why are the neutrino mixings  $\theta_{Atmos}$  and  $\theta_\odot$  so much larger than the corresponding mixing angles in the quark sector ? (iii) How do neutrinos fit into the big picture of particle physics that addresses other issues in particle physics and cosmology such as hierarchy problem, origin of matter, inflation etc. While there are many approaches to understanding the smallness of neutrino masses, the seesaw mechanism[2] which introduces three right handed neutrinos with a large Majorana masses to suppress the light neutrino mass is no doubt the most appealing and as such has received the most attention. The addition of the right handed neutrinos

not only restores quark lepton symmetry to unified theories but it also imposes nontrivial restrictions on the new physics scenarios beyond the standard model.

I focus on both the bottom-up and top-down approaches. The former consists of searching for symmetries and patterns in the neutrino mass matrix whereas the latter starts with a high scale grand unified theory and isolate predictions that can distinguish between different models and then use symmetries to understand the naturalness of the model parameters. Both represent progress since the disparate mixing patterns between quarks and leptons is so counter intuitive in a quark-lepton unified theory.

## 2. Seesaw mechanism

The basic idea of seesaw mechanism is to introduce three right handed neutrinos to the standard model and give them a large Majorana mass  $M_R$ . This combined with the now allowed Dirac mass  $M_D$  that arises from the Yukawa coupling  $\bar{L}HN_R$ , one get the seesaw mechanism with the formula for neutrino masses given by [2]:

$$M_\nu = -M_D^T M_R^{-1} M_D \quad (1)$$

This provides a natural way to understand the small neutrino masses and implies interesting new physics beyond the standard model.

### 2.1. Generic tests of seesaw

Seesaw being a high scale phenomenon its effects at low energies tend to be small since they are suppressed by  $m_W^2/M_R^2$ . However in the presence of supersymmetry, there are enhanced lepton flavor violating effects in processes such as  $\mu \rightarrow e\gamma$  etc. and changes in the slepton spectrum. It is also possible to rule out the conventional seesaw if either or both of the following is established: (i) the neutrinos are Dirac fermions and/or (ii) there is  $Z'$  in the TeV scale with couplings similar to the left-right model. One way to establish if the neutrino is a Dirac fermion using current and planned experiments is a negative result of the  $\beta\beta_{\nu\nu}$  down to the level of neutrino mass sensitivity of ten milli-eV or so and if simultaneously, the long baseline experiments establish that the  $\Delta m_{31}^2$  is negative (or inverted mass hierarchy).

### 2.2. Seesaw scale

A simple minded estimate the rough scale of right handed neutrino masses can be made using the present observed value for the  $\Delta m_A^2$  required for understanding atmospheric neutrino deficit if we assume that the largest element of  $M_D$  to be  $m_t \sim 100$  GeV, ignoring mixing effects, one can conclude that  $M_R$  is around  $10^{15}$  GeV or so. This is tantalizingly close to the conventional grand unification scale. Thus the seesaw scale may well be related to the GUT scale, explaining why  $M_R \ll M_{Pl}$  suggesting GUT embedding of the seesaw mechanism that unifies both quark and lepton flavor physics. An advantage of this approach is that due to the high symmetry of the theory, one may be able to predict the various observed mass and mixing parameters.

### 2.3. New symmetry associated with seesaw

The addition of  $N_R$ 's not only restores the quark-lepton symmetry, but also generates new gauge symmetries, e.g.  $B - L$  which was a global symmetry in the standard model but becomes a gaugeable symmetry since one has the condition  $Tr(B-L)^3 = 0$ , implying cancellation of gauge anomalies. The gauge group of weak interactions expands to become the left-right symmetric group  $SU(2)_L \times SU(2)_R \times U(1)_{B-L}$  which is a subgroup of the  $SU(2)_L \times SU(2)_R \times SU(4)_c$  group of Pati and Salam. This leads to a picture of weak interactions which is fundamentally different from that envisaged in the standard model in that *weak interactions becomes parity conserving*. Furthermore, in this theory, the electric charge formula is given by :  $Q = I_{3L} + I_{3R} + \frac{B-L}{2}$ , where each term has a physical meaning unlike the case of the standard model. Once the gauge symmetry  $SU(2)_R \times U(1)_{B-L}$  is broken down, one finds the relation  $\Delta I_{3R} = -\Delta \left( \frac{B-L}{2} \right)$ . This connects  $B - L$  breaking, *i.e.*  $\Delta(B - L) \neq 0$ , and hence the neutrino mass to the breakdown of parity symmetry,  $\Delta I_{3R} \neq 0$ .

### 3. Seesaw and quark-lepton flavor structure

Seesaw mechanism by itself however does not throw any light on the detailed flavor structure of leptons. In a top down theory such as an SO(10) GUT model, one can either look for a dynamical mechanism that gives rise to large lepton mixings while keeping the quark mixings small or use flavor symmetries that endow appropriate flavor structure to  $M_R$  which will decouple neutrino mixing pattern from quarks despite quark lepton unification. The dynamical mechanisms can come either from type II seesaw mechanism[3] which relates neutrino mass matrix to couplings of a standard model triplet to leptons or to double seesaw mechanism which relates it to new standard model singlet fermions[4].

Other approaches tried in literature are not related to symmetries e.g. the anarchy approach[5] where the neutrino mass matrix elements are allowed to be random numbers and one then studies the probability that the observed large leptonic mixings (within two  $\sigma$  range of observations) emerges out of these. A generic feature of such models is that the mixing angle  $\theta_{13}$  is typically near the present upper limit. Another approach is to assume texture zeroes in the neutrino mass matrix in the basis where the charged lepton mass matrix is diagonal[6].

### 4. SO(10) Grand Unification and lepton flavor structure

The main reason for considering SO(10) group as appropriate for understanding neutrino masses is that its **16** dimensional spinor representation consists of all fifteen standard model fermions plus the right handed neutrino. It also contains the  $B - L$  symmetry and implies that the seesaw scale is at or below the GUT scale. In the context of supersymmetric SO(10) models, the way B-L breaks has profound consequences for low energy physics. For instance, if B-L is broken by a Higgs field belonging to the **16**

dimensional Higgs field, then the field that acquires a nonzero vev has the quantum numbers of the  $\nu_R$  field i.e. B-L breaks by one unit. In this case higher dimensional operators of the form  $\Psi\Psi\Psi\Psi_H$  will lead to R-parity violating operators in the effective low energy MSSM theory such as  $QLd^c, u^cd^cd^c$  etc which can lead to large breaking of lepton and baryon number symmetry and hence unacceptable rates for proton decay. This theory also has no dark matter candidate without making additional assumptions. On the other hand, one may break B-L by a **126** dimensional Higgs field. The member of this multiplet that acquires vev has  $B - L = 2$  and leaves R-parity as an automatic symmetry at low energies and a naturally stable dark matter in this case.

In order to study the predictions of the theory, one can either go the route of breaking B-L symmetry by **16**-Higgs[7] or by **126** Higgs[8, 9]. In the former case, one not only need to assume matter parity to have stable dark matter but one also needs to impose extra horizontal symmetries to make the theory predictive. In the **126** case on the other hand, one does not need to assume any new symmetry and only a CP like  $Z_2$  symmetry if CKM physics is to be incorporated.

In order to study the predictions of the minimal **126**-Higgs models, we first note that in generic SO(10) models, seesaw formula gets modified to the form[3]  $M_\nu = fv_L$ . In ref.[8], one considers only two Higgs multiplets that contribute to fermion masses i.e. one **10** and one **126**. A unique property of the **126** multiplet is that it not only breaks the B-L symmetry and therefore contributes to right handed neutrino masses, but it also contributes to charged fermion masses by virtue of the fact that it contains MSSM doublets which mix with those from the **10** dimensional multiplets and survive down to the MSSM scale. This leads to a tremendous reduction of the number of arbitrary parameters[8]. If we ignore CP violation for a moment, there are only two real Yukawa coupling matrices: (i)  $h$  for the **10** Higgs and (ii)  $f$  for the **126** Higgs. SO(10) has the property that the Yukawa couplings involving the **10** and **126** Higgs representations are symmetric. Therefore if we assume that CP violation arises from other sectors of the theory (e.g. squark masses) and work in a basis where one of these two sets of Yukawa coupling matrices is diagonal, then it will have only nine parameters. To determine the light neutrino masses, we use the type II seesaw formula, where the  $\mathbf{f}$  is nothing but the **126** Yukawa coupling. Thus all parameters that give neutrino mixings except an overall scale are determined. A simple way to see how large mixings arise in this model is to note that when the triplet term dominates the seesaw formula, we have the neutrino mass matrix  $M_\nu \propto f$ , where  $f$  matrix is the **126** coupling to fermions discussed earlier.

$$M_\nu = c(M_d - M_\ell) \quad (2)$$

Using the generic hierarchical forms forms for  $M_{d,\ell}$  characterized by a small parameter  $\lambda \sim 0.22$  it is easy to see that  $b - \tau$  mass convergence of supersymmetric theories leads to

$$M_\nu = c(M_d - M_\ell) \approx m_0 \begin{pmatrix} \lambda^3 & \lambda^3 & \lambda^3 \\ \lambda^3 & \lambda^2 & \lambda^2 \\ \lambda^3 & \lambda^2 & \lambda^2 \end{pmatrix}. \quad (3)$$

This gives both the  $\theta_{12}$  and  $\theta_{23}$  to be large and it predicts  $\sin\theta_{13} \equiv U_{e3}$  is near 0.18.

There have been two approaches to CP violation in this class of SO(10) models: (i) introducing complex couplings within the minimal  $\mathbf{10}+\mathbf{126}$  Higgs fields[11] and (ii) introducing a  $\mathbf{120}$  Higgs field[12]. In the class (i) models, there is a very specific range of model parameters where one can get CKM CP violation, a point specifically emphasized in the detailed analysis in the last paper of ref.[11]. In the second class of models, the couplings matrices  $h$  and  $f$  are real and symmetric whereas the  $\mathbf{120}$  coupling matrix becomes imaginary and antisymmetric. In this case, one can predict  $U_{e3}$ ,  $\theta_A$  as well as the Dirac CP phase for neutrinos.

#### 4.1. $\mathbf{16}_H$ based models

The other class of SO(10) models for neutrinos that has been widely discussed in the literature includes  $\mathbf{10}_H$ ,  $\mathbf{16}_H$ ,  $\overline{\mathbf{16}}_H$  and  $\mathbf{45}_H$  only [7]. An advantage of these models is that they use low dimensional Higgs multiplets. However, since in these models the only renormalizable term is the  $\mathbf{16}_m\mathbf{16}_m\mathbf{10}_H$ , this can neither explain the observed quark and lepton masses nor can it explain the neutrino masses. One has to therefore include higher dimensional operators in the Yukawa coupling such as  $\mathbf{16}_m\mathbf{16}_m\mathbf{16}_H\mathbf{16}_H$ ,  $\mathbf{16}_m\mathbf{16}_m\overline{\mathbf{16}}_H\overline{\mathbf{16}}_H$ ,  $\mathbf{16}_m\mathbf{16}_H\mathbf{16}_m\mathbf{16}_H$ ,  $\mathbf{16}_m\overline{\mathbf{16}}_H\mathbf{16}_m\overline{\mathbf{16}}_H$ ,  $\mathbf{16}_m\mathbf{16}_m\mathbf{10}_H\mathbf{45}_H$ , where  $\mathbf{16}_m$  stands for various fermion generations. Of these, the first two give symmetric Yukawa couplings and the next two have no symmetry property and the last one can be both symmetric as well as antisymmetric. Since each coupling is a  $3 \times 3$  matrix, there are many more free parameters in such models than observables, one needs additional discrete symmetries to reduce the number of parameters. These models have certain advantages: (i) it is possible to implement the doublet-triplet splitting in a simple way such that the low energy theory below the GUT scale is the MSSM and (ii) the threshold corrections to the gauge couplings are not excessive, so that no particular constraint on symmetry breaking is necessary for the gauge couplings to remain perturbative. Most  $\mathbf{16}$ -Higgs based SO(10) models lead to small value for  $\theta_{13}$ , although it is possible to have variations of the model which have bigger value for it.

### 5. Bottom up approach and leptonic symmetries

In this approach, one looks for symmetries of leptons that would naturally lead to the unusual mixing pattern for leptons and the attempt to gain insight into quark flavor structure from this knowledge. A tantalizing indication of a symmetry comes from the following two observations: (i)  $\theta_{AT} \simeq 45^\circ$  and  $\theta_{13} \leq 0.2$ . In the limit that  $\theta_{13} = 0$ , the neutrino Majorana mass matrix is invariant under a  $\mu - \tau$  exchange symmetry[13]. Departures from it can lead to verifiable correlation between the  $\theta_A - \pi/4$  and  $\theta_{13}$ . Thus this is an approximate symmetry whose existence can be tested in the next round of neutrino experiments. As far as what insight it may provide into quark flavor puzzle, the first step would be to embed it into a more quark lepton unified framework. This has been discussed in a recent series of papers. What is now clear is that even though

none of the charged fermion masses indicate any such symmetry, it is possible to embed these models into grand unified theories. The next step would be to see if they indicate some still higher flavor symmetries that may shed light on the flavor puzzle issue in general.

A much more striking fact is that the solar angle has the value  $\sin^2\theta_\odot \sim \frac{1}{3}$ , a fact which leads to the so-called tribimaximal mixing pattern for neutrinos[14] i.e.

$$U_{PMNS} = \begin{pmatrix} \frac{\sqrt{2}}{\sqrt{3}} & \frac{1}{\sqrt{3}} & 0 \\ -\frac{\sqrt{1}}{\sqrt{6}} & \frac{\sqrt{1}}{\sqrt{3}} & \frac{\sqrt{1}}{\sqrt{2}} \\ \frac{\sqrt{1}}{\sqrt{6}} & -\frac{\sqrt{1}}{\sqrt{3}} & \frac{\sqrt{1}}{\sqrt{2}} \end{pmatrix} \quad (4)$$

. There have been many speculations that this is an indication that the  $\mu - \tau$  exchange symmetry is part of a bigger symmetry such as  $S_3$  or  $A_4$ [15] to mention two examples. The challenge then would be to embed it into a quark-lepton unified framework.  $S_3$  flavor models for quarks already exist in literature and it will be interesting to merge them together.

To give a flavor for the  $S_3$  symmetry example, we note that the mass matrix that leads to tbm has the form:

$$\mathcal{M}_\nu = \begin{pmatrix} a & b & b \\ b & a+c & b-c \\ b & b-c & a+c \end{pmatrix} \quad (5)$$

It turns out that this can be obtained from a mixed type I+II seesaw as follows:  $\mathcal{M}_\nu = M_0 - M_D^T M^{-1} M_D$  where  $M_0$  has the general  $S_3$  invariant form. If there is only one right handed neutrino (or three, of which two have large mass) and  $M_D = (0, m, -m)$ , then one gets the desired form for tri-bimaximal mixing. Note that the dominance of one right handed neutrino could be an indication that the  $S_3$  symmetry is broken in the right handed neutrino sector to  $\mu - \tau$  symmetry. It is possible to construct a detailed model where the charged lepton masses are diagonal so that one has tri-bimaximal mixing.

### 5.1. Quark-lepton complementarity and large solar mixing

There has been a recent suggestion[16] that perhaps the large but not maximal solar mixing angle is related to physics of the quark sector. According to this suggestion, the deviation from maximality of the solar mixing may be related to the quark mixing angle  $\theta_C \equiv \theta_{12}^q$  and is based on the observation that the mixing angle responsible for solar neutrino oscillations,  $\theta_\odot \equiv \theta_{12}^\nu$  satisfies an interesting complementarity relation with the corresponding angle in the quark sector  $\theta_{Cabibbo} \equiv \theta_{12}^q$  i.e.  $\theta_{12}^\nu + \theta_{12}^q \simeq \pi/4$ . It is interesting to pursue the possibility that there is a deep meaning behind it. If Nature is quark lepton unified at high scale, then a relation between  $\theta_{12}^\nu$  and  $\theta_{12}^q$  can be obtained in a natural manner provided the neutrinos obey the inverse hierarchy. However, in such models one generally gets a modified QLC relation due to the fact that true QLC requires that we have  $U_{PMNS} = U_{bm} U_{CKM}^\dagger$  whereas in models one gets  $U_{PMNS} = U_{CKM}^\dagger U_{bm}$  (where  $U_{bm}$  stands for the bimaximal mixing matrix.). This model gives a variation of the quark-lepton complementarity relation and predicts  $\sin^2\theta_\odot \simeq 0.34$  which agrees

with present data at the  $2\sigma$  level. It also predicts a large  $\theta_{13} \sim 0.18$ , both of which are predictions that can be tested experimentally in the near future.

## 6. Conclusion

Neutrino model building- very much a work in progress ! though we have learnt several important things: (i) Seesaw is a simple paradigm with many interesting features; (ii) Quark lepton symmetry and  $B - L$  are nature's new symmetries; (iii) SO(10) GUT is a natural group and testable; (iv) Bottom up scenarios do reveal many new symmetries which can throw light on the flavor structure of quarks. High precision searches for  $\theta_{13}$ , mass ordering, CP phase,  $\beta\beta_{0\nu}$  will "weed" out a lot of models.

This work is supported by National Science Foundation (NSF) Grant No. PHY-0354401.

- [1] For review and references to literature, see R. N. Mohapatra et al. hep-ph/0510213 and R. N. Mohapatra and A. Y. Smirnov, Ann. Rev. Nucl. and Part. Science, **56**, (2006).
- [2] P. Minkowski, Phys. Lett. **B67** , 421 (1977); M. Gell-Mann et al, *Supergravity* (P. van Nieuwenhuizen et al. eds.), North Holland, Amsterdam, 1980, p. 315; T. Yanagida, in *Proceedings of the Workshop on the Unified Theory and the Baryon Number in the Universe* (O. Sawada and A. Sugamoto, eds.), KEK, Tsukuba, Japan, 1979, p. 95; S. L. Glashow, in *Proceedings of the 1979 Cargèse Summer Institute on Quarks and Leptons* (M. Lévy et al. eds.), Plenum Press, New York, 1980, pp. 687; R. N. Mohapatra and G. Senjanović, Phys. Rev. Lett. **44** 912 (1980).
- [3] G. Lazarides et al. Nucl.Phys.**B181**, 287 (1981); R. N. Mohapatra and G. Senjanović, Phys. Rev. **D 23**, 165 (1981);
- [4] R. N. Mohapatra, Phys. Rev. Lett. **56**, 561 (1986); R. N. Mohapatra and J. W. F. Valle, Phys. Rev. **D 34**, 1642 (1986).
- [5] L. J. Hall et al. Phys. Rev. Lett. **84**, 2572 (2000); A. de Gouvea and H. Murayama, Phys. Lett. B **573**, 94 (2003).
- [6] P. H. Frampton et al. Phys. Lett. B **536**, 79 (2002).
- [7] E. Witten, Phys. Lett. B **91**, 81 (1980); C. H. Albright et al., Phys. Rev. Lett. **81**, 1167 (1998); C. H. Albright and S. M. Barr, Phys. Rev. D **58**, 013002 (1998); K. S. Babu et al., Nucl. Phys. B **566**, 33 (2000); X. Ji et al., Phys.Lett. **B633** 755 (2006).
- [8] K. S. Babu and R. N. Mohapatra, Phys. Rev. Lett. **70**, 2845 (1993).
- [9] B. Bajc et al., Phys. Rev. Lett. **90**, 051802 (2003).
- [10] H. S. Goh et al. Phys. Lett. B **570**, 215 (2003).
- [11] H. S. Goh et al, Phys. Rev. D **68**, 115008 (2003); K. S. Babu and C. Macesanu, Phys. Rev. D **72**, 115003 (2005); S. Bertolini et al. arXiv:hep-ph/0605006.
- [12] B. Dutta et al., Phys. Lett. **B603**, 35 (2004).
- [13] See Ref.[1] for references.
- [14] P. Harrison, D. Perkins and W. G. Scott, Phys. Lett. **B 530**, 167 (2002); P. F. Harrison and W. G. Scott, Phys. Lett. **B 535**, 163 (2002), Z. z. Xing, Phys. Lett. **B 533**, 85 (2002).
- [15] W. Grimus and L. Lavoura, hep-ph/0509239; I. de Medeiros Varzielas, S. F. King and G. G. Ross, hep-ph/0512313; K. S. Babu and X. G. He, hep-ph/0507217; E. Ma, Phys.Rev.**D 73** 057304 (2006); F. Caravaglios and S. Morisi, hep-ph/0503234; R. N. Mohapatra, S. Nasri and H. Yu, Phys. Lett.**B639**, 318 (2006) .
- [16] See Ref.[1] for references.

# Future Neutrino Cross Section and Nuclear Effects Studies

**Jorge G. Morfin**

Fermi National Accelerator Laboratory,  
P.O. Box 500, Batavia, IL,  
60510

E-mail: [morfin@fnal.gov](mailto:morfin@fnal.gov)

**Abstract.** A careful study of neutrino scattering physics is an essential part of the program to answer many open questions being addressed by several different physics communities. A deeper understanding of nuclear effects induced by neutrinos and considerably more accurate measurements of neutrino exclusive cross sections are crucial for minimizing systematics of neutrino oscillation experiments and understanding the mechanism by which core-collapse supernovae explode.

## 1. Introduction

What are the open questions in neutrino physics? According to the multi-divisional study on the physics of neutrinos they are the following:

- What are the masses of the neutrinos?
- What is the pattern of mixing among the different types of neutrinos?
- Are neutrinos their own antiparticles?
- Do neutrinos violate the symmetry CP?
- Are there “sterile” neutrinos?
- Do neutrinos have unexpected or exotic properties?
- What can neutrinos tell us about the models of new physics beyond the Standard Model?

The answer to almost every one of these questions involves understanding how neutrinos interact with matter! In particular, the requirements on the neutrino scattering program from the particle physics community are quite stringent. For high-statistics  $\nu_\mu$  neutrino oscillation disappearance studies, such as the MINOS experiment currently running at Fermilab, we need accurate measurements of nuclear effects with neutrinos for a neutrino energy calibration. For upcoming  $\nu_e$  appearance experiments a careful measurement of pion production cross sections, both coherent and resonant, are essential for both the  $\nu$  to  $\bar{\nu}$  exposures.

Currently there are three experiments designed specifically to address the topic of low-energy neutrino-nucleus scattering: the  $\nu$ -SNS experiment at ORNL and the SciBooNE and MINER $\nu$ A experiments at Fermilab.

## 2. The $\nu$ -SNS Experiment at ORNL [1]

The construction of the Spallation Neutron Source at ORNL provides an extraordinary opportunity to make the high precision neutrino measurements required to satisfy the needs of important astrophysics problems to be addressed over the next few years. As a byproduct the SNS will produce, the worlds most intense flux of decay-at- rest neutrinos which have an energy spectrum that fortuitously overlaps with the energy of interest for nuclear astrophysics, supernovae dynamics, and nuclear theory. A multi- institutional collaboration with more than 40 scientists is actively involved in the proposal to build the facility.

At present, only neutrino cross sections on  $C^{12}$  have been measured well (roughly 4-10 % errors). The only other reported results are for  $H^2$ ,  $Fe^{56}$  and  $I^{127}$ , all with  $\sim 40\%$  uncertainty. The anticipated neutrino flux at the SNS facility will allow the measurement of the charged-current neutrino-nucleus cross section for any nuclear target to a statistical accuracy of better than 10% in one year of running.

### 2.1. Proposed Facility

The neutrino detector and shielding enclosure would be located inside the SNS target hall. It would be at a mean distance of  $\sim 20\text{m}$  from the spallation target, and at an angle of  $165\text{deg}$  relative to the incoming proton beam direction. The available floor space is  $4.5\text{m} \times 4.5\text{m}$  with a clear height of  $6.5\text{m}$ .

At full power (1.0 MW) the SNS will bombard a mercury target with a 1.0 mA, 1.0 GeV proton beam. The resulting neutrino flux at the detector location will be  $1.0 \times 10^7 \nu/\text{s}/\text{cm}^2$  of each flavor, providing several tens of neutrino interactions per day for a ten ton detector. This must be compared with the cosmic ray muon [or neutron] flux through this volume of  $2.5 \times 10^8$  [ $1.4 \times 10^6$ ] events per day. Such cosmic ray events must be suppressed through a combination of the SNS time structure, an active veto counter, and shielding.

The facility would consist of two detectors for neutrino cross section measurements that would operate simultaneously. The available volume inside the shielded enclosure ( $3.5 \times 3.5 \times 5.5 \text{ m}^3$ ) is sufficient for two detectors with a mass of  $\sim 20$  tons each. Each will be designed to allow for reuse of the detectors with different target material.

One of the detectors would be a homogeneous scintillation detector filling the bottom half of the  $\nu$ -SNS enclosure. A  $43 \text{ m}^3$  steel tank would be viewed by 600 8-inch PMTs, resulting in a fiducial volume of about  $15 \text{ m}^3$ . This detector would be used to measure neutrino-nucleus cross sections on liquid target materials like carbon (mineral oil), oxygen (water) or deuterium (heavy water). Monte Carlo simulations indicate a rate of 1300 events/year for charged-current interactions on carbon.

The second detector is based on gas proportional counters interleaved with thin sheets of solid target materials. This detector would be mounted above the homogeneous detector and would be slightly smaller in size.

### 2.2. The $\nu$ -SNS Scientific Program

The first neutrino cross section measurement would be made with iron as the target material in the segmented detector due to the great importance of the iron cross sections for understanding the electron capture that drives core collapse at the onset of the supernova and for understanding the role that neutrino-nucleus interactions have in driving the supernova explosion. Simultaneously a cross section measurement on carbon, using mineral oil, would be made in the liquid detector. Since carbon is the only nucleus that has been previously measured, an accurate initial measurement of this cross section will allow us to understand the neutrino flux normalization, calibrate the detector, and understand the background environment. Cross sections on iron and carbon with an accuracy of about 10% should be achievable within the first full year of operation.

A program of neutrino cross section measurements that are important for understanding nucleosynthesis as well as supernova dynamics would follow these initial measurements on iron and carbon. Accurate neutrino cross section measurements on such relatively simple nuclei spanning a wide mass range ( $A = 16, 58, \text{ and } 208$ ) would be a crucial first step toward assessing and eventually improving the reliability of neutrino-nucleus cross section calculations.

$\nu$ -SNS will also make definitive measurements of nuclear excitations that would be difficult to generate or analyze with any other type of experiment. When combined with reliable nuclear theory, this will enable a more quantitative understanding of neutrino cross sections throughout the periodic table.

In order to make precise neutrino-nucleus cross section measurements both statistical and systematic errors must be minimized. The combination of SNS time structure, passive shielding and active veto allows us to make measurements that are largely background free. As a result the statistical accuracy is well-defined by the number of signal counts. The expected statistical significance for one year of operation at full SNS power ranges from  $\leq 1.4\%$  for lead to  $\sim 7.4\%$  for oxygen.

### 3. The SciBooNE Experiment at the FNAL Booster Neutrino Beam <sup>1</sup>

As we proceed up the neutrino energy scale, we come to the concept of installing the K2K SciBar detector in the FNAL Booster Neutrino Beamline in an experiment called SciBooNE [3]. The marriage of a high rate, low energy neutrino beam and the fine granularity of SciBar is a unique opportunity for precise measurements of neutrino cross sections since both are already built and have been operated very successfully. The energy range covered by SciBooNE is very appropriate for understanding the backgrounds of T2K [2].

The current schedule assumes that the SciBooNE detector will be installed and begin commissioning in the spring of 2007 and exposed to  $2 \times 10^{20}$  POT in one year of running.

#### 3.1. The Booster Neutrino Beam at FNAL

To create the Booster Neutrino Beam (BNB), 8 GeV protons are extracted from the Booster and steered to strike a beryllium target. This target sits at the upstream end of a magnetic horn to focus the mesons, primarily  $\pi^+$ , produced by the  $p$ -Be interactions. Following the horn is a 50 m long decay pipe that gives  $\pi^+$  a chance to decay and produce neutrinos, before the mesons encounter an absorber. By reversing the polarity of the horn current,  $\pi^-$  are focused and hence a predominantly antineutrino beam is created.

The pion and kaon production cross sections from  $p$ -Be interactions are the most important input to the neutrino flux prediction, and the most uncertain. These cross sections have been measured by the HARP experiment at CERN [4]. This will allow a very precise prediction of neutrino and antineutrino fluxes in the BNB.

The entire range of the T2K energy spectrum is encompassed within the spectrum of SciBooNE. This indicates why SciBooNE is of direct interest to T2K.

#### 3.2. The SciBooNE Detector

The SciBooNE detector will be located 100 m downstream from the neutrino production target. The detector complex will consist of three detectors: a scintillator tracking detector (SciBar), an electromagnetic calorimeter (EC) and a muon range detector (MRD).

SciBar [5] is a fully active, finely segmented tracking detector which was operated at K2K from October 2003 to November 2004.

The tracker consists of extruded scintillator strips, each  $1.3 \times 2.5 \times 300 \text{ cm}^3$ . The scintillators are arranged vertically and horizontally to construct a  $3 \times 3 \times 1.7 \text{ m}^3$  volume with a total mass of

<sup>1</sup> My thanks to Katsuki Hiraide, Kyoto University, for supplying much of the text for this section on SciBooNE.

15 tons, and a fiducial mass of 9.38 tons. Each strip is read out by a wavelength-shifting (WLS) fiber attached to a 64-channel multi-anode PMT (MA-PMT). Charge and timing information from each MA-PMT is recorded by custom electronics.

The EC is installed downstream of SciBar, and consists of 32 vertical and 30 horizontal modules made of scintillating fibers embedded in lead foils. Each module has dimensions of  $4.0 \times 8.2 \times 262 \text{ cm}^3$ , and is read out by two 1" PMTs on both sides. The EC has a thickness of  $11X_0$  along the beam direction. The energy resolution of the EC is  $14\%/\sqrt{E} [\text{GeV}]$ .

The MRD is located downstream of EC. The MRD will consist of 12 layers of iron plates sandwiched between layers of plastic scintillator. The cross sectional area of each plate is approximately  $3.5 \times 4.0 \text{ m}$ , and each plane has a thickness of 5 cm of iron.

### 3.3. SciBooNE Physics

If we make the assumption that in the one year run,  $0.5 \times 10^{20}$  protons on target (POT) will be delivered in neutrino mode and  $1.5 \times 10^{20}$  POT will be delivered in antineutrino mode, SciBooNE would study, among others, the following channels with the given statistics.

- Charged Current Coherent Pion Measurement

Recently, K2K observed no evidence for coherent charged pion production in neutrino-carbon interaction in the energy range of a few GeV [6]. SciBooNE will have antineutrino mode running as well as neutrino mode running, and hence can perform further studies of CC coherent pion production in the low energy range in both neutrino- and antineutrino-carbon interaction with the same detector.

After subtracting the background,  $\sim 160$  ( $\sim 240$ ) CC coherent pion events are expected in the region with  $Q^2 < 0.10 (\text{GeV}/c)^2$  in neutrino (antineutrino) mode, based on the Rein and Sehgal model. The purity for CC coherent pion production in the sample is estimated to be 44% (49%) in neutrino (antineutrino) mode.

- Charged Current Single Pion (CC- $1\pi^+$ ) Cross Section

The expected number of CC- $1\pi^+$  interactions in SciBar is  $\sim 14,000$  assuming  $0.5 \times 10^{20}$  POT. Selecting two track events and requiring that both are MIP-like yield a sample of  $\sim 2,900$  events that are 47% pure CC- $1\pi^+$  events. With this cut efficiency, we still expect less than 5% statistical uncertainty per energy bin. Further requiring large energy deposited near the vertex can separate  $\nu p \rightarrow \mu p \pi^+$  from  $\nu n \rightarrow \mu n \pi^+$ .

- Neutral Current Single Pion (NC- $1\pi^0$ ) Cross Section

Since the neutrino spectrum in the BNB is so well matched to that of T2K, a measurement of the NC- $1\pi^0$  production rate at SciBooNE is directly applicable to T2K. The difference between these two beams in the high energy tail does mean, however, that the NC- $1\pi^0$  production rate at SciBooNE will not be exactly the same as that in the T2K beam. With the expected sample of  $\sim 1,900$  such interactions for SciBooNE (assuming  $0.5 \times 10^{20}$  POT), a 15% cross section measurement can be obtained.

- Antineutrino Cross Sections

The state of antineutrino cross section knowledge in the few GeV range is very poor with only a handful of low statistics measurements. The proposed SciBooNE antineutrino run of  $1.5 \times 10^{20}$  POT will provide healthy numbers for an antineutrino CC-QE measurement and sufficient numbers for CC- $1\pi$  and NC- $1\pi^0$  measurements.

## 4. The MINER $\nu$ A Experiment at the FNAL Main Injector Neutrino Beam (NuMI)

The NuMI Facility at Fermilab, based on the 120 GeV protons from the Main Injector (MI) accelerator, is providing an extremely intense beam of neutrinos for the MINOS Neutrino Oscillation Experiment, yielding several orders of magnitude more events per kg of detector

per unit of time than the earlier Tevatron neutrino beam. It is an ideal place for a high statistics (anti)neutrino-nucleon/nucleus scattering experiments. The MINER $\nu$ A (Main Injector Experiment:  $\nu$  A) [10] experiment, a collaboration of elementary-particle and nuclear physicists, will install a fully active fine-grained solid scintillator detector in this beam. The overall goals of the experiment are to measure absolute exclusive cross-sections, study nuclear effects in  $\nu$  - A interactions (with A varying from He to Pb), perform a systematic study of the resonance-DIS transition region and the lower  $Q^2$  DIS region including the extraction of high- $x_{Bj}$  parton distribution functions.

#### 4.1. The Fermilab NuMI Facility

The Fermilab NuMI facility is made up of the technical beamline components including target, two magnetic focusing horns, evacuated decay pipe, monitoring devices, shielding and the underground facilities to contain the beamline components. A large, on-site experimental detector hall  $\sim$  100 meters underground currently contains the MINOS near detector and will house the MINER $\nu$ A detector just upstream of the MINOS near detector.

The neutrino energy distribution of the NuMI beam can be chosen by changing the distance of the target and second horn with respect to the first horn, as in a zoom lens, or, with reduced intensity but quicker tuning time, by simply varying the distance of target from the first horn and leaving the second horn in a fixed position. Depending on the chosen configuration, event rates will vary from 60K to 520K per ton of detector and  $10^{20}$  protons on target (POT). The Main Injector is now delivering protons to MINOS at a rate equivalent to around  $2.5 \times 10^{20}$  POT/year and will slowly build up to higher proton intensities reaching  $\sim 4.0 \times 10^{20}$  POT/year by the time MINER $\nu$ A starts taking data.

For the MINOS experiment the beamline will be operating mainly in its lowest possible neutrino energy configuration to be able to reach desired low values of  $\delta m^2$ . For the proposed NO $\nu$ A experiment [12], the beam will be operating in the full ME configuration.

#### 4.2. The MINER $\nu$ A Detector

The MINER $\nu$ A detector is a hybrid of a fully-active fine-grained detector and a traditional calorimeter and is made up of a number of sub-detectors with distinct functions in reconstructing neutrino interactions. The fiducial volume for most analyses is the inner ‘‘Active Target’’ where all the material of the detector is the scintillator strips themselves. The scintillator detector does not fully contain events due to its low density and low  $Z$ , and therefore, the MINER $\nu$ A design surrounds the scintillator fiducial volume with sampling detectors. To construct these sampling detectors, the scintillator strips are intermixed with absorbers. For example, the side and downstream (DS) electromagnetic calorimeters (ECALs) have lead foil absorbers. Surrounding the ECALs are the hadronic calorimeter (HCAL) where the absorbers are steel plates. On the sides of the detector the outer detector (OD) plays the role of the HCAL. In the upstream end of the detector are the nuclear targets of pure C, Fe and Pb as well as a LHe target. The He target vessel is directly upstream of the main MINER $\nu$ A detector. Upstream of the detector and LHe target vessel is a veto of steel and scintillator strips to shield MINER $\nu$ A from incoming soft particles produced upstream in the hall. A complete description of MINER $\nu$ A is found in the proposal [11] and TDR [14].

The core active element will be extruded triangular-shaped scintillator strips read out *via* wavelength-shifting fibers. Readout of the fibers will be done with multi-anode photomultiplier tubes (MAPMTs), connected to the wavelength shifting fibers *via* an optical cable system.

There are three distinct orientations of strips in the inner detector and veto, separated by  $60^\circ$ , and labeled X, U, V. A single module of MINER $\nu$ A has two X layers to seed two-dimensional track reconstruction, and one each of the U and V layers to reconstruct three-dimensional tracks.

Monte Carlo studies of this detector and subsequent prototype studies have confirmed that light-sharing with the triangular-shaped scintillator extrusions (3.1 cm base and 1.7 cm height) yield reconstructed point resolution of just under 3 mm. The electromagnetic ( $\pi^0$ ) energy resolution is  $6\%/\sqrt{E_{em}}$  while the hadron energy resolution is  $4\% + 18\%/\sqrt{E_{had}}$ .

#### 4.3. Overview of the MINER $\nu$ A Physics Program

For a four-year run with 1-year of LE running parasitically with MINOS and 3-years of ME running parasitically with NO $\nu$ A we expect a total of **9.0M** in the 3-ton fiducial volume of the active scintillator target and a total of another **5.5M** total events on the four nuclear targets of the MINER $\nu$ A experiment.

The high-statistics studies listed below are important for both the particle and nuclear physics communities, providing information complementary to JeffersonLab charged lepton studies in the same kinematic range

- Precision measurement of the quasi-elastic neutrino–nucleus cross-section, including its  $E_\nu$  and  $q^2$  dependence, and study of the nucleon axial form factors. Over **800 K** events are expected in the fiducial volume during the four-year MINER $\nu$ A run.
- Determination of cross-sections in the resonance-dominated region for both neutral-current (NC) and charged-current (CC) interactions, including study of isospin amplitudes, measurement of pion angular distributions, isolation of dominant form factors, and measurement of the effective axial mass. A total of **1.7M** one-pion events make up the low- $W$  resonance sample.
- Clarification of the  $W$  ( $\equiv$  mass of the hadronic system) transition region where resonance production merges with neutrino deep-inelastic scattering, including tests of phenomenological characterizations of this transition such as quark/hadron duality. A sample of **2.1 M** multi-pion events is expected with  $W \leq 2.0$  GeV.
- Precision measurement of coherent single-pion production cross-sections, with particular attention to target  $A$  dependence. Coherent  $\pi^0$  production, via the neutral current, is a significant background for next-generation neutrino oscillation experiments seeking to observe  $\nu_\mu \rightarrow \nu_e$  oscillation. A sample of **89 K** CC events is expected off carbon. The expected NC sample is roughly half the CC sample.
- Examination of nuclear effects in neutrino interactions, including final-state modifications in heavy nuclei, by employing helium, carbon, iron and lead targets. These effects play a significant role in neutrino oscillation experiments measuring  $\nu_\mu$  disappearance as a function of  $E_\nu$ . It has recently been suggested [13] that, for a given  $Q^2$ , shadowing can occur at much lower energy transfer ( $\nu$ ) for neutrinos than for charged leptons. This effect is unaccounted for in neutrino event generators. With sufficient  $\bar{\nu}$  running, a study of flavor-dependent nuclear effects can also be performed. Due to the different mix of quark flavors, this is another way in which neutrino and charged-lepton nuclear effects differ. MINER $\nu$ A will collect over **0.6, 0.4, 2.0 and 2.5 M** CC events off He, C, Fe and Pb targets respectively in addition to the carbon of the scintillator.
- Study of nuclear effects on  $\sin^2 \theta_W$  measurements, and the NC/CC ratio for different nuclear targets.
- With a sample of over **4.3 M** CC DIS events, a much-improved measurement of the parton distribution functions, particularly at large  $x_{Bj}$ , will be possible using a measurement of all three  $\nu$  structure functions. Although we expect over **150 K** CC  $\bar{\nu}$  events in the four year MINER $\nu$ A  $\nu$  run, an additional dedicated  $\bar{\nu}$  run would be required to measure the three  $\bar{\nu}$  structure functions with similar precision.
- Examination of the leading exponential contributions of perturbative QCD.

- With nearly **240 K** fully reconstructed exclusive events, precision measurement of exclusive strange-production channels near threshold. This will significantly improve our knowledge of backgrounds in nucleon-decay searches. Also, determination of  $V_{us}$ , and searches for strangeness-changing neutral-currents and candidate pentaquark resonances will be undertaken. Measurement of hyperon-production cross-sections, including hyperon polarization, is feasible with exposure of MINER $\nu$ A to  $\bar{\nu}$  beams

These are worthy research topics in their own right, and improved knowledge in most is essential to minimizing systematic uncertainties in neutrino-oscillation experiments.

## 5. Conclusions

There is an obvious and crucial need for the measurement of exclusive cross sections and the study of nuclear effects in the 10 MeV to 10 GeV energy range

- $\nu$ -SNS will measure  $\nu$  capture cross sections in the energy range relevant for the study of uipernovae core collapse.
- SciBooNE in the Fermilab Booster Neutrino Beam will measure both  $\nu$  and  $\bar{\nu}$  cross sections for energies relevant for T2K oscillation studies.
- MINER $\nu$ A in the Fermilab NuMI beam will measure cross sections and study nuclear effects to both  $\nu$  and  $\bar{\nu}$  at energies relevant for both NuMI and T2K studies and study nucleon structure from quasi-elastic, resonance, through the transition region to DIS.

- [1] Yu. Efremenko et al, Nucl. Phys. Proc. Suppl. **138**, 343 (2005) and [www.phy.ornl.gov/nusns/proposal.pdf](http://www.phy.ornl.gov/nusns/proposal.pdf).
- [2] K. Nishikawa *et al.* [T2K Collaboration], "Letter of Intent for a Neutrino Oscillation Experiment at JHF," KEK Report (2003), <http://neutrino.kek.jp/jhfnu/>.
- [3] SciBooNE Collaboration, arXiv:hep-ex/0601022.
- [4] HARP website, <http://harp.web.cern.ch/harp/>.
- [5] K. Nitta *et al.*, Nucl. Instrum. Meth. A **535** (2004) 147.
- [6] M. Hasegawa *et al.* [K2K Collaboration], Phys. Rev. Lett. **95** (2005) 252301.
- [7] B. Mukherjee *et al.*, *Cyclotrons and Their Applications 2001, Sixteenth International Conference*, ed. F. Marti, p.108 (2001).
- [8] see, for example, W. Y. Lee *et al.*, Phys. Rev. Lett. **37** (1976) 186.
- [9] E. Ables *et al.* [MINOS Collaboration], FERMILAB-PROPOSAL-0875 and A. Marchionni [MINOS Collaboration], FERMILAB-CONF-05-429-AD-E
- [10] The MINER $\nu$ A Collaboration consists of groups from the following institutions: U Athens, U California/Irvine, U Dortmund, Fermilab, Hampton U, IL Inst. Tech., Inst. for Nuc. Research - Moscow, James Madison U, U Minnesota-Duluth, Jefferson Lab, U Nacional Ingenieria de Lima, N. Illinois U, Northwestern U, Pontifica U Catolica de Lima, U Pittsburgh, U Rochester, Rutgers U, U Texas-Austin, Tufts U, William and Mary U.
- [11] D. Drakoulakos *et al.* [Minerva Collaboration], arXiv:hep-ex/0405002. <http://minerva.fnal.gov/>
- [12] D. S. Ayres *et al.* [NOvA Collaboration], arXiv:hep-ex/0503053.
- [13] S. Boyd, S. Kulagin, J. G. Morfin and R. Ransome, "Studying Neutrino-induced Nuclear Effects with the MINER $\nu$ A Detector". MINER $\nu$ A Note 700, September, 2004. <http://minerva-docdb.fnal.gov/cgi-bin/ShowDocument?docid=52>
- [14] The MINER $\nu$ A Technical Design Report, 1 December 2006, <http://minerva-docdb.fnal.gov/cgi-bin/ShowDocument?docid=700>
- [15] K. Nitta *et al.* (K2K SciBar), Nucl. Instrum. Meth. **A536**, 147 (2004)

# T2K and beyond

**Takeshi Nakadaira**

High Energy Accelerator Research Organization(KEK), 1-1 Oho, Tsukuba, Ibaraki 305-0801  
Japan

E-mail: nakadair@neutrino.kek.jp

**Abstract.** The project status of T2K is presented. T2K will search for the  $\nu_\mu \rightarrow \nu_e$  oscillation using the high intensity  $\nu_\mu$  beam produced by J-PARC. The experimental setup and the prospects are discussed. The possible long-term future plans are also presented.

## 1. Introduction

The Tokai-to-Kamioka experiment (T2K) [1, 2] is the successor experiment of K2K, the KEK to Kamioka long-baseline neutrino oscillation experiment(1999–2005) [3]. T2K will utilize the neutrino beam which is  $\sim 50$  times intense compared with K2K, and the neutrino beam energy is optimized for the neutrino oscillation measurement based on the known oscillation parameters.

The high-intensity  $\nu_\mu$  beam will be generated at Japan Proton Accelerator Research Complex (J-PARC) [4] in Tokai village towards the Super-Kamiokande (SK) [5]. We will investigate the neutrino oscillation during the flight length of 295 km. The T2K collaboration consists of  $\sim 200$  members from 58 institutes in 11 countries.

## 2. Physics motivation

The main goal of T2K is to determine the oscillation parameters,  $\theta_{13}$ , and  $\delta$ , in neutrino mixing matrix [6] which is parametrized as

$$\begin{pmatrix} \nu_e \\ \nu_\mu \\ \nu_\tau \end{pmatrix} = \begin{pmatrix} 1 & 0 & 0 \\ 0 & \cos \theta_{23} & \sin \theta_{23} \\ 0 & -\sin \theta_{23} & \cos \theta_{23} \end{pmatrix} \begin{pmatrix} \cos \theta_{13} & 0 & \sin \theta_{13} e^{-i\delta} \\ 0 & 1 & 0 \\ -\sin \theta_{13} e^{-i\delta} & 0 & \cos \theta_{13} \end{pmatrix} \times \begin{pmatrix} \cos \theta_{12} & \sin \theta_{12} & 0 \\ -\sin \theta_{12} & \cos \theta_{12} & 0 \\ 0 & 0 & 1 \end{pmatrix} \begin{pmatrix} \nu_1 \\ \nu_2 \\ \nu_3 \end{pmatrix},$$

where  $\nu_x (x = e, \mu, \tau)$  and  $\nu_i (i = 1, 2, 3)$  are the flavor eigenstate and the mass eigenstate, respectively.  $\theta_{12}, \theta_{23}$  and  $\theta_{13}$  are the mixing angles and  $\delta$  is the complex phase of the neutrino mixing matrix. Here,  $\theta_{13}$  is the only remaining mixing angle, which has not been measured. The results from the reactor experiments [7, 8] and K2K [9] indicate that  $\sin^2 2\theta_{13}$  is expected to be smaller than 0.15. Also, there is no information about the  $CP$  phase  $\delta$ .

T2K search for the  $\nu_\mu$  to  $\nu_e$  oscillation to obtain the information about  $\theta_{13}$  and  $\delta$ . Because the matter effect [10] is negligibly small in the T2K condition, the oscillation probability is

approximated around the first oscillation maximum assuming  $\Delta m_{32}^2 \sim \Delta m_{31}^2$  as

$$P(\nu_\mu \rightarrow \nu_e) \approx \sin^2 2\theta_{13} \sin^2 2\theta_{23} \sin^2 \left( \frac{\Delta m_{31}^2}{4E} \right) \mp 4J_r \sin \delta \left( \frac{\Delta m_{21}^2}{2E} \right) \sin^2 \left( \frac{\Delta m_{31}^2}{4E} \right),$$

where  $E$  and  $L$  are the neutrino energy and flight length, respectively.  $\Delta m_{ij}^2 (i, j = 1, 2, 3)$  is the mass squared difference between two mass eigenstates. The second term is  $CP$  asymmetric, and its sign is  $- (+)$  for  $\nu (\bar{\nu})$ .  $J_r \equiv \cos \theta_{12} \sin \theta_{12} \cos \theta_{23} \sin \theta_{23} \cos^2 \theta_{13} \sin \theta_{13}$  is the Jarlskog parameter of neutrino mixing matrix. The magnitude of  $CP$  asymmetry is also depends on  $\theta_{13}$  because the  $J_r$  is proportional to  $\sin \theta_{13}$ .

### 3. Principle of T2K

The experimental principle of T2K is quite similar to K2K. We estimate the neutrino flux at the SK by extrapolating the flux measured at the near detector, which is 280 meters away from the target. Then, we measure the neutrino oscillation parameters from the comparison between the observation by SK and the expectation from the  $\nu$  beam flux.

Based on the current knowledge of the  $\Delta m_{23}^2$ , the first oscillation maximum for  $L = 295$  km corresponds to the neutrino energy of  $\sim 0.6$  GeV. We tune the peak energy of the  $\nu$  beam at this energy to improve the sensitivity for the neutrino oscillation. The dominant process in  $\nu$ -nucleon interactions for this energy region is charged-current quasi-elastic (CC-QE) interaction. The CC-QE interactions in SK are easily identified by selecting the events with a single Cherenkov ring. Because the CC-QE interaction is a two-body process, we can reconstruct the neutrino energy with  $\sim 10$  % precision by assuming the CC-QE kinematics. The methods of the CC-QE event selection and the energy reconstruction by SK are established very well in the study of atmospheric neutrinos.

The non CC-QE  $\nu$ -nucleon interactions, such as a charged-current pion production ( $\nu N \rightarrow \ell N' \pi$ ), are the background for the neutrino energy reconstruction. Furthermore, the neutral-current events with  $\pi^0$  production ( $\nu N \rightarrow \nu N' \pi^0$ ) are the dominant background source of  $\nu_e$  detection, since  $\pi^0$  can be miss-identified as a  $\nu_e$  when one of the  $\gamma$ s from  $\pi^0$  decay is missed or two  $\gamma$  Cherenkov rings are overlapped. Thus, the fraction of the neutrino with the energy greater than a few GeV is required to be small to reduce the non CC-QE interactions.

### 4. Experimental apparatuses

J-PARC is the multipurpose proton accelerator which consists of the 400 MeV LINAC, 1 MW 3 GeV Rapid Cycle Synchrotron (RCS) and 0.75MW 50 GeV Synchrotron(MR). At the beginning, the energy of the LINAC and MR are 200 MeV and 30 GeV, respectively.

The  $\nu$ -beam line in J-PARC generate almost pure  $\nu_\mu (\bar{\nu}_\mu)$  beam by the conventional method. The protons hit the graphite target and the generated  $\pi^+$  ( $\pi^-$ ) are focused by 3 electromagnetic horns. Then,  $\nu_{\mu s} (\bar{\nu}_{\mu s})$  are produced by the decay of the pions while traveling in the decay tunnel. The neutrino energy at SK is pseudo-monochromatic because “off-axis” (OA) scheme [11] is adopted. The peak of  $\nu$  energy spectrum at SK is adjusted to the oscillation maximum by changing off-axis angle from  $2^\circ$  to  $2.5^\circ$ .

The J-PARC accelerator construction started in 2001. Now, the installation of the beam instruments such as magnets is in progress, and the accelerator commissioning starts in 2006. During the preparation of the MR beam line components, one of the problems which we encountered is that some of RF cores discharges with 15 kV/gap in long term tests. The cause of this failure have already been identified, but the MR commissioning will start with the current RF system on schedule, because we found it works in low beam power operation. The R&D work to solve this problem is in progress, and we aim to replacing the current RF system with new one around 2010.

The  $\nu$  beam-line construction was started in 2004. The civil construction and the development of the beam instruments are going well. The first module of the superconducting combined-function magnet for the proton beam transport is produced, and excited to the full operation current successfully. The mechanical prototype of the graphite target, which has enough thermal shock resistance against 0.75 MW beam, is fabricated. The prototype of the first electromagnetic horn succeeds in the test operation with 320 kA.

The characteristics of the neutrino beam is measured by two detectors located at the 280 meters from the target [12]. One is the on-axis detector which consists of 14 modules of iron-scintillator stacks. The on-axis detector will measure the  $\nu$  beam profile to determine the  $\nu$  beam direction within 1 mrad. The other is the off-axis detector to measure the  $\nu$  flux in the far-detector direction. The tracking system, which consists of TPCs and the layers of finely segmented scintillating bars, and the electromagnetic calorimeter are installed in the magnetic field of 0.2 T to measure  $\nu_\mu$ ,  $\bar{\nu}_\mu$  and  $\nu_e + \bar{\nu}_e$  fluxes separately. The muons are detected by the Muon Range Detector. The cross sections of  $\nu$ -nucleon interactions are also studied by the off-axis detector. The detector which is optimized for measuring the rate of neutral current  $\pi^0$  production is also installed in the magnet.

The far detector for T2K is SK, which is a 50 kt water Cherenkov detector. The reconstruction to recover the damage by the accident in 2001 is completed in Apr. 2006. The full operation with the original 40% photo-coverage starts in Jul. 2006, and it becomes ready for T2K.

The intermediate detector located at 2 km from the target is proposed [13, 14]. The energy spectrum at the 2 km detector position is more similar to that at SK than the 280 m detector position. The 2 km detector is expected to reduce the uncertainties from the extrapolation of the neutrino flux. The current design of the detector configuration consists of a liquid argon TPC, a water Cherenkov detector and a muon range detector. The facilities for the intermediate detector is planning to be requested in Japan after the commissioning of J-PARC facilities.

### 5. Prospects in T2K Phase-I

The feasibility of T2K for  $5 \times 10^{21}$  Protons-On-Target (POT), which is corresponds to  $\sim 5$  years operation with the full intensity beam, is studied. In the study, we assumed  $\sin^2 2\theta_{13} = 0.1$ ,  $\sin^2 2\theta_{23} = 1.0$  and  $\Delta m_{13}^2 = 2.5 \times 10^{-3} \text{ eV}^2$ . Figure 1 shows the energy distribution of the  $\nu_e$  candidate events observed by SK in the Monte Carlo simulation. The expected  $\nu_\mu \rightarrow \nu_e$  signals which has the reconstructed energy from 0.35 GeV to 0.85 GeV is 103 events, while the background from the intrinsic  $\nu_e$  in the beam and the backgrounds from  $\nu_\mu$  interactions are 13 and 10 events, respectively. The 90% CL sensitivity to  $\sin^2 2\theta_{13}$  is 0.008 where  $\delta = 0$  and 10% systematic uncertainty for the background subtraction are assumed.

T2K also provides the precise measurement of  $\nu_\mu$  disappearance. The statistics become 50 times larger than K2K final result. The expected errors for the oscillation parameters are  $\delta(\sin^2 2\theta_{23}) \sim 0.01$  and  $\delta(\Delta m_{23}^2) < 1 \times 10^{-4} \text{ eV}^2$ .

### 6. Beyond T2K Phase-I

If the obtained  $\sin^2 2\theta_{13}$  is greater than 0.01, it paves the way for the  $CP$  violation search in  $\nu$  sector. The  $CP$  asymmetry arise in the difference of the  $\nu_\mu \rightarrow \nu_e$  oscillation probabilities between neutrinos and anti-neutrinos.

$$A_{CP} \equiv \frac{P(\nu_\mu \rightarrow \nu_e) - P(\bar{\nu}_\mu \rightarrow \bar{\nu}_e)}{P(\nu_\mu \rightarrow \nu_e) + P(\bar{\nu}_\mu \rightarrow \bar{\nu}_e)} \approx \frac{\Delta m_{12}^2 L}{E} \cdot \frac{\sin 2\theta_{12}}{\sin \theta_{13}} \cdot \sin \delta$$

In the 2nd phase of T2K, it is planned to increase the proton beam intensity up to 4MW by upgrading the J-PARC accelerator. The 1 Mt water Cherenkov detector is also proposed. The statistics after both accelerator and far detector upgrade is expected to be increased by

more than a factor of 100 with respect to T2K-I. Figure.3 shows the  $3\sigma$  sensitivity for the  $\sin\delta$  assuming the data which is taken for 2 years with  $\nu_\mu$ -beam and 6 years with  $\bar{\nu}_\mu$ -beam in T2K phase-II. If the  $\sin\delta$  is greater than 0.3 and the systematic uncertainties controlled less than 2%, the  $CP$  asymmetry in  $\nu$  oscillation will be observed.

The ideas to build another far detector at the second oscillation maximum point, which is located at  $\sim 1000$  km away from J-PARC, are proposed [15, 16]. The contribution of the  $CP$  asymmetric term to the  $\nu_\mu \rightarrow \nu_e$  oscillation probability become 3 times larger than that at the first oscillation maximum point because the magnitude of the  $CP$  asymmetric term is proportional to the baseline length. Because the matter effect become significant in the second oscillation maximum point, It may be possible to resolve the mass hierarchy if  $\delta$  is suitable.

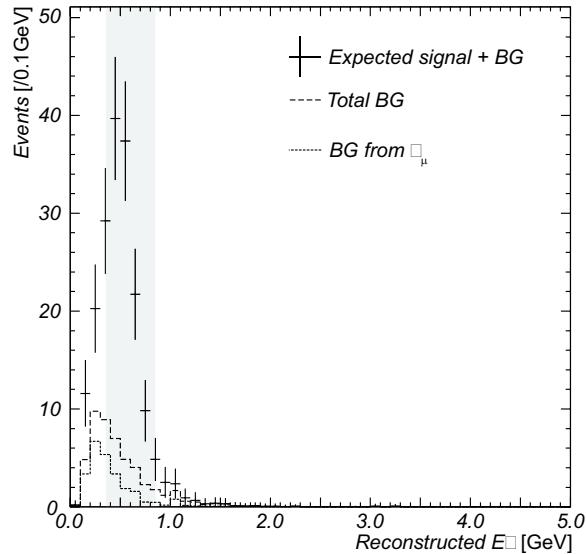


**Figure 1.** The data points shows the energy distribution of the  $\nu_e$  candidate events observed by SK in the Monte Carlo simulation, where  $\sin^2 2\theta_{13} = 0.1$  and  $\Delta m^2 = 2.5 \times 10^{-3}$  [eV<sup>2</sup>] are assumed. The dotted histogram shows the background originated from  $\nu_\mu$ . The dashed histogram shows all the background events including the beam intrinsic  $\nu_e$ . The MC statistics corresponds to a 5-years operation.

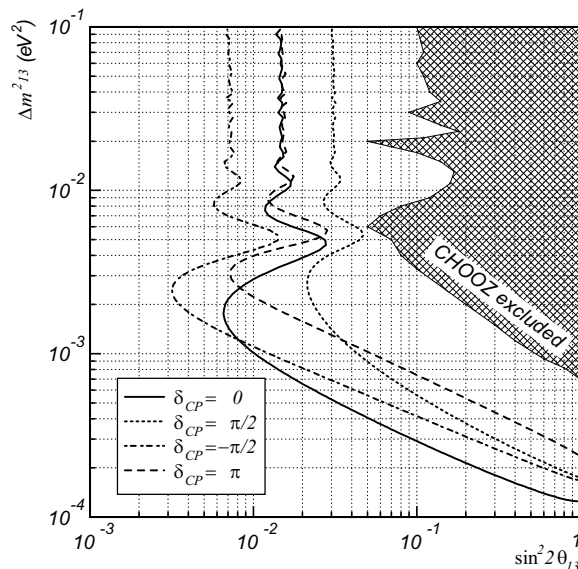


**Figure 2.** The 90% CL sensitivity to  $(\sin^2 2\theta_{13}, \Delta m_{13}^2)$  for the  $5 \times 10^{21}$  POT data acquisition, where the 10% systematic uncertainty for the background estimation and  $\sin^2 2\theta_{23} = 1$  are assumed. The solid (dotted, dash-dotted, dashed) line shows the sensitivity on condition that  $CP$  phase  $\delta$  is 0 ( $\pi/2$ ,  $-\pi/2$ ,  $\pi$ ). The hatched region is excluded by the CHOOZ experiment.

## 7. Summary

T2K is the long-baseline neutrino experiment to study the neutrino oscillation using the high intensity  $\nu_\mu$  beam by J-PARC. The accelerator operation will start in 2008, while the parallel R&D is going on to realize the design intensity. The neutrino beam-line is constructed on schedule and will be completed in 2009.

The first phase of T2K will also start in 2009. The main topic of T2K-I is the  $\nu_\mu \rightarrow \nu_e$  oscillation search to determine  $\theta_{13}$ .  $\theta_{23}$  and  $\Delta m_{23}^2$  will be measured precisely via  $\nu_\mu$  disappearance. An intermediate detector at 2 km position is planned to reduce the systematic uncertainties due to the neutrino flux extrapolation.

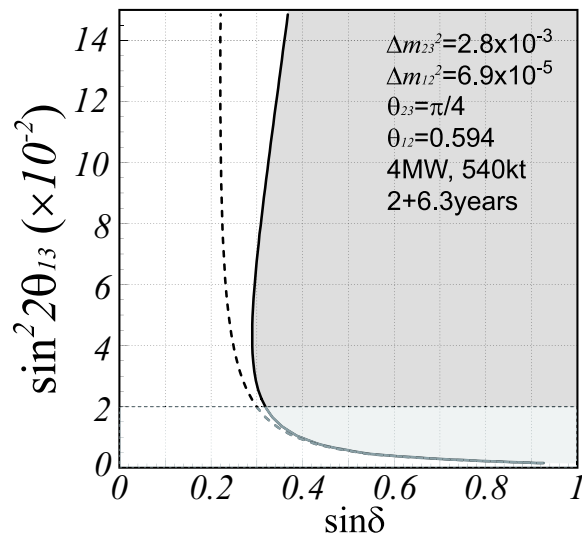


**Figure 3.** The sensitivity for the  $CP$  violation parameter,  $\sin \delta$ , assuming the data which is taken for 2 years  $\nu_\mu$ -beam and 6 years  $\bar{\nu}_\mu$ -beam after the accelerator and detector upgrade. The solid line shows the  $3\sigma$  sensitivity assuming the 2% systematic uncertainty for the background event estimation. The dashed line shows the  $3\sigma$  sensitivity assuming only the statistical error.

If  $\sin^2 \theta_{13}$  obtained by T2K-I is greater than 0.01, T2K Phase-II can study the  $CP$  asymmetry between  $\nu_\mu \rightarrow \nu_e$  and  $\bar{\nu}_\mu \rightarrow \bar{\nu}_e$  oscillations by upgrading the accelerator and the far detector. The far detector at the second oscillation-maximum point may resolve the mass hierarchy unambiguity.

## Reference

- [1] Y. Itow *et al.*, arXiv:hep-ex/0106019.
- [2] “Tokai-to-Kamioka (T2K) Long Baseline Neutrino Oscillation Experiment Proposal”, Submitted to Program Advisory Committee for Nuclear and Particle Physics Experiments at the J-PARC 50GeV Proton Synchrotron, 2006.
- [3] M. H. Ahn [K2K Collaboration], Phys. Rev. D. in press [arXiv:hep-ex/0606032].
- [4] <http://j-parc.jp/index-e.html>
- [5] Y. Fukuda *et al.*, Nucl. Instrum. Meth. A **501** (2003) 418.
- [6] Z. Maki, N. Nakagawa, and S. Sakata, Prog. Theor. Phys. **28** (1962) 870.
- [7] M. Apollonio *et al.*, Eur. Phys. J. C **27** (2003) 331 [arXiv:hep-ex/0301017].
- [8] A. Piepke [Palo Verde Collaboration], Prog. Part. Nucl. Phys. **48** (2002) 113.
- [9] S. Yamamoto *et al.* [K2K Collaboration], Phys. Rev. Lett. **96** (2006) 181801 [arXiv:hep-ex/0603004].
- [10] J. Arafune, M. Koike and J. Sato, “CP violation and matter effect in long baseline neutrino oscillation Phys. Rev. D **56**, 3093 (1997) [Erratum-ibid. D **60**, 119905 (1999)] [arXiv:hep-ph/9703351].
- [11] D. Beavis, A. Carroll, I. Chiang, *et al.*, Proposal of BNL AGS E-889 (1995).
- [12] D. Karlen, The proceedings of 4th International Workshop on Neutrino-Nucleus Interactions in the Few-GeV Region (NuInt05), Okayama, Japan, 2005.
- [13] K. Okumura, *ibid.*
- [14] A. Mereaglia, *ibid.*
- [15] M. Ishitsuka, T. Kajita, H. Minakata and H. Nunokawa, Phys. Rev. D **72** (2005) 033003 [arXiv:hep-ph/0504026].
- [16] K. Hagiwara, N. Okamura and K. i. Senda, arXiv:hep-ph/0607255.

# New techniques: EXO and other tracking detectors

**Andreas Piepke**

Department of Physics and Astronomy, University of Alabama, Tuscaloosa, AL 35487, USA

E-mail: [andreas@bama.ua.edu](mailto:andreas@bama.ua.edu)

**Abstract.** Neutrinoless double beta ( $\beta\beta 0\nu$ ) decay has become an area of interest of the neutrino physics community. A new generation of  $\beta\beta$ -experiments is under design or construction to provide clear and unambiguous evidence for double beta decay, should it exist. These experiments aim to optimize the key aspects of  $\beta\beta 0\nu$ -experiments: source strength, detection efficiency, energy resolution, and background. This article will focus on tracking detectors, with emphasis on the EXO experiment.

## 1. Introduction

Neutrino flavor oscillations and thus non-zero masses of at least two mass eigenstates have been widely accepted throughout our field. The three flavor mixing model is the new paradigm of neutrino physics. It allows an elegant and simple description of all oscillation experiments but LSND. Depending on the outcome of the ongoing MiniBooNE experiment, it may thus require revision. Within the three flavor model two mass differences ( $\Delta m_{12}$ ,  $\Delta m_{23}$ ), two mixing angles ( $\theta_{12}$ ,  $\theta_{23}$ ), and the mass hierarchy of the first two mass eigenstates ( $m_1 < m_2$ ) suffice to describe the diverse array of oscillation experiments, covering a wide area of techniques, sources, and energies. The third mixing angle ( $\theta_{13}$ ), the absolute values of the neutrino masses ( $m_1$ ,  $m_2$ ,  $m_3$ ), the mass hierarchy ( $m_1 < m_2 < m_3$  *normal*,  $m_3 < m_1 < m_2$  *inverted*,  $m_1 \approx m_2 \approx m_3$  *degenerate*), the CP-phases, and behavior of neutrinos under CPT-conjugation remain undetermined.

This article will focus on two double beta decay modes: the allowed two neutrino double beta decay ( $\beta\beta 2\nu$ ),  $A(Z, N) \rightarrow A(Z + 2, N - 2) + 2 e^- + 2 \bar{\nu}_e$  (Z: nuclear charge, N: neutron number,  $A=Z+N$ ), resulting in a continuous sum energy spectrum of the emitted electrons, and the the neutrino less mode ( $\beta\beta 0\nu$ )  $A(Z, N) \rightarrow A(Z + 2, N - 2) + 2 e^-$ , which violates conservation of Lepton number, of B-L conservation and requires neutrinos to be massive Majorana particles. In the latter decay the electron sum energy has a discrete distribution. Assuming that  $\beta\beta 0\nu$ -decay is mediated by the exchange of light neutrinos, its decay rate is given by:  $(T_{1/2}^{\beta\beta 0\nu})^{-1} = G^{\beta\beta 0\nu} |M^{\beta\beta 0\nu}|^2 \langle m_{\beta\beta} \rangle^2$ . Using theoretically calculated phase space,  $G^{\beta\beta 0\nu}$ , nuclear matrix element,  $M^{\beta\beta 0\nu}$ , a measured decay rate (or limit of it) can be translated into an average Majorana neutrino mass,  $\langle m_{\beta\beta} \rangle$ . While theory claims to have good control over the accuracy of  $G^{\beta\beta 0\nu}$  the calculation of  $M^{\beta\beta 0\nu}$  remains a difficult and controversial issue. A dedicated talk covered this topic. It should therefore suffice to say that estimates for the uncertainty of theoretically calculated nuclear matrix elements range from a depressing factor 3 to a more aggressive  $\pm 30\%$  in a more recent systematic evaluation [1]. The detection of  $\beta\beta 0\nu$ -decay would prove the Majorana character of neutrinos, independent of any uncertainties of the

computed parameters entering above equation. Such demonstration of Lepton number violation would, in itself, be a worthy price.

The effective Majorana neutrino mass, the quantity of interest, is given by:

$$\langle m_{\beta\beta} \rangle = \left| \sum_i \eta_i U_{ei}^2 m_i \right|, \quad (1)$$

where the sum goes over all active flavors,  $\eta_i$  denotes the complex CP-phases,  $U_{ei}$  the elements of the upper row of the mass mixing matrix, and  $m_i$  the physical neutrino masses.

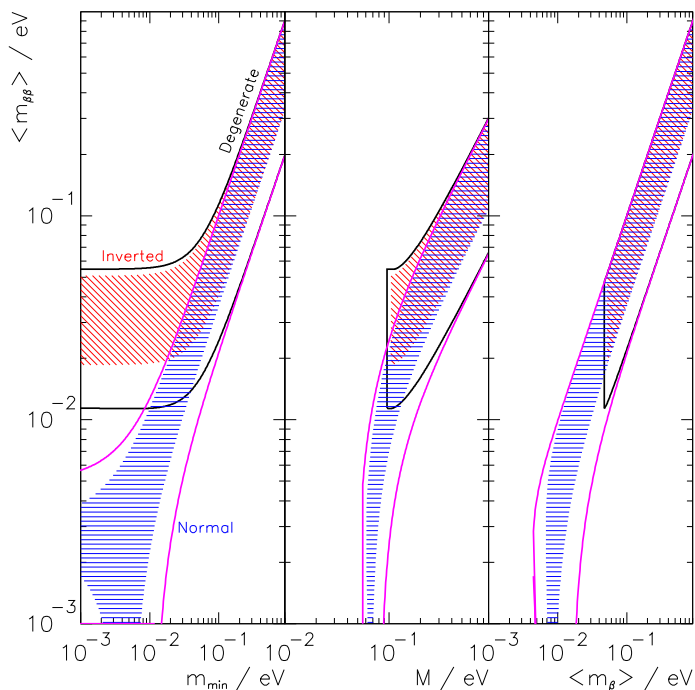


**Figure 1.** Dependence of  $\langle m_{\beta\beta} \rangle$  on the mass of the lightest neutrino  $m_{min}$  (left panel).  $\langle m_{\beta\beta} \rangle$  as a function of  $M = m_1 + m_2 + m_3$  is shown in the middle panel. The right panel depicts  $\langle m_{\beta\beta} \rangle$  as a function of  $\langle m_{\beta} \rangle$ . In all panels the width of the hatched areas is due to the unknown Majorana phases and thus irreducible. The allowed areas given by the solid lines are obtained by taking into account the errors of the oscillation parameters.

Equation 1 can be used to derive a relation between  $\langle m_{\beta\beta} \rangle$  and the minimal neutrino mass,  $m_{min}$ , utilizing the known oscillation parameters. This projection is different for the three mass scenarios mentioned before. The global three flavor oscillation analysis of reference [2] has been used as input data for figure 1. It covers the first MINOS data release. The left panel of figure 1 shows the parameter values of  $\langle m_{\beta\beta} \rangle$  (as a function of  $m_{min}$ ), consistent with oscillation data. From figure 1 one can see that a sensitivity of 10 meV is required to conclusively probe the degenerate and inversely hierarchical mass scenarios.

Figure 1 further shows the interplay of  $\langle m_{\beta\beta} \rangle$  with two other observable neutrino mass quantities: the total neutrino mass  $M = m_1 + m_2 + m_3$ , evaluated by observational cosmology (middle panel), and  $\langle m_{\beta} \rangle = [\sum_i |U_{ei}|^2 m_i^2]^{1/2}$  determined in beta-endpoint experiments (right panel). These two panels can be used to directly compare projected sensitivities of these different experimental approaches.

To compensate for the lack of a clear experimental  $\beta\beta 0\nu$ -decay signature and the uncertainty of the nuclear matrix elements it would seem prudent to conduct several experiments world wide, using different decaying nuclides. In case of an observation only redundancy will allow to make an unambiguous case. Truly redundant results will require at least one competitive tracking detector in the suit of world wide experiments.

## 2. Tracking detectors

A variety of new experiments is being planned to explore the degenerate and inversely hierarchical mass scenarios. These projects will further test the evidence for  $\beta\beta 0\nu$ -decay in  $^{76}\text{Ge}$ , brought forward by part of the Heidelberg component of the Heidelberg-Moscow experiment [3]. No project sensitive to the normal hierarchy has been proposed to date.

For  $\langle m_{\beta\beta} \rangle = 10$  meV  $\beta\beta 0\nu$ -half lives are of order  $10^{28}$  y for isotopes of practical interest. Large detectors, containing order of tons of the decaying substance, are thus needed to arrive at a detectable decay rate of at least a few per year. Most next generation experiments plan to use large quantities of isotopically enriched source material in order to reduce the target for background radiation while maximizing source strength. Typical decay energies are between 2 and 3 MeV. Natural, anthropogenic, and cosmogenic radioactivity, as well as cosmic radiation contribute to the background. In the presence of a finite energy resolution  $\beta\beta 2\nu$ -decay constitutes a background for the discrete spectrum of the  $\beta\beta 0\nu$ -mode. Its contribution depends in the 5.8<sup>th</sup> power on the energy resolution. Good energy resolution is of the utmost importance to reduce all continuous backgrounds under the  $\beta\beta 0\nu$ -line and to suppress the otherwise irreducible  $\beta\beta 2\nu$ -background. Source strength, detection efficiency, energy resolution, and background are the key parameters of these experiments.

The two main approaches, used in real-time double beta decay experiments, are calorimetric and tracking. In calorimetric experiments the source usually doubles as detection medium, thus optimizing the electron detection efficiency. These experiments rely on their excellent energy resolution. The detectors are typically simple in design, reducing the risk of introducing unwanted radioactivity into the technical components near the active volume. Examples are Ge semiconductor detectors and bolometers. Limited tracking is achieved through detector granularity and time analysis of the collected charge. Separate articles are devoted to this approach.

Tracking detectors offer more active background rejection, however, at the expense of technical complexity making background control harder. This article will focus on three new projects: MOON, Super-NEMO, and EXO.

The somewhat unbalanced lengths of the following sections has something to do with the different state of preparation of the various projects and the fact that the author of this article is a member of the EXO collaboration. No judgment is implied or intended.

### 2.1. MOON

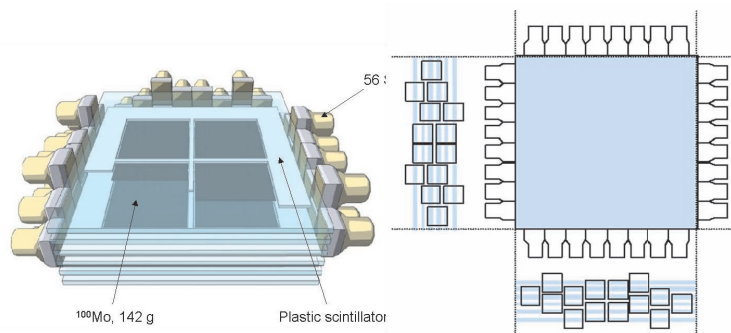


**Figure 2.** Sketch of a prototype detector module of MOON 1.

The Japanese-US-Czech-Russian MOON collaboration proposes to build a multi layer passive source tracking detector based on plastic scintillator calorimetry [4], an expansion of the 2-layer detector ELEGANT V. The goal is to use of order 1 ton of enriched isotope to achieve a mass sensitivity of 30 meV within 5 ton · y of exposure.

In this design single electron background events can be distinguished from double events. In

case of a measurement of double beta decay both the single electron spectra and the angular correlation of the electrons will be recorded.  $^{82}\text{Se}$ ,  $^{100}\text{Mo}$ , and  $^{150}\text{Nd}$  sources are being considered. Thin ( $20\text{ mg/cm}^2$ ) double beta unstable sources would be sandwiched between two thin detector planes, used for position and particle identification. Detector options are scintillating fibers or wire chambers. These will be surrounded by thick plastic scintillator acting as calorimeter. The typical size of the plastic scintillator would be  $1.3\text{ m} \times 1.3\text{ m} \times 0.015\text{ m}$ . 150 of these units would be combined to form a module, containing about 30 kg of double beta unstable isotope. The concept is sketched in figure 2. Light read out would be by photo multiplier. A valid hit would require two planes, adjacent to a source film, and their associated calorimeters to be active. All other planes would be used as anti-coincidence to reduce  $\gamma$ -background. Energy resolution around 2.9% (in units of  $\sigma$ ), at the 3 MeV Q-value of  $^{100}\text{Mo}$ , has been achieved with a prototype detector, called MOON 1. Based on tests with various plastic scintillators, the collaboration hopes to achieve a resolution of 2.5% or better, including the contribution due to electron scattering within the source foil. In MOON 1, containing 6 layers of plastic scintillator, background is further suppressed by means of an active outer NaI-shield, followed by passive Cu and Pb radiation shields. Background is assumed to be mainly due to residual  $^{214}\text{Bi}$  (a  $^{238}\text{U}$  daughter) contained in the source. For a design background of  $0.3\text{ /ton y}$  the collaboration estimates a purity requirement of  $20\text{ }\mu\text{Bq/kg}$ , or 1.6 ppt U assuming chain equilibrium. The MOON collaboration plans to prepare an experiment proposal after the work on MOON 1 has been concluded.

## 2.2. Super-NEMO

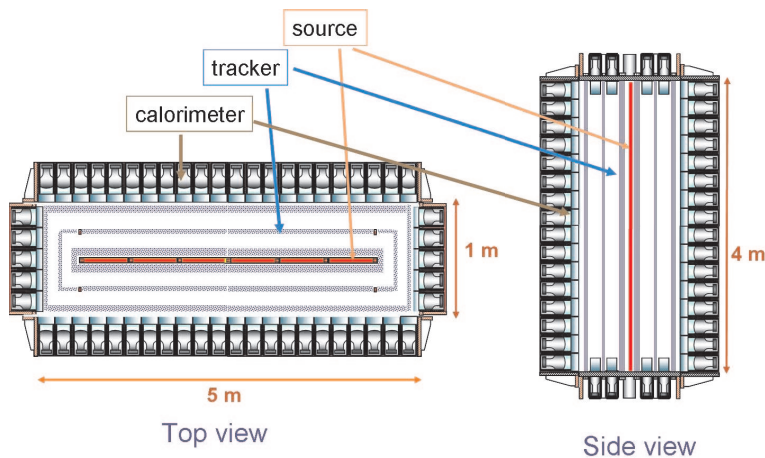


**Figure 3.** Cross section of a Super-NEMO detector module. The thin source foil is placed into a gas filled multi wire tracking detector. Electron calorimetry is provided by scintillator modules covering the module walls.

A large international collaboration explores an extended and improved version of the successful NEMO 3 experiment [5]. Their goal is to use about 100 kg of enriched isotope(s) in a passive source tracking calorimeter. The use of  $^{82}\text{Se}$  and  $^{150}\text{Nd}$  is being envisioned, with the goal of achieving a neutrino mass sensitivity of 40 meV. Isotopical enrichment of Se is by ultra centrifugation. The collaboration is exploring the use of a French laser enrichment facility for the production of a large amount of  $^{150}\text{Nd}$ . An active R&D program is funded in France, Spain and the UK.

As in the previous project, Super-NEMO would have double electron detection capability. Thin, 5 kg, source foils are to be installed into large modular multi wire gas tracking detectors, its walls covered with scintillator calorimeters for energy measurement. Read out would be via 300 to 1000 PMTs per module. Figure 3 shows a sketch of this concept. A magnetic field will be used for particle identification. A total of 20 modules is envisaged at this time. Passive shielding

would be provided by 2 ktons of water for the 20 modules. The collaboration hopes to achieve an energy resolution of 1.7% (in units of  $\sigma$ ) at 3 MeV. Research on different calorimeter technologies is ongoing. Resolution scattering of  $\beta\beta 2\nu$ -events into the  $\beta\beta 0\nu$ -analysis interval is an important background. The  $\beta\beta 2\nu$ -background into the 200 keV  $\beta\beta 0\nu$ -analysis interval is expected to be about 1 event/year for 100 kg of  $^{82}\text{Se}$ . Radiopurity requirements for the source foils are of the order 0.5 to 0.8 ppt for Th and U, respectively. Careful Rn reduction is important, just like in any other double beta experiment. Possible sites for the experiment are: Frejus, Gran Sasso, Canfranc, and Bulby.

The collaboration aims at having a proposal ready by 2008, start of data taking is envisaged for 2010-2011.

### 2.3. EXO

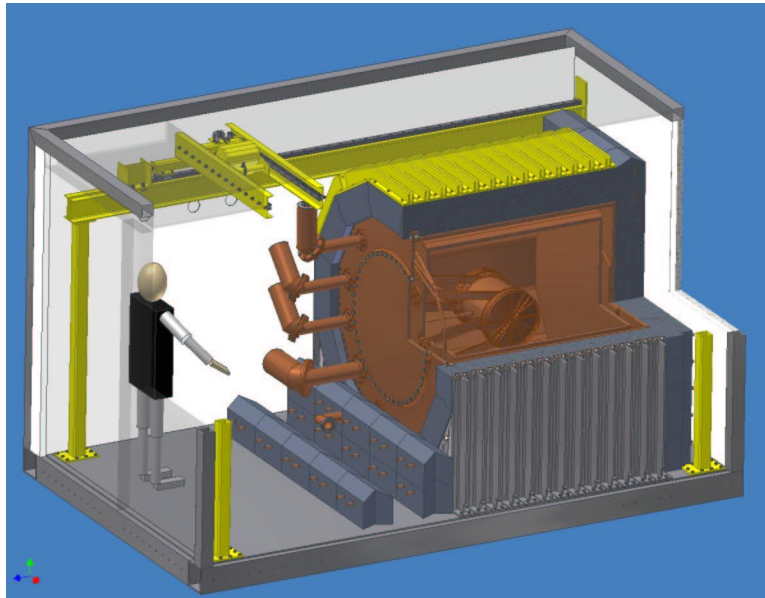


**Figure 4.** EXO-200 detector and its components. The cylindrical TPC and the 12-sided cryostat are made from high purity Cu. The tightly fitted passive lead shield minimizes  $\gamma$ -ray leakage and traps internal Radon. A steel support structure is attached to the outside of the lead.

Goal of the US-Canadian-Russian-Swiss EXO collaboration is to use 1 to 10 tons of enriched  $^{136}\text{Xe}$  in an active source TPC, equipped with final state Ba-tagging [6]. Liquid and high pressure Xe options are under investigation. Due to lack of space only the liquid option will be discussed here. Based on a recent mass determination [7],  $^{136}\text{Xe}$  has a fairly high Q-value of  $2457.8 \pm 0.4$  keV. As a noble gas enrichment can be done economically by ultra centrifugation, requiring no chemical conversion. The enrichment of ton quantities is technically and fiscally feasible. As a gas, Xe can be re-purified during operation of the experiment.

Electrons can be drifted through liquid Xe. Liquid Xe is further a high light yield scintillator (in the UV). It has been shown that liquid Xe detectors, with simultaneous read-out of ionization and scintillation, can achieve an energy resolution of about 1.5% ( $\sigma$ ) at  $Q_{\beta\beta}$  [8]. When used in a TPC with read out of the scintillation light three dimensional track reconstruction is possible. This allows tagging of  $\gamma$ -ray induced background due to its extended vertex.

Double beta decay of  $^{136}\text{Xe}$  results in the formation of a doubly charged  $^{136}\text{Ba}^{++}$  ion. Owing to their different ionization potentials  $\text{Ba}^{++}$  is stable in Xe.  $\text{Ba}^+$  single ions can be detected through optical pumping with blue and red lasers. This opens the possibility to capture the Ba ion at the decay vertex, transfer it into an ion trap, and then detect it by laser pumping. Such additional event signature would yield a large suppression of all random backgrounds.

The EXO collaboration estimates that a neutrino mass sensitivity of about 10 meV can be

achieved within 5 years of data taking, when using 10 tons of enriched Xe equipped with final state Ba tagging. The background was assumed to be dominated by  $\beta\beta 2\nu$ -decay. Research toward this goal is two pronged: construction of a high resolution, low background liquid Xe TPC, using 200 kg of enriched  $^{136}\text{Xe}$ , and development of the single Ba atom transfer and detection technology. The former aspect of the project is called EXO-200. Its goal is to demonstrate that a large Xe TPC with good energy resolution, high tracking power, and sufficiently low background can be build and stably operated. The development of the Ba tagging explores two options: in situ detection of single Ba ions in gaseous Xe, and retrieval of Ba ions from liquid Xe, followed by detection in an ion trap.

*2.3.1. EXO-200* The EXO-200 detector is fully funded and under construction. It is to be installed in the WIPP underground facility near Carlsbad, NM at an overburden of 1600 mw.e.. 200 kg of enriched Xe are at hand. It will be contained in a thin walled cylindrical copper vessel, with a high voltage cathode in the middle. The high purity copper has been custom manufactured and will only be transported in a concrete shielded container to avoid activation by the cosmic radiation. Either side of the TPC will have 114 x- and the same number of y-wires (arranged at  $60^\circ$  angle to each other), grouped in three, for charge read-out and position reconstruction. The spatial resolution will be about 1 cm. Scintillation light will be read out by 258 large area avalanche photo diodes on each side. These low-mass devices offer good UV sensitivity, high quantum efficiency, and low background. It is estimated that about 115 kg of Xe will be fully active. The counting chamber will be submerged in HFE-7000, a highly radiopure heat transfer fluid, thermally coupled to the heat exchanges. It further serves as the innermost radiation shield (50 cm thickness). A double walled copper cryostat, containing the HFE-7000, is serviced by 3 refrigerators to have triple redundant cooling. The cryostat vessels have a combined thickness of 5 cm. 25 cm of low activity lead form the outer radiation shield. The setup is depicted in figure 4. Plastic scintillator modules will be installed outside the lead to provide an active muon veto. The experiment is to be housed in modular cleanrooms.

At this time part of the lead, the copper cryostat and the xenon piping have been installed in the cleanrooms at Stanford, CA. The pre-instrumented cleanrooms will later be transferred to WIPP.

All construction materials used in EXO-200 go through a rigorous radioactivity testing process. The required level of radiopurity is determined by means of a Monte Carlo simulation. Testing to the required sensitivity is then performed by means of  $\alpha$ -spectroscopy,  $\gamma$ -ray spectroscopy, mass spectroscopy, and neutron activation analysis. Th and U sensitivities as low as 0.3 ppt have been achieved in the course of this work. More than 250 materials measurements have been conducted thus far in preparation for EXO-200. Depending on the material and its location, tracking background suppression factors between 3 and 60 have been determined by Monte Carlo, using a simple track length test. All materials are selected so that their summed background will to not exceed 30 events per year in the  $\beta\beta 0\nu$ -analysis window, and 10 events per day in the  $\beta\beta 2\nu$ -window. It is assumed that all are at their screening limits. This is conservative as not all materials will be at or close to their screening limits.

The current schedule calls for the start of operations underground sometimes in 2007. The EXO collaboration hopes to achieve a neutrino mass sensitivity of about 0.3 eV within 2 years of running EXO-200.

*2.3.2. Ba tagging* In a liquid Xe detector collision broadening requires removal of the Ba ions from the detector, transfer into an ion trap, followed by laser detection. Each step has to be performed with high efficiency. Extraction of the Ba ion will be done by means of a movable negatively biased probe. For events of sufficient energy the probe will be steered into the vicinity of the reconstructed event vertex, the Ba ion will be attracted to it and then removed together

with the probe. The removal of  $^{222}\text{Ra}$  ions (chemically similar to Ba) from liquid Xe, by means of a charged probe, has been experimentally demonstrated. The Ra was injected into Xe by means of  $\alpha$  recoil and then detected via its subsequent alpha decay.

Ba single ion detection has been achieved using the EXO linear RFQ trap. The trapping potential is arranged such as to allow the Ba ions, after loading, to gradually fall into the potential minimum where the laser detection happens. High loading efficiencies have been reported for such traps. Measurements of the loading efficiency are now being planned with this trap.

Once attached to the probe, Ba forms a strong bond with it and is difficult to release. To achieve release three options are under study: (1) the charged probe is covered with a thin layer of Xe ice (about 100 atomic layers). To release the Ba the Xe ice is thawed at the entrance of the trap. (2) On a field emission tip the Ba attaches to the very sharp tip. For release a very large positive field is created. (3) With a resonance ionization tip (a 200  $\mu\text{m}$  fiber with semitransparent metalization at its end) the Ba ion is first electrically attracted to the metalization, where it is neutralized. A powerful desorption laser pulse evaporates the Ba in the trap. A second pulse (at a different wavelength) resonantly ionizes the Ba while it is still close to the tip. The appropriate lasers needed to test this method are now at hand.

In parallel a grabber transfer system is under construction. This device, equipped with a liquid Xe vessel, a charged probe, and the linear trap will allow to exercise the entire capture, release, detection sequence, verify the concept and allow to measure its efficiency.

The collaboration hopes to be ready to submit a full experiment proposal one to two years after data taking commenced with EXO-200.

### 3. Conclusion

The next generation of double beta decay experiments will, hopefully, play an important role in the effort to obtain complete understanding of the physics of neutrinos. Neutrino oscillation experiments have defined the task. Their data suggests that Majorana masses down to 10 meV have to be probed in order to fully cover the degenerate and inversely hierarchical mass patterns. Tracking detectors can play an important role in providing redundant and unambiguous evidence for double beta decay, if it indeed exists. Many groups are working hard to make this a reality within the next  $\sim 5$  years. It is hoped that the funding agencies will be supportive of this effort!

### Acknowledgments

I would like to thank Hiro Ejiri and Dominique Lalanne for providing high quality transparencies for my talk and valuable input data for this proceedings article.

- [1] Rodin V A, Faessler A, Simkovic F and Vogel P, 2006 *Nucl. Phys. A* **766** 107 (*Preprint nucl-th/0503063*)
- [2] Fogli G L, Lisi E, Marrone A, Melchiorri A, Palazzo A, Serra P, Silk J and Slosar A, 2006 *Preprint hep-ph/0608060*
- [3] Klapdor-Kleingrothaus H V, Krivosheina I V, Dietz A and Chkvorets O, 2004 *Phys. Lett. B* **586** 198
- [4] Nakamura H et al., 2006 submitted to *Nucl. Inst. Meth. (Preprint nucl-ex/0609008)*
- [5] Arnold R et al. 2005 *Phys. Rev. Lett.* **95** 182302
- [6] Danilov M et al., 2000 *Phys. Lett. B* **480** 12 *Preprint hep-ex/0002003*
- [7] Redshaw M, McDaniel J, Wingfield E and Meyers E G, 2006 to be submitted to *Phys. Rev. C*
- [8] Conti E et al., 2003 *Phys. Rev. B* **68** 054201 *Preprint hep-ex/0303008*

# Supernova neutrino observations: What can we learn?

**Georg G. Raffelt**

Max-Planck-Institut für Physik (Werner-Heisenberg-Institut)  
Föhringer Ring 6, 80805 München, Germany

E-mail: [raffelt@mppmu.mpg.de](mailto:raffelt@mppmu.mpg.de)

**Abstract.** Twenty years after SN 1987A, the vast international programme of experimental neutrino physics and neutrino astronomy suggests that large detectors will operate for a long time. It is realistic that a high-statistics neutrino signal from a galactic SN will be observed. I review some of the generic lessons from such an observation where neutrinos largely play the role of astrophysical messengers. In principle, the signal also holds valuable information about neutrino mixing parameters. I explain some recent developments about the crucial importance of collective neutrino oscillations in the SN environment.

## 1. Introduction

Twenty years ago, the neutrino burst from supernova (SN) 1987A in the Large Magellanic Cloud was observed. On 23 February 1987 at 7:35 h universal time, the Kamiokande II [1, 2] and IMB [3, 4] water-Cherenkov detectors each registered a burst clearly attributed to SN 1987A. A contemporaneous signal in the Baksan scintillator detector [5, 6] may have been caused by the neutrino burst as well. A significant event cluster in the LSD experiment [7, 8] was observed several hours earlier and had no counterpart in the other detectors and vice versa. It can be associated with SN 1987A only if one invokes very non-standard double-bang scenarios of stellar collapse [9]. A lively account of the exciting and somewhat confusing history of the SN 1987A neutrino detection was given by M. Koshiba [10] and A. Mann [11].

This unique observation of stellar-collapse neutrinos helped to pave the way for a new era of neutrino physics. Today, the discovery of neutrino masses, lepton mixing, and flavor oscillations are quickly fading to become yesterday's sensation while the experimental efforts are turning to yet more challenging issues, notably the question of leptonic CP violation, the absolute neutrino masses, and their Majorana nature. A broad programme of experimental neutrino physics, dedicated SN neutrino observatories, and the construction of IceCube as a high-energy neutrino observatory almost guarantee the operation of large detectors for a long time so that the eventual observation of a high-statistics SN neutrino burst is a realistic possibility. A review of the ongoing, planned or proposed neutrino experiments with SN detection capabilities was given by K. Scholberg at this conference [12].

In our galaxy, the SN rate is perhaps 1–3 per century, so that the observation of a SN neutrino burst is a once-in-a-lifetime opportunity. What can we learn? There is no simple answer to this question because what we will learn depends on the detectors operating at that time, what they will observe, what else we then know about neutrinos, and which non-neutrino observations will

be available. Galactic SNe are typically obscured, but even then probably would be seen, for example, in x- or  $\gamma$ -rays. Moreover, a gravitational wave signal could be observed.

Forecasting all possible scenarios would be both impossible and moot. Rather, I will focus on a number of generic issues. First, in Sec. 2 I review current estimates of the galactic SN rate and about their distance distribution. In Sec. 3 I will review some of the obvious lessons from a SN neutrino observation. Here, neutrinos largely play the role of astrophysical messengers. In Sec. 4 I turn to flavor oscillations where the observations could reveal crucial information about neutrino mixing parameters. Until recently, the impact of collective neutrino oscillations in the SN context had been underestimated. Therefore, the overall picture of SN neutrino oscillations is in a state of flux. Sec. 5 is given over to a summary and conclusions.

## 2. Next supernova: Where and When?

Existing and near-future neutrino detectors [12] do not reach beyond the galaxy and its satellites. Super-Kamiokande would observe about  $10^4$  events from a SN at a typical galactic distance of 10 kpc. The next significant target would be the Andromeda region at a distance of 760 kpc, reducing the rate by  $(10/760)^2 = 1.7 \times 10^{-4}$ , i.e., Super-K would register 1–2 events. If a megatonne detector is built with perhaps 30 times the Super-K fiducial volume, it would provide several tens of events. Even such a low-statistics observation would be very useful as we shall see below. From the nearest galaxies beyond Andromeda, even a megatonne detector would register only 1–2 events. It was noted, however, that correlating them with astronomical SN observations may allow one to reduce background enough to build up SN neutrinos at a rate of perhaps 1 neutrino per year from galaxies out to several Mpc [13].

One classic method to estimate our galaxy's SN rate is to scale from external galaxies. Another classic approach is to extrapolate the five historical SNe of the past millenium to the entire galaxy, leading to a larger but more uncertain estimate. The most recent estimate derives from the  $\gamma$ -rays emitted by  $^{26}\text{Al}$  (half-life  $7.2 \times 10^5$  years) that is produced in massive stars. Finally, the non-observation of a galactic neutrino burst since 30 June 1980 when the Baksan Scintillator Telescope (BST) took up operation, and the almost complete coverage of the neutrino sky by different detectors since then, provides the upper limit shown in Table 1.

Therefore, one expects 1–3 core-collapse SNe per century in our galaxy and its satellites. With a megatonne-class detector one would reach Andromeda (M31) and its immediate neighbors such as Triangulum (M33), roughly doubling the expected rate. On the other hand, the last SN from that region was observed in 1885! However, we also note that SNe can be quite frequent in some galaxies. The record holders are NGC 6946 with SNe 1917A, 1939C, 1948B, 1968D, 1969P,

**Table 1.** Estimated rate of galactic core-collapse SNe per century.

Method	Rate	Authors	Refs.
Scaling from external galaxies	$2.5 \pm 0.9$	van den Bergh & McClure (1994)	[14, 17]
	$1.8 \pm 1.2$	Cappellaro & Turatto (2000)	[15, 16]
Gamma-rays from galactic $^{26}\text{Al}$	$1.9 \pm 1.1$	Diehl et al. (2006)	[17]
Historical galactic SNe (all types)	$5.7 \pm 1.7$	Strom (1994)	[18]
	$3.9 \pm 1.7$	Tammann et al. (1994)	[19]
No neutrino burst in 25 years <sup>a</sup>	$< 9.2$ (90% CL)	Alekseev & Alekseeva (2002)	[20]

<sup>a</sup>We have scaled the limit of Ref. [20] to 25 years of neutrino sky coverage.

1980K, 2002hh and 2004et and the galaxy NGC 5236 (M83 or Southern Pinwheel) with SNe 1923A, 1945B, 1950B, 1957D, 1968L and 1983N [21]. These time sequences provide a healthy lesson in Poisson statistics: even if the average rate is quite large, one may still wait for a long time for the next SN, or conversely, we could be lucky and observe one soon, even if the average rate is as small as suggested by Table 1.

What would be a typical distance for a SN in our own galaxy? Core-collapse marks the final evolution of massive stars and thus must occur in regions of active star formation, i.e., in the spiral arms. As proxies for the distribution one can use either observations in other galaxies or in our galaxy the distribution of pulsars, SN remnants, molecular and ionized hydrogen, and OB-star forming regions [22]. All of these observables are consistent with a deficit of SNe in the inner galaxy and a maximum at 3.0–5.5 kpc galactocentric distance. Small regions of high star-forming activity have been found within 50 pc from the galactic center that may contribute up to 1% of the galactic star-formation rate [23], although this finding does not seem to contradict the overall picture of a reduced SN rate in the inner galaxy.

As a representative example we follow Ref. [24] and consider a common parametrization for the galactic surface density of core-collapse (cc) events,

$$\sigma_{\text{cc}}(r) \propto r^{\xi} \exp(-r/u) , \quad (1)$$

where  $r$  is the galactocentric radius. For the birth location of neutron stars, a fiducial distribution of this form was suggested with the parameters  $\xi = 4$  and  $u = 1.25$  kpc [25]. They are consistent with several SN-related observables, even though large uncertainties remain. Thermonuclear SNe, that are believed to originate from old stars in binary systems, more closely follow the matter distribution. It can be parameterized as [22]

$$\sigma_{\text{Ia}}(r) \propto \exp\left(-\frac{r}{4.5 \text{ kpc}}\right) . \quad (2)$$

We show the SN distance distributions corresponding to these models in Fig. 1. The tails at large distances are unphysical due to a complete lack of data.

The average distance for the assumed distribution is  $\langle d_{\text{cc}} \rangle = 10.7$  kpc with a rms dispersion of 4.9 kpc. This agrees with the fiducial distance of 10 kpc that is frequently assumed in the literature. On the other hand, the dispersion is very large so that the number of neutrinos detected even from a “typical” galactic SN can vary by more than an order of magnitude.

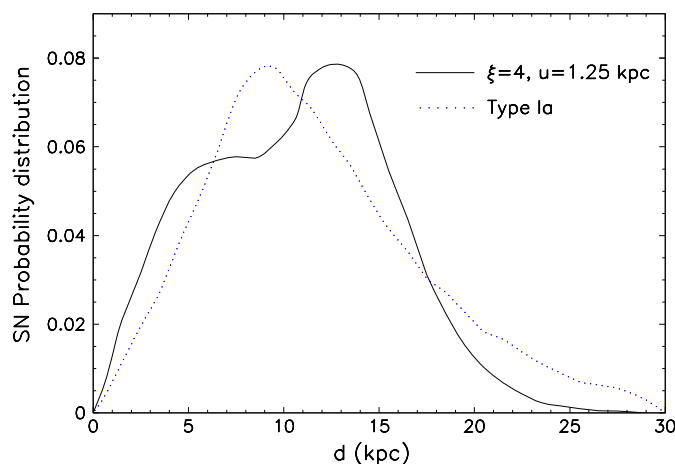


**Figure 1.** Distance distribution of core-collapse (solid) and thermonuclear SNe (dotted) according to the assumed galactic surface distributions of Eqs. (1) and (2), respectively [24].

### 3. Basic lessons from a SN neutrino observation

#### 3.1. Early warning, distance and direction

Turning to the many uses of a SN neutrino observation, we first note that it occurs several hours before the optical explosion, allowing one to issue an alert. The Supernova Early Warning System (SNEWS) provides this service to the neutrino and astronomy communities [28].

Most galactic SNe are optically obscured. While it is implausible that the SN will remain invisible in the entire electromagnetic spectrum, it is interesting if it can be located by its neutrinos alone [29, 30]. The best existing pointing capability is provided by  $\nu + e \rightarrow \nu + e$  scattering in Super-K where an accuracy of about  $8^\circ$  (95% CL half-cone opening angle) can be achieved. If neutron tagging becomes possible by adding gadolinium [31], the accuracy increases to about  $3^\circ$ . For a megatonne-class detector with 30 times the Super-K fiducial volume, these numbers improve to  $1.4^\circ$  (no neutron tagging) and  $0.6^\circ$  (90% tagging efficiency).

The distance of SN 1987A, besides its obvious association with the Large Magellanic Cloud, could be directly determined with light echoes from its inner ring [32, 33]. If the next galactic SN is obscured, nothing of the sort may be possible and one may actually have to rely on the neutrinos to estimate its distance. However, SNe are no good neutrino standard candles. The total emitted energy depends on the poorly known nuclear equation of state as well as the total mass of the progenitor star. The signal registered by the standard  $\bar{\nu}_e + p \rightarrow n + e^+$  reaction is also subject to details of the flavor-dependent neutrino emission and on flavor oscillations. Altogether, one could probably estimate the distance within a factor of two or so.

The prompt  $\nu_e$  burst, on the other hand, comes close to being a standard candle [34, 35, 36]. Here the problem is that the world lacks a big  $\nu_e$  detector because in water-Cherenkov and scintillator detectors the main channel is inverse beta decay. In a large liquid Argon TPC the charged-current absorption  $\nu_e + {}^{40}\text{Ar} \rightarrow {}^{40}\text{K} + e^-$  would provide an exquisite  $\nu_e$  signal [37]. In a megatonne water-Cherenkov detector with neutron tagging, the signal from  $\nu + e$  scattering could be isolated and a distance determination within 5–10% may become possible, in particular if the neutrino mass hierarchy and the 13-mixing angle were known [36].

#### 3.2. Neutrino spectrum

The SN 1987A neutrino observations provided a unique confirmation of the overall picture of core-collapse and neutron-star formation. The signal lasted for about ten seconds, a time scale predicted by the diffusive neutrino energy transport in a nuclear-density hot compact star. The energies in the ten MeV range, representative of the temperature at the “neutrino sphere,” roughly agrees with expectations. (The physics of core-collapse phenomena was presented by H.-T. Janka at this conference; for a recent review see [27].)

In detail, however, the  $\bar{\nu}_e$  energies implied by Kamiokande-II [1, 2] and IMB [3, 4] do not agree well with each other or with expectations. In particular, the Kamiokande-II energies are significantly lower than expected [38, 39, 40, 41]. To interpret the SN 1987A data in any useful way one must make a prior assumption about the spectral shape [40]. The tension in the data and with theoretical models may well be a fluke of small-number statistics, but a serious comparison of the neutrino spectrum with theory for sure requires better data. Even a low-statistics signal of a few tens of events from a SN in Andromeda in a megatonne detector would provide valuable information. Without better data one has to rely on theoretical models, for example, to interpret future measurements of the cosmic Diffuse Supernova Neutrino Background (DSNB) from all past SNe (see C. Lunardini’s presentation at this conference [42]).

A large detector might reveal new subdominant spectral components. A few 100–200 MeV events contemporaneous with the ordinary burst could reveal that energy leaks out directly from the inner core in some novel form of radiation. For example, right-handed neutrinos produced in the SN core could decay into active ones [43] or neutrinos with Dirac magnetic moments could escape from the SN interior and spin-precess into active ones on the way to us [44, 45].

### 3.3. Signal duration

The signal duration of the SN 1987A burst agrees well with expectations. This observation is the basis for perhaps the most useful particle-physics lesson from SN 1987A: apparently there was no other energy-loss channel but the ordinary neutrinos [46, 47, 48, 49]. This “energy-loss argument” has been applied to a large number of cases, notably axions, Majorons, right-handed neutrinos, and Kaluza-Klein gravitons, often providing the most restrictive limits on the underlying particle-physics model. Extensive reviews are Refs. [50, 51, 52] and some more recent applications are discussed in Refs. [53, 54, 55, 56].

Far-reaching conclusions about fundamental physics are here based on a sparse sample of data. Even a relatively low-statistics observation would be enough to remove any lingering doubt if these energy-loss limits are actually correct. Beyond a general confirmation, a high-statistics observation would not improve such limits very much because their uncertainties are typically dominated by physics in the SN core. This includes uncertainties about the temperature, density and composition of the medium as well as uncertainties of how to calculate interaction and emission rates in a nuclear medium.

### 3.4. High-statistics light curve

If one were to observe a high-statistics neutrino light curve, crucial details of the core-collapse paradigm could be tested. In particular, one could probably separate the early accretion phase from the later Kelvin-Helmholtz cooling phase after the explosion has been launched. If the standard delayed-explosion scenario is indeed correct, one could probably see the different phases in the neutrino light curve and confirm or refute this scenario [57]. Besides Super-K, the IceCube detector would be well suited to this task even though it does not provide spectral information, but a high-statistics “bolometric” neutrino light-curve that reflects the time-structure of the burst with high significance.

A detailed cooling profile would allow one to test the theory behind neutrino transport in a hot nuclear medium. Moreover, one may be able to detect short-term time variations that are caused by the large-scale convection pattern during the accretion phase. A sudden termination would reveal late black-hole formation. Of course, there could be completely unexpected features.

Even a high-statistics signal has only limited time-of-flight sensitivity to neutrino masses. Even the most ambitious forecasts do not seriously go below 1 eV [58, 59, 60], not good enough in the light of cosmological limits [61, 62] and the expected sensitivity of the KATRIN tritium decay experiment [63]. A few tens of events from a SN in Andromeda would also provide a sensitivity of about 1 eV. One man’s trash is another man’s treasure: we now expect the time-of-flight dispersion caused by neutrino masses to be so small that fast time variations at the source will faithfully show up at the detector.

## 4. Neutrino flavor oscillations

### 4.1. Ordinary MSW oscillations

Since SN 1987A, many of the “simple” questions about neutrinos have been answered, but more challenges lie ahead. The observation of a galactic SN burst may help us to address some of them. The neutrinos pass through the mantle and envelope of the progenitor star and encounter a vast range of matter densities, implying two MSW resonances. One of them corresponds to the “atmospheric mass difference” (H-resonance), the other, at lower density, to the “solar mass difference” (L-resonance). Of particular interest is the MSW effect at the H-resonance driven by the unknown 13-mixing angle. This resonance occurs in the neutrino sector for the normal mass hierarchy, and among anti-neutrinos for the inverted hierarchy. It is adiabatic for  $\sin^2 \Theta_{13} \gtrsim 10^{-3}$  and non-adiabatic for  $\sin^2 \Theta_{13} \lesssim 10^{-5}$ . Therefore, the neutrino burst is, in principle, sensitive to the mass hierarchy and the 13-mixing angle [64, 65].

One important simplification is that the neutrino energies are far below the  $\mu$  and  $\tau$  mass thresholds. Therefore, the species  $\nu_\mu$ ,  $\bar{\nu}_\mu$ ,  $\nu_\tau$ , and  $\bar{\nu}_\tau$  have only neutral-current interactions. Their fluxes and spectra emerging from the SN and their detection cross sections are the same. They are collectively denoted as  $\nu_x$  or equivalently  $\bar{\nu}_x$ . On the other hand,  $\nu_e$  and  $\bar{\nu}_e$  have charged-current interactions, notably with protons, neutrons and nuclei with different abundances so that we finally need to distinguish between the three species  $\nu_e$ ,  $\bar{\nu}_e$  and  $\nu_x$ . Oscillation effects can be summarized in terms of the energy-dependent  $\nu_e$  survival probability  $p(E)$  as

$$F_{\nu_e}(E) = p(E)F_{\nu_e}^0(E) + [1 - p(E)]F_{\nu_x}^0(E), \quad (3)$$

where the superscript zero denotes the primary fluxes. An analogous expression pertains to  $\bar{\nu}_e$  with the survival probability  $\bar{p}(E)$ . Table 2 summarizes the survival probabilities for different mixing scenarios where  $\Theta_\odot$  refers to the ‘‘solar’’ mixing angle [64, 65].

The most pronounced and most robust flavor-dependent structure of a SN neutrino signal is the prompt  $\nu_e$  burst. Unfortunately, the main detection channel in all existing and near-future detectors is  $\bar{\nu}_e + p \rightarrow n + e^+$ . In Super-K, the prompt  $\nu_e$  burst would generate of order 10 events from  $\nu e$  scattering so that the burst perhaps could be just barely detected. Of course, in a megatonne water-Cherenkov detector with neutron tagging, the  $\nu_e$  burst would be an extremely useful tool both for studying flavor oscillations and determining the SN distance [30]. Likewise, a large liquid Argon TPC would be a powerful and useful  $\nu_e$  detector [37].

For the time being, inverse beta decay will provide the dominant signal. Oscillation effects are more subtle in this channel because the primary spectra and fluxes of  $\bar{\nu}_e$  and  $\bar{\nu}_x$  are probably more similar than had been thought until recently [66, 67]. Moreover, the relative spectral energies and fluxes change during the accretion and cooling phases. At present, reliable predictions for the time-dependent quantities  $\langle E_{\bar{\nu}_e} \rangle / \langle E_{\bar{\nu}_x} \rangle$  and  $F_{\bar{\nu}_e} / F_{\bar{\nu}_x}$  are not available and in fact may differ for different SNe because the progenitor mass may play some role.

Therefore, one must focus on model-independent signatures. One is the matter regeneration effect if the neutrinos are observed through the Earth. Flavor oscillations would manifest themselves by characteristic energy-dependent signal modulations [68, 69, 70, 71, 72, 73], an effect that would be especially apparent in a large scintillator detector because of its superior energy resolution. One could also compare the signals of different detectors if one of them sees the SN shadowed and the other not [70]. We have provided an online tool that allows one, for chosen detector locations, to calculate the probability for the next galactic SN to be shadowed in none, one, or both detectors [24]. Both for SN and geo-neutrino detection, several big scintillator detectors in different locations would be more useful than one large detector such as the proposed LENA [74] in a single location.

Another characteristic signature of flavor oscillations could be a pronounced dip or double-dip feature in the late neutrino signal caused by shock-wave propagation. When the shock wave passes the H-resonance region, the MSW adiabaticity is temporarily broken. Moreover, for some time several H-resonances obtain because the density profile is not monotonic. If one were to

**Table 2.** Survival probabilities for neutrinos,  $p$ , and antineutrinos,  $\bar{p}$ , in various mixing scenarios. The channels where one expects Earth effects, shock-wave propagation effects, and where the full  $\nu_e$  burst is present or absent are indicated.

Scenario	Hierarchy	$\sin^2 \Theta_{13}$	$p$	$\bar{p}$	Earth effects	Shock wave	$\nu_e$ burst
A	Normal	$\gtrsim 10^{-3}$	0	$\cos^2 \Theta_\odot$	$\bar{\nu}_e$	$\nu_e$	absent
B	Inverted	$\gtrsim 10^{-3}$	$\sin^2 \Theta_\odot$	0	$\nu_e$	$\bar{\nu}_e$	present
C	Any	$\lesssim 10^{-5}$	$\sin^2 \Theta_\odot$	$\cos^2 \Theta_\odot$	$\nu_e$ and $\bar{\nu}_e$	—	present

observe such features, they could serve as a diagnostic both for neutrino oscillation parameters and the astrophysics of shock-wave propagation [75, 76, 77, 78].

The SN matter profile need not be smooth. Behind the shock-wave, convection and turbulence can cause significant stochastic density variations that tend to wash out the neutrino oscillation signatures [79, 80]. The quantitative relevance of this effect remains to be understood.

#### 4.2. Collective neutrino oscillations

The trapped neutrinos in a SN core as well as the neutrinos streaming off its surface are so dense that they provide a large matter effect for each other. The nonlinear nature of this neutrino-neutrino effect renders its consequences very different from the ordinary matter effect in that it results in collective oscillation phenomena [81, 82, 83, 84, 85, 86, 87, 88, 89, 90, 91, 92, 93] that can be of practical interest in the early universe [94, 95, 96, 97] or in core-collapse SNe [98, 99, 100, 101, 102, 103, 104, 105, 106, 107]. The crucial importance of “bipolar oscillations” for SN neutrinos was first recognized in Refs. [104, 105, 106] and some of their salient features explained in Ref. [107].

What are the conditions for neutrino-neutrino matter effects to be relevant? Considering for simplicity a two-flavor situation, vacuum oscillations are driven by the frequency  $\omega = \Delta m^2/2E$ . The ordinary matter effect is important when  $\lambda \gtrsim \omega$  where  $\lambda = \sqrt{2}G_F n_e$ . Neutrino-neutrino effects are important when  $\mu \gtrsim \omega$  where  $\mu = \sqrt{2}G_F n_\nu$ . It is crucial to note that ordinary matter effects do not override neutrino-neutrino effects. As stressed in Ref. [104], it is a misconception that neutrino-neutrino effects would be negligible when  $\lambda \gg \mu$ .

The low-energy weak-interaction Hamiltonian is of current-current form so that the interaction energy between two particles of momenta  $\mathbf{p}$  and  $\mathbf{q}$  is proportional to  $(1 - \mathbf{v}_\mathbf{p} \cdot \mathbf{v}_\mathbf{q})$  where  $\mathbf{v}_\mathbf{p} = \mathbf{p}/E_\mathbf{p}$  is the velocity. In isotropic media the  $\mathbf{v}_\mathbf{p} \cdot \mathbf{v}_\mathbf{q}$  term averages to zero. On the other hand, collinear-moving relativistic particles produce no weak potential for each other. For neutrinos streaming off a SN core, the  $(1 - \mathbf{v}_\mathbf{p} \cdot \mathbf{v}_\mathbf{q})$  term implies that the neutrino flux declines not only with the geometric  $r^{-2}$  factor, but the average interaction energy  $\mu$  has another  $r^{-2}$  factor that accounts for the increasing collinearity of the neutrino trajectories with distance from the source [99]. Considering the atmospheric mass difference of  $1.9\text{--}3.0 \times 10^{-3} \text{ eV}^2$  and using a typical energy of 15 MeV, we may use  $\omega = 0.3 \text{ km}^{-1}$  as a typical value, where we here express frequencies and energies in  $\text{km}^{-1}$  that is a useful unit in the SN context. Moreover, if we use  $10^{51} \text{ erg s}^{-1}$  as a typical neutrino luminosity, and if we use 10 km as the neutrino-sphere radius, we may use  $\mu = 0.3 \times 10^5 \text{ km}^{-1}$  at the neutrino sphere so that indeed  $\mu \gg \omega$ . With the  $r^{-4}$  scaling of the effective  $\mu$ , collective neutrino oscillations will be important out to a radius of about 200 km.

There are two extreme cases of collective oscillation effects that have been discussed in the literature. *Synchronized oscillations* occur when the neutrino-neutrino interaction “glues” the neutrino flavor polarization vectors together enough so that they evolve the same. In other words, even though the vacuum oscillation frequency  $\Delta m^2/2E$  is different for different modes, they all oscillate with the same “synchronized frequency” that is an average of the vacuum or in-medium frequencies (“self-maintained coherence”). Of course, if the vacuum or in-medium mixing angle is small, this synchronization effect has no macroscopic significance.

The generic case of *bipolar oscillations* occurs in a neutrino gas with equal densities of, say,  $\nu_e$  and  $\bar{\nu}_e$ . In an inverted-mass situation with a small mixing angle, the ensemble will undergo oscillations of the sort  $\nu_e \bar{\nu}_e \rightarrow \nu_\mu \bar{\nu}_\mu \rightarrow \nu_e \bar{\nu}_e \rightarrow \dots$ , approximately with the “bipolar frequency”  $\kappa = \sqrt{2\omega\mu}$  that is much faster than the vacuum oscillation frequency. The period of this phenomenon depends logarithmically on the mixing angle, explaining why this phenomenon is not much affected by the presence of ordinary matter [104, 105, 107]. For the normal hierarchy, the ensemble performs small-amplitude harmonic oscillations with the frequency  $\kappa$  so that macroscopically “nothing” happens.

The next complication are “multi-angle effects,” probably first stressed in Ref. [92] and numerically explored in Ref. [105]. In a non-isotropic neutrino gas, the self-term is not the same for all modes because of the  $(1 - \mathbf{v}_p \cdot \mathbf{v}_q)$  factor. The result is an instability that causes a neutrino gas with equal densities of  $\nu$  and  $\bar{\nu}$  to de-cohere kinematically in flavor space between different directions of motion. Independently of the mass hierarchy and with the smallest initial anisotropy, complete flavor equipartition obtains. The time scale, again, is set by the bipolar frequency  $\kappa$ . The overall time to achieve equilibrium depends logarithmically on the mixing angle and the initial anisotropy [93].

Bipolar oscillations are a collective pair-conversion effect; there is no enhanced flavor conversion. For equal densities of  $\nu_e$  and  $\bar{\nu}_e$ , the net electron lepton number vanishes. “Pair oscillations” do not change of overall flavor lepton number. One requirement is that there is a sufficient “pair excess” in some flavor. This is not the case in the interior of a SN core where all neutrinos are in thermal equilibrium, and only the  $\nu_e$  have a large chemical potential that increases the number density of  $\nu_e$  (relative to  $\nu_\mu$  or  $\nu_\tau$ ) while at the same time suppressing the  $\bar{\nu}_e$  density. Therefore, bipolar oscillations do not seem to be relevant in the interior of a SN core. Synchronized oscillations will occur, but with an extremely small in-medium mixing angle.

On the other hand, there is an excess of both  $\nu_e$  and  $\bar{\nu}_e$  in the neutrinos streaming off a SN core, where generically  $F_{\nu_e} > F_{\bar{\nu}_e}$ . If this asymmetry is too large, the oscillations are still of the synchronized type, even though there is a pair excess. Bipolar conversions will begin playing a role beyond a radius where the effective  $\mu$  is small enough that the asymmetry no longer prevents them. The critical region is between a few tens of km above the neutrino sphere and about 200 km. Without the “multi-angle effect,” the outcome would be generic in that complete pair-conversion  $\nu_e \bar{\nu}_e \rightarrow \nu_x \bar{\nu}_x$  would occur for the inverted mass hierarchy, and essentially nothing new would happen for the normal hierarchy. Including multi-angle effects, the outcome does not seem generic but rather depends on details [105].

As for observable flavor oscillation effects from the next galactic SN, the deleptonization burst likely remains unaffected because it is characterized by an excess of  $\nu_e$  and a suppression of  $\bar{\nu}_e$ . During the accretion phase, some degree of flavor-swapping may occur and since the relevant region is within the stalled shock wave, one may speculate if some effect on the SN dynamics itself obtain in the spirit of Ref. [108]. After a successful explosion, nucleosynthesis in the neutrino-driven wind above the neutron star may well be affected, a possibility that was the main motivation for the exploratory study of Ref. [105, 109]. Possible modifications of what will be observed in the neutrino signal of the next galactic SN have not yet been studied. Some interesting work remains to be done!

## 5. Summary

Twenty years after SN 1987A we are well prepared for the observation of another neutrino burst from a collapsing star. The scientific harvest would be immense. Without any doubt, neutrinos would be excellent astrophysical messengers and allow us to follow stellar collapse and many of its details “in situ.” From the particle-physics perspective, many of the unique lessons from SN 1987A could be corroborated. In principle, the neutrino burst also holds information about the neutrino mass hierarchy that is extremely difficult to determine in the laboratory. On the other hand, collective neutrino oscillation effects that had not been fully appreciated may change some of the previous paradigm. In preparation for the next galactic SN burst, both theorists and experimentalists have more work to do than just wait!

## Acknowledgments

This work was partly supported by the Deutsche Forschungsgemeinschaft under Grants No. SFB-375 and TR-27 and by the European Union under the ILIAS project, contract No. RII3-CT-2004-506222.

## References

- [1] K. Hirata et al. (KAMIOKANDE-II Collaboration), “Observation of a neutrino burst from the supernova SN 1987A,” *Phys. Rev. Lett.* **58**, 1490 (1987).
- [2] K. S. Hirata et al., “Observation in the Kamiokande-II detector of the neutrino burst from supernova SN1987A,” *Phys. Rev. D* **38**, 448 (1988).
- [3] R. M. Bionta et al., “Observation of a neutrino burst in coincidence with supernova 1987A in the Large Magellanic Cloud,” *Phys. Rev. Lett.* **58**, 1494 (1987).
- [4] C. B. Bratton et al. (IMB Collaboration), “Angular distribution of events from SN 1987A,” *Phys. Rev. D* **37**, 3361 (1988).
- [5] E. N. Alekseev, L. N. Alekseeva, V. I. Volchenko and I. V. Krivosheina, “Possible detection of a neutrino signal on 23 February 1987 at the Baksan underground scintillation telescope of the Institute of Nuclear Research,” *Pisma Zh. Eksp. Teor. Fiz.* **45**, 461 (1987) [*JETP Lett.* **45**, 589 (1987)].
- [6] E. N. Alekseev, L. N. Alekseeva, I. V. Krivosheina and V. I. Volchenko, “Detection of the neutrino signal from SN 1987A in the LMC using the INR Baksan underground scintillation telescope,” *Phys. Lett. B* **205**, 209 (1988).
- [7] V. L. Dadykin et al., “Detection of a rare event on 23 February 1987 by the neutrino radiation detector under Mont Blanc,” *Pisma Zh. Eksp. Teor. Fiz.* **45**, 464 (1987) [*JETP Lett.* **45**, 593 (1987)].
- [8] M. Aglietta *et al.*, “On the event observed in the Mont Blanc Underground Neutrino observatory during the occurrence of Supernova 1987A,” *Europhys. Lett.* **3**, 1315 (1987).
- [9] V. S. Imshennik and O. G. Ryazhskaya, “A rotating collapsar and possible interpretation of the LSD neutrino signal from SN 1987A,” *Pisma Astron. Zhurnal*, **30**, 17 (2004) [*Astron. Lett.* **30**, 14 (2004)] [[astro-ph/0401613](#)].
- [10] M. Koshiya, “Observational neutrino astrophysics,” *Phys. Rept.* **220**, 229 (1992).
- [11] A. K. Mann, *Shadow of a star: The neutrino story of supernova 1987A* (Freeman, 1997).
- [12] K. Scholberg, “Supernova neutrino detection,” [astro-ph/0701081](#).
- [13] S. Ando, J. F. Beacom and H. Yuksel, “Detection of neutrinos from supernovae in nearby galaxies,” *Phys. Rev. Lett.* **95**, 171101 (2005) [[astro-ph/0503321](#)].
- [14] S. van den Bergh and R. D. McClure, “Rediscussion of extragalactic supernova rates derived from Evans’s 1980–1988 observations,” *Astrophys. J.* **425**, 205 (1994).
- [15] E. Cappellaro, R. Evans and M. Turatto, “A new determination of supernova rates and a comparison with indicators for galactic star formation,” *Astron. Astrophys.* **351**, 459 (1999) [[astro-ph/9904225](#)].
- [16] E. Cappellaro and M. Turatto, “Supernova types and rates,” [astro-ph/0012455](#).
- [17] R. Diehl et al., “Radioactive  $^{26}\text{Al}$  and massive stars in the Galaxy,” *Nature* **439**, 45 (2006). For a review of supernova rates from various methods see the supplementary material provided in the electronic version of the Nature article and in [astro-ph/0601015](#).
- [18] R. G. Strom, “Guest stars, sample completeness and the local supernova rate,” *Astron. Astrophys.* **288**, L1 (1994).
- [19] G. A. Tammann, W. Löffler and A. Schröder, “The galactic supernova rate,” *Astrophys. J. Suppl.* **92**, 487 (1994).
- [20] E. N. Alekseev and L. N. Alekseeva, “Twenty years of galactic observations in searching for bursts of collapse neutrinos with the Baksan underground scintillation telescope,” *Zh. Eksp. Teor. Fiz.* **95**, 10 (2002) [*J. Exp. Theor. Phys.* **95**, 5 (2002)] [[astro-ph/0212499](#)].
- [21] Padova-Asiago supernova catalogue <http://web.pd.astro.it/supern>
- [22] K. M. Ferriere, “The interstellar environment of our Galaxy,” *Rev. Mod. Phys.* **73** (2001) 1031 [[astro-ph/0106359](#)].
- [23] D. F. Figer, R. M. Rich, S. S. Kim, M. Morris and E. Serabyn, “An extended star formation history for the Galactic Center from Hubble Space Telescope/NICMOS observations,” *Astrophys. J.* **601** (2004) 319 [[astro-ph/0309757](#)].
- [24] A. Mirizzi, G. G. Raffelt and P. D. Serpico, “Earth matter effects in supernova neutrinos: Optimal detector locations,” *JCAP* **0605**, 012 (2006) [[astro-ph/0604300](#)]. For the online tool see <http://www.mppmu.mpg.de/supernova/shadowing>
- [25] I. Yusifov and I. Küçük, “Revisiting the radial distribution of pulsars in the Galaxy,” *Astron. Astrophys.* **422** (2004) 545 [[astro-ph/0405559](#)].
- [26] D. R. Lorimer, “The Galactic population and birth rate of radio pulsars,” in: *Young neutron stars and their environments*, IAU Symposium No. 218 (14–17 July 2003, Sydney, Australia), ed. by F. Camilo and B. M. Gaensler (San Francisco, Astronomical Society of the Pacific, 2004) p. 105 [[astro-ph/0308501](#)].
- [27] H. T. Janka, K. Langanke, A. Marek, G. Martinez-Pinedo and B. Mueller, “Theory of core-collapse supernovae,” [astro-ph/0612072](#).
- [28] P. Antonioli *et al.*, “SNEWS: The SuperNova Early Warning System,” *New J. Phys.* **6**, 114 (2004) [[astro-](#)

- ph/0406214]. See also <http://snews.bnl.gov>
- [29] J. F. Beacom and P. Vogel, “Can a supernova be located by its neutrinos?,” *Phys. Rev. D* **60**, 033007 (1999) [astro-ph/9811350].
  - [30] R. Tomás, D. Semikoz, G. G. Raffelt, M. Kachelriess and A. S. Dighe, “Supernova pointing with low- and high-energy neutrino detectors,” *Phys. Rev. D* **68**, 093013 (2003) [hep-ph/0307050].
  - [31] J. F. Beacom and M. R. Vagins, “Antineutrino spectroscopy with large water Cherenkov detectors,” *Phys. Rev. Lett.* **93**, 171101 (2004) [hep-ph/0309300].
  - [32] N. Panagia et al., “Properties of the SN 1987A circumstellar ring and the distance to the Large Magellanic Cloud,” *Astrophys. J.* **380**, L23 (1991)
  - [33] A. Gould and O. Uza, “Upper limit to the distance to the Large Magellanic Cloud,” *Astrophys. J.* **494**, 118 (1998) [astro-ph/9705051].
  - [34] T. A. Thompson, A. Burrows and P. A. Pinto, “Shock breakout in core-collapse supernovae and its neutrino signature,” *Astrophys. J.* **592**, 434 (2003) [astro-ph/0211194].
  - [35] K. Takahashi, K. Sato, A. Burrows and T. A. Thompson, “Supernova neutrinos, neutrino oscillations, and the mass of the progenitor star,” *Phys. Rev. D* **68**, 113009 (2003) [hep-ph/0306056].
  - [36] M. Kachelriess, R. Tomas, R. Buras, H. T. Janka, A. Marek and M. Rampp, “Exploiting the neutronization burst of a galactic supernova,” *Phys. Rev. D* **71**, 063003 (2005) [astro-ph/0412082].
  - [37] I. Gil-Botella and A. Rubbia, “Oscillation effects on supernova neutrino rates and spectra and detection of the shock breakout in a liquid argon TPC,” *JCAP* **0310**, 009 (2003) [hep-ph/0307244].
  - [38] H.-T. Janka and W. Hillebrandt, “Neutrino emission from type II supernovae: an analysis of the spectra,” *Astron. Astrophys.* **224**, 49 (1989)
  - [39] B. Jegerlehner, F. Neubig and G. Raffelt, “Neutrino oscillations and the supernova 1987A signal,” *Phys. Rev. D* **54**, 1194 (1996) [astro-ph/9601111].
  - [40] A. Mirizzi and G. G. Raffelt, “New analysis of the SN 1987A neutrinos with a flexible spectral shape,” *Phys. Rev. D* **72**, 063001 (2005) [astro-ph/0508612].
  - [41] M. L. Costantini, A. Ianni, G. Pagliaroli and F. Vissani, “Is there a problem with low energy SN1987A neutrinos?,” astro-ph/0608399.
  - [42] C. Lunardini, “The diffuse supernova neutrino flux,” astro-ph/0610534.
  - [43] S. Dodelson, J. A. Frieman and M. S. Turner, “Constraints to the decays of Dirac neutrinos from SN 1987A,” *Phys. Rev. Lett.* **68**, 2572 (1992).
  - [44] R. Barbieri and R. N. Mohapatra, “Limit on the magnetic moment of the neutrino from supernova SN 1987A observations,” *Phys. Rev. Lett.* **61**, 27 (1988).
  - [45] D. Nötzold, “New bounds on neutrino magnetic moments from stellar collapse.,” *Phys. Rev. D* **38**, 1658 (1988).
  - [46] J. R. Ellis and K. A. Olive, “Constraints on light particles from Supernova SN 1987A,” *Phys. Lett. B* **193**, 525 (1987).
  - [47] G. Raffelt and D. Seckel, “Bounds on exotic particle interactions from SN 1987A,” *Phys. Rev. Lett.* **60**, 1793 (1988).
  - [48] M. S. Turner, “Axions from SN 1987A,” *Phys. Rev. Lett.* **60**, 1797 (1988).
  - [49] R. Mayle, J. R. Wilson, J. R. Ellis, K. A. Olive, D. N. Schramm and G. Steigman, “Constraints on axions from SN 1987A,” *Phys. Lett. B* **203**, 188 (1988).
  - [50] D. N. Schramm, “Neutrinos from Supernova SN 1987A,” *Comments Nucl. Part. Phys.* **17**, 239 (1987).
  - [51] G. G. Raffelt, “Astrophysical methods to constrain axions and other novel particle phenomena,” *Phys. Rept.* **198**, 1 (1990).
  - [52] G. G. Raffelt, “Particle physics from stars,” *Ann. Rev. Nucl. Part. Sci.* **49**, 163 (1999) [hep-ph/9903472].
  - [53] C. Hanhart, D. R. Phillips, S. Reddy and M. J. Savage, “Extra dimensions, SN 1987A, and nucleon nucleon scattering data,” *Nucl. Phys. B* **595**, 335 (2001) [nucl-th/0007016].
  - [54] C. Hanhart, J. A. Pons, D. R. Phillips and S. Reddy, “The likelihood of GODs’ existence: Improving the SN 1987A constraint on the size of large compact dimensions,” *Phys. Lett. B* **509**, 1 (2001) [astro-ph/0102063].
  - [55] H. K. Dreiner, C. Hanhart, U. Langenfeld and D. R. Phillips, “Supernovae and light neutralinos: SN 1987A bounds on supersymmetry revisited,” *Phys. Rev. D* **68**, 055004 (2003) [hep-ph/0304289].
  - [56] P. Fayet, D. Hooper and G. Sigl, “Constraints on light dark matter from core-collapse supernovae,” *Phys. Rev. Lett.* **96**, 211302 (2006) [hep-ph/0602169].
  - [57] T. Totani, K. Sato, H. E. Dalhed and J. R. Wilson, “Future detection of supernova neutrino burst and explosion mechanism,” *Astrophys. J.* **496**, 216 (1998) [astro-ph/9710203].
  - [58] T. Totani, “Electron neutrino mass measurement by supernova neutrino bursts and implications on hot dark matter,” *Phys. Rev. Lett.* **80**, 2039 (1998) [astro-ph/9801104].
  - [59] J. F. Beacom and P. Vogel, “Mass signature of supernova  $\nu_\mu$  and  $\nu_\tau$  neutrinos in Super-Kamiokande,” *Phys.*

- Rev. D **58**, 053010 (1998) [hep-ph/9802424].
- [60] E. Nardi and J. I. Zuluaga, “Constraints on neutrino masses from a galactic supernova neutrino signal at present and future detectors,” Nucl. Phys. B **731**, 140 (2005) [hep-ph/0412104].
- [61] J. Lesgourgues and S. Pastor, “Massive neutrinos and cosmology,” Phys. Rept. **429**, 307 (2006) [astro-ph/0603494].
- [62] S. Hannestad, “Primordial neutrinos,” hep-ph/0602058.
- [63] G. Drexlin et al. (KATRIN Collaboration), “KATRIN: Direct measurement of a sub-eV neutrino mass,” Nucl. Phys. Proc. Suppl. **145**, 263 (2005).
- [64] A. S. Dighe and A. Y. Smirnov, “Identifying the neutrino mass spectrum from the neutrino burst from a supernova,” Phys. Rev. D **62**, 033007 (2000) [hep-ph/9907423].
- [65] A. Dighe, “Supernova neutrinos: Production, propagation and oscillations,” Nucl. Phys. Proc. Suppl. **143**, 449 (2005) [arXiv:hep-ph/0409268].
- [66] M. T. Keil, G. G. Raffelt and H.-T. Janka, “Monte Carlo study of supernova neutrino spectra formation,” Astrophys. J. **590**, 971 (2003) [astro-ph/0208035].
- [67] G. G. Raffelt, M. T. Keil, R. Buras, H.-T. Janka and M. Rampp, “Supernova neutrinos: Flavor-dependent fluxes and spectra,” Proc. of the 4th Workshop on Neutrino Oscillations and their Origin: NooN 2003 (10–14 February 2003, Kanazawa, Japan), eds. Y. Suzuki, M. Nakahata, Y. Itow, M. Shiozawa and Y. Obayashi (World Scientific, Singapore, 2004), pp. 380–387 [astro-ph/0303226].
- [68] C. Lunardini and A. Yu. Smirnov, “Supernova neutrinos: Earth matter effects and neutrino mass spectrum,” Nucl. Phys. B **616** (2001) 307 [hep-ph/0106149].
- [69] C. Lunardini and A. Y. Smirnov, “Probing the neutrino mass hierarchy and the 13-mixing with supernovae,” JCAP **0306** (2003) 009 [hep-ph/0302033].
- [70] A. S. Dighe, M. T. Keil and G. G. Raffelt, “Detecting the neutrino mass hierarchy with a supernova at IceCube,” JCAP **0306** (2003) 005 [hep-ph/0303210].
- [71] A. S. Dighe, M. T. Keil and G. G. Raffelt, “Identifying earth matter effects on supernova neutrinos at a single detector,” JCAP **0306**, 006 (2003) [hep-ph/0304150].
- [72] A. S. Dighe, M. Kachelriess, G. G. Raffelt and R. Tomàs, “Signatures of supernova neutrino oscillations in the earth mantle and core,” JCAP **0401**, 004 (2004) [hep-ph/0311172].
- [73] M. Lindner, T. Ohlsson, R. Tomàs and W. Winter, “Tomography of the Earth’s core using supernova neutrinos,” Astropart. Phys. **19** (2003) 755 [hep-ph/0207238].
- [74] T. Marrodán Undagoitia, F. von Feilitzsch, M. Göger-Neff, K. A. Hochmuth, L. Oberauer, W. Potzel and M. Wurm, “Low energy neutrino astronomy with the large liquid-scintillation detector LENA,” J. Phys. Conf. Ser. **39**, 287 (2006).
- [75] R. C. Schirato, G. M. Fuller, “Connection between supernova shocks, flavor transformation, and the neutrino signal,” astro-ph/0205390.
- [76] R. Tomàs, M. Kachelriess, G. Raffelt, A. Dighe, H. T. Janka and L. Scheck, “Neutrino signatures of supernova shock and reverse shock propagation,” JCAP **0409** (2004) 015 [astro-ph/0407132].
- [77] G. L. Fogli, E. Lisi, A. Mirizzi and D. Montanino, “Probing supernova shock waves and neutrino flavor transitions in next-generation water-Cherenkov detectors,” JCAP **0504** (2005) 002 [hep-ph/0412046].
- [78] S. Choubey, N. P. Harries and G. G. Ross, “Probing neutrino oscillations from supernovae shock waves via the IceCube detector,” Phys. Rev. D **74**, 053010 (2006) [hep-ph/0605255].
- [79] G. L. Fogli, E. Lisi, A. Mirizzi and D. Montanino, “Damping of supernova neutrino transitions in stochastic shock-wave density profiles,” hep-ph/0603033.
- [80] A. Friedland and A. Gruzinov, “Neutrino signatures of supernova turbulence,” astro-ph/0607244.
- [81] J. Pantaleone, “Neutrino oscillations at high densities,” Phys. Lett. B **287**, 128 (1992).
- [82] S. Samuel, “Neutrino oscillations in dense neutrino gases,” Phys. Rev. D **48**, 1462 (1993).
- [83] V. A. Kostelecký, J. Pantaleone and S. Samuel, “Neutrino oscillation in the early universe,” Phys. Lett. B **315**, 46 (1993).
- [84] V. A. Kostelecký and S. Samuel, “Neutrino oscillations in the early universe with an inverted neutrino mass hierarchy,” Phys. Lett. B **318**, 127 (1993).
- [85] V. A. Kostelecký and S. Samuel, “Nonlinear neutrino oscillations in the expanding universe,” Phys. Rev. D **49**, 1740 (1994).
- [86] V. A. Kostelecký and S. Samuel, “Self-maintained coherent oscillations in dense neutrino gases,” Phys. Rev. D **52**, 621 (1995) [hep-ph/9506262].
- [87] V. A. Kostelecký and S. Samuel, “Neutrino oscillations in the early universe with nonequilibrium neutrino distributions,” Phys. Rev. D **52**, 3184 (1995) [hep-ph/9507427].
- [88] S. Samuel, “Bimodal coherence in dense selfinteracting neutrino gases,” Phys. Rev. D **53**, 5382 (1996) [hep-ph/9604341].
- [89] V. A. Kostelecký and S. Samuel, “Nonequilibrium neutrino oscillations in the early universe with an inverted

- neutrino mass hierarchy,” *Phys. Lett. B* **385**, 159 (1996) [hep-ph/9610399].
- [90] J. Pantaleone, “Stability of incoherence in an isotropic gas of oscillating neutrinos,” *Phys. Rev. D* **58**, 073002 (1998).
- [91] S. Pastor, G. G. Raffelt and D. V. Semikoz, “Physics of synchronized neutrino oscillations caused by self-interactions,” *Phys. Rev. D* **65**, 053011 (2002) [hep-ph/0109035].
- [92] R. F. Sawyer, “Speed-up of neutrino transformations in a supernova environment,” *Phys. Rev. D* **72**, 045003 (2005) [hep-ph/0503013].
- [93] G. G. Raffelt and G. Sigl, “Self-induced decoherence in dense neutrino gases,” hep-ph/0701182.
- [94] C. Lunardini and A. Y. Smirnov, “High-energy neutrino conversion and the lepton asymmetry in the universe,” *Phys. Rev. D* **64**, 073006 (2001) [hep-ph/0012056].
- [95] A. D. Dolgov, S. H. Hansen, S. Pastor, S. T. Petcov, G. G. Raffelt and D. V. Semikoz, “Cosmological bounds on neutrino degeneracy improved by flavor oscillations,” *Nucl. Phys. B* **632**, 363 (2002) [hep-ph/0201287].
- [96] Y. Y. Y. Wong, “Analytical treatment of neutrino asymmetry equilibration from flavour oscillations in the early universe,” *Phys. Rev. D* **66**, 025015 (2002) [hep-ph/0203180].
- [97] K. N. Abazajian, J. F. Beacom and N. F. Bell, “Stringent constraints on cosmological neutrino antineutrino asymmetries from synchronized flavor transformation,” *Phys. Rev. D* **66**, 013008 (2002) [astro-ph/0203442].
- [98] J. T. Pantaleone, “Neutrino flavor evolution near a supernova’s core,” *Phys. Lett. B* **342**, 250 (1995) [astro-ph/9405008].
- [99] Y. Z. Qian and G. M. Fuller, “Neutrino-neutrino scattering and matter enhanced neutrino flavor transformation in Supernovae,” *Phys. Rev. D* **51**, 1479 (1995) [astro-ph/9406073].
- [100] G. Sigl, “Neutrino mixing constraints and supernova nucleosynthesis,” *Phys. Rev. D* **51**, 4035 (1995) [astro-ph/9410094].
- [101] S. Pastor and G. Raffelt, “Flavor oscillations in the supernova hot bubble region: Nonlinear effects of neutrino background,” *Phys. Rev. Lett.* **89**, 191101 (2002) [astro-ph/0207281].
- [102] A. B. Balantekin and H. Yüksel, “Neutrino mixing and nucleosynthesis in core-collapse supernovae,” *New J. Phys.* **7**, 51 (2005) [astro-ph/0411159].
- [103] G. M. Fuller and Y. Z. Qian, “Simultaneous flavor transformation of neutrinos and antineutrinos with dominant potentials from neutrino neutrino forward scattering,” *Phys. Rev. D* **73**, 023004 (2006) [astro-ph/0505240].
- [104] H. Duan, G. M. Fuller and Y. Z. Qian, “Collective neutrino flavor transformation in supernovae,” astro-ph/0511275.
- [105] H. Duan, G. M. Fuller, J. Carlson and Y. Z. Qian, “Simulation of coherent non-linear neutrino flavor transformation in the supernova environment. I: Correlated neutrino trajectories,” *Phys. Rev. D* **74**, 105014 (2006) [astro-ph/0606616].
- [106] H. Duan, G. M. Fuller, J. Carlson and Y. Z. Qian, “Coherent development of neutrino flavor in the supernova environment,” astro-ph/0608050.
- [107] S. Hannestad, G. G. Raffelt, G. Sigl and Y. Y. Y. Wong, “Self-induced conversion in dense neutrino gases: Pendulum in flavour space,” *Phys. Rev. D* **74**, 105010 (2006) [astro-ph/0608695].
- [108] G. M. Fuller, R. Mayle, B. S. Meyer, J. R. Wilson, “Can a closure mass neutrino help solve the supernova shock reheating problem?”, *Astrophys. J.* **389**, 517 (1992).
- [109] Y. Z. Qian, G. M. Fuller, G. J. Mathews, R. Mayle, J. R. Wilson and S. E. Woosley, “A connection between flavor mixing of cosmologically significant neutrinos and heavy element nucleosynthesis in supernovae,” *Phys. Rev. Lett.* **71**, 1965 (1993).

## NEUTRINOS FROM THE EARTH

**R. S. Raghavan**

Virginia Polytechnic Institute and State University, Blacksburg VA 24060

raghavan@vt.edu

The structure and composition of the interior of the Earth and the larger context of the evolution of the Earth and planets in the solar system is a subject of vital interest to mankind. Neutrino physics and the technology of particle physics have recently made fundamental contributions by directly looking into the interior of the sun. A similar possibility arises regarding the Earth since all the component layers of the Earth's interior contain naturally radioactive elements U, Th and K that have played a vital part in the heat output and the evolution of the Earth. These nuclides emit copious fluxes of antineutrinos ( $\bar{\nu}_e$ ) as realized long ago by Eder<sup>1</sup> and by Marx<sup>2</sup>. By detecting these "geo-neutrinos" one could make a global observation of the deep interior details of the Earth and make substantial advances in geophysical research. For this program the upcoming DUSEL laboratory in the US is exciting and timely because 1) the U. S. sites are more favorable for geoneutrino research than those elsewhere in the world (for background as well as geological relevance); 2) the required neutrino technology is mature; and 3) preliminary evidence for geoneutrinos has been obtained in the Kamland detector.

**Structure and Evolution of the Earth:** Models based on seismic data divide the earth into three basic regions: the core, mantle and crust ( Fig. 1). All regions are solid except for the liquid core. Two different types of crust cover the Earth's surface<sup>3</sup>: continental (40%)<sup>4</sup> and oceanic (60%)<sup>5</sup>. Continuous renewal of the oceanic crust at mid ocean ridges makes the oceanic crust homogeneous and relatively young, ~only 80 MYr old. In contrast, the continental crust is variable and much older, ~2000 Myr. Our knowledge of the Earth's interior, derived from material extracted in man-made probe holes, from lava flows that bring material from the upper mantle to the surface and from seismic studies, suggests that the crust and mantle are composed mainly of silica enriched in U, Th and K while the core is composed mainly of Fe. Table 1 shows the estimated concentration of U, Th and K in different Earth regions.

The chemical abundances of the sun's outer layer can be measured from optical absorption spectra and by analysis of undifferentiated meteorites such as type I carbonaceous chondrites<sup>6</sup>. These abundances should be similar to those on the Earth since both were formed out of the same process. Models referred to as "Bulk Silicate Earth"(BSE)<sup>7</sup> are based on such chondrite abundances. Table 1 includes the estimated concentration of U, Th and K in the BSE model. The ratio of Th/U between 3.7 and 4.1 is better established than the total abundances<sup>8</sup>.

**Thermodynamics of the Earth:** The rate of radiogenic heat released from U, Th and K decays are 98.1 $\mu$ W/kg, 26.4 $\mu$ W/kg and 0.0035 $\mu$ W/kg respectively<sup>3,5</sup>. Table 2 summarizes the total radiogenic heat in the Earth regions based on the mass of these elements in Table 1. The radiogenic heat production within the Earth can be compared to the heat dissipation rate

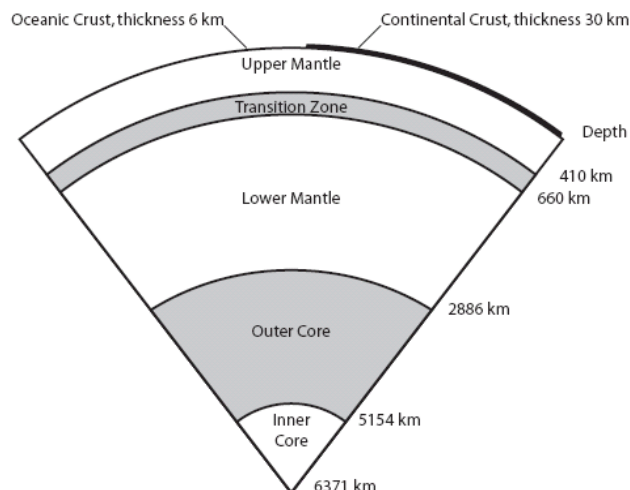


Fig. 1 Radial Distributions of major regions of the geophysical structure as determined by seismic data.

Table 1 Estimated concentrations of radioactive elements in different regions of the Earth

Region	Total mass [ $10^{21}$ kg]	Concentration		
		U[ppb]	Th[ppb]	K[ppm]
Oceanic crust[7]	6	100	220	1250
Continental crust[8]	19	1400	5600	15600
Mantle	3985	13.6	53.0	165
BSE[9]	4010	20.3	79.5	240

Table 2 Radiogenic heat production rates in different regions of the Earth

Region	U	Th	K	Total
	[TW]	[TW]	[TW]	[TW]
Oceanic crust	0.06	0.03	0.03	0.12
Continental crust	2.61	2.81	1.04	6.46
Mantle	5.32	5.57	2.30	13.19
BSE	7.99	8.42	3.37	19.78

measured at the surface. Table 3 shows the estimated<sup>9</sup> heat dissipation rate based on rock conductivity and temperature gradients in bore holes measured at 20,201 sites. The majority of the heat is lost through the oceanic crust despite the fact that the continental crust contains the majority of the radiogenic elements. A recent evaluation of the same data<sup>10</sup> however, suggests that the heat loss in the oceanic crust is less, resulting in a total heat dissipation rate of 31 TW.

The Urey ratio, the ratio between the mantle heat dissipation and production, indicates what fraction of the current cooling is due to primordial heat. Subtracting the continental crust rate of 6.5TW the mantle is dissipating heat at a rate of 37.7 TW and generating heat at the rate of 13.3TW (Urey ratio = 0.35). It is believed that the mantle convects, although the exact nature of the convection is unclear. Models give ratios  $> \sim 0.69$ <sup>11</sup> which are consistent with the value

obtained from heat considerations. A direct measurement of the terrestrial radiogenic heat production rate would therefore be very interesting.

Table 3 Crustal conductive heat dissipation rates

Region	Heat Dissipation Rate [W m <sup>-2</sup> ]	Area [m <sup>2</sup> ]	Global Heat Dissipation Rate [TW]
Oceanic crust	$101 \pm 2.2 \times 10^{-3}$	$3.1 \times 10^{14}$	$31.2 \pm 0.7$
Continental crust	$65 \pm 1.6 \times 10^{-3}$	$2.0 \times 10^{14}$	$13.0 \pm 0.3$
Whole Earth	$87 \pm 2.0 \times 10^{-3}$	$5.1 \times 10^{14}$	$44.2 \pm 1.0$

**Geo-Reactor in the Earth's Core?** In addition to neutrino signals from the Earth's U and Th content, a recent proposal suggests the possibility of another source of neutrino signal from the Earth by positing the existence of an active fission reactor at the Earth's core.<sup>12</sup> The proposal is controversial, however, it is possible to make a definitive experimental test of the proposal in the same detector built for observing geoneutrinos. The geo-reactor signal (identical to that from a power reactor on the surface) can be separated in principle from geoneutrinos since it extends well beyond the spectrum from U and Th (see below). However, the principal impediment is the strong backgrounds from nearby power reactors (see below).

**The Geo-neutrino Signal:** Each of the <sup>238</sup>U, <sup>232</sup>Th and <sup>40</sup>K decay chains contain at least one  $\beta$ -decay thus, at least one  $\bar{\nu}_e$ . Fig 2 shows the  $\bar{\nu}_e$  spectrum for the three chains. The neutrinos are practically unimpeded by the Earth's mass and reach the surface (except for neutrino oscillations which introduces a ~5% correction.)

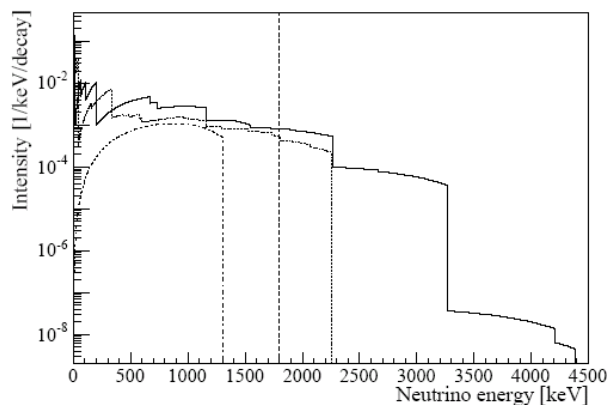


Fig. 2 The  $\bar{\nu}_e$  energy spectra from <sup>238</sup>U (solid), <sup>232</sup>Th (dash) and <sup>40</sup>K (dot-dash) decay chains. The vertical line marks the threshold for the detection reaction  $\bar{\nu}_e + p \rightarrow e^+ + n$ .

The most convenient and well established method<sup>13</sup> of detecting  $\bar{\nu}_e$  is the inverse beta decay on protons:  $\bar{\nu}_e + p \rightarrow e^+ + n$ . The positron appears as a prompt signal which is followed after several  $\mu$ s by a neutron induced signal, thus affording a delayed coincidence signature that reduces background enormously. This is of great advantage in detecting low energy (few MeV) neutrinos since the normal background due to natural radioactivity in the ambience and cosmic ray secondaries is normally a formidable obstacle. The disadvantage of the above reaction is that the threshold is the neutron-proton

(atomic) mass difference (0.782 MeV) plus the energy needed to create an  $e^+e^-$  pair (1.022 MeV) for a total of 1.8 MeV. Thus  $\bar{\nu}_e$  from <sup>40</sup>K with energy 1.3 MeV cannot be detected by this reaction. At present there is no satisfactory method to detect  $\bar{\nu}_e$  of energy <1.8 MeV. The  $\bar{\nu}_e$  energy can be directly measured by the energy of  $e^+$ , the *visible* energy of which is  $E_{e^+} + 0.782 = E_{\bar{\nu}_e}$  MeV since in a large scale detector one observes calorimetrically the  $e^+ + e^-$  annihilation energy.

Using the detailed decay chains and the frequencies of  $\bar{\nu}_e$  emission in each chain, the specific  $\bar{\nu}_e$  emissions above threshold are  $n(U) = 0.4$  per decay of <sup>238</sup>U and  $n(Th) = 0.156/\text{decay}$  of <sup>232</sup>Th. The signal observed in a detector on the surface is due typically to geo-sources up to ~500 km

from the detector, weighted by factors depending on the geometry of the source<sup>14</sup> (spherical shells in the crusts and an approximately solid sphere from the mantle).

Geo-neutrino spectra expected in two operating detectors for typical models of the U, Th distribution in the earth<sup>15</sup> are shown in Fig. 3. Note that the U part can be separated from U+Th part so that for the first time, a whole-earth measurement of the U/Th ratio can be made via geo-neutrinos. The most encouraging experimental development is the recent result from Kamland<sup>16</sup> (see Fig. 4), announcing preliminary evidence for observation of geoneutrinos that can be compared to Fig. 3. The experimental spectrum indicates strong hints of the U and U+Th features as well as the effect of high background from nearby reactors as shown in the lower panel of Fig. 4.

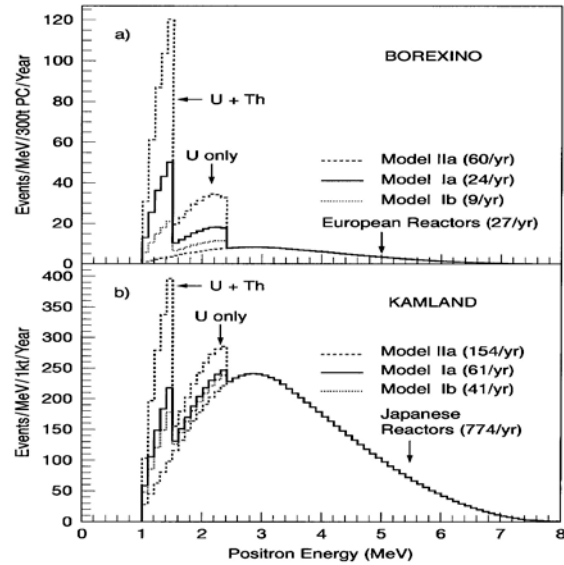


Fig. 3 Geoneutrino spectra expected in detectors operating at present and in the near future. (Ref.15)

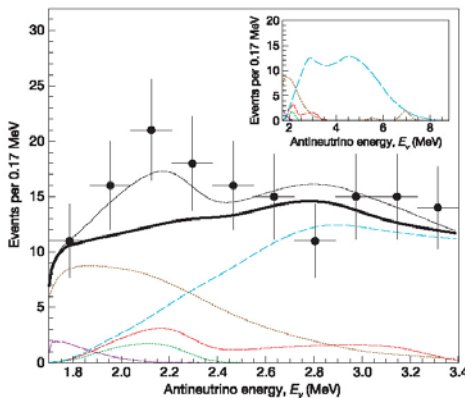


Fig. 4 Experimental  $\bar{\nu}_e$  spectra in observed in the Kamland detector: Thin blue line is the expected geoneutrino spectrum superimposed on reactor background spectrum (thick black line).

Focusing for the present on the A) to D) above, the boundaries for detector design are set by the low  $\bar{\nu}_e$  fluxes (see Fig. 4) that dictate detectors containing protons on the  $10^{32}$  scale—i.e. kilotons of proton rich target materials. The most economical way—the only way at present to achieve this design is to use organic liquid scintillators (LS) typically containing H atoms in the ratio or H/C~0.5 at best. The required LS technology is mature some 60 years and large scale detectors (of several 100 tons) with ultra -low background are in operation, pioneered by the Borexino project. Kamland which currently operates with nominal 1 kton scintillator is a direct result and has successfully recorded a preliminary result on geoneutrinos as mentioned above.

The LS technique is ideal for the detecting the  $\bar{\nu}_e + p \rightarrow e^+ + n$  reaction via a delayed coincidence signature. The delay time is due to the diffusion of the neutron, (with initial energies of several keV) that slows down in the organic liquid to thermal energies. It can then be absorbed by the protons in the liquid via the capture reaction  $n+p \rightarrow 2.2 \text{ MeV} \gamma$  which can be detected some

**Detectors:** The goals of an experimental geoneutrino program of multiple detectors at suitable geographical locations can be set as: A) Measure the total geoneutrino rate and at a minimum, test the models of  $\bar{\nu}_e$  emission rates from the continental crust B) Measure the U/Th ratio C) Measure the  $\bar{\nu}_e$  emission rates from the oceanic crusts (thus, essentially from the mantle) with a detector placed in a location where the continental crustal  $\bar{\nu}_e$  flux is very small. D) Test the hypothesis of a fission reactor in the Earth's core; E) Develop new reactions and techniques to observe the expected large  $\bar{\nu}_e$  flux from  $^{40}\text{K}$ .

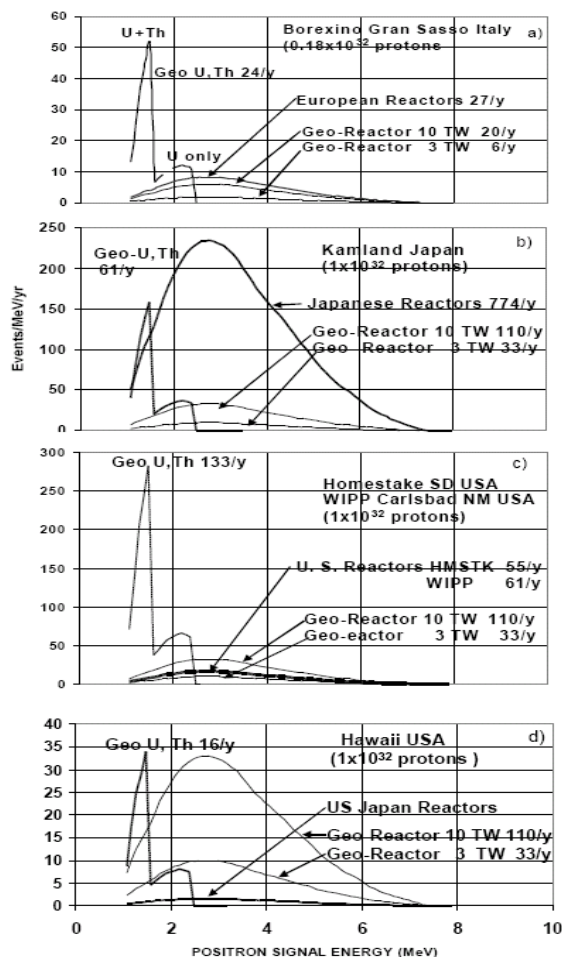


Fig. 5 Event rates and spectra of  $\bar{\nu}_e$  from the Earth and Homestake and Henderson as well as in from nuclear power reactors at various locations (Ref.21)

heavy particles under the Cerenkov threshold. Thus proton decay modes such as  $p \rightarrow K + \pi^0$  can be observed with low background with nearly ten times the efficiency possible in a Megaton Cerenkov detector.

**Background:** The basic advantage of the  $\bar{\nu}_e + p$  reaction above is the delayed coincidence which suppresses most correlated and uncorrelated radiation from the ambient radioactivity and cosmic ray muons. The use of Gd or Cd can reduce the random coincidence background considerably by shortening the neutron diffusion. Neutron producing cosmogenic spallation that generates exotic activities such as  ${}^9\text{Li}$  that decay by beta-neutron emission reproduce the tag exactly. Heavy nuclei that can induce such spallation activities must be avoided. Thus the detector should be located sufficiently deep underground, e.g., at depths of the order of 3000-4000 mwe. Internal radioactivity could be a problem since alpha particles in naturally radioactive contaminants can produce  $(\alpha, n)$  reactions with high cross section on  ${}^{13}\text{C}$  (~1% abundance) which is unavoidable in a LS detector using organic solvents. Thus scintillator radiopurity approaching levels required for solar neutrino detection as demonstrated by the Borexino Project<sup>22</sup> may have to be achieved.

~100  $\mu\text{s}$  later and used to specifically tag the  $\bar{\nu}_e$  signal. Doping with metal (Gd, Cd) atoms (neutron capture cross sections some  $\sim 10^3$  times larger than for n+p) is employed so that the delay time can be significantly reduced and thus also the time open to random coincidence background.

Several kiloton scale LS detectors are being considered for geo-neutrino research, e.g. the LBL proposal<sup>17</sup> in the framework of the Homestake DUSEL<sup>18</sup>, HANO HANO (10 kT)<sup>19</sup> developed for operation in the seas off Hawaii focusing primarily on the  $\bar{\nu}_e$  flux from the oceanic crust, and EARTH<sup>20</sup>, to be located in Curacao that expects to add directionality to its detection scheme. In addition to these specific geo-neutrino detectors, ideas for a very large detector on the scale of 50-100 kT are being studied in Europe (LENA = Low energy neutrino astronomy) and in the U. S. (HSD—Hyper-Scintillation Detector). With such sizes, most of the items in the goals for geoneutrino research above can be fulfilled in a definitive fashion. The additional attraction is their high multidisciplinary function at low and high energies for which the LS technique offers very specific advantages, for example, for  $\bar{\nu}_e$  detection from active and relic supernovae as well as pair annihilation neutrinos  $e^+ + e^- \rightarrow \bar{\nu}_e + \nu_e$ <sup>21</sup> from pre-explosion high temperature stars at the end of the C, O and Si burning.

The scintillation approach can observe

**DUSEL and International Geographical Location** The geographical location of the detector is a critical aspect from the point of view of the geo-science obtainable from it as well as the background incurred due to the proximity of nearby high-power nuclear reactors. A detector located at sites proposed for DUSEL and at Borexino at LNGS Italy, will focus primarily on geoneutrinos from the continental crust. The Kamland detector would be sensitive to the proximity of the oceanic crust besides that of the Asian continental crust. The former can be probed by Hanohano in Hawaii and the latter exclusively in the Himalayan neighborhood. A search for  $\bar{\nu}_e$  from a possible geo-reactor would be independent of geographical location.

Beyond the background sources discussed above, most of which depend on the depth and detector materials, a crucial  $\bar{\nu}_e$  background arises from nearby high power nuclear reactors that produce large  $\bar{\nu}_e$  fluxes indistinguishable from the weak geoneutrino and even worse, a possible spectrally identical georeactor  $\bar{\nu}_e$  signal. Thus the location of the experiment vis a vis power reactor locations is crucial. A recent study<sup>23</sup> compares several U.S. and international locations and the inherent  $\bar{\nu}_e$  background relative to geo signals expected at these locations as seen in Fig. 5. The spectra for Homestake apply as well to the Henderson site. The US sites are generally more favorable from this point of view than either the Italian or Japanese sites.

In summary, from both the science and background points of view the proposed DUSEL sites adequately fulfill background related constraints on the underground depth and distance from power reactors. The continental sites are ideal for making definitive measurements of the  $\bar{\nu}_e$  from the continental crust especially with the a large detector such as HSD that can be applied to many other questions in particle physics, astrophysics and cosmology.

- [1] G. Eder, Nucl. Phys. **78**, 657 (1966)
- [2] G. Marx, Czech. J. Phys. **B19**, 1471 (1969)
- [3] G. Schubert et al, *Mantle Convection in the Earth and Planets* (Cambridge U. P) 2001
- [4] S. R. Taylor and S. M. McLennan, *The Continental Crust: Its Composition and Evolution: An Examination of the Geochemical Record Preserved in Sedimentary Rocks* (Blackwell Scientific Publications, Oxford, 1985)
- [5] R. L. Rudnick and D. M. Fountain, Rev. Geophys. **33**, 267 (1995)
- [6] E. Anders and N. Grevesse, Geochim. Cosmochim. Acta **53**, 197 (1989)
- [7] W. F. McDonough and S. S. Sun Chem. Geol. **120**, 223 (1995)
- [8] A. Rocholl and K. P. Jochum, Earth Planet. Sci Lett **117**, 265 (1993)
- [9] H. Pollock, S. J. Hurter and J. R. Johnson, Rev. Geophys. **31**, 267 (1993)
- [10] A. Hofmeister, R. Criss, Tectonophys. **395**, 159 (2005)
- [11] See e.g. F. M. Richter, Earth Planet. Sci. Lett. **68**, 471 (1984)
- [12] J. M. Herndon, Proc. Nat. Acad. Sci. **100**, 3047 (2003)
- [13] F. Reines and C. L. Cowan Jr., Science **124**, 103 (1956); Phys. Rev. **113**, 273 (1959)
- [14] L. Krauss, S. Glashow and D. Schramm, Nature **310**, 191 (1984)
- [15] R. S. Raghavan et al, Phys. Rev. Lett. **80**, 635 (1998).
- [16] T. Araki et al, Nature **436**, 499 (2005)
- [17] N. Tolich et al, LBL Proposal for "A geoneutrino experiment at Homestake" talk at Homestake DUSEL workshop
- [18] See <http://www.int.washington.edu/DUSEL/homestake.html>
- [19] S. Dye, Hawaii Conf. on Geoneutrinos <http://www.phys.hawaii.edu/~sdye/hnsc.html#agn>
- [20] R. de Meijer, Hawaii Conf on Geoneutr. <http://www.phys.hawaii.edu/~sdye/hnsc.html#agn>
- [21] Odrziwolek et al, Astro-ph/0405006
- [22] G. Alimonti et al, Astroparticle Phys. **16**, 205 (2002)
- [23] R. S. Raghavan, hep-ex/0208038

# Status of Double Chooz

## D. Reyna for the Double Chooz Collaboration

Argonne National Laboratory, HEP Division, 9700 S. Cass Ave., Argonne, IL 60439

E-mail: reyna@anl.gov

**Abstract.** The Double Chooz experiment will be the next reactor based neutrino oscillation measurement. The collaboration has made significant progress toward the initiation of the experimental construction. Here, we present details of the design, testing and development that have been ongoing, as well as the expected schedule for construction and installation of the experiment. We are currently on our target path to begin data taking in 2008.

## 1. Introduction

The Double Chooz experiment will be the next reactor based neutrino oscillation measurement. The multi-national collaboration includes 26 institutions from France, Germany, Italy, Spain, Russia, the U.K. and the United States. This collaboration will attempt to make almost an order of magnitude improvement on our knowledge of the last unmeasured neutrino mixing parameter  $\theta_{13}$ [1] by looking for the disappearance of electron antineutrinos emitted by the cores of nuclear power reactors. To minimize the time and expense required to construct this experiment, the collaboration proposes to perform this measurement at the site of the successfully concluded CHOOZ experiment[2] in the Ardennes region of France. In addition, by using the baseline designs of the CHOOZ experiment, which provides the current best limit on the value for  $\theta_{13}$ , and making improvements to those aspects which dominated the systematic errors, we are confident that the desired goals can be achieved. A much more complete description of the experiment can be found in [3].

## 2. Experimental Design

The experiment will be located on the site of the Chooz nuclear power plant, which is operated by the French company Electricité de France (EDF). The source of antineutrinos will be the two N4 class PWR reactors of 4.27 GW<sub>th</sub> each. The detection technique will be similar to the previous CHOOZ experiment by identifying the inverse beta-decay event signature in monolithic liquid scintillator detectors viewed by 8" photomultiplier tubes.

Since the previous limit on  $\theta_{13}$  by the CHOOZ experiment was equally limited by statistical and systematic errors, the design of the Double Chooz experiment has evolved in ways that will improve or eliminate the largest sources of the systematic errors, allowing the useful application of increased statistics. The dominant error in CHOOZ was the knowledge of the antineutrino flux and spectrum from the reactor cores. To eliminate this effect, a second detector—identical in construction to the first—will be constructed and installed at a laboratory 280m from the reactor cores. This second (Near) detector will provide an unoscillated reference measurement which can be compared with a similarly constructed (Far) detector to be installed at the original CHOOZ

laboratory, located an average of 1051m from the reactor cores—very near to the oscillation maximum. The near laboratory location has been chosen by working closely with the engineers of EDF to minimize the average distance from the cores, maintain the same ratio of fluxes between the two cores as seen by the far detector, and satisfy the needs of the reactor complex for safety and security. The laboratory will be constructed at the bottom of a 40m shaft and is intended to maintain a minimum overburden of 30m of rock (approximately 80 meters of water equivalent) in all directions.

The detector design has also evolved in order to minimize the effects of random singles backgrounds which adversely impacted the CHOOZ experiment. The largest source of these backgrounds in CHOOZ was the radioactivity of the PMT glass itself, emitting gammas directly into the active scintillator. To reduce this, the PMTs for Double Chooz will be installed in a 1.05m thick non-scintillating mineral oil buffer which will completely surround the active scintillating region. In addition, the natural radioactivity of the surrounding rock will be shielded in Double Chooz by the use of 17cm of steel surrounding the entire active detector system. The use of steel, instead of the 1 meter thick low-radioactivity sand shielding used in CHOOZ will reduce the external gamma background by almost two orders of magnitude while simultaneously allowing the central fiducial volume to be increased by a factor of two. The combination of the steel shielding and the mineral oil buffer will dramatically reduce the random singles rate. It is expected that this will allow the elimination of several analysis criteria used for event selection in the CHOOZ analysis which relied on reconstructed vertex positions and had systematic errors on the order of 1–1.5%. Including all modifications, the final detector design to be used for both detectors in Double Chooz (shown in Fig. 1) can be described, from the center outward, as follows:

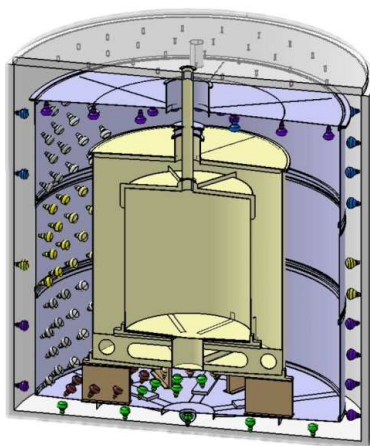


**Figure 1.** Design graphic for the complete Double Chooz Detector. This design has a total diameter of  $\sim 7\text{m}$  and a total height of just over 7m.

**Central Detector** The fiducial “target” volume is contained within an 8mm thick transparent acrylic vessel. The target contains  $10.3\text{ m}^3$  of Gd-loaded dodecane+PXE scintillator. The target is surrounded by a layer of unloaded dodecane+PXE scintillator, used to detect gammas from the n-Gd capture events which exit the target region—reducing the loss in detection efficiency near the edge of the target volume. This so-called “gamma catcher” is contained within a second transparent acrylic vessel of thickness 12mm and volume  $22.6\text{ m}^3$ . The acrylic vessel is surrounded by the non-scintillating dodecane buffer, mentioned above, which is contained within a 1.05m thick mineral oil buffer system. The entire detector is housed within a large, cylindrical structure with a hemispherical top.

steel tank, 534 8" PMTs—providing an active coverage of  $\sim 13\%$ —collect the light from the central scintillating volumes.

**Inner Veto** A 50cm thick cylindrical “veto” region, filled with liquid scintillator, will surround the central detector at the far site. A slightly thicker inner veto—as much as 100cm—will be used at the near site to reduce the effect of the increased muon rate at the shallower depth. This system provides the dual purpose of identifying muons which pass near the central detector and can create spallation neutrons—a correlated background—as well as attenuate and identify any background coming from outside the detector area. Information from the inner veto will be used, offline, to further reduce the effects of correlated and uncorrelated backgrounds that may lie within the event sample. The inner veto is completely surrounded by the steel shielding mentioned above.

**Outer Veto** Placed above the previously described systems, an active external tracking system will be used to further identify “near-miss” muons. By covering an extended region from 2–4m beyond the edge of the inner veto, the rate of unidentified spallation neutrons entering the central detector can be reduced by an additional factor of 5–10. In addition, providing an entry point and/or track direction for muons which cross the central detector is expected to provide useful information for the rejection of correlated events arising from cosmogenic radioactive isotopes such as  ${}^9\text{Li}$ .

The projected systematic errors for Double Chooz, compared with those from the original CHOOZ experiment, are shown in Table 1.

**Table 1.** Total systematic error on the normalization between the detectors.

		CHOOZ	Double Chooz	
	$\nu$ flux and $\sigma$	1.9%	0–0.1%	
Reactor Induced	Reactor Power	0.7%	0–0.1%	Two identical detectors
	Energy per fission	0.6%	0–0.1%	
	Solid Angle	0.3%	0–0.1%	
Detector Induced	Volume	0.3%	0.2%	Identical measurement device
	Density	0.3%	0–0.1%	Accurate temperature control
	H/C/Gd Ratios	1.2%	0–0.1%	Single scintillator batch
	Spatial Effects	1.0%	0–0.1%	Identical target geometry
	Live Time	few%	0.25%	Redundant measurements
	Analysis	Event Selections	1.5%	0.2–0.3%
Total		2.7%	0.6%	

### 3. Prototype and Testing

In preparation for the construction of the experiment, almost every system has gone through extensive design and development work. Prototype electronics boards have been constructed, PMTs from multiple manufacturers have been compared, and procedures for everything from measuring the mass of the scintillator to demagnetizing the steel shielding have been tested—just to name a few. Two systems, however, deserve special comment: the liquid scintillator development and the design of the double-walled acrylic vessel.

**Liquid Scintillator Development** The performance of the liquid scintillator, particularly the Gd-doped target scintillator, is of critical importance to the success of the experiment. Stable, high quality liquid scintillator has become rather commonplace, however doping these

optical degradation of the Gd-doped scintillator in the original CHOOZ experiment which ultimately terminated data taking after 1 year. To achieve the Double Chooz goals, a stable scintillator will be required which can provide high performance for at least 3–5 years.

With that understanding, groups from MPIK–Heidelberg and LNGS/INR have been working for more than 4 years to understand the previous degradations and to develop new chemical compositions which will satisfy the Double Chooz requirements. A base scintillator composed of PXE and dodecane has been chosen due to its high flashpoint and relative compatibility with the acrylic vessels. Two Gd formulations have been developed which show good performance—one based on carboxylic acids and the other on Gd- $\beta$ -diketonates. Both of these candidates have been extensively tested under multiple environmental conditions and have already demonstrated stability for periods of greater than 400 days. The preferred candidate is currently in transition to industrial production. Samples of 50g and 400g have been produced by an industrial firm and synthesized into ~80 liters of scintillator. A final complete test batch of 700g (~150 liters of scintillator) is currently being synthesized completely by the industrial firm as a last test of the procedures. Once successful production at these scales has been established, the final production run of 100 kg (needed for both detectors) will begin.

**Acrylic Vessel Design** The nested acrylic cylinders, which will contain the target and gamma-catcher liquids, present challenges from the perspective of both fabrication and longevity. The material must be transparent to wavelengths above 400nm and must resist leakage for more than 10 years. By far the most significant constraint, however, is that the acrylic must demonstrate a level of chemical compatibility with all of the central detector liquids such that over the 5 year lifespan of the experiment, no degradation of either the liquids (scintillation and absorbency) or the acrylics (cracking and crazing) will occur.

These requirements put severe limits on the quality of the acrylic welding processes and the levels of residual stresses which can exist within the acrylic structure itself. A significant amount of effort has gone into studying the response of the acrylic under various chemical and environmental conditions. In addition, a detailed finite element analysis has been performed to study not only the static forces on the acrylic structure, but also the stresses that will be born during transport from the factory to the experimental laboratories.

As a final test of our understanding of the acrylic, the scintillator and ancillary systems, a 1:5 scaled prototype of the liquid vessels has been constructed. This model contained a nested acrylic structure which was filled with the Gd-doped carboxylate type scintillator in the central volume and the expected unloaded PXE/dodecane scintillator in the outer volume. The acrylic was placed inside a stainless steel vessel which contained non-scintillating mineral oil which was itself contained within another steel vessel filled with scintillator. This prototype assembly enabled testing of all expected cleaning and installation procedures for the components. In addition, a complete liquid handling system was required.

Such a test setup—almost an experiment on its own—has been very educational for the collaboration. In addition to the opportunity to practice installation and filling procedures, some weaknesses in the liquid connections and pressure relief systems were seen.

#### 4. Expected Schedule and Results

As of this writing, funding from most of the European groups has either already been established or is in the final stages of approval. In addition, the French scientific agencies have committed to doubling their contribution, as needed, in order to insure that the intended experimental schedule is maintained. As such, work by EDF to renovate the infrastructure at the far laboratory has already commenced. It is expected that the collaboration will gain beneficial occupancy in November of 2006. Detailed engineering layouts of the completed laboratory have already been

performed and procedures for transport and installation of all liquids and major components have been established. Complete installation of the detector will take about one year such that data taking with the far detector alone is expected to begin in 2008.

The near laboratory is undergoing a final refinement of the civil design by the engineers of EDF. Construction of the laboratory will begin after completion of the final design and the competitive bidding process—expected by the end of 2007. The completed laboratory is expected to be available to the collaboration by the fall of 2008. After a similar 1 year detector construction program, the collaboration should begin full 2 detector data taking near the end of 2009. The expected sensitivity from Double Chooz is shown in Fig. 2. Notice that running the far detector alone will be sufficient to confirm and even surpass the previous CHOOZ results in only a few months. This is primarily due to the significantly increased statistics from both reactor power and fiducial volume, as well as the improvements to the detector designs.

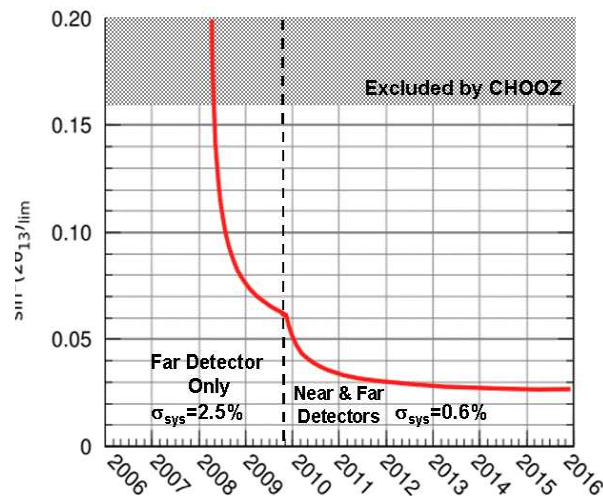


**Figure 2.** Expected sensitivity of Double Chooz under the current schedule. The 90% confidence level limit on  $\sin^2(2\theta_{13})$  is shown for an assumed null measurement and  $\Delta m^2 = 2.5 \times 10^{-3} \text{ eV}^2$  known to 20%.

## 5. Conclusion

The Double Chooz collaboration has made significant progress in the design and prototyping of the experiment and its necessary components. Construction is already underway at the EDF facility in France. We expect to provide a substantial improvement to the previous limit on  $\theta_{13}$ , surpassing the previous bounds within 6 months with the far detector alone. With the expected schedule, Double Chooz should provide a 90% confidence limit on  $\sin^2(2\theta_{13})$  of  $\sim 0.05$  in 2009 and between 0.02–0.03 in 2011.

## References

- [1] W. M. Yao *et al.* [Particle Data Group], Chapter 13: “Neutrino Mixing”, *J. Phys. G* **33**, 1 (2006).
- [2] M. Apollonio *et al.* [CHOOZ Collaboration], *Eur. Phys. J. C* **27**, 331 (2003).
- [3] F. Ardellier *et al.* [Double Chooz Collaboration], arXiv:hep-ex/0606025.

## John Bahcall and Ray Davis: a Brief Tribute

**R.G. Hamish Robertson**

Center for Experimental Nuclear Physics and Astrophysics, and Department of Physics,  
University of Washington, Seattle, WA 98195

E-mail: [rghr@u.washington.edu](mailto:rghr@u.washington.edu)

**Abstract.** Ray Davis and John Bahcall inspired a generation of physicists and astronomers, and changed science in important ways. Their deaths in the past year are a great loss.

Although 20 years separated them in age, by a sad coincidence two giants of our field passed away within the last year.<sup>1</sup> John Bahcall (Fig. 1) died August 17, 2005, aged 70, succumbing to a rare blood disorder, and Ray Davis (Fig. 2) died May 31, 2006, aged 91, of complications from Alzheimer's disease.



**Figure 1.** John N. Bahcall 1934 - 2005.

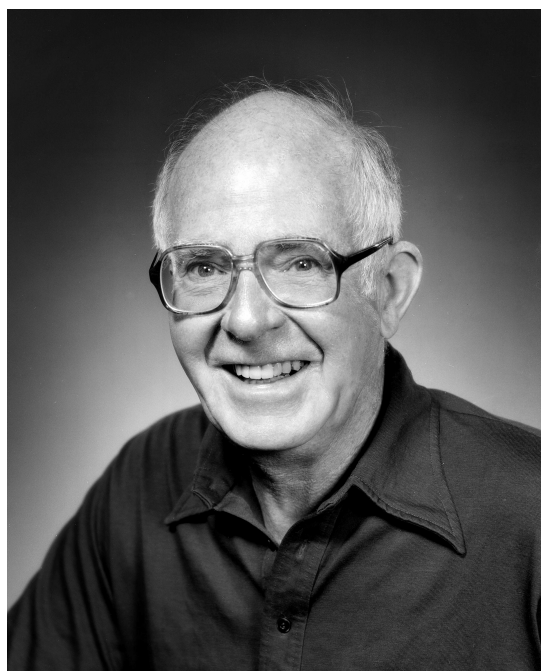


**Figure 2.** Raymond A. Davis, Jr. 1914 - 2006.

Davis and Bahcall began their lifelong friendship in 1962, when Davis wrote to Bahcall asking about the rate of electron capture by  ${}^7\text{Be}$  in the sun [1]. Davis began with a 1000-gallon tank

<sup>1</sup> Hans Bethge, *Proceedings of Neutrino Physics and Astrophysics, July 13-19, 2006*

of perchloroethylene in the Barberton limestone mine in Ohio. He made measurements (a limit of 300 SNU) that convinced him the method was sound and immediately began to argue for a 100,000-gallon tank, which would still have been too small, given what had just been learned by Kavanagh at Caltech about the  ${}^7\text{Be}(p,\gamma){}^8\text{B}$  cross section. But in 1963 Bahcall made the crucial calculation (inspired, he said, by a question from Ben Mottelson) that the analog state was very important. By 1964 funds and a site, the Homestake mine, were in place for the full-scale experiment. The first results from the new tank were available in 1968, an upper limit of 3 SNU. That was already somewhat in conflict with Bahcall's calculation of  $7.5 \pm 3$  SNU and the Solar Neutrino Problem was born. In 1970 risetime discrimination methods reduced the counter backgrounds tenfold and the solar signal (not a limit) was observed for the first time. The lower counter backgrounds focused attention on  ${}^{37}\text{Ar}$  backgrounds and, among other things, it was decided to fill the cavity with water to reduce fast neutrons. Ray was full of fun and it was, after all, 90 degrees down there all the time, so he cooled off by swimming in the water shield.

The exquisite miniature proportional counters, made of synthetic fused silica with zone-refined iron cathodes, were also moved underground. Counting continued steadily for 24 years, the experiment operating on something like \$50k a year from DOE. Failure of both eductor pumps shut the experiment down for 2 years in the mid 80s for lack of funds to replace them.

Meanwhile John and many other theorists labored at the theory. Many small effects that had been neglected were discovered, and many new experimental data of ever-increasing precision were obtained, but the predicted SNU rate never changed much. The Gallium experiments SAGE and GALLEX in the early 90s also gave results below the prediction. The hope was that they would come in either much above the  $pp$ -only expectation, which was 70 SNU, or much below, pointing in that case to neutrino oscillations as the culprit, but of course, they came in at exactly 70 SNU. Kamiokande gave a result that really could be reconciled with Cl-Ar only by oscillations or experimental error. At the end, the beautiful tension between experiment and theory was finally to be resolved with the Sudbury Neutrino Observatory, which showed clearly the presence of non-electron neutrinos in the solar flux. John and Ray were both very influential in getting SNO supported and funded. Two-thirds of the solar flux turned out to be mu and tau neutrinos. The agreement with the calculations of Bahcall for the neutral-current rate, about  $\pm 15\%$  now, translates to an incredible sub-1% precision on the central temperature of the sun, predicted in the face of decades of not-too-subtle dismissal by many scientists of the capabilities of astrophysical theory.

Davis won the 2002 Nobel Prize in Physics for detecting solar neutrinos. He shared the prize with Masatoshi Koshiba, and Riccardo Giacconi.

It is easy to forget while we savor the triumph of their work on solar neutrinos that they both did much more. John was the author of more than 500 papers and books; the architect of the Standard Solar Model, vindicated in spectacular fashion along with the discovery of neutrino oscillations and mass; a leading figure, with Lyman Spitzer, in the Hubble Space Telescope; *the* authoritative figure in Astronomy, president of the AAS and Chair of the NAS Decadal study that shaped modern astronomy; the winner of innumerable prizes. Except one. Many of us felt that when the Nobel Committee recognized Davis and Koshiba for opening the field of experimental neutrino astronomy, they carefully left the door open for a subsequent Prize that might have gone to John. We shall not know.

Ray showed experimentally, using his novel radiochemical approach and a nuclear reactor, that neutrinos were not the same as antineutrinos. He developed both of the extraction technologies that were subsequently used in the SAGE and GALLEX experiments, although he was skeptical there would ever be a gallium experiment after the experiences in the US in the mid-80s. Ray used to say, "Gallium is the metal of the future. And it always will be!"

Each was a leader, in his own charismatic way. Bahcall was always the activist, positive, promoting the science, mentoring a generation of physicists (and not just theorists, I can attest).

On the very day John slipped away, Raju Raghavan and I were by an odd chance sitting across a table in Sudbury sharing stories of how we first met John and how our lives were thus changed. He had a way of doing that with young people, and our stories are far from unique. John loved to encourage the experimentalists, and he never saw a solar neutrino experiment he didn't like. And he could come out swinging if anything threatened an experiment. Vladimir Gavrin wrote [2],

“One of the bright examples was his help to save the gallium in SAGE. For five years he fought together with Russian scientists against numerous encroachments on SAGE gallium. These were difficult times in Russia and he wrote in The New York Times ‘It just astonishes me, that such magnificent science can continue at all in such a lawless country.’ Currently Russia has almost returned to the frames of civil community. John always provided support when his help was needed. He involved the world scientific community to support SAGE at that time with the result that a letter was written from 12 Nobel Prize Winners to Russian Prime Minister Chernomyrdin in 1997 to preserve the gallium in SAGE. Thanks to his efforts, the issue about preserving gallium in SAGE was raised in 1998 in the Intergovernmental Russian-American Commission Gore-Chernomyrdin, and that was extremely helpful. Also his letter to the President of Kabardino-Balkarian Republic played a significant role when local people stopped our  $^{51}\text{Cr}$  source on its way to the Baksan Neutrino Observatory.”

Davis led by example, showing how experimental science should be done: care, pragmatism, and a lifelong demonstration that it was never necessary, in achieving your own goals, to diminish anyone else. He would take the most pointed criticism in good stride, and gave thoughtful and gracious responses to all. It struck me that I have never seen a picture in which he was not smiling. When I asked Tom Bowles for his recollections, he said, “Ray was always straightforward about everything and in good spirits. I don't ever recall seeing him upset.”

In the excitement of our field, in the many people who acknowledge John and Ray as their inspirations and guides, they are both still very much with us.

### *References*

- [1] Bahcall JN and Davis R, Jr., *Essays in Nuclear Astrophysics*, ed Barnes CA, Clayton DD and Schramm D (Cambridge University Press, 1982), 243.
- [2] Gavrin VN, private communication 2005.

Tribute to Hans Bethe  
(Remarks to Neutrino Conference)  
L. Rosen

During the War years at Los Alamos, Hans Bethe was a super giant among a host of giants. Many of us had learned nuclear physics from three papers, in Reviews of Modern Physics, which were authored or co-authored by Bethe. They were known as the Bethe Bible and contained all that was then known about the subject.

I believe that most, if not all, would agree that Bethe, as T-Division Leader, was, next to Oppenheimer the most important factor in the early success of the Manhattan Project. My work had one notable interaction with Bethe during the war years.

I was assigned to one of the “implosion” groups. There were times when we waited for the next design of explosives. During those intervals we did whatever experiment we chose. I chose to measure the attenuation of electromagnetic signals by high explosives. I never heard a word about my measurements, until after the Trinity event.

At the Trinity site, containment of the plutonium, in case of failure to detonate, had been abandoned. The bomb was on top of the tower. Everything was in readiness awaiting the results of a final, full scale experiment. The results were a “show-stopper”. The rise-time of the signal, which reflected the compression time, was longer than could be tolerated due to spontaneous fission. Oppenheimer turned to Bethe for an explanation of why the new results differed from extrapolation of smaller scale experiments. Bethe secluded himself for several hours and returned with a complete theory of the transmission of electromagnetic energy through an environment created by chemical explosives. He used his recollection of results from my experiments to anchor his theory with the conclusion that all was well. No-one could compete with Bethe’s calculational abilities. It is not much of an exaggeration to say that he missed nothing and remembered everything.

Bethe was a strong advocate for peaceful co-existence and an implacable foe of tyranny. He was not enthusiastic about H-bomb development until the Soviet threat emerged and there was a credible approach to igniting deuterium and tritium. Thereafter he made his signature contributions to the computational program, as a consultant to the Laboratory Director and T-Division. He returned annually to the Laboratory from the next 40 years.

Following our proposal for a meson factory, the AEC asked Bethe to chair a panel for advising them on the feasibility, scientific utility and priority that should be accorded the facility we had proposed. Bob Wilson and Bob Christy were among the distinguished scientists on this panel, but Bethe was the driving force. Their assessment was, I believe critical to AEC sponsorship of LAMPF. Bethe's favorite for LAMPF were the nucleon-nucleon problem and neutrino physics.

Soon after we achieved full energy beam, I was driving Bethe to the site. As we passed huge letters on the canyon wall announcing 800 MeV, Bethe mused "I am looking forward to seeing what I have wrought". He was pleased with what he saw.

On another visit I told Bethe about an experiment, to measure the cross section for scattering electron neutrinos by electrons, and that his predicted cross section, his solar energy production theory, was correct. Well, he said, "that's a relief. Now I don't have to give back my Nobel Prize".

Immediately following the end of the Cold War there appeared an editorial in the Bulletin of the Atomic Scientist which argued that now it is no longer necessary or desirable for Los Alamos to be engaged in fundamental science. George Cowan, Metropolis, and I wrote a rebuttal and sent it to Bethe for his criticism and hoped for concurrence. Bethe rewrote most of it and we submitted it to the Bulletin.

Recently, in an interview with Los Alamos Science, the Editor, asked me what advice I might give to the new management of LANL. I suggested they read the rebuttal to the editorial in the Bulletin, of which Bethe was first author. May I quote several brief excerpts?

“The demise of the Cold War provides unique opportunities for improving the quality of life throughout the world. It also provides opportunity for destroying some national treasures which may be critical to accomplishing the above goal.

“Admiral Watkins and others have correctly, in our opinion, identified the national laboratories as national treasures. However, voices are now heard suggesting, even demanding, that Los Alamos be henceforth devoted to weapons work, and nothing else. There was no such restriction on Los Alamos, even at the height of the Cold War. It was understood then, and also during World War II, that major advances in technology require understanding and pursuit of the science that underlies the technology. It was also understood that even science which is not directly related to a specific technology can contribute greatly to that technology and vice-versa.

“This country faces many problems on the way to becoming again pre-eminent in civilian technology. Creative technology is the key to economic competitiveness. Many of the technological problems are of long range. These cannot be solved by industry alone, because industry must look at the bottom line every year. Multidisciplinary laboratories are required which do not need to make an annual profit.

“We have learned from our Los Alamos experience that the major key to progress in science and technology is highly gifted and dedicated people, together with an environment which fosters cross-fertilization, involving a broad spectrum of sciences and technologies, of ideas and concepts and skills; and also dreams and aspirations. Such an environment cannot, for long, exist in a single purpose, narrowly focused, institution.

Such was the wisdom of Hans Bethe.

# New techniques in $0\nu\beta\beta$ germanium experiments

**Stefan Schönert**

Max-Planck-Institute für Kernphysik Heidelberg, Saupfercheckweg 1, 69117 Heidelberg, Germany

E-mail: [stefan.schoenert@mpi-hd.mpg.de](mailto:stefan.schoenert@mpi-hd.mpg.de)

**Abstract.** This paper summarizes recent progress novel experimental concepts developed in the framework of the GERDA and MAJORANA projects using high-purity germanium detectors for the search of  $0\nu\beta\beta$  decays.

## 1. Introduction

High-purity germanium (HP-Ge) detectors enriched in the isotope  $^{76}\text{Ge}$  have been used for the search of neutrinoless double beta decay  $0\nu\beta\beta$  in the Heidelberg-Moscow (HDM) [1] and IGEX [2] experiments. Both projects have been completed several years ago. Until today, the achieved sensitivities are the most stringent in the field. A part of the HDM collaboration claims evidence for a  $0\nu\beta\beta$  signal after a reanalysis of the full data set [3].

Two new experimental projects are under preparation. The European Germanium Detector Array (GERDA) [4] and the US lead MAJORANA [5] experiment. Both projects pursue a phased approach with the ultimate goal of commonly operating a one ton experiment to explore the mass range predicted by neutrino oscillation experiments assuming an inverted mass hierarchy. Novel background techniques will be used to reduce or actively suppress backgrounds which could mimic  $0\nu\beta\beta$  events.

## 2. Characteristics of $^{76}\text{Ge}$

The isotope  $^{76}\text{Ge}$  has several features which makes it a highly attractive element to be used for  $0\nu\beta\beta$  search. Some of the features are listed below.

- Favorable nuclear matrix element  $|M^{0\nu}| = 2.5$  [6]
- Reasonable slow  $2\nu\beta\beta$  rate ( $T_{1/2} = 1.4 \cdot 10^{21}$  y) and high  $Q_{\beta\beta}$  value (2039 keV).
- Germanium is both source and detector
- Elemental germanium maximizes the source-to-total mass ratio
- Intrinsic high-purity germanium diodes
- HP-Ge detector technologies are well established
- Industrial techniques and facilities available to enrich from 7% up to 90%
- Excellent energy resolution: FWHM 3.3 keV at 2039 keV (0.16%)
- Powerful background rejection possible: granularity (segmentation and close packing), timing, pulse shape discrimination, argon scintillation
- Best limits on  $0\nu\beta\beta$  - decay used Ge  $T_{1/2} > 1.9 \cdot 10^{25}$  y (90%CL)

### 3. Sensitivity and background considerations

Figure 1 displays the achievable half-life limit as a function of exposure given in kg-years under the assumption of background free operation. As long as no events occur in the energy analysis window, the sensitivity increases linearly with exposure. A background level of  $\sim 10^{-3}$  counts/(kg·y·keV) must be reached for an exposure of 100 kg-years and  $\sim 10^{-4}$  counts/(kg·y·keV) for 1000 kg-years. An energy resolution of approximately 3.3 keV FWHM at  $Q_{\beta\beta}$  has been assumed. Novel background reduction and active suppression methods are required to improve the current state-of-the-art levels  $\sim 10^{-1}$  counts/(kg·y·keV) by two to three orders of magnitude. An exposure of 100 kg-years is required to explore the degenerate mass hierarchy, while the inverted mass hierarchy requires about  $5 \cdot 10^3$  years to be fully covered.

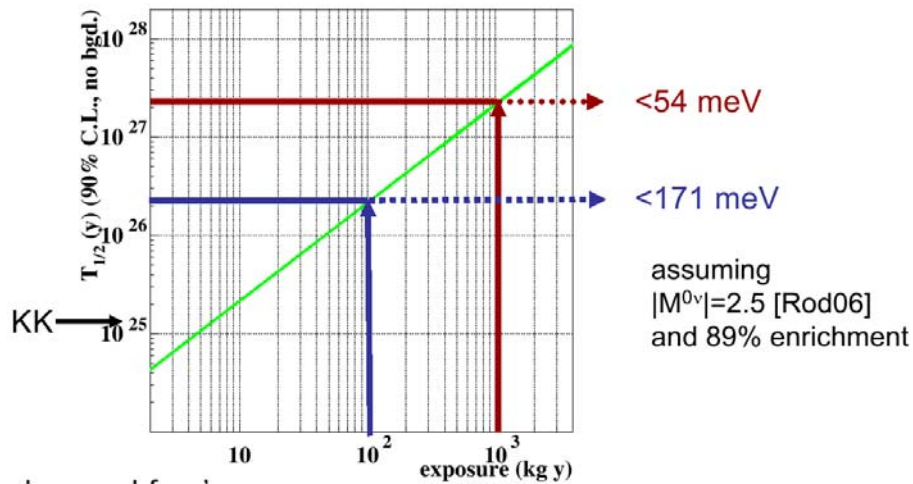


**Figure 1.** Achievable  $T_{1/2}$  limit versus exposure in kg-years assuming background free operations. 'KK' indicates the half-life of the HDM claim. The corresponding limits on the effective neutrino mass are indicated and are based on the matrix elements of Ref.[6]. Isotope enrichment of 89% has been assumed.

### 4. Experimental implementations and background reduction strategies

The MAJORANA project plans to use arrays of enriched germanium detectors housed in electro-formed copper cryostat's. The shield against external radiation consists of electro-formed copper and lead and housed deep underground to be shielded against cosmic muon interactions. The proposal which is currently under review foresees a staged approach based on 60 kg arrays (60/120/180 kg). The GERDA experiment is located at the LNGS underground laboratory. Bare enriched detectors submerged in high-purity liquid argon serving simultaneously as cooling medium and as shield against external radiation. All 18 kg of enriched germanium crystals which have formerly been used in the HDM and IGEX experiment will be used in phase I of GERDA. New detectors will be added in phase II and doubling the target mass to about 40 kg.

The physics goal of both experiments is to first explore the degenerate mass scale, study backgrounds and novel experimental techniques. A letter of intend has been worked out amongst the two collaborations to haven an open exchange of knowledge and technologies and at a later stage to consider to select the best technique and to explore the inverse hierarchy mass range in a joint experiment using about one ton of enriched crystals. Figure 2 displays schematically the two experimental setups.

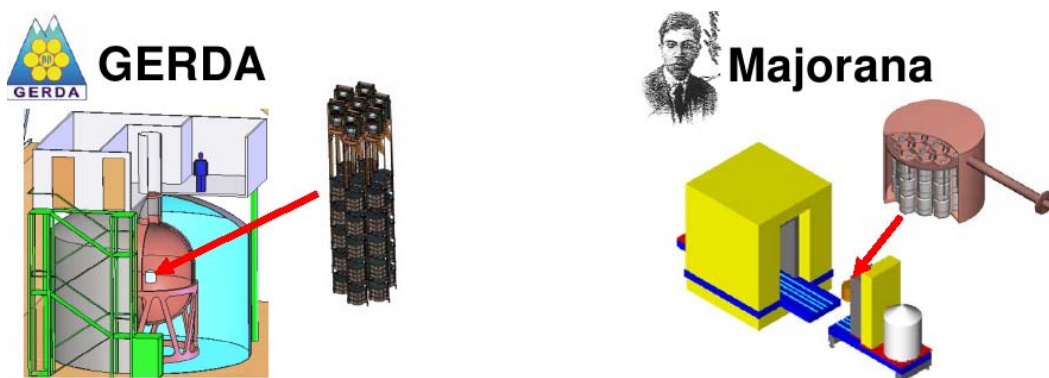


**Figure 2.** Schematic view of the GERDA and MAJORANA experiment .

The main difference of the experimental concepts is the shielding against external radiation. While GERDA uses high-purity liquid argon (backup: nitrogen) enclosed in a large water tank, MAJORANA relies on high-purity electro-formed copper with an external lead shield. Given the Z-dependence of muon induced neutron production, MAJORANA requires a greater depth in comparison to GERDA in order to avoid backgrounds induced by neutron capture on  $^{76}\text{Ge}$ . Figure 3 summarizes the main backgrounds and reduction strategies.

Source	Action GERDA	Action Majorana
$\gamma$ 's external to crystals from $^{208}\text{Tl}$ ( $^{232}\text{Th}$ ), $^{214}\text{Bi}$ ( $^{226}\text{Ra}$ ), $^{60}\text{Co}$ ,...	Shield: high-purity liquid argon (nitrogen) / water shield	Shield: Electroformed copper, lead
Front-end electronics	ASIC (77/85° K)	Discrete low-level design
$\mu$ induced prompt signals	Underground location LNGS (3400 mwe); Water Cherenkov $\mu$ -veto	Underground location >4500 mwe; plastic scintillator $\mu$ -veto
$\mu$ induced delayed signals (e.g. $n+^{76}\text{Ge}\rightarrow^{77}\text{Ge}^{53\text{s}}$ , $^{77}\text{As}$ )	Low-Z material shield (Ar/water)	high-Z shield: deep underground location >4500 mwe
Internal to crystal: cosm. $^{60}\text{Co}$ ( $t_{1/2}= 5.27$ y)	Minimize time above ground after crystal growing (30d $\rightarrow$ 2.5 $\cdot$ 10 $^{-3}$ cts/(keV kg y)	same
Internal to crystal: cosm. $^{68}\text{Ge}$ ( $t_{1/2}= 270$ d)	Minimize time above ground after end of enrichment; shielded transp. container (180d $\rightarrow$ 12 $\cdot$ 10 $^{-3}$ cts/(keV kg y)	same

6

**Figure 3.** Backgrounds and reduction strategies of GERDA and MAJORANA.

### 5. Novel background suppression methods

Despite careful selection of the material in close vicinity of the detectors, residual background events are expected. In particular isotopes induced by cosmic ray interactions during detector operations above ground are of major concern. Novel background suppression techniques

will be employed using the characteristic signature of  $0\nu\beta\beta$  signal and background events. Interactions which lead to background events typically have an initial energy which is higher than  $Q_{\beta\beta}$ . Different to  $0\nu\beta\beta$  events, which are point-like on the scale of the crystal dimension, background events have energy depositions at several sites inside as well as outside of the crystals. This signature can be used for background suppression by analyzing the pulse shape of the charge signal, by segmenting of the electrodes of the diode, by anti-coincidence amongst crystals in an array, or by detecting the energy deposition in the surrounding material in case of liquid argon [7]. Figure 4 shows results from prototype measurement of a bare crystal operated in liquid argon detecting the scintillation light with a photomultiplier tube.

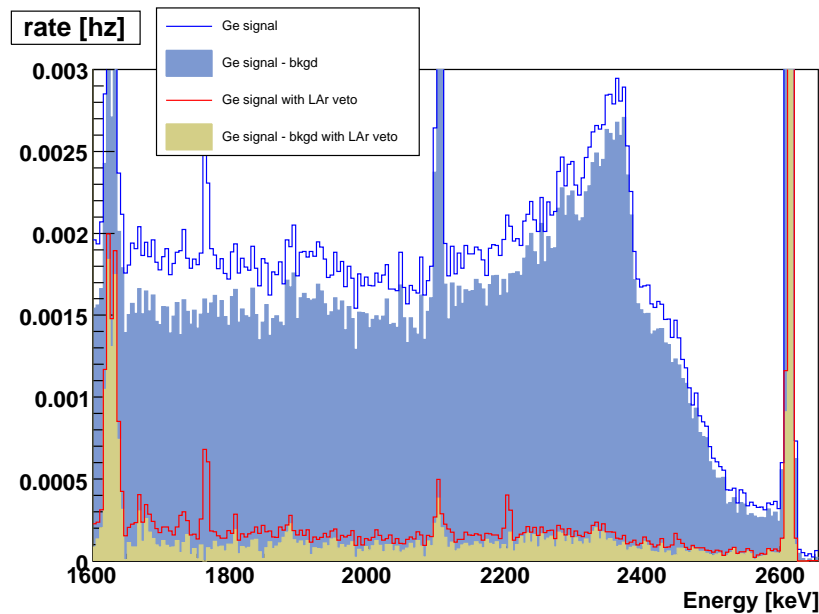


**Figure 4.** Background suppression of the 2.614 MeV Compton continuum from an  $^{228}\text{Th}$  source external to the crystal using the liquid argon scintillation light as veto signal. The Compton spectrum at  $Q_{\beta\beta}$  has been suppressed by a factor of 20 limited by the size of the setup [8].

## 6. Outlook

The GERDA experiment is under construction in Hall A of the LNGS. 18 kg of enriched crystals are prepared for operations in phase I of GERDA. Detector commissioning is planned for 2008. The DOE Office of Nuclear Physics has identified  $0\nu\beta\beta$  as a mission need, and approved Majorana to pursue R&D and to prepare for a Conceptual Design Review (CDR). The site under consideration is SNOLab or DUSEL with a required depth larger than 4500 mwe.

- [1] Klapdor-Kleingrothaus, H. V. et al., Eur. Phys. J. A12 (2001) 147-154.
- [2] C. Aalseth et. al., Phys. Rev. D65 (2002) 092007
- [3] H.V. Klapdor-Kleingrothaus, et al. NIM A522 (2004) 371-406,
- [4] Abt et al., hep-ex/0404039, <http://www.mpi-hd.mpg.de/GERDA/>
- [5] Gaitskell et al., nucl-ex/0311013 (2003)
- [6] V.Rodin et al., NPA 766 (2006) .
- [7] P. Peiffer et al., Nucl. Phys. B Suppl., Vol. 143, 511
- [8] M. Di Marco et al., physics/0701001

# Supernova neutrino detection

**Kate Scholberg**

Department of Physics, Duke University, Durham, NC, 27708, USA

E-mail: [schol@phy.duke.edu](mailto:schol@phy.duke.edu)

**Abstract.** The gravitational core collapse of a star produces a huge burst of neutrinos of all flavors. A number of detectors worldwide are sensitive to such a burst; its detection would yield information about both particle physics and astrophysics. Sensitivity to all flavors, and ability to tag different interactions will be key for extraction of information. Here I will survey the capabilities of current and future detectors for detection of supernova neutrinos from the Milky Way and beyond.

## 1. The supernova neutrino signal

The gravitational collapse of the core of a massive stars entails a vast release of energy. Because particles with only weak interactions can readily escape the star on a timescale of tens of seconds, an overwhelming fraction of the binding energy is carried away by neutrinos. The neutrino burst from a Galactic supernova can be detected in terrestrial detectors. As of this writing, the only supernova for which neutrinos have been detected is SN1987A, for which a total of 19 neutrinos were observed in two water Cherenkov detectors[1, 2]; scintillation detectors[3, 4] also reported observations. These observations confirmed the expected general features of gravitational collapse, but the data were insufficient to distinguish fine details of different models.

The baseline model predicts a burst of neutrinos of total energy a few times  $10^{53}$  ergs. The expected proto-neutron star core temperature corresponds to neutrino energies in the few to tens of MeV range. In the most straightforward picture, one expects  $\langle E_{\nu_{\mu,\tau}} \rangle > \langle E_{\bar{\nu}_e} \rangle > \langle E_{\nu_e} \rangle$ , because neutrino species with fewer interactions with the core's matter will emerge from deeper, and hence hotter regions of the star. However, some recent studies (*e.g.*[5]) bring into question the robustness of this prediction, since scattering may degrade this hierarchy of energies. The timescale of the burst is tens of seconds (consistent with the 1987A measurements), with a higher rate during the first few seconds. The neutrinos will emerge from the collapsed core well before any supernova photons. Possibly, the flux could be modulated by formation of a black hole or other events early in the neutron star's life. The neutrino burst includes all flavors of  $\nu$  and  $\bar{\nu}$ , and the generic expectation is for the neutrino energy to be roughly equipartitioned among the different flavors.

## 2. What we can learn

A nearby core collapse supernova would be a neutrino experimentalist's dream, as well as an astrophysicist's. The huge burst will certainly help us learn about the core collapse process itself. The neutrino burst's time, flavor and energy structure will bring information about the explosion mechanism, accretion, possible quark matter or black hole formation, and so on. In

addition, we can learn about neutrinos themselves. For instance, absolute neutrino mass leads to an energy-dependent time of flight delay as neutrinos travel from their source to Earth; however, it will be difficult to improve on current laboratory limits. The parameters governing neutrino oscillations will imprint themselves on the neutrino signal. As the neutrinos propagate through the stellar matter, they may undergo MSW-type resonance transitions in regions of specific matter density; in particular, there may be signatures of the unknown mixing angle  $\theta_{13}$  and neutrino mass hierarchy (*e.g.* [6]). Other properties of neutrinos may also yield interesting effects, as will various proposed exotic physics scenarios: in particular, the observed cooling timescale allows one to set limits on coupling to axions, large extra dimensions, and other exotic physics (*e.g.* [7, 8]), since any large coupling would allow extra energy to escape from the star, and lead to neutrino signal abbreviated with respect to the observed burst. Again, the measured time, flavor and energy structure of the burst will contain the signatures of unknown physics.

However, a difficulty here is that both core collapse physics and neutrino physics affect the nature of the burst, and it may not be trivial to disentangle the two. To learn about neutrinos, one must make assumptions about the nature of the collapse, and vice versa. Nevertheless, some features of the collapse are more robust than others, allowing model-independent studies. Also, one may cancel supernova model-dependent uncertainties in the study of neutrino oscillations by comparing fluxes measured at different locations on the Earth, and one may even look for matter-induced oscillation features in the spectrum of neutrinos measured in a single detector [9, 10]. Clearly, the more information we can gather about the flavor, energy and time structure of the burst, in as many detectors around the world as possible, the better chance we will have of disentangling the various effects.

One other potential scientific gift from a neutrino burst is an early warning of a supernova's occurrence: the neutrinos emerge promptly from the dense core, while astronomers must wait hours for the first photons to appear as the shock wave emerges from the stellar envelope. The SNEWS[11] network exists to provide such an early warning to astronomers (and others), which may allow observations from the very early (and previously rarely-observed) turn-on of the supernova light. Clearly, the more information that can be gathered, in all wavelengths (and also perhaps in gravitational waves), the better. Because core collapses are rare events (a few per century), it is essential to be prepared.

### 3. Detector technologies

From a neutrino experimentalist's point of view, the basic strategy is to prepare to collect as many neutrino events as possible, of as many flavors as possible. A back of the envelope calculation shows that one typically gets a few hundred neutrino interactions per kton of detector material for a core collapse event at the center of the Milky Way, 8.5 kpc away. For a successful observation, the detector background rate must not exceed the supernova signal rate in a 10 second burst: this criterion is easy to satisfy for underground detectors, and is even thinkable for many near-surface detectors[12]. One would like to have event-by-event timing resolution, ability to measure neutrino energies, and if possible, ability to use the neutrino information to point back to the supernova. Sensitivity to all flavors of the burst is extremely desirable:  $\nu_\mu$  and  $\nu_\tau$  flavors comprise two-thirds of the burst's energy, but because supernova neutrino energies rarely exceed a few tens of MeV, these components of the flux are overwhelmingly below charged current (CC) interaction threshold, and neutral current (NC) sensitivity is required to detect them. As a final point, it will be especially valuable for detectors to have *ability to tag* interactions as  $\nu_e$ ,  $\bar{\nu}_e$ , and  $\nu_{\mu,\tau}$  as well as just to collect them.

#### 3.1. Inverse beta decay:

Currently the world's primary sensitivity to supernova neutrinos is via that old workhorse of neutrino physics, inverse beta decay:  $\bar{\nu}_e + p \rightarrow e^+ + n$ . In this reaction, the produced positron

has the energy of the neutrino, less 1.8 MeV; the positron's energy loss is the primary means of detection. There are furthermore two possible tags of inverse beta decay: a prompt positron annihilation produces two 0.511 MeV  $\gamma$  rays, and the neutron may also be observable via its time-delayed capture on a nucleus. Capture of a neutron by a free proton produces a 180  $\mu$ s-delayed 2.2 MeV  $\gamma$  ray.

In any detector with lots of free protons, inverse beta decay typically dominates by orders of magnitude. The reaction has a mild energy-dependent anisotropy[13]. Examples of detectors leaning heavily on this reaction are hydrocarbon-based, and usually scintillating (e.g. LVD, KamLAND, Borexino, and mini-BooNE.) Scintillation detectors can often achieve quite low (sub-MeV) energy thresholds, and therefore have potential for a neutron capture and/or  $\gamma$  tagging. However because scintillation light is emitted isotropically, pointing capability is generally poor.

Water Cherenkov detectors (e.g. Super-Kamiokande) also have a high rate of inverse beta decays, but have difficulty with tagging neutrons due to high energy thresholds. A recent suggestion to spike water with gadolinium trichloride[14] which may allow tagging. Gd has a huge neutron capture cross-section; the resulting  $\gamma$ -rays can then be observed via the Cherenkov radiation from Compton scatters. The Gd-capture technique has been successfully used in small scintillation detectors (e.g. CHOOZ) and is currently under study for Super-Kamiokande.

The use of water Cherenkov detectors for supernova neutrino detection can be extended to detectors like AMANDA/IceCube that are made of long strings of sparsely distributed photomultiplier tubes embedded in ice or water. Such sparse PMT array detectors are nominally high energy ( $>$  GeV) neutrino detectors. They cannot record MeV neutrinos on an event-by-event basis; nevertheless they may be able to observe a coincident increase in single count rate from many phototubes due to a large number of inverse-beta-decay-induced Cherenkov photons in the surrounding ice or water[15].

### 3.2. Other charged current reactions:

Charged current interactions can occur for bound as well as free nucleons. Reactions of both  $\nu_e$  and  $\bar{\nu}_e$  can occur, with the production of an electron or positron:  $\nu_e + (N, Z) \rightarrow (N - 1, Z + 1) + e^-$ ;  $\bar{\nu}_e + (N, Z) \rightarrow (N + 1, Z - 1) + e^+$ .

Cross-sections are typically smaller for bound than for free nucleons, but can nevertheless be non-negligible. The charged lepton is usually observable, and CC interactions sometimes can be tagged in other ways, e.g. via detection of ejected nucleons or nuclear de-excitation  $\gamma$  rays. CC cross-sections and the nature of the observables are dependent on the nuclear physics of the specific nucleus involved, and in many cases there are large uncertainties. Examples of CC interactions useful for supernova neutrino detection are NC breakup in heavy water, ( $\nu_e + d \rightarrow p + p + e^-$ ,  $\bar{\nu}_e + d \rightarrow n + n + e^+$ ), interactions with oxygen in water, ( $\nu_e + {}^{16,18}\text{O} \rightarrow {}^{16,18}\text{F} + e^-$ ,  $\bar{\nu}_e + {}^{16}\text{O} \rightarrow {}^{16}\text{N} + e^+$ ), and interactions with carbon in scintillator ( $\nu_e + {}^{12}\text{C} \rightarrow {}^{12}\text{N} + e^-$ ,  $\bar{\nu}_e + {}^{12}\text{C} \rightarrow {}^{12}\text{B} + e^+$ ). Interactions with heavier nuclei may also yield high rates: for example, various lead-based detectors have been proposed (OMNIS, LAND, HALO)[16]. A particularly nice tagged  $\nu_e$  channel is available in argon,  $\nu_e + {}^{40}\text{Ar} \rightarrow e^- + {}^{40}\text{K}^*$ ; the  ${}^{40}\text{K}^*$  de-excitation  $\gamma$ 's would be observable in various proposed large liquid argon detectors (Icarus, LANNDD)[17]. Finally, radiochemical detectors based on Ga, Cl, and other isotopes could potentially yield excess events (although without time resolution); and it is in principle possible to run some of these in a quasi-real-time mode.

### 3.3. Elastic scattering:

Elastic neutrino-electron scattering (ES),  $\nu_{e,x} + e^- \rightarrow \nu_{e,x} + e^-$ , which occurs via both CC and NC channels, has a relatively small cross-section: the rate is a few percent of the inverse beta decay rate in scintillator and water Cherenkov detectors. Nevertheless the ES component of the

supernova neutrino signal will be especially interesting, because it is *directional*: the electrons get kicked forward by the neutrinos with an average angle of about  $25^\circ$ . If the direction of the kicked electron can be determined (e.g. from a Cherenkov cone), elastic scattering can be used to learn the location of the supernova, and is in fact the best way of using a neutrino detector to point back to the supernova's location[18].

#### 3.4. Neutral current reactions:

Only the  $\nu_e$  and  $\bar{\nu}_e$  components of the supernova neutrino signal are accessible via CC interactions. Because NC interactions are flavor-blind, they measure the total flux, including the  $\nu_\mu$  and  $\nu_\tau$  components. Various NC interactions on nuclei have cross-sections that yield reasonable rates, and as for the CC case, sometimes a nice tag is possible via ejected nucleons or de-excitation  $\gamma$ 's. For example, a 15.5 MeV de-excitation  $\gamma$ -ray tags the NC excitation of  $^{12}\text{C}^*$ ,  $\nu_x + ^{12}\text{C} \rightarrow \nu_x + ^{12}\text{C}^*$ ; a cascade of 5-10 MeV de-excitation  $\gamma$ s may also tag  $\nu_x + ^{16}\text{O} \rightarrow \nu_x + ^{12}\text{O}^*$  in a water Cherenkov detector [19].

A particularly promising future possibility for NC supernova neutrino detection is a lead-based neutrino detector, for which the cross-section is high for NC as well as CC channels. For  $\nu_x + ^{210}\text{Pb} \rightarrow \nu_x + ^{210}\text{Pb}^*$ , the lead nucleus subsequently emits a neutron. The one neutron emission channel is expected to be predominant for NC[20, 21], in contrast to a high rate of double-neutron emission for the CC reaction. The relative rates for the different channels in lead depend on neutrino energy, which promises some spectral information and hence sensitivity to oscillation effects. There have been proposals to employ metallic lead and lead in form of perchlorate. A promising recent proposal is HALO[22], which is planned to make use the  $^3\text{He}$  NCD counters from SNO when SNO shuts down at the end of 2006. As for the CC  $\nu$ -nucleus reactions, here again rates and signatures depend on specific nuclear physics.

Another NC channel which has been not been explored until fairly recently is neutrino-proton NC elastic scattering,  $\nu + p \rightarrow \nu + p$ [23]. The rate is relatively high, but because the free proton target is heavy, recoil kinetic energies are low. The recoils may nevertheless be observable in large low threshold scintillation detectors, e.g. KamLAND, even after accounting for "quenching" in scintillator. Neutral current coherent neutrino-nucleus elastic scattering,  $\nu + A \rightarrow \nu + A$ , occurs at even higher rates than  $\nu p$  scattering, but because the targets are yet heavier, recoil energies are yet tinier— in the tens of keV range. This might seem a hopeless situation, but such tiny recoils are within the reach of novel detectors developed for pp solar neutrinos or WIMP detection[24]. For example, a detector like CLEAN[25], which can potentially expand to a 10 ton scale, would observe a few events per ton from an 8.5 kpc supernova.

#### 3.5. Detector summary:

Current and proposed detectors are summarized in Table 1. The numbers of events given for a Galactic center supernova should be taken as uncertain by at least 50%; not only are there uncertainties in the collapse models, in many cases the numbers of observable events depend on assumed thresholds, efficiencies, enrichment, and other detector-configuration-specific properties.

As emphasized above, in order to understand the rates and signatures, we must understand the nuclear physics involved. In many cases, the cross-sections have never been measured experimentally, and theoretically there are large uncertainties. One way of decreasing uncertainties is to use a stopped-pion neutrino source to measure relevant cross-sections: such a source provides  $\nu_\mu$ ,  $\nu_e$ , and  $\bar{\nu}_e$  in nearly the same energy range as expected for a supernova. A future program of measurements on various targets, such as that planned for the Spallation Neutron Source[26], will be vital for extracting physics from the next supernova.

**Table 1.** Summary of current and proposed detectors.

Detector	Type	Mass (kton)	Location	Events at 8.5 kpc	Status
Super-K	H <sub>2</sub> O	32	Japan	7000	Running
SNO	D <sub>2</sub> O	1 (D <sub>2</sub> O)	Canada	400	Running until
		1.4 (H <sub>2</sub> O)		450	end 2006
LVD	C <sub>n</sub> H <sub>2n</sub>	1	Italy	200	Running
KamLAND	C <sub>n</sub> H <sub>2n</sub>	1	Japan	300	Running
Borexino	C <sub>n</sub> H <sub>2n</sub>	0.3	Italy	100	200x
Baksan	C <sub>n</sub> H <sub>2n</sub>	0.33	Russia	50	Running
Mini-BooNE	C <sub>n</sub> H <sub>2n</sub>	0.7	USA	200	Running
AMANDA/ IceCube	Long string	0.4/PMT	South Pole	N/A	Running
SAGE	Ga	Russia	0.06	1	Running
Icarus	LAr	2.4	Italy	200	200x
SNO+	C <sub>n</sub> H <sub>2n</sub>	1	Canada	300	Proposed
CLEAN	Ne,Ar	0.01	Canada/USA?	30	Proposed
HALO	Pb	0.1	Canada	40	Proposed
MOON	<sup>100</sup> Mo	0.03	?	20	Proposed
NO $\nu$ A	C <sub>n</sub> H <sub>2n</sub>	20	USA	4000	Proposed
OMNIS	Pb	2-3	USA?	>1000	Proposed
LANNDD	LAr	70	USA?	6000	Proposed
MEMPHYS	H <sub>2</sub> O	440	Europe	>100,000	Proposed
UNO	H <sub>2</sub> O	500	USA	>100,000	Proposed
Hyper-K	H <sub>2</sub> O	500	Japan	>100,000	Proposed
LENA	C <sub>n</sub> H <sub>2n</sub>	60	Europe	18,000	Proposed
HSD	C <sub>n</sub> H <sub>2n</sub>	100	USA	30,000	Proposed

#### 4. Beyond the Milky Way

Even the largest detectors running today are sensitive only to supernovae within a few hundred kpc, which pretty much covers only our own Galaxy. The next nearest large concentration of stars is the Andromeda galaxy, about 770 kpc away; at this distance, Super-K would expect only  $\sim 1$  event. Unfortunately, the expected rate of Milky Way supernovae is only a few per century, so if luck is against us, the wait may well be longer than a typical physicist's career. Several next-generation very large detectors have been proposed which would have supernova neutrino sensitivity: these include Mton-scale water detectors (Hyper-K, UNO, MEMPHYS) and 100 kton-scale large LAr and scintillator detectors (LANNDD, LENA).<sup>1</sup> However even the largest of these mega-detectors would see only tens of events from a core collapse in Andromeda.

But while  $1/D^2$  hurts, the increase of potential sources as  $D^3$  helps: a recent study[27] has pointed out a regime for which the probability of detecting a few events per supernova in a Mton detector is reasonably close to 1 at the same time as the overall rate of expected core collapses is reasonably close to 1 per year. So if one can operate a large, low background detector (possibly using optical or gravitational wave (GW) detections nearby in time to reduce the background), one can expect to collect a thin but steady dribble of supernova neutrinos.

<sup>1</sup> One might consider siting these detectors to optimize the probability of Earth shadowing[28].

We can look even farther out: stellar cores have been giving up their binding energy to neutrinos ever since the first stars formed, and we are awash in a sea of these ancient neutrinos. This diffuse supernova neutrino background (DSNB) (formerly known as the “relic” supernova neutrino background) provides a steady source of neutrinos. But because there is no hope of tagging DSNB neutrinos with optical or GW events, detection feasibility rests on reducing background to essentially zero. This may indeed be possible for  $\bar{\nu}_e$  using a large scintillator or Gd-spiked water detector to tag  $\bar{\nu}_e$ , in the few tens of MeV regime, which is nearly free of solar or atmospheric neutrino background. Detection of DSNB neutrinos is very interesting from the point of view of learning about cosmology via knowledge of the past supernova rate. However, when considering use of the DSNB to learn about neutrinos, stellar collapse physics and so on, one must consider the overall rate. One expects a low, but sure return on one’s investment at  $\sim 0.1$  event/kton/yr of DSNB. In contrast, in the very long term, on average one expects about 10 events/kton/yr of Galactic supernova neutrinos. Counting on a signal from the latter is risky in the short term, because there may be large Poissonian gaps. But surely, over centuries, the Galactic supernova detection approach wins. Clearly the best strategy is diversification of one’s experimental portfolio: a large, clean detector that runs for decades will yield rich and reliable returns.

## 5. Conclusion

Several supernova-neutrino detectors are running and ready to observe a galactic burst. A variety of new detectors are proposed: those with broad flavor sensitivity and tagging ability will be especially valuable for extracting physics from the signal. The neutrinos will come. We need to build detectors to gather them all: the Galactic bursts, the fainter flashes from just beyond, and the dim but steady background glow.

- [1] R. M. Bionta *et al.*, Phys. Rev. Lett. **58**, 1494 (1987).
- [2] K. Hirata *et al.* [KAMIOKANDE-II Collaboration], Phys. Rev. Lett. **58**, 1490 (1987).
- [3] E. N. Alekseev, L. N. Alekseeva, V. I. Volchenko and I. V. Krivosheina, JETP Lett. **45**, 589 (1987) [Pisma Zh. Eksp. Teor. Fiz. **45**, 461 (1987)].
- [4] M. Aglietta *et al.*, Europhys. Lett. **3**, 1315 (1987).
- [5] M. T. Keil, G. G. Raffelt and H. T. Janka, Astrophys. J. **590**, 971 (2003) [arXiv:astro-ph/0208035].
- [6] A. S. Dighe and A. Y. Smirnov, Phys. Rev. D **62**, 033007 (2000) [arXiv:hep-ph/9907423].
- [7] G. G. Raffelt, arXiv:astro-ph/9707268.
- [8] S. Hannestad and G. Raffelt, Phys. Rev. Lett. **87**, 051301 (2001) [arXiv:hep-ph/0103201].
- [9] C. Lunardini and A. Y. Smirnov, Nucl. Phys. B **616**, 307 (2001) [arXiv:hep-ph/0106149].
- [10] A. S. Dighe, M. T. Keil and G. G. Raffelt, JCAP **0306**, 006 (2003) [arXiv:hep-ph/0304150].
- [11] P. Antonioli *et al.*, New J. Phys. **6**, 114 (2004) [arXiv:astro-ph/0406214].
- [12] M. K. Sharp, J. F. Beacom and J. A. Formaggio, Phys. Rev. D **66**, 013012 (2002) [arXiv:hep-ph/0205035].
- [13] P. Vogel and J. F. Beacom, Phys. Rev. D **60**, 053003 (1999) [arXiv:hep-ph/9903554].
- [14] J. F. Beacom and M. R. Vagins, Phys. Rev. Lett. **93**, 171101 (2004) [arXiv:hep-ph/0309300].
- [15] F. Halzen, J. E. Jacobsen and E. Zas, Phys. Rev. D **53**, 7359 (1996) [arXiv:astro-ph/9512080].
- [16] C. K. Hargrove, I. Batkin, M. K. Sundaresan and J. Dubeau, Astropart. Phys. **5**, 183 (1996).
- [17] A. Bueno, I. Gil-Botella and A. Rubbia, arXiv:hep-ph/0307222.
- [18] J. F. Beacom and P. Vogel, Phys. Rev. D **60**, 033007 (1999) [arXiv:astro-ph/9811350].
- [19] E. Kolbe, K. Langanke and P. Vogel, Phys. Rev. D **66**, 013007 (2002).
- [20] G. M. Fuller, W. C. Haxton and G. C. McLaughlin, Phys. Rev. D **59**, 085005 (1999) [arXiv:astro-ph/9809164].
- [21] J. Engel, G. C. McLaughlin and C. Volpe, Phys. Rev. D **67**, 013005 (2003) [arXiv:hep-ph/0209267].
- [22] C. Virtue, [http://snolab2006.snolab.ca/talks/HALO\\_aug06.ppt](http://snolab2006.snolab.ca/talks/HALO_aug06.ppt)
- [23] J. F. Beacom, W. M. Farr and P. Vogel, Phys. Rev. D **66**, 033001 (2002) [arXiv:hep-ph/0205220].
- [24] C. J. Horowitz, K. J. Coakley and D. N. McKinsey, Phys. Rev. D **68**, 023005 (2003) [arXiv:astro-ph/0302071].
- [25] D. N. McKinsey and K. J. Coakley, Astropart. Phys. **22**, 355 (2005) [arXiv:astro-ph/0402007].
- [26] Yu. Efremenko, Nucl. Phys. Proc. Suppl. **138**, 343 (2005).
- [27] S. Ando, J. F. Beacom and H. Yuksel, Phys. Rev. Lett. **95**, 171101 (2005) [arXiv:astro-ph/0503321].
- [28] A. Mirizzi, G. G. Raffelt and P. D. Serpico, JCAP **0605**, 012 (2006) [arXiv:astro-ph/0604300].

# Status and Prospects of the NOvA Experiment

**P. Shanahan**<sup>1</sup>

Fermilab – MS 220, P.O. Box 500, Batavia, IL 60510 USA

E-mail: shanahan@fnal.gov

**Abstract.** NOvA is a proposed experiment to search for  $\nu_{\mu} \rightarrow \nu_e$  oscillations using the NuMI neutrino beam, and two detectors separated by a baseline of 810 km. A better signal-to-background ratio than that of current experiments will be achieved by using detectors with a low  $Z/A$  ratio, and by situating the far detector off the beam axis. NOvA will have sensitivity to the related physics of the neutrino mass hierarchy and leptonic CP violation depending on the values of the mixing angle  $\theta_{13}$  and the CP violation angle  $\delta$ .

## 1. Introduction

The proposed NOvA<sup>2</sup> (NuMI Off-axis  $\nu_e$  Appearance) experiment will search primarily for the oscillation of muon neutrinos into electron neutrinos and the corresponding mixing angle  $\theta_{13}$ . NOvA will use the Fermilab NuMI (Neutrinos at the Main Injector) neutrino beam over a baseline of 810 km, and detectors at Fermilab and the Ash River site in northern Minnesota. The detector design is optimized for the identification of electrons in the final state of  $\nu_e$  charged current (CC) interactions. The Far detector will be located 12 km from the central axis of the beam to suppress backgrounds from intrinsic beam  $\nu_e$  and high-energy neutral current interactions. Operation of a partially completed Far Detector is currently scheduled to begin in mid-FY2011, with completion of the full detector the following year.

Depending on the size of any observed electron neutrino appearance signal, NOvA will have the potential to investigate the associated physics, such as the CP violating phase  $\delta$  and whether the Neutrino Mass Hierarchy is normal or inverted. NOvA will also be able to make a high precision measurement of the atmospheric mixing parameters  $\Delta m_{23}^2$  and  $\sin^2(2\theta_{23})$ .

## 2. The NuMI Beam

The NuMI beam starts with the production of hadrons from the interaction of the 120 GeV protons from the Fermilab Main Injector (MI) in a graphite target, during a pulse approximately 10  $\mu$ s in duration. The charged hadrons are focused with two parabolic magnetic horns into a 670 m long decay pipe that ends with an aluminum and steel absorber. The relative placement of the target and horns along the beam axis determines the resulting neutrino energy spectrum. An array of ionization chambers just upstream of the absorber, and several more at different locations downstream of varying longitudinal depths of bedrock, allow the hadron and muon fluxes in the beam to be monitored [1]. The NuMI beam was commissioned in 2005, and has been used by the MINOS experiment for its first result on  $\nu_{\mu}$  disappearance [2].

<sup>1</sup> For the NOvA Collaboration

<sup>2</sup> pronounced “NOVA”

To date the NuMI beam has operated with spills as frequently as every 2 seconds, with up to  $3 \times 10^{13}$  protons-on-target (POT) each, achieving a maximum primary beam power of 290 kW. Upgrades to the Main Injector and other components of the Fermilab accelerator complex will increase the NuMI beam power before and during the planned operation of NOvA. The current phase, Proton Plan I, includes upgrades to the MI RF system and other components to allow the MI to accept and accelerate up to 11 cycles of the 8 GeV Booster per MI cycle, leading to a maximum power of 430 kW. Further upgrades proposed for after the end of TeVatron collider operations use the existing anti-proton Recycler and Accumulator rings as proton accumulators in the MI injection phase, to achieve 700 kW and 1 MW of beam power, respectively [3].

### 3. Detectors

#### 3.1. Location

The proposed location of the NOvA Far Detector is determined by the simultaneous optimization of two physics criteria: the maximization of matter effects, and the maximization of the  $\nu_{\mu} \rightarrow \nu_e$  appearance signal relative to the backgrounds.

The size of the matter effect grows with the baseline. Within other constraints including site access and location within the United States, this corresponds to a distance of about 800 km from the NuMI target. The maximization of signal over background is achieved with a location of the detector off the beam axis, which yields a more monochromatic unoscillated  $\nu_{\mu}$  spectrum due to the kinematics of the 2-body pion decay, compared to the intrinsic beam  $\nu_e$  spectrum which is dominated by 3-body decays. As is shown in figure 1, the further off axis from the beam, the lower in energy and more narrow the peak of the neutrino interaction energy spectrum, and the lower the high-energy tail that is the dominant source of backgrounds from neutral current interactions. A distance corresponding to an off-axis angle of 14 mrad maximizes the overlap of the neutrino interaction rate with the oscillation probability, while greatly suppressing the high-energy tail. The combined optimization of baseline and off-axis distance leads to the choice of a Far Detector site near the Ash River in northern Minnesota, 810 km from the NuMI target.

#### 3.2. Design

The design of the NOvA detector enhances identification of  $\nu_e$  CC events by the separation of electromagnetic and hadronic showers. This is achieved with nearly totally active detector of relatively low  $Z/A$  ratio, allowing a high number of samples per radiation length that is not cost-prohibitive for a detector of large mass.

The detectors will be composed of liquid scintillator contained in planes of an extruded PVC cell structure, read out on one end of each cell via a wavelength-shifting fiber. To reduce the effective attenuation in light level from activity furthest from the readout end of a cell, the fiber will be looped along the length of the cell and both ends read out. The basic active cell unit will be approximately 6 cm deep along the beam direction, and 3.8 cm wide along the measurement coordinate, with PVC walls of between 2 and 4.5 mm thickness. The PVC accounts for approximately 27% of the total detector mass. A single extrusion will consist of 16 cells, up to 24 of which will make up a single plane of the detector. The orientation of the cells will alternate between horizontal and vertical.

The wavelength shifting fibers will be read out by 32-pixel Avalanche Photo-Diodes (APDs), operated at a gain of 100, and cooled to -15 deg C to reduce the noise to approximately 10 percent of the lowest signal expected for a minimum ionizing particle. The APD output will be amplified and shaped by an ASIC being designed for NOvA, and digitized by a commercial ADC.

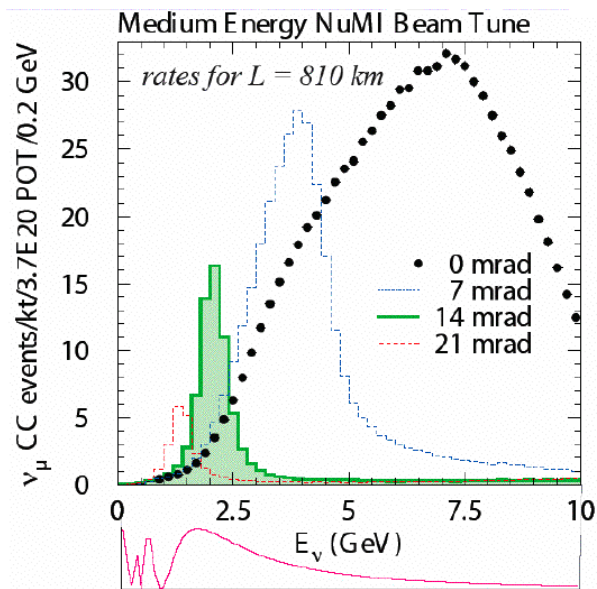


Figure 1. The unoscillated  $\nu_\mu$  CC interaction spectrum for various distances from the beam axis, 810 km from the NuMI target (*top*), and the relative  $\nu_\mu \rightarrow \nu_e$  oscillation probability (*bottom*).

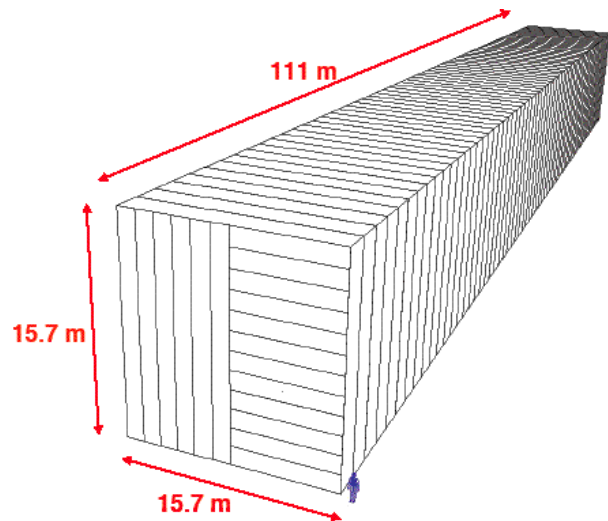


Figure 2. The NOvA Far Detector (20 kT).

The Far Detector will be situated below grade, with an overburden of between 10 and 20 radiation lengths to reduce backgrounds due to cosmic rays. A Far Detector of 20 kT total mass will comprise roughly 1300 planes approximately 15.7 m on a side (figure 2). The effective attenuation will yield 20 photoelectrons for a minimum ionizing particle traversing normal to the cell at the end far from the readout. The Near Detector will have the same structure, although with smaller and few planes, and a muon ranger to compensate. The fully active part of the detector will consist of 186 planes of scintillator and PVC, and will be followed by a muon ranger of 10 planes of iron alternating with planes of Scintillator and PVC. The Near Detector will be located underground in the NuMI complex, at an off-angle location similar to that of the Far Detector.

### 3.3. Performance

The more than 6 planes per radiation length of the NOvA detector design yields a detailed sampling of the development of electromagnetic showers from the electron in  $\nu_e$  CC interactions. Figure 3 shows an event display of a CC interaction of a 2.9 GeV  $\nu_e$ . The electron and a  $\pi^+$  are visible in the final state, with the electron displaying the typical “fuzzy track” that distinguishes it clearly from most other particles. The remaining challenge is the rejection of neutral current events where the bulk of visible energy is in the form of a neutral pion. This background is suppressed by the use of several variables that are sensitive to the presence of 2 electromagnetic showers from the decay photons of the  $\pi^0$ , and the overall visible energy in the event.

The design of the NOvA detector, and the reconstruction and event selection algorithms, have been chosen to maximize the ratio of the number of selected  $\nu_\mu \rightarrow \nu_e$  signal events to the square-root of the number of background events, for  $\Delta m^2 = 0.0025 \text{ eV}^2$  and  $\sin^2(2\theta_{13}) = 0.1$ .

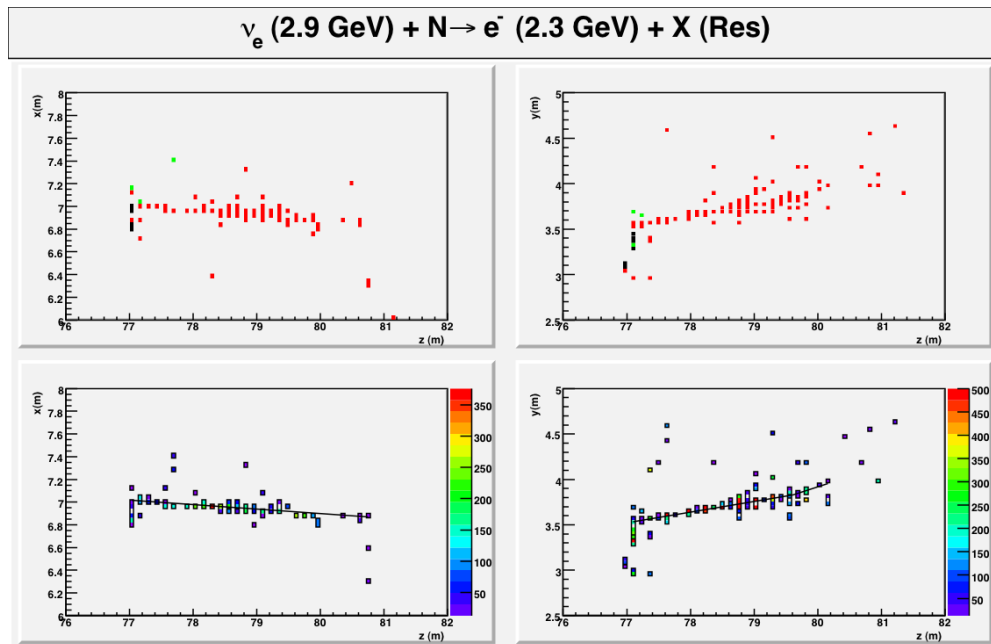


Figure 3. A display of a simulated  $\nu_e$  CC interaction in the two detector views, with resonant production of pion. Top: Simulated energy depositions in scintillator color-coded according to source: red for  $e$ ,  $\gamma$ , green for primary proton and  $\pi$ , and black for secondary hadronic activity. Bottom: the reconstructed event, with the pulseheight of the digitizations indicated by the color scale. The black line represents the reconstructed electron track.

#### 4. Physics Reach

The following physics sensitivities assume a 1MW NuMI upgrade, permitting an exposure of  $60 \times 10^{20}$  POT in 6 years, divided equally between neutrino and anti-neutrino running and a 25 kT far detector. The relevant mixing parameters are assumed to be  $\Delta m^2 = 0.0025 \text{ eV}^2$  and  $\sin^2(2\theta_{23}) = 1$ . The plots and numbers shown are derived from a full simulation of the NuMI beam and the NOvA detectors, and an event selection based on reconstruction of simulated interactions.

Figure 4 shows the NOvA reach in  $\sin^2(2\theta_{13})$ , in the form of a  $3\sigma$  sensitivity to  $\theta_{13} \neq 0$ , for neutrino-only and equal neutrino and anti-neutrino running. For a normal mass hierarchy ( $\Delta m^2_{23} > 0$ ), matter effects increase (decrease) the oscillation probability for neutrinos (anti-neutrinos), and vice-versa for the inverted mass hierarchy. Furthermore, the variation in the vacuum oscillation probability as a function of the CP violating angle  $\delta$  is roughly opposite for neutrinos and anti-neutrinos near the oscillation maximum [4]. Thus the advantage to the shared running is a more consistent sensitivity to the mixing, about  $\sin^2(2\theta_{13}) \sim 0.01$  for the parameters given, with respect to both  $\delta$  and the mass hierarchy.

The mass hierarchy enters the oscillation probability via matter effects, and is proportional to the baseline  $L$  at a fixed  $L/E$  [4]. NOvA will therefore have a unique reach in sensitivity to the Mass Hierarchy, due to its long baseline compared to other experiments. Figure 5 shows the 95% confidence level for the resolution of the mass hierarchy.

NOvA also will be able to address the dominant mixing mode in  $\nu_\mu$  disappearance, offering a great improvement in the precision of the oscillation parameters over that expected when the current generation of experiments is complete. Figure 6 shows the contours for  $\Delta m^2$  and  $\sin^2(2\theta_{23})$  that NOvA is expected to achieve using only quasi-elastic  $\nu_\mu$  CC events, which allow a more precise determination of neutrino energy and therefore  $L/E$ .

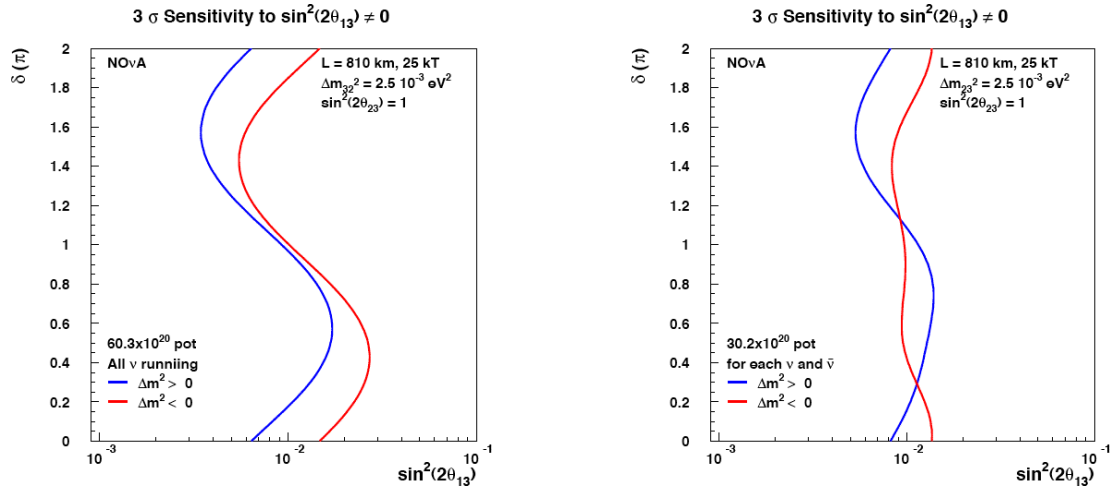


Figure 4. NOvA sensitivity to  $\sin^2(2\theta_{13})$  for neutrino-only running (*left*) and equal neutrino and anti-neutrino running (*right*), as a function of the CP-violating phase  $\delta$ .

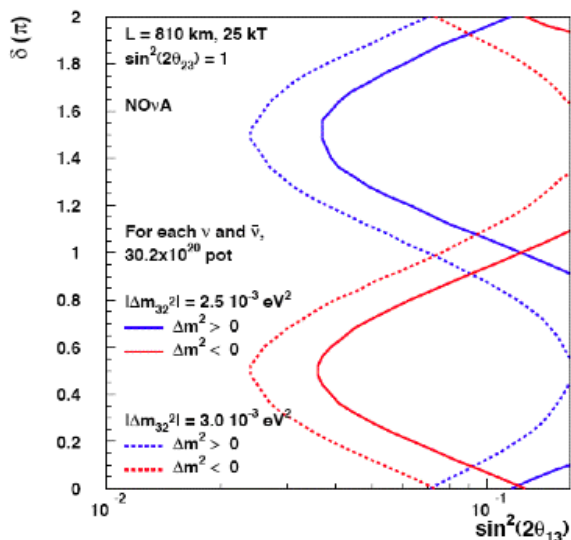


Figure 5. The NOvA 95% confidence level resolution contour as a function of  $\delta$  and  $\sin^2(2\theta_{13})$ .

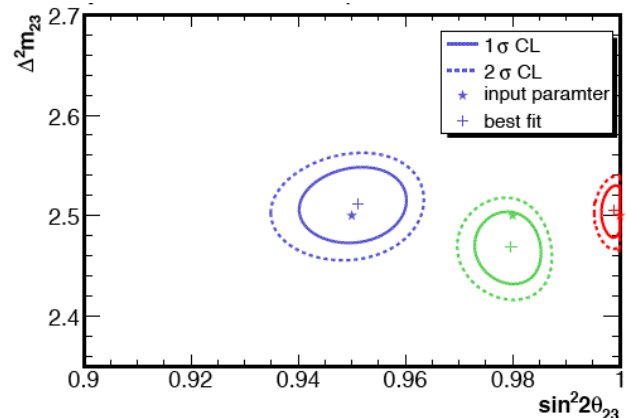


Figure 6. NOvA confidence level contours for the oscillation parameters for  $\nu_\mu$  disappearance.

## 5. Beyond NOvA

Among several additional possible projects for the use of the NuMI beam is a proposal for a liquid Argonne TPC detector of between 15 and 50 kT total mass [5]. The sampling of the LAr TPC detector is approximately 3.5% of a radiation length, allowing a more aggressive separation of showers from electrons and  $\pi^0 \rightarrow \gamma\gamma$ . In a manual scan of simulated events, a selection efficiency of  $\nu_e$  CC events of 81% was achieved, with a level of non- $\nu_e$  background less than one half of that of the intrinsic beam  $\nu_e$ . Figure 7 shows the expected sensitivity to the CP violating phase  $\delta$ , for several

different possible values of  $\delta$  and  $\sin^2(2\theta_{13})$ , for the NOvA run exposure used in Section 4. Figure 8 shows the same assuming additional NuMI running with both NOvA and a 25 kT LAr TPC detector. The two detectors and extra running would permit a greatly improved sensitivity to leptonic CP violation.

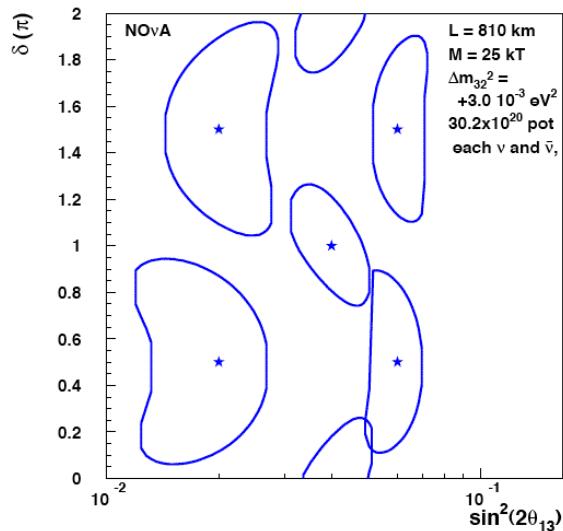


Figure 7. NOvA 1 sigma contours to the CP violation angle  $\delta$ .

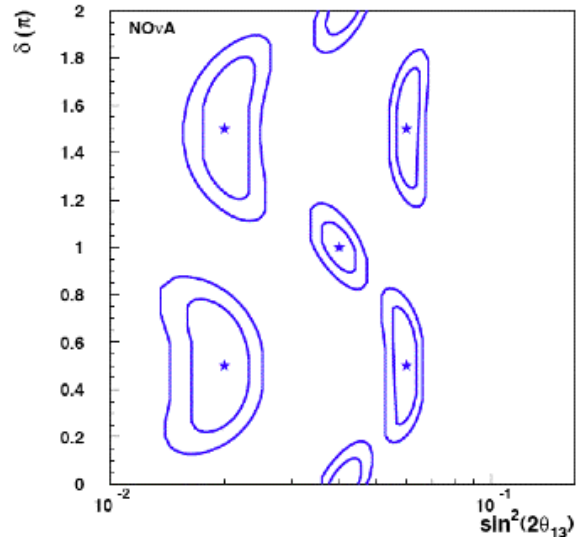


Figure 8. 1 and 2 sigma contours for NOvA combined with a LAr TPC detector taking data during an additional  $60 \times 10^{20}$  proton-on-target NuMI Run.

## 6. Conclusions

NOvA will have a greatly improved sensitivity to  $\nu_{\mu} \rightarrow \nu_e$  over current experiments, in part due to its low  $Z/A$  ratio and off-axis location. NOvA will have a unique level of sensitivity to matter effects among present and approved experiments, and therefore the neutrino mass hierarchy, due to its uniquely long baseline. Depending on the size of the remaining unmeasured mixing angle,  $\theta_{13}$ , the detection of CP violation in the lepton sector could be within the reach of NOvA.

The author is grateful to the NOvA collaboration for the opportunity to represent it at Neutrino 2006. Work supported by the U.S. Department of Energy under contract No. DE-AC02-07CH11359.

## References

- [1] Kopp S et al. 2006 *Nucl. Instrum. Meth. A* **568** 503-19  
Zwaska R.M. 2005 Accelerator Systems and Instrumentation for the NuMI Neutrino Beam [dissertation] (Austin, TX: University of Texas)
- [2] Michael D et al. 2006 *Phys. Rev. Lett.* **97** 191801.
- [3] sNuMI Working Group 2006 sNuMI Conceptual Design Report *Preprint* ProtonPlan2-doc-101 (beamdocs.fnal.gov)
- [4] Minikata H and Nunokawa H 2001 Exploring Neutrino Mixing with Low Energy Superbeams *JHEP* **0110** 001  
NOvA Collaboration 2005 Proposal to Build a 30 Kiloton Off-Axis Detector to Study  $\nu_{\mu} \rightarrow \nu_e$  in the NuMI Beamline *Preprint* hep-ex/0503053.
- [5] Finley D et al. A Large Liquid Argon Time Projection Chamber for Long-Baseline, Off-Axis Neutrino Oscillation Physics with the NuMI Beam *Preprint* FERMILAB-FN-0776-E

# The nuclear matrix elements for double beta decay

**Fedor Šimkovic**

Department of Nuclear Physics and Biophysics, Comenius University  
Mlynská dolina, 842 48 Bratislava, Slovakia

E-mail: simkovic@fmph.uniba.sk

**Abstract.** The status of the calculation of the neutrinoless double beta decay ( $0\nu\beta\beta$ -decay) nuclear matrix elements (NME's) is reviewed. The spread of published values of NME's is discussed. The main attention is paid to the recent progress achieved in the evaluation of the  $0\nu\beta\beta$ -decay NME's in the framework of the quasiparticle random phase approximation (QRPA). The obtained results are compared with those of the nuclear shell model. The problem of reliable determination of the  $0\nu\beta\beta$ -decay NME's is addressed. The uncertainty in NME's are analyzed and further progress in calculation of the  $0\nu\beta\beta$ -decay NME's is outlined.

## 1. Introduction

The discovery of neutrino oscillations has opened a new excited era in neutrino physics and represents a big step forward in our knowledge of neutrino properties. The data of solar (SNO), atmospheric (Super-Kamiokande) accelerator (K2K) and reactor (KamLAND) (anti)-neutrino experiments are perfectly described by the three-neutrino mixing. The existence of neutrino masses qualifies as the first evidence of new physics beyond the standard model (SM).

Neutrino oscillation experiments, while being extremely valuable, can not answer some fundamental questions in neutrino physics. First, they are only sensitive to mass squared differences and thus can not fix the overall mass scale of neutrinos. Second, they can not distinguish between Dirac and Majorana neutrinos. The neutrinoless double beta decay ( $0\nu\beta\beta$ -decay),

$$(A, Z) \rightarrow (A, Z + 2) + 2e^-, \quad (1)$$

is expected to be of crucial importance in answering these questions.

By assuming the dominance of the light neutrino mass mechanism the inverse value of the  $0\nu\beta\beta$ -decay half-life for a given isotope  $(A, Z)$  is given by

$$\frac{1}{T_{1/2}^{0\nu}(A, Z)} = \left| \frac{m_{\beta\beta}}{m_e} \right|^2 |M^{0\nu}(A, Z)|^2 G_{01}^{0\nu}(E_0, Z). \quad (2)$$

Here,  $m_e$  is the mass of electron.  $G^{0\nu}(E_0, Z)$  and  $|M^{0\nu}(A, Z)|$  are, respectively, the known kinematic phase-space factor ( $E_0$  is the energy release) and the nuclear matrix element (NME). The main aim of the experiments on the search for  $0\nu\beta\beta$ -decay is the measurement of the effective Majorana neutrino mass  $m_{\beta\beta}$ :

$$m_{\beta\beta} = U_{e1}^2 m_1 + U_{e2}^2 m_2 + U_{e3}^2 m_3, \quad (3)$$

Here,  $m_i$  and  $U_{li}$  ( $i = 1, 2, 3$ ) are, respectively, mass of the neutrino and the element of the Pontecorvo–Maki–Nakagawa–Sakata (PMNS) unitary neutrino matrix.

The  $0\nu\beta\beta$ -decay is a process known for almost 70 years, which has been searched for, but not seen yet. The most stringent lower bounds on the half-life of  $0\nu\beta\beta$ -decay were obtained in the Heidelberg-Moscow  $^{76}\text{Ge}$ , CUORICINO  $^{130}\text{Te}$ , NEMO3  $^{100}\text{Mo}$ ,  $^{82}\text{Se}$ , DAMA  $^{136}\text{Xe}$  and CAMEO  $^{116}\text{Cd}$  experiments [1]:

$$\begin{aligned} T_{1/2}^{0\nu}(^{76}\text{Ge}) &\geq 1.9 \cdot 10^{25} \text{ years}, & T_{1/2}^{0\nu}(^{130}\text{Te}) &\geq 1.8 \cdot 10^{24} \text{ years} \\ T_{1/2}^{0\nu}(^{136}\text{Xe}) &\geq 1.2 \cdot 10^{24} \text{ years}, & T_{1/2}^{0\nu}(^{100}\text{Mo}) &\geq 4.6 \cdot 10^{23} \text{ years}, \\ T_{1/2}^{0\nu}(^{116}\text{Cd}) &\geq 1.7 \cdot 10^{23} \text{ years}, & T_{1/2}^{0\nu}(^{82}\text{Se}) &\geq 1.0 \cdot 10^{23} \text{ years}. \end{aligned} \quad (4)$$

A few authors of the Heidelberg-Moscow collaboration have claimed [2] evidence for the  $0\nu\beta\beta$ -decay of  $^{76}\text{Ge}$  with  $T_{1/2}^{0\nu} = (0.69 - 4.18) \cdot 10^{25}$  years at the  $4.2\sigma$  confidence level. A such a claim with its profound implications requires to be confirmed or rule out by other experiment. The disproof or the confirmation of the claim is expected to come from the GERDA I experiment [3] (now at preparation at Gran Sasso) in the near future.

The primary concern are the nuclear matrix elements. Clearly, the accuracy of the determination of the effective Majorana mass from the measured  $0\nu\beta\beta$ -decay half-life is mainly determined by our knowledge of the nuclear matrix elements. Reliable nuclear matrix elements are required as they guide future choices of isotopes for the  $0\nu\beta\beta$ -decay experiments.

## 2. Nuclear matrix elements

The  $\beta\beta$ -decay can be observed because the pairing force renders the even-even nuclei with even number of protons and neutrons more stable than the odd-odd nuclei with broken pairs. Thus, the single beta decay transition from the even-even parent nucleus ( $A, Z$ ) to the neighbouring odd-odd nucleus ( $A, Z+1$ ) is forbidden energetically and the  $\beta\beta$  decay to the daughter nucleus ( $A, Z+2$ ) is the only possible decay channel. There are few tenths of nuclear systems, which offer an opportunity to study it.

The two-neutrino double beta decay ( $2\nu\beta\beta$ -decay), which involves the emission of two electrons and two antineutrinos,

$$(A, Z) \rightarrow (A, Z + 2) + 2e^- + 2\bar{\nu}_e, \quad (5)$$

is the most rare nuclear decay allowed in the standard model. This second-order weak decay process has been observed so far in ten nuclides ( $^{48}\text{Ca}$ ,  $^{76}\text{Ge}$ ,  $^{82}\text{Se}$ ,  $^{96}\text{Zr}$ ,  $^{100}\text{Mo}$ ,  $^{116}\text{Cd}$ ,  $^{128}\text{Te}$ ,  $^{130}\text{Te}$ ,  $^{150}\text{Nd}$  and  $^{238}\text{U}$ ) and in two excited states ( $^{100}\text{Mo}$ ,  $^{150}\text{Nd}$ ), often by different groups and using different methods.

The inverse half-life of  $2\nu\beta\beta$ -decay is free of unknown parameters on the particle physics. It can be expressed as a product of an accurately known phase-space factor  $G_{01}^{2\nu}(E_0, Z)$  and the double Gamow-Teller transition matrix element  $M_{GT}^{2\nu}(A, Z)$ ,

$$\frac{1}{T_{1/2}^{2\nu}(A, Z)} = |M_{GT}^{2\nu}(A, Z)|^2 G_{01}^{2\nu}(E_0, Z). \quad (6)$$

The measured  $2\nu\beta\beta$ -decay half-lives give us directly the value of  $M_{GT}^{2\nu}(A, Z)$ , i.e, the  $2\nu\beta\beta$ -decay offers a severe test of nuclear structure calculations. In Fig. 1 we present the  $2\nu\beta\beta$ -decay NME's extracted from the average and recommended half-live values of Ref. [4]. We note that the matrix element for  $^{100}\text{Mo}$  is about 10 times larger than the one for  $^{130}\text{Te}$ . The large spread of the  $2\nu\beta\beta$ -decay NME's has origin in the shell dependence of the involved nuclei. The energy

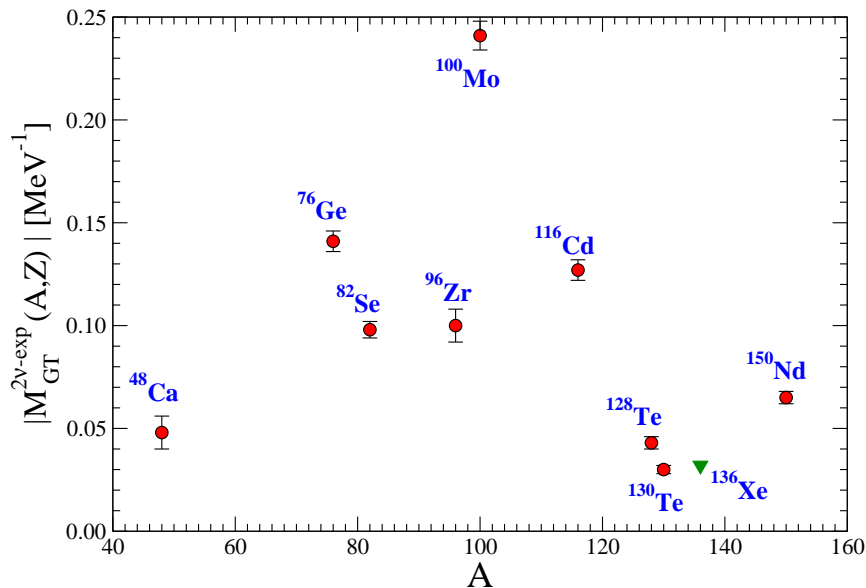


**Figure 1.** The  $2\nu\beta\beta$ -decay nuclear matrix elements extracted from the average and recommended half-life values [see Ref. [4]].  $g_A = 1.25$  is assumed.

position and structure of the intermediate  $1^+$  states play a crucial role in the evaluation of  $M_{GT}^{2\nu}(A, Z)$ .

From the measurement of half-life of the  $0\nu\beta\beta$ -decay [see Eq. (2)] only the product  $|m_{\beta\beta}| |M^{0\nu}(A, Z)|$  can be determined. Thus, without accurate calculation of the  $0\nu\beta\beta$ -decay NME's, it is not possible to reach qualitative conclusions about neutrino masses and the type of neutrino mass spectrum. The calculation of the  $0\nu\beta\beta$ -decay matrix elements is a difficult problem because ground and many excited states of open-shell nuclei with complicated nuclear structure have to be considered.

The two basic approaches used so far for the evaluation of the double beta decay NME's are the Quasiparticle Random Phase Approximation (QRPA) and the nuclear shell model (NSM). Both methods have the same starting point, namely a Slater determinant of independent particles. However, there are substantial differences between both approaches, namely the kind of correlations they include are complementary. The QRPA treats a large single particle model space, but truncates heavily the included configurations. NSM, by a contrast, treats a small fraction of this model space, but allows the nucleons to correlate in arbitrary ways [5].

Due to its simplicity the QRPA is a popular technique to calculate the  $0\nu\beta\beta$ -decay NME's. The overwhelming majority of the published results were obtained within this many-body approach. However, various implementations of the QRPA introduced by different authors have produced a spread of results with a factor of three or as much as five. Some authors simplified this problem by assuming that the published range of calculated NME's defines a plausible approximation to the uncertainty in our knowledge of the matrix elements [6]. This position is unsound. In Ref. [7] a list of main reasons leading to a spread of the previous QRPA and renormalized QRPA (RQRPA) NME's was presented. It was shown that in most, albeit not all, cases the differences among them can be understood.

Actually, it is not appropriate to consider that all  $0\nu\beta\beta$ -decay calculations are of even quality. Some of them requires that the measured  $2\nu\beta\beta$ -decay half-life is reproduced, other do not pay attention to this issue. In many works a simplified form of transition operator was considered. In particular, the two-nucleon short-range correlations and induced current terms of the nucleon

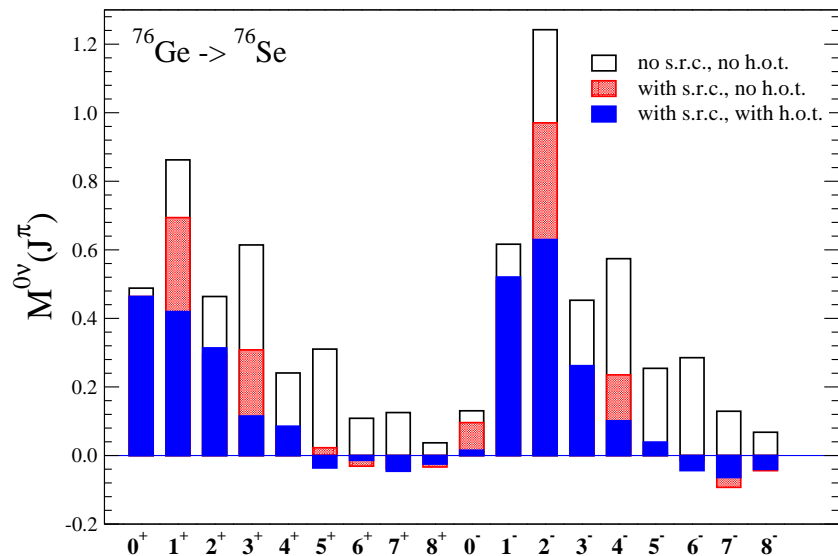


**Figure 2.** The effects of higher-order terms of nucleon currents (h.o.c.) and of the nucleon-nucleon short range repulsion (s.r.c.) on the multipole distribution of the  $0\nu\beta\beta$ -decay matrix element in the QRPA.

current were not taken into account. However, their consideration, which is of course a question of physics, reduces the value of  $M^{0\nu}(A, Z)$  by about factor of two and change the multipole distribution of the  $0\nu\beta\beta$ -decay NME (see Fig. 3).

One of the most important factors of the QRPA calculation of the  $0\nu\beta\beta$ -decay NME's is the way how the particle-particle strength of the nuclear Hamiltonian  $g_{pp}$  is fixed. It has been shown that by adjusting  $g_{pp}$  to the  $2\nu\beta\beta$ -decay rates the uncertainty associated with variations in QRPA calculations of the  $0\nu\beta\beta$ -decay NME's can be significantly eliminated [7]. In particular, the results obtained in this way are essentially independent of the size of the basis, the form of different realistic nucleon-nucleon potentials, or on whether QRPA or RQRPA is used (see Fig. 2). Recently, this has been confirmed also for the self-consistent RQRPA (SRQRPA) [9].

Some author's believe that fitting of  $g_{pp}$  to  $\beta^+$  (or electron capture (EC)) and single  $\beta^-$ -decay of the ground state of the intermediate nucleus is a more meaningful procedure [8] than the procedure of adjusting the interaction constant  $g_{pp}$  to known  $2\nu\beta\beta$ -decay half-lives. However, there is no reason to give preference to the lowest state of the intermediate nucleus [7]. The  $\beta^-$  and  $\beta^+/EC$  matrix elements move with  $g_{pp}$  in opposite directions, what makes it difficult to adjust  $g_{pp}$  by choosing one of them. It was also noticed that practically for all multipolarities significant amount of strength is concentrated up to 10-15 MeV and that the contributions of the  $1^+$  multipole to the  $2\nu\beta\beta$ - and  $0\nu\beta\beta$ -decay matrix elements are correlated. Thus, there is no reason to choose any one particular state or transition for adjustment.

Fig. 3 presents the  $0\nu\beta\beta$ -decay NME's of most nuclei of experimental interest evaluated using the QRPA and the RQRPA within the procedure of fixing  $g_{pp}$  to known  $M_{GT}^{2\nu}(A, Z)$  [7]. Their variance includes the error coming from the experimental (statistical and systematic) uncertainty in  $M^{2\nu}(A, Z)$  and uncertainty from theory itself. For  $^{136}\text{Xe}$  the error bars encompass the whole interval related to the unknown rate of the  $2\nu\beta\beta$  decay. These results provide hope that with a consistent treatment 20-30 % uncertainties are possible.

After some break of about 10 years the Strasbourg-Madrid group presented new results for the  $0\nu\beta\beta$ -decay NME's [5], which are based on good spectroscopy for parent, intermediate and daughter nuclei. The NSM code can deal with problems involving basis of  $10^{10}$  Slater

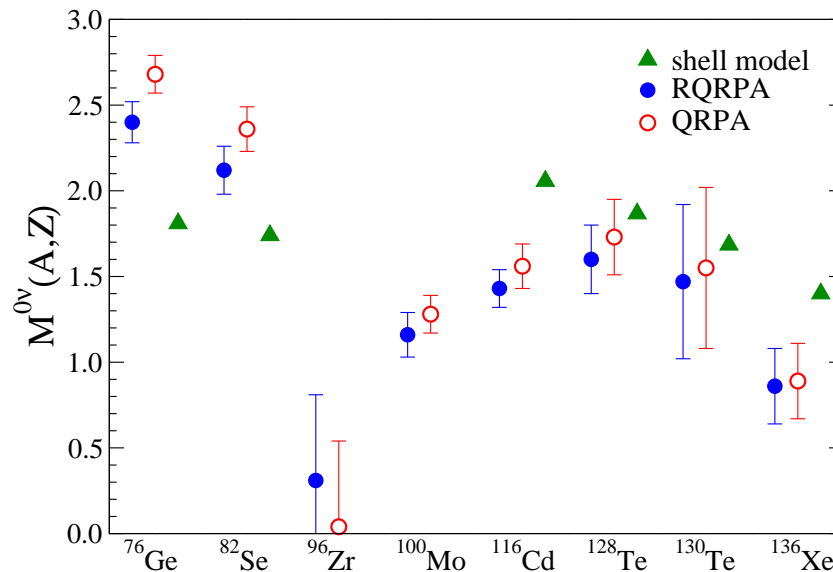


**Figure 3.** The  $0\nu\beta\beta$ -decay nuclear matrix elements  $M^{0\nu}(A, Z)$  (and their variance) obtained within the QRPA and the RQRPA [7] and the NSM [5]. The NSM results are scaled by factor 0.7 in order to account approximately for the effect of induced nucleon currents. For the axial coupling constant  $g_A$  the value  $g_A = 1.25$  was assumed.

determinants, using relatively modest computational resources. In Fig. 3 the comparison of recent NME's of Rodin et al. [7] based on the QRPA and the RQRPA with those of the available most recent NSM results [5] is presented. The NSM values are reduced by 30% in order to account approximately for the effect of the induced nucleon currents, not considered in the calculation. It is surprising that these very different methods yield similar results. It might indicate that both approaches capture most of the important physics. However, this fact deserves further investigation, which should include analysis of the truncation of the model space by the NSM, analysis of the multipole decomposition of the  $0\nu\beta\beta$ -decay NME's and the study of the role of spin-orbit partners missing in the NSM calculations. By glancing the Fig. 3 one also finds that once the NSM calculations for  $^{96}\text{Zr}$  and  $^{100}\text{Mo}$  become available the comparison of these two approaches will be more meaningful.

In Fig. 3 we notice that there is only a small variation of the  $0\nu\beta\beta$ -decay NME's going from one nucleus to another one in comparison with the variation of the  $2\nu\beta\beta$ -decay NME's (see Fig 1). The explanation of it can be that the  $0\nu\beta\beta$ -decay NME's are not sensitive to the spectroscopy of the intermediate nucleus due to a large average exchange momentum of mediated neutrinos (about 100 MeV).

### 3. Reducing the uncertainty in NME's

It is clear that further progress in the calculation of the  $0\nu\beta\beta$ -decay NME's is needed. In particular, the problem of the two-nucleon short-range correlations should be better understood. An open issue is what is the effect of deformation on the  $0\nu\beta\beta$ -decay NME's.

Till now, the effect of deformation has been ignored in the treatment of  $\beta\beta$  nuclei of experimental interest. However, many of the nuclei undergoing double beta decay are deformed. The values of experimental quadrupole deformation parameter  $\beta$  for different  $\beta\beta$  nuclei are given in Table 1. They were derived from laboratory moments [10] and from experimental values of B(E2) strengths [11]. We note that especially nuclei involved in the double beta decay transition

**Table 1.** The experimental values of quadrupole deformation parameter  $\beta$  of the  $\beta\beta$  nuclei of interest and the BCS overlap factors, which represent approximately the suppression of the  $\beta\beta$  NME's.  $Q_{\beta\beta}$  denotes the Q-value of the double beta decay process ( $E_0 = Q_{\beta\beta} + 2m_e$ ).

Transition	$Q_{\beta\beta}$ [MeV]	$\beta_{initial}$		$\beta_{final}$		$i \langle BCS   BCS \rangle_f$
		Ref. [10]	Ref. [11]	Ref. [10]	Ref. [11]	
$^{48}\text{Ca} \rightarrow ^{48}\text{Ti}$	4.272	0.000	0.101	+0.17	0.269	0.51, 0.44
$^{76}\text{Ge} \rightarrow ^{76}\text{Se}$	2.039	+0.095	0.262	+0.163	0.309	0.74, 0.67
$^{82}\text{Se} \rightarrow ^{82}\text{Kr}$	2.995	+0.104	0.194		0.202	0.80
$^{96}\text{Zr} \rightarrow ^{96}\text{Mo}$	3.350		0.081	+0.068	0.172	0.46
$^{100}\text{Mo} \rightarrow ^{100}\text{Ru}$	3.034	+0.139	0.231	+0.136	0.217	0.85, 0.84
$^{116}\text{Cd} \rightarrow ^{116}\text{Sn}$	2.805	+0.113	0.191	+0.043	0.112	0.61, 0.52
$^{128}\text{Te} \rightarrow ^{128}\text{Xe}$	0.867	+0.011	0.136		0.184	0.66
$^{130}\text{Te} \rightarrow ^{130}\text{Xe}$	2.529	+0.035	0.118		0.169	0.65
$^{136}\text{Xe} \rightarrow ^{136}\text{Ba}$	2.468		0.086		0.124	0.72
$^{150}\text{Nd} \rightarrow ^{150}\text{Sm}$	3.367	+0.367	0.285	+0.230	0.193	0.16, 0.37

$^{150}\text{Nd} \rightarrow ^{150}\text{Sm}$  exhibit large deformations.

Recently, it was found that differences in deformation between the initial and final nuclei have large effects on the  $2\nu\beta\beta$ -decay NME's [12]. The calculations were performed in the framework of the deformed QRPA with separable proton-neutron residual interaction, which is relevant only for allowed Gamow-Teller transitions. The origin of this suppression mechanism is a strong sensitivity of the overlap of initial and final BCS vacua (which enters directly into the overlap of intermediate nuclear states generated from the initial and final nuclei via QRPA diagonalization) to the deformations of the initial and final nuclei. The effect of deformation can be large also in the case of the  $0\nu\beta\beta$ -decay NME's as they need to be scaled by this factor as well. The values of the BCS overlap factor, which give us some estimate of the effect of deformation on the  $0\nu\beta\beta$ -decay transitions, are presented in Table 1. The smallest values of this factor are for  $A=48$ , 96 and 150 nuclear systems. Of course, the correct treatment of nuclear deformation requires to exploit, e.g., the deformed QRPA approach based on realistic nucleon-nucleon interaction. For further progress in the field, it would be useful to improve and complete the experimental information on nuclear deformations.

The improvement of the calculation of the nuclear matrix elements is a very important and challenging problem. The uncertainty associated with the calculation of the  $0\nu\beta\beta$ -decay NME's can be diminished by suitable chosen nuclear probes [13]. A complementary experimental information from related processes like charge-exchange reactions, muon capture and charged current (anti)neutrino-nucleus reactions is highly required. It is desired to understand the extent to which a given method can reproduce other observables. However, we note that there are no observables directly related to the  $0\nu\beta\beta$ -decay NME except of the measured half-life and differential characteristics of this process.

The problem of the uncertainty in the  $0\nu\beta\beta$ -decay NME might be better understood by observation of the  $0\nu\beta\beta$ -decay of at least three different nuclei. The ratios of corresponding  $0\nu\beta\beta$ -decay half-lives can be a model independent test of the theoretically calculated NME's.

#### 4. Distinguishing the $0\nu\beta\beta$ -decay mechanisms

The helicity flip Majorana mass mechanism with three light neutrinos is the most popular  $0\nu\beta\beta$ -decay mechanism. It is because existing experimental results fit rather nicely into a picture with

three light massive neutrinos, which corresponds to the simplest scenario for three generations. However, the neutrino sector may contain more than three neutrinos by including mixing to sterile neutrinos. The sterile right-handed neutrinos, not participating in the electroweak interactions, are natural candidates for the extension of the standard model (SM) field contents.

A simplest scenario would be that in addition to the three conventional light neutrinos there exists only one Majorana neutrino mass eigenstate  $\nu_h$ , dominated by the sterile neutrino species, with an arbitrary mass  $m_h$ , which may mix with all the active neutrinos,  $\nu_{e,\mu,\tau}$ . If the contribution of  $\nu_h$  neutrino state to the  $0\nu\beta\beta$ -decay dominates we can write [14]

$$[T_{1/2}^{0\nu}]^{-1} = G_{01}^{0\nu}(E_0, Z) \left| U_{eh}^2 \frac{m_h}{m_e} M^{0\nu}(A, Z, m_h) \right|^2. \quad (7)$$

In the limit  $m_h = 0$  we find  $M^{0\nu}(A, Z, m_h)$  to be equal to  $M^{0\nu}(A, Z)$  of Eq. (2).

The left-right symmetric models allow us to explain the smallness of the neutrino mass within the so called see-saw mechanism in the most natural way. It is supposed that the neutrino mixing does take place according to

$$\nu_{eL} = \sum_k^{light} U_{ek}^L \chi_{kL} + \sum_k^{heavy} U_{ek}^L N_{kL}, \quad \nu_{eR} = \sum_k^{light} U_{ek}^R \chi_{kR} + \sum_k^{heavy} U_{ek}^R N_{kR}, \quad (8)$$

where,  $\chi_k$  ( $N_k$ ) are fields of light (heavy) Majorana neutrinos with masses  $m_k$  ( $m_k \ll 1$  MeV) and  $M_k$  ( $M_k \gg 100$  GeV), respectively, and  $U_{ek}^L, U_{ek}^R$  are unitary mixing matrices. In the case of the most general lepton mixing the flavor neutrino fields are superposition of three light and three heavy Majorana neutrinos with definite mass.

In this model the  $0\nu\beta\beta$ -decay amplitude consists of contributions associated with different effective lepton number violating parameters (LNV). In addition to  $m_{\beta\beta}$  the most relevant LNV parameters are

$$\varepsilon_{LR} = \sum_k^{light} U_{ek}^L U_{ek}^R, \quad \eta_N^{LL} = \sum_k^{heavy} U_{ek}^L U_{ek}^L \frac{m_p}{M_k}, \quad \eta_N^{RR} = \sum_k^{heavy} U_{ek}^R U_{ek}^R \frac{m_p}{M_k}. \quad (9)$$

Here,  $m_p$  is the mass of proton.

If one assumes that one mechanism at a time dominates, the half-life of the  $0\nu\beta\beta$ -decay can be written as

$$(T_{1/2}^{0\nu})^{-1} = |LNV|^2 \sum_i P_i^{0\nu} G_i^{0\nu}. \quad (10)$$

The sum over  $i$  runs over different phase space integrals  $G_i^{0\nu}$  weighted by a corresponding product  $P_i^{0\nu}$  of different NME's.

Although the occurrence of  $0\nu\beta\beta$ -decay implies the existence of massive Majorana neutrinos, their exchange need not be the only to the decay rate. Almost any physics that violates the total lepton number can cause the  $0\nu\beta\beta$ -decay. The GUT's and R-parity violating SUSY models offer a plethora of  $0\nu\beta\beta$ -decay mechanisms triggered by exchange of neutrinos, neutralinos, gluinos, leptoquarks etc. Thus, one can not unambiguously infer  $m_{\beta\beta}$  from the  $0\nu\beta\beta$ -decay half-life.

Once the  $0\nu\beta\beta$ -decay will be observed the main question will be what is the dominant mechanism of this process. In order to solve this difficult task it will be necessary to use the phenomenological constraints imposed by other experiments (neutrino oscillations,  $\mu \rightarrow e$  conversion,  $\mu \rightarrow \gamma$  decay, processes at accelerators etc.), to consider appropriate particle physics models with their constraints, to measure differential characteristics and the  $0\nu\beta\beta$ -decay transitions to excited  $0^+$  and  $2^+$  states and finally, to perform reliable calculation of different  $0\nu\beta\beta$ -decay NME's originating from different exchange potentials.

## 5. Conclusion and outlook

Many new projects for measurements of  $0\nu\beta\beta$ -decay have been proposed, which hope to probe effective neutrino mass  $m_{\beta\beta}$  down to 10-50 meV. Nuclear matrix elements need to be evaluated with uncertainty of less than 30% to establish the neutrino mass spectrum and CP violating phases. The improvement of the calculation of the nuclear matrix elements is a very important and challenging problem.

Recently, there has been significant progress in understanding the source of the spread of calculated NME's. Nevertheless, there is no consensus among nuclear theorists about their correct values, and corresponding uncertainty. However, a comparison of the QRPA and the RQRPA results of Ref. [7] with recent NSM calculations is encouraging. There is a reason to be hopeful that the uncertainty will be reduced.

Unfortunately, there are not many theorists working on the nuclear physics aspects of double beta decay. More collaborations, more postdoctoral and Ph.D projects would make progress faster. A cumulative effort of specialist in the field might result in reliable NME's, which will be needed when  $0\nu\beta\beta$ -decay data will appear.

An important cross-check for nuclear models would be to explore the structure of the intermediate odd-odd nuclei by the charge exchange reactions. There are possibilities for improving the QRPA calculation of NME's, e.g., by taking into account the deformation of parent and daughter nuclei. Further progress in the NSM calculation will be possible due to increasing computer speed and memory. This will allow to extend the considered model spaces. The exactly solvable models can also help to find the ultimate solution of this important problem. It is also clear that in order to have confidence in calculated NME's multiple  $0\nu\beta\beta$ -decay experimental results are required.

## 6. Acknowledgement

I acknowledge the support of the EU ILIAS project under the contract RII3-CT-2004-506222 and the VEGA Grant agency of the Slovak Republic under the contract No. 1/0249/03.

## References

- [1] Heidelberg-Moscow collaboration, Baudis L *et al.* 1999 *Phys. Rev. Lett.* **83** 41; CUORE Collaboration, Arnaboldi C *et al.* 2004 *Phys. Lett. B* **584** 260; DAMA Collaboration, Bernabei R *et al.* 2002 *Phys. Lett. B* **546** 23; NEMO Collaboration, Arnold R *et al.* 2005 *Phys. Rev. Lett.* **95** 182302; CAMEO Collaboration, Danevich F A *et al.* 2003 *Phys. Rev. C* **68** 035501
- [2] Klapdor-Kleingrothaus H V, Krivosheina I V, Dietz A, and Chkvorets O 2004 *Phys. Lett. B* **586** 198
- [3] GERDA Collaboration, Abt I *et al.* 2004 *Preprint* hep-ex/0404039
- [4] Barabash A S 2006 *Czech. J. Phys.* **56** 437
- [5] Caurier E, Martinez-Pinedo G, Nowacki F, Poves A, and Zuker A P 2005 *Rev. Mod. Phys.* **77** 427 A. Poves, talk at 3rd ILIAS/N6-ENTApP: <http://www2.iap.fr/users/sigl/entapp/entapp-2006.html>.
- [6] Bahcall J N, Murayama H, and Pena-Garay C 2004 *Phys. Rev. D* **70** 033012
- [7] Rodin V A, Faessler A, Šimkovic F, and Vogel P 2003 *Phys. Rev. C* **68** 044302; 2006 *Nucl. Phys. A* **766** 107; 2006 *Czech. J. Phys.* **56** 495
- [8] Civitarese O, Suhonen J 2005 *Nucl. Phys. A* **761** 313; 2005 *Phys. Lett. B* **626** 80
- [9] Beneš P, Šimkovic F, Faessler A, and Kaminski W A 2006 *Prog. Part. Nucl. Phys.* **57** 257
- [10] Raghavan P 1989 *At. Dat. Nucl. Dat. Tabl.* **42** 189; Stone N J 2001 *Oxford University preprint*
- [11] Raman S *et al.* 1987 *At. Dat. Nucl. Dat. Tabl.* **36** 1
- [12] Šimkovic F, Pacearescu L, and Faessler A 2004 *Nucl. Phys. A* **733** 321
- [13] Zuber K 2005 *Preprint* nucl-ex/0511009
- [14] Beneš P, Faessler A, Kovalenko S, and Šimkovic F 2005 *Phys. Rev. D* **71** 077901

## The CNGS project and OPERA experiment at LNGS

**Chiara Sirignano for the OPERA Collaboration**

Dipartimento di Fisica "E.R.Caianiello", Salerno University, 84081 Baronissi  
(Salerno)-ITALY

E-mail: sirignano@sa.infn.it

**Abstract.** The OPERA (CNGS1) experiment will study neutrino oscillations; in particular it was designed to observe  $\nu_\mu \rightarrow \nu_\tau$  oscillation signal via the direct observation of  $\nu_\tau$  interactions in a target of nuclear emulsions films and lead. The experiment will make use of a high energy  $\nu_\mu$  beam (CNGS) produced at CERN and of a detector placed in the Gran Sasso Underground laboratory (LNGS); the sub-micron spatial resolution provided by nuclear emulsions will allow to identify oscillation signal with a very low background level. In these months the OPERA collaboration is carrying out the detector assembly and the physical data acquisition is expected to start in August 2006. In order to cope with the expected neutrino interaction rate and allow a quasi-online analysis of the events, the emulsion read out have to be very fast; the limited number of signal events expected requires to the system high efficiency, purity and precision.

### 1. Introduction

OPERA is a long-baseline experiment devoted to the direct observation of  $\nu_\tau$  appearance from  $\nu_\mu \rightarrow \nu_\tau$  oscillations in the CNGS beam from the CERN SPS to the LNGS; the whole project was designed to search for  $\nu_\mu \rightarrow \nu_\tau$  oscillation in the parameter region indicated by the Super Kamiokande, Macro and Soudan2 atmospheric neutrino analysis [1], [2], [3]; it will be also possible to search for the sub leading  $\nu_\mu \rightarrow \nu_e$  oscillations, which could be observed if  $\theta_{13}$  is close to the present limit from CHOOZ [4] and Palo Verde [5] experiments.

The detection of the  $\nu_\tau$  interactions will be realized by looking for the charged  $\tau$  lepton produced in CC interaction and its decay products. In order to observe and fully reconstruct the decay topologies it is necessary a spatial resolution at the micrometer scale and such resolution is possible by detecting the charged particle tracks in emulsion sheets interspersed with thin lead plates acting as target material. In order to reach these goals a pure  $\nu_\mu$  beam will be sent from CERN to LNGS where the OPERA experiment is under preparation. The distance between CERN and LNGS is  $L = 732$  km and the  $\nu_\mu$  beam flux is optimized to yield a maximum number of  $\nu_\tau$  CC interactions at Gran Sasso. Table 1 shows some basic parameters of the beam; the mean energy is  $\langle E \rangle = 17$  GeV, the resulting  $L/\langle E \rangle$  ratio is 43 km/GeV and CNGS operates in the "off peak" mode due to the high energy needed for  $\nu_\tau$  production. The CNGS civil engineering has been completed; all beam parts were produced

and installed on schedule. The commissioning started in May 2006 and the first beam is expected on 18<sup>th</sup> August 2006.

$\nu_\mu$ CC + NC int/year	~ 6200
Proton on target /year	$4.5 \times 10^{19}$
$\nu_\tau^{prompt}$	Negligible
$(\nu_e + \bar{\nu}_e) / \nu_\mu$	0.87%
$\nu_\mu / \sqrt{\nu_\mu}$	2.1%
$\nu_\tau$ CC int/year	~25
$(\Delta m^2 = 2.4 \times 10^{-3} \text{ eV}^2, \text{maximal mixing})$	

Table 1 – CNGS beam mean features.

The experiment design is based on the ECC detector, a modular structure made of sandwich of passive material interspersed with emulsion layers. By assembling a large quantity of such modules, it has been possible to conceive and realise a ~ 2000 ton fine-grained vertex detector optimised for the study of  $\nu_\tau$  appearance. This technique, known as Emulsion Cloud Chamber (ECC), was validated for  $\nu_\tau$  search in the DONUT experiment [6]. The ECC used in Opera is a stack of 56 lead plates (1mm thickness) and 57 nuclear emulsion films. A brick has a size of 10.2 cm×12.7 cm with a length of 7.5 cm and a weight of 8.3 kg. In a separate package, two additional emulsion sheets, called changeable sheets, are glued on its downstream face. The total thickness of one brick is 10 X<sub>0</sub>, which is enough to identify electrons, measure their energies and measure the momentum of charged particles by multiple scattering [7]. The total number of bricks (206336) will be produced by an automatic machine called BAM (Brick Assembly Machine), designed by external firms following specifications listed in a technical document.

Within a brick, the achieved spatial resolution is  $\Delta x = 1 \mu\text{m}$  and the angular resolution is  $\Delta\theta = 2 \text{ mrad}$ . With these values, the reconstruction of the  $\nu_\tau$  interaction vertex and of the  $\tau$  decay topology will be possible. The brick was designed also as a stand alone detector that allows momentum measurement of charged particles by multiple scattering, separation of low energy  $\pi$  and  $\mu$  by  $dE/dx$  measurements and identification of electrons and photons by measurement of the electromagnetic shower. To provide  $\nu_\tau$  interaction triggers and to identify the brick in which the interaction took place, the detector is equipped by a target tracker and a muon spectrometer. Once the presence of tracks coming out of an interaction is confirmed, the brick is unpacked and all emulsion sheets are developed through a sophisticated chemico-physical process and sent to the scanning laboratories for analysis.

## 2. OPERA detector

The OPERA detector, shown in Fig. 1, consists of 2 Super Modules (SM) each of them composed by a target section followed by a muon spectrometer. In front of the SM1 there is a Veto plane made of Resistive Plate Chamber, detecting charged particles entering the detector. The target section is made of 31 brick walls interleaved with 31 Target Tracker planes. Each Wall consists of 3328 bricks removable by the side using an automatic system called Brick Manipulator System (BMS). The whole target section on each SM contains 103168 Bricks equivalent to about 900 tons. A Target Tracker plane consists of 4 horizontal + 4 vertical modules to measure x-y coordinate and will indicate in real time the neutrino interaction, pointing to the corresponding brick to be removed and analyzed. The

Muon Spectrometer consists of a  $10 \times 10 \text{ m}^2$  section dipole magnet formed by 22 iron planes interleaved by 22 RPC planes. In front, in the gap and behind the magnet there are 3 couples of Precision Tracker (PT) planes made of streamer tubes. The role of the PT is to measure the angle of

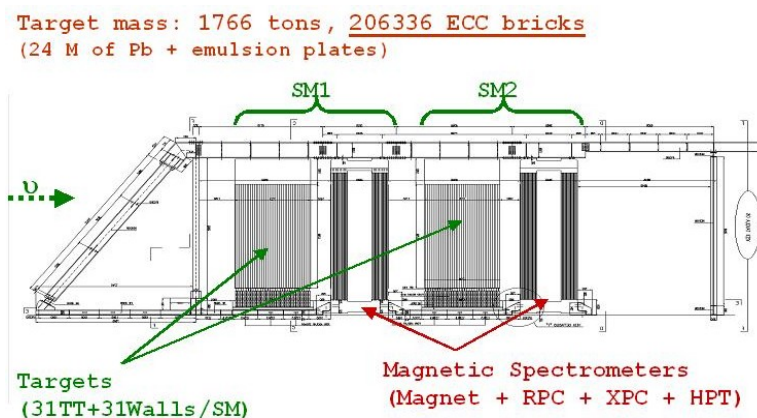


Fig. 1 – OPERA detector full design

the passing through muons. In order to improve the angular resolution on the measurement of the incoming particle, in front of the magnet it is positioned an additional couple of RPC planes with inclined read out strips with respect to the horizontal and vertical ones: these planes are called XPC. The muon spectrometer is able to measure the charge and momentum of the muon produced by the neutrino interactions in the target section. Once the neutrino interacts in the target section, the TT planes will indicate the brick where the interaction has happened. The “triggered brick” will be removed by the BMS and sent to the brick analysis procedure. It will not be replaced by a fresh one.

The construction status in June 2006 is well advanced. The brick supporting structure and all the tracker planes are installed. The XPC’s and three of the high PT planes of the first super-module are installed. The magnets, including the RPC’s for the whole detector and the mechanical structure are completed. The brick production will be completed by BAM. This machine consists of robots designed for the mechanical packing; the final system was successfully tested and is under installation at the Gran Sasso laboratory. Inside the detector the produced bricks will be handled by the brick manipulator system (BMS). Two large robots, each one operating at one side of the detector, consist of a drum for the brick transfer and a brick storage carousel. A pushing arm will be used to insert the bricks in any given row. The extraction of a brick in the region of interest indicated by the electronic detectors will be done by a vacuum sucker. BMS robots were successfully installed during 2006 and the commissioning phase is currently going on.

Starting from May 2006 the commissioning of the whole OPERA detector is going on smoothly using cosmic rays signal and electronic detector performances have been evaluated.

### 3. Event reconstruction and oscillation search

In order to perform Opera event analysis it was necessary to develop an automatic emulsion scanning system having remarkable speed and precision in the reconstruction of neutrino interactions. A long and complex R&D phase has been accomplished among European and Japanese Scanning laboratories to reach OPERA requirements. The European Scanning System [8], [9] consists of a microscope equipped with a computer-controlled motorised stage, a dedicated optical system and a CMOS camera mounted on top of the optical tube. Several images of the emulsion are grabbed at equally spaced

depth levels and processed. The scanning procedure accomplishes several tasks in on-line and off-line mode; since the system has a DAQ speed of 20 cm<sup>2</sup>/h/side tasks are decoupled and performed in an asynchronous way. Event location is performed by selecting stopping tracks, possibly intersecting each other; vertex reconstruction proceed among a selected emulsion volume and can be achieved by the computation of impact parameters between couple of stopping tracks.

The precision obtained in the vertex point determination is affected by particle scattering through lead plates and can be evaluated by Monte Carlo simulations. All those analysis steps, apart from the last one, will be accomplished by fast and quasi on-line scanning, whose direction and low level selections are completely accomplished by the central Opera DB. Several tests were needed to tune this complicate procedure. This motivated several exposures to pion beams at CERN and to NuMI neutrino beam line at Fermi Lab. The whole scanning procedure has been tuned and several hundred pion interactions and a few tens of neutrino interactions have been reconstructed.

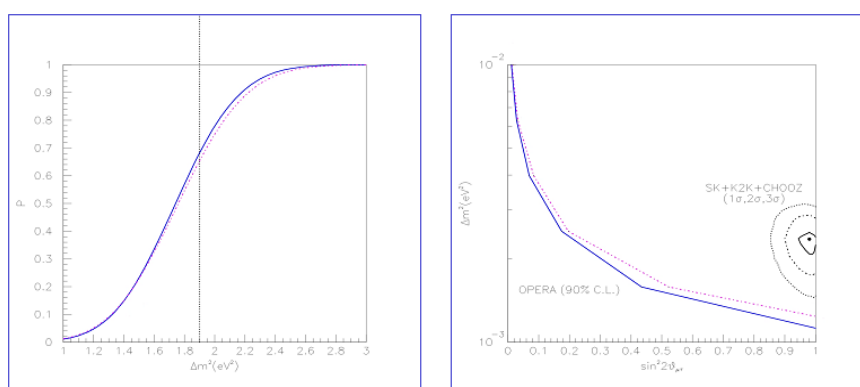


Fig. 2– OPERA discovery potential and exclusion plot.

The tau decay detection and reconstruction efficiency has been studied by detailed Monte Carlo simulations. We can consider two different topologies: the so-called short decays, when the tau particle decays in the same lead plate where the primary interaction takes place while the remaining ones are long decays. In short decays, the only topological signature is a non-zero impact parameter of the decay products with respect to the primary neutrino vertex. In long decays, the tau track direction can be measured together with the kink angle of the charged decay products. The resulting tau detection efficiencies for the detected channels, weighted with their branching ratios, are listed in Table 2. The first OPERA run is scheduled for the second half of August 2006. After the commissioning of the CNGS beam, a low intensity run with integrated  $0.3 \times 10^{19}$  pot will be performed. This physics run is important for the validation and monitoring of the CNGS beam, which will be done by checking the interaction rates, the energy distribution and by analyzing the muon charge to determine the content of  $\nu_{\mu}$ . The collected sample of interactions in the bricks will be sufficient to check the full analysis procedure and control the vertex finding efficiencies estimated by simulation. The resulting sensitivity and the  $4\sigma$  discovery probability, the probability that one can claim to have seen a signal larger than a  $4\sigma$  fluctuation of the background, are shown in Fig 2. This probability is described by the solid lines dependent on the value of  $\Delta m^2$ . If no  $\nu_{\tau}$  appearance will be seen, an exclusion region (90 % CL) can be given. As mentioned before OPERA will also search for  $\nu_{\mu} \rightarrow \nu_e$  oscillations. If  $\theta_{13}$  is close to the CHOOZ limit ( $\sin^2 2\theta_{13} < 0.14$  for  $\Delta m^2 = 2.5 \times 10^{-3} \text{ eV}^2$ ) [4], OPERA has the potential to observe the appearance of  $\nu_e$ . In case no  $\nu_e$  are observed and assuming  $\Delta m^2 = 2.5 \times 10^{-3} \text{ eV}^2$ , OPERA will be able to set a limit  $\sin^2 2\theta_{13} < 0.06$  (90% CL) [10].

#### 4. Conclusions

The OPERA – CNGS project is well advanced in the beam commissioning and in the detector installation at LNGS. The first run is expected starting from August 2006. The emulsion scanning infrastructure is operational and ready to accomplish the task of fast, precise and reliable neutrino interaction reconstruction. In case of success the experiment, it will give an unambiguous proof of  $\nu_\mu \rightarrow \nu_\tau$  oscillation hypothesis in the parameter region indicated by the Super Kamiokande, Macro and Soudan2 atmospheric neutrino analysis.

$\tau$ decay channel	Signal		Background
	$(\Delta m^2 = 2.4 \times 10^{-3} \text{ eV}^2)$	$(\Delta m^2 = 3.0 \times 10^{-3} \text{ eV}^2)$	
$\tau \rightarrow \mu$	3.6	5.6	0.23
$\tau \rightarrow e$	4.3	6.7	0.23
$\tau \rightarrow h$	3.8	5.9	0.32
$\tau \rightarrow 3h$	1.1	1.7	0.22
ALL	12.8	19.9	1.0

Table 2 – Opera oscillation expected signal in case of full mixing, 5 years run @  $4.5 \times 10^9$  pot.

#### References

- [1] Y. Ashie et al., Phys. Rev. Lett.93:101801, (2004).
- [2] M. Ambrosio et al., Phys. Lett. B 434,(1998), 451; Eur. Phys. J. C 36, (2004),323.
- [3] W. W. Allison et al., Phys. Rev. D 72,(2005), 052005.
- [4] M. Appollonio et al., "Search for neutrino oscillations on a long baseline at the CHOOZ nuclear power station", Eur. Phys.J. C 27, (2003), 331-374.
- [5] F. Boehm et. al., "Final results from Palo Verde Neutrino Oscillation Experiment",Phys. Rev. D 64, (2001), 112001
- [6] K. Kodama et. al., "Observation of tau neutrino interactions", Physics Letters B 504, (2001), 218-224
- [7] G. De Lellis et al., "Momentum measurement by the angular method in the Emulsion Cloud Chamber", Nucl.Instrum.Meth.A 512 (2003) 539.
- [8] N.Armenise et al., "High speed particle tracking in nuclear emulsion by last-generation automatic microscopes", Nucl.Instrum.Meth.A 551 (2005) 261-270
- [9] L. Arrabito et al., "Hardware performance of a scanning system for high speed analysis of nuclear emulsions", Nucl.Instrum.Meth. A 568 (2006) 578.
- [10] M. Komatsu, P. Migliozzi, F. Terranova, "Sensitivity to THETA(13) of the CERN to Gran Sasso Neutrino Beam", J. Phys. G29, (2003)

This document was created with Win2PDF available at <http://www.win2pdf.com>.  
The unregistered version of Win2PDF is for evaluation or non-commercial use only.

J. Steinberger, v2006, Santa Fe, June 2006

## The electron and the muon neutrinos are different particles; the story of the second neutrino

This story begins with a paper of G. Feinberg <sup>1)</sup>. At the time, the neutrino, the Fermi theory of  $\beta$ -decay, as well as the universal Fermi interaction, which linked the muon-neutrino current to the electron-neutrino and the nucleon-neutrino currents, and so created the Puppi triangle of three weak interactions, were well established and confirmed. But it had also already been noticed that at high energies the Fermi interaction violates unitarity, and the idea of an intermediate meson had been put forward. The paper of Feinberg pointed out that this theory would predict also the radiative decay of the muon and, on the basis of the Feynman diagrams of Fig. 1, predicted the branching ratio  $\alpha/24\pi = 10^{-4}$ . However, Lokanathan and I <sup>2)</sup> had already searched for this decay and observed an upper limit of  $2 \times 10^{-5}$ , that is five times smaller.

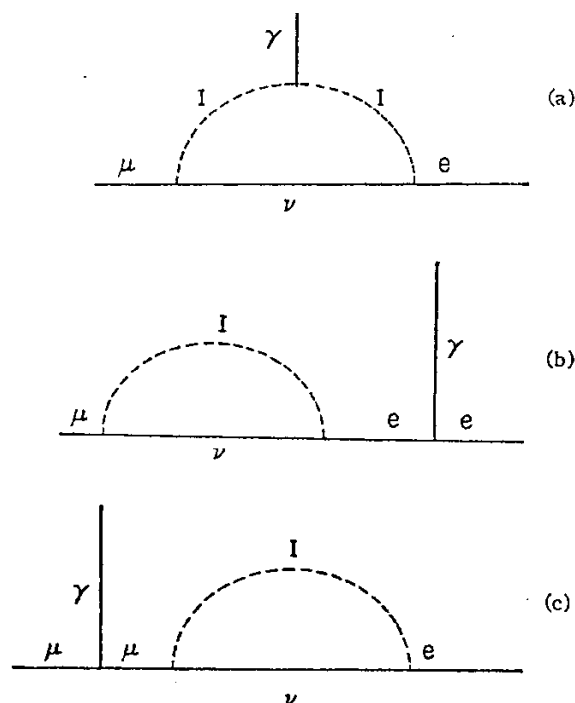


**Fig. 1:** Feynman diagrams for  $\mu \rightarrow e + \gamma$  through an intermediate boson.  $I$  labels the intermediate boson field.

One-half year later, Oneda and Pati <sup>3)</sup> noted that the problem pointed out by Feinberg, that is the non-observed radiative muon decay, could be overcome by making the neutrino associated with muon decay a different particle than that associated with beta decay,  $\nu_\mu \neq \nu_e$ .

This was followed by the article of Bruno Pontecorvo <sup>4)</sup> in which he proposed specific experiments to check if the two neutrinos are the same or if they are different, in particular to make beams of neutrinos produced in the decay of muons, and to look if these neutrinos associated with muons will produce electrons and positrons in interacting with nucleons,

$$\nu + n \rightarrow e^- + p \quad \text{and} \quad \bar{\nu} + p \rightarrow e^+ + n,$$

in the same manner as beta-decay neutrinos would be expected to do, in the frame of the Fermi theory. This is the experiment which we did in 1962 <sup>5)</sup>.

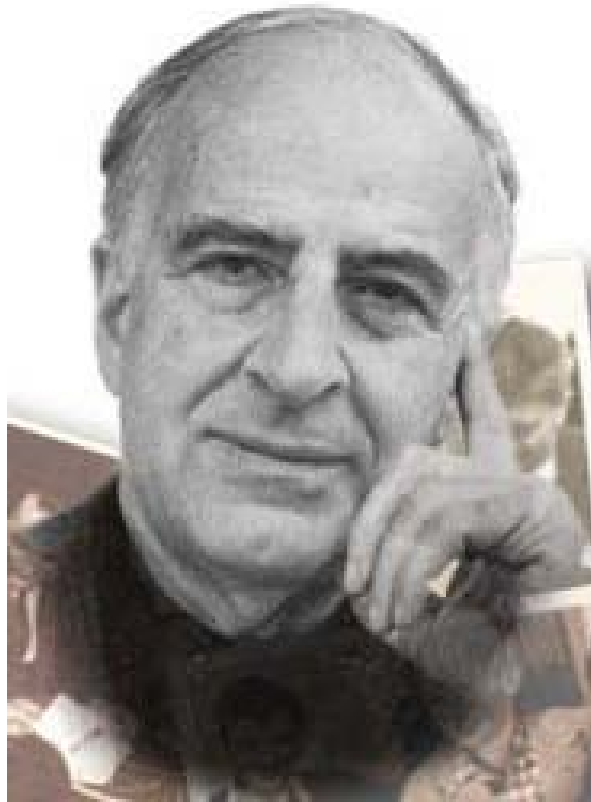


**Fig. 2:** Bruno Pontecorvo (Courtesy JINR, Dubna)

In some sense, our experiment began on one of the customary Friday afternoon Columbia University physics department coffees, this one early in 1960. Unfortunately for me, I was not present. The work of Pontecorvo had not yet travelled to the US. T.D. Lee asked the question: All we know of the weak interaction is based on the study of particle decays. How can we learn about the weak interaction at higher energies than are involved in the decays of pions, kaons and hyperons? Stimulated by this question, Mel Schwartz reflected and came to the idea of doing experiments using beams of neutrinos of higher energy <sup>6)</sup>. This short note by Mel in Physical Review Letters was followed by a considerably longer letter by Lee and Yang <sup>7)</sup>, in which they detail nine specific questions on the weak interaction which might be answered by neutrino beam experiments:

1. The identity of the neutrinos.
2. Conservation of leptons.
3. Possible existence of a neutral lepton current.
4. Point structure of the lepton current.
5. Universality of weak interactions involving electrons and muons.
6. S-symmetry.
7. Conserved vector current and proportionality with electromagnetic current.
8. Possible existence of weakly coupled Boson  $W^{+/-}$ .
9. Interactions with extremely large momentum transfers.

Certainly neutrino experiments contributed to the resolution of several of these questions. But it is also true that not even Lee and Yang could anticipate all that could be learned with the help of neutrino beams, for instance the nucleon structure functions (before it was known that the nucleons were not elementary particles), or the first validation of the theory of the strong interaction, QCD, in the neutrino deep-inelastic scaling violations.

It should also be remembered that here, as is often the case in the history of advances in physics, the moment was ripe. On the basis of the invention of the alternating gradient synchrotron by Courant, Livingston and Snyder <sup>8)</sup> in 1952, two accelerators, the PS at CERN and the AGS at Brookhaven National Laboratory, were nearing completion, and these, for the first time, offered sufficiently high proton beam energies and intensities to make neutrino beam experiments a practical possibility.

Following the suggestions by Pontecorvo <sup>4)</sup> and Schwartz <sup>6)</sup>, neutrino beam experiments were initiated both at the Columbia University Nevis Laboratory, for the Brookhaven AGS, and at CERN, for the PS. The Columbia team <sup>5)</sup> consisted of Mel Schwartz, two faculty colleagues, Leon Lederman and myself, one post-doc from France, Jean-Marc Gaillard, two doctoral students, Dinos Goulianos and Nariman Mistry, and one Brookhaven colleague, Gordon Danby.

In order to fit the experiment into the available space at the AGS, the proton beam energy had to be reduced to 15 GeV, one-half of its maximum. The layout, see Fig. 3, (Fig. 1 of the publication <sup>5)</sup>).

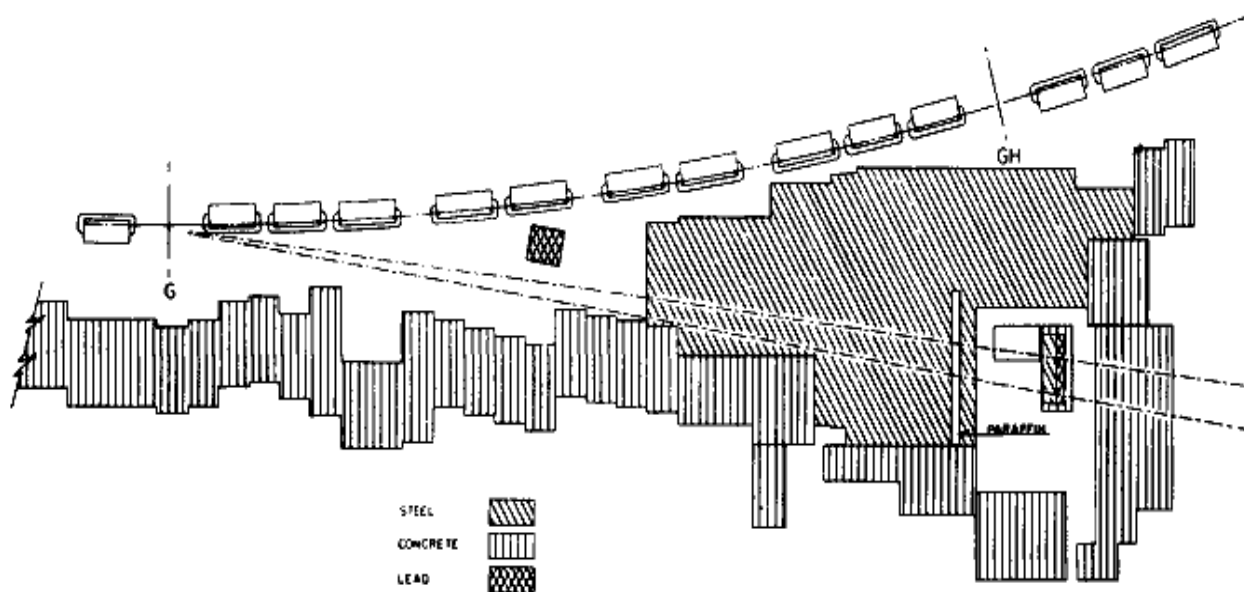


**Fig. 3:** Plan view of AGS neutrino beam experiment

The proton beam strikes an internal beryllium target, since the technique of beam extraction was still waiting to be invented by Piccioni a year or two later. The 31 m decay path for the pions and kaons, whose spectrum is shown in Fig. 4, Fig. 2 of the paper, is followed by 13.5 m of iron shielding, the scrap of battleships, kindly supplied by the US Navy, which at the time funded the Nevis Laboratory. One of the problems in doing the experiment was that the initial shielding was found to be inadequate; the shielding was improved during the experiment.

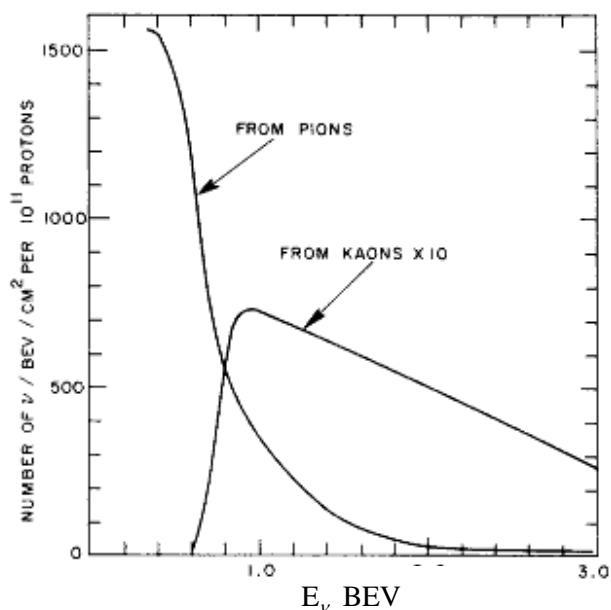


**Fig. 4:** Energy distribution of the neutrinos expected, with 15 GeV protons on a Be target

Given the successful Fermi theory of weak interactions, the neutrino interaction cross-sections were known, and given their small size, the target mass had to be maximized and the target incorporated into the detector. For the detector we consequently chose the newly invented spark chamber, with the metal foils replaced by 2.5 cm thick aluminium plates. The detector consisted of ten chambers, five sitting on the other five. Each was made of nine square plates, each side 112 cm long, for a total (target) mass of 10 tons. Between the spark chambers, and following them, scintillator planes for triggering were inserted, as well as anticoincidence counters in front, on top, and behind a shield, as can be seen in Fig. 5, Fig. 3 of the paper.

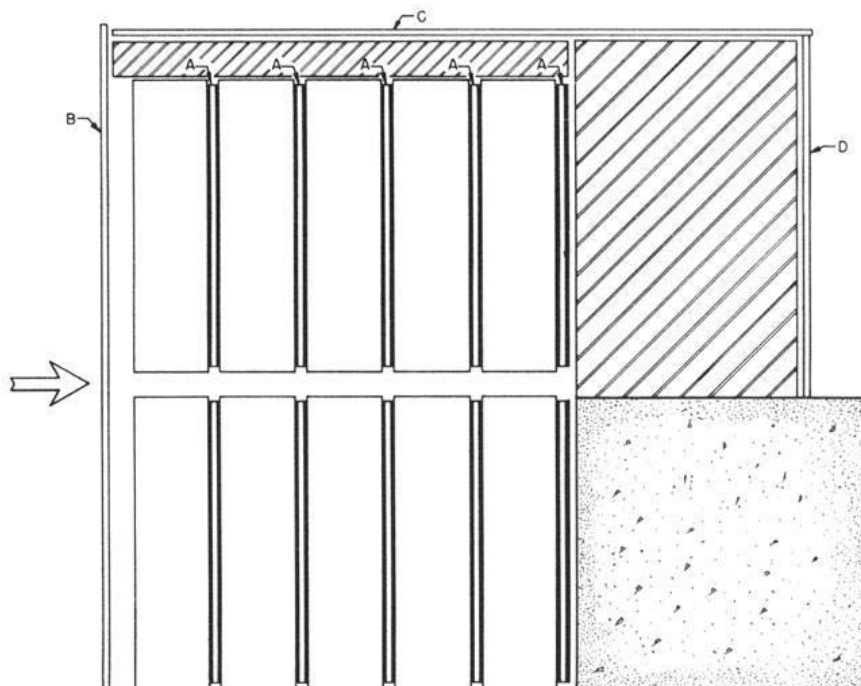


**Fig. 5:** Spark chamber and counter arrangement. A are the triggering slabs, B, C, and D are anticoincidence slabs. This is the front view, seen by the four-camera stereo system.

The experiment ran for several months, early in 1962. With a total of  $3.5 \times 10^{17}$  protons on target, 113 events were obtained, which originated within a fiducial volume 10 cm from front and back walls and 5 cm from top and bottom. If an event consisted of a single track, this was required to be at an angle of less than  $60^\circ$  with respect to the neutrino beam. Ignoring single track events with lengths corresponding to less than 300 MeV/c momentum, there remained:

- a) 34 single track events,
- b) 22 ‘vertex’ events, characterized by more than one track, and
- c) 8 ‘showers’, that is events, in general single tracks, but too irregular in structure to be normal mu mesons, and which perhaps could be electron or photon showers. Of these, six were so located that, for comparison with events of type a) and b), their *potential* ranges within the chambers corresponded to muons of more than 300 MeV/c.

An event of type b) is shown in Fig. 6.

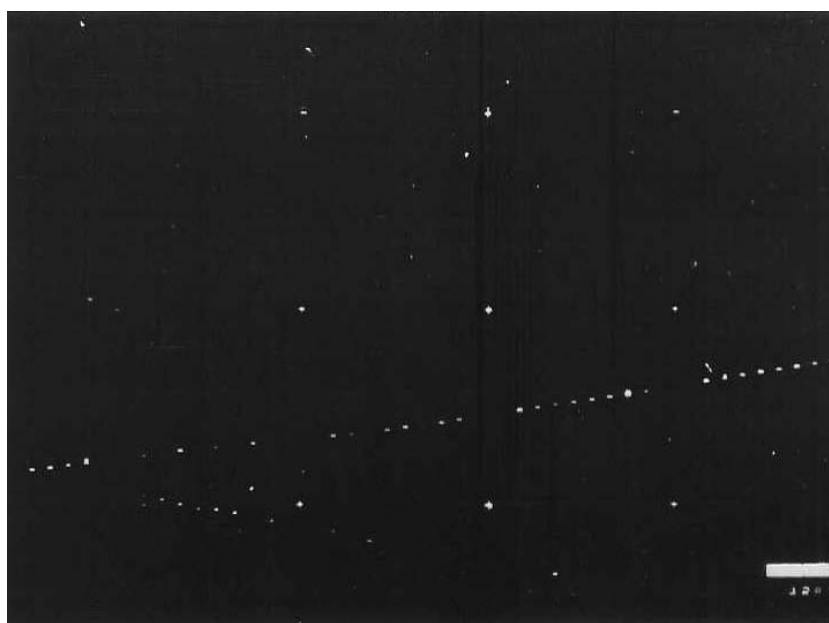


**Fig. 6:** Type b) event, consisting of a penetrating track as well as an additional shorter track

Events of type c) constituted the candidates for events in which the neutrinos produced electrons or positrons. To analyse these, an auxiliary exposure of the detector in a 400 MeV electron beam was performed. Figure 7, Fig. 9 of the paper, compares what would have been expected for the case of equal production rates for electrons and muons, with the actual observations, that is, with the six events of type c). Comparing these two distributions, it could be concluded that the neutrinos accompanying muons in pion and kaon decay are different from those accompanying electrons in beta decay.

Following this experimental result, it was clear that there are two lepton families, each composed of a charged and neutral lepton. Following the SLAC discovery in 1969 that hadrons are complex particles, made of ‘partons’, a few years later understood to be third integral electric charge quarks, it was clear that each ‘family’ consists of four types of particles: a lepton doublet plus a quark doublet. With the discovery of the tau lepton, in 1973, and later the bottom and top quarks, it became clear that there are at least three families. One of the most important results achieved at the LEP collider, in 1989 and the years following, based on the measurement of the decay width of the  $Z_0$ , is that the contribution to this width by  $Z_0$  decay to neutrinos corresponds exactly to three neutrino families, so that the total number of families is three.

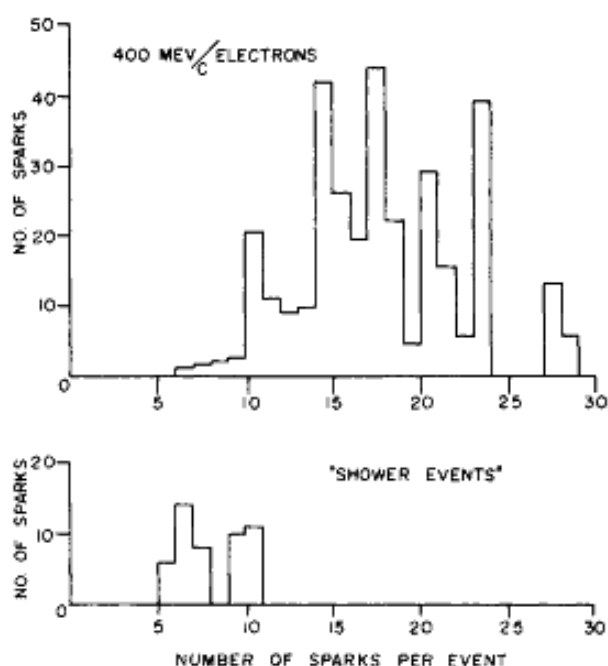


**Fig. 7:** Spark distribution of 400 MeV/c electrons normalized to expected number of showers. Also shown are the 'shower' events.



**Fig. 8:** The second neutrino team in 1962, and 26 years later, in Stockholm. From left to right: myself, Goulianos, Gaillard, Mistry, Danby, W. Hayes (technician), Lederman, Schwartz.

The last of the particles constituting the three families, the tau neutrino, was observed in 2001 at Fermilab by the DONUT Collaboration<sup>9)</sup>. In the experiment, as shown in Fig. 9, a tau-neutrino beam is produced by 800 GeV protons striking a 1 m long tungsten beam-dump target. The neutrinos are invited to interact in a hybrid target of emulsion modules interleaved with scintillating fibre planes. Up to four emulsion modules, each 7 cm thick and separated by 20 cm were used. The emulsion modules were of two types, either 1 mm stainless steel plates interleaved with 100 micron emulsions layers on each side of a 200 micron plastic sheet, or entirely of emulsion plates with 350 microns of emulsion on each side of a 100 micron plastic sheet. The emulsion neutrino target was followed by a magnetic spectrometer to track the decay products of the tau leptons produced in the interaction, and by a muon identifier.

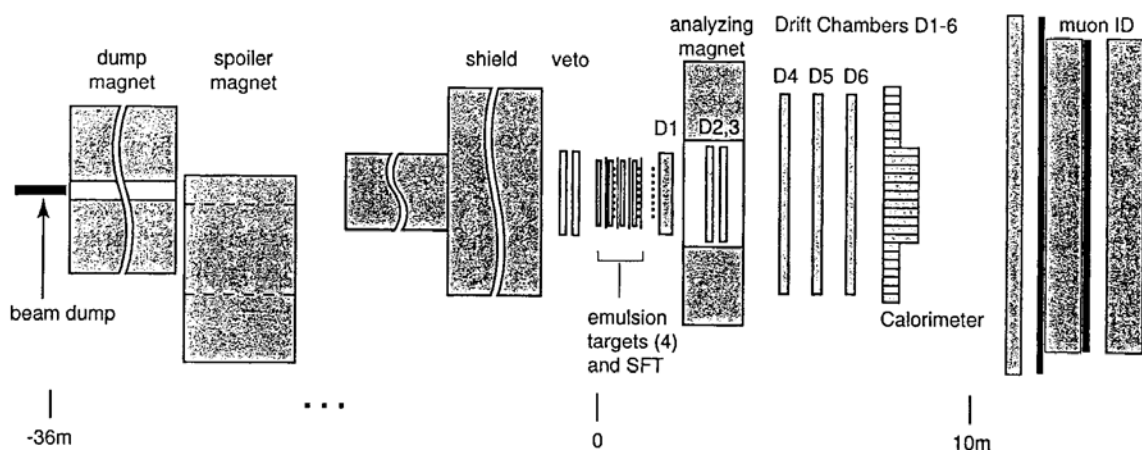


**Fig. 9:** (Fig 1. of Ref. [9].) Experimental beam and spectrometer. At the left, 800 GeV protons were incident on the beam dump, which was 36 m from the first emulsion target. Muon identification was done by range in the system at the right.

The observed muon tracks were followed back into the emulsion, in the search for possible tau decays. Four events of tau leptons produced in neutrino interactions were identified. These are shown in Fig. 10.

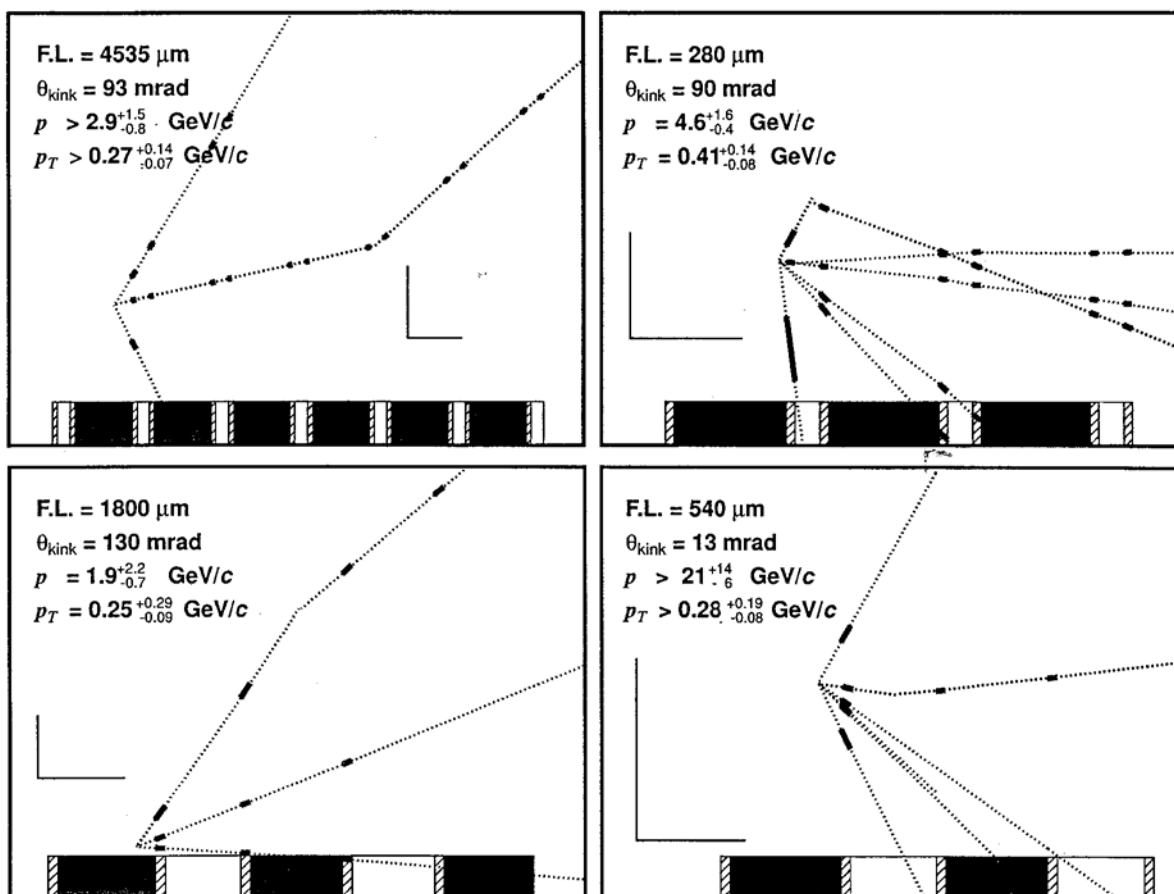


**Fig. 10:** (Fig 2 of Ref. [9]). The four tau-neutrino charged-current interaction events. The neutrinos are incident from the left. The scales are given by the perpendicular lines, with the vertical line representing 0.1mm and the horizontal line 1.0 mm. The target material is shown by the bar at the bottom of the figure, steel is shaded, emulsion is crosshatched, and plastic has no shading.

To conclude, the past century has witnessed a formidable progress in our understanding of the particles which everything is made of, and their interactions. Neutrino-beam experiments have played a major role in this advance. It is very sad that, for reasons of health, this historical review of the experiment which demonstrated the existence of a second neutrino, could not be given by Melvin Schwartz, who not only had the idea for this experiment, but also dominated it technically.

### References:

- [1] G. Feinberg, Decays of the  $\mu$  meson in the intermediate-meson theory, Phys. Rev. **110**, 1482 (1958).
- [2] S. Lokanathan and J. Steinberger, Phys. Rev. **98**, 240(A) (1955).
- [3] S. Oneda and J.C. Pati, V-A four-fermion interaction and the intermediate charged vector meson, Phys. Rev. Lett. **2**, 125 (1959).
- [4] B. Pontecorvo, Electron and muon neutrinos, Zh. Eksp. Teor. Fiz. **37**, 1751 (1959).
- [5] G. Danby, J-M. Gaillard, Zk. Goulianos, L.M. Lederman, N. Mistry, M. Schwartz, and J. Steinberger, Observation of high-energy neutrino interactions and the existence of two kinds of neutrinos, Phys. Rev. Lett. **9**, 36 (1962).
- [6] M. Schwartz, Feasibility of using high-energy neutrinos to study the weak interaction, Phys. Rev. Lett. **4**, 306 (1960).
- [7] T.D. Lee and C.N. Yang, Theoretical discussion on possible high-energy neutrino experiments, Phys. Rev. Lett. **4**, 307 (1960).
- [8] Ernest D. Courant, M. Stanley Livingston and Hartland Snyder, The strong focusing synchrotron—a new high-energy accelerator, Phys. Rev. **88**, 1190 (1952).
- [9] K. Kodema *et al.*, Observation of tau neutrino interactions, Phys. Lett. **B 504**, 218 (2001).

# Evidence for Neutrino Mass Leads to Kamiokande-II

SUZUKI ATSUTO

KEK, High Energy Accelerator Research Organization, Oho 1-1, Tsukuba, Ibaraki, 305-0801, JAPAN

E-mail: atsuto.suzuki@kek.jp

**Abstract.** The observations of solar neutrino deficit and atmospheric neutrino anomaly opened up a new vista of neutrino physics, and encouraged new experiments such as Super-Kamiokande, SNO, K2K, KamLAND and so on. Kamiokande-II played key roles to establish these two anomalies. This is the reason for the title of this article.

## 1. Kamiokande to Kamiokande-II

Kamiokande is an imaging water Cherenkov detector with 3000 tons of pure water in the main detector tank located at a depth of 2700 m.w.e. in the Kamioka mine. The unique feature of this experiment is the use of the world's largest 20-inch diameter photomultiplier tubes (PMT's), which provide a large coverage of the photosensitive area over the inner detector surface. The original motivation which stimulated the construction of the Kamiokande detector was searches for nucleon decay. With this main physics target we thought the Kamiokande data-taking should continue at the longest for 5 years. The detector design was paid attention to saving the construction cost. For instance the water purification system was designed to be quite simple so as to satisfy minimum specifications. The roof of a 3000 ton steel tank was covered with several black-polyethylene sheets. The mine air could easily sneak into the detector through many pinholes and joints of these sheets. The experiment started on July 6, 1983.

After running the detector for several months, careful analyses of cosmic-ray muons which were stopped in the detector and were accompanied by  $\mu \rightarrow e$  decay electrons, gave us hints to detect the  $^8\text{B}$  solar neutrinos. From fig. 1 one can see that the lower end of the energy spectrum reaches down to  $\sim 15$  MeV. Below this energy, the number of background events rises up enormously. This figure implies the possibility to detect the  $^8\text{B}$  solar neutrinos with a maximum energy of 14 MeV, with the aid of reasonable reduction of background events. This was the motivation for upgrading the Kamiokande detector.

## 2. Kamiokande-II

AT ICOBAN'84 Koshiya gave a talk concerning the possibility to detect the  $^8\text{B}$  solar neutrinos in addition to proton decay [1]. He asked people there to join in upgrading the Kamiokande detector for this purpose (Kamiokande-II). Soon after this workshop, A.K. Mann of the Univ. Pennsylvania expressed a desire for collaboration between Japan and the United States, and to prepare new signal discriminators and timing electronics for each PMT. The detector design of Kamiokande-II was investigated until July, 1984. Fig. 2 shows a schematic outline of the Kamiokande-II detector. There were 3 major improvements in Kamiokande-II: (1) constructing

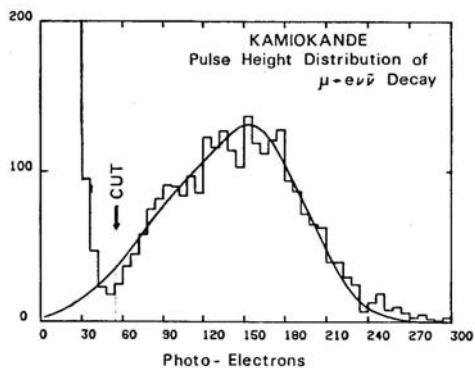


**Figure 1.** Energy spectrum of observed electrons from cosmic-ray  $\mu \rightarrow e\nu\bar{\nu}$  decays. 110 photoelectrons correspond to  $\sim 30$  MeV.

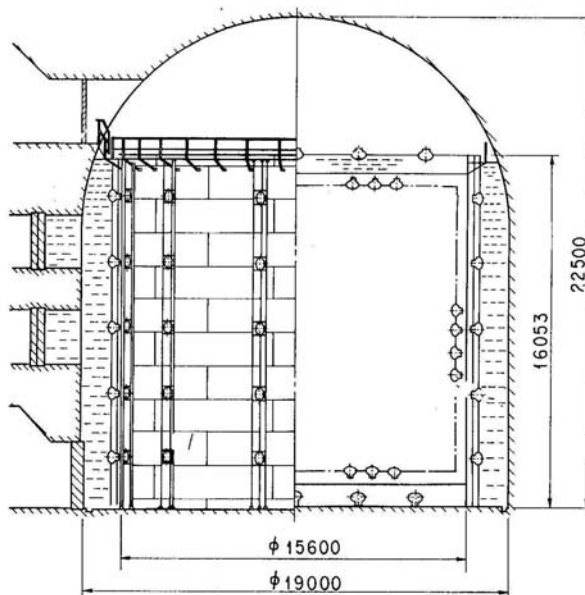


**Figure 2.** Schematic view of the Kamiokande-II detector.

a hermetic-live anticounter to veto cosmic-ray muons and to shield  $\gamma$ 's and neutrons entering from the outside of the detector; (2) enabling the water purification system to reduce radio activities sufficiently; and (3) installing the multi-hit time and charge measurement systems with multi-depth analog buffers.

The Kamiokande-II construction began in September, 1984. In April, 1985 the renewed water purification system turned on, although the detector water was insufficient in quality of radio impurity. The trigger rate under a 8.5 MeV detection threshold energy decreased rapidly with the same decay time as that of  $^{222}\text{Rn}$ . However we often suffered water leak troubles in the purification system. This obligated us to supply fresh water into the detector tank. Consequently a big jump-up of the trigger rate occurred due to much  $^{222}\text{Rn}$  in the fresh water. Fortunately such troubles calmed down until the end of December, 1986. Figs. 3 and 4 show the itinerary of our fights against water. Supernova SN1987A exploded during the period of a somewhat stable detector condition. Upgrading the Kamiokande detector toward realizing solar neutrino detection was paid back dramatically.

### 3. Reconfirmation of the solar neutrino deficit

Kamiokande-II permitted a study of low-energy contained electrons produced through the neutrino elastic scattering reaction  $\nu + e^- \rightarrow \nu + e^-$ . This was the first experiment to have a chance to confirm the solar neutrino deficit observed in the radiochemical  $^{37}\text{Cl}$  solar neutrino experiment (Homestake) of R. Davis, Jr., and collaborators [2][3]. In Kamiokande-II the initial position and momentum vector of the recoiling electron are measured. This therefore makes it possible to point the incident neutrinos back to the Sun. In addition, the observed electrons yield information concerning the energy spectrum of the incident  $\nu$ . This provides confident evidence of the  $^8\text{B}$  solar neutrinos which come from the fusion processes occurring inside the Sun.

The detector performance of Kamiokande-II was first presented at the 7th Workshop of Grand Unification/ICOBAN'86 [4]. The first report concerning the search for  $^8\text{B}$  solar neutrinos was

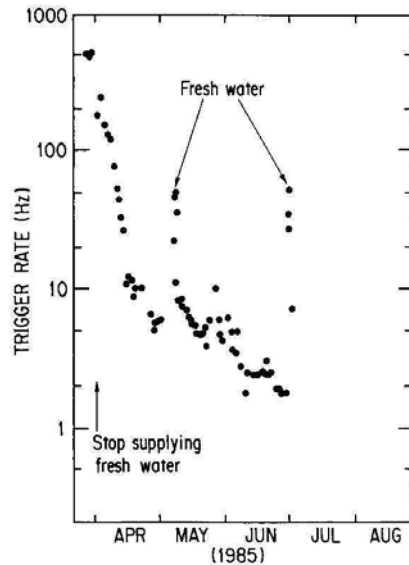


**Figure 3.** Change in the trigger rate after starting recirculation of the detector water. The threshold energy of the event trigger is 8.5 MeV.

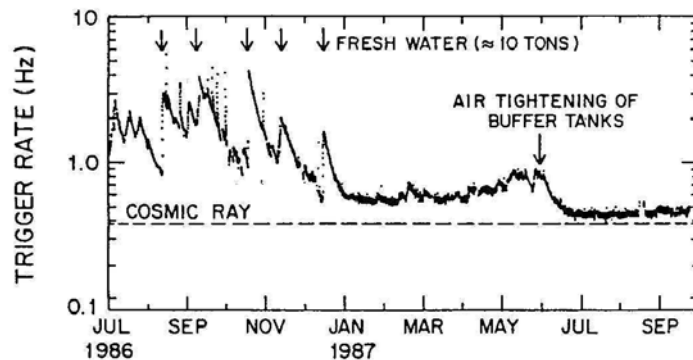


**Figure 4.** Change in the trigger rate since 1986.

reported in the 12th Int. Conf. on Neutrino'86 [5]. The finite-flux value of  $^8\text{B}$  solar neutrinos was published in 1989 [6] and 1990 [7]. The  $^8\text{B}$  neutrino flux obtained in a Kamiokande-II 1040-day data sample was  $0.46 \pm 0.13(\text{stst.}) \pm 0.08(\text{sys.})$  of the value predicted by the standard solar model [8]. Thus Kamiokande-II reconfirmed the solar neutrino deficit which was a long-standing puzzle for almost 20 years. This solar neutrino deficit was also confirmed by two experiments of Gallex [9] and SAGE [10] which used  $^{71}\text{Ga}$  as a target. A remarkable feature of the  $^{71}\text{Ga}$  experiment is the high sensitivity to the  $pp$  solar neutrinos produced in the primary stage of solar fusion process. In 1995 the results of the ratio of observation to prediction from the standard solar model were  $0.29 \pm 0.03$  for Homestake,  $0.48 \pm 0.08$  for Kamiokande-II,  $0.60 \pm 0.09$  for Gallex and  $0.52 \pm 0.09$  for SAGE. The distributions of  $\cos\theta_{SUN}$  for different live day data samples of Kamiokande-II are summarized in Fig. 5.

Where have solar neutrinos gone? The most plausible solution to the solar neutrino deficit based on non-standard neutrino physics was neutrino oscillations in vacuum or in matter. Fig. 6 shows the 90% confidence-level (C.L.) allowed regions of  $\nu_e \leftrightarrow \nu_\mu$  oscillations for the results of 4 experiments in the vacuum and matter schemes. The combined results of 4 experiments are shown by dark colored regions. Solar neutrino experiments provided the first promising data which indicated massive neutrinos. However it was uncertain at that time whether the solar neutrino deficit was trouble with solar physics or trouble with neutrino physics.

#### 4. Observation of the Atmospheric Neutrino Anomaly

Atmospheric neutrinos are generated from the decay of  $\pi$ 's,  $K$ 's and  $\mu$ 's produced in primary and secondary cosmic-ray interactions in the atmosphere. In the energy range below  $E_\nu \sim 1\text{GeV}$ , where all secondaries decay, it is roughly expected that  $(\nu_\mu + \bar{\nu}_\mu)/(\nu_e + \bar{\nu}_e) \simeq 2$ . This is because  $\pi^\pm \rightarrow \mu^\pm + \nu_\mu(\bar{\nu}_\mu)$  and  $\mu^\pm \rightarrow e^\pm + \nu_e(\bar{\nu}_e) + \nu_\mu(\bar{\nu}_\mu)$ . In 1988 Kamiokande published the paper entitled "Experimental study of the atmospheric neutrino flux", where it was pointed out the number of  $\mu$ -like single ring events ( $\nu_\mu, \bar{\nu}_\mu$  events) with  $\langle E_\nu \rangle \sim 700$  MeV (sub-GeV) was

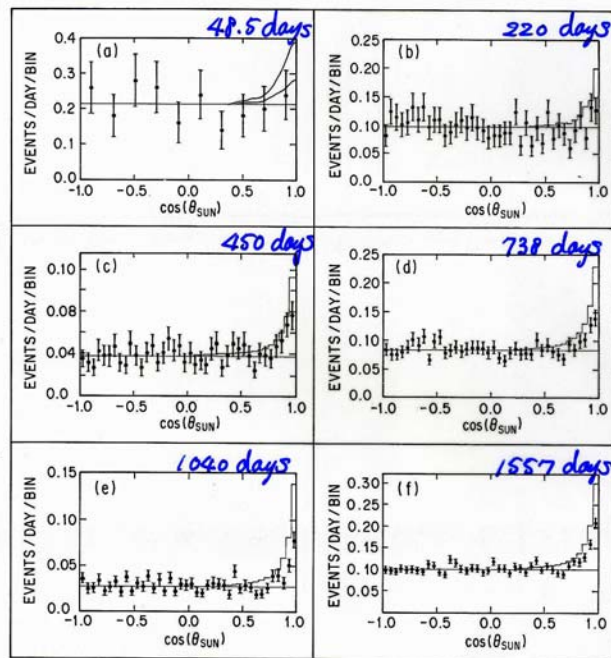


**Figure 5.**  $\cos \theta_{SUN}$  distributions for 48.5 days with  $E_e \geq 9$  MeV, 220 days with  $E_e \geq 9.6$  MeV, 450 days with  $E_e \geq 10.1$  MeV, 738 days with  $E_e \geq 10.1$  MeV for 450 days and  $E_e \geq 7.5$  MeV for 288 days, 1040 days with  $E_e \geq 9.3$  MeV for 450 days and  $E_e \geq 7.5$  MeV for 590 days and 1557 days with  $E_e \geq 9.3$  MeV for 449 days and  $E_e \geq 7.5$  MeV for 794 days.

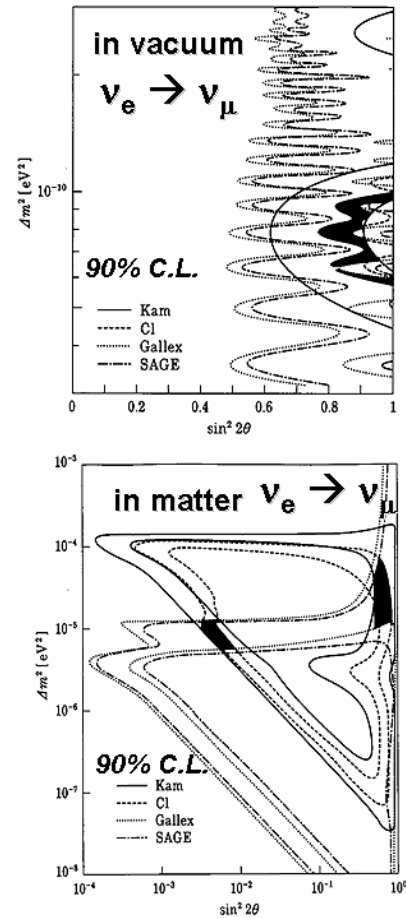


**Figure 6.** The 90 % C.L. allowed regions of the Homestake, Kamiokande, Gallex and SAGE experiments, and the combined data in vacuum and in matter.

smaller than the prediction as shown in Fig.7 [11]. The conclusion of this paper was that we were unable to explain the data as the result of systematic detector effects or uncertainties in the atmospheric neutrino fluxes. Accumulating more data, Kamiokande detected a small atmospheric  $(\nu_\mu + \bar{\nu}_\mu)/(\nu_e + \bar{\nu}_e)$  ratio in 1992 [12].  $R(\mu/e) \equiv [(\nu_\mu + \bar{\nu}_\mu)/(\nu_e + \bar{\nu}_e)]_{data}/[(\nu_\mu + \bar{\nu}_\mu)/(\nu_e + \bar{\nu}_e)]_{MC}$  was  $0.60^{+0.06}_{-0.05}(stat) \pm 0.05(syst)$ .  $R(\mu/e)$  should be 1, if the observation is equal to the prediction. This effect was called the atmospheric neutrino anomaly. In these days the atmospheric neutrino anomaly was not a common understanding in the neutrino community. Although IMB supported the Kamiokande result, 3 other experiments which used a tracking-type detector, showed no anomaly of  $R(\mu/e) \sim 1$ . Fig. 8 is the list of  $R(\mu/e)$  in these experiments in 1992. We often heard that the atmospheric neutrino anomaly was a water Cherenkov effect. There was the climate suspecting the efficiency of discriminating  $\mu/e$  for a water Cherenkov detector. The Kamiokande and IMB groups collaborated with the beam test experiment at KEK to investigate the detector performance, using known particles and constructing a 1000 ton water Cherenkov detector. Electrons, muons and pions produced by the KEK 12 GeV proton-synchrotron are used for verifying the  $\mu/e$  identification efficiency, the detection efficiency for

low momentum charged particles and the properties of pion-nucleus interactions. The results obtained in this beam-test showed enough capability of the  $\mu/e$  discrimination, and were well fitted to the Monte Carlo predictions of Kamiokande and IMB. This gave the confidence in the atmospheric neutrino anomaly.

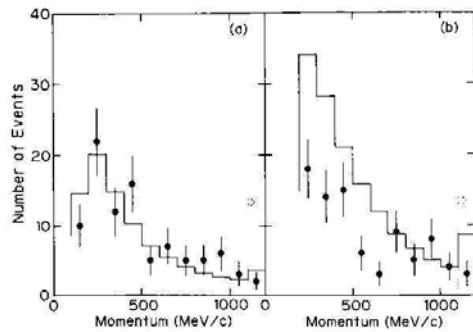


**Figure 7.** Momentum distributions of electron-like (left) and muon-like (right) sub-GeV events. The histograms show the distributions expected from atmospheric neutrino fluxes.

	NUSEX	Frejus	Soudan 2	IMB 3	Kamiokande
Exposure (kton-yr)	0.74	1.56	1.01	7.7	7.7
$\mu - e$ ID (efficiency)	good	95% ( $\nu_\mu$ ) 85% ( $\nu_e$ )	95%	92%	98%
Data					
e-like	18	57	35.3	325	248
$\mu$ -like	32	108	33.5	182	234
$\nu$ MC*					
e-like	20.5	70.6	28.7	257.3	227.6
$\mu$ -like	36.8	125.8	42.1	268.0	356.8
$(\mu/e)_{DATA}$	<b>0.99</b>	<b>1.06</b>	<b>1.90</b>	<b>3.50</b>	<b>5.10</b>
$(\mu/e)_{MC}$			<b>0.64</b>	<b>0.54</b>	<b>0.60</b>
(stat.)	+ 0.35 - 0.25	+ 0.19 - 0.16	$\pm 0.17$	$\pm 0.05$	$\pm 0.06$ $\pm 0.05$
(sys.)	$\pm$ small	$\pm 0.15$	$\pm 0.09$	$\pm 0.12$	$\pm 0.05$

**Figure 8.** Summary of atmospheric neutrino data from 5 experiments.

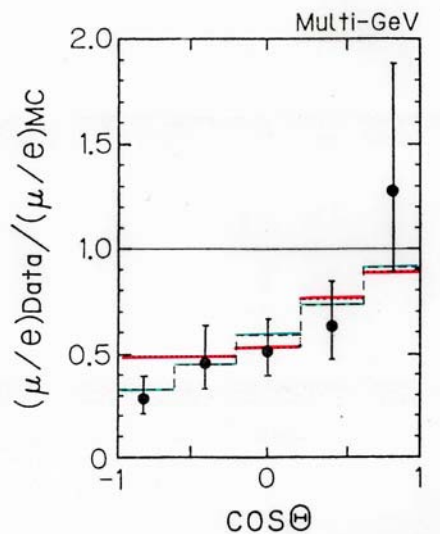


**Figure 9.** Zenith-angle distribution of  $R(\mu/e)$  for the multi-GeV events. Also shown are the expectations from the MC simulations with neutrino oscillations for  $\nu_\mu \leftrightarrow \nu_e$  by dashes and  $\nu_\mu \leftrightarrow \nu_\tau$  by dots.

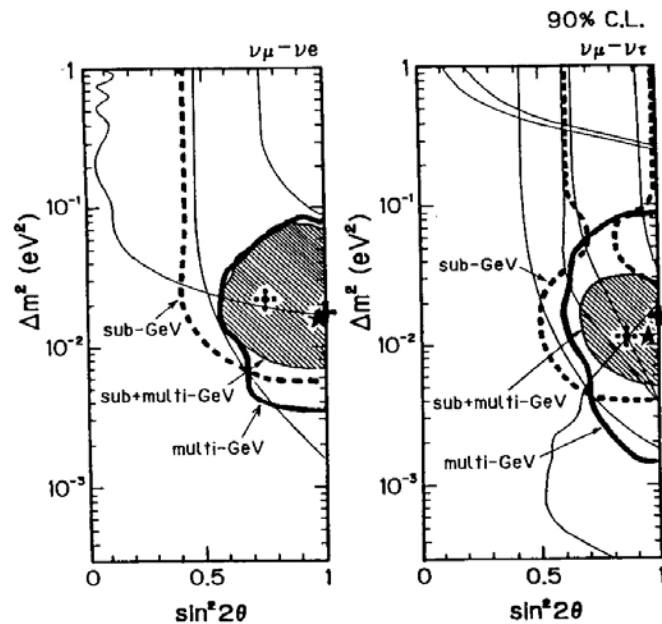


**Figure 10.** The 90% C.L. allowed neutrino oscillation parameters obtained from the multi-GeV (thick curves), sub-GeV (thick-dotted curves) and combined data (shaded areas). The best fit values are also shown for the sub-GeV (dashed crosses), multi-GeV (full crosses) and combined (stars) data.

In 1994 Kamiokande also showed the atmospheric neutrino anomaly for higher energy events with  $\langle E_\nu \rangle \sim 6$  GeV (multi-GeV). The observed  $R(\mu/e) = 0.57^{+0.08}_{-0.07}(stat) \pm 0.07(syst)$  [13]. And

Kamiokande demonstrated a clear non-uniform zenith-angle dependence of  $R(\mu/e)$  shown in Fig. 9. A possible explanation of this non-uniform zenith-angle distribution of  $R(\mu/e)$  together with the small  $R(\mu/e)$  sought in neutrino oscillations. The zenith-angle dependence of  $R(\mu/e)$  was analyzed assuming neutrino oscillations and yielded the best-fitted parameter sets  $(\Delta m^2, \sin^2 2\theta)$  of  $(1.8 \times 10^{-2}, 1.0)$  for  $\nu_\mu \leftrightarrow \nu_e$  and  $(1.6 \times 10^{-2}, 1.0)$  for  $\nu_\mu \leftrightarrow \nu_\tau$ . Combined the sub-GeV and multi-GeV data, the allowed oscillation parameter regions were shown in Fig. 10. The atmospheric neutrino anomaly was getting the position of the second indication of non-standard neutrino physics.

## 5. Conclusions

Kamiokande-II reconfirmed the solar neutrino deficit and became a motive power to understand solar physics and neutrino physics. Kamiokande-II detected the atmospheric neutrino anomaly. These two anomalies strongly suggested finite neutrino masses, and gave a confident motivation for constructing the next generation water Cherenkov detector, Super-Kamiokande. Fig. 11 is the slide which was used around 1994. It is not too much to say that the solar and atmospheric neutrino anomalies invited the discovery rush by the next generation experiments of Super-Kamiokande, SNO, K2K and KamLAND.

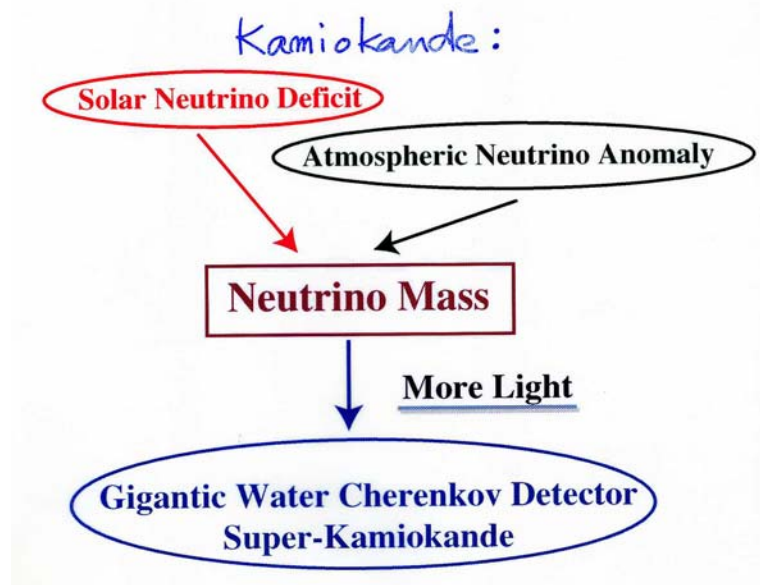


Figure 11. Slide which was used around 1994.

- [1] Koshiha M 1984 *Proc. ICOBAN'84, Utha.*
- [2] Davis R Jr. *et al.* 1968 *Phys. Rev. Lett.* **20** 1205
- [3] Rowley J.K *et al.* 1984 *Proc. AIP Conf. No.126*
- [4] Beier E.W 1986 *Proc. ICOBAN'86, Toyama*
- [5] Suzuki A 1986 *Proc. Neutrino'86, Sendai*
- [6] Hirata K.S *et al.* 1989 *Phys. Rev. Lett.* **63** 16
- [7] Hirata K.S *et al.* 1989 *Phys. Rev. Lett.* **65** 1297
- [8] Bahcall J.N and Ulrich P.K 1988 *Rev. Mod. Phys.* **60** 297
- [9] Anselmann P *et al.* 1994 *Phys. Lett.* **B327** 377
- [10] Abdurashitov J.N *et al.* 1994 *Phys. Lett.* **B328** 234
- [11] Hirata K.S *et al.* 1988 *Phys. Lett.* **B205** 416
- [12] Hirata K.S *et al.* 1992 *Phys. Lett.* **B280** 146
- [13] Fukuda Y *et al.* 1994 *Phys. Lett.* **B335** 237

# Neutrino cross section measurements with MiniBooNE

Rex Tayloe<sup>1</sup>

Physics Department, Indiana University, Bloomington, IN 47405, USA

E-mail: rtayloe@indiana.edu

**Abstract.** The MiniBooNE neutrino oscillation experiment has collected a large sample of charged- and neutral-current neutrino interaction events. These samples are important to understand the normalization and backgrounds in neutrino oscillation searches. They also reveal insight into the structure of the nucleus and nucleon. The MiniBooNE experiment is briefly described and neutrino interaction rates presented. Preliminary results are reported for neutral-current elastic scattering and neutral-current production of  $\pi^0$ .

## 1. Introduction

The MiniBooNE experiment [2], located at Fermilab and running since 2002, was designed to provide a precision search for neutrino oscillations of the type reported by the LSND experiment [3]. For maximum sensitivity to oscillations, the MiniBooNE experiment has been designed for high neutrino interaction rates and good particle identification capability [4]. This also allows for measurements of neutrino interaction cross sections with excellent statistical and systematic precision.

These measurements are important for systematic cross checks of detector efficiencies and background estimations for the MiniBooNE oscillation search. In addition, these measurements will also help future experiments such as MINOS [5], NOvA [6], and T2K [7] that are planned to run in the same neutrino energy range ( $E_\nu \approx 1 - 5$  GeV) by providing valuable cross section data.

In addition, the physics addressed by these measurements is interesting beyond simple utility for oscillation experiments. The neutrino provides a weak probe of the nucleus and/or nucleon in these processes. Does the neutrino “see” the same nucleus/nucleon as does the proton or electron in the scattering of these particles? In many cases neutrino scattering allows for the clearest view of the fundamental physics.

## 2. Experiment

The MiniBooNE experiment employs horn-focusing of pions produced in 8 GeV proton interactions on beryllium to yield a 99%-pure muon-flavor neutrino with an average neutrino energy of  $\approx 0.7$  GeV. There are very few neutrinos in this beam with  $E_\nu > 2$  GeV which results in low event rates from potential high-multiplicity backgrounds “feeding-down” to low energy.

<sup>1</sup> for the MiniBooNE collaboration [1]

The detector consists of a spherical tank containing 800 tons of mineral oil ( $\text{CH}_2$ ) viewed by 1280 20-cm-diameter photomultiplier tubes for 10% photocathode coverage of the surface area of the tank. In addition, a veto region with 240 photomultiplier tubes provides a signal for particles that enter or exit the main tank region. The time and charge recorded by these tubes in response to the Cerenkov radiation and the small amount of scintillation light that is emitted from charged particles enable the reconstruction of neutrino interactions of various types.

### 3. Neutrino Interactions in MiniBooNE

Both charged- and neutral-current neutrino interactions are observed in the MiniBooNE detector. The rates of these interactions (before efficiency corrections) are estimated via the NUANCE [8] neutrino interaction code. Charged-current quasielastic (CCQE) scattering is the most abundant process, comprising 42% of the total neutrino interaction rate. Charged-current production of a single pion ( $\text{CC}1\pi$ ) is second-most abundant at 26% of the interaction rate. The neutral-current elastic-scattering process (NC elastic) makes up 18% of the events and neutral-current production of pions is about 10%. The remainder of the events (4%) consist of charged- and neutral-current production of multiple pions and deep-inelastic-scattering processes.

#### 3.1. CCQE and $\text{CC}1\pi$

The CCQE and  $\text{CC}1\pi$  reactions are extremely important to identify and understand in MiniBooNE for the neutrino oscillation search. The  $\nu_\mu$  CCQE reaction ( $\nu_\mu C \rightarrow \mu^- X$ ) provides an important cross check of the  $\nu_\mu$  flux. The  $\nu_e$  CCQE reaction ( $\nu_e C \rightarrow e^- X$ ) is the oscillation signal channel. It is important for MiniBooNE to understand this reaction on carbon for which data does not exist.

The  $\text{CC}1\pi$  reaction ( $\nu_\mu C \rightarrow \mu^- \pi^+ X$ ) is the largest background for  $\nu_\mu$  CCQE and provides important information about  $\Delta$  production which is needed to constrain the  $\Delta \rightarrow N\gamma$  background in the oscillation search. In addition, *coherent*  $\text{CC}\pi^+$  production, is an interesting subject and the K2K experiment has set an upper limit [9].

MiniBooNE has extracted approximately 60k CCQE events and 40k  $\text{CC}1\pi$  from one-half of the existing neutrino data set and a first measurement of the ratio of these two channels has been made. Results from this analysis is available in Ref. [10]. That data is showing a suppression relative to a prediction from a relativistic fermi-gas model in the low 4-momentum-transfer ( $Q^2$ ) region. This effect is currently under further scrutiny and the analysis of the full MiniBooNE neutrino data set is currently in progress.

#### 3.2. NC elastic

The NC elastic reaction ( $\nu_\mu n, p \rightarrow \nu n, p$ ) is a unique weak-neutral-current probe of the nucleon. Unlike the CC channel, it is sensitive to the isoscalar content of the nucleon and may show the effects of strange quarks. The NC elastic reaction is identified in MiniBooNE by selecting for low-energy events with a small fraction of prompt light (the signature for proton/neutron scintillation only) and no associated muon decay.

The low-energy sample is shown in Fig. 1. A clear separation is visible in phototube hit times and the fraction of prompt hits between events with proton/neutron scintillation only (NC elastic events) and the ubiquitous muon-decay (Michel) electrons.

A NC elastic event sample has been extracted from approximately 10% of the total MB data sample. This sample consists of approximately 4000 events with an expected background of approximately 20%. The distributions of phototube hit multiplicity and total charge from this preliminary sample are shown together with the predicted distributions from the Monte Carlo (MC) simulation program in Fig. 2. Data-MC agreement is reasonable, however, the data shows more events in the lower extremes of the plots. The physics contained in these distributions is under investigation.

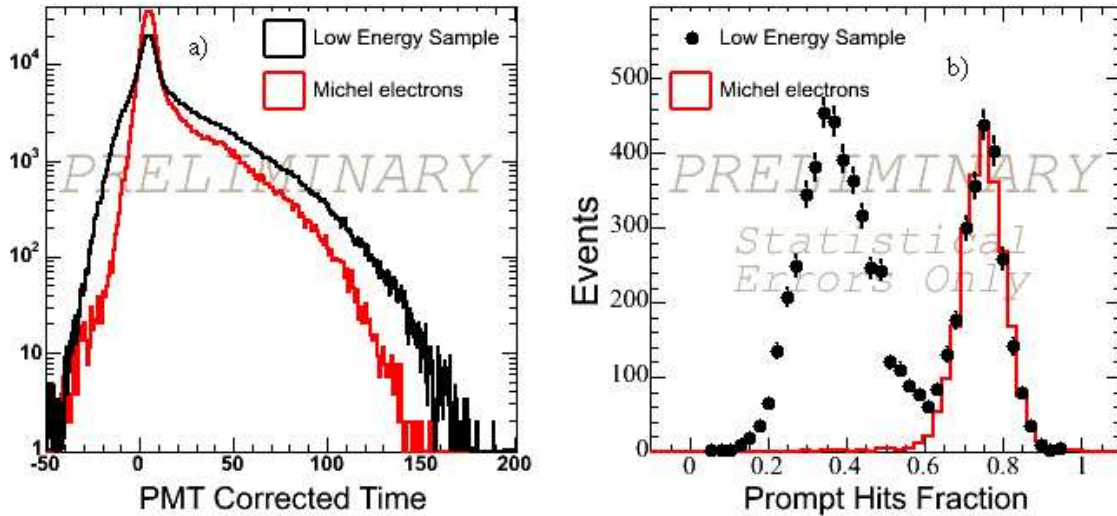


**Figure 1.** The distribution of phototube hit times a) and the fraction of prompt (between -5 and 15 ns) hits b) for the low energy (NC elastic) and muon-decay electron (Michel) samples.

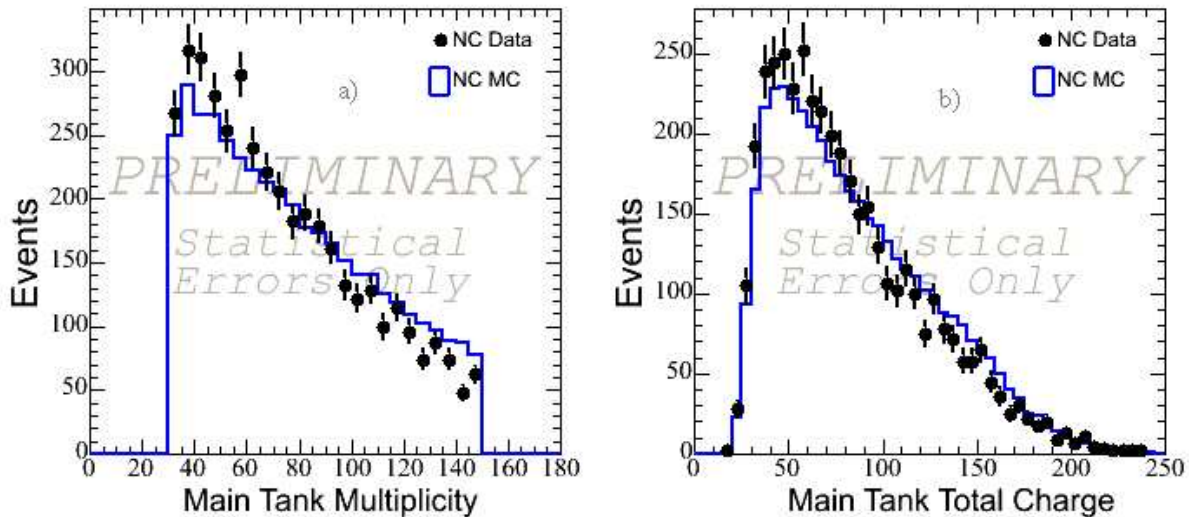


**Figure 2.** Phototube multiplicity a) and total phototube charge b) in the main tank for the NC elastic event sample. The data is shown as points with statistical errors only. The simulated data is shown as solid histograms.

### 3.3. NC $\pi^0$

The NC  $\pi^0$  production reaction ( $\nu_\mu C \rightarrow \nu\pi^0 X$ ) is a crucial channel for MiniBooNE as it contributes substantially to the  $\nu_\mu \rightarrow \nu_e$  oscillation search. Both resonant and coherent channels contribute to the process. The coherent channel — predicted to compose  $\approx 5 - 20\%$  of the total rate — is dominated by the axial current and, therefore, is unconstrained by any electron-scattering data. The existing data on the coherent process is extremely sparse and requires better measurements. The resonant and coherent rates may be separately extracted from the data via the different pion angular distributions in each process.

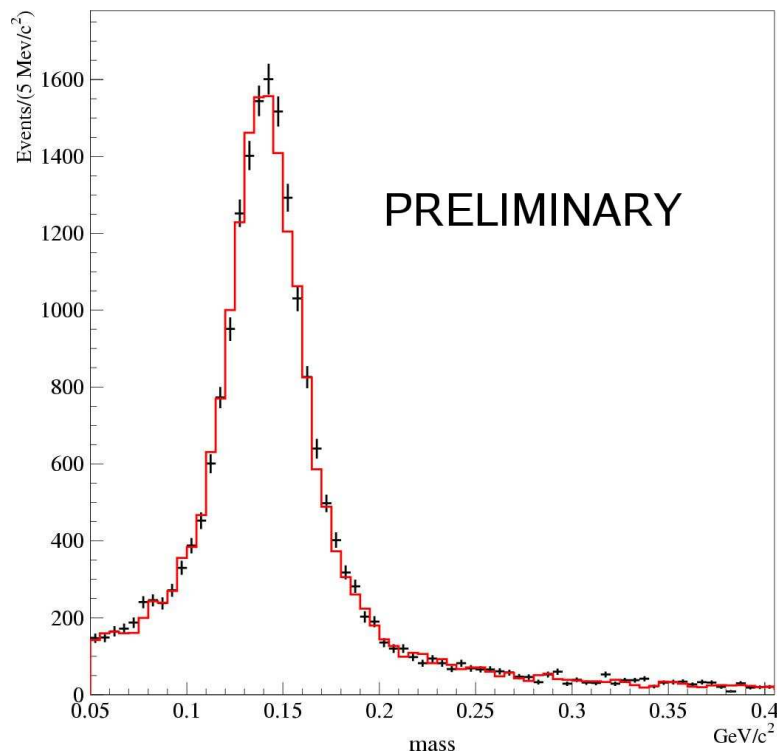


**Figure 3.** Preliminary reconstructed  $\pi^0$  mass distribution of NC  $\pi^0$  events. The data points are shown with statistical errors only. The simulated data after a fit to resonant, coherent, and background fractions is shown as a solid histogram.

The NC  $\pi^0$  reaction is extracted from the MiniBooNE event sample by search for events with no muon decays and a “2-ring” event topology consistent with the prompt decay of a  $\pi^0$  ( $\pi^0 \rightarrow \gamma\gamma$ ). The MiniBooNE NC  $\pi^0$  sample consists of 29k events and has a calculated background fraction of only 10%.

The reconstructed invariant mass of the  $\pi^0$  may be calculated from the energy and angle of the photons identified in the 2-ring event. This (preliminary) distribution is shown in Fig. 3 and compared to simulated data. The agreement is good.

The simulated data in Fig. 3 has been adjusted to the data via a fit that allows the resonant, coherent, and background fractions in the NC  $\pi^0$  sample to float. The results of that (preliminary) fit are shown in Fig. 4. The fit is performed to the quantity  $E(1 - \cos\theta)$  where  $E$  is the  $\pi^0$  energy and  $\theta$  is the lab production angle of the  $\pi^0$ . The coherent NC  $\pi^0$  process is expected to scale with this variable [11]. In this procedure, it is assumed that the  $\Delta$  that decay into  $\pi^0$  do so isotropically and the simulated  $\pi^0$  momenta have not been corrected to that observed in the data. These issues are currently under investigation. The resulting fit shows that the data is incompatible to a high confidence level with zero coherent NC  $\pi^0$  production.

#### 4. Summary and Conclusions

The MiniBooNE experiment has collected large samples of both charged-current and neutral-current neutrino-carbon interactions. Both charged-current quasielastic and charged-current  $\pi^+$  production channels show a low- $Q^2$  suppression that is currently under further investigation.

A sample of neutral-current neutrino-nucleon elastic-scattering events has been cleanly identified and compared with data. The investigation of systematic errors and extraction of the cross section is in progress.

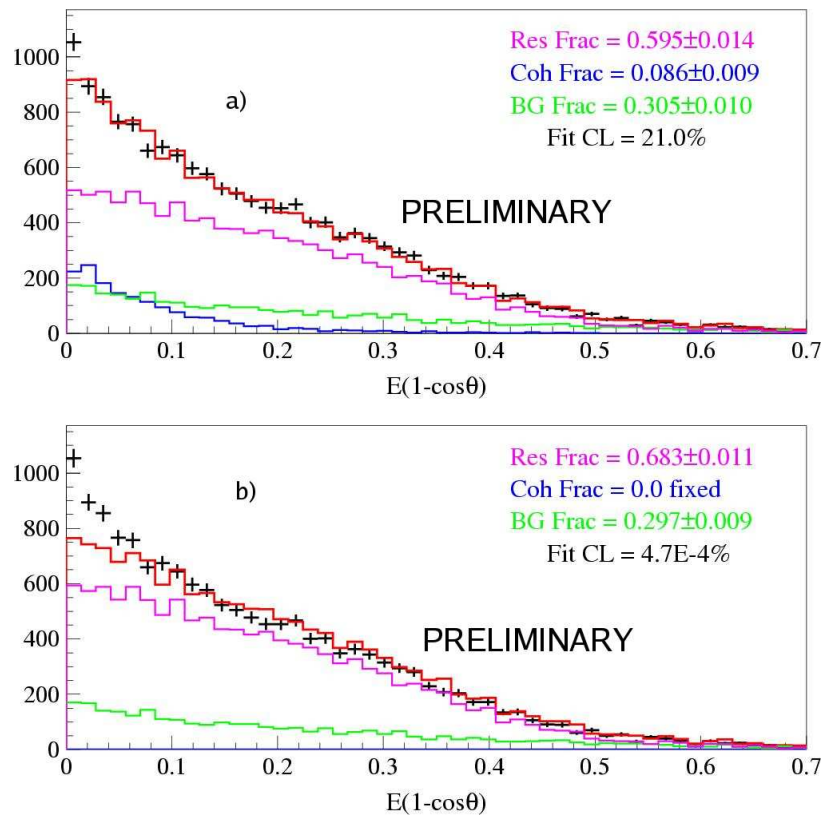


**Figure 4.** Preliminary distribution of  $E(1 - \cos \theta)$  for NC  $\pi^0$  events. The data are shown as points with statistical errors only. The resulting simulated data distribution is overlaid and the individual resonant, coherent, and background components indicated. Plot a) shows simulated data with all three components allowed to vary. In plot b), the coherent fraction was fixed to be zero.

A large sample of neutral-current neutrino  $\pi^0$  events has been identified in MiniBooNE. This allows for a measurement of the background that this reaction contributes to the  $\nu_\mu \rightarrow \nu_e$  oscillation search. The reconstructed  $\pi^0$  mass distribution agrees well with simulation. A fit has been performed and a non-zero contribution from coherent NC  $\pi^0$  is evident in the data.

### Acknowledgments

This work has been supported by NSF Grant NSF-PHY-0457219.

### References

- [1] <http://www-boone.fnal.gov/cgi-bin/collaboration>
- [2] R. Tayloe [MiniBooNE Collaboration], Nucl. Phys. Proc. Suppl. **118**, 157 (2003).
- [3] A.A. Aguilar *et al.* [LSND Collaboration], Phys. Rev. D **64**, 112007 (2001).
- [4] B. Fleming, "Progress on a Neutrino Oscillation Search at MiniBooNE", *these proceedings*.
- [5] P. Adamson *et al.* [MINOS Collaboration], [arXiv:hep-ex/0512036].
- [6] D. S. Ayres *et al.* [NOvA Collaboration], arXiv:hep-ex/0503053.
- [7] Y. Itow *et al.*, [arXiv:hep-ex/0106019].
- [8] D. Casper, Nucl. Phys. Proc. Suppl. **112**, 161 (2002).
- [9] M. Hasegawa *et al.* [K2K Collaboration], Phys. Rev. Lett. **95**, 252301 (2005).
- [10] arXiv:hep-ex/0602050.
- [11] D. Rein and L. M. Sehgal, Nucl. Phys. B **223**, 29 (1983).

# What we know and do not know about neutrino production in stars

**Sylvaine Turck-Chièze**

SAP/DAPNIA/CEA CE Saclay Bat 709 91191 Gif sur Yvette, France

E-mail: cturck@cea.fr

**Abstract.** This review summarizes the necessary ingredients for determining the neutrino production rates in stars. Then the case of the Sun is studying. A detailed comparison between solar neutrino predictions and each neutrino detection shows the interest of the seismic model versus standard model. After the determination of  $\theta_{12}$ ,  $\Delta m_{12}^2$  and the inclusion of electronic neutrino transformation, the global agreement is a noticeable success with nevertheless some identified questions. The second part of the review is dedicated to the important lacks in solar and stellar modelling and to the way we are presently attacking the different problems. Such situation encourages to pursue the effort on stellar neutrino detections and neutrino predictions, astrophysics modelling with evident consequences for stellar evolution, supernovae explosion and neutrino properties.

## 1. Introduction

Stellar neutrinos have been studying for decades through solar and type II supernova neutrinos. These two cases are totally different due to the energy released by this elusive particle which does not modify the solar equilibrium but plays a fundamental role in the supernova explosion.

It was a great event to detect few supernova neutrinos in 1987 and they have produced a lot of works on the knowledge of supernovae and neutrinos. But it is clear that the solar neutrinos have played a dominant role in the neutrino community during the last 30 years. They were already a subject of discussion in the thirties when H. Bethe was proposing the nuclear energy as THE missing element to understand the age of the Sun and then he has always studied stars to look for their properties. Then our dedicated colleagues R. Davis and J. Bahcall have never released their efforts up to get firm conclusions, solar neutrinos have been wonderful opportunities for advance on neutrino properties and subtle guides for progress in stellar evolution. We are all extremely grateful toward these three great physicists for their role in this field thanks to their determination, inspiration and permanent works dedicated to this field. Nevertheless, it seems to me that we are today only at the beginning of the road. The real goal is to establish the strict number of neutrinos and their mass in order to use these particles as probes for activities we have maybe not yet imagined. We are facing great challenges and the best way to advance is to go step by step in looking for coherence without neglecting any established fact.

This review will be separated in three parts: the first section will be devoted to the way we calculate neutrino productions in stars and the application to the Sun, the second one to what we do not know yet on stars, how we progress and the consequences for supernovae neutrinos, finally the last section will be dedicated to the perspective on neutrino properties and neutrino astronomy.

## 2. Neutrino production in stars: application to the solar case

The determination of the neutrino production rates supposes to know the cross section of each reaction rate (NP) producing neutrinos, the number of species of the reactants (A) and also the temperature and density profile (A) in the region where the neutrino is emitted (NP). Moreover if one would like to compare predictions with detected neutrinos one needs to add the knowledge of the cross section neutrino- detector (NP) and the radial profile of electron and neutron density in the star (A) for determining the theoretical oscillation parameters (PP). I have noted in parenthesis the abbreviations NP for nuclear physics PP for particle physics and A for astrophysics.

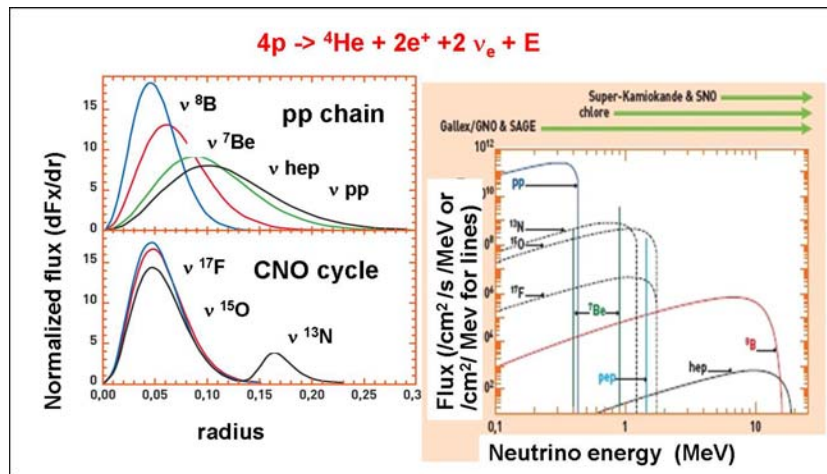


**Figure 1.** Location of emission of solar neutrinos and sensitivity of the different detectors

One notes that a precise prediction of emitted neutrinos requires information coming from the three disciplines at the same level of accuracy. Figure 1 shows the different regions of emission for each source of neutrinos in the solar case. They result from the details of the reaction rate cross section: those neutrinos which strongly depend on temperature are emitted in the real center of the Sun contrary to the pp neutrinos which are emitted in the whole nuclear core; they are consequently extremely dependent on stellar conditions and on the properties of the plasma. Table 1 and references therein illustrates the case of boron 8 neutrinos which is the only case where we can directly compare prediction with detection! For more than two decades, the neutrino predictions coming from the astrophysical community were in disagreement with the measured neutrino fluxes. It is why we have improved along time the prediction estimate in injecting the progress done on the characteristics of the plasma thanks to the nuclear new experiments, atomic calculations and helioseismic observations. Before 1993, the calculation was a pure theoretical calculation extracted from the four structural equations of stellar evolution. Then we have first used seismology as a guide for questioning some inconsistency as the observed quasi primordial photospheric helium which has pushed the introduction of the microscopic diffusion. It has resulted a better agreement between solar model predictions in particular between Bahcall team and our Saclay models. In 2001, after extraction of a precise sound speed down to  $0.05 R_{\odot}$  [6], we have added, for what we call the seismic model, a supplementary constraint: to impose a temperature profile which respects the observed sound speed obtained by the knowledge of the acoustic modes. We notice that its prediction agrees extremely well with the measured value (inside the error bars) obtained with the SNO detector (filled with heavy water) which is sensitive to all the different neutrino flavours. This is the great success of the last 5 years: a real consistency between the two solar probes even there is still fluctuations in the predictions of the standard model.

**Table 1.** Time evolution of the neutrino flux prediction associated to the reaction  ${}^7\text{Be}(p, \gamma){}^8\text{B} \rightarrow {}^8\text{Be}^* + e^+ + \nu_e \rightarrow {}^4\text{He}$ , for Saclay solar models.  $T_c$  and  $Y$  initial are the corresponding central temperature, initial helium content. Problem solved: origin of the improvements introduced in the corresponding solar model and maintained in the following ones. Comparison with the recent results of the SNO detector [1] and references therein

Flux	Boron flux	Tc	Y initial	Model	Problem solved	References
1988	$3.8 \pm 1.1$	15.6	0.276	Standard model	CNO opacity, ${}^7\text{Be}(p, \gamma)$	[2]
1993	$4.4 \pm 1.1$	15.43	0.271	Standard model	Fe opacity, screening	[3]
1998	4.82	15.67	0.273	Standard model	Microscopic diffusion	[4]
1999	4.82	15.71	0.272	Standard model	Turbulence in tachocline	[5]
2001	$4.98 \pm 0.73$	15.74	0.276	Seismic model	Best physics + sound speed	[6]
2003	$5.07 \pm 0.76$	15.75	0.277	Seismic model	magnetic field, relativ. EOS	[7]
2004	$4.35 \pm 1.2$	15.54	0.262	Standard model	new CNO value, ${}^7\text{Be}$ & ${}^{14}\text{N}(p, \gamma)$	[8]
2004	$5.31 \pm 0.6$	15.75	0.277	Seismic model	${}^7\text{Be}(p, \gamma)$ , ${}^{14}\text{N}(p, \gamma)$	[8]
SNO results $5.44 \pm 0.99$ (CC+ES 2001) $5.09 \pm 0.44 \pm 0.45$ (NC 2002)						
$5.27 \pm 0.27 \pm 0.38$ (2004) $4.94 \pm 0.06 \pm 0.34$ (2005) active neutrinos						

**Table 2.** Neutrino predictions of the present standard model and of the seismic model compared to detections. For water experiments, the results are given in flux, the values must be multiplied by  $10^6$  and are expressed in  $\text{cm}^{-2}\text{s}^{-1}$

	Predictions without neutrino oscillation	Predictions with neutrino oscillation
Chlorine detector		[9]
Standard model	6.315 SNU	2.24 SNU
Seismic model	$7.67 \pm 1.1$ SNU	$2.76 \pm 0.4$ SNU
Detection		$2.56 \pm 0.23$ SNU
Gallium detectors		[10]
Standard model	120.9 SNU	64.1 SNU
Seismic model	$123.4 \pm 8.2$ SNU	$67.1 \pm 4.4$ SNU
Experiment		$67.7 \pm 3.6$ SNU
Water detectors	SNO [1]	SNO and SuperKamiokande [11]
Standard model	4.35	1.35 (for $\nu_e$ detected only)
Seismic model	$5.31 \pm 0.6$	$1.65 \pm 0.19$
SNO	$5.27 \pm 0.27 \pm 0.38$	$1.76 \pm 0.06 \pm 0.09$
SuperKamiokande		$2.35 \pm 0.08$ including some $\nu_\mu, \nu_\tau$

For the other neutrino detectors, we add to the neutrino predictions the energy dependent reduction factor due to neutrino oscillations, derived from [12] and confirmed by Kamland for the MSW part. With such hypothesis, the electronic neutrinos are partially transformed in muon or tau neutrinos through vacuum oscillation for pp and  ${}^7\text{Be}$  neutrinos and mainly through MSW oscillation for  ${}^8\text{B}$  neutrinos. We introduce also for gallium and chlorine the neutrino interacting cross section with the detectors. Doing so, the agreement between the predictions of the seismic model and all the detectors is satisfactory (inside the error bars) as shown in table 2. The

present standard model which includes the reduction by 30% of the CNO composition, leads to a greater discrepancy between predictions and detection of neutrino fluxes. This point has been also noticed by Bahcall and collaborators in [13]. The error bar of the predictions coming from the standard model is not so easy to establish, at least for the astrophysics part, it is why we have not mentioned it in table 2 So let summarize this section in answering to the initial question.

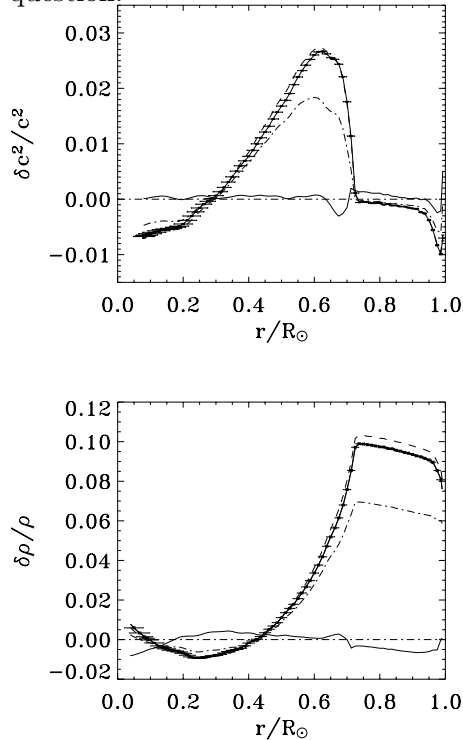


**Figure 2.** Squared sound speed and density profile discrepancies between models and seismic observation established with GOLF and MDI aboard SoHO [6] for three new updated standard models all including a revision of the CNO composition (full line with seismic error bars, dot line, dot dashed line, see details in [8]) and for the seismic model (full line).

#### *What we know on neutrino predictions*

During the last two decades, three fundamental ingredients of the neutrino production have been clearly improved:

- In NP, the solar nuclear reaction rates through experiments, theoretical extrapolation and screening estimates together with the neutrino-species cross sections for all the solar neutrino detectors with unprecedented accuracy (see review of R. Menagazzo these proceedings). The main efforts must be concentrated now on more advanced stages of stellar evolution,
- in A, the observed sound speed profile is properly established down to  $0.05 R_\odot$  [6]. This puts an adding constraint on the temperature profile in the region where neutrinos are emitted, if the product abundance  $\times$  opacity is under control.
- in PP, the transformation from electronic neutrinos to muon or tau neutrinos through MSW is demonstrated by SNO, confirmed by Kamland for the high energy part and the corresponding reduction could be properly introduced after the establishment of the emitted neutrinos.

#### *What we do not know*

- In A, a detailed knowledge of the solar abundance is important to establish the proper photon-nucleus interaction, the consequent solar central temperature and also the CNO neutrinos. After reestimate of solar iron in 1993, a new reestimate of CNO photospheric abundance leads to a reduction of at least 30% announced by Holweger then by Asplund et

al. [14]. The recent value seems strongly established as they use a better description of turbulent atmosphere but is not in agreement with some new tentative to extract those abundances from helioseismology. Moreover the density profile (figure 2) is not yet sufficiently established to guarantee that the standard hypotheses are sufficient. We will see on the next paragraph why it is important to go further.

- In PP, the reduction of electronic neutrino at low energy by 57% instead 31% is not established and the global agreement for all the neutrino detectors could be artificial as the oscillations parameters are extracted partly from the observations.

### 3. Dynamical processes in stars

In some sense, the previous paragraph summarizes the success of nuclear stellar evolution: understanding the large scales which justify that the Sun is a billion years star as a lot of others in the Universe. But the fascinating development of helioseismology is justified by observations of internal motions due to the fact that the Sun is rotating and that it is an active star (see reviews of [15],[16]). This point is important for understanding the small timescales of stars: centuries, decades and probably even explosion times. This progress is important for two reasons:

- the dynamical processes are needed for a better understanding of the real interaction between the Sun and our planet. We would like to establish especially what is the quantitative role of the Sun in the Earth warming [17],
- these dynamical processes are significantly more important in massive stars. Massive stars are rotating quicker than the Sun and these phenomena have strong effects on the internal structure. Moreover, all the forgotten processes will impact on the presupernova type II structure and consequently on their neutrino productions and explosion mechanisms.

The Sun stays a reference for the whole Astrophysics. In fact it is up to now the only star for which we are able to check in situ the theoretical hypotheses of stellar evolution. Some crucial quantities are now observed as the sub-surface meridional flows, the zonal flows and the profile of the rotation down to the limit of the core. We can even follow them with time along the 11 year cycle and some smaller periodicity of 1.3 year near the tachocline region is suggested by the helioseismic observations in different instruments. More and more realistic dynamo models are developed to explain not only the mean 11 year period but series of cycles. But the prediction stays difficult and controversial because direct measurement of the internal magnetic field has not been obtained yet. An upper limit of 3 MG for the core is deduced from the estimated deformation of the Sun [18]. So, the pursuit of helioseismic observations with improved instruments is crucial to get the complete dynamics down to the core and to catch the different actors. Gravity modes have been searched for more than 20 years but we know now that they are detectable. Gravity mode multiplet candidates have been identified with the GOLF spectrometer in the upper frequency range [19]. Such modes are very sensitive to the core and to the whole static and dynamics radiative zone [20, 21, 22]. In the lower asymptotic regime of the spectrum one has detected a strong signal compatible with the asymptotic behaviour of the dipole modes [23]. These two analyses both suggest that the rotation is higher in the solar core than in the rest of the radiative zone as a relic of the young Sun [17]. Such information is extremely important to put constraints on magnetic fields in the solar nuclear core.

In parallel 3D MHD calculations of portions of Sun are developing. They have the objective to reproduce and explain the solar internal dynamics. A new challenge is to reproduce the flat radiative rotation profile [24] and the thin tachocline potentially sustained by the development of a magnetic field in the radiative zone to block the extension of the differential rotation downward [25]. Moreover transport of angular momentum begins to be introduced in stellar evolution equations and the role of gravity waves becomes important for the Sun and massive stars including in the supernovae explosions.

## 4. Perspective for the coming years

### 4.1. *the low neutrino energy spectrum*

In fact we have today direct access to only one source of neutrinos: the boron 8 one. Next year we will detect with Borexino and may be Kamland the second source due to the  $(p, {}^7\text{Be})$  interaction, this progress is extremely important to see the coherence or not with the previous conclusions, to check the astrophysical prediction and the presence or not of sterile neutrinos. To obtain an independent measurement of the pp neutrinos is a very fundamental objective, it is also useful to validate the "known" neutrino properties. Today the agreement between prediction and detection is at the level of 10% on the mean value of three types of detection. Going further, in analyzing the different sources independently may reveal other subleading effects like magnetic interaction or other astronomical properties as mentined in the previous section. The oscillation parameters must be checked on the whole energy spectrum to see properly the shape of the oscillation probability spectrum.

### 4.2. *neutrino fluxes variability*

After more than thirty years of neutrino detection, we do not know if some fluxes are varying or not. If boron 8 neutrinos seem stable, several reports have mentioned possible variability in chlorine detection or in gallium detection (see Caldwell talk these proceedings and Gavrin talk these proceedings). Today it is extremely difficult to demonstrate such variability or to be sure that it is only statistical effects and we use generally a mean value on a long period of time or between two detectors for the chemical neutrino detection. We need to progress on this point because consequences of potential variabilities are important: effect of 11 year solar cycle, effect of internal radiative zone reconfiguration, effect of neutrino properties at low energy. To progress on this point one needs a better signal/noise and an effort on the low energy spectrum with not too poor statistics.

### 4.3. *temperature profile*

We notice today that the quality of the boron 8 neutrino detection leads to a very proper determination of the central temperature. 10% of accuracy leads a determination of the central temperature better than 0.5% if there is no other source of uncertainty. If the absolute value is difficult to guarantee as mentioned in table 1, the relative accuracy is sufficient to transform this source of neutrinos as a remarkable temporal thermometer of the very central region. In extrapolating this remark to CNO neutrinos and at lower level to pp neutrinos, if there is any variability of the temperature in the region of emission of any neutrinos on timescale of decades or more, neutrinos would be the best probe to follow it in time, so I consider that we enter in the area where solar neutrinos are among others an important astronomical observatory for the developing field called *space climate* whose the objective is to better follow the influence of the Sun on the Earth warming.

### 4.4. *CNO neutrinos*

The mass of the Sun is sufficiently low for burning hydrogen mainly through pp reaction chains, it is not the case for massive stars where the first stage is dominated by the faster CNO cycle. Today there is some doubt on the solar CNO composition. Measuring CNO neutrinos is a very interesting challenge for particle physics with nuclear and astrophysics interesting clues.

These different remarks show that continuing the solar neutrinos program is extremely exciting for the three disciplines: astronomy, nuclear physics and particle physics. Numerous waited results and challenges continue to keep this field extremely attractive.

In parallel real progress for better understanding massive stars and final stage of evolution will appear thanks to the space asteroseismic COROT and KEPLER missions which encourage large neutrino detectors for detecting far supernovae neutrino explosions.

## 5. Acknowledgments

I would like to thank all my colleagues quoted in the references who contribute on different aspects of this field: theory, seismic observation and instrumentation.

## 6. References

- [1] SNO collaboration  
Ahmed et al. 2004 *Phys. Rev. Lett.* **92** 181301  
Aaharmim et al. 2005 *Phys. Rev. C* **72** 055502 and references therein
- [2] Turck-Chièze S. et al. 1988 *ApJ*. **335** 415
- [3] Turck-Chièze S. & Lopes I. 1993 *ApJ*. **408** 347
- [4] Brun A. S., Turck-Chièze S. & Morel, P. 1998 *ApJ*. **506** 913
- [5] Brun A. S., Turck-Chièze S. & Zahn, J. P. 1999 *ApJ*. **525** 1032
- [6] Turck-Chièze S. et al. 2001 *ApJ*. **555** L69
- [7] Couvidat S., Turck-Chièze S. & Kosovichev A. 2003 *ApJ*. **599** 1448
- [8] Turck-Chièze S. et al. 2004 *Phys. Rev. Lett.* **93** 1102
- [9] Lande K. et al. for the Homestake collaboration 1999 *Nucl. Phys. Suppl.* **77** 13
- [10] Gavrin these proceedings for the mean values between GALLEX, GNO and SAGE
- [11] Hosaka et al. for the Superkamiokande collaboration, *Phys. Rev. D* **73** 112001
- [12] Bahcall, J. N., Pena-Garay, C. 2004 *New J. of Phys.* **6** 63
- [13] Bahcall, J. N. et al. 2006 *ApJS*. **165** 400
- [14] Asplund, M., Grevesse, N. & Sauval, A. J. 2004 *A & A* **417** 751
- [15] Christensen-Dalsgaard, 2002 *Rev Mod Phys* **74**, 1073
- [16] Turck-Chièze S. et al., 2005, Cosmic Vision ESA astro-ph/0510854, ESA-SP 588 39th ESLAB symposium: Trends in Space Science and Cosmic Vision 2020, p 193
- [17] Turck-Chièze S. et al., 2006, The DynaMICS perspective ESA-SP 624 in *SoHO18/GONG 2006/HELAS1*, in press.
- [18] Friedland, A., Gruzinov, A., 2004, *ApJ* **601**, 570
- [19] Turck-Chièze, S., Garcia, R.A., Couvidat, S., et al. 2004, *ApJ* **604**, 455
- [20] Cox, A. N. & Guzik, J. A. 2004, *ApJ* **613** L169
- [21] Rashba, T. I., Semikoz, V. B., Valle, J. W. F. 2006, *MNRAS* **370** 845
- [22] Mathur, S. et al. 2006 ESA-SP 624, in *SoHO18/GONG2006/HELAS1* in press.
- [23] Garcia, R. A., Turck-Chièze, S., Jimenez-Reyes, S. et al. 2006 ESA-SP 624, in *SoHO18/GONG2006/HELAS1* in press.
- [24] Couvidat, S., et al. 2003b, *ApJ* **597**, L77
- [25] Brun, A. S. & Zahn, J.-P. 2006, *A&A* accepted

# Properties of the Tau-Neutrino

George S. Tzanakos†

University of Athens, Department of Physics, Division of Nuclear and Particle Physics, Panepistimioupoli, Zografou, 15771 Athens, Greece

tzanakos@phys.uoa.gr

**Abstract.** The  $\nu_\tau$  was postulated to exist after the discovery of the tau-lepton in 1975. First  $\nu_\tau$  CC interactions was observed in 2000 by the DONuT experiment at Fermilab, which also set a limit on the magnetic moment. Electron positron collider experiments have studied the tau-lepton decays and measured the Michel parameters, the tau lifetime, and the number of the light neutrino species. In addition a direct upper limit of the tau-neutrino mass was measured. This paper gives a short review of the known properties of the tau-neutrino, along with preliminary results from DONuT on the measurement of the  $\nu_\tau$  CC DIS cross section.

## 1. Introduction

The discovery of the  $\tau$ -lepton [1] in 1975 lead to the postulation of the existence of a weak isospin  $\frac{1}{2}$  partner, the tau-neutrino,  $\nu_\tau$ . Twenty five years later, in 2000, the  $\nu_\tau$  was observed in the laboratory via its charged current interaction with nuclei [2] signaled by the production of the  $\tau$ -lepton, in a way similar to the observation of the electron neutrino [3] and the muon neutrino [4] in 1956 and 1962 respectively. The difficulty in the detection of the  $\nu_\tau$  was two-fold: (i) Production of a  $\nu_\tau$  beam from an active proton beam dump facility with  $\nu_\tau$ 's produced in  $D_s$  decays. (ii) Detection of the  $\tau$ -lepton in a  $\nu_\tau$ -Nucleus CC interaction. This would require a detector with high spatial resolution. The DONuT (Direct Observation of the NuTau) was proposed in 1994 in an attempt to observe the  $\nu_\tau$ -Nucleus CC interactions. In the following we will first present the initial indirect evidence for the  $\nu_\tau$ , then discuss the DONuT experiment, the data analysis and preliminary latest results including a first measurement of the  $\nu_\tau$  CC DIS cross section and the limit on the  $\nu_\tau$  magnetic moment. Then we will discuss properties of the  $\nu_\tau$  coming from  $\tau$ -lepton decay studies at collider experiments.

## 2. Early Indirect Evidence

The indirect evidence for the existence of the  $\nu_\tau$  comes mainly from the studies of the  $\tau$ -lepton decays. It was shown that the anomalous  $e\mu$  pairs produced in  $e^+e^-$  annihilation [1] were due to the production of a pair of sequential leptons  $\tau^+$ ,  $\tau^-$ , with a mass about 1.9 GeV/c<sup>2</sup> and spin  $\frac{1}{2}$ . Thus, it should have a partner, " $\nu_\tau$ ", with V-A coupling. Initial studies of  $\tau$  decays with the DELCO experiment [5] in 1979 gave a Michel parameter  $\rho = 0.72 \pm 0.15$ , evidence of V-A coupling. First measurements of the strength of the coupling came from MARK II experiment [6] which measured a statistically significant nonzero value of the tau lifetime  $\tau_\tau = (4.6 \pm 1.9) \times 10^{-13}$ s, consistent with the expectation of  $2.91 \times 10^{-13}$ s for  $\tau$ - $\mu$  universality. The " $\nu_\tau$ " helicity was measured by ARGUS in 1990 [7] by studying the decay  $\tau^- \rightarrow a_1^- \nu_\tau \rightarrow (\rho^0 \pi^-) \nu_\tau \rightarrow \pi^+ \pi^- \pi^- \nu_\tau$ . In this decay the  $\rho^0$  can pair with either  $\pi^-$ , namely there should be two diagrams to be added, leading to a parity violating asymmetry which would manifest itself as

an asymmetry in the orientation of the 3-pion plane with respect to the  $\tau$  direction in the 3-pion rest frame. This asymmetry is predicted to be proportional to the quantity  $\gamma_{AV} = 2g_A g_V / (g_A^2 + g_V^2)$ . Measurement of this quantity gave  $\gamma_{AV} = 1.14 \pm 0.34_{-0.17}^{+0.34}$ , consistent with the Standard Model prediction of  $\gamma_{AV} = 1$  for a negative helicity  $\nu_\tau$ . The  $\nu_\tau$  spin was shown to be  $\frac{1}{2}$ , with the assumption of zero  $\nu_\tau$  mass, from the analysis of the decay  $\tau^- \rightarrow \rho^- \nu_\tau$  by the ARGUS collaboration [8]. The question whether the  $J=1/2$ , negative helicity, V-A partner of the  $\tau$ -lepton could be identified with  $\nu_\mu$  or  $\nu_e$  was settled by Fermilab experiment E531 [9], which measured the possible direct couplings  $G_F'$  of the  $\tau$  to  $\nu_\mu$  and  $\nu_e$  and found that  $G_F'/G_F < 0.002$  and  $0.073$  correspondingly, showing clearly that the  $\tau$ -lepton does not couple directly to  $\nu_\mu$  or  $\nu_e$ . Finally, in 1989, the ALEPH experiment was the first to measure the number of light neutrino species to be  $N_\nu = 3.27 \pm 0.30$  [10], ruling out the possibility of a fourth type of light neutrino at 98% CL.

### 3. The DONuT Experiment

The DONuT (Direct Observation of the NuTau) Experiment was designed to observe directly the CC interactions of the tau-neutrino. An 800 GeV proton beam dump was used to produce  $\nu_\tau$ 's from  $D_s$  decays and a hybrid emulsion magnetic spectrometer to detect  $\nu_\tau$  - Nucleus CC interactions.

#### 3.1. Beam and Detector

The beam layout is shown in Figure 1. A 0.5 m long tungsten beam dump is followed by two sweeping magnets and passive shielding. An emulsion target is located at a distance 36 m from the dump, followed by a magnetic spectrometer. Production of  $\nu_\tau$ 's comes from  $D_s \rightarrow \tau + \nu_\tau$ , with the  $\tau$  decaying again into nutau and leptons or hadrons. There are prompt muon and electron neutrinos produced by D mesons, as well as non-prompt muon neutrinos coming from the decays of pions and kaons that decay before absorption. The beam dump was optimized to reduce as much as possible the non-prompt contamination of the neutrino beam. The sweeping magnets and passive shield were designed to minimize the muon flux at the emulsion target. Details can be found in ref. [11].

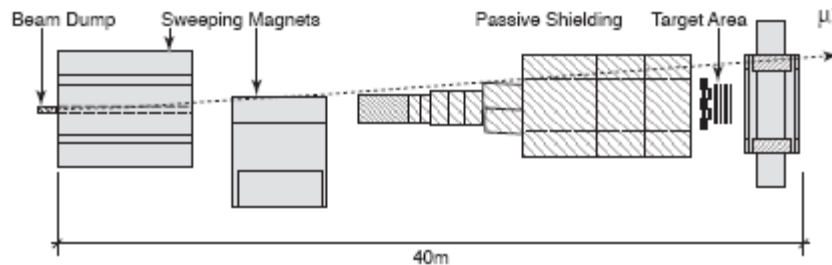


Fig 1. The DONUT Beam configuration

Figure 2 shows the hybrid emulsion spectrometer layout. It consisted of a veto wall, the emulsion target section and a magnetic spectrometer. Integrated with the target is a plastic scintillator hodoscope for triggering purposes, and scintillating fiber tracker (SFT). The magnetic spectrometer consisted of a large aperture magnet, followed by drift chamber planes (DC), lead glass and scintillating glass electromagnetic calorimeter (EMCAL), and a muon identifier (MID) system. Electrons were identified by their showers in the calorimeter as well as in SFT region. The purpose of the spectrometer is to trigger for interesting events, do electron and muon identification, track reconstruction, momentum and energy measurements, neutrino interaction vertex reconstruction, and vertex location in the emulsion. Detailed description of the hybrid emulsion spectrometer can be found in [11].

The neutrino target consisted of 250 Kg of nuclear emulsion organized in a modular fashion and interleaved with planes of scintillating fibers. Details of the emulsion target and its performance can be found in [12]. The basic building block was a sheet of acrylic with a layer of emulsion on either side.

The bulk of the mass was provided by using a sheet of steel, 1 mm thick. In this way three types of targets were built: Bulk emulsion, ECC800, and ECC200 [12]. The spatial and vertex position resolutions were found to be  $0.3 \mu\text{m}$  and  $0.8 \mu\text{m}$ , respectively. Planes of scintillating fibers in U, V, and X orientations, were used to improve the vertex reconstruction accuracy and therefore the vertex prediction in the emulsion, necessary in the semi-automatic emulsion scanning.

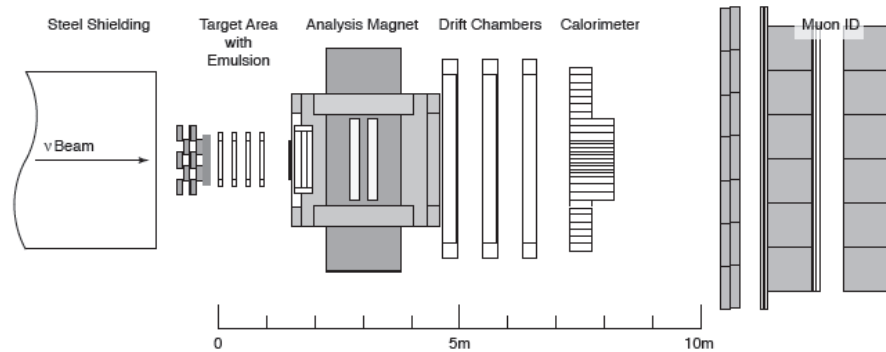


Fig. 2 The DONUT hybrid emulsion spectrometer

### 3.2. Data Analysis

The event reconstruction used the SFT and DC systems and the magnet information to reconstruct tracks and determine momentum. The SFT tracks were employed to reconstruct the event vertex in the emulsion (vertex prediction), which, in turn, was used in the emulsion scanning to locate the actual vertex. The final reconstruction was done by matching the emulsion tracks to the electronic (SFT) track information. Having identified the neutrino interaction, a subsequent emulsion scanning was used to (i) measure all emulsion tracks and estimate momentum from multiple Coulomb scattering and (ii) follow each track and look for kinks (1-prong decays) or tridents (3-prong decays).

After filtering, stripping, and scanning, we ended up with  $\sim 10^3$  predicted vertices in the spectrometer, from the total run with  $3.54 \times 10^{17}$  protons on target (POT). From these 868 reside within the fiducial volume. Emulsion vertex location was attempted and vertex found in 579 events. As will be shown later 9  $\nu_\tau$  candidates were isolated.

Lepton identification has played a key role in the CC/NC separation and the further identification of CC  $\nu_\mu$ ,  $\nu_e$ , and  $\nu_\tau$ . Electrons were identified by their showering in the SFT and EMCAL systems. The muon identification required a minimum number of hits in the MID system. The neutrino event identification was based on the different topological characteristics of the interaction and was done by various methods, including scanning by physicists and the use of Artificial Neural Networks (ANN). The separation of  $\nu_\mu$  CC events was based mainly on the identification of muon tracks. For the  $\nu_e$  CC/NC separation we used information from the SFT, DC, EMCAL, and MID systems. Out of 579 located events 210 were classified as  $\nu_\mu$  CC, 143 as  $\nu_e$  CC, 9 as  $\nu_\tau$  CC, and 191 as NC. These numbers agree with the expected composition to better than 10%. The ratio of negative to positive muons is estimated to be  $1.40 \pm 0.17$ , consistent with expectations from the Monte Carlo. We have estimated the fraction of prompt to total  $\nu_\mu$  CC interactions to be  $0.57 \pm 0.07$ .

### 3.3. The $\nu_\tau$ signal

The CC interaction of  $\nu_\tau$  produces a  $\tau$ -lepton that decays within a short distance, typically 2 mm. Thus, the identification of  $\nu_\tau$  CC interactions is based on the detection of kinks or tridents. Tau production can be mimicked by charm produced by  $\nu_e$  or  $\nu_\mu$  with missing or misidentified primary lepton, and also by hadronic interactions that appear in the emulsion as a 1- or 3-prong decays. The

extraction of the tau signal was based in applying 1-dimensional topological and kinematical cuts as well as on multivariate statistical analysis [13], which determines the likelihood of events belonging to one of the following three categories: tau, charm, hadronic interactions. It uses a set of parameters measured for each event, namely, the decay length of the parent track, the kink angle, the daughter momentum, the parent track angle with respect to the neutrino direction, and the azimuthal angle difference between the lepton and the recoil tracks, whereas for tridents the daughter momentum and kink angle were replaced with the sum of the impact parameters of the three daughters with respect to the primary vertex.

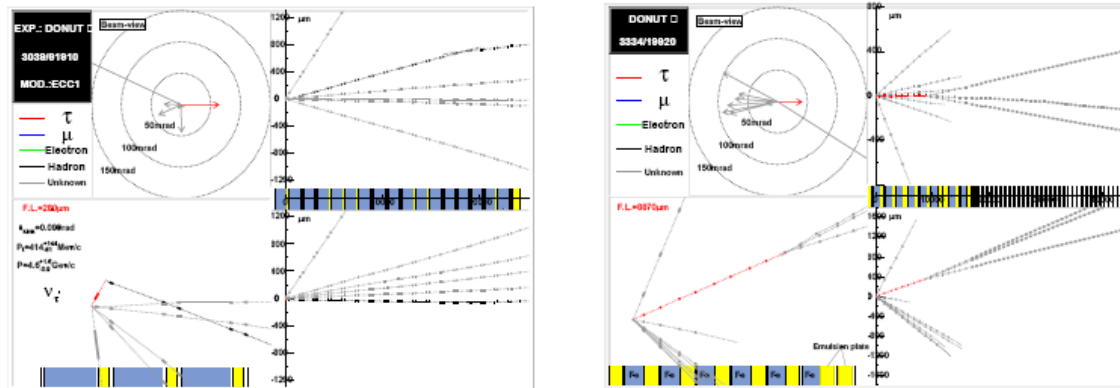


Fig. 3. Two events: a kink (1-prong) and a trident (3-prong). The target structure is shown at the bottom of each figure. The top left of each figure shows the azimuthal and polar (circles) configuration of the interaction. In the azimuthal view the tau direction is opposite to the rest of the particles.

Table I lists the kink events, their parameters, and the probabilities,  $P_\tau$ ,  $P_c$ ,  $P_l$ , of being tau, charm, or hadronic interaction correspondingly. Table II shows the selected trident events, their parameters, and their probabilities of being taus, charm, or interactions correspondingly. In total, there are 9 events identified as tau neutrino CC interactions with probabilities listed as explained just above. Two such events, a kink and a trident are displayed in Figure 3.

Run	Event	$L_{Dec}$ (mm)	$\theta_{kink}$ (rad)	IP ( $\mu\text{m}$ )	Daughter	$P$ (GeV/c)	$P_T$ (GeV/c)	$P_\tau$	$P_c$	$P_l$
3024	30175	4.47	0.093	416.0	e	5.2	0.48	0.53	0.47	0.0
3039	01910	0.28	0.089	23.5	h	4.6	0.41	0.96	0.04	0.0
3140	22143	4.83	0.012	60.2	$\mu^+$	22.2	0.27	0.97	0.03	0.0
3333	17665	0.66	0.011	7.70	e	59.0	0.65	0.98	0.02	0.0
3024	18706	1.70	0.014	22.6	e	50.0	0.70	1.00	0.0	0.0
3139	22722	0.44	0.027	11.8	h	15.8	0.43	0.50	0.29	0.21

Table I: The list of kink (1-prong) events. The charge of the daughter is known in only one case.

Run	Event	FL (mm)	$\theta_d$ (rad)	IP ( $\mu\text{m}$ )	P (GeV/c)	$P_T$ (GeV/c)	$P_\tau$	$P_C$	$P_I$
3296	18816	0.80	0.054	38.2	5.0	0.27	0.71	0.29	0.0
			0.190	148.1	1.3	0.25			
			0.130	112.0	1.9	0.25			
3334	19920	8.88	0.017	147.4	11.6	0.20	1.0	0.0	0.0
			0.011	98.0	15.7	0.17			
			0.011	94.1	3.2	0.04			
3250	01713	0.83	0.133	109.9	1.3	0.17	0.87	0.12	0.01
			0.192	160.7	2.4	0.46			
			0.442	354.7	0.5	0.21			

Table II: List of the trident (3-prong) events

### 3.4. The $\nu_\tau$ CC interaction cross section

The CC  $\nu_\tau$  interaction cross section was measured relative to the electron and muon neutrino-nucleon CC interaction cross sections. Electron and muon neutrinos in DONuT come from charm decays in the beam dump, characterized thus as prompt neutrinos. In addition, muon neutrinos come also from pion and kaons decays in the dump. The fraction of these non-prompt muon neutrinos has been measured in the experiment. In DONuT, the electron and muon neutrino cross sections per nucleon are linear in energy, namely,  $\sigma^i \equiv \sigma_c^i E$ , where  $\sigma_c^i$  is the energy-independent known proportionality factor of the DIS cross section. The tau neutrino cross section has the form  $\sigma^\tau \equiv \sigma_c^\tau E K_\tau(E)$ , where  $K_\tau(E)$  is an energy dependent threshold factor. The number of observed neutrino interactions of flavor  $\nu$  per proton in the beam dump is:

$$N_\nu^{obs} = R_\nu(E) N^{pot} \varepsilon_\nu, \text{ where } R_\nu(E) = \int dE \Phi_\nu^{tgt}(E) \sigma_\nu(E) N_{nucl},$$

$E$  is the neutrino energy,  $\varepsilon_\nu$  is the total efficiency of identifying the interaction,  $\Phi_\nu$  is the neutrino flux on the target per proton,  $\sigma_\nu$  is the CC cross section per nucleon, and  $N_{nucl}$  the number of nucleons in the target. In the experiment  $N_\nu^{obs}$  is measured, whereas the efficiencies are estimated from the data and computed with the Monte Carlo. The fluxes are calculated from known charm production reactions  $pN \rightarrow \bar{c}c + X$ . The number of interactions in the located sample of 579 events was 143  $\nu_e$ , 210  $\nu_\mu$  and 9  $\nu_\tau$  CC events. Backgrounds for these categories have been estimated. The corresponding efficiencies were estimated to be 0.57 for  $\nu_e$ , 0.56 for  $\nu_\mu$ , and 0.49 for  $\nu_\tau$ . The prompt  $\nu_\mu$  fraction was estimated to be  $0.57 \pm 0.07$ . The total number of  $\nu_\tau$  interactions was calculated by taking into account the corresponding probabilities event-by-event. With this information the DIS cross section proportionality factor ratios are preliminarily estimated to be:  $\sigma_c^\tau / \sigma_c^e = 0.99 \pm 0.37$  (stat) and  $\sigma_c^\tau / \sigma_c^\mu = 0.98 \pm 0.36$ (stat), where the systematic uncertainties for these results cancel out

### 3.5. The $\nu_\tau$ magnetic moment

The DONuT experiment searched for an anomalous increase of the number of electron-neutrino interactions above the value predicted by the Standard Model in an attempt to measure the magnetic moment of the  $\nu_\tau$ . Results from this search have been published in ref [14]. According to the Standard Model, neutrinos interact with electrons via  $Z^0$  exchange. The magnetic moment,  $\mu_\nu$ , adds an extra interaction term due to photon exchange via a loop diagram. In the high energy limit this contribution to the cross section is given by:

$$\frac{d\sigma_\mu}{dT_e} = \left(\frac{\mu_\nu}{\mu_B}\right)^2 \pi \left(\frac{\alpha}{m_e}\right)^2 \left(\frac{1}{T_e} - \frac{1}{E_\nu}\right)$$

where  $T_e$  is the scattered electron energy in the laboratory frame. The total cross section is obtained by integrating over  $T_e$ . There is no interference term with the Standard Model process because the neutrino undergoes a spin-flip when a photon is exchanged. From kinematical constraints the electron scattering angle with respect to the incoming neutrino direction in the laboratory frame is limited to be:  $\theta_e^2 < 2m_e / E_e$ . Therefore, for  $E_e \geq 1$  GeV we have  $\theta_e < 30$  mrad, namely the interaction has to show a single forward electron shower. This angular constraint helps separate the signal from the background of  $\nu_e$  – nucleon CC interactions. The DONuT data analysis found one candidate in view of 2.3 expected events [14]. This sets an upper 90% CL limit on  $\mu_\nu$  of  $3.9 \times 10^{-7} \mu_B$ , which is flavor blind. Given that much stringent limits hold for  $\nu_e$  and  $\nu_\mu$ , we can interpret this as a limit, currently the most sensitive, on the magnetic moment of the tau-neutrino.

#### 4. The tau-neutrino mass

The tau-neutrino average mass squared is related to the masses,  $m_i$ , of the mass eigenstates by the relationship  $\langle m_\tau^2 \rangle = \sum_i |U_{\tau i}|^2 m_i^2$  where  $U_{\tau i}$  the matrix elements of the mixing matrix. Measurement of

the mass of the tau neutrino have resulted from the study of the  $\tau$ -lepton decays, in particular  $\tau^- \rightarrow 2\pi^- \pi^+ \nu_\tau$  and  $\tau^- \rightarrow 3\pi^- 2\pi^+(\pi^0) \nu_\tau$  [15], with the ALEPH detector at LEP, at  $\sqrt{s} \cong m_Z$ . The method is based on the description of either of these decays as a two body decay:  $\tau^- \rightarrow h^-(E_h, \mathbf{p}_h) + \nu_\tau$ . By fitting the distribution of events in the  $(m_h, E_h)$  plane the experiment obtained an upper limit of 18.2 MeV/c<sup>2</sup> at 95% confidence level for the  $m_\tau = \sqrt{\langle m_\tau^2 \rangle}$ . This is presently the most sensitive direct limit, about two orders of magnitude less sensitive that the corresponding limit for the muon neutrino that comes from pion decay. This measurement constraints the quantity  $\sum_i |U_{\tau i}|^2 m_i^2$ , where the summation is over all masses,  $m_i$ , that cannot be resolved experimentally. Similar constraints come from measurements of the masses of the weak interaction eigenstates  $\nu_e$  and  $\nu_\mu$  [16]. Notice that the true  $\langle m_\tau^2 \rangle$  cannot exceed the  $\max\{m_i^2\}$ .

#### 5. Present SM properties of the tau-neutrino

5.1.1. *V-A coupling.* The coupling was studied by making precise measurements of the Michel parameters. The state of the art has resulted by studying the  $\tau$  – lepton decay in several experiments: ALEPH, DELPHI, L3, OPAL, Argus, SLD, MAC and CLEO. The most precise measurements comes from ALEPH [17]. Using 155 pb<sup>-1</sup> of data the ALEPH collaboration studied the  $\tau$  - decays from  $e^+e^- \rightarrow \tau^+\tau^-$  in the decay channels  $e^- \bar{\nu}_e \nu_\tau, \mu^- \bar{\nu}_\mu \nu_\tau, \pi^- \nu_\tau, K^- \nu_\tau, \pi^- \pi^0 \nu_\tau, \pi^- \pi^0 \pi^0 \nu_\tau, \pi^- \pi^+ \pi^- \nu_\tau$ , and their charge conjugates. It has reported measurements of the Michel parameters under the assumption of  $e$ -  $\mu$  universality and  $\xi_\pi = \xi_\rho = \xi_{a1}$ , shown in Table III, and, in addition, the  $\nu_\tau$  helicity  $-\langle h_{\nu_\tau} \rangle = \xi_h = 0.992 \pm 0.007$  (stat)  $\pm 0.006$  (sys)  $\pm 0.005$  (3-pion model). The Particle Data Group (PDG)[18] has summarized the data from all the experiments in the form of a “fit” as well as in the form of an average. Table III shows the results from ALEPH, the PDG Fit and PDG average along with the predictions from the Standard Model. From these measurements we can conclude that there are no significant deviations from the SM, assuming the V-A structure of the CC interactions.

Parameter	SM	ALEPH	PDG Fit	PDG Average
$\rho$ (e or $\mu$ )	3/4	0.742 $\pm$ 0.014 $\pm$ 0.006	0.745 $\pm$ 0.008	0.749 $\pm$ 0.008
$\xi$ (e or $\mu$ )	1	0.986 $\pm$ 0.068 $\pm$ 0.031	0.985 $\pm$ 0.030	0.981 $\pm$ 0.031
$\eta$ (e or $\mu$ )	0	0.012 $\pm$ 0.026 $\pm$ 0.004	0.013 $\pm$ 0.020	0.015 $\pm$ 0.021
$(\delta\xi)$ (e or $\mu$ )	3/4	0.776 $\pm$ 0.045 $\pm$ 0.024	0.746 $\pm$ 0.021	0.744 $\pm$ 0.022

Table III: The Michel parameters from the tau decays

5.1.2. *Test of Universality.* The strength of the coupling is extracted from the  $\tau$ -lepton lifetime:  $\tau_\tau \approx (m_\mu/m_\tau)^5 \tau_\mu \text{BR}(\tau \rightarrow e) = 2.91 \times 10^{-13}$  s. Data come from DELPHI, ALEPH, L3, OPAL, and CLEO, the most precise being the DELPHI data:  $\tau_\tau = (2.909 \pm 0.014 \pm 0.010) \times 10^{-13}$  s, whereas the PDG average is  $\tau_\tau = (2.906 \pm 0.010) \times 10^{-13}$  s, where the error is combined both statistical and systematic errors in quadrature. Again we can see here an excellent agreement with the SM.

5.1.3. *Number of light neutrinos.* The most precise measurement comes from  $e+e-$  collider experiments on the  $Z^0$  pole. These experiments measure the  $Z^0$  width as well as the visible partial widths of the  $Z^0$  decays into quarks and leptons. From these measurements the invisible partial width  $\Gamma_{\text{inv}}$  is extracted. The number of neutrinos  $N_\nu$  then is computed from  $N_\nu = (\Gamma_{\text{inv}}/\Gamma_l)(\Gamma_l/\Gamma_\nu)_{\text{SM}}$ , where the SM model ratio is used to reduce model dependence. The resulting number of light neutrinos from the LEP experiments is  $N_\nu = 2.984 \pm 0.008$  [19], consistent with  $N_\nu = 3$ .

## 6. Conclusions

In conclusion, the DONuT experiment has directly observed the tau-neutrino as a particle via its CC interaction with nuclei. Nine  $\nu_\tau$  CC interactions have been identified in DONuT, with the produced  $\tau$ -lepton decaying into 1-prong (kink) in 6 of the cases and into 3-prongs (tridents) in the remaining three cases. A preliminary first measurement of the DIS  $\nu_\tau$ -N cross section is consistent, within a large statistical error, with the SM. On the other hand, several tau-lepton decay studies in collider experiments have produced very precise measurements of the Michel parameters, the tau-neutrino helicity, the tau-decay lifetime, and the number of light neutrinos, all in excellent agreement with the Standard Model. Putting together all the above mentioned properties one can justify assigning this neutral particle of spin  $\frac{1}{2}$  and negative helicity as the weak isospin  $\frac{1}{2}$  partner of the  $\tau$ -lepton. The author wishes to thank his DONuT collaborators and to acknowledge the hospitality of the Neutrino 2006 organizers.

## References

- † For the DONuT Collaboration: Aichi (Japan), Athens (Greece), UC/Davis (USA), Fermilab (USA), Gyeongsang (Korea), Kansas State (USA), Kobe (Japan), Kon-kuk (Korea), Minnesota (USA), Nagoya (Japan), Pittsburgh (USA), and Tufts (USA).
- [1] M. L. Perl et al., Phys. Rev. Lett. 35, 1489 (1975).
  - [2] K. Kodama et al., Phys. Lett. B504, 218 (2001).
  - [3] C. L. Cowan et al., Science 124, 103 (1956).
  - [4] G. Danby et al., Phys. Rev. Lett. 9, 36 (1962).
  - [5] W. Bacino et al., Phys. Rev. Lett. 42, 749 (1979).
  - [6] G. J. Feldman et al., Phys. Rev. Lett. 48, 66 (1982).
  - [7] H. Albrecht et al., Phys. Lett. B250, 164 (1990).
  - [8] H. Albrecht et al., Z. Phys. C56, 339 (1992); DESY 92-082.
  - [9] N. Ushida et al., Phys. Rev. Lett. 57, 2897 (1986).
  - [10] D. Decamp et al., Phys. Lett. B231, 519 (1989); CERN-EP/89-132.
  - [11] K. Kodama et al., Nucl. Instr. Meth. A516, 21 (2004).
  - [12] K. Kodama et al., Nucl. Instr. Meth. A493, 45 (2002).
  - [13] J. Sielaff, Ph.D. Thesis, Univ. of Minnesota, 2002; E. Maher, Ph.D. Thesis, Univ. of Minnesota, 2005; K. Kodama et al., (DONuT Collaboration), to be submitted to Phys. Rev. D.
  - [14] R. Schwienhorst et al., Phys. Lett. B513, 23 (2001).
  - [15] R. Barate et al., Eur. Phys. J. C 2, 395 (1998).
  - [16] P. Vogel and A. Piepke, in W.-M. Yao et al. (*Particle Data Group*), J. Phys. G 33, 1 (2006)
  - [17] A. Heister et al., Eur. Phys. J. C22 : 217 (2001).
  - [18] A. Stahl, in W.-M. Yao et al. (*Particle Data Group*), J. Phys. G 33, 1 (2006)

- [19] J. Dress, XX Intl Symposium on Lepton and Photon Interactions at High Energy, Rome, Italy (2001); D. Karlen, in W.-M. Yao *et al.* (*Particle Data Group*), J. Phys. G **33**, 1 (2006).

# The Cascades Proposal for the Deep Underground Science and Engineering Laboratory

W. C. Haxton<sup>1</sup> and J. F. Wilkerson<sup>2</sup>

Institute for Nuclear Theory<sup>1</sup> and Center for Experimental Nuclear Physics and Astrophysics<sup>2</sup>,  
University of Washington, Seattle, WA 98195

E-mail: haxton@phys.washington.edu, jfw@u.washington.edu

**Abstract.** One of the options for creating a Deep Underground Science and Engineering Laboratory (DUSEL) is a site in the Mt. Stuart batholith, a granodiorite and tonalite rock mass in the Cascade mountain range in Washington State. The batholith's 100-year history in hard-rock tunneling includes the construction of the longest and deepest tunnels in the U.S., the parallel Cascade and Pioneer tunnels. The laboratory plan would utilize these two tunnels to produce a laboratory that has many desirable features, including dedicated, clean, horizontal access, container-module transport, and low operations costs. Various aspects of the site help to reduce geotechnical, environmental, and safety risks.

## 1. Introduction

In 2003 a search was done over most of the western U.S. to identify sites suitable for a horizontal-access DUSEL, a laboratory that will host future neutrino, dark matter, geoscience, geomicrobiology, and engineering projects [1]. The Mt. Stuart batholith, a granodiorite formation in the Cascade Range, was one of the identified sites. Because of a combination of railroad and water projects, this batholith has been frequently tunneled over the past 100 years. In the most famous of these projects, the 1926-29 excavation of the parallel Cascade and Pioneer tunnels, a world record for the rate of advance through hard rock was established. These remain the longest (12.5 km) and deepest (1040 m) transportation tunnels in the U.S. DUSEL-inspired interest in the Mt. Stuart batholith increased in August 2005 when the owner of the Cascade and Pioneer tunnels, Burlington Northern & Santa Fe, decided that development of the Pioneer Tunnel for science would be compatible with railroad operations in the Cascade Tunnel, and that such development might simplify tunnel maintenance and improve safety. Subsequent work on DUSEL-Cascades [2] has focused on using the Pioneer Tunnel as the portal to a three-level laboratory, a horizontal Level I at 1040m that would be ideal for large-detector construction, an intermediate Level II (1760 m) that would be coupled to Level I by two hoists, and a very deep Level III (2330 m) that would be developed a decade or more in the future.

The site has a number of attributes important to a project like DUSEL:

- The site has a low-elevation portal (685 m) and mild climate, and is located in the western foothills of the Cascades. Thus the site is accessible year around, with the drive from the Seattle-Tacoma airport (1.5 hours) generally snow-free.
- All surface development would occur on land owned by BNSF, and all underground development would occur in areas where BNSF owns the mineral rights. Current site use

includes a range of railroad industrial activities very similar to those required for DUSEL.

- The site is within a federal energy corridor. Redundant power feeds to DUSEL with automatic pickup are possible because substations are located at both portals. Power rates are very favorable, about \$0.016/kW-hr. There is the potential to tie into ESnet, Pacific Wave, and other international high-speed data corridors, to facilitate remote visualization and detector operations.
- The site's location relative to potential neutrino beams will position the U.S. to play an important role in long-baseline physics. The baseline to FermiLab, 2630 km, is very close to ideal for an on-axis superbeam experiment, as noted in the S1 study [1]. Its neutrino-factory baselines are unique, with "magic" (7500 km) baselines to both KEK and CERN, and with a FermiLab baseline that will optimize the followup CP-violation experiment. It is the only practical site on the globe matching APS Multi-Divisional Neutrino Study [3] neutrino-factory baseline specifications for each of the three high-energy accelerator laboratories.
- The site is adjacent to a major international cargo-container route: a significant fraction of the cargo entering the U.S. from Asia comes by ship to the Seattle and Tacoma ports, then by rail through the Cascade Tunnel to Chicago and points east. One of the driving principles of the DUSEL-Cascades design is to tie the laboratory seamlessly to this transportation corridor, so that groups from distant laboratories can construct large modules at home, then efficiently transport the modules to DUSEL-Cascades.
- The site is near a major urban center with a concentration of high tech industries, such as aerospace, biotechnology, micro-electronics, and communications. There are six major research institutions within 200 miles.
- Risk factors are low. The site has a favorable construction history and the rock on Level I is accessible. The site is clean and can be developed without creating rock piles or other environmental legacies. The ownership is stable. The site's parallel tunnels can be exploited to minimize underground ES&H hazards. The site is private with a relatively uncomplicated set of permitting issues. The design minimizes long-term operations and experimental costs. The proximity to Puget Sound will be helpful to DUSEL recruiting, opening opportunities for academic, industrial, and outreach partnerships and providing employment opportunities for spouses.

## **2. Geologic, environmental, and geotechnical characterization**

### *2.1. Regional geologic context*

The Mt. Stuart batholith is a 600 km<sup>2</sup> granitic formation, dominantly granodiorite and tonalite with schist wallrock, located in a convergent tectonic margin. The host rock, Chiwaukum schist and banded gneiss, was intruded by the Mt. Stuart batholith and other plutons during regional metamorphism in the Late Cretaceous period, about 93 My ago. Geologic work in the area began 120 years ago and includes surface mapping, borehole studies, and construction of nine significant tunnels.

The portal is located in a region of moderate seismic activity, separated by approximately 70 km from the nearest identified active crustal fault. No earthquake over magnitude 4.0 has occurred within 35 km over recorded history. The U.S. Geologic Survey Seismic Hazard Mapping Index for the site is 15% of g peak acceleration (10% probability over 50 years). The corresponding 1997 Uniform Building Code risk zone is 2B. (The range is 1 to 5, with 1 the lowest.) The portal location was selected by BNSF in 1927 to be free of rock falls and avalanches.

### *2.2. Environmental characterization*

An analysis of the rock shows that the principal minerals are plagioclase, quartz, biotite, hornblende, and K-feldspar. No asbestiform minerals were identified. The principal health

hazard from the rock will be quartz dust produced in construction, which is readily controllable by standard industry practices.

The Pioneer Tunnel serves as the drainage gallery for the tunnel complex. Tests of the drainage from the Pioneer Tunnel were done by RETEX Group Inc., assisted by collaboration scientists from Pacific Northwest National Laboratory and by BNSF. Analysis included pH (7.29), temperature (15.6 C), hardness (28.4 mg/L), and a variety of metals. Sulfide content is very low, below analytical sensitivity. All results met the applicable EPA or Washington State chronic standards.

Subsurface radioactivity was determined by gamma counting and XRF as a function of depth, by counting rock samples taken from a recent deep glacial cut into the batholith. The activities for U ( $\sim 0.5$  ppm), Th ( $\sim 0.7$  ppm), and  $K_2O$  ( $\sim 1.4\%$ ) are very low for granitic rock.

Subsurface temperatures have been mapped from the surface to 1040 m, and thermal gradients for projections to greater depth determined from these data, with suitable corrections for the effects of surface topography. The Level I (1040 m) rock temperature is 21 C, and the estimated Level II (1760 m) and Level III (2330 m) temperatures are  $34 \pm 3$  C and  $45 \pm 4$  C, respectively.

The site is free of spotted owl or other protected nesting areas. The area's drainage basin is the Tye River, but the portal is well above waterfalls and other natural barriers. Thus there are no Chinook or bull trout impacts associated with water release.

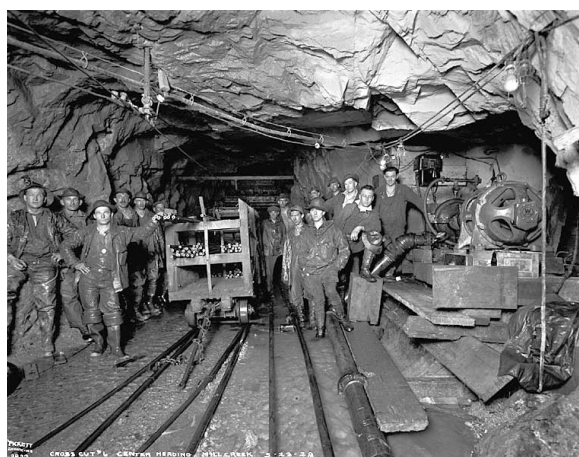


**Figure 1.** Archival Pioneer Tunnel photo showing an enlarged-span equipment bay [4].



**Figure 2.** Station 308 in the Pioneer Tunnel during recent reconnaissance [5].

### 2.3. Geotechnical characterization

Part of the site's attractiveness is that it is effectively a greenfield – the site does not impose any significant constraints on DUSEL design – without the usual geotechnical uncertainties inherent in a greenfield. The geotechnical database includes historical records from construction and tunnel repairs, borehole studies conducted to determine thermal gradients, extensive surface mappings (including a survey of surface outcroppings commissioned by our collaboration in 2004), and surveys of the Pioneer Tunnel. Because the Pioneer Tunnel is largely unlined, it serves as a “test adit,” providing continuous access to the rock along the DUSEL entrance tunnel and demonstrating the stability of openings after 80 years.

The original construction records describe localized draining of newly opened rock. Baxter [6] notes “Practically all of the water encountered was ground-water filling fissures in the rock. These fissures were of all sizes... [and] acted in the same manner: A maximum flow when first

encountered; a radical decrease in the flow in the next few days (sometimes hours), with a gradual decrease over weeks and months, at times drying up entirely.” Level I rock is now dewatered. While fissures in granite tend to tighten with depth, new rock opened in the construction of Levels II and III would likely exhibit similar transient drainage of the local rock mass: the contractor would need to provide adequate pumping capacity during excavation.

The surface mappings of joints and fissures, compiled into stereonet [7], showed four major joints sets, three of which are steeply dipping and one (the most common) shallow dipping. Joint observations in the tunnel proved consistent with surface patterns: joint conditions were found to improve with depth, with many joints/fractures either healed or discontinuous.

The most important database comes from recent geotechnical surveys along a 4500-ft section of the Pioneer Tunnel near maximum depth. Tunnel walls were mapped, rock samples collected, and laboratory tests performed for 45 tunnel stations located at 100-ft intervals. Photographs from this reconnaissance (see Fig. 2) and from original construction (see Fig. 1) are available [4, 5]. The resulting rock characterizations are summarized in Table 1. The results may be conservative because laboratory tests were done with samples taken from exposed tunnel walls (rather than from corings). Regardless, the rock quality is very high, comparable to that found at the Tochibora Mine, a proposed HyperKamiokande site: the average RQD (Rock Quality Designation) for the 45 stations is 94% (excellent rock) and the average RMR (Rock Mass Rating) is 83 (Class I rock).

**Table 1.** Large Detector Sites

Site	Mozumi Mine	Tochibora Mine	Pioneer Tunnel
Principal rock type	Hornblende gneiss	Hornblende biotite gneiss	Granodiorite
Peak overburden (m)	870	600-700	~ 1000
Density (g/cm <sup>3</sup> )	2.65	2.65	2.69-3.04
Compressive strength (kpsi)	15.2-17.4	21.7-36.3	16.4 → 35
Discontinuity spacing (m)	0.2-0.6	0.6-2.0	0.2-2.0
condition	Slightly rough	Very rough	Rough, healed/discontinuous
orientation	Favorable	V. Favorable	Favorable/v. favorable
RQD	78%	85%	94%
RMR	79	89	83
Rock Mass Classification	II	I	I

The tunnel, unsupported over 87% of its length, is in generally good condition after 80 years. In a number of locations the Pioneer Tunnel was widened to spans of 5-10 m to accommodate equipment or to form junctions with cross cuts (e.g., see Fig. 1). Standard tables of stand-up times indicate an RMR of at least 85 for any stable 80-year span above 5m, and 90+ for any span above 7.5m. This empirical demonstration of rock competence is consistent with the laboratory results described above.

### 3. The Development Plan

The development plan for DUSEL-Cascades is based on several principles:

- Careful engineering for efficient science, enhanced safety, and economical lifetime operations: The design provides for dedicated horizontal access with tracked transport and standardized turning radii to allow efficient, safe equipment transport; a ducted ventilation system capable of isolating emergencies occurring in laboratory rooms or in Level II hallways; a dedicated exhaust path that will help keep exit-ways open in an emergency; the capacity to

sequester new construction from active laboratory areas; and vertical alignment of the three laboratory levels for efficient connections and efficient exploitation of Level I's receiving and industrial support facilities.

- **Maximize cleanliness:** Environmental radioactivity is often the primary background in underground experiments. As a dedicated facility with all-electric operations, finished hallways, and ducted ventilation, DUSEL-Cascades will be clean from the portal onward. The design allows individual rooms (or portions of rooms) to be held at Class 1-10, provides for a common Class 1000 clean area, a “white area” at Class 100,000, and “dirty-side” operations that will in fact be quite clean, if compared to laboratories operating in shared mine facilities.
- **Complementing SNOLab:** North America will soon have a very deep vertical-access facility at SNOLab. DUSEL-Cascades will complement SNOLab by providing a horizontal-access level at Kamioka depths, ideal for long-baseline megadetector construction, and an intermediate level at Frejus depths (4.05 km-water-equivalent) that can accommodate container-scale experimental modules. A third level at SNOLab depths is planned, when North America finds itself in need of additional very deep space.
- **Use of the site's unique transportation system:** The design envisions efficient transport of 20-ft container modules from distant laboratories to any DUSEL level. Level I is effectively a siding on the BNSF railroad: loads can be moved by rail to the portal, mounted onto laboratory flatcars, then tracked to Level I laboratory rooms. Tracked container transport is extended to deeper levels by a large-diameter, roll-in/roll-out hoist that effectively serves as a track switching device between levels.
- **International cooperation:** The combination of large detector capabilities, efficient cargo container transport, complementarity to SNOLab, and magic baselines will position DUSEL-Cascades to play an important role in international science. Seattle is the mainland U.S. port closest to Asia, which currently lacks a deep laboratory. We envision DUSEL-Cascades being operated cooperatively, part of a network of international laboratories (SNOLab, Kamioka, Gran Sasso, etc.) that would collectively endeavor to accommodate new experiments in the most efficient way.

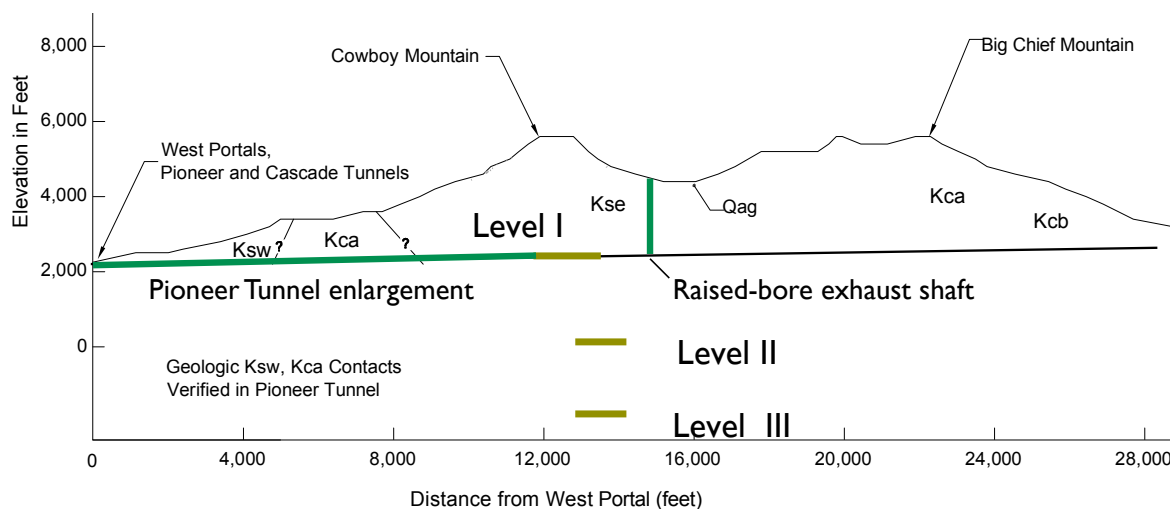
Figure 3 shows the orientation of the three levels under Cowboy Mountain. As noted previously, significant work has been done to characterize rock properties on Level I. The Pioneer Tunnel also provides a convenient platform for borehole studies of the deeper rock that will house Levels II and III; both downhole and crosshole exploration programs can be conducted at relatively low cost. The deeper levels are connected to Level I – the industrial level providing access to the surface, power, drainage, ventilation, and receiving services – by a large-diameter container- and man-hoist, and by an emergency/mining hoist. Levels II and III are designed so that new, specialized cavities can be constructed “downstream” of other laboratory operations. Thus these deeper levels can expand to accommodate newly approved experiments.

Figure 4 shows the plan for Level I, including a possible megadetector site. The baseline design includes enlargement of the Pioneer Tunnel (most likely by tunnel boring machine) to form the entrance hallway, with fully finished walls and a concrete tracked invert under which drainage would run; raise-bore construction of an exhaust shaft to the surface; and construction of a series of cross cuts/refuges between the Pioneer and Cascade Tunnels, so that the latter can serve as a secondary escape route for the former.

Detailed discussions of this project can be found elsewhere [7]. This work was supported in part by the Office of Nuclear Physics, U.S. Department of Energy.

## References

- [1] See the S1 report *Deep Science*, <http://www.dusel.org/>



**Figure 3.** Pioneer Tunnel topography and the arrangement of laboratory levels, the entrance tunnel, and the exhaust shaft.

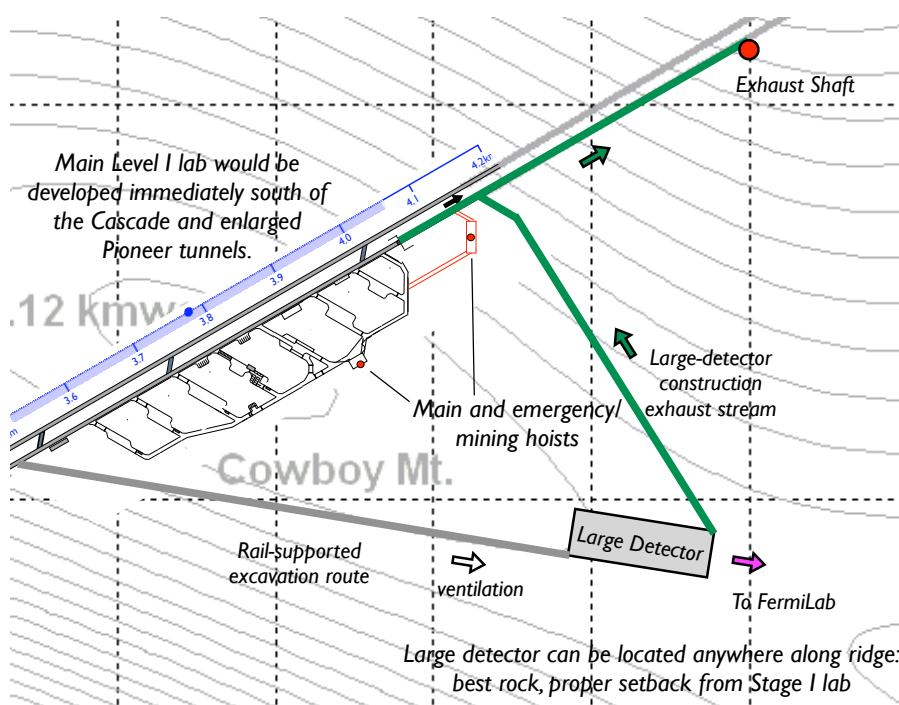


**Figure 4.** The proposed arrangement of rooms and support facilities on Level I. The site provides a large area, south of the tunnel, where a megadetector could be constructed. The layout shows how transportation to and exhaust from that construction site could be routed to avoid interference with other Level I activities.

- [2] Haxton W C, Philpott K A, Holtz R, Long P, and Wilkerson J F 2007 *Nucl. Instruments and Methods in Physics Research A* **570** 414
- [3] APS Multi-Divisional Neutrino Study, <http://www.aps.org/neutrino/>; also see Huber P and Winter W 2003 *Phys. Rev. D* **68** 037301
- [4] Photograph by Lee Pickett, University of Washington Digital Library.
- [5] Photograph by Red Robinson, Shannon & Wilson, Inc.
- [6] Baxter J C 1932 *Transactions of the American Society of Civil Engineers* **96** 950
- [7] See <http://www.int.washington.edu/s3/>

# Double Beta Decay Measurement with COBRA

**Jeanne R. Wilson**

Department of Physics and Astronomy, University of Sussex, Brighton, BN1 9QH, UK

E-mail: [j.wilson@sussex.ac.uk](mailto:j.wilson@sussex.ac.uk)

## Abstract.

The COBRA experiment aims to use a large array of CdZnTe semiconductor detectors to search for neutrinoless double beta decay. Extensive simulation studies and data collected with a small proto-type experiment have been used to address the major design specifications for a large scale experiment sensitive to  $^{116}\text{Cd}$  half-lives in excess of  $10^{26}$  years. The current and future prospects of the COBRA experiment are presented.

## 1. Introduction

The idea of COBRA is to use a large array of CdZnTe semiconductor crystals[1]. There are actually 9 double beta isotopes, 5 in the form of  $\beta^-\beta^-$  emitters, intrinsic to the detector material, but measurements will focus on  $^{116}\text{Cd}$ . This has the highest Q-value at 2.8 MeV, beyond all the single gamma-lines from the natural decay chains which would be problematic in contaminating signal regions at lower energies.

CdZnTe, in common with other semiconductors can be produced cleanly with low levels of intrinsic radioactive background and offers good energy resolution. Unlike many semiconductors though, CdZnTe can be operated at room temperature without the need for expensive cryogenics close to the detectors. The COBRA detector will be formed from many  $1\text{ cm}^3$  crystals as current fabrication methods are not suited to producing larger crystals with good detector properties. However, the modular design is advantageous as it can be easily extended and provides a means of background reduction through rejection of events with coincident energy deposits in separate crystals.

## 2. Status

A small proto-type for the COBRA experiment is operating in the LNGS laboratory in Italy, which provides a shielding equivalent to  $\approx 3500\text{ m}$  of water. Initially, the proto-type consisted of four  $1\text{ cm}^3$  crystals with which 4.34 kg.days of data were collected. This was the first operation of CdZnTe crystals in a low background, underground environment and the data were used to study the detector properties and the major sources of background in the crystals. Despite the small detector mass, less than 25 g, the data revealed a number of interesting results including a measurement of the 4-fold forbidden beta decay of  $^{113}\text{Cd}$ [2] which yields  $T_{1/2} = (8.2 \pm 0.2(\text{stat.})_{-1.0}^{+0.2}(\text{sys.})) \cdot 10^{15}$  years and new half-life limits on some  $\beta^+$ -electron-capture decay modes of  $^{64}\text{Zn}$  and  $^{120}\text{Te}$ [3].

Earlier this year, installation of a larger proto-type consisting of a  $4 \times 4 \times 4$  array of  $1\text{ cm}^3$  crystals commenced. Figure 1 shows the first layer of this array and a diagram of the detector

set-up. With this set-up the major detector operation issues can be addressed and the power of the coincidence method of background reduction (as discussed in section 3.2) will be investigated.



**Figure 1.** A photograph of the first layer of the 64-crystal proto-type (left) and an artistic impression of the whole array in the copper mounting structure (right).

### 3. Experimental Requirements

The half-life predictions for neutrinoless double beta decay cover a wide range due to the uncertainties associated with the nuclear matrix element. However, for a neutrino mass of about 50 meV as suggested by neutrino oscillation data, the half-life of  $^{116}\text{Cd}$  is of order  $10^{26}$  years.

As with all neutrinoless double beta decay searches, the COBRA experiment will require low backgrounds, good energy resolution and a large detector mass to achieve this. Figure 2 shows the predicted sensitivity for a 418 kg detector consisting of 64,000  $1\text{ cm}^3$  crystals enriched to 90% in  $^{116}\text{Cd}$  for three different scenarios. To obtain sensitivity to  $T_{1/2} = 10^{26}$  y in 5 years of operation, a resolution of  $\Delta E < 2\%$  (FWHM), and a background rate in the signal region of  $< 0.001$  counts/keV/kg/year are required.

#### 3.1. Energy Resolution

One motivation for good energy resolution is to reduce the width of the signal region and hence the background contributions, in particular those from the irremovable  $2\nu\beta\beta$  decays. The fraction of these decays in the signal region can be shown to be[4]

$$F = \frac{AQ}{m_e} \left( \frac{\Delta E}{Q} \right)^6 \quad (1)$$

where  $m_e$  is electron mass,  $\Delta E$  is the FWHM energy resolution and  $Q$  is the endpoint energy of the  $2\nu\beta\beta$  spectrum.  $A$  has some dependence on the resolution and takes a value in the range 7–8.5 for FWHM values in the range 5–1%.

The energy resolution and stability of the detectors is calibrated regularly with the help of  $^{137}\text{Cs}$ ,  $^{60}\text{Co}$  and  $^{228}\text{Th}$  sources. Currently the best detectors in operation have a FWHM of 1.9% at 2.8 MeV resulting in a contribution of approximately  $1.3 \times 10^{-5}$  events/kg/year to the signal region (using  $T_{1/2}^{2\nu\beta\beta} = 2.6 \times 10^{19}$  years for  $^{116}\text{Cd}$ [5]). Even this modest background could be reduced as resolution depends on the grade of detector material and better detectors are available. Studies have also shown that a modest cooling of the detectors, of order 10–20°C could further improve the resolution.

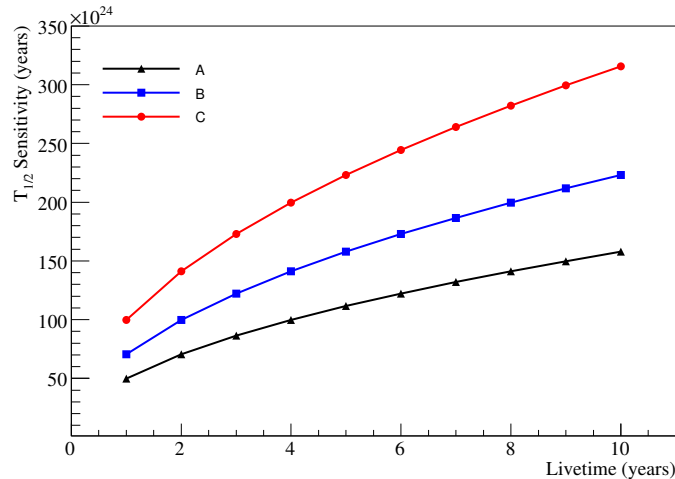


**Figure 2.** The expected half-life sensitivity for  $0\nu\beta\beta$ -decay of  $^{116}\text{Cd}$  in an array of 64,000  $1\text{ cm}^3$  detectors, enriched to 90% in  $^{116}\text{Cd}$  for three scenarios:

A =  $10^{-3}$  background counts/keV/kg/year,  $\Delta E = 2\%$  at 2.8 MeV.

B =  $10^{-3}$  background counts/keV/kg/year,  $\Delta E = 1\%$  at 2.8 MeV.

C =  $5 \times 10^{-4}$  background counts/keV/kg/year,  $\Delta E = 1\%$  at 2.8 MeV.

### 3.2. Background Reduction

Due to the large cross-section of  $^{113}\text{Cd}$  for thermal neutron capture, special attention is required to exclude neutrons created in the rock forming the laboratory walls. Therefore, a comprehensive study was performed to optimise the design of a shield for external backgrounds[6]. The final design is 80 cm thick and consists of a number of layers of passive shielding materials such as iron, lead and Bi and Li doped polyethelene and an active liquid scintillator component closest to the detectors. The scintillator does not only serve as a veto for any residual gammas that pass through from the outer layers of shielding; it will also detect gammas emerging from the detector region and will therefore help to veto internal backgrounds and can also be used in the identification of possible  $\beta\beta$  decays to excited states which are accompanied by de-excitation gammas.

Simulations of the optimised shielding design were performed for a number of years of the measured LNGS neutron background and no events were observed in the detectors which were not picked up in the active veto layer. Thus this shield should keep the background below one event per year for the 64,000 crystal set-up. The same simulation package, based on the GEANT4 framework, was used to study the contributions of various  $\alpha$ ,  $\beta$  and  $\gamma$  background sources, in the detector materials and also on the surfaces. These simulations have been used to determine the required purity of the CdZnTe, plastic mounting material, air and Cu and Pb shielding components.

COBRA will also be able to reject background events from residual radioactive contamination based on coincident energy deposits between different crystals in the array. Simulation studies for the 64,000 crystal array show that by vetoing events that deposit energy in multiple crystals, the number of events contributing to the 2–3 MeV signal region can be reduced by more than 50% for  $^{232}\text{Th}$  events arising in the CdZnTe and by about 15% for  $^{238}\text{U}$ . In this energy range the main contribution (about 70%) to the  $^{238}\text{U}$  events is from the beta decay of  $^{214}\text{Bi}$ . The daughter of this decay,  $^{214}\text{Po}$  has a half life of just  $164\ \mu\text{s}$  and produces a 7.7 MeV  $\alpha$  which can be used to tag the preceding decay. Simulations show this timing coincidence can be used to veto over 40%

of  $^{214}\text{Bi}$  decays originating in the crystal material. Samples of event pairs identified through this tag from current data show a time distribution between the first ( $\beta$ ) and second ( $\alpha$ ) event in good agreement with the known half-life of  $^{214}\text{Po}$ , confirming that these events can be identified in the data.

### 3.3. Pixellisation

Crystals with coplanar-grid anodes are currently used in the COBRA proto-type. However, investigations are also underway into the feasibility of using pixellated detectors. Pixellisation would allow background reduction through particle identification and would provide a unique signal for double beta decay events. For example, the range in CZT for the electrons produced in a 2.8 MeV  $\beta\beta$  decay is 1–1.5 mm, whereas an alpha particle of the same energy would only travel about 15  $\mu\text{m}$ . Thus a pixellisation of order 200  $\mu\text{m}$ 's would yield 5–10 points along the  $\beta$  particle tracks but the alpha event would be largely confined to a single pixel. This will be particularly beneficial for eliminating backgrounds such as the  $^{214}\text{Bi}$ -decays discussed in the previous section.

## 4. Summary

The COBRA experiment aims to search for neutrinoless double beta decay of  $^{116}\text{Cd}$  with a sensitivity to half-lives greater than  $10^{26}$  years with a large array of CdZnTe crystals. Resolutions of FWHM=2% at the peak energy (2.8 MeV) have already been obtained and improvements are expected. The background in the signal region will be minimised through careful selection of materials, a comprehensive shielding with active veto, and the use of timing and spatial coincidences to reject radioactive decay events. A new proto-type experiment is being deployed to investigate these issues.

## Acknowledgments

This research was supported by PPARC and the Deutsche Forschungsgemeinschaft (DFG). We thank V. Tretyak for providing the Decay0 code and eV-PRODUCTS for their support. In addition, we thank the Forschungszentrum Karlsruhe, especially K. Eitel, for providing the material for the neutron shield. We thank the mechanical workshop of the University Dortmund for their support and the Laboratori Nazionali del Gran Sasso (LNGS) for offering the possibility to perform measurements underground.

## References

- [1] Zuber K., 2001 *Phys. Lett. B* **519** 262
- [2] Goeßling G. et al, 2005 *Phys. Rev. C* **72** 064328
- [3] To be published shortly.
- [4] Elliott S. and Vogel P., 2002 *Annu. Rev. Nucl. Part. Sci.* **52** 115
- [5] Ejiri H. et al, 1995, *J. Phys. Soc. Jpn.* **64** 339
- [6] Stewart D. et al, 2006, submitted to *Nucl. Instr. and Meth. A.* (arXiv:nucl-ex/0607032)

## Inventing the neutrino

L. Wolfenstein  
 University Professor, Emeritus, Carnegie Mellon University, Physics  
 Department, 5000 Forbes Avenue, Pittsburgh, PA 15213

E-mail:Lincoln@cmuhep2.phys.cmu.edu

### Abstract

A short history of the neutrino is presented honoring the pioneers from Wolfgang Pauli to Raymond Davis.

In November of 1930 Wolfgang Pauli sent a letter to a meeting of nuclear physicists (he addressed them as “radioactive ladies and gentlemen”) in which he proposed the existence of a new neutral particle that no one had detected. He wrote “I admit that my remedy may appear to have a small a priori probability, however, only those who wager can win” (1). This last phrase could be taken as the motto of neutrino physics.

The problem that motivated Pauli was the continuous electron spectrum in beta-decay. When a nucleus made a transition from one state to another there should be a fixed amount of energy. Pauli proposed that when the electron had less than maximum energy the rest of the energy was taken by this new particle. That this was a serious problem is illustrated by the fact that Bohr’s solution was that energy conservation no longer held at the nuclear level. That was too radical for Pauli (2).

Pauli called the new particle a “neutron”. In 1932 Chadwick discovered the particle we all know as the neutron. When someone asked Enrico Fermi as to the difference between Chadwick’s neutron and Pauli’s, he is reported to have said Chadwick’s was “grande” but Pauli’s neutron was “piccolo”, a “neutrino”. And so it has been ever since.

In 1933 Fermi formulated his theory of beta-decay (3). He used to say that once he understood quantum electrodynamics (in 1931 he gave a set of beautiful lectures on QED at the University of Michigan summer school) he knew what to do. The electron and neutrino were created in the nuclear transition just as the photon is created in an atomic transition. Of course, a new fundamental interaction was needed and a new fundamental constant  $G_f$ . I like to say that the work of Pauli and Fermi constitutes the beginning of particle physics.

An important consequence of Fermi’s theory was that it could be used to calculate the cross-section for neutrinos hitting neutrons and protons in terms of  $G_f$  which had been determined from the rate of beta decay. This was done by Bethe and Peierls (4) in 1934 with the result that the cross-section was less than  $10^{-43}$  cm<sup>2</sup>; this particle would never be detected.

In his original paper Fermi also discusses the mass of the neutrino. By comparing the theoretical electron spectrum with observations he concluded that the mass was “equal to zero or, in any case, small compared to the mass of the electron”.

Evidence in favor of the neutrino hypothesis came over time from studies of the recoil nucleus from beta-decay (5). However only 25 years after Pauli came the definite detection by Cowan and Reines, to be reviewed in the next talk. Another 40 years elapsed before Fred Reines finally got his Nobel Prize in 1995.

The next episode in the neutrino story started with the pi-mu puzzle. The mesons observed in cosmic rays were presumed to be Yukawa’s, now called pions, but the negative mesons were found not to be captured by light nuclei in the famous experiment of Conversi,

Pancini and Piccioni. The definitive answer was given in 1948 by the emulsion experiments of the Powell group. There the pion was seen to stop in emulsion and a long muon track emerged (6). There was nothing seen in the direction opposite to the muon; it didn't take a Pauli to call this nothing a neutrino.

The question gradually arose whether this was the same neutrino as the one in beta-decay (7). A possible experiment to determine this was outlined by Mel Schwartz (8) and led to the discovery of the mu-neutrino to be discussed in the talk by Jack Steinberger. The New York Times reported that the physicists had discovered a "new kind of nothing". For this Mel, Jack and Leon Lederman received the Nobel Prize in 1988. Why the second neutrino got the prize before the first I will not explain.

The study of the interactions of the mu-neutrino with matter led to the discovery of neutral currents in 1973, but only after they had been predicted in Weinberg's electroweak gauge theory. For many years after 1973, the major results in neutrino physics came from extraterrestrial sources: cosmic rays interacting with the atmosphere, the sun and supernova 1987a.

The solar neutrino discoveries provide one of the greatest scientific events of the last 50 years. The story starts in the 19<sup>th</sup> century with the question of how the sun's energy is produced. This is the energy the earth depends on; what is its origin? The best answer that could be found by scientists like Lord Kelvin was gravitational contraction; the sun could shine for less than 50 million years.

The answer came in the 1930's with the discovery of nuclear fusion reactions. In particular, Bethe and Critchfield (9) proposed the pp cycle of reactions to fuse hydrogen into helium, but how could you tell if this was the right answer; how could you see into the center of the sun? The answer was that neutrinos emerged from the center of the sun with negligible absorption and reached the earth 8 minutes after the reactions took place. Detailed calculations of the neutrino flux from the pp cycle were made in the 1960's by John Bahcall, whose absence today we regret most deeply.

Given this wonderful opportunity to see inside the sun you would imagine that many scientists would carry out solar neutrino experiments. In fact for 20 years one man almost alone searched for these neutrinos. His name was Raymond Davis, who died within the last month. To be fair Fred Reines and his collaborators set up more than one experiment. However, once Davis first results arrived in 1968, it was clear that the Reines experiments were too small to see solar neutrinos.

The Davis experiment used the capture of electron neutrinos in chlorine transforming it to argon, a reaction suggested independently by Pontecorvo and Luis Alvarez (10). Bahcall's final calculation predicted that a little more than one argon atom a day would be produced in 100,000 gallons of carbon tetrachloride. Davis found a little less than half an atom a day. And so the solar neutrino problem was born.

I like to say that the solar neutrino problem is the prototypical problem of astrophysics. We apply the laws of physics that hold on earth to explain the stars, but do we know all the laws? Are we using our physics to understand the stars or are we using the cosmos as a laboratory to study the laws of physics? Was the problem the sun or the neutrino?

The definitive answer came with the Sudbury neutrino observatory (SNO) experiment first suggested by the late Herb Chen. The total flux of neutrinos of all flavors as measured by the neutral current reaction agreed with the theoretical expectation, but only a third arrived electron neutrinos. Two-thirds of the neutrinos had oscillated to tau and mu neutrinos on their way out from the center of the sun. Thus the wonderful success story: we have learned that our theory of the sun appears to be all right and at the same time that neutrinos have masses and large flavor mixing.

However it is really necessary to complete the story. Although we think we now understand that results, the fact is that most of the experiments concern the very rare (2 out of

10,000) Boron-8 neutrinos. The only direct evidence for the main neutrinos from Beryllium and the pp reactions comes from the gallium experiment which integrates over the whole spectrum above 200 keV. It is essential that in the future that we have direct observations of these neutrinos to make sure that we have not missed something and to convince the general scientific community that we have confirmed the theory of solar energy. Once an experiment detects clearly the pp neutrinos, that result should be shown in every astronomy textbook from that day forward.

In conclusion here today we honor the pioneers of neutrino physics: Wolfgang Pauli, Enrico Fermi, Bruno Pontecorvo, Fred Reines, John Bahcall, Raymond Davis and others, those who wagered and won!

This work was supported in part by The Department of Energy under contract number DE-FG02-91ER40682

1. This is from the translation by L. Brown, Sept. 1978 Phys. Today, 21-24,
2. See W. Pauli "On the earlier and more recent history of the neutrino" in K. Winter (ed) 2000 Neutrino Physics, Cambridge U. Press, 1-22,
3. E. Fermi, (1933) Ric. Scientifica 4, 491-495, (1934) Nuovo Cimento 11, 1-19
4. H. A. Bethe and R. Peierls, (1934) Nature 133, 532
5. B. Pontecorvo, (1948) Rep. on Progr in Physics 11, 32-42
6. C.M.G. Lattes et al, 1947 Nature 159, 694
7. S. Oneda and J. C. Pati, (1959) Phys. Rev. Lett 2, 125, G. Feinberg, (1958) Phys. Rev 110, 1482, B. Pontecorvo, (1960) Soviet Physics JETP 37, 1236
8. M. Schwartz, (1960) Phys. Rev. Lett. 4, 396
9. H. A. Bethe and C.L. Critchfield, (1938) Phys. Rev. 54, 248
10. B. Pontecorvo, (1946) Chalk River Report PD-205, L. Alvarez, (1949) Univ. of California, Rad Lab Report

# Research program towards observation of neutrino-nucleus coherent scattering

H T Wong<sup>1,\*</sup>, H B Li<sup>1</sup>, S K Lin<sup>1</sup>, S T Lin<sup>1</sup>, D He<sup>2</sup>, J Li<sup>2</sup>, X Li<sup>2</sup>, Q Yue<sup>2</sup>, Z Y Zhou<sup>3</sup> and S K Kim<sup>4</sup>

<sup>1</sup> Institute of Physics, Academia Sinica, Taipei 11529, Taiwan.

<sup>2</sup> Department of Engineering Physics, Tsing Hua University, Beijing 100084, China.

<sup>3</sup> Department of Nuclear Physics, Institute of Atomic Energy, Beijing 102413, China.

<sup>4</sup> Department of Physics, Seoul National University, Seoul 151-742, Korea.

E-mail: htwong@phys.sinica.edu.tw (\*Corresponding Author)

**Abstract.** The article describes the research program towards an experiment to observe coherent scattering between neutrinos and the nucleus at the power reactor. The motivations of studying this process are surveyed. In particular, a threshold of 100-200 eV has been achieved with an ultra-low-energy germanium detector prototype. This detection capability at low energy can also be adapted for searches of Cold Dark Matter in the low-mass region as well as to enhance the sensitivities in the study of neutrino magnetic moments.

Neutrino coherent scattering with the nucleus[1]  $\nu + N \rightarrow \nu + N$  is a fundamental neutrino interaction which has never been experimentally observed. The Standard Model cross section for this process is given by:

$$\left(\frac{d\sigma}{dT}\right)_{\text{SM}}^{\text{coh}} = \frac{G_{\text{F}}^2}{4\pi} m_{\text{N}} [Z(1 - 4\sin^2\theta_{\text{W}}) - N]^2 \left[1 - \frac{m_{\text{N}} T_{\text{N}}}{2E_{\nu}^2}\right] \quad \& \quad \sigma_{\text{tot}} = \frac{G_{\text{F}}^2 E_{\nu}^2}{4\pi} [Z(1 - 4\sin^2\theta_{\text{W}}) - N]^2 \quad ,$$

where  $m_{\text{N}}$ ,  $N$  and  $Z$  are the mass, neutron number and atomic number of the nuclei, respectively,  $E_{\nu}$  is the incident neutrino energy and  $T_{\text{N}}$  is the measure-able recoil energy of the nucleus. This formula is applicable for  $E_{\nu} < 50$  MeV where the momentum transfer ( $Q^2$ ) is small such that  $Q^2 R^2 < 1$ , where  $R$  is the nuclear size. Although the cross-section is relatively large due to the  $\sim N^2$  enhancement by coherence, the small kinetic energy from nuclear recoils poses severe experimental challenges both to the detector sensitivity and to background control. Various detector techniques have been considered[2] to meet these challenges.

Measurement of the coherent scattering cross-section would provide a sensitive test to the Standard Model[3], probing the weak nuclear charge and radiative corrections due to possible new physics above the weak scale. The coherent interaction plays important role in astrophysical processes where the neutrino-electron scatterings are suppressed due to Fermi gas degeneracy. It is significant to the neutrino dynamics and energy transport in supernovae and neutron stars[4]. Being a new detection channel for neutrinos, it may provide new approaches to study other aspects of neutrino physics, such as that for supernova neutrinos[5]. Coherent scattering with the nuclei is also the detection mechanism adopted in the direct Dark Matter searches[6], such that its observations and measurements with the known particle neutrino is an important milestone. Furthermore, neutrino coherent scattering may be a promising avenue towards a

compact and relatively transportable neutrino detector, an application of which can be for the real-time monitoring on the operation of nuclear reactors[7].

Nuclear power reactors provide powerful and controllable source of electron anti-neutrinos, and can serve as optimal tool for the studies of neutrino-nucleus scatterings. A research program on low energy neutrino physics[8] is intensely pursued by the TEXONO Collaboration at the Kuo-Sheng (KS) Nuclear Power Station in Taiwan. The expected observable spectra due to  $\bar{\nu}_e$ -e and  $\bar{\nu}_e$ -N scatterings with Standard Model (SM) and magnetic moment (MM) interactions at KS are displayed in Figure 1. The maximum nuclear recoil energy  $T_{\max}$  in  $\bar{\nu}_e$ -N coherent scatterings is given by:  $T_{\max} = \frac{2E_\nu^2}{M_N + 2E_\nu}$  which corresponds to  $T_{\max} = 1.9$  keV in the case of Ge target ( $A=72.6$ ) exposed to the typical reactor neutrino spectra.

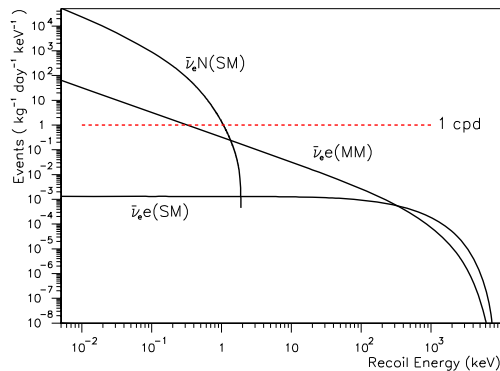


**Figure 1.** The differential cross-section of the various neutrino interaction channels, at KS-Lab with Ge as the target isotope. The background level of 1 cpd is also shown.

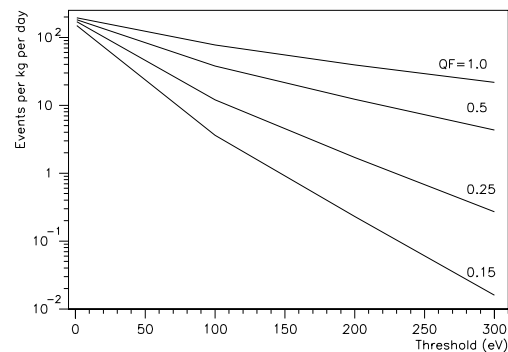


**Figure 2.** The variations of the neutrino coherent scattering event rates versus threshold at different quenching factors for a 1 kg ULEGe detector at KS Lab.

High-Purity Germanium(HPGe) detectors have been widely and successfully used in various areas of low energy neutrino physics and cold dark matter searches. These detectors are kilogram-scale in mass, and with a detection threshold (“noise edge”) of several keV. A sensitive direct search of neutrino magnetic moments[9] was recently performed with a 1 kg HPGe detector at KS[10]. A physics threshold of 12 keV and a background level of  $\sim 1 \text{ day}^{-1} \text{ kg}^{-1} \text{ keV}^{-1}$  (cpd) comparable to underground dark matter experiments were achieved. For ionization detectors like germanium, the measure-able energy of nuclear recoil events is only a fraction of their energy deposited due to charge recombination or “quenching” at large  $dE/dx$ . The expected event rates for neutrino-nucleus coherent scattering at different threshold and quenching factors (QF) at KS are depicted in Figure 2. The QF for Ge is typically 0.25 in the several keV region, such that the maximum measure-able energy for nuclear recoil events is only about 500 eV.

“Ultra-Low-Energy” Germanium (ULEGe) detectors, developed originally for soft X-rays detection, are candidate technologies to meet these challenges of probing into a previously unexplored energy domain[11]. These detectors typically have modular mass of 5-10 grams while detector array of up to  $N=30$  elements have been successfully built. Various prototypes based on this detector technology have been constructed. As illustrations, the measured energy spectrum with a 10 g ULEGe prototype is depicted in Figure 3. Pulse shape discrimination (PSD) criteria were applied as illustrated in Figure 4 by correlating two output with different electronics amplifications and shaping times. Calibration was achieved by external  $^{55}\text{Fe}$  X-ray sources (5.90 and 6.49 keV) together with X-rays from titanium (4.51 and 4.93 keV), calcium (4.01 keV), sulphur (2.46 keV) and aluminium (1.55 keV). A random trigger uncorrelated to the detector provided the zero-energy condition. The electronic noise edge can be suppressed

by PSD and a threshold of 100 eV was achieved.

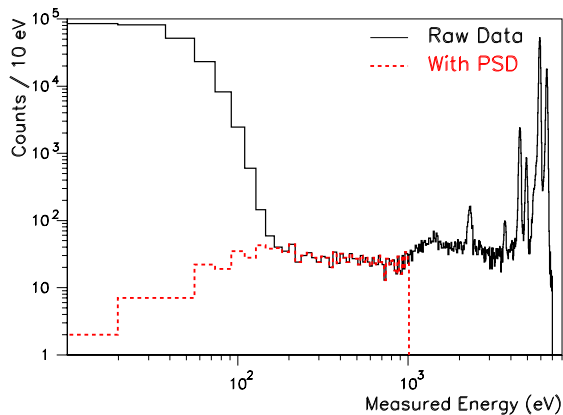


**Figure 3.** Measured energy spectra with  $^{55}\text{Fe}$  source with X-rays from Ti by the ULEGe prototype. A threshold of 100 eV was achieved, and the electronic noise edge was suppressed by PSD.

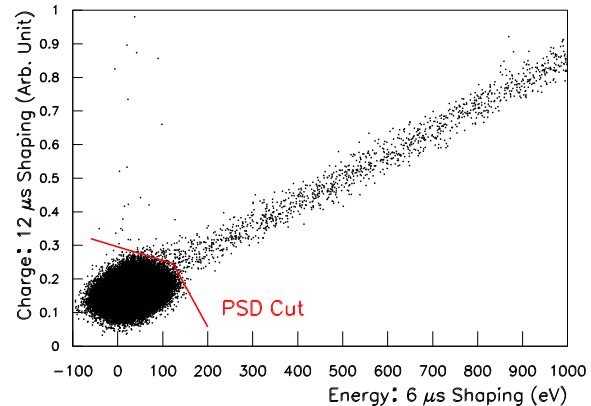


**Figure 4.** Pulse shape discrimination: correlations of signals with different electronic amplifications and shaping times lead to suppression of the noise edge.

The goal of the  $\nu$ -N coherent scattering experiment is to develop a ULEGe detector with a total mass of  $\sim 1$  kg and a modular threshold as low as 100 eV, with a background level below 1 keV in the range of 1 cpd. From Figure 2 and at the typical  $QF=0.25$ , the event rate for such configurations at KS will be  $11 \text{ kg}^{-1}\text{day}^{-1}$ , implying a signal-to-background ratio of  $>22$ . A by-product of such an detector would be to further enhance the searches of neutrino magnetic moment at reactors. An improved sensitivity range down to  $\sim 10^{-11} \mu_B$  can be expected[9]. Such detector can also be used for Cold Dark Matter searches[6], probing the unexplored low WIMP-mass region, as indicated in Figure 5.

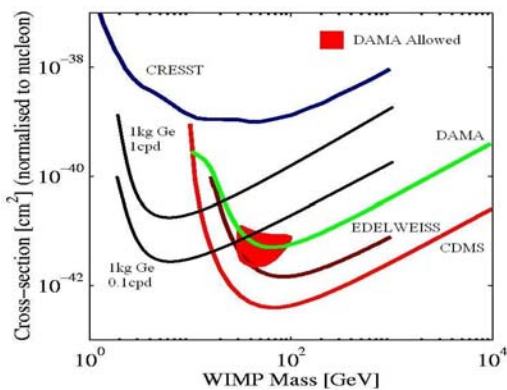


**Figure 5.** Expected sensitivity region for Cold Dark Matter searches using a ULEGe detector with a total mass of 1 kg.

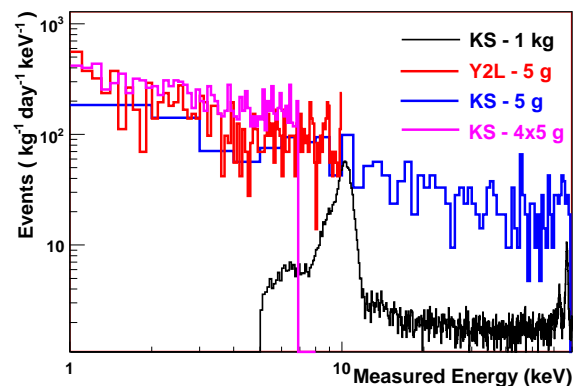


**Figure 6.** Measured background spectra, normalized by mass, at KS and Y2L with different Ge detectors.

An R&D program towards realizations of these experiments is being pursued. A quenching factor measurement for nuclear recoils in Ge with sub-keV ionization energy is being prepared at a neutron beam facility. Background studies are performed at both KS as well as the Yang-Yang Underground Laboratory (Y2L) in South Korea with the different prototypes. The measured

spectra above 1 keV on the various configurations are presented in Figure 6, while sub-keV background are under intense studies. The factor-of-ten difference in the mass-normalized background levels between the 1 kg and 5 g detectors is due to self-shielding of the detector. Such effects are reproduced by realistic simulation studies on the variations of  $\gamma$  and neutron background levels with detector mass, as depicted in Figure 7.

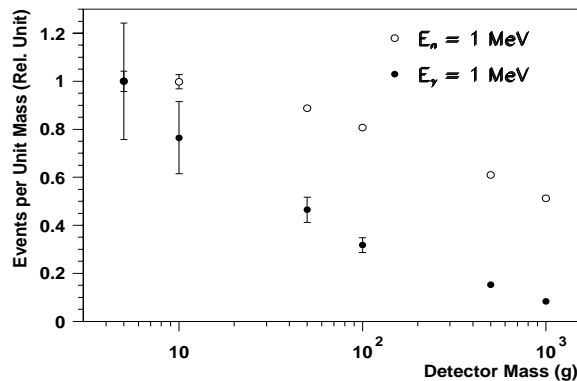


**Figure 7.** Simulated results on the variations of background per unit mass versus detector mass at the same external  $\gamma$  and neutron background level.

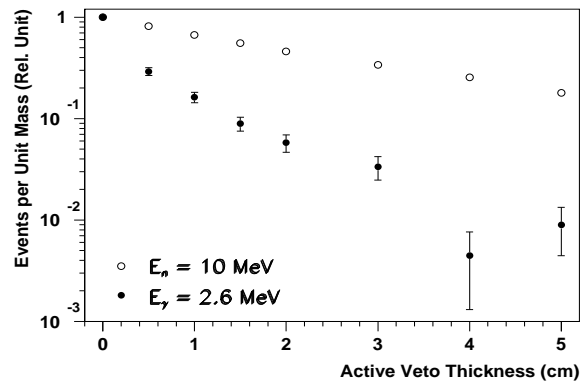


**Figure 8.** Simulated results on the background suppression for  $\gamma$  and neutron sources at the inner ULEGe target due to an enclosing structures of active Ge-vetos.

Consequently, in the scaling-up to the kilogram mass-range, the individual elements of the ULEGe should be assembled in a compact array in order to maintain the same background level of  $\sim 1$  cpd achieved in the 1 kg HPGe detector. The “segmented” Ge technology with the integrated circuitry approach is an attractive alternative. Configurations can be envisaged to have active veto HPGe layers enclosing hermetically the ULEGe inner target. Simulation results of Figure 8 show that a Ge-veto thickness of 3 cm can further suppress the background at the inner target by about a factor of 30 and 3 for typical  $\gamma$  and neutron background, respectively. A prototype segmented ULEGe detector with a veto ring and dual-readout channels from both the signal and high-voltage electrodes is being constructed.

## References

- [1] Freedman D S 1974 *Phys. Rev.* **D 9**, 1389; Gaponov Y V and Tikhonov V N 1977 *Sov. J. Nucl. Phys.* **26**, 31; Sehgal L H and Wanninger M 1986 *Phys. Lett.* **B 171**, 107.
- [2] Drukier A and Stodolsky L 1984 *Phys. Rev.* **D 30**, 2295; Canbrea B, Krauss L M and Wilczek F 1985 *Phys. Rev. Lett.* **55**, 25; Barbeau P et al. 2003 *IEEE Tran. Nucl. Sci.* **50**, 1285; Hagmann C and Bernstein A, 2004 *IEEE Tran. Nucl. Sci.* **51**, 2151.
- [3] Krauss L M 1991 *Phys. Lett.* **B 269**, 407; Barranco J, Miranda O G and Rashba T I 2005 *J. High Energy Phys.* **12**, 021; Papavassiliou J, Bernabéu J and Passera M 2005 *Preprint hep-ph/0512029*; Scholberg K 2006 *Phys. Rev.* **D 73**, 033005.
- [4] Wilson J R 1974 *Phys. Rev. Lett.* **32**, 849; Freedman D Z, Schramm D N and Tubbs D L 1977 *Annu. Rev. Nucl. Sci.* **27**, 167.
- [5] Aune S et al. 2005 *Preprint hep-ex/0503031*; Scholberg K, *these Proceedings*.
- [6] Akerid D 2006 *these Proceedings*; Smith N 2006 *these Proceedings*;
- [7] Cribier M 2006 *these Proceedings*.
- [8] Wong H T 2004 *Mod. Phys. Lett.* **A 19**, 1207.
- [9] Wong H T and Li H B 2005 *Mod. Phys. Lett.* **A 20**, 1103.
- [10] Li H B et al. 2003 *Phys. Rev. Lett.* **90**, 131802; Xin B et al. 2005 *Phys. Rev.* **D 72**, 012006; Wong H T 2006 *Preprint hep-ex/0605006*.
- [11] Wong H T et al. 2006 *J. Phys. Conf. Ser.* **39**, 266.

# High Energy Neutrino Emissions from GRBs: Predictions and Issues

**Bing Zhang**

Department of Physics and Astronomy, University of Nevada Las Vegas

E-mail: bzhang@physics.unlv.edu

**Abstract.** Gamma-ray bursts (GRBs) are believed to be cosmic ray accelerators and high energy neutrino emitters. Within the framework of the standard GRB fireball model, neutrinos of a wide range of energy are produced from different emission sites. The published predictions of GRB neutrino emission are reviewed, especially in view of the latest GRB observations with Swift. Issues regarding the uncertainties in those predictions are discussed.

## 1. Introduction

Gamma-ray bursts (GRBs) are short, energetic bursts of gamma-rays that mark the most violent, cataclysmic explosions in the universe. Followed by the broad-band afterglows, these event are observationally accessible in essentially all electromagnetic wavelengths. Within the standard fireball model of GRBs [1], GRBs are originated from a relativistic ejecta that moves towards the Earth. gamma-rays are emitted by the shock-accelerated electrons in the so-called internal shocks, while afterglow photons are emitted by the electrons accelerated from an external forward shock as the fireball is decelerated by the circumburst medium.

The external shock afterglow model has been successful to interpret much of the broad-band afterglow data. The latest observations with NASA's dedicated mission Swift reveal a rich phenomenology of GRB afterglows, which requires additional emission components other than the external shock to interpret the X-ray (and probably also the optical) afterglows [2,3]. In any case, one could safely accept that the external shock indeed exists. There is no direct proof for the existence of internal shocks, on the other hand. They are introduced to mainly interpret the erratic, irregular gamma-ray lightcurves during the burst. Alternative suggestions to interpret the prompt emission include other energy dissipation mechanisms such as magnetic reconnection.

The suggestion that GRBs are high energy neutrino emitters has been rooted in the belief that GRB outflows are baryonic in nature (not dominated by a Poynting flux) and that shocks are the sites of energy dissipation. While electrons must have been accelerated to high energies to radiate and give rise to the observed GRBs, associated ions (mainly protons) must have been also accelerated to high energies. The interactions between these high energy protons and soft photons or other nucleons would give rise to intense emission of high energy neutrinos. Originally, the suggestion that GRBs are neutrino emitters was derived from the argument that GRBs are likely sources of ultra-high energy cosmic rays (UHECRs) [4]. More generally, GRBs can be important neutrino emitters even if the shocks cannot accelerate particles to the desired high energies of UHECRs, as long as shocks are in operation.

## 2. GRBs as emitters of neutrinos of different energies

Widely discussed processes for high energy neutrino emission include

- $p\gamma$  process:  $p\gamma \rightarrow \Delta^+ \rightarrow n\pi^+ \rightarrow ne^+\nu_e\bar{\nu}_\mu\nu_\mu$ ;
- $pp$  process:  $pp \rightarrow \pi^\pm/K^\pm \dots \rightarrow \mu\nu_\mu \dots \rightarrow e\nu_e\bar{\nu}_\mu\nu_\mu \dots$ ;
- $pn$  process:  $pn \rightarrow \pi^\pm/K^\pm \dots \rightarrow \mu\nu_\mu \dots \rightarrow e\nu_e\bar{\nu}_\mu\nu_\mu \dots$ .

The dominant  $p\gamma$  process occurs at the  $\Delta$ -resonance, which has the threshold condition  $\epsilon_p\epsilon_\gamma \sim 0.2 \text{ GeV}^2$  in the center of mass frame. In the case of GRBs, this is usually translated in the observer's frame to  $\epsilon_p\epsilon_\gamma \sim 0.2 \text{ GeV}^2\Gamma^2$  if both protons and photons are generated in relativistic shocks, where  $\Gamma$  is the bulk Lorentz factor. The threshold condition for both  $pp$  and  $pn$  interactions is that the relative drift energy between these baryons exceed the pion rest mass, i.e.,  $\epsilon' \geq 140 \text{ MeV}$ . Since both  $p$  and  $n$  have a rest mass close to 1 GeV, the threshold of  $pp$  and  $pn$  interaction only demands semi-relativistic relative motions.

In a GRB event, there are multiple sites where neutrinos with different energies are generated. Below is a non-exhaustive list which encompasses most of the processes discussed in the literature, in a sequence of ascending neutrino energy, which is essentially also in a sequence of ascending distance from the central engine:

- MeV neutrinos: Long GRBs are believed to be originated from stellar collapses, while short GRBs are likely related to mergers of compact objects. In both cases, they should be associated with thermal MeV neutrinos. In most models, the central engine involves a black hole - torus system, and the thermal neutrino annihilation is one of the leading processes for launching the fireball. For long GRBs, MeV neutrino signals are expected such as those in supernovae. However, these thermal neutrinos are extremely difficult to detect from cosmological distances, due to the very low cross section for  $\nu N$  interactions at these energies.
- multi-GeV neutrinos: GRB fireballs may be neutron-rich. During the fireball acceleration phase, neutrons can decouple from protons when the elastic scattering condition breaks down. The relative drift between both species results in inelastic  $pn$  interactions giving rise to 5-10 GeV neutrinos [5]. A similar process also occurs within sub-photospheric internal shocks, which extends significantly the parameter space for the inelastic neutrino collision condition [6].  $pp$  interactions within the internal shocks can also give rise to a 30 GeV neutrino burst, although magnetic fields can inhibit the inter-penetration of charged species streams with different velocities [7];
- multi-TeV neutrinos: Within the collapsar scenario, the relativistic jet launched from the base of the flow (presumably the black hole and the torus) has to penetrate through the stellar envelope before breaking out and generating the GRB. The internal shocks below the envelope accelerate protons that interact with thermal photons within the envelope (i.e.  $p\gamma$  interaction). Regardless of whether the jet finally penetrates through the envelope or gets choked, it will generate strong multi-TeV neutrino signals [8]. The signature is enhanced or even dominated by  $pn, pp$  interactions and could be used as a diagnostic about the type of progenitor stars [9];
- $\sim \text{PeV}$  neutrinos:  $p\gamma$  interactions within the conventional internal shocks which produce prompt gamma-rays typically generate  $10^{14} - 10^{16} \text{ eV}$  neutrinos [10]. For a long-duration GRB with a dense medium (e.g. in the stellar wind environment), the internal shock gamma-rays may overlap the external shock region (both the forward and the reverse shock) and interact with the protons accelerated in those shocks. These interactions also give rise to  $\sim \text{PeV}$  range neutrinos [11].
- $\sim \text{EeV}$  neutrinos:  $p\gamma$  interactions within the external reverse shock give rise to even higher energy neutrinos. For a constant density medium the typical energy is  $10^{17} - 10^{19} \text{ eV}$ , while

for a wind medium, the typical energy is  $\sim 3 \times (10^{15} - 10^{17})$  eV and extending above it [12]. In the forward shock region, assuming the blast wave can accelerate protons to ultrahigh energies, a neutrino afterglow is expected with the peak energy  $\sim 10^{18}$  eV [13].

The latest observations by Swift provide two new interesting possibilities of GRB neutrino emissions.

- Erratic X-ray flares are observed in about half GRBs [14]. The properties of these flares strongly suggest that they are of “internal” origin, marking the reactivation of the GRB central engine [2,15,16]. If these late internal emissions are also from internal shocks,  $p\gamma$  interactions would generate high energy neutrinos as well, which peaks at a higher energy than the traditional internal shock component for the GRB prompt emission [17].
- The discovery of the nearby low-luminosity (LL) GRB 060218 suggests a much higher local event rate of LL-GRBs [18]. Although these X-ray flashes are less energetic individually, the high event rate compensates the energy deficit, making LL-GRBs form an interesting second high-energy component in the diffuse neutrino spectrum [19,20].

The flux levels of the above mentioned various neutrino emission components have been calculated. Neutrinos from individual GRBs can be only detected from nearby, bright events (e.g. GRB 030329 [9]). For the majority of GRBs, what is observationally interesting is the diffuse neutrino background from all GRBs. For sources that are optically thin for  $p\gamma$  and  $pp$  interactions (which are also likely the best candidates of high energy neutrino sources such as GRBs and AGNs), an upper limit of diffuse neutrino background could be placed using the observed UHECR data [21].

$$E_\nu^2 \Phi < E_\nu^2 \Phi_\nu^{WB} = 2 \times 10^{-8} \zeta_z \left[ \frac{E_p^2 d\dot{N}_p/dE_p|_{z=0}}{10^{44} \text{ ergs Mpc}^{-3} \text{ yr}^{-1}} \right] \text{ GeV cm}^{-2} \text{ s}^{-1} \text{ sr}^{-1} . \quad (1)$$

A good list of neutrino telescopes are being constructed [22]. In order to reach the WB limit and therefore to place an interesting limit on the diffuse neutrino flux, kilometer-size (giga-ton) detectors are needed. The Antarctic Muon and Neutrino Detector Array (AMANDA) has been in operation since 2000, and has achieved an effective detector mass of  $\sim 0.1$  Gton. The extension of AMANDA, Icecube, is planned to reach the  $\sim 1$  Gton effective detector mass by 2008-2009. Other neutrino detectors include ANTARES (Astronomy with a Neutrino Telescope and Abyss Environment Research), NESTOR (Neutrino Extended Submarine Telescope with Oceanographic Research), RICE, ANITA, KM3Net, etc. Although no neutrino signals from GRBs have been reported so far, it looks promising that breakthrough will be made in the next several years.

Among the neutrino emission components discussed above, the most promising components from observational point of view are the  $\sim$  PeV neutrino emission from internal shocks [10] (or “overlapping” external shocks [11]) and the multi-TeV emission from slow jets inside the stellar envelopes [8,9]. This is because at lower energies (below TeV) the atmospheric neutrino background sharply increases with decreasing energies, and at higher energies (above several PeV) a much larger effective detector mass is needed.

### 3. Uncertainties in the neutrino flux predictions

In view that directly detecting the GRB neutrino background (or posing a stringent upper limit) becomes plausible in the near future, it would be informative to collect various issues regarding the predicted neutrino fluxes. This would serve to answer the questions such as “what if the neutrino background is not detected at the predicted level?”, etc. This section is dedicated to this topic.

The most important issue is the composition of the GRB ejecta. As discussed above, the observationally most interesting component ( $\sim$  PeV component) solely relies on the assumption that GRB prompt emission is produced in internal shocks. While this is the most popular model of prompt emission, there is no robust proof. A list of concerns regarding the internal shock model have been raised in the literature.

- Gamma-ray polarization and reverse shock modeling both suggest that the GRB central engine is likely strongly magnetized [23]. Weak or negligible reverse shock emission from many GRBs is at least consistent with a Poynting flux dominated flow [24,25].
- Independent arguments have been raised to suggest a prompt emission radius orders of magnitude larger than the standard internal shock radius [26].
- At least for X-ray flares, mechanisms involving magnetic fields are needed, and there is a clean argument based on energetics only to suggest that the GRB outflow is launched via magnetic processes [16].
- The internal shock model predicts much wider distributions of spectral peak energy ( $E_p$ ) within a same burst and among different bursts, which are inconsistent with the data [27].
- It has been argued recently by several different groups that some empirical relations invoking prompt emission parameters are more naturally interpreted by invoking energy dissipation near the photosphere of the fireball where internal shocks are no longer necessarily needed [28].

Although none of the above objections can rule out the internal shock model, they do raise the caution that the  $\sim$  PeV neutrino signals [10] are not guaranteed. Positive detections of these signals, on the other hand, would greatly support the internal shock model and would rule out the Poynting-flux-dominated model of GRBs. The  $\sim$  PeV neutrino signals due to overlapping the prompt gamma-ray front and the external shock region [11] are more robust if overlapping indeed happen, since it is almost certain that an external forward shock exists. The condition for overlapping, on the other hand, is not easy to satisfy in the constant density ISM medium but is likely satisfied in a stellar wind medium. Recent Swift observations however suggest that a wind-type medium, if any, is very rare [2,25].

Even if GRBs are baryonic in nature, the predictions of the  $\sim$  PeV neutrino flux is still subject to uncertainties. Two effects, in particular, affect the predicted neutrino flux level significantly [19]. First, in order to maximize the predicted neutrino flux, usually a  $p = 2$  proton spectrum is assumed. Studies of prompt and afterglow emissions suggest that  $p$  is typically steeper than 2 for electrons. If protons also have  $p > 2$ , the predicted neutrino spectrum no longer has a flat plateau, and the flux would drop at high energies above the peak. Second, usually the neutrino spectrum for a burst with typical parameters is taken to estimate the diffuse neutrino flux [10]. In principle, one needs to average over bursts with a wide range of distributions of luminosity and other parameters. Such an analysis [19] suggests that the predicted diffuse background emission sensitively depends on some unknown parameters, especially the bulk Lorentz factor of GRBs. The predicted diffuse neutrino flux level is therefore rather uncertain. On the other hand, the detection (or tight upper limit) would present severe constraints on the bulk Lorentz factor distribution of GRBs.

#### 4. Conclusions

There are good reasons to believe that GRBs are one of the best candidates for high energy neutrino emission. Within the standard GRB fireball framework, neutrinos from MeV to EeV are produced. The detectability of these signals depend on detectors' capability, and it is optimistic that neutrinos in the TeV-PeV range may be detectable in the near future. The predicted flux levels in this energy range, on the other hand, suffer important uncertainties of some unknown

# *POSTERS*

# Radio Ice Cherenkov Experiment Flux Limits

**J. Adams for the RICE Collaboration**

University of Canterbury, Private Bag 4800, Christchurch, New Zealand

RICE is an array of radio receivers deployed in the ice at the South Pole. It is designed to detect neutrinos with energies in the PeV range and higher with the long attenuation length of radio frequencies in ice meaning that the effective volume of RICE extends well beyond the instrumented volume of ice. Development, calibration and status of RICE is detailed in [1, 2, 3]. The concept behind RICE is that an UHE  $\nu_e$  that undergoes a charged current interaction in the ice will transfer most of its energy to the resulting electron. The electron initiates a shower of Cherenkov emitting particles. The Cherenkov pulse that is observed will be a superposition of the signal from each track and will be coherent at radio wavelengths.

Our limits are obtained by considering the neutrino detection efficiency, expressed as an energy dependent effective volume, for the array which is determined by a detailed Monte-Carlo simulation. We compare the number of expected detections for a given input spectrum with the observed number of detections and obtain an upper limit on the normalization of the input spectrum. The total livetime for the 1999–2005 dataset is 13200 hours. Our upper limits, based on the observation of zero candidates, are shown in Figure 1 for various diffuse neutrino flux models and for a stacked sum of five GRBs in Figure 2.

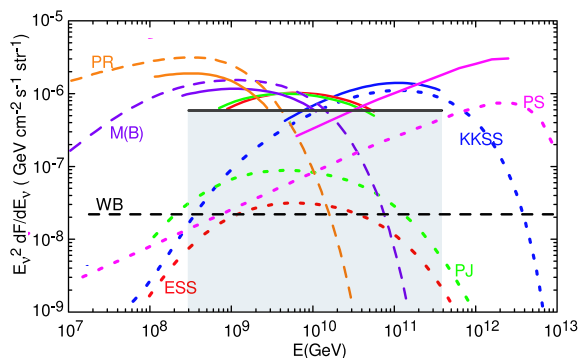


**Figure 1.** Upper bounds on total (all flavour) neutrino fluxes for AGN models (PR, M(B)), GZK neutrino models (ESS,PJ, KKSS) and topological defect models (PS). Dashed curves are for model fluxes and thick curves are the corresponding bounds. The black curve is a model independent summary of current RICE results. Further details and references in [3].

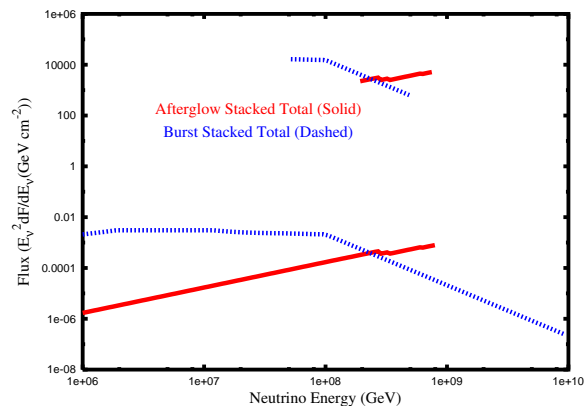


**Figure 2.** RICE upperbounds on the neutrino flux from a stacked sum of five GRBs for which full spectral information was available. Neutrinos produced with the burst photons (solid) and in after-glow associated processes (dashed) are considered. Further details can be found in [4].

- [1] I. Kravchenko et al (The RICE collaboration), *Astropart. Phys.*, 19, 15–36, (2003)
- [2] I. Kravchenko et al (The RICE collaboration), *Astropart. Phys.*, 20, 195–213, (2003)
- [3] I. Kravchenko et al (The RICE collaboration), *Phys.Rev. D*73 (2006) 082002
- [4] D. Besson, S. Razzaque, J. Adams and P. Harris, Accepted by *Astropart. Phys.* astro-ph/0605480

## First data from the ANTARES neutrino telescope

V. Bertin<sup>1</sup> on behalf of the ANTARES Collaboration

<sup>1</sup>C.P.P.M., CNRS/IN2P3 et Université de la Méditerranée,  
Case 902, 163, avenue de Luminy, 13288 Marseille cedex 9, France

E-mail: bertin@cppm.in2p3.fr

**Abstract.** This contribution reviews the recent progress achieved towards building the ANTARES neutrino telescope. The first results obtained by the operation of a Mini Instrumentation Line with Optical Modules, “MILOM”, and the first complete detector line are highlighted.

### 1. The ANTARES detector

The European Collaboration ANTARES aims at building and operating a large undersea neutrino telescope located at a depth of 2500 m in the Mediterranean Sea, offshore from Toulon in France [1]. Neutrinos will be detected through their interaction in the matter surrounding the detector, producing muons radiating Cherenkov light while propagating in the sea water. Photons are recorded by a lattice of Optical Modules (OMs) [2], consisting of 10” hemispherical photomultiplier tubes (PMTs) [3] housed in pressure resistant glass spheres, installed on a set of mooring lines. The reconstruction of the muon track direction, pointing to a fraction of a degree towards the direction of the parent neutrino source for high energy neutrinos, is achieved from the measurement of the arrival times of the Cherenkov photons on the OMs, as well as their position in space.

The complete ANTARES detector will consist of 12 lines of 25 storeys, each storey being equipped with a triplet of Optical Modules looking at 45° downward and an electronics container mounted on a titanium frame, giving a grand-total of 900 OMs. On each storey, the local electronics container includes the front-end electronics of the PMTs, an Ethernet board for the data acquisition and the detector Slow Control, electronics boards for clock distribution and for Dense Wavelength Division Multiplexing of the Ethernet transmission, and a tiltmeter-compass board measuring the local tilt and orientation of the storey. Some storeys also support a hydrophone for acoustic positioning or an LED Optical Beacon used for inter-string time calibration.

The vertical distance between storeys is 14.5 m, the first one being placed at 100 m above the sea bed, leading to a total height of the detector strings of 480 m. Each string is anchored on the sea floor at a distance of 70 m from its neighbours. Every line is individually connected to a Junction Box by an interconnection cable a few hundred metres long. The Junction Box is itself linked to the shore by a 40 km long electro-optical cable equipped with 48 optical fibres.

The construction of the ANTARES detector started in October 2001 with the deployment of the main electro-optical cable from the ANTARES site, located in the Mediterranean Sea (42°48’N-6°10’E) offshore Toulon (France) at a depth of 2475 m, to the beach of La Seyne-sur-Mer where the shore station of the experiment is situated. In December 2002, the Junction Box was connected at the end of this cable and immersed on the site. In Spring 2003, two small test lines, the Prototype Sector

Line (PSL) and the Mini Instrumentation Line (MIL), were installed, connected and operated for a few months. The genuine operation of the ANTARES neutrino telescope really started in April 2005 after the connection of the Mini Instrumentation Line with Optical Modules (MILOM) and more recently the installation of the first full complete detector line, Line 1, in March 2006. The second line, Line 2, was in integration phase in June 2006, at the time of the Neutrino'06 Conference, it has been successfully deployed on the ANTARES site at the end of July 2006 as scheduled. Thanks to two assembly sites running in parallel, the ANTARES detector is foreseen to be fully deployed and operational by the end of 2007 for several years of physics data taking.

The main performance parameters expected for the complete ANTARES neutrino telescope are summarized in figure 1. The left plot shows the effective area for neutrinos as a function of the neutrino energy for various incident angles. The effective area reaches 1 m<sup>2</sup> for  $E_\nu > 100$  TeV, the energy above which the Earth shadowing starts to be of some importance. The right plot shows the angular resolution for the reconstructed muon compared to the true muon direction and to the parent neutrino direction, as a function of the neutrino energy. While the angular resolution is dominated by the physical angle between the muon and the parent neutrino at low energy, it is dominated by the reconstruction for  $E_\nu \geq 10$  TeV and is expected to be as good as 0.3°. In this regime, the angular resolution is mainly dominated by two effects: the scattering and the chromatic dispersion of the Cherenkov light during its travel into the sea water, contributing for a time arrival spread of  $\sigma \sim 1$  ns; the transit time spread (TTS) of the PMT signals being  $\sigma \sim 1.3$  ns.

To achieve this good angular resolution, the ANTARES detector is designed such as additional electronics contributions to the time calibration contribute for less than  $\sim 0.5$  ns to the time-stamping of the detected photons. In addition, the relative position reconstruction of the OM has to be controlled with a precision of  $\sim 10$  cm.

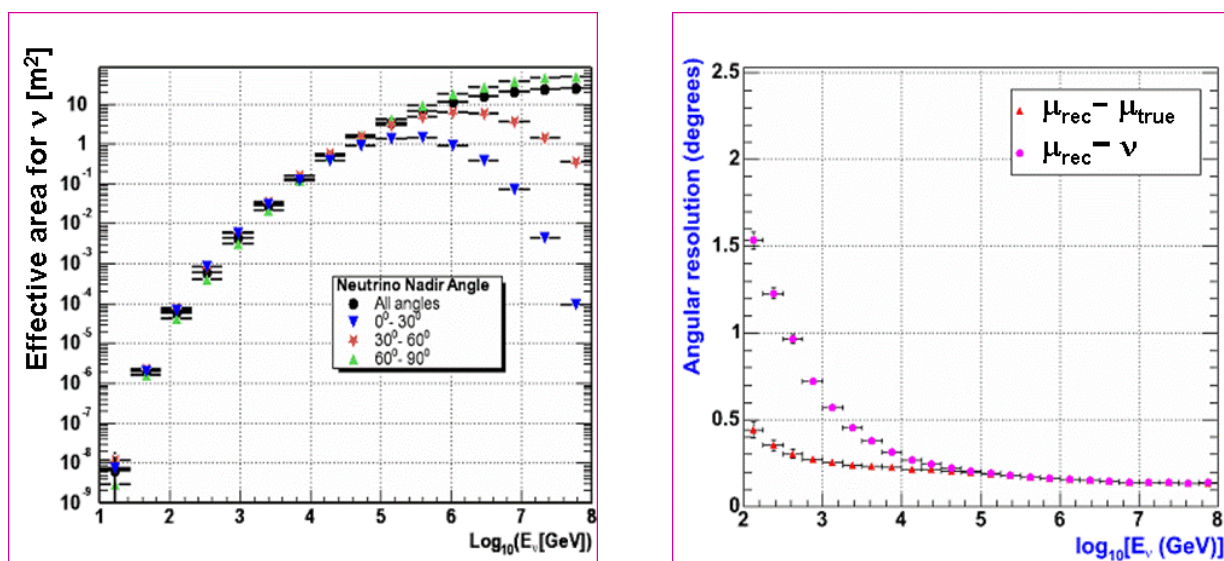


**Figure 1.** Expected performance for the complete 12 lines ANTARES neutrino telescope. The left figure shows the effective area for neutrinos as a function of the neutrino energy for several incident angles. The right figure shows the angular resolution of the reconstructed muon compared to the true muon direction and to the parent neutrino as a function of the neutrino energy.

## 2. Results from the first ANTARES lines

### 2.1. The MILOM line

The current data taking of the ANTARES detector started in March 2005 with the operation of the MILOM [4]. This instrumentation line, partly devoted to multi-disciplinary and environmental studies,

consists of an instrumented releasable anchor, the Bottom String Socket (BSS), and three storeys respectively located at 100 m, 117 m and 169 m above the sea bed. The middle storey is a standard ANTARES storey housing a triplet of Optical Modules. The main other devices are a water current profiler located on the top storey, an LED Optical Beacon held on the bottom storey, an acoustic positioning transducer attached to the BSS and a seismometer buried into the sea floor 50 m away from the MILOM.

2.1.1. *Optical background measurements.* The operation of the MILOM allowed a continuous monitoring of the background rates of the Optical Modules. A typical OM counting rate display exhibits a baseline of  $\sim 60$ -80 kHz largely dominated by optical background due to  $^{40}\text{K}$  decays and bioluminescence activities coming from bacteria, as well as bursts of a few seconds duration produced by bioluminescent emission of macro-organisms [5]. Figure 2 (left) shows the baseline rates recorded by the three OMs of the MILOM during a period of three months in Autumn 2005. A seasonal variation of the bioluminescence component of the baseline is clearly observed. The 15% higher counting rate of OM1 during the full period is due to a lower threshold set on the readout of this Optical Module. Figure 2 (right) shows the burstfraction, defined as the fraction of the time when the counting rate is higher than the baseline by 20% during a 15 min interval, as a function of the water current intensity. A strong correlation of these two quantities is clearly observed.

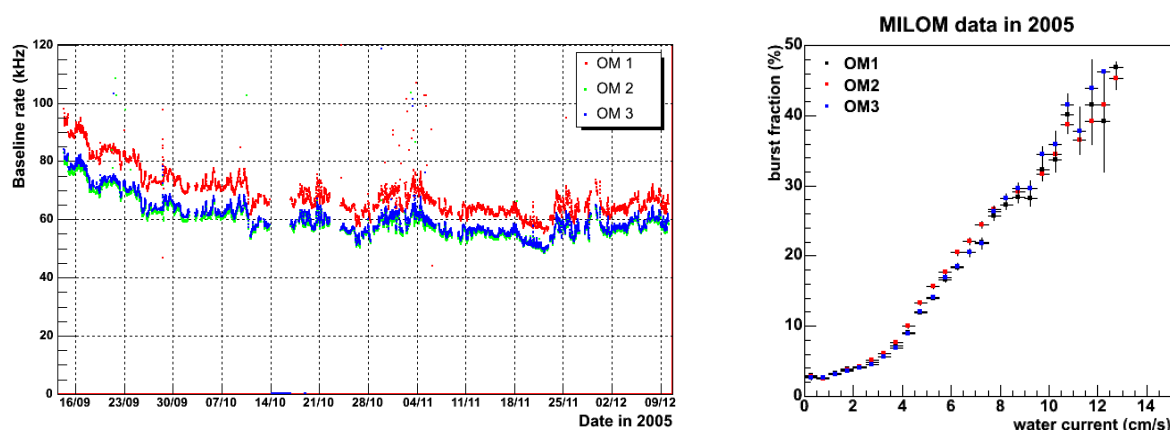


**Figure 2.** Baseline rates recorded by the three OMs of the MILOM during Autumn 2005 (left) and burstfraction as function of the water current intensity (right).

The time coincidences between pairs of neighbouring Optical Modules have also been studied. These distributions exhibit a flat background of random coincidences and a Gaussian peak of few ns width due to genuine coincidences of  $^{40}\text{K}$  radioactive decays producing two detected photons. The  $^{40}\text{K}$  coincidence rate is measured to be  $13.0 \pm 0.5$  Hz and is in good agreement with a simulation the signals induced by  $^{40}\text{K}$  decays which leads to a coincidence rate of 12 Hz with a 4 Hz systematic error due to uncertainties in the effective area and angular response of the OMs.

2.1.2. *Time calibration with the LED Optical Beacon.* The time calibration of the MILOM Optical Modules has been checked by flashing the LED Optical Beacon located on the bottom storey. This device consists of a glass cylinder container containing 36 blue LEDs synchronised in time in order to produced intense light flashes with a time dispersion  $< 0.5$  ns. The time calibration of the OMs can be checked either by looking at the arrival time of the signal on the PMT relative to the time of the flash, or by the time difference of the flash arrival time measured by two adjacent OMs. Due to the large intensity of the light flashes and the short 15 m distance of propagation of the light into the water, the time stamping of the OM signal is dominated by its electronics contribution and not by the TTS of the

PMT in this case. The measured distributions confirm that the electronics contribution to the time calibration is  $\leq 0.5$  ns as expected.

## 2.2. The Line 1

The first complete line of the ANTARES neutrino telescope, Line 1, has been deployed on the site on February 14<sup>th</sup> 2006 and connected two weeks later on March 2<sup>nd</sup> by using the Remote Operated Vehicle *Victor* of IFREMER. This line is made of a BSS and of 25 storeys, holding a total of 75 OMs. It also includes 4 LED Optical Beacons and 5 acoustic positioning hydrophones spread along the line, as well as an acoustic transducer on its BSS.

**2.2.1. Time calibration with the MILOM LED Optical Beacon.** The time calibration of the Line 1 OMs can also be checked by flashing the LED Optical Beacon located on the MILOM bottom storey. Figure 3 (left) shows the detection time spread of the LED Optical Beacon flashes by an OM of Line 1 located on a storey at the same altitude than the MILOM LED Optical Beacon. In this case, the measured distribution width is  $\sigma = 0.7$  ns for a “horizontal” travel path of  $\sim 80$  m of the light in the sea water. Figure 3 (right) shows in comparison the detection time spread for an OM of Line 1 located at a higher altitude corresponding to a “diagonal” travel path of the flash light of  $\sim 150$  m. A wider distribution is clearly observed due to the smaller intensity of the detected signal, as well as a tail of delayed photons coming from scattering light. All measured distributions have been found in good agreement with expectations.

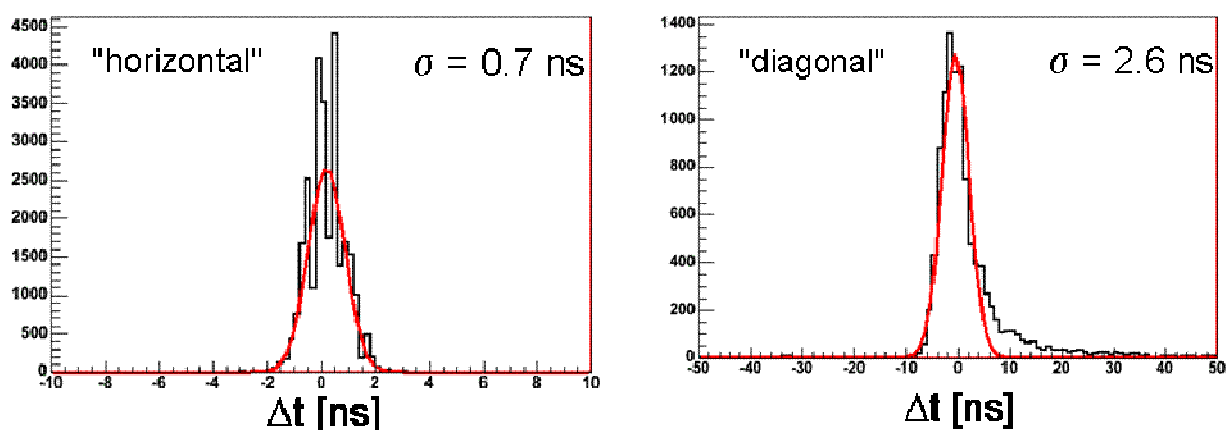


**Figure 3.** Detection time spread of the MILOM LED Optical Beacon flashes by an OM of Line 1 located at the same altitude as the LED Optical Beacon at an “horizontal” distance of  $\sim 80$  m (left) and by an OM at a higher altitude at a “diagonal” distance of  $\sim 150$  m (right).

**2.2.2. Acoustic positioning measurements.** The reconstruction of the detector geometry in real time is primarily based on acoustic triangulation of a small number of hydrophones scattered along every line. The triangulation is performed from distance measurements of each hydrophone to several fixed acoustic emitters located either on every line anchor base (transducers) or on autonomous pyramidal structures anchored around the detector field (transponders). A relative positioning of the hydrophones in space with a precision of few cm is necessary in order to obtain a precision of  $\sim 10$  cm on the OM positions as a result of the line shape reconstruction performed by the addition of the tilts and heading measurements of every storey. The concomitant operation of MILOM and Line 1 has allowed a check of the acoustic system performance by performing the Line 1 hydrophone triangulation based on the acoustic emission of the MILOM transducer and two autonomous transponders. The good resolution of the acoustic system, found to be well within the specification, can be appreciated on figure 4 which shows the radial displacement of the lowest hydrophone of Line 1, located on its bottom storey at 100 m above the sea bed, with respect to the line axis during a period of two weeks.

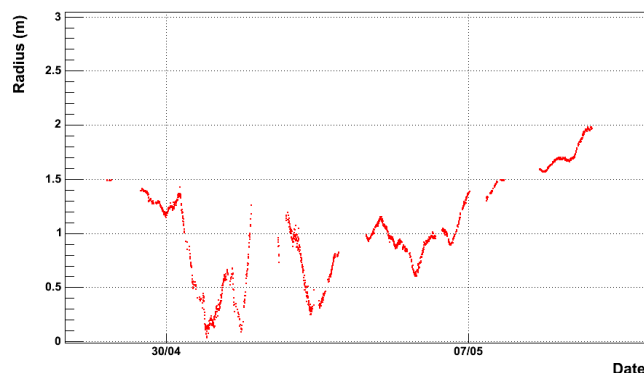


**Figure 4.** Radial displacement of the Line 1 lowest hydrophone with respect to the line axis measured by the acoustic relative positioning system during a period of two weeks.

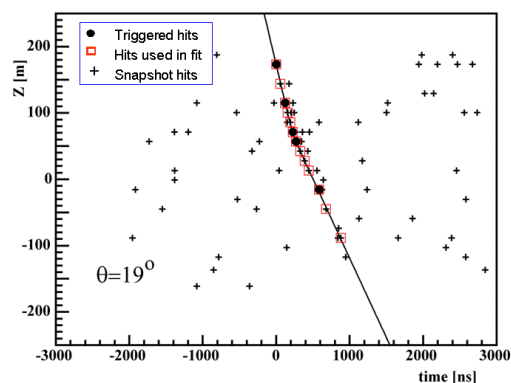


**Figure 5.** Example of a downward-going atmospheric muon track reconstruction with the ANTARES Line 1.

**2.2.3. Reconstruction of atmospheric muons.** Although the OMs point at  $45^\circ$  downwards, the ANTARES detector has a none negligible efficiency for the detection and the reconstruction of downward-going atmospheric muons. The event selection is first performed by an online filter algorithm, running at the shore station, which looks for a set of  $\geq 4$  local coincidence hits, the triggered hits, causally compatible with a muon track passing through the detector during a  $4 \mu\text{s}$  time window. The muon reconstruction is then performed with a  $\chi^2$  fit of the hit times as function of their altitudes, to a hyperbola corresponding to the intersection of the muon Cherenkov light front with the line plane, in order to determine the zenith angle of the muon track. An example of such a muon track fit is shown on figure 5. Several thousand of atmospheric muons have already been reconstructed after a few weeks of operation of the Line 1, the first being detected only two days after its connection. The study of the muon angular distribution is in progress. The preliminary results already show that the muon reconstruction is working well and that the hunt for the first undersea neutrino can be started.

### 3. Conclusion

The ANTARES Collaboration has made a major step forward during the last year by the operation of a Mini Instrumentation Line with Optical Modules, the MILOM, for more than a year, and the installation of the first complete line of the detector in Spring 2006. All studies performed with these two lines show that the detector behaves well within the design specification and that all technical problems are solved. The detector should be fully installed by the end of 2007 and in operation for science during at least five years. It is also considered as a milestone towards the building of a  $\text{km}^3$  underwater detector for which a design study is under preparation.

### References

- [1] Aslanides E *et al.*, ANTARES Collaboration 1999 the ANTARES Proposal *Preprint astro-ph/9907432*
- [2] Amram P *et al.* ANTARES Collaboration 2002 *Nucl. Inst. Meth. A* **484** 369 (*Preprint astro-ph/0112172*)
- [3] Aguilar J A *et al.* ANTARES Collaboration 2005 *Nucl. Inst. Meth. A* **555** 132 (*Preprint physics/0510031*)
- [4] Aguilar J A *et al.* ANTARES Collaboration 2006 First results of the Instrumentation Line for the deep-sea ANTARES neutrino telescope *Preprint astro-ph/0606229*
- [5] Amram P *et al.* ANTARES Collaboration 2000 *Astropart. Phys.* **13** 127 (*Preprint astro-ph/9910170*)

# Expressions for Neutrino Wave Functions and Transition Probabilities at Three Neutrino Oscillations in Vacuum and Some of Their Applications

Kh. M. Beshtoev    beshtoev@cv.jinr.ru

Joint Institute for Nuclear Research, Joliot Curie 6, 141980 Dubna, Moscow region, Russia

## 1. Introduction

The suggestion that there could be neutrino-antineutrino oscillations was considered by Pontecorvo in 1957. It was subsequently considered by Maki et al. and Pontecorvo that there could be mixings (and oscillations) of neutrinos of different flavors (i.e.,  $\nu_e \rightarrow \nu_\mu$  transitions). In the general case there can be two schemes (types) of neutrino mixings (oscillations): mass mixing schemes and charge mixings scheme [1]. In the both cases the form of the mixing matrix is the same. In this work three neutrino vacuum transitions and oscillations in the general case are considered in three cases: with  $CP$  violation, without  $CP$  violation and when direct  $\nu_e \leftrightarrow \nu_\tau$  transitions are absent (i.e.,  $\beta(\theta_{13}) = 0$ ). Then using the existing experimental data some analysis is fulfilled. It is also found out that the probability of  $\nu_e \leftrightarrow \nu_e$  neutrino transitions is a positively defined value only if the angle of  $\nu_e, \nu_\tau$  mixing  $\beta \leq 15^\circ \div 17^\circ$ .

## 2. General Expressions for Neutrino Wave Functions and Transition Probabilities at Three Neutrino Transitions (Oscillations) in Vacuum in Dependence on Time

**Expressions for Neutrino Wave Functions of  $\nu_e, \nu_\mu, \nu_\tau \rightarrow \nu_e, \nu_\mu, \nu_\tau$  Transitions (Oscillations) in Vacuum with  $CP$  Violation, without  $CP$  Violation and when  $\beta(\theta_{13}) = 0$ .**

In these cases expression for wave functions at three neutrino transitions (oscillations) in matrix form is

$$\begin{pmatrix} \Psi_{\nu_e \rightarrow \nu_e, \nu_\mu, \nu_\tau}(t) \\ \Psi_{\nu_\mu \rightarrow \nu_e, \nu_\mu, \nu_\tau}(t) \\ \Psi_{\nu_\tau \rightarrow \nu_e, \nu_\mu, \nu_\tau}(t) \end{pmatrix} = \begin{pmatrix} b_{\nu_e \nu_e}(t) & b_{\nu_e \nu_\mu}(t) & b_{\nu_e \nu_\tau}(t) \\ b_{\nu_\mu \nu_e}(t) & b_{\nu_\mu \nu_\mu}(t) & b_{\nu_\mu \nu_\tau}(t) \\ b_{\nu_\tau \nu_e}(t) & b_{\nu_\tau \nu_\mu}(t) & b_{\nu_\tau \nu_\tau}(t) \end{pmatrix} \begin{pmatrix} \Psi_{\nu_e}(0) \\ \Psi_{\nu_\mu}(0) \\ \Psi_{\nu_\tau}(0) \end{pmatrix},$$

where  $b_{ij}(t)$  is function of rotation angles  $\alpha, \beta, \gamma$  and  $CP$  violation parameter  $\delta$ , rotation angles  $\alpha, \beta, \gamma$  and rotation angles  $\alpha, \gamma$ . Evident forms of  $b_{ij}(t)$  are given in [2].

**Expressions for probability of  $\nu_e, \nu_\mu, \nu_\tau \rightarrow \nu_e, \nu_\mu, \nu_\tau$  transitions (oscillations) in vacuum without  $CP$  violation and in the case when  $\beta(\theta_{13}) = 0$  is also computed** (see an evident form for these transition probabilities in [2]).

## 3. Some Analysis of Neutrino Oscillation Possibilities for the Sun neutrinos.

Using the existing experimental data and expression for probability of  $\nu_e \rightarrow \nu_e$  transitions the analysis has been fulfilled (the detailed form see in [2]). This analysis definitely shows that direct transitions  $\nu_e \leftrightarrow \nu_\tau$  cannot be closed for the Solar neutrinos, i.e.,  $\beta(\theta_{13}) \neq 0$ . It is also shown that the possibility that  $\beta(\theta_{13}) = 0$  can not be realized by using the resonance mechanism of neutrino oscillations in the solar matter.

## 4. Limitation on value of angle $\beta(\theta_{13})$

By using the expression for probability  $P_{\nu_e \rightarrow \nu_e}(t)$  of  $\nu_e \leftrightarrow \nu_e$  transitions the limitation on value of angle  $\beta$  is obtained. If  $\beta > 15^\circ \div 17^\circ$ , then  $P_{\nu_e \rightarrow \nu_e}(t)$  becomes negative at some values of  $t$ . Since the value for the probability of  $\nu_e \leftrightarrow \nu_e$  transitions  $P_{\nu_e \rightarrow \nu_e}(t)$  must be the positively defined one then, if in reality neutrino oscillations take place, the value for  $\beta$  must be  $\beta \leq 15^\circ \div 17^\circ$  [2].

1. Kh. M. Beshtoev, JINR Communication E2-2004-58, Dubna, 2004; hep-ph/0506248, 2005.

2. Kh. M. Beshtoev, JINR Communication E2-2006-16, Dubna, 2006; hep-ph/0508122, 2005.

# First observations of separated atmospheric $\nu_\mu$ and $\bar{\nu}_\mu$ events in the MINOS detector.

A. S. T. Blake<sup>1</sup> (for the MINOS collaboration).

<sup>1</sup> Cavendish Laboratory, University of Cambridge, J. J. Thomson Avenue, CB3 0HE, UK.

**Abstract.** The first MINOS results on atmospheric neutrinos are presented.

In recent years, the observed deficit in the atmospheric  $\nu_\mu$  flux has become firmly established [1, 2, 3, 4, 5, 6], with the favoured interpretation being  $\nu_\mu \leftrightarrow \nu_\tau$  oscillations. The MINOS far detector, located at a depth of 700m (2100 m.w.e.) in the Soudan mine, Minnesota, has been collecting atmospheric neutrino data since August 2003. The detector is a steel-scintillator sampling calorimeter weighing 5.4 kilotons. It is the first massive underground detector to be magnetized, enabling the first direct observations of atmospheric  $\nu_\mu$  and  $\bar{\nu}_\mu$  interactions.

An analysis of contained vertex charged current  $\nu_\mu$  and  $\bar{\nu}_\mu$  interactions has been performed, using 418 days (6.18 kiloton-years) of far detector data. The work is described in detail in [7]. A total of 107 events are observed, compared with a Monte Carlo expectation of  $127 \pm 13$  events for the case of no oscillations. The background contribution from cosmic muons is measured to be  $4.4 \pm 0.5$  events. A total of 77 events are found to have a well measured direction from timing, with 49 down-going and 28 up-going events. The ratio of up-going to down-going events in the data compared to the expectation is:

$$R_{u/d}^{data}/R_{u/d}^{MC} = 0.62_{-0.14}^{+0.19}(stat) \pm 0.02(sys).$$

An extended maximum likelihood analysis of the observed  $L/E$  distribution is found to exclude the null oscillation hypothesis at the 98% confidence level.

The  $\nu_\mu$  and  $\bar{\nu}_\mu$  charged current interactions are separated using the curvature of the muons in the MINOS magnetic field. A total of 52 events are found to have a well measured charge, with 34  $\nu_\mu$  and 18  $\bar{\nu}_\mu$  events. The ratio of  $\bar{\nu}_\mu$  to  $\nu_\mu$  events in the data compared to the expectation (which assumes the same oscillation parameters for neutrinos and anti-neutrinos) is:

$$R_{\bar{\nu}_\mu/\nu_\mu}^{data}/R_{\bar{\nu}_\mu/\nu_\mu}^{MC} = 0.96_{-0.27}^{+0.38}(stat) \pm 0.15(sys).$$

Although the statistics are limited, the current data are consistent with the hypothesis that neutrinos and anti-neutrinos oscillate with the same parameters.

## References

- [1] Ashie Y et al (Super-Kamiokande) 2004 *Phys. Rev. Lett.* **93** 101801.
- [2] Ashie Y et al (Super-Kamiokande) 2005 *Phys. Rev. D* **71** 112005.
- [3] Abe K et al (Super-Kamiokande) 2006 *Preprint hep-ex/0607059*.
- [4] Ambrosio M et al (MACRO) 2003 *Phys. Lett. B* **566** 35.
- [5] Sanchez M et al (Soudan 2) 2003 *Phys. Rev. D* **68** 113004.
- [6] Michael D G et al (MINOS) 2006 *Preprint hep-ex/0607088*.
- [7] Adamson P et al (MINOS) 2006 *Phys. Rev. D* **73** 072002.

## The MINOS Near Detector

**J. Boehm<sup>a</sup> and P. Vahle<sup>b</sup> for the MINOS Collaboration**

<sup>a</sup> Department of Physics, Harvard University Cambridge MA 02138 USA

<sup>b</sup> Department of Physics and Astronomy, University College London  
Gower Street, London UK WC1E 6BT

boehm@physics.harvard.edu, vahle@hep.ucl.ac.uk

The Main Injector Neutrino Oscillation Search (MINOS) is a two detector long baseline neutrino oscillation experiment that samples the intense beam of neutrinos produced by the Neutrinos in the Main Injector (NuMI) facility at Fermi National Accelerator Laboratory. The upstream MINOS Detector, or Near Detector, determines the composition and energy of the beam before oscillations have developed. The MINOS Far detector, located in Soudan Minnesota, is then used to search for distortions of the beam spectrum or composition.

The MINOS Near Detector is a 980 ton tracking, sampling calorimeter composed of alternating layers of steel and plastic scintillator. Light produced in the scintillator is collected and transported by wavelength shifting fibers then read out using multi-anode photomultiplier tubes. A magnetic field allows for both identification of neutrino from anti-neutrino and provides a measure of muon energy from curvature. When operating in stable conditions, the Near Detector records 7-8 neutrino interactions per 10 $\mu$ s spill, approximately once every two seconds. In one year of running nearly  $1.4 \times 10^{20}$  protons were delivered to the NuMI target, and over 35 million neutrino induced events were recorded in the Near Detector. This high statistics data set is also used to study the beam spectrum and composition, the performance of the detector, and the properties of neutrino interactions.

Previous oscillation experiments have been dominated by the systematic uncertainty in the neutrino flux when measuring the neutrino oscillation parameters. In MINOS, the Near Detector measures the neutrino energy spectrum, reducing the systematic error induced by incorrectly modeled neutrino flux. These data have also allowed MINOS to demonstrate the stability and integrity of the signal with respect to variations in both time and intensities. Six different beam configurations obtained by changing the position of the target relative to the first focusing horn and/or the horn current were used to explore hadron production in different regions of  $p_T$  and  $p_z$  space. The data collected in these studies have allowed MINOS to tune the hadronic production model and improve the agreement between data and Monte Carlo for all beam configurations in the energy region of 0 and 30 GeV. The flexibility of the NuMI beam has also allowed MINOS to probe the response of the detectors and the reconstruction software under a wide range of intensities. Beyond operations in the NuMI beam line, the MINOS Near Detector also has observed neutrinos produced in the MiniBoone beam line. Study of such events provides measurement of  $K^+$  production at the MiniBoone target and will be used as a tool to help understand signal and background of  $\nu_e$  selection techniques in the MINOS detector. As understanding of the detector and the beam develops, the MINOS Near Detector will measure cross sections and structure functions of neutrino interactions on iron in a kinematic range previously unexplored.

# Neutrino Mass Experiment at The University of Texas at Austin (NEXTEX)

Manfred Fink<sup>1</sup>, Jacek Borysow<sup>2</sup>, Herrmann Wellenstein<sup>3</sup>, Timothy Gay<sup>4</sup>, and Richard Mawhorter<sup>5</sup>

1University of Texas at Austin, Austin, TX, 2Michigan Tech. University, Houghton, MI, 3University of Nebraska at Lincoln, Lincoln, NE, 4Brandeis University, Waltham, MA, 5Pomona College CA.  
[jborysow@mtu.edu](mailto:jborysow@mtu.edu)

**Abstract.** NEXTEX is the next generation experiment designed to determine the electron antineutrino mass to at least 0.5 eV. The experiment is based on the shape of the beta endpoint energy spectrum from gaseous tritium molecules. Two high throughput electrostatic differential electron analyzers coupled with spherical deflection accelerator are key components of the apparatus. The voltages at the electrodes of the spectrometers ultimately determine the energy of the electrons reaching the detector. The correlations between voltages and the energy of the transmitted electrons will be calibrated with diffraction on the  $T_2$  gas of electrons emitted from the auxiliary gun. The coherent electron diffraction pattern from  $T_2$  will provide a series of calibration markers for the spectrum with uncertainties better than 100 mV. Extremely low background count-rates from cosmic rates of less than one count a day at the detector has been already demonstrated. A numerical model predicts residual background from tritium sources of few counts per day. The tritium source and its recycling system is designed to prevent the formation of HT to better than 1% during the fiduciary runs.

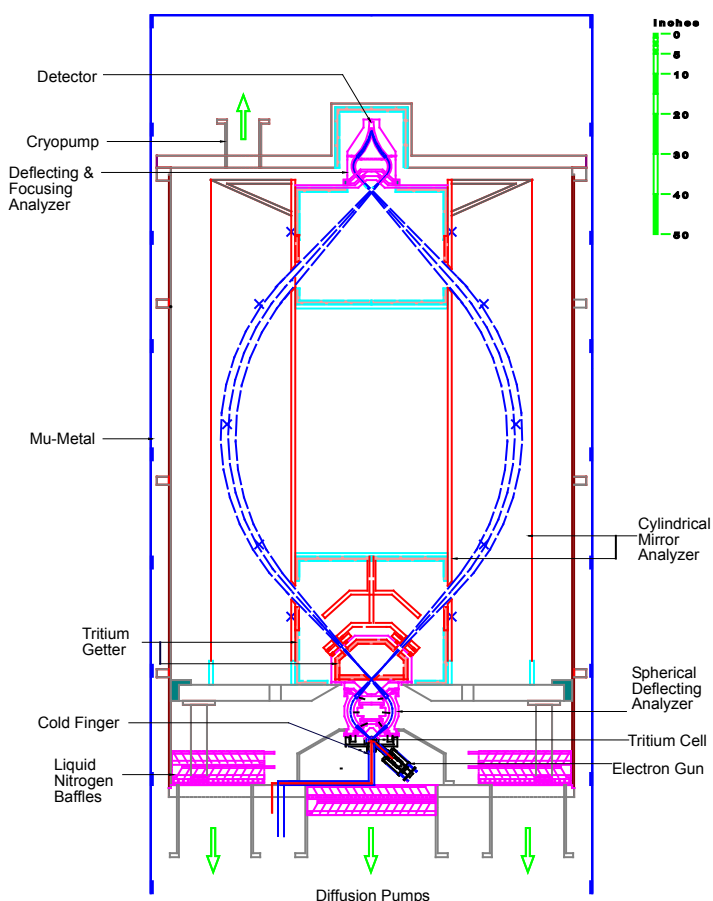


**Fig. 1.** Electron trajectories through the triple Spectrometer of NEXTEX.

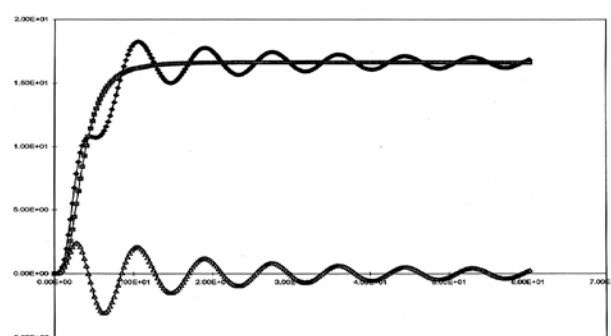


**Fig. 2.** Electron diffraction from Tritium

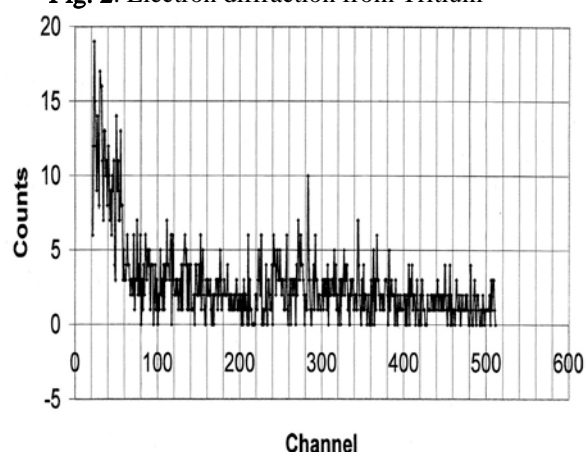


**Fig. 3.** Dark count per day of SiLi detector. The electron energy to be detected is at channel 480

Supported by The National Science Foundation grant PHY-0457194

## “Choozing Double Chooz...”

**Anatael Cabrera & Guillaume Mention**

AstroParticule et Cosmologie (APC), Paris, France & DAPNIA, CEA-Saclay, France

E-mail: anatael@in2p3.fr & mention@in2p3.fr

The potential of reactor anti-neutrino disappearance experiments has not been yet fully exploited. High precision neutrino oscillation measurements could be achieved by a multi-detector experiment, whereby the sensitivity of the experiment becomes independent from the -up to now- dominant uncertainties related to the absolute neutrino flux from the reactor. This strategy has been adopted by the Double Chooz (*DC*) collaboration in order to measure (or limit) the PMNS matrix  $\theta_{13}$  mixing angle. A non-zero  $\theta_{13}$  is necessary to measure leptonic CP violation through neutrino oscillations by future neutrino beam long-baseline experiments.

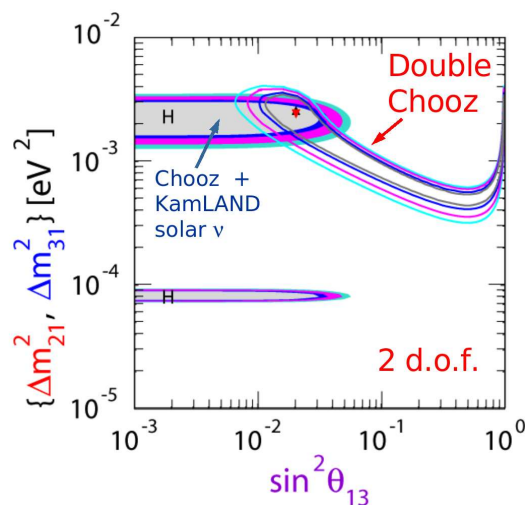


**Figure 1.** Double Chooz sensitivity contour plot:  $\Delta m^2$  vs  $\sin^2(\theta_{13})$ .

The *DC* collaboration (institutions from France, Germany, Russia, Spain, USA and Italy) will start the installation of the far detector by late 2006. The far detector is located at the former CHOOZ experiment site (1.050 km) while the near detector is  $\sim 250$ -300 m away from the Chooz nuclear reactors (France). *DC* is particularly attractive because of its capability to explore  $\sin^2(2\theta_{13})$  down to  $\sim 0.02$  to 90% C.L., for  $\Delta m^2 = 2.5 \times 10^{-3} \text{ eV}^2$ , as shown in Figure 1 [*hep-ex/060625*], within an unrivaled time scale: five years of data taking from early 2008 - when the far detector becomes available. *DC* has carried out intensive R&D (liquid scintillator, background studies, inter-detector calibration, etc.) to reach the targeted level of precision. Some of such developments were also presented -as posters- in this conference.

## CUORICINO latest results and background analysis

**Capelli Silvia on behalf of CUORICINO Coll.**

Univ. degli Studi e Sez. INFN di Milano Bicocca, P.za della Scienza 3 20126 Milano, Italy

E-mail: capelli@mib.infn.it

**Abstract.** The latest CUORICINO results for  $^{130}\text{Te}$  Neutrinoless Double Beta Decay ( $\beta\beta(0\nu)$ ) and the background analysis performed on the measured data will be presented.

CUORICINO is a running experiment, aimed to look for the  $\beta\beta(0\nu)$  of the isotope  $^{130}\text{Te}$ . This search is performed by means of  $\sim 41$  kg of  $\text{TeO}_2$  bolometers, working at about 10mK. The detector, arranged in a tower like structure, is provided with Pb, Cu, anti-Rn and anti-n shields.

The statistics collected from April 2003 up to March 2006 is of  $8.38 \text{ kg } ^{130}\text{Te} \cdot \text{y}$ , with a long stop between runI and runII, made in order to recover lost channels. The live time in standard conditions is of about 60%.

The lifetime for the searched decay is evaluated by means of a Maximum Likelihood procedure. The Q value used in the evaluation is of 2530.3 keV. A flat background was considered. In order to account for the different detector energy resolutions we used, as response function, the sum of N Gaussians, having each a FWHM equal to the average FWHM measured on the 2615 keV line of a  $^{232}\text{Th}$  calibration source for that detector during the run considered. The 2505 keV sum peak of the 2  $^{60}\text{Co}$  gamma lines is included in the fit. The intensity of this peak and its position are left as free parameters in the fit, together with the  $\beta\beta(0\nu)$  peak intensity and the background coefficients. The analysis gave a lower limit for the halflife of  $^{130}\text{Te}$  for  $\beta\beta(0\nu)$  decay of  $2.4 \times 10^{24} \text{y}$  at 90% C.L. and a background in this region of  $0.18 \pm 0.01 \text{ c/keV/kg/y}$ . The systematics that can affect the result, such as the error on the  $\beta\beta(0\nu)$  transition energy value ( $2530.3 \pm 2 \text{ keV}$ ), the peak shape, the error on the energy calibration and the not flat background, have been studied. The corresponding error on the halflife should be less than 5%.

The collected data have also been analysed in order to disentangle the different sources of the measured background. By analysing coincidences, rates in different energy regions, gamma and alpha peaks position, intensity, rates and shapes and by comparison of the measured spectrum with MonteCarlo spectra obtained for different sources and localizations, the most probable sources contributing to the measured bkg have been evaluated. All the gamma lines observed in the measured spectrum are identified. The observed alfa peaks seems to be due to  $^{232}\text{Th}$  and  $^{238}\text{U}$  contaminations in the crystals bulk ( $\sim 10^{-13} \text{ g/g}$ ) and surface. The main fraction of the counts in the region between 3 and 4 MeV seems to arise from a source located outside the crystals, the most probable one being Cu surface. The main sources for the background in the  $\beta\beta(0\nu)$  region have been therefore evaluated to be  $\beta$  and  $\alpha$  from crystal surface ( $\sim 10\% \pm 5\%$ ),  $\alpha$  from materials facing the crystals ( $\sim 50\% \pm 20\%$ ) and  $^{208}\text{Tl}$  multi-Compton events due to  $^{232}\text{Th}$  sources far away from the crystals ( $\sim 30\% \pm 10\%$ ).

[1] Arnaboldi C. et al. 2005 *Phys.Rev.Lett.***95** 142501

# Searching for signatures of dark matter in the cosmic ray spectrum measured by AMS-01

G. Carosi<sup>1\*</sup>, S. Xiao<sup>1</sup>, P. Fisher<sup>1</sup>, G. Rybka<sup>1</sup> and F. Zhou<sup>1</sup>

<sup>1</sup>Massachusetts Institute of Technology: 77 Massachusetts Ave, Cambridge, MA, USA 02139

\*Now at: LLNL, L-270, 7000 East Ave, Livermore, CA, USA 94550

E-mail: carosi2@llnl.gov

**Abstract.** A search for signatures of WIMP dark matter annihilating to charged cosmic rays via  $W^+W^-$  production was performed using data from the AMS-01 magnetic spectrometer, which flew for 10 days on the space shuttle Discovery in 1998. A brief description of the detector along with the analysis method and results is given.

If dark matter consists of majorana Weakly Interacting Massive Particles (WIMPs) one can look for them annihilating with each other to charged cosmic rays in the galactic halo. Direct annihilation to an  $e^\pm$  or  $p^\pm$  pair is highly helicity suppressed so we focused our search on annihilation through  $W^+W^-$  bosons (requiring  $M_{WIMP} > 80$  GeV). The  $W^+W^-$  then decay to stable charged particles ( $e^\pm$  and  $p^\pm$ ) with characteristic spectra correlated to  $M_{WIMP}$ . Even after propagation through the galaxy these decay products could show up as anomalous features in the flat power-law spectrum from astrophysical sources [1].

The AMS-01 experiment consisted of a permanent magnet with a uniform 0.14 Tesla field in a 1 m<sup>3</sup> volume, a scintillator time of flight system, a 6 layer silicon tracker, an aerogel cerenkov detector and an anti-coincidence counter. Its maximum detectable rigidity was  $\approx 360$  GV. For detector and mission details see [2].

Though annihilation signals would be clearer in the lower background  $e^+$  spectra AMS-01 couldn't distinguish  $e^+$  from the large  $p^+$  background at energies  $> 3$  GeV. Instead we utilized the  $Z = -1$  spectrum. PYTHIA was used to generate  $Z = -1$  decay spectra for  $W^+W^-$  bosons decaying at various center of mass energies. These spectra were then convolved with Green's functions of particles transported to earth using the GALPROP galactic propagation software. The final  $e^+$  and  $\bar{p}$  spectra for each WIMP mass was then convolved with an AMS acceptance matrix (from Monte-Carlo) and added. These expected signals from WIMPs of various masses were then compared with data with and without an additional astrophysical power-law background. The results showed that the dark-matter alone could not describe the data, that the power-law alone was a good fit and that the addition of WIMP annihilation did not improve the fit. As a result we could place limits on the rate of  $W^+W^-$  production in the galaxy and, subsequently on the cross-section of WIMP annihilation through this channel. For further details see [3].

[1] G. Jungman, M. Kamionkowski and K. Griest, *Physics Reports*, 267:195–373, 1996

[2] M. Aguilar et al. (AMS Collaboration). *Physics Reports*, 366(6):331-405, 2002

[3] G. Carosi. Ph.D dissertation. MIT, Dept. of Physics, 2006: [http://web.mit.edu/gcarosi/www/gp\\_thesis.pdf](http://web.mit.edu/gcarosi/www/gp_thesis.pdf)

# Present status of the MEG experiment at PSI

F Cei<sup>1</sup>, for the MEG Collaboration

<sup>1</sup> Department of Physics, University of Pisa, Largo B. Pontecorvo, 3, 56127 Pisa, ITALY

E-mail: [fabrizio.cei@pi.infn.it](mailto:fabrizio.cei@pi.infn.it)

**Abstract.** We describe the present status of the MEG experiment, whose aim is to search for the lepton flavour violating (LFV) process  $\mu^+ \rightarrow e^+ \gamma$  with a sensitivity down to  $10^{-13}$ . Recent theoretical calculations indicate a strong connection between LFV processes and neutrino oscillations [1]. We discuss the detection techniques and the performances of the experiment.

The MEG experiment at PSI [2] (Fig. 1) aims to be sensitive to the  $\mu^+ \rightarrow e^+ \gamma$  branching ratio down to  $10^{-13}$ , a level within the predictions of many SUSY theories [3] and two orders of magnitude better than the present limit [4]. A positive muon beam ( $\approx 10^8 \mu^+ \text{ s}^{-1}$ ) will be brought to stop in a thin target, slanted by  $22^\circ$ , where muons will decay.

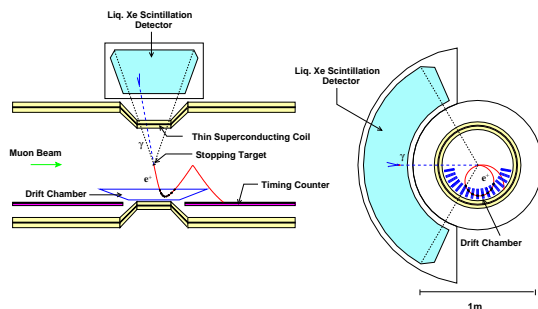


**Figure 1.** Layout of MEG experiment.

The  $e^+$  and the  $\gamma$  (emitted back-to-back, both with 52.8 MeV kinetic energy) will be detected by 1) a magnetic spectrometer (composed by an almost solenoidal magnet (COBRA) with an axial gradient field and a system of 16 drift chambers, DCH) for measuring the momentum and a pair of double-layer arrays of plastic scintillators (Timing Counter, TC) for measuring the absolute timing and by 2) a  $\approx 800$  l volume liquid xenon (LXe) calorimeter, equipped with 846 PMTs, for the measurement of  $\gamma$  energy, direction and timing.

The LXe was chosen because of its large light yield, homogeneity and fast scintillation light decay time ( $\sim 20$  ns). Challenging energy, angular and timing resolutions are required for all detectors in order to single out the possible  $\mu^+ \rightarrow e^+ \gamma$  candidates and reject the background. A 5 % energy and 140 ps timing resolution at 55 MeV [5] for  $\gamma$ 's in LXe calorimeter and a  $< 100$  ps timing resolution (all FWHM) in TC for  $e^+$ 's were obtained in various experimental tests. The expected resolutions for DCH system are  $\Delta p \approx 0.7 \div 0.9$  % and  $\Delta \theta \approx 9 \div 12$  mrad (all FWHM).

The MEG experiment is in advanced state of building and is planned to start at the end of 2006; it is expected to be completed in 2008, before the first results of LHC experiments.

## References

- [1] Masiero A *et al* 2004 *JHEP* **0403** 046; Hisano J and Nomura D 1999 *Phys. Rev. D* **59** 116005
- [2] MEG Collaboration, Baldini A *et al* , Proposal to INFN, available at the web-site: <http://meg.psi.ch>
- [3] Barbieri R and Hall L J 1994 *Phys. Lett. B* **338** 212; Barbieri R *et al* 1995 *Nucl. Phys. B* **445** 219
- [4] MEGA Collaboration, Ahmed M *et al* 2002 *Phys. Rev. D* **65** 112002
- [5] Baldini A *et al* 2005 *Nucl. Inst. and Meth. A* **545** 753

## Indium-Loaded Liquid Scintillator for Solar Neutrino Spectroscopy

Zheng Chang<sup>1</sup>, Jay Benziger<sup>2</sup>, Alexander Garnov<sup>3</sup>, Christian Grieb<sup>1</sup>, Richard L. Hahn<sup>3</sup>, Raju S. Raghavan<sup>1</sup> and Minfang Yeh<sup>3</sup>

<sup>1</sup>Department of Physics, Virginia Polytechnic Institute & State University, Blacksburg, VA 24061, USA

<sup>2</sup>Dep. of Chem. Engineering, Princeton University, Princeton, NJ 08544

<sup>3</sup>Chem. Dept., BNL, Upton, NY 11973

E-mail: zchang@vt.edu

The synthesis of 125 tons of high quality indium-loaded liquid scintillator (InLS) is a key technology for the success of the LENS experiment. A new improved synthesis procedure (VT recipe) has been recently developed to meet the stringent requirements of LENS. This procedure contains two improvements: 1) liquid-liquid extraction with a high concentration of  $\text{NH}_4\text{Ac}$ , and 2) vacuum evaporation to produce solid indium carboxylate. Consequently, the final InLS can be readily prepared by dissolving the solid Indium carboxylate in a desired scintillation solvent (e.g. pseudocumene). We have produced InLS samples with light yield ( $S$ ) over 55%, optical attenuation length ( $L_{1/e}$ )  $> 8$  m at 430 nm, and the contents of water and acid  $< 0.5$  and  $0.4$  equivalents per In respectively. The samples showed good physical and chemical stability for more than 8 months.

A large number of samples were prepared with the improved procedure to search the optimum synthesis conditions. Chemical analyses were conducted to understand the dependence of the scintillation properties ( $S$  and  $L_{1/e}$ ) on the compositions of the InLS. The effects of the impurities in the organic reactants and the speciation of the In carboxylates in the InLS were also studied with GC-MS and electrospray MS. We found the best InLS samples were obtained with the pH in the liquid-liquid extraction at 6.88. With an In loading over 8 wt.%, these samples had a light yield  $S > 55\%$  and  $L_{1/e}$  at 430 nm  $> 10$  m. The  $S$  and  $L_{1/e}$  values have been monitored over 8 months. It was found that  $S$  remained unchanged and  $L_{1/e}$  decreased slightly and remained  $> 8$  m thereafter. Composition analysis showed that for the InLS prepared at the optimum conditions, the apparent molecular formula of the indium complexes is  $\text{In}(\text{MVA})_2(\text{OH})$  (where MVA refers to 2-methylvaleric acid root). Mass spectrometry analysis suggested that most of the indium species in the freshly prepared InLS are monomers. Dimers, trimer and other oligomers were observed in small quantities several months after the preparation. This can explain the slight degradation in  $L_{1/e}$ . However, further oligomerization was prevented as there is only one hydroxyl group contained in the In complexes. This may explain why the attenuation degradation has stopped after several months.

The experimental results proved that the VT recipe is the best InLS recipe ever developed to this date. We are continuing to monitor the scintillation properties of the InLS and refine the synthesis procedure. Future investigations include the design of a synthesis procedure at the 200% scale and the setup of quality control parameters for industry scale preparation.

# Non-proliferation studies with Double Chooz detectors

**S. Cormon, M. Fallot and J. Martino on behalf of the Double Chooz collaboration**

SUBATECH, 4 rue Alfred Kastler, La Chantrerie BP 20722 44307 Nantes Cedex 3, France

E-mail: fallot@subatech.in2p3.fr

**Abstract.** The near detector of Double Chooz will provide the most accurate measurement of the spectrum and the flux of the electronic anti-neutrinos ( $\bar{\nu}_e$ ) emitted by a nuclear power plant. This enables the collaboration to address certain safeguards issues for the International Atomic Energy Agency's (IAEA) benefit.

The flux and the energy spectrum of the  $\bar{\nu}_e$  emitted by a nuclear power plant depend on the thermal power delivered by the plant and on the isotopic composition of its fuel which evolves in time. Reactor  $\bar{\nu}_e$  come from the decay of the fission products (FP) produced mainly by  $^{235}\text{U}$ ,  $^{239}\text{Pu}$ ,  $^{241}\text{Pu}$  and  $^{238}\text{U}$  fissions. The arising FP distribution and delivered energy is an intrinsic property of the fissioning isotope : their associated  $\bar{\nu}_e$  flux and energy spectra differ from each-other, especially at high  $\bar{\nu}_e$  energy. The evolution over time of the  $\bar{\nu}_e$  spectrum from a reactor is governed by the evolution of the FP concentrations in the core, given by the Bateman equations. We started a simulation work using the widely used particle transport code MCNPX [1] coupled with an evolution code solving the Bateman equations for the FP within a package called MURE (MCNP Utility for Reactor Evolution) [2]. As a starting point, simple Fermi decays to the ground state of daughter nuclei are implemented. To improve accuracy by taking into account decays towards excited states, as well as the type of  $\beta$  transition, the code will be interfaced with databases (ENDF/B-VI.8, JENDL3.3, JEFF3.1, JEF2.2). For unknown decay properties of exotic nuclei, more elaborate theoretical calculation for allowed and first forbidden transitions will be performed in collaboration with CEA/DAPNIA/SPhN, and an experimental program has started to complete databases. The extended MURE simulation will allow to perform sensitivity studies for relevant scenarios for IAEA. Preliminary results show that nuclei with half-lives lower than 1s emit about 60% (50%) of the  $^{235}\text{U}$  ( $^{239}\text{Pu}$ )  $\bar{\nu}_e$  spectrum above 6MeV. Simulations will also be performed to evaluate the possibility to use  $\bar{\nu}_e$  for power monitoring. Indeed, Huber and Schwetz [3] predict that, considering our actual knowledge of the  $\bar{\nu}_e$  flux, a measurement with a 3% precision of the thermal power delivered by a nuclear plant could already be performed with a detector of a few cubic meters placed at a few 10's of meters from the core.

## References

- [1] Monte Carlo N-Particle eXtended, *LA-UR-05-2675*, J-S. Hendricks et al.,
- [2] O. Méplan et al., *ENC.proceedings*, Versailles (2005),
- [3] P. Huber and T. Schwetz, *Phys. Rev. D* **70**(2004).

## Short Term Quality Control and Assurance in Borexino

Ferenc Dalnoki-Veress<sup>1</sup>, S. Nisi<sup>3</sup>, C. Salvo<sup>2</sup>, M. Laubenstein<sup>3</sup>, A. Ianni<sup>3</sup>, G. Di Pietro<sup>4</sup>

Princeton University<sup>1</sup>, I.N.F.N. Genova<sup>2</sup>, L.N.G.S.<sup>3</sup>, Università degli Studi di Milano<sup>4</sup>

fdalnoki@Princeton.EDU

Abstract. This poster describes the short term quality control (QC) and assurance implemented in order to maintain the radiopurity goals in the Borexino liquid detector components.

Now in the process of being filled at Laboratori Nazionale del Gran Sasso, Italy, Borexino is a real-time solar neutrino liquid scintillator detector designed to measure the sub-MeV region of the solar neutrino spectrum. Through an extensive campaign of purification and measurements with the 4 tonne prototype (CTF) Borexino has demonstrated a liquid scintillator radiopurity of  $10^{-16}$  g/g Th/U equivalent and  $10^{-18}$   $^{14}\text{C}/^{12}\text{C}$  and  $10^{-14}$  g/g Th/U ultra-pure water [1]. However, this achievement is only one component of the goal since there must be a detailed QC initiative to maintain this level of radiopurity over the lifetime of the experiment and during installation and commissioning. For example, we must limit the air intake at the level of 9 mL ( $^{85}\text{Kr}$ ) in the inner core of the detector and rock dust containing ppm level Th/U at the level of nBq/kg. From this perspective, it is clear that there must be a two-streamed approach to quality implementation, a QA scheme where the process is reviewed, and a QC program where the process is independently tested to *gain confidence* that radiopurity is not breached in the particular process. *Gain confidence* because at this level of activity it is clearly not possible to measure the radiopurity of any substance on a short time-scale.

However, we can indirectly ascertain whether quality has been compromised using various techniques. For example, a task involving the installation of a new component of the purification plant requires a detailed plan for installation, cleanliness protocol, He leak checking to  $<10^{-9}$  mBar l/s to verify that the part has been properly installed and will not introduce contamination present in air. The components are cleaned until the water resistivity exceeds 14 M $\Omega$ .cm, and the level of dust is lower than class 30 (implying  $<0.4$  ppb dust by volume) evaluated according to Mil-STD-1246C. Particle analysis is done by filtration followed by optical microscopic analysis of the filter. In addition, Scanning Electron Microscopy (SEM) analysis coupled with Energy Dispersive X-Ray Fluorescence has helped us determine the nature of the particles that we see in various liquid samples. The types of particles seen with the SEM fall broadly in two classes: particles which are *rock or concrete-like* and particles which are *stainless-steel-like* (Fe, Ni, Cr present). It is natural for us to expect *stainless-steel-like* particles because all of the piping in the Borexino plant is stainless steel. We have also developed techniques to analyze the Th/U content of the liquid scintillator (metallic ions are back extracted with acidified UPW) using ICPMS at the level of ppt.

### References

- [1] Borexino collaboration, G. Alimonti et al., *Astropart. Phys.*, 16 (2002) 205-234

**eV See-Saw  
Sterile Neutrinos and the  
LSND Anomaly  
(and Extra Gauged  $U(1)$ s)**

André de Gouvêa  
*Northwestern University*

## Massive Neutrinos and the Seesaw Mechanism

A simple<sup>a</sup>, renormalizable Lagrangian that allows for neutrino masses is

$$\mathcal{L}_\nu = \mathcal{L}_{\text{old}} - \lambda_{\alpha i} L^\alpha H N^i - \sum_{i=1}^3 \frac{M_i}{2} N^i N^i + H.c.,$$

where  $N_i$  ( $i = 1, 2, 3$ , for concreteness) are SM gauge singlet fermions.  $\mathcal{L}_\nu$  is the most general, renormalizable Lagrangian consistent with the SM gauge group and particle content, plus the addition of the  $N_i$  fields.

After electroweak symmetry breaking,  $\mathcal{L}_\nu$  describes, besides all other SM degrees of freedom, six Majorana fermions: **six neutrinos**.

---

<sup>a</sup>Only requires the introduction of three fermionic degrees of freedom, no new interactions or symmetries. Other “similar” option is to introduce a Higgs  $SU(2)$  Triplet.

## To be determined from data: $\lambda$ and $M$ .

The data can be summarized as follows: there is evidence for three neutrinos, mostly “active” (linear combinations of  $\nu_e$ ,  $\nu_\mu$ , and  $\nu_\tau$ ). At least two of them are massive and, if there are other neutrinos, they have to be “sterile.”

This provides very little information concerning the magnitude of  $M_i$  (assume  $M_1 \sim M_2 \sim M_3$ )

Theoretically, there is prejudice in favor of very large  $M$ :  $M \gg v$ . Popular examples include  $M \sim M_{\text{GUT}}$  (GUT scale), or  $M \sim 1$  TeV (EWSB scale). Furthermore,  $\lambda \sim 1$  translates into  $M \sim 10^{14}$  GeV, while thermal leptogenesis requires the lightest  $M_i$  to be around  $10^{10}$  GeV.

**we can impose very, very few experimental constraints on  $M$**

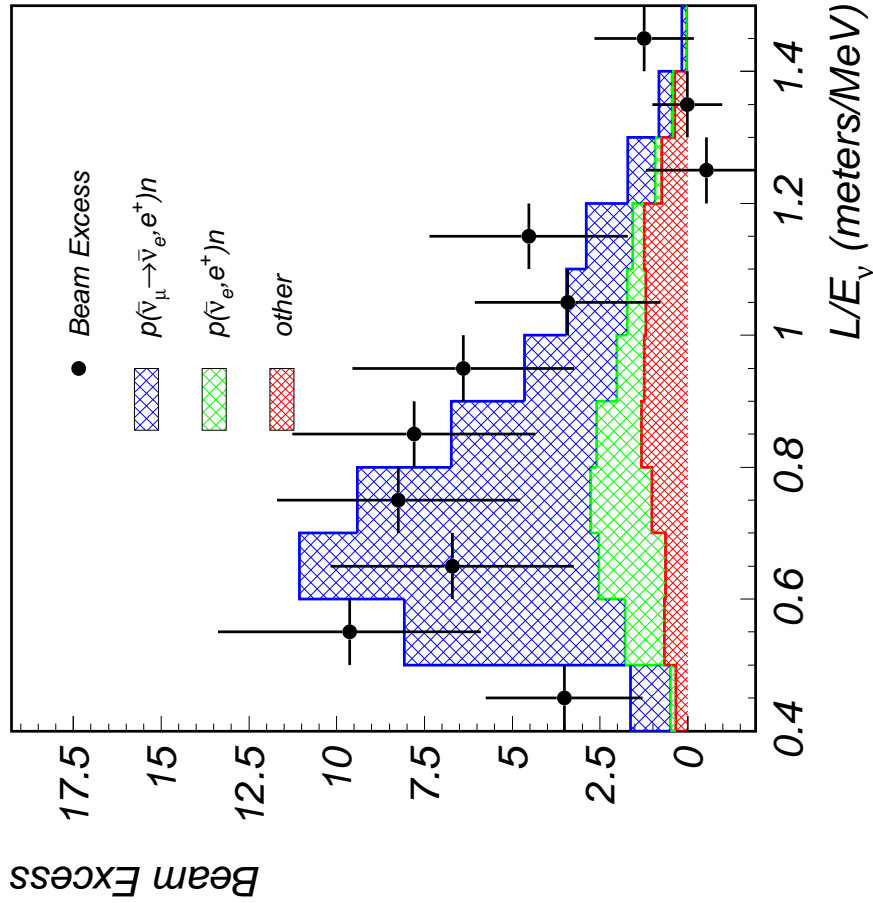
---

## What We Know About $M$ :

- $M = 0$ : the six neutrinos “fuse” into three Dirac states. Neutrino mass matrix given by  $\mu_{\alpha i} \equiv \lambda_{\alpha i} \nu$ . The symmetry of  $\mathcal{L}_\nu$  is enhanced:  $U(1)_{B-L}$  is an exact global symmetry of the Lagrangian if all  $M_i$  vanish. Small  $M_i$  values are ‘tHooft natural.
- $M \gg \mu$ : the six neutrinos split up into three mostly active, light ones, and three, mostly sterile, heavy ones. The light neutrino mass matrix is given by  $m_{\alpha\beta} = \sum_i \lambda_{\alpha i} M_i^{-1} \lambda_{\beta i}$ . This is the **seesaw mechanism**. Neutrinos are Majorana fermions. Lepton number is not a good symmetry of  $\mathcal{L}_\nu$ , even though  $L$ -violating effects are hard to come by.
- $M \sim \mu$ : six states have similar masses. Active–sterile mixing is very large. This scenario is (generically) ruled out by active neutrino data (atmospheric, solar, KamLAND, K2K, etc).

# The LSND anomaly

**strong evidence for  $\bar{\nu}_\mu \rightarrow \bar{\nu}_e$**



If oscillations  $\Rightarrow \Delta m^2 \sim 1 \text{ eV}^2$

- × does not fit into 3  $\nu$  picture;
- × 2 + 2 scheme ruled out (solar, atm);
- ? 3 + 1 scheme disfavored (sbl searches);
- × 3  $\nu$ 's CPTV ruled out (KamLAND, atm);
- ×  $\mu \rightarrow e \nu_e \bar{\nu}_e$  ruled out (KARMEN, TWIST);
- 3 + 1 + 1 scheme works (finely tuned?);
- 4  $\nu$ 's CPTV
- “heavy” decaying sterile neutrinos;
- Lorentz violation (NuTeV, Chorus, Nomad);
- something completely different.

The “best” solution to the LSND anomaly we have been able to concoct is **3+2 neutrino oscillations** (or 3+3, 3+4, etc).

**There are many left-over theoretical complaints.**

- What are these sterile neutrinos? [LEP data tell us there are only three light neutrinos that couple to the Z-boson...]
- Why are they so light? Sterile neutrinos are “theoretically expected” to be very heavy...
- Can we say anything about the expected sterile–active neutrino mixing? Can LSND oscillations be predicted?
- ...

**The main point: LSND anomaly provides one of the only experimental positive hint for a new neutrino physics scale. Use it to fix the mostly unknown seesaw energy scale:**

$$M \sim \sqrt{\Delta m_{\text{LSND}}^2} \sim 1 \text{ eV.}$$

In return, an **eV-seesaw** naturally explains why there are sterile neutrino around 1 eV (and what they are). Solves two out of the three “theoretical complaints” in the previous “page.”

More exciting, however, is that it turns out that the active sterile mixing angles are mostly determined from the “active” mixing angles, and the masses.  $\Rightarrow$  falsifiable hypothesis!

The key property of  $\mathcal{L}_\nu$  is that it **does not** lead, after EWSB, to the most general active–sterile mass-matrix:

$$\mathcal{M} = \begin{pmatrix} 0 & \mu^T \\ \mu & M \end{pmatrix}, \quad \mu = \text{Dirac mass matrix}; \quad M = N_i \text{ Majorana mass matrix.}$$

In the limit  $\mu \ll M$  (the seesaw limit),

$$m_\nu^{\alpha\beta} = \sum_i \frac{\mu_{\alpha i} \mu_{\beta i}}{M_i} = \sum_i U_{\alpha i} U_{\beta i} m_i,$$

where  $U$  is the active neutrino mixing matrix (MNS matrix). In this case, it is easy to solve for  $\mu$  in terms of active neutrino observables and  $M$ :<sup>a</sup>

$$\mu_{\alpha i} = U_{\alpha i} \sqrt{M_i m_i}$$

---

<sup>a</sup>This is a fixed ansatz, which is fixed henceforth. More general solution does not lead to any qualitative changes to rest of the discussion.

## Active–sterile mixing:

$$\langle \nu_\alpha | M_i \rangle \equiv \vartheta_{\alpha i} = \frac{\mu_{\alpha i}}{M_i} + \mathcal{O}\left(\frac{\mu^2}{M^2}\right) = U_{\alpha i} \sqrt{\frac{m_i}{M_i}} + \mathcal{O}\left(\frac{m}{M}\right),$$

such that, for example,  $|U_{e4}|^2 = |U_{ej}|^2 \frac{m_j}{M_j}$ , where  $M_j$  is the lightest of the  $M_i$ .

(  $\nu_4, \nu_5$  and  $\nu_6$ , are mass eigenstates with masses, respectively,  $m_4 < m_5 < m_6$ . In the seesaw limit,  $m_4 =$  lightest  $M_i$ ,  $m_5 =$  second lightest  $M_i$  and  $m_6 =$  heaviest  $M_i$ , where  $i = 1, 2, 3$ . The  $i$  index refers to the position of  $M_i$  in  $\mathcal{M}$ )

## Can this explain the LSND data?

Depends on the active neutrino mass hierarchy. It is easy to explore 3+1 schemes, which are obtained if some  $M_i \sim 1$  eV, while the other two are large enough, say  $> 10$  eV.

Normal hierarchy:  $m_3^2 \sim \Delta m_{13}^2$ , and

$$\sin^2 2\theta_{\text{LSND}} = 4|U_{e3}|^2|U_{\mu 3}|^2 \frac{\Delta m_{13}^2}{M_3^2} < 5 \times 10^{-4} \quad \rightarrow \text{too small}$$

For an inverted mass hierarchy ( $m_1^2 \sim m_2^2 \sim \Delta m_{13}^2 \gg m_3^2$ )

$$|U_{e4}|^2 \simeq 0.020 \left( \frac{|U_{e2}|^2}{0.3} \right) \sqrt{\left( \frac{\Delta m_{13}^2}{3 \times 10^{-3} \text{ eV}^2} \frac{0.92 \text{ eV}^2}{M_2^2} \right)},$$

$$|U_{\mu 4}|^2 \simeq 0.024 \left( \frac{|U_{\mu 2}|^2}{0.42} \right) \sqrt{\left( \frac{\Delta m_{13}^2}{3 \times 10^{-3} \text{ eV}^2} \frac{0.92 \text{ eV}^2}{M_2^2} \right)}.$$

$\rightarrow$  works quite well!

Finally, 3+2 or 3+3 solutions to LSND are generically expected in the eV-seesaw. For example, say  $M_3 = 5 \text{ eV}$ ,  $M_2 = 1 \text{ eV}$ ,  $M_1 \sim 10 \text{ eV}$  (or larger) and the active neutrino masses are quasi-degenerate.

$$\Delta m_{15}^2 \sim 25 \text{ eV}^2,$$

$$\Delta m_{14}^2 \sim 1 \text{ eV}^2,$$

$$|U_{e4}|^2 \sim 0.02, \quad |U_{\mu 4}|^2 \sim 0.03,$$

$$|U_{e5}|^2 \sim 0.001, \quad |U_{\mu 5}|^2 \sim 0.01.$$

**It Works!**

## Other predictions: Tritium beta-decay

Heavy neutrinos participate in tritium  $\beta$ -decay. Their contribution can be parameterized by

$$m_{\beta}^2 = \sum_{i=1}^6 |U_{ei}|^2 m_i^2 \simeq \sum_{i=1}^3 |U_{ei}|^2 m_i^2 + \sum_{i=1}^3 |U_{ei}|^2 m_i M_i,$$

as long as  $M_i$  is not too heavy (above tens of eV). For example, in the 3+2 scenario of the previous slide,  $m_{\beta}^2 \simeq 0.7 \text{ eV}^2 \left( \frac{|U_{e1}|^2}{0.7} \right) \left( \frac{m_1}{0.1 \text{ eV}} \right) \left( \frac{M_1}{10 \text{ eV}} \right)$ .

NOTE: next generation experiment (KATRIN) will be sensitive to  $O(10^{-1}) \text{ eV}^2$ .

## Other predictions: Neutrinoless Double-Beta Decay

The exchange of Majorana neutrinos mediates lepton-number violating neutrinoless double-beta decay,  $0\nu\beta\beta$ :  $Z \rightarrow (Z + 2)e^-e^-$ .

For light enough neutrinos, the amplitude for  $0\nu\beta\beta$  is proportional to the effective neutrino mass

$$m_{ee} = \left| \sum_{i=1}^6 U_{ei}^2 m_i \right| \sim \left| \sum_{i=1}^3 U_{ei}^2 m_i + \sum_{i=1}^3 \nu_{ei}^2 M_i \right|.$$

However, upon further examination,  $m_{ee} = 0$  in the eV-seesaw. **The contribution of light and heavy neutrinos exactly cancels!** This seems to remain true to a good approximation as long as  $M_i \ll 1$  MeV.

$$\left[ \mathcal{M} = \begin{pmatrix} 0 & \mu^T \\ \mu & M \end{pmatrix} \rightarrow m_{ee} \text{ is identically zero!} \right]$$

## On Early Universe Cosmology / Astrophysics

A combination of the SM of particle physics plus the “concordance cosmological model” severely constrain light, sterile neutrinos with significant active-sterile mixing. Taken at face value, not only is the  $eV$ -seesaw ruled out, but so are all oscillation solutions to the LSND anomaly.

Hence,  $eV$ -seesaw  $\rightarrow$  **nonstandard particle physics and cosmology.**

**On the other hand...**

- Right-handed neutrinos may make good warm dark matter particles.
- Sterile neutrinos are known to help out with  $r$ -process nucleosynthesis in supernovae, ...
- ... and may help explain the peculiar peculiar velocities of pulsars.

Asaka, Blanchet, Shaposhnikov, hep-ph/0503065.

## Down-Sides

- No clear connection between the seesaw scale and other interesting energy scales (GUT scale, EWSB scale, etc). → Relationship to UV physics is more subtle.
- We haven't "explained" why the neutrino masses are so small:  $\lambda \sim 10^{-11}$  for  $M \sim 1$  eV. → "More" new physics needed (flavor physics, UV connection?)
- Traditional thermal leptogenesis does not work. → However, there are other CP-invariance violating phases. Any relation to baryon asymmetry of the Universe?
- ...

## Very Light Right-Handed Fermions?

It could be that right-handed neutrino masses are, similar to all other fermion masses, forbidden: new local or global symmetries!

$$\frac{M}{2}NN \rightarrow \frac{y}{2}\chi NN,$$

or more generically, it could be that neutrino masses and the LSND anomaly represent our first window to a new “sterile” sector of Nature (what else is it good for?)

$$\mathcal{L} = \mathcal{L}_{SM} + \mathcal{L}_{\text{sterile}} + \mathcal{L}_{\text{mix}}$$

Why very light?  $\rightarrow$  right-handed neutrino masses could be “seesawed,” e.g.

$$\frac{M}{2}NN \rightarrow \frac{\lambda}{2\Lambda}(\chi N)^2$$

## Example: Non-Anomalous, Gauged $U(1)_\nu$

Add to the SM a new, non-anomalous  $U(1)_\nu$  under which both SM fermions and the right-handed neutrinos transform. Charges are heavily constrained by anomaly cancellations and the fact that quarks and charged leptons have relatively large masses.

One can choose  $U(1)_\nu$  charges so that all neutrino masses are forbidden by gauge invariance. This way, neutrino masses are only generated after  $U(1)_\nu$  is spontaneously broken,<sup>a</sup> and only through higher dimensional operators, suppressed by a new ultraviolet scale  $\Lambda$ .

Neutrino masses are small either because  $\Lambda$  is very large (this is the “usual” high energy seesaw) or because it is a consequence of a very high dimensional operator:  $m_\nu \propto \left(\frac{\mu}{\Lambda}\right)^{|p|}$ , where  $p$  is a large integer exponent.

---

<sup>a</sup> Assume  $U(1)_\nu$  is spontaneously broken when SM singlet scalar  $\Phi$  gets a vev,  $\langle \Phi \rangle \equiv \varphi$ .

After  $U(1)_\nu$  breaking  $\rightarrow$  see-saw Lagrangian plus “left–left” neutrino mass:

$$\mathcal{L} \supset \sum_{ik} \epsilon^{|p_{ik}|} \bar{L}_i (\lambda^\nu)^{ik} n_k \tilde{H} + \sum_{ij} \epsilon^{|q_{ij}|} \bar{L}_i^c \frac{(h^L)^{ij}}{\Lambda} L_j H H + \sum_{kk'} \epsilon^{|r_{kk'}|} \Lambda \bar{n}_k^c (h^R)^{kk'} n_{k'},$$

$\lambda^\nu$  – neutrino Yukawa coupling,  $h^L$  – “left–left” coupling, and  $h^R$  – “right–right” Majorana mass term).  $i, j = 1, 2, 3$ ,  $k, k' = 1 \dots N$ . Only allowed for integer values of  $p, q$ , and  $r$ .

After electroweak symmetry breaking,  $(3 + N) \times (3 + N)$  neutrino mass matrix  $M_\nu$ :

$$M_\nu \sim \begin{pmatrix} \frac{v^2}{\Lambda} h^L \epsilon^{|q|} & v \lambda^\nu \epsilon^{|p|} \\ v (\lambda^\nu \epsilon^{|p|})^\top & \Lambda h^R \epsilon^r \end{pmatrix}.$$

Lots of possibilities. If there are **no integer  $q$  and  $r$**   $\rightarrow$  **Dirac Neutrinos**, with suppressed masses ( $m_\nu \propto v \epsilon^{|p|}$ )

[M.C. Chen, B. Dobrescu, AdG, work in progress]

## Summary, Conclusions

- The introduction of right-handed neutrinos renders the neutrinos massive. Furthermore, the introduction of the most general, renormalizable Lagrangian consistent with the enlarged field content and gauge invariance describes, after EWSB, six Majorana fermions.
- This seesaw Lagrangian contains several free parameters, which are to be determined from experiment. In particular, the seesaw energy scale  $M$  is only very poorly bound.
- Theoretical prejudice favors  $M \gg \text{EWSB scale}$ . However, there is no concrete reason for  $M$  very large — **any value of  $M$  is “natural.”** Remember, the symmetry of the Lagrangian is enhanced when  $M = 0$ .
- The LSND anomaly may come to the rescue. It provides experimental evidence for a new physics scale, which happens to be around 1 electron-volt — is  $M \sim 1 \text{ eV}$ ?

The eV-seesaw is falsifiable, but not currently ruled out. It will be severely tested in the near future.

- Mini-BooNE has to see a signal, consistent with neutrino oscillations;
- Either the active neutrino mass hierarchy is inverted, or the active neutrino masses are quasi-degenerate;
- Effective neutrino mass probed by tritium  $\beta$ -decay is “large;”
- Neutrinos are Majorana fermions, but their contribution to neutrinoless double beta decay vanishes (very tricky to experimentally see “Majoraneness” of the neutrinos);
- Strong active-sterile mixing of supernova neutrinos;
- Concordance cosmology is incomplete.

Finally, sterile–active, sterile–sterile neutrino mixing “non-generic” — strongly correlated to active–active mixing.

Work based on A. de Gouvêa, “See-saw energy scale and the *LSND anomaly*,” *Phys. Rev. D* **72**, 033005 (2005) [arXiv:hep-ph/0501039].

For related work (and work in progress) see also

- T. Asaka, S. Blanchet and M. Shaposhnikov, “The nuMSM, dark matter and neutrino masses,” *Phys. Lett. B* **631**, 151 (2005) [arXiv:hep-ph/0503065].
- T. Asaka and M. Shaposhnikov, “The nuMSM, dark matter and baryon asymmetry of the universe,” *Phys. Lett. B* **620**, 17 (2005) [arXiv:hep-ph/0505013].
- W. S. Hou and A. Soddu, “eV seesaw with four generations,” hep-ph/0512278.
- S. Gopalakrishna, A. de Gouvêa and W. Porod, “Right-handed sneutrinos as nonthermal dark matter,” *JCAP* **0605**, 005 (2006) [arXiv:hep-ph/0602027].
- M. Shaposhnikov and I. Tkachev, “The nuMSM, inflation, and dark matter,” hep-ph/0604236.
- A. de Gouvêa, J. Jenkins and N. Vasudevan, hep-ph/060mnnn (to appear).
- M.-C. Chen, A. de Gouvêa, and B. Dobrescu, hep-ph/060mnnn (to appear).

# Looking at a supernova shock in neutrinos

**Amol Dighe**

Tata Institute of Fundamental Research, Homi Bhabha Road, Colaba, Mumbai 400005, India

E-mail: amol@tifr.res.in

**Abstract.** We analyze how the neutrino flavor conversion inside a core collapse supernova is affected by the shock wave, and show how the time dependent neutrino spectra can be used to reconstruct features of the shock wave while it is still inside the mantle.

The neutrino signal from a core collapse supernova contains encoded information about the primary neutrino spectra, neutrino mixing parameters as well as the density profile encountered by the neutrinos. Decoding this information from the large neutrino flux expected from a galactic supernova has been a topic of much interest in the past few years [1].

A few seconds after bounce in a core-collapse supernova, the shock wave passes the density region corresponding to resonant neutrino oscillations with the “atmospheric” neutrino mass difference:  $\rho \sim 10^3\text{--}10^4$  g/cc. The transient violation of the adiabaticity condition manifests itself in an observable modulation of the neutrino signal, as long as  $\sin^2 \theta_{13} \gg 10^{-5}$ . If there is a reverse shock in addition to the forward one, for some time interval the neutrinos pass two subsequent density discontinuities, giving rise to a “double dip” feature in the average neutrino energy as a function of time. It may even allow one to trace the positions of the forward and reverse shocks while they are in this density region [2].

The neutrino mass eigenstates in matter stay coherent between the multiple resonances they encounter, giving rise to oscillations in the survival probabilities of neutrino species. These “phase effects” are present if the multiple resonances encountered by neutrinos are semi-adiabatic, which typically happens for  $10^{-5} \lesssim \sin^2 \theta_{13} \lesssim 10^{-3}$ . The observation of these effects would, however, need extremely high energy resolution and a large number of events [3].

Not only do neutrinos provide us the only way of looking at the shock wave while still deep inside the mantle, the mere identification of the shock wave features in the  $\nu_e$  ( $\bar{\nu}_e$ ) spectrum also confirms the normal (inverted) mass ordering of neutrinos.

## Acknowledgments

I would like to thank the Partner Group project between the Max Planck institute of Physics and Tata Institute of Fundamental Research for financial support.

## References

- [1] Dighe A 2005 Supernova neutrinos: Production, propagation and oscillations *Nucl. Phys. Proc. Suppl.* **143** 449 (*Preprint* hep-ph/0409268)
- [2] Tomàs R, Kachelriess M, Raffelt G, Dighe A, Janka H -T and Scheck L 2004 Neutrino signatures of supernova shock and reverse shock propagation *J. Cosmol. Astropart. Phys.* **0409** 015 (*Preprint* astro-ph/0407132)
- [3] Dasgupta B and Dighe A 2005 Phase effects in neutrino conversions during a supernova shock wave *Preprint* hep-ph/0510219

## Cross sections for neutron interactions in the CUORE neutrinoless double beta decay experiment

M.J. Dolinski<sup>1,3</sup>, M. Devlin<sup>2</sup>, N. Fotiadis<sup>2</sup>, P.E. Garrett<sup>1,4</sup>, R.O. Nelson<sup>2</sup>, E.B. Norman<sup>1</sup>, W. Younes<sup>1</sup>

<sup>1</sup> Lawrence Livermore National Laboratory, Livermore, CA 94550 U.S.A.; <sup>2</sup> Los Alamos National Laboratory, Los Alamos, NM 87545 U.S.A.; <sup>3</sup> Department of Physics, University of California, Berkeley, CA 94720 U.S.A.

Email: dolinski@berkeley.edu

**Abstract.** We describe experiments to determine the cross sections for neutron reactions on tellurium isotopes. These cross sections will be used to improve Monte Carlo simulations for CUORE, a next generation double beta decay experiment.

Underground neutron fluxes and related backgrounds for neutrinoless double beta decay experiments will be an important consideration for next generation experiments. These backgrounds are being explored through Monte Carlo simulations, but often the parameters used in these calculations rely on nuclear models. We are using the GEANIE germanium detector array at the Los Alamos Neutron Science Center to measure cross sections for neutron-induced reactions on Te isotopes. A spectrum of  $\gamma$ -rays produced through interactions of 1-200 MeV neutrons with a target of  $^{130}\text{Te}$  is shown in figure 1.

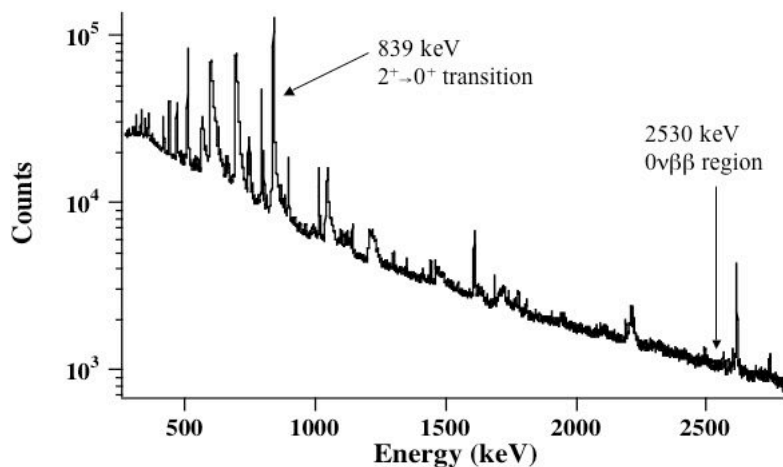


**Figure 1.** This spectrum represents about half of the total data from the  $^{130}\text{Te}$  run. Visible lines include neutron interactions on  $^{130}\text{Te}$  as well as traces of other Te isotopes in the target, neutron interactions with the Ge in the detectors, and room backgrounds. The first excited state transition in  $^{130}\text{Te}$  at 839 keV is labeled. In addition, there is no peak in the region of interest for  $0\nu\beta\beta$ . Other isotopes of Te will follow.

This work was supported in part by U.S. DOE under contract numbers W-7405-ENG-36 (LANL) and W-7405-ENG-48 (LLNL).

<sup>4</sup> Now at Department of Physics, University of Guelph, Guelph, Ontario, Canada, N1G 2W1

# The Cryogenic Pumping Section of KATRIN and the Test Experiment TRAP

**F. Eichelhardt for the KATRIN Collaboration**

Institute for Experimental Nuclear Physics, University of Karlsruhe, Germany

E-mail: frank.eichelhardt@hvt.fzk.de

**Abstract.** The **K**arlsruhe **T**ritium **N**eutrino experiment (KATRIN) employs a **C**ryogenic **P**umping **S**ection (CPS) at  $\approx 4.5$  K to suppress the tritium penetration into the spectrometers. A test experiment (TRAP - Tritium Argon frost Pump) has been set up to investigate the tritium pumping performance of the CPS.

## 1. Introduction

The KATRIN experiment (**K**arlsruhe **T**ritium **N**eutrino experiment) investigates spectroscopically the electron spectrum from tritium beta decay near its kinematical endpoint of 18.6 keV. With a strong windowless gaseous tritium source and a tandem of two electrostatic spectrometers, KATRIN will allow a model independent measurement of neutrino masses with an expected sensitivity of  $0.2 \text{ eV}/c^2$  (90% CL).

In the 10 m long source tube a constant tritium column density of  $5 \cdot 10^{17} \text{ cm}^{-2}$  is maintained by continuous tritium inlet of  $1.8 \text{ mbar } \ell/\text{s}$  in the middle and by continuous pumping of the tritium at its ends. Between source and spectrometer the magnetic transport system is located, which guides the decay electrons adiabatically from the source to the spectrometers while at the same time suppressing the tritium flow rate below  $10^{-14} \text{ mbar } \ell/\text{s}$ . A first flow rate reduction of  $10^7$  is achieved by a differential pumping section with turbomolecular pumps. The remaining  $10^7$  suppression will be accomplished by the **C**ryogenic **P**umping **S**ection (CPS), which is basically a tube covered with pre-condensed Ar as adsorbent and kept at  $\approx 4.5$  K.

## 2. The TRAP Test Experiment

The pumping properties of the CPS are influenced by the tritium decay heat, which is deposited in the Ar adsorbent and increases the desorption rate of both argon and tritium. Since no experimental data is publicly available on the low flow rate level of  $\leq 10^{-14} \text{ mbar } \ell/\text{s}$ , the test experiment TRAP is being performed at the Tritium Laboratory Karlsruhe (TLK). TRAP is a model pump for the CPS with the same gas conductivity and tritium surface density. The main goal is to measure the tritium flow rate suppression factor of the CPS and to test the regeneration procedure, which involves heating of the tube surfaces and purging of the tubes with He gas at 300 K.

Several tritium measurement runs have been performed with TRAP so far, showing a tritium flow rate suppression factor of  $\geq 1.5 \cdot 10^7$ , which is sufficient for KATRIN. In addition, the regeneration procedure of the cryopump was proved to be applicable for the CPS.

## The T2K 2KM water Cherenkov detector

M. Fechner<sup>1,2</sup>, N. Tanimoto<sup>2</sup>, for T2K's 2KM working group.

<sup>1</sup> DAPNIA, CEA Saclay, 91191 Gif-sur-Yvette Cedex, France

<sup>2</sup> Department of Physics, Duke University, Box 90305, Durham NC 27708, USA

E-mail: fechner@phy.duke.edu, tanimoto@phy.duke.edu

T2K is a next generation long-baseline oscillation experiment that will start in 2009, using an intense  $\nu_\mu$  beam produced at J-PARC (Japan). The far detector is Super-Kamiokande (SK), the 50 kt water Cherenkov detector located 295 km from J-PARC ; the beam will be  $2.5^\circ$  off-axis to the detector, with a peak neutrino energy of 700 MeV. The goals of T2K are the precise measurement of  $\Delta m_{23}^2$  and  $\theta_{23}$  from  $\nu_\mu$  disappearance, and the search for  $\nu_e$  appearance, which would bring new information on  $\theta_{13}$ , the last remaining unknown mixing angle.

A 1 kt water Cherenkov detector located 2 km away from the  $\nu$  source has many advantages : it uses the same target as SK, the same event reconstruction techniques, and sees almost the same flux spectrum as SK : the spectral differences (so called Far/Near differences) are about 5%. At 2 km there is one interaction per beam spill, leading to 200,000 interactions per year in the 100 t fiducial volume.

In order to take maximum advantage of the intense  $\nu$  beam, we should measure the background in the beam before oscillations ; the total error on the background should be  $< 10\%$ . With systematics on fiducial volume of  $\sim 4\%$  and on energy scale of  $2\%$  at each detector, we should control the extrapolation error to  $\sim 5\%$  or less.

We developed a full GEANT4 simulation of the 2km detector, tuning it to data from the 1kton water Cherenkov of the K2K experiment. Using this tool, as well as the standard SK tools, we studied the background for  $\nu_e$  appearance at 2km and SK, obtaining very similar distributions (see poster). To show the effectiveness of the 2KM detector, a simple scaling extrapolation, only taking into account spherical attenuation and the ratio of fiducial masses but without any other correction, leads to excellent agreement between both detectors, with a total systematic error smaller than 8% (see poster). This is conservative and can be reduced to  $\sim 5\%$ .

We thank J. Bouchez, T. Kajita, E. Kearns, K. Scholberg, C. Walter for their contributions.

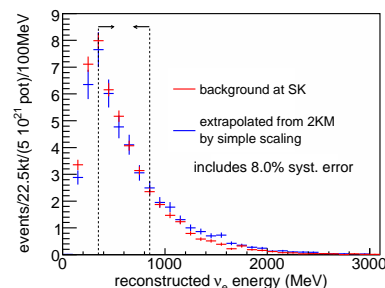


**Figure 1.** Background at SK, and scaled background from the measurement at 2KM. The agreement is very good over a wide energy range.

# CNO and *pep* neutrino spectroscopy in Borexino: measurement of the cosmogenic $^{11}\text{C}$ background with the Counting Test Facility

**Davide Franco** *on behalf of the Borexino Collaboration*

University of Milano and INFN, via Celoria 16, I-20133 Milano, Italy

E-mail: [davide.franco@mi.infn.it](mailto:davide.franco@mi.infn.it)

**Abstract.** Borexino is an organic liquid scintillator detector for low energy neutrino spectroscopy at the Gran Sasso underground laboratories. Besides the main goal, the measurement of the mono-energetic  $^7\text{Be}$  solar neutrino flux in real time, Borexino has the potential to detect *pep* and CNO neutrinos. For this purpose, two conditions are required: an extremely low radioactive contamination level and the efficient identification of the cosmic muon induced  $^{11}\text{C}$  background. We demonstrated with the Borexino Counting Test Facility that  $^{11}\text{C}$  decay events can be efficiently identified and removed event by event.

## 1. Analysis and results

Borexino [1] has the potential to extend the energy region of observation beyond the  $^7\text{Be}$ - $\nu$  electron recoil energy spectrum, in order to detect neutrinos from the *pep* fusion reaction and the CNO cycle in the Sun. The expected rate for *pep* and CNO neutrinos in Borexino between [0.8,1.3] MeV is  $0.015 \text{ day}^{-1} \text{ ton}^{-1}$ . Concentrations of  $10^{-17} \text{ g/g}$  for  $^{238}\text{U}$  and  $^{232}\text{Th}$  and  $10^{-15} \text{ g/g}$  for  $^{nat}\text{K}$  contribute to the *pep*+CNO window with  $0.006 \text{ day}^{-1} \text{ ton}^{-1}$ . In the same window, the expected contamination from  $^{11}\text{C}$ , produced deep underground by residual cosmic muons interacting with  $^{12}\text{C}$  atoms in the scintillator, is  $0.074 \pm 0.008 \text{ day}^{-1} \text{ ton}^{-1}$  [2].

Since in 95% of the  $^{11}\text{C}$  is produced in association with neutron,  $^{11}\text{C}$  event can be identified by detecting the three-fold coincidence (TFC) given by the parent cosmic muon, the neutron capture on hydrogen and the  $^{11}\text{C}$  decay. The TFC technique has been tested in the Borexino prototype (CTF), where 4 tons of scintillator are housed in a 1 m radius nylon vessel, surrounded by 100 photomultiplier tubes and shielded by 4.5 m of water. CTF measured a  $^{11}\text{C}$  production rate of  $0.130 \pm 0.026 \text{ (stat)} \pm 0.014 \text{ (syst)} \text{ day}^{-1} \text{ ton}^{-1}$  [3] in the entire energy spectrum, in agreement with the prediction performed with a muon beam on a scintillator target [2]. For the first time, *in situ* muon induced  $^{11}\text{C}$  has been identified event by event in a large underground scintillator detector. We expect that Borexino will reach a signal-to-background ratio equals to 1 in the *pep*+CNO window by discarding events in proximity of the TFC, losing only 14% of the mass time detector fraction.

[1] Alimonti G et al. 2002 *Astrop. Phys. B* **16** 205

[2] T. Hagner *et al.*, *Astropart. Phys.* **14**, 33 (2000).

[3] Back H. et al. *Preprint*: hep-ex/0601035

[4] Galbiati G et al. 2005 *Phys. Rev. C* **71** 055805

# Horizontal muon flux measured with the LVD detector at LNGS

**Marco Garbini, on behalf of LVD Collaboration**

Museo Storico della Fisica e Centro Studi e Ricerche “E. Fermi” Roma & INFN Bologna, Italy

E-mail: garbini@bo.infn.it

**Abstract.** We report the measure of underground horizontal ( $\cos(\theta) < 0.3$ ) muon flux with the Large Volume Detector (LVD) at the I.N.F.N. Gran Sasso National Laboratory. The analysis is based on the whole muon data collected by LVD since start of data taking in 1992.

The underground muon flux at depth  $x$  and zenith angle  $\theta$  is due to the sum of two main components expressed as  $I_\mu(x, \theta) = I_\mu^{(\mu)}(x, \theta) + I_\mu^{(\nu)}(x, \theta)$ , where  $I_\mu^{(\mu)}(x, \theta)$  is the contribution of high energy downward going muons coming from the decay of charged  $\pi$  and  $K$  mesons in the atmosphere and  $I_\mu^{(\nu)}(x, \theta)$  represents the contribution of muons produced by charged current interactions of  $\nu_\mu$  in the material surrounding the detector. For traversed rock depth greater than 13 *km w. e.* the Earth provides a shield against cosmic muons; thus the flux of neutrino induced muons becomes dominant.

The Large Volume Detector (LVD) [1] is located in the underground I.N.F.N. Gran Sasso National Laboratory at a minimum depth of about 3000 *m w. e.*. LVD is a massive ( $\sim 1$  kt) liquid scintillator detector mainly devoted to study Supernova neutrinos. It is also equipped with a tracking system made of limited streamer tubes; it allows the reconstruction of the direction of the muon tracks. With the knowledge of the Gran Sasso mountain profile LVD can measure the muon flux as a function of the muons traversed rock depth in a wide range of depths (3 – 20 *km we*). In particular muons coming from the horizontal direction are associated to depths larger than 13 *km w. e.* so they are mainly due to neutrino interaction in the rock surrounding the detector.

We analyzed the data collected by LVD since June 1992 until September 2002, for a total live time of  $8 \times 10^4$  *h*. We selected the angular region in the plane  $(\theta, \phi)$  corresponding to slant depth greater than 13 *km w.e.* ( $\cos(\theta) < 0.3$ ). At the end of the analysis a sample of 24 neutrino induced muons is obtained. The corresponding horizontal muon flux is:

$$\Phi_{\nu_\mu} = (4.94 \pm 1.14(stat) \pm 0.39(sys) \times 10^{-13} cm^{-2} sr^{-1} s^{-1} \quad (1)$$

The result is in agreement with other experimental results. Moreover the neutrino induced muons flux does not depend on the traversed rock depth, as expected.

[1] Aglietta M et al. 1994 *Astropart. Phys.* **2** 103

## Pulse shape and segmentation analysis in germanium detectors for $\beta\beta$ decay

V. M. Gehman, for the Majorana Collaboration

Los Alamos National Laboratory, Los Alamos, NM 87545, USA

E-mail: vmg@lanl.gov, vmg@u.washington.edu

The next generation of  $0\nu\beta\beta$  experiments will endeavor to reach down through the quasi-degenerate mass scale in sensitivity, greatly improving the current limits on the  $0\nu\beta\beta$  lifetime and the effective Majorana neutrino mass. This will require a variety of background reduction techniques that will depend on the isotope under consideration and the experimental technique employed. The Majorana Project will exploit several of these techniques. In particular, the combination of pulse shape analysis (PSA) with the segmentation of germanium diode detectors will be paramount to reducing backgrounds. This is possible because  $\beta\beta$  events are single-site energy depositions, whereas likely backgrounds of similar energy will be predominantly multi-site in nature. We use double-escape peaks (DEPs) as surrogate single-site events and full-energy  $\gamma$  peaks as surrogate multi-site events.<sup>1</sup> We describe three measurements using two different detectors in combination with three different  $\gamma$  sources: a Clover detector from Canberra (an array of four two-fold segmented detectors in a single cryostat) and a  $^{232}\text{Th}$  source, the Clover detector and a  $^{56}\text{Co}$  source, and the Segmented, Enriched Germanium Assembly (SEGA, a 2 x 6 segmented detector made from 86% enriched  $^{76}\text{Ge}$  made specially for the Majorana collaboration by Ortec) in combination with the Triangle Universities Nuclear Laboratory's (TUNL) High-Intensity Gamma Source (HI $\gamma$ S), at the Duke Free Electron Laser Laboratory.

The Clover/ $^{232}\text{Th}$  data were taken to demonstrate the combined efficacy of PSA and segmentation analysis.<sup>2</sup> The Clover/ $^{56}\text{Co}$  data were taken to examine the energy dependence of PSA because  $^{56}\text{Co}$  has  $\gamma$  lines with DEPs from 1.6 - 2.4 MeV, comfortably spanning the region of interest ( $Q_{\beta\beta}$  for  $^{76}\text{Ge}$  is 2.039 MeV). The survival probability for DEP events (65 - 70%) had no dependence on energy. The  $^{56}\text{Co}$  source has  $\gamma$  lines from approximately 0.1 - 3.6 MeV. The survival probability for  $\gamma$  events at low-energy is roughly the same as that of the DEPs and falls as a function of  $\gamma$  energy, settling to an asymptotic value (25 - 30%) at approximately 0.7 MeV. This is because the average spatial extent of a  $\gamma$  event is very small at low-energy, and grows with energy until it reaches the resolution of the PSA cuts. The SEGA/FEL data were taken to examine PSA/segmentation in a modestly segmented, enriched detector at  $Q_{\beta\beta}$  for  $^{76}\text{Ge}$ , using HI $\gamma$ S as a  $\gamma$  source of tunable energy. The  $\gamma$  energies were chosen such that the  $\gamma$  line and DEP were observed at  $Q_{\beta\beta}$  in the two modes of the experiment. In the SEGA/FEL experiment, we found  $\gamma$  and DEP survival probabilities of 87% and 55% respectively.

This work is ongoing, first, we continue exploring novel PSA techniques for both detectors. Second, the HI $\gamma$ S experiment included an array of NaI detectors to capture the DEP annihilation  $\gamma$  rays, providing a cleaner sample of DEP events on which to train the PSA. This data stream has not yet been added to the analysis, and work on that effort continues.

<sup>1</sup> C. E. Aalseth *et al*, *IEEE Nucl. Sci. Symp.* **03CH375152** (2004) 1250

<sup>2</sup> S. R. Elliott *et al*, *Nucl. Inst. Meth. A* **558** (2006) 504

# The KATRIN sensitivity to the neutrino mass and to right-handed currents in beta decay

J Bonn<sup>1</sup>, K Eitel<sup>2</sup>, F Glück<sup>3,4</sup>, D Sevilla-Sanchez<sup>1</sup> and N Titov<sup>5,6</sup>

<sup>1</sup> Johannes Gutenberg-Universität Mainz, Institut für Physik, Germany

<sup>2</sup> Forschungszentrum Karlsruhe, Institut für Kernphysik, Germany

<sup>3</sup> Universität Karlsruhe (TH), Institut für Experimentelle Kernphysik, Germany

<sup>4</sup> Research Institute for Nuclear and Particle Physics, Theory Dep., Budapest, Hungary

<sup>5</sup> Westfälische Wilhelms-Universität Münster, Institut für Kernphysik, Germany

<sup>6</sup> Institute for Nuclear Research, Troitsk, Russia

E-mail: jbonn@uni-mainz.de, Klaus.Eitel@ik.fzk.de, Ferenc.Glueck@ik.fzk.de, sevilla@uni-mainz.de, titov@inr.ru

## Abstract.

The aim of the Karlsruhe TRItium Neutrino experiment KATRIN is the determination of the absolute neutrino mass scale down to 0.2 eV, with smaller model dependence than from cosmology and neutrinoless double beta decay. For this purpose, the integral electron energy spectrum is measured close to the endpoint of molecular tritium beta decay. The endpoint, together with the neutrino mass, should be fitted from the KATRIN data as a free parameter. The right-handed couplings change the electron energy spectrum close to the endpoint, therefore they have some effect also to the precise neutrino mass determination. The statistical calculations show that, using the endpoint as a free parameter, the unaccounted right-handed couplings constrained by many beta decay experiments can change the fitted neutrino mass value, relative to the true neutrino mass, by not larger than about 5-10 %. Using, incorrectly, the endpoint as a fixed input parameter, the above change of the neutrino mass can be much larger, order of 100 %, and for some cases it can happen that for large true neutrino mass value the fitted neutrino mass squared is negative. Publications using fixed endpoint and presenting large right-handed coupling effects to the neutrino mass determination are not relevant for the KATRIN experiment.

## 1. Neutrino mass determination and the endpoint

In the KATRIN experiment the absolute neutrino mass is determined by the measurement of the integral energy spectrum of the electrons coming from beta decay of tritium molecules. The electrons are guided from the tritium source to the detector by magnetic field. Between the source and the detector a large negative potential (-18.6 kV) is applied at the main spectrometer, with the aim that only those electrons can reach the detector that have a decay kinetic energy above the value corresponding to this potential. The transversal energy component (relative to magnetic field) of the electrons is converted into longitudinal energy by using the inverse magnetic mirror effect, due to small magnetic field inside the main spectrometer (the electric field can change only the longitudinal energy component of the electrons). Thus it is possible to measure the integral electron energy spectrum simultaneously with high statistics and with high precision. For further information about the KATRIN experiment see Refs. [1] and [2].

The differential electron energy spectrum can be written (in a first approximation, close to the endpoint) as

$$w_{diff}(E) = E_\nu \sqrt{E_\nu^2 - m_\nu^2}, \quad (1)$$

where  $E$  is the relativistic total electron energy,  $E_\nu = E_0 - E$  and  $m_\nu$  denote the neutrino energy and mass, and  $E_0$  is the nominal endpoint (maximum of  $E$ , if the neutrino mass is zero). There are several theoretical modifications to this simplified spectrum, the most important of them is due to the recoil molecular ion final state distribution (see Ref. [3] for a recent calculation). Degenerate neutrino masses are assumed (the KATRIN experiment is able to find a non-zero neutrino mass only above 0.2 eV).

The KATRIN experiment measures the integral energy spectrum, therefore one has to multiply the differential spectrum by the response function of the spectrometer (see Ref. [2] for details), and to integrate from the minimal electron energy  $E_U = e|U_A - U_S|$ , where  $U_A$  and  $U_S$  denote the electric potential in the middle of the main spectrometer and in the tritium source, respectively. The expected absolute detection rate of the KATRIN experiment can be seen in Fig. 1 for different neutrino mass and endpoint values. The most sensitive region for the neutrino mass determination is around  $E_U - E_0^* \approx -5$  eV, where the signal is twice as large as the background (Ref. [4]). It is clear from the figure that there is a positive correlation between the neutrino mass and the endpoint: a larger fixed endpoint value results in a larger fitted neutrino mass value.

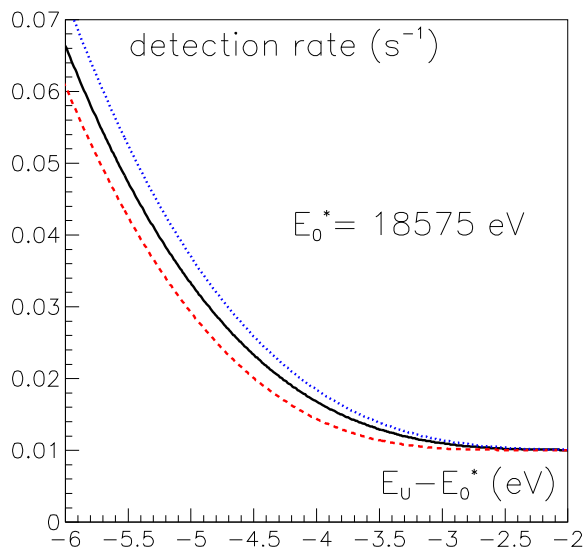


**Figure 1.** Expected detection rate of the KATRIN experiment as function of the minimal detected electron energy  $E_U$ , for different neutrino mass and endpoint values. Full (black) curve:  $m_\nu = 0$ ,  $E_0 = E_0^*$ ; dashed (red) curve:  $m_\nu = 1$  eV,  $E_0 = E_0^*$ ; dotted (blue) curve:  $m_\nu = 0$ ,  $E_0 = E_0^* + 0.15$  eV. The new KATRIN design parameters of Ref. [2] together with  $0.01 \text{ s}^{-1}$  background rate have been employed.

In the KATRIN experiment (like in several earlier neutrino mass experiments) the endpoint is a free parameter, to be determined from the KATRIN spectrum data. Nevertheless, let us assume for a moment that the endpoint is a fixed input parameter. Then a  $\Delta E_0$  error of the endpoint results in a  $\Delta m_\nu^2 \text{ (eV}^2\text{)} \approx 7\Delta E_0 \text{ (eV)}$  error for the neutrino mass squared (using the last 20 eV of the spectrum for the data analysis). From the triton-Helium3 nuclear mass differences one has at present a  $\Delta E_0 = 1.2$  eV error for the endpoint [5]. In addition, it is difficult to determine the absolute potential values with a precision better than 100 mV. On the other hand, the KATRIN experiment aims to measure the neutrino mass squared with an accuracy of  $\sigma(m_\nu^2) = 0.025 \text{ eV}^2$ . To obtain this precision, the accuracy of the endpoint value (as fixed parameter) should be at least 4 meV. Therefore, it is obvious: **for the data analysis of the KATRIN experiment the endpoint cannot be used as an external fixed input parameter; it should be used necessarily as a free parameter, determined from**

the KATRIN data. Analyses assuming the endpoint as a fixed parameter are not relevant for the KATRIN experiment.

## 2. Right-handed couplings and the electron energy spectrum

In the presence of right-handed weak couplings the differential electron spectrum is changed to the following form:

$$w_{diff}(E) = E_\nu \sqrt{E_\nu^2 - m_\nu^2} \left( 1 + b' \frac{m_\nu}{E_\nu} \right). \quad (2)$$

This formula is valid close to the endpoint. A similar change of the electron spectrum is due to the Fierz parameter  $b$ . The parameter  $b'$  is a linear combination of the right-handed vector ( $R_V$ ), axial-vector ( $R_A$ ), scalar ( $R_S$ ) and tensor ( $R_T$ ) couplings:

$$b' \approx -2 \frac{\Re e(L_V R_V^* + L_V R_S^*) |M_F|^2 + \Re e(L_A R_A^* + L_A R_T^*) |M_{GT}|^2}{|L_V|^2 |M_F|^2 + |L_A|^2 |M_{GT}|^2} \quad (3)$$

(only the dominant terms are shown in this formula, which is in agreement with Ref. [6]). The left-handed  $L_j$  and right-handed  $R_j$  couplings have the following simple relations with the widely used couplings  $C_j$  and  $C'_j$  introduced by Lee and Yang in Ref. [7]:  $C_j = (L_j + R_j)/\sqrt{2}$ ,  $C'_j = (L_j - R_j)/\sqrt{2}$ . As it is explained in Ref. [8], there are several advantages using the couplings  $L_j$  and  $R_j$ . In the Standard Model only the left-handed vector and axial-vector couplings  $L_V$  and  $L_A$  are non-zero.

There are many experimental observables (like beta asymmetry, neutrino-electron correlation, beta polarization etc.) that provide constraints for the couplings  $R_j$ . Unfortunately, these observables are quadratic in the  $R_j$  couplings (with zero neutrino mass the right-handed couplings have no interference with the dominant left-handed couplings), therefore the 95 % confidence limits are not too small:  $|R_V| < 0.08$ ,  $|R_A| < 0.10$ ,  $|R_S| < 0.07$ ,  $|R_T| < 0.10$  (see the recent overview in Ref. [9]; the  $L_V = 1$  normalization is used here). The signs of the couplings  $R_j$  are not known; in order to obtain conservative limit for  $b'$  we assume that these signs are equal (in this case there is no sign cancellation in Eq. 3). Then we get the following constraints for  $b'$ :

$$|b'| < 0.26 \quad (95\% \text{ CL}); \quad |b'| < 0.31 \quad (99.7\% \text{ CL}). \quad (4)$$

## 3. Right-handed couplings and neutrino mass determination in KATRIN

Let us assume that the real value of the parameter  $b'$  is nonzero, and the KATRIN data are analyzed with  $b' = 0$  theory (Standard Model). In this case, the fitted neutrino mass value should deviate from the real mass value. Fig. 2 shows the  $\Delta m_\nu/m_\nu = (m_\nu^{(\text{fit})} - m_\nu^{(\text{real})})/m_\nu^{(\text{real})}$  relative deviation due to the unaccounted right-handed parameter  $b' = \pm 0.28$ . The KATRIN design parameters and the statistical method described in Ref. [2] have been used for this calculation. The fitted parameter in these calculations is the neutrino mass squared, not the mass. One has to emphasize also that the endpoint was taken as a free parameter. According to Fig. 2 **the relative change of the neutrino mass due to the unaccounted right-handed couplings is of order of 5-10 %**. For small neutrino mass values (below 0.5 eV) the shift  $m_\nu^{(\text{fit})} - m_\nu^{(\text{real})}$  is smaller than the expected experimental error of the mass, for larger mass values (above 0.5 eV) the shift of the mass is larger than the experimental error.

Taking the endpoint as a fixed input parameter, the results are completely different. To illustrate this difference, let us consider a special numerical example: we assume that the real neutrino mass is  $m_\nu^{(\text{real})} = 0.35$  eV, and the real value of the parameter  $b'$  is  $b'_{\text{real}} = \pm 0.28$ . Then we make a computer experiment: we generate the KATRIN data by using these real values, but

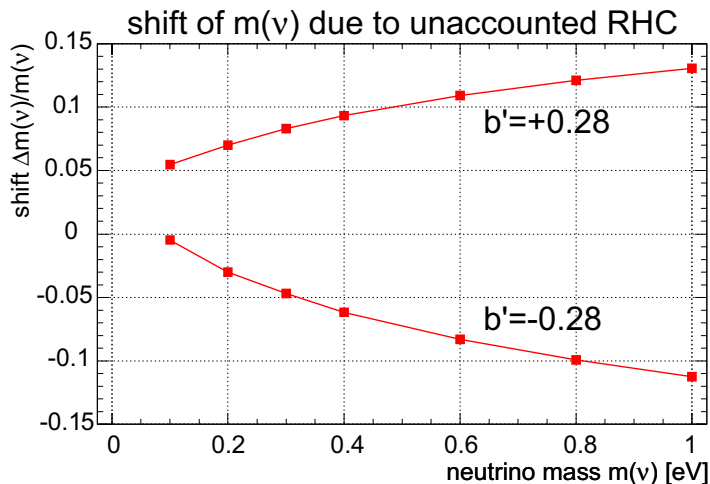


**Figure 2.** Relative shift  $(m_\nu^{(\text{fit})} - m_\nu^{(\text{real})})/m_\nu^{(\text{real})}$  of neutrino mass due to unaccounted right-handed couplings, as function of  $m_\nu^{(\text{real})}$ .

we analyze the data assuming  $b' = 0$ . Table 1 shows the fitted neutrino mass values of these calculations with fixed and with free endpoint. **With free endpoint the fitted mass values are close to the real mass. On the other hand, in the case of fixed endpoint the fitted neutrino mass with  $b'_{\text{real}} = -0.28$  is completely different from the real mass value. In the case of  $b'_{\text{real}} = +0.28$  the fitted mass squared becomes negative, in spite of the positive real mass value. Using the endpoint as a free parameter such a large deviation between real and fitted mass or mass squared values does not occur.**

$b'_{\text{real}}$	$E_0$ fixed	$E_0$ free
-0.28	$m_\nu^{(\text{fit})} = 0.6$ eV	$m_\nu^{(\text{fit})} = 0.33$ eV
+0.28	$m_\nu^{2(\text{fit})} = -0.1$ eV <sup>2</sup>	$m_\nu^{(\text{fit})} = 0.38$ eV

**Table 1.** Fitted neutrino mass (or mass squared) values with  $m_\nu^{(\text{real})} = 0.35$  eV.

Several theoretical publications present large right-handed coupling effects to the neutrino mass determination (Refs. [10, 11, 12]). Refs. [10, 11] tried to explain the negative mass squared anomaly of several neutrino mass experiments by assuming the presence of non-zero right-handed couplings. **Nevertheless, all these 3 publications used in their analyses fixed endpoint, therefore they are not relevant for the neutrino mass experiments (like KATRIN) using free endpoint.** We mention that in Ref. [13] right-handed couplings were searched in the data of the Mainz neutrino mass experiment, using free endpoint in the analysis; the data did not favor the existence of non-zero right-handed couplings.

## References

- [1] Doe P 2006, Direct neutrino mass measurements, *in this proceedings*.
- [2] KATRIN Collaboration, KATRIN Design Report 2004, Wissenschaftliche Berichte FZK 7090 (2004); NPI ASCR Rez EXP-01/2005; MS-KP-0501; see also in: <http://www-ik.fzk.de/~katrin/index.html>.
- [3] Doss N et al. 2006 *Phys. Rev. C* **73** 025502.
- [4] Otten E W, Bonn J and Weinheimer Ch. 2006 *Int. J. Mass Spectrom.* **251** 173.
- [5] Nagy Sz. et al. 2006 *Europhys. Lett.* **74** 404.
- [6] Enz C P 1957 *Nuovo Cimento* **6** 250.
- [7] Lee T D and Yang C N 1956 *Phys. Rev.* **104** 254.
- [8] Glück F, Joo I and Last J 1995 *Nucl. Phys. A* **593** 125.
- [9] Severijns N, Beck M and Naviliat-Cuncic O 2006 *Rev. Mod. Phys.*, to appear.

- [10] Stephenson G J and Goldman T 1998 *Phys. Lett. B* **440** 89.
- [11] Stephenson G J, Goldman T and McKellar B H J 2000 *Phys. Rev. D* **62** 093013.
- [12] Ignatiev A Yu and McKellar B H J 2006 *Phys. Lett. B* **633** 89.
- [13] Kraus C 2000 *Diplomework, Mainz* .

# Accurate incident neutrino momentum determination

**T. Goldman**

T-16/MS-B283 Theoretical Division, Los Alamos National Laboratory, POB 1663, Los Alamos, NM 87545, USA

E-mail: tgoldman@lanl.gov

**Abstract.** When neutrinos produced from the decay of pions in a bunched, accelerated pion beam interact in a downstream target, the arrival time and location define the energy of the incident neutrino independently of whether the scattering event occurs by a charged or neutral current interaction and the details of the final state.

Some time ago, Los Alamos proposed[1] a pion post accelerator (PiLAC) to be appended to the Los Alamos Meson Physics Facility, LAMPF. Pion decay occurs during the acceleration and is almost exclusively into muons and muon-antineutrinos (or antimuons and muon-neutrinos depending on the charge of the pion) with a purity at the part in ten thousand level. Thus, a PiLAC also provides an intense, collimated beam of neutrinos with an energy spectrum ranging up to  $\sim 43\%$  of the output energy value in the highly relativistic limit for the pions. The neutrino spectrum can be adjusted to be flat in energy, or even increasing with energy by varying the accelerating gradients for the pions. The gradients necessary ( $\sim 18$  MeV/m) are below those previously achieved[2] using superconducting RF cavities and since widely exceeded (at KEK, CEBAF, SNS and TESLA; see, e.g., Ref.[3]).

For a constant accelerating gradient,  $G = dE_\pi/dx$ ,  $E_x = E_I + Gx$ . for pions with injection energy  $E_I$ . When a pion of this energy decays, the neutrino energy of the neutrino emitted (axially symmetrically) at polar angle  $\phi$  with respect to the beam axis in the pion rest frame is given by

$$E_\nu = E_0 \sqrt{2\gamma^2 - 1 + 2\beta\gamma^2 \cos(\phi) - (\gamma^2 - 2)\sin^2(\phi)} \quad (1)$$

where  $E_0 \equiv \frac{m_\pi^2 - m_\mu^2}{2m_\pi} \sim 29.8$  MeV, and the neutrino appears at lab angle  $\theta$  with respect to the beam at the decay point where  $\tan(\theta) = \frac{\sin(\phi)}{\gamma[1 + \beta\cos(\phi)]}$ . (Here,  $\beta = p_x/E_x$  and  $\gamma = E_x/m$ .) Since the paths for a neutrino to reach the detection point are unique combinations of  $\beta < 1$  (as the pion accelerates) and  $\beta = 1$  (for the neutrino) segments, the interaction time uniquely identifies the pion decay location and angle for the decay into the incident neutrino, hence its momentum and energy can be determined from the time and location of the scattering event in a downstream detector.

## Acknowledgments

This research is supported by the Department of Energy under contract W-7405-ENG-36.

[1] Blind Barbara B 2004 Overview of the PiLAC project, *Report* LA-UR-04-3797

[2] Brown P, Brunner O, Butterworth A, Ciapala E, Fritscholz H, Geschonke G, Peschardt E and Sladen J 1999 Performance of the LEP200 superconducting RF system *Preprint* CERN-SL-RF-99-075

[3] Liepe M and Knobloch J 2006 *Nucl. Instr. Meth. A* **557** 354

## Scintillating bolometers for $\beta\beta$ Decay search

P Gorla<sup>1</sup>, J Beeman<sup>2</sup>, S Capelli<sup>3</sup>, M Pavan<sup>3</sup>, S Pirro<sup>3</sup> and E Previtali<sup>3</sup>

1. Laboratori nazionali del Gran Sasso of INFN

2. Nuclear Science Division, Lawrence Berkeley National Laboratory, Berkeley, CA, USA

3. Dipartimento di Fisica dell'Università di Milano-Bicocca and INFN-Milano I-20126, Italy

E-mail: [paolo.gorla@lngs.infn.it](mailto:paolo.gorla@lngs.infn.it)

### Abstract.

We present the results achieved in the development of scintillating bolometers for double beta decay searches. A bolometric light detector was developed using an extremely pure germanium crystal. The excellent results represent the first proof of the feasibility of this kind of technique.

In the field of Double Beta Decay (DBD), high resolution detectors in which a large part of the background can be discriminated result very appealing [1]. This possibility can be fulfilled with a scintillating bolometer containing a DBD emitter whose transition energy exceeds the natural 2615 keV gamma line of  $^{208}\text{Tl}$ . A 140 g  $\text{CdWO}_4$  crystal ( $^{116}\text{Cd}$  has a DBD transition energy of 2802 keV) was operated as bolometer and the scintillation light was read by a bolometric Light Detector (LD). The LD was a 1 mm thick pure germanium disk (Fig. 2) coated with a layer of  $\text{SiO}_2$  in order to increase the light collection. The adopted temperature sensors were NTD Ge thermistors optimized to work at  $T \sim 11$  mK. The scatter plot in Fig. 1 shows that

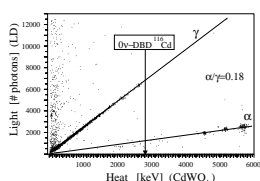


**Figure 1.** Scatter plot of Heat vs Light.

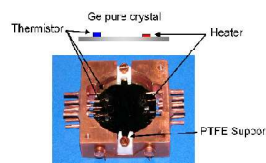


**Figure 2.** The Ge bolometric Light Detector.

the  $\alpha$ -continuum is ruled out thanks to the scintillation detection. The background above the 2615 keV, due to degraded  $\alpha$  particles, is completely suppressed, demonstrating the power of this technique [1]. The natural  $\beta$  decay of  $^{113}\text{Cd}$  (12.2 % i.a.) with  $Q_\beta=318$  keV and  $T_{1/2}=7.7 \times 10^{15}$  y is clearly visible.

### Acknowledgments

This work has been partially supported by the ILIAS integrating activity (Contract No. RII3-CT-2004-506222) as part of the EU FP6 programme in Astroparticle Physics.

### References

- [1] S. Pirro *et al.*, (2005) [arXiv:nucl-ex/0510074]

## Measuring the Neutrino Luminosity of the Sun with LENS & the MINILENS prototype

**Christian Grieb<sup>1</sup>, Igor Barabanov<sup>2</sup>, Jeff Blackmon<sup>3</sup>, Art Champagne<sup>4</sup>, Zheng Chang<sup>1</sup>, V Gurentsov<sup>2</sup>, Mark Pitt<sup>1</sup>, Raju S Raghavan<sup>1</sup>, Charles Roscoe<sup>3</sup>, Derek Rountree<sup>1</sup>, Bruce Vogelaar<sup>1</sup> and Qinglin Zeng<sup>3</sup>**

<sup>1</sup>Department of Physics, Virginia Polytechnic Institute & State University, Blacksburg, VA 24061, USA

<sup>2</sup>Institute of Nuclear Research, Academy of Sciences, Moscow 117312, Russia

<sup>3</sup>Oak Ridge National Laboratory, Oak Ridge, TN 37831, USA

<sup>4</sup>University of North Carolina, Chapel Hill, NC 27599, USA

E-mail: christian.grieb@gmail.com

The science goal of LENS is to measure the Solar Neutrino Spectrum for  $E_\nu > 114$  keV, and the pp- and  ${}^7\text{Be}$ - $\nu$  flux to  $\sim 3\%$ . This will allow determining the Neutrino Luminosity of the sun to  $\sim 4\%$ . The balance of  $\nu$ -luminosity and photon luminosity is the final precision test of the correctness of neutrino physics and detailed questions of the present, past and future of the sun's energy production mechanisms. This direct spectroscopic measurement of sub-MeV solar neutrinos which contain specific fluxes at several energies will provide the ideal tool for probing flavor survival and non-standard  $\nu$  phenomena at the earth. No spectral data is yet available below  $\sim 5$  MeV.

The experimental tool used in the LENS detector for the detection of solar neutrinos is the tagged capture of  $\nu_e$ 's on  ${}^{115}\text{In}$  via charged current (cc):  $\nu_e + {}^{115}\text{In} \rightarrow {}^{115}\text{Sn}^* + e^- \rightarrow {}^{115}\text{Sn} + 2\gamma$ . The tagged cc-capture technique has two outstanding advantages over competing scattering experiments: First, there is a one-to-one correspondence between the incoming neutrino energy and the measurable electron energy  $E_\nu = E_e + Q_d$  ( $Q_d$ : capture threshold), and second, the  $\gamma$ -cascade allows the application of time/space coincidence techniques to suppress ubiquitous radioactive backgrounds as well as the inherent background from the beta decay of  ${}^{115}\text{In}$ .

An R&D program for LENS initiated at Virginia Tech in 2004-5 has made major breakthroughs in the detector design, Indium liquid scintillator chemistry and background rejection. A new type of liquid scintillator detector, the "Scintillation Lattice" will provide extraordinary spatial resolution in a large mass of liquid scintillator through segmentation rather than time of flight information, which allows adequate background rejection using the time/space coincidence tag. Extensive Monte Carlo studies have established the feasibility of LENS with less than 200t of scintillator.

MINILENS will be the first step in the realization of the full scale experiment: a modest detector in a scalable design with 250l of scintillator containing 20-40 kg of Indium viewed by  $\sim 100$  5" phototubes. It will set the stage for constructing LENS by establishing the technology, design, background suppression and *signal detection* in LENS, using cosmic ray induced "proxy pp neutrino" events. These occur when muon secondary protons excite the 713keV isomer in  ${}^{115}\text{Sn}$  via (p,n) on  ${}^{115}\text{In}$ . The excitation of this state can be tagged by the track of the proton and using the neutron via (n, $\gamma$ ) on In ( $\sigma=3000\text{b}$ ). The isomer with a lifetime  $\tau=230\mu\text{s}$  emits a 100keV conversion electron and then follows the same tag cascade as a  $\nu$  capture event, thus being a proxy for a 214keV pp solar  $\nu$ .

# Precision Neutrino Oscillation Physics with MINOS

**J Hartnell<sup>1</sup>, M Ishitsuka<sup>2</sup>, T M Raufer<sup>3</sup> for the MINOS Collaboration**

<sup>1</sup> CCLRC Rutherford Appleton Laboratory, Chilton, Didcot, OX11 0QX, UK

<sup>2</sup> Physics Department, Indiana University, Bloomington, IN 47405

<sup>3</sup> Sub-department of Particle Physics, University of Oxford, Oxford, OX1 3RH, UK

E-mail: j.j.hartnell@rl.ac.uk, ishi@indiana.edu, t.raufer1@physics.ox.ac.uk

**Abstract.** MINOS is a long-baseline neutrino oscillation experiment utilising Fermilab's NuMI beam and two functionally identical steel/scintillator calorimeter detectors. Here we describe the short and long term physics goals of MINOS and we give a brief overview of the beam and detector technology used to achieve them.

In the Standard Model neutrinos are regarded as exactly massless particles. However, there is no fundamental reason to forbid finite masses. If neutrinos have finite mass, and their flavour eigenstates are the superposition of the mass eigenstates, then flavour oscillations occur. The survival probability of a neutrino in a  $\nu_\mu \rightarrow \nu_\mu$  two flavour oscillation scenario is given as  $P(\nu_\mu \rightarrow \nu_\mu) = 1 - \sin^2(2\theta_{23})\sin^2(1.267\Delta m_{32}^2 \frac{L(km)}{E(GeV)})$ .

MINOS measures the energy spectrum of the neutrino beam twice: at 1 km and at 735 km from the source. An energy dependent deficit of  $\nu_\mu$  is observed at the far detector [1]. A fit to the above formula yields the oscillation parameters  $\theta_{23}$  and  $\Delta m_{32}^2$ . The measurement is currently statistically limited but a factor of 10 more data is expected to be collected by 2010.

Longer term physics goals include: sizable improvements to the limit on the third mixing angle  $\theta_{13}$  by measuring  $\nu_e$ -appearance; and the search for oscillations into sterile neutrinos.

The NuMI facility at Fermilab produces intense pulses of neutrinos by extracting 120 GeV protons from the Main Injector and directing them onto a graphite target. The secondary pions and kaons are focused using two magnetic horns and subsequently travel down a 675 m water cooled vacuum pipe where they decay to give predominantly muon neutrinos. The remaining protons, pions and kaons are stopped by the hadron absorber; whereas the muons are removed from the beam by several hundred meters of rock.

The MINOS detectors are magnetised, tracking calorimeters that are made from hundreds of steel-scintillator planes. Each plane of scintillator is divided up into 4 cm wide strips; the strips are orientated perpendicularly in consecutive planes to allow 3D track reconstruction. The scintillation light is extracted from the point of interaction using wave-length shifting fibres and then transmitted on to multi-anode photo-multiplier tubes.

The MINOS experiment started taking beam data in January 2005 and has accumulated approximately  $1 \times 10^{20}$  protons-on-target in its first year of operation. The next few years will see precise measurements of  $\Delta m_{32}^2$ , new limits on  $\theta_{13}$  and searches for new physics.

## References

- [1] Michael D G et al. 2006 *Preprint* hep-ex/0607088, submitted to Phys. Rev. Lett.

## The K2K calibration source manipulator

**P-A Amaudruz, F Berghaus, S Chen, R L Helmer, C Holmberg,  
K Hoyle, I Kato, P Kitching, A Konaka, M Lenckowski, D Morris  
and S Oser**

TRIUMF, 4004 Wesbrook Mall, Vancouver, Canada, V6T 2A3

**Abstract.** A manipulator used to move optical calibration sources throughout the volume of a water Cherenkov detector is described.

Part of the optical calibration of the water Cherenkov near detector for the K2K experiment is accomplished by placing an isotropic light source in the water. Because there is only a single access port at the top of the detector, previous calibrations have been confined to data taken along the central axis. To investigate the detector response at other positions, we have built a manipulator system that permits locating the source throughout the detector volume.

The manipulator consists of a 6 meter long vertical column suspended in the detector from a platform mounted on the detector cover. A three-jointed articulating arm is mounted from the bottom of the column. The source is mounted at the outer end of the third arm, and can be placed anywhere within 4.3 m from the bottom of the column. The arms are sealed so as to be neutrally buoyant in water. All components are fabricated from stainless steel or plastic in order not to contaminate the water.

Four motors are used to rotate the column and drive the arm segments so as to position the source in the desired location. A chain and sprocket arrangement transfers the motion of the motor drives to the appropriate arms. Each motor contains an encoder to record arm rotation angles, and a redundant, second encoder is mounted on each motor shaft. More precise position readback is achieved using solid state accelerometers based on MEMS technology. The angular position of each arm can be read out to 0.1 degrees with these devices, corresponding to less than 1 cm positioning uncertainty in the source location.

Besides the necessity of positioning the source accurately, it is of paramount importance to prevent any impact between the manipulator and other detector components. The control system takes advantage of the redundancy in the feedback of arm positions to achieve these goals. The accelerometer signals are read out and processed by two 8051 microprocessors. The data are converted into angles for each arm, and boundary conditions are calculated internally to determine if there are violations that require motion limiting. A destination algorithm is used to move the source from one position to another within the detector.

MatLab was used to build the user interface for the system. The interface displays both profile and polar views of the manipulator arm to assist the operator in understanding how the arms move and what boundary conditions (e.g. approaching too closely to the PMTs) may be restricting movement.

Data were collected at over two hundred positions throughout the detector volume during a two month long run before the experiment ended. These data are now being analyzed.

# MaGe, a Simulation Framework for $^{76}\text{Ge}$ -based Neutrinoless Double-beta Decay Experiments

**Reyco Henning for the MaGe Collaboration**

Lawrence Berkeley National Laboratory, Berkeley, CA

The Majorana and Gerda experiments will search for the  $0\nu\beta\beta$ -decay of  $^{76}\text{Ge}$  using arrays of High Purity Germanium (HPGe) detectors. These experiments are described elsewhere in these proceedings. An important requirement is the ability to characterize the signal contamination by radioactive backgrounds in detector components and cosmic-ray induced neutron interactions. Monte Carlo simulation is critical during the design phase to estimate this contamination, provide radiopurity requirements for detector components, and to determine the minimum acceptable depth underground to locate these experiments.

The Majorana and Gerda collaborations are pursuing the development of a joint Monte Carlo package, MaGe, to achieve these goals. MaGe is Geant4 [1] and ROOT [2]-based and uses the powerful abstraction and object-oriented capabilities of C++ and STL to provide a common interface for different event generators, detector geometries and output formats. This allows the reuse of code and increases efficiency. The common interfaces also simplify cross comparisons.

Majorana has performed studies to compare the background reduction efficiency of different detector segmentation schemes for an exhaustive list of potential sources in the detector bulk and surfaces. The studies have shown that  $^{208}\text{Tl}$  in the copper shield is a dominant source and that surface alpha contamination has to be limited to  $10^{-4}\mu\text{Bq}/\text{cm}^2$ , a level similar to that achieved in the Sudbury Neutrino Observatory Neutral Current Detectors [3].

Majorana is also studying cosmic-ray induced interactions in the detector. Initial studies have shown that Geant4, with corrections, reproduces the experimental results for both neutron production from electron and muon beamdumps, as well as neutron inelastic scattering in HPGe detectors, allowing the estimation of systematic uncertainties in the simulation of the Majorana detector.

The Gerda collaboration has pursued Monte Carlo studies of the Cherenkov photon production in their water buffer shield. These studies optimized the positions of the photomultipliers and showed that in inclusion of VM2000-foil doubles the number of collected photons.

Gerda Monte Carlo studies have also shown that the detector can be operated at Gran Sasso depths, if segmentation, active shielding, and dedicated delayed coincidence cuts are applied. The latter tags events from  $^{77\text{m}}\text{Ge}$  produced by the capture of thermal neutrons on  $^{76}\text{Ge}$ . Additional studies have shown that crystal segmentation is sufficient for rejecting background in Gerda components.

Majorana and Gerda will continue pursuing their joint simulation effort and anticipate merging collaborations to pursue a 1 ton scale experiment.

[1] S. Agostinelli et al. *Nucl. Instr. and Meth. A*, **506** : 250, 2003.

[2] Rene Brun and Fons Rademakers. *Nucl. Instr. and Meth. A*, **389** : 81, 1997.

[3] Laura Stonehill. PhD thesis, University of Washington, 2005.

# Neutrino Background from Population III Stars

**Fabio Iocco**

Università di Napoli “Federico II”, Napoli, Italy

KIPAC @ Stanford/SLAC, CA, USA

E-mail: iocco@na.infn.it

**Abstract.** Population III Stars (PopIII) are the first generation of stars formed from the collapse of the very first structures in the Universe. Their peculiar chemical composition (metal-free, resembling the Primordial Nucleosynthesis yields) affects their formation and evolution and makes them unusually big and hot stars. They are good candidates for the engines of Reionization of the Universe although their direct observation is extremely difficult. Here we summarize a study of their expected diffuse low-energy neutrino background flux at Earth.

PopIII are the pregalactic generation of stars which formed from the pristine metal-free gas left from Primordial Nucleosynthesis. The dust- and metal-free gas from which they originated made them unusually heavy ( $\mathcal{O}(200 M_{\odot})$ ), extremely short lived ( $\mathcal{O}(10^6)$  yrs), and with a high rate of Pair Instability Supernovae (PISNe). Their peculiarities make them extremely difficult to observe directly and so far no unambiguous observation has been reported. Such massive stars should have a high Supernova rate, and it is therefore reasonable to expect a huge  $\nu$  emission associated with the PopIII phenomenon. We study their MeV-energy neutrino flux to understand if it can be considered as a direct observable for such a generation of stars, motivated also by the recent interest in modeling the diffuse fluxes due to different cosmic sources. Our simple model, which may be regarded as an upper limit to the actual flux, makes strong assumptions on the Stellar Formation Rate (SFR), the Initial Mass Function (IMF) of the PopIII and uses the results of 3-D simulations of PISNe explosions to model the  $\nu$  contributions. In the model we propose and fully describe in [1] we assume that the whole PopIII generation is formed by only  $300 M_{\odot}$  stars, which give the most spectacular contribution in neutrinos,  $\approx 10^{55}$  ergs, according to [2]; we also assume that a fraction  $f_{\text{III}} = 10^{-3}$  of the total baryonic mass of the Universe contributes to the stellar phenomenon (actually ends up in a star) which we model as a delta-like function at the redshift suggested from WMAP3 as the central value for Reionization,  $\bar{z} = 12$ . The neutrino contributions we take into account are the  $\nu_e$  flux due to H-burning ( $E < 2$  MeV), the  $\nu$  and  $\bar{\nu}$  of all flavours by purely leptonic processes and  $\nu$  and  $\bar{\nu}$  of all flavours produced during the PISNe collapse ( $E \leq 20$  MeV), energies at the *source*. We find that, as expected, the energy at the Earth is lower because of cosmological redshift effect: the  $\nu$  flux drops below  $1 \text{ cm}^{-2} \text{ s}^{-1}$  at  $E \approx 5$  MeV, the total background being always dominated by cosmic SNe and galactic stellar neutrinos. Although the anti-neutrino flux shows the same magnitude it is interesting to notice that the PopIII flux dominates the cosmic background up to  $E \approx 2$  MeV.

## References

- [1] F. Iocco, G. Mangano, G. Miele, G.G. Raffelt and P.D. Serpico, *Astropart. Phys.* **23** (2005) 303.
- [2] C.L. Fryer, S.E. Woosley and A. Heger, *Astrophys. J.* **550** (2001) 372.

## Neutrinoless double beta decay experiment DCBA using a magnetic momentum-analyzer

N Ishihara<sup>1</sup>, Y Kato<sup>1</sup>, T Inagaki<sup>1</sup>, T Ohama<sup>1</sup>, S Takeda<sup>1</sup>, Y Yamada<sup>1</sup>, N Ukishima<sup>2</sup>, Y Teramoto<sup>2</sup>, Y Morishima<sup>3</sup>, I Nakano<sup>3</sup>, S Kitamura<sup>4</sup>, Y Sakamoto<sup>5</sup>, Y Nagasaka<sup>6</sup>, N Tamura<sup>7</sup>, K Tanaka<sup>8</sup> and R Ito<sup>9</sup>

<sup>1</sup>High Energy Accelerator Research Organization (KEK), Tsukuba, 305-0801 Japan

<sup>2</sup>Osaka City University, Sumiyoshi, Osaka, 558-8585 Japan

<sup>3</sup>Okayama University, Okayama, 700-8530 Japan

<sup>4</sup>Tokyo Metropolitan University, Arakawa, Tokyo, 116-8551 Japan

<sup>5</sup>Tohoku Gakuin University, Izumi, Sendai, 981-3193 Japan

<sup>6</sup>Hiroshima Institute of Technology, Saeki, Hiroshima, 731-5193 Japan

<sup>7</sup>Niigata University, Niigata, 950-2181 Japan

<sup>8</sup>BTE, Minato, Tokyo, 105-0011 Japan

<sup>9</sup>ZTJ, Chiyoda, Tokyo, 101-0047 Japan

E-mail: nobuhiro.ishihara@kek.jp

**Abstract.** A magnetic momentum-analyzer is being developed at KEK for neutrinoless double beta decay experiment called DCBA (Drift Chamber Beta-ray Analyzer, inverted ABCD). A lot of thin plates of <sup>150</sup>Nd compound are installed in tracking detectors located in a uniform magnetic field. The three-dimensional position information is obtained for the helical track of a beta ray. More R&D will be studied using the second test apparatus DCBA-T2, which is now under construction.

In double beta decay experiments, the main method distinguishing 0ν mode from 2ν mode is to find a spike spectrum at Q-value in respect of kinetic energy sum of two beta rays. In DCBA, the kinetic energy of each beta ray is calculated from the data of measured momentum. The accuracy of the momentum directly depends on the position resolution of tracking detector. The resolution of X-coordinate is due to the spread of drift velocity in the electron drift space, in which a beta ray ionizes chamber gas (85%He + 15%CO<sub>2</sub>). The electric field in the drift space should be carefully tuned. The Y-coordinates of a track are determined by the positions of anode wires. The position accuracy of every anode wire is precise as 0.03 mm (rms). The resolution of Y-coordinate is rather determined by the fitting error in analysis. The Z-coordinates are obtained from pickup wire signals. A pickup wire plane is located at 2 mm distance from an anode wire plane in the opposite side of source plate. There is a small capacitance between an anode wire and a crossing pickup wire. Electron avalanche signals on a surface of an anode wire propagate several pickup wires through capacitances. The Z-coordinate of a track point is therefore obtained as the center of mass of signals from several pickup wires. The position resolutions have been preliminary obtained as 0.57 mm, 0.49 mm and 0.70 mm for X, Y and Z, respectively, using the straight track of cosmic rays. Electron tracks in a uniform magnetic field have been obtained using internal conversion electrons from <sup>207</sup>Bi. Test apparatus DCBA-T2 will provide the data of energy resolution. In the future, a module of DCBA-F will consist of about 80 m<sup>2</sup> source plates of <sup>150</sup>Nd, a lot of drift chambers and a super-conducting solenoid. It is finally expected that 20 modules of DCBA-F will provide the sensitivity of 0.02 eV for effective neutrino mass.

# Supernova detection with KamLAND

**Kazumi Tolich for the KamLAND Collaboration**

Physics Department, Stanford University, Stanford, California 94305, USA

E-mail: [kazumi@stanford.edu](mailto:kazumi@stanford.edu)

If KamLAND detected neutrinos or antineutrinos from a supernova explosion, we would be able to obtain valuable knowledge on the supernova explosion mechanism. From a standard supernova, defined to be 10 kpc away, with  $3 \times 10^{53}$  ergs of energy and equal luminosity in all flavors of neutrinos and antineutrinos, we expect to see the following events over a few seconds assuming no neutrino oscillations:  $\sim 310$  neutron inverse beta decays with the mean energy of  $\sim 16$  MeV and  $\sim 300$  proton recoil reactions above a 0.2 MeV threshold. The proton recoil events, which have low energies, are particularly interesting since they yield both the luminosity and temperature of all neutrino flavors combined. Due to the low energy threshold, KamLAND is the only currently running experiment that can detect the proton recoil reactions. The current radioactivity level in KamLAND limits the energy threshold to be  $\sim 0.6$  MeV, however, ongoing effort to purify the scintillator will significantly reduce the background level in the low energy region, increasing our ability of observing more proton recoil reactions.

KamLAND uses three different methods to search for a supernova explosion. The first method is performed in real time at the electronics level. This method looks for a burst of antineutrino events by searching for eight high energy events in  $\sim 0.8$  s. Upon detecting such a burst, the KamLAND trigger electronics lowers the energy threshold for one minute to detect as many proton recoil reactions as possible.

The second method analyzes the time and approximate energy of each event from the trigger electronics data within a few seconds of the trigger data being collected. This method searches for neutron inverse beta decays by looking for pairs of events: a high energy event followed by a neutron capture energy event in a temporal coincidence of 1 ms. When the trigger data analyzer detects five candidate pairs of events in one second, the person monitoring the detector is alerted to a possible supernova detection, and the data acquisition system prevents the run from being stopped for one minute.

The third method uses the time, energy, and position of each event, reconstructed using data from all the photo multiplier tubes within about 20 minutes from the data being collected. The method searches for neutron inverse decays by looking for two events in spatial and temporal coincidence: An event with an energy greater than 5 MeV must be followed by another event with an energy between 1.8 MeV and 2.6 MeV less than 2 m apart, and within  $0.5 \mu\text{s}$  to 1 ms. When the analyzer finds two such coincidences in 10 seconds, the person monitoring the detector is alerted.

In case of a supernova detection, to synchronize our data with other experiments, we record the absolute time accurate to  $\sim 150$  ns to the coordinated universal time by using the Global Positioning System.

# Tau Neutrino Appearance in Atmospheric Neutrinos<sup>1</sup>

Tokufumi Kato for the Super-Kamiokande Collaboration

Department of Physics and Astronomy, Stony Brook University, Stony Brook, NY 11794

E-mail: fumi@nngroup.physics.sunysb.edu

A search for the appearance of tau neutrinos from  $\nu_\mu \leftrightarrow \nu_\tau$  oscillations in the atmospheric neutrinos has been carried out using the atmospheric neutrino data from the Super-Kamiokande-I experiment. An estimated total of 78  $\nu_\tau$  events is expected in the data sample presented. A  $\nu_\tau$  enriched sample is selected by statistical analysis methods, likelihood and neural network, with a set of five variables characterizing the decays of tau leptons. After applying  $\nu_\tau$  event selection criteria with the likelihood cut or neural network cut (Figure ), the zenith angle distribution of the selected sample is fitted with a combination of the expected  $\nu_\tau$  signals resulting from oscillations and the predicted atmospheric neutrino background events including oscillations (Figure ). The various systematic uncertainties are also considered. The Super-Kamiokande-I atmospheric neutrino data for 1489.2 days, which find a best fit  $\nu_\tau$  appearance signal of  $138 \pm 48$  (stat.)  $^{+15}_{-32}$  (sys.), disfavor the hypothesis of no tau neutrino appearance by 2.4 sigma.

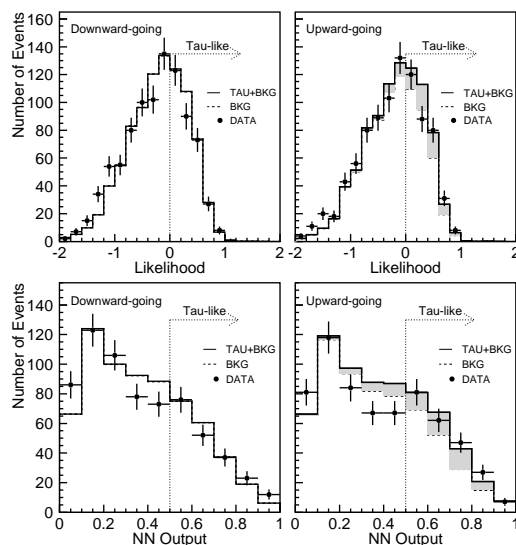


**Figure 1.** The likelihood (top) and NN output (bottom) distributions of downward-going (left) and upward-going (right) events. The events for likelihood  $\mathcal{L} > 0$  or NN output  $> 0.5$  are defined to be tau-like.

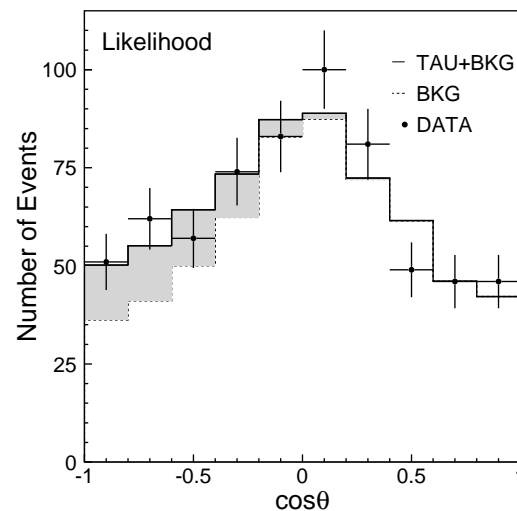


**Figure 2.** The zenith angle distributions for the likelihood analysis. A fitted excess of tau-like events is observed in upward-going direction (shaded area).

<sup>1</sup> The paper was presented at the Proceedings of Neutrino Physics and Astrophysics, July 13-19, 2006

# Global three-parameter model for neutrino oscillations using Lorentz violation [hep-ph/0606154]

Teppei Katori, V. Alan Kostelecký, and Rex Tayloe

Physics Department, Indiana University, Bloomington, IN 47405, U.S.A.

E-mail: katori@iucf.indiana.edu

**Abstract.** A model of neutrino oscillations is presented that has only three degrees of freedom and is consistent with existing data. The model is a subset of the renormalizable sector of the Standard-Model Extension (SME), and it offers an alternative to the standard three-neutrino massive model. All classes of neutrino data are described, including solar, reactor, atmospheric, and LSND oscillations. The disappearance of solar neutrinos is obtained without matter-enhanced oscillations. Quantitative predictions are offered for the ongoing MiniBooNE experiment and for the future experiments OscSNS, NOVA, and T2K.

## 1. Tandem Model

The tandem model has an effective Hamiltonian for neutrino oscillations, which is described by the mixture of 3 different energy depending terms, namely neutrino mass term, CPT-odd Lorentz violating terms, and CPT-even Lorentz Violating terms.

$$(h_{\text{eff}})_{ab} \sim \frac{m_{ab}^2}{2E} + \frac{1}{E}[(a_L)^\mu p_\mu - (c_L)^{\mu\nu} p_\mu p_\nu]_{ab} \sim \begin{pmatrix} cE & a & a \\ a & 0 & a \\ a & a & \frac{m^2}{2E} \end{pmatrix}$$

Through the diagonalization process, the tandem model can reproduce all classes of neutrino oscillation data at relevant energy region, including LSND signal (Fig. 1).

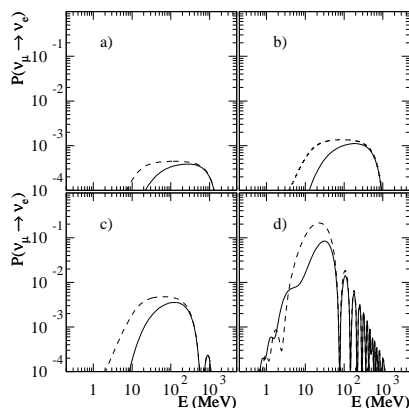


**Figure 1.** Oscillation probabilities as a function of  $E$  for neutrinos (solid) and antineutrinos (dashed) in (a) KARMEN, (b) LSND, (c) the proposed OscSNS experiment, and (d) the current running MiniBooNE experiment. The effects of experimental position and energy resolution are not shown. The tandem model yields an acceptable value for oscillation probability for LSND, but smaller value for KARMEN. And the model predicts small, yet nonzero signals for ongoing MiniBooNE experiment and future OscSNS experiment. On the other hand, this model gives null signals for long baseline  $\nu_e$  appearance experiments, such as NOVA and T2K.

## Low background phase of KamLAND

**Gregory Keefer for the KamLAND Collaboration**

Physics Department, The University of Alabama, Tuscaloosa, Alabama 35487, USA

E-mail: keefe002@bama.ua.edu

The removal of radioactive isotopes from liquid scintillator has been studied extensively in preparation for KamLAND's low background phase. Lower backgrounds will reduce the reactor and geo neutrino background caused by  $^{210}\text{Po}$ ,  $^{13}\text{C}(\alpha, n)^{16}\text{O}$  and increase our sensitivity to solar neutrinos below 1.5 MeV.  $^{40}\text{K}$ ,  $^{85}\text{Kr}$ ,  $^{210}\text{Pb}$ ,  $^{210}\text{Po}$ , and  $^{210}\text{Bi}$  impurities currently inhibit a direct solar neutrino measurement. Background studies indicate KamLAND must reduce current concentrations of  $^{210}\text{Pb}$  by a factor of  $10^5$  from  $4.1 \times 10^{-5}$  Bq/kg,  $^{40}\text{K}$  by a factor of 100 from  $7.1 \times 10^{-8}$  Bq/kg and  $^{85}\text{Kr}$  by  $10^5$  from  $9.0 \times 10^{-4}$  Bq/kg.

The isotopes  $^{210}\text{Pb}$  and  $^{210}\text{Po}$  are difficult to measure in the lab due to their long lifetimes. To solve this problem we make the assumption that all Pb isotopes have equal removal efficiencies. The short lived isotopes from  $^{220,222}\text{Rn}$  decay are used to study scintillator purification techniques. Liquid scintillator is doped in the lab to contain the same concentrations found in KamLAND.

In the following I report results obtained during test purifications of dodecane, the major component of KamLAND scintillator. Lead impurities are present both in ionic form (main component) and in the form of organometallic compounds. Experiments designed to address separately the ionic/polar form and the organic form of Pb indicate that approximately 5% is in organic form. This result was verified by applying  $\text{FeCl}_3$  to address organo-metallic bonds, which, once broken could then be extracted with silica gel or distillation. Studies on the independent scintillator components show that the pseudocumene and PPO suppress the formation of organo-metallic Pb. We also find that the ratio of ionic/organo-metallic molecules is different for isotopes born through beta or alpha decay, the later producing more organic Pb molecules.

The methods found most effective during our preparatory studies are distillation, nitrogen purging, adsorption and heating. Distillation yields the largest reduction efficiency for all isotopes studied. Nitrogen purging addresses only the gas components while adsorption targets the ionic/polar forms of Pb. Heating was found to break organo-metallic Pb bonds, subsequently creating an ionic/polar form of the Pb.

Independent studies of scintillator purification have been conducted at Caltech, Tohoku University and The University of Alabama. In the presence of a gas flow during distillation reduction factors of up to  $10^5$  for Kr and  $10^3$  for  $^{222}\text{Rn}$  have been observed. In the absence of a carrier gas the reduction is a factor of 2. After multiple distillations we achieved reduction factor of up to in  $10^4$  for  $^{212}\text{Pb}$ .

Adsorption experiments yield a factor 30 reduction in  $^{212}\text{Pb}$ , 3 for  $^{222}\text{Rn}$ , 18 for  $^{214}\text{Pb}$  and 71 for  $^{214}\text{Bi}$ . Heating the doped dodecane to 120 C before adsorption increases the  $^{212}\text{Pb}$  reduction to 300. Our studies indicate that all of these methods are complementary in Pb removal. Silica gel adsorption is considered as a back-up for the distillation system currently under construction.

# Cross Section for Deep Inelastic Neutrino Scattering in MINOS

**Minsuk Kim (for the MINOS Collaboration)**

University of Pittsburgh, Department of Physics and Astronomy, Pittsburgh, PA 15260, U.S.A.

E-mail: [mskim@fnal.gov](mailto:mskim@fnal.gov)

**Abstract.** The flux is a necessary ingredient to measure the cross section in the near detector. This document briefly describes how to extract the neutrino flux in NuMI (Neutrinos at Main Injector) beams.

Experiments with solar, atmospheric and reactor neutrinos have provided compelling evidence for the existence of neutrino oscillations driven by nonzero neutrino masses and neutrino mixing. Evidence for oscillations of neutrinos was obtained also in the first long-baseline accelerator neutrino experiment K2K (KEK to Kamioka with  $L \sim 250$  km). The studies of the neutrino flavor transitions offer the possibility to obtain information about the neutrino masses and mixing. New experimental studies have been planned to measure with greater precision the properties of the neutrino flavor transitions. In particular, the MINOS experiment using the NuMI beamline neutrinos (Fermilab to Minnesota with  $L \sim 735$  km) is producing important results and will collect much more data to yield more results with higher precision. The flavor composition, and energy spectrum of a neutrino beam in a detector (located at a distance  $L$  from the source) is determined from the observation of neutrino interactions, and clearly determination of the neutrino reaction and production cross sections required for a precise understanding of neutrino-oscillation physics.

$$\sigma_{total}(E_\nu) = \frac{N(E_\nu)}{A \cdot \Phi(E_\nu)} \quad (1)$$

The total neutrino cross section can be obtained from data using the formula above, where  $N(E_\nu)$  is the observed number of events as a function of neutrino energy.  $\Phi(E_\nu)$  is the neutrino flux, and  $A$  is the correction function that accounts for finite resolution, efficiencies and acceptance. The uncertainty of cross section is dominated by systematic errors in the determination of the neutrino flux. The shape of the flux can be determined by measurements of quasi-elastic interactions observed in a massive, high-resolution near detector, or extracted by the low- $\nu$  flux extraction method making use of the fact that the low- $\nu$  part of the neutrino (anti-neutrino) cross section is constant, i.e. independent of energy and equal for neutrinos and anti-neutrinos [1]. These fluxes should be accurately reproduced by Monte Carlo calculations.

## References

- [1] Janet M. Conrad, Michael H. Shaevitz and Tim Bolton 1998 *Rev. Mod. Phys.* D **70**, 1341-92

## Physics potential of future reactor neutrino experiments

**P Huber<sup>1</sup>, J Kopp<sup>2</sup>, M Lindner<sup>2,3</sup>, A Merle<sup>2</sup>, W Rodejohann<sup>2</sup>,  
M Rolinec<sup>2</sup>, T Schwetz<sup>4</sup> and W Winter<sup>5</sup>**

<sup>1</sup> Dep. of Physics, University of Wisconsin, 1150 University Avenue, Madison, WI 53706, USA

<sup>2</sup> Physik-Department, TU München, James-Frank-Straße, 85748 Garching, Germany

<sup>3</sup> Max-Planck-Institut für Kernphysik, Saupfercheckweg 1, 69117 Heidelberg, Germany

<sup>4</sup> Scuola Internazionale Superiore di Studi Avanzati Via Beirut 2-4, I-34014 Trieste, Italy

<sup>5</sup> School of Natural Sciences, IAS, Einstein Drive, Princeton, NJ 08540, USA

The sensitivity of a  $\theta_{13}$ -measurement at a two-detector reactor neutrino experiment is limited by different factors, depending on the total exposure. For low exposure ( $\lesssim 2 \cdot 10^1$  GW t yrs), the overall event rate is most important, while for medium exposure ( $2 \cdot 10^1 - 10^3$  GW t yrs) the systematical normalization errors become dominant. For very high exposure ( $\gtrsim 10^3$  GW t yrs), the sensitivity is limited by the statistics in each energy bin. Only uncorrelated spectral errors can spoil the performance here. Next-generation experiments such as Double Chooz operate in the medium exposure region, while more advanced setups like Triple Chooz [1], R2D2 [2], or setups involving mobile nuclear reactors and large liquid scintillator detectors [3] can reach the high exposure region, yielding sensitivities of  $\sin^2 2\theta_{13} \approx 10^{-3}$ .

Upcoming reactor neutrino experiments can put limits on  $\theta_{13}$  which are comparable to or even better than those of first-generation superbeams since the latter suffer from correlations between  $\theta_{13}$  and  $\delta_{CP}$ . Their discovery reach, i.e. their potential to distinguish  $\theta_{13} \neq 0$  from the zero hypothesis, depends crucially on the true value of  $\delta_{CP}$ . In the distant future, accelerator experiments will outperform reactor experiments, but an early reactor result is important to select the optimum technology for future beam projects: For very small  $\theta_{13}$ , a neutrino factory will be needed, while for larger values other setups may yield better results.

Precise knowledge about  $\theta_{13}$  is important to estimate the potential of future  $0\nu\beta\beta$  decay experiments [4]: Small  $\theta_{13}$  implies that the effective  $\nu_e$  masses  $m_{ee}$  for the normal and inverted mass hierarchies are clearly separated, and that, for the normal hierarchy, the band of allowed  $m_{ee}$  values is much narrower.

An interesting application of reactor experiments can be to constrain the scenario of mass-varying neutrinos [5], in which the mixing parameters in matter and air may be very different. By comparing two experiments, for which neutrinos pass through different proportions of air and matter on their way to the detector, a direct test of mass-varying neutrinos is possible.

For future low-energy neutrino detectors, a new energy calibration technique can be employed: Self-calibration with Geo- or solar neutrinos. These have characteristic steps or peaks in their spectra, which can be easily located in the data, thus fixing the energy calibration.

### References

- [1] Huber P, Kopp J, Lindner M and Rolinec M 2006 *JHEP* **05** 072 (*Preprint* hep-ph/0601266)
- [2] Huber P, Lindner M and Schwetz T 2005 *JHEP* **02** 029 (*Preprint* hep-ph/0411166)
- [3] Kopp J F, Lindner M, Merle A and Rolinec M 2006 *Preprint* hep-ph/0606151 submitted to *JHEP*
- [4] Lindner M, Merle A and Rodejohann W 2006 *Phys. Rev. D* **73** 053005 (*Preprint* hep-ph/0512143)
- [5] Schwetz T and Winter W 2006 *Phys. Lett. B* **633** 557 (*Preprint* hep-ph/0511177)

## Calibrating the Heavy Water Cherenkov Detector in Phase III of the SNO Experiment

Alain Bellerive<sup>2</sup>, Monica Dunford<sup>3</sup>, Kevin Graham<sup>1</sup>, Aksel Hallin<sup>1</sup>, Josh Klein<sup>4</sup>, Mark Kos<sup>1</sup>, Carsten Krauss<sup>1</sup>, Christine Kraus<sup>1</sup>, Ryan MacLellan<sup>1</sup>, Jose Maneira<sup>5</sup>, Gabriel Orebi Gann<sup>6</sup>, Stan Seibert<sup>4</sup>, Olivier Simard<sup>2</sup>, Peter Skensved<sup>1</sup> *for the SNO collaboration*

<sup>1</sup> Queens University, Kingston, Canada

<sup>2</sup> Carleton University, Ottawa, Canada

<sup>3</sup> University of Pennsylvania, Philadelphia, USA

<sup>4</sup> University of Texas, Austin, USA

<sup>5</sup> LIP, Lisboa, Portugal

<sup>6</sup> University of Oxford, Oxford, UK

E-mail: Corresponding author: [tine@owl.phy.queensu.ca](mailto:tine@owl.phy.queensu.ca)

The Sudbury Neutrino Observatory (SNO) is a 1000 tonne heavy water Cherenkov detector, that is currently taking data with an array of 36 <sup>3</sup>He and 4 <sup>4</sup>He counters. Neutron capture in these counters (Neutral-Current Detection Array, NCDs) detects neutrons from  $\nu$ -deuteron neutral-current interactions of solar neutrinos. Cherenkov light signals from  $\nu_e$  deuteron charged-current interactions and  $\nu_e$  elastic scattering are detected by the heavy water Cherenkov detector. The calibration methods for this third phase of the SNO experiment are described.

The calibration of the optical properties of the SNO experiment is essential for the Cherenkov signals. The addition of the NCDs complicates the vertex and energy reconstruction of Cherenkov events. A manipulator system which permits positioning of a source in two perpendicular planes is used to deploy optical,  $\gamma$  or neutron sources.

A dye laser with 6 different wavelengths between 337 and 620 nm and a diffusing sphere is used for optical calibrations. New methods have been developed to take shadowing and reflections of the NCDs into account. The energy calibration is performed with a <sup>16</sup>N source which emits 6.13 MeV  $\gamma$ 's and is used to determine the energy response and to monitor the stability over time. A new energy estimation algorithm that takes into account the variation of the efficiency of individual photomultiplier tubes has been developed. Two independent energy estimations are performed, one using the prompt light only, the other one taking all late light into account. An increased frequency of calibrations (especially for neutron calibrations) and the improvements in the calibrations methods are an essential part of the forthcoming analysis of the solar <sup>8</sup>B neutrino flux with the NCDs.

# The PICASSO Dark Matter Experiment - Getting Ready for Phase II

Carsten B. Krauss, Queen's University, Kingston, Ontario, Canada –  
for the PICASSO collaboration

Queen's University, Department of Physics, Kingston, ON, K7L 2N6, Canada

E-mail: ckrauss@owl.phy.queensu.ca

**Abstract.** PICASSO is a dark matter search experiment that uses the superheated droplet technique to find spin-dependently interacting WIMPs. A set of 11 detectors with a total active mass of 19.4 g was used to prove the validity of the technique. The data from this run disfavors WIMP-proton cross sections larger than 1.3 pb for a WIMP mass of 29 GeV. Currently phase II of PICASSO is getting started. It will consist of 32 4.5 l detectors with a projected active mass of 2.5 kg and improved detectors.

In two publications the PICASSO collaboration has shown that the superheated droplet detection technique is capable of setting limits on the spin-dependent neutralino-nucleon interaction [1][2]. The exclusion limit extracted from the 2004 19.4 g active mass running at SNO is shown as black line in figure 1. This data was taken with three one liter detectors purified with the HTiO method developed for SNO [3]. Since then new 4.5 l detector containers with nine piezo-electric sensors have been developed. The purification was improved by more controlled environmental conditions during the manufacturing process and a new, more efficient method to remove heavy ions from the U and Th chain from the CsCl salt used in the detectors. The purification is now completely performed in a new cleanroom facility where the ingredients are kept under a Nitrogen cover gas during the entire handling and purification. The manufacturing process was improved to increase the droplet size which improves the active mass per volume (loading) while reducing the sensitivity to alpha decays at the same time. The projected

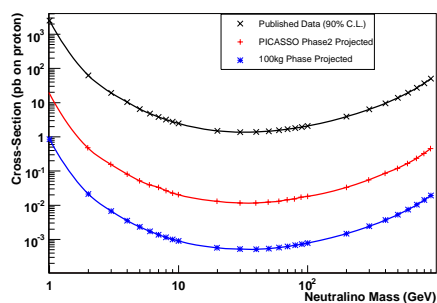


**Figure 1.** published PICASSO exclusion curve (black) and projected sensitivity for the 32 detector phase (red) and sensitivity for a possible 100 kg active mass PICASSO experiment.

sensitivity with the new detectors for a excluding WIMP-proton interactions at 90% C.L. is plotted in figure 1 in red. Also shown is a projected large scale PICASSO experiment with 100 kg active mass and another improvement of the the purification by a factor of 100 (blue).

[1] Barnabe-Heider M *et al* 2005 *Phys. Lett. B* **624** 186-194

[2] Barnabe-Heider M *et al* 2005 *Nucl. Instrum. Meth. A* **555** 184-204

[3] Andersen T C *et al* 2003 *Nucl. Instrum. Meth. A* **501** 386-398

# Detector-related backgrounds in the Karlsruhe Tritium Neutrino Experiment

**Michelle Leber for the KATRIN collaboration**

Center for Experimental Nuclear Physics and Astrophysics, University of Washington, Box  
354290 Seattle, WA 98195-4290, USA

E-mail: [mleber@u.washington.edu](mailto:mleber@u.washington.edu)

**Abstract.** The Karlsruhe Tritium Neutrino Experiment, or KATRIN, is a next generation tritium beta decay experiment to directly measure neutrino mass with an expected sensitivity of 0.2 eV[1]. Neutrino mass does not fit into the Standard Model, and determining this mass may set the scale of new physics. To achieve this level of sensitivity, backgrounds in the experiment must be minimized. A complete Geant4[2] simulation of KATRIN's focal plane detector and surrounding region is being developed. These simulations will help guide the design and selection of shielding and detector construction materials to reduce backgrounds from cosmic rays and natural radioactivity.

The KATRIN experiment will use a silicon semiconductor diode array to detect  $\beta$ -decay electrons. Cosmic rays, natural radioactivity, and cosmogenics in the detector region are all potential background sources. These can be reduced with a passive shield of lead and copper and a plastic scintillator. Natural radioactivity and cosmogenics can be minimized by careful material selection. Materials must also be compatible with a 6 Tesla field and ultra-high vacuum. Once all backgrounds are understood, an optimum low-background region-of-interest (ROI) will be identified. The detector-related background is specified as  $\lesssim 1$  mHz. The  $\beta$ -decay electrons can be accelerated after the electrons pass through the spectrometer to energies above the endpoint energy, 18.6 keV, so that they fall within this low-background ROI. This is accomplished by floating the inner detector system at up to 30 kV. To better understand backgrounds related to the KATRIN detector, a Geant4-based[2] code to simulate all possible backgrounds is being developed.

[1] KATRIN Design Report 2004 see <http://www-ik.fzk.de/~katrin/>

[2] Agostinelli S *et al.* 2003 *Nuclear Instr. Methods A* **506** 250-303

Allison J *et al.* 2006 *IEEE Transactions on Nuclear Science* **53** No. 1 270-8

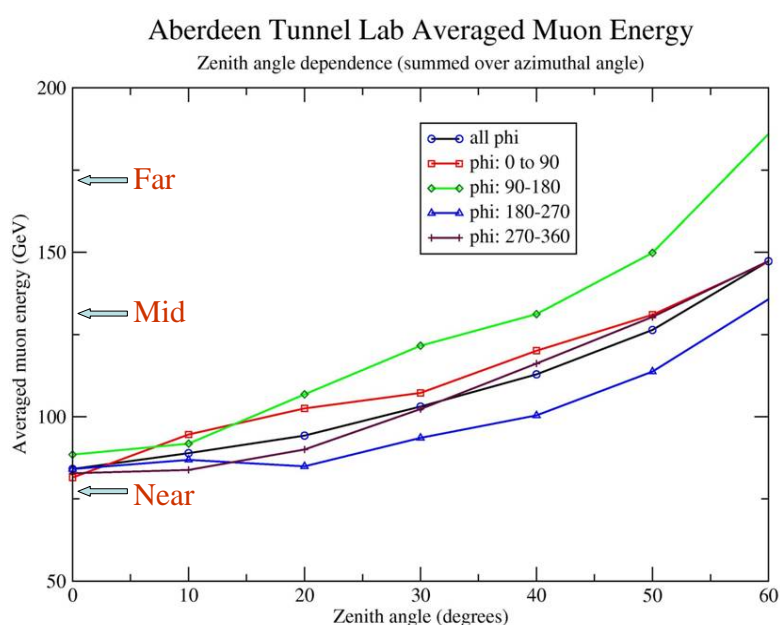
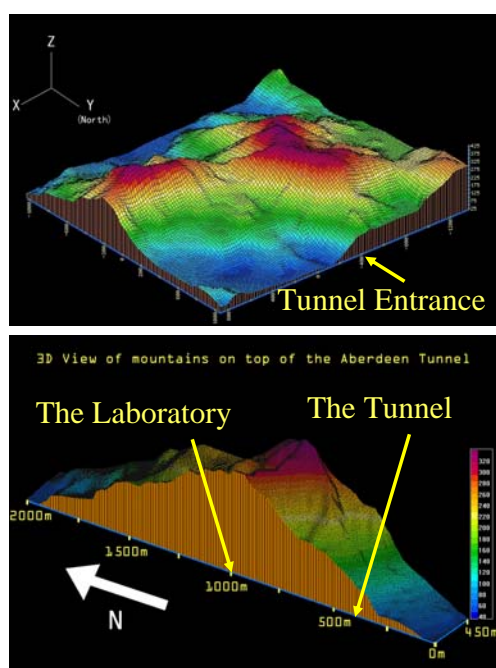
## Acknowledgments

This work was supported in part by the U.S. Department of Energy under Grant DE-FG02-97ER41020.

## ABSTRACT

An underground laboratory (Aberdeen Tunnel Laboratory) was built inside a traffic tunnel (Aberdeen Tunnel) in the Hong Kong Island in the early 80's for the study of cosmic-ray muon anisotropy. The laboratory has an overburden of about 250 m of rock, which is comparable to those of the detector halls proposed for the Daya Bay Neutrino Experiment in Guangdong Province, China. Given the very similar geographical location, the geology and background radiation to those in Daya Bay, the Aberdeen Tunnel Laboratory is an ideal testing ground for the Daya Bay Experiment. This project aims to study the neutrons initiated from cosmic muons by detecting the neutrons with a 0.5 ton neutron detector comprising of Gd-doped liquid scintillators viewed by PMTs. The events will be triggered by a muon tracker consisting of 3 horizontal layers of crossed stainless steel proportional counters and plastic scintillators, with 2 layers above and 1 layer below the neutron detector. It is hoped that the results will help in understanding and minimizing the neutron background in Gd-doped liquid scintillator based neutrino detectors. This paper presents an overview of the laboratory, the geology and radiation background, and the proposed detectors.

## THE ABERDEEN TUNNEL LABORATORY



The mountain profile above the Laboratory is like a saddle. So by appropriately choosing the zenith angle of the arriving muon events, it is possible to study the muon-induced neutrons at different overburdens, corresponding to the “Near-”, “Mid-” and “Far-site” detectors in the Daya Bay Experiment.

## BACKGROUND

The Daya Bay Experiment is designed to measure the smallest neutrino mixing angle  $\theta_{13}$  by measuring the disappearance rate of anti-neutrinos emitted from the nuclear power reactors in the Daya Bay region. The neutrinos will be detected through the inverse beta-decay reaction which will generate a positron and a neutron. Knowledge of the background neutron flux in the future underground detector halls in Daya Bay is therefore critical in the design of the experiment.

## KEY OBJECTIVES

- To build a Gd-doped liquid scintillator type neutron detector completed with a muon tracking system.
- To obtain the muon flux and energy spectra in the laboratory having an overburden of  $\sim 240$  m of rock.
- To study the production of neutrons in the laboratory environment and in the neutron detector.
- To study other background radiation effects such as gammas and radon from rocks.
- To act as a satellite laboratory for the Daya Bay Experiment for testing equipments and verifying experimental data.
- To develop simulation packages such as GEANT4, MUSIC that could be applied in the Daya Bay Experiment.

## THE DETECTOR



Proportional counters

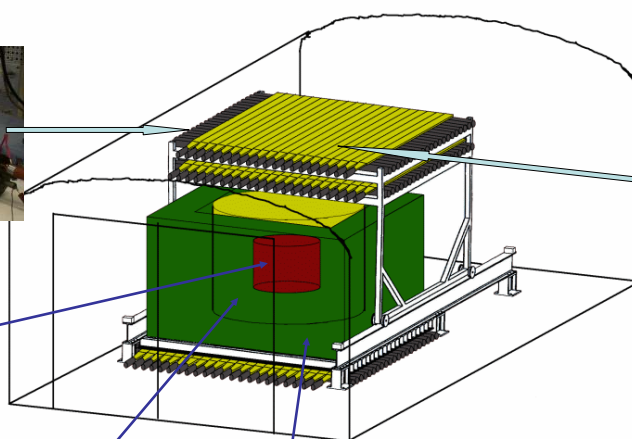
Neutron detector:  
Gd-doped liquid  
scintillator

Gamma catcher: normal  
liquid scintillator

Water buffer



Plastic scintillators



Dimension of Laboratory	3.2m x 6.7m x 2.3m (W x D x H)
Neutron detector	1 m diameter x 1 m high
Gamma catcher	1.5 m diameter x 1.4 m high
Buffer	0.25 m thick of water
Active area of muon tracker	$\sim 2$ m x 2 m
Distance between top & bottom layers	2 m



**Please also visit the other 3 posters of ours for related works and results. Thank you!**  
 Proceedings of Neutrino Physics and Astrophysics, July 13-19, 2006

# Geophysics with Hawaiian Anti-neutrino Observatory (Hanohano)

## J. Maricic for the Hanohano Collaboration

Drexel University, Philadelphia, PA, 19104, University of Hawaii, Honolulu, HI, 96822

jelena.maricic@physics.drexel.edu

**Abstract.** The design studies are under way for the deep ocean anti-neutrino observatory located in the vicinity of the Big Island (Hawaii) with the main goal of measuring geo-neutrino flux from the mantle and core which can exclusively be done in a location far from the continental plates such as Hawaiian Islands chain. Hanohano will also accomplish the definitive measurement of the electron anti-neutrino signal from the core to observe or eliminate a hypothetical natural reactor in the Earth's core.

## 1. Introduction

Uranium and thorium content of the Earth is directly related to the Earth's heat flow, which is not a well known quantity [1]. One suggested way of estimating the uranium and thorium content of the Earth is via detection of anti-neutrinos produced in the radioactive decays of these elements [2] which has been done in [3] for the first time. The hypothetical nuclear reactor in the Earth's core can also be detected through its anti-neutrino flux and attempt has been made in [4]. Hawaiian Anti-neutrino Observatory (Hanohano) will be a liquid scintillator detector designed with a goal to make a definitive measurement of geo-neutrino flux due to uranium and thorium in the Earth's mantle and core and to observe or eliminate a putative reactor in the Earth's core via its anti-neutrino flux. Experience from the KamLAND detector in Japan is used to estimate needed baseline to achieve desired sensitivity as well as for the background rate estimates.

## 2. Hanohano detector

In order to accomplish 16% measurement of the U/Th content of the mantle plus core, Hanohano must have at least 10 kiloton-years of exposure. It should be placed at 4 km depth to reduce cosmic ray induced backgrounds, thus the suggested location is in the vicinity of the Big Island in Hawaii. It is expected that Hanohano should reach the same level of radio-purity levels as in KamLAND, except for radon where the significant improvement is needed (at least a factor of 40). 1 TW or larger core nuclear reactor may be detected with  $5\sigma$  confidence level with Hanohano detector.

## References

- [1] D.L. Anderson, *Theory of Earth*, Blackwell Science (1990).
- [2] G. Eder, *Terrestrial Neutrinos*, Nucl. Phys. **78**, 657 (1966).
- [3] T. Araki et al., Nature (London) **436**, 499 (2005).
- [4] Jelena Maricic, Ph.D. Thesis, University of Hawaii (2005).



## The Majorana Experiment

**J. Esterline<sup>1</sup>, V.M. Gehman<sup>4,8</sup>, K. Gusev<sup>2</sup>, T. Hossbach<sup>3,9</sup>,  
R.A. Johnson<sup>4,\*</sup>, K. Kazkaz<sup>4</sup>, J. Kephart<sup>5,9,10</sup>, M. Kidd<sup>1</sup>, G. King<sup>3</sup>,  
M.G. Marino<sup>4,\*</sup>, A.G. Schubert<sup>4,\*</sup>, M. Shirchenko<sup>2</sup>, J. Thompson<sup>6</sup>,  
V. Timkin<sup>2</sup>, B. White<sup>7</sup>, on behalf of the Majorana Collaboration**

<sup>1</sup> Duke University, Durham, NC

<sup>2</sup> Joint Institute for Nuclear Research, Dubna, Russia

<sup>3</sup> University of South Carolina, Columbia, SC

<sup>4</sup> University of Washington, Seattle, WA

<sup>5</sup> North Carolina State University, Raleigh, NC

<sup>6</sup> Brown University, Providence, RI

<sup>7</sup> University of Tennessee, Knoxville, TN

<sup>8</sup> Los Alamos National Laboratory, Los Alamos, NM

<sup>9</sup> Pacific Northwest National Lab, Richland, WA

<sup>10</sup> Triangle Universities Nuclear Lab, Durham, NC

\* Poster presented by R. Johnson, M. Marino, and A. Schubert

E-mail: mgmarino@u.washington.edu

Recent results from Super-Kamiokande, SNO, KamLAND, MINOS, [1-4] and other experiments have demonstrated that neutrinos are massive and change flavor. Probing the absolute scale of neutrino masses can be accomplished via neutrinoless double-beta decay searches; discovery of neutrinoless double-beta ( $0\nu\beta\beta$ ) decay would also establish the Majorana nature of the neutrino. The Majorana collaboration proposes to search for this process by employing high-purity, segmented, enriched (86%  $^{76}\text{Ge}$ ) germanium as both source and detector. Recent improvements in signal processing, detector design, and advances in controlling intrinsic and external backgrounds will augment this well-established technique [5,6]. The objective of the first experimental phase of the Majorana experiment is to build a 120-kg detector of 86% enriched  $^{76}\text{Ge}$  to search for  $0\nu\beta\beta$  decay. The physics goals for this first phase are to probe the quasi-degenerate neutrino mass region above 100 meV, demonstrate that backgrounds at or below 1 count/tonne/year in the  $0\nu\beta\beta$  decay peak 4-keV region of interest can be achieved that would justify scaling up to a 1 tonne or larger mass detector, and to definitively test the Klapdor-Kleingrothaus claim to have observed  $0\nu\beta\beta$  decay in  $^{76}\text{Ge}$  in the mass region around 400 meV [5]. Such low backgrounds and an exposure of 464 kg-years would enable the Majorana experiment to achieve a sensitivity to the  $^{76}\text{Ge}$   $0\nu\beta\beta$  decay half-life of  $5.5 \times 10^{26}$  years at the 90% CL and a Majorana neutrino mass sensitivity of 120 meV (using the latest RQRPA nuclear matrix element calculations [7]).

[1] Y. Ashie *et al.* (Super-Kamiokande), Phys. Rev. D71, 112005 (2005), hep-ex/0501064.

[2] S. N. Ahmed *et al.* (SNO), Phys. Rev. Lett. 92, 181301 (2004), nucl-ex/0309004.

[3] T. Araki *et al.* (KamLAND), Phys. Rev. Lett. 94, 081801 (2005), hep-ex/0406035.

[4] D.G. Michael *et al.* (MINOS), hep-ex/0607088.

[5] H. V. Klapdor-Kleingrothaus *et al.*, European Physical Journal A 12, 147 (2001a).

[6] C. E. Aalseth *et al.*, Physical Review D 65, 092007 (2002).

[7] V. A. Rodin, *et al.*, nucl-th/0503063

# Cryogenic Double Beta Decay Experiments: CUORE and CUORICINO

**Reina Maruyama, for the CUORE Collaboration [1]**

Lawrence Berkeley National Laboratory & University of Wisconsin, Madison, USA

E-mail: rmaruyama@lbl.gov

**Abstract.** Cryogenic bolometers, with their excellent energy resolution, flexibility in material, and availability in high purity, are excellent detectors for the search for neutrinoless double beta decay. Kilogram-size single crystals of  $\text{TeO}_2$  are utilized in CUORICINO for an array with a total detector mass of 40.7 kg. CUORICINO currently sets the most stringent limit on the halflife of  $^{130}\text{Te}$  of  $T_{1/2}^{0\nu} \geq 2.4 \times 10^{24}$  yr (90% C.L.), corresponding to a limit on the effective Majorana neutrino mass in the range of  $\langle m_\nu \rangle \leq 0.2\text{--}0.9$  eV. Based on technology developed for CUORICINO and its predecessors, CUORE is a next-generation experiment designed to probe  $\langle m_\nu \rangle$  in the range of 10–100 meV. Latest results from CUORICINO and overview of the progress and current status of CUORE are presented.

## 1. Introduction

The search for neutrinoless double beta decay ( $0\nu\beta\beta$ ) has become one of the top priorities in the field of neutrino physics since the discovery of neutrino oscillations in atmospheric[2], solar[3], and reactor[4] experiments. An overview and current status of double-beta decay physics and experiments were given in earlier talks by Hirsch, Simkovic, Elliott, and Barabash[5]. The need to verify the claim of the observation of  $0\nu\beta\beta$  by a subset of Heidelberg-Moscow germanium experiment[6] has also been presented in these talks. The most stringent limit on the effective mass of Majorana neutrinos comes from two  $^{76}\text{Ge}$  experiments, Heidelberg-Moscow[7] and IGEX[8]. CUORICINO which is searching for  $0\nu\beta\beta$  in  $^{130}\text{Te}$  follows closely behind[9]. NEMO-3 is capable of a multiple-isotope search for double-beta decay events, and with its tracking capabilities, has excellent sensitivity to  $2\nu\beta\beta$ [11].

A number of experiments are currently at various stages of development to probe the degenerate mass hierarchy region of the neutrino mass spectrum and into the inverted hierarchy, many of which are represented at this conference[12]. CUORE (Cryogenic Underground Observatory for Rare Events) is one such experiment, to be located at the Gran Sasso National Laboratory (LNGS). It will consist of 988 bolometers of  $\text{TeO}_2$  crystals, with a total mass of 741 kg. Because of the high isotopic abundance of 34%, 204 kg of  $^{130}\text{Te}$  is available for  $0\nu\beta\beta$  without isotopic enrichment, making CUORE both timely and significantly less expensive than other experiments. CUORE's modular design and flexibility will also allow future searches in other isotopes of interest. It is imperative to carry out double beta decay searches in multiple isotopes, both to improve the nuclear matrix calculations necessary to extract the effective neutrino mass, and to ensure that the observation of a line at the expected energy is not a result of an unidentified background.

Double beta decay experiments can be divided into three categories: indirect measurements such as geochemical analyses, direct measurements with the source being separate from the detector, and direct measurements with a detector that also acts as the source. Bolometers belong to the last category[16]. When the source is the same as the detector, the source mass is maximized while materials that could potentially contribute to the background are minimized. In bolometers, the deposited energy is measured thermally, therefore the entire energy of a decay event is fully accounted for. At low temperatures (the operating temperature for CUORICINO is 8 mK), the heat capacity of crystals is proportional to the cube of the ratio of the operating and Debye temperatures. The energy released in a single particle interaction within the crystal is clearly measurable as change in temperature of the entire crystal. The temperature change is measured by neutron transmutation doped (NTD) germanium thermistors which are optimized to operate at these temperatures[14, 15]. The energy resolution of cryogenic bolometers rivals that of germanium detectors, and 5 keV FWHM resolution at 2.5 MeV is readily achievable.

## 2. CUORICINO: Results and Performance

CUORICINO started taking data in April 2003 at LNGS and is now producing competitive results with those achieved by the germanium experiments. It will continue to run until CUORE has been constructed and is ready to take data. First results from CUORICINO were published recently which included data from a total exposure of 3.09 kg·yr of  $^{130}\text{Te}$ [9]. Here we report on an update that includes the data up to May 2006 with a total of 8.38 kg·yr of  $^{130}\text{Te}$  (see Fig. 1)[17]. No evidence for excess counts is observed at 2530 keV, the expected Q-value for  $0\nu\beta\beta$  for  $^{130}\text{Te}$ . The absence of any excess events above backgrounds in the region of interest gives a limit of  $T_{1/2}^{0\nu} \geq 2.4 \times 10^{24}$  yr (90% C.L.) on the  $0\nu\beta\beta$  decay rate of  $^{130}\text{Te}$ . This corresponds to an effective neutrino mass of  $\langle m_\nu \rangle \leq 0.18 - 0.94$  eV, the range reflecting the spread in QRPA nuclear matrix element calculations (see [9] for list). The background measured in the  $0\nu\beta\beta$  region of interest is  $0.18 \pm 0.01$  counts/keV·kg·yr.

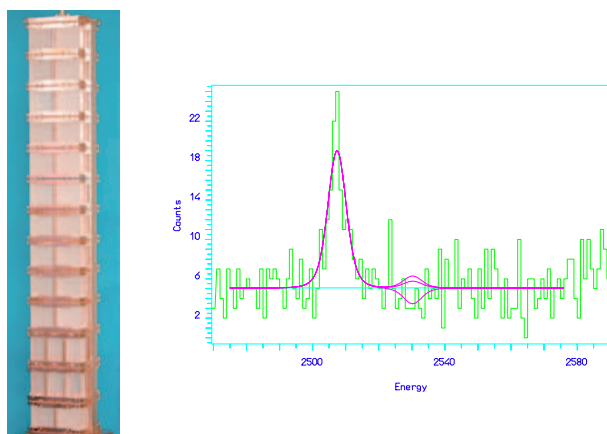


**Figure 1.** Left: Photo of the CUORICINO tower before Cu thermal shields were installed. Right: CUORICINO summed background energy spectrum in the  $^{130}\text{Te}$   $0\nu\beta\beta$  region. The peak at 2505 keV is the sum peak from two  $^{60}\text{Co}$  gamma lines.  $0\nu\beta\beta$  signal from  $^{130}\text{Te}$  is expected at 2530 keV. No evidence of DBD is seen.

CUORICINO is roughly one-twentieth the size of CUORE, and much of the technology that will be used in CUORE was used to build CUORICINO. It consists of 62  $\text{TeO}_2$  crystals with a total mass of 40.7 kg. The crystals are arranged in a tower, 11 levels each containing four crystals  $5 \times 5 \times 5 \text{ cm}^3$  in

size, weighing  $\sim 330$  g (see Fig. 1). All  $5 \times 5 \times 5$  cm<sup>3</sup> crystals and all but four of the  $3 \times 3 \times 6$  cm<sup>3</sup> crystals are made from tellurium of natural abundance. Two of the  $3 \times 3 \times 6$  cm<sup>3</sup> crystals are enriched to 75% <sup>130</sup>Te and two are enriched to 82.3% <sup>128</sup>Te. The average resolution in the  $0\nu\beta\beta$  region, measured with the 2615 keV <sup>208</sup>Tl line during calibration runs, is  $\sim 8$  keV. In 3 years of running with the present background level, CUORICINO will achieve a half-life sensitivity for  $0\nu\beta\beta$  decay of  $7.1 \times 10^{24}$  yr, corresponding to an effective mass on the order of 300 meV.

### 3. CUORE

CUORICINO also serves as an excellent test bed and prototype for CUORE. All critical subsystems of the proposed CUORE detector are based on the design of CUORICINO. CUORE will consist of an array of 988,  $5 \times 5 \times 5$  cm<sup>3</sup> TeO<sub>2</sub> bolometers arranged in 19 CUORICINO-like towers. The total crystal mass of TeO<sub>2</sub> will be 741 kg, with 204 kg of <sup>130</sup>Te (see Fig. 2). The entire detector will be housed in a single dilution refrigerator at 10 mK.

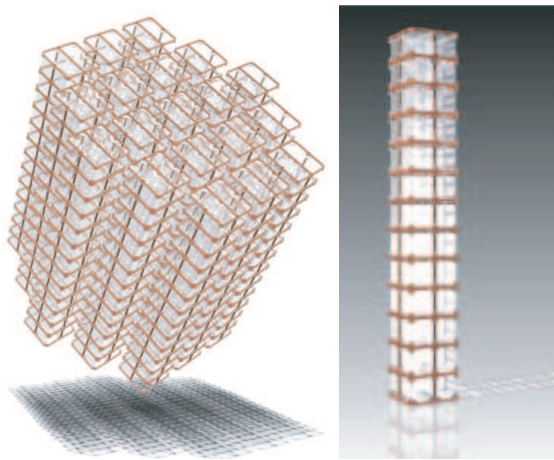


**Figure 2.** Left: The CUORE detector consisting of a close-packed array of 19 towers with a total of 988 crystals. Right: One of the 19 towers of the CUORE detector array, similar to the one operating in the CUORICINO experiment.

In 5 years of running with a background of 0.01 counts/keV·kg·yr and a resolution of 5 keV, CUORE expects to have a sensitivity to the half-life of  $0\nu\beta\beta$  of  $T_{1/2}^{0\nu} \sim 2.1 \times 10^{26}$  yr. This corresponds to an effective neutrino mass of  $\langle m_\nu \rangle \leq 19 - 100$  meV, with the spread coming from the uncertainty in matrix element calculations. If we are able to reduce the background to 0.001 counts/keV·kg·yr, the sensitivity will extend to  $T_{1/2}^{0\nu} = 6.5 \times 10^{26}$  yr (11–57 meV). The main technical challenges will be to control the background levels, ensure that the narrow energy resolution achieved with many of the crystals are uniformly implemented in all crystals, and that all crystals are well calibrated for energy.

A combination of CUORICINO background data, measurements from an independent R&D setup in Hall C in LNGS, direct counting with germanium detectors on- and off-site, neutron activation analysis, and other techniques are used to characterize materials and components to be used in CUORE. The results of these measurements as well as other potential sources of radioactive background (e.g. environmental activity) are used as input for Monte Carlo simulation. Estimates of the relative contributions of the main background sources in the ROI in CUORICINO is as follows:  $10 \pm 5\%$  from U/Th contaminations on the TeO<sub>2</sub> surfaces,  $50 \pm 20\%$  from Cu surfaces (both from the crystal support structure and thermal shielding), and  $30 \pm 10\%$  from the bulk of the Cu shields.

The sources of backgrounds are divided into three main categories: contamination in the bulk, surfaces, and environmental radioactivity. Because the Q-value for <sup>130</sup>Te  $0\nu\beta\beta$  decay is higher than most gamma-lines from U and Th, the only tails of known lines that may contribute to the background are <sup>60</sup>Co and <sup>208</sup>Tl, which are  $2035$  keV and  $2615$  keV, respectively.

Alpha events with lines at higher energies can contribute if they deposit only a part of their energy in the crystals, therefore surface contaminations on or near the crystals is of particular concern.

Other components facing the detector (Teflon stand-offs, heaters used for gain stabilization, and gold wires for signal and other electrical controls) were also tested in the R&D setup in Hall C by covering crystal surfaces with a large amount of these materials. The background seen from these materials was found to be negligible.

Simulations are being refined as more data are being collected with the CUORICINO detector and elsewhere. As of April 2006, we have demonstrated that background reductions of a factor of  $\sim 8$  and detector resolutions of 5 keV are achievable. Figure 3 shows the background spectrum obtained from CUORICINO and the R&D setup in Hall C. The shielding around the Hall C setup is insufficient to shield much of the  $\gamma$ 's below 2.6 MeV, however significant reduction in the  $\alpha$  events above 2.6 MeV is clearly seen. Effort is underway to further reduce the background by careful material selection and handling procedures. In addition, background rejection through anticoincidence among adjacent crystals will be more effective in the much larger CUORE array and will aid in achieving the background goals.

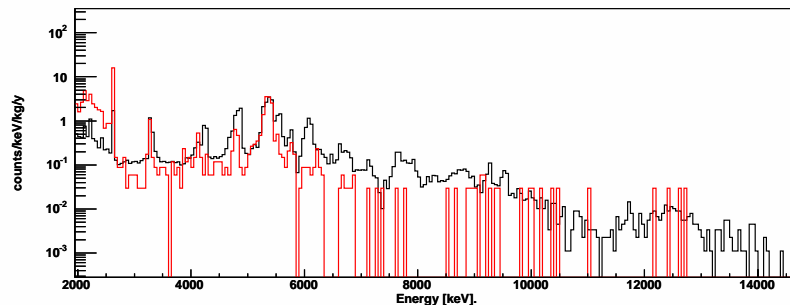


**Figure 3.** CUORICINO background energy spectrum (black) and background spectrum from the R&D setup in Hall C (red).

We have estimated that for the muon flux observed in LNGS ( $2.5 \times 10^{-8} \mu/(\text{cm}^2 \text{s})$ ), muons would produce  $\sim 0.04$  neutrons/day in the polyethylene shield and  $\sim 25$  neutrons/day in the lead shield. This indicates that neutrons will play a secondary role in the total background compared with other sources of background. In addition, we are planning a series of experiments at the GEANIE facility at Los Alamos National Laboratory to measure cross-sections for neutron-induced reactions on the abundant Te isotopes for neutrons from 1-100 MeV[18]. The results of these measurements will then be used in our MC calculations to refine background estimates.

#### 4. Beyond CUORE

The main goal and design of CUORE is to search for  $0\nu\beta\beta$  decay in  $^{130}\text{Te}$ . Its sensitivity can be increased three times ( $\sim 60\%$  improvement in the sensitivity to neutrino mass) by replacing the detectors with enriched crystals. Event identification using multiple signatures from a single event is a powerful tool in reducing backgrounds. Work is underway to further reduce backgrounds by using Surface Sensitive Bolometers (SSB) and/or scintillating bolometers[18]. Every factor of ten reduction in background would increase the halflife sensitivity by a factor of three.

SSB allows us to distinguish surface events and bulk events, especially for  $\alpha$ -particles. It consists of the main DBD absorber and thin absorbers attached to the crystal surfaces. The

surface events from either the main crystal absorber or elsewhere would trigger the SSB, and those events could be rejected. In addition, the additional heat capacity from the thin absorbers alters the pulse shape of the signal from the main absorber[19].

Scintillating bolometers would combine heat and scintillation approach already successfully applied in dark matter experiments such as CRESST and ROSEBUD. Scintillation and heat signals have different sensitivities for nuclear recoils,  $\alpha$  particles, and ionizing events such as  $0\nu\beta\beta$  decay. A  $\text{CaF}_2$  bolometer has successfully been used[20], and the collaboration is currently investigating  $\text{TeO}_2$  doped with Nb and Mn[21].

The modular design of the CUORE detector also allows for searches of  $0\nu\beta\beta$  in other isotopes. It is possible to create thermal detectors from a variety of materials, and CUORE could investigate  $0\nu\beta\beta$  in other nuclei. Several DBD candidates have been tested as thermal detectors:  $\text{CaF}_2$ , Ge,  $\text{MoPbO}_4$ ,  $\text{CdWO}_4$ , and  $\text{TeO}_2$ . Possible crystals for Nd are under development.

## 5. Conclusion

Cryogenic bolometers, with their flexibility in material choice and the ability to scale up to the ton-scale are ideal for large-scale detectors for double-beta physics experiments. CUORE aims to probe the Majorana nature of the neutrino, with a sensitivity to the neutrino mass deep into the inverted mass hierarchy. CUORICINO is currently running as the most sensitive  $0\nu\beta\beta$  experiment, and will continue until CUORE comes online. Much of the technology has been tested for CUORE, and a factor of 8 reduction from the radioactive background observed in CUORICINO has been achieved. CUORE has been approved by the advisory Commissione II of INFN (Italian Institute of Nuclear Physics) and funding has been allocated in 2005. The CUORE experiment was approved by the Scientific Committee of LNGS in 2004, and preparations of the laboratory space and the construction of CUORE are underway.

## References

- [1] For more information and complete list of authors, see the CUORE website: <http://crio.mib.infn.it/wig/Cuorepage/CUORE.php>.
- [2] Super-Kamiokande Collaboration, S. Fukuda *et al.*, Phys. Rev. Lett. **86** (2001) 5656.
- [3] SNO Collaboration, Q.R. Ahmad *et al.*, Phys. Rev. Lett. **89** (2002) 011301.
- [4] KamLAND Collaboration, K. Eguchi *et al.*, Phys. Rev. Lett. **90** (2003) 021802.
- [5] See presentations at Neutrino'06 by M. Hirsch, F. Simkovic, S. Elliott, and A. Barabash.
- [6] H.V. Klapdor-Kleingrothaus *et al.*, Mod. Phys. Lett. A **16** (2001) 2409; H.V. Klapdor-Kleingrothaus, A. Dietz, I. Krivosheina and O. Chkvorets, Phys. Lett. B **586** (2004) 198; H.V. Klapdor-Kleingrothaus *et al.*, Nucl.Instrum.and Meth. **522** (2004) 367.
- [7] H.V. Klapdor-Kleingrothaus *et al.* Eur. Phys. J. A **12** (2001) 147.
- [8] C.E. Aalseth *et al.*, Phys. Rev. D **65** (2002) 092007.
- [9] CUORICINO Collaboration, C. Arnaboldi *et al.*, Phys. Rev. Lett. **95** (2005) 142501.
- [10] CUORE Collaboration, R. Ardito *et al.*, hep-ex/0501010.
- [11] R. Arnold *et al.* Phys. Rev. Lett. **95** (2005) 182302.
- [12] See presentations at Neutrino'06 by S. Schoenert, A. Piepke, and J. Wilson.
- [13] C. Arnaboldi *et al.*, Phys. Lett. B **584** (2004) 260.
- [14] E.E. Haller *et al.*, Proc. Fourth Int. Conf. on Neutron Transmutation Doping of Semiconductor Materials, Nat. Bureau of Standards, June 1,2 1982, Gaithersburg MD, R.D. Larrabee ed., (Plenum Press 1984) p 21.
- [15] E. Haller, J. Appl. Phys. **77** (1995) 2857.
- [16] S.H. Moseley, J.C. Mather and D. McCammon, J. Appl. Phys. **56** (1994) 1257.
- [17] S. Capelli, Poster presentation at Neutrino'06 Conference (Santa Fe, NM, USA).
- [18] M. Dolinski, S. Sangiorgio, P. Gorla, Poster presentations at Neutrino'06 Conference (Santa Fe, NM, USA);
- [19] I. Bandac *et al.*, submitted to Journal of Applied Physics (2006).
- [20] A. Alessandrello *et al.*, Phys.Lett. B **420** (1998) 109
- [21] I. Dafinei *et al.*,  $\text{TeO}_2$  scintillating crystal growth and properties, presented at the Int.Conf. on Inorganic Scintillators and their Industrial Applications SCINT2005,; Crimea, Alushta (Ukraine), Sept.19-23, 2005

# Tagging radon daughters in low-energy scintillation detectors

**Kevin B McCarty**

Princeton University Physics Department, Princeton, NJ 08544, USA

Email: kmccarty@princeton.edu

**Abstract.** One problematic source of background in scintillator-based low-energy solar neutrino experiments such as Borexino is the presence of radon gas and its daughters. The mean lifetime of the  $\alpha$ -emitter  $^{214}\text{Po}$  in the radon chain is sufficiently short, 0.24 ms, that its decay, together with that immediately preceding of  $^{214}\text{Bi}$ , is easily recognized as a “coincidence event.” This fact, combined with the capability of  $\alpha/\beta$  pulse-shape discrimination, makes it possible to tag decays of  $^{222}\text{Rn}$  and its first four daughters via a likelihood-based method.

## 1. Introduction

Low-energy scintillation detectors, such as the solar neutrino detector Borexino [1], are plagued by radon and its daughter isotopes. These isotopes (including  $\alpha$ -emitters, due to the phenomenon of  $\alpha$  quenching in organic scintillators) generate background in the sub-MeV energy window.

Happily, the four daughters produced following a  $^{222}\text{Rn}$  decay are short-lived,  $\tau_{1/2} < 30$  min. Given observation of a  $^{214}\text{Bi}/^{214}\text{Po}$  coincidence event (“BiPo”), it is thus very probable that the original  $^{222}\text{Rn}$  decay and the following decays of  $^{218}\text{Po}$  and  $^{214}\text{Pb}$  took place within the previous 4 hours. If the rate of other background events is not too high, the decay events of radon and its daughters may be picked out—not statistically, but individually. A likelihood-based method used in doing so takes into account the observed positions, energies, and  $\alpha/\beta$  discrimination parameter values of each event during the 4-hr time window preceding the BiPo, as well as the time separation of each possible pair of events.

## 2. Monte Carlo simulation and Counting Test Facility data

A simple Monte Carlo simulation of Borexino data, with pessimistic assumptions about the background, yielded a success rate for the likelihood-based algorithm of  $> 96\%$  in identifying each of the three isotopes  $^{222}\text{Rn}$ ,  $^{218}\text{Po}$ ,  $^{214}\text{Pb}$ . The probability for a neutrino event to be falsely identified as a radon-chain decay was  $< 1\%$ . A 1/20-scale Counting Test Facility prototype [2] is less shielded from external  $\gamma$  rays and therefore has a higher average event rate per unit mass. Analogous simulations for CTF predicted a success rate of  $\sim 95\%$  for the two  $\alpha$ -emitters, and  $87\%$  in identifying  $^{214}\text{Pb}$   $\beta$  decays. An analysis of 177 BiPo coincidences in real CTF data further indicated the potential utility of the method [3]. The possibility of similar event tagging in the  $^{238}\text{Th}$  chain may also be foreseen.

## References

- [1] Alimonti G *et al.* 2002 *Astropart. Phys.* **16** 205
- [2] Alimonti G *et al.* 1998 *Nuc. Inst. Meth. A* **406** 411
- [3] McCarty K 2006 *The Borexino Nylon Film and the Third Counting Test Facility* (Ph. D. thesis, Princeton University) chapter 8 pp 388–400

## Pulse-shape analysis of NCD-array data at SNO

**H. Deng<sup>4</sup>, S. McGee<sup>5</sup>, M. Miller<sup>2</sup>, N. Oblath<sup>5,\*</sup>, J. Secret<sup>4</sup>, N. Tolich<sup>1</sup> and H. Wan Chan Tseung<sup>3</sup> for the SNO Collaboration**

<sup>1</sup>Lawrence Berkeley National Laboratory, Berkeley, CA 94720, USA

<sup>2</sup>Massachusetts Institute of Technology, Cambridge, MA 02139, USA

<sup>3</sup>University of Oxford, Oxford OX1 2JD, UK

<sup>4</sup>University of Pennsylvania, Philadelphia, PA 19104, USA

<sup>5</sup>University of Washington, Seattle, WA 98195, USA

E-mail: \*Corresponding author: nsoblath@u.washington.edu

In November 2004, Phase III of the Sudbury Neutrino Observatory (SNO) experiment began after the installation of the Neutral-Current Detection (NCD) Array in the D<sub>2</sub>O-filled acrylic vessel. The array is composed of 40 ultra-clean proportional counters, each about 10 m in length. Signal is detected by 36 <sup>3</sup>He-filled counters with 4 <sup>4</sup>He-filled counters deployed as controls. The former detect neutrons via the following interaction:  $n + {}^3\text{He} \rightarrow p + {}^3\text{H} + 764 \text{ keV}$ .

Phase III is unique in the SNO experiment in that the Neutral-Current (NC) signal can be statistically and systematically separated from the Elastic-Scattering and Charged-Current signals by simply counting the number of  $\nu_{\text{solar}}$ -induced dissociated neutrons captured in the NCD Array. To make a measurement of the NC signal it is necessary to understand and quantify which events in the NCD Array are neutrons and which are backgrounds.

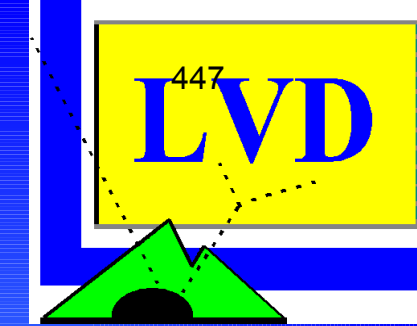
A significant background to the neutron interaction in the NCD Array is the  $\alpha$ -particles from the decay chains of <sup>238</sup>U and <sup>232</sup>Th embedded in the nickel bodies of the NCDs, and of <sup>210</sup>Po residing on the inner surfaces. Other potential backgrounds include electronic discharges and multiply-scattered  $\beta$ s and  $\gamma$ s. To separate these events, members of the SNO collaboration are pursuing numerous paths to find the most discriminating Pulse-Shape-Analysis technique.

Two basic methods are being pursued. The first method minimizes the  $\chi^2$  of the fit of a data pulse to a library of neutron and alpha pulses. This method is very CPU intensive. The second, less processor-intensive method characterizes the pulse shape according to a variety of parameters including width, energy and higher-order moments. In this method discrimination is performed by comparing the pulse shape parameters to distributions of these parameters obtained from either simulations or a combination of data from control counters and runs with sources deployed.

In addition, there is a contribution to the neutron signal in the NCD Array from neutrons generated in SNO's acrylic vessel. These neutrons will interact predominantly in the ends of the NCD strings. Therefore, a determination of the vertical ( $z$ ) position of the neutron interaction within the NCD string is another goal of this work.



NEUTRINO 2006



# Galactic Supernovae monitoring at LVD

The LVD collaboration

# Scintillator R&D and construction of a prototype for the Double Chooz experiment

C Buck<sup>1</sup>, A di Vacri<sup>2</sup>, G Mention<sup>3</sup> and D Motta<sup>3</sup>

<sup>1</sup>Max Planck Institut für Kernphysik (MPIK), Heidelberg – Germany

<sup>2</sup>Laboratori Nazionali del Gran Sasso (LNGS), Assergi – Italy

<sup>3</sup>Commissariat à l'Énergie Atomique (CEA), Saclay – France

E-mail: christian.buck@mpi-hd.mpg.de, assunta.divacri@lngs.infn.it,  
guillaume.mention@cea.fr and dario.motta@cea.fr

Double Chooz is the next generation reactor neutrino experiment dedicated to the search for the  $\theta_{13}$  neutrino mixing angle. It will be based on the comparison of two identical detectors, one near ( $\sim 250$ – $300$  m) and one far (1,051 m), to improve the sensitivity to the oscillation amplitude  $\sin^2(2\theta_{13})$  of nearly an order of magnitude with respect to the current best limit.

A H-rich liquid scintillator is used as target, and Gd is dissolved to 1 g/L in order to enhance the delayed neutron capture associated with the electronic anti-neutrino charged current interaction. Past reactor experiments have produced Gd-doped scintillators showing relatively fast degradation of transparency. In Double Chooz, the long-term stability of the target scintillator is of fundamental importance, both to assure a sufficiently long running time (several years) and to avoid systematics due to a possible different evolution of the liquids in the two detectors.

Gd-loaded scintillators are being produced since 2003 within the Double Chooz collaboration. Two families of chemical formulations have been developed to dissolve Gd in the organic scintillator base. One is based on carboxylic acids as ligand, the other on the chemistry of metal beta-diketonates. The chemical parameters controlling the long term stability of these systems are now well understood and both formulations have shown to be sound for Double Chooz.

An experimental program is being carried out to assess, through optical monitoring of the liquids, the long term stability of the scintillators under experimental conditions as close as possible to those of the real experiment. As a part of this program, a 1/5<sup>th</sup>-scaled mechanical replica of the Double Chooz detector was built at Saclay. The target volume, delimited by an acrylic vessel, was filled with 110 L of a Gd-doped scintillator. Similar tests in 30 L acrylic vessels allow the parallel validation of the other scintillator formulations. Validation procedures sharing the same technology are being developed to certify all the materials which could be in contact with the Gd-doped scintillator.

## References

- [1] F Ardellier *et al.*, proposal, “Double Chooz: A search for the Neutrino Mixing Angle  $\theta_{13}$ ”, hep-ex/0606025.
- [2] C Buck, F X Hartmann, D Motta, S Schönert, U Schwan, “Metal beta-diketonate scintillators”, Presentation at the Workshop on Future Low Energy Neutrino Experiments, TU Munich, Munich, 9-11 October (2003).

# Lorentz violation and neutrino oscillations

**Matthew Mewes**

Marquette University, P.O. Box 1881, Milwaukee, WI 53201

**Abstract.** Lorentz violation naturally leads to neutrino oscillations and provides an alternative mechanism that may explain current data. This contribution to the proceedings of The XXII International Conference on Neutrino Physics and Astrophysics provides a brief review of possible signals of Lorentz violation in neutrino-oscillation experiments.

General violations of Lorentz invariance are described by a theoretical framework known as the Standard-Model Extension (SME) [1, 2, 3]. This program has revealed many observable consequences and led to numerous high-precision tests of this fundamental symmetry. One prediction in the neutrino sector is oscillations caused by Lorentz violations rather than neutrino mass. This alternative mechanism results in experimental signatures that distinguish it from the more conventional explanation and lead to potential tests of Lorentz invariance using neutrino-oscillation data. The resulting sensitivities rival the most precise tests in any system. Here we highlight some of the key results of the detailed discussion given in Ref. [4].

One potential signal of Lorentz violation in neutrinos is oscillations with unusual energy dependences. Normally, oscillation lengths are inversely proportional to energy, so the wavelength of neutrino oscillations shrink with an increase in energy. In contrast, Lorentz violation can cause oscillation lengths that remain constant or grow with energy. This can lead to *spectral anomalies* or distortions in the expected energy spectrum.

Anisotropies are another important possibility that arises from a breakdown of rotational symmetry. These can cause direction-dependent oscillations and can have profound consequences. For example, in terrestrial experiments, direction-dependent oscillations can lead to sidereal variations in the observed fluxes as oscillation probabilities fluctuate due to a change in propagation direction resulting from the rotation of the Earth.

Two strategies have been proposed for searches for Lorentz violation. The first involves looking for model-independent features in the oscillation data that can only occur if Lorentz symmetry is violated. The other strategy involves comparing data with simple candidate test models. Several models have been proposed that roughly reproduced current observations, some of which may help resolve the LSND anomaly [5, 6, 7, 8]. In either approach, extreme sensitivities are expected from current and future neutrino-oscillation experiments.

[1] Colladay D and Kostelecký V A 1997 *Phys. Rev. D* **55** 6760

[2] Colladay D and Kostelecký V A 1998 *Phys. Rev. D* **58** 116002

[3] Kostelecký V A 2004 *Phys. Rev. D* **69** 105009

[4] Kostelecký V A and Mewes M 2004 *Phys. Rev. D* **69** 016005

[5] Kostelecký V A and Mewes M 2004 *Phys. Rev. D* **70** 031902

[6] Kostelecký V A and Mewes M 2004 *Phys. Rev. D* **70** 076002

[7] Auerbach L B *et al.* 2005 *Phys. Rev. D* **72** 076004

[8] Katori T, Kostelecký V A and Tayloe R 2006 Global three-parameter model for neutrino oscillations using

Lorentz violation, *Preprint*, hep-ph/0606154

# Search for the Neutron Disappearance using the KamLAND Detector

**Tatjana Miletic for the KamLAND Collaboration**

Drexel University, Philadelphia

tanya@drexel.edu

**Abstract.** Data from the Kamioka Liquid scintillator Anti-Neutrino Detector (KamLAND) have been analyzed to search for the signature of neutrons disappearing to invisible channels. Improved limits have recently been set by KamLAND on these nucleon decay lifetimes. This poster presented the data analysis that resulted in these limits, as well as the ongoing research that aims to improve the calibrations and efficiency estimates for further nucleon decay searches with KamLAND.

## 1. Data Analysis and Results

Invisible decay modes of neutrons are detectable with KamLAND, although no energetic charged particles are produced directly in the decay for single neutron and two neutron intra-nuclear disappearance that would produce holes in the s-shell energy level of  $^{12}\text{C}$ . The de-excitation of the corresponding daughter nucleus results in a sequence of space and time correlated events observable in the liquid scintillator detector. We report on new limits for one and two-neutron disappearance:  $\tau(n \rightarrow inv) > 5.8 \times 10^{29}$  years and  $\tau(nn \rightarrow inv) > 1.4 \times 10^{30}$  years at 90% CL. These results represent an improvement factors of  $\sim 3$  and  $> 10^4$  over previous experiments.

## 2. Ongoing Efforts to Improve the Results

Detector purification is under way for the low background phase of KamLAND. Removing  $^{85}\text{Kr}$ ,  $^{40}\text{K}$ ,  $^{210}\text{Pb}$ ,  $^{210}\text{Bi}$ ,  $^{210}\text{Po}$ ,  $^{222}\text{Rn}$  from the scintillator will allow the data taking threshold to be reduced to give KamLAND the capability of detecting  $^7\text{Be}$  solar neutrinos. Reduced backgrounds will also allow the improvement of the current KamLAND result for  $\Delta m_{12}^2$ , geo-antineutrino flux and improve detection efficiency for some neutron decay modes. A new measurement of scintillation quenching of protons in KamLAND is available which will reduce the systematic error. More data from recent runs is available.

## References

- [1] Search for the invisible decay of neutrons with KamLAND, Phys. Rev. Lett. 96, 101802 (2006)

# Borexino

**Lino Miramonti *on behalf of the Borexino Collaboration***

Department of Physics of University of Milano and INFN, via Celoria 16, I 20133 Milano, Italia

E-mail: [lino.miramonti@mi.infn.it](mailto:lino.miramonti@mi.infn.it)

**Abstract.** Borexino is a massive calorimetric liquid scintillation detector whose installation has been completed in the underground Gran Sasso Laboratory. The focus of the experiment is on the direct and real time measurement of the flux of neutrinos produced in the  ${}^7\text{Be}$  electron capture reaction in the Sun. Furthermore, recent studies about the reduction of the  ${}^{11}\text{C}$  background through suitable rejection techniques demonstrated the possibility to open an interesting additional observation window in the energy region of the pep and CNO solar neutrinos. Beyond the solar neutrino program, the detector will be also a powerful observatory for antineutrinos from Supernovae, as well as for geoneutrinos, profiting from a very low background from nuclear reactors.

## 1. Goals

The Borexino main goal is to detect neutrinos from the Sun via the scattering process  $e^- \nu_x \rightarrow e^- \nu_x$ . The neutrino signature is given by the scintillation light produced as the recoil electron deposits its energy in the medium. The detector is designed to work with a very low energy threshold (250 keV), thus providing important information on the low energy portion of the solar neutrino spectrum. Recent studies proved the capability to reduce the  ${}^{11}\text{C}$  background through suitable rejection techniques and demonstrated the possibility to exploit the energy region of the pep and CNO solar neutrinos.

Borexino will also be able to observe antineutrinos coming from Supernovae and from the Earth (geoneutrinos); the detector is far away from nuclear reactors, which represent the most important background to electron antineutrino detection.

## 2. Status

The installation of the detector has been completed in July 2004. Several campaigns of data-taking with the empty detector have been performed in order to check the overall performance of the apparatus, DAQ, electronics and software. Some runs were performed inserting a radioactive source into the detector (i.e. a vial containing liquid scintillator loaded with Rn) to check the light collection efficiency of the detector and to test the position reconstruction algorithm. Currently (September 2006) the detector is being filled with ultra pure water and the filling with pseudocumene is foreseen starting from the end of this year. Borexino will be ready to take data by the spring of 2007.

[1] Alimonti G et al. 2002 *Astroparticle Physics B* **16** 205

[2] Borexino Web site: <http://borex.lngs.infn.it/>

# The XENON dark matter experiment: status of the XENON10 phase

**Maria Elena Monzani (on behalf of the XENON collaboration)**

Columbia Astrophysics Laboratory, Columbia University, New York, NY 10027

monzani@astro.columbia.edu

**Abstract.** The XENON experiment searches for Weakly Interacting Massive Particles (WIMPs) with liquid Xenon as the active target. The proposed XENON1T detector is designed to achieve a sensitivity more than a factor of thousand beyond current limits. The collaboration is now testing the 10 kg target: the XENON10 detector was recently installed at the Gran Sasso Underground Laboratory and the first phase of data taking is underway.

## 1. The XENON experiment

The purpose of XENON experiment is the direct detection of Weakly Interacting Massive Particles (WIMPs), populating the halo of our galaxy. The detector is designed to observe the small energy released by a WIMP when scattering off a Xe nucleus [1]. It features a time projection chamber operated in dual (liquid/gas) phase, optimized to simultaneously detect the primary scintillation in the liquid and the ionization signal (through secondary scintillation in the gas) produced by low energy recoils down to 16 keV.

The discrimination of signal and background is based on the distinct ratio of the ionization and scintillation signals produced by nuclear (from WIMPs and neutrons) and electron (from gamma, beta and alpha backgrounds) recoil events [2]. The background will be additionally suppressed by passive gamma and neutron shields and by the detector's 3-D position sensitivity.

## 2. Status of the project

Using a target mass of 1 ton distributed in 10 identical modules, the proposed XENON1T will achieve a sensitivity of  $10^{-46}$  cm<sup>2</sup> for spin-independent cross-sections, which is several orders of magnitude below the current best limit of  $1.6 \times 10^{-43}$  cm<sup>2</sup> [3]. A phased program is currently testing the 10 kg target (XENON10); this stage will be followed by a 100 kg (XENON100) module [1].

The XENON10 detector was assembled and preliminarily tested at Columbia University in January 2006. It was shipped to the Gran Sasso National Laboratory in Italy in March, where it was installed and tested in a temporary location in the underground lab. In July, the detector was moved in its final location in a shielded environment: the first XENON Dark Matter Search run is currently underway.

## References

- [1] XENON: A Liquid Xenon Experiment for Dark Matter. Submitted to NSF, Particle and Nuclear Astrophysics, Proposal 0201740 (September 2001).
- [2] M. Yamashita et al., *Astropart. Phys.* 20 (2003) 79.
- [3] D.S. Akerib et al. (CDMS Collaboration), *Phys. Rev. Lett.* 96 (2006) 011302.

## The T2KLAr: a liquid Ar TPC for the T2K experiment

Maria Elena Monzani<sup>1</sup> and Anselmo Meregaglia<sup>2</sup>

<sup>1</sup> Columbia Astrophysics Laboratory, Columbia University, New York, NY 10027

<sup>2</sup> Institute for Particle Physics, ETH Hönggerberg, CH-8093 Zürich, SWITZERLAND

monzani@astro.columbia.edu

**Abstract.** The T2K experiment is a second generation neutrino oscillation experiment using the existing Super-Kamiokande experiment as the main detector. The presence of a LAr detector located in the 2km site would enhance the performances of the T2K experiment, improving its ultimate sensitivity on  $\theta_{13}$ .

### 1. The T2K neutrino oscillation experiment

The primary aim of the T2K experiment is to improve our knowledge of neutrino oscillation parameters like  $\sin^2\theta_{23}$ ,  $\delta m^2_{23}$  and  $\sin^2\theta_{13}$ . This will be done using the high-intensity 50GeV proton beam (delivered by the new Japanese nuclear physics facility being built at Tokai) to generate an intense muon neutrino beam aiming approximately at the Super-Kamiokande site (a slightly off-axis geometry is used to produce a more monochromatic beam) [1].

A detector site 2km from the neutrino production point of the experiment was proposed, to measure the neutrino flux seen at Super-K with very high precision. This flux will be observed by a 1 kton water Cherenkov detector optimized to match Super-K resolution, and with a 100 ton liquid argon time projection chamber, which will provide fine grain imaging and low particle detection thresholds for a precise study of neutrino interactions at the relevant energies [2].

### 2. The 2km Liquid Ar detector

The presence of a 2km LAr detector would be an important asset for the T2K experiment, especially for its role in reducing the systematics enhancing the ultimate sensitivity on  $\theta_{13}$ . Thanks to the detector capability of measuring the different components of the background separately, a LAr TPC would play an important part also during the first phase of the experiment, when the sensitivity on  $\theta_{13}$  will be dominated by statistics [3]. The large sample of neutrino interactions in the GeV region would provide crucial information for the study of different type of reactions and of nuclear effects, whereas the inner target would give a direct measurement of the cross sections ratio between Water and Argon. Such a detector would also be an important milestone for the LAr TPC technique providing an extremely valuable experience for future large LAr detectors.

### References

- [1] K. Kaneyuki et al. (T2K Collaboration), Nucl.Phys.Proc.Suppl.145 (2005), 178
- [2] A. Ereditato and A. Rubbia, Nucl.Phys.Proc.Suppl.139 (2005), 301
- [3] A. Meregaglia, Nucl.Phys.Proc.Suppl.155 (2006), 248



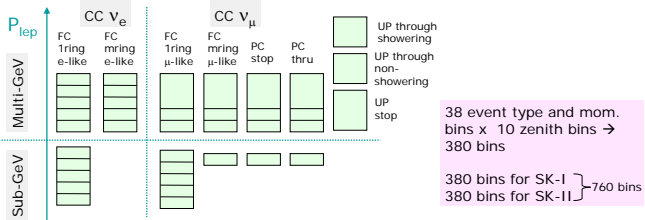
# Oscillation Analysis with and without Solar Term Using Super-K-I and Super-K-II Atmospheric Neutrino data

S. Moriyama on behalf of the Super-Kamiokande Collaboration  
Kamioka Observatory, Institute for Cosmic Ray Research, University of Tokyo, Japan



# 1. Two flavor oscillation analysis

## ◆ Binning and systematic errors for the zenith angle fit



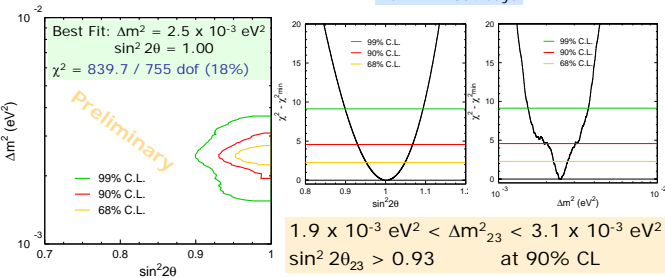
Since various detector related systematic errors are different, we do not combine the SK-I and SK-II bins.

neutrino flux (14) } Identical for SK-I and SK-II  
 neutrino interaction (12) }  
 solar activity (1) } Regarded as independent between SK-I and SK-II  
 event selection and reconstruction (21) }

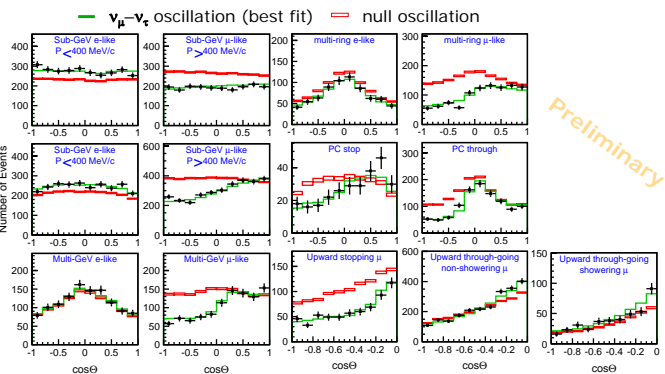
The total number of systematic errors is : Flux (14) + Interaction (12) + SK-I (22) + SK-II (22) = 70

## ◆ Results from SK-I + SK-II data

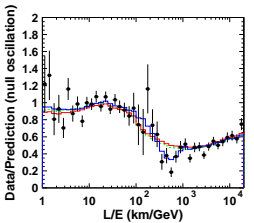
Data sets  
 SK-I : 1489 days  
 SK-II : 804 days



$1.9 \times 10^{-3} \text{ eV}^2 < \Delta m_{23}^2 < 3.1 \times 10^{-3} \text{ eV}^2$   
 $\sin^2 2\theta_{23} > 0.93$  at 90% CL



## ◆ Results from L/E analysis (flight length/neutrino energy)

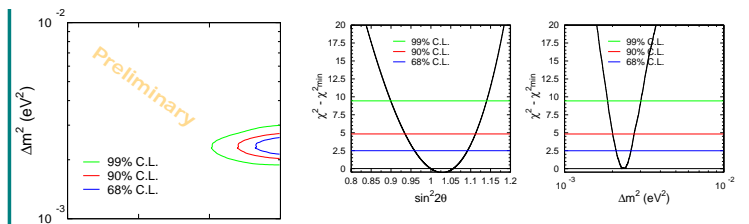


$\nu_\mu$  disappearance probability as a function of neutrino flight length L over neutrino energy E.

A dip in the L/E distribution was observed in the data as predicted from the sinusoidal flavor transition probability of neutrino oscillation.

For neutrino oscillations, the best fit parameters are  
 $\Delta m_{23}^2 = 2.3 \times 10^{-3} \text{ eV}^2$  ( $2.0 \times 10^{-3} < \Delta m^2 / \text{eV}^2 < 2.8 \times 10^{-3}$  at 90% C.L.)  
 $\sin^2 2\theta_{23} = 1.00$  ( $\sin^2 2\theta_{23} > 0.93$  at 90% C.L.)  
 $\chi^2_{\text{min}} = 83.9/83 \text{ d.o.f.}$  ( $\sin^2 2\theta_{23} = 1.03, \chi^2_{\text{min}} = 83.4/83 \text{ d.o.f.}$ )

— Oscillation  $\chi^2_{\text{osc}} = 83.9/83 \text{ d.o.f.}$   
 — Decay  $\chi^2_{\text{dec}} = 107.1/83 \text{ d.o.f.}, \Delta\chi^2 = 23.2(4.8)$   
 — Decoherence  $\chi^2_{\text{dec}} = 112.5/83 \text{ d.o.f.}, \Delta\chi^2 = 27.6(5.3)$



$\nu_\mu \leftrightarrow \nu_\tau$  2 flavor oscillation with full mixing is consistent with data

# 2. Analysis with solar term

## ◆ Sub-dominant oscillations driven by $\Delta m_{12}^2$

According to the LMA-MSW oscillation parameters obtained by solar  $\nu$  experiments and KamLAND, the oscillation of **low energy atmospheric electron neutrinos** might be observable even if  $\sin^2 \theta_{13} = 0$ .

## ◆ Oscillation effects on e-like events

$P_2$  :  $2\nu$  transition prob.  $\nu_e \rightarrow \nu_{\mu,\tau}$  in matter driven by  $\Delta m_{12}^2$

$$P(\nu_e \rightarrow \nu_e) = 1 - P_2$$

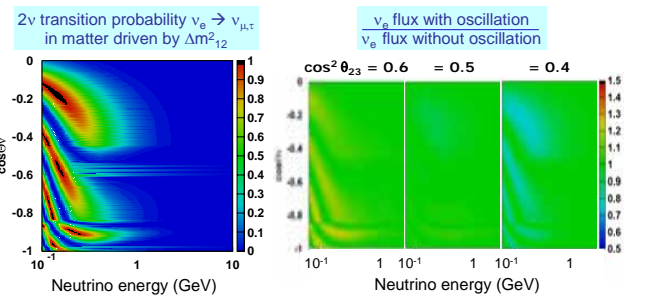
$$P(\nu_e \rightarrow \nu_\mu) = P(\nu_\mu \rightarrow \nu_e) = \cos^2 \theta_{23} P_2$$

$$P(\nu_e \rightarrow \nu_\tau) = P(\nu_\tau \rightarrow \nu_e) = \sin^2 \theta_{23} P_2$$

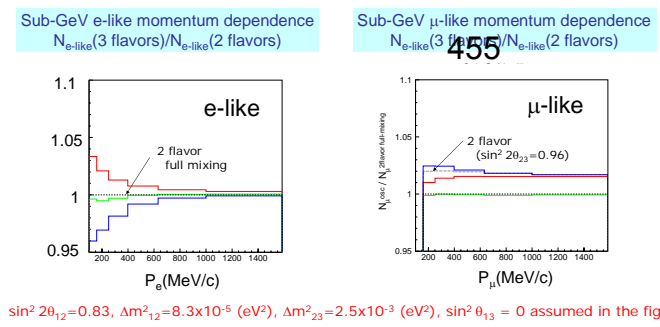
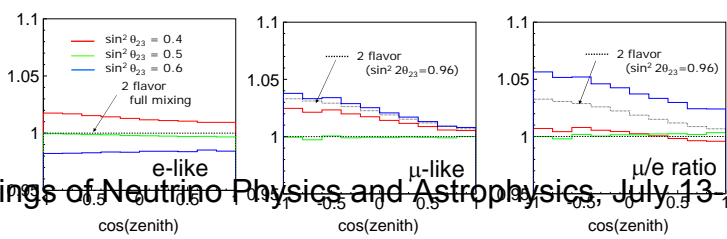
$$P_2 = r P(\nu_e \rightarrow \nu_e) = r \cos^2 \theta_{23} P_2$$

$$r = (\nu_\mu \text{ flux}) / (\nu_e \text{ flux}) \sim 2 \text{ at low energy}$$

$\cos^2 \theta_{23} = 0.5$  ( $\theta_{23} = 45 \text{ deg.}$ ) :  $\nu_e$  increase ~ decrease  
 $\cos^2 \theta_{23} > 0.5$  ( $\theta_{23} < 45 \text{ deg.}$ ) :  $\nu_e$  increase > decrease  
 $\cos^2 \theta_{23} < 0.5$  ( $\theta_{23} > 45 \text{ deg.}$ ) :  $\nu_e$  increase < decrease



Sub-GeV e-like zenith angle  $N_{e\text{-like}}(3 \text{ flavors})/N_{e\text{-like}}(2 \text{ flavors})$   
 Sub-GeV  $\mu$ -like zenith angle  $N_{\mu\text{-like}}(3 \text{ flavors})/N_{\mu\text{-like}}(2 \text{ flavors})$   
 Sub-GeV  $\mu/e$  ratio zenith angle  $N_{\mu\text{-like}}(3 \text{ flavors})/N_{e\text{-like}}(3 \text{ flavors})$   
 $N_{\mu\text{-like}}(2 \text{ flavors})/N_{e\text{-like}}(2 \text{ flavors})$



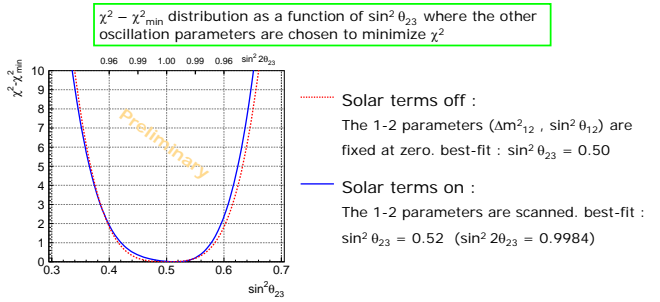
Discrimination between  $\theta_{23} < \pi/4$  and  $> \pi/4$  might be possible by studying low energy atmospheric  $\nu_e$  and  $\nu_\mu$  events.

## ◆ Oscillation analysis with $\sin^2 \theta_{12}$ and $\Delta m_{12}^2$

Oscillation maps :  
 $\Delta m_{12}^2 = 10^{-4.16} \sim 10^{-4.04} \text{ eV}^2$  (5 points)  
 $\sin^2 \theta_{12} = 0.22 \sim 0.40$  (7 points)  
 $\sin^2 \theta_{13} = 0$  (fixed)  
 $\Delta m_{23}^2 = 10^{-3} \sim 10^{-2.2} \text{ eV}^2$  (41 points)  
 $\sin^2 \theta_{23} = 0.3 \sim 0.7$  (41 points)  
 4 dimensional analysis

Calculate the minimum  $\chi^2$  : projection to the  $\sin^2 \theta_{23}$  axis, Deviation from the full mixing ?  
 Treatment of solar term contribution from solar neutrino and KamLAND exp.  
 Add  $\chi^2_{\text{solar } \nu}$  + KamLAND to  $\chi^2_{\text{atmospheric}}$  for each  $(\Delta m_{12}^2, \sin^2 \theta_{12})$  point

## ◆ Effect of the solar terms on determination of $\sin^2 \theta_{23}$



No significant evidence for the deviation from  $\sin^2 2\theta_{23} = 1$

# 3. Conclusions

## ◆ Atmospheric neutrino oscillation analysis without solar terms

Atmospheric neutrino data of SK-I and SK-II are well explained with  $\nu_\mu \leftrightarrow \nu_\tau$  2 flavor oscillations. The oscillation parameters were determined as  $1.9 \times 10^{-3} \text{ eV}^2 < \Delta m_{23}^2 < 3.1 \times 10^{-3} \text{ eV}^2$  and  $\sin^2 2\theta_{23} > 0.93$  at 90% C.L.

## ◆ $\nu_\mu$ disappearance probability as a function of L/E

A dip in the L/E distribution was observed in the data as predicted from the neutrino oscillations. Some other models were disfavored. The oscillation parameters were determined as  $2.0 \times 10^{-3} \text{ eV}^2 < \Delta m_{23}^2 < 2.8 \times 10^{-3} \text{ eV}^2$  and  $\sin^2 2\theta_{23} > 0.93$  at 90% C.L.

## ◆ Effect of the solar terms on determination of $\sin^2 \theta_{23}$

The effect of sub-dominant oscillations driven by  $\Delta m_{12}^2$  was examined with the atmospheric neutrino data. The result gives no significant evidence for the deviation of  $\sin^2 \theta_{23}$  from the maximal mixing.

## The Double Chooz simulation strategy

Dario Motta<sup>1</sup>, Anatael Cabrera<sup>2</sup>

<sup>1</sup> DAPNIA/SPP, CEA/Saclay, 91191 Gif-sur-Yvette CEDEX, France

<sup>2</sup> APC, Collge de France, 11 place Marcelin Berthelot, 75231 PARIS CEDEX 05, France

E-mail: dario.motta@cea.fr, anatael@in2p3.fr

The Double Chooz experiment (DC hereafter) aims to search for a non-vanishing PMNS  $\theta_{13}$  neutrino oscillation parameter from precise comparison of  $\bar{\nu}_e$  fluxes and spectra measured by two identical detectors at different distances from the Chooz reactors (France). Details in [1, 2].

The design of the DC experiment has been based on detailed simulation studies aimed at optimizing the detector performance, while reducing the systematics and backgrounds. Details of all sub-systems and of the calibration devices are now being worked out with the aid of simulations to assess the accuracy within which the two detectors need to be identical.

The DC Monte Carlo simulation is based on GLG4sim [3], a public simulation package built on Geant4 (G4) [4]. Major extensions have been developed to implement a detailed micro-physical optical model of both scintillators and photomultiplier tubes (PMTs) [1]. This model accounts for the details of light production, wavelength-shift, absorption, reflection and refraction at all interfaces, including PMTs. The model is used to predict the intrinsic detector response, investigate the impact of detector-to-detector variations, set the calibration strategy, optimize the scintillator formulation and study possible aging scenarios. A full read-out system simulation converts the photon-hits into digitized signals, including charge and time smearing. The simulated DC signals can then be reconstructed like real data. The reconstruction algorithm uses the signals from all PMTs to maximize a charge and time likelihood function.

Understanding the response to neutrons is critical in DC, hence a new model has been developed to improve the G4 description of the radiative emission upon n-capture by Gd [1].

Substantial efforts have been devoted to the simulation of backgrounds, in particular the  $\mu$ -induced ones. For the latter, an accurate  $(E, \theta, \phi)$  resolved  $\mu$  flux at far and near site (overburden of 300 and 80 mwe respectively) has been calculated [5, 6]. The generated fluxes are used to predict the  $\mu$ -induced fast neutron background; the production of long-lived,  $(\beta/n)$ -decaying nuclei ( ${}^9\text{Li}$ ,  ${}^8\text{He}$ ) by showering muons; the Bremsstrahlung gammas from  $\delta$ /knock-on  $e^-$  by near-miss muons. These studies are combined with the Monte Carlo of the inner and outer veto systems to evaluate their performance and hence optimize the design with respect to the  $\mu$  detection efficiency and background rejection.

### References

- [1] Ardellier F, et al, 2006, Double Chooz: a search for the neutrino mixing angle  $\theta_{13}$  *Preprint* hep-ex/0606025
- [2] Reyna D, these proceedings
- [3] Horton-Smith G, <http://neutrino.phys.ksu.edu/~GLG4sim/>
- [4] Agostinelli S, et al., *Nucl. Instr. Meth. A* **506** (2003), 250
- [5] Tang A, Horton-Smith G, Kudryavtsev V A and Tonazzo A, these proceedings, (*Preprint* hep-ph/0604078)
- [6] Reyna D. 2006 *Preprint* hep-ph/0604145

## Dark Matter Detection with Bubble Chambers

**E.Behnke<sup>1</sup>, J.I.Collar<sup>2</sup>, P.S.Cooper<sup>3</sup>, K.Crum<sup>2</sup>, M.Crisler<sup>3</sup>, M.Hu<sup>3</sup>,  
I.Levine<sup>1</sup>, S.Mishra<sup>2</sup>, D.Nakazawa<sup>2</sup>, B.Odom<sup>2</sup>, E.Ramberg<sup>3</sup>,  
J.Rasmussen<sup>2</sup>, N.Riley<sup>2</sup>, A.Sonnenschein<sup>3</sup>, M.Szydaxis<sup>2</sup>,  
R. Tschirhart<sup>3</sup> and N.Vander Werf<sup>1</sup>**

<sup>1</sup>Department of Physics and Astronomy, Indiana University South Bend, South Bend, IN 46634, USA

<sup>2</sup>Department of Physics, Enrico Fermi Institute and Kavli Institute for Cosmological Physics, University of Chicago, Chicago, IL 60637, USA

<sup>3</sup>Fermi National Accelerator Laboratory, Batavia, IL 60510, USA

(COUPP Collaboration)

COUPP[1] (Chicagoland Observatory for Underground Particle Physics) uses stable room-temperature bubble chambers to search for Weakly Interacting Massive Particles (WIMPs) which might compose a significant fraction of the galactic dark matter. The superheated refrigerant used,  $\text{CF}_3\text{I}$ , is a fire-extinguishing agent and an optimal target for both spin-dependent and spin-independent WIMP couplings. At the moderate degrees of superheat necessary to detect low-energy nuclear recoils such as those expected from WIMPs, this fluid exhibits a measured intrinsic rejection of minimum-ionizing backgrounds better than  $10^{10}$ . The metastable superheated state is, however, sensitive to alpha-recoils. This leads to the requirement to reach ultra-trace levels of alpha-emitters within the active volume of the chambers. The eventual goal is to match the radio-purity in alpha-emitters of modern large neutrino detectors.

COUPP presently operates a 2 kg chamber at the 300 m.w.e. depth of the Fermilab neutrino tunnel. Information has been obtained on the presence and control of radon-induced backgrounds. More than 250 kg-days of exposure has been collected. A very competitive sensitivity to spin-dependent couplings can be extracted, even in the presence of identifiable backgrounds. Measures against these backgrounds are currently being implemented. Calibrations of the device with gamma and neutron sources have been performed.

The short-term goals for COUPP are to reduce the alpha-recoil backgrounds in the 2kg chamber to a level of less than one event per kg per day, and to apply the upgrades tested on it to larger chambers currently under construction. A pion beam calibration able to separate the response to iodine and fluorine recoils is planned using a dedicated chamber. With the addition of a muon veto, presently being commissioned, it is in principle possible to reach improved sensitivities to both WIMP couplings in the present Fermilab location. The collaboration is constructing larger devices, totaling up to 80 kg of  $\text{CF}_3\text{I}$ . Devices of this mass will be able to exploit a number of signatures characteristic of WIMP-induced recoils, leading to a diminished sensitivity to alpha and neutron recoils and to a much improved WIMP sensitivity. Long-term plans involve the deep-underground installation of a target mass of order one ton, using a number of different refrigerant targets enclosed in suitable hydrogenated shielding and leading to an exhaustive exploration of supersymmetric WIMP models.

[1] <http://www-coupp.fnal.gov/>

## Thermal neutrinos from pre-supernova

A. Odrzywolek<sup>1</sup>, M. Miaszerek<sup>1</sup>, M. Kutschera<sup>1,2</sup>

<sup>1</sup> M. Smoluchowski Institute of Physics, Jagiellonian University, Reymonta 4, Cracov, Poland

<sup>2</sup> H. Niewodniczanski Institute of Nuclear Physics, PAS, Radzikowskiego 152, Cracov, Poland

E-mail: odrzywolek@th.if.uj.edu.pl

**Abstract.** We would like to discuss prospects for neutrino observations of the core-collapse supernova progenitor during neutrino-cooled stage. We will present new theoretical results on thermal neutrino and antineutrino spectra produced deep inside the pre-supernova core. Three competing processes: pair-, photo and plasma-neutrino production, are taken into account. The results will be used to estimate signal in existing and future neutrino detectors. Chance for supernova prediction is estimated, with possible aid to core-collapse neutrino and gravitational wave detectors in the form of early warning.

In our short contribution we would like to answer some comments and questions asked during poster session [1]. Two days of the silicon burning with  $\langle L_\nu \rangle = 3 \times 10^{45}$  erg/s quoted in [2] was randomly chosen typical example model [3]. Duration of the Si burning depends on evolutionary track of the massive star, particularly mass of the Si core at the onset of the ignition. Total average neutrino luminosity  $\langle L_\nu \rangle$  depends on (1) the burning time  $\tau_{\text{Si}}$  and (2) amount of fuel (Si core mass  $M_{\text{Si}} \simeq M_{\text{Fe}}$ ):

$$\langle L_\nu \rangle = M_{\text{Fe}} \Delta E_b / \tau_{\text{Si}}. \quad (1)$$

$\Delta E_b$  is the nuclear binding energy difference between fuel ("Si") and ash ("Fe"). From evolutionary calculations of [4] we get core mass in the range 1.2 ... 1.65  $M_\odot$  and  $\tau_{\text{Si}}$  from 18 days to 17 hours, respectively. Therefore  $\langle L_\nu \rangle$  vary from  $3.1 \times 10^{44}$  to  $9.8 \times 10^{45}$  erg/s.

Electron antineutrinos from pair-annihilation are of particular interest [5]. One can quickly estimate fraction of given flavor from the following: (1) reaction rate is proportional to squared matrix element  $M^2 \sim 8G_F^2(C_V^2 + C_A^2)$ , where mass term was dropped (2) number of emitted neutrinos and antineutrinos is equal. Therefore, rate of the reaction rates is  $R_e/R_{\mu,\tau} \simeq (C_V^e)^2 + (C_A^e)^2 / (C_V^{\mu,\tau})^2 + (C_A^{\mu,\tau})^2 = 4.5$ . Total neutrino flux is:  $F_{\text{tot}} = 2R_e + 4R_{\mu,\tau} = (2 + 4/4.5)R_e = 2.9R_e$ . Finally  $F_{\bar{\nu}_e}/F_{\text{tot}} \simeq 0.35 \sim 1/3$ , i.e. about one third is emitted as electron antineutrinos. This statement may be altered by the neutrino oscillations.

### Acknowledgments

Supported by grant of Polish Ministry of Science and Higher Education No. 1 P03D 005 28.

### References

- [1] <http://ribes.if.uj.edu.pl/poster/PosterA0.pdf>
- [2] Odrzywolek A, Miaszerek M, Kutschera M 2004 *Astropart. Phys.* **21** 303-313
- [3] Weaver T A, Zimmerman G B, Woosley S E, 1978, *ApJ* **225** 1021
- [4] Woosley S E, Heger A, Weaver T A 2002 *Rev. Mod. Phys.* **74** 1015
- [5] Beacom J F, Vagins M R 2004 *PRL* **93** 171101

# Neutrinos from WIMP annihilations in the Sun including neutrino oscillations

Mattias Blennow<sup>1</sup>, Joakim Edsjö<sup>2</sup> and Tommy Ohlsson<sup>1</sup>

<sup>1</sup> Department of Theoretical Physics, School of Engineering Sciences, Royal Institute of Technology (KTH) – AlbaNova University Center, SE-106 91 Stockholm, Sweden

<sup>2</sup> Department of Physics, Stockholm University – AlbaNova University Center, SE-106 91 Stockholm, Sweden

E-mail: emb@kth.se, edsjo@physto.se, tommy@theophys.kth.se

**Abstract.** The prospects to detect neutrinos from the Sun arising from dark matter annihilations in the core of the Sun are reviewed. Emphasis is placed on new work investigating the effects of neutrino oscillations on the expected neutrino fluxes.

## 1. WIMP capture and annihilation in the Sun

Weakly Interacting Massive Particles (WIMPs) in the Milky Way halo can scatter in the Sun and be gravitationally bound to it. Eventually, they will scatter again and sink to the core of the Sun. In the core, WIMPs will accumulate and can annihilate and produce neutrinos.

## 2. Neutrino interactions

On the way out of the Sun, neutrinos can participate in both charged- and neutral-current interactions. Neutral-currents degrade the energy of the neutrinos, whereas charged-currents give a charged lepton. Electrons and muons are stopped before they can give neutrinos, which means that electron and muon neutrinos are lost, while tau leptons will decay and produce new neutrinos (regeneration).

Then, what about the spectra beyond the Sun? At the surface of the Sun, some of the neutrinos have interacted, and thus, the flux at high energies is degraded. However, some of these neutrinos reappear at low energies both from neutral-current interactions and tau decays.

## 3. Neutrino oscillations

We use a completely general three-flavor neutrino oscillation scheme (with matter effects included) and a realistic solar model [1]. Thus, at the surface of the Sun, we obtain the fluxes in a general format (including both amplitudes and phases of the neutrino oscillations). Furthermore, in our computations, neutrino oscillations and interactions are treated simultaneously. We have used the following values of standard neutrino oscillation parameters (which are the central values from Ref. [2] with no CP violation in neutrino oscillations and a normal neutrino mass hierarchy):  $\theta_{12} = 33.2^\circ$ ,  $\theta_{13} = 0$ ,  $\theta_{23} = 45.0^\circ$ ,  $\delta = 0$ ,  $\Delta m_{21}^2 = 8.1 \cdot 10^{-5} \text{ eV}^2$ ,  $\Delta m_{31}^2 = 2.2 \cdot 10^{-3} \text{ eV}^2$ .

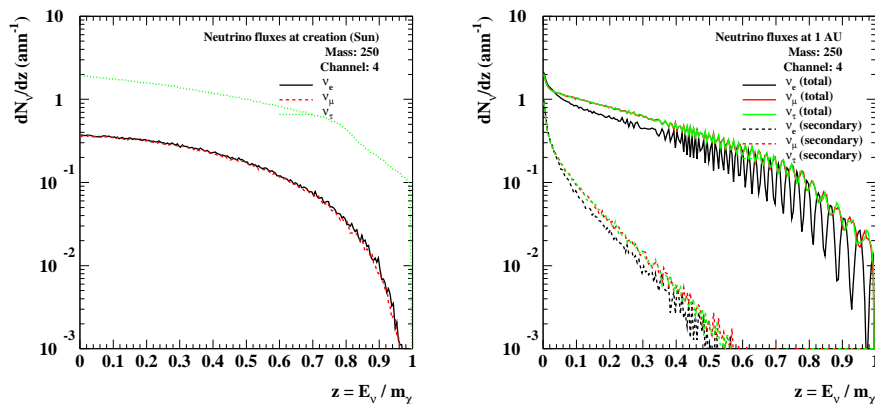


**Figure 1.** *Left:* Initial neutrino fluxes at the center of the Sun. *Right:* Neutrino fluxes at 1 AU.

#### 4. Propagation to and in the Earth

First, for the propagation to the Earth, vacuum neutrino oscillations to the Earth are included in the same three-flavor neutrino setup. In addition, effects of the eccentricity of the Earth's orbit are included. In Fig. 1, we plot the initial neutrino fluxes at the center of the Sun, *i.e.*, at the point of production, as well as we show an example of the propagation of neutrinos from the center of the Sun to the distance of the Earth, *i.e.*, on the distance of 1 AU).

Second, for the propagation in the Earth, matter effects are included in the neutrino oscillations as well. Our simulations are made with a time stamp to include effects of the Earth's distance to the Sun (due to the eccentricity of the orbit) and rotation (affects the distance traversed in the Earth).

#### 5. Summary and conclusions

For typical WIMP masses (*i.e.*,  $10\text{--}10^5$  GeV), neutrino oscillations effectively: 1. average  $\nu_\mu$  and  $\nu_\tau$  on the way out of the Sun, 2. average  $\nu_e$  and  $\nu_\mu/\nu_\tau$  on the way to the Earth, and 3. wash out the remaining oscillation patterns in the spectra due to the eccentricity of the Earth's orbit.

Note that the full scheme described above is implemented as a complete event-based Monte Carlo code. In addition, it should be mentioned that other computations of neutrinos from WIMP annihilations have been performed, such as the study by Cirelli *et al.* [3]. However, their results are not event-based.

#### Acknowledgments

This work was supported by the Royal Swedish Academy of Sciences (KVA) and the Swedish Research Council (Vetenskapsrådet), Contract No. 621-2002-3577, 621-2003-6025, 621-2005-3588.

#### References

- [1] J. N. Bahcall, A. M. Serenelli and S. Basu, "New solar opacities, abundances, helioseismology, and neutrino fluxes," *Astrophys. J.* **621** (2005) L85 [arXiv:astro-ph/0412440].
- [2] M. Maltoni, T. Schwetz, M. A. Tortola and J. W. F. Valle, "Status of global fits to neutrino oscillations," *New J. Phys.* **6** (2004) 122 [arXiv:hep-ph/0405172].
- [3] M. Cirelli, N. Fornengo, T. Montaruli, I. Sokalski, A. Strumia and F. Vissani, "Spectra of neutrinos from dark matter annihilations," *Nucl. Phys. B* **727** (2005) 99 [arXiv:hep-ph/0506298].

# Determining the Low Energy Backgrounds at the Sudbury Neutrino Observatory

H.M. O’Keeffe<sup>1\*</sup>, B. Aharmim<sup>2</sup>, R. Ford<sup>3</sup>, J. Farine<sup>2</sup>, N.A. Jelley<sup>1</sup>,  
J.T.M. Goon<sup>4</sup>, S.R. Seibert<sup>5</sup>, on behalf of the SNO collaboration.

1 University of Oxford, Oxford, UK

2 Laurentian University, Sudbury, Ontario, Canada

3 Sudbury Neutrino Observatory, Lively, Ontario, Canada

4 Louisiana State University, Baton Rouge, USA

5 University of Texas at Austin, Austin, USA

E-mail: \*Corresponding author: h.okeeffe1@physics.ox.ac.uk

**Abstract.** Naturally occurring radioisotopes can produce neutrons by photodisintegration and Cherenkov events via beta/gamma decays. The techniques used to measure the radioisotopes in the heavy water target and light water shield in the third phase of SNO is discussed.

Trace amounts of uranium and thorium present in the SNO detector can produce neutrons via photodisintegration of the deuteron and Cherenkov events from beta/gamma decays. These signals are identical to the observed neutrino interactions. Two independent methods are used to measure the amount of activity present in the detector: *in-situ* analysis of PMT data and *ex-situ* assay techniques.

The *in-situ* analysis of data exploits differences in isotropy and radial distributions to provide a measure of  $^{214}\text{Bi}$  and  $^{208}\text{Tl}$  present in the heavy water target and light water shield of the detector. *Ex-situ* assay techniques extract parent radioisotopes directly from the detector water and the resulting samples are counted using low background counters. Three different types of assay are regularly performed: absorption on Hydrous Titanium Oxide (HTiO), absorption by Manganese Oxide coated beads (MnOx) and radon degassing. HTiO and MnOx principally measure the thorium levels and uranium activity is measured by radon degassing. Recent improvements in these assay techniques have improved the limit of sensitivity to  $^{224}\text{Ra}$  to better than 1 atom per tonne.

Preliminary results for the third phase of SNO have found that all impurities are below target levels in the heavy and light water regions and good agreement between *in-situ* and *ex-situ* techniques has been observed.

# Hadronic Cross Sections for Neutrino Production in

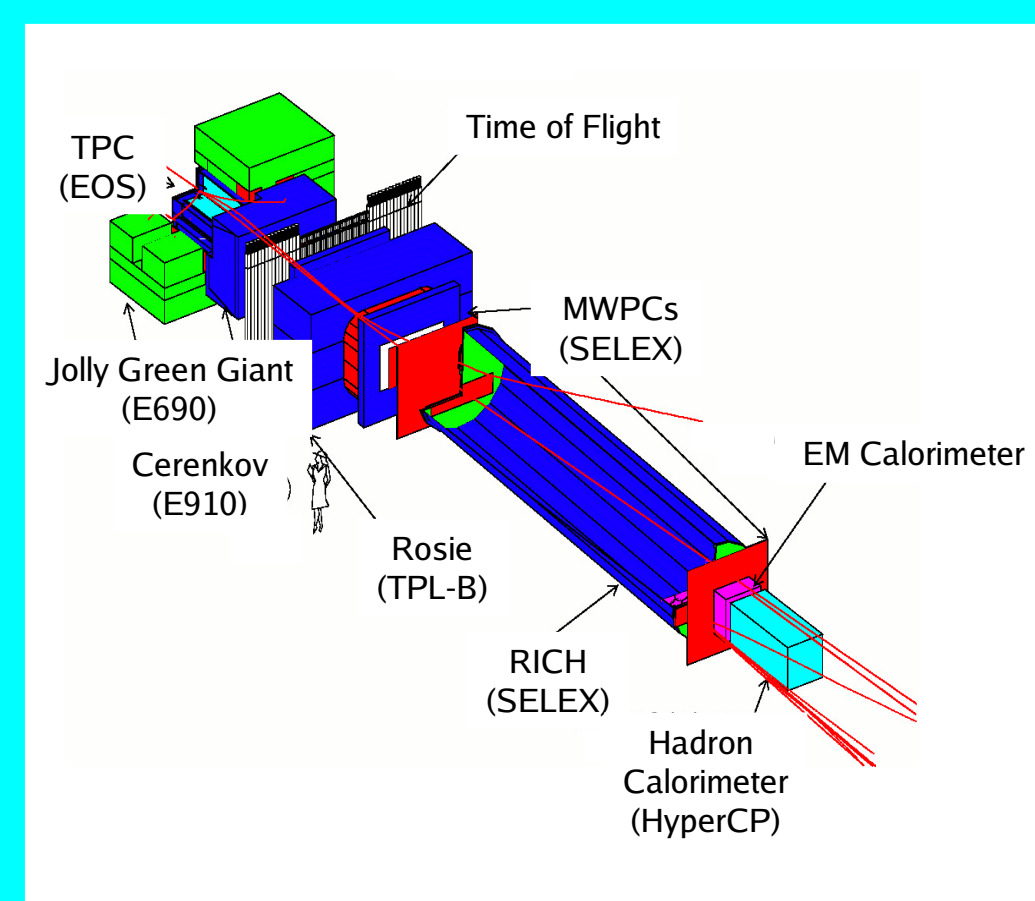
Jonathan M. Paley, Indiana University, for the MIPP Collaboration

# MIPP

R.L. Abrams<sup>9</sup>, U. Akgun<sup>12</sup>, G. Aydin<sup>12</sup>, W. Baker<sup>9</sup>, P.D. Barnes Jr.<sup>7</sup>, T. Bergfeld<sup>13</sup>, A. Bujak<sup>6</sup>, D. Carey<sup>6</sup>, C. Dukes<sup>14</sup>, F. Duna<sup>12</sup>, G. Feldman<sup>7</sup>, Y. Fisyak<sup>1</sup>, N. Graf<sup>6</sup>, A. Godley<sup>13</sup>, Y. Gunaydin<sup>12</sup>, H.R. Gustafson<sup>3</sup>, L. Gutay<sup>6</sup>, E. Hartouni<sup>9</sup>, P. Hanlet<sup>6</sup>, M. Heffner<sup>7</sup>, J. Hlyen<sup>7</sup>, C. Johnstone<sup>2</sup>, D. Kaplan<sup>9</sup>, O. Kamaev<sup>6</sup>, J. Klay<sup>7</sup>, M. Kostin<sup>2</sup>, D. Lange<sup>6</sup>, A. Lebedev<sup>6</sup>, M. Longo<sup>9</sup>, C. Maternick<sup>14</sup>, M. Messier<sup>7</sup>, H. Meyer<sup>6</sup>, D.E. Miller<sup>6</sup>, S.R. Mishra<sup>13</sup>, N. Mokhov<sup>12</sup>, K. Nelson<sup>14</sup>, T. Nigmatov<sup>6</sup>, A. Norman<sup>14</sup>, Y. Onef<sup>12</sup>, J. Paley<sup>7</sup>, A. Para<sup>6</sup>, H.K. Park<sup>6</sup>, A. Penzo<sup>12</sup>, R.J. Peterson<sup>13</sup>, R. Raja<sup>6</sup>, D. Rajaram<sup>6</sup>, C. Rosenfeld<sup>13</sup>, H. Rubini<sup>6</sup>, S. Seun<sup>12</sup>, N. Solomey<sup>7</sup>, R. Soltz<sup>7</sup>, E. Swallow<sup>7</sup>, Y. Torun<sup>12</sup>, R. Winston<sup>10</sup>, D. Wright<sup>10</sup> and K. Wu<sup>13</sup>

1 - Brookhaven National Laboratory, 2 - Fermi National Laboratory, 3 - Harvard University, 4 - Elmhurst College, 5 - Illinois Institute of Technology, 6 - Indiana University, 7 - Lawrence Livermore National Laboratory, 8 - Purdue University, 9 - University of Michigan, 10 - University of Chicago, 11 - University of Colorado, 12 - University of Iowa, 13 - University of South Carolina, 14 - University of Virginia

## The MIPP Spectrometer



- Full acceptance spectrometer
  - Two analysis magnets deflect in opposite directions
  - TPC + 4 Drift Chambers + 2 PWCs
- Excellent Particle ID (PID) separation (2-3  $\sigma$ )
  - TPC: < 1 GeV/c
  - ToF: 1-3 GeV/c
  - DCkov: 3-17 GeV/c
  - RICH: 17-80 GeV/c



The EOS TPC being prepared in a clean-room before it was installed in the MIPP hall.



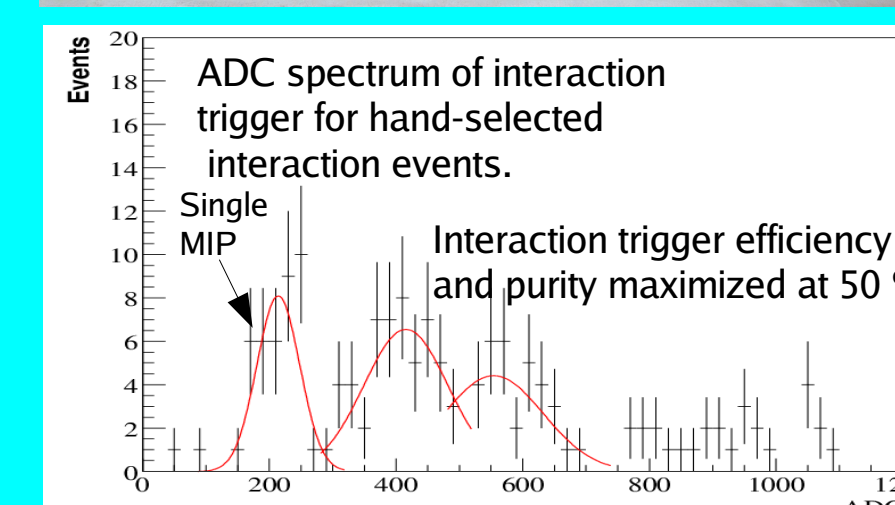
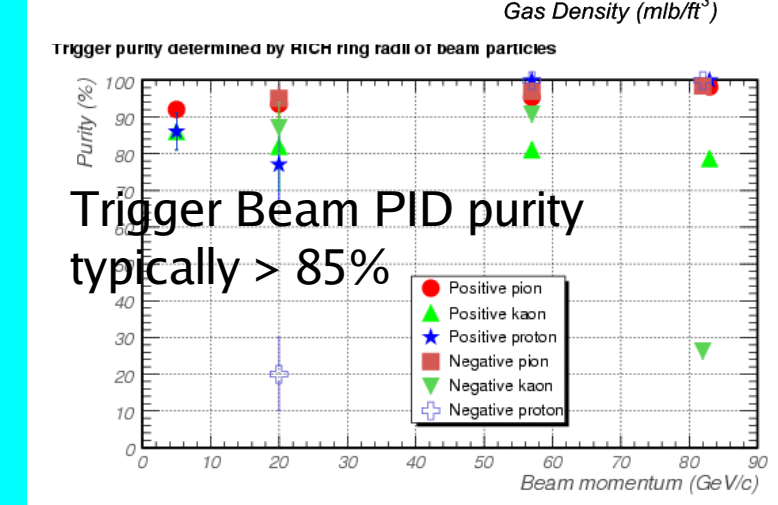
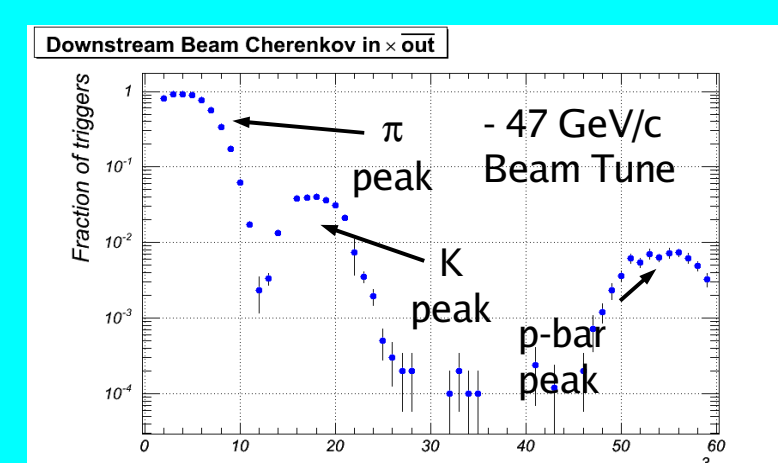
The SELEX RICH detector vessel being installed in the MIPP hall, before the hall was enclosed.

Most components of the MIPP spectrometer are taken from previous experiments!

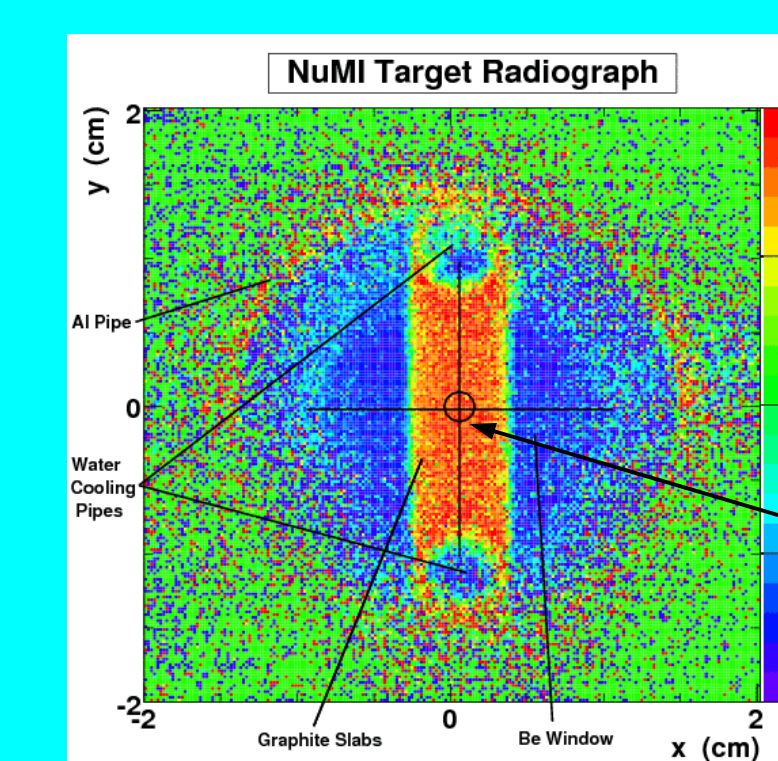
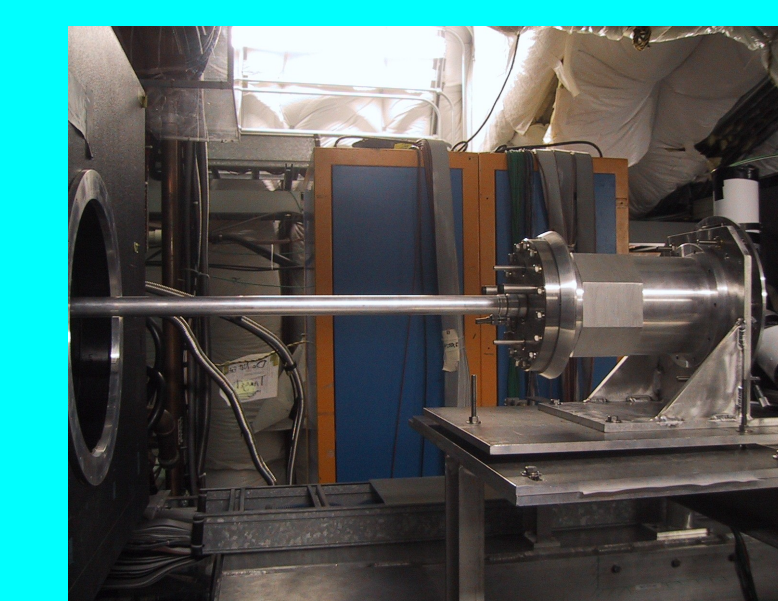


## MIPP Event Trigger

- Primary 120 GeV/c proton beam from Fermilab Main Injector, secondary target and beamline upstream provides lower momentum p's,  $\pi$ 's and K's.
- Must tag incoming particle id!
- Two Ckov detectors upstream of target used to tag beam species.
- DAQ rate is low (~30 Hz), so we enhance our sample of interaction events using a track multiplicity trigger.
- An interaction trigger was constructed using a thin piece of scintillator and spare MINOS parts (optical fibers and connectors).

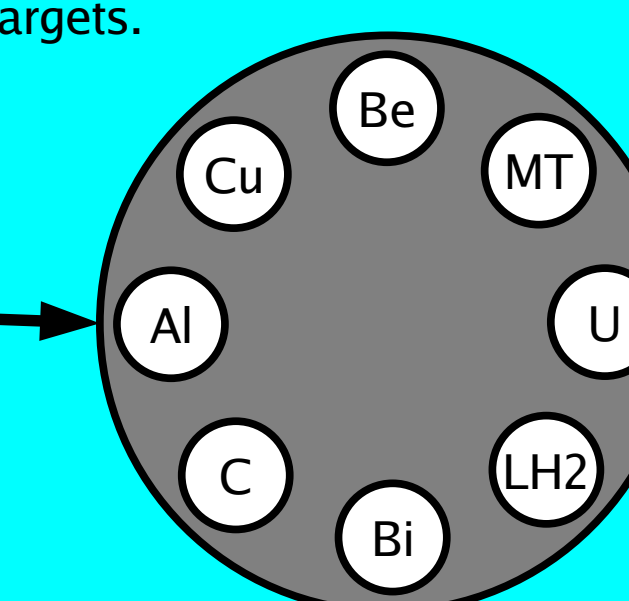


## The MINOS and Other physics Targets in MIPP



- Six week run with a spare MINOS target installed in the MIPP hall.
- Collected ~1.6 x 10<sup>6</sup> events of Main Injector 120 GeV/c protons on the MINOS target.
- Target wheel installed ~2 cm upstream of TPC allows switching between various thin targets.
  - 3.2 x 10<sup>6</sup> p's,  $\pi$ 's and K's at 120, 60, 35 and 20 GeV/c on thin C and Be targets.
- Other physics interests: several million events of p's,  $\pi$ 's and K's at momenta ranging from 5-120 GeV/c on thin (<2%  $\lambda$ ) LH<sub>2</sub>, Bi, and U targets.

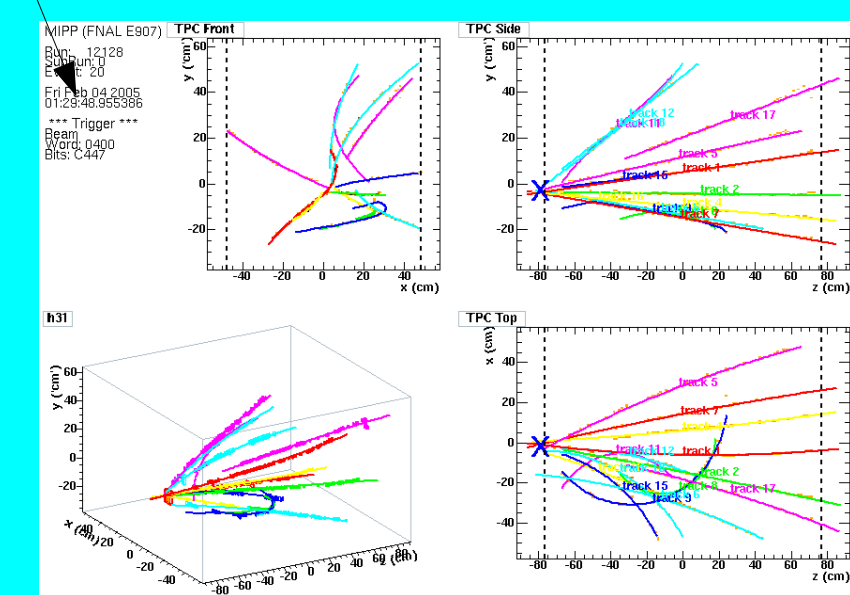
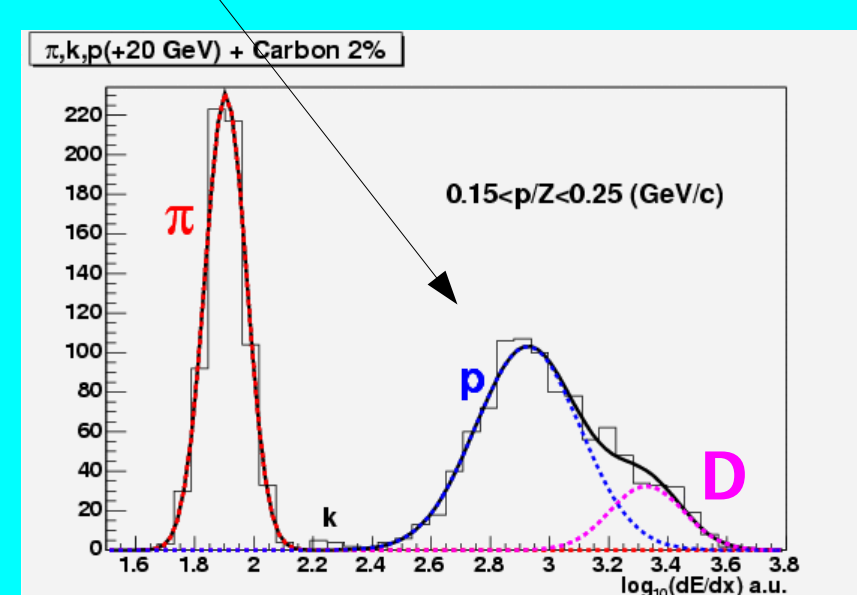
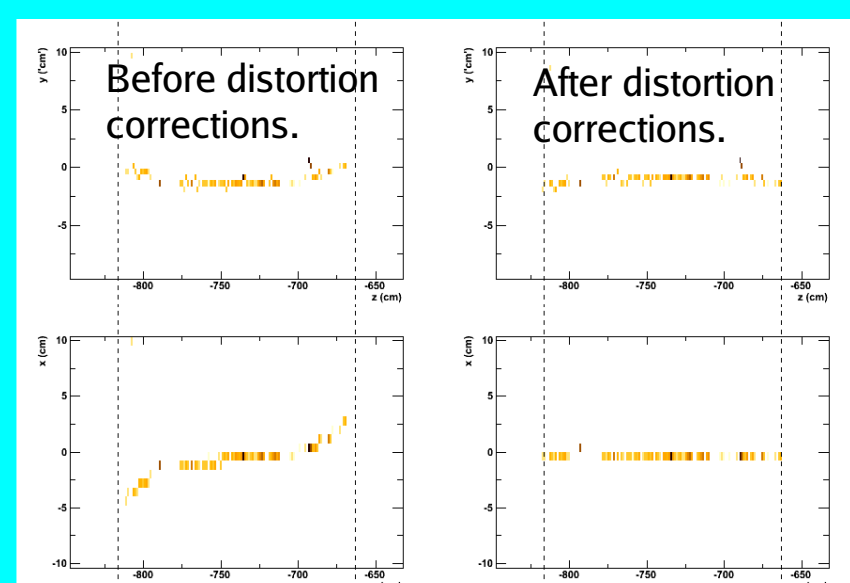
Beam is aligned to within 0.5 mm of the target center ( $\Delta x = 0.002$  cm,  $\Delta y = 0.051$  cm)



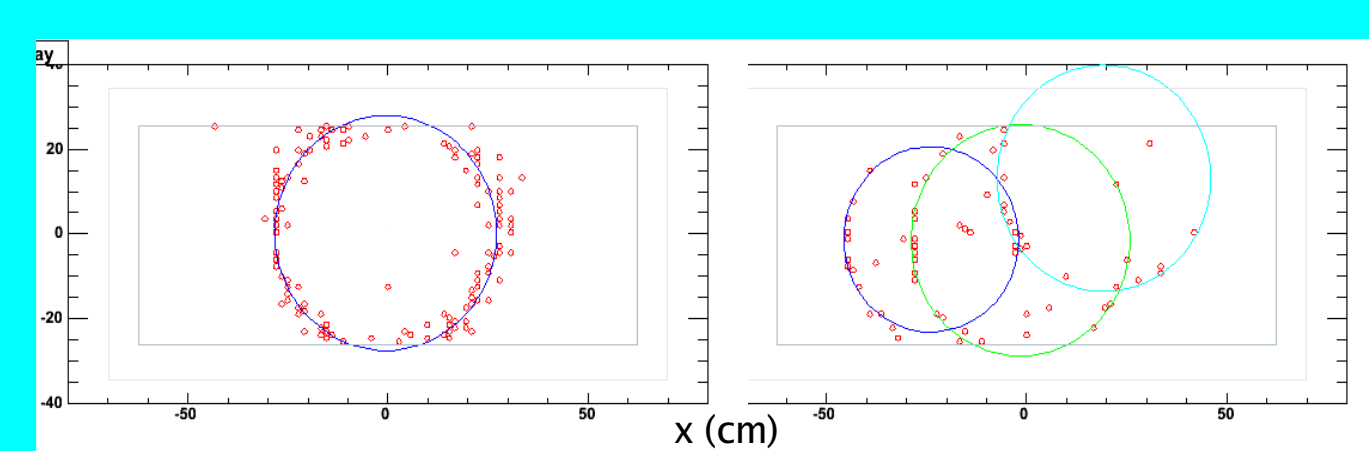
## Detector Performance

### Time Projection Chamber (TPC)

- The TPC data are "distorted" due to the non-uniform magnetic field. These distortions are corrected as shown on the right.
- Track finding efficiency now ~100%. Vertex-constrained fits are a work-in-progress.
- Preliminary results of <dE/dx> (uncalibrated and with poor momentum resolution) are very promising.

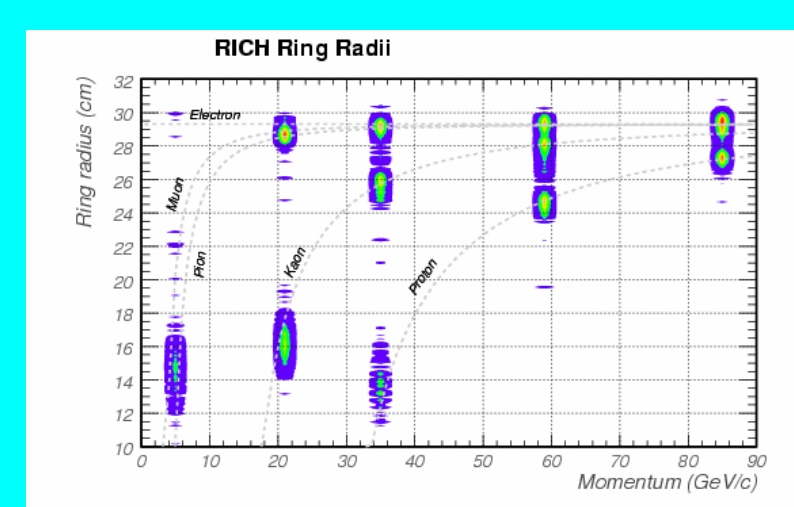


### Ring Imaging Cherenkov (RICH) Detector

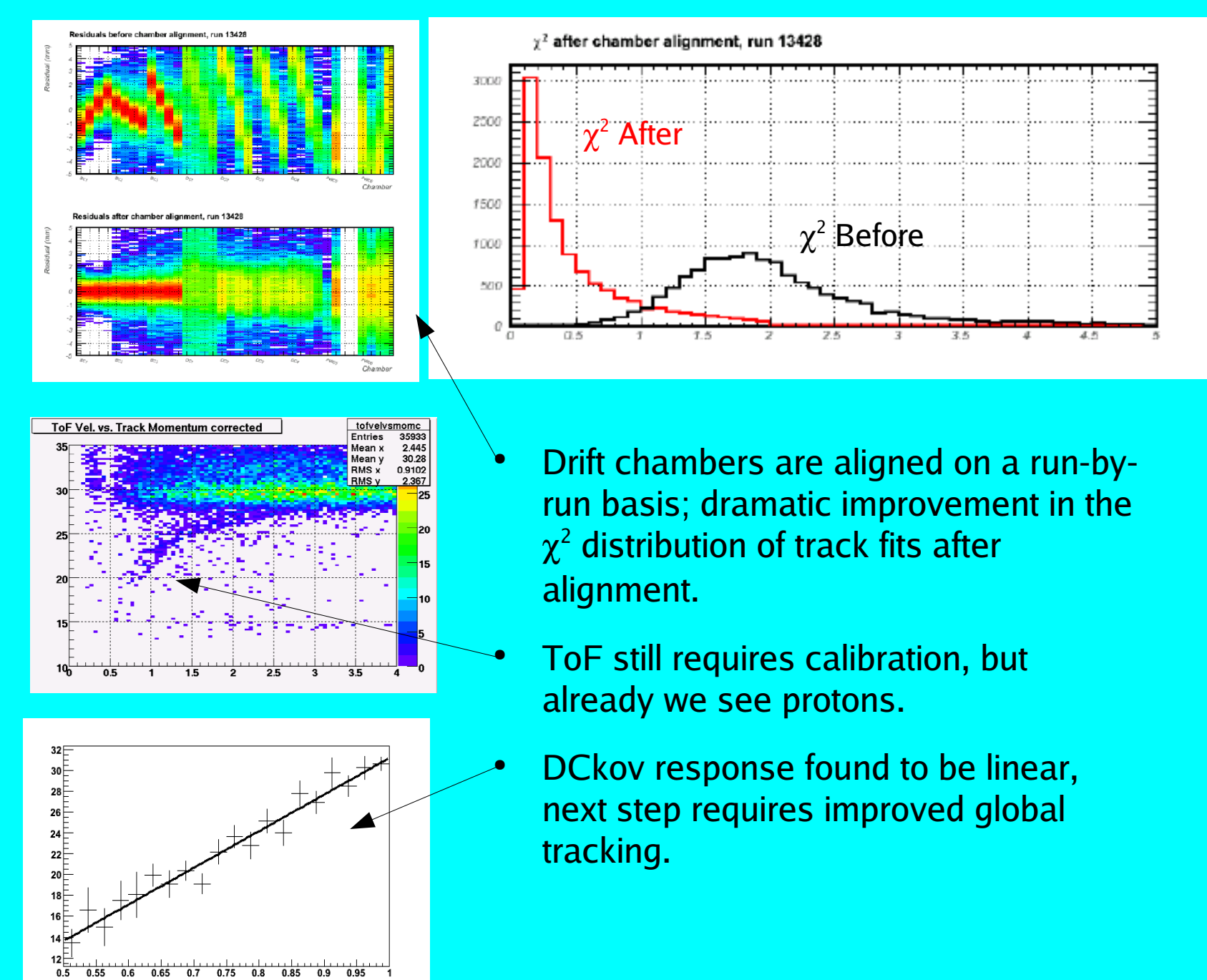


- The RICH detector was extremely stable during the data run.
- RICH rings are found and fit to a circle of radius  $R$ 

$$R \sim \sqrt{2(1 - 1/n\beta)}$$
- Matching rings to track trajectories, we are able to separate  $\pi$ 's and K's above ~17 GeV/c!

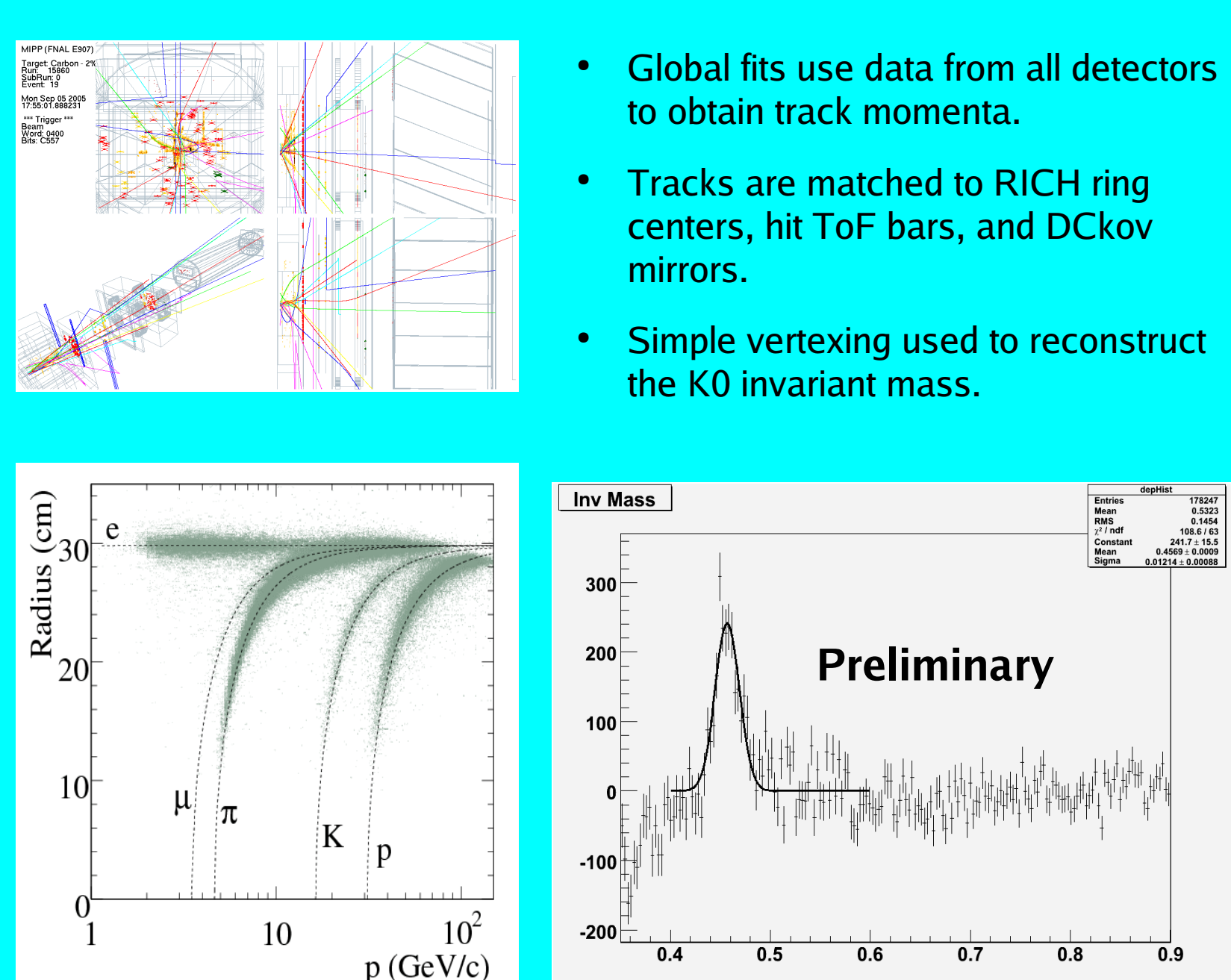


### Drift Chambers, ToF and DCKov Detectors



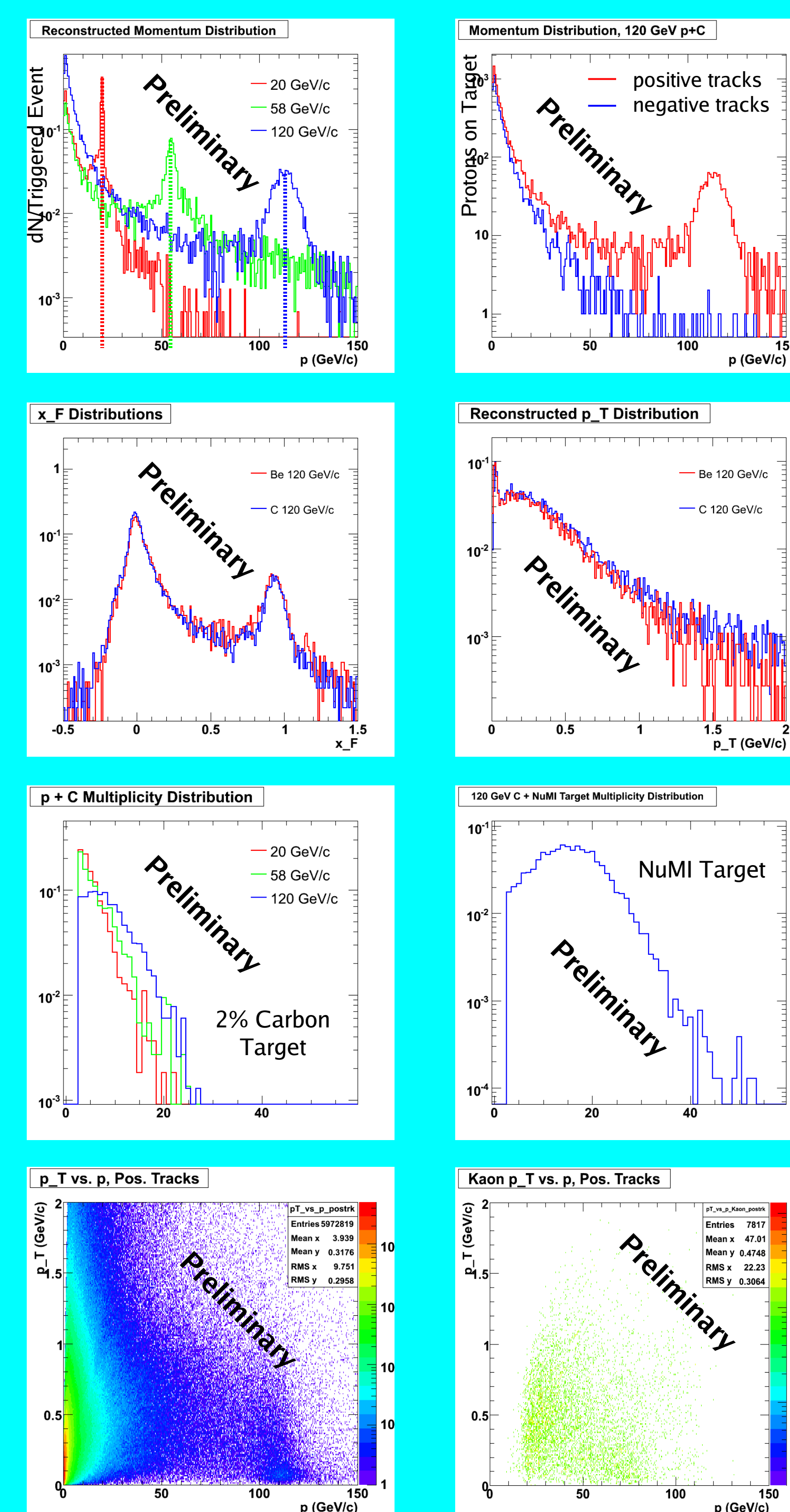
- Drift chambers are aligned on a run-by-run basis; dramatic improvement in the  $\chi^2$  distribution of track fits after alignment.
- ToF still requires calibration, but already we see protons.
- DCKov response found to be linear, next step requires improved global tracking.

### Putting It All Together...



- Global fits use data from all detectors to obtain track momenta.
- Tracks are matched to RICH ring centers, hit ToF bars, and DCKov mirrors.
- Simple vertexing used to reconstruct the K0 invariant mass.

## Preliminary Results

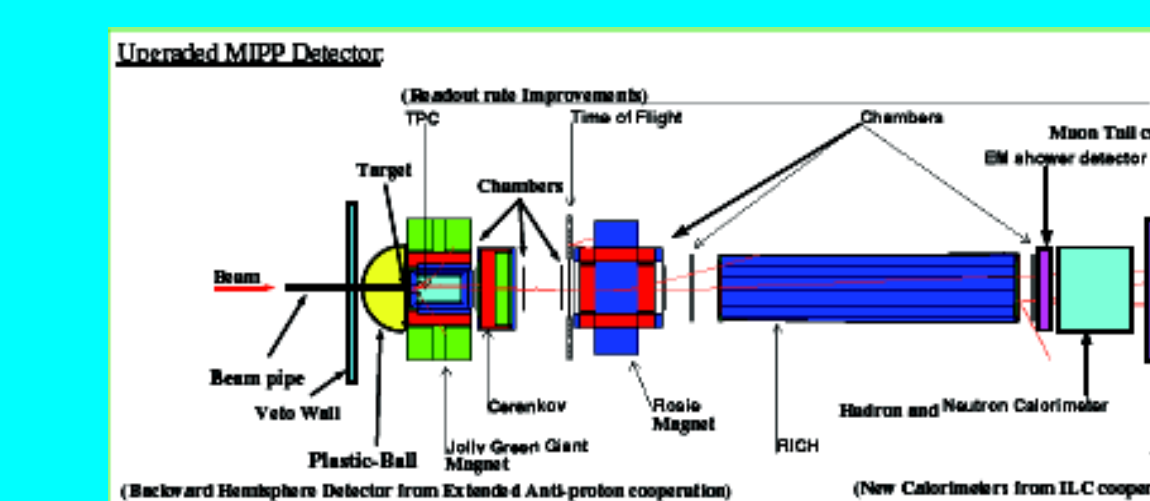


- Current momentum resolution is ~3% at 20 GeV/c and ~7% at 120 GeV/c.
- ~100% efficient at charge determination up to 120 GeV/c.
- MIPP measures  $x_F$  between -0.25 and 1.
- Thin C-target data will be essential in building cascade models of more complicated graphite-based targets (eg, the MINOS target).
- Thin Be-target data may also be used to enhance our thin C-target data sample.
- Multiplicity distributions of hadronic interactions with both thin and MINOS targets.
- Inclusive  $p_x$  vs  $p$  spectra for the MINOS target for all momenta.
- Using the RICH to select  $\pi$ 's and K's,  $p_x$  vs  $p$  spectra for these particles off the MINOS target.
  - Measurements of  $\pi/\pi^+$ ,  $\pi/K$  and  $\pi^+/K^+$  ratios for  $p > 20$  GeV/c will help MINOS constrain the predicted high-energy tail of the nm energy-spectrum.
- Hope to have preliminary  $p_x$  vs.  $p$  spectra of full momentum range by Dec. 2006.

## Analysis Goals

- Kalman-filter based reconstruction is currently being incorporated to improve momentum resolution.
- $\pi/K$  and  $\pi/\pi^+$  ratios off of NuMI target.
- $p_x$  vs  $p$  spectra for the NuMI, thin C and thin Be targets.
- Novel precise measurement (~50 ppm) of the charged Kaon mass.
- HBT (pion interferometry).
- A-dependence of inclusive and exclusive cross-sections.
- Testing the Scaling Law of inclusive cross-sections.
- Provide data for studies of non-perturbative QCD.

## MIPP Upgrade



- Current experiment is limited by DAQ rate, dominated by the TPC readout rate (~30 Hz).
- An upgrade of the TPC electronics, using the ALICE ALTR0 chip, can increase this readout rate by up to 50x.
- Further upgrades include repair of analysis magnet coils, wire-chamber electronics upgrade, improved interaction trigger, recoil proton detector, addition of large veto wall, and an improved beamline.
- Estimated total cost: \$500K.
- Expanded run plan would support US and world-wide neutrino program by including more data on the MINOS/NOVA and C and Be targets, as well as cross-section measurements for O<sub>2</sub> and N<sub>2</sub>.
- Beam would span the full range of momenta from a few GeV/c up to 120 GeV/c.
- MIPP welcomes new institutions to join the upgrade effort!

## Search for the neutrinoless $\beta\beta$ decay in $^{76}\text{Ge}$ with the GERDA experiment

C Cattadori, M Knapp, K Kröniger, X Liu, L Pandola, A Pullia, C Tomei, C Ur and F Zocca for the GERDA Collaboration

**Abstract.** The GERmanium Detector Array, GERDA, [1] is designed to search for neutrinoless double beta ( $0\nu\beta\beta$ )–decay of  $^{76}\text{Ge}$ . The importance of such a search is emphasized by the evidence of a non-zero neutrino mass from flavour oscillation experiments and by the recent claim [2] based on data of the Heidelberg-Moscow experiment. GERDA will be installed in the Hall A of the Gran Sasso underground Laboratory (LNGS), Italy. The construction of GERDA will start in 2006.

The GERDA experiment is designed to collect an exposure of 100 kg·y quasi background free, reaching a sensitivity on the  $^{76}\text{Ge}$  half-life of about  $10^{26}$  years. This leads to a requirement of a background index of the order of  $10^{-3}$  counts/(kg·y·keV) at the  $Q_{\beta\beta}$ –value of 2039 keV. The experiment is foreseen to proceed in two phases. In the first phase, enriched detectors which were previously operated by the Heidelberg-Moscow and IGEX collaborations (about 18 kg total mass) will be redeployed. The goal of the first phase is to confirm or reject the claim from [2] with an exposure of about 20 kg·y. In the second phase, custom made detectors will be installed which are truly coaxial and segmented.

The main design feature of GERDA is to use liquid Argon as the shield against  $\gamma$  radiation. High purity germanium detectors are immersed directly in the cryogenic liquid which also acts as the cooling medium. The cryogenic volume is surrounded by a buffer of ultra-pure water acting as an additional  $\gamma$ -ray and neutron shield. The detectors are surrounded by low- $Z$  material (water and liquid Argon) to reduce the production rate of neutrons by cosmic ray muons with respect to conventional high- $Z$  passive shieldings (lead). Furthermore, the water buffer is equipped with photomultipliers and operated as a Čerenkov muon veto. Additional background reduction comes from the careful material selection, anti-coincidence cuts applied on signals from different detectors, segmentation and pulse shape analysis.

The existing enriched detectors to be used for the phase-I are going to be dismantled from their cryostat, re-furbished and tested inside the cryogenic liquid bath. Meanwhile, 37 kg of germanium, enriched to a level of 86% in  $^{76}\text{Ge}$ , have been procured for the production of the new segmented detectors. The material is currently stored underground to prevent cosmogenic activation. A 18-fold segmented prototype of natural germanium is currently under test, to characterize the core/segment energy resolution and the background reduction.

Front-end electronics has been developed which is able to operate at the cryogenic temperature of liquid Argon. Its rise time and noise level that meet the GERDA specifications.

[1] Gerda Collaboration, Abt I et al., Proposal, a <http://www.mpi-hd.mpg.de/ge76/home.html>

[2] Klapdor-Kleingrothaus H V et al., *Phys. Lett. B* **586**, 198 (2004)

# Mass Eigenstate Composition of $^8\text{B}$ Solar Neutrinos

Hiroshi Nunokawa<sup>1</sup>, Stephen Parke<sup>2</sup> and Renata Zukanovich Funchal<sup>3</sup>

<sup>1</sup> Departamento de Física, Pontifícia Universidade Católica do Rio de Janeiro, C. P. 38071, 22452-970, Rio de Janeiro, Brazil: email: nunokawa@fis.puc-rio.br

<sup>2</sup>Theoretical Physics Department, Fermi National Accelerator Laboratory, P.O. Box 500, Batavia, IL 60510, USA: email: parke@fnal.gov

<sup>3</sup>Instituto de Física, Universidade de São Paulo, C. P. 66.318, 05315-970 São Paulo, Brazil: email: zukanov@if.usp.br

**Abstract.**  $91\pm 2\%$  of  $^8\text{B}$  Boron solar neutrinos observed by SNO are  $\nu_2$  mass eigenstates.

Around the MSW “triangle”, where  $\langle P(\nu_e \rightarrow \nu_e) \rangle = 0.35$ , the composition of  $^8\text{B}$  Boron solar neutrinos is either 65% or 100%  $\nu_2$  except at the top and bottom right hand corners of this triangle. Nature’s choice for the solar oscillation parameters is at the top right hand corner, the LMA corner, where the fraction of  $\nu_2$  is  $91\pm 2\%$ , see Fig. 1. Details of this two flavor calculation can be found in [1] using the analytical formulation of [2] and the global solar analysis of SNO, [3]. For non-vanishing  $\theta_{13}$ , the  $\nu_2$  fraction is reduced by  $\sin^2 \theta_{13}$ , see Ref. [1].

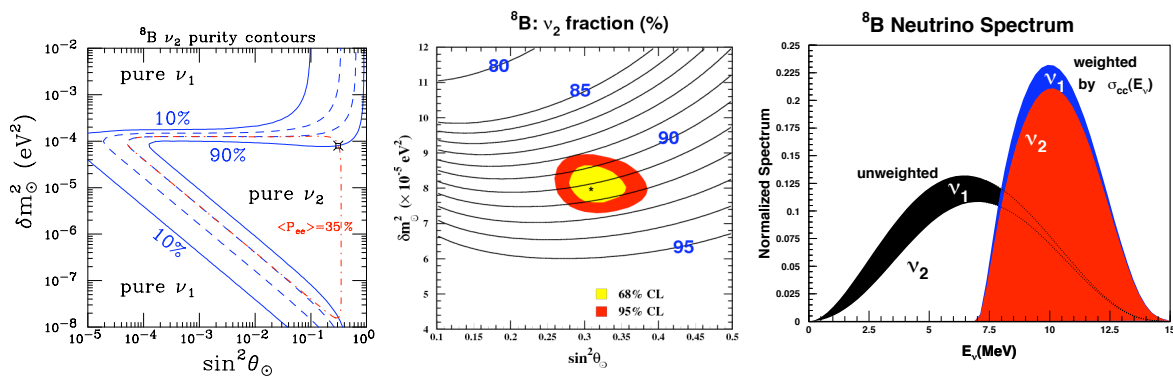


**Figure 1.** Left panel: The mass eigenstate composition of  $^8\text{B}$  Boron solar neutrinos in  $\delta m_\odot^2$  v  $\sin^2 \theta_\odot$  plane showing the MSW triangle (red) dotdashed line. Middle panel: Focusing in on the current allowed region. Right panel: The normalized  $^8\text{B}$  spectrum broken into its  $\nu_1$  and  $\nu_2$  components both unweighted, left, and weighted, right, by the charge current cross section using a 5.5 MeV threshold on the kinetic energy of the recoil electron and the best fit point for the solar oscillation parameters given in [3]. These weighted mass eigenstate fractions are the fractions that SNO is sensitive to. All panels of this figure are for vanishing  $\sin^2 \theta_{13}$ .

[1] H. Nunokawa, S. J. Parke and R. Zukanovich Funchal, “What fraction of boron-8 solar neutrinos arrive at the earth as a  $\nu(2)$  mass eigenstate?,” Phys. Rev. D **74**, 013006 (2006) [arXiv:hep-ph/0601198].

[2] S. J. Parke, Phys. Rev. Lett. **57**, 1275 (1986); S. J. Parke and T. P. Walker, Phys. Rev. Lett. **57**, 2322 (1986).

[3] B. Aharmim *et al.* [SNO Collaboration], Phys. Rev. C **72**, 055502 (2005) [arXiv:nucl-ex/0502021].

## Calibration of the Neutral Current Detection Array in the SNO experiment

G.A. Cox<sup>8</sup>, B.T. Cleveland<sup>5</sup>, M. Di Marco<sup>6,9</sup>, H.C. Evans<sup>6</sup>,  
 E. Guillian<sup>6</sup>, A.L. Hallin<sup>6</sup>, M. Huang<sup>7</sup>, C. Howard<sup>6</sup>, N.A. Jelley<sup>5</sup>,  
 J. Law<sup>2</sup>, J.C. Loach<sup>5</sup>, H.M. O’Keeffe<sup>5</sup>, C. Kraus<sup>6</sup>, C.B. Krauss<sup>6</sup>,  
 S. McGee<sup>8</sup>, S.J.M. Peeters<sup>5,\*</sup>, G. Prior<sup>6</sup>, K. Rielage<sup>4</sup>, D. Reitzner<sup>2</sup>,  
 P. Skensved<sup>6</sup>, J. Wendland<sup>1</sup> on behalf of the SNO collaboration

1 University of British Columbia, Vancouver, Canada

2 University of Guelph, Guelph, Canada

3 Lawrence Berkeley National Laboratory, Berkeley, USA

4 Los Alamos National Laboratory, Los Alamos, USA

5 University of Oxford, Oxford, UK

6 Queen’s University, Kingston, Canada

7 University of Texas, Austin, US

8 University of Washington, Seattle, US

9 present address: University of Geneva, Geneva, Switzerland

E-mail: \*Corresponding author: s.peeters1@physics.ox.ac.uk

**Abstract.** Since November 25th, 2004, the Sudbury Neutrino Observatory has been taking production data in its third and final phase. For this phase a ‘Neutral-Current Detection (NCD) Array’, consisting of 36 strings of <sup>3</sup>He proportional counters and 4 strings of <sup>4</sup>He proportional counters, was deployed in SNO’s D<sub>2</sub>O volume. It supplements the Cherenkov detector, consisting of 9456 photomultiplier tubes, present in the previous two phases by offering an independent measurement of the solar neutral current rate. The <sup>3</sup>He counters detect neutrons from neutrino-deuteron neutral current interactions in the D<sub>2</sub>O. We describe the calibration of this array.

The neutron detection efficiency is calibrated and monitored with contained (<sup>252</sup>Cf and AmBe) sources that are regularly deployed throughout the D<sub>2</sub>O volume. The data from these sources are analysed using both a normal counting technique and (when appropriate) a Time Series Analysis (TSA). TSA is an alternative method based on characteristic event time patterns generated by the <sup>252</sup>Cf source from the multiple neutrons produced per fission. Both analysis methods agree with each other and the SNO Monte-Carlo. A soluble <sup>24</sup>Na source was successfully injected and mixed throughout the D<sub>2</sub>O volume in October 2005. The 2.7 MeV gamma ray released in its (15 hour half-life) decay can photo-disintegrate the deuteron, thus creating a neutron source with the same geometrical distribution as the neutrons produced by neutrinos. A pulse injection system is used to determine the electronics characteristics of the NCD array. The threshold, the gain and the linearity of the read-out systems, as well as the properties of the amplifiers are monitored weekly. The neutron detection efficiency of the SNO Neutral-Current Detection Array is well understood. The ongoing calibrations have demonstrated the stable operation of the Neutral-Current Detection Array throughout the data taking period.

# Results of a 3-ton experiment with a Gd loaded liquid scintillator target performed in the frame of LVD at LNGS

M.Aglietta<sup>1</sup>, G.Bari<sup>2</sup>, G.Bruno, W.Fulgione<sup>1</sup>, E.Kemp<sup>3</sup>, A.Porta<sup>1</sup>,  
 A.Malguine<sup>4</sup> for the LVD collaboration, and C.Cattadori<sup>5</sup>,  
 N.Danilov<sup>4,7</sup>, A.DiVacri<sup>6</sup>, Yu.Krilov<sup>4,7</sup>, E.Yanovich<sup>4</sup>

<sup>1</sup> IFSI-To INAF and INFN-Torino (I), <sup>2</sup> INFN-Bologna (I), <sup>3</sup> Universidade Estadual de Campinas Campinas (BR), <sup>4</sup> Institute of Nuclear Research Moscow (RU), <sup>5</sup> INFN-Milano Bicocca (I), <sup>6</sup> LNGS INFN (I), <sup>7</sup> Institute of Physical Chemistry Moscow (RU)

E-mail: porta@to.infn.it, divacri@lngs.infn.it

**Abstract.** In the frame of the LVD experimental program in the INFN Gran Sasso National Laboratory (LNGS), we performed a 3-ton Gd experiment, by loading (up to 0.1% in weight) the LVD organic liquid scintillator with a Gd organic salt developed and produced as the result of a joint INFN/INR research activity. Performances, feasibility and preliminary results on stability have been presented.

LVD main target is the detection of neutrino bursts from Gravitational Stellar Collapses in our galaxy. The main reaction is the inverse beta decay  $p(\bar{\nu}_e, e^+)n$  followed by neutron capture on H  $p(n, \gamma)d$ , with  $E_\gamma=2.2$  MeV. Doping the LVD liquid scintillator ( $C_nH_{2n}, \bar{n} \simeq 9.6$ ) with gadolinium, the dominant n-capture reaction becomes  $Gd(n, \gamma_i)Gd$  with some advantages: a shorter mean capture time and a higher energy released ( $\simeq 8$  MeV) by the  $\gamma$  cascade.

Two LVD counters (1.2 ton of liquid scintillator (LS) each) were doped starting from a concentrated master solution (30 l at a Gd concentration of 40 g/l). The master solution has been obtained by diluting the Gd carboxylate salt ( $Gd(2Methyl-Valerate)_3$ ) in the standard LVD LS. The Gd salt has been chosen and optimized to maximize the solubility, minimize light quenching while keeping good optical properties of final Gd doped LS.

In the doped counters, the neutron mean capture time decreases by a factor  $\sim 8$  (from 185  $\mu s$  to 25  $\mu s$ ), improving of the same factor the S/N. The neutron detection efficiency, measured by a  $^{252}Cf$  source placed in the centre of the counter, increases by  $\sim 25\%$  (from 70% to 87%). The counter optical gain decreases by  $\sim 17\%$ .

The stability of the Gd doped LS is continuously monitored:

- on large scale by recording the detector response to cosmic muons, the neutron detection efficiency and the mean n-capture time;
- on small scale by directly measuring transmittance, light yield and fluors concentration of liquid scintillator samples periodically extracted from the counters.

Results regarding 170 days of stability survey, do not evidence any change in Gd LVD liquid scintillator performances.

# Experiment for Discrimination between Special Relativity Theory and Covariant Ether Theories

W. Potzel<sup>1</sup>, A.L. Kholmetskii<sup>2</sup>, U. van Bürck<sup>1</sup>, R. Röhlberger<sup>3</sup>, and E. Gerdau<sup>4</sup>

<sup>1</sup>Physik-Department, Technische Universität München, D-85747 Garching, Germany

<sup>2</sup>Department of Physics, Belarus State University, 220080 Minsk, Belarus

<sup>3</sup>Deutsches Elektronen Synchrotron DESY, D-22607 Hamburg, Germany

<sup>4</sup>Institut für Experimentalphysik, Universität Hamburg, D-22761 Hamburg, Germany

wpotzel@ph.tum.de

**Abstract.** Some covariant ether theories assume the existence of an “absolute” inertial frame, leading to a frequency shift of electromagnetic radiation proportional to the “absolute” velocity of the frame of experiment. Two experiments are discussed which are able to measure such a possible frequency shift.

Experimental data obtained in high-energy cosmic-ray physics triggered a discussion about a possible violation of the Lorentz invariance. In this context, some space-time theories with a covariant description of a hypothetical “absolute space” in the Universe (covariant ether theories, CETs) have attracted attention. In contrast to Special Relativity Theory, in CETs, an “absolute” inertial frame is allowed to exist. A very important consequence of CETs is the appearance of a frequency (energy) shift between emitter and receiver of electromagnetic radiation, which is proportional to the “absolute” velocity of the reference frame in which the experiment is carried out, e. g., the Earth [1, 2]. Such a shift appears, for example, when source and receiver rotate on a fast-spinning rotor at different distances from a common rotational axis. The shift is proportional to  $c^3$ :  $\Delta E/E = u^2 v/4c^3$  where  $u$  is the linear velocity at the perimeter of the rotor and  $v$  is the absolute velocity of the Earth.

We favour two experimental schemes: a) Using synchrotron radiation in the x-ray regime (14.4 keV) and applying the Nuclear Lighthouse effect [3] the time evolution of the nuclear decay by coherent  $\gamma$ -ray emission of two targets is recorded: one target is fixed at the perimeter ( $u$  is maximal) the other close to the axis of the rotor ( $u \sim 0$ ). The coherent radiation emitted by the two targets will result in a characteristic interference pattern from which  $\Delta E/E$  can be derived if present. b) Using visible light from a laser and a beam splitter, light reflected from the rotor surface ( $u$  is maximal) in off-specular directions is caused to interfere with light (from the same laser) reflected by a stationary mirror ( $u=0$ ). Again, the characteristic interference pattern will allow to determine  $\Delta E/E$ . Computer simulations show that using modern technology an energy resolution of  $\Delta E/E$  at the level of  $10^{-16}$  can be expected which is sufficient to reveal – if present at all - the effect predicted by CETs.

## References

- [1] A.L. Kholmetskii, *Physica Scripta* **67** (2003) 381.
- [2] A. L. Kholmetskii et al., *Hyperfine Interactions* **156/157** (2004) 9.
- [3] R. Röhlberger et al., *Phys. Rev. Lett.* **84** (2000) 1007.

# Recent proton decay results from Super-Kamiokande

**J L Raaf for the Super-Kamiokande Collaboration**

Boston University, Department of Physics, 590 Commonwealth Avenue, Boston, MA 02215

E-mail: jltraaf@bu.edu

**Abstract.** Recent experimental limits on the search for proton decay are presented. Data from Super-Kamiokande, a water Cherenkov detector with a fiducial volume of 22,500 tons of ultra pure water, are used in the analysis. Analyses from SK-I (40% photomultiplier coverage) plus SK-II (20% photomultiplier coverage) are reported with results from  $p \rightarrow e^+\pi^0$ ,  $p \rightarrow \mu^+\pi^0$ , and  $p \rightarrow \bar{\nu}K^+$ .

## 1. Introduction

In the Standard Model, protons have a lifetime which is finite but unobservably long. The long lifetime arises from baryon number (B) conservation; however, the conservation of baryon number is considered an open experimental question, since it was introduced to the Standard Model empirically. Grand unified theories (GUTs) attempt to unify the three fundamental interactions in the Standard Model, motivated in part by the desire to constrain some of the seemingly arbitrary quantities in the model. An important decay mode in many GUTs is  $p \rightarrow e^+\pi^0$ , which can proceed via exchange of an extremely heavy X boson. Many other decay modes are also predicted; different modes are favored by different GUTs.

## 2. Results

The Super-Kamiokande (SK) detector is well-suited to proton decay searches, with  $7.5 \times 10^{33}$  protons in the 22.5 kiloton fiducial volume. The backgrounds to proton decay in SK arise from atmospheric neutrino interactions; they are carefully accounted for in all proton decay searches.

The results presented here are the combined results of SK-I and SK-II datasets. The main difference between SK-I and SK-II is the photocathode coverage of the detector (40% for SK-I, 20% for SK-II). Table 1 shows the limits set on the proton lifetime for recent Super-Kamiokande searches.

**Table 1.** Summary of recent Super-K proton decay searches.

Mode	Dataset	Lifetime (yrs)	Reference
$p \rightarrow e^+\pi^0$	SK-I + SK-II	$8.4 \times 10^{33}$	[1]
$p \rightarrow \mu^+\pi^0$	SK-I + SK-II	$6.6 \times 10^{33}$	[1]
$p \rightarrow \bar{\nu}K^+$	SK-I	$2.3 \times 10^{33}$	[2]

### Acknowledgments

We gratefully acknowledge the cooperation of the Kamioka Mining and Smelting Company. The Super-Kamiokande experiment was built from and has been operated with funding from the Japanese Ministry of Education, Culture, Sports, Science, and Technology, the United States Department of Energy, and the U.S. National Science Foundation.

### References

- [1] Clark S T 2006 *Searches for proton decay with the Super-Kamiokande detector* PhD thesis, Boston University
- [2] Kobayashi K *et al.* 2005 Search for nucleon decay via modes favored by supersymmetric grand unification models in Super-Kamiokande-I *Phys. Rev. D* **72** 052007

# High energy neutrino Astronomy

**Soebur Razzaque**

Department of Astronomy and Astrophysics, and Department of Physics, Pennsylvania State University, University Park, Pennsylvania 16802, USA

E-mail: soeb@astro.psu.edu

**Abstract.** Astrophysical candidate sources of ultra-high energy cosmic rays inevitably produce high-energy neutrinos in and/or around them. While cosmic rays are scattered in the inter-galactic magnetic fields, neutrinos point back to their origin. Hence neutrinos can be used to probe astrophysical sources just like in usual photon astronomy. Here we present the expected neutrino signals from different astrophysical objects and discuss their possible applications to study these intriguing sources.

## 1. Introduction

Neutrinos, produced by cosmic-ray interactions at the sources, can probe Astronomical objects at very high energies. They interact weakly with matter and travel long distances as opposed to high energy  $\gamma$ -rays which are absorbed by background photons. Moreover,  $\nu$ 's point back to their sources unlike cosmic-rays which deflect in magnetic field. Thus high energy  $\nu$ 's are unique probe to learn physical processes going deep inside some of the most fascinating objects such as  $\gamma$ -ray bursts (GRBs), active galaxis (AGNs), core-collapse supernovae (SNe) and neutron stars.

## 2. Results and Conclusions

High energy  $\nu$  fluxes are predicted from long duration ( $> 2$  s) GRBs in different astrophysical models where a SN explosion precedes the GRB event [2], and a relativistic GRB jet is buried inside the progenitor star [3]. Expected high energy  $\nu$ 's from a short duration ( $\leq 2$  s) GRB is calculated in Ref. [7], and from giant flares of a highly magnetized neutron star in Ref. [1]. A model of SNe endowed with buried jet may be tested with high energy  $\nu$ 's [5]. Upcoming neutrino telescopes such as IceCube and KM3NeT will be able to probe nearby GRBs [4, 6].

## Acknowledgments

Research supported in part through NSF AST 03-07376 and NASA NAG 5-13286

## References

- [1] Ioka K, Razzaque S, Kobayashi S and Meszaros P 2005 *Astrophys. J.* **633**, 1013
- [2] Razzaque S, Meszaros P and Waxman E 2003 *Phys. Rev. Lett.* **90**, 241103
- [3] Razzaque S, Meszaros P and Waxman E 2003 *Phys. Rev. D* **68**, 083001
- [4] Razzaque S, Meszaros P and Waxman E 2004 *Phys. Rev. D* **69**, 023001
- [5] Razzaque S, Meszaros P and Waxman E 2004 *Phys. Rev. Lett.* **93**, 181101 [Erratum-ibid. **94**, 109903]
- [6] Razzaque S, Meszaros P and Waxman E 2006 *Phys. Rev. D* **73**, 103005
- [7] Razzaque S and Meszaros P 2006 *Astrophys. J.* **650**, 998

## A new technique for the identification of surface contamination in low temperature bolometric experiments

S Sangiorgio<sup>1</sup>, C Arnaboldi<sup>2</sup>, C Brofferio<sup>2</sup>, C Bucci<sup>3</sup>, S Capelli<sup>2</sup>, L Carbone<sup>2</sup>, M Clemenza<sup>2</sup>, O Cremonesi<sup>2</sup>, E Fiorini<sup>2</sup>, L Foggetta<sup>1</sup>, A Giuliani<sup>1</sup>, P Gorla<sup>3</sup>, C Nones<sup>2</sup>, A Nucciotti<sup>2</sup>, M Pavan<sup>2</sup>, M Pedretti<sup>1</sup>, G Pessina<sup>2</sup>, S Pirro<sup>2</sup>, E Previtali<sup>2</sup>, C Salvioni<sup>1</sup>, M Sisti<sup>2</sup>

<sup>1</sup> Dipartimento di Fisica e Matematica, Università degli Studi dell'Insubria, Como and INFN, Milano, Italy

<sup>2</sup> Dipartimento di Fisica, Università di Milano-Bicocca and INFN, Milano, Italy

<sup>3</sup> Laboratori Nazionali del Gran Sasso, Assergi (L'Aquila), Italy

E-mail: samuele.sangiorgio@mib.infn.it

**Abstract.** In the framework of the bolometric experiment CUORE, a new and promising technique has been developed in order to control the dangerous contamination coming from the surfaces close to the detector. In fact, by means of a composite bolometer, it is possible to partially overcome the loss of spatial resolution of the bolometer itself and to clearly identify events coming from outside.

The reduction of the background in the CUORE experiment[1] is subject of a wide R&D program. The goal is a reduction of a factor 10–100 from the present Cuoricino[2] limit of 0.18 c/keV/kg/y. Many indications suggest that the most dangerous component of this background in the  $\beta\beta 0\nu$  region comes from contamination of the surface close to the detector.

In the last two years we developed a new kind of bolometers which is able to discriminate between bulk and external events. This result is achieved by means of a composite device where a main bolometer is fully shielded by slab bolometers. The slab bolometers are not independent from the main absorber but are glued on it. Provided that the slabs heat capacity is small enough, pulse shape discrimination can be used to distinguish from events that take place inside the main absorber and events coming from external sources and impacting first on the covering slabs. We usually refer to this new detector as *Surface Sensitive Bolometer* (SSB)[3].

Working principle tests were performed on several small scale prototypes in the Cryogenic Detector Laboratory at Insubria University (Como, Italy). Investigation on suitable materials and optimization of detector parameters were also carried out. Full scale CUORE-like SSBs have been already tested successfully at Gran Sasso Underground Laboratory and other measurements are under way to improve device understanding and rejection methods.

### References

- [1] C. Arnaboldi et al., *Nucl. Instrum. Meth. A* **518** 775 (2004)
- [2] C. Arnaboldi et al., *Phys. Lett. B* **584**, 260 (2004)
- [3] L. Foggetta et al., *Appl. Phys. Lett.* **86**, 134106 (2004)

# The improvement of the detector susceptibility for carrying out the neutrino investigations on the electron magnetic spectrometer

G.V. Sapozhnikov <sup>a</sup>, A.V. Kholzakov <sup>a</sup>, I.N. Shabanova <sup>b</sup>, A.E. Kazanzev <sup>b</sup>

<sup>a</sup> Surface Physics Institute, Udmurt State University, 1 Universitetskaya St, 426034 Izhevsk, Russia

<sup>b</sup> Physical Technical Institute, 132 Kirov st., 426000 Izhevsk, Russia

E-mail: xps@fti.udm.ru

**Abstract.** For the precise determination of the energy of electrons that are formed during the beta-decay with the use of the electron magnetic spectrometer, an experimental unit for the system of highly susceptible high-speed parallel electron recording based on microchannel plates has been developed and tested.

**Key words:** electron magnetic spectrometer, rest mass of electron anti-neutrino.

## 1. Introduction

At present, the Udmurt State University together with the Physical-Technical Institute Ural Branch Russian Academy of Science have build and are adjusting the unique 100-cm electron magnetic spectrometer with double focusing by the uniform field  $\pi\sqrt{2}$  that has the resolution of  $10^{-4}$  (fig.1) [1]. The analysis of work on the building and use of electron magnetic spectrometers showed a significant advantage of a magnetic energy analyzer over an electrostatic one. It provides higher resolution and better contrast over the entire energy region. These specific features allow estimating the anti-neutrino electron mass using tritium beta-decay. The upper limit of the neutrino rest mass decreases down to 0.1 eV.

## 2. Experimental

The objective of this part of the work was the development of the high-sensitive high-speed system based on micro-channel plates for a parallel registration of electron spectra (fig.2).

The electrons having departed from the sample as the result of the photo-effect enter the energy analyzer chamber through the entrance slit, where they are dispersed by energies in the magnetic field and focused on the spectrometer focal plane (fig.3).

The presence of the focal plane in spectrometers with magnetic focusing gives a unique opportunity of the simultaneous record of all the electrons focused on it, which is not possible to carry out on electrostatic spectrometers. A change in the electron flow density over the width of the focal plane gives the information on the electron structure of the surface elements. It is offered to use the supersensitive electron magnetic spectrometer for determine neutrino flow from the Sun, antineutrino flow from nuclear reactors and other sources. The possibility of choosing focusing allows simultaneous registration of electrons with different energies due to the presence of the focal plane. For the signal increase, a herringbone assembly from two micro-channel plates is used; each plate has multiplication factor of  $10^6$  and the number of channels can be almost unlimited. Then electrons hit the substrate with resistive layer. In our sensor, a PbO resistive film with surface resistance of  $100 \text{ k}\Omega/\square$  is used, which provides the signal recording time of the order of  $10^{-5}$  s.

## 3. Results

The experiments on estimating the energy range width in the spectrometer focal plane have been carried out, which show that the use of this sensor allows simultaneous spectra recording from the region  $\Delta E = 200$  eV. When micro-channel plates with a larger radius are used, recording simultaneous spectra from the entire spectrometer focal plane is possible.

#### 4. Conclusions

The system for high-speed parallel electron spectra recording is developed in order to increase the susceptibility and the time resolution of the x-ray electron magnetic spectrometer designed for investigating fast processes on the surfaces (fig.4). When the rest mass of electron at tritium  $\beta$ -decay is estimated, it is important to investigate small radiation doses during fast processes, which is also possible to carry-out on this spectrometer.

#### References

1. V.A. Trapeznikov. Electron spectroscopy of small radiation doses // UFN, 1998, №7, с.793-799.



Fig.1. 100-cm electronic magnetic spectrometer

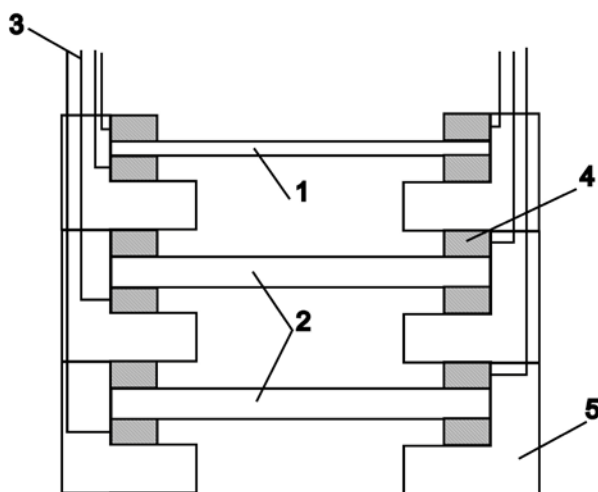


Fig. 2. The schematic diagram of the system for high-speed parallel record of electron spectra (1 – a resistive position-sensitive sensor, 2 – microchannel plates – 12, 3 – electrodes, 4 – coverings of MCP, 5 – a fluoroplastic frame)

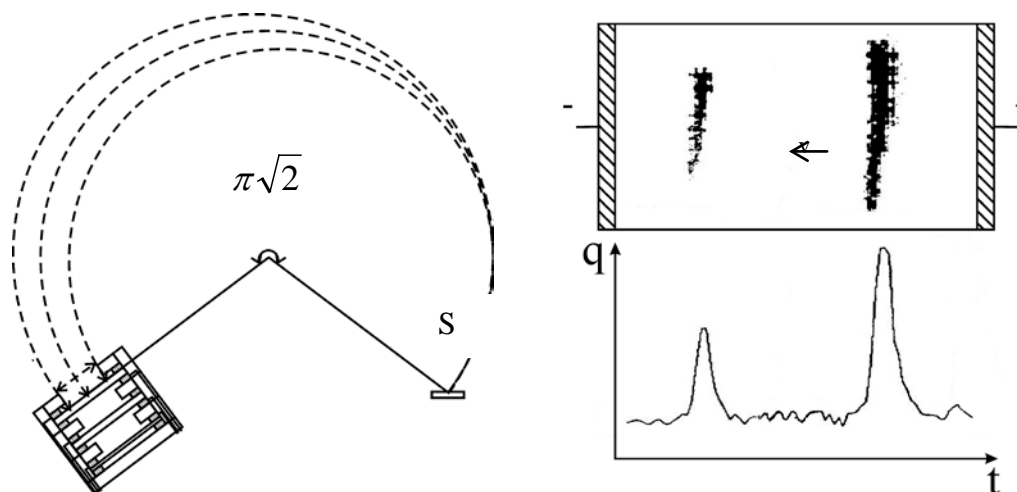


Fig. 3 Scheme of the electron registration with the use of the resistive position-sensitive sensor

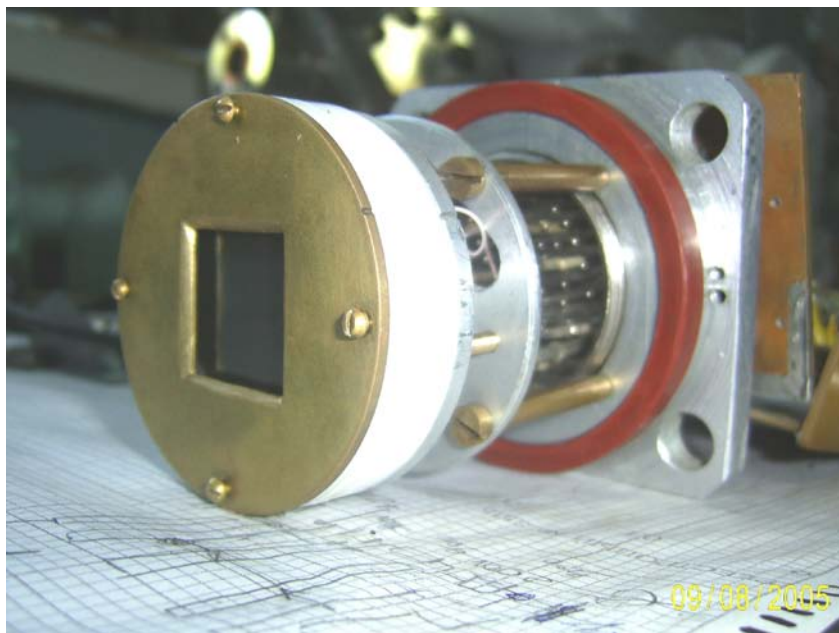


Fig.4. The view of the high susceptible, high-speed system detector for the parallel registration of electron spectra.

## The MARE project : a new $^{187}\text{Re}$ neutrino mass experiment with sub eV sensitivity

D. Schaeffer<sup>1</sup>, F. Gatti<sup>2</sup>, G. Gallinaro<sup>2</sup>, D. Pergolesi<sup>2</sup>, P. Repetto<sup>2</sup>, M. Ribeiro-Gomes<sup>2</sup>, R. Kelley<sup>3</sup>, C.A. Kilbourne<sup>3</sup>, F.S. Porter<sup>3</sup>, C. Enss<sup>4</sup>, A. Fleischmann<sup>4</sup>, L. Gastaldo<sup>4</sup>, E. Andreotti<sup>5</sup>, L. Foggetta<sup>5</sup>, A. Giuliani<sup>5</sup>, M. Pedretti<sup>5</sup>, M. Prest<sup>5</sup>, C. Rusconi<sup>5</sup>, S. Sangiorgio<sup>5</sup>, C. Arnaboldi<sup>1</sup>, C. Brofferio<sup>1</sup>, S. Capelli<sup>1</sup>, O. Cremonesi<sup>1</sup>, E. Fiorini<sup>1</sup>, P. Gorla<sup>1</sup>, S. Kraft<sup>1</sup>, A. Nucciotti<sup>1</sup>, M. Pavan<sup>1</sup>, G. Pessina<sup>1</sup>, E. Previtali<sup>1</sup>, M. Sisti<sup>1</sup>, K.D. Irwin<sup>6</sup>, B. Margesin<sup>7</sup>, A. Monfardini<sup>7</sup>, J. Beyer<sup>8</sup>, M. Galeazzi<sup>9</sup>, P. de Bernardis<sup>10</sup>, M. Calvo<sup>10</sup>, S. Masi<sup>10</sup>, S. Petcov<sup>11</sup>, K. Heeger<sup>12</sup>, R. Maruyama<sup>12</sup>, D. McCammon<sup>12</sup>

<sup>1</sup> Università di Milano-Bicocca and Sezione INFN di Milano-Bicocca, Italy

<sup>2</sup> Università di Genova and Sezione INFN di Genova, Italy

<sup>3</sup> Goddard Space Flight Center, NASA, Maryland, USA

<sup>4</sup> University of Heidelberg, Kirckhof-Institute of Physics, Germany

<sup>5</sup> Università di Insubria, Como and Sezione INFN di Milano-Bicocca, Italy

<sup>6</sup> National Institute of standards and Technology, Boulder, Colorado, USA

<sup>7</sup> ITC-IRST, Trento and Sezione INFN di Padova, Italy

<sup>8</sup> Physikalisch-Technische Bundesanstalt, Berlin, Germany

<sup>9</sup> University of Miami, Florida, USA

<sup>10</sup> Università di Roma "La Sapienza", Roma and Sezione INFN di Roma 1, Italy

<sup>11</sup> Scuola Internazionale Superiore Studi Avanzati, Trieste, Italy

<sup>12</sup> University of Wisconsin, Madison, Wisconsin, USA

E-mail: david.schaeffer@mib.infn.it

**Abstract.** A large worldwide collaboration is growing around the project of Micro-calorimeter Arrays for a Rhenium Experiment (MARE) for a direct calorimetric measurement of the neutrino mass with a sensitivity of about  $0.2 \text{ eV}/c^2$ . Many groups are joining their experience and technical expertise in a common effort towards this challenging experiment which will use the most recent and advanced developments of the thermal detection technique.

Single nuclear  $\beta$  decay is the most direct clue to investigate the electron neutrino mass, and by far, the most sensitive process due to the very low energy available to the particle in the final states. Unfortunately, even taking advantage of the lowest Q-value  $\beta$  processes in nature ( $Q = 2.5 \text{ keV}$  for  $^{187}\text{Re}$  and  $Q = 18.6 \text{ keV}$  for  $^3\text{H}$ ), sensitivities, up to now, are not much lower than  $\sim 1 \text{ eV}$ . In this context, the KATRIN experiment, the largest spectrometer for measuring  $\beta$  spectrum of  $^3\text{H}$ , could (if successful) reduce this limit by a factor of 10. Experiments with different systematics are needed. Experts in calorimetric technique are pushing their efforts for a huge programme of R&D in order to increase the sensitivity on the neutrino mass from the  $\beta$  decay of  $^{187}\text{Re}$  to  $\sim 0.2 \text{ eV}/c^2$ , making MARE as a complement of KATRIN.

[1] The updated version of the MARE proposal at <http://crio.mib.infn.it/wig/silicini/proposal>

# Prospects for Measuring Neutrino-Nucleus Coherent Scattering at a Stopped-Pion Neutrino Source

**Kate Scholberg**

Department of Physics, Duke University, Durham, NC, 27708, USA

E-mail: [schol@phy.duke.edu](mailto:schol@phy.duke.edu)

Coherent elastic neutral current neutrino-nucleus scattering has never been observed. In this process, a neutrino of any flavor scatters off a nucleus at low momentum transfer  $Q$  such that the nucleon wavefunction amplitudes are in phase and add coherently. The cross-section is large, but resulting nuclear recoil energies are below the detection thresholds of most conventional high-mass neutrino detectors. However, in recent years there has been a surge of progress in development of novel ultra low threshold detectors, many with the aim of WIMP recoil detection or pp solar neutrino detection. Thresholds of 10 keV or even lower for detection of nuclear recoils may be possible. A promising source of neutrinos for measurement of coherent elastic cross-sections is that arising from a stopped-pion beam, such as the Spallation Neutron Source (SNS). Monoenergetic 29.9 MeV  $\nu_\mu$ 's are produced from pion decay at rest,  $\pi^+ \rightarrow \mu^+ \nu_\mu$ , and  $\bar{\nu}_\mu$  and  $\nu_e$  from  $\mu^+ \rightarrow \nu_e e^+ \bar{\nu}_\mu$  follow on a muon-decay timescale ( $\tau = 2.2 \mu\text{s}$ .) The neutrino spectral shape is shown in Figure 1. Neutrinos in this energy range will produce nuclear recoils from coherent scattering with tens of keV. If the beam is pulsed in a short ( $< \mu\text{s}$ ) time window, the pion decay  $\nu_\mu$  will be prompt with the beam, and the muon decay products will be delayed. The expected rates for the SNS are quite promising[1]: for a ton-scale detector with a few to 10 keV threshold,  $10^4 - 10^5$  signal events per year are expected: see Figure 1.

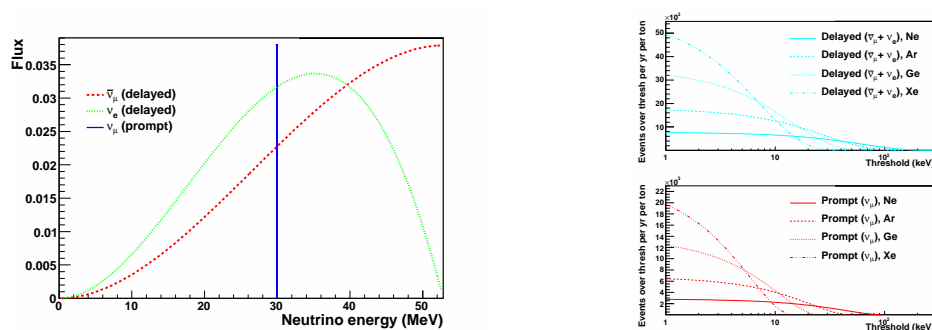


**Figure 1.** Left: SNS spectrum. Right: Expected yield over recoil energy threshold at the SNS (bottom:  $\nu_\mu$ , top: sum of  $\nu_e$  and  $\bar{\nu}_\mu$ .)

The neutrino-nucleus coherent elastic scattering cross-section is cleanly predicted by the Standard Model (SM); therefore a measured deviation from prediction could be a signature of new physics.

[1] K. Scholberg, Phys. Rev. D **73**, 033005 (2006) [arXiv:hep-ex/0511042].

# Optical simulations of a liquid scintillator detector for reactor neutrino experiments

Gabriel Orebi Gann<sup>1</sup>, Stanley Seibert<sup>2</sup> and Christopher Tunnell<sup>3</sup>

<sup>1</sup> Department of Physics, University of Oxford, Oxford, OX1 3RH, UK

<sup>2,3</sup> Department of Physics, University of Texas at Austin, Austin, TX 78712, USA

E-mail: <sup>1</sup>[g.orebi-gann1@physics.ox.ac.uk](mailto:g.orebi-gann1@physics.ox.ac.uk), <sup>2</sup>[volsung@physics.utexas.edu](mailto:volsung@physics.utexas.edu),

<sup>3</sup>[tunnell@mail.utexas.edu](mailto:tunnell@mail.utexas.edu)

**Abstract.** Described below are simulations of certain optical properties of a spherical liquid scintillator reactor neutrino experiment. Considered are the addition of concentrators to the photomultiplier tubes (PMTs) and an LED calibration system.

## 1. Concentrators

A comparison was made of PMTs with and without concentrators in order to determine their effect on the resolving power of the detector. The charge spectra and energy resolution for PMTs with and without concentrators were investigated. For events out to 1.75m radius, the improvement in resolution is fairly constant at 32-33%. Towards the edge of the acrylic vessel the improvement drops because the angular acceptance of the concentrators limits photon collection.

## 2. LED calibration system

A set of LEDs permanently mounted to the PMT support structure would provide a simple, adaptable system for non-intrusive in-situ calibration. The LEDs could continuously monitor PMT timing and optical properties of detector media at different wavelengths. One aim of the system is to be able to extract attenuation lengths of the optical media in the detector. A moveable laser source would be deployed within the detector periodically to establish a baseline set of optics parameters, including the PMT angular response function. The LED system can then be used to continuously monitor the optical quality of the gadolinium-loaded scintillator during normal data taking.

## 3. Conclusions

Adding concentrators to photomultiplier tubes increases light collection by over 80% and improves the energy resolution of the detector by over 30%. In addition, an LED calibration system has been modelled which could be used to monitor the optical stability of the detector, to calibrate PMT timings and to extract attenuation lengths and angular response curves.

## Acknowledgments

The authors wish to thank the Braidwood Collaboration, Glenn Horton-Smith and E. Falk Harris for their contributions.

# High energy neutrino flavor ratios, neutrino mixing angles, and astrophysical diagnostics

**Pasquale Dario Serpico**

Max-Planck-Institut für Physik (Werner-Heisenberg-Institut) — Munich, Germany

E-mail: [serpico@mppmu.mpg.de](mailto:serpico@mppmu.mpg.de)

**Abstract.** Forthcoming neutrino telescopes (NTs) will be sensitive to the flavor content of high energy neutrino fluxes. We have shown that, when accounting for current experimental ranges for neutrino mixing parameters, astrophysical sources may present a more rich phenomenology than usually thought. In particular, one might access model-independent information on neutrino mixing parameters at km<sup>3</sup> NTs, like the octant of  $\theta_{23}$ . Ongoing and planned laboratory neutrino experiments will help us to shed light on the properties of cosmic accelerators.

The flavor ratios of high energy neutrino fluxes have been recognized as an important tool for astrophysical diagnostics or to probe new physics. We have recently pointed out that, even barring the possibility of exotic physics, varying the neutrino mixing parameters in the experimentally allowed regions a much rich phenomenology than previously thought is possible. In particular, peculiar astrophysical sources like neutron or muon-damped beams may be identified unambiguously at neutrino telescopes and might even allow one to determine in a model-independent way qualitative features of neutrino mixing parameters, like the octant of  $\theta_{23}$  or the existence of a non-vanishing  $\{\theta_{13}, \delta_{\text{CP}}\}$  sector [1,2]. To that purpose, a  $\mathcal{O}(10\%-20\%)$  determination of the ratio of track to shower events at km<sup>3</sup> Cherenkov NTs may suffice. In less fortunate cases, one might still gain insights on the neutrino mixing parameters from combining the information to be collected at the next generation reactor and accelerator experiments with the one from astrophysical neutrino fluxes [3]. This is due to the significantly different dependence on the mixing parameters for the two kinds of sources. For the fluxes arriving at a NT matter effects are negligible because of the extremely low densities of cosmic environments, and the interference terms sensitive to the mass splittings and to the sign of  $\delta_{\text{CP}}$  (i.e. the CP-violating terms) average out because the distances involved far exceed the experimentally known oscillation lengths.

From a complementary perspective, accurate laboratory measurements of the neutrino mixing parameters are relevant to perform astrophysical diagnostics, not to mention searches for new physics: Since the flux flavor ratios *do depend* on mixing angles, degeneracies with astrophysical parameters exist. A synergy between NTs and the Lab may help to understand better both neutrino physics and the mechanisms and environments of the cosmic accelerators.

## References

- [1] P. D. Serpico and M. Kachelrieß, Phys. Rev. Lett. **94**, 211102 (2005) [hep-ph/0502088].
- [2] P. D. Serpico, Phys. Rev. D **73**, 047301 (2006) [hep-ph/0511313].
- [3] W. Winter, hep-ph/0604191.

## Borexino Geo/Solar Antineutrino discovery potential (on the basis of CTF results)

**O. Yu. Smirnov<sup>a</sup> and A. Ianni<sup>b</sup>, for the Borexino collaboration**

a)Joint Inst. for Nuclear Research, 141980 Dubna, Russia

E-mail: [osmirnov@jinr.ru](mailto:osmirnov@jinr.ru)

b)INFN, Gran Sasso Laboratory, S.S. 17-bis Km 18+910 67010 Assergi, Italy

E-mail: [aldo.ianni@lngs.infn.it](mailto:aldo.ianni@lngs.infn.it)

The Counting Test Facility [1], CTF, is 4 tones prototype of the Borexino [2] Solar neutrino detector. Despite of its relatively small size the CTF detector demonstrated sensitivity to a number of processes in a field of rare events physics. Here we report results of recent studies devoted to the search for the antineutrino interactions in the CTF [3].

The inverse beta-decay of the antineutrino  $\bar{\nu}_e + p \rightarrow n + e^+$  is a dominant type of antineutrino interactions in liquid scintillator detectors. The capture of the thermalized neutron on the proton  $n + p \rightarrow d + \gamma$  with a mean life-time of  $\sim 250 \mu\text{s}$  and energy release  $E_\gamma = 2.2 \text{ MeV}$  provides a robust tag for this reaction in low-threshold LS detector.

One antineutrino candidate event was observed during 7.8 ton x year exposure of the CTF detector with an expected background of  $0.8 \pm 0.3$  from the known sources. This implies that an upper limit on solar neutrino transition probability  $\nu \rightarrow \bar{\nu}$  is no more than 0.02 at 90% C.L. The limit, being weaker than that of other experiments, is the first one that includes the low energy region above the inverse beta-decay energy of  $E > 1.8 \text{ MeV}$ . The expected Borexino sensitivity to electron antineutrino from the Sun with 5 years x 300 ton of Borexino exposure is at the level of  $10^{-5}$ .

An upper bound on the terrestrial Uranium antineutrino flux,  $\Phi(U)$ , that can be obtained using the same data is  $1.8 \times 10^8 \text{ cm}^{-2}\text{s}^{-1}$ . KamLAND's current upper limit is 20 times better with an exposure approximately 150 times greater. The CTF result shows how important the purity of the LS and a low reactor background are for the detection of geoneutrinos. Borexino is expected to have even lower radioactive contamination than CTF and the same specific background from reactors. In addition, the Borexino detector is located at the LNGS far away from the nuclear reactors (the mean distance from the nuclear reactors is  $\simeq 800 \text{ km}$ ), and has an advantage of lower antineutrino background in comparison to the KamLAND detector. The expected signal in Borexino for a LS target mass of 300 tons in the 1.0-2.6 MeV energy range is 5.7 events from reactor antineutrinos and 6.3 from geoneutrinos for one year of data taking. The relative precision of the geoneutrino flux measurements, estimated using available data is  $\sim 25\%$  in five years.

Together with KamLAND data, the Borexino measurements will provide unique information on the distribution of U and Th in the Earth interior.

[1] Borexino collaboration, A. Alimonti et al., NIM A406 (1998)411.

[2] Borexino collaboration, A. Alimonti et al., Astrop. Phys. 16(2002)205-234.

[3] Borexino collaboration, M.Balata et al., to appear in EJP C, 2006.

# Large neutrino mixing from small flavor mixing

G. J. Stephenson, Jr.<sup>1</sup>, T. Goldman<sup>2</sup> and B. H. J. McKellar<sup>3</sup>

<sup>1</sup>Physics and Astronomy, University of New Mexico, Albuquerque, NM 87545, USA,

<sup>2</sup>T-16/MS-B283 Theoretical Division, Los Alamos National Laboratory, POB 1663, Los Alamos, NM 87545, USA, <sup>3</sup>University of Melbourne, Parkville, Victoria 3052, Australia

E-mail: <sup>1</sup>GJS@phys.unm.edu, <sup>2</sup>tgoldman@lanl.gov, <sup>3</sup>b.mckellar@physics.unimelb.edu.au

**Abstract.** We show that, in a general quark-lepton symmetric scenario, large MNS mixing among active neutrino flavors can be induced by small mixing in the sterile sector with CKM or smaller mixing in the Dirac mass sector. The model independent bound does not show any conflict between  $\nu_e$ - and  $\nu_\mu$ -disappearance limits and the LSND rate for  $\nu_e$ -appearance from a  $\nu_\mu$  beam.

Quark-lepton symmetry requires that the three pairs of Weyl spinors describing the quarks and charged leptons be matched in the neutrino sector where only three Weyl spinors describing the active neutrinos reside in the Standard Model. These three additional Weyl spinors encompass sterile neutrinos which may have an arbitrary Majorana mass matrix. We have found[1] that when the rank of this matrix is one, the neutrino mass eigenstates form two pseudo-Dirac pairs as well as one very light and one very heavy Majorana neutrino in the typical seesaw form[2]. As we have also shown analytically in the simpler two-flavor case, it is then straightforward to find wide parameter ranges wherein a small misalignment between the flavor bases in the active and sterile neutrinos produces a large mixing among the active flavor states. This occurs with or without the analog of CKM mixing in the Dirac mass matrix that couples the active and sterile states.

We have also derived a model-independent bound on the probability for  $\nu_e$ -appearance from a  $\nu_\mu$  beam,  $P(\nu_\mu \rightarrow \nu_e)$ , using the limits on  $\nu_e$ - and  $\nu_\mu$ -disappearance,  $1 - P(\nu_e \rightarrow \nu_e)$  and  $1 - P(\nu_\mu \rightarrow \nu_\mu)$  from experiments[3, 4]. Ignoring CP violation, this bound is

$$P(\nu_\mu \rightarrow \nu_e) < \sqrt{[1 - P(\nu_e \rightarrow \nu_e)][1 - P(\nu_\mu \rightarrow \nu_\mu)]} \quad (1)$$

which is weaker than the model-dependent bounds derived from sequential fits of two-channel mixing in experiments. The LSND result is consistent with this bound.

## Acknowledgments

This research is supported in part by the Department of Energy under contract W-7405-ENG-36, the National Science Foundation under NSF Grant #PHY0099385 and the Australian Research Council.

[1] Stephenson, Jr. G J, Goldman T, McKellar B H J and Garbutt M 2005 *Int. J. Mod. Phys. A* **20** 6373

[2] Mohapatra R N and Senjanovic G 1980 *Phys. Rev. Lett.* **44** 912

[3] CHOOZ Collaboration 1997 *Phys. Lett. B* **240** 397

[4] Rebel B J for the MINOS Collaboration 2007 First MINOS Results with the NuMI Beam, *Preprint hep-ex/0701049*

# Neutrinos and electrons in background matter

**Alexander Studenikin**

Department of Theoretical Physics and Skobeltsyn Institute of Nuclear Physics, Moscow State University, 119992 Moscow, Russia

E-mail: studenik@srd.sinp.msu.ru

**Abstract.** We present a rather powerful method in investigations of different phenomena that can appear when neutrinos and electrons propagate in background matter. This method is based on the use of the modified Dirac equations for particles wave functions, in which the correspondent effective potentials accounting for the matter influence on particles are included.

Within the standard model interaction of electron neutrinos and electrons with matter composed of neutrons, the modified Dirac equations are [1, 2, 3]

$$\left\{ i\gamma_\mu \partial^\mu - \frac{1}{2}\gamma_\mu (c_l + \gamma_5) \tilde{f}^\mu - m_l \right\} \Psi^{(l)}(x) = 0, \quad (1)$$

where for the case of neutrinos  $m_l = m_\nu$  and  $c_l = c_\nu = 1$ , whereas for electrons  $m_l = m_e$  and  $c_l = c_e = 1 - 4\sin^2 \theta_W$ . For unpolarized matter  $\tilde{f}^\mu = \frac{G_F}{\sqrt{2}}(n_n, n_n \mathbf{v})$ ,  $n_n$  and  $\mathbf{v}$  are, respectively, the neutron number density and average speed. We have obtained the wave functions for neutrinos and electrons in the following form [1, 2, 3]

$$\Psi_{\varepsilon, \mathbf{p}, s}^{(l)}(\mathbf{r}, t) = \frac{e^{-i(E_\varepsilon^{(l)} t - \mathbf{p}\mathbf{r})}}{2L^{\frac{3}{2}}} \begin{pmatrix} \sqrt{1 + \frac{m_l}{E_\varepsilon^{(l)} - c\alpha_n m_l}} \sqrt{1 + s \frac{p_3}{p}} \\ s \sqrt{1 + \frac{m_l}{E_\varepsilon^{(l)} - c\alpha_n m_l}} \sqrt{1 - s \frac{p_3}{p}} e^{i\delta} \\ s\varepsilon \sqrt{1 - \frac{m_l}{E_\varepsilon^{(l)} - c\alpha_n m_l}} \sqrt{1 + s \frac{p_3}{p}} \\ \varepsilon \sqrt{1 - \frac{m_l}{E_\varepsilon^{(l)} - c\alpha_n m_l}} \sqrt{1 - s \frac{p_3}{p}} e^{i\delta} \end{pmatrix}, \quad (2)$$

where the energy spectra are

$$E_\varepsilon^{(l)} = \varepsilon \sqrt{\mathbf{p}^2 \left(1 - s\alpha_n \frac{m}{p}\right)^2 + m^2} + c_l \alpha_n m_l, \quad \alpha_n = \frac{1}{2\sqrt{2}} G_F \frac{n_n}{m_l}, \quad (3)$$

here  $p$ ,  $s$  and  $\varepsilon$  are particles momenta, helicities and signs of energy, respectively.

The developed approach establishes a basis for investigation of different phenomena which can arise when neutrinos and electrons move in dense media, including those peculiar for astrophysical and cosmological environments. In particular, within this approach we have investigated new types of electromagnetic radiation which can be emitted by neutrinos and electrons moving in dense matter (the ‘‘spin light’’ of neutrino and electron in matter,  $SL\nu$  and  $SLe$ ).

[1] Studenikin A and Ternov A 2005 *Phys.Lett. B* **608** 107

[2] Grigoriev A, Studenikin A and Ternov A 2005 *Phys.Lett. B* **622** 199

[3] Studenikin A 2006 *J.Phys.A: Math. Gen.* **39** 6769

## KASKA experiment: A reactor $\sin^2 2\theta_{13}$ project

H Furuta<sup>9</sup>, K Akiyama<sup>5a</sup>, M Aoki<sup>6</sup>, Y Fukuda<sup>5</sup>, Y Funaki<sup>9</sup>, T Hara<sup>3</sup>,  
 T Haruna<sup>10</sup>, N Ishihara<sup>1</sup>, M Katsumata<sup>6</sup>, T Kawasaki<sup>6</sup>, M Kuze<sup>9</sup>,  
 J Maeda<sup>9</sup>, T Matsubara<sup>9</sup>, T Matsumoto<sup>10b</sup>, H Miyata<sup>9</sup>, Y Nagasaka<sup>2</sup>,  
 T Nakagawa<sup>10c</sup>, N Nakajima<sup>6</sup>, H Nakano<sup>6</sup>, K Nitta<sup>9</sup>, Y Nomachi<sup>4</sup>,  
 K Sakai<sup>6</sup>, Y Sakamoto<sup>7</sup>, K Sakuma<sup>10d</sup>, F Suekane<sup>8</sup>, T Sumiyoshi<sup>10</sup>,  
 H Tabata<sup>8</sup>, N Tamura<sup>6</sup> and Y Tsuchiya<sup>8</sup>

<sup>1</sup> High Energy Accelerator Research Organization (KEK), <sup>2</sup> Hiroshima Inst. of Tech., <sup>3</sup> Kobe Univ., <sup>4</sup> Osaka Univ., <sup>5</sup> Miyagi Univ. of Education, <sup>6</sup> Niigata Univ., <sup>7</sup> Tohoku Gakuin Univ., <sup>8</sup> Tohoku Univ., <sup>9</sup> Tokyo Inst. of Tech., <sup>10</sup> Tokyo Metropolitan Univ.

Present address: <sup>a</sup> Tohoku U., <sup>b</sup> KEK, <sup>c</sup> Hewlett-Packard, Japan, <sup>d</sup> Ministry of Economy, Trade and Industry of Japan.

E-mail: furuta@nucl.phys.titech.ac.jp

**Abstract.** KASKA is a reactor neutrino experiment to measure  $\theta_{13}$  accurately. The sensitivity reach of  $\sin^2 2\theta_{13}$  will be 0.015 in its first phase. Higher accuracy  $\theta_{13}$  measurement, precise  $\theta_{12}$  measurement and first  $\Delta m_{13}^2$  measurement are also in consideration in future extensions of the experiment. A brief description of the KASKA project and its R&D activities are presented.

One of the most urgent issues in neutrino physics now is to measure the last neutrino mixing angle  $\theta_{13}$ .  $\sin^2 2\theta_{13}$  can be measured by disappearance rate of  $\bar{\nu}_e$  flux at a distance of 1~2 km from reactors. KASKA experiment improves the sensitivity by one order of magnitude compared with the current limit using the world largest nuclear reactor complex, Kashiwazaki-Kariwa nuclear power station and optimum baseline and near/far-detector systematic cancellations. A detailed description of the KASKA experiment is shown in the reference-[1]. A 70 m deep boring study was performed at a near detector location in Kashiwazaki-Kariwa nuclear power station. Cosmic-rays and  $\gamma$ -ray backgrounds as well as geology were measured using plastic scintillators and a NaI counter [2]. Both types of backgrounds data were consistent with expectation and used to tune the Monte Carlo simulations for KASKA detector development. A prototype detector made of 120 cm diameter acrylic sphere which is viewed by 16 8" photomultipliers was constructed to study properties of KASKA detector. The efficiency of the  $\gamma$ -catcher layer [1] for  $\gamma$ -rays from neutron absorption on Gd was studied by putting an Am/Be source at the center of the sphere. A clear 8 MeV peak and a low energy tail due to escape  $\gamma$ s were observed in the energy spectrum. Since the energy combination of the cascade  $\gamma$ 's from neutron absorption on Gd is not well known, these data are important to evaluate detector performance. The prototype was moved to the Joyo reasearch fast reactor, whose thermal power is 140 MW, and is now placed at a distance of 25 m from the reactor core to detect plutonium-rich reactor  $\bar{\nu}_e$ . The data taking is expected to start from the fall of 2006.

[1] KASKA Collaboration, 'Letter of Intent for KASKA', hep-ex/0607013.

[2] H.Furuta et. al., to appear on Nucl. Instr. Meth., hep-ex/0607015.

# A CDM candidate in supersymmetric extra U(1) models<sup>1</sup>

**Daijiro Suematsu**

Institute for Theoretical Physics, Kanazawa University, Kanazawa 920-1192, Japan

E-mail: suematsu@hep.s.kanazawa-u.ac.jp

**Abstract.** A singlino dominated neutralino is studied as a CDM candidate in supersymmetric models with a  $Z'$  in TeV regions. If a gaugino for the  $Z'$  is much heavier than other gauginos, the lightest neutralino can be dominated by a singlino. Assuming that and imposing the CDM abundance required from the WMAP data, we predict masses of the  $Z'$ , the lightest neutralino and neutral Higgs scalar. These models can be a good target in LHC experiments.

Recent astrophysical observations suggest the existence of cold dark matter (CDM). This means that the SM should be extended. Here we consider supersymmetric extra U(1) models which can resolve the famous  $\mu$  problem in the MSSM. In comparison with the MSSM these models have additional fields in each sector of neutral gauge fields, neutral Higgs fields and neutralinos. Since these extended sectors affect composition of the lightest neutralino and its interaction, the annihilation cross section can behave differently from that in the MSSM.

In order to study these aspects, we consider a case that the lightest neutralino is singlino dominated by assuming that a gaugino for the extra U(1) is much heavier than other gauginos [1]. Since their annihilation processes are expected to be mediated through a  $Z'$  exchange and an additional Higgs exchange, phenomenologically allowed parameter regions are expected to be shifted from those in the MSSM.

In this study we adopt an extra U(1) whose charge  $Q_x$  is defined as linear combinations of  $U(1)_\psi$  and  $U(1)_\chi$  derived from  $E_6$  as  $Q_x = Q_\psi \cos \theta - Q_\chi \sin \theta$ . Imposing phenomenological constraints such as the CDM abundance predicted from the WMAP data, neutral Higgs mass bound,  $Z'$  mass bound, chargino mass bound, sfermion mass bound and so on, we find that the allowed parameter space appears in different regions from those in the MSSM [2]. The models may be examined in the forth coming LHC experiments through detection of the  $Z'$  and masses of the neutral Higgs scalar and neutralinos.

## References

- [1] Suematsu D 2006 *Phys. Rev. D* **73** 035010
- [2] Nakamura S and Suematsu D 2006 Supersymmetric extra U(1) models with a singlino dominated LSP *Preprint hep-ph/0609061*

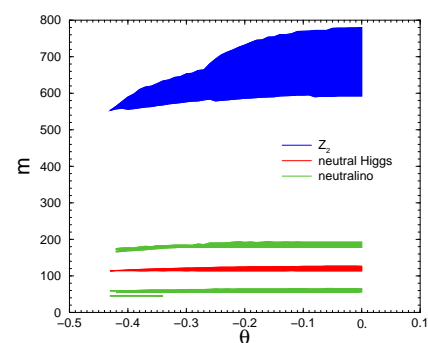


**Figure 1.** Masses of the  $Z'$ , the lightest neutral Higgs and the lightest neutralino.

<sup>1</sup> This is partially based on the work with S. Nakamura and supported by a Grant-in-Aid for Scientific Research (C) from the Japan Society for Promotion of Science (No.17540246).

## Search for supernova burst neutrino

**A. Takeda<sup>a</sup> and M. Ikeda<sup>b</sup> on behalf of the Super-Kamiokande Collaboration**

<sup>a</sup>Institute for Cosmic Ray Research, University of Tokyo, Japan

<sup>b</sup>Department of Physics, Okayama University, Japan

E-mail: [takeda@suketto.icrr.u-tokyo.ac.jp](mailto:takeda@suketto.icrr.u-tokyo.ac.jp)

**Abstract.** A search for the supernova burst neutrinos was conducted using data from the Super-Kamiokande (SK) detector. We used the data set of SK taken from May 1996 to July 2001 (SK-I) and from December 2002 to October 2005 (SK-II). There is no evidence of such a supernova explosions during the data period. The preliminary 90% C.L. upper limit on the rate of supernova explosions out to distances of 100 kiloparsecs is found to be  $< 0.32 \text{ SN} \cdot \text{year}^{-1}$ . In addition of the 4.26 year's worth of data from Kamiokande-II and III, the limit on the rate of supernova explosions within our galaxy is determined to be  $< 0.20 \text{ SN} \cdot \text{year}^{-1}$ .

Super-Kamiokande (SK) detector is an imaging water Čerenkov detector containing 50,000 tons of pure water [1]. The data used in this analysis was taken in two periods. The first period referred to as Super-Kamiokande-I (SK-I) is from 1st of April, 1996, to 15th of July, 2001 with 40% photo coverage. The second period, Super-Kamiokande-II (SK-II) is from 10th of December, 2002, to 6th of October, 2005 with 19% photo coverage. Because of rapid variation of the water transparency, the data before the 31st of May, 1996 in SK-I, and the data before the 23rd of December, 2002 in SK-II have not been used for analysis due to uncertainties in the energy calibration. Vertex and energy reconstruction techniques are the same as those used in our solar neutrino analysis [2]. Fiducial volume for the supernova search is also 22.5 kton, though the energy thresholds are 6.5 MeV for SK-I and 7.0 MeV for SK-II data.

SK is sensitive to type II supernova explosions via mainly  $\bar{\nu}_e + p \rightarrow e^+ + n$  reaction. According to the calculation performed by the Livermore group [3], during the initial 10 mil-

liseconds of explosions, electron neutrino generated in the neutronization burst can be main component, and expected to be observed via elastic scattering,  $\nu_x + e^- \rightarrow \nu_x + e^-$ . After the neutronization, all flavors of neutrinos are produced by electron-positron annihilation.

We searched for time-clustered events in the obtained data using several time windows referring to the time profile.

- (i) Model-independent windows: Thresholds are 3, 4, and 8 events per 0.5, 2 and 10 seconds, respectively. Time-clustered events which is independent from any supernova model were searched.
- (ii) Short time windows: Thresholds are 2 events per 1, 10, and 100 milliseconds. The physics motivation of this short time window search is to detect a neutronization burst which is supposed to be a prompt burst of  $\nu_e$  in a supernova neutrino burst.
- (iii) Long time windows: Threshold is 2 events per 20 seconds. The energy threshold was set to 17 MeV to obtain the maximum value of (detection

probability)/ $\sqrt{(\text{number of chance coincidence})}$ As the result, we conclude that there was

To distinguish real signals from background clusters, a spatial distribution ( $R_{mean}$ ) cut was applied to candidate clusters.  $R_{mean}$  is defined by the averaged spatial distance between each event. Since actual neutrinos from a supernova explosion interact with free protons and the resulting positions are generated uniformly in the detector,  $R_{mean}$  should have a larger value than that resulting from spatially clustered events such as spallation products. In addition, for the short time window search, a direction distribution ( $Sumdir$ ) cut was also applied because the main reaction is neutrino-electron scattering and the recoiled electrons have almost the same direction as in incident neutrinos.  $Sumdir$  is defined by the vector sum of reconstructed direction vectors of each event divided by multiplicity of the cluster, and should be close to 1 in the case of real supernova cluster.

no real signal of supernova burst during the data taking period between April 1996 and December 2005 which corresponds to live-time 2589.2 days. The preliminary 90% C.L. upper limit on the rate of supernova explosions out to distances of 100 kiloparsecs is found to be  $< 0.32 \text{ SN} \cdot \text{year}^{-1}$ . In addition of the 4.26 year's worth of data from Kamiokande-II and III [4], the limit on the rate of supernova explosions within our galaxy is determined to be  $< 0.20 \text{ SN} \cdot \text{year}^{-1}$ .

- [1] S. Fukuda *et al.*, Nucl. Instr. and Meth. **A 501** (2003) 418.
- [2] Y. Fukuda *et al.*, Phys. Rev. Lett. **81** (1998) 1158; S. Fukuda *et al.*, Phys. Rev. Lett. **86** (2001) 5651.
- [3] T. Totani *et al.*, Phys. Rev. Lett. **80** (1998) 2039
- [4] Y. Suzuki, in *Proc. of the International Symposium on Neutrino Astrophysics: Frontiers of Neutrino Astrophysics*, edited by Y. Suzuki and K. Nakamura, (Universal Academy Press Inc., Tokyo, 1993), number 5 in Frontier Science Series, p. 61.

# **Muon Simulations for Super-Kamiokande, KamLAND and CHOOZ**

*Alfred Tanq<sup>1</sup>, Glenn Horton-Smith<sup>1</sup>, Vitaly A. Kudryavtsev<sup>2</sup> and Alessandra Tonazzo<sup>3</sup>*

*<sup>1</sup>Kansas State University, USA*

*<sup>2</sup>University of Sheffield, UK*

*<sup>3</sup>APC and Université Paris, France*

## Energy calibration and monitoring of the KATRIN experiment

T Thuemmler<sup>1</sup>, M Beck<sup>1</sup>, J Bonn<sup>2</sup>, B Hillen<sup>1</sup>, H W Ortjohann<sup>1</sup>, B Ostrick<sup>1,2</sup>, E W Otten<sup>2</sup>, M Prall<sup>1</sup>, N Titov<sup>1</sup> and C Weinheimer<sup>1</sup> for the KATRIN collaboration

<sup>1</sup> Nuclear Physics Institute, University of Muenster, 48149 Muenster, Germany

<sup>2</sup> Physics Institute, University of Mainz, 55128 Mainz, Germany

E-mail: [thuemmler@uni-muenster.de](mailto:thuemmler@uni-muenster.de), [weinheimer@uni-muenster.de](mailto:weinheimer@uni-muenster.de)

**Abstract.** A new high precision voltage divider has been built for monitoring the analysing potential of the KATRIN main spectrometer. In addition a condensed <sup>83m</sup>Kr calibration source has been set up at the modified 1 eV resolving Mainz spectrometer, our measurements show that energy calibration and monitoring for KATRIN is feasible at the few ppm level.

The KATRIN experiment aims for a sensitivity of 0.2 eV on the absolute mass of the electron anti-neutrino using a high luminosity windowless gaseous tritium source and an electrostatic retardation spectrometer of MAC-E-Filter type [1]. For the aimed sensitivity the few systematic uncertainties have to be limited to  $\Delta m^2 < 0.007 \text{ eV}^2$ , as simulation studies show. This value is connected to a gaussian fluctuation  $\sigma$  of the high voltage (HV) by  $\Delta m_\nu^2 = -2 \cdot \sigma^2$ . Hence it is crucial to monitor and calibrate the HV at the endpoint of the tritium  $\beta$ -spectrum of 18.6 keV with few ppm precision and stability. Devices capable of this are not commercially available, so we set up a new precision high voltage divider in cooperation with PTB (German National Metrology Institute) [2]. Carefully selecting 100 precision resistors and matching them according to warmup drift and temperature coefficient leads to an overall drift at the sub-ppm level. The resistors are housed inside a shielded stainless steel vessel filled with temperature controlled and circulating N<sub>2</sub> insulation gas. A second divider for field shaping electrodes and a third pure capacitive one to prevent damage by voltage spikes are included. Calibration of the divider setup at PTB yields sub-ppm stability for up to 35 kV. The spectrometer setup of the former Mainz Neutrino Mass Experiment has been modified to 1 eV resolution and will serve as a monitor spectrometer connected to the KATRIN analysing potential. Several calibration sources with monoenergetic and quasi-monoenergetic electrons close to the tritium endpoint energy are under development at different collaboration institutes [3]. Measurements have been performed using a condensed <sup>83m</sup>Kr source on a graphite substrate attached to the Mainz spectrometer. Preliminary results for the K-32 conversion electrons at 17.824 keV show a reproducibility and medium term stability of < 3 ppm. We conclude that it is feasible to calibrate and monitor the retarding potential of the KATRIN main spectrometer online at ppm level. Supported by the German BMBF (05CK5MA/0) and by the virtual institute VIDMAN of HGF.

[1] Angrik J *et al* KATRIN design report 2004 *FZK Scientific Report* **7090** <http://www-ik.fzk.de/katrin>

[2] Marx R 2001 *IEEE Transactions on Instr. and Meas.* **50** No. 2 426

[3] Dragoun O *et al* 2004 *Czech J. Phys.* **54** 833

# Application of the diffraction phenomenon for increasing the neutrino flux density

V.A. Trapeznikov<sup>1,2</sup>

<sup>1</sup>Physical-technical Institute, the Ural Branch of the Russian Academy of Sciences, 132 Kirov Str, Izhevsk, 426001, Russia

<sup>2</sup>The Udmurt State University, Izhevsk, 426034, Russia

E-mail: xps@fti.udm.ru

**Abstract.** The investigations of the neutrino physics are connected with great difficulties due to an extremely small section of the interaction of neutrino with a substance. It necessitates enlarging the volumes of a detecting substance to huge sizes. An increase in the density of low-energy neutrino at the detector entrance by several orders (to 1 MeV) is offered with the use of the diffraction phenomenon on the bent crystals in neutrino spectrometers in accordance with the inverse schemes of the methods of Johann and Cauchois. This scheme was used for investigating x-ray radiation from the source situated beyond the focal circle at an unlimited distance from the spectrometer [1]. For the neutrino investigation a large number of crystals with crystal-holders will be needed; the crystal-holders should be situated on one platform with a general direction of a cumulative neutrino beam towards one detector.

**Key words:** section of interaction of neutrino and substance, inverse  $\beta$ -decay, x-ray and neutrino diffraction, x-ray spectrometer with bent crystals, inverse scheme of the methods of Johann and Cauchois, neutrino spectrometer.

## 1. Introduction

The investigations of the neutrino physics are connected with great difficulties due to an extremely small section of the interaction of neutrino with a substance. It necessitates enlarging the volumes of a detecting substance in experimental set-ups to huge amounts equal to tens of thousand tons like for the “Super-Kamiokande” device [2] or using tens of thousands of cubic kilometers of seawater for recording neutrino [3] or using some other similar devices [4].

Parallel to increasing the capacities of the detector for the neutrino registration, it is offered to increase the density of the low-energy neutrino flux by several orders of magnitude (to 1 MeV) at the detector entrance by the application of the diffraction phenomenon on bent crystals in accordance with the methods of Johann [5] and Cauchois [6]; the methods involve the inverse scheme like in the investigation of x-ray-radiation coming from the source placed beyond the focal circle at an unlimited distance from the detector [1]. From this experimental method, only its slitless part is used since there is no slit that can become an obstacle for neutrino.

In the case of the neutrino experiment, using a set-up with a significant number of crystals with respective crystal-holders is offered; the crystal-holders are situated on one platform with a general direction of a cumulative neutrino beam towards one detector.

The adjustment of this system is carried out with the help of x-ray radiation with the quantum energy corresponding to the energy of studied neutrino, which is obtained from the  $\beta$ -decay spectra by their mirror reflection (see figure 1).

In this case, the sum of the energies of the  $\beta$  and  $\nu$  spectra, the intensities of which are equal, is equal to the maximal energy of the  $\beta$ -spectrum (without losses to neutrino); the  $\beta$  and  $\nu$  spectra are situated on different sides relative to the reflection axis. In the experiment under discussion, it is suggested that at  $\beta$ -decay, one neutrino falls on one electron. In the general case, it is admitted that “more than one neutrino” can fall on one emitted electron during  $\beta$ -decay [8].

The experimental set-up for the  $\beta$ -decay investigation is based on a 100 cm x-ray electron magnetic spectrometer with adapters [9, 10] or a 10-cm spectrometer for a portable variant [11].

## 2. The x-ray experiment

Let us discuss some experimental results on obtaining x-ray spectra on the spectrometer with bent crystals in accordance with Johann's method in order to analyze the radiation beyond the focal circle [1].

To determine the capacities of the spectrometer based on the inverse scheme, a vacuum x-ray spectrometer [12] with the ion registration was used, which was designed for the operation in accordance with the usual scheme (figure 2a). The device (figure 2b) was altered by placing an x-ray tube and a counter SBT-9 on the holder for a cathode (the cathode was removed) and by setting a standard slit UF-13 with variable width from 0.1 to 4 mm in the focus on the circle. An irradiator was placed either directly behind the slit or at the distance of several centimeters from it. The irradiators were x-ray tubes BSV-E with copper and cobalt anodes with the focus size of  $\sim 1.5$  mm or a Co-plate acting as an anode in the fluorescent method, which was irradiated by copper irradiation from a tube BHV-7. The plate surface of  $\varnothing \sim 15$  mm was irradiated.

$K\alpha_{1,2}$  doublets of Co and Cu and  $K\beta_{2,5}$  – line of Cu were registered. In the primary and secondary methods, the operation modes of the x-ray tubes were 12 kV, 14 mA and 21 kV, 30 mA, respectively. The radiation analyzers were quartz crystals, in which the reflections were from the surface  $(1\bar{3}\bar{4}0)$ ,  $R = 720$  mm, and mica,  $R = 470$ . The counter window was at the distance of 50 mm from the crystal. In the primary method, the time of the radiation registration at one point was 15 s, and in the secondary method, it was 1 – 2 min. In the experiments, the crystal was scanned when the rest of the set-up assemblies were immobile, or the slit was scanned when the other set-up assemblies were immobile.

The primary and secondary Co-spectra obtained when the crystal was scanned at different widths of the slit are shown in fig. 3a and b, where the quantum energy  $E$  is plotted down the abscissa axis, and the radiation intensity, imp./s, is plotted down the ordinate axis.

In figure 3, one can see that at a forty-fold increase in the slit width, i.e., when it is practically absent, a spectrum is observed. However, its resolution is significantly worse and the intensity ratio 'signal - background' decreases by a factor of 5 due to the significant background intensity growth. We believe that the latter will not take place in a neutrino experiment because of a very small section of the interaction of neutrino with a substance and, consequently, because of the absence of the neutrino scattered radiation.

## 3. Low-energy neutrino diffraction

It seems more convenient to start the problem statement in the investigation of the neutrino physics by means of the diffraction on crystals with the estimation of the advantages of using low-energy neutrino (up 1 MeV) in comparison with the use of high-energy neutrino (more than 1 MeV with the appearance of Cerenkov's effect).

According to the data of work [4], for the electron neutrino with the energy of 1 MeV, the state density of the reactor neutrino is better than for the high-energy electron neutrino with the energy of 10 MeV (see figure 4). As it follows from fig. 4, the density of states,  $N_{\nu_e}$ , is decreasing by four orders with the energy increase in the range of 1 – 10 MeV.

The registration of the track appearance from the high-energy neutrino, when Cerenkov's effect takes place, corresponds to 'one neutrino – one track' pattern. For the low-energy neutrino, which are larger in number by four orders than the high-energy ones, the number of excited electrons increases by two orders more due to the appearance of Auger and Coster-Cronig effects for heavy atoms. For example, for lead, more than 540 Auger-transitions are known. The gain in the number of registered electrons is six orders of magnitude for the case of the use of low-energy neutrino. At the same time, the appearance of Cerenkov's effect is known as most probable for neutrino large energies. Thus, the competition between low- and high-energy neutrino is in favor of low-energy neutrino.

The main advantage of the use of low-energy neutrino is the possibility of the crystal application for their diffraction, i.e. for increasing the density of the neutrino beam. For high-energy neutrino, the wave-length ( $\lambda$ ) in Bragg-Wolf equation  $n\lambda = 2d \cdot \sin \vartheta$  will be too small, which will not allow using this method due to significantly high orders of reflection ( $n$ ) that will negatively influence the intensity.

The set-up scheme for the investigation of the neutrino diffraction consists of the following main assemblies: 1 – neutrino source; 2 – programmed device for establishing the crystals in the position necessary for carrying-out the neutrino diffraction and the direction of neutrino from separate crystals to the “gathering point”; 3 – assembly of all the crystals in the form of a cube with the number of crystals needed for the signal appearance from the source; the number of crystals equals to the cube of one from the natural numbers or more (1, 8, 27, 64, 125...1000...10<sup>6</sup>...); 4 – cumulative neutrino flux directed into the detector; 5 – neutrino detector that is a thick-walled tube from superconducting material, for example, lead oxide, with a built-in quadrupole lens placed along the tube centre, which directs electrons to the electron spectrometer; 6 – 100 cm electron magnetic spectrometer.

For the neutrino spectrum investigation at  $\beta$ -decay of tritium, the most suitable crystal is quartz, the prism face of which is (1010), the interplanar distance is 4.2 Å with the interval of the spectrum investigations from 0.3 to 8 Å, which is quite sufficient for the investigation of the most intensive part of the neutrino spectrum.

The entire system for neutrino diffraction is adjusted with the help of the x-ray radiation with the energy corresponding to the neutrino energy.

For registering the neutrino spectrum with the help of the electron spectrum on the 100 cm electron magnetic spectrometer, the simultaneous registration of all regions of the spectrum is provided with the use of multi-anode micro-channel plates. When it is necessary to receive a very weak signal arising due to the appearance of a neutrino source, the entire system of micro-channel plates closes on one anode.

In addition to scanning separate crystals within the aperture angle of the quadrupole lens, the scanning of the entire cube with the crystals within several grades is provided. The scanning of the entire set-up containing the 10 cm electron spectrometer where the large compensation Helmholtz coils are replaced by smaller ones is also possible, when it is placed on a movable platform, which gives the opportunity to receive neutrino signals within the whole planet Earth and beyond its bounds.

When the number of crystals is sufficient for focusing neutrino beams, a new renewable neutrino energy source will be obtained on the steam generator receptor.

#### 4. Acknowledgments

The author expresses his gratitude for helpful discussion of the article and for the assistance in work to I.N. Shabanova, V.A. Zhuravlev, B.A. Budenkov, N.S. Terebova, L.G. Makarova and G.P. Kiyko.

#### References

- [1] Trapeznikov V.A., Sapozhnikov V.P. 1970 The application of the x-ray spectrometer with a bent crystal for analyzing the radiation that is beyond the focal circle *Pribory i tekhnika eksperimenta*, **3**, 227
- [2] Totsuka Y. 1987 University of Tokio Report NJCCR- Report 227-90-20
- [3] Lo Presti 2000 Low Power Electronics for a Submarine Neutrinos Detector *Nuclear Physics B (Proc. Suppl.)* **87** 523
- [4] Borovoy A.A., Khakimov S.K. 1990 *Neutrino experiments on nuclear reactors* (Moscow Energoatomizdat)
- [5] Johann H. 1931 *Zs. f. Physik* **60** 185
- [6] Cauchois Y. *Journ. De Phys. et Radium*, S. VII, t. III, №7, p.320 (1932); t. IV, №2, p.61 (1933)
- [7] Dorofeyev O.F., Lobanov A.Ye., 2005  $\beta$ -decay in the field of the electromagnetic wave and experiments on measuring the neutrino mass *Yadernaya fizika* **68**, №6 1074

- [8] Fermi E. *Yadernaya fizika* 1951 (Moscow Izd-vo: Inostrannaya literature)
- [9] Trapeznikov V.A. 1998 Electron spectroscopy of small doses of radiation *Uspekhi fizicheskikh nauk* **168** №7 793
- [10] Trapeznikov V.A., Shabanova I.N., Zhuravlev V.A. 2004 Application of electron spectroscopy for inverse  $\beta$ -decay study *J. of Electron Spectroscopy and Related Phenomena* **137-140** 731
- [11] Manakov Yu.G., Nurullina R.A., Shabanova I.N., Trapeznikov V.A. 2006 New developments for creating energy analyzers of the next generation for the neutrino physics investigation *abstracts "Neutrino 2006"*
- [12] Trapeznikov V.A., Nemnonov S.A., 1968 Vacuum x-ray spectrometer with a bent crystal *Fizika metallov i metallovedeniye* **25** 157

### Captions for the illustrations

Figure 1. The electron spectra ( $e^-$ ) and neutrino spectra ( $\nu$ ) obtained in the  $\beta$ -decay tritium [7].

Figure 2. The scheme of ray paths in Johann method:

- a) usual variant;
- b) variant with the source of radiation placed beyond the focal circle.

Figure 3. Co  $K\alpha_{1,2}$  spectra obtained at different widths of the slit (the sizes are in mm) during scanning the crystal:

- a) primary spectra;
- b) secondary spectra.

Figure 4. The plot of the energy dependence of the state density of the reactor anti-neutrino [4].

# Galactic supernovae monitoring at LVD

**C.Vigorito on behalf of the LVD Collaboration**

University and INFN Torino, via P.Giuria 1 , 10125 Torino, IT

E-mail: vigorito@to.infn.it

## 1. The detector

The Large Volume Detector (LVD), located in hall A of the INFN Gran Sasso National Laboratory (Italy), is a multipurpose detector mainly designed to search for neutrinos from Gravitational Stellar Collapses (GSC) in our Galaxy [1, 2]. The detector has been in operation since 1992, under different increasing configurations reaching the final one with an active mass  $M=1000$  ton in 2001. LVD consists of an array of 840 scintillator counters,  $1.5 m^3$  each, arranged in a compact and modular geometry, viewed by 3 photomultipliers. All counters are operated at a common threshold  $\epsilon_H \simeq 5 MeV$ . To tag the delayed  $\gamma$  pulse due to  $n$ -capture, counters are equipped with an additional discrimination channel, set at a lower threshold  $\epsilon_L \simeq 1 MeV$ .

## 2. The supernova monitor

Supernova monitoring at LVD is performed both on-line and off-line for different purposes: **on-line** to generate prompt alert in the case of a  $\nu$ -burst candidate; **off-line** to check recorded data over long duration and multiple runs. The search for candidates is based on a 2 steps analysis of the pulses sequence including all triggers in the 7-100  $MeV$  range. Step 1 is the pure statistical selection of pulse clusters in fixed time windows (20 s) with an imitation frequency IMF below a defined threshold; if  $IMF < 1 event \cdot month^{-1}$  an automated web alert is sent to the SNEWS network of neutrino detectors [3]. Step 2 includes the complete analysis of candidates at  $IMF < 1 event \cdot year^{-1}$  studying the energy spectrum, the topological distribution of pulses in the detector and the time distribution of delayed pulses. Candidates characteristics are finally compared with the behaviour of pure background clusters to disentangle possible good signals.

## 3. Conclusions

After almost 15 years of data taking no burst candidate eligible for a true supernova signal has been detected. Over 4503 days of observation and taking into account the detector sensitivity [4], the obtained upper limit to the Gravitational Stellar Collapse in the Milky Way (source distance  $D \leq 20 kpc$ ) is: **0.18 event  $\cdot$  year $^{-1}$  at 90% c.l.**

## References

- [1] LVD Coll. 1992 *Il nuovo Cimento A* **105** 1793
- [2] LVD Coll. 2005 *Proc. 29<sup>th</sup> ICRC Pune* **5** 59
- [3] Antonioni P. et al. 2004 *New Journal of Physics* **6** 114
- [4] LVD Coll. 2005 *Proc. 29<sup>th</sup> ICRC Pune* **5** 307

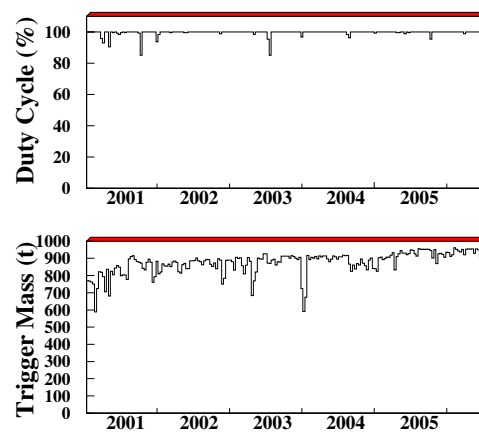


**Figure 1.** Duty cycle and trigger mass of LVD over last 5 years.

## Cosmic ray muons and muon bremsstrahlung gammas at very high energies in the atmosphere

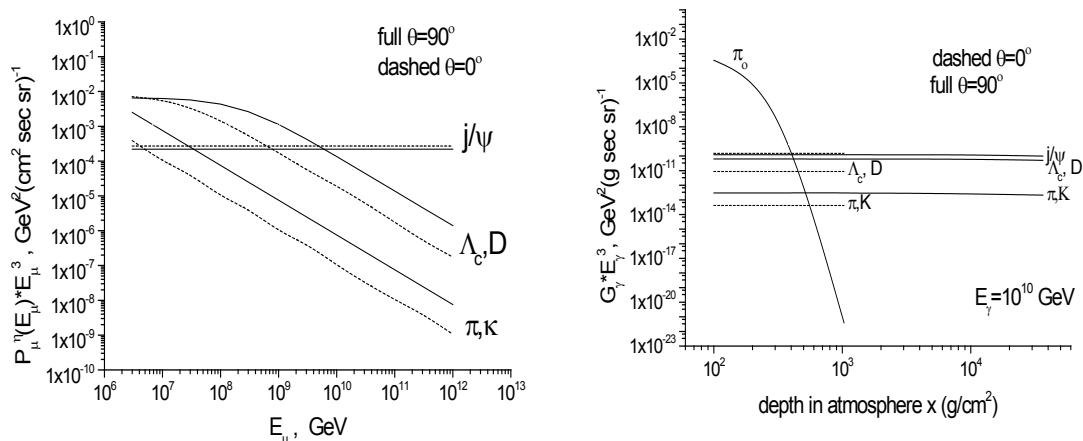
L.V. Volkova

Institute for Nuclear Research of RAS, 60<sup>th</sup> October pr. 7a, Moscow 117312, Russia

E-mail: [volkova@inr.npd.ac.ru](mailto:volkova@inr.npd.ac.ru)

**Abstract.** Fluxes of cosmic ray muons and production functions of muon bremsstrahlung gammas and of gammas from  $\pi^0$ -decays are calculated at different angles and levels in the atmosphere ( $3 \cdot 10^6$ - $10^{12}$  GeV). It is shown that charm and  $j/\psi$  production in nucleon-nucleus interactions is to be taken into account when EAS data are interpreted. The calculations are based on data from experiments on accelerators and their extrapolation to higher energies.

In the figures the calculated differential energy fluxes of muons coming to the sea level (left) and production functions of gammas produced in muon bremsstrahlung and  $\pi^0$ -decays (right) are given. All the used assumptions and parameters can be found in [1-4]. The letters near the curves show the sources of muon production in the atmosphere.



The author thank RFBR (grant 06-02-16029-a) and LSS-5573.2006.2 for financial support.

### References

- [1] Review of particle physics. Particle Data Group 2004 *Physics Letters B* **592** 1-1109
- [2] Volkova L V and Zatsepin G T 2001 *Physics of Atomic Nuclei* **64** 266-74
- [3] The HERA-B Collaboration 2005 *Preprint* hep-ex/0512029 v1 13 Dec 2005
- [4] Zhangbu Xu 2004 *Preprint* nucl-ex/0410005 v2 7 Oct 2004

# Constraints on sterile neutrinos using Super-Kamiokande I atmospheric neutrino data

W. Wang (on behalf of the Super-Kamiokande collaboration)

Department of Physics, Boston University, Boston, MA 02215, US

## 1. Introduction

In this paper, the oscillation analysis of muon neutrino mixing with tau neutrino is presented and compared with its mixing with sterile neutrino ( $\nu_s$ ) using Super-K I atmospheric neutrino data [1]. We include neutral current enhanced samples in our analysis in addition to the charged current samples in Ref. [2]. The details of the pull method used in our oscillation analysis is also documented in Ref [2].

## 2. Results

With a degree-of-freedom of 426, the least chi-square of  $\nu_\mu - \nu_\tau$  model is 455.6 and  $\nu_\mu - \nu_s$  model gives a least chi-square value of 504.8. The chi-square difference is 49.2, which corresponds to  $7\sigma$  exclusion level. Fig. 1 (a) shows the best-fit results of two models in bins that contribute the most to  $\Delta\chi^2$ . Fig. 1 (b) shows the allowance of admixture based on a  $2 + 2$  mass hierarchy model [3]. Our observation allows 25% admixture at 90% C.L.

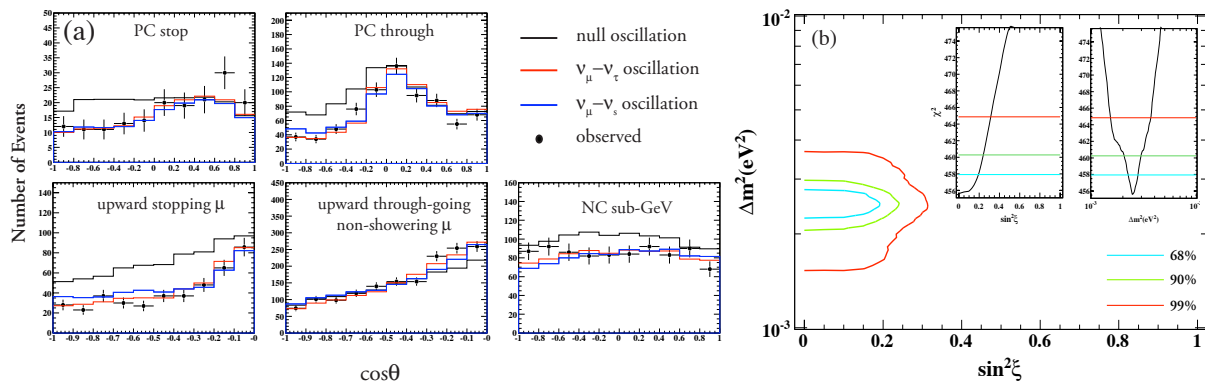


**Figure 1.** (a) Comparison of best-fits (zenith angle distributions); (b) Admixture allowance

## Acknowledgments

The author is supported by the United States Department of Energy.

- [1] Y. Ashie et al. A measurement of atmospheric neutrino oscillation parameters by Super-Kamiokande I. *Phys. Rev.*, D71:112005, 2005.
- [2] J. Hosaka et al. Three flavor neutrino oscillation analysis of atmospheric neutrinos in Super-Kamiokande. *Phys. Rev.*, D74:032002, 2006.
- [3] G. L. Fogli, E. Lisi, and A. Marrone. Four-neutrino oscillation solutions of the atmospheric neutrino anomaly. *Phys. Rev. D*, 63(5):053008, Feb 2001.

## Dual-phase argon ionization detector for measurement of coherent elastic neutrino scattering and medium-energy nuclear recoils

Winant, C.D.<sup>(1,2)</sup>, Bernstein, A.<sup>(1)</sup>, Haggmann, C.<sup>(1)</sup>, Madden, N.<sup>(1)</sup>, Stoeffl, W.<sup>(1)</sup>

(1) Lawrence Livermore National Laboratory, 7000 East Ave., Livermore CA 94550

(2) [winant2@llnl.gov](mailto:winant2@llnl.gov)

UCRL-PROC-224459

**Abstract.** We propose to build and deploy a 10-kg dual-phase argon ionization detector for the detection of coherent neutrino-nucleus scattering, which is described by the reaction;  $(\nu) + (Z,N) \rightarrow (\nu) + (Z,N)$ . Our group would be the first to make this measurement. Its detection would validate (or refute) central tenets of the Standard Model. The existence of this process is also relevant to astrophysics, where coherent neutrino scattering is assumed to impede energy transport within neutron stars. We have built a gas-phase argon ionization detector to determine the feasibility of measuring small recoil energies ( $\sim 1$ keV) predicted from coherent neutrino scattering, and to characterize the recoil spectrum of the argon nuclei induced by scattering from medium-energy neutrons. We present calibrations made with  $^{55}\text{Fe}$ , a low energy x-ray source, and describe a planned measurement of the recoil spectra from the 60keV Lithium-target neutron generator at LLNL. A high signal-to-noise measurement of the recoil spectrum will not only serve an important milestone in achieving the sensitivity necessary for measuring coherent neutrino-nucleus scattering, but will break new scientific ground by providing a first ever measurement of low-energy quenching factors in argon.

Coherent scattering occurs when the momentum transfer from a neutrino to the nucleus is much smaller than the inverse size of the recoil nucleus. A detection of coherent neutrino-nucleus scattering would verify an unconfirmed Standard Model prediction [1], explore non-standard neutrino-quark interactions, confirm stellar collapse and supernova energy transport and neutrino opacity models, and could be applied to the measurement of the flavor-blind neutrino spectrum from next nearby supernova, or could be used to promote non-intrusive reactor power monitoring [2].

We propose detecting the ionization induced by recoiling argon nuclei using a 10 kg dual-phase argon detector. The principle of dual-phase detection has been described elsewhere [3]. We propose using a 3 GW commercial nuclear reactor as a source of antineutrinos. We have designed and built a gas-phase prototype of the detector with which we have measured the 200-electron equivalent ionization signals from a 6keV  $^{55}\text{Fe}$  source with a signal-to-noise threshold of 50 electrons. This prototype also enables study of scintillation properties of Argon and investigation of electron and nuclear recoils in Argon. We will measure medium energy neutron-nuclear recoils in our prototype detector using the recently-commissioned LLNL compact pulsed neutron source.

### References

- [1] Freedman, D. Phys. Rev. D 9, 1389–1392 (1974)
- [2] Haggmann, C. A., Bernstein, A. IEEE transactions on Nuclear Science, 51(5), 2151 (2004)
- [3] Bolozdynya, A.I., NIM A 422, 314-320 (1999)

# The KamLAND Muon Tracking System

## Lindley Winslow for the KamLAND Collaboration

University of California, Berkeley and Lawrence Berkeley National Lab

LAWinslow@lbl.gov

The KamLAND detector with an overburden of 2700 m.w.e. measures a muon rate of 0.33 Hz through the inner detector. The neutrons and light nuclei produced by these muons are a significant background to both the reactor neutrino analysis and future solar neutrino analysis. A new detector is being constructed on deck to track a subset of muons as they pass through the inner detector or the surrounding rock. These data will be used to study KamLAND's muon detecting and tracking efficiencies and the production of neutrons and light nuclei from muon spallation.

### 1. Detector Design

The detector has two components, scintillator paddles and proportional tube modules. A proportional tube module contains 15 wires 3m in length with effective wire spacing of 1.5cm. Perpendicular modules will be used to obtain a (x, y) position along the track and the layer of scintillator paddles directly above these will trigger the event. A second point along the track will be given by another layer of detectors, consisting of two perpendicular layers of modules and a layer of scintillators. This second layer of detectors sits 2m below the first layer. Each of these layers of proportional tube modules has a total of 13 modules when these layers are arranged perpendicularly they form an active area of approximately 2.5m x 2.5m.

The proportional tube modules will use an Ar(90%) CO<sub>2</sub>(10%) mixture as the operating gas. Pulses on the wire pass through discriminators attached to the ends of the modules. An ECL signal is sent from the discriminator boards to LeCroy 4448 Coincidence registers. The system is then readout by the MIDAS Data Acquisition System. The current electronics readout does not allow us to store timing information so the wire spacing will limit our tracking accuracy.

Simulations of this configuration show that we can expect 1,000 events per day through the system of which 200 will pass through the inner detector of KamLAND. Extrapolating the uncertainty in these tracks 13m down to the center of KamLAND gives us a 20cm uncertainty on the impact parameter for these muons.

### 2. Physics Goal

KamLAND's geometry is well suited for detecting point like events with MeV scale energies. Muons are more difficult to reconstruct since they deposit light along a track and deposit several orders of magnitude more light. Studies of muon track theta and phi distributions are consistent with Monte Carlo predictions but there are reconstruction problems as muons approach the detector boundaries. This new system will allow us to study these reconstruction inefficiencies and therefore improve our studies of neutrons and light nuclei from muon spallation. It will also give us the ability to study the effects of muons passing through the rocks surrounding KamLAND.

# Optimization of a neutrino factory experiment

Walter Winter

School of Natural Sciences, Institute for Advanced Study, Einstein Drive, Princeton, NJ 08540

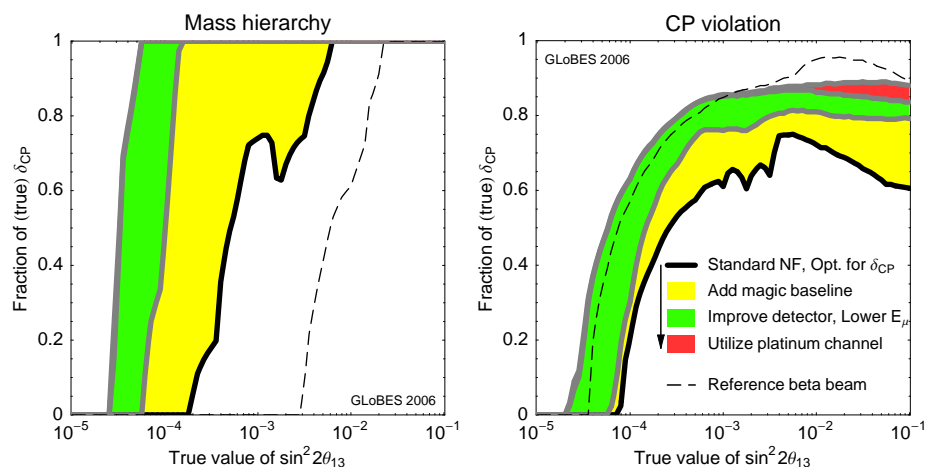
E-mail: winter@ias.edu

**Abstract.** We discuss the optimization of a neutrino factory experiment for neutrino oscillation physics in terms of muon energy, baselines, and oscillation channels.

For the optimization of a neutrino factory in Ref. [1], we first of all consider a single baseline for the  $\sin^2 2\theta_{13}$ , mass hierarchy, and CP violation sensitivities. For the sensitivity to  $\sin^2 2\theta_{13}$ , a baseline of  $L \simeq 7500$  km is optimal because correlations and degeneracies are minimal at this “magic” baseline. For the mass hierarchy sensitivity, very long baselines  $L \gg 6000$  km are preferred in general. And for CP violation, a shorter baseline of 3000 to 5000 km is preferable, which also improves the statistics for the  $\sin^2 2\theta_{13}$  sensitivity. Therefore, we conclude that two baselines, one with 3000 to 5000 km and one with  $L \simeq 7500$  km, have an excellent physics potential for neutrino oscillation physics, where the muon energy should be  $E_\mu \gtrsim 40$  GeV.

As far as possible improvements of a neutrino factory oscillation experiment are concerned, the main factor may be the muon neutrino detector with charge identification. For example, energy threshold and energy resolution of a magnetized iron calorimeter may be improved. We have identified the threshold as major impact factor for the physics potential, and we have demonstrated that a lower threshold can improve the physics potential significantly even if a larger background from charge mis-identification is allowed. For such an improved detection system, the muon energy may be lowered to about 20 GeV without loss of physics potential.

In addition to the “golden” ( $\nu_e \rightarrow \nu_\mu$ ) channel, the “silver” ( $\nu_e \rightarrow \nu_\tau$ ) and platinum ( $\nu_\mu \rightarrow \nu_e$ ) channels may provide additional complementary information. We demonstrate in Ref. [1] that especially the platinum channel may have an interesting CP violation potential for large  $\sin^2 2\theta_{13}$  which cannot be achieved otherwise. The overall physics potential of a neutrino factory including possible optimization is summarized in the following figure (from Ref. [1]):



I would like to acknowledge support from the W. M. Keck Foundation, and through NSF grant PHY-0503584.

[1] P. Huber, M. Lindner, M. Rolinec, and W. Winter, *Preprint hep-ph/0606119*

## EXO-200: A LXe Detector for Double Beta Decay

Jesse Wodin and Andrea Pocar for the EXO Collaboration

Physics Department, Stanford University, Stanford, CA 94305, USA

EXO-200 is the first phase of the Enriched Xenon Observatory (EXO) searching for double beta decay of  $^{136}\text{Xe}$ . It employs 200 kg of enriched xenon (isotopically enriched to 80% in  $^{136}\text{Xe}$ , already in hand for the project) in liquid form (LXe). The xenon, contained in a cylindrical time projection chamber (TPC) with 3-dimensional ionization and scintillation readout, is both the target and active medium. The simultaneous, event-by-event collection of deposited ionization and scintillation light was shown to significantly improve the energy resolution of LXe detectors. The TPC is currently under construction at Stanford, where its functionality will be tested prior to being housed underground at the Waste Isolation Pilot Plant (WIPP), New Mexico. EXO-200 will have a sensitivity to Majorana neutrino masses of  $\sim 0.3$  eV in two years and will also serve as a prototype for a 1-10 ton scale EXO experiment. The enriched xenon target is contained in a cylindrical, thin (1.5 mm) copper vessel, approximately 40 cm long and 40 cm in diameter. Scintillation light is collected by 518 Large Area Avalanche PhotoDiodes (LAAPDs) mounted on two planes at the bases of the cylinder and read out in groups of 7. The TPC has two symmetric drift volumes along the cylinder axis, with a central cathode grid. Each drift region works as a gridded ionization chamber with crossed "x" and "y" wires (100  $\mu\text{m}$  in diameter), read out in groups of 3. "Y" wires collect the induced charge drifting by them and collected on the "x" wires behind them. All wire planes and the cathode are  $>90\%$  transparent to the scintillation light. Overall, a  $>15\%$  optical coverage is expected, which includes the use of a teflon reflector on the cylinder wall and LAAPD reflectance. Long electron lifetimes in LXe were demonstrated by recirculating the xenon through a hot zirconium SAES getter. The xenon vessel is placed within a double-walled, vacuum insulated copper cryostat. Each copper layer is 2.5 cm thick. The inner cryostat is further thermally insulated with layers of superinsulation. The volume between the xenon vessel and the cryostat is filled with a fluorinated organic fluid (3M HFE-7000) which has a density of 1.8 at the LXe temperature of  $-100^\circ\text{C}$ ; such fluid provides a large thermal mass for temperature stability of the detector and provides excellent screening from gamma-ray backgrounds from the cryostat materials. The cryostat is surrounded by 25 cm of lead, specifically selected for its low  $^{210}\text{Pb}$  content. All construction materials are being chosen after fulfilling extremely strict radio-purity requirements. Analysis tools used by the EXO collaboration include neutron activation analysis (NAA), direct  $\gamma$  counting,  $\alpha$  counting, radon emanation assays, and mass spectroscopy (ICP-MS and GDMS). The detector will be operated 655 m ( $\sim 1600$  m.w.e.) underground at WIPP, where vertical residual muon flux was measured  $3 \times 10^{-7} \text{ s}^{-1} \text{ m}^{-2} \text{ sr}^{-1}$  (Nucl. Instr. Meth. A 538(2005)516). The cryostat, xenon and HFE plumbing, and part of the lead are installed in the Stanford modular clean rooms, while the TPC and xenon vessel are currently being assembled. The detector is expected to be shipped in its clean rooms to WIPP by the end of 2006.

factors, such as the composition of the GRB ejecta, the bulk Lorentz factor of the outflow, as well as the spectral index of the shock accelerated protons. In any case, future observations with Icecube and other neutrino detectors would bring important information about GRBs, regardless whether a positive detection or a stringent upper limit are made.

### References:

- [1] Mészáros P 2002 *Ann. Rev. Astron. Astrophys.* **40** 137; Zhang B. and Mészáros, P. 2004 *Int. J. Mod. Phys. A.* **19** 2395; Piran T 2005 *Rev. Mod. Phys.* **76** 1143; Mészáros P 2006 *Rev. Prog. Phys.* **69** 2259
- [2] Zhang B. et al. 2006 *Astrophys. J.* **642** 354
- [3] Nousek J A et al. 2006 *Astrophys. J.* **642** 389; Chincarini G et al. 2005, astro-ph/0506453; O'Brien P et al. 2006 *Astrophys. J.* **647** 1213; Willingale R et al. 2007 *Astrophys. J.* submitted (astro-ph/0612031); Zhang B 2007 *Chinese J. Astron. astrophys.* **7** 1 (astro-ph/0701520)
- [4] Waxman E 1995, *Phys. Rev. Lett.* **75** 386; Milgrom M and Usov V V 1995, *Astrophys. J.* **449** L37; Vietri D 1995, *Astrophys. J.* **453** 883
- [5] Bahcall J N and Mészáros P 2000 *Phys. Rev. Lett.* **85** 1362; Derishev E V et al. 1999 *Astrophys. J.* **521** 640
- [6] Mészáros P and Rees M J 2001 *Astrophys. J.* **541** L5
- [7] Paczyński B and Xu G 1994 *Astrophys. J.* **427** 708
- [8] Mészáros P and Waxman E 2001 *Phys. Rev. Lett.* **87** 171102
- [9] Razzaque S, Mészáros P and Waxman E 2003 *Phys. Rev. Lett.* **90** 241103; Razzaque S, Mészáros P and Waxman E 2004 *Phys. Rev. D* **69** 023001
- [10] Waxman E and Bahcall J N 1997 *Phys. Rev. Lett.* **78** 2292; Rachen J P and Mészáros P 1998 *Phys. Rev. D* **58** 123005
- [11] Fan Y Z, Zhang B and Wei D M *Astrophys. J.* **629** 334
- [12] Waxman E and Bahcall JN 2000 *Astrophys. J.* **541** 707; Dai Z G and Lu T. 2001 *Astrophys. J.* **551** 249
- [13] Dermer C D 2002 *Astrophys. J.* **574** 65; Li Z, Dai Z G and Lu T 2002 *Astron. Astrophys.* **396** 303
- [14] Burrows, D N et al. 2005 *Science* **309** 1833; Falcone A D et al. 2006 *Astrophys. J.* **641** 1010; Romano P et al. 2006 *Astron. Astrophys.* **450** 59; Chincarini G et al. 2007, in preparation
- [15] Fan Y Z and Wei D M 2005 *Mon. Not. R. Astron. Soc.* **364** L42; Perna R, Armitage P J and Zhang B 2006 *Astrophys. J.* **636** L29
- [16] Fan Y Z, Zhang B and Proga D 2005 *Astrophys. J.* **635** L129; Proga D and Zhang B 2006 *Mon. Not. R. Astron. Soc.* **370** L41; Dai Z G et al. 2006 *Science* **311** 1127
- [17] Murase K and Nagataki S 2006 *Phys. Rev. Lett.* **97** 051101
- [18] Campana, S et al. 2006 *Nature* **442** 1008; Cobb B E. et al. 2006 *Astrophys. J.* **645** L113; Pian E et al. 2006 *Nature* **442** 1011; Soderberg A et al. 2006 *Nature* **442** 1014; Liang E W et al. 2006 *Astrophys. J.* submitted (astro-ph/0605200)
- [19] Gupta N and Zhang B 2007 *AstroPart. Phys.* in press (astro-ph/0606744)
- [20] Murase K et al. 2006 *Astrophys. J.* **651** L5
- [21] Waxman E and Bahcall J 1999 *Phys. Rev. D* **59** 023002; Bahcall J N and Waxman E 2001 *Phys. Rev. D* **64** 023002
- [22] Halzen F 2007 *Science* **315** 66; Waxman E 2007 *Science* **315** 63
- [23] Coburn W and Boggs S E 2003 *Nature* **423** 415, cf. Rutledge R E and Fox D B 2004 *Mon. Not. R. Astron. Soc.* **350** 1288; Zhang B, Kobayashi S and Mészáros P 2003 *Astrophys. J.* **595** 950; Fan Y-Z et al. 2002 *Chinese J. Astron. Astrophys.* **2** 449; Kumar P and Panaitescu A 2003 *Mon. Not. R. Astron. Soc.* **346** 905
- [24] Zhang B and Kobayashi S 2005 *Astrophys. J.* **628** 315; Roming P W A et al. 2006 *Astrophys. J.* **652** 1416
- [25] Molinari E et al. 2006, preprint (astro-ph/0612607); Jin Z-P and Fan Y-Z 2007, preprint (astro-ph/0701715)
- [26] Kumar P et al. 2006 *Mon. Not. R. Astron. Soc.* **367** L52; Kumar P et al. 2007 *Mon. Not. R. Astron. Soc.*, in press; Lyutikov M 2006 *Mon. Not. R. Astron. Soc.* **369** L5
- [27] Zhang B and Mészáros P 2002 *Astrophys. J.* **581** 1236; Asano K and Kobayashi S 2003 *Pub. Astron. Soc. Japan* **55** 579
- [28] Mészáros P et al. 2002 *Astrophys. J.* **578** 812; Rees M J and Mészáros P 2005 *Astrophys. J.* **628** 847; Ryde F et al 2006 *Astrophys. J.* **652** 1400; Thompson C, Mészáros P and Rees M J 2006 *Astrophys. J.* submitted (astro-ph/0608282)